Volume 194 Number 1

THE BIOLOGICAL BULLETIN

FEBRUARY, 1998

Published by the Marine Biological Laboratory

THE
BIOLOGICAL BULLETIN

PUBLISHED BY
THE MARINE BIOLOGICAL LABORATORY

FEBRUARY, 1998

Printed and Issued by
LANCASTER PRESS, Inc.
3575 HEMPLAND ROAD
LANCASTER, PA

Cover

Hydroides elegans is a polychaete annelid and a common member of warm-water, marine fouling communities around the world. This microserpulid worm can be reared on the bench, at room temperature, in the wells of a plastic ice-cube tray. In nature, the worms spawn their gametes into the sea, where fertilization occurs. Some 4–6 days after fertilization, the feeding larvae become competent to settle, and they do so rapidly upon contact with a biofilmed surface. *H. elegans* is small, manageable, and has a generation time of 3 weeks or less; it is therefore the quintessential marine polychaete with which to study developmental and genetic processes.

Metamorphosis in *H. elegans* is characterized in a report by Capizio-Ituarte and Hadfield in this issue; key morphogenetic events are used to assay the responses of larvae to biofilms and to artificial ionic inducers of metamorphosis.

Counterclockwise from upper left:

1. Adult *H. elegans* in their calcareous tubes display their branchial crowns; the operculum that characterizes the species is visible in the midst of the crown.
2. Competent, 5-day-old larva showing the characteristic prototroch (photo by B. Nedved).
3. Anterior portion of a worm only 24 hours after metamorphosis. Note the pair of radioles that will form the branchial crown in the adult; the collar helps to shape the calcareous tube.

CONTENTS

THE BIOLOGICAL BULLETIN

THE BIOLOGICAL BULLETIN is published six times a year by the Marine Biological Laboratory, 7 MBL Street, Woods Hole, Massachusetts 02543.

Subscriptions and similar matter should be addressed to Subscription Manager, THE BIOLOGICAL BULLETIN, Marine Biological Laboratory, 7 MBL Street, Woods Hole, Massachusetts 02543. Subscription per year (six issues, two volumes): $195 for libraries; $95 for individuals. Subscription per volume (three issues): $97.50 for libraries; $50 for individuals. Back and single issues (subject to availability): $40 for libraries; $20 for individuals.

Communications relative to manuscripts should be sent to Michael J. Greenberg, Editor-in-Chief, or Pamela L. Clapp, Managing Editor, at the Marine Biological Laboratory, 7 MBL Street, Woods Hole, Massachusetts 02543. Telephone: (508) 289-7428. FAX: 508-457-1924. E-mail: pclapp@mbl.edu.

http://www.mbl.edu/BiologicalBulletin/

The home page for the electronic companion to THE BIOLOGICAL BULLETIN—*the Marine Models Electronic Record*—and other BIOLOGICAL BULLETIN publications is available on the World Wide Web at the address shown above.

THE BIOLOGICAL BULLETIN is indexed in bibliographic services including *Index Medicus* and MEDLINE, *Chemical Abstracts, Current Contents, CABS (Current Awareness in Biological Sciences),* and *Geo Abstracts.*

Printed on acid free paper,
effective with Volume 180, Issue 1, 1991.

POSTMASTER: Send address changes to THE BIOLOGICAL BULLETIN, Marine Biological Laboratory, 7 MBL Street, Woods Hole, MA 02543.

Periodicals postage paid at Woods Hole, MA, and additional mailing offices.
ISSN 0006-3185

INSTRUCTIONS TO AUTHORS

The Biological Bulletin accepts outstanding original research reports of general interest to biologists throughout the world. Papers are usually of intermediate length (10–40 manuscript pages). A limited number of solicited review papers may be accepted after formal review. A paper will usually appear within four months after its acceptance.

Very short, especially topical papers (less than 9 manuscript pages including tables, figures, and bibliography) will be published in a separate section entitled "Research Notes." A Research Note in *The Biological Bulletin* follows the format of similar notes in *Nature.* It should open with a summary paragraph of 150 to 200 words comprising the introduction and the conclusions. The rest of the text should continue on without subheadings, and there should be no more than 30 references. References should be referred to in the text by number, and listed in the Literature Cited section in the order that they appear in the text. Unlike references in *Nature,* references in the Research Notes section should conform in punctuation and arrangement to the style of recent issues of *The Biological Bulletin.* Materials and Methods should be incorporated into appropriate figure legends. See the article by Lohmann *et al.* (October 1990, Vol. **179:** 214–218) for sample style. A Research Note will usually appear within two months after its acceptance.

The Editorial Board requests that regular manuscripts conform to the requirements set below; those manuscripts that do not conform will be returned to authors for correction before review.

1. ***Manuscripts.*** Manuscripts, including figures, should be submitted in triplicate. (Xerox copies of photographs are not acceptable for review purposes.) The submission letter accompanying the manuscript should include a telephone number, a FAX number, and (if possible) an E-mail address for the corresponding author. The original manuscript must be typed in no smaller than 12 pitch or 10 point, using double spacing (*including* figure legends, footnotes, bibliography, etc.) on one side of 16- or 20-lb. bond paper, 8 by 11 inches. Please, no right justification. Manuscripts should be proofread carefully and errors corrected legibly in black ink. Pages should be numbered consecutively. Margins on all sides should be at least 1 inch (2.5 cm). Manuscripts should conform to the *Council of Biology Editors Style Manual,* 5th Edition (Council of Biology Editors, 1983) and to American spelling. Unusual abbreviations should be kept to a minimum and should be spelled out on first reference as well as defined in a footnote on the title page. Manuscripts should be divided into the following components: Title page, Abstract (of no more than 200 words), Introduction, Materials and Methods, Results, Discussion, Acknowledgments, Literature Cited, Tables, and Figure Legends. In addition, authors should supply a list of words and phrases under which the article should be indexed.

2. ***Title page.*** The title page consists of a condensed title or running head of no more than 35 letters and spaces, the manuscript title, authors' names and appropriate addresses, and footnotes listing present addresses, acknowledgments or contribution numbers, and explanation of unusual abbreviations.

3. ***Figures.*** The dimensions of the printed page, 7 by 9 inches, should be kept in mind in preparing figures for publication. We recommend that figures be about 1 times the linear dimensions of the final printing desired, and that the ratio of the largest to the smallest letter or number and of the thickest to the thinnest line not exceed 1:1.5. Explanatory matter generally should be included in legends, although axes should always be identified on the illustration itself. Figures should be prepared for reproduction as either line cuts or halftones. Figures to be reproduced as line cuts should be unmounted glossy photographic reproductions or drawn in black ink on white paper, good-quality tracing cloth or plastic, or blue-lined coordinate paper. Those to be reproduced as halftones should be mounted on board, with both designating numbers or letters and scale bars affixed directly to the figures. All figures should be numbered in consecutive order, with no distinction between text and plate figures and cited, in order, in the text. The author's name and an arrow indicating orientation should appear on the reverse side of all figures.

Color: The Biological Bulletin will publish color figures and plates, but must bill authors for the actual additional cost of printing in color. The process is expensive, so authors with more than one color image should—consistent with editorial concerns, especially citation of figures in order—combine them into a single plate to reduce the expense. On request, when supplied with a copy of a color illustration, the editorial staff will provide a pre-publication estimate of the printing cost.

4. ***Tables, footnotes, figure legends, etc.*** Authors should follow the style in a recent issue of *The Biological Bulletin* in preparing table headings, figure legends, and the like. Because of the high cost of setting tabular material in type, authors are asked to limit such material as much as possible. Tables, with their headings and footnotes, should be typed on separate sheets, numbered with consecutive Roman numerals, and placed after the Literature Cited. Figure legends should contain enough information to make the figure intelligible separate from the text. Legends should be typed double spaced, with consecutive Arabic numbers, on a separate sheet at the end of the paper. Footnotes should be limited to authors' current addresses, acknowledgments or contribution numbers, and explanation of unusual abbreviations. All such footnotes should appear on the title page. Footnotes are not normally permitted in the body of the text.

5. ***Literature cited.*** In the text, literature should be cited by the Harvard system, with papers by more than two authors cited as Jones *et al.*, 1980. Personal communications and material in preparation or in press should be cited in the text only, with author's initials and institutions, unless the material has been formally accepted and a volume number can be supplied. The list of references following the text should be headed Literature Cited, and must be typed double spaced on separate pages, conforming in punctuation and arrangement to the style of recent issues of *The Biological Bulletin*. Citations should include complete titles and inclusive pagination. Journal abbreviations should normally follow those of the U. S. A. Standards Institute (USASI), as adopted by BIOLOGICAL ABSTRACTS and CHEMICAL ABSTRACTS, with the minor differences set out below. The most generally useful list of biological journal titles is that published each year by BIOLOGICAL ABSTRACTS (BIOSIS List of Serials; the most recent issue). Foreign authors, and others who are accustomed to using THE WORLD LIST OF SCIENTIFIC PERIODICALS, may find a booklet published by the Biological Council of the U.K. (obtainable from the Institute of Biology, 41 Queen's Gate, London, S.W.7, England, U.K.) useful, since it sets out the WORLD LIST abbreviations for most biological journals with notes of the USASI abbreviations where these differ. CHEMICAL ABSTRACTS publishes quarterly supplements of additional abbreviations. The following points of reference style for THE BIOLOGICAL BULLETIN differ from USASI (or modified WORLD LIST) usage:

A. Journal abbreviations, and book titles, all underlined (for *italics*)

B. All components of abbreviations with initial capitals (not as European usage in WORLD LIST *e.g., J. Cell. Comp. Physiol.* NOT *J. cell. comp. Physiol.*)

C. *All* abbreviated components must be followed by a period, whole word components *must not* (*i.e., J. Cancer Res.*)

D. Space between all components (*e.g., J. Cell. Comp. Physiol.*, not *J.Cell.Comp.Physiol.*)

E. Unusual words in journal titles should be spelled out in full, rather than employing new abbreviations invented by the author. For example, use *Rit Vísindafjélags Islendinga* without abbreviation.

F. All single word journal titles in full (*e.g., Veliger, Ecology, Brain*).

G. The order of abbreviated components should be the same as the word order of the complete title (*i.e., Proc.* and *Trans.* placed where they appear, not transposed as in some BIOLOGICAL ABSTRACTS listings).

H. A few well-known international journals in their preferred forms rather than WORLD LIST or USASI usage (*e.g., Nature, Science, Evolution* NOT *Nature, Lond., Science, N.Y.; Evolution, Lancaster, Pa.*)

6. ***Reprints, page proofs, and charges.*** Authors of articles in black and white (no color figures) receive their first 50 reprints (without covers) free of charge. Color reprints and additional black-and-white reprints may be purchased; authors will receive order forms. Reprints normally will be delivered about 2 to 3 months after the issue date. Authors (or delegates for foreign authors) will receive page proofs of articles shortly before publication. They will be charged the current cost of printers' time for corrections to these (other than corrections of printers' or editors' errors). Other than these charges for authors' alterations, *The Biological Bulletin* does not have page charges.

Reference: *Biol. Bull.* **194**: 1–6. (February, 1998)

Mechanical Significance of Obliquely Striated Architecture in Nematode Muscle

A. H. JAY BURR* AND CARL GANS

Department of Biological Sciences, Simon Fraser University, Burnaby, British Columbia, V5A 1S6, Canada; and Department of Zoology, University of Texas, Austin, Texas 78746

In certain invertebrate muscles, adjacent narrow columns of sarcomeres are displaced along the fiber axis, providing an obliquely striated myofilament pattern in certain section planes. Although this architecture is described in many phyla and has been the subject of much discussion (1–12), its mechanical significance has yet to be resolved. In nematodes, where ultrastructural details of the obliquely striated muscle have long been known (12–19), another unique and prominent feature is the attachment of every sarcomere to the plasmalemma and basal lamina via dense bodies (Z-disc analogs). Unfortunately, the importance of this feature to the transmission of the contractile force to the cuticle is not understood outside the Caenorhabditis elegans *literature: it was overlooked in recent reviews covering obliquely striated muscle (9–11). Here we consider transmission of force and oblique striation together. We compare the contractile architecture in* C. elegans *with that in the more complex muscle type of larger nematodes. Both types are designed to transmit the force of contraction laterally to the cuticle rather than longitudinally to the muscle ends. In the second type, folding of the contractile structure around an inward extension of the basal lamina enables a higher number of sarcomeres to be linked to cuticle per unit length. We suggest that the mechanical significance of the oblique arrangement of sarcomeres in both types is that it distributes the force application sites of the sarcomeres more evenly over the basal lamina and cuticle. With this muscle architecture, smooth bending of the nematode body tube would be possible, and kinking would be prevented.*

In nematodes, four bands of muscles lie longitudinally along the cuticle. Bending is caused by compression of the cuticle due to contraction of either the dorsal or ventral muscle pairs with opposing action from the hydrostatic skeleton (20–21). The undulatory locomotion (see Fig. 2A) is due to smooth waves of bending that apply the propulsive forces to the substrate (22).

In all nematodes, the longitudinal muscle bands are composed of a single layer of cells, and the contractile filaments form a layer along the distal surface of each cell. The structure of the filament layer is diagrammed in Figure 1 for the two main types of muscle fiber architecture found in nematodes: platymyarian, represented here by *Caenorhabditis elegans*, and coelomyarian, represented by *Mermis nigrescens*. The structures of other platymyarian and coelomyarian nematode species are closely similar to these examples (12–15, 19).

In both types of architecture the myofilaments lie parallel to the long axis of the muscle fiber and the body axis (vertical in Fig. 1). Observe the one complete sarcomere shown in the frontal plane of the *Mermis* diagram and the partial ones in the other section planes. Clusters of thin filaments attach to each bar-shaped electron-dense structure. Called dense bodies or Z-bars, the latter are equivalent to the Z-discs of vertebrate cross-striated muscle in that they provide attachment sites for the actin filaments and form the boundaries between the narrow sarcomeres (16). Within each sarcomere, the thick filaments are linked to each other and to the plasmalemma by the M-line material (Fig. 1).

Probably the most significant and distinguishing structural feature of obliquely striated muscle of nematodes is the direct attachment of each dense body, and thereby each sarcomere, to the muscle cell membrane (Fig. 1). In cross-striated muscle there is no equivalent attachment—only a loose linkage of Z-discs with others along the same myofibril, between neighboring myofibrils, and to sites on the sarcolemma. These connections are made via

Received 12 May 1997; accepted 1 October 1997.

*To whom correspondence should be addressed. E-mail: burr@sfu.ca

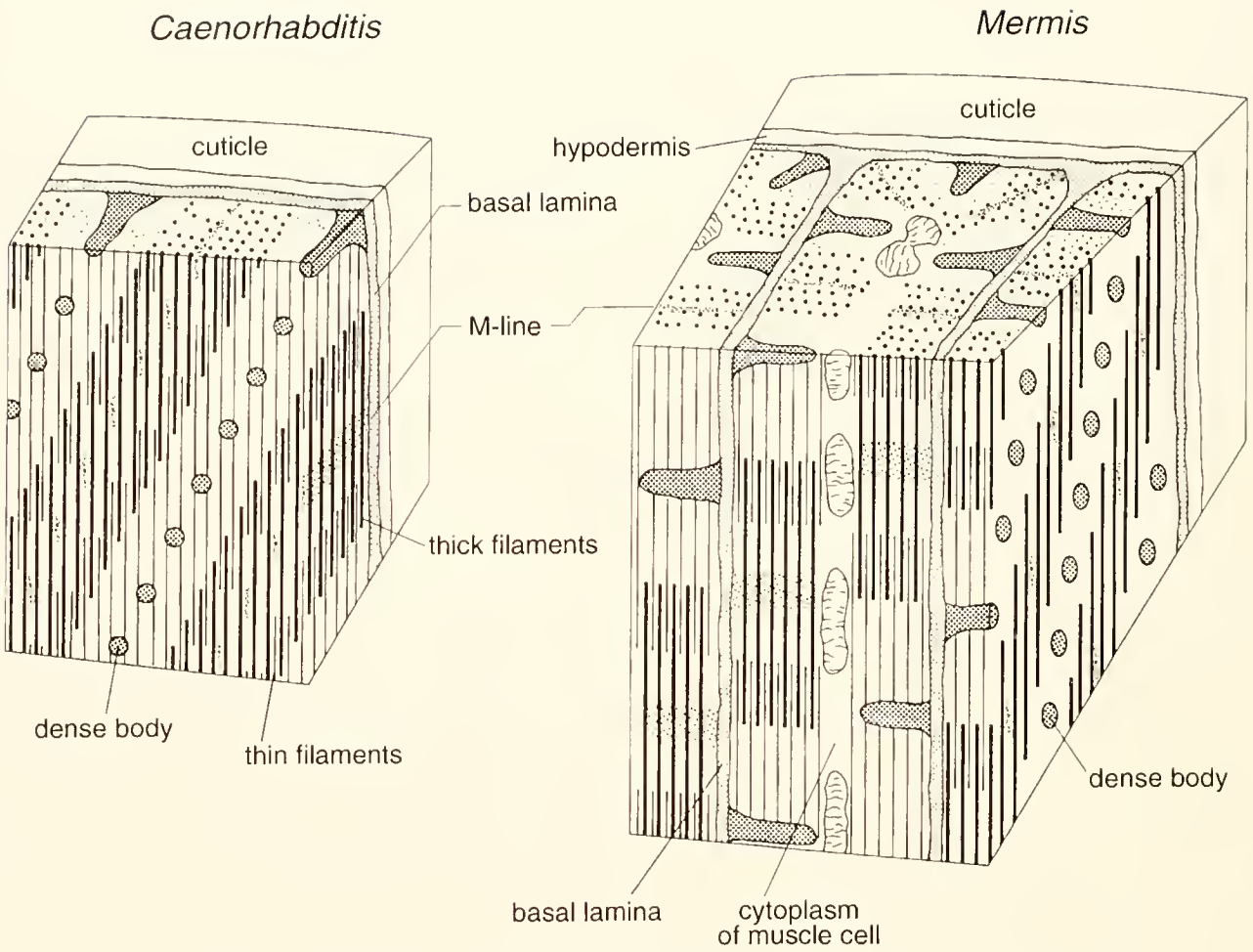

Figure 1. Contractile architecture of the two main types of nematode body-wall muscle: platymyarian (example: *Caenorhabditis elegans*) and coelomyarian (example: *Mermis nigrescens*). The anterior-posterior axis is vertical. For clarity, only two thin filaments of the bundle that attach to each dense body (13–14, 29) are illustrated in the tangential section of the *Caenorhabditis* diagram. In the equivalent, radial plane of the *Mermis* diagram, the thin filaments have been omitted altogether. The scale of the diagrams was shortened in the vertical direction to allow illustration of a complete sarcomere. *Methods:* The *C. elegans* structure was redrawn at a new orientation from illustrations by Francis and Waterston (16). That of *Mermis* was drawn from transmission electron micrographs of orthogonal sections (29).

an exosarcomeric lattice of intermediate filaments (23). The intermediate filament lattice can transmit forces along a myofibril, but only when a sarcomere is stretched beyond its normal operating range (24), and there is no evidence for lateral transmission of forces to the sarcolemma. In smooth muscle, also, there is no equivalent lateral attachment. The myofilament strands containing actin-myosin contractile units are anchored at their ends to the plasmalemma by membrane-associated dense bodies, or adherens junctions. However, cytoplasmic dense bodies that serially link contractile units within the strands are not directly attached to the plasmalemma (25–26).

By contrast, in nematode body wall muscle, all dense bodies appear firmly attached to the sarcolemma. Like the force-transmitting attachment plaques at the ends of cross-striated muscle cells, the electron-dense, α-actinin-containing dense bodies are fastened to the plasmalemma and basal lamina by a broad base composed of vinculin, talin, and integrin (16–18, 27). These components also play a role in sarcomere localization and assembly during embryonic development (27). The dense bodies are analogous to focal adhesions of vertebrate non-muscle cells in that they attach actin filaments through the plasmalemma to the basal lamina via the same protein components (28).

In the platymyarian type of nematode muscle cell, the contractile structure consists of a layer, about 1 μm in thickness, of myofilaments parallel to the very thin epidermis (hypodermis) and cuticle (Fig. 1). The ~1-μm dense

bodies traverse the entire depth of the filament layer and thereby attach the myofilaments perpendicularly to the sarcolemma and basal lamina. The basal lamina underlying the muscle, in turn, is fastened to the cuticle across the 0.15-μm-thick epidermal cell cytoplasm via 1-μm-spaced, 1-μm-wide circumferential bands of hemidesmosomes and intermediate filaments (16–17). Thus, the ends of each sarcomere are tightly anchored to the cuticle via dense bodies, basal lamina, and hypodermal cytoskeleton, and the shortening of a sarcomere would compress the cuticle locally.

In the coelomyarian muscle type, seen in *Mermis nigrescens* (19, 29) and various other large nematodes including *Ascaris lumbricoides* (reclassified *suum*) (12–14), the plate of myofilaments is folded lengthwise so that most of the contractile layer lies radially (Fig. 1). The thickness of the myofilament plate is the same (1–2 μm) in *Mermis* and *C. elegans;* however, it is two times thicker in the much larger *Ascaris* (13). In the folded contractile layer of coelomyarian muscle, the dense bodies connect the thin filaments perpendicularly to the basal lamina, as in platymyarian muscle, but most of the basal lamina is in the form of a longitudinal ribbon that extends radially inwards between the cells (Fig. 1). This rearrangement markedly increases the number of sarcomeres that can be connected to a unit length of cuticle, thus increasing the maximum contractile force. These ribbons of basal lamina would transmit compressive forces radially to the circumferential basal lamina lining the hypodermis. There, as in the platymyarian arrangement, hemidesmosomes and intermediate filaments are present in the thin hypodermal cytoplasm (12, 30) which would transmit compressive forces across it to the cuticle.

Hence, the links between thin filaments and the cuticle are the same in the two types, but with the radial extension of the basal lamina in coelomyarian muscle. In both types, the density and thickness of the dense bodies suggest rigidity, and the increased electron density seen in the basal lamina adjacent to the dense bodies and in the cuticle near the intermediate filaments (12, 18–19, 29–30) suggests that these attachment sites are reinforced to distribute stress. In the coelomyarian type, the radial extension of the basal lamina would add an extra element of elasticity to the link between sarcomere and cuticle.

The M-line material in the center of the A band (Fig. 1) attaches the thick filaments to the basal lamina and thus could also transmit forces to the basal lamina; however, it is unlikely to contribute significantly to the compressive forces acting on the basal lamina. Nematode M-lines are similar in density and thickness to those in cross-striated muscle fibrils. The relatively thicker and more electron-dense dense bodies are more probably the primary force transmitters. Like dense bodies, the M-line material is attached via β-integin and talin, but vinculin and α-actinin are missing (16, 28). M-lines are thought to keep the thick filaments roughly in register and centered within the sarcomere. The forces transmitted via the M-line in nematode muscle are probably limited to what is needed to maintain the average position of the thick filaments in a sarcomere centered between the dense bodies.

A system of inelastic fibers that interconnect dense bodies along the oblique row in *Ascaris* (12) is now known to be intermediate filaments (30). These are coiled except in fully extended muscle, so their role—like that of the exosarcomeric intermediate filament lattice of cross-striated muscle—may be to limit over-extension (8, 12, 15, 30).

The mechanical linkage in cross-striated muscle cells is very different. The sarcomeres of vertebrate myofibrils are assembled into cylindrical columns, the myofibrils. Tensile forces are transmitted longitudinally by the end-to-end contacts across the Z-discs bounding the sarcomeres and across the attachment plaques connecting between cell ends. In contrast, the contractile apparatus of nematodes appears to be designed for transmitting compressive forces laterally to the cuticle. In *C. elegans*, the attachment sites of sarcomeres via dense bodies to the basal lamina are far more numerous than the attachment plaques at the ends of the cells. In *Mermis*, the lateral attachments to the basal lamina extend over the entire 6-mm length of the extremely narrow (2 μm) band of contractile filaments. These dimensions are to be compared to the 5-10 mm arc lengths of the smooth bends which are propagated along the body. These geometries suggest that comparatively little of the contractile force developed within the longitudinal muscles is transmitted serially (from sarcomere to sarcomere and cell to cell) to the muscle ends. Rather, shortening of each sarcomere would directly compress the adjacent basal lamina to which it is individually and tightly attached. From the basal lamina, this compression would be transmitted to the cuticle by the many short intermediate filaments traversing the 1.5-μm hypodermis. Thus, the most significant mechanical distinction between obliquely striated muscle of nematodes and cross-striated muscle is that each sarcomere is connected perpendicularly to the site of force application, rather than serially to the muscle ends.

The functional consequence of this lateral, parallel application of contractile force to the cuticle is evident in the motion caused by the longitudinal muscles. Nematode locomotion typically involves smooth dorsoventral bending of the body tube (Fig. 2A). Although the straps of longitudinal muscles run the entire length of the body, compression of the cuticle occurs locally, on the inside of bends, for two or more separated bends along the length. This could occur only if local, lateral application of contractile force was significant. Localized bending is

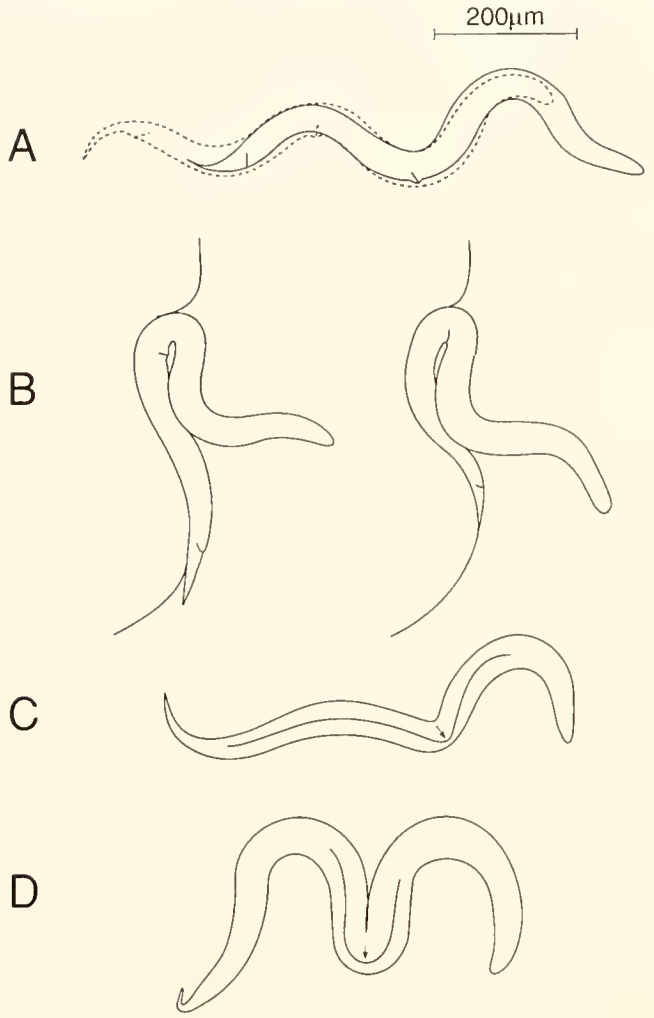

Figure 2. Propulsive motion of wild-type and mutant *Caenorhabditis elegans*. (A) Free forward motion of wild-type on surface of agar gel (two views 1.2 s apart). (B) Propulsion of wild-type in contact with surface of a bubble (two views 1.0 s apart). The external capillary force causes buckling of the body tube. Marks indicate location of vulva (midbody) and anus of this young adult hermaphrodite. There is some foreshortening due to out-of-plane orientation. (C) Kink that occurs during forward locomotion of a *lin-39* mutant of *C. elegans* crawling on agar. Dorsal is upwards. (D) Sharp kink that occurs during reverse locomotion of the same individual. Arrows point to the position of the refractile intestinal lumen, visible under the illumination conditions. *Methods:* Locomotory motion of *C. elegans* wildtype (Bristol, N2 strain), and the *lin-39* (n1760 null allele) mutant kindly provided by Scott Clark (32), was recorded on videotape with a CCD camera mounted at the focal plane of a 3.2 power microscope objective with diffused illumination from below. Body outlines were traced from a video monitor during frame-by-frame replay using a Mitsubishi Model HS-U62(C) video recorder. *C. elegans* strains were cultivated on agar petri plates with a culture of *Escherichia coli* mutant strain OP-50 for food (34).

especially evident in the unique locomotion of *Mermis*. Free-living stages of *Mermis nigrescens* (about 100 mm in length and 0.4 mm in diameter) are capable of remarkable local control of six to eight body waves so as to apply lateral force to various point contacts in grass as the body tube glides by (29).

The lateral attachment is also important to prevent buckling of the inherently flexible cuticle during contraction of the longitudinal muscles. Buckling would be predicted to occur if the muscle attachments were to span long intervals of the cuticle, in particular, if the ratio of length over width of the compressed zone exceeded 7, the value that shifts the Euler column formula into the long-column phase governed by buckling (31). The narrow cuticular tube of wild-type *C. elegans* buckles only when unusual external forces are applied—for example, when the worm becomes trapped by surface tension against a bubble (Fig. 2B). However, in the presence of the *lin-39* (n1760) mutation, buckling occurs during normal locomotion. The mutation leaves a substantial length of the ventral muscle detached from the cuticle in the midbody region (32). The detached sarcomeres remain interconnected serially like vertebrate myofibrils, through dense bodies and attachment plaques between cells. During contraction, the muscle strand applies forces to the cuticle anterior and posterior to the midbody region. When these mutants locomote, the body tube is seen to buckle as the wave of contraction passes into the midbody (Fig. 2C and 2D). Kinking is greatest in dorsal bends where the detached ventral muscle bands could slip the farthest across the pseudocoelom from their normal position, thus producing a greater component of force perpendicular to the cuticle. Arrows indicate displacement of the intestine (refractile lumen) by the muscle. Mutations in the *mua* (muscle attachment) genes similarly result in muscle detachment and kinking (Plenefisch and Hedgecock, pers. comm.).

Oblique striations are observed in longitudinal sections of *C. elegans* and radial sections of *Mermis* (Fig. 1). The oblique pattern is due to the displacement of adjacent columns of sarcomeres along one of the longitudinal dimensions. The actual angle of oblique striation could not be shown in Figure 1 but is seen in Figure 3A, a diagram illustrating to scale a surface view of the basal lamina and the dense body attachment sites. In all nematodes described the striation angle is 5°–7° with respect to the myofilaments (13–14, 16, 33) and depends on degree of contraction (12).

Contraction of obliquely striated muscle occurs by a sliding filament mechanism. But unlike cross-striated muscle, the angle of striation with respect to the filament axis increases with contraction while the amount of stagger between adjacent sarcomeres decreases. To date, the discussion of this motion in the literature (1–2, 8, 11–12) has not considered the constraining role of the lateral attachment of the sarcomeres to the basal lamina and cuticle. This attachment maintains the staggered position and spacing of the columns of sarcomeres at rest. During

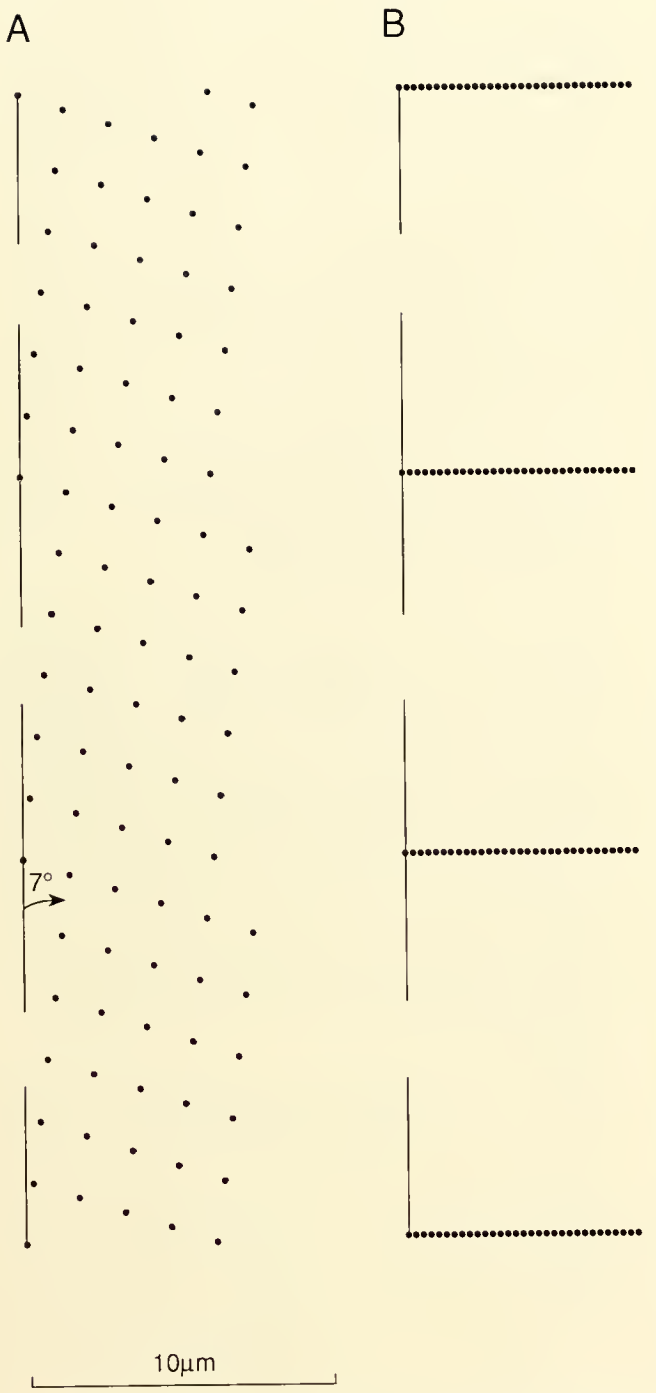

Figure 3. Surface view of nematode body wall muscle cell showing distribution of dense body attachment sites (dots) to the basal lamina: (A) with observed 7° oblique striation, and (B) rearranged as if it were cross-striated. The lines in the first column of sarcomeres indicate orientation of the thin filaments. Three complete sarcomeres are illustrated in each diagram. Longitudinal dimension is vertical. The pattern in (A) was drawn to scale from a surface view of *C. elegans* body-wall muscle photographed under phase optics published by Francis and Waterston (16). The same pattern is seen in radial sections of coelomyarian muscle.

the shortening of sarcomeres, the change in both stagger and striation angle must be governed by the elastic properties of the basal lamina and cuticle. Figure 3A illustrates the actual distribution of dense body attachment sites on the basal lamina. The system can be modeled by transferring the pattern of attachment sites onto a rubber membrane that has been previously stretched along the myofilament axis. The rubber membrane is thus equivalent to the basal lamina and cuticle under isometric tension. When the rubber membrane is allowed to shorten (equivalent to muscle contraction), the pattern width increases, the amount of stagger decreases, and the striation angle increases. Thus, the elastic properties of the membrane govern how the pattern is deformed during shortening. The previously hypothesized link between shearing and angle of striation in obliquely striated muscle (3) must, at least in nematodes, be the elastic basal lamina and cuticle to which the sarcomeres are attached.

What is the significance of the oblique arrangement of sarcomeres? We propose that it distributes the attachment sites more evenly over the basal lamina. Compare the distributions with sarcomere attachment sites displaced longitudinally (Fig. 3A) and arranged orthogonally as if cross-striated (Fig. 3B). With oblique striation, the sarcomere compression zones overlap, the attachment sites are spread apart, and a more even loading pattern is generated within the basal lamina. The lateral transmission of sarcomere contraction and the staggering of the sarcomere attachment sites should result in essentially continuous compressive loading of the adjacent cuticle and a smooth bend in the body tube.

Oblique striation has been described for muscles of platyhelminths, nematodes, gastrotrichs, nematomorphs, priapulids, pogonophora, chaetognathes, annelids, molluscs, brachiopods, and an echinoderm (3–7, 9), and dense bodies are an obvious feature in all taxa. A provocative question is to what extent the lateral transmission of contractile force and the even distribution of attachment sites on the basal lamina—discovered in nematode body wall muscles—are significant architectural features of other obliquely striated muscles.

Acknowledgments

We thank Scott Clark for providing the *lin-39* strains, Gwen Bollerup for collection of *Mermis*, Hella Prochaska for assistance with electron microscopy, and Bonny Milsome for the art work. Supported by grants from the Natural Sciences and Engineering Research Council of Canada to AHJB and from the Leo Leeser Foundation for Tropical Biology to CG.

Literature Cited

1. **Rosenbluth, J. 1972.** Obliquely striated muscle. Pp. 389–420 in *The Structure and Function of Muscle*, 2nd ed., vol. 1, part 1, G. H. Bourne, ed. Academic Press, New York.

2. **Knapp, M. F., and P. J. Mill. 1971.** The contractile mechanism in obliquely striated body wall muscle of the earthworm, *Lumbricus terrestris*. *J. Cell Sci.* **8:** 413–425.
3. **Lanzavecchia, G. 1977.** Morphological modulations in helical muscles (Aschelminthes and Annelida). *Int. Rev. Cytol.* **51:** 133–186.
4. **Toida, N., H. Kuriyama, N. Tashiro, and Y. Ito. 1975.** Obliquely striated muscle. *Physiol. Rev.* **55:** 700–756.
5. **Lanzavecchia, G., R. Valvassori, M. de Eguileor, and P. Lanzavecchia, Jr. 1979.** Three-dimensional reconstruction of the contractile system of the Nematomorpha muscle fiber. *J. Ultrastruct. Res.* **66:** 201–227.
6. **Candia Carnevali, M. D., A. Saita, and A. Fedrigo. 1986.** An unusual Z-system in the obliquely striated muscles of crinoids: three-dimensional structure and computer simulations. *J. Muscle Res. Cell Motil.* **7:** 568–578.
7. **Ward, S. M., J. M. Allen, and G. McKerr. 1992.** Physiology of obliquely striated muscle fibers within *Grillotia erinaceus* metacestodes (Cestoda: Trypanorhyncha). *Parasitology* **104:** 337–346.
8. **De Eguileor, M., R. Cotelli, R. Valvassori, M. Brivio, and L. Di Lernia. 1988.** Functional significance of intermediate filament meshwork in annelid helical muscles. *J. Ultrastruct. Mol. Struct. Res.* **100:** 183–193.
9. **Paniagua, R., M. Royuela, R. M. Garcia-Anchuello, and B. Fraile. 1996.** Ultrastructure of invertebrate muscle cell types. *Histol. Histopathol.* **11:** 181–201.
10. **Vigoreau, J. O. 1994.** The muscle Z band: lessons in stress management. *J. Muscle Res. Cell Motil.* **15:** 237–255.
11. **Prosser, C. L. 1991.** Animal Movement. Pp. 83–84 in *Neural and Integrative Animal Physiology*, C. L. Prosser, ed. Wiley-Liss, New York.
12. **Rosenbluth, J. 1967.** Obliquely striated muscle. III. Contraction mechanism of *Ascaris* body muscle. *J. Cell Biol.* **34:** 15–33.
13. **Rosenbluth, J. 1965.** Ultrastructural organization of obliquely striated muscle fibers in *Ascaris lumbricoides*. *J. Cell. Biol.* **25:** 495–515.
14. **Hope, W. D. 1969.** Fine structure of the somatic muscles of the free-living marine nematode *Deontostoma californicum* Steiner and Albin, 1933 (Leptosomatidae). *Proc. Helminthol. Soc.* **36:** 10–29.
15. **Hirumi, H., D. J. Raski, and N. O. Jones. 1971.** Primitive muscle cells of nematodes: morphological aspects of platymyarian and shallow coelomyarian muscles in two plant parasitic nematodes, *Trichodorus christiei* and *Longidorus elongatus*. *J. Ultrastruct. Res.* **34:** 517–543.
16. **Francis, G. R., and R. H. Waterston. 1985.** Muscle organization in *Caenorhabditis elegans:* localization of proteins implicated in thin filament attachment and I-band organization. *J. Cell Biol.* **101:** 1532–1549.
17. **Barstead, R. J., and R. H. Waterston. 1989.** The basal component of the nematode dense body is vinculin. *J. Biol. Chem.* **264:** 10177–10185.
18. **Francis, R., and R. H. Waterston. 1991.** Muscle cell attachment in *Caenorhabditis elegans*. *J. Cell Biol.* **114:** 465–479.
19. **Valvassori, R., M. de Eguileor, and G. Lanzavecchia. 1981.** Studies on the helical and paramyosinic muscle. VIII. Ultrastructural analysis of body wall muscles from *Mermis* sp. *J. Ultrastruct. Res.* **76:** 82–88.
20. **Harris, J. E., and H. D. Crofton. 1957.** Structure and function in nematodes: internal pressure and cuticular structure in *Ascaris*. *J. Exp. Biol.* **34:** 116–130.
21. **Niebur, E., and P. Erdös. 1991.** Theory of the locomotion of nematodes. Dynamics of undulatory progression on a surface. *Biophys. J.* **60:** 1132–1146.
22. **Gray, J., and H. W. Lissmann. 1964.** The locomotion of nematodes. *J. Exp. Biol.* **41:** 135–154.
23. **Price, M. G. 1991.** Striated muscle endosarcomeric and exosarcomeric lattices. *Adv. Struct. Biol.* **1:** 175–207.
24. **Wang, K., R. McCarter, J. Wright, J. Beverly, and R. Ramirez-Mitchell. 1993.** Viscoelasticity of the sarcomere matrix of skeletal muscles. The titin-myosin composite filament is a dual-stage molecular spring. *Biophys. J.* **64:** 1161–1177.
25. **Small, J. V. 1995.** Structure-function relationships in smooth muscle: the missing links. *Bioessays* **17:** 785–792.
26. **Stromer, M. H. 1995.** Immunocytochemistry of the muscle cell cytoskeleton. *Microsc. Res. Techn.* **31:** 95–105.
27. **Moerman, D. G., and A. Fire. 1997.** Muscle: structure, function, and development. Pp. 417–470 in *C. elegans II*, D. L. Riddle, T. Blumenthal, B. J. Meyer, and J. R. Priess, eds. Cold Spring Harbor Laboratory Press, Cold Spring Harbor, NY.
28. **Moulder, G. L., M. M. Huang, R. H. Waterston, and R. J. Barstead. 1996.** Talin requires β-integrin, but not vinculin, for its assembly into focal adhesion-like structures in the nematode *Caenorhabditis elegans*. *Mol. Biol. Cell* **7:** 1181–1193.
29. **Gans, C., and A. H. J. Burr. 1994.** Unique locomotory mechanism of *Mermis nigrescens*, a large nematode that crawls over soil and climbs through vegetation. *J. Morphol.* **222:** 133–148.
30. **Bartnik, E., M. Osborn, and K. Weber. 1986.** Intermediate filaments in muscle and epithelial cells of nematodes. *J. Cell Biol.* **102:** 2033–2041.
31. **Timoshenko, S., and G. H. MacCullough. 1940.** *Elements of Strength of Materials*, VanNostrand, New York.
32. **Clark, S. G., A. D. Chisholm, and H. R. Horvitz. 1993.** Control of cell fates in the central body region of *C. elegans* by the homeobox gene *lin-39*. *Cell* **74:** 43–55.
33. **Mackenzie, J. M., and H. F. Epstein. 1980.** Paramyosin is necessary for determination of nematode thick filament length *in vivo*. *Cell* **22:** 747–755.
34. **Brenner, S. 1974.** The genetics of *Caenorhabditis elegans*. *Genetics* **77:** 71–94.

Reference: *Biol. Bull.* **194:** 7–13. (February, 1998)

Distinctive Cytoskeletal Organization in Erythrocytes of the Cold-Seep Vesicomyid Clam, *Calyptogena kilmeri*

WILLIAM D. COHEN[1,*] AND MARIO N. TAMBURRI[2]

[1] *Department of Biological Sciences, Hunter College of CUNY, 695 Park Ave., New York, New York 10021; and* [2] *Monterey Bay Aquarium Research Institute, P.O. Box 628, Moss Landing, California 95039*

Abstract. Erythrocytes have long served as model cells, useful for analyzing cytoskeletal structure and function. In non-mammalian vertebrates, erythrocytes are typically highly flattened, nucleated ellipsoids in which a marginal band (MB) of microtubules interacts with the membrane skeleton (MS) to generate and maintain cell shape. Though relatively rare, erythrocytes also occur in representatives of many invertebrate phyla, including the arcid and vesicomyid molluscs, but the structure and function of these cells are not well understood. Previous work has shown arcid erythrocytes to be highly flattened ellipsoids containing the MB-MS cytoskeletal system, similar to vertebrates but with an additional interesting feature: a functional centriole-containing centrosome associated with each MB. In the present study we have examined, for the first time, erythrocyte morphology and cytoskeletal structure in a vesicomyid. Using *Calyptogena kilmeri*, the dominant invertebrate at many Pacific cold seeps, we have found that the erythrocytes are only slightly flattened and do not contain MBs. Rather, their cytoskeletons display a peripheral centriole-containing centrosome with radiating fibers, a distinctive type of organization not observed previously in mature erythrocytes from any species.

Introduction

Hemoglobin-bearing erythrocytes are found in all vertebrates and have long been utilized for studies of cytoskeletal organization and function. In adult mammals the erythrocytes are typically anucleate discoids, with a cytoskeletal system consisting principally of the membrane skeleton (MS). In adult non-mammalian vertebrates and mammalian embryos the mature erythrocytes are nucleated, flattened ellipsoids or discoids, and the cytoskeleton characteristically includes a marginal band (MB) of microtubules. The MB resists mechanically and osmotically induced shape deformation in normal mature cells, and abnormally pointed MBs generate abnormally pointed cells, presumably by MS deformation (Joseph-Silverstein and Cohen, 1984). Mechanical interaction between these two cytoskeletal components is thus believed to be important for morphogenesis and maintenance of cell shape in nucleated erythrocytes (Cohen, 1991; Winckler and Solomon, 1991).

Invertebrates with erythrocytes are relatively rare, but phylogenetically diverse; they include representatives of the annelids, brachipods, echinoderms, echiurans, molluscs, priapulids, and sipunculans. These invertebrate erythrocytes vary with respect to morphology and type of respiratory protein, and the MB-MS cytoskeletal system may or may not be present. The role of these cells is incompletely understood, with several workers suggesting that erythrocytes may be multifunctional in some species (*e.g.,* Terwilliger *et al.,* 1985). Comparative studies of cytoskeletal organization in invertebrate erythrocytes might, therefore, help to shed light on the functions of these cells.

Among the molluscs, erythrocytes appear in representatives of the arcid and vesicomyid bivalves (Terwilliger *et al.,* 1983; Cohen and Nemhauser, 1985; Nagel, 1985). Previous work on arcid species—including *Anadara transversa, A. ovalis,* and *Noetia ponderosa* from coastal

Received 2 July 1997; accepted 5 December 1997.

*To whom correspondence should be addressed. E-mail: cohen@genectr.hunter.cuny.edu

waters of the eastern United States—has demonstrated that the MB-MS system is present and functional in maintenance of cell shape (Cohen and Nemhauser, 1980; Nemhauser *et al.,* 1983; Joseph-Silverstein and Cohen, 1984, 1985). Each MB also has an associated centrosome containing a pair of centrioles, an unusual feature not observed in mature erythrocytes of vertebrates (Cohen and Nemhauser, 1980; Cohen, 1991). This centrosome remains functional as a microtubule organizing center—as demonstrated by experimentally induced MB reassembly in the living cells (Nemhauser *et al.,* 1983)—and is presumed to be the same centriole that was involved in MB biogenesis during erythrocyte differentiation. Erythrocytes of the Australian species *A. trapezia* and several related Japanese bivalves have a virtually identical centrosome-containing cytoskeleton (Ochi, O., and Cohen, W. D., 1984, and Cohen, W. D., 1989, unpubl. obs.), indicating that this feature is a general characteristic of arcid erythrocytes.

In contrast with the arcids, cytoskeletal structure in vesicomyid erythrocytes has never been described. Of those vesicomyids with erythrocytes, *Calyptogena magnifica* is best known because it populates well-explored Pacific hydrothermal vent communities (Boss and Turner, 1980; Johnson *et al.,* 1988b; Fisher *et al.,* 1988) and because its erythroid hemoglobin has been studied (Terwilliger *et al.,* 1983). Most (perhaps all) other *Calyptogena* species with erythrocytes inhabit "cold seeps," sites that have high levels of hydrogen sulfide, low levels of oxygen, and high hydrostatic pressures in common with hydrothermal vents (McHugh *et al.,* 1992; Barry *et al.,* 1997a; Vrijenhoek *et al.,* 1994). The principal difference between the two environments is that hydrothermal vents are characterized by fluctuating and frequently elevated temperatures (Johnson *et al.,* 1988a), whereas cold-seep temperatures are similar to those of surrounding waters and are relatively constant. Vesicomyid bivalves inhabiting cold seeps in the Monterey Canyon—including *Vesicomya gigas, V. steamsii, Calyptogena kilmeri,* and *C. pacifica*—experience a temperature range of only 4–6°C (Barry, J. P., pers. comm.). Of these species, *C. kilmeri* is the most abundant at several cold-seep sites routinely sampled by the remotely operated vehicles (ROVs) of the Monterey Bay Aquarium Research Institute.

Seeking to determine whether molluscan erythrocytes have a common cytoskeletal organization, we undertook to compare the structure of vesicomyid erythrocytes with that known for erythrocytes of the arcids. We report here the first examination of cell morphology and cytoskeletal structure in vesicomyid erythrocytes, those of *C. kilmeri.*

Materials and Methods

Experimental material

Clams (*C. kilmeri,* Fig. 1) were collected by the ROV *Ventana* from the Monterey Bay cold-seep locale known as "Clam Field" (Barry *et al.,* 1997b). They were maintained for one to several days in laboratory seawater tanks at 6°C, approximately the temperature of their native habitat. The animals were opened with a scalpel, and the bright red, flowing blood (hemolymph) was collected in a plastic tray and used immediately in experiments. Depending on the experiment, hemolymph was collected either at 22°C (room temperature) or at 6°C (coldroom).

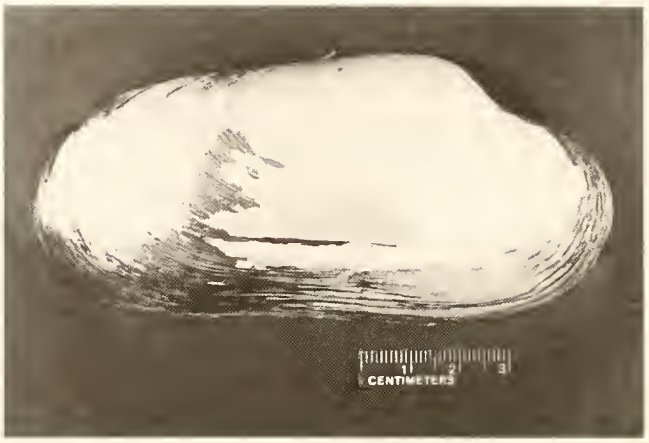

Figure 1. *Calyptogena kilmeri.* Animals were collected by a remotely operated vehicle (ROV) and maintained in aquaria in a closed filtered seawater system at 6°C.

Erythrocyte cytoskeletons were prepared, in general, by lysis of cells with nonionic detergents under microtubule-stabilizing conditions. Immediately after collection (<30 s) the hemolymph was diluted about 1:20 into Brij lysis medium or Triton lysis medium. The Brij lysis medium contained 100 m*M* piperazine-N,N′-bis(ethanesulfonic acid) [PIPES buffer], 5 m*M* ethylene glycol-bis-(β-aminoethyl ether) n,n′-tetraacetic acid [EGTA], 1 m*M* $MgCl_2$, pH 6.8, plus 0.6% Brij-58. The Triton lysis medium was similar except that it contained 0.4% Triton X-100 instead of Brij-58. In some cases, 0.1% glutaraldehyde was included in the medium for additional rapid post-lysis stabilization. These media had been effective previously for preparing erythrocyte cytoskeletons from a wide range of vertebrates and invertebrates, including the archid genera *Noetia* and *Anadara* (Nemhauser *et al.,* 1983; Cohen and Nemhauser, 1985; Cohen, 1991).

Microscopy

Cells for morphological examination were either unfixed, or fixed immediately (<30 s) by dilution (about 1:20) of hemolymph into marine molluscan Ringer's solution (Cavanaugh, 1975) containing 0.1% glutaraldehyde. Information on cell shape was obtained by observing cells while they were stationary in the medium on a slide, as well as while they were tumbling in flow. Observations

and photomicrographs of the cells and their cytoskeletons were made with a Zeiss Axioscope equipped with an Olympus 35-mm camera system with focusing eyepiece, and phase contrast optics including a 100× Plan-Neofluar objective (NA 1.3).

For transmission electron microscopy of cytoskeletons, fresh hemolymph obtained at 6°C was diluted into Triton lysis medium containing 0.1% glutaraldehyde, incubated 1 h at about 22°C, stored 3 days at 0°C with glutaraldehyde added to 1%, and post-fixed 1 h in 1% OsO_4 buffered with 0.1 *M* KH_2PO_4-KOH at pH 6.8. After ethanol dehydration, the material was embedded in Polybed 812 (Polysciences, Inc.), thin sectioned with a diamond knife, stained with uranyl acetate and lead citrate, and examined with a Hitachi H-600 transmission electron microscope.

Results

Cell morphology

The erythrocytes were generally ellipsoidal, but irregular in size and contour (Fig. 2a). Observations made as they tumbled in flow under coverslips showed that the cells were somewhat flattened, but relatively thick (Fig. 2b, c). The shape of the *C. kilmeri* erythrocytes was the same whether examined in living cells or in cells fixed immediately upon collection of the hemolymph.

Cytoskeletal structure

In different experiments, erythrocyte cytoskeletons were prepared from hemolymph collected either at room temperature (~22°C) or at cold-seep temperature (cold-room at ~6°C); the lysis media were also maintained either at ~22°C or ~6°C. Examination by high resolution, phase contrast light microscopy revealed, in most cells, a peripheral pair of closely opposed phase-dense "dots" of uniform size (Fig. 3a–d; arrowheads). In highly flattened samples, this structure was clearly resolvable as a centriole-containing centrosome from which straight fibrous material radiated (Figure 3e-g). However, circumferential MBs of microtubules were not present.

The cytoskeletal structure observed was not induced by temperature during the experimental procedure. Peripheral pairs of centrioles with radiating fibers were observed in the cytoskeletons whether the hemolymph was collected at ~22°C or ~6°C, or whether lysis was achieved with media at either temperature. We did note, however, that cytoskeletons tended to collapse closer to the nucleus more frequently when the cells were collected and lysed at the lower temperature; thus, our stabilization media were not as effective at that temperature.

Although the paired, phase-dense "dots" were similar to those observed previously in phase contrast and subsequently identified as centrioles in *Noetia* and *Anadara* (Cohen and Nemhauser, 1980, 1985), transmission electron microscopy of thin sections was used to verify their identification in *Calyptogena*. The cytoskeletons were found to contain classic pairs of centrioles measuring about 0.22 × 0.32 μm (Fig. 4a–c), with typical 9-triplet ultrastructure (Fig. 4d), and microtubules observed frequently in their vicinity did not emanate directly from the centriolar triplets (Fig. 4a–c). In many cases a mass of electron-dense material was observed in association with one or both centrioles (*e.g.*, Fig. 4b, d, arrowheads).

Discussion

With their generally ellipsoidal and partially flattened irregular shape, the *C. kilmeri* erythrocytes differed considerably in morphology from those of arcids, which are much flatter and smoother in contour when first removed from the animal (Cohen and Nemhauser, 1985). In addition, the shape of the vesicomyid cells remained stable,

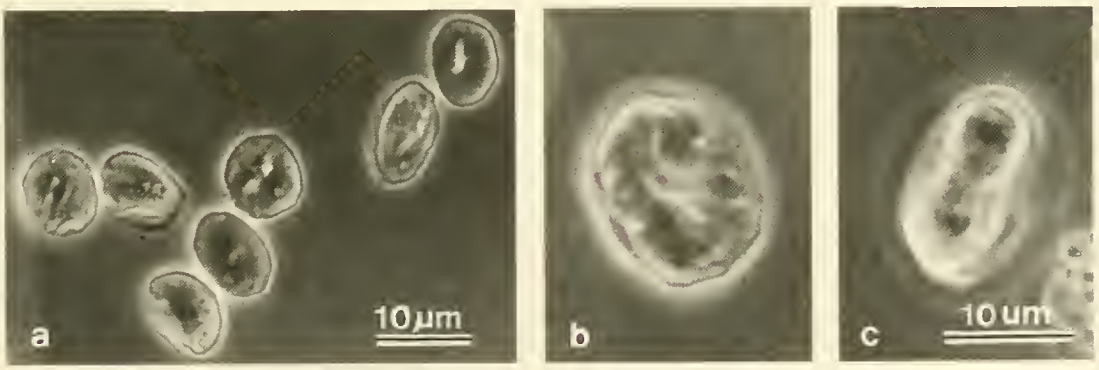

Figure 2. Fixed erythrocytes of *Calyptogena kilmeri*, observed by phase contrast microscopy. (a) Erythrocytes were generally ellipsoidal, but irregular in size and contour; (b, c) face and edge views, respectively, of the same cell, observed as it tumbled in flow. The erythrocytes are thus found to be somewhat flattened but relatively thick, and the shape of unfixed cells is similar (not shown).

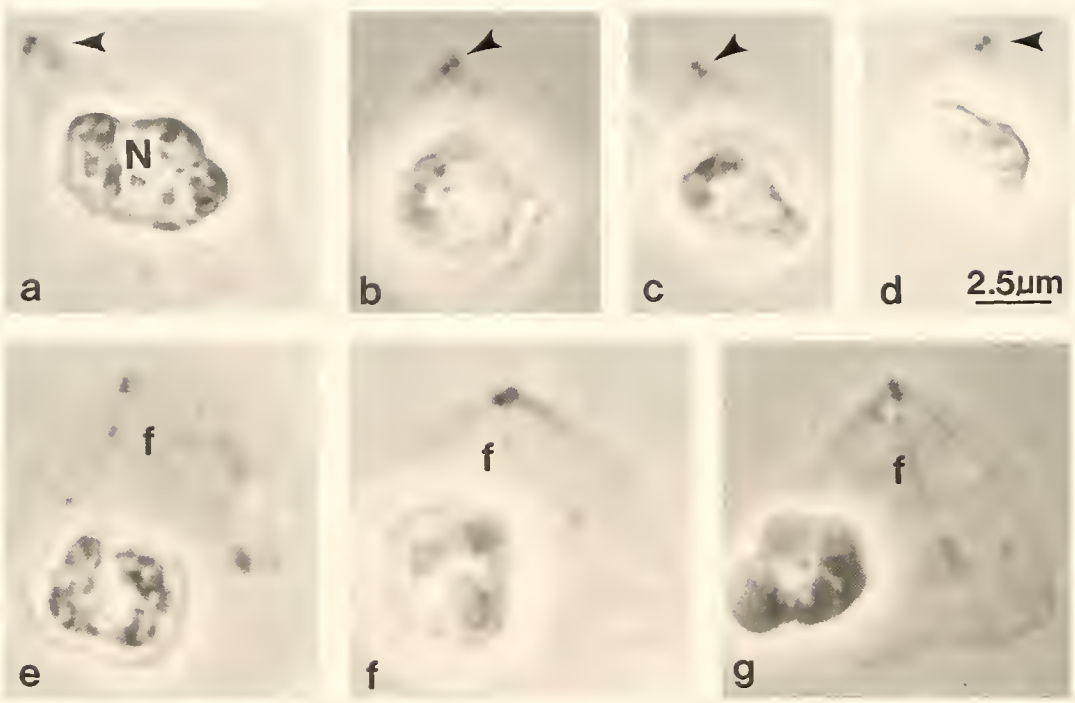

Figure 3. Cytoskeletons of *Calyptogena kilmeri* erythrocytes; phase contrast microscopy. (a–d) Examples of cytoskeletons in which centrioles are resolved as a pair of phase-dense "dots" (arrowheads); (e–g) cytoskeletons flattened under the coverslip to improve visualization of fibers (f) radiating from the centrosomal region. Marginal bands of microtubules are not present. Conditions: (a) and (e–g), Brij lysis medium, no glutaraldehyde; (b, c), Triton lysis medium + glutaraldehyde; (d), Brij lysis medium + glutaraldehyde.

whereas arcid erythrocytes, if left in their own hemolymph, undergo a spontaneous, reversible morphological transformation to lumpy spheroids within about 5 min (Sullivan, 1961; Dadacay *et al.*, 1996).

Cytoskeletal structure in these vesicomyid erythrocytes was distinctive. Fibers radiated from prominent centrosomes containing centriole pairs similar to those of arcid erythrocytes, but, in contrast to the arcid cells, the vesicomyid erythrocytes contained no MB. So far as we have been able to determine, this kind of organization has not been observed previously in erythrocytes of any other species. Our survey encompasses annelid, brachiopod, echinoderm, echiuran, molluscan, priapulid, and sipunculan representatives among the invertebrates (Table I), as

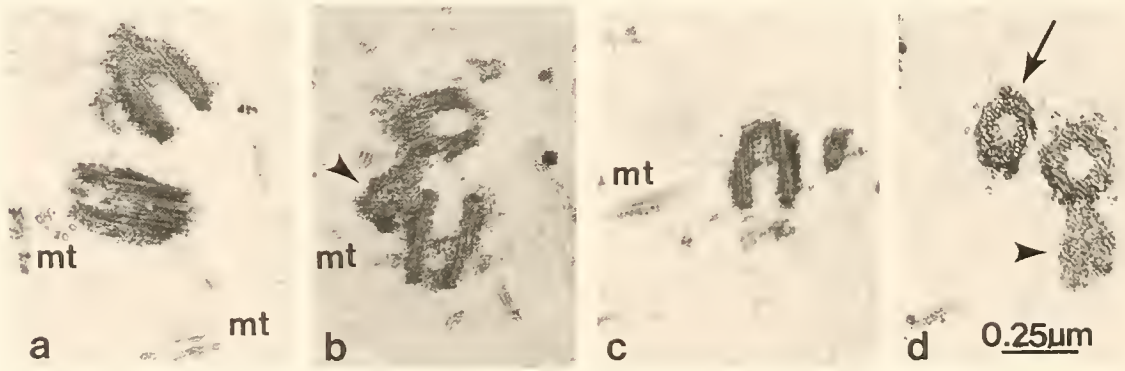

Figure 4. Centrioles in cytoskeletons as observed by transmission electron microscopy of thin sections. (a–c) Longitudinal and oblique views; (d) cross-sectional view showing 9-triplet cylindrical ultrastructure. Adjacent microtubules or microtubule bundles (mt) did not emanate from the centriolar triplets (a–c). Electron-dense material was sometimes observed close to the centrioles (b, d; arrowheads).

Table 1

Survey of cytoskeletal organization in invertebrate erythrocytes

Phylum,[1] species	RP[2]	MB[3]	PC[4]	Reference
Annelida				
Travisia japonica	Hb	+	+	Ochi, 1969; Ochi, unpubl. obs., 1980
Pista pacifica	Hb	−	−	Nemhauser, 1981; Terwilliger *et al.*, 1985
Glycera dibranchiata	Hb	−	−	Nemhauser, 1981; Pierce and Maugel, 1985
Brachiopoda				
Laqueus californicus	He	−	−	Nemhauser, 1981; Meglitsch, 1967
Echinodermata (Holothuroidea)				
Cucumaria miniata	Hb	+	?	Fontaine and Lambert, 1973
Molpadia arenicola	Hb	+	?	Clifford, 1969
Eupentacta quinquesemita[5]	Hb	+	+	Fontaine and Hall, 1981
Echiuroida				
Urechis caupo	Hb	−	−	Nemhauser, 1981; Terwilliger *et al.*, 1985
Mollusca (Arcidae & Vesicomyidae)				
Anadara transversa	Hb	+	+	Cohen and Nemhauser, 1985
A. ovalis	Hb	+	+	Nemhauser, 1981
A. lienosa	Hb	+	+	"
A. braziliana	Hb	+	+	"
A. trapezia	Hb	+	+	Cohen, W. D., unpubl. obs., 1988
Noetia ponderosa	Hb	+	+	Nemhauser *et al.*, 1983
Barbatia virescens	Hb	+	+	Cohen and Nemhauser, 1985; Ochi, O., and Cohen, W. D., unpubl. obs. 1984
Arca boucardi	Hb	+	+	"
Pseudogrammatodon dalli	Hb	+	+	"
Calyptogena kilmeri	Hb	−	+	this paper
Priapulida				
Priapulus caudatus	He	+	?	Mattison and Fange, 1973
Sipuncula				
Phascolopsis gouldii	He	+	?	Nemhauser *et al.*, 1980
Themiste dyscrita	He	−	−	Nemhauser, 1981[6]; Terwilliger *et al.*, 1985[7]

[1] Where erythrocytes are restricted to a class or family, this is indicated in parentheses.

[2] Abbreviations: RP = respiratory protein; Hb = hemoglobin; He = hemerythrin; MB = marginal band of microtubules; PC = peripheral centriole-containing centrosome.

[3] MB observed (+) or not observed (−).

[4] PC consistently observed (+) or not observed (−); ? = insufficient data.

[5] Cells with MBs and PC in this species are described as *immature* flattened ellipsoids.

[6] Only coelomic erythrocytes observed.

[7] Both coelomic and circulatory erythrocytes observed.

well as a wide range of vertebrates including fish, amphibians, reptiles, birds, newborn marsupials, and placental mammals (Cohen and Nemhauser, 1985; Cohen *et al.*, 1990). In many of the arcid species in Table 1, erythrocyte cytoskeletons bearing partial resemblance to those of *C. kilmeri* are found in natural subpopulations of singly pointed erythrocytes in which the centrosome occupies the pointed end. In these cytoskeletons, however, unlike those of *C. kilmeri*, the opposite end contains the curved portion of the incomplete MB. Cytoskeletons of arcid erythrocytes in the early stages of experimentally induced MB reassembly (Nemhauser *et al.*, 1983) also bear some resemblance to those observed in this study of *C. kilmeri* erythrocytes.

As observed by transmission electron microscopy, the centriole pairs were typical in dimensions and in frequent near right-angle orientation (*e.g.*, Fig. 4a, b). That microtubules in their vicinity were not continuous with centriolar triplets is consistent with cytoskeletal organization by centrosomes in other systems, based on pericentriolar distribution of gamma tubulin. However, as in the arcids, a distinctive surrounding region of pericentriolar material, such as is typical of mitotic centrosomes, was not observed in the *Calyptogena* erythrocyte cytoskeletons. Discrete electron-dense masses were frequently found in association with one or both centrioles (*e.g.*, Fig. 4b, d), but microtubules did not emanate from them. The question arises as to the relationship between these erythrocyte centrosomes and those of precursor cells. We assume that, both in arcid and vesicomyid erythrocytes, the peripheral centriole pairs are the same ones initially located more centrally at the erythroblast mitotic spindle poles, each

daughter cell having received one pair. This implies the existence of control mechanisms that reprogram or switch centrosome function from mitotic spindle organization to erythrocyte morphogenesis and shape maintenance.

Among the species in Table 1, in addition to *C. kilmeri*, there are five in which erythrocyte MBs are lacking. However, these species also lack the centrosomal organization found in *C. kilmeri* erythrocytes, verified by examination of cytoskeletons as in the present work (Nemhauser, 1981). The best studied of these cases are instructive. The hemoglobin-bearing erythrocytes of *Pista pacifica*, *Glycera dibranchiata*, and *Urechis caupo* are all spherical (Terwilliger *et al.*, 1985; Pierce and Maugel, 1985), and the coelomic hemerythrin-containing cells of *Themiste dyscrita* are described as varying from disks to spheres (Terwilliger *et al.*, 1985). Absence of the MB is thus correlated with absence or loss of morphological asymmetry. Conversely, MB presence is correlated with maintenance of marked erythrocyte flatness, as in the Arcidae (Cohen and Nemhauser, 1985). The unusual cytoskeletal organization of *C. kilmeri* erythrocytes might then be viewed as functioning to maintain an equally unusual intermediate morphological state, that of limited cell flattening.

The value of erythrocyte flattening to an organism can be at least twofold. First, reduction of diffusion distances is generally acknowledged to facilitate respiratory gas exchange, and second, flattening reduces the work required to maintain "blood" flow by reducing its viscosity (Fischer, 1978). The latter helps to explain why blood cells other than erythrocytes, including mammalian platelets, non-mammalian vertebrate thrombocytes, and invertebrate clotting cells such as *Limulus* amebocytes (Armstrong, 1985) are also highly flattened. All of these cell types also contain MBs. Conversely, for organisms with spherical erythrocytes, we might speculate that rapid respiratory gas exchange and the requirement for reduced viscosity are not as critical.

In interpreting the data, potential artifacts must be considered. We note that the habitat of *C. kilmeri* is characterized in part by relatively high pressures, with a depth range of ~0.5–5 km for cold-seep vesicomyids in general, and ~0.9 km at "Clam Field" (Orange, D. L., and Barry, J. P., pers. comm.). Since our findings were obtained from animals brought to sea level, it might be hypothesized that arcid-like MBs with associated centrosomes occur in vesicomyid erythrocytes under native conditions and become disorganized by the pressure reduction. We believe this to be quite unlikely; as shown in many studies (summarized in Dustin, 1978, 1984), it is *increased* hydrostatic pressure that can cause microtubule disorganization. Data relevant to this question might be obtainable by fixing material *in situ* at the time of specimen collection, but we have found that fixation of whole, unlysed bivalve erythrocytes (both arcid and vesicomyid) traps sufficient hemoglobin to obscure cytoskeletal elements in thin sections for transmission electron microscopy and to render immunofluorescence light microscopy ineffective. Indeed, blood must be withdrawn and the cells lysed, as in the present work, if the entire cytoskeleton is to be viewed. Such procedures would be problematic at the depths and under the challenging physical conditions characteristic of the cold seeps.

A second possible source of artifact would be a spontaneous change of erythrocyte shape occurring in the hemolymph shortly after collection, as observed previously in arcid erythrocytes (Cohen and Nemhauser, 1985; Dadacay *et al.*, 1996) and in coelomic erythrocytes of a sipunculan, *T. dyscrita* (Terwilliger *et al.*, 1985). In the present work, this is not a factor. Although, in the absence of prior data, precautions were taken by preparing cytoskeletons and fixed cells immediately upon obtaining the hemolymph, such shape alteration was not observed in the vesicomyid erythrocytes.

Acknowledgments

We thank K. R. Buck for patient technical assistance, and Drs. R. Kochevar and J. P. Barry for their efforts in making this work possible. We are indebted to the crew and pilots of the *Pt. Lobos* and the ROV *Ventana* for aid in specimen collection, and to MBARI for providing workspace and other support. Additional support from NSF MCB-9118773 and PSC-CUNY 666180 (WDC) is also gratefully acknowledged.

Literature Cited

Armstrong, P. B. 1985. Adhesion and motility of the blood cells of *Limulus*. Pp. 77–124 in *Blood Cells of Marine Invertebrates*, W. D. Cohen, ed. Alan R. Liss, New York.

Barry, J. P., H. G. Greene, D. L. Orange, C. H. Baxter, B. H. Robison, R. E. Kochevar, J. W. Nybakken, D. L. Reed, and C. M. McHugh. 1997a. Biologic and geologic characteristics of cold seeps in Monterey Bay, California. *Deep-Sea Res.* **43:** 1739–1762.

Barry, J. P., R. E. Kochevar, and C. H. Baxter. 1997b. The influence of pore-water chemistry and physiology in the distribution of vesicomyid clams at cold seeps in Monterey Bay: implications for patterns of chemosynthetic community organization. *Limnol. Oceanogr.* **42:** 318–328.

Boss, K. J., and R. D. Turner. 1980. The giant white clam from the Galapogos Rift, *Calyptogena magnifica* species novum. *Malacologia* **20:** 161–194.

Cavanaugh, G. M. 1975. *Formulae and Methods VI.* The Marine Biological Laboratory, Woods Hole, MA.

Clifford, C. H. 1969. Morphological and biochemical features of the coelomocytes of the sea cucumber *Molpadia arenicola* (Echinodermata: Holothuroidea). Master's Thesis, Scripps Institution of Oceanography, University of California, San Diego, CA.

Cohen, W. D. 1991. The cytoskeletal system of nucleated erythrocytes. *Int. Rev. Cytol.* **130:** 37–83.

Cohen, W. D., and I. Nemhauser. 1980. Association of centrioles

with the marginal band of a molluscan erythrocyte. *J. Cell. Biol.* **86:** 286–291.

Cohen, W. D., and I. Nemhauser. 1985. Marginal bands and the cytoskeleton in blood cells of marine invertebrates. Pp. 1–49 in *Blood Cells of Marine Invertebrates,* W. D. Cohen, ed. Alan R. Liss, New York.

Cohen, W. D., M. F. Cohen, C. H. Tyndale-Biscoe, J. L. VandeBerg, and G. B. Ralston. 1990. The cytoskeletal system of mammalian primitive erythrocytes: studies in developing marsupials. *Cell Motil. Cytoskeleton* **16:** 133–145.

Dadacay, A-V. M., J. C. Huerta, C. J. Theiner, S. Swarnakar, and W. D. Cohen. 1996. Reversible alteration of molluscan erythrocyte morphology by a natural hemolymph activity. *Biol. Bull.* **191:** 276–277.

Dustin, P. 1978. *Microtubules.* Springer-Verlag, Berlin.

Dustin, P. 1984. *Microtubules,* (2nd ed.). Springer-Verlag, Berlin.

Fisher, C. R., J. J. Childress, A. J. Arp, J. M. Brooks, D. L. Distel, J. A. Dugan, H. Felbeck, L. W. Fritz, R. R. Hessler, K. S. Johnson, M. C. Kennicutt II, R. A. Lutz, S. A. Macko, A. Newton, M. A. Powell, G. N. Somero, and T. Soto. 1988. Variation in the hydrothermal vent clam, *Calyptogena magnifica,* at the Rose Garden vent on the Galapogos spreading center. *Deep-Sea Res.* **35:** 1811–1831.

Fischer, T. M. 1978. A comparison of the flow behavior of disc shaped versus elliptic red blood cells (RBC). *Blood Cells* **4:** 453–461.

Fontaine, A. R., and P. Lambert. 1973. The fine structure of the haemocyte of the holothurian *Cucumaria miniata* (Brandt). *Can. J. Zool.* **51:** 323–332.

Fontaine, A. R., and B. D. Hall. 1981. The hemocyte of the holothurian *Eupentacta quinquesemita:* ultrastructure and maturation. *Can. J. Zool.* **59:** 1884–1891.

Johnson, K. S., J. J. Childress, and C. L. Beehler. 1988a. Short-term temperature variability in the Rose Garden hydrothermal vent field: an unstable deep-sea environment. *Deep-Sea Res.* **35:** 1711–1721.

Johnson, K. S., J. J. Childress, R. R. Hessler, C. M. Sakamoto-Arnold, and C. L. Beehler. 1988b. Chemical and biological interactions in the Rose Garden hydrothermal vent field, Galapogos spreading center. *Deep-Sea Res.* **35:** 1723–1744.

Joseph-Silverstein, J., and W. D. Cohen. 1984. The cytoskeletal system of nucleated erythrocytes. III. Marginal band function in mature cells. *J. Cell. Biol.* **98:** 2118–2125.

Joseph-Silverstein, J., and W. D. Cohen. 1985. Role of the marginal band in an invertebrate erythrocyte: evidence for a universal mechanical function. *Can. J. Biochem Cell Biol.* **63:** 621–630.

Mattison, A., and R. Fange. 1973. Ultrastructure of erythrocytes and leucocytes of *Priapulus caudatus* (De Lamarck) (Priapulida). *J. Morphol.* **140:** 367–380.

McHugh, C. M., W. B. F. Ryan, and B. Hecker. 1992. Contemporary sedimentary processes in the Monterey Canyon-Fan System. *Mar. Geol.* **107:** 35–50.

Meglitsch, P. A. 1967. *Invertebrate Zoology.* Oxford University Press, New York.

Nagel, R. L. 1985. Molluscan hemoglobins. Pp. 227–247 in *Blood Cells of Marine Invertebrates,* W. D. Cohen, ed. Alan R. Liss, New York.

Nemhauser, I. 1981. Marginal band systems in blood cells of invertebrates. Doctoral dissertation, Graduate Center, City University of New York, New York.

Nemhauser, I., R. Ornberg, and W. D. Cohen. 1980. Marginal bands in blood cells of invertebrates. *J. Ultrastruct. Res.* **70:** 308–317.

Nemhauser, I., J. Joseph-Silverstein, and W. D. Cohen. 1983. Centrioles as microtubule organizing centers for marginal bands of molluscan erythrocytes. *J. Cell. Biol.* **96:** 979–989.

Ochi, O. 1969. Blood pigments and erythrocytes found in some marine annelids. *Mem. Ehime Univ. Nat. Sci., Ser. B (Biol.)* **VI:** 23–131.

Pierce, S. K., and T. Maugel. 1985. A comparison of the water-regulating responses of bivalve and polychaete red cells to osmotic stresses. Pp. 167–189 in *Blood Cells of Marine Invertebrates,* W. D. Cohen, ed. Alan R. Liss, New York.

Sullivan, G. E. 1961. Functional morphology, microanatomy, and histology of the "Sydney cockle", *Anadara trapezia* (Deshayes) (Lamellibranchia: Arcidae). *Aust. J. Zool.* **9:** 219–257.

Terwilliger, R. C., N. B. Terwilliger, and A. Arp. 1983. Thermal vent clam (*Calyptogena magnifica*) hemoglobin. *Science* **219:** 981–983.

Terwilliger, N. B., R. C. Terwilliger, and E. Schabtach. 1985. Intracellular respiratory proteins of Sipuncula, Echiura, and Annelida. Pp. 193–225 in *Blood Cells of Marine Invertebrates,* W. D. Cohen, ed. Alan R. Liss, New York.

Vrijenhoek, R. C., S. J. Schutz, R. G. Gustafson, and R. A. Lutz. 1994. Cryptic species of deep-sea clams (Mollusca: Bivalvia: Vesicomyidea) from hydrothermal vent and cold-water seep environments. *Deep-Sea Res.* **41:** 1171–1189.

Winckler, B., and F. Solomon. 1991. A role for microtubule bundles in the morphogenesis of chicken erythrocytes. *Proc. Natl. Acad. Sci.* **88:** 6033–6037.

Reference: *Biol. Bull.* **194:** 14–24. (February, 1998)

Stimulation of Metamorphosis in the Polychaete *Hydroides elegans* Haswell (Serpulidae)

EUGENIO CARPIZO-ITUARTE AND MICHAEL G. HADFIELD*

Kewalo Marine Laboratory, University of Hawaii, 41 Ahui St., Honolulu, Hawaii 96813

Abstract. The serpulid polychaete *Hydroides elegans* is a common, cosmopolitan warm-water biofouling organism. Competent larvae of *H. elegans* metamorphose rapidly after induction by marine biofilms. Only 15 min after coming in contact with the metamorphic cue, larvae have completed secretion of the primary tube; secretion of the secondary, calcareous tube begins 1.5 h after the primary tube has been deposited. Metamorphosis is characterized by disappearance of the prototroch and differentiation of the tentacular crown in the head region, the collar and thoracic membrane in the thoracic region, and the pygidium at the tip of the abdomen. These morphogenetic events were used to gauge the responses of larvae to biofilms, as well as to the artificial inducers Cs^+ and K^+. A maximal metamorphic response to the two ions requires exposure to different concentrations and durations, *i.e.*, a 3-h pulse of 10 m*M* CsCl, or a 24-h continuous exposure to 50 m*M* excess KCl. The metamorphic response to Cs^+ or K^+ is much slower than the response to biofilms, demonstrating that the tissues respond differently to artificial inducers. The differences in the kinetics of the responses to the natural and cationic inducers suggest that the induction mechanisms are not the same. When these artificial inducers were used, some, but not all, of the metamorphosed juveniles never attached to the substratum or secreted a primary tube, probably as a result of secondary effects of the ions on processes of tube formation. The exact mechanisms by which Cs^+ and excess K^+ induce metamorphosis are still unclear, although we assume, as do others, that these agents act by depolarizing the membranes of excitable sensory cells and not by interacting with specific receptors.

Received 15 July 1997; accepted 12 December 1997.

*To whom correspondence should be addressed. E-mail: hadfield@hawaii.edu

Introduction

The influence of ions on invertebrate metamorphosis, first reported by Müller and Buchal (1973) for the larvae of *Hydractinia echinata* more than 2 decades ago, has been demonstrated for a large number of species (summarized in Herrmann, 1995; Woollacott and Hadfield, 1996). Monovalent cations, particularly K^+ and Cs^+, are clearly established as potent inducers of metamorphosis in several groups, although they are ineffective in some species and actually inhibit metamorphosis in others (Rittschof *et al.*, 1986; Eyster and Pechenik, 1988; Morse *et al.*, 1988; Rowley, 1989). Metamorphosis in response to excess K^+ has been reported for seven phyla, and to Cs^+ in at least four phyla. How and where these ions act in the metamorphic pathway and how their action is related to that of natural inducers remain unclear.

The most direct approach to metamorphosis-inducing mechanisms of cations and other artificial inducers would be a series of electrophysiological studies of larval sensory organs made during the development of competence. Unfortunately, the small size of most invertebrate larvae makes such studies difficult or impossible. The more usual approach is illustrated by some studies on gastropod larvae. Larvae of the tropical nudibranch *Phestilla sibogae* respond to choline (Hirata and Hadfield, 1986) and excess K^+ induction (Yool *et al.*, 1986; Pechenik *et al.*, 1995) only after they are competent to respond to the natural inducer (an extract of coral). In contrast, larvae of the prosobranch gastropod *Crepidula fornicata* do not become responsive to natural cues until 12 to 24 h after they can be induced to metamorphose by excess K^+ (Pechenik and Gee, 1993). Differences in the timing of sensitivity to the different inducers has been interpreted as indicative of operation at different sites in an inductive-transduction pathway, but the mechanisms by which vari-

ous artificial inducers act may also develop at different rates.

In the present research, we exposed larvae of *Hydroides elegans* to a natural biofilm and produced a detailed timetable of the resulting events of settlement and metamorphosis. We then compared this developmental timetable with one describing the metamorphic events induced by the monovalent cations Cs^+ and K^+ when groups of sibling larvae were exposed to the different inducers at the same ages. Because nearly all who have used potassium as an inducer of metamorphosis in invertebrate larvae hypothesize a role for depolarization in induction (*e.g.*, Yool *et al.*, 1986), inductions were also carried out in the presence of a K^+-channel blocker. These investigations took advantage of previous work in our laboratory that demonstrated that larvae of *H. elegans* settle preferentially on well-developed marine biofilms, where dominant bacterial species or their extracellular products appear to be the source of a metamorphic cue (Hadfield *et al.*, 1994).

Materials and Methods

Collection of adults and culture of larvae

Adults of *Hydroides elegans* were collected from Pearl Harbor, Hawaii, and kept at the Kewalo Marine Laboratory of the University of Hawaii in 125 × 46 × 15 cm trays supplied with running seawater. When gametes were needed, several worms were removed from their calcified tubes, whereupon they released eggs or sperm into the seawater, where fertilization occurred. Embryos were cultured at 5–10/ml in glass beakers at room temperature (24°–26°C) in 2 l of natural seawater that had been passed through a 0.22-μm filter (FSW). After 48 h, when they had achieved the trochophore stage, the larvae were collected on a 41-μm mesh sieve and transferred to a beaker containing 2 l of freshly filtered seawater. The larvae were fed daily on *Isochrysis galbana* "Tahitian Strain" at a density of about 60,000 cells/ml. The larvae were subsequently transferred to fresh seawater and fed daily until they attained metamorphic competence as three-segmented nectochaetes, usually 4–5 days after fertilization. Competence is defined as the ability of larvae to settle and metamorphose when exposed to a well-developed marine biofilm.

Induction of metamorphosis

Microscope slides were suspended in laboratory tanks supplied with running seawater; after 3 days the slides had accumulated sufficient biofilm to induce metamorphosis of 5-day-old competent larvae. Ten to twenty larvae were added to a drop of seawater on a biofilmed slide, and a supported coverslip was placed over the drop. The seawater beneath the coverslip was replaced periodically by adding fresh seawater with a pasteur pipette at one end of the coverslip and removing the seawater from the other end with absorbent paper. Under these conditions, larvae remained healthy beneath the coverslips for up to 20 h and completed normal metamorphosis. For 14 h after being placed on the biofilmed slides, the larvae were videotaped at 16× magnification through a compound microscope. Images were recorded for 30–60 s approximately every 15 min during the first hour, and about once per hour after that. The series of events from exposure to the biofilm to completion of metamorphosis was characterized by frame-by-frame analysis of the videotape.

Assay methods

Competent larvae aged 4–6 days were used in all experiments except those in which the ontogeny of the metamorphic response was examined; in the latter, testing for induction began 3 days after fertilization. All assays were conducted in 5-ml plastic petri dishes using either FSW or artificial seawater (ASW) (Cavanaugh, 1956). Twenty to sixty competent larvae were pipetted into each dish containing a test solution, and the number of larvae that had metamorphosed was determined 12, 24, 48, or 72 h after the initial induction by observing the larvae through a dissecting microscope. Larvae were considered to have metamorphosed when they had resorbed the prototroch, showed the characteristic differentiation of the body regions that distinguish the juvenile worm and had developed branchial rudiments that indicate early juvenile development.

Five different experiments were conducted to test the effects of Cs^+ and excess K^+ as artificial inducers.

Continuous exposure. Larvae were exposed to the test solution throughout the experimental period. Response to excess K^+ was tested in seawater with KCl concentration increased by 10, 20, 30, 50, 60, 80, 100, or 150 m*M*. Effects of Cs^+ were tested by adding CsCl to seawater at 2.5, 5, and 10–80 m*M* in 10-m*M* steps.

Pulse exposure. Larvae were exposed to the test solution for a determined period and then transferred to seawater free of added ions. In some experiments, larvae were removed from the solution by collecting them on 41-μm mesh, and in the remainder most of the water was removed from the larval dish with a 5-ml automatic pipettor with a filter across its tip. In both cases the solution was replaced with fresh FSW in which the larvae remained until the end of the experiment. Pulse durations of 20, 40, and 60 min, and 3, 4, 6, 24, and 48 h, were used with 20, 30, and 40 m*M* excess K^+, and shorter pulses of 3,

10, 15, 60, and 120 min were employed with 60, 70, and 80 m*M* excess K^+. In the cesium experiments, pulse durations were 1, 1.5, 2, 3, 4.5, 6, 7, and 24 h with 10 m*M* CsCl as the metamorphic inducer.

Interactions among inducers. Larvae were exposed to a marine biofilm (the natural inducer) in seawater containing 50 m*M* excess KCl for 24 h, or 10 m*M* CsCl for 3 h. After these periods, the biofilm was retained, but the medium was replaced with unaltered seawater. Metamorphic responses were compared with those of larvae induced with a biofilm alone, with excess K^+ (50 m*M*) for 24 h, or with Cs^+ (10 m*M*) for 3 h alone.

Effects of the potassium-channel blocker tetraethylammonium chloride (TEA). Four concentrations of TEA (1, 10, 15, and 30 m*M*) were tested for their effect on metamorphosis in the presence and absence of inducers. When excess K^+ or Cs^+ was used, TEA remained in the treatment for the same amount of time as the inducer (24 h for excess K^+ and 3 h for Cs^+), after which solutions were replaced with fresh FSW. When a biofilm was used as the inducer, the larvae remained in the presence of biofilm and TEA during the experiment (12 h).

Ontogeny of the response to inducers. To observe the ontogeny of the metamorphic response to ionic inducers, optimum concentrations of the ions, determined as described above, were used. From a single batch of developing larvae, a subset was induced to metamorphose every day beginning 3 days after fertilization. For this experiment, larvae were cultured at an initial density of 5/ml. After each experiment, the density of the larvae remaining in the stock culture was readjusted to maintain 5/ml. An additional experiment was performed to quantify how fast larvae respond to a biofilm as inducer. Larvae (ages 3, 4, and 5 days) were exposed to a biofilm, and the number of larvae that began to secrete a primary tube was determined at 5-min intervals during the first 15 min, at 30-min intervals for the next 3 h, then at 6, 8, 20, and 22 h, and at 24 h when the experiment terminated.

In all experiments, pieces of plastic mesh coated with bacterial biofilm in the laboratory seawater tables were used as a positive control to determine that the larvae were metamorphically competent. A negative control, included to measure spontaneous metamorphosis, consisted of placing larvae in FSW or ASW in clean plastic petri dishes during the experimental period. In experiments with pulse exposures to excess K^+ or Cs^+, larvae in the negative controls were sieved, or the water was removed, in the same way and at the same time as in the experimental treatments to duplicate the manipulation of the larvae in the experimental treatments.

Stock solutions of 1 *M* KCl, 0.542 *M* CsCl, and 1 *M* TEA (Sigma Chem. Co.) dissolved in FSW or ASW were used to make up test solutions. Each experiment was repeated at least three times, except that the response to biofilms with respect to larval age was tested in only one experiment. Data presented here are those from experiments in which minimum and maximum values were recorded in the negative (FSW or ASW) and positive controls (substratum coated with bacterial biofilm), respectively.

Statistical analyses

Proportional response data were arc-sine transformed, and statistical differences among treatments were tested with one-way ANOVA or Kruskal-Wallis ANOVA of ranks when equal-variance tests failed. Pairwise multiple comparisons were tested using the Student-Newman-Keuls method. All tests were conducted with the aid of SigmaStat software.

Results

Induction and completion of metamorphosis

When 3-, 4-, and 5-day-old larvae of *Hydroides elegans* were exposed to a natural biofilm, only 5-day-old larvae responded to the metamorphic cue during the first hour. Typically 80% of the 5-day-old larvae settled and began metamorphosis; no metamorphosis was detected when 3-day-old larvae were exposed to a biofilm, and only low percentages (39%) of 4-day-old larvae responded to the inducer after 22 h (Fig. 1).

Five-day-old competent larvae started to crawl on the bottom of the dish within 5 min of being exposed to a biofilm. Each larva secreted a sticky thread from its posterior end, and then immediately began secreting the primary tube. Larvae appeared to secrete the primary tube from most of the trunk surface and to shape it by rolling and moving back and forth within it, and periodically erecting their setae, apparently to push the tube material away from the body. Secretion of the primary tube, completed 10–15 min after the initial response to the biofilm, defines the permanent attachment of the larva. As the primary tube is being secreted, the prototroch is resorbed, the larval body elongates, the collar region becomes apparent due to anterior and posterior constrictions, and the pair of lobes that will form the branchial radioles becomes apparent on the anterior surface of the head (Fig. 2). At this point, metamorphosis is complete.

Secretion of the calcareous tube at the anterior edge of the primary tube begins about 1.7 h after the induction of metamorphosis, and new material is then added to the calcareous tube more or less continuously. As the calcareous tube is being secreted, the branchial radioles grow out from the anterior lobes signaling the initiation of juvenile development. The primary tube is never

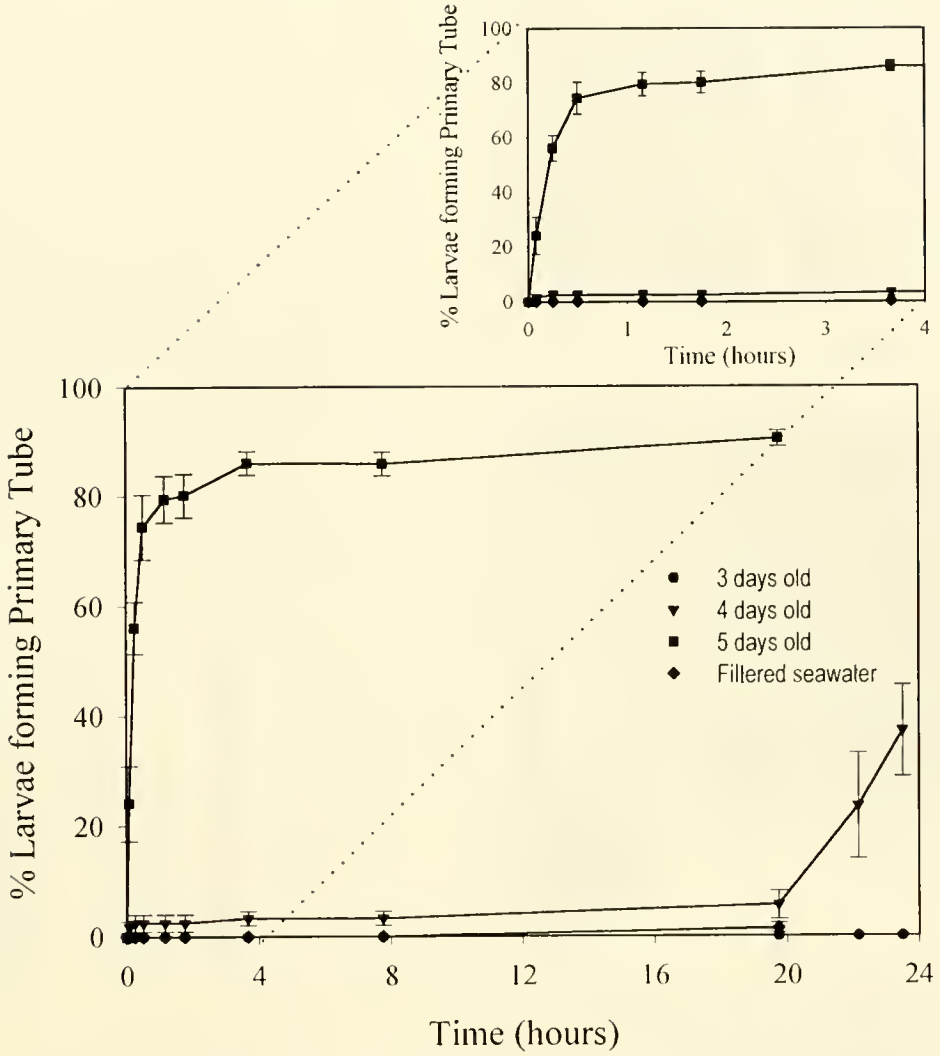

Figure 1. Percentage of larvae of *Hydroides elegans* that settled and formed a primary tube after exposure to a marine biofilm. Larvae were 3, 4, or 5 days old at the beginning of the experiment. As a control, 5-day-old larvae were maintained in filtered (22 μm) seawater without an inducer. Plotted are mean percentages of larvae making a primary tube ± 1 SE (n = 4 replicates/treatment). Insert: detail of the response of larvae during the first 4 h after exposure to a biofilm; symbols are the same as in the main figure.

calcified, and the juvenile has moved completely out of it by 7 h after beginning to metamorphose (Fig. 2).

Continuous and pulse exposure to metamorphic inducers

Effects of excess K^+. Excess K^+ in seawater caused competent larvae of *Hydroides elegans* to metamorphose (Fig. 3A). This response was dependent on both duration of exposure and concentration. Up to 77% of competent larvae metamorphosed within 72 h when exposed to 50 mM excess K^+ for 24 h. Concentrations higher than 50 mM K^+ resulted in fewer metamorphosed larvae, and concentrations higher than 60 mM were toxic. Periods of exposure to excess K^+ longer than 24 h resulted in lower frequencies of metamorphosis. Pulse exposure (3, 10, 15, 60, and 120 min) to excess K^+ (≥60 mM) induced only low percentages of metamorphosis (about 6.5%).

In K^+ treatments, some of the metamorphosed larvae (35%–63%) were unable to secrete primary and secondary tubes, even after they were returned to filtered seawater. Despite their tubeless state, some of these worms survived when fed single-celled algae; they grew for up to 2 months, when the cultures were discarded.

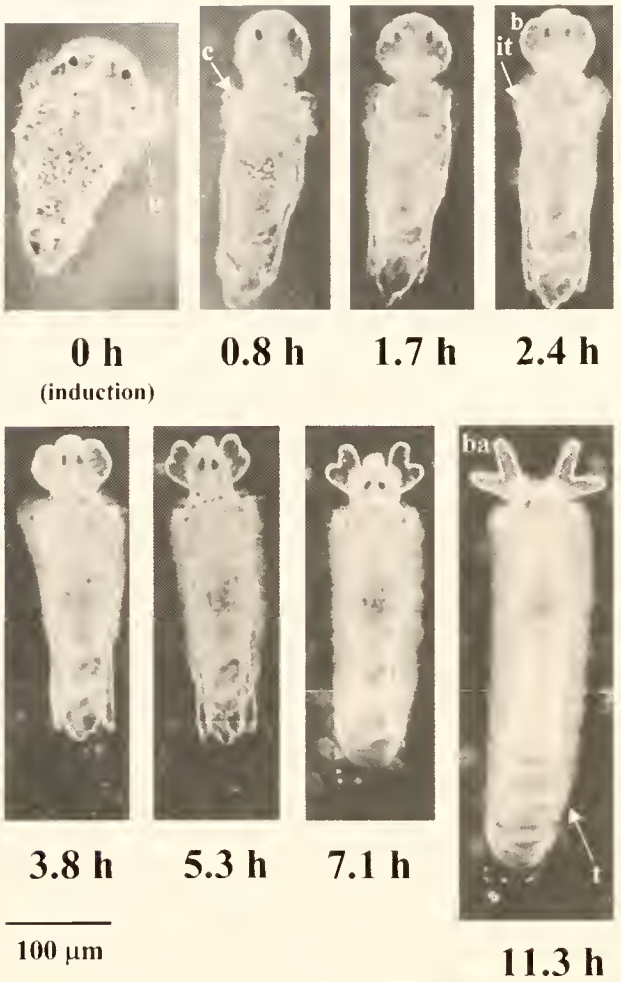

Figure 2. Time course of metamorphosis in *Hydroides elegans*. Frames represent a competent larva at the moment of induction to metamorphosis (0 h) and selected stages for the first 11.3 h after induction. p: prototroch, c: collar, b: branchial lobes, it: initiation point of calcareous tube, ba: branchial radioles, t: calcareous tube covering the worm.

Effects of Cs^+. Larvae of *H. elegans* metamorphosed when exposed to Cs^+ in seawater. This response was dependent on concentration and duration of exposure. When the larvae were continuously exposed for 24 h to different concentrations of CsCl, the maximum response occurred with 5 m*M* Cs^+ 48 h after induction (24% metamorphosis) (Fig. 3B). Larvae exposed for 24 h to concentrations of CsCl higher than 5 m*M* showed increasing signs of toxicity. In 10 m*M* CsCl, the branchial crown began to form, but never developed further. In the 20-m*M* treatment, the larvae became immobile on the bottoms of the dishes, and at concentrations of 30 m*M* and higher, they died. CsCl applied in pulses of 3–4.5 h produced maximal responses (49%) (Fig. 4A); increases in neither concentration nor length of exposure produced a higher percentage of metamorphosis. At 50 m*M* Cs^+, elongated larvae were observed on the bottoms of the dishes; at higher concentrations, the larvae died (Fig. 4B).

Interactions among inducers

Metamorphosis in response to a biofilm was greater than 90% in both the presence and absence of excess K^+, and these values were significantly higher at 48 h ($P < 0.05$) than those obtained when the larvae were exposed to excess

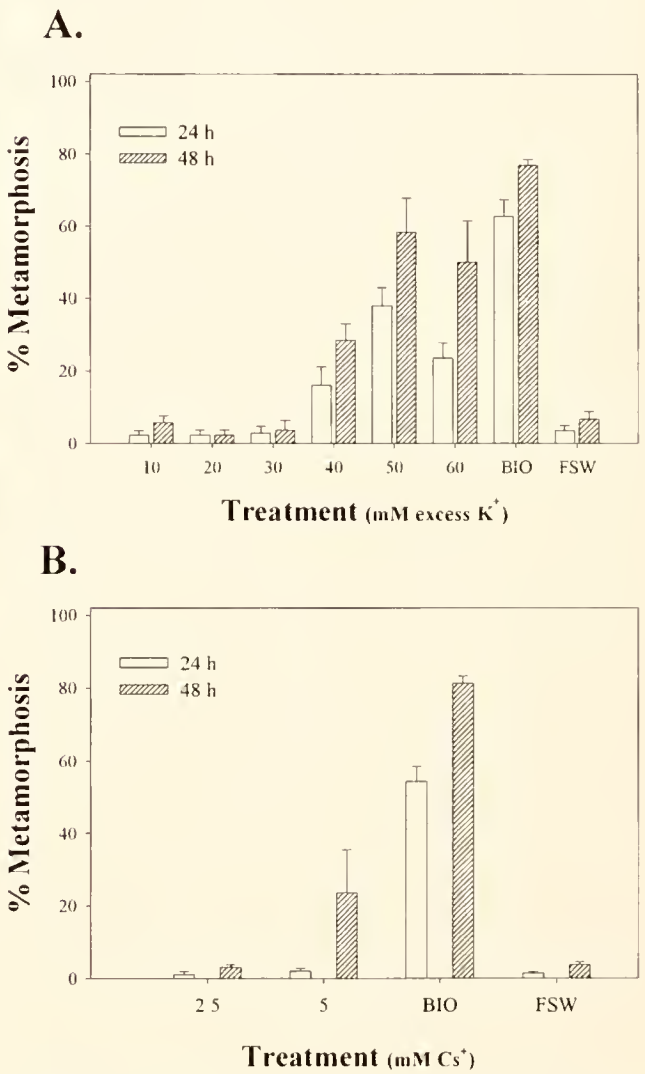

Figure 3. Metamorphosis of *Hydroides elegans* exposed to ionic inducers. (A) Exposure to excess K^+ in FSW for 24 h; (B) exposure to CsCl in FSW for 24 or 48 h. Bars indicate mean percentages of larvae that metamorphosed ± 1 SE (n = 4 replicates/treatment), evaluated 24 and 48 h after removal of excess K^+, or initial exposure to CsCl. BIO = substratum coated with a marine biofilm; FSW = seawater filtered through 0.22-µm filter.

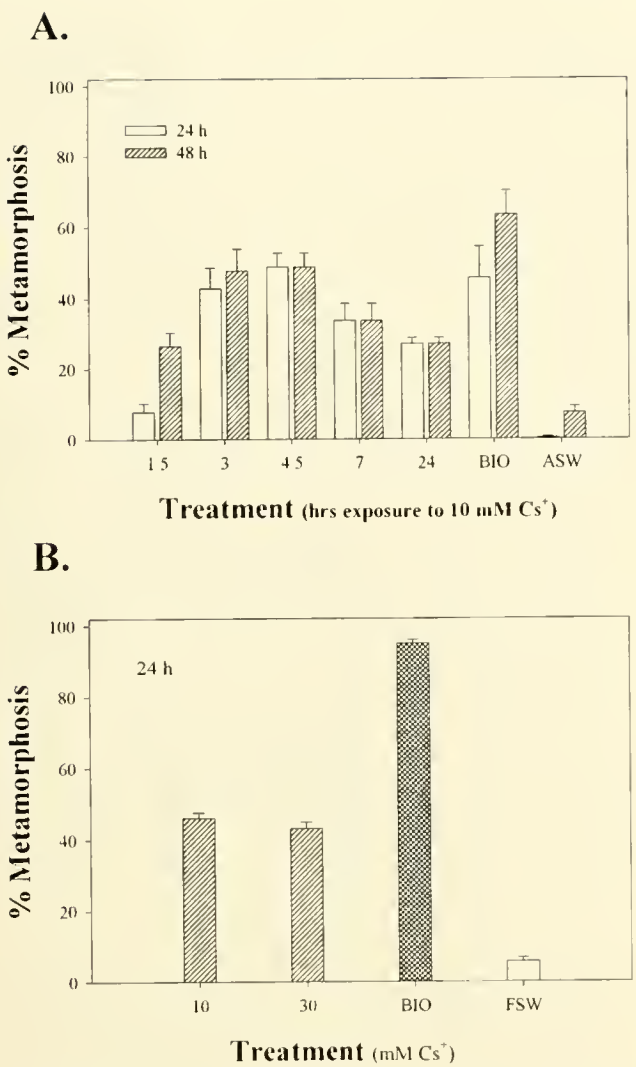

Figure 4. Dose-response relationship for cesium applied as a pulse. Metamorphosis of *Hydroides elegans* after exposure to (A) 10 m*M* CsCl for 1.5 to 24 h; (B) 10 or 30 m*M* CsCl for 3 h. Concentrations higher than 30 m*M* were toxic. Bars indicate mean percentages of larvae that metamorphosed ± 1 SE (n = 4 replicates/treatment), evaluated 24 or 48 h after the beginning of the pulse. BIO = substratum coated with a marine biofilm; FSW = seawater filtered through 0.22-μm filter; ASW = artificial seawater.

K^+ alone (66%) (Fig. 5A). When larvae of *H. elegans* were exposed to a biofilm in the presence of Cs^+, metamorphosis was higher than with biofilm or Cs^+ tested separately (Fig. 5B). These values were significantly different at 24 and 48 h of initial exposure to the inducers ($P < 0.05$). When larvae were induced to metamorphose by a biofilm that had been pre-soaked in seawater containing CsCl, percentages of metamorphosis were similar to those observed with biofilm not exposed to Cs^+, demonstrating that cesium ion has no direct effect on the biofilm.

Effects of tetraethylammonium chloride (TEA)

TEA inhibited metamorphosis in a concentration-dependent manner when larvae were induced with excess K^+ or Cs^+. Significant inhibition of metamorphosis ($P < 0.05$) was found when 10 m*M* TEA was tested in the presence of excess K^+ for 24 h (Fig. 6A), and when

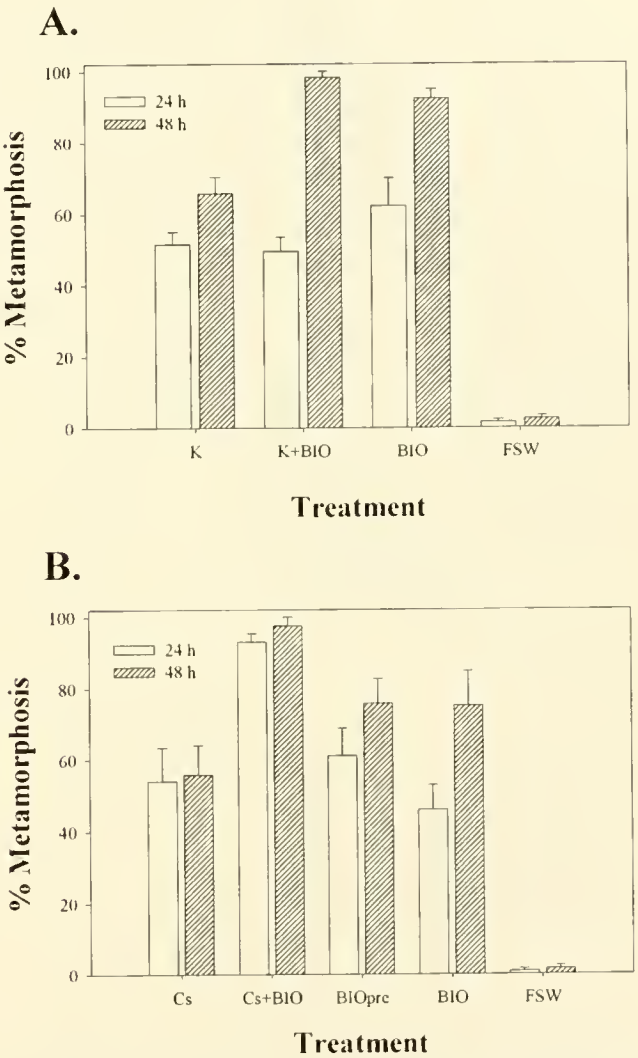

Figure 5. Synergism in the effects of ionic inducers and biofilm on metamorphosis of *Hydroides elegans*. (A) Metamorphosis of larvae exposed to 50 m*M* excess K^+ for 24 h in the presence or absence of a marine biofilm. (B) Metamorphosis of larvae exposed to a 3-h pulse of 10 m*M* CsCl in seawater in the presence or absence of a marine biofilm. Bars indicate mean percentages of larvae that metamorphosed ± 1 SE (n = 4 replicates/treatment), evaluated 24 and 48 h after initial contact with the inducers. K = 50 m*M* excess K^+ for 24 h; Cs = 3-h pulse of 10 m*M* CsCl; BIO = substratum coated with a marine biofilm; FSW = seawater filtered through 0.22-μm filter; BIOpre = substratum coated with a marine biofilm, soaked in 10 m*M* CsCl for 3 h and returned to FSW before addition of larvae.

30 m*M* TEA was tested in combination with a 3-h pulse of Cs^+ (Fig. 6B). Metamorphosis was reduced, but to a lesser extent, when larvae were exposed simultaneously to a biofilm and to 10 or 15 m*M* TEA ($P < 0.05$) (Fig. 6C). At the doses tested, 30 m*M* TEA was toxic after 24 h when tested with an organic biofilm or excess K^+.

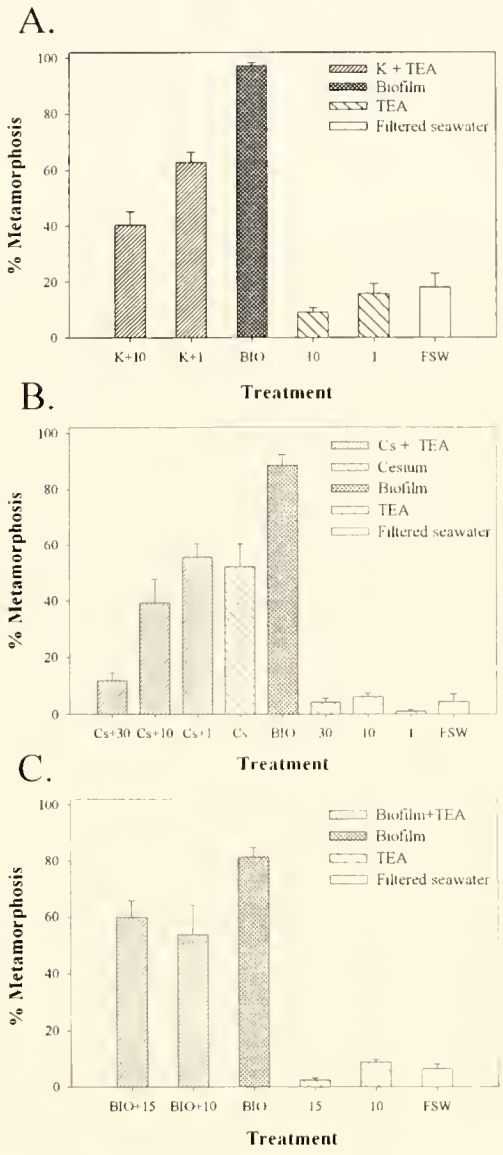

Figure 6. Inhibition of metamorphosis of *Hydroides elegans* by the ion channel blocker tetraethylammonium chloride (TEA). (A) Effect of TEA on metamorphosis in the presence or absence of 50 m*M* excess K^+ in seawater for 24 h. (B) Effect of TEA on metamorphosis in the presence or absence of a 3-h pulse of 10 m*M* CsCl in seawater. (C) Effect of TEA in the presence or absence of a marine biofilm for 12 h. Bars indicate mean percentages of larvae that metamorphosed ± 1 SE (n = 4 replicates/treatment), evaluated 48 h after initial exposure to excess K^+, 24 h after initial exposure to CsCl, and 12 h after initial exposure to a marine biofilm. K = 50 m*M* excess K^+ for 24 h; Cs = 3-h pulse of 10 m*M* CsCl; 1, 10, 15 and 30 = m*M* concentrations of TEA; BIO = substratum coated with a marine biofilm; FSW = seawater filtered through 0.22-μm filter.

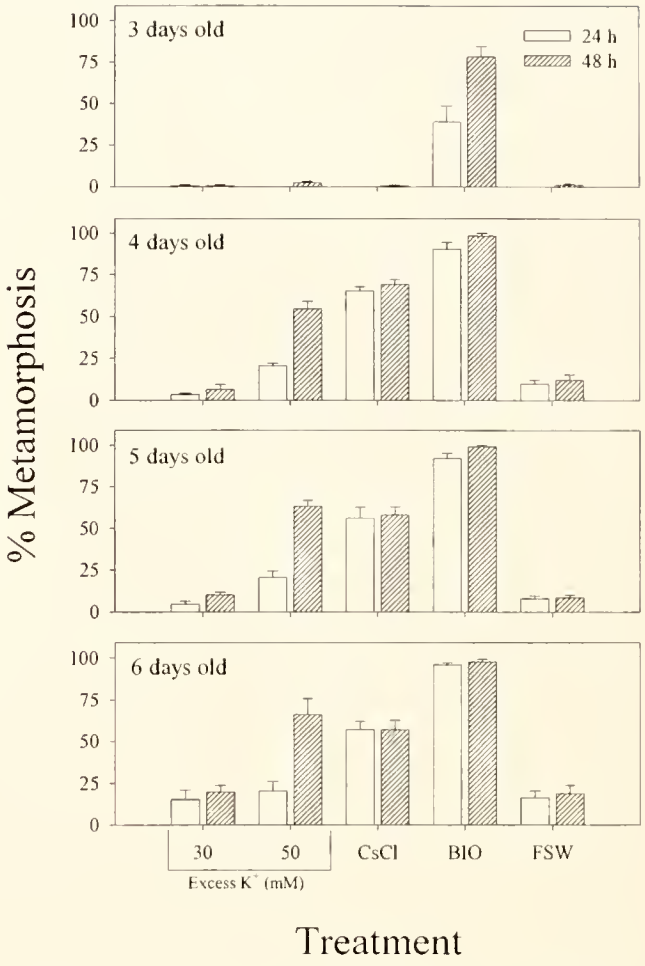

Figure 7. Metamorphosis of 3- to 6-day-old larvae of *Hydroides elegans* from a single batch when exposed to different inducers. Larvae were removed from the 10 m*M* CsCl after 3 h and from 30 and 50 m*M* excess K^+ after 24 h. Bars indicate mean percentages of larvae that metamorphosed ± 1 SE (n = 4 replicates/treatment). BIO = substratum coated with a marine biofilm; FSW = seawater filtered through 0.22-μm filter.

Ontogeny of the metamorphic response to biofilm, Cs^+, and excess K^+

The metamorphic responses of larvae, as a function of age (beginning at day 3) and inducing agent, were compared. The earliest response was to biofilm, where 39% of larvae metamorphosed after 24 h of exposure, *i.e.*, at an age of 4 days. In contrast, only negligible numbers of larvae exposed to either Cs^+ or K^+ on day 3 metamorphosed, even after 48 h (Fig. 7); indeed the first responses to Cs^+ and excess K^+ were recorded only 24 h after an

initial exposure on day 4. The delayed response to ions is more striking when maximal values are compared. When metamorphosis was induced with excess K^+, maximal values were reached 48 h after induction, much later than with a biofilm or Cs^+. With all three inducers, maximal values of metamorphosis were obtained with larvae 4 days old or older, and the percentage of metamorphosis was always higher in response to a biofilm than to Cs^+ or excess K^+. Larvae remained responsive to the inducers through the last day of the experiment, when they were 6 days old.

Discussion

Morphogenesis during metamorphosis

When larvae of *Hydroides elegans* are exposed to a well-developed marine biofilm, they respond rapidly by exploring the surface of the substratum for 1–2 min, attaching, secreting a primary tube, and beginning to metamorphose, all within 1–15 min of initial exposure (Fig. 1). The main morphogenetic events of metamorphosis are completed within 11–12 h of initial contact with a biofilm (Fig. 2). These developmental events progress more slowly when metamorphosis is induced with ions (excess K^+ and Cs^+). Wisely (1958), in an earlier report on metamorphosis in this species, described secretion of an "adhesive substance," but did not mention the behavioral phase when larvae appear to examine the substratum.

In *H. elegans,* secretion of the primary tube and simultaneous elongation of the larva and resorption of the prototroch cilia are irreversible steps. The subsequent differentiation of the tentacular crown defines early juvenile development.

The observation that competent larvae of *H. elegans* respond to bacterial biofilms within 15 min, together with evidence presented by Hadfield *et al.* (1994) that settlement of *H. elegans* increases linearly with bacterial cell count, demonstrates that bacteria are an important source of stimulus for settlement and metamorphosis in this species. In addition, Walters *et al.* (1997) found that larvae of *H. elegans* do not settle preferentially on or near conspecific individuals, living or dead, in the field or in laboratory dishes, and that natural settlement patterns are explained by hydrodynamic processes and the presence of biofilms. We thus suggest that the latent response of larvae of *H. elegans* to extracts of adult worms described by Bryan *et al.* (1997) probably results from the buildup of bacteria in their test vessels. The gregarious response of larvae of *Hydroides dianthus* described by Scheltema *et al.* (1981) and Toonen and Pawlik (1996) is apparently a character not shared by all species in this genus.

The data provided here on induction of metamorphosis of *H. elegans* with excess K^+ or Cs^+ expand on a growing literature on this subject (see summaries in Herrmann, 1995; Woollacott and Hadfield, 1996). *Hydroides elegans* is not the first polychaete to be found sensitive to potassium or cesium (Herrmann, 1995). Yool *et al.* (1986) were able to induce maximum percentages of metamorphosis in larvae of *Phragmatopoma californica* at lower potassium concentrations (5–20 m*M*) than those found to be optimal for *H. elegans* (50 m*M*). In addition, percentages of metamorphosis were lower in *H. elegans* (77% *versus* 100% for *P. californica*). Differences in K^+ sensitivity between species could explain these results: species-specific metamorphic responses to excess K^+ were recently reported by Pearce and Scheibling (1994) for the echinoids *Strongylocentrotus droebachiensis* and *Echinarachnius parma.*

The metamorphic response of larvae of *H. elegans* to excess K^+ was slower than to Cs^+ or a biofilm. The larvae took 72 h to achieve maximum levels of metamorphosis in response to K^+, and metamorphosis was typically completed 24 h or longer after removing them from seawater with excess K^+. A similar delay in the metamorphic response was found in *Phestilla sibogae,* when induction was compared between the natural inducer (a coral metabolite) and choline (Hirata and Hadfield, 1986) or excess K^+ (Pechenik *et al.,* 1995). In contrast, larvae of the prosobranch *Crepidula fornicata* become sensitive to induction by excess K^+ 12–24 h before they are responsive to natural inducers (Pechenik and Gee, 1993). These differences may arise from nothing more complex than the degree of exposure of sensory cells to the external medium or the resistance of sensory cells to depolarization by external ion shifts—in other words, to plasticity in induction mechanisms at the species level, as suggested by Woollacott and Hadfield (1996).

It has been proposed that excess K^+ induces metamorphosis by depolarization of externally accessible excitable cells (Baloun and Morse, 1984; Yool *et al.,* 1986). However, the possibility remains that K^+ acts on the entire nervous system, producing a generalized activation (Todd *et al.,* 1991), or that the ions exert a direct effect on target tissues (Yool *et al.,* 1986).

The observation that most larvae of *H. elegans* metamorphose without tube formation when induced by potassium ions may indicate that at least part of the action of this ion is directly on target tissues. However, it is more likely that the altered ionic makeup of the seawater disrupts secretion of the primary-tube proteins (possibly by inhibiting proper cross-linking) by epidermal cells. The lengthy exposure to excess K^+ required to induce maximum metamorphosis concomitantly leads to large numbers of tubeless metamorphosed worms. Although failure to produce a primary tube prevents a larva from attaching to hard substrata, the morphogenetic events of metamorphosis are completed. In other words, metamorphic

morphogenesis is not dependent on secretion of the primary tube. Potassium ions produced an analogously disturbed metamorphosis in the brachiopod *Terebratalia transversa;* many of the larvae underwent partial metamorphosis, characterized by protegulum (or initial shell) formation without settlement (Freeman, 1993). Clearly, care must be used in ascribing singular modes of action to events elicited when an entire sensitive larva is immersed in seawater with an altered ion composition.

Larvae of *H. elegans* metamorphosed faster in response to Cs^+ than to excess K^+. These results are difficult to interpret because of the required short-pulse exposure necessary with cesium compared to the 24-h exposure required for maximum response to potassium. That the larvae first become sensitive to these ions at about the same age suggests either a similar inductive mechanism or a common site of action in the metamorphic pathway; reasoning presented below supports the latter hypothesis.

The one or more mechanisms by which Cs^+ induces metamorphosis in marine invertebrate larvae have not been determined with certainty, although Cs^+ has been tested with positive results in coelenterates (Freeman and Ridgway, 1987; Hujer and Lesh-Laurie, 1995), phoronids (Herrmann, 1995), a sponge (Woollacott and Hadfield, 1996), and a polychaete (Herrmann, 1986). Cesium is a recognized potassium-channel blocker and, when externally applied, leads to depolarization of the plasma membrane in some systems (Hille, 1992). This depolarization can activate voltage-dependent calcium channels, releasing calcium ions into the cytoplasm and modulating a wide variety of cell processes, including secretion, contraction, and the cell cycle (Clapham, 1995). Cesium activation of calcium-mediated mechanisms in invertebrate larvae has been documented mainly in hydrozoans. Leitz and Müller (1987) found a fast increase of inositol trisphosphate (IP_3) concentration after incubation of planulae of *Hydractinia echinata* in 116 m*M* CsCl. IP_3 is known to induce release of Ca^{2+} from internal stores by activating receptors on the endoplasmic reticulum. Freeman and Ridgway (1990) observed that calcium transients were produced when larvae of the hydrozoan *Mitrocomella polydiademata* were induced to metamorphose by Cs^+. Ilan *et al.* (1993) demonstrated a role for intracellular calcium in regulating metamorphosis in the polychaete *Phragmatopoma californica;* larvae metamorphosed in response to elevated external Ca^{2+} concentrations and to calcium ionophores. A role for calcium during metamorphosis of *H. elegans* appears certain despite the fact that our preliminary experiments with this species produced results that were different from those reported by Ilan *et al.* (1993) for *P. californica.* In *H. elegans,* metamorphosis was inhibited when induced in the presence of calcium ionophore A23187 or one of the calcium-channel blockers nefedipine and verapamil. These results and the effects of TEA, discussed below, suggest that the mechanism of action of Cs^+ on larvae of *H. elegans* may be different from the way it acts on planula larvae and, perhaps, on larvae of *P. californica.* Experiments are under way in our laboratory to clarify the role of Ca^{2+} in the metamorphosis of *H. elegans.*

If, as is generally assumed, the natural inducer (a marine biofilm) and potassium ions both lead to metamorphosis by initiating membrane depolarization and generation of a receptor potential in excitable, external sensory cells, the inhibition of such induction by TEA, a potassium-channel blocker, is understandable. TEA, by blocking K^+ channels, inhibits ion flow and membrane depolarization. The observation that TEA also inhibits cesium-induced metamorphosis appears contradictory at first, because Cs^+ is itself a potassium-channel blocker in some organisms (Hille, 1992). However, potential explanations are at hand. The concentration of cesium found to induce metamorphosis in *H. elegans* (10 m*M*) is much lower than the concentration of potassium ion found necessary to induce metamorphosis (50 m*M* in excess of that normally present in seawater) and is thus unlikely to act by simply depolarizing the membrane of a receptor cell. It is more likely that Cs^+ enters receptor cells through potassium channels, as has been shown to occur in *Drosophila* potassium channels expressed in *Xenopus* oocytes (Heginbotham and MacKinnon, 1993), and acts inside the cells. TEA blockage of K^+ channels in larvae of *H. elegans* would thus directly inhibit cesium inflow and metamorphic induction. A possible target for Cs^+ inside the cells may be the ATP-driven Na^+/K^+ pump, whose major function is maintenance of the transmembrane gradient and thus the resting membrane potential (Petersen, 1992).

When competent larvae were exposed to a biofilm in the presence of Cs^+ or excess K^+, a synergistic effect was noted (24 h after removal from excess K^+). This synergism may be understood as a partial depolarization of excitable cells that reduces the threshold necessary to activate metamorphosis by the natural biofilm inducer; this mechanism was suggested by Woollacott and Hadfield (1996) as a possible explanation for the interaction of ions and biofilm in the induction of metamorphosis of larvae of a sponge. The more apparent synergism noted between Cs^+ and a biofilm probably arises from the more rapid (compared to potassium) action of cesium as an inducer. Given the 24-h exposure necessary to achieve maximum metamorphosis with potassium, most larvae will already have metamorphosed from continued contact with the biofilm.

Larvae must be exposed to excess potassium longer than to biofilms to achieve metamorphosis, and it is therefore impossible to distinguish between the possibilities

(1) that larval sensitivity to K^+ develops later than sensitivity to biofilms and (2) that the larval response to K^+ simply takes longer. The response to a biofilm that can be seen after a 24-h exposure in 3-day-old larvae does not occur when potassium (or cesium) is used as an inducer (Fig. 7). However, it may be that the larvae that respond to a biofilm when exposed at day 3 became competent only in the last moments of exposure; that is, when they were almost 4 days old. Because the larvae tested with potassium were removed from the inducer at this time, they were deprived of the necessary 24-h exposure after becoming competent, and thus never metamorphosed at all. The argument is similar for cesium. Day 3 larvae were exposed to cesium for only 3 h, and thus were not in the inducer when they became metamorphically competent (Fig. 7). The result is that no larvae metamorphosed after 24 or 48 h. Differences in the age at onset of sensitivity to biofilms and the ions cannot be discerned from our experimental results.

Despite possible variation in the age at which larvae of *Hydroides elegans* become sensitive to different inducers, the hypothesis that metamorphic induction is primarily a chemoreceptive process, including depolarization of an excitable receptor cell and transmission of the metamorphic signal via the nervous system, is still the most parsimonious. Moreover, the ability of larvae of *H. elegans* to metamorphose without primary tube formation as a response to potassium or cesium demonstrates that steps in the settlement process may be separated, with some processes proceeding while others do not. Our current work includes exploration of the transduction pathway associated with metamorphic induction. We seek to understand the mechanisms by which the chemoreceptive act of induction is transduced into a cellular signal as well as the manner in which the metamorphic stimulus activates new gene transcription or translation.

Acknowledgments

The authors are indebted to Dr. Andrea Baloun Yool for her knowledgeable support of our attempts to unravel the mechanisms of metamorphic induction in marine invertebrates. Contributions of colleagues in the Hadfield lab have been many, and we are grateful indeed for all of them. Comments of the editor and two anonymous reviewers led to improvements in the paper. This research was supported by ONR grant No. N00014-95-1015 to MGH; EC-I is the recipient of a scholarship for graduate studies from Conacyt/UABC, Mexico.

Literature Cited

Baloun, A. J., and D. E. Morse. 1984. Ionic control of settlement and metamorphosis in larval *Haliotis rufescens* (Gastropoda). *Biol. Bull.* **167:** 124–138.

Bryan, J. P., P-Y. Qian, J. L. Kreider, and F-S. Chia. 1997. Induction of larval settlement and metamorphosis by pharmacological and conspecific associated compounds in the serpulid polychaete *Hydroides elegans*. *Mar. Ecol. Prog. Ser.* **146:** 81–90.

Cavanaugh, G. M. 1956. *Formulae and Methods VI.* Marine Biological Laboratory, Woods Hole, Massachusetts. Pp. 62–69.

Clapham, D. E. 1995. Calcium signaling. *Cell* **80:** 259–268.

Eyster, L. S., and J. A. Pechenik. 1988. Comparison of growth, respiration, and feeding of juvenile *Crepidula fornicata* (L.) following natural or KCl-triggered metamorphosis. *J. Exp. Mar. Biol. Ecol.* **118:** 269–279.

Freeman, G. 1993. Metamorphosis in the brachiopod *Terebratalia:* evidence for a role of calcium channel function and dissociation of shell formation from settlement. *Biol. Bull.* **184:** 15–24.

Freeman, G., and E. B. Ridgway. 1987. Endogenous photoproteins, calcium channels and calcium transients during metamorphosis in hydrozoans. *Roux's Arch. Dev. Biol.* **196:** 30–50.

Freeman, G., and E. B. Ridgway. 1990. Cellular and intracellular pathways mediating the metamorphic stimulus in hydrozoan planulae. *Roux's Arch. Dev. Biol.* **199:** 63–79.

Hadfield, M. G., C. C. Unabia, C. M. Smith, and T. M. Michael. 1994. Settlement preferences of the ubiquitous fouler *Hydroides elegans*. Pp. 65–72 in *Recent Developments in Biofouling Control*, M. F. Thompson, R. Nagabhushanam, R. Sarojini, and M. Fingerman, eds. Oxford and IBH Publishing Co., New Delhi.

Heginbotham, L., and R. MacKinnon. 1993. Conduction properties of the cloned Shaker K^+ channel. *Biophys. J.* **65:** 2089–2096.

Herrmann, K. 1986. Die metamorphose von *Polygordius appendiculatus* (Polychaeta, Archiannelida): Induction und ablauf. *Publ. Wiss. Film (Sekt. Biol.* Ser. 18) **36:** 1–15 (cited by Herrmann, 1995).

Herrmann, K. 1995. Induction and regulation of metamorphosis in planktonic larvae: *Phoronis müilleri* (Tentaculata) as archetype. *Helgol. Wiss. Meeresunters.* **49:** 255–281.

Hille, B. 1992. *Ionic Channels of Excitable Membranes.* 2nd ed. Sinauer, Sunderland, MA. 607 pp.

Hirata, K. Y., and M. G. Hadfield. 1986. The role of choline in metamorphic induction of *Phestilla* (Gastropoda, Nudibranchia). *Comp. Biochem. Physiol.* **84:** 15–21.

Hujer, A., and G. E. Lesh-Laurie. 1995. Effect of mono- and divalent cations on polyp morphogenesis in isolated tentacles of *Aurelia aurita* (Scyphozoa). *Roux's Arch. Dev. Biol.* **205:** 122–127.

Ilan, M., R. A. Jensen, and D. E. Morse. 1993. Calcium control of metamorphosis in polychaete larvae. *J. Exp. Zool.* **267:** 423–430.

Leitz, T., and W. A. Müller. 1987. Evidence for the involvement of PI-signaling and diacylglycerol second messengers in the initiation of metamorphosis in the hydroid *Hydractinia echinata* Fleming. *Dev. Biol.* **121:** 82–89.

Morse, D. E., N. Hooker, A. N. C. Morse, and R. A. Jensen. 1988. Control of larval metamorphosis and recruitment in sympatric agariciid corals. *J. Exp. Mar. Biol. Ecol.* **166:** 193–217.

Müller, W. A., and G. Buchal. 1973. Metamorphose-Induktion bei-Planularven: II. Induktion durch monovalente Kationen: Die Bedeutung des Gibbs-Donnan-Verhaltnisses und der Na^+/K^+ ATPase. *Roux's Arch. Dev. Biol.* **173:** 122–135.

Pearce, C. M., and R. E. Scheibling. 1994. Induction of metamorphosis of larval echinoids (*Strongylocentrotus droebachiensis* and *Echinarachnius parma*) by potassium chloride (KCl). *Invertebr. Reprod. Dev.* **26:** 213–220.

Pechenik, J. A., and C. C. Gee. 1993. Onset of metamorphic competence in larvae of the gastropod *Crepidula fornicata* (L.), judged by a natural and an artificial cue. *J. Exp. Mar. Biol. Ecol.* **167:** 59–72.

Pechenik, J. A., M. G. Hadfield, and L. S. Eyster. 1995. Assessing

whether larvae of the opisthobranch gastropod *Phestilla sibogae* Bergh become responsive to three chemical cues at the same age. *J. Exp. Mar. Biol. Ecol.* **191:** 1–17.

Petersen, O. H. 1992. Ion channels. Ten years of patch-clamp studies. *Biochem. Pharmacol.* **43:** 1–3.

Rittschof, D., J. Maki, R. Mitchell, and J. D. Costlow. 1986. Ion and neuropharmacological studies of barnacle settlement. *Neth. J. Sea Res.* **20:** 269–275.

Rowley, R. J. 1989. Settlement and recruitment of sea urchins (*Strongylocentrotus* spp.) in a sea-urchin barren ground and a kelp bed: Are populations regulated by settlement or post-settlement processes? *Mar. Biol.* **100:** 485–494.

Scheltema, R. S., I. P. Williams, M. A. Shaw, and C. Loudon. 1981. Gregarious settlement by the larvae of *Hydroides dianthus* (Polychaeta: Serpulidae). *Mar. Ecol. Prog. Ser.* **5:** 69–74.

Todd, C. D., M. G. Bentley, and J. N. Havenhand. 1991. Larval metamorphosis of the opisthobranch mollusc *Adalaria proxima* (Gastropoda: Nudibranchia): the effects of choline and elevated potassium ion concentration. *J. Mar. Biol. Assoc. U.K.* **71:** 53–72.

Toonen, J. P., and J. R. Pawlik. 1996. Settlement of the tube worm *Hydroides dianthus* (Polychaeta: Serpulidae): cues for gregarious settlement. *Mar. Biol.* **126:** 725–733.

Walters, L. J., M. G. Hadfield, and K. A. del Carmen. 1997. The importance of larval choice and hydrodynamics in creating aggregations of *Hydroides elegans* (Polychaeta: Serpulidae). *Invertebr. Biol.* **116:** 102–114.

Wisely, B. 1958. The development and settling of a serpulid worm, *Hydroides norvegica gunnerus* (Polychaeta). *Aust. J. Mar. Freshwater Res.* **9:** 351–361.

Woollacott, R. M., and M. G. Hadfield. 1996. Induction of metamorphosis in larvae of a sponge. *Invertebr. Biol.* **115:** 257–262.

Yool, A. J., S. M. Grau, M. G. Hadfield, R. A. Jensen, D. A. Markell, and D. E. Morse. 1986. Excess potassium induces larval metamorphosis in four marine invertebrate species. *Biol. Bull.* **170:** 255–266.

Reference: *Biol. Bull.* **194:** 25–35. (February, 1998)

Effects of Salinity on Sperm Motility, Fertilization, and Development in the Pacific Herring, *Clupea pallasi*

FREDERICK J. GRIFFIN[1], MURALI C. PILLAI[1,2], CAROL A. VINES[1], JUHA KÄÄRIÄ[3], THEA HIBBARD-ROBBINS[1], RYUZO YANAGIMACHI[4], AND GARY N. CHERR[1,5,*]

[1] *University of California at Davis, Bodega Marine Laboratory, Bodega Bay, California;* [2] *Department of Biology, Sonoma State University, Rohnert Park, California;* [3] *University of Turku, Turku, Finland;* [4] *Department of Anatomy and Reproductive Biology, University of Hawaii School of Medicine, Honolulu, Hawaii; and* [5] *Department of Environmental Toxicology, University of California, Davis, California*

Abstract. We investigated the effects of salinity on fertilization and early development in a population of Pacific herring, *Clupea pallasi*, that migrate from oceanic waters into the San Francisco Bay estuary to spawn. The salinity range for fertilization fell between 8 and 28 ppt, with an optimal range of about 12 to 24 ppt. In comparison, the range for a population of *C. harengus membras* (Airisto Sound, Finland) that reside year-round in the Baltic Sea was 4 to 24 ppt. Roles for both Na^+ and K^+ were indicated in *C. pallasi* fertilization since increasing Na^+ in the presence of 10 m*M* K^+ (concentration of seawater) mimicked the effects of increased overall salinity, whereas reduced effects were obtained if $[K^+]$ was held at 5 m*M* (that of half-strength seawater). The initiation of *C. pallasi* sperm motility by components of the egg chorion, a prerequisite for fertilization, was inhibited at both elevated (28 and 32 ppt) and reduced (4 and 8 ppt) salinities. Embryonic development through larval hatching in *C. pallasi* exhibited a salinity tolerance similar to that of fertilization; optimum development was obtained at salinities between 8 and 24 ppt. A comparison of developmental progression in 3.5, 14, and 28 ppt seawater revealed that salinity effects became evident during the post-gastrulation stages of development and that progression to hatching was delayed in both the lower and higher salinities for those embryos that completed development.

Received 17 October 1996; accepted 11 November 1997.

* To whom correspondence should be addressed. E-mail: gncherr@ucdavis.edu.

Abbreviations: ASW, artificial seawater; FSW, filtered seawater; HR, herring Ringer's; SMIF, sperm motility initiation factor.

Introduction

Pacific herring, *Clupea pallasi*, inhabit the continental shelves of the North Pacific Ocean from California to Korea, and the White and Kara Sea regions of the Arctic Ocean (Dushkina, 1973; Grant, 1984; Grant and Utter, 1984). Once considered a subspecies of the Atlantic herring (*C. harengus*), as currently is the Baltic herring, *C. pallasi* is now recognized to be different behaviorally, morphologically, and genetically from *C. harengus* (Grant, 1984; Grant and Utter, 1984; Haegele and Schweigert, 1985). Pacific herring spawn during the winter and spring, predominantly in protected waters of bays and estuaries. Males release sperm into the water while females deposit adhesive eggs onto shallow subtidal and lower intertidal substrates where fertilization and embryonic development take place (see Haegele and Schweigert, 1985). Herring are unique among fish in that sperm are immotile when released from males and remain so after dilution into the surrounding media (Yanagimachi and Kanoh, 1953). They are typical in that their eggs are surrounded by a thick chorion with only one access site to the egg surface (the micropylar canal), and that sperm must be motile to traverse this canal and achieve fertilization (Yanagimachi and Kanoh, 1953; Yanagimachi, 1956; 1957).

Although salinity has been shown to influence fertiliza-

tion and embryonic development in *C. pallasi*, the importance of this environmental factor has been questioned due primarily to the overall broad range of salinities (5–35 ppt) observed at spawning sites throughout the species' range (Blaxter and Holliday, 1963; Haegele and Schweigert, 1985). Laboratory studies, however, with specific populations or stocks suggest that this broad tolerance range may not apply to all Pacific herring. An optimum laboratory salinity range of 10–36 ppt has been reported for the embryonic development of White Sea herring (Dushkina, 1973), and herring from the Strait of Georgia in British Columbia have shown a developmental tolerance of 12–26 ppt (Alderdice and Velsen, 1971) with a much narrowed optimum of 12–17 ppt (reviewed by Alderdice and Hourston, 1985).

Research into the mechanisms of fertilization in *C. pallasi* has provided insight as to how salinity could adversely affect the establishment of a new generation. Herring sperm become motile upon physical contact with the micropyle region of the egg chorion, and both K^+ and Na^+ ions have been implicated in this initiation of sperm motility (Yanagimachi and Kanoh, 1953; Yanagimachi, 1956; 1957; Yanagimachi *et al.*, 1992). The presence of extracellular K^+ is required for initiation of motility at the micropyle region of an egg (Yanagimachi *et al.*, 1992). In contrast, Na^+ is not required and, in fact, the deletion of Na^+ or the addition of a Na^+ ionophore (in low external Na^+ concentrations) initiates spontaneous sperm motility in the absence of the chorion factor (Yanagimachi *et al.*, 1992).

In the present report we (1) describe the salinity tolerance range for fertilization in *C. pallasi* from San Francisco Bay, California; (2) provide evidence that a synergistic effect between elevated Na^+ and K^+ ions at elevated salinities is responsible for decreased fertilization in *C. pallasi;* (3) demonstrate that decreased fertilization at elevated salinities is due to an inhibition of sperm motility; and (4) determine the effects of lowered and elevated salinity on embryonic development in *C. pallasi.* Lastly, we compare the salinity tolerance range for fertilization of an eastern population of Baltic herring (*C. h. membras*) with that of San Francisco Bay *C. pallasi.*

Materials and Methods

Collection of animals and gametes

Pacific herring, *Clupea pallasi,* were collected by otter trawl from the San Francisco Bay estuary in collaboration with biologists from the California Department of Fish and Game. The fish were maintained at 4°C in moist conditions and brought to the University of California Bodega Marine Laboratory within 3–4 h of collection. Eggs were obtained either by stripping or by dissection of ovaries as described previously (Yanagimachi, 1957; Griffin *et al.*, 1996). "Dry" eggs, in ovarian fluid, were maintained in a humid chamber at 4°C until used. Testes were dissected from males and maintained separately in a moist environment at 4°C until used (Yanagimachi *et al.*, 1992). To obtain sperm, milt was collected by stripping or by dissection of testes, diluted to approximately 10^9 sperm/ml into herring Ringer's (HR), and kept at 4°C: this maintains sperm in an isotonic medium and in an inactivated state (Yanagimachi *et al.*, 1992). HR was prepared according to Yanagimachi (1957) and contained 206 m*M* NaCl, 7.2 m*M* KCl, 2.1 m*M* $CaCl_2$, 3.3 m*M* $MgCl_2 \cdot 6H_2O$, pH adjusted to 7.8 using 1 m*M* $NaHCO_3$. Sperm were used for experiments within 1 h after isolation into HR.

Baltic herring (*C. h. membras*) from Airisto Sound (Turku, Finland) were collected in trapping pens at spawning sites within Airisto Sound, the gonads dissected, and then shipped overnight under moist conditions, at 4°C, to the Bodega Marine Laboratory. Gametes were isolated as described for *C. pallasi.*

Fertilization assays under different salinity conditions

Fertilization curves based on sperm concentration were generated for each set of gametes to determine the lowest sperm concentration that yielded between 50% and 90% fertilization. This was done to ensure that effects of experimental manipulations were not masked by an excess of sperm. For *C. pallasi,* the ratio was determined in half-strength filtered (0.45-μm) seawater ($^1/_2$ FSW), pH 7.8, previously shown to be optimal for fertilization in this species (Yanagimachi *et al.*, 1992). For *C. h. membras,* $^1/_4$-strength FSW was utilized, based on the reported salinities of 6–7 ppt in Airisto Sound, Finland (Vuorinen and Ranta, 1987). Different salinities of seawater were prepared by adding appropriate quantities of double-distilled water to full-strength FSW, after which salinity in parts per thousand (ppt) was determined with a refractometer. Since the salinity tolerance range is reported to expand close to optimal temperatures and to contract as temperature increases or decreases away from the optimum (Alderdice and Velsen, 1971), the effects of temperature were eliminated by conducting experiments within normative environmental temperatures (Alderdice and Velsen, 1971; Haegele and Schweigert, 1985). Unaltered salinities of FSW at the facility during fertilization experiments ranged from 32 to 34 ppt; if the salinity was above 32 ppt, distilled water was used to bring it down to 32 ppt. For all fertilization experiments, stock sperm (in HR) were diluted into 10 ml of the appropriate dilution of FSW (in polystyrene culture dishes) and incubated for 10 min at 12°C, after which about 100 eggs were distributed evenly into the dishes. Eggs were co-incubated with sperm for 10 min, quickly rinsed twice with the same-

salinity FSW to remove excess sperm, and incubated at 12°C, 10 h light/14 h dark, in temperature- and light-controlled incubators (Revco and Lab-Line Ambi-Hi-Lo). For each salinity treatment, fertilization was determined by scoring the percentage of eggs with elevated chorions at 30 min post-insemination (see Fig. 1); these zygotes were followed through first cleavage to ensure that they had been fertilized. Experiments were conducted in triplicate ($n = 3$) using gametes from different animals; each n was, in turn, the average of three replicates using gametes from the same animals. Data presented are the averages ± standard deviations of the replicates (n). Significance of differences was determined with a Student's t test using the values from each n.

Effects of extracellular Na^+ and K^+ concentration on fertilization

Artificial seawaters containing different concentrations of Na^+ and K^+ were prepared from half-strength ASW (artificial seawater; from Cavanaugh, 1975) containing either 5 m*M* or 10 m*M* K^+. To obtain final Na^+ concentrations of 200–400 m*M*, the ½ ASWs were supplemented with Na^+ in 50-m*M* increments using a stock solution of 4.4 *M* NaCl. Fertilization assays in these media were conducted as described above.

In vitro *sperm motility assessments under different salinity conditions*

Sperm motility was assessed *in vitro* using Pacific herring sperm motility initiation factor (SMIF) according to Yanagimachi *et al.* (1992) and Pillai *et al.* (1993).

Figure 1. Fertilized (f) and unfertilized (u) eggs of *Clupea pallasi*. Fertilized eggs are translucent with an easily seen perivitelline space between chorion and egg. Bar = 1 mm.

Chorions from *C. pallasi* eggs were obtained as described by Griffin *et al.* (1996), and SMIF was isolated from these chorions according to Pillai *et al.* (1993). Different-salinity FSWs were mixed with SMIF (at 50–100 μg protein SMIF/ml, final concentration), and 50 μl of each was placed into individual wells of a multi-well immunoslide (Polysciences, Inc., PA). Stock sperm (10^9 sperm/ml in HR) diluted (final concentration of 5×10^6 sperm/ml) into different-salinity FSWs were then added to the wells containing SMIF (in the same-salinity FSWs) as a 1.5-μl bolus. Using darkfield microscopy and a 20× objective lens, the interface between the bolus of sperm and the SMIF solution was monitored for 15 s. In the absence of motility the bolus spread into the SMIF as a monolayer of sperm, preserving a discrete interface between the two. The initiation of motility, characterized by a counterclockwise corkscrew or circular swimming pattern, disrupted this interface; the degree of disruption was related to the percentage of motile sperm. Motility was scored by using the following qualitative motility index: 0 = no motility, 1 = up to 25% of the cells motile, 2 = up to 50% of the cells motile, 3 = up to 75% of the cells motile, 4 = >75% of the cells motile (Griffin *et al.*, 1996).

Embryonic development and hatching of C. pallasi

For assessing the effects of altered salinities on embryonic development and hatching, *C. pallasi* eggs were fertilized in ½ FSW and then cultured in different-salinity seawaters as described above. During the embryonic development experiments, unaltered salinities ranged from 28–32 ppt. When the full-strength salinity was below 32 ppt, the salinity was not adjusted upward, but the lower starting salinity was noted. The FSW of the cultures was exchanged every 24 h and salinities, dissolved oxygen, and pH were measured at the end of each experiment. Any experiment that exhibited significantly decreased dissolved oxygen or altered pH was not included in data analyses. Development experiments were conducted on batches of embryos that were different from those used for the fertilization experiments described above.

Embryonic development and hatching were followed using either an Olympus stereo-zoom microscope equipped with darkfield optics or an Olympus BHS compound microscope equipped with Nomarski optics. Development was assessed on the basis of comparisons with control embryos and using terminology and stages employed by Kimmel *et al.* (1995) for the zebrafish (see Results). Larval hatching was quantified by counting empty chorions still attached to the bottom of the dishes *versus* chorions containing unhatched embryos. In the experiments from which the salinity tolerance curve was generated, hatching success in all salinities was assessed when greater than 40% of the embryos in the ½ FSW had

hatched. In the experiments to ascertain whether salinity delayed hatching, the cultures were scored at 24-h intervals for 3 days after hatching reached 40% in ½ FSW cultures. In these experiments the salinity of FSW was 28 ppt; therefore, the different-salinity FSWs were 3.5 ppt (⅛ FSW), 14 ppt (½ FSW), and 28 ppt (full-strength FSW). The total number of chorions was counted each day to determine if embryos or empty chorions had been inadvertently removed during water exchanges in cultures.

Results

The salinity tolerance ranges for fertilization in *C. pallasi* from San Francisco Bay, California, USA, and *C. h. membras* from Airisto Sound, Turku, Finland, overlap, but are significantly different (Figs. 2, 3). The optimum salinity for *C. h. membras* in our experiments was 8 ppt (56.3% ± 12.7% fertilization), with decreases in fertilization to 15.0% ± 2.2% at 4 ppt and 10.5% ± 3.8% at 24 ppt (Fig. 2). Fertilization in *C. pallasi* peaked at 16 ppt (86.0% ± 7.5%) with decreases to 17.1% ± 4.6% at 8 ppt and 10.5% ± 6.2% at 32 ppt. After normalization of the data such that the highest fertilization percentage observed for each species was designated as 100% (Fig. 3), the significance of the differences in salinity tolerance was determined. In 8 ppt, fertilization of *C. h. membras* was significantly higher ($P < 0.001$) than that of *C. pallasi* (see Fig. 3). At 24 ppt, the difference between the two species was also significant ($P < 0.01$), but reversed: fertilization was 71.1% ± 12.9% in *C. pallasi*, but 20.3% ± 13% in *C. h. membras*. Within the mid-range, 16 ppt, there was also a difference in fertilization ($P < 0.05$): 100% for *C. pallasi* and 78.6% ± 12.5% for *C. h. membras*. The salinity response curves for *C. pallasi* and *C. h. membras* were very similar, except that the *C. pallasi* curve was shifted 4–8 ppt hypersaline to the one for *C. h. membras*. Thus, although each species exhibited an optimal range of nearly 20 ppt, the position of that range differed between *C. h. membras* and *C. pallasi*.

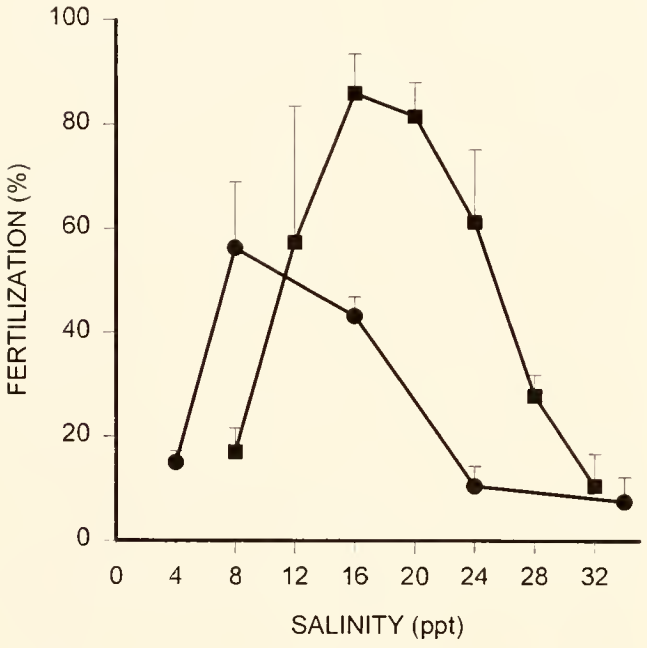

Figure 2. Fertilization in *Clupea pallasi* from San Francisco Bay (■) and *C. h. membras* from Airisto Sound, Finland (●) in seawater of different salinities; $n = 3$. Vertical lines = std. dev.

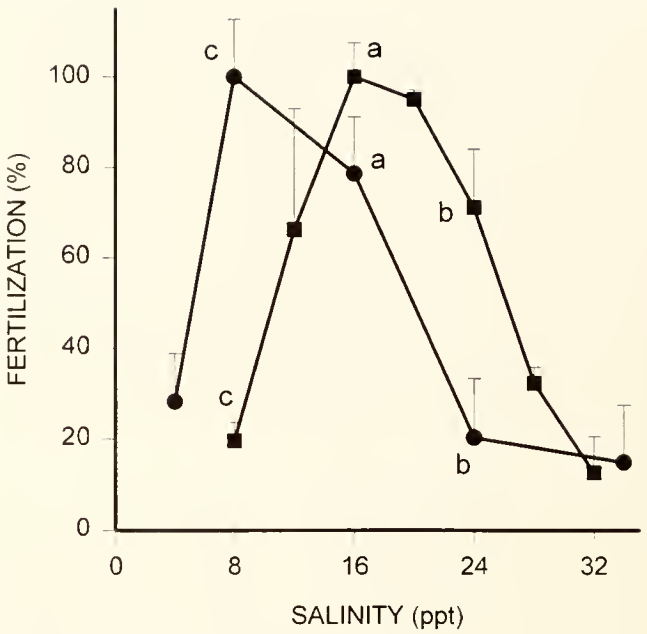

Figure 3. Normalized fertilization percentages for *Clupea pallasi* (■) and *C. h. membras* (●) at different salinities. Percentages are normalized from data in Figure 2; $n = 3$. Vertical lines = std. dev. a-a, $P < 0.05$; b-b, $P < 0.01$; c-c, $P < 0.001$ (Student's t test).

The decrease in *C. pallasi* fertilization at increased salinity was a function of the external concentrations of both Na^+ and K^+ (Fig. 4). In 211 m*M* Na^+ (concentration of ½ ASW), fertilization was similar in the presence of 5 m*M* K^+ (concentration in ½ ASW) and in 10 m*M* K^+ (concentration in full-strength seawater): 67% ± 8.7% fertilization was obtained in ½ ASW when the $[K^+]$ was 5 m*M*, and 74.7% ± 1.5% of the eggs fertilized when the $[K^+]$ was 10 m*M*. Likewise, raising the external $[Na^+]$ to 400 m*M* while keeping $[K^+]$ at 5 m*M* did not significantly change fertilization levels. Fertilization was significantly affected ($P < 0.005$) at $[Na^+]$s of 300, 350, and 400 m*M* when the $[K^+]$ was raised to 10 m*M* (Fig. 4).

Sperm behavior around the micropyles of eggs (*C. pallasi*) in both high- and low-salinity seawaters suggested that the numbers of motile sperm were reduced compared to those at optimal salinity (16 ppt). To more accurately

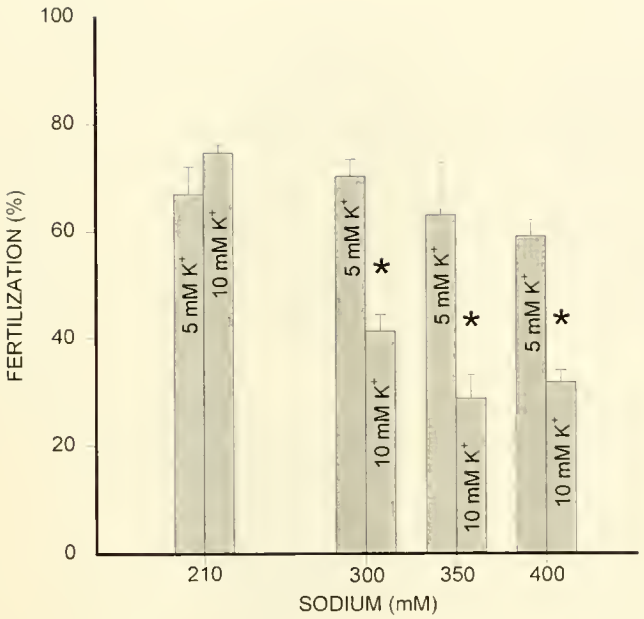

Figure 4. Effects on fertilization of increasing [Na^+] in half-strength filtered seawater containing 5 m*M* K^+ and 10 m*M* K^+; $n = 3$. Vertical lines = std. dev. Fertilization is significantly lower (*) in the 10 m*M* K^+ treatment than in the 5 m*M* K^+ treatment at the same salinity ($P < 0.01$, Student's t test).

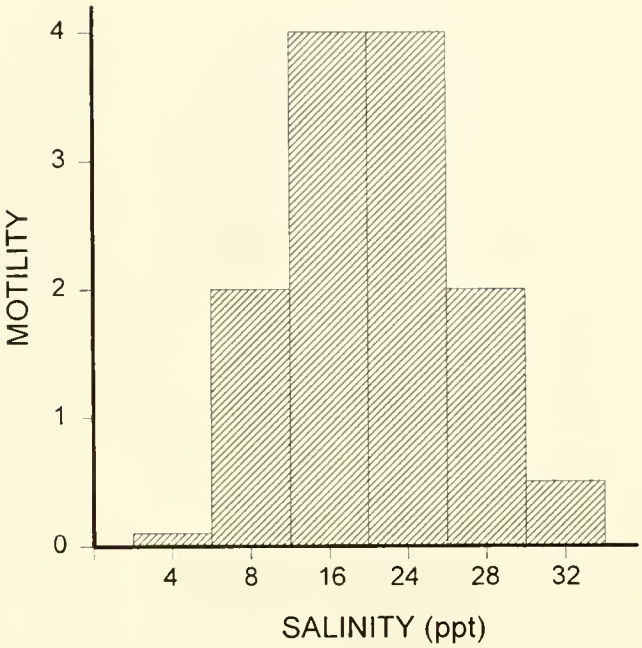

Figure 5. Sperm motility as a function of salinity. Sperm motility was induced *in vitro* with sperm motility initiation factor at the salinities listed above; $n = 3$. Motility was scored as 4 > 75% motile, 3 = 50%–75% motile, 2 = 25%–50% motile, and 1 < 25% motile.

evaluate the effects of salinity on herring sperm, motility was assayed *in vitro*, using *C. pallasi* sperm and SMIF that was isolated from *C. pallasi* eggs. When sperm were exposed to SMIF at differing salinities, motility was a function of external salinity (Fig. 5) and mirrored the range observed for fertilization at different salinities (compare Figs. 2 and 5). Motility was greatest at 16 and 24 ppt and lowest at extreme salinities of 4 and 32 ppt, although at neither extreme was motility completely inhibited.

First described by McMynn and Hoar (1953), the events and stages of embryonic development in *C. pallasi* closely follow those recently described in detail for the zebrafish by Kimmel *et al.* (1995), and so their terminology has been adopted in the current study. Five stages were scored during experiments on salinity tolerance of embryonic development. (1) First cleavage occurred at about 3 h post-insemination in ½ FSW at 12°C. (2) The onset of gastrulation occurred at about 16–17 h and corresponded with the embryo reaching 50% epiboly; gastrulation was completed by 20–21 h. (3) The 5-somite stage of segmentation was seen at 42–48 h and was marked by the appearance of optic vesicles. (4) Retinal pigmentation (entrance into the pharyngula period) was initiated by day 5 and progressed through day 6 of development. (5) Hatching of the larva occurred at 8–10 days post-fertilization in ½ ASW.

Embryonic development, like fertilization, was affected by external salinity. When measured as a function of the effect on an embryo's ability to complete development through hatching, the optimal salinities were between 8

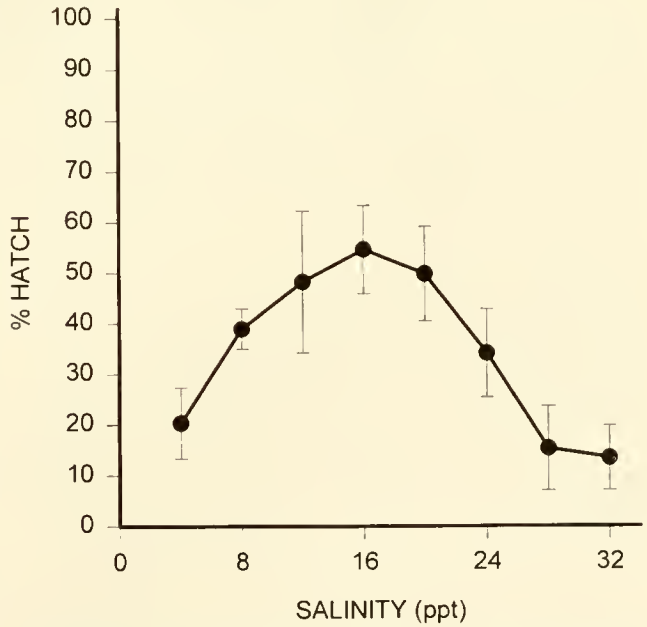

Figure 6. Effects of salinity on hatching of *Clupea pallasi* larvae as of day 9 post-fertilization; $n = 3$. Vertical lines = std. dev.

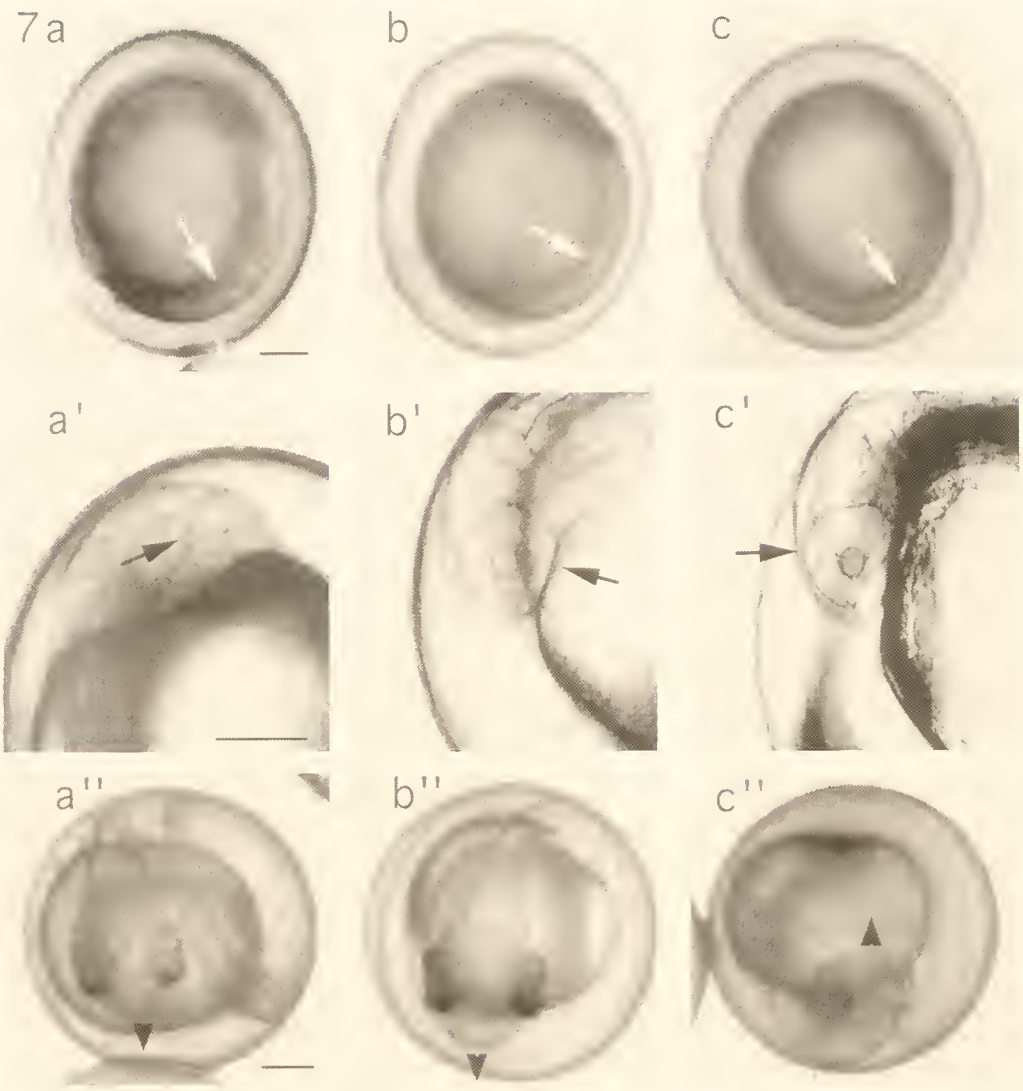

Figure 7. Comparison of development in 3.5 ppt (a-a″), 14 ppt (b-b″), and 28 ppt (c-c″) seawater. Bars = 200 μm. (a-c) Embryos at 21 h post-fertilization nearing the completion of epiboly (arrows = edge of epibolic front; arrowheads [panel b] show future head and tail regions of embryo). (a′-c′) Sixty-six hour embryos at lens stage of eye development (arrows). (a″-c″) Five-day (126-h) embryos with pigmented retinas (arrowheads indicate direction the embryonic head faces).

and 24 ppt (Fig. 6). Salinities both below and above the 8–24 ppt range hindered development; 20.3% ± 7.0% of the cultured embryos hatched in 4-ppt FSW, which was significantly less ($P < 0.01$) than the 38.9% ± 4.0% that hatched in 8-ppt FSW. Likewise, only 15.3% ± 8.3% and 13.4% ± 6.4% of embryos hatched in 28- and 32-ppt FSW, respectively, significantly lower ($P < 0.01$) than the percentage that hatched in 24-ppt FSW (34.1% ± 8.7%).

To further examine the effects of low and high salinity, the course of development of embryos was followed in three FSW salinities: 28 ppt (full-strength seawater; see Materials and Methods), 14 ppt, and 3.5 ppt. Salinity had no observable significant effect on first cleavage (not shown), epiboly, optic vesicle formation, or initiation of retinal pigmentation. The percentage of fertilized embryos that completed development through epiboly in all salinities was 74%–84%, with no significant difference between salinities (Fig. 7a–c). Near the end of day 3 (66 h), lens development was evident (Fig. 7a′-c′); by day 5, retinal pigmentation was evident in embryos at all three salinities (Fig. 7a″-c″). A salinity-associated delay in hatching and in the ability to hatch was observed (Fig. 8). At 9 days post-fertilization, 42.5% ± 4.6% of embryos in the 14-ppt cultures had hatched, whereas 17% ± 6.9% and 18.2% ± 3.4% had hatched in the 3.5- and 28-ppt

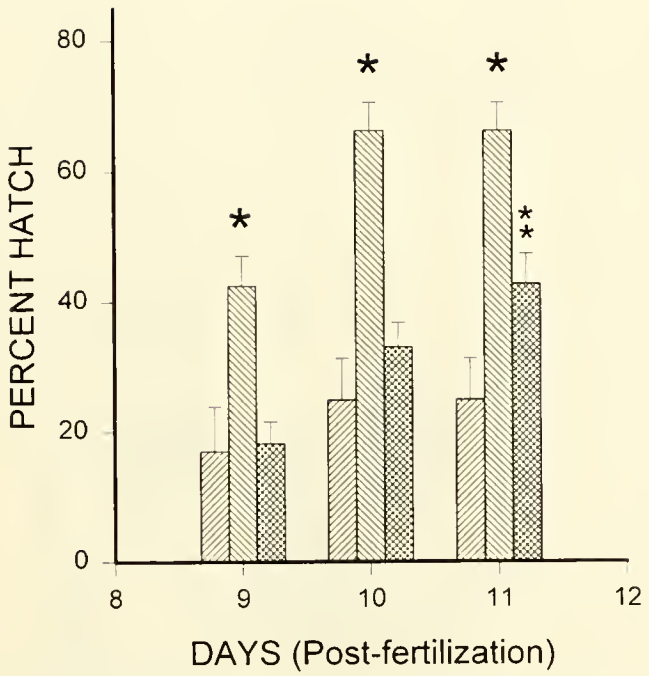

Figure 8. Effects of salinity on time to hatching and on percent hatching of *Clupea pallasi* embryos in 3.5 ppt (▨), 14 ppt (▤), and 28 ppt (□) seawater. The total percentage of hatched larvae was significantly greater (*) in 14 ppt seawater at all three days ($P < 0.001$, Student's t test). On day 11, % total hatch in the 28 ppt group was significantly higher (*) than in the 3.5 ppt group ($P < 0.005$, Student's t test).

FSWs. At day 10 the percentages increased to 24.9% ± 6.4% (3.5 ppt), 66.3% ± 4.3% (14 ppt), and 33% ± 3.8% (28 ppt). No further hatching was observed in either the 3.5- or 14-ppt cultures; however, hatching continued at 28 ppt, and by the 11th day, 42.8% ± 4.7% of the embryos had hatched. No further hatching was observed in any of the cultures. These data suggest that salinity does influence time to hatching, and thus the effect of salinity on development is not as absolute as a simple salinity tolerance curve would predict (see Fig. 6).

In addition to the delay in hatching time, both abnormal hatching and hatched abnormal embryos were observed. Figure 9 depicts larval cultures captured by video at day 10. Larvae in 14-ppt FSW swam vigorously, with few possessing abnormalities (Fig. 9a). In the other two salinities a number of abnormalities occurred, including immotile hatched larvae (see Fig. 9b), scoliotic hatched larvae (see Fig. 9c), and larvae that initiated but failed to complete hatching (see Fig. 9c). The larvae that initiated hatching but died prior to its completion were seen only in 3.5-ppt FSW cultures; by the 10th day, 30.3% ± 7.4% of the embryos had initiated, but failed to complete, the process. Again, these embryos did not survive. Scoliotic larvae varied in the degree of deformity, but none swam normally and none survived. Percentages of scoliotic larvae in both 3.5- and 28-ppt cultures averaged about 10%, whereas only 1%–2% were scoliotic at 14 ppt.

Discussion

Freshwater input has been implicated as an important component of some locations where *C. pallasi* is known to spawn (Taylor, 1971; Barnhart, 1988), and low-salinity water can stimulate spawning in the field (Rabin and Barnhart, 1986) as well as in the laboratory (Outram, 1951). There is also the suggestion in the literature that a spawning site, and therefore the salinity at which spawning occurs, may be a function of the reproductive stock (population) from which the fish derive; although some populations spawn at sites of lowered salinity, others consistently spawn where the salinity approaches that of normal, or full-strength, seawater (Dushkina, 1973; Kijima *et al.*, 1992; Kobayashi, 1993). Such isolation has been suggested to occur not only between populations that reproduce in widely separated geographical regions (Kobayashi, 1993), but also within geographical zones. Oceanic and estuarine populations of *C. pallasi* have been identified in the waters around Japan (Kijima *et al.*, 1992; Kobayashi, 1993), and populations that spawn at different salinity sites have been delineated within the White Sea, Barents Sea, Sea of Okhotsk, and Sea of Japan (Dushkina, 1973). The reproductive "stock" (population) concept is well accepted, even within regions where salinities are not known to vary widely from site to site; within British Columbia waters of the northeastern Pacific Ocean there are up to 23 reproductive stocks that are each faithful to defined spawning subregions (Hay *et al.*, 1984; Hay, 1985). What is undocumented for *C. pallasi* is whether salinity differences between sites, where they exist, lie within a broad permissive range for this euryhaline species or reflect the salinity tolerance limitations on fertilization and embryonic development in specific populations.

The results in the present study indicate that the salinity tolerances for fertilization and embryonic development in the San Francisco Bay population of Pacific herring are limited in comparison with those reported overall for the species. Furthermore, the present results both agree and disagree with previous findings. The range (between 12 and 24 ppt) at which both fertilization and development were optimal was similar to that reported for British Columbia herring (12–26 ppt with 12–17 ppt optimum) by Alderdice and Velsen (1971) and Alderdice and Hourston (1985), but more stringent than that reported by McMynn and Hoar (1953) for development of British Columbia Pacific herring (6–34 ppt) or by Dushkina (1973) for Pacific herring in the White Sea (10–36 ppt).

These differences might reflect actual abilities of populations to tolerate different salinities. Similar population

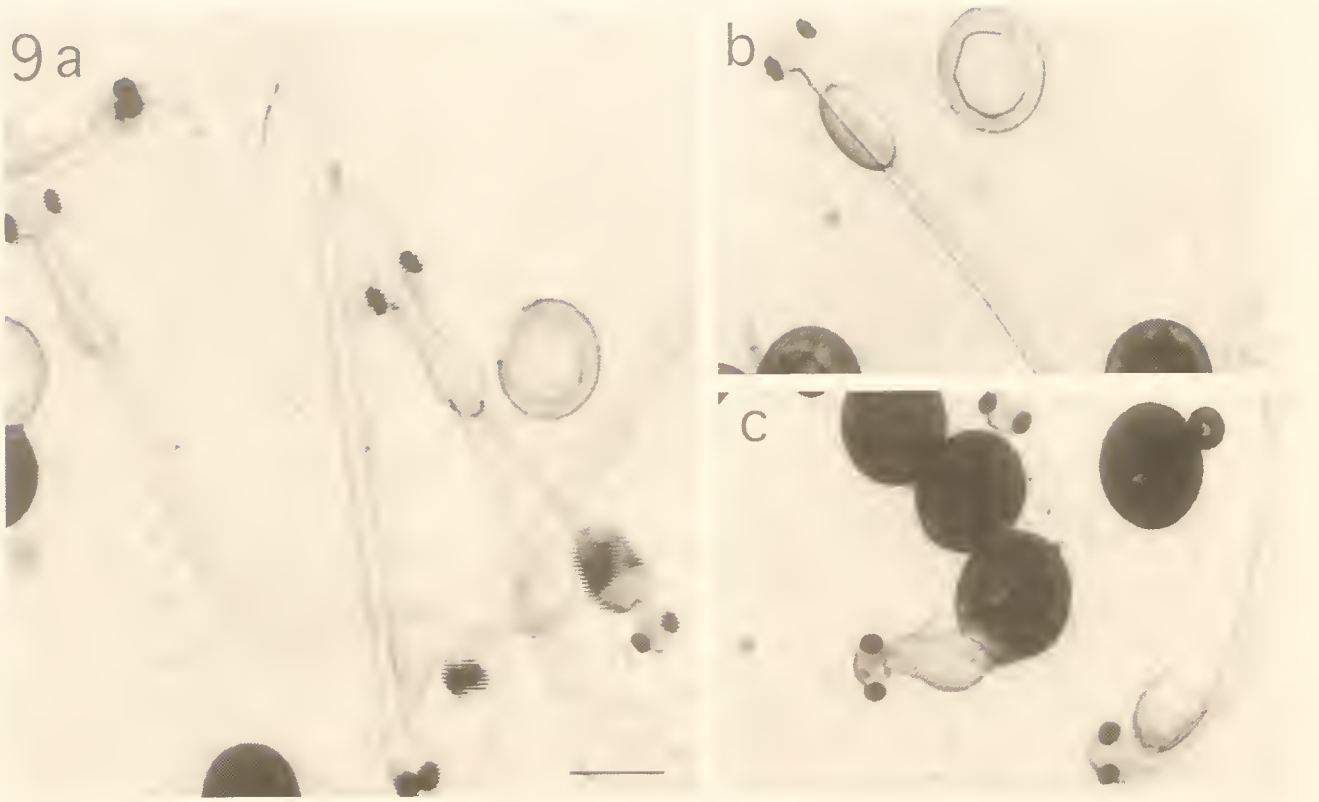

Figure 9. Representative images, obtained by video frame capture, from cultures of *Clupea pallasi* embryos maintained at three salinities. In the 14 ppt (a) and 28 ppt (b) cultures, larvae, empty (transparent) chorions of hatched larvae, and chorions (darkened, opaque) from which embryos have not hatched are evident. In the 3.5 ppt culture (c), a hatched scoliotic larva with a bent tail, a partially hatched larva, and chorions of unhatched embryos are present. Bar = 1 mm.

or subspecies differences are reported to exist within *C. harengus*, which overall possesses a broader fertilization and developmental salinity tolerance range than *C. pallasi* (see Blaxter and Holliday, 1963; Ojaveer, 1981; Haegele and Schweigert, 1985). The comparison of salinity tolerance curves for fertilization in San Francisco Bay *C. pallasi* and *C. h. membras* from Airisto Sound supports this possibility. Alternatively, the differences may reflect physiological, nongenetic responses to the different salinity regimes to which the fish are exposed. Pacific herring that reproduce in the San Francisco Bay estuary constitute the southernmost eastern Pacific population of *C. pallasi*, isolated by a large geographical distance from other Pacific populations (Haegele and Schweigert, 1985). The fish migrate from oceanic waters of the eastern Pacific into the San Francisco Bay estuary where salinities fluctuate both seasonally and annually (2–32 ppt), dependent on both natural precipitation and freshwater diversions imposed by humans (Peterson *et al.*, 1989). In contrast, the *C. h. membras* population that reproduces in Airisto Sound resides in lowered salinity waters (4–10 ppt) of the Baltic Sea throughout the year (Haapala and Alenius, 1994). The fact that the salinity tolerance range for fertilization in *C. h. membras* has not narrowed suggests that the position of the range is more responsive to the salinity history of the population than is the breadth of the range.

The discrepancies between the results in the present study and those previously reported for *C. pallasi* (Dushkina, 1973) may also be in part due to experimental techniques. Fertilization assays conducted in the present study used sperm-egg ratios that yielded between 50% and 90% fertilization, rates that lie on the exponential, most sensitive, portion of a fertilization curve (Cherr *et al.*, 1990). The importance of utilizing such ratios is indicated by one of our experimental trials in which eggs were fertilized at sperm concentrations of 10^6 sperm/ml and 10^5 sperm/ml (Fig. 10). Although fertilization at the optimal salinity (16 ppt) differed by only 4%, the salinity tolerance curves for the two sperm concentrations were vastly different. At a sperm concentration of 10^5 sperm/ml, extremes at both ends of the salinity spectrum reduced fertilization to below 20%, whereas at a sperm concentration of 10^6

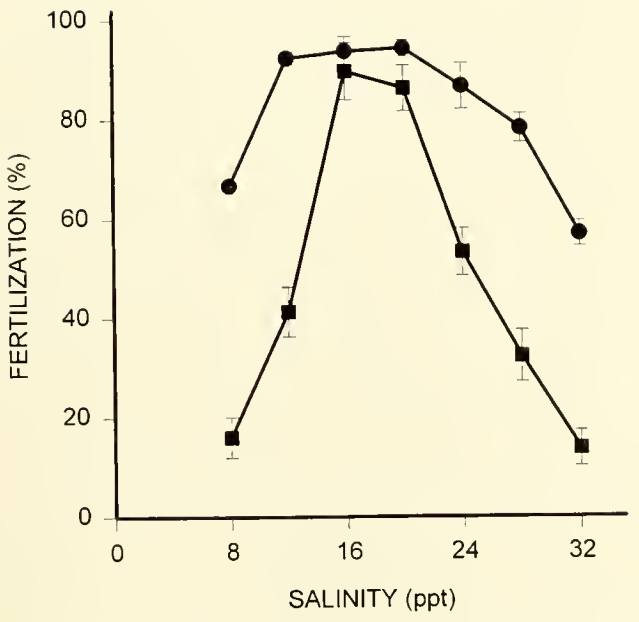

Figure 10. The effects of salinity on fertilization of *Clupea pallasi* eggs inseminated with 1×10^5 sperm/ml (■) and 1×10^6 sperm/ml (●); $n = 3$. Vertical lines = std. dev.

sperm/ml, fertilization remained above 50% even at 8 and 32 ppt salinity. This becomes very important in natural spawnings if the numbers of sperm reported at a British Columbia site (range of 100–150 sperm/ml) represent normal sperm concentrations in the wild (Hourston and Rosenthal, 1976).

Previous studies have shown that *C. pallasi* sperm maintain the ability to fertilize longer in lowered salinity water (*e.g.*, 10–15 ppt) than in full-strength seawater (Yanagimachi and Kanoh, 1953; Morisawa *et al.*, 1992). In the present study, fertilization reductions for *C. pallasi* at both high and low salinities correlated with the inhibition of sperm motility observed during *in vitro* assays with isolated SMIF (sperm motility initiation factor; Pillai *et al.*, 1993). Although the mechanism or mechanisms by which motility was inhibited were not investigated, three possibilities seem plausible: (1) The ability of SMIF to elicit motility could be affected; since the presence of SMIF in the micropyle area is essential for sperm motility (Yanagimachi *et al.*, 1992), its removal or inactivation would prevent fertilization. (2) External changes in Na^+, K^+, or both could perturb ionic movements across the sperm plasma membrane that are necessary for motility; support for this possibility comes from the current finding that fertilization is inhibited at elevated ($\geq$300 m*M*) Na^+ in the presence of high (10 m*M*) K^+ and from a previous report that sperm become spontaneously motile (in the absence of SMIF) when placed in choline-substituted ASW that lacks Na^+ ions (Yanagimachi *et al.*, 1992). (3) There could be a general osmotic inhibition of motility at altered salinities; osmolality has been shown to affect sperm motility in a variety of freshwater and marine fish, but not in Pacific herring (Morisawa *et al.*, 1992). Osmolality alone was not sufficient to initiate sperm motility; only very low levels of motility were obtained when sperm were placed into hyperosmotic solutions of mannitol or even hyperosmotic solutions of NaCl and KCl (Morisawa *et al.*, 1992). Osmolality (under all three conditions) did influence the activity of sperm activating substance (now termed HSAP; Oda *et al.*, 1995) that was isolated from herring eggs (Morisawa *et al.*, 1992).

The effects of salinity on embryonic development in *C. pallasi* are not as absolute as those on fertilization. McMynn and Hoar (1953) reported that *C. pallasi* embryos possess a salinity tolerance range of 6–34 ppt, with an optimum at 11.5 ppt; however, the percent hatch achieved ranged from 0.2 to 11.8% in all salinities. Despite the inability of the study to decipher salinity effects on development, the authors reported two particularly sensitive stages of development—the completion of epiboly [called blastopore closure by McMynn and Hoar (1953)] and near the time of larval hatching (McMynn and Hoar, 1953). In the present study, there was no significant salinity effect through gastrulation (completion of epiboly). Effects of salinity were evidenced by (a) a delayed time to hatch and (b) a reduced number of larvae that successfully hatched. It is likely that these failures to complete development at both 3.5 and 28 ppt are manifestations of earlier developmental problems that we did not detect. It is also possible that energy reserves used to maintain ionic balances within the developing embryos at the extreme salinities depleted those needed for developmental progression, thus prolonging and ultimately halting development. Delay in the developmental program could lead to malformed embryos (*e.g.*, scoliotic larvae) or simply to larvae without the necessary energy reserves to survive hatching. Knowing whether the effects on development are the cumulative result of long-term or constant exposure to altered salinity or are a function of the developmental stage at which exposure occurs will be important in understanding the mechanisms by which salinity affects development.

Although we do not believe that salinity is the only factor governing successful reproduction of Pacific herring, it does appear to be an important component of both fertilization and embryonic development. Furthermore, comparisons of fertilization in the San Francisco Bay population with that of a Baltic population of *C. h. membras* and with published reports of other Pacific herring populations suggest that salinity tolerance ranges may differ between populations. The effects of salinity pressure on development may be more subtle than those on fertilization, yet may have more impact on recruitment in the

environment. Altered salinity not only reduces the number of normal, competent larvae that hatch, it also delays the hatching of those embryos. The costs of such delays, separations from larval schools, depleted energy reserves, and extended time in the chorion (where embryos are subject to both predation and exposure) influence chance for survival. A full understanding of the importance of salinity to herring reproduction will require knowledge of key physiological requirements for successful reproduction and recruitment and correlation of those requirements with environmental conditions in the bays and estuaries where defined populations of herring spawn.

Acknowledgments

The authors thank Dr. D. Hay for stimulating discussions about the relationships that inevitably must be discovered between biological investigations in the laboratory and in the field. We also thank Ken Oda, Diana Watters, and Tom Moore of the California Department of Fish and Game for generously providing experimental animals, and Ms. Lina Kwong for her assistance in the laboratory. We are grateful to Chuck Armor of the California Department of Fish and Game and Tim Vedlinski of the U.S. Environmental Protection Agency for their input on aspects of the experimental design. This research was funded by the California Department of Fish and Game (Interagency Agreement Number FG3345BD). Additional support was provided by the California Sea Grant College Program (National Oceanic and Atmospheric Administration, U.S. Department of Commerce, under grant No. NA36RG0537, project No. R/F161); by the Sonoma State University AAFDP; by the Coastal Toxicology component of the University of California Toxic Substances Research and Teaching Program; and by the TOP Foundation, Turku, Finland.

Literature Cited

Alderdice, D. F., and F. P. J. Velsen. 1971. Some effects of salinity and temperature on early development of Pacific herring (*Clupea pallasi*). *J. Fish. Res. Board Can.* **28:** 1545–1562.

Alderdice, D. F., and A. S. Hourston. 1985. Factors influencing development and survival of Pacific herring (*Clupea harengus pallasi*) eggs and larvae to beginning of exogenous feeding. *Can. J. Fish. Aquat. Sci.* **42:** 56–68.

Barnhart, R. A. 1988. Species profiles: life histories and environmental requirements of coastal fishes and invertebrates (Pacific Southwest)—Pacific herring. *U.S. Fish Wildl. Serv. Biol. Rep.* **82(11.79).** U.S. Army Corps of Engineers, TR EL-82-4. p. 14.

Blaxter, J. H. S., and F. G. T. Holliday. 1963. The behavior and physiology of herring and other clupeids. Pp. 202–394 in *Advances in Marine Biology*, Vol 1, F. S. Russell, ed. Academic Press, New York.

Cavanaugh, G. M., ed. 1975. *Formulae and Methods of the Marine Biological Laboratory Chemical Room.* Marine Biological Laboratory, Woods Hole, MA, pp. 67–69.

Cherr, G. N., J. Sholfner-McGee, and J. M. Shenker. 1990. Methods for assessing fertilization and embryonic development in toxicity tests using the California mussel (*Mytilus californianus*). *Environ. Toxicol. Chem.* **9:** 1137–1145.

Dushkina, L. A. 1973. Influence of salinity on eggs, sperm and larvae of low-vertebral herring reproduction in the coastal waters of the Soviet Union. *Mar. Biol.* **19:** 210–223.

Grant, W. S. 1984. Biochemical population genetics of Atlantic herring, *Clupea harengus*. *Copeia* **1984:** 357–364.

Grant, W. S., and F. Utter. 1984. Biochemical population genetics of Pacific herring (*Clupea pallasi*). *Can. J. Fish. Aquat. Sci.* **41:** 856–865.

Griffin, F. J., C. A. Vines, M. C. Pillai, R. Yanagimachi, and G. N. Cherr. 1996. Sperm motility initiation factor is a minor component of the Pacific herring egg chorion. *Dev. Growth Differ.* **38:** 193–202.

Haapala, J., and P. Alenius. 1994. Temperature and salinity statistics for the northern Baltic Sea 1961–1990. *Finn. Mar. Res.* **262:** 51–121.

Haegele, C. W., and J. F. Schweigert. 1985. Distribution and characteristics of herring spawning grounds and description of spawning behavior. *Can. J. Fish. Aquat. Sci.* **42:** 39–55.

Hay, D. E. 1985. A stock hypothesis based on spawn and winter distribution. Proceedings of the Fifth Pacific Coast Herring Workshop, *Can. Manuscr. Rep. Fish. Aquat. Sci.* **1871:** 145–148.

Hay, D. E., C. D. Levings, and M. J. Hamey. 1984. Distribution of a herring fishery relative to submerged vegetation, herring spawn distribution and oceanographic conditions. *Can. Manuscr. Rep. Fish. Aquat. Sci.* **1760:** 53 pp.

Hourston, A. S., and H. Rosenthal. 1976. Sperm density during active spawning of Pacific herring (*Clupea harengus pallasi*). *J. Fish. Res. Board Can.* **33:** 1788–1790.

Kijima, A., M. Bajajima, and Y. Fujio. 1992. Genetic differentiation among localities in the natural Pacific herring around Japan and genetic characterization of the artificial seeds compared with the natural population. *Tohoku J. Agric. Res.* **42:** 3–4.

Kimmel, C. B., W. W. Ballard, S. R. Kimmel, B. Ullmann, and T. F. Schilling. 1995. Stages of embryonic development of the zebrafish. *Dev. Dyn.* **203:** 253–310.

Kobayashi, T. 1993. Biochemical analysis of genetic variability and divergence of populations in Pacific herring. *Bull. Natl. Res. Inst. Far Seas Fish.* **30:** 1–77.

McMynn, R. G., and W. S. Hoar. 1953. Effects of salinity on the development of the Pacific herring. *Can. J. Zool.* **31:** 417–432.

Morisawa, M., S. Tanimoto, and H. Ohtake. 1992. Characterization and partial purification of sperm activating substance from eggs of the Pacific herring, *Clupea palasii*. *J. Exp. Zool.* **264:** 225–230.

Oda, S., Y. Igarashi, H. Ohtake, K. Sakai, N. Shimizu, and M. Morisawa. 1995. Sperm-activating proteins from unfertilized eggs of the Pacific herring, *Clupea pallasii*. *Dev. Growth Differ.* **37:** 257–261.

Ojaveer, E. 1981. Influence of temperature, salinity, and reproductive mixing of Baltic herring groups on its embryonal development. *Rapp. P.-V. Reun. Cons. Int. Explor. Mer* **178:** 409–415.

Outram, D. M. 1951. Observations on the retention and spawning of the Pacific herring. *Prog. Rep. Biol. Stn., Nanaimo and Prince Rupert* **87:** 32–33.

Peterson, D., D. R. Cayan, J. F. Festa, F. H. Nichols, R. A. Walters, J. V. Slack, S. E. Hager, and L. E. Schemel. 1989. Climate variability in an estuary: effects of riverflow on San Francisco Bay. In: *Aspects of Climate Variability in Pacific and Western Americas. Geophys. Monog.* **55:** 419–442.

Pillai, M. C., T. S. Shields, R. Yanagimachi, and G. N. Cherr. 1993.

Isolation and partial characterization of the sperm motility initiating factor from the eggs of the Pacific herring, *Clupea pallasi*. *J. Exp. Zool.* **265:** 336–342.

Rabin, D. J., and R. A. Barnhart. 1986. Population characteristics of Pacific herring, *Clupea harengus pallasi*, in Humboldt Bay, California. *Calif. Fish Game* **72:** 4–16.

Taylor, F. H. C. 1971. Variation in hatching success in Pacific herring *Clupea pallasi*, eggs with water depth, temperature, salinity, and egg mass thickness. *Rapp. P.-V. Reun. Cons. Int. Explor. Mer* **160:** 34–41.

Vuorinen, I., and E. Ranta. 1987. Dynamics of marine meso-zooplankton at Seili, northern Baltic Sea, in 1967–1975. *Ophelia* **28:** 31–48.

Yanagimachi, R. 1956. The effects of single salt solutions on the fertilizability of the herring egg. *J. Fac. Sci. Hokkaido Univ. Ser. IV Zool.* **12:** 317–324.

Yanagimachi, R. 1957. Some properties of the sperm activating factor in the micropyle area of the herring egg. *Annot. Zool. Jpn.* **30:** 114–119.

Yanagimachi, R., and Y. Kanoh. 1953. Manner of sperm entry in herring egg, with special reference to the role of calcium ions in fertilization. *J. Fac. Sci. Hokkaido Univ. Ser. IV Zool.* **11:** 487–494.

Yanagimachi, R., G. N. Cherr, M. C. Pillai, and J. D. Baldwin. 1992. Evidence suggesting the presence of a sperm-attracting substance around the micropyles of salmonid and herring eggs. *Dev. Growth Differ.* **34:** 447–461.

Reference: *Biol. Bull.* **194:** 36–43. (February, 1998)

Bacterial Symbionts Colonize the Accessory Nidamental Gland of the Squid *Loligo opalescens* via Horizontal Transmission

MELISSA R. KAUFMAN[1,*], YUZURU IKEDA[1,*,†], CHRIS PATTON[1], GILBERT VAN DYKHUIZEN[2], AND DAVID EPEL[1,‡]

[1] *Hopkins Marine Station of Stanford University, Pacific Grove, California 93950; and* [2] *Monterey Bay Aquarium, Monterey, California 93940*

Abstract. The accessory nidamental gland (AN gland), a reproductive organ of the mature female squid *Loligo opalescens*, harbors a dense culture of bacteria of unknown function. A multilayered sheath surrounding the *L. opalescens* egg case is similarly colonized by bacteria that presumably originate in the AN gland, as evidenced by their presence in the egg case at oviposition. This study investigates how these bacteria are transmitted to juvenile squid and examines some morphological consequences of bacterial colonization of AN gland tissues. By observing the structure of the AN gland in adults and the development and bacterial colonization of the gland in juveniles raised in captivity, we determined that the AN gland was absent in newly hatched squid and did not appear until 87 days post-hatching. At 129 days post-hatching, the organ displayed tubules composed of a single layer of epithelial cells and expressing numerous cilia and microvilli. These tubules were not yet fully formed and thus were open to the mantle cavity and external seawater, possibly to aid in the acquisition of microorganisms. Since the AN gland developed a considerable time after hatching, it most likely acquires its symbionts horizontally from environmental seawater and not vertically from the egg case sheath. The switch from expression of cilia to production of microvilli on the epithelial cell surface may dictate the competence of the tissue for bacterial colonization. Electron microscopic examination of juvenile and adult AN glands revealed that an analogous process occurs during the development of the related light organ of other cephalopod species that harbor symbiotic bacteria.

Received 7 July 1997; accepted 13 November 1997.

* Both authors contributed equally to this study.

† Present Address: Department of Fisheries, Faculty of Aquaculture, Kyoto University, Kyoto 606-01, Japan.

‡ To whom correspondence should be addressed. E-mail: depel@leland.stanford.edu

Abbreviations: AN gland = accessory nidamental gland.

Introduction

When spawning, *Loligo opalescens* attaches its eggs to the sandy seafloor, building large masses of capsules that appear to be resistant to fungal, bacterial, and predator attack during their month-long embryonic development (Fields, 1965). Each egg capsule, containing about 200 embryos, is surrounded by a mucopolysaccharide sheath that disintegrates during the gestation period. Within the egg case, the embryos are embedded in gelatinous substances released from three accessory reproductive organs—the oviducal and nidamental glands, and presumably, the accessory nidamental (AN) gland (Arnold, 1984; Boletzky, 1986). This AN gland, in cephalopods such as *L. pealei* (Bloodgood, 1977), *Sepia officinalis* (Van den Branden *et al.*, 1980), and *L. forbesi* (Lum-Kong and Hastings, 1992), harbors a dense culture of symbiotic bacteria, suggesting that it may have a conserved function. Recently, a dense culture of bacteria was also described in layers of the egg capsule sheath in *L. opalescens* (Biggs and Epel, 1991). Because these bacteria were present in the egg capsules at oviposition, a transfer of bacteria from the AN gland of the spawning mother to the egg capsule was proposed. In addition, a protective role in defending the vulnerable embryos against microbial attack was postulated for these egg-capsule-associated bacteria. This

role is analogous to the anti-fungal protection provided by symbiotic bacteria associated with shrimp and lobster eggs (Gil-Turnes *et al.*, 1989; Gil-Turnes and Fenical, 1992).

This study addresses the primary events in the bacterial colonization of the naïve AN gland tissues after hatching of the juvenile squid. Bacteria from the egg sheath might be transmitted directly to the juvenile female at hatching ("vertical transmission"). Alternatively, transmission of bacteria from the water column might occur during or after hatching ("horizontal transmission").

An ultrastructural analysis was conducted to observe AN gland development and bacterial colonization in newly hatched juveniles, older juveniles raised in captivity, and glands from mature females. Our results indicate that the newly hatched squid do not contain a differentiated AN gland, and thus vertical transmission cannot occur. Rather, when the gland appears many weeks post-hatching, it is probably infected horizontally with bacteria from the water column.

Electron microscopic studies indicate that the bacterial colonization occurs in epithelial cell layers that have differentiated structures such as ciliated epithelium to facilitate inoculation. This host tissue competence is similar to that described for the *Euprymna scolopes-Vibrio fischeri* symbiosis in which the light organ of the squid becomes infected with bacteria (Montgomery and McFall-Ngai, 1994).

Materials and Methods

Squid culture

Adult specimens of *L. opalescens* Berry were captured live in Monterey Bay. Fresh egg capsules spawned by the captive squid were collected as previously described (Biggs and Epel, 1991). To obtain freshly hatched juvenile squid, three to five of the freshly laid egg capsules were cultured in a beaker containing 800 ml of UV-sterilized seawater until hatching occurred. The seawater in the beaker was exchanged daily and aerated. Water temperature was 15°–17°C and light conditions were 12L:12D throughout the incubation period.

Juveniles used for the microscopic observations of the later stages were raised in a flowing seawater system at the Monterey Bay Aquarium to the maximum date of 129 days post-hatching by methods previously described (Chen *et al.*, 1996). Larger juveniles (1-cm mantle length) were transferred into 180-gallon flowing seawater tanks. Juveniles older than 60 days were fed Selco-enriched adult brine shrimp (*Artemia*), a local species of mysid (*Acanthomysis sculpta*), and guppies (*Poecilia reticulata*) of appropriate size.

Microscopic observations

For light microscopy of newly hatched juveniles, whole hatchlings were fixed in glutaraldehyde (2% in sterile seawater for overnight at 4°C), treated with osmium tetroxide (1% adjusted to oceanic salinity/pH for 1 h), dehydrated in a graded series of acetone (20%–100% in 10% steps), and embedded in Spurr's plastic (Spurr, 1969). Blocks were sectioned transversely in 1-μm intervals and stained with toluidine blue (1 mg toluidine blue/100 ml distilled water, 1–2 mg sodium borate, pH 9.1–9.3).

Older juveniles were fixed in 10% formalin, post-fixed with glutaraldehyde, and embedded in Spurr's plastic as above. For older juveniles too large for serial sectioning, a small section of visceral tissue that included the region of the AN gland was dissected under a stereoscopic microscope and then fixed with glutaraldehyde. So that fe-

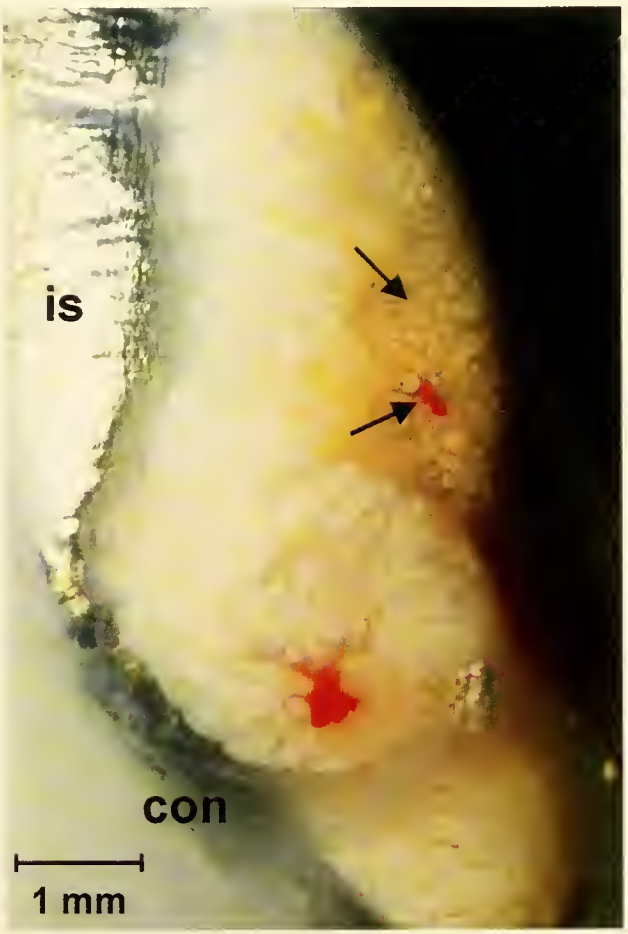

Figure 1. Light micrograph of adult female accessory nidamental gland and associated ink sac. Arrows indicate differential coloring of tubules, which may reflect different levels of colonization by pigmented bacteria. The ink sac (is) and connective tissue (con) located adjacent to the gland are labeled. The second lobe of this bilobed organ can be seen in the lower right portion of the photograph. Magnification bar = 1 mm.

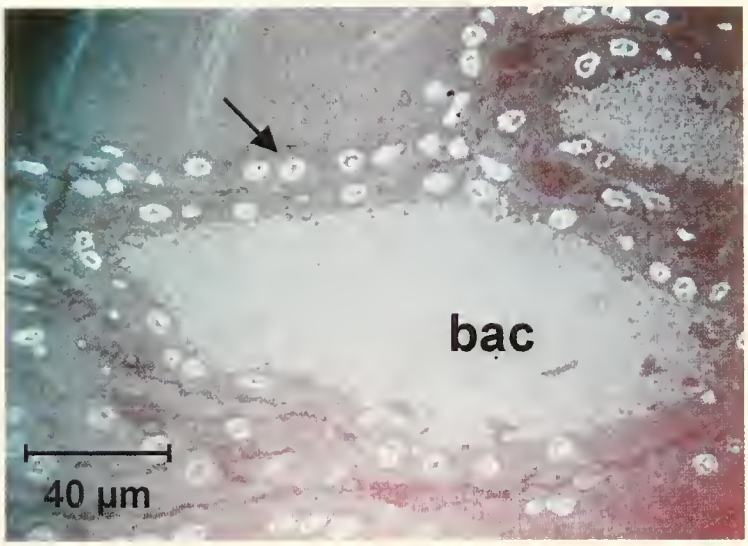

Figure 2. Fluorescent micrograph of 1-μm section of fixed and DAPI-stained tissues of the accessory nidamental gland. Bacteria (bac) densely populate the tubule, which is composed of columnar epithelial cells indicated by the arrow. Magnification bar = 40 μm.

males could be selected, the gonad at the anterior end of the mantle cavity was first examined in thin sections by light microscopy; if it was judged to be an ovary, the sectioning was continued until the region of accessory nidamental gland was observed. The following juveniles were examined (age post-hatching followed by number of specimens in parentheses): 0 days (10); 46 days (1); 75 days (2); 87 days (1); 100 days (2); 129 days (1). Accessory nidamental glands from adult females were dissected and fixed in glutaraldehyde prior to embedding in either Spurr's resin as described above or LR White resin as described previously (Biggs and Epel, 1991).

Transmission electron microscopy

Freshly dissected adult AN gland tissue was cut into 2-mm sections and immediately placed into fixative containing 4 ml 50% gluteraldehyde, 2.38 g HEPES (1 m*M*), and 80 ml sterile seawater (pH 7.2) and incubated on a rotator overnight at 4°C. Fixed glands were rinsed in sterile seawater and post-fixed in osmium tetroxide (1%) for 1 h at room temperature. After two seawater rinses (5 min each), glands were dehydrated in an acetone series (20% to 70%, 10 min each) and held overnight in 70% acetone at 4°C. The acetone dehydration was continued (70% to 100%) using acetone dehydrated with $CuSO_4$. Spurr's resin was measured volumetrically and degassed under a vacuum. Glands were incubated in a 50:50 mix of acetone:Spurr's for 2 h at room temperature, 25:75 mix for 2 h, and 100% Spurr's overnight. Samples were then suspended in fresh Spurr's, placed into BEEM embedding capsules, and polymerized by baking at 70°C overnight. A Porter-Bloom MT2B microtome was used to cut 1-μm sections, which were floated onto Formvar and carbon-coated copper grids (Polysciences). After staining with uranyl acetate and lead citrate, the sections were viewed on a Phillips 201 transmission electron microscope operating at 80 kV.

Results

In the adult female squid, the AN gland is adjacent to the ink sac and digestive organs on the ventral side of the mantle cavity (Fig. 1). The mature gland is composed of thousands of tubules, many of which are heavily colonized by bacteria at the time of spawning (Fig. 2; also see Bloodgood, 1977). Densities of the pigmented bacteria varied within individual tubules, perhaps contributing to the array of colors from orange to dark red displayed on the gland surface (Fig. 1).

To study the mode of infection following hatching, the region near the ink sac and gut tissues was observed in newly hatched juveniles. The gonads were undifferentiated, making it impossible to define the sex of these juveniles, so 10 specimens were analyzed to ensure that some percentage of the sample would be female. In the 1-day post-hatching specimens, no structure indicative of the AN gland could be distinguished (Fig. 3). Only a large ink sac surrounded with muscular tissue and the digestive organ were observed in all the juveniles analyzed.

In the older juveniles (46- to 129-days post-hatching) cultured at the Monterey Bay Aquarium, it was possible

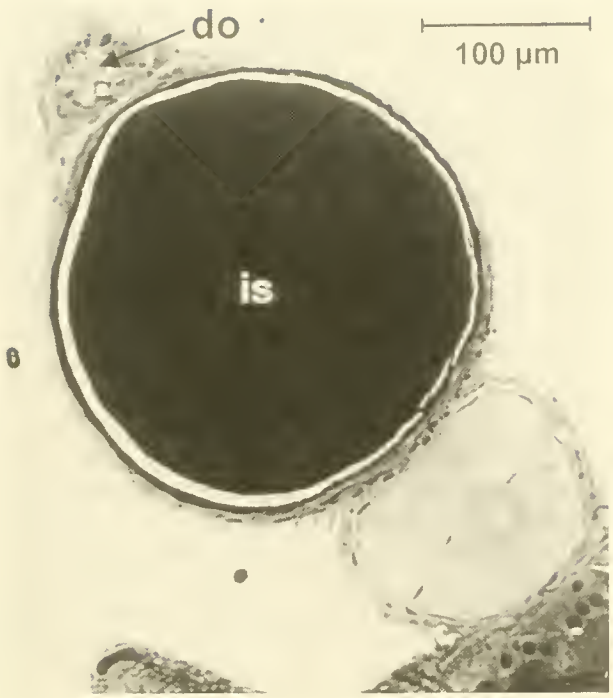

Figure 3. Light micrograph of 1-μm section of 1-day post-hatching *Loligo opalescens* showing the visceral mass, including the ink sac (is) and digestive organ (do). Magnification bar = 100 μm.

to track development of the AN gland. In these specimens, the gonads had differentiated and the sex of the individuals could be determined. In the 46- and 75-day-old female juveniles, the ink sac and digestive organ increased in size, but no AN gland was observed (data not shown). In the 87-day-old juvenile, an early developmental stage of the AN gland was seen flanking the ink sac (Fig. 4). At this stage the gland was a paired structure attached to the outer muscular wall of the ink sac (Fig. 4A) and consisted of a single layer of epithelial cells (Fig. 4B).

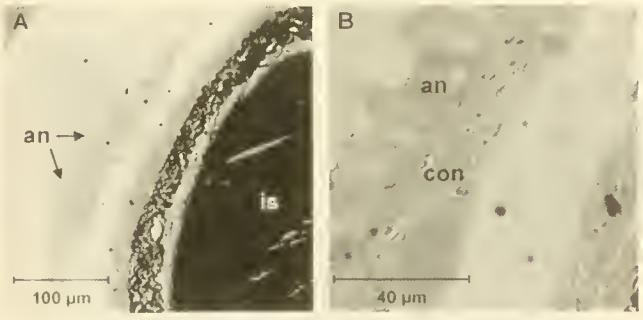

Figure 4. Light micrographs of 1-μm sections of accessory nidamental (AN) gland of 87-day-old juvenile. (A) Gland (an) and associated ink sac (is). Magnification bar = 100 μm. (B) Early tissues of AN gland (an), including the basal connective tissues (con). Magnification bar = 40 μm.

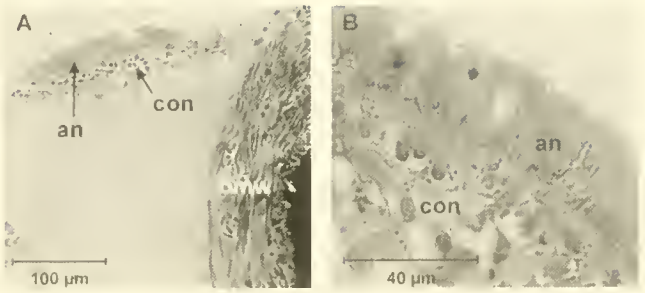

Figure 5. Light micrographs of 1-μm sections of epithelial cells of the accessory nidamental (AN) gland in 100-day-old juvenile. (A) View highlighting gland attachment to the outer muscular wall (omw) of the ink sac. Magnification bar = 100 μm. (B) Cells of AN gland (an) organizing into tubules atop differentiating connective tissues (con). Magnification bar = 40 μm.

No bacteria were evident on the surface of the 87-day AN gland epithelial cells. Between each epithelial cell, typical cell junction complexes were seen and a relatively undifferentiated connective tissue layer was in contact with the basal surface of the cells (Fig. 4B). By 100 days, differentiation of connective tissue pushed the epithelial cell layer towards the mantle cavity. A second layer of epithelial cells was observed, and cilia were occasionally seen on the apical surface (Fig. 5A, B). No bacteria were yet observed in association with the tissue of the AN gland.

In the 129-day-old juvenile, the cell layers of the AN gland were deeply invaginated, forming the primordial tubules (Fig. 6A). In many of these tubules, the end of the structure remained open to the mantle cavity (Fig.

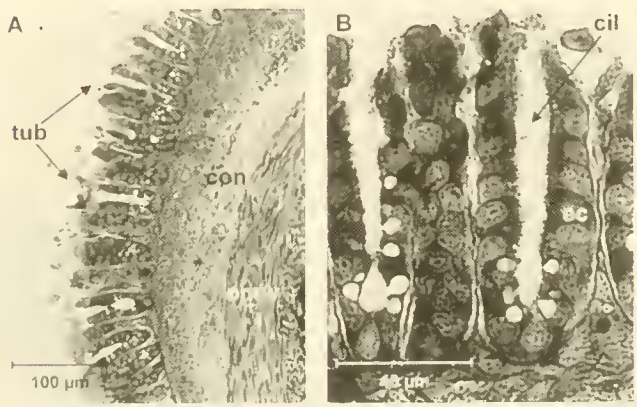

Figure 6. Light micrographs of 1-μm sections of tubules of accessory nidamental (AN) gland in 129-day juvenile. (A) Arrows indicate tubules (tub) open to the mantle cavity. Underlying connective tissue (con) is indicated as well as the outer muscular wall (omw) of the ink sac. Magnification bar = 100 μm. (B) High magnification of tubule structure open to the mantle cavity. Arrow points to cilia (cil) protruding into the tubule. Squid epithelial cells (ec) line the tubule. Magnification bar = 40 μm.

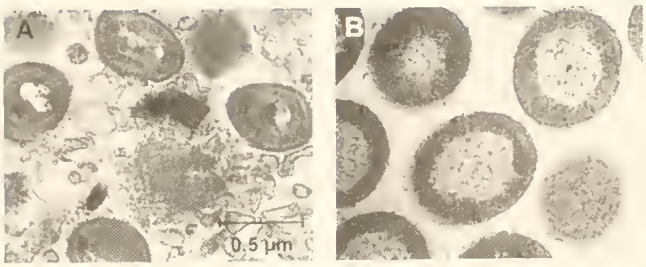

Figure 7. Transmission electron micrographs of bacteria present in accessory nidamental gland at (A) 129 days and (B) in the adult female. Note difference in morphological types and sizes between the juvenile and adult organisms. Magnification bar = 0.5 μm.

6B). Many cilia and some microvilli were observed on the inner surface of both the completely formed and the unformed tubules. The connective tissue layer on the basal surface also continued to undergo significant differentiation. Electron micrographs showed that some of the tubules contained a few bacteria, but these were dissimilar in ultrastructure to the bacteria seen in feral squid from Monterey Bay (in Fig. 7, compare A with B). The bacteria seen in the 129-day specimen have a distinct, gram-positive cell wall; in contrast, organisms found in both the adult gland and purified culture have a gram-negative double membrane. Protozoa were also observed in the lumen of the 129-day AN gland (data not shown). Because the tubule was not completely formed, the presence of the bacteria and protozoa might be adventitious and, therefore, is not evidence for specific infection of the differentiated gland in the 129-day-old squid.

The structures of the epithelial cell components of the AN gland are distinctly different in the 129-day-old squid and the colonized tissue of the adult. The cilia in the juvenile AN gland are more numerous, presumably to facilitate water flow and bacterial colonization (Fig. 8A). In the adult gland laden with microbes, the primary components of the cells are microvilli, with 7- to 10-fold fewer cilia than in the uninfected squid (Fig. 8B).

Micrographs also revealed "secretory vesicles" within the lumen of the mature AN gland (Fig. 9). These globular structures were seen in a layer between the surface microvilli and the bacteria in the center portion of the tubule. The composition and role of these vesicles has not been resolved, but their ubiquity in the adult gland suggests that the AN gland likely contributes both bacteria and structural material to the egg capsule sheath.

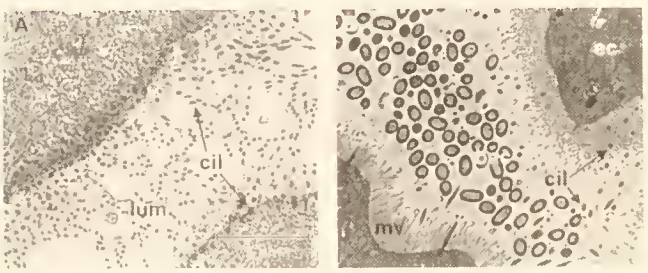

Figure 8. Transmission electron micrographs showing morphology of lumen of accessory nidamental gland at two stages of development. (A) At 129 days, vast numbers of cilia (cil) in the lumen (lum) are surrounded by squid epithelial tissue (ec). (B) In the sexually mature female, microvilli (mv) outnumber the cilia and a dense colony of symbiotic bacteria (bac) resides in the lumen. Magnification bar = 5 μm.

Discussion

In the *L. opalescens* egg case, the most probable mode of transmission of bacteria to the female accessory nidamental gland might intuitively appear to be vertical transmission, in which the juveniles encounter the bacteria upon hatching. However, by showing that the AN gland is not differentiated until about 11 weeks post-hatching, this study provides direct evidence that there is no vertical transmission of microorganisms to early hatchlings. Horizontal transmission to juveniles thus most likely occurs from the water column at a later point in development. This time is significantly after hatching: distinct morpho-

Figure 9. Electron micrograph of "secretory vesicles" at the cell surface of the epithelial cells of the accessory nidamental gland. Arrows designate two examples of this secreted material. Magnification bar = 2 μm.

logical differentiation of epithelial cells is first visible at about 60 days, progressing at 129 days to the formation of tubules similar to those seen in adult squid (see schematic in Fig. 10).

Our analysis of hatchlings and juveniles indicates that a primordial, or rudimentary, AN gland first appears between 75 and 87 days post-hatching. By 129 days post-hatching, tubules resemble the adult morphology and contain numerous cilia (see Fig. 10).

The differentiated AN gland in the 129-day-old female contained small numbers of bacteria, but they bore no ultrastructural relationship to the bacteria seen in adult females brought in from Monterey Bay (Fig. 7). Protozoa were also present in the gland of the 129-day-old female (data not shown), suggesting that the gland was open to the seawater and that a variety of microorganisms could get trapped within the tissue. It is probable that specific infection occurs much later, as the squid approaches sexual maturity. Another possibility is that the appropriate species of bacteria were not present in the artificial conditions of husbandry in the laboratory. It is unknown whether the tubules of the adult gland remain exposed to circulating seawater or close at one or both ends during later gland development. One possibility that remains to be investigated is that the bacteria are acquired at hatching and harbored in an as-yet-unidentified site within the squid hatchling to serve as a reservoir for seeding the developing AN gland.

Bacterial-squid symbiosis has been well studied in the luminous light organ of several cephalopod species (Boletzky, 1970; Herring *et al.*, 1981; McFall-Ngai and Montgomery, 1990; Pringgenies and Jorgensen, 1994). In the case of the sepiolid squid *Euprymna scolopes*, the symbiotic bacteria necessary for luminescence are acquired from the surrounding seawater within hours of hatching (McFall-Ngai and Ruby, 1991).

Although bacterial transmission is horizontal in both the AN gland and the light organ, the time of bacterial colonization differs greatly. This difference is consistent with the different roles for the microorganisms in the

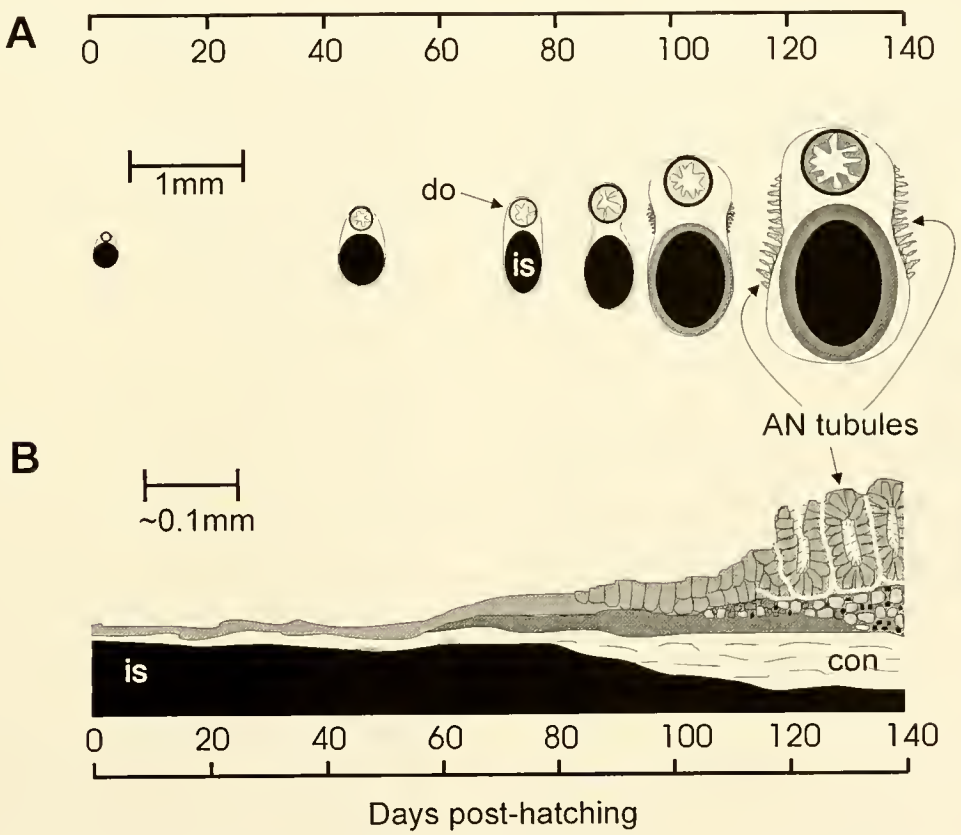

Figure 10. Development of accessory nidamental gland in *Loligo opalescens*. Numbered bars indicate days post hatching. (A) Transverse sections showing the locations of the digestive organ (do) and the ink sac (is) over time are illustrated schematically. (B) Composite drawing, based on light micrographs, showing differentiation and development of gland tissue and associated connective tissue layers. Locations of the ink sac (is) and connective tissue (con) are indicated.

two tissues. The symbiotic bacteria in the light organ of *E. scolopes* provide counterillumination (McFall-Ngai and Montgomery, 1990), which is advantageous just after hatching, when juveniles are especially vulnerable to their predators. In contrast, the role of the AN gland and its associated bacteria is apparently related to sexual maturation and reproduction, which occurs at 1–2 years of age.

Our electron micrographs of tissue from the juvenile and adult AN gland show differences that are remarkably similar to the tissue changes necessary for colonization of *E. scolopes* by *Vibrio fischeri*, in which a cilia-rich epithelium is replaced by a microvilli-rich one (Montgomery and McFall-Ngai, 1993). In the case of the *L. opalescens* AN gland, primary colonization by the squid symbiont probably requires regression of the cilia-rich cells and proliferation of the microvilli-expressing cells. These changes are likely to facilitate bacterial colonization. Preceding infection, the cilia most likely wash copious quantities of seawater through the tubules to "pan" for the specific squid endosymbiont (Ruby, 1996). It is interesting that the squid light organ has been postulated to have its evolutionary origin in the AN gland (Buchner, 1965; Bloodgood, 1977; Montgomery and McFall-Ngai, 1993).

The role of the secretions of the AN gland tissue is still unknown. Proof that the gland contributes gelatinous materials for egg capsule production (Boletzky, 1986) is lacking. Micrographs of adult glands show "secretory vesicles" (Fig. 9) that may be either gland secretions or lipids (Lum-Kong, 1992). It has also been suggested that the AN gland functions in hormonal control of female sexual maturation or mediates reproductive behavior by secreting a pheromone that triggers mating (Richard *et al.*, 1979; Bloodgood, 1977; Lum-Kong and Hastings, 1992).

We suggest that a major role of the AN gland may be cultivating bacteria for deposition to the egg capsules. The precise function of the bacteria is unknown, but the speculation first raised by Biggs and Epel (1991) that microbes provide protective products to the embryos is under investigation and continues to be an attractive hypothesis.

Acknowledgments

This study would not have been possible without the samples of older juveniles of *L. opalescens* provided by F. E. Anderson. We are indebted to S. v. Boletzky for his valuable information about juvenile ultrastructure. We are grateful to M. McFall-Ngai and N. Ruby for their insight and suggestions. The staff and students at Hopkins Marine Station are acknowledged for their fruitful discussion and encouragement. This research is a result of financial support provided by the National Science Foundation Postdoctoral Fellowship in Marine Biotechnology (M.R.K.), the Vital Spark Foundation (D.E. and M.R.K.), and is funded in part by a grant from the National Sea Grant College Program, National Oceanic and Atmospheric Administration, U.S. Department of Commerce, under grant number NA36RG0537, project number R/MP-62 through the California Sea Grant College (D.E. and M.R.K.) The views expressed herein are those of the authors and do not necessarily reflect the views of NOAA or any of its subagencies. The U.S. Government is authorized to reproduce and distribute for governmental purposes.

Literature Cited

Arnold, J. M. 1984. Cephalopods. Pp. 419–454 in *The Mollusca*, Vol. 7 (Reproduction), A. S. Tompa, N. H Verdonk, and J. A. M. van den Biggelaar, eds. Academic Press, New York.

Biggs, J., and D. Epel. 1991. Egg capsule sheath of *Loligo opalescens* Berry: structure and association with bacteria. *J. Exp. Zool.* **259:** 263–267.

Bloodgood, R. 1977. The squid accessory nidamental gland: ultrastructure and association with bacteria. *Tissue Cell* **9:** 197–208.

Boletzky, s. V. 1970. On the presence of light organs in *Semirossia steenstrup. Bull. Mar. Sci.* **20:** 374–388.

Boletzky, s. V. 1986. Encapsulation of cephalopod embryos: a search for functional correlations. *Am. Malacol. Bull.* **4:** 217–227.

Buchner, P. 1965. Symbiosis in luminous animals. Pp. 543–571 in *Endosymbiosis of Animals with Plant Microorganisms*, P. Buchner, ed. Interscience, New York.

Chen, D. S., G. Van Dykhuizen, J. Hodge, and W. F. Gilly. 1996. Ontogeny of copepod predation in juvenile squid (*Loligo opalescens*). *Biol. Bull.* **190:** 69–81.

Fields, G. 1965. The structure, development, food relations, reproduction, and life history of the squid *Loligo opalescens* Berry. *Calif. Fish. Bull.* **131:** 1–108.

Gil-Turnes, M. S., and W. Fenical. 1992. Embryos of *Homarus americanus* are protected by epibiotic bacteria. *Biol. Bull.* **182:** 105–108.

Gil-Turnes, M. S., M. E. Hay, and W. Fenical. 1989. Symbiotic marine bacteria chemically defend crustacean embryos from a pathogenic fungus. *Science* **246:** 116–118.

Herring, P. J., M. Clarke, s. V. Boletzky, and K. P. Ryan. 1981. The light organs of *Sepiola atlantica* and *Spirula spirula* (Mollusca: Cephalopoda): bacterial and intrinsic systems in the order Sepiodea. *J. Mar. Biol. Assoc. U.K.* **61:** 901–916.

Lum-Kong, A. 1992. A histological study of the accessory reproductive organs of female *Loligo forbesi* (Cephalopoda: Loliginidae). *J. Zool., Lond.* **226:** 469–490.

Lum-Kong, A., and T. S. Hastings. 1992. The accessory nidamental gland of *Loligo forbesi* (Cephalopoda: Loligonidae): characterization of symbiotic bacteria and preliminary experiments to investigate factors controlling sexual maturation. *J. Zool., Lond.* **228:** 395–403.

McFall-Ngai, M. J., and M. K. Montgomery. 1990. The anatomy and morphology of the adult bacterial light organ of *Euprymna scolopes* Berry (Cephalopoda: Sepiolidae). *Biol. Bull.* **179:** 332–339.

McFall-Ngai, M. J., and E. G. Ruby. 1991. Symbiont recognition and subsequent morphogenesis as early events in an animal-bacterial mutualism. *Science* **254:** 1491–1494.

Montgomery, M. K., and M. J. McFall-Ngai. 1993. Embryonic development of the light organ of the sepiolid squid *Euprymna scolopes* Berry. *Biol. Bull.* **184:** 296–308.

Montgomery, M. K., and M. McFall-Ngai. 1994. Bacterial symbionts induce host organ morphogenesis during early postembryonic development of the squid *Euprymna scolopes*. *Development* **120:** 1719–1729.

Pringgenies, D., and J. P. Jorgensen. 1994. Morphology of the luminous organ of the squid *Loligo duvauceli* d'Orbigny, 1839. *Acta Zool.* **75:** 305–309.

Richard, A., C. Van den Branden, and W. Decleir. 1979. The cycle of activity in the accessory nidamental gland from cephalopods. Pp. 173–180 in *Cyclic Phenomena in Marine Plants and Animals*, E. Naylor and R. G. Hartnoll, eds. Pergamon, New York.

Ruby, E. G. 1996. Lessons from a cooperative, bacterial-animal association: *The Vibrio fischeri-Euprymna scolopes* light organ symbiosis. *Annu. Rev. Microbiol.* **50:** 591–624.

Spurr, A. 1969. A low-viscosity epoxy resin embedding medium for electron microscopy. *J. Ultrastruct. Res.* **26:** 31–43.

Van den Branden, C., M. Gillis, and A. Richard. 1980. Carotinoid producing bacteria in the accessory nidamental gland of *Sepia officinalis* L.. *Comp. Biochem. Physiol.* **66B:** 331–334.

Reference: *Biol. Bull.* **194:** 44–52. (February, 1998)

Temperature and Embryonic Development in Relation to Spawning and Field Occurrence of Larvae of Three Antarctic Echinoderms

DAMON STANWELL-SMITH* AND LLOYD S. PECK

British Antarctic Survey, High Cross, Madingley Road, Cambridge, CB3 0ET, United Kingdom

Abstract. The effects of temperature on development and viability were measured at 14 levels between −2°C and +3°C on embryos of two asteroids (*Odontaster validus* and *Odontaster meridionalis*) and an echinoid (*Sterechinus neumayeri*) from Signy Island, Antarctica. Development rates were 2 to 10 times slower than those for temperate or tropical echinoderms, with times to hatching up to 240 h. Development rates for the two asteroids differed by 1.15 ×, and rates for both species approximately doubled over the experimental temperature range. In *O. validus*, embryo viability was independent of temperature, but in *O. meridionalis* viability declined with increasing temperature. Development rates for *S. neumayeri* were little affected by temperature above +0.2°C, but declined rapidly at lower temperatures. Conversely, the number of nonviable eggs was low and constant below +1.7°C, but rose rapidly at higher temperatures. A window of optimal temperature, between +0.2°C and +1.7°C, has therefore been proposed for development time and embryo viability in this population of *S. neumayeri*. Spawning trials and field observations of larvae indicated that the time of gamete release and periods of larval development in *S. neumayeri* coincided with austral summer sea temperatures in the same window. Embryos of *O. meridionalis* and *O. validus* are released in winter, when temperatures are constantly below −1.6°C. Comparison of the different strategies suggests that larval food supply and predation during planktonic phases are not the dominant ecological factors for these species.

Received 13 January 1997; accepted 7 November 1997.

* To whom correspondence should be addressed. E-mail: dpss@pcmail.nerc-bas.ac.uk

Introduction

Temperature and food availability are recognized as the two major factors affecting the development of marine invertebrate larvae (Thorson, 1950). The thermodynamic effect of temperature on physiological rates is a fundamental structuring element in biological processes and is perhaps the more straightforward of the two factors to understand. The powerful effect of temperature on larval development has long been recognized (Orton, 1920; reviewed by Pechenik, 1987). Nutrient availability, from reserves in brooded and lecithotrophic larvae and via feeding by planktotrophic larvae, is also clearly essential to sustain development to maturity. These factors should be of great importance in polar environments where temperatures are low and summer phytoplankton blooms short. However, the relative importance of temperature and resource availability to Antarctic larvae is not yet generally agreed upon (Clarke, 1992; Hoegh-Guldberg and Pearse, 1995).

The aim of this study was to investigate how the interaction of these two factors influences geographical distributions and reproductive strategies. Echinoderms were chosen because many of their Antarctic representatives have planktonic larvae (Bosch and Pearse, 1990). The three species used were the common cushion stars *Odontaster validus* Koehler and *Odontaster meridionalis* (Smith), and the regular urchin *Sterechinus neumayeri* (Meisner). All are ubiquitous and abundant in Antarctic waters, and their distributions overlap at Signy Island; all have been the subjects of previous research (McClintock *et al.*, 1988; Bosch and Pearse, 1990; Brey *et al.*, 1995). Both species of *Odontaster* have circum-antarctic distributions (McClintock *et al.*, 1988). *O. meridionalis* has a northerly limit at South Georgia (54°S, 36°W) and Ker-

guelen Island (49°S, 63°W), and occurs at depths between 15 and 590 m; whereas *O. validus* has been reported from Shag Rocks (53°S, 42°W) and Bouvetøya (54°S, 03°E), from 0 to 914 m (Clark, 1963). The obligate sponge-feeding *O. meridionalis* usually occurs at much lower densities than the predatory or scavenging *O. validus* (Dayton *et al.*, 1974). *S. neumayeri* is a nonspecific grazer (Pearse and Giese, 1966) and has a circum-antarctic distribution as far north as Kerguelen Island, from 0 to 400 m in depth (Brey and Gutt, 1991).

The larvae of both *Odontaster* and *Sterechinus* are pelagic and planktotrophic. Asteroid gastrulae develop into bipinnaria, whereas the echinoid gastrulae become plutei, both about 1 mm long (Bosch, 1989; Bosch *et al.*, 1987). *Odontaster* bipinnaria occur during the Antarctic winter, defined here as the mean period for which fast ice is present (Murphy *et al.*, 1995), usually under the sea-ice and at a time when very little phytoplankton is in the water column (Clarke and Leakey, 1996). The possibility of starvation in *O. validus* larvae has been investigated by Olson *et al.* (1987). Bacterivory has been proposed as a supplementary food source for asteroid larvae (Rivkin *et al.*, 1986), although its importance to Antarctic larvae has been questioned (Pearse *et al.*, 1991). However, the plutei of *S. neumayeri* develop and feed during the austral summer, a period of high phytoplankton standing crop and many associated zooplanktonic larval predators (Morgan, 1995). The larval phase of almost all marine invertebrates is the most vulnerable stage in their life history (Thorson, 1950). The ecological question is therefore, Why does such different seasonal timing occur in functionally similar echinoderm larvae from the same environment?

Materials and Methods

Spawning induction

Ten adults of each of the three species (*Odontaster validus*, *Odontaster meridionalis*, and *Sterechinus neumayeri*) were collected at monthly intervals by scuba divers in Borge Bay, Signy Island, Antarctica (60° 43′S, 45° 37′W). Collection depths and periods were as follows: *O. meridionalis*, 8–10 m from January 1994 to February 1995; *O. validus*, 36 m from February 1993 to February 1995; *S. neumayeri*, 16–18 m from February 1993 to February 1995. The animals were immediately transferred to a flow-through aquarium at the British Antarctic Survey research station for about 24 h, then put into 500-ml beakers of filtered (1.2 μm; Whatman GF/C) seawater standing in a shallow tank of running seawater. The gonadal regions of the starfish were injected with 1–2 ml of 1-methyl adenine (1MA, 10^{-4} *M* in seawater) (Chia and Walker, 1991), which induced spawning within a few hours if the animals were gravid (Bosch, 1989). To induce spawning in *S. neumayeri*, about 2 ml of 0.5 *M* KCl in seawater was injected into the coelom (Bosch *et al.*, 1987); gravid individuals spawned within a few hours of the injection.

Culture methods

An aluminium thermogradient block with apertures for 70 universal tubes (30-ml volume), in five rows of 14 tubes, was kept in a controlled temperature (CT) room set at +2°C. Thermocirculators at each end of the block were set at −2°C and +3°C respectively to represent the annual range of sea temperature around the Antarctic Peninsula and Sub-antarctic Islands (Foster, 1984). A 13-step temperature gradient was maintained with very low fluctuation. Construction notes and methods, with illustrations, are given by Baker (1974). The overall temperature range and variation at each step were monitored for 48 h before each experiment, and data were stored on a Grant Instruments "Squirrel" data logger. A precision electronic thermometer was used to measure the temperature of each culture prior to sampling. The culture water was exchanged every 48 h with precooled and aerated filtered (1.2 μm; Whatman GF/C) seawater. The five apertures at each temperature step were used as follows: two replicate larval cultures were maintained, and replacement water at the same temperature as the cultures was kept in adjacent apertures; the spare (fifth) tube was used for monitoring with the thermometer probe. The CT room was kept dark during the experimental period to minimize the possible conflicting effect of an artificial diurnal light pattern.

The development experiment was conducted on eggs and sperm collected at the peak of spawning for each species. These peak periods were different for each species, so the dates for the experiments varied accordingly: *O. meridionalis* embryos were incubated for 235 h starting on 22 July 1993; *O. validus*, 244 h starting on 15 June 1994; and *S. neumayeri*, 155 h starting on 17 October 1994. Eggs were collected in 1000-ml beakers and held in monolayers on the bottom of each beaker. Sperm were diluted with filtered seawater until translucent grey. To fertilize the eggs a few drops of the sperm were stirred into each beaker (following Strathmann, 1987). After a rapid wash in filtered seawater, the newly fertilized eggs were immediately transferred to the precooled universal (30-ml) vials in the thermogradient block. To prevent overcrowding, no more than a monolayer of embryos was put in the bottom of each vial (MacBride, 1900); this equated to about 250 embryos per incubation tube.

The remaining embryos were kept as controls in two 3000-ml beakers on a flow-through seawater table in the aquarium. A monolayer of eggs developed at ambient sea temperature and were stirred at the same time as the experimental cultures in the thermogradient block were

checked. Fertilization was confirmed after about 30 min by the presence of a fertilization membrane, as observed with a compound microscope at 400× magnification. The cultures at each temperature were observed alternately, to minimize disturbance (Bosch *et al.*, 1987).

Culture observation

Development in the cultures was monitored by pipetting about 100 embryos into a precooled cavity slide and photographing them at 12× magnification with a Wild M5 microscope, set up in the CT room. The cultures were observed every 4 h for the first 12 h, then every 12 h until the approach of hatching. When hatching was imminent, 4-h intervals were reinstated. The control cultures were observed at the same intervals and by the same method as the experimental cultures. Photographs were taken on Ektachrome ISO 200 transparency film, which was subsequently projected for calculating the various stages of development. The use of photography enabled development to be assessed rapidly, with minimal disturbance to the embryos. The times for 50% of the embryos to reach eight cells, blastulae, and hatching were recorded, together with the number of eggs and embryos failing to develop.

Data for each species were analyzed with Arrhenius plots (log of development rate as a function of the reciprocal of absolute temperature). Linear regressions were used where suitable, and compared using Minitab ver. 10 for regression analysis (Sokal and Rohlf, 1981). A broken stick model (one break) was fitted to *S. neumayeri* development times on the Arrhenius plot by the maximum likelihood method, using Genstat ver. 5.3 (Payne *et al.*, 1993).

Field observation of larvae

A two-year survey of the planktonic invertebrate larvae around Signy Island was carried out at the same time as the experiments described (Stanwell-Smith *et al.*, in press). Diver-towed nets and a handheld, diver-operated suction pump were used for regular sampling (method details in Stanwell-Smith *et al.*, 1997). Samples were collected at five sites at intervals of 2 to 4 weeks, both at 20 cm above the sea bed and 20 cm below the sea surface. A total of 317 net tows were made by divers. All relevant data were pooled to produce overall values of larval abundance in the water column.

Results

Development and embryo viability

The embryos were transparent, enabling easy identification of different development stages of each species. At the lowest incubation temperature (−2.02°C) the development times of *O. meridionalis* embryos were the longest, taking about 50 h for 50% of the embryos to reach the 8-cell stage, and 240 h for 50% to hatch (Fig. 1). A steady reduction in development time with increasing temperature was also observed. For all three species, times to hatching approximately halved over the experimental temperature range (−2.02°C to +2.83°C). In *O. meridionalis* the number of eggs remaining unfertilized had a strong positive correlation with temperature ($y = 2.59x + 11.15$, $r^2 = 0.95$. Fig. 2). Thus, the number of nonviable eggs increased with temperature from about 6% at −2.02°C to about 18% at +2.83°C; this was the reverse of the trend for development time. Development times for *O. validus* were similar to those of *O. meridionalis*, and the time to 50% hatching also shortened with increasing temperature (Fig. 1). However, in contrast to *O. meridionalis*, *O. validus* showed no relationship between temperature and its percentage of nonviable eggs ($y = -0.31x + 12.87$, $r^2 = 0.03$; Fig. 2), which averaged about 13%. The eggs that failed to fertilize constituted more than 95% of the embryos that did not hatch during the experimental period; the other 5% was composed of occasional embryos that divided only once or twice before ceasing development.

The time for *S. neumayeri* embryos to reach the 8-cell stage was between 15 and 40 h, and was similar to that for the starfish. Times declined by about half over the experimental temperature range, in a fashion similar to that seen in Figure 1 for hatching. The methods used here were unable to detect temperature-related differences in

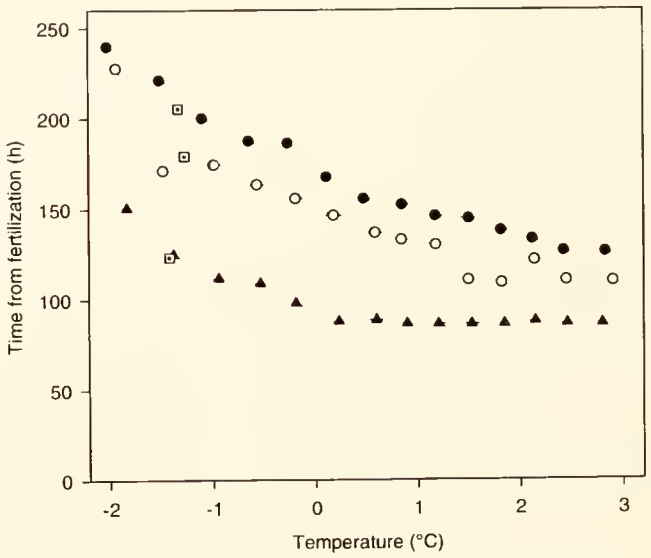

Figure 1. The time taken for 50% of *Odontaster meridionalis* (●), *O. validus* (○) and *Sterechinus neumayeri* (▲) embryos to hatch, as indicated by the loss of the fertilization envelope (Chia and Walker, 1991). Data were taken from photographs of larvae in cultures. The control cultures times are also indicated (⊡).

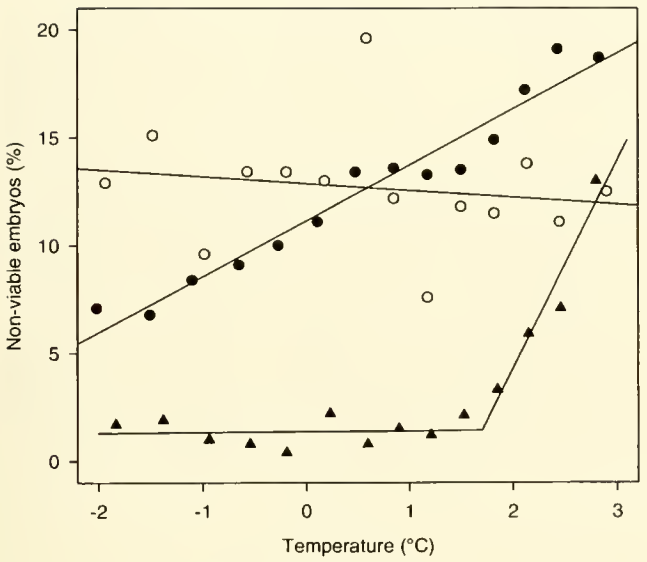

Figure 2. The number of nonviable eggs and embryos in each culture at each temperature step. *Odontaster meridionalis* (●) was fitted by linear regression ($y = 2.59x + 11.15$, $r^2 = 0.95$), as was *O. validus* (○) ($y = -0.31x + 12.87$, $r^2 = 0.03$). *Sterechinus neumayeri* (▲) data were fitted with a broken stick model by the maximum likelihood method (94% of variance accounted for).

development rates to the blastula stage for *S. neumayeri*, and results indicated that embryos took just over 40 h to reach this stage. Clearly, very small differences in development rate could have gone undetected. Data for 50% hatching times presented a different picture. Development time declined rapidly between −1.8°C (153 h) and +0.2°C (88 h). Above 0.2°C, times to hatching were independent of temperature. The percentage of nonviable eggs in *S. neumayeri* was very low and constant (about 1%) below +1.7°C (Fig. 2). Above 1.7°C, the proportion of nonviable eggs rose rapidly to about 13% at +2.83°C. A broken stick model (one break) fitted by the maximum likelihood method showed a break point at +1.7°C, and the fit accounted for 94% of the variance in the data.

Arrhenius plot

An Arrhenius plot is a simple description of the relationship between reaction rate and absolute temperature. Although originally developed for estimating activation free energies in enzyme kinetics, Arrhenius plots are often applied to the temperature behavior of complex biological systems (Clarke, 1983). When development rates based on the 50% hatch times (log transformed) for the three species were plotted against the reciprocal of absolute temperature (Fig. 3), data for both of the *Odontaster* species yielded straight-line relationships, and their slopes were not significantly different from one another ($F = 1.3$, df = 1, 24, $P = 0.27$). A common slope was calculated and fitted to the two data sets by analysis of covariance. The resulting intercepts were significantly different (difference = −0.0135, $t = -6.78$, $P < 0.0001$), indicating that *O. validus* embryos were, on average, developing at a rate 1.15 times faster than *O. meridionalis*.

A broken stick model was fitted to the data for the development rate of *S. neumayeri* (Fig. 3); the fit accounted for 98% of the variance. Maximum likelihood showed that the break point occurred at +0.2°C. Below this temperature, development rate increased rapidly with temperature ($y = 0.242x - 4.53$, $r^2 = 0.97$), but above it development rate did not alter significantly with temperature ($y = 0.006x - 4.47$, $r^2 = 0.23$).

Q_{10} *values*

The Q_{10} coefficient is a measure of the change in rate of a process with temperature (Cossins and Bowler, 1987). It is expressed as the factorial rate change over a 10°C temperature step and was originally devised for biochemical systems. It is useful here for comparing development rates between species and emphasising differences between rates. In physiological systems, Q_{10} values are usually between 2 and 3 (Clarke, 1983), and a Q_{10} of 1 indicates no change with temperature. Although the temperature range here is

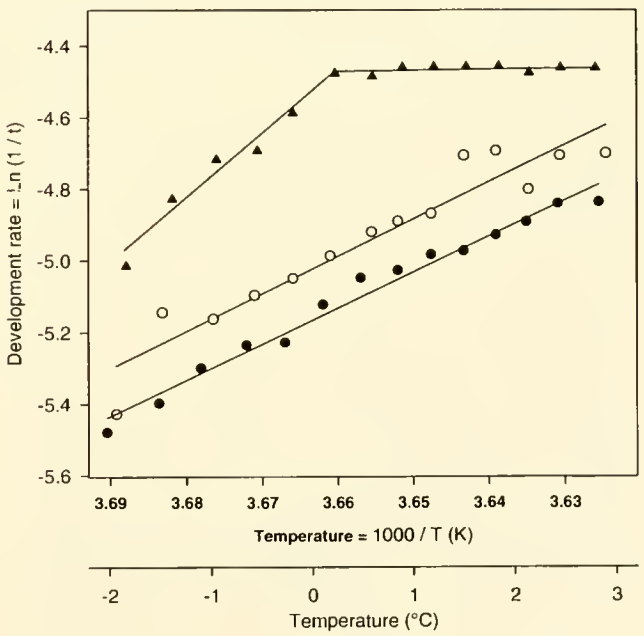

Figure 3. Arrhenius plot of the development rates of *Odontaster meriodonalis* (●), *O. validus* (○) and *Sterechinus neumayeri* (▲). Broken stick model fitted by the maximum likelihood method (98% of variance accounted for). Straight lines fitted by linear regression: *O. validus* ($y = 0.14x - 5.02$, $r^2 = 0.91$), *O. meriodonalis* ($y = 0.13x - 5.16$, $r^2 = 0.98$). Actual temperatures are also shown on second axis for clarity. Development rate was calculated as the reciprocal time to 50% hatching.

narrow (about −2.9°C to +2.0°C), the Q_{10} for development times to 50% hatching were calculated. Q_{10} = 3.8 for *O. meridionalis*, 4.5 for *O. validus*, and 13.6 below +0.2°C and 1.1 above +0.2°C for *S. neumayeri*.

Spawning and field observations

The results from the regular spawning trials were compared with environmental data from Clarke *et al.* (1988) and Clarke and Leakey (1996), particularly for sea temperature and microplankton chlorophyll *a* biomass for the period January 1993 to February 1995 at Signy Island (Fig. 4). Spawning was successfully induced in both the starfish species during the winter months (May—July). A few *S. neumayeri* individuals could be induced from June onward. Of these, only males spawned in June, July, and August; females could be induced from September onward. In both sexes, peak spawning induction occurred in November. Field observations of gastrulae have been combined with those for bipinnaria (for asteroids) or plutei (for echinoids) in the kite diagrams (Fig. 4), giving values for overall pelagic larval abundances in the water column. *Odontaster* larvae occurred between June and September of both years at densities up to 0.76 m^{-3}. *S. neumayeri* larvae were present between December and February in much lower numbers than the starfish (up to 0.09 m^{-3}), and were observed only during the 1993–1994 austral summer. It is clear that the timing of spawning

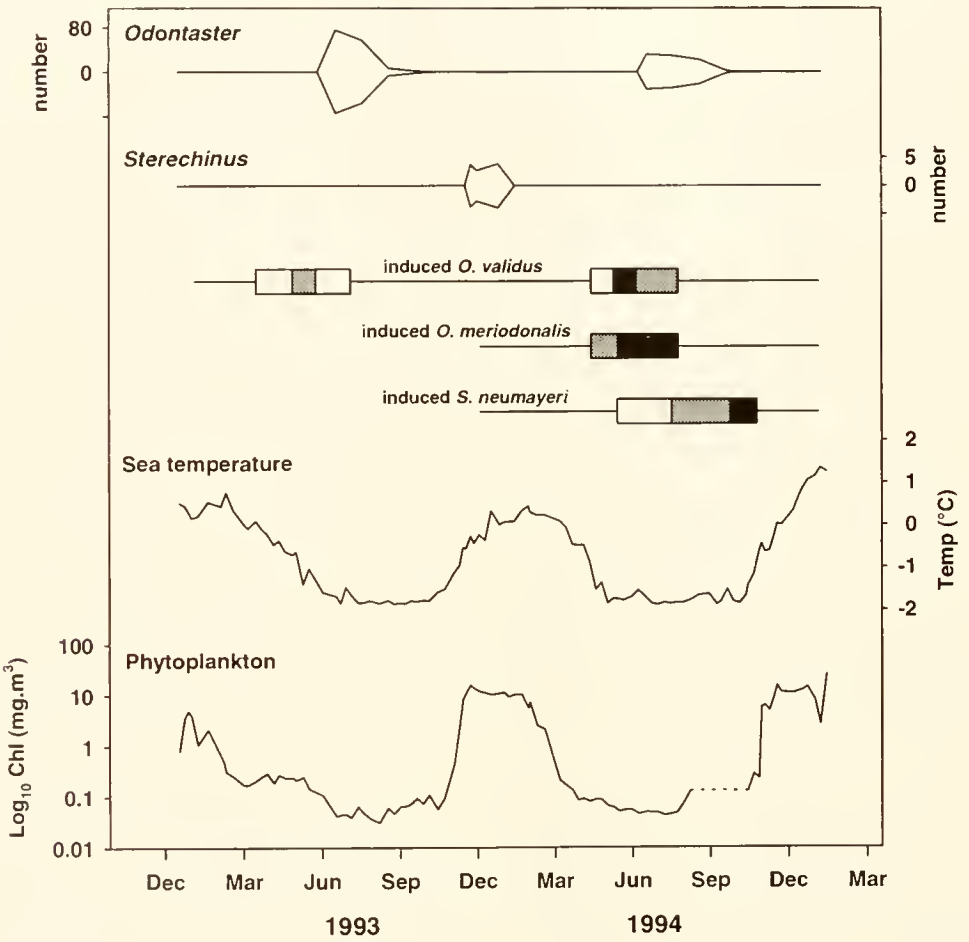

Figure 4. Field data collected between January 1993 and February 1995. The kite diagrams show the number of larvae caught (per 5000 l seawater filtered). The shaded bars show when spawning could be induced in the three echinoderm species: □ = 0%–25% animals spawned, ▨ = 25%–75% spawned, ■ = 75%–100% spawned. Note that the entire length of the lines indicate experimental duration (*Odontaster validus* was sampled for two years; *O. meriodonalis* and *Sterechinus neumayeri* were only sampled during the second year of the study). The chlorophyll *a* plot shows the microphytoplankton chlorophyll standing crop (>20 μm filter, mg·m^{-3}), with a dotted line indicating missing data. Temperature and chlorophyll data adapted from Clarke and Leakey (1996).

induction closely matches the observed seasonal pattern of larval occurrence in the wild.

Discussion

A reduction in development time with temperature (= increasing development rate) was observed in all three species (Fig. 1). This was expected, as development rates in Antarctic ectotherms are much lower than in temperate and tropical species (Clarke, 1992) and our data for *S. neumayeri* below 0.2°C agree with the general relationship found for echinoids (Fig. 5) from all latitudes by Bosch *et al.* (1987). Above 0.2°C the development rates depart from the general relationship. Development in *S. neumayeri* was 2 to 10 times slower than rates for temperate and tropical species at their normal habitat temperatures.

The changes in development rates with temperature of the two *Odontaster* species were not significantly different from one another, but *O. meridionalis* was 1.15 times slower at all measured temperatures (Fig. 3). Its slightly lower Q_{10} value may also indicate less influence of temperature on development rate. If temperature were the sole criterion, it would be advantageous for both species to release larvae in the warmer seas of the austral summer, when development would proceed at a rate about 1.5 times faster than in winter. However, other factors must be considered. The number of nonviable embryos released by the two species varied. For *O. meridionalis*, the number of fertilized eggs that did not develop further rose significantly as the temperature increased, from 7% at −2°C to 19% at +2.5°C (Fig. 2). For *O. validus*, however, the number of nonviable embryos did not increase with temperature, averaging about 12.5% throughout. This suggests that, for *O. meridionalis* at least, larvae gain some survival advantage by developing in the colder waters of winter.

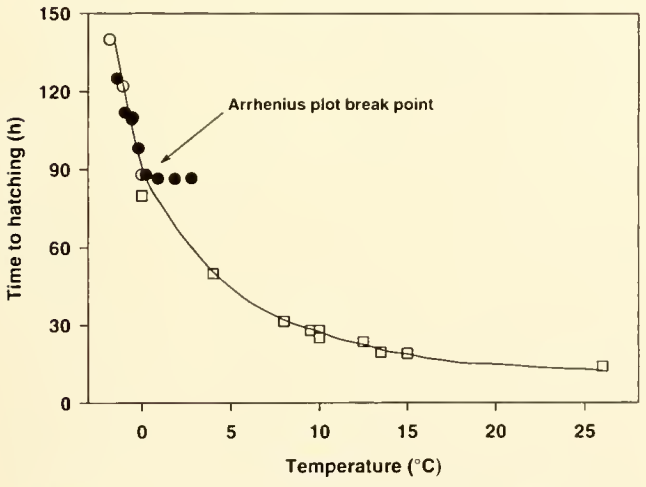

Figure 5. Duration of embryonic development to hatching as a function of temperature of several species of echinoids at different latitudes (adapted from Bosch *et al.*, 1987). Results from tropical and temperate species (□), *Sterechinus neumayeri* from McMurdo Sound (○), and *S. neumayeri* from the present study (●). The line was fitted by eye.

Looking at the field data (Fig. 4), it is clear that both *Odontaster* species spawn in the wild during the austral winter months and can be induced to spawn from May to August. As measured by Bosch (1989), the interval for *O. meriodonalis* and *O. validus* to develop from fertilized egg to feeding bipinnaria was about 35 days, which agrees with the timing of larval presence in the water column in the present study (June to September). These starfish probably obtain a reduction in mortality by avoiding pelagic predators associated with the summer phytoplankton bloom (Clarke, 1988). *O. meridionalis* also has reduced mortality at winter temperatures, as a result of the relationship between embryo viability and temperature (Fig. 2). The disadvantages of a winter spawning strategy include a slower (by a factor of 1.5) development rate and a diminished food supply. Slowed development rates may carry with them the extra energetic requirement of an increased overall maintenance metabolic cost when summed from fertilization to settlement (Clarke, 1992). It is possible that higher overall metabolic costs and reduced food availability are a disadvantage for winter larvae. However, Rivkin *et al.* (1986) produced evidence that asteroid larvae could feed on bacteria, and Peck (1993) found that larvae of the Antarctic nemertean *Parborlasia corrugatus* were capable of feeding on particles less that 1 μm in diameter. Bosch *et al.* (1991) showed that algae, bacteria, dissolved organic matter, and endogenous reserves could all make significant contributions to the nutrition of larvae of the Antarctic starfish *Porania antarctica*. In contrast, Pearse *et al.* (1991) found that bacterial ingestion by *O. validus* larvae was of little importance, and that temperate echinoderm larvae did not ingest bacteria at all. More recently still, Hoegh-Guldberg and Manahan (1995) and Prothero-Thomas (pers. comm) have found that metabolic rates are so low in Antarctic echinoderm larvae that they may not need to feed at all during development. Irrespective of these considerations, the wide distribution and abundance of *O. validus* and *O. meridionalis* demonstrate the success of their winter spawning strategy.

S. neumayeri has a different strategy. Below +0.2°C, its development rate was strongly influenced by temperature. The calculated Q_{10} of 13.6 is very high—beyond the range typically accepted as normal for biological systems (Clarke, 1983), suggesting that this response is not that usually presented by an enzyme-mediated reaction system. Other factors such as changes in membrane perme-

ability (Hochachka, 1991) may be important at temperatures at the lower end of a species tolerance range and, in the case of the Signy population of *S. neumayeri*, below +0.2°C. This would also suggest that below the break point for development rate data in the Arrhenius plot (Fig. 3), *S. neumayeri* is developing at the lower end of its range of temperature tolerance (Hoegh-Guldberg and Pearse, 1995). Above +0.2°C the development rate was independent of temperature up to the maximum temperature in the investigation (+2.8°C). The inference based on this observation is that development rate has reached its upper limit at 0.2°C, and further temperature rises are incapable of increasing the rate.

From temperature alone it would seem that *S. neumayeri* could maximize its rate of larval development by spawning when the sea was at or above +0.2°C, as in the austral spring/summer period at Signy Island. Once again the system is more complex than this. Embryo mortality in *S. neumayeri* is independent of temperature below +1.7°C, but increases rapidly above this: the next 1°C rise in temperature produces a 6-fold increase. The results (Figs. 2, 3) suggest there is a sea-temperature window between +0.2°C and +1.7°C in which development rate and embryo viability are optimized. The field data (Fig. 4) concur, showing that *S. neumayeri* produces embryos and larvae within the proposed temperature window. It is competent to spawn and can be induced to do so from May to October, when sea temperatures range between −1.8°C and −1.6°C. However, the period of maximum spawning competence was later than this, in November, when sea temperatures were approaching 0°C. (Such optimal temperature windows for development were also observed by Orton, 1920.)

Wild larvae were only found in the water column from about December to January, at temperatures around +0.5°C (Stanwell-Smith *et al.*, in press). Bosch *et al.* (1987) measured the development time from fertilization to plutei stage as about 20 days, suggesting the successful larvae seen in the water column had developed from gametes released in November, and that earlier spawnings in field populations are absent or rare. The rising sea temperatures observed in November may therefore be a cue for spawning in the Signy Island *S. neumayeri* population. The phytoplankton levels are also increasing at this time and have been closely correlated with spawning times in the patellid limpet *Nacella concinna* (Stanwell-Smith and Clarke, 1997), thus suggesting another possible cue (Starr *et al.*, 1990).

S. neumayeri larvae were also observed in plankton samples from McMurdo Sound during the end of November and the beginning of December (Bosch *et al.*, 1987), which was within the same interval that *S. neumayeri* larvae were observed in the present study (Fig. 4). The temperature at McMurdo remains constant at about −1.9°C (Littlepage, 1965), so this conflicts with the suggestion of optimizing a temperature "window." Spawning synchrony maximizes fertilization success in free-spawning animals (Levitan, 1995) and thus high-latitude populations would benefit from environmental spawning cues of some sort. Deep-sea echinoids exhibit aggregation prior to gamete release (Young *et al.*, 1992) as well as spawning synchrony. The thermal stability at McMurdo, as in the deep sea, suggests an alternative cue to temperature—perhaps phytoplankton?

Temperature and development were investigated in *O. validus* and *O. meridionalis* from populations at McMurdo Sound, Antarctica, by Hoegh-Guldberg and Pearse (1995). Their data show a different relationship than found for these same species at Signy Island, but are similar to the data for *S. neumayeri* (Fig. 3). Arrhenius plots of development rate were fitted with a broken stick model. The break point in the Hoegh-Guldberg and Pearse (1995) data occurred at 0°C, and the effect of temperature on development rate above that point was small. If the lower part of the broken plot were translated to the right in the Signy Island population, the break point for those embryos would be above +2.8°C. The plot for the Signy Island starfish would not, therefore, include a temperature range high enough to show a dramatic change in development rate. A translation of this type might be expected (Precht *et al.*, 1973) when going from a population adapted to the McMurdo marine environment, where temperatures are permanently about −1.9°C (Littlepage, 1965), to Signy Island, where the annual temperature ranges from a winter low at −1.8°C to a summer maximum between +0.5°C and +1.0°C (Clarke and Leakey, 1996). Applying the same logic to the McMurdo *S. neumayeri* data suggests that embryonic development rates in McMurdo populations of this urchin should have a break point at a lower temperature than that found in the present study (+0.2°C).

There are both advantages and disadvantages associated with the winter spawning strategy of the two starfish, *O. validus* and *O. meriodonalis*, and the summer spawning strategy of the urchin, *S. neumayeri*. However, neither the advantages nor the disadvantages are overwhelming. The data therefore suggest that the important selection criteria for these echinoderms are not associated with predation from bloom-associated predators or with the abundance of food. Other factors that could be important are egg quality, which should be related to previous adult nutrition, and predation by benthic suspension feeders during the settlement phase.

The relationships found here between development rate and temperature and between embryonic mortality and temperature may be important factors affecting distributions of Antarctic echinoderms. Variations in these characters between populations adapted to different tempera-

ture regimes clearly indicate their role in delineating the ability of a species to colonize a given habitat. The study also shows evidence for local population adaptation in embryonic development.

Acknowledgments

Sincere thanks to the Signy team that provided invaluable support for these experiments; Andrew Clarke for much advice and discussion; Alistair Murray for the Genstat calculations; and Nadine Johnston, Paul Tyler, and Simon Brockington for comments that improved the manuscript. John Pearse and an anonymous reviewer made valuable comments on the manuscript. This study is part of the Nearshore Marine Biology Program of the British Antarctic Survey.

Literature Cited

Baker, J. H. 1974. The use of a temperature-gradient incubator to investigate the temperature characteristics of some bacteria from Antarctic peat. *Br. Antarct. Surv. Bull.* **39:** 49–59.

Bosch, I. 1989. Reproduction and development of shallow-water asteroids and an echinoid in McMurdo Sound, Antarctica. Ph.D. Thesis. Univ. California, Santa Cruz.

Bosch, I., and J. S. Pearse. 1990. Developmental types of shallow-water asteroids of McMurdo Sound, Antarctica. *Mar. Biol.* **104:** 41–46.

Bosch, I., K. A. Beauchamp, M. E. Steele, and J. S. Pearse. 1987. Development, metamorphosis and seasonal abundance of embryos and larvae of the Antarctic sea urchin *Sterechinus neumayeri*. *Biol. Bull.* **173:** 126–135.

Bosch, I., S. J. Colwell, J. S. Pearse, and V. B. Pearse. 1991. Nutritional flexibility in yolk-rich planktotrophic larvae of an antarctic echinoderm. *Antarct. J. U.S.* **26:** 168–170.

Brey, T., and J. Gutt. 1991. The genus *Sterechinus* (Echinodermata: Echinoidea) on the Weddell Sea shelf and slope (Antarctica): distribution, abundance and biomass. *Polar Biol.* **11:** 227–232.

Brey, T., J. S. Pearse, L. Basch, J. B. McClintock, and M. Slattery. 1995. Growth and production of *Sterechinus neumayeri* (Echinoidea: Echinodermata) in McMurdo Sound, Antarctica. *Mar. Biol.* **124:** 279–292.

Chia, F. S., and C. W. Walker. 1991. Echinodermata: Asteroidea. Pp. 301–353 in *Reproduction of Marine Invertebrates*, Vol. VI. A. C. Giese and J. S. Pearse, eds. Boxwood Press, Pacific Grove, CA.

Clark, H. E. S. 1963. The fauna of the Ross Sea. Part 3: Asteroidea. *N.Z. Dept. Sci. Ind. Res. Bull.* **151:** 1–84.

Clarke, A. 1983. Life in cold water: The physiological ecology of polar marine ectotherms. *Oceanogr. Mar. Biol. Annu. Rev.* **21:** 341–453.

Clarke, A. 1988. Seasonality in the Antarctic marine environment. *Comp. Biochem. Physiol.* **90 B (3):** 461–473.

Clarke, A. 1992. Reproduction in the cold: Thorson revisited. *Invertebr. Reprod. Dev.* **22:** 175–184.

Clarke, A., and R. J. G. Leakey. 1996. The seasonal cycle of phytoplankton macronutrients and the microbial community in a near shore Antarctic marine ecosystem. *Limnol. Oceanogr.* **41:** 1281–1294.

Clarke, A., L. J. Holmes, and M. G. White. 1988. The annual cycle of temperature, chlorophyll and major nutrients at Signy Island, South Orkney Islands, 1969-82. *Br. Antarct. Surv. Bull.* **80:** 65–86.

Cossins, A. R., and K. Bowler. 1987. *Temperature Biology of Animals.* Chapman and Hall, London. 339 pp.

Dayton, P. K., G. A. Robilliard, R. T. Paine, and L. B. Dayton. 1974. Biological accommodation in the benthic community at McMurdo Sound, Antarctica. *Ecol. Monogr.* **44:** 105–128.

Foster, T. D. 1984. The marine environment. Pp. 345–371 in *Antarctic Ecology*, Vol. 2. R. M. Laws, ed. Academic Press, London.

Hochachka, P. W. 1991. Temperature: The ectothermy option. Pp. 313–322 in *Biochemistry and Molecular Biology of Fishes*, Vol. 1. P. W. Hochachka and T. P. Mommsen, eds. Elsevier Science, Amsterdam.

Hoegh-Guldberg, O., and D. Manahan. 1995. Coulometric measurement of oxygen consumption during development of marine invertebrate embryos and larvae. *J. Exp. Biol.* **198:** 19–30.

Hoegh-Guldberg, O., and J. S. Pearse. 1995. Temperature, food availability, and the development of marine invertebrate larvae. *Am. Zool.* **35:** 415–425.

Levitan, D. R. 1995. The ecology of fertilization in free-spawning invertebrates. Pp. 123–156 in *Ecology of Marine Invertebrate Larvae*. L. R. McEdward, ed. CRC Press, Boca Raton, FL.

Littlepage, J. L. 1965. Oceanographic investigations in McMurdo Sound, Antarctica. *Antarct. Res. Ser.* **5:** 1–37.

MacBride, E. W. 1900. Note on the rearing of echinoid larvae. *J. Mar. Biol. Assoc. U.K.* **6:** 94–97.

McClintock, J. B., J. S. Pearse, and I. Bosch. 1988. Population structures and energetics of the shallow-water antarctic sea star *Odontaster validus* in contrasting habitats. *Mar. Biol.* **99:** 235–246.

Morgan, S. G. 1995. Life and death in the plankton: larval mortality and adaptation. Pp 279–321 in *Ecology of Marine Invertebrate Larvae*. L. R. McEdward, ed. CRC Press, Boca Raton, FL.

Murphy, E. J., A. Clarke, C. Simon, and J. Priddle. 1995. Temporal variation in Antarctic sea-ice: analysis of a long term fast-ice record from the South Orkney Islands. *Deep-Sea Res. Part I.* **42:** 1045–1062.

Olson, R. R., I. Bosch, and J. S. Pearse. 1987. The hypothesis of antarctic larval starvation examined for the asteroid *Odontaster validus*. *Limnol. Oceanogr.* **32:** 686–690.

Orton, J. H. 1920. Sea-temperature, breeding and distribution in marine animals. *J. Mar. Biol. Assoc. U.K.* **20:** 339–366.

Payne, R. W., P. W. Lane, P. G. N. Digby, S. A. Harding, P. K. Leech, G. W. Morgan, A. W. Todd, R. Thompson, W. G. Tunnicliffe, S. J. Welham, and R. P. White. 1993. *Genstat 5 Release 3 Reference Manual*, Oxford University Press, Oxford, UK. 796 pp.

Pearse, J. S., and A. C. Giese. 1966. Food, reproduction and organic constitution of the common antarctic echinoid *Sterechinus neumayeri* (Meisner). *Biol. Bull.* **130:** 387–401.

Pearse, J. S., I. Bosch, V. B. Pearse, and L. V. Basch. 1991. Differences in feeding on algae and bacteria by temperate and antarctic sea star larvae. *Antarct. J. U.S.* **26:** 170–172.

Pechenik, J. A. 1987. Environmental influences on larval survival and development. Pp. 551–608 in *Reproduction of Marine Invertebrates*, Vol. IX. A. C. Giese and J. S. Pearse, eds. Boxwood Press, Pacific Grove, CA.

Peck, L. S. 1993. Larval development in the Antarctic nemertean *Parbolasia corrugatus* (Heteronemertea: Lineidae). *Mar. Biol.* **116:** 301–310.

Precht, H., J. Christophersen, H. Hensel, and W. Larcher. 1973. *Temperature and Life.* Springer-Verlag, Berlin, 779 pp.

Rivkin, R. B., I. Bosch, J. S. Pearse, and E. J. Lessard. 1986. Bacterivory: A novel feeding mode for asteroid larvae. *Science* **233:** 1311–1314.

Sokal, R. R., and F. J. Rohlf. 1981. *Biometry.* 2nd ed. Freeman, Oxford. 859 pp.

Stanwell-Smith, D., and A. Clarke. 1997. The timing of reproduction in the Antarctic limpet *Nacella concinna* (Strebel, 1908) (Patellidae) at Signy Island, in relation to environmental variables. *J. Molluscan. Stud.***63:** 627–631.

Stanwell-Smith, D., A. Hood, and L. S. Peck. 1997. *A Field Guide of the Pelagic Invertebrate Larvae of the Maritime Antarctic.* British Antarctic Survey Press, Cambridge, UK. 162 pp.

Stanwell-Smith, D., L. S. Peck, A. Clarke, A. W. A. Murray, and C. D. Todd. The distribution, abundance and seasonality of pelagic marine invertebrate larvae in the maritime Antarctic. *Philos. Trans. Roy. Soc. Lond. B* (in press).

Starr, M., J. H. Himmelmann, and J.-C. Therriault. 1990. Direct coupling of marine invertebrate spawning with phytoplankton blooms. *Science* **247:** 1071–1074.

Strathmann, M. F. 1987. *Reproduction and Development of Marine Invertebrates of the Northern Pacific Coast.* Univ. Washington Press, Seattle. 670 pp.

Thorson, G. 1950. Reproductive and larval ecology of marine bottom invertebrates. *Biol. Rev.* **25:** 1–45.

Young, C. M., P. A. Tyler, J. L. Cameron, and S. G. Rumrill. 1992. Seasonal breeding aggregations in low-density populations of the bathyal echinoid *Stylocidaris lineata. Mar. Biol.* **113:** 603–612.

Reference: *Biol. Bull.* **194:** 53–62. (February, 1998)

Recovery of Claw Size and Function Following Autotomy in *Cancer productus* (Decapoda: Brachyura)

RACHEL E. BROCK[1] AND L. DAVID SMITH[2,*]

Department of Zoology, University of Alberta, Edmonton, Alberta T6G 2E9, and Bamfield Marine Station, Bamfield, British Columbia VOR 1B0, Canada

Abstract. We examined recovery of claw size and function following autotomy in red rock crabs *Cancer productus*. We also tested for costs of regeneration to growth and documented the frequency of claw injury in *C. productus* populations in Barkley Sound, Canada. Field and laboratory results indicated that crabs required at least three molts to recover a full-length cheliped. For injured crabs, regenerating claws were significantly less powerful than contralateral, normal (*i.e.*, uninjured) claws even two instars after autotomy. Greater mechanical advantage in normal claws of injured (*versus* uninjured) crabs, however, suggests some morphological response by the remaining normal claw to increased exercise. Despite this compensatory response, our experiments indicate that injured crabs remain at a significant disadvantage while foraging. After adjusting for differences in propodus length, both regenerating and normal claws of injured crabs delivered significantly lower crushing forces than did claws of intact crabs. Energetic costs, in the form of reduced body size increase at the molt, were detected only for crabs regenerating both claws. High incidences of single claw loss in *C. productus* in Barkley Sound, together with our experimental data, suggest that much of the population experiences a prolonged foraging handicap following injury.

Introduction

Many animals possess the ability to self-amputate, or autotomize, an appendage in response to injury or its threat (Robinson *et al.*, 1970; Medel *et al.*, 1988; McCallum *et al.*, 1989; Smith, 1995). Although the absence of an appendage can impair subsequent performance (*e.g.*, Vitt *et al.*, 1977; Sekkelsten, 1988; Smith and Hines, 1991*a*; Davenport *et al.*, 1992; Smith, 1992, 1995; Juanes and Smith, 1995), the handicap is considered temporary because, in most cases, individuals are able to regenerate the missing structure. Regeneration of a normal-length limb generally requires a minimum of two molts (*e.g.*, Miller and Watson, 1976; Savage and Sullivan, 1978; Smith, 1990); however, the actual time to replace an appendage completely can vary dramatically (*e.g.*, <1 y in juvenile king crabs, *Paralithodes camtschatica*, 4–7 y in young adults; Edwards, 1972). If the regenerative process is prolonged and the regenerating appendage functions at a level significantly below that of a normal one, then the long-term cost of autotomy to individual performance could be high. In this study, we examine recovery of claw size and function following autotomy in *Cancer productus*, a common shallow-water molluscivorous crab in the eastern Pacific Ocean.

In crustaceans, recovery of a normal-length limb following autotomy is dependent on the molt frequency and the proportion of limb length replaced at each ecdysis (Goss, 1969; Skinner, 1985). These factors, in turn, can vary with species, age of the animal, and extent of injury. For example, blue crabs (*Callinectes sapidus*) are able to recover 85% to 90% of their normal limb length in the first post-autotomy molt and nearly 100% in the second molt (Smith, 1990). In contrast, spider crabs (*Chionoecetes opilio*) recover about 48% and 73% of the normal

Received 16 July 1997; accepted 3 November 1997.

[1] Present address: Department of Wildlife, Fish and Conservation Biology, University of California, Davis, CA 95616.

[2] Present address: Marine Science Center, Northeastern University, Nahant, MA 01908.

* To whom correspondence should be addressed. E-mail: ldsmith@lynx.neu.edu

limb length in the first and second molt (Miller and Watson, 1976). Because molting frequency typically declines with age in most crustaceans (Hartnoll, 1982), regeneration will take longer in older individuals (Smith and Hines, 1991*b*). The effect of limb autotomy on the molt cycle is more complex; it can accelerate or delay ecdysis, depending on the number of limbs removed and the stage at which injury occurs (Hopkins, 1982; Spivak, 1990; Smith, 1990).

In many brachyuran crab populations, cheliped (claw) autotomy is the most common form of limb injury (Smith and Hines, 1991*b*; Juanes and Smith, 1995). This type of injury can have profound fitness consequences given the functional importance of chelipeds (*e.g.*, Lee and Seed, 1992; Lee, 1995; Seed and Hughes, 1995) and their relative contribution to total body mass (*e.g.*, *ca.* 50% in *Menippe mercenaria*, Simonson and Steele, 1981). In molluscivorous crabs, chelipeds must generate sufficient closing force to break the defensive armor of their prey (Vermeij, 1983; Boulding and LaBarbara, 1986). Because closing force is a function of muscle mass as well as the size, dentition, and leverage properties (*e.g.*, mechanical advantage) of the claw (Brown *et al.*, 1979; Elner and Campbell, 1981), one would expect the smaller regenerating claw to deliver less crushing force than a contralateral limb of normal size. Regenerating claws, however, might also fail to operate at their size-specific functional capacity if their leverage properties or muscle development differ from those of equivalently sized, normal chelipeds. In either case, smaller closing forces generated by regenerating chelipeds could limit the type or size of prey taken (Elner, 1980).

The potential exists for the contralateral normal cheliped to compensate for reduced function in the regenerating cheliped through either behavioral or morphological changes. Smith and Palmer (1994) have shown that exercise in *Cancer productus* can increase cheliped size and strength in subsequent instars. If reduced function in regenerating chelipeds leads to an increased workload for contralateral claws, the latter may become relatively larger and more powerful. Performance levels of regenerating chelipeds and the effect of injury on the contralateral cheliped have not, however, been examined in brachyuran crabs.

Regeneration of a missing appendage involves energetic trade-offs, and cheliped replacement has been shown to reduce size increase at the molt (Bennett, 1973; Chittleborough, 1975; Kuris and Mager, 1975; Hopkins, 1982; Smith, 1990). Because smaller animals are often at a disadvantage in encounters with predators and competitors (Werner and Gilliam, 1984; Garvey *et al.*, 1994), diverting resources meant for growth to regeneration has potentially serious ecological consequences.

In this study, we document the recovery of functional performance in injured *Cancer productus* individuals by comparing the mechanical advantage and maximum crushing force of regenerating claws with the same characteristics in normal claws of injured and intact crabs. We estimate the number of instars required by *C. productus* to regenerate a normal-length cheliped as a function of body size, and we determine the energetic cost of regeneration by comparing growth increments after one molt for regenerating and nonregenerating crabs. Finally, to assess the extent of handicap in *C. productus* populations, we document the frequency of claw loss and regeneration in two populations in Barkley Sound, British Columbia. Our data show that (1) regenerating claws are weaker than the contralateral normal claw, (2) both regenerating and normal claws of injured crabs operate below their size-specific functional capacity, (3) this disadvantage persists for several instars following autotomy, and (4) claw injury is common in the field. As a consequence, the functional cost of autotomy to foraging may be more extensive than previously thought.

Materials and Methods

Claw regeneration and growth increments

Two hundred forty-three crabs ranging in carapace width from 19 to 146 mm were kept between June and August 1993 in laboratory seawater tables at Bamfield Marine Station in Bamfield, British Columbia. Among these were crabs with two normal-size chelipeds (intact) and those missing or regenerating one or both chelipeds (injured). Crabs were held individually in plastic freezer containers (l × w × h = 12 cm × 10 cm × 13 cm for smaller crabs; 30 cm × 18 cm × 10 cm for larger crabs) with mesh sides in constantly flowing seawater (32 ppt salinity, ~12°C temperature). Crabs were fed mussels, *Mytilus californianus* and *M. trossulus*, *ad libitum* every other day. Each crab received mussels within a size range that it could easily crush.

Cheliped propodus lengths (distance from the proximal end of the manus to the distal tip of the fixed finger) of crabs regenerating one or both chelipeds were measured after each molt to determine percent claw regeneration ([regenerating propodus length/normal propodus length] ×100). "Normal" propodus lengths were estimated by regressing carapace width (CW, distance between anterolateral spines, in millimeters) against propodus length for intact crabs with two normal claws (propodus length = 0.456 CW − 2.11, n = 305 chelae, R^2 = 0.98). Mechanical advantage, an indicator of grip strength (Warner and Jones, 1976; Seed and Hughes, 1995), was measured in regenerating and normal claws. Mechanical advantage (L_1/L_2) was calculated by dividing dactyl height (L_1, the distance between the dactyl pivot point and the attachment site of the dactyl with the closer apodeme) by dactyl

length (L_2, the distance between the dactyl pivot point and the dactyl tip) for each claw type. For all crabs that molted while in captivity, we recorded increases in carapace width (in millimeters) and blotted wet weight (in grams) [(postmolt−premolt size)/premolt size] ×100.

Crushing force in regenerating and intact crabs

Crushing forces were determined for regenerating and normal claws of injured crabs and for normal claws of intact crabs by encouraging crabs to grasp a device that registered the force applied. The device consisted of a stationary lower ring and a movable upper ring; the latter was attached at a 90° angle to a 2-mm-thick flexible steel beam by means of a set screw (Smith and Palmer, 1994). Crabs were maneuvered so that the fixed finger of the cheliped fit into the lower ring and the dactyl into the upper ring, each at their midpoint. The distance between the inner margins of the rings was set at about 60% of the maximum gape (determined by regression of maximum gape of normal claws *versus* CW) at the midpoint of the claw. Crabs were held stationary with their chela at a right angle to the rings and allowed to squeeze the rings for 10 s. Forces were transduced by two strain gauges (BAE-13-250BB-350TE; 350 Ω, William Bean, Inc., Detroit, MI) glued to opposite sides of the beam. The signal was amplified by a Wheatstone bridge powered by two 6-V batteries and registered onto a Hewlett-Packard 8045A X-Y chart recorder. Crushing forces (newtons) were calculated after calibrating with known weights.

Crushing force measurements for selected crabs were conducted over a period of 1 month. Crabs were given at least 24 h to recuperate between trials. For crabs with regenerating claws, normal and regenerating claws were measured on alternate trial days. For crabs with two normal claws, right and left claws were tested on alternate trial days. Crabs that molted less than 2 weeks prior to or 1 week subsequent to the tests were excluded from analysis, as were crabs that crushed in less than 50% of the trials (mean number of trials per claw in which crushing occurred ± 1 SD = 4.7 ± 1.6). Because differences in the crab's motivational state produced highly variable crushing forces, only the maximum crushing force for each claw was included in our analyses.

Frequency of autotomy and regeneration

We compared the frequency of cheliped autotomy and regeneration in two populations of *Cancer productus* from Barkley Sound, British Columbia. Crabs were collected by hand at low tide from Grappler Inlet (48° 50′N, 125° 07′W) and Dixon Island (48° 51′N, 125° 07′W) in June 1993. We measured crabs for carapace width and recorded their sex (Dixon Island population only). Crabs were divided into small (CW < 65 mm) and large (CW ≥ 65 mm) size classes for analysis. This division roughly corresponded with the onset of sexual maturity in *C. productus* (Orensanz and Gallucci, 1988). Chelipeds were classified either as (1) missing (stump, papilla, or limb bud), (2) regenerating (functional but shorter than normal-length limbs), or (3) normal (full length with no evidence of regeneration).

All statistical analyses were performed using Statistical Analysis Systems software (SAS Institute, 1985).

Results

Claw regeneration rate

Field and laboratory data indicate that *Cancer productus* requires at least three instars to regenerate 100% of the normal, contralateral cheliped length. In the field, the percentage of cheliped length regenerated in large crabs was bimodally distributed with peaks at 60% and 85% the length of a normal cheliped (Fig. 1). Small crabs appeared to regenerate slightly more (70% and 90%) of their normal cheliped length than large crabs over successive molts (Fig. 1). Increases in cheliped length in laboratory-reared crabs mirrored regeneration patterns observed in field populations. In the laboratory, the greatest percent increase (± 1 SD) in limb length (66% ± 11%, n = 8) occurred in the first molt following autotomy, when the regenerate expanded from a bud to a short, functional limb. The mean percent increase in limb length over subsequent molts was substantially less (8% ± 7%, n = 22). Seven of the individuals with regenerated chelipeds increased less than 4% in cheliped length after the molt. The percentage of cheliped length regenerated in the first post-autotomy molt varied inversely with crab body size (Fig. 2).

Claw performance and mechanical advantage

Recovery of measurable crushing force in regenerating claws required at least two instars following autotomy. In experiments designed to record claw crushing forces, injured crabs (*i.e.*, those with one normal and one regenerating cheliped) exerted measurable crushing force in all trials significantly less often than did crabs with two normal claws (χ^2 = 12.3, df = 2, P = 0.002; Table I). Among injured crabs, individuals that had regenerated <75% of a normal cheliped length squeezed the rings significantly less often than crabs that had regenerated ≥75% of a normal cheliped length (Table I). Normal and regenerating claws of injured crabs did not differ in their frequency of successful crushing attempts (Fisher's exact tests, Table I).

Because only two measurable crushing forces were available for injured crabs with <75% of the cheliped length regenerated, we report crushing forces only of

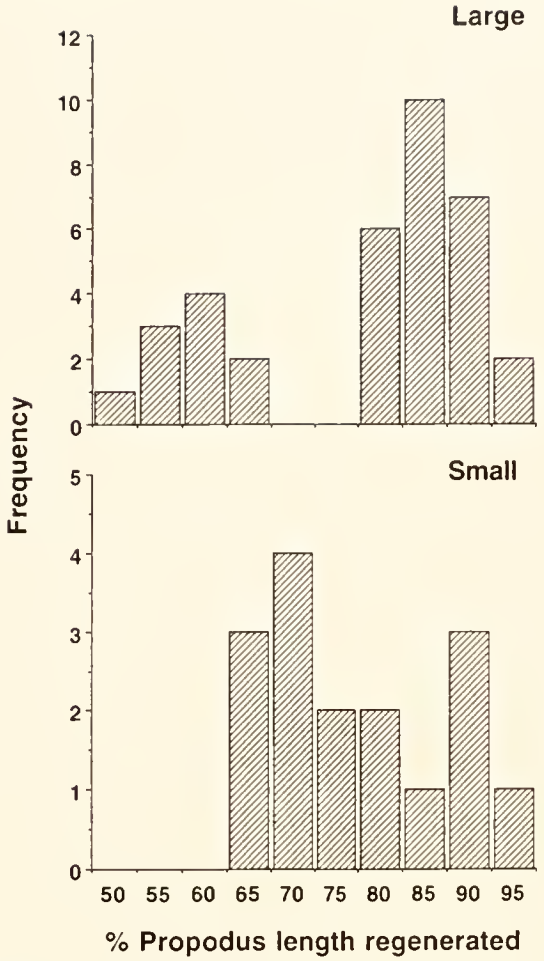

Figure 1. The frequency distribution of percent cheliped length regenerated in small (carapace width [CW] <65 mm) and large (CW ≥ 65 mm) *Cancer productus* individuals collected from Grappler Inlet and Dixon Island. Percent cheliped length regenerated was calculated from propodus length using the equation ([regenerating propodus length/ normal propodus length] × 100). Normal propodus lengths were estimated by regressing CW against propodus length for intact crabs with two normal chelipeds.

claws that had regenerated more than 75% of the normal claw length. Within these individuals (34 to 98 mm, CW range), the mean crushing force (± 1 SD) of the regenerating claw (23.9 ± 11.3 N) was significantly less than that of the opposing normal-size claw (31.0 ± 15.9 N) (Paired *t* test, $t = 2.84$, $n = 12$, $P = 0.016$). The mean mechanical advantage of the regenerating claw (0.378 ± 0.032) was also less than that of the contralateral normal claw (0.425 ± 0.048) (Paired *t* test, $t = 2.97$, $n = 12$, $P = 0.013$).

We compared crushing forces and mechanical advantages of the different claw types (*i.e.*, normal claws from intact crabs, normal and regenerating claws from injured crabs) after adjusting for propodus length (mean propodus length = 27.1 mm; range, 10 to 42 mm) (Sokal and Rohlf, 1981). Crushing force correlated positively with the covariate, propodus length ($F = 219.6$, df = 1, $P < 0.001$), and slopes of the regression of crushing force *versus* propodus length were homogeneous among claw types (claw type × propodus length interaction, $F = 0.59$, df = 2, 57, $P = 0.56$). Among individuals, least squares mean crushing force was dependent on claw type (one-way ANCOVA, $F = 6.41$, df = 2, $P = 0.003$) (Fig. 3A). Normal claws of intact crabs were significantly stronger than either regenerating ($F = 7.1$, df = 1, $P = 0.010$) or normal ($F = 11.1$, df = 1, $P = 0.0015$) claws of injured crabs (linear contrasts followed by sequential Bonferroni, experimentwise alpha = 0.05; Rice, 1989) (Fig. 3A). For injured crabs, size-adjusted crushing forces of normal and regenerating claws did not differ ($F = 0.14$, df = 1, $P = 0.71$).

Among experimental animals, mechanical advantage did not correlate with the covariate, propodus length ($F = 1.5$, df = 1, $P = 0.23$). Least squares mean mechanical advantage differed among claw types (one-way ANCOVA, $F = 4.0$, df = 2, $P = 0.023$), but did not follow the same pattern as crushing force (Fig. 3B). Instead, size-adjusted mean mechanical advantage (± 1 SE) was highest for normal claws opposite regenerating claws (0.42 ± 0.008) and lowest for regenerating claws (0.38 ± 0.01) (linear contrast, $F = 7.6$, df = 1, $P = 0.008$; Fig.

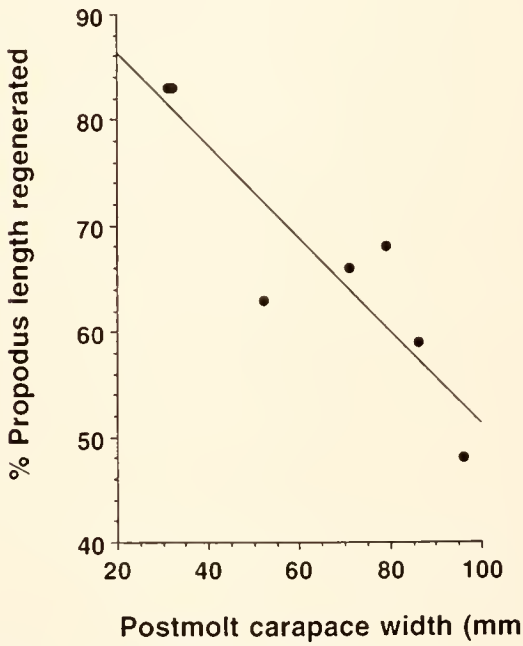

Figure 2. Percent propodus length regenerated in first post-autotomy molt of crabs missing one cheliped as a function of carapace width (CW, in mm). Smaller *Cancer productus* individuals regenerate proportionally more than larger individuals (% propodus length regenerated = −0.438 CW + 95.1, $n = 7$, $R^2 = 0.81$, slope SE = 0.0947, $P = 0.006$).

Table I

Comparison of crushing success of intact crabs with normal claws and injured crabs with one normal and one regenerating claw

	Intact crabs[a]	Injured crabs, <75% regenerated[b]		Injured crabs, ≥75% regenerated[c]	
Crushing success	Two normal claws	Normal claw	Regenerating claw	Normal claw	Regenerating claw
Yes	25 (83.3%)	2 (22.2%)	0 (0.0%)	9 (42.9%)	10 (47.6%)
No	5 (16.7%)	7 (77.8%)	9 (100.0%)	12 (57.1%)	11 (52.4%)
Fisher's exact test	not applicable	$P = 0.47$		$P = 1.0$	

Injured crabs were subdivided into those individuals with regenerating claws whose propodus lengths were < and ≥75% of a normal, contralateral propodus length. Values represent the number (and percentage, in parentheses) of crabs which exerted (Yes) or failed to exert (No) measurable crushing force in all trials (mean number of trials ± 1 SD = 5.2 ± 1.4). Different superscripted letters denote significant differences in crushing success of paired claws among different crab categories ($P < 0.05$, STP test; Sokal and Rohlf, 1981). Fisher's exact tests compare normal and regenerating claws within categories of injured crabs.

3B). Size-adjusted mean mechanical advantage of normal claws of intact crabs (0.39 ± 0.008) did not differ from that of regenerating claws of injured crabs ($F = 1.1$, df = 1, $P = 0.30$) and was marginally nonsignificant compared to normal claws of injured crabs ($F = 3.6$, df = 1, $P = 0.063$) (linear contrasts followed by sequential Bonferroni, experimentwise alpha = 0.05).

Among injured crabs collected from Dixon Island and Grappler Inlet, mechanical advantage increased as the cheliped grew through successive regenerative molts (mechanical advantage = 0.00124% propodus length regenerated + 0.267; $n = 80$, $R^2 = 0.19$, slope SE = 0.000292, $P < 0.001$) (Fig. 4). This positive relationship is not simply a function of increasing body size over successive molts, because although mechanical advantage correlated positively with carapace width for regenerating claws ($P = 0.028$), there was no such relationship for normal claws ($P = 0.96$) of injured crabs. Instead, claw dimensions relevant to mechanical advantage are likely changing during regeneration. As evidence, mechanical advantage correlated positively with dactyl height (L_1) of regenerating claws (Pearson correlation coefficient, $r = 0.26$, $n = 80$, $P = 0.017$), but not with dactyl height of normal claws of injured crabs ($r = 0.19$, $n = 78$, $P = 0.10$). Mechanical advantage did not correlate significantly with dactyl length (L_2) of regenerating ($r = 0.016$, $P = 0.89$) or normal ($r = -0.082$, $P = 0.48$) claws of injured crabs.

Growth increments

The energetic cost of cheliped replacement to growth depended on whether one or both claws were regenerating (one-way ANOVA, $F = 6.46$, df = 3, $P < 0.001$). Carapace width increments (proportions arcsine-transformed prior to analysis) at the molt did not differ between intact crabs and those regenerating a single cheliped, regardless of whether regeneration began from a limb bud or a partially regenerated limb (Table II). In contrast, regeneration of both claws significantly reduced carapace width increments relative to those of intact or singly injured crabs. Similar trends were observed for wet-weight increments at the molt, but differences among claw conditions were marginally nonsignificant (Kruskal-Wallis test, $\chi^2 = 7.70$, df = 3, $P = 0.053$) (Table II).

Frequency of autotomy and regeneration

About one-third of *Cancer productus* individuals collected from Dixon Island (32%; $n = 183$) and Grappler Inlet (29%; $n = 126$) were missing or regenerating one or both chelipeds (two-way logistic regression, site effect, $\chi^2 = 0.03$, df = 1, $P = 0.87$; Table III). Large crabs were nearly two times more likely to be injured than small crabs (size effect, $\chi^2 = 17.4$, df = 1, $P < 0.001$), and this size dependence was consistent between sites (size × site interaction, $\chi^2 = 0.38$, df = 1, $P = 0.54$; Table III). For combined sizes, the frequency of crabs missing chelipeds did not differ from that of crabs regenerating chelipeds at either site (G-tests, df = 1, $P > 0.1$). The majority of injured crabs (97% at Dixon; 86% at Grappler) were missing or regenerating one claw only; loss of both claws was rare (Table III). In the Dixon Island population (data unavailable for Grappler Inlet), right and left chelipeds were missing and regenerating with equal frequency (G-tests, df = 1, $P > 0.1$), and the frequency of autotomy was independent of sex ($\chi^2 = 0.40$, df = 1, $P = 0.53$; 96 males and 87 females).

Discussion

Foraging costs during claw regeneration

Previous experiments have shown that crabs with missing (Smith and Hines, 1991*a*) or damaged (Juanes and Hartwick, 1990) claws forage less successfully than do crabs with both claws intact. Our results demonstrate that functional costs persist well into the regenerative process.

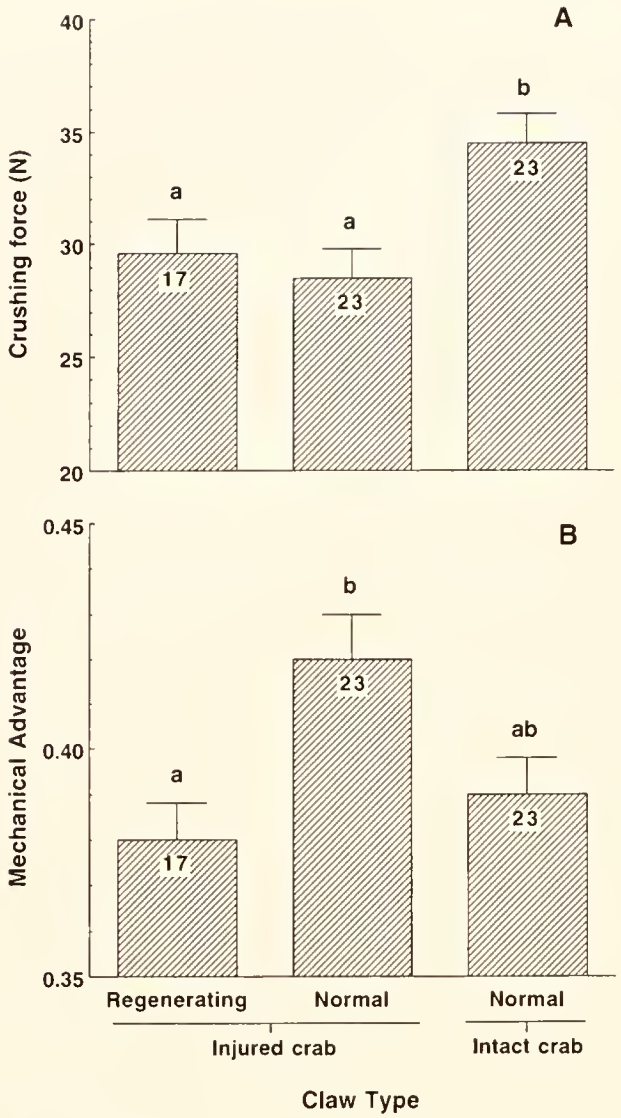

Figure 3. Comparison of (A) crushing force (in newtons) and (B) mechanical advantage of regenerating and normal chelipeds of injured crabs and normal chelipeds of intact crabs. Only regenerating chelipeds with propodus lengths at least 75% of contralateral normal propodus length were included. Crushing forces and mechanical advantages (± 1 SE) were adjusted for the covariate, propodus length, using least squares estimation (one-way ANCOVAs; mean propodus length = 27.1 mm) (Sokal and Rohlf, 1981). Mechanical advantage = L_1/L_2; where L_1 is the distance between the dactyl pivot point and the dactyl attachment site with the closer apodeme and L_2 is the distance between the dactyl pivot point and the dactyl tip. Different letters above bars denote means that differ significantly (linear contrasts followed by sequential Bonferroni, experimentwise alpha = 0.05; Rice 1989). Sample size (n) is given for each claw type.

After the first post-autotomy molt, regenerating claws of *Cancer productus* individuals could not grip forcefully; hence, they would be of little assistance while foraging. Measurable crushing forces were detected in regenerating claws only after the second post-autotomy molt (*i.e.*, when >75% of the normal cheliped length had been regenerated) (Table 1). Even then, regenerating claws exerted significantly less crushing force than did contralateral intact claws. Reduced performance in regenerating claws is not surprising, because crushing force is correlated with claw size (Vermeij, 1977; Elner, 1980; Lee and Seed, 1992; Lee, 1993), and regenerating claws are smaller than their intact counterparts. Regenerating claws should also be constrained to handle smaller prey because of the smaller gape between the fixed and movable fingers. Elner (1980) noted that *Carcinus maenas* males with proportionately smaller chelae (*i.e.*, presumably those with regenerating claws) chose smaller mussel prey and had a lower energy intake per day than did equivalent-size males with normal claws.

Our experiments revealed two less obvious but potentially important effects of autotomy on foraging ability. First, normal claws of injured crabs showed a morphological response to loss of function by the regenerating claw (Fig. 3B). Specifically, we observed a strong trend (P = 0.063) toward greater mechanical advantage in the normal claws of injured rather than intact crabs. Second, both normal and regenerating claws in injured crabs operated below their size-specific crushing capacity (Fig. 3A). These results are intriguing, because previous work has

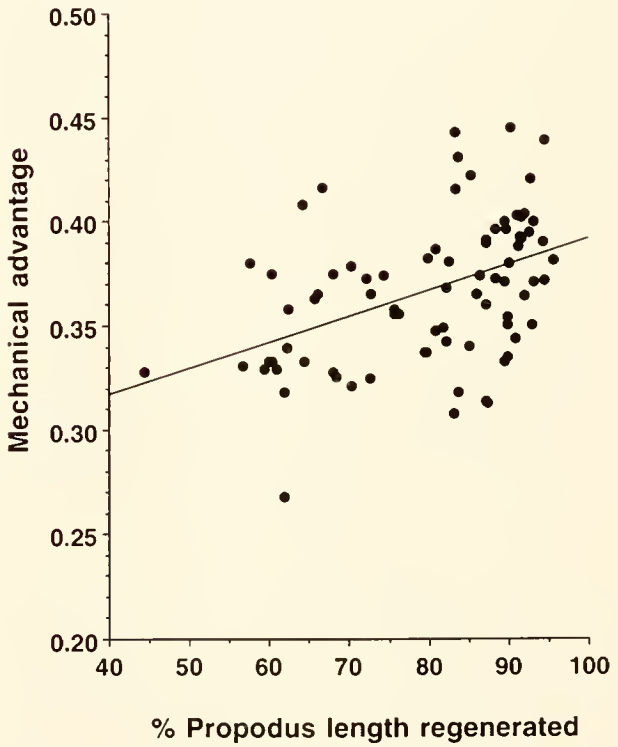

Figure 4. Mechanical advantage as a function of percent propodus length regenerated. Mechanical advantage increases as the cheliped goes through successive regenerative molts ($P < 0.001$, $R^2 = 0.19$).

Table II

Comparison of mean percent carapace width (CW) and wet weight (weight) increments after one molt among crabs with two normal chelipeds and those initially missing or regenerating one cheliped or regenerating two chelipeds

	Crab cheliped status[1]								
	2 claws normal		1 claw missing 1 claw normal		1 claw regenerating 1 claw normal		2 claws regenerating		
Size category	Mean	*n*	Mean	*n*	Mean	*n*	Mean	*n*	*P*
CW[2]	28.7[a] (27.0–30.5)	29	26.4[a] (22.4–30.6)	5	24.9[a] (22.3–27.5)	12	18.1[b] (13.8–23.0)	3	0.001
Weight	98.5 (24.3)	21	99.8 (11.5)	4	87.8 (28.8)	11	56.6 (8.4)	2	0.053

CW (mm) and wet weight (g) increments calculated as [(postmolt − premolt value)/premolt value] × 100. Variances for carapace width increments were homogeneous; those for wet weights were not (F_{max}-tests, alpha = 0.05). For carapace width, mean percent increments, sample sizes (*n*), 95% confidence intervals (in parentheses), and significance level (*P*) of the ANOVA are presented. For wet weight, mean percent increments, sample sizes (*n*), standard deviations (in parentheses), and significance level of Kruskal-Wallis test are presented. Different superscripted letters denote significant differences in carapace width increment among crabs with different degrees of injury (Ryan's Q test; Day and Quinn, 1989).

[1] Missing chelipeds include limb stumps possessing a papilla or limb bud. Regenerating chelipeds have undergone at least one post-autotomy molt, but remain shorter than normal chelipeds.

[2] Means and confidence limits for carapace widths were backtransformed for presentation (arcsine-transformed mean square error = 0.00266, error df = 45, F = 6.5).

shown that *Cancer productus* responded to increased exercise by developing larger and stronger claws in subsequent instars (Smith and Palmer, 1994). Furthermore, if one claw was immobilized, the remaining functional claw became larger and stronger by the next instar (Smith and Palmer, 1994). Given that an injured crab is (1) without a claw for the period immediately following autotomy until the next molt and (2) without a fully functional claw for at least two instars while the appendage regenerates, the remaining normal claw should be subject to prolonged exercise.

Despite their greater mechanical advantage, normal claws of injured crabs were still relatively weaker than equivalent-size normal claws of intact crabs (Fig. 3A). At least three possible explanations exist for this finding. First, among the size range of mussels presented, injured crabs may have selected smaller mussels than did intact crabs (*e.g.*, Elner, 1980). In crushing smaller prey, both

Table III

Frequencies (n) and percentages (%) of crabs missing and regenerating one or both chelipeds at Dixon Island and Grappler Inlet sites, Barkley Sound, Canada, in June 1993

	Dixon Island						Grappler Inlet					
	Small		Large		Total		Small		Large		Total	
Category	*n*	%	*n*	%	*n*	%	*n*	%	*n*	%	*n*	%
Total intact	73	81.1	51	54.8	124	67.8	63	77.8	26	57.8	89	70.6
Total injured[1]	17	18.9	42	45.2	59	32.2	18	22.2	19	42.2	37	29.4
1 missing	8	8.9	19	20.4	27	14.8	6	7.4	7	15.5	13	10.3
2 missing	1	1.1	0	0.0	1	0.5	1	1.2	1	2.2	2	1.6
1 regenerating	8	8.9	22	23.7	30	16.4	11	13.6	8	17.8	19	15.1
2 regenerating	0	0.0	1	1.1	1	0.5	0	0.0	3	6.7	3	2.4
Total caught	90	100.0	93	100.0	183	100.0	81	100.0	45	100.0	126	100.0

Crabs were divided into two size classes on the basis of carapace width: small = <65 mm; large = ≥65 mm. Values are also given for both size classes combined (Total).

[1] Missing = crabs with scarred stump, papilla, or limb bud. Regenerating = crabs possessing a functional but shortened cheliped. No injured crabs were found missing one cheliped and regenerating the other cheliped.

normal and regenerating claws of injured crabs would receive less exercise than the normal claws of an intact crab, and consequently would remain weaker. We cannot address this question, because systematic records were not kept of the sizes of mussels eaten by injured *versus* intact crabs. Second, unlike the crabs in a study conducted by Smith and Palmer (1994), the crabs in the present experiments were not given mussels whose size was near the upper limit of the crabs' crushing ability; consequently, both the range of exertion needed to forage and the degree of morphological differentiation expressed in the earlier study were greater than in ours. Finally, it is possible that synthesis of new tissue in the regenerating limb might impede extensive muscle development in the contralateral limb. Although a substantial body of work has examined muscle fiber transformation during claw reversal in heterochelous species (*e.g.*, Mellon and Stephens, 1980; Quigley and Mellon, 1986; Govind *et al.*, 1987), there is a dearth of information concerning the influence of regeneration on muscle development in claws of homochelous species such as *Cancer*.

Given the high frequency of claw loss in these (Table III) and other populations of molluscivorous crabs (see review by Juanes and Smith, 1995), a compensatory morphological response by normal claws of injured crabs would be advantageous. The response, however, probably only partially offsets the functional loss of a cheliped. As a consequence, crabs with a regenerating claw should be expected to (1) require longer handling times to subdue hard-shelled prey, (2) modify their tactics for gaining entry to hard-shelled prey, or (3) modify their diet to include smaller or less well defended prey items. Shell-opening tactics in crustaceans are complex (Lau, 1987), and it is possible that behavioral adjustments may compensate for limited crushing power (Hughes and Seed, 1981; Cunningham and Hughes, 1984; Smith and Hines, 1991*a*; Seed and Hughes, 1995). Direct comparisons of foraging behavior, handling times, and prey choice between injured and intact crabs are needed to determine the true costs of autotomy and regeneration to foraging performance.

Morphological changes during regeneration

As chelipeds regenerate, they become more efficient and forceful foraging tools, in part because of changes in their leverage properties. Mechanical advantage increased as the cheliped regenerated (Fig. 4), primarily because L_1 (the distance between the dactyl pivot point and the attachment site of the dactyl with the closer apodeme) increased faster than L_2 (the distance between the dactyl pivot point and the dactyl tip). L_1 approximates chela height, and Lee (1993) has shown that chela height is a good estimator of claw strength within species. The allometric change observed in the lever arms was specific to claw regeneration; no such change was observed during the growth of normal claws of injured crabs. The change in mechanical advantage during claw regeneration may reflect a use-induced increase in the underlying muscle as the claw becomes larger and more functional with each molt, or other, as yet unknown, developmental phenomena.

Regeneration time

The length of time required to regenerate a missing limb to normal size can vary dramatically between life-history stages and species of crabs (Juanes and Smith, 1995). Certainly, disadvantages arising from cheliped loss will be lessened if regeneration of the missing appendage(s) is rapid. Both field and laboratory data indicated that *Cancer productus* individuals were able to replace a full-length cheliped in about three molts. The number of instars needed for complete regeneration in *C. productus* thus falls within the range observed for other crab species—for example, two instars for juvenile *Callinectes sapidus* (Smith, 1990); four to seven instars for *Paralithodes camtschatica* (Edwards, 1972). *C. productus* undergoes about 13 molts over 3 years with the ninth (puberty) molt occurring 10 to 11 months after settlement (Orensanz and Gallucci, 1988). If this molting schedule holds for regenerating crabs, then juvenile crabs could recover claws in as little as 2 to 3 months. In contrast, adults could require years. Given that some individuals in our experiments showed almost no size increase (<4%) in their claws after the initial post-autotomy molt, it is possible that some *C. productus* individuals never recover a full-length claw.

It is interesting that in *Cancer productus* and in other crab species (*e.g.*, Skinner and Graham, 1972), individuals regenerate more than half the length of a normal claw in the first molt, but fail to complete the task in the next molt. This phenomenon of rapid, but incomplete, replacement of a missing appendage followed by slower subsequent growth is not confined to crustaceans. For example, Fielman *et al.* (1991) suggested that ophiuroids regenerate lost disc and arm tissue until a "minimal functional configuration" is achieved, then regeneration rates slow. Indeed, selection pressures may be great for replacing the majority of the skeletal framework quickly so that injured animals can "make do." Beyond this, pressure for complete recovery of function diminishes. Energetic resources can then be shunted to other tasks such as growth or reproduction. This scenario may also explain why the proportion of cheliped length regenerated decreased with increased body size in *C. productus* (Figs. 1, 2). If larger crabs are able to forage on a greater range of prey sizes and are at less risk of predation than smaller individuals,

selection for rapid replacement of a missing cheliped may be less intense than for smaller crabs.

Energetic costs to regeneration

Energetic costs, in the form of smaller growth increments at the molt, were seen only in cases of multiple autotomy (Table II). A similar, additive effect of limb loss on growth increment has been observed in other crab species (*e.g.*, Bennett, 1973; Kuris and Mager, 1975; Hopkins, 1982; Smith, 1990). We detected reduced growth increments, though, in crabs that had already undergone one post-autotomy molt. The energetic cost of replacing both chelipeds thus persists well into the regenerative process for *Cancer productus*. It should be noted that in most studies examining the effect of limb regeneration on growth, injured crabs were fed *ad libitum*. In field situations, reduced foraging performance in injured crabs could magnify energetic costs of limb replacement.

Injury frequency in the population

If cheliped loss is high in crab populations, and if foraging ability is compromised for injured crabs under field conditions, then predator-prey dynamics and community structure may be profoundly affected. We observed high frequencies of cheliped damage in *Cancer productus* populations in Barkley Sound: up to 45% of the larger and 22% of the smaller crabs were missing or regenerating a single claw (Table III). A substantial component of the *Cancer productus* population, then, may have to switch to smaller size classes or different types of prey. Injured crabs, in turn, may become more vulnerable to their own predators, if search or handling times increase. The fact that we found few crabs missing or regenerating both chelipeds (≤4%) suggests that, at the least, multiple autotomy places individuals at a selective disadvantage. Our data suggest that the consequences of claw autotomy for the individual crab are prolonged. The direct and indirect effects of reduced foraging performance in injured crabs on community dynamics remain to be explored.

Acknowledgments

We thank Dr. A. R. Palmer and the Bamfield Marine Station for providing research facilities, and Dr. D. Lello and two anonymous reviewers for comments on the manuscript. This research was partially supported by a scholarship from the Western Canadian Universities Marine Biological Society to R. E. Brock and a Bamfield Marine Station Research Associate Award to L. D. Smith.

Literature Cited

Bennett, D. B. 1973. The effect of limb loss and regeneration on the growth of the edible crab, *Cancer pagurus* (L.). *J. Exp. Mar. Biol. Ecol.* **13:** 45–53.

Boulding, E. G., and M. LaBarbara. 1986. Fatigue damage: repeated loading enables crabs to open larger bivalves. *Biol. Bull.* **171:** 538–547.

Brown, S. C., S. R. Cassuto, and R. W. Loos. 1979. Biomechanics of chelipeds in some decapod crustaceans. *J. Zool. Lond.* **188:** 143–159.

Chittleborough, R. G. 1975. Environmental factors affecting growth and survival of juvenile western rock lobsters *Panulirus longipes* (Milne-Edwards). *Aust. J. Mar. Freshwater Res.* **26:** 117–196.

Cunningham, P. N., and R. N. Hughes. 1984. Learning of predatory skills by shorecrabs *Carcinus maenas* feeding on mussels and dogwhelks. *Mar. Ecol. Prog. Ser.* **16:** 21–26.

Davenport, J., M. Spikes, S. M. Thornton, and B. O. Kelly. 1992. Crab-eating in the diamondback terrapin *Malaclemys terrapin:* dealing with dangerous prey. *J. Mar. Biol. Assoc. U. K.* **72:** 835–848.

Day, R. W., and G. P. Quinn. 1989. Comparisons of treatments after an analysis of variance in ecology. *Ecol. Monogr.* **59:** 433–463.

Edwards, J. S. 1972. Limb loss and regeneration in two crabs: the king crab *Paralithodes camtschatica* and the tanner crab *Chionoecetes bairdi. Acta Zool.* **53:** 105–112.

Elner, R. W. 1980. The influence of temperature, sex, and chelae size in the foraging strategy of the shore crab, *Carcinus maenas* (L.). *Mar. Behav. Physiol.* **7:** 15–24.

Elner, R. W., and A. Campbell. 1981. Force, function and mechanical advantage in the chelae of the American lobster *Homarus americanus* (Decapoda: Crustacea). *J. Zool. Lond.* **193:** 269–286.

Fielman, K. T., S. E. Stancyk, W. E. Dobson, and L. A. Jerome Clements. 1991. Effects of disc and arm loss on regeneration by *Microphiopholis gracillima* (Echinodermata: Ophiuroidea) in nutrient-free seawater. *Mar. Biol.* **111:** 121–127.

Garvey, J. E., R. A. Stein, and H. M. Thomas. 1994. Assessing how fish predation and interspecific prey competition influence a crayfish assemblage. *Ecology* **75:** 532–547.

Goss, R. J. 1969. Molting, metamorphosis and regeneration in arthropods. Pp. 91–113 in *Principles of Regeneration.* Academic Press, New York.

Govind, C. K., DeF. Mellon, Jr., and M. M. Quigley. 1987. Muscle and muscle fiber type transformation in clawed crustaceans. *Am. Zool.* **27:** 1079–1098.

Hartnoll, R. A. 1982. Growth. Pp. 111–196 in *The Biology of Crustacea.* Vol. 2. D. E. Bliss, ed. Academic Press, New York.

Hopkins, P. M. 1982. Growth and regeneration patterns in the fiddler crabs *Uca pugilator. Biol. Bull.* **163:** 301–319.

Hughes, R. N., and R. Seed. 1981. Size selection of mussels by the blue crab *Callinectes sapidus:* energy maximizer or time minimizer? *Mar. Ecol. Prog. Ser.* **6:** 83–89.

Juanes, F., and E. B. Hartwick. 1990. Prey size selection in Dungeness crabs: the effect of claw damage. *Ecology* **71:** 744–758.

Juanes, F., and L. D. Smith. 1995. The ecological consequences of limb damage and loss in decapod crustaceans: a review and prospectus. *J. Exp. Mar. Biol. Ecol.* **193:** 197–223.

Kuris, A. M., and M. Mager. 1975. Effect of limb regeneration on size increase at molt of the shore crab *Hemigrapsus oregonensis* and *Pachygrapsus crassipes. J. Exp. Zool.* **193:** 353–360.

Lau, C. J. 1987. Feeding behaviour of the Hawaiian slipper lobster, *Scyllarides squammosus,* with a review of decapod crustacean feeding tactics on molluscan prey. *Bull. Mar. Sci.* **41:** 378–391.

Lee, S. Y. 1993. Chela height is an acceptable indicator of chela strength in *Carcinus maenas* (Linneaus, 1758) (Decapoda, Brachyura). *Crustaceana* **65:** 115–116.

Lee, S. Y. 1995. Cheliped size and structure: the evolution of a multifunctional decapod organ. *J. Exp. Mar. Biol. Ecol.* **193:** 161–176.

Lee, S. Y., and R. Seed. 1992. Ecological implications of cheliped

size in crabs; some data from *Carcinus maenas* and *Liocarcinus holsatus*. *Mar. Ecol. Prog. Ser.* **84:** 151–160.

McCallum, H. I., R. Endean, and A. M. Cameron. 1989. Sublethal damage to *Acanthaster planci* as an index of predation pressure. *Mar. Ecol. Prog. Ser.* **56:** 29–36.

Medel, R. G., J. E. Jimenez, S. F. Fox, and F. M. Jaksic. 1988. Experimental evidence that high population frequencies of lizard tail autotomy indicate inefficient predation. *Oikos* **53:** 321–324.

Mellon, DeF., Jr., and P. J. Stephens. 1980. Modifications in the arrangement of thick and thin filaments in transforming shrimp muscle. *J. Exp. Zool.* **213:** 173–179.

Miller, R. J., and J. Watson. 1976. Growth per molt and limb regeneration in the spider crab, *Chionecetes opilio*. *J. Fish. Res. Board. Can.* **33:** 1644–1649.

Orensanz, J. M., and V. F. Gallucci. 1988. Comparative study of postlarval life-history schedules in four sympatric species of *Cancer* (Decapoda: Brachyura: Cancridae). *J. Crustac. Biol.* **8:** 187–220.

Quigley, M. M., and DeF. Mellon, Jr. 1986. Myofiber death plays a role in determining fiber type composition in the claw closer muscles of the snapping shrimp, *Alpheus heterochelis*. *J. Exp. Zool.* **239:** 299–305.

Rice, W. R. 1989. Analyzing tables of statistical tests. *Evolution* **43:** 223–225.

Robinson, M. H., L. G. Abele, and B. Robinson. 1970. Attack autotomy: a defense against predators. *Science* **169:** 300–301.

SAS Institute. 1985. *SAS User's Guide: Statistics*, Version 5 Edition. SAS Institute Inc., Cary, NC.

Savage, T., and J. R. Sullivan. 1978. Growth and regeneration of the stone crab, *Menippe mercenaria*. *Fla. Mar. Res. Publ.* **32:** 1–23.

Seed, R., and R. N. Hughes. 1995. Criteria for prey size-selection in molluscivorous crabs with contrasting claw morphologies. *J. Exp. Mar. Biol. Ecol.* **193:** 177–195.

Sekkelsten, G. I. 1988. Effect of handicap on mating success in male shore crabs, *Carcinus maenas*. *Oikos* **51:** 131–134.

Simonson, J. L., and P. Steele. 1981. Cheliped asymmetry in the stone crab, *Menippe mercenaria*, with notes on claw reversal and regeneration. *Northeast Gulf. Sci.* **5:** 21–30.

Skinner, D. M. 1985. Molting and regeneration. Pp. 43–146 in *The Biology of Crustacea*. Vol. 9. D. E. Bliss, ed. Academic Press, New York.

Skinner, D. M., and D. E. Graham. 1972. Loss of limbs as a stimulus to ecdysis in Brachyura (true crabs). *Biol. Bull.* **143:** 222–223.

Smith, L. D. 1990. Patterns of limb loss in the blue crab, *Callinectes sapidus* Rathbun, and the effects of autotomy on growth. *Bull. Mar. Sci.* **46:** 23–36.

Smith, L. D. 1992. The impact of limb autotomy on mate competition in blue crabs, *Callinectes sapidus* (Rathbun). *Oecologia* **89:** 494–501.

Smith, L. D. 1995. Effects of limb autotomy and tethering on juvenile blue crab survival from cannibalism. *Mar. Ecol. Prog. Ser.* **116:** 65–74.

Smith, L. D., and A. H. Hines. 1991a. The effect of cheliped loss on blue crab *Callinectes sapidus* Rathbun foraging rate on soft-shelled clams *Mya arenaria* L. *J. Exp. Mar. Biol. Ecol.* **151:** 245–256.

Smith, L. D., and A. H. Hines. 1991b. Autotomy in blue crab (*Callinectes sapidus* Rathbun) populations: geographic, temporal and ontogenetic variation. *Biol. Bull.* **180:** 416–431.

Smith, L. D., and A. R. Palmer. 1994. Effects of manipulated diet on size and performance of brachyuran crab claws. *Science* **264:** 710–712.

Sokal, R. R., and F. J. Rohlf. 1981. *Biometry*. W. H. Freeman, New York.

Spivak, E. D. 1990. Limb regeneration in a common South American littoral crab *Cyrtograpsus angulatus*. *J. Nat. Hist.* **24:** 393–402.

Vermeij, G. J. 1977. Patterns in crab claw size: the geography of crushing. *Syst. Zool.* **26:** 138–151.

Vermeij, G. J. 1983. Shell-breaking predation through time. Pp. 649–669 in *Biotic Interactions in Recent and Fossil Benthic Communities*. M. J. S. Tevesz and P. L. McCall, eds. Plenum, New York.

Vitt, L. J., J. D. Congdon, and N. A. Dickson. 1977. Adaptive strategies and energetics of tail autotomy in lizards. *Ecology* **58:** 326–337.

Warner, G. F., and A. R. Jones. 1976. Leverage and muscle type in crab chelae (Crustacea: Brachyura). *J. Zool. (Lond.)* **180:** 57–68.

Werner, E. E., and J. F. Gilliam. 1984. The ontogenetic niche and species interactions in size-structured populations. *Annu. Rev. Ecol. Syst.* **15:** 393–425.

Reference: *Biol. Bull.* **194:** 63–71. (February, 1998)

Comparative Analysis of Escape Behavior in Male, and Gravid and Non-Gravid, Female Lobsters

S. J. CROMARTY*, J. MELLO, AND G. KASS-SIMON†

Biological Sciences Department, University of Rhode Island, 100 Flagg Rd, Kingston, Rhode Island 02881-0816.

Abstract. Few studies exist in which the parameters of a single behavior have been quantitatively compared for male and female lobsters. Here, we have examined the effects of sex and gravidity on the parameters of the escape behavior of the American lobster, *Homarus americanus*, elicited by a visual threat.

Both non-gravid females and male lobsters readily tailflipped in response to the stimulus, but gravid females failed, with one exception, to initiate a swim, even when stimulus strength was increased.

Although the total distance swum by males and non-gravid females was not statistically different, males covered more ground in the initial power swim and during the subsequent swims than did non-gravid females. Males swam for a longer time, performing more tailflips, than females. Relative to their length and weight, males swam a greater distance at each stroke during the initial power swim and the subsequent swims, although, females might have compensated by swimming at a higher frequency. There were no significant differences in swimming velocity or acceleration, nor in the calculated force or work performed by the two sex classes (male and non-gravid females).

Therefore, apart from egg-bearing, which severely inhibits the escape response, it remains to be seen whether the subtle physiological and anatomical sexual dimorphism that produces longer and more swim strokes in males but higher frequency tailflips in females results in the same chances of survival for the sexes.

Received 14 May 1997; accepted 24 October 1997.

* Present address: Department of Neurobiology, Harvard Medical School, 220 Longwood Ave., Boston, MA 02115. E-mail: scromart@warren.med.harvard.edu

† To whom correspondence should be addressed. E-mail: avf101@uriacc.uri.edu

Abbreviations: FEP, Fisher exact probability test; SS1, subsequent swims of first half; SS2, subsequent swims of second half.

Introduction

There are very few quantitative studies comparing sexual differences in agonistic and avoidance behavior among lobsters (Scrivener, 1971; Stein, 1976; Atema *et al.*, 1979; Waddy and Aiken, 1991). Anecdotal evidence and references in the literature suggest that gravid female lobsters are much more aggressive than either males or non-ovigerous females. Gravid females are described as being asocial, secretive, and defensive; when approached, they are reported to backup and raise their wide-open claws (Atema and Voigt, 1995).

Sexual dimorphism of mature individuals is well documented. Males develop larger claws, and females have broader abdomens (Templeman, 1935; McLeese and Wilder, 1964; Lang *et al.*, 1977; Waddy and Aiken, 1991). Other physiological differences of yet-undetermined significance also exist. Males have higher hemolymph concentrations of octopamine, serotonin, tryptophan, and an unidentified compound known as compound S than do females (Fadool *et al.*, 1989).

The sexual anatomical dimorphism has led to the idea that there were sexual differences in aggressive behavior and in the establishment of dominance. The suggestion has been made that the larger claws of males were important in establishing dominance over other males or females, because lobsters with larger claws usually win in a fight (Scrivener, 1971). Alternatively, larger claws among males could be used as a sexual signal (Atema and Voigt, 1995), as is the case in crayfish where females select males with larger claws (Stein, 1976). In the female, on the other hand, sexual dimorphism has been associated

with reproduction—the wider female abdomen increases egg-carrying capacity (Templeman, 1935; McLeese and Wilder, 1964; Waddy and Aiken, 1991).

As part of a larger study to determine whether and to what extent male and female lobsters differ in their nonsexual behaviors, we have quantitatively compared the escape response in males, gravid females, and non-gravid females. Lobsters of the three "sex classes" were presented with a threatening visual stimulus. We recorded the escape behavior sequences and post-stimuli behaviors, which included whether animals re-approached and attacked the stimulus (after tailflipping) or whether they avoided the stimulus and continued to back away from it after the initial response. We now present evidence that among these three classes of lobsters, in addition to differences in the propensity to flee between gravid and non-gravid animals, there are significant differences in the parameters of the escape response between males and non-gravid females.

Materials and Methods

Animals

Adult American lobsters (carapace length 78–85 mm) were obtained through the Rhode Island Department of Environmental Management from a nearshore lobster vessel fishing in Narragansett Bay, Rhode Island. Animals were housed at the Narragansett Bay Campus of the University of Rhode Island, in separate but connecting tanks in a free-flow seawater system, at ambient temperatures ranging from 16° to 23°C and under an illumination cycle of 14 h light to 10 h dark.

Animals were fed three times per week on a mixed diet of squid, crab, and fish, but they were not fed for 48 h prior to an experiment. Four to six hours before an experiment, the animals were moved to the Kingston campus of the university, where they were placed in separate holding tanks (30 cm^3), and visually isolated from one another. Each tank was supplied with its own air supply, and water was obtained from the same source that supplied the tanks at the Bay Campus. Individuals were kept at the same temperature (20°C) as the animals held at the Bay Campus. Three hours prior to an experiment, lobsters whose claws and antennae were intact were placed in the experimental tank and left undisturbed. One hour before the experiment, the physical condition of each animal was checked. Animals were used only once and only if they moved around the tank or exhibited antennule flicking.

Experiments

Experiments were conducted from April to October to avoid possible seasonal differences in behavior. Seasonal changes in the physiology and morphology of crayfish nerve terminals have been documented (Lnenicka and Zhao, 1991). The protocol for inducing escape responses in lobsters is described in detail elsewhere (Cromarty *et al.*, 1991). In summary, experiments were run between 1200 and 1700 h in an aquarium filled with filtered recirculated seawater from Narragansett Bay. Salinity was measured before each experiment and ranged between 29‰ and 34‰. Water was replaced or added as necessary to maintain salinities within this range. The experimental tank was kept between 18° and 20°C by a Frigid Units AE-234 AG-602 chiller. The experimental setup consisted of an open-ended tank (1.0 m L × 0.3 m W × 0.3 m H) emersed into a larger main tank (2.2 m L × 0.75 m W × 0.91 m H). The layout was designed so that a threatening stimulus could be introduced at the open end of the experimental tank. A weighted wooden partition with a pulley acted as a blind (and a separation from the main tank) at the open end (Fig. 1A). To ensure that lobsters were initially at the closed, non-stimulus end, a light was placed at the open end. The partition was raised once the lobster had reached the closed end, while the light was moved to the closed, non-stimulus end. This served to 'push' the animal back towards the open (stimulus) end. A piece of PVC tubing (0.15 m L × 0.10 m W) weighted with pebbles to a total weight of 1.45 kg served as the threatening visual stimulus. The stimulus was raised above the open end of the tank as depicted in Figure 1A. The stimulus was released into the water at a preset distance of 10 cm (measured from the open edge of the tank to the lobster) whenever a lobster approached the open end. In a second set of experiments, a larger stimulus of PVC tubing (0.30 m L × 0.20 m W, weighing 2.45 kg) was used on an additional set of gravid lobsters.

Cameras were placed in two positions (a Sony camcorder above the tank and a Panasonic WV-CD20 camera to the side) and experiments were recorded (Panasonic AG-6010 and Panasonic NV-8950) simultaneously from the horizontal and vertical perspectives. Video recordings of each lobster were analyzed frame-by-frame. For measurements of distance traveled, a metric grid divided into 0.5-cm units was painted onto the side of the experimental tank. Transparent overlays on the video monitor were later used to record escape swimming distance of each animal. Distance traveled along the length of the tank was measured by using the position of the tip of the lobster's rostrum as a guide. The number of tailflips was counted. Time was automatically recorded on the videotape. An independent observer inspected all recordings and rejected runs in which the experimental parameters were not strictly adhered to; *e.g.*, cases in which the stimulus was released closer than 10 cm to the experimental animal.

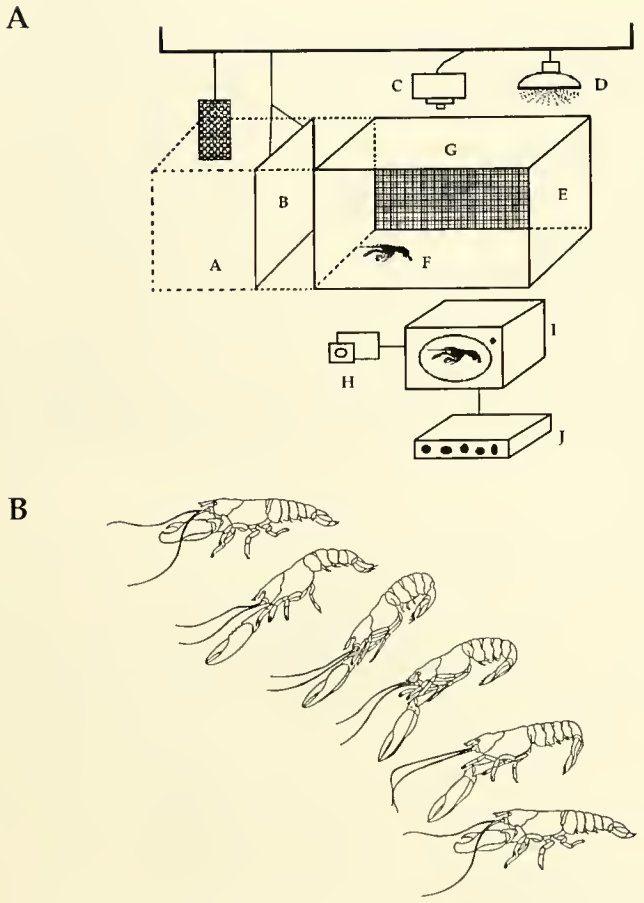

Figure 1. (A) Diagram of the experimental tank (E). The stimulus was a piece of PVC tubing weighted with pebbles (A); the partition (B) was lifted while the lobster (F) was at the opposite end of the tank. A light served as the mechanism to "push" the animal to the open end, and the stimulus was released when the lobster was within 10 cm of the edge of the open end. The escape reaction of each lobster was photographed against a grid (G) with divisions of 0.5 cm. The recording system consisted of two cameras, one vertical (C) and one horizontal (H); monitor (I); and time-lapse VCR (J). (B) Schematic breakdown of a single tailflip as it was seen in the video analysis (original drawings done by K. Davignon, Graphics specialist, URI).

After each experiment, the animal's molt stage was determined by examining cuticular changes and setal development in the pleopods (Aiken, 1973, 1980). Only stage C (intermolt) animals were used, since the probability of escape depends on the molt stage of the lobster (Cromarty *et al.*, 1991; Cromarty *et al.*, 1995). Measurements of carapace length, cutter length, lobster weight and volume, temperature, and salinity were recorded at the end of each experimental trial. Gravid lobsters were difficult to obtain; thus, to ensure that equal numbers of animals were tested in each sex class (males, non-gravid females, gravid females), only 10 lobsters in each class (total $n = 30$) were chosen for stimulus trials. Only one gravid lobster escaped in the first set of experiments, so an additional 10 gravid females were used in a second set of experiments with a larger stimulus. Abdominal width was not measured in the original experiments, but this measurement was later made on an additional 16 animals of each sex whose weights were equivalent to those of the original specimens.

Analysis of the escape response follows the methods used in our earlier analysis of escape behavior in juveniles (Cromarty *et al.*, 1991). The response was broken into two elements—the initial tailflip, henceforth designated as the "power swim," and the many subsequent tailflips, designated as "subsequent swims." The number of subsequent swims in this study ranged from one to three. A tailflip, or swim, is defined as beginning immediately after the start of abdominal flexion and ending at abdominal extension (Fig. 1B). The following characteristics of the escape response were analyzed for each lobster: distance traveled (centimeters), number of tailflips, duration of the response (seconds), frequency of tailflips (tailflips/second), velocity (meters/second), acceleration (meters per second squared), force (mass × acceleration), work (force × distance), distance traveled per unit of weight per tailflip (meters/kilogram/number of tailflips), distance traveled per unit of weight (meters/kilogram), and distance per lobster body length (dimensionless). The latter two parameters were calculated to determine whether variability in the weight and size of individual lobsters altered the relative significance of a parameter, even though the mean values were not significantly different among all three classes of experimental animals.

In evaluating acceleration, the added-mass forces (Batchelor, 1967) that act on accelerating bodies in fluids were ignored since these are a multiple of mass and would act equally on all animals of the same weight. Another variable which we did not include in our calculations was body rotation. Body rotation during swimming was slight in our experiments and not measurable by our methods. Animals whose gross swimming pattern deviated from a rectilinear motion were not included in the analysis. (The analysis of the escape response is meant to reflect relative changes in lobster escape behavior and not kinematic relationships such as those investigated by other researchers [Batchelor, 1967; Daniel and Meyhöfer, 1989; Nauen and Shadwick 1992].)

Each of the escape parameters was analyzed for (1) the entire escape response, (2) the initial power swim, (3) the subsequent swims over the entire subsequent swimming distance, and (4) the subsequent swims in each half of that distance, since earlier experiments showed that there were differences in the distance traveled by lobsters. We therefore divided the distance traveled in the subsequent

swims by half and analyzed each half (Cromarty *et al.*, 1991). Because the distance was divided equally in half for each escape sequence for each animal, no data were available to compare distance traveled between the two halves of the subsequent swims for male and non-gravid lobsters.

Statistical analysis

Differences in weight, carapace length, and cutter length among the three sex classes were determined by parametric analysis of variance (ANOVA). In the additional set of measured lobsters (16 of each sex), abdominal width, carapace length, and weight were analyzed with parametric ANOVA. The Fisher exact probability test (FEP) was used to determine differences in the probabilities of escape between the three sex classes.

A separate Kruskal-Wallis test (KW) was run for each escape parameter (except the subsequent swims). The first and second halves of the subsequent swims were compared with an ANOVA and a one-way repeated measures follow-up test (Keppel, 1982). ANOVAs were run on SPSS software (SPSS Inc., Chicago). Values were considered significant at $P \leq 0.05$ for all the statistical tests.

Results

Weight (in grams), carapace length (in millimeters), cutter length (in millimeters)

There were no significant differences in the weights (mean ± SEM for all) of gravid (464 ± 17.3), non-gravid (452 ± 9.3), and male (464 ± 30.1) lobsters (ANOVA, $F(2, 27) = 0.15$, $P = 0.86$). No significant differences were found in the carapace lengths of gravid (79 ± 0.6), non-gravid (80 ± 1), and male (82 ± 2) lobsters (ANOVA, $F(2, 27) = 0.80$, $P = 0.45$), and similarly there were no significant differences in the cutter lengths of gravid (109 ± 3), non-gravid (110 ± 1), and male (113 ± 3) lobsters (ANOVA, $F(2, 27) = 0.92$, $P = 0.41$).

Abdominal width (in millimeters)

In the set of data collected to determine if there were differences in abdominal width between the sexes, we first needed to demonstrate that these lobsters were similar in weight and size (carapace length) to those used in the escape behavior experiments.

No differences were found between the weights (mean ± SEM, in grams) of the measured females (461 ± 9.4; $n = 16$) and the experimental females (460 ± 9.5; $n = 20$); ANOVA, $F(1, 34) = 0.11$, $P = 0.92$. Similarly, no differences were found in the weights of the measured males (421 ± 18.9; $n = 16$) and the experimental males (464 ± 30.1; $n = 10$); ANOVA, $F(1, 24) = 1.81$, $P = 0.19$. Furthermore, there were no differences in carapace length (mean ± SEM, in millimeters)—male or female—between the two groups. Females: measured (79.6 ± 0.5; $n = 16$) *versus* experimental (79.7 ± 0.6; $n = 20$); ANOVA, $F(1, 34) = 0.003$, $P = 0.95$. Male: measured (77.9 ± 1.3; $n = 16$) *versus* experimental (82.0 ± 2.0; $n = 10$); ANOVA, $F(1, 24) = 2.72$, $P = 0.11$. Therefore, abdominal widths from this data set were analyzed and are assumed to reflect the abdominal widths of the animals that were used in the experiments on escape behavior.

In this data set, significant differences in abdominal width were found between male (42.93 ± 0.52) and female (53.38 ± 0.97) lobsters (ANOVA, $F(1, 30) = 89.33$, $P = 0.0001$), suggesting that a similar sexual dimorphism also existed in the experimental escape animals.

Escape behavior in response to a threatening stimulus

The probability of responding to a threat with an escape response was unequal among the three sex classes (Table 1). Gravid female lobsters were significantly less likely to escape than either males (Fisher exact probability test, FEP, $P < 0.0004$) or non-gravid females (FEP, $P < 0.0001$) when presented with a stimulus (0.30 m L × 0.15 m W) weighing 1.45 kg. No gravid lobsters escaped when presented with this stimulus. Eight of ten males and five of ten non-gravid females tailflipped when presented with this stimulus. The difference was not significantly different (FEP, $P = 0.17$).

When 10 gravid females were presented with a larger and heavier stimulus (0.30 m L × 0.15 m W), weighing 2.45 kg, only one gravid animal tailflipped. This female traveled approximately 80 cm, tailflipping six times with a large loss of eggs. The larger stimulus was not presented to males or non-gravid females since the smaller stimulus was sufficient to initiate their escape behavior.

Table I

Escape and post-threat behavior of each sex class after the small escape stimulus was presented (ten lobsters in each class were tested)

	Immediate response	Secondary responses		
Sex class	Tailflip*	Back up	Approach	Approach and attack
Gravid females	0	6	4	4
Non-gravid females	5	3	7	4
Males	8	5	5	4

* Some lobsters initially tailflipped and then reapproached and/or attacked the stimulus.

Post-stimulus behavior

After the stimulus was presented, lobsters would either (1) tailflip away from the stimulus, (2) tailflip first and then continue backing slowly away, (3) tailflip first and then approach, (4) tailflip, and then approach and attack. "Approach" is distinguished from "approach and attack" by the absence of any physical contact on the part of the lobster and might just as well be due to curiosity as to agonistic causes, unlike "approach and attack," which clearly suggests agonistic responses. For example, four lobsters in each of the three sex classes (that had originally tailflipped), immediately returned, approached and attacked the stimulus (Table I).

Post-threat behaviors were evaluated by Fisher exact probability tests (2×2 contingency tables). No significant differences were found in post-threat behavior among the three sex classes. All probability values were greater than $P = 0.15$, regardless of whether the comparisons were between gravid and non-gravid females, gravid females and males, or non-gravid female and males.

Escape parameters for male and non-gravid adult lobsters

Only non-gravid females and males were compared because only one gravid female could be induced to tailflip.

Total escape response (initial power swim plus subsequent swims). Total distance traveled during an escape, number of tailflips, swimming velocity, acceleration, force, work, distance traveled per kilogram of weight,

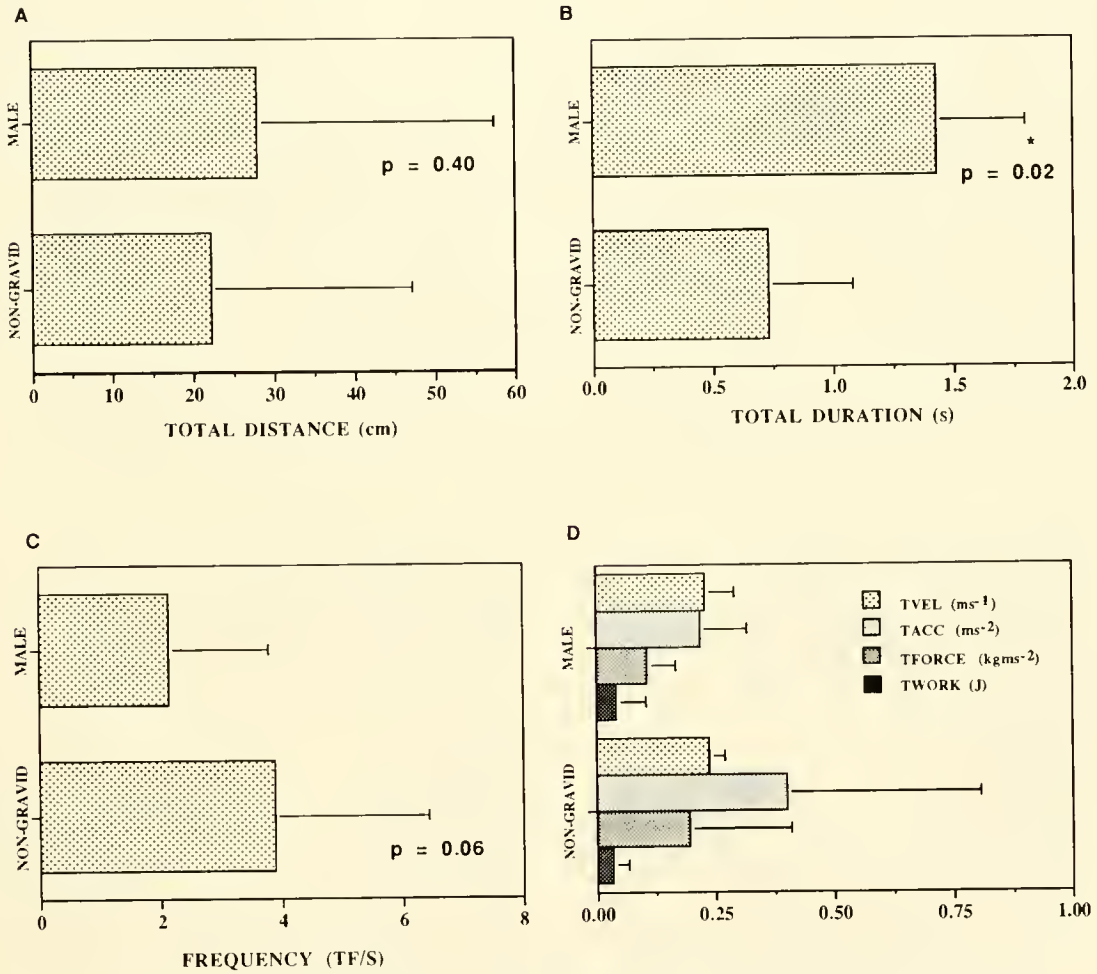

Figure 2. Comparison of parameters (mean ± SD) of the entire escape response for male ($n = 8$) and non-gravid female ($n = 5$) lobsters. An asterisk (*) indicates significant differences at $P \leq 0.05$. (A) Distance traveled in centimeters (cm). (B) Duration of swimming sequence in seconds (s). (C) Frequency (TF/s). (D) TVEL = total velocity (m/s); TACC = total acceleration (m/s^2); TFORCE = total force (newtons [$kg/(m/s^2)$]); and TWORK = total work (joules [force × distance]).

and distance traveled per lobster body length were not significantly different (KW, $P > 0.05$; see Fig. 2A and 2D for examples). The total time spent escaping was, however, significantly greater for male lobsters (KW, $P = 0.02$, Fig. 2B). Distance traveled per kilogram of weight per tailflip was not significantly different (KW, $P = 0.40$). Although the difference was not significant at the 0.05 level, non-gravid females may perform more tailflips per second than male lobsters (KW, $P = 0.06$, Fig. 2C).

Initial power swim. Distance traveled was significantly higher for males than for non-gravid females (KW, $P = 0.04$; Fig. 3A). Although males tended to have longer power swim durations, the difference was not significantly different at the $P = 0.05$ level (KW, $P = 0.08$, Fig. 3B). Distance swum per body length and distance swum per kilogram of weight were also both significantly greater for males (KWs, $P = 0.03$ and 0.05 respectively). Although the mean values for power swim velocity, acceleration, force, and work all were higher for male lobsters, the differences were not significant, because of the large variance within each class.

Total subsequent swims. The time spent in subsequent swims and the number of tailflips were significantly higher for male lobsters than for non-gravid females (KWs, $P = 0.04$ and 0.03, Fig. 3C and D respectively). Distance swum per body length and distance swum per kilogram of weight for the subsequent swims were also statistically higher for males (KWs, $P = 0.01$ and 0.02 respectively). No other parameters were found to be statistically different for the total subsequent swims.

Comparison of SS1 and SS2 between and within sex classes. In the first half of the subsequent swims (SS1),

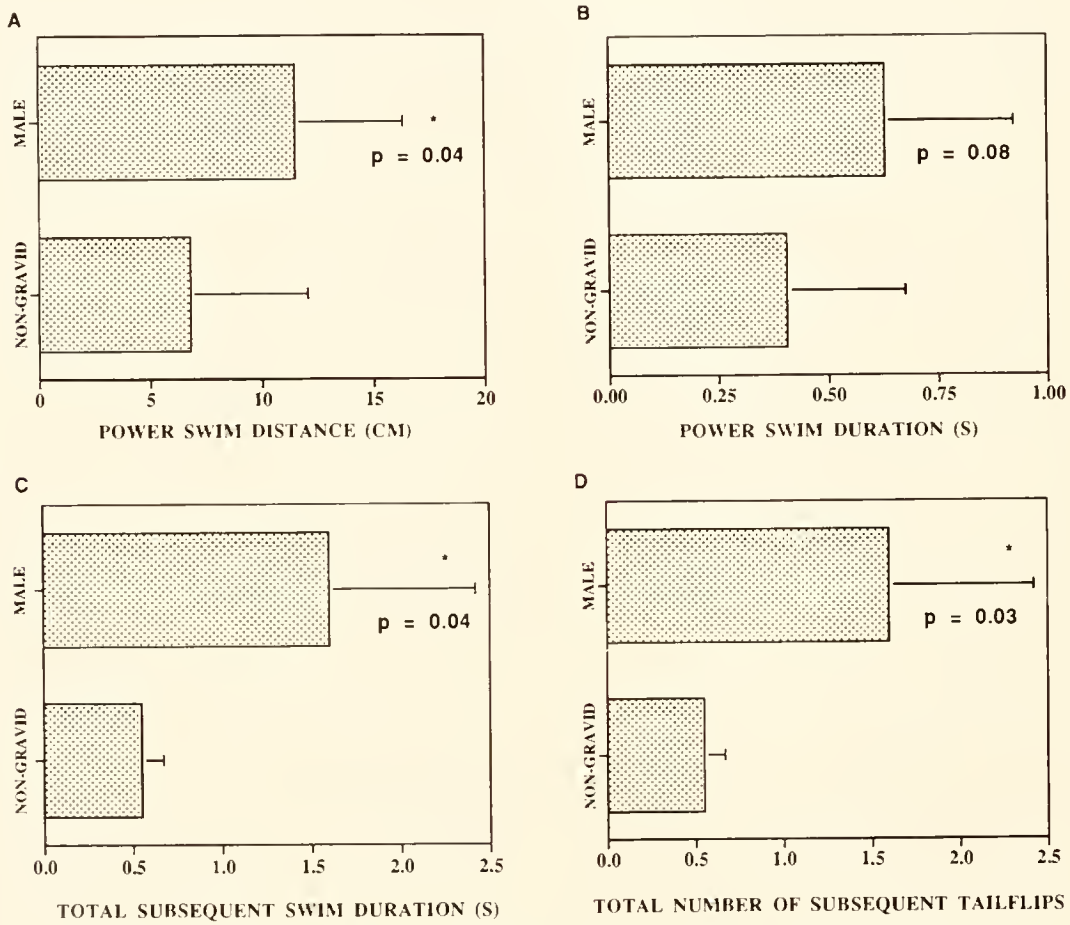

Figure 3. Comparison of parameters (mean ± SD) of the power swim and total subsequent swims for male ($n = 8$) and non-gravid female ($n = 5$) lobsters. An asterisk (*) indicates that the results are significantly different at $P \leq 0.05$. (A) Distance traveled during the power swim in centimeters (cm). (B) Time spent escaping during the power swim in seconds (s). (C) Duration of swimming sequence during the total subsequent swims in seconds (s). (D) Number of tailflips during the total subsequent swims in centimeters (cm).

male lobsters spent more time escaping (duration) and produced more tailflips (KWs; $P = 0.05$ and 0.03, Fig. 4A and C respectively). Similar differences were found in the second half of the subsequent swims (SS2), with males again spending more time escaping and taking more tailflips (KWs, $P = 0.04$ and 0.04, Fig. 4B and D respectively). When SS1 and SS2 were compared to each other, for each sex, no significant differences were observed. There was no reduction in any of the parameters between the first and second halves of the subsequent swims for either males or females. No other parameters, either of total subsequent swims or within SS1 or SS2, were statistically different.

Discussion

Among crustaceans, there are four major morphological and physiological determinants that affect agonistic and escape behavior: age, size, molt-stage, and sex. Thus, large adults are more likely to win in aggressive encounters (Scrivener, 1971) and are dominant over smaller juveniles (Atema and Cobb, 1980); and soft-shelled premolt animals win over soft-shelled postmolt animals (Tamm and Cobb, 1978). In avoidance or escape behavior, small juveniles swim faster and farther than large adults, which tend not to respond to a threat with escape swimming (Cromarty *et al.*, 1995). In addition, soft-shelled juveniles swim faster and farther than hard-shelled juveniles (Cromarty *et al.*, 1991), but hard-shelled adults swim farther than soft-shelled ones (Cromarty *et al.*, 1995).

In this study we have shown that males and non-gravid females are equally likely to initiate escape swimming when threatened. The probability of eliciting escape behavior in gravid females is, however, significantly lower. These animals, like large adult males (>600 g), are essentially inhibited from swimming, even when presented

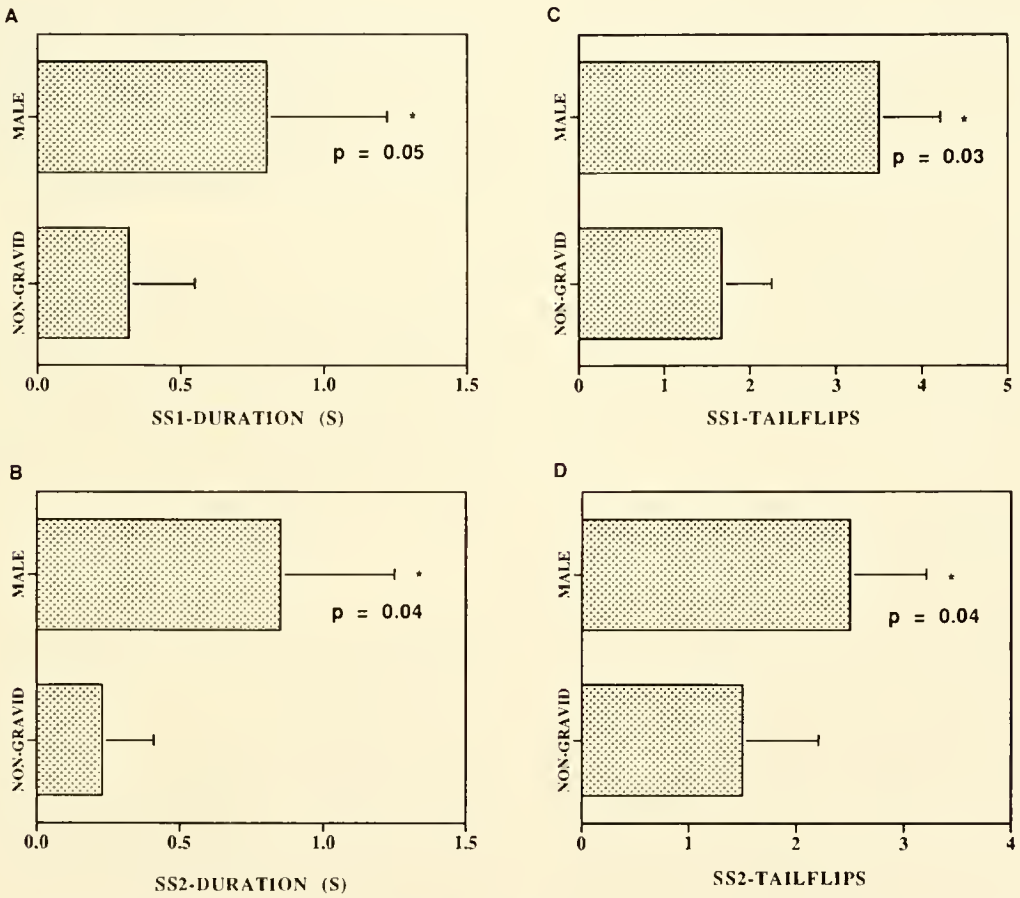

Figure 4. Comparison of parameters (mean ± SD) of the first (SS1) and second (SS2) halves of subsequent swims for male ($n = 8$) and non-gravid female ($n = 5$) lobsters. An asterisk (*) indicates these results are significantly different at $P \leq 0.05$. (A, B) Duration, in seconds (s), of swimming sequence during SS1 (A) and SS2 (B). (C, D) Number of tailflips during SS1 (C) and SS2 (D).

with larger stimuli (see Cromarty *et al.*, 1997). The physiological bases for these inhibitions are not yet known and may or may not be due to the same physiological mechanisms; these could involve inhibition of (a) sensory input to the central nervous system (Watson, 1992, for a review) or (b) neurons within the central nervous system (Beall *et al.*, 1990), or at peripheral synapses (Schwanke *et al.*, 1990; Cromarty *et al.*, 1995; Cromarty and Kass-Simon, 1996), or in both locations.

Although the same physiology may ultimately be involved in both cases, the adaptive significance in each instance appears to be different. In the case of the adult male lobsters, the large size of the claws could make escape swimming more difficult (Lang *et al.*, 1977), but would increase the odds of a favorable outcome in confrontations with a predator or conspecific opponent. In the case of the ovigerous females, escape swimming would have a deleterious effect. The single gravid female that responded to a threat with swimming lost many eggs, underscoring the idea that in this case, swimming inhibition evolved to ensure reproductive success.

Differences in the characteristics of escape behavior between non-gravid females and males are more subtle. Although the total distance that each group swam did not prove to be different, males covered more ground than did non-gravid females, both in the single initial power swim and in the sum of the subsequent swims. This suggests that, like the molt-related differential effects on the power swim and subsequent swims found in juvenile lobsters (Cromarty *et al.*, 1991), sex-related differential effects on the neuronal pathway appear to be mediating the two components of the escape swimming. It thus appears that, as in crayfish (Wine and Krasne, 1972), in lobster, escape behavior is most likely mediated by both giant (initial power swim) and non-giant fibers (subsequent swims).

Male lobsters appeared to outperform females in several other parameters. On average, they swam for a significantly longer time by performing more tailflips than non-gravid females. They also covered a greater distance relative to their body length and weight than females, in both the initial power swim and in the sum of the subsequent swims. Females, on the other hand, may have compensated by swimming at a higher frequency than males. Since the weight averages for all groups were not statistically different, these performance differences may reflect differences in body architecture, muscle properties (composition or physiology), titers of circulating neurohumors, or a combination of these factors. The broader females (see results) would experience more drag, so that the distance covered for each body length would be reduced; males, on the other hand, might have greater abdominal strength and thus be more efficient swimmers. Moreover, since males have higher circulating concentrations of putative excitatory neurohormones (Fadool *et al.*, 1989), their actions might enhance central or peripheral synapses (Kravitz, 1988, for review; Schwanke *et al.*, 1990). In this regard, although our experiments were run on isolated individuals, it should be noted that in crayfish (Yeh *et al.*, 1996), the lateral giant neuron, which is responsible for escape responses elicited by tactile or mechanical deflection of the telson, is affected by the animal's social experience, with dominant animals having an enhanced response to stimuli.

However, although there may be subtle sex-related differences in the characteristics of escape swimming, significant differences between the two sexes were absent not only in the total distance swum, but also in the velocity or acceleration of the swim, and in the calculated force or work performed. Our relatively small sample size may preclude a definitive conclusion about sexual differences in escape behavior. A larger sample size, or an analysis of additional escape parameters, might reveal differences between the sexes, given that there are inherent sexual abdominal dimorphisms.

It remains to be seen, therefore, whether the anatomical and physiological sexual differences that result in more and longer tailflips in males, but perhaps a higher frequency of swimming in females, have any effect on the relative chances of the sexes for survival.

Acknowledgments

We thank Kathy Castro of the University of Rhode Island Fisheries Department for her assistance in collecting lobsters and measuring their abdomens. We also thank Dr. Michael Clancy and Malia Schwartz for critiquing an earlier draft of the manuscript. This research was supported by a Whitehall Foundation grant to G.K.S., and Sigma Xi and Lerner Gray grants to S.I.C.

Literature Cited

Aiken, D. E. 1973. Proecdysis, setal development, and molt prediction in the American lobster (*Homarus americanus*). *J. Fish. Res. Board Can.* **30:** 1334–1337.

Aiken, D. E. 1980. Molting and growth. Pp. 91–163 in *The Biology and Management of Lobsters*, vol. 1, J. S. Cobb and B. F. Phillips, eds. Academic Press, New York.

Atema, J., and J. S. Cobb. 1980. Social behavior. Pp. 409–450 in *The Biology and Management of Lobsters*, vol. 1, J. S. Cobb and B. F. Phillips, eds. Academic Press, New York.

Atema, J., and R. Voigt. 1995. Behavior and sensory biology. Pp. 313–348 in *The Biology of the Lobster*, Homarus americanus, J. Factor, ed. Academic Press, New York.

Atema, J., S. Jacobsen, E. Karnofsky, S. Olesko-Szuts, and L. Stein. 1979. Pair formation in the lobster, *Homarus americanus:* behavioral development, and mating. *Mar. Behav. Physiol.* **6:** 277–296.

Batchelor, G. K. 1967. *An Introduction to Fluid Dynamics.* Cambridge University Press, London.

Beall, S. P., D. J. Langley, and D. H. Edwards. 1990. Inhibition of escape tailflip in crayfish during backward walking and the defense posture. *J. Exp. Biol.* **152:** 577–582.

Cromarty, S. I., and G. Kass-Simon. 1996. Electrophysiological correlates of the escape response in the adult American lobster (*Homarus americanus*) over the molt cycle. *Soc. Neurosci. Abstr.* **26:** 440.

Cromarty, S. I., J. S. Cobb, and G. Kass-Simon. 1991. Behavioral analysis of the escape response in juvenile American lobsters, *Homarus americanus* over the molt cycle. *J. Exp. Biol.* **158:** 565–581.

Cromarty, S. I., J. S. Cobb, and G. Kass-Simon. 1995. Adult and juvenile lobsters (*Homarus americanus*), differ markedly in the neuromuscular physiology and behavior of the escape response over the molt cycle. *Soc. Neurosci. Abstr.* **25:** 201.

Daniel, T. L., and E. Meyhöfer. 1989. Size limits in escape locomotion of carridean shrimp. *J. Exp. Biol.* **143:** 245–265.

Fadool, D. A., P. R. Brown, J. S. Cobb, and G. Kass-Simon. 1989. HPLC analysis of lobster haemolymph over the molt cycle. *Comp. Biochem. Physiol.* **93C:** 225–230.

Keppel, G. 1982. *Design and Analysis: A Researcher's Handbook,* 2nd Ed. Prentice Hall, Englewood Cliffs, New Jersey.

Kravitz, E. A. 1988. Hormonal control of behavior: amines and the biasing of behavioral output in lobsters. *Science* **241:** 1775–1782.

Lang, F., C. K. Govind, W. J. Costello, and S. I. Greene. 1977. Developmental neuroethology: changes in escape and defensive behavior during growth of the lobster. *Science* **197:** 682–684.

Lnenicka, G. A., and Y. Zhao. 1991. Seasonal differences in the physiology and morphology of crayfish motor terminals. *J. Neurobiol.* **22:** 561–569.

McLeese, D. W., and D. G. Wilder. 1964. Lobster storage and shipment. *Bull. Fish. Res. Board Can.* No. 147. 69 pp.

Nauen, J. C., and R. E. Shadwick. 1992. Biomechanics of tail-flipping by the spiny lobster *Panulirus interruptus. Am. Zool.* **32:** 127A.

Schwanke, M. L., J. S. Cobb, and G. Kass-Simon. 1990. Synaptic plasticity and humoral modulation of neuromuscular transmission in the lobster claw opener during the molt cycle. *Comp. Biochem. Physiol.* **97C:** 143–149.

Scrivener, J. C. E. 1971. Agonistic behavior of the American lobster, *Homarus americanus* (Milne-Edwards). *Fish. Res. Board. Can. Tech. Rep.* **235:** 1–128.

Stein, R. A. 1976. Sexual dimorphism in crayfish chelae: functional significance linked to reproductive activities. *Can. J. Zool.* **54:** 220–227.

Tamm, G. R., and J. S. Cobb. 1978. Behavior and the crustacean molt cycle: changes in aggression of *Homarus americanus. Science* **200:** 79–81.

Templeman, W. 1935. Local differences in the body proportions of the lobster *Homarus americanus. J. Biol. Board Can.* **2:** 223–226.

Waddy, S. L., and D. E. Aiken. 1991. Mating and insemination in the American lobster, *Homarus americanus.* Pp. 126–144 in *Crustacean Sexual Biology,* R. T. Bauer and J. W. Martin, eds. Columbia University Press, New York.

Watson, A. H. D. 1992. Presynaptic modulation of sensory afferents in the invertebrate and vertebrate nervous system. *Comp. Biochem. Physiol.* **103A:** 227–239.

Wine, J. J., and F. B. Krasne. 1972. The organization of escape behaviour in the crayfish. *J. Exp. Biol.* **56:** 1–18.

Yeh, S.-R., R. A. Fricke, and D. H. Edwards. 1996. The effect of social experience on serotonergic modulation of the escape circuit of crayfish. *Science* **271:** 366–369.

Reference: *Biol. Bull.* **194:** 72–82. (February, 1998)

Neural Control of the Lateral Abdominal Arterial Valves in the Lobster *Homarus americanus*

GLEN W. DAVIDSON[1], JERREL L. WILKENS[2,*], AND PETER LOVELL[2]

[1] *School of Biomedical Sciences, Curtin University of Technology, GPO Box 1987, Perth, Western Australia; and* [2] *Department of Biological Sciences, University of Calgary, 2500 University Drive N.W., Calgary, Canada T2N 1N4*

Abstract. A dorsal abdominal artery in *Homarus americanus* runs the length of the abdomen, giving rise to one pair of large lateral arteries in each segment. These lateral arteries supply hemolymph to the abdominal muscles and the swimmerets. In addition, many small vessels leave the dorsal abdominal artery ventrolaterally to supply the gut and gonads. Bicuspid muscular valves are located at the junction of each segmental lateral artery with the dorsal abdominal artery, but not at the origin of the gut vessels. Nerves originating from the ventral abdominal ganglia travel along the lateral arteries to innervate the valves, providing both inhibitory and excitatory inputs. Inhibitory input produces hyperpolarizing inhibitory junctional potentials that relax the valve muscles, and in intact *in situ* perfused arteries causes increases in outflow from the affected lateral artery. Excitatory input produces depolarizing excitatory junctional potentials that close the valves and reduce perfusate outflow. The valve nerves also branch to innervate valves up to two segments anterior and one segment posterior. Application of exogenous γ-aminobutyric acid hyperpolarizes valve muscle fibers. This and the hyperpolarizing effect of valve nerve stimulation are reversibly abolished by the application of picrotoxin (10^{-5} *M*). Acetylcholine (10^{-5} *M*), but not glutamate, causes depolarization and contraction of valves. The role of the valves in controlling the distribution of hemolymph flow is discussed.

Received 8 May 1997; accepted 15 October 1997.

* To whom correspondence should be addressed. E-mail: wilkens@acs.ucalgary.ca

Abbreviations: Ach, acetylcholine; DAA, dorsal abdominal artery; EJP, excitatory junction potential; GABA, γ-aminobutyric acid; 5-HT, 5-hydroxytryptamine; IJP, inhibitory junction potential; LAA, segmental lateral abdominal artery; LAAV, lateral abdominal arterial valve.

Introduction

In decapod crustaceans, seven arteries deliver hemolymph from the heart to the systemic circulation. These arteries branch into progressively finer vessels in the tissues until they open into small capillary-sized vessels that are bounded by a thin intima (Martin and Hose, 1995). The smallest vessels are the functional equivalent of vertebrate capillaries, and it is here that exchange of metabolites, gases and ions occurs between the hemolymph and the tissues.

The crustacean circulation is an open system, lacking a tubular venous return to the heart. Instead, "venous" hemolymph collects into progressively larger sinuses and is returned to the heart *via* the gills. Despite very early observations on the anatomy and innervation of various flow-rectifying structures, such as cardioarterial (CA) and segmental lateral arterial valves of the dorsal abdominal artery (Alexandrowicz, 1932a), the control of hemolymph circulation in crustaceans has been poorly understood until recently. Inhibitory innervation of the sternal CA valve in *Homarus americanus* causes valve relaxation and increased outflow in this artery (Kuramoto *et al.*, 1992, 1995). The 11 CA valves in the isopod *Bathynomus doederleini* receive varying patterns of innervation (Kihara *et al.*, 1985), and the activity of the inhibitory nerve to the CA valve of the artery supplying hemolymph to the swimmerets is coordinated with the activity of the swimmerets themselves (Fujiwara-Tsukamoto *et al.*, 1992).

Changes in regional blood flow have been measured in intact *Cancer magister* using ultrasonic techniques (Airriess and McMahon, 1994, 1996; McGaw *et al.*, 1994). During hypoxia, hemolymph is diverted away from the viscera and brain and toward the locomotory and ventilatory appendages. Injection of dopamine into intact nor-

moxic *C. magister* produces a similar response, suggesting hormonal control of hemolymph distribution. However, the sites of regulation of hemolymph flow distribution were not identified in these animals. In *H. americanus,* a number of neurotransmitters and hormones, with peptides being the most effective, have been shown to alter the peripheral resistances of *in situ* perfused arterial trees (Wilkens, 1997). Two possible mechanisms for regulation of regional blood flow in decapods exist: (1) the centrally located muscular CA valves may differentially regulate blood flow in arteries leaving the heart, as seen in *B. doederleini* and *Panulirus japonicus* (Kuramoto and Ebara, 1984, 1989), and (2) the relative resistances of arterial pathways may be altered by peripheral mechanisms.

How can the peripheral resistance of arteries be controlled? Unlike the blood vessels of vertebrates, the walls of all crustacean arteries, except the dorsal abdominal artery (DAA), lack muscle layers. A layer of striated muscle fibers has been found in the DAA of a number of macruran species including *H. americanus* (Burnett, 1984; Martin *et al.,* 1989; Wilkens *et al.,* 1997a). Since hormones and nervous inputs cannot act directly on vessels that lack muscular walls, other mechanisms for controlling arterial resistance and regional hemolymph flow must exist. Muscular arterial valves have been identified at the junction of each lateral abdominal artery (LAA) with the DAA in *Panulirus interruptus* (Alexandrowicz, 1932a). In decapod crustaceans, the DAA supplies blood to the abdominal positioning muscles and swimmeret muscles via the LAAs, and to the gut through many small arterioles that arise from the ventral wall of the DAA. The lateral abdominal arterial valves (LAAV) may be the sites where the distribution of hemolymph is differentially regulated between the locomotory and vegetative organs. This paper investigates the role of the LAAVs in controlling hemolymph flow in this part of the circulation in *H. americanus.*

Materials and Methods

Lobsters (approximately 500 g) were purchased from a commercial supplier and maintained in a recirculating seawater system at 12°C prior to experimentation. Animals were fed frozen smelt twice weekly. Data presented here are based on observations taken from 12 animals.

In preparation for surgery, lobsters were restrained with elastic bands and cold-anesthetized by burial in crushed ice in an acrylic plastic box (50 × 20 × 20 cm) for 20 to 30 min. While a lobster was still buried in ice, its hemolymph was replaced by saline (Cole, 1941, pH = 7.6). To exsanguinate an animal, the heart was exposed by removing the overlying dorsal carapace and dermis. Ice-chilled saline was pumped through a polyethylene cannula, tipped with a 21-gauge needle, directly into the ventricle *via* an ostium. The heart continued to pump slowly, and hemolymph returning to the pericardium was allowed to escape into the container. Perfusion was continued until all traces of hemolymph were removed. Following exsanguination, the ice was replaced with artificial seawater at 12°C. The dorsal cuticle was removed from each abdominal segment and the DAA and proximal sections of each LAA were exposed by dissecting away the dermis and superficial abdominal positioning muscles.

In situ *preparations*

The DAA was cannulated *in situ* at a point close to the bulbus arteriosis with polyethylene tubing (PE 160), and the cannula was secured with surgical silk. A peristaltic pump was used to perfuse the artery with saline at a flow rate of 1.5–2.5 ml min^{-1}. To measure pressure in the DAA, a small transverse incision was made in the dorsal wall of the artery, posterior to the branching point of the third pair of LAAs. A saline-filled polyethylene cannula (PE 160), previously heated and drawn to about one-third of the arterial diameter, was inserted through the slit and secured with surgical silk. This cannula was connected to a Hewlett-Packard pressure transducer (267BC) and amplifier (311A). All of the LAAs except one were tied off with surgical silk. A small incision was made in the dorsal wall of the LAA remaining patent. A short length of polyethylene cannula drawn to a taper and connected to an ultrasonic flow transducer (Transonics, 1 mm i.d.) was inserted into the LAA through the incision and secured with surgical silk. The flow probe was then connected to a Transonics (T106) flow meter.

The effects of stimulating the nerves to the valve of the patent LAA and of various test compounds on LAA flow and DAA luminal pressure were measured. The LAAV nerves were stimulated as described below. To apply drugs, the perfusate (2.0 ml min^{-1}) was switched from saline to one containing the desired compound. After application of a drug, the preparation was perfused with regular saline until all variables had recovered to pretreatment levels. The drugs tested were acetylcholine (ACh), γ-aminobutyric acid (GABA), 5-hydroxytryptamine (5-HT) and picrotoxin (Sigma).

In vitro *preparations*

Following exsanguination, the DAA was separated from the underlying gut and gonads by cutting the fine arterioles that arise from its ventrolateral surface to supply these organs. Each lateral artery was cut 0.5–1.0 cm from its junction with the DAA. The DAA with attached proximal sections of the LAAs was placed in an acrylic tissue bath (volume 15 ml) lined with Sylgard and filled with aerated saline at 12°–15°C. The vessel was cannulated

anteriorly using a polyethylene cannula as described above and flushed by pumping saline at a flow rate of 4–5 ml min^{-1}. Next, the artery was secured by micropins placed in the severed ends of the LAAs, the cannula was removed, and the DAA was opened longitudinally by cutting along the dorsal midline. The DAA was pinned open with the luminal surface uppermost, exposing the valves (see Fig. 1).

The LAAV nerves were stimulated using a glass suction electrode (tip diameter 50 μm) and a Grass S48 stimulator. Trains of impulses (1-ms duration) were applied to the nerve at varying frequencies (1–80 Hz). Fluctuations produced in the membrane potential of individual valve muscle fibers by nerve stimulation were recorded intracellularly. Glass microelectrodes (tip resistance 15–25 MΩ) were pulled from thin-walled borosilicate glass tubing. These were filled with 3 *M* KCl and connected to a WPI M4-A electrometer. Signals from the electrometer were displayed on a Tektronix 5103N oscilloscope and recorded on a Vetter 420L four-channel video recording system. Hard copy was printed with a Gould 2400 chart recorder. Between recordings, the vessel was superfused at a flow rate of 2.5 ml min^{-1} with chilled saline to maintain the bath temperature between 12° and 15°C.

The effects of various drugs on the membrane potential of valve muscle were tested by direct application to the bath over an exposed valve. Prior to testing, all solutions (drug in saline) were maintained at the same temperature as the bath. In random order, 0.5 ml of each solution was applied with a pasteur pipette. The bath was perfused with fresh, aerated saline after each drug.

Morphology

The orientation of LAAV muscle bundles and the innervation of the valves were examined using a Wild M-5 stereomicroscope. Nerve tissue was stained for 24–48 h at 4°C with methylene blue (10 drops of 0.1% stock added to 100 ml of saline). Fading of the stain upon exposure to light was prevented by placing tissue samples in 4% ammonium molybdate in saline at 4°C for 1 h prior to examination.

Results

Morphology

The DAA originates from the posterior wall of the bulbus arteriosus of the heart and passes along the dorsal midline of the abdomen. The diameter of the vessel decreases posteriorly. Within each of the first five anterior

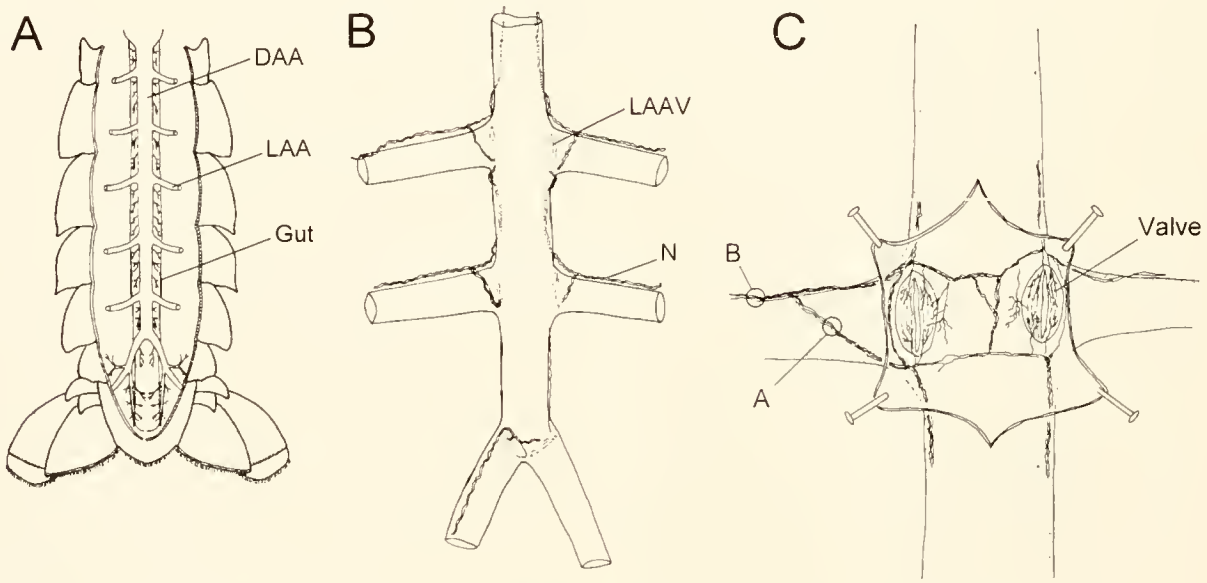

Figure 1. (A) Dorsal view of the dorsal abdominal vasculature in *Homarus americanus*. The dorsal abdominal aorta (DAA) lies along the dorsal surface of the hindgut (Gut). Within each of the first five abdominal segments, a pair of lateral abdominal arteries (LAA) branch off the DAA at roughly right angles. The bifurcating pair of arteries at the posterior margin of the fifth segment are homologous to the more anterior LAAs. (B) The innervation patterns of the LAA valves. The valve nerves (N) approach each valve in connective tissue along the anterior edge of each LAA. (C) A dorsal view of the junction of one pair of segmental lateral abdominal arteries with the dorsal abdominal aorta. The dorsal wall of the DAA has been cut longitudinally and the flaps have been pinned back to reveal the lateral abdominal artery valves (Valve). A and B indicate the sites of nerve stimulation proximal and distal to the point where the incoming nerve bifurcates.

abdominal somites, a pair of LAAs branch at roughly right angles from the DAA (Fig. 1A). Each LAA extends laterally for a short distance, then descends and arborizes to supply hemolymph to the abdominal muscles and the swimmerets (Wilkens *et al.*, 1997b). Branches of the LAAs also supply the gonads. At the posterior margin of the 5th abdominal segment the DAA bifurcates at an acute angle into two smaller arteries that supply the uropods and telson. These two arteries are the modified LAAs of the 6th abdominal segment. A bicuspid muscular valve is situated at the junction of each LAA with the DAA, and also at the junctions of the two posterior arteries with the DAA. The valve muscle fibers lie in an anteroposterior direction, and the valve aperture appears as a horizontal slit. A rich array of very small vessels arises from the ventrolateral wall of the DAA to supply hemolymph to the gut and posterior portions of the gonads. No valves exist at the origins of these gut vessels (Wilkens, 1997).

Segmental nerves, embedded in connective tissue, approach each LAAV along the anterior edge of each LAA. The valve nerves originate from the second root of each abdominal ganglion in the next anterior segment. Methylene blue staining revealed multiple axons in these nerves (Fig. 1B). As the nerve approaches a valve, it bifurcates. One branch continues to follow the anterior edge of the LAA until it reaches a dense cluster of axons at the anterior edge of the valve. The second branch passes posteriorly over the dorsal surface of the LAA to a cluster of axons at the posterior edge of the valve. The distance of the point of bifurcation from the valve was quite variable. In some instances the bifurcation was several millimeters away from the valve, whereas in others it occurred at the junction of the LAA and DAA. Proximal to the bifurcation, both branches appeared to contain three axons (Fig. 1C). Two of the three axons arise from the distal LAAV nerve proper. The third axon, not originating in the LAAV nerve, spans the bifurcation of the other two axons, passing over the dorsal surface of the LAA. The origin and target of this third axon could not be discerned, but it appeared to link the clusters of axons at the anterior and posterior edges of a particular LAAV. The nerves terminate at synapses on the two muscular flaps of each valve anteriorly, posteriorly, and medially. Contralateral valves within each segment were connected by many small axons traversing the ventral luminal wall of the DAA in a "figure eight" fashion (Fig. 1C). The pattern of innervation described for each abdominal segment was bilaterally symmetrical. Ipsilateral valves in adjacent segments were connected by two to four axons running longitudinally along the external ventrolateral wall of the DAA (Fig. 1B). In the first abdominal segment, the LAA nerves supply the LAAVs of this segment and also pass forward along the DAA to terminate on the sternal cardioarterial valve (SCA).

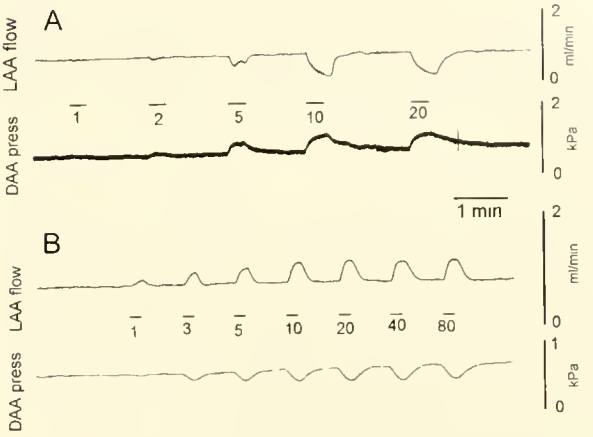

Figure 2. The effect of proximal excitatory (A) and distal inhibitory (B) valve nerve stimulation on LAA flow and DAA pressure in an in situ saline-perfused preparation of the dorsal abdominal vasculature in *Homarus americanus*. The stimulating locations are as shown in Figure 1C. Stimulating frequencies are indicated along each set of records.

The innervation of the two valves located at the posterior bifurcation of the DAA was difficult to visualize, but in one preparation both valves were innervated by a single nerve approaching along the dorsolateral surface of one of the posterior vessels (Fig. 1B), a position homologous to the route of the nerve in the more anterior LAAs.

In situ *preparations*

The valve flaps were clearly visible through the transparent wall of the LAA. Spontaneous rhythmic contractions of LAAVs were frequently observed in saline-perfused arteries. With each contraction, the LAA flow decreased and the luminal pressure in the DAA increased (not illustrated). Conversely, valve relaxation was accompanied by increased LAA flow and a drop in DAA luminal pressure. These pressure fluctuations caused substantial changes in the diameter of the DAA.

Stimulation of the LAAV nerve at a site distal to the bifurcation (site B in Fig. 1C) always resulted in a relaxation of the valve, an increase in flow through that LAA, and a concomitant decrease in DAA lumen pressure (Fig. 2A, typical of 20 observations on six arteries). Stimulation proximal to the bifurcation of the nerve (site A in Fig. 1C) resulted in contraction of the valve, a decrease in LAA flow, and an increase in DAA lumen pressure (Fig. 2B, three arteries). The biphasic change in membrane potential observed during stimulation at A (see Fig. 4C) was not reflected in the LAA flow and DAA pressure responses to stimulation at this site. The maximal change in LAA flow to proximal stimulation occurred at the stimulation frequency of 20 Hz.

Figure 3 demonstrates the effects of the neurotransmitter ACh on flow through the LAA *in situ* ($n = 2$). ACh caused valve closure and a decrease in flow through the LAA.

In vitro *preparations*

The mean resting membrane potential of LAAV muscle fibers was -40 ± 1.7 mV ($n = 12$ fibers from five animals). The effect of LAAV nerve stimulation on the membrane potential of valve muscle fibers is shown in Figure 4. Lateral abdominal arterial valve nerves were stimulated at the two sites marked in Figure 1C: one proximal (site A) and the other distal (site B) to the nerve bifurcation. Stimulation at A did not produce unitary excitatory junction potentials (EJPs), but did produce frequency-dependent summing depolarizations. The rates of onset and recovery of excitatory responses, and their amplitudes, were lower than for inhibitory input. EJPs produced only graded depolarizations; all-or-none action potentials were never observed. EJPs were recorded only in very fresh preparations, with the excitatory response being lost after a short time *in vitro*.

Without exception, stimulation at point B distal to the bifurcation of the LAAV nerve produced inhibitory junction potentials (IJPs) in the muscle fibers of the ipsilateral valve (Fig. 4B, $n = 8$), the contralateral valve in the same segment ($n = 3$), and both the ipsilateral and contralateral valves in the next anterior segment ($n = 6$). IJPs produced at these different sites were usually of similar magnitude. In two preparations, IJPs were also recorded from the contralateral valve two segments anterior. The magnitude of the IJPs in this valve was smaller than in the other four sites (not shown). In one other preparation, IJPs were recorded in the ipsilateral valve one segment posterior. Stimulation of the LAAV nerve at point B in the first abdominal segment produced IJPs in the sternal cardioarterial valve in addition to the ipsilateral and contralateral LAAVs in that segment (not illustrated). In all cases the magnitude of the hyperpolarization at a given site increased with increasing stimulation frequency up to 40–80 Hz, indicating summation of IJPs.

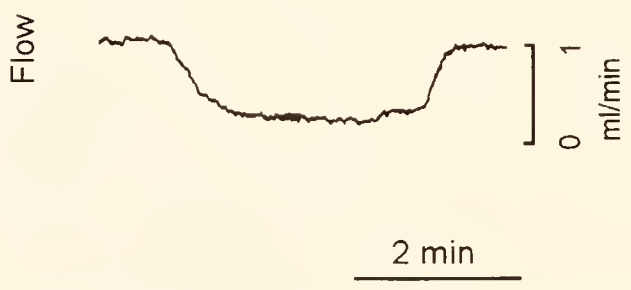

Figure 3. The effect of ACh (10^{-4} *M*) on the flow through a lateral abdominal artery. In this case, 5 ml of test substance was perfused into the abdominal artery at 2 ml min^{-1}, followed by saline.

In one preparation, stimulation at point A produced a biphasic response in the muscle fibers of the ipsilateral valve (Fig. 4C); in five others, stimulation at point B produced biphasic responses. In the illustrated record, low stimulation frequencies (<5 Hz) produced IJPs only. As stimulation frequency increased, the response became biphasic, with progressively shorter periods of hyperpolarization followed by depolarization. In most preparations, maximum depolarization occurred at a stimulating frequency of 40 Hz. In preparations exhibiting biphasic responses, the eventual loss of EJPs left only the IJPs in the ipsilateral and the contralateral valves.

Figure 5 illustrates that valve muscles receive dual inhibitory inputs that show facilitation when repetitively stimulated. These recordings were taken from the valve contralateral to the site of stimulation. A single 8-V stimulus resulted in a 1.5-mV hyperpolarization, while a 9-V stimulus recruited the second inhibitory axon and resulted in a 3-mV hyperpolarization. When stimulated by 8-V twin pulses (time delay between pulses = 170 ms), the first and second IJPs were 2 and 6 mV, respectively. Twin pulse stimulation at 9 V produced hyperpolarizations of 4 and 9.5 mV after the first and second pulses, respectively.

The bath application of a few drops of saline had no effect on membrane potential (Fig. 6A), but the same amount of ACh (10^{-5} *M*) caused a rapid depolarization of muscle fibers, with a gradual repolarization back to the resting membrane potential (Fig. 6B). GABA (10^{-5} *M*) elicited a rapid hyperpolarization of fiber membrane, with a slow recovery back to rest (Fig. 6C). The results shown are consistent with those taken from three animals. The IJPs were blocked by picrotoxin (Fig. 7). Fifty milliliters of 10^{-5} *M* picrotoxin was applied to the bath at a flow rate of 2.5 ml min^{-1} for 20 min, after which superfusion of the bath with saline resumed. Twenty minutes after the first application of picrotoxin, IJP magnitude was greatly reduced, and after 30 min it was virtually eliminated. Twenty minutes after resuming perfusion with fresh saline, IJP magnitude had partially recovered to pretreatment levels.

Spontaneous rhythmic oscillations in membrane potential of up to 28 mV and oscillation periods of 5–9 s were often observed (Fig. 8). These oscillations could persist for several hours and were usually accompanied by visible rhythmic contraction and relaxation of the valve flaps. The activity of spontaneously contracting LAAVs was modified by both ACh and GABA. ACh depolarized the valve muscle fibers, blocking the spontaneous oscillations in membrane potential; rhythmic oscillations gradually returned as ACh was washed out. Application of GABA to spontaneously oscillating muscle fibers produced a biphasic response: an initial period of membrane hyperpo-

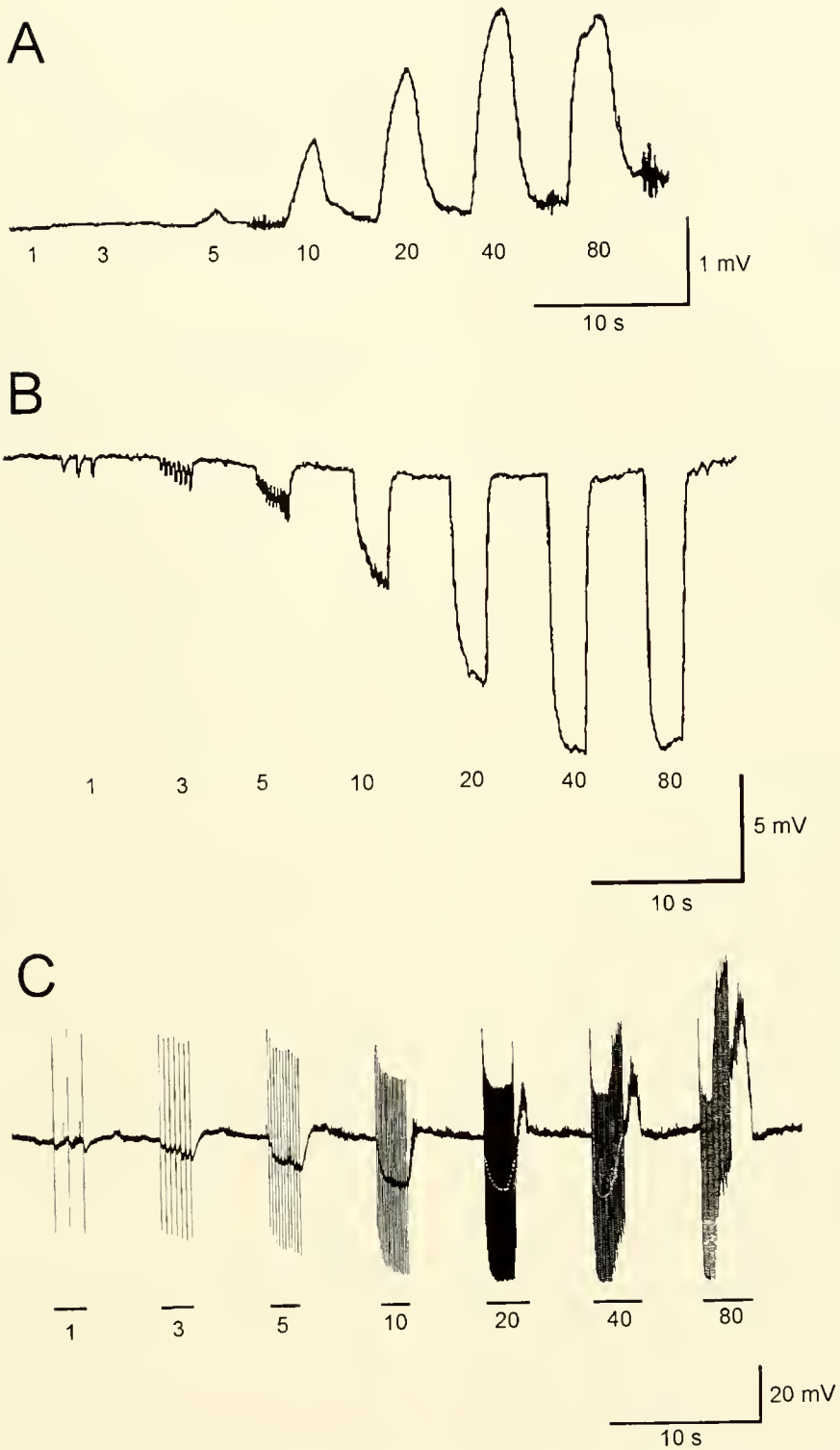

Figure 4. (A) Intracellular recordings from a valve muscle fiber during stimulation of the valve nerve at site A (Fig. 1C), and (B) at site B (Fig. 1C) at different frequencies. (C) Record of biphasic membrane potential responses to stimulation of valve nerve at site A (Fig. 1C). Only IJPs were produced below 5 Hz stimulation, summed IJPs followed by a small depolarization occurred at 5 and 10 Hz, and summed IJPs followed by repolarization during the period of stimulation and large EJPs occurred during stimulation at 20 Hz and higher. The vertical lines on each trace are stimulus artifacts. The inhibitory waveform during the 20 and 40 Hz stimulation was lost in these computer-scanned records; these two records are retouched to reveal the negative waveforms.

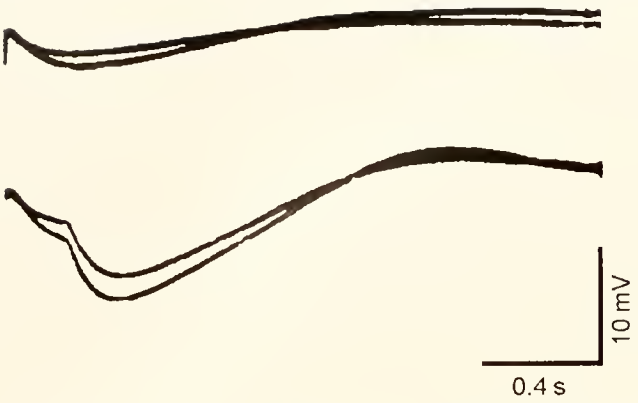

Figure 5. The effect of a single pulse (top trace) and twin pulse (lower trace, delay = 170 ms) stimulation of the lateral abdominal arterial valve nerve on muscle fiber membrane potential. Stimulation at two different voltages (8 and 9 V) in each pair of traces.

larization and decreased oscillation frequency, followed by a period of increased frequency of spontaneous depolarizations.

Discussion

This study focuses on the control of hemolymph distribution into and from the DAA, but to put these results into perspective relative to the overall control of hemolymph distribution, it is useful to review the general distribution of hemolymph among the seven arteries that leave the heart. Several crustacean species are known to have a muscular cardioarterial valve at the origin of each artery at the ventricle. These valves are in a position to control the distribution of cardiac output to large regions of the body (Kuramoto and Ebara, 1984; Kihara *et al.*, 1985; Fujiwara-Tsukamoto *et al.*, 1992; Kuramoto *et al.*, 1995). This holds true for *Homarus americanus*, except for the sternal and dorsal abdominal arteries that arise from the bulbus arteriosis at the back of the heart. The bulbus and ventricle are separated by a nonmuscular flap valve that serves to rectify hemolymph flow leaving the ventricle posteriorly (Kuramoto *et al.*, 1992). A different mechanism is responsible for partitioning of flow between these two posterior arteries. The outflow from the bulbus into the sternal artery is regulated by the muscular sternal cardioarterial valve (Kuramoto *et al.*, 1992, 1995), but there is no valve at the origin of the DAA. Instead the segmental LAAVs provide the only sites to regulate flow into and through the DAA. The DAA supplies hemolymph to the abdominal muscles and swimmerets through the segmental pairs of LAAs, and to the gut and gonads through a perfusion of small-diameter vessels that exit the ventrolateral wall of the DAA. Contraction of the LAAVs by neural (present results) or hormonal (Wilkens, 1997) inputs will decrease the flow into the DAA and redirect flow into other vascular beds, including those supplied by the small vessels to the gut and those supplied by the sternal artery. Conversely, a generalized neural-induced relaxation of the LAAVs will reduce the resistance of the DAA and favor an increased hemolymph flow into the LAAs that supply the abdominal muscles and swimmerets. Thus, LAAVs play important roles in controlling the distribution of hemolymph from the DAA.

The nerves supplying the LAAVs were first identified in *Potamobius astacus* by Alexandrowicz (1932a), who referred to them as the nervi segmentales aortae abdominalis. It is shown here that valve muscles of *H. americanus* receive both inhibitory and excitatory innervation. Stimulation of the inhibitory nerves causes hyperpolarization of valve muscle fibers and relaxation of the valves. This results in increased outflow through the LAAs. Valve fibers receive at least two inhibitory neurons. Excitatory nerves cause fiber depolarization, contraction of the valves, and reduction in LAA outflow. The sternal arterial valve in *H. americanus* appears to receive only inhibitory nervous input (Kuramoto *et al.*, 1992, 1995), a conclusion supported by the present results. One of the inhibitory neurons to this valve arises from an anterior projection from the LAA nerve from the first abdominal segment.

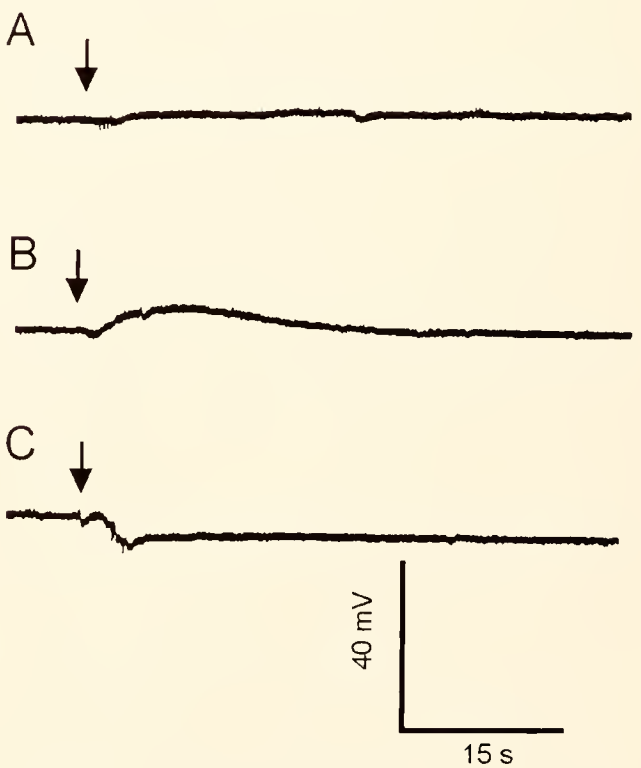

Figure 6. The effect on fiber membrane potential of adding 0.5 ml of (A) saline, (B) ACh (10^{-5} *M*), and (C) GABA (10^{-5} *M*) solution from a pasteur pipette directly over a lateral abdominal arterial valve muscle. Arrow indicates the time of application.

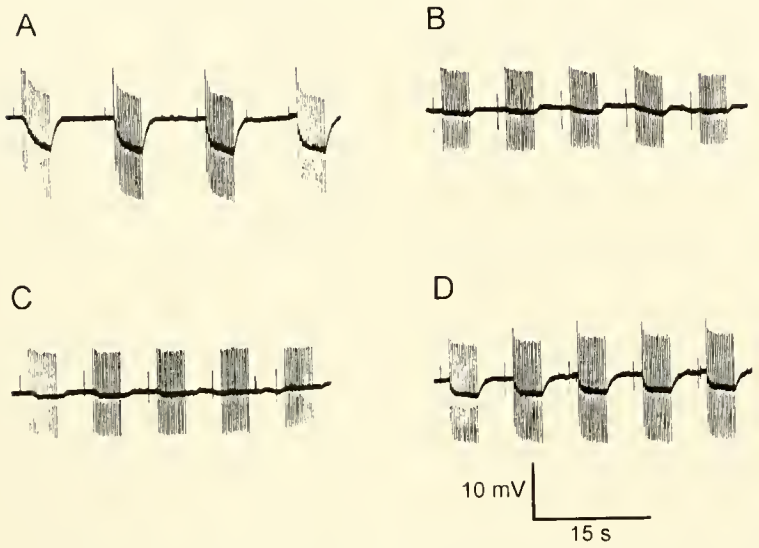

Figure 7. The effect of picrotoxin (10^{-5} *M*) on IJP amplitude during train stimulation (3.5-s train, 10 Hz) of the lateral abdominal arterial valve nerve. (A) Control responses; picrotoxin was added to the bath immediately after this recording. (B) Responses after 20-min exposure to picrotoxin. The bath was flushed with saline (2.5 ml min^{-1}) beginning at 20 min. (C) Recording after 10 min of saline wash. (D) IJP amplitude had partially recovered after 20 min of washing. The vertical lines on each trace are stimulus artifacts.

The nature of the innervation of the other cardioarterial valves in not known for lobsters. In the isopod *B. doederleini,* Kihara *et al.* (1985) found that some cardioarterial valves are dually and antagonistically innervated, whereas others receive only excitatory or inhibitory innervation.

It seems reasonable to assume that the complexity of the innervation of a valve is related to the degree of control required of that valve, and of the overall architecture of the arterial system of which the valve is a part. For example, the sternal artery in *H. americanus* supplies a number of critical structures, including the mouthparts, scaphognathites, walking legs, gut, and ventral nerve cord. It is unlikely that completely stopping hemolymph flow into this artery would ever be desirable, which may help explain the absence of excitatory nervous control of this valve. Flow into the sternal artery would, however, be indirectly reduced if the cardioarterial valves of other arteries and LAAVs were to dilate, lowering the relative flow resistances of other arterial pathways out of the heart. On the other hand, the DAA supplies two different vascular beds, and the complex control that includes both excitatory and inhibitory innervation would allow redistribution between them. We presume that the neural control of the LAAVs in *H. americanus* is related to swimmeret activity, as in *B. doederleini* (Fujiwara-Tsukamoto *et al.,* 1992), with increased inhibitory input during swimmeret and abdominal muscle activity and reduced inhibitory input during periods of low physical activity. Restriction of the flow out the LAAs by nervous and hormonal excitation of the valve muscles would favor flow into the smaller diameter and higher resistance gut vessels, presumably during digestive episodes.

The distribution of the LAAV nerves, with the projection of at least inhibitory axons to segments anterior to a particular nerve, may contribute to anterior waves of valve opening during anteriorly directed metachronal waves of swimmeret beating. However, the spontaneous membrane potential oscillations recorded *in vitro* seem unrelated to swimmeret activity because the frequency of the oscillations is lower than typical swimmeret beat frequencies (0.5–2 Hz; Cattaert and Clarac, 1983; Mulloney *et al.,* 1987; Barthe *et al.,* 1993), and the oscillations persist when the swimmerets are not active (see below). Further investigation is required to test this suggestion.

Biphasic changes in membrane potential were sometimes found during nerve stimulation, with a period of hyperpolarization preceding depolarization. The simplest interpretation of this observation is that both inhibitory and excitatory axons were stimulated and that the latency was shorter for the inhibitory inputs. This interpretation is similar to the time course of change in heart rate in crayfish (Wilkens and Walker, 1992; also seen in *H. americanus,* Wilkens, unpubl. obs.). At the heart, the response to cardioinhibitory nerve stimulation is quicker than that to cardioacceleratory nerve stimulation. Biphasic responses were not apparent in recordings of LAA flow and DAA pressure, where only the effects of valve contraction were apparent. A more detailed analysis, including the use of neurotransmitter blockers, will help understand the basis for these biphasic responses.

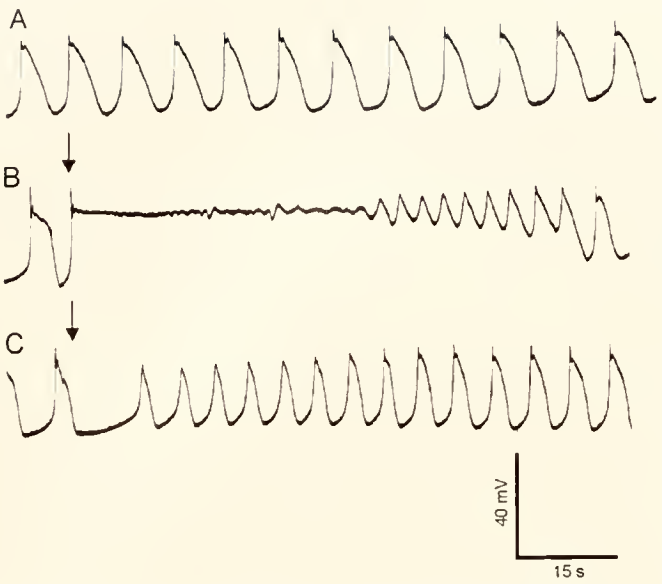

Figure 8. (A) Spontaneous membrane potential oscillations recorded from a lateral abdominal arterial valve muscle fiber when perfused with saline. (B) Application of 0.5 ml of ACh (10^{-3} *M*, arrow) depolarized the fiber and temporarily blocked the spontaneous oscillations. C) The application of 0.5 ml of GABA (10^{-3} *M*, arrow) at first prolonged the interoscillation interval and then increased the rate of oscillations. All records are taken from a single fiber.

It is most likely that GABA is the neurotransmitter released at the inhibitory LAAV neuromuscular junctions in *H. americanus*. This assumption is based on a number of observations. First, the magnitudes of hyperpolarizations of membrane potential resulting from nerve stimulation are similar to those produced by application of GABA. Second, during GABA-initiated hyperpolarization of LAAV muscle, electrical stimulation of the LAAV nerve had little effect, but as the membrane potential recovered from GABA, IJPs could again be elicited by nerve stimulation. Third, picrotoxin was effective in reversibly blocking nerve-induced and GABA-induced hyperpolarizations of the LAAVs. In another study, GABA hyperpolarized the sternal arterial valve and masked inhibitory postsynaptic potentials (IPSPs) arising from inhibitory nerve stimulation (Kuramoto *et al.*, 1992). In crustacean neuromuscular systems, picrotoxin depresses the increased membrane Cl^- conductance caused by GABA in a reversible noncompetitive manner (Takeuchi and Takeuchi, 1969). In view of the proposed homology between the sternal artery and LAAs (Wilkens *et al.*, 1997b), it is noteworthy that the nerve-induced hyperpolarization of the sternal cardioarterial valve is mimicked by dopamine and is not blocked by picrotoxin (Kuramoto *et al.*, 1992).

ACh, but not glutamic acid, caused depolarization of the valve muscle fibers, resulting in decreased flow through the LAA due to contraction of the LAAV. The magnitudes of these effects were similar to those caused by selective stimulation of the LAAV nerve, suggesting cholinergic innervation. This suggestion should be tested with further work using ACh blockers. The depolarization of valve fibers by ACh must account for the increase in the resistance to flow through the DAA (Wilkens, 1997). In *B. doederleini*, the inhibitory innervation of cardioarterial valves is cholinergic (Okada *et al.*, 1997). It appears that there is variability among the Crustacea in the physiological effects of ACh.

Spontaneous nonspiking oscillations in LAAV muscle membrane potential, with concurrent contraction and relaxation of the valves, were often observed in the present study. Spontaneous slow depolarizing and spiking potentials have been reported to occur in the sternal cardioarterial valve in *H. americanus* (Kuramoto *et al.*, 1992, 1995), and are produced in the cardioarterial valves of other arteries in both *H. americanus* and *Panulirus japonicus* (Wilkens and Kuramoto, unpubl. obs.). The records of arterial flow taken from intact *H. americanus* and *Cancer magister* often reveal cyclic fluctuations of flow (McMahon, 1992; McGaw *et al.*, 1994). Assuming that these rhythmic fluctuations are a result of rhythms of LAAV tension, we can ask about their physiological role. In the abdomen, the slow rhythmic opening and closing of the LAAVs may serve to maintain a low basal hemolymph flow to the abdomen and swimmerets during periods of locomotory inactivity and of increased digestive activity when it is predicted that the LAAVs would be closed.

Control of hemolymph distribution within a particular region would require peripheral mechanisms of flow control. Apart from the LAAVs of macrurans, very little is known about such peripheral sites of control of hemolymph flow in decapods. Taylor and Taylor (1986) identified structures in the gills of *Carcinus maenas* (L.) which they suggested might be efferent valves. In an abstract, Taylor *et al.* (1995) indicate that some cardioactive hormones can modulate vascular resistance to perfusion in crab gills *in vitro*. The resistances of perfused arterial trees in *H. americanus* (Wilkens, 1997) and *Procambarus clarkii* (Lovell and Wilkens, unpubl. data) are altered by several hormones.

Of the seven arteries leaving the heart in *H. americanus*, only the DAA has a layer of striated muscle in the artery wall (Wilkens *et al.*, 1997a). A muscular layer has also been identified in the dorsal abdominal arterial wall in the ridgeback prawn *Scyonia ingentis* (Martin *et al.*, 1989) and the spiny lobster *Panulirus interruptus* (Burnett, 1984). Indeed, this may be a common feature of all the macrurans. These muscle fibers are arranged circumferentially; their contraction will reduce the diameter of the vessel, and spontaneous rhythmic contractions of the DAA have been observed *in vitro* (Wilkens *et al.*, 1997b; Davidson and Lovell, unpubl. data).

Burnett (1984) postulated that the muscular DAA is a vestigial remnant of the tubular heart found in more primitive malacostracans, such as stomatopods. Wilkens *et al.* (1997b) supported this hypothesis and suggested in addition that the LAAVs may have been ancestral cardioarterial valves. In agreement with this suggestion, the anatomical pattern of innervation of the LAAVs in *H. americanus* is similar to that of the cardioarterial valves in the stomatopod *Squilla mantis* (Alexandrowicz, 1932b). The stomatopod cardiovascular system is thought to resemble a more primitive architecture (McLaughlin, 1980). In *S. mantis*, a branch of each of the segmental nerves supplying a cardioarterial valve passes across the heart to innervate the contralateral valve in the same segment, much in the same way that LAAV nerves innervate both valves within a segment in *H. americanus*. Wilkens *et al.* (1997b) further suggested that the sternal artery is homologous to the abdominal LAAs. This view is supported by observation that the anterior projection of the LAAV nerve in the first abdominal segment synapses on the sternal cardioarterial valve in the same manner that LAAVs in adjacent abdominal segments are connected. Interestingly, neural-induced relaxation of LAAVs in the first abdominal segment would presumably be accompanied by relaxation of the sternal cardioarterial valve due to their common innervation. Thus, in the absence of other control mechanisms such as hormones, changes in the resistances of the DAA and SA pathways may occur in parallel, rather than being regulated independently. There is no evidence that the sternal cardioarterial valve receives excitatory input.

The contraction and relaxation of the locomotory muscles in decapods may augment venous blood flow (Blatchford, 1971; Wood and Randall, 1981; McMahon and Burnett, 1990). Flow of dye injected into the ventral blood sinuses of the abdomen of *H. americanus* was shown to increase about 10-fold during abdominal flexion (Burger and Smythe, 1953). Extracardiac pumping would be possible only if valves are present to prevent the retrograde flow of blood. One function of the LAAVs may thus be to prevent blood backflow during the vigorous abdominal movements of swimming and escape tail flips. Passive flexion of the abdomen in semi-intact preparations of *H. americanus* causes a small rise in DAA resistance (Wilkens *et al.*, 1996), and tail flips cause pulses of increased pressure in the DAA in *P. clarkii* (Lovell and Wilkens, unpubl. obs.).

Taken together, the observations discussed here show that the LAAVs may be important in passively rectifying hemolymph flow and actively regulating the distribution of flow between the different vascular beds of the abdomen. It is yet to be investigated whether the nervous inputs to these valves are active as predicted during normal behaviors, and whether a similar valvular mechanism is involved in the control of peripheral resistance in the other arterial systems.

Acknowledgments

This study was supported by a grant from the Natural Science and Engineering Research Council (NSERC) of Canada to JLW.

Literature Cited

Airriess, C. N., and B. R. McMahon. 1994. Cardiovascular adaptations enhance tolerance of environmental hypoxia in the crab *Cancer magister*. *J. Exp. Biol.* **190:** 23–41.

Airriess, C. N., and B. R. McMahon. 1996. Short-term emersion affects cardiac function and regional hemolymph distribution in the crab *Cancer magister*. *J. Exp. Biol.* **199:** 569–578.

Alexandrowicz, J. S. 1932a. The innervation of the heart of Crustacea. I. Decapoda. *Q. J. Microscop. Sci.* **75:** 181–249.

Alexandrowicz, J. S. 1932b. The innervation of the heart of Crustacea. II. Stomatopoda. *Q. J. Microscop. Sci.* **75:** 511–548.

Barthe, J. Y., M. Bevengut, and F. Clarac. 1993. *In vitro*, proctolin and serotonin induced modulations of the abdominal motor system activities in crayfish. *Brain Res.* **623:** 101–109.

Blatchford, J. G. 1971. Haemodynamics of *Carcinus maenas* (L.). *Comp. Biochem. Physiol.* **39A:** 193–302.

Burger, J. W., and C. McC. Smythe. 1953. The general form of circulation in the lobster, *Homarus*. *J. Cell. Comp. Physiol.* **42:** 369–383.

Burnett, B. R. 1984. Striated muscle in the wall of the dorsal abdominal aorta of the California spiny lobster *Panulirus interruptus*. *J. Crust. Biol.* **4:** 560–566.

Cattaert, D., and F. Clarac. 1983. Influence of walking on swimmeret beating in the lobster *Homarus gammarus*. *J. Neurobiol.* **14:** 421–439.

Cole, W. 1941. A perfusing solution for the lobster (*Homarus*) heart and the effects of its constituent ions on the heart. *J. Gen. Physiol.* **25:** 1–6.

Fujiwara-Tsukamoto, Y., K. Kuwasawa, and J. Okada. 1992. Anatomy and physiology of neural regulation of hemolymph flow in the lateral arteries of the isopod crustacean, *Bathynomus doederleini*. In *Phylogenetic Models in Functional Coupling of the CNS and the Cardiovascular System*, R. B. Hill, K. Kuwasawa, B. R. McMahon, and T. Kuramoto, eds. *Comp. Physiol.* **11:** 70–85. Basel, Karger.

Kihara, A., K. Kuwasawa, and T. Yazawa. 1985. Neural control of the cardio-arterial valves in an isopod crustacean, *Bathynomus doederleini*: excitatory and inhibitory junctional potentials. *J. Comp. Physiol. A.* **157:** 529–536.

Kuramoto, T., and A. Ebara. 1984. Neurohormonal modulation of the cardiac outflow through the caradioarterial valve in the lobster. *J. Exp. Biol.* **11:** 123–130.

Kuramoto, T., and A. Ebara. 1989. Contraction of flap muscle in the cardioarterial valve of *Panulirus japonicus*. *Comp. Biochem. Physiol.* **93A:** 419–422.

Kuramoto, T., H. Hirose, and M. Tani. 1992. Neuromuscular transmission and hormonal modulation in the cardioarterial valve of the lobster, *Homarus americanus*. In *Phylogenetic Models in Functional Coupling of the CNS and the Cardiovascular System*, R. B. Hill, K. Kuwasawa, B. R. McMahon, and T. Kuramoto, eds. *Comp. Physiol.* **11:** 62–69. Basel, Karger.

Kuramoto, T., J. L. Wilkens, and B. R. McMahon. 1995. Neural control of cardiac outflow through the sternal valve in the lobster *Homarus americanus*. *Physiol. Zool.* **68:** 443–452.

Martin, G. G., and J. E. Hose. 1995. Circulation, the blood, and disease. Pages 465–495 in *Biology of the lobster* Homarus americanus, J. R. Factor, ed., Academic Press, New York.

Martin, G. G., J. E. Hose, and C. J. Corzine. 1989. Morphological comparison of major arteries in the ridgeback prawn, *Scyonia ingentis*. *J. Morph.* **200:** 175–183.

McGaw, I. J., C. N. Airriess, and B. R. McMahon. 1994. Patterns of hemolymph-flow variation in decapod crustaceans. *Mar. Biol.* **121:** 53–60.

McLaughlin, P. A. 1980. *Comparative Morphology of Recent Crustacea.* Freeman, San Francisco. 177 pp.

McMahon, B. R. 1992. Factors controlling the distribution of cardiac output in decapod crustaceans. In *Phylogenetic Models in Functional Coupling of the CNS and the Cardiovascular System,* R. B. Hill, K. Kuwasawa, B. R. McMahon, and T. Kuramoto, eds. *Comp. Physiol.* **11:** 51–61. Karger, Basel.

McMahon, B. R., and L. E. Burnett. 1990. The crustacean open circulatory system: a reexamination. *Physiol. Zool.* **63:** 35–71.

Mulloney, B., L. D. Acevedo, and A. G. Bradbury. 1987. Modulation of the crayfish swimmeret rhythm by octopamine and the neuropeptide proctolin. *J. Neurophys.* **58:** 584–597.

Okada, J., K. Kuwasawa, A. Kihara, Y. F. Tsukamoto, and T. Yazawa. 1997. Cholinergic inhibitory innervation of the cardioarterial valves in the isopod *Bathynomus doederleini*. *Zool. Sci.* **14:** 571–579.

Takeuchi, A., and N. Takeuchi. 1969. The action of picrotoxin on the inhibitory neuromuscular junction of the crayfish. *J. Physiol.* **205:** 377–391.

Taylor, H. H., and E. W. Taylor. 1986. Observations of valve-like structures and evidence for rectification of flow within the gill lamellae of the crab *Carcinus maenas* (Crustacea, Decapoda). *Zoomorphology* **106:** 1–11.

Taylor, H. H., L. E. Burnett, K. Krajniak, W. W. Burggren, and C. Reiber. 1995. Vasomotor responses in crab gills. *Physiol. Zool.* **68:** 66 (abst.).

Wilkens, J. L. 1997. Possible mechanisms of control of vascular resistance in the lobster *Homarus americanus*. *J. Exp. Biol.* **200:** 487–493.

Wilkens, J. L., and R. L. Walker. 1992. Nervous control of crayfish cardiac hemodynamics. In *Phylogenetic Models in Functional Coupling of the CNS and the Cardiovascular System,* R. B. Hill, K. Kuwasawa, B. R. McMahon, and T. Kuramoto, eds. *Comp. Physiol.* **11:** 115–122. Basel, Karger.

Wilkens, J. L., T. Kuramoto, and B. R. McMahon. 1996. The effects of six pericardial hormones and hypoxia on the semi-isolated heart and sternal arterial valve of the lobster *Homarus americanus*. *Comp. Biochem. Physiol.* **114C:** 57–65.

Wilkens, J. L., G. W. Davidson, and M. J. Cavey. 1997a. Vascular peripheral resistance and compliance in the lobster *Homarus americanus*. *J. Exp. Biol.* **200:** 477–485.

Wilkens, J. L., T. Yazawa, and M. J. Cavey. 1997b. Evolutionary derivation of the American lobster cardiovascular system: an hypothesis based on morphological and physiological evidence. *Invertebr. Biol.,* **116:** 30–38.

Wood, C. M., and D. J. Randall. 1981. Hemolymph gas transport, acid-base balance, and anaerobic metabolism during exercise in the land crab (*Cardisoma guanhumi*). *J. Exp. Zool.* **218:** 7–22.

Reference: *Biol. Bull.* **194:** 83–91. (February, 1998)

Chemical Fate of a Metamorphic Inducer in Larvae-like Buds of the Cnidarian *Cassiopea andromeda*

JÜRGEN FLECK*

Lehrstuhl für Spezielle Zoologie, Ruhr-Universität Bochum, D-44780 Bochum, Germany

Abstract. Larvae-like vegetative buds of the scyphozoan *Cassiopea andromeda* metamorphose into polyps in the presence of oligopeptides that have a well-defined primary structure. Buds were incubated with the hexapeptide ^{14}C-dansyl-GPGGPA, a representative inducer. Autoradiography of longitudinal sections of these buds revealed rapid internalization of peptide by the buds. Silver grain density was highest in the pre-pedal disc region (or aboral knob) of metamorphosing buds. Larvae and buds sporadically explore their habitat with this aboral knob, searching for a suitable solid substrate to which irreversible attachment will be made. Buds were incubated for 3, 8, or 16 h with ^{14}C-dansyl-GPGGPA, then homogenized and the supernatants analyzed to determine the chemical fate of the inducer. The signal molecule was shown to be partly degraded to ^{14}C-dansyl-GP, partly to ^{14}C-dansyl-G, and in part still present in its original structure. These cleavage products were also found in the surrounding medium after an incubation time of 8 h with ^{14}C-dansyl-GPGGPA, but did not induce metamorphosis. This study suggests that exposure of metamorphosis-inducing peptides to buds of *Cassiopea andromeda* results in signal termination.

Introduction

Studies dealing with chemical inducers of metamorphosis of marine invertebrate larvae often focus on their signal transduction systems. Such research has been carried out with the scyphozoan *Cassiopea* spp. In *Cassiopea*, settlement of vegetative buds and larvae and dramatic morphogenetic transition to a primary polyp can be observed in less than 24 h by exposing the animals to oligopeptides of a well-defined primary structure (Fitt and Hofmann, 1985; Fitt *et al.*, 1987; Hofmann and Brand, 1987; Fleck and Hofmann, 1990; Fleck and Bischoff, 1993; Hofmann *et al.*, 1996). Substitution of the amino terminals of metamorphosis-triggering peptides with ligands of increasing hydrophobic character enhances the biological activity, whereas carboxyterminal blockade inactivates it (Hofmann and Brand, 1987; Fleck and Hofmann, 1990; Fleck and Bischoff, 1993; Hofmann *et al.*, 1996).

Biologically active peptides for *Cassiopea* spp. can be easily marked by inserting a radioactively labeled group. Coupling of ^{14}C-dansyl chloride to the amino terminus of the hexapeptide GPGGPA results not only in a labeled inducer molecule but also in a highly efficient trigger of metamorphosis in buds of *Cassiopea andromeda* (Fleck and Hofmann, 1995).

Using this molecule in studies *in vivo*, Fleck and Hofmann (1995) demonstrated specific and saturable binding to buds, suggesting that peptide-induced metamorphosis is receptor mediated. Bioactive peptides are proposed to bind primarily to cell membrane receptors located in the pre-pedal disc region (aboral knob) (Fleck, 1994; Arthecker, 1995; Hofmann and Hellmann, 1995). Swimming with this morphological structure facing forward, buds and larvae explore their habitat in search of a suitable substrate and eventually attach. The natural signal for metamorphic induction of the hydroid *Hydractinia echinata* is also recognized at the aboral end of the larvae (Schwoerer-Böhning *et al.*, 1990). Although the possibility that peptidic cues have to interact with intracellular receptors in order to trigger metamorphosis of *Cassiopea* spp. cannot be excluded, none of the currently available

Received 22 September 1995; accepted 17 September 1997.

* E-mail: Juergen.Fleck@ruhr-uni-bochum.de

Abbreviations: ABS, seawater containing antibiotics; PKC, protein kinase C; TLC, thin layer chromatography.

data favor such a signal transduction mechanism. However, it remains unknown on what part of buds or larvae and in what tissue layers the receptors for the inducers are located.

Tumor-promoting phorbol esters, which are known to activate protein kinase C (PKC, see review by Hug and Sarre, 1993), are another class of biologically active compounds in *Cassiopea* spp. (Bischoff *et al.*, 1991; Fleck and Bischoff, 1993). Studies conducted with phorbol esters, biologically active peptides, and PKC inhibitors indicated that PKC is an important part of the signal transduction pathway in induction of metamorphosis (Bischoff *et al.*, 1991; Fleck and Bischoff, 1993; Fleck, in press). This enzyme has also been shown to be involved in the initiation of metamorphosis in other cnidarian larvae (Freeman and Ridgway, 1990; Hassel *et al.*, 1996; Henning *et al.*, 1996; Walther *et al.*, 1996, Fleck, 1997).

The chemical fate of the metamorphic inducer—after it has produced its biological effect—is a critical matter for signal transduction systems (Carr *et al.*, 1990). Carr *et al.* (1990) reported that chemoactive agents in various organisms are chemically changed by degradative enzymes to yield products that can be either more or less stimulatory than the original compound.

Reports on changes in the chemical structure of the biologically active compounds during interaction with larvae are rare, since even the chemical structure of most natural inducers is not known (see review by Pawlik, 1992). Some inducers are compounds whose chemical fate is difficult to monitor because the molecules are difficult to label; others are of such a simple chemical structure that no further change is to be expected (see review by Pawlik, 1992). This issue is also unexplored for scyphozoans, *i.e.*, it remains unresolved if the inducer molecule is inactivated by either being taken up by larvae or buds of *Cassiopea* or being chemically modified outside of or within larvae or buds.

This paper shows uptake of radioactively labeled peptide and chemical alteration of the signal molecule ^{14}C-dansyl-GPGGPA when exposed to buds of *Cassiopea andromeda* in order to induce metamorphosis. Autoradiographical techniques were used to determine the location—area and tissue—of the receptors for the inducer.

Materials and Methods

Animals

Vegetative buds of *Cassiopea andromeda* were collected from a culture of budding polyps kept in the laboratory at a constant temperature of 23°C in North Sea water. The buds were washed in seawater containing antibiotics (ABS: 100 mg penicillin, 100 mg neomycin, and 130 mg streptomycin dissolved in 1 l seawater) before being used in the assays.

Preparation of ^{14}C-dansyl-GPGGPA

Synthesis of the metamorphosis-inducing oligopeptide ^{14}C-dansyl-GPGGPA is described elsewhere (Fleck and Hofmann, 1995). The total amount of product after purification and lyophilization was about 585 μg (1.9 MBq).

Preparation of bud sections for autoradiographic analysis

Solutions of the inducer peptide were prepared in two glass dishes each containing ^{14}C-dansyl-GPGGPA dissolved in 1 ml ABS in a final concentration of 5.3×10^{-5} mol/l (114 KBq). Forty buds of *Cassiopea andromeda* were incubated in each of the two dishes. A few buds (3–4) were removed after 10, 20, 30, 60, and 120 min and every 2 h thereafter up to a total incubation time of 32 h. The buds were subsequently transferred into 2.5% glutaraldehyde in 0.1 *M* cacodyle buffer and fixed overnight. This procedure was followed by one wash in 0.1 *M* cacodyle buffer and one wash in distilled water, and then by successive rinses in increasing concentrations of ethanol. Embedding was carried out in Epon for 3 days at a temperature of 60°C. The buds were sectioned (1 μm) with an ultramicrotome (Om U3, Reichert). The sections were transferred to slides previously coated with chrome alum gelatin. The slides were covered with stripping film AR 10 (Kodak) in red light and then kept at −20°C for 3 months in darkness. At the end of the exposure, the filmed slides were developed in D19b developer (Kodak) for 5 min, fixed, and dried with cold air from a hair drier. The sections were then stained for 25 min with a solution composed of the following components: 50 ml distilled water, 1.5 ml 0.2 mol/l sodium hydrogen phosphate containing 0.1 mol/l citric acid (pH 7.2), 1.5 ml methanol, and 5 ml Giemsas-solution. After rinsing the slides with distilled water and drying, the specimens were analyzed with a BH-2 light microscope (Olympus).

Silver grain density in the ectoderm and endoderm of the pedal disc, stalk, and presumptive head was determined directly by microscopy (magnification 1000×). Label was counted in five longitudinal sections through the center of buds that had been incubated for either 10 or 30 min in ABS containing ^{14}C-dansyl-GPGGPA. Whole sections were photographed at a magnification of 200×. The number of grains was related to the area (in square centimeters) of the different segments of the developing polyp (pedal disc, stalk, presumptive head). The means of the number of labels of the five sections of each of the three morphological parts were analyzed by analysis of variance (ANOVA): 2-way ANOVAs were performed for the 10-min and 30-min incubation, with segment and tissue (ectoderm, endoderm) as factors, and another 2-way ANOVA was carried out with incubation time and segment as the factors. The Student-Newman-Keuls method

was used for all pairwise multiple comparison procedures ($P < 0.05$).

Determination of the chemical fate of ^{14}C-dansyl-GPGGPA

One thousand buds of *C. andromeda* were incubated in small glass dishes containing ^{14}C-dansyl-GPGGPA dissolved in ABS to make a final concentration of 9×10^{-6} mol/l (17.8 KBq). Inducer peptide at this concentration effects metamorphosis of 100% of buds within 24 h (Fleck and Hofmann, 1995). Incubations were terminated after 3, 8, or 16 h. The animals were washed four times with 5 ml ABS, either in PD 10 columns (Pharmacia) or, if irreversibly attached, in the glass dishes themselves. The buds were homogenized in 1 ml 0.1 *M* HCl by intensive flushing with a glass pipette. The homogenate was transferred to an Eppendorf tube and centrifuged for 5 min at 24000 × *g*. The supernatant, containing cytosol and very small cellular particles, and the pellet, containing cell fragments, were separated. The pellet was completely dissolved in 1 ml 1.35 *M* NaOH overnight. The radioactivity of 100 μl of the supernatant, and of the dissolved pellet, was determined in 2 ml Quickszint 212 (Zinsser) in plastic vials in a Rack Beta liquid scintillation counter (LKB). Both the remaining supernatant (900 μl 0.1 *M* HCl) and pellet (900 μl 1.35 *M* NaOH) were desalted and separated in Mobicol mini columns (Biometra) containing about 300 μl of the reversed phase gel Octyl Si = 100 (Serva). After application of the sample, the gel was washed sequentially with 2 ml distilled water, and then 30, 50, 70, and 100% methanol. Radioactivity of 100 μl of each eluate was measured in 2 ml Quickszint 212 in the scintillation counter. Eluates containing radioactivity were then lyophilized in a Speed Vac concentrator (Savant) coupled to an LO 3 freeze dryer (Wkf). The lyophilisate of each radioactive eluate was dissolved in an appropriate volume of distilled water corresponding to the radioactivity previously determined. Samples (2 μl) of each radioactive lyophilisate were separated by thin layer chromatography (TLC) on silica gel aluminum foils (Merck) in *n*-propanol:distilled water of 3:1 (total volume 60 ml). Autoradiography was conducted by exposing the chromatograms to Fuji RX X-ray film in a cassette with intensifier screen (Sigma) for 7–14 days at a temperature of −45°C. The film was subsequently developed in D19b developer (Kodak) and fixed in Unifix fixer (Kodak) for 5 min in absolute darkness. The film was then kept, for 2 min, in a stop bath containing a small volume of acetic acid in distilled water. Finally the film was intensively washed with water and dried at 30°C.

The experiment to determine the chemical fate of the inducer peptide was performed in replicate. In addition, the following control experiments were carried out:

a) The chemical stability of ^{14}C-dansyl-GPGGPA in ABS was determined by incubating the inducer peptide in 100 μl ABS at a concentration of 1.7×10^{-6} mol/l (0.4 KBq) for 8 h at room temperature. Thereafter the solution was separated by reversed phase chromatography in Octyl Si = 100 in mini columns and further prepared for TLC and autoradiography as described above.

b) As a test of the chemical stability of ^{14}C-dansyl-GPGGPA during homogenization of the buds in 0.1 *M* HCl, the peptide (1.7×10^{-7} mol/l; 0.4 KBq) was added directly to 1000 buds of *Cassiopea andromeda* which were taken up in 1 ml 0.1 *M* HCl. Homogenization in a glass pipette and all further steps up to autoradiographic analysis of the homogenate were carried out as reported above.

c) The chemical stability of ^{14}C-dansyl-GPGGPA in bud homogenate was determined by exposing the radioactively labeled peptide at a concentration of 5.1×10^{-7} mol/l (1.2 KBq) to 1 ml 0.1 *M* HCl containing 1000 homogenized buds of *Cassiopea andromeda* for 8 h at room temperature. Afterwards the homogenate was prepared as described above.

Results

Induction of metamorphosis by ^{14}C-dansyl-GPGGPA

The radioactively labeled inducer peptide ^{14}C-dansyl-GPGGPA triggered metamorphosis of buds of *Cassiopea andromeda*. Buds started to metamorphose when incubated in ABS containing ^{14}C-dansyl-GPGGPA at either test concentration (9×10^{-6} mol/l or 5.3×10^{-5} mol/l). Reversible attachment (stage A, Fig. 1) of the buds to the walls of the glass dishes or to the surface of the solutions took place within 4–6 h. Irreversible attachment (stage B, Fig. 1) was established after 8 h, whereas buds developed up to stage C and D (Fig. 1) when exposed to the inducer for 16–32 h.

Uptake of radioactively labeled peptide by metamorphosing buds

Autoradiographic analysis revealed silver grains in all longitudinal sections of buds, regardless of whether they were exposed to ^{14}C-dansyl-GPGGPA for 10 min or for 32 h (Fig. 2a).

Labeling was discovered in the ectoderm and endoderm. The ectoderm is composed of three cell types: tall columnar cells, nematoblasts and nematocytes, and mucus cells (Hofmann and Honegger, 1990). Silver grains were found in all of these cell types. Accumulation of labeling in a special cell type could not be observed (Fig. 2b). The same was true for the endoderm consisting of columnar cells and cells exhibiting heterolysosomes, digestive

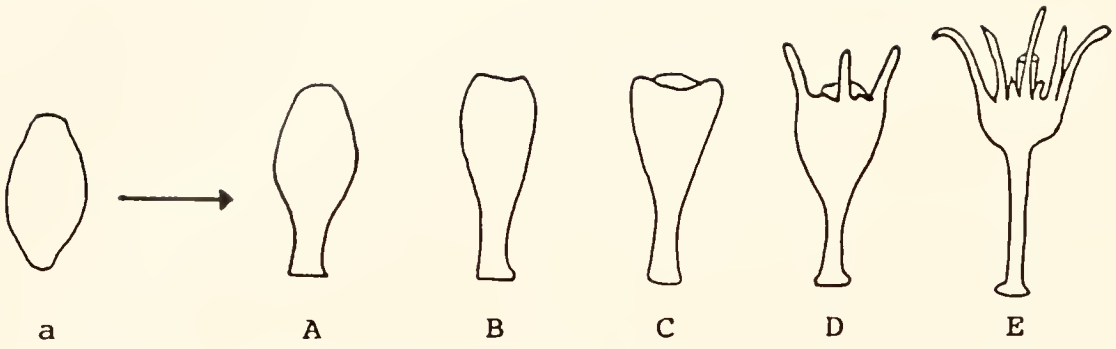

Figure 1. Development of buds (stage a) of *Cassiopea* spp. in the presence of metamorphic inducers. Irreversible attachment takes place at stage B.

vacuoles, and vesicles (Hofmann and Honegger, 1990; Fig. 2b).

Analysis of the silver grain density in sections of buds exposed to ^{14}C-dansyl-GPGGPA for 10 min or 30 min revealed a significant increase in the total number of labels with the duration of the incubation. Comparison of the degree of labeling of the segments for the two incubation times showed that after 30 min the number of silver grains significantly increased in all segments except the head. The ectoderm was found to label more than the endoderm for both 10-min and 30-min incubation (Fig. 3). The density of silver grains was highest in the pedal disc, followed by the stalk and the head. This profile appeared in the 10-min and 30-min specimens (Fig. 3). Comparison of the data of the 10-min incubation showed significant differences in the labeling of the segments in ectoderm and endoderm except for (1) pedal disc endoderm *versus* head ectoderm and (2) stalk endoderm *versus* head endoderm (Fig. 3). This was also true for the 30-min incubation except for (1) stalk ectoderm *versus* pedal disc endoderm and (2) stalk endoderm *versus* head endoderm (Fig. 3).

Chemical fate of ^{14}C-dansyl-GPGGPA

When buds that had been previously exposed to ^{14}C-dansyl-GPGGPA for 3, 8, or 16 h were homogenized in 0.1 *M* HCl, more than 85% of the total radioactivity was

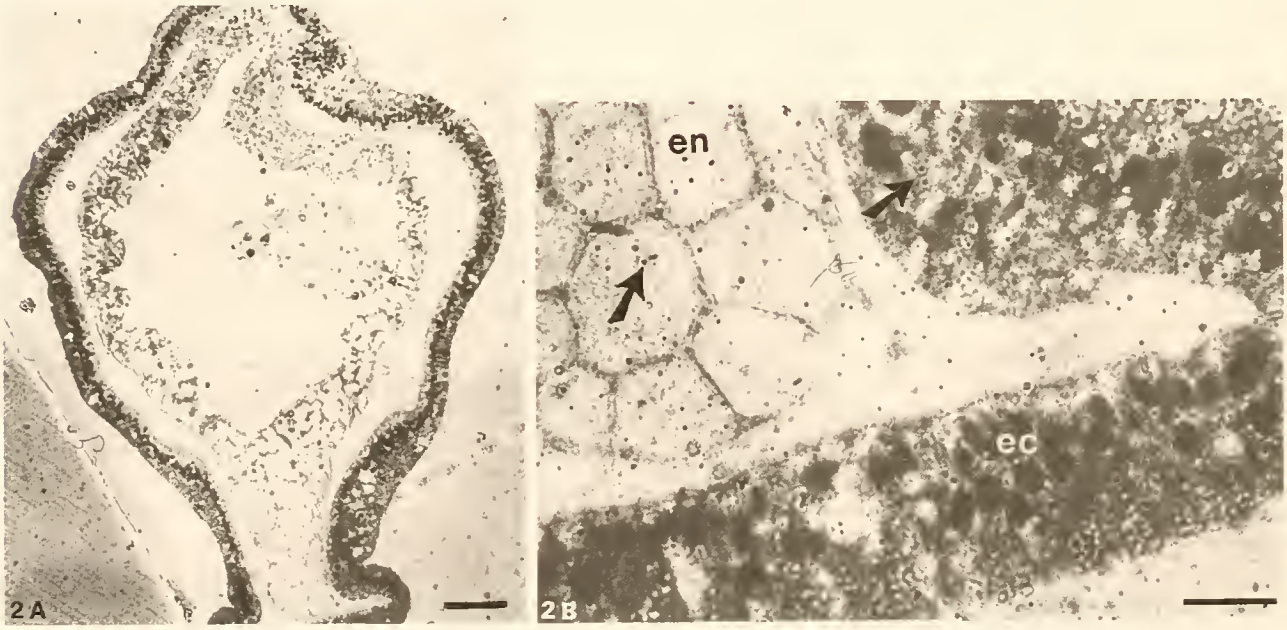

Figure 2. (A) Total view of a longitudinal section through the center of a bud of *Cassiopea andromeda* exposed to ^{14}C-dansyl-GPGGPA (5.3×10^{-5} mol/l) for 30 min. Silver grains are not visible at this magnification (200×). Scale bar, 50 μm. (B) Distribution of silver grains (arrows) in the corresponding pedal disc of (A). en, endoderm; ec, ectoderm. Magnification 1000×; scale bar, 10 μm.

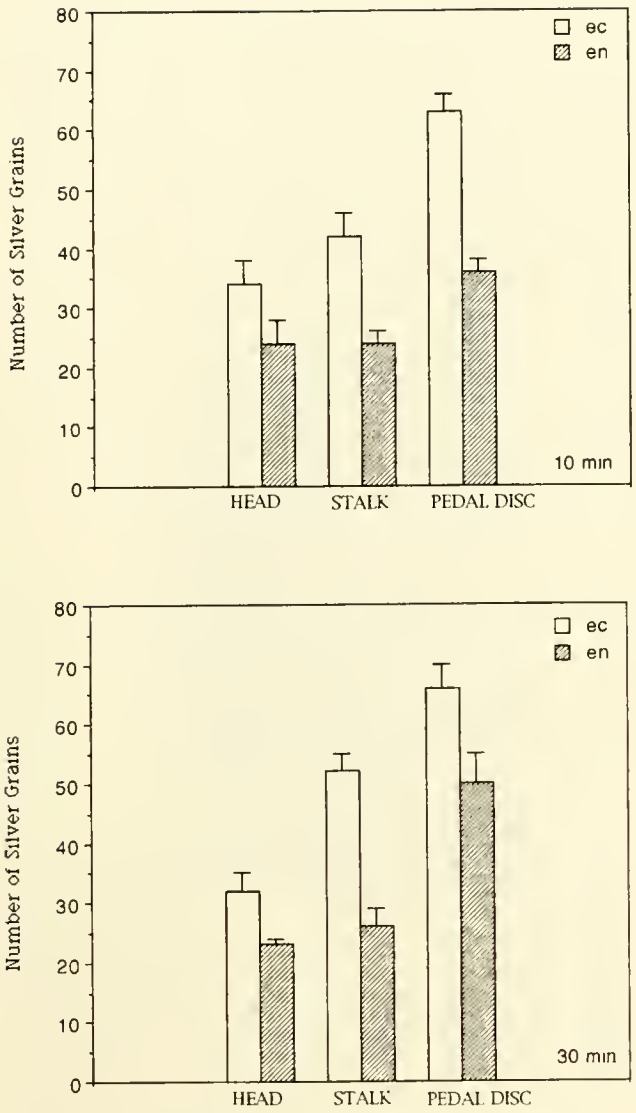

Figure 3. Number of silver grains per cm^2 photo area of longitudinal sections of buds of *Cassiopea andromeda* exposed to ^{14}C-dansyl-GPGGPA (5.3×10^{-5} mol/l; 114 kBq) either for 10 or 30 min. Data are means ± SD of the number of silver grains in 5 sections of one bud. Two-way ANOVAs were carried out for both incubation times, with segment (head, stalk, pedal disc) and tissue (ectoderm, endoderm) as factors. All pairwise multiple comparison procedures were performed with the Student-Newman-Keuls method. ec, ectoderm; en, endoderm.

found in the supernatant after centrifugation of the homogenate. The pellet dissolved in 1.35 *M* NaOH contained less than 14% of the total radioactivity. Therefore, only the supernatant of the homogenate of buds was separated by reversed phase chromatography in mini columns.

Total radioactivity in the 0.1 *M* HCl supernatant increased in a nonlinear manner with the duration of the incubation (Fig. 4). Reversed phase chromatography of the 0.1 *M* HCl supernatant revealed radioactivity in the distilled water eluate and in the 50% methanol eluate (Fig. 4), but at longer incubations, an increasing portion of radioactivity could not be eluted from the reversed phase gel (Fig. 4).

The 50% methanol eluates were lyophilized, redissolved, and subjected to TLC. Autoradiography showed ^{14}C-dansyl-GPGGPA, ^{14}C-dansyl-GP, and ^{14}C-dansyl-G for each incubation time (Fig. 5, lanes B, C, D). The distilled water eluates contained high amounts of salts, and these autoradiograms showed no well-defined spots. Therefore, identification of the radioactive compounds was impossible.

To determine whether degradation products of the hexapeptide occur in the incubation solution in the presence of metamorphosing buds, a 20-μl sample of the incubation solution was analyzed following an 8-h incubation of 1000 buds in 900 μl of ABS containing ^{14}C-dansyl-GPGGPA (9×10^{-6} mol/l; 17.8 KBq). The sample was separated on a mini column by reversed phase chromatography in Octyl Si = 100. Radioactive eluates were checked by TLC followed by autoradiography of the TLC aluminium foil. The autoradiogram showed that traces of ^{14}C-dansyl-GP and ^{14}C-dansyl-G were present in the medium simultaneously with the hexapeptide (Fig. 6, lane A).

The control experiments revealed that (i) ^{14}C-dansyl-GPGGPA was chemically stable in ABS at room temperature for at least 8 h (Fig. 6, lanes B, C, and D); (ii) the chemical stability of ^{14}C-dansyl-GPGGPA was not affected by the homogenization of the buds in 0.1 *M* HCl (data not shown); and (iii) ^{14}C-dansyl-GPGGPA was chemically stable in bud homogenate for an incubation time of at least 8 h (Fig. 6, lanes E and F).

Discussion

The present study, applying the same radioactively labeled inducer to buds of *Cassiopea andromeda* as used for binding experiments *in vivo* (Fleck and Hofmann, 1995), shows that biologically active oligopeptides might face a chemical fate similar to that of many signal molecules. Autoradiography of longitudinal sections of buds incubated in solutions containing ^{14}C-dansyl-GPGGPA revealed uptake of the peptide (Fig. 2). Analysis of homogenates of buds that had been exposed to the hexapeptide for 3, 8, or 16 h showed that the inducer was partly degraded to ^{14}C-dansyl-GP and ^{14}C-dansyl-G (Fig. 5). Those cleavage products are not able to induce metamorphosis (Fleck, 1994). Internalization and degradation may therefore represent a mechanism for signal termination.

Uptake of peptidic signal molecules is common in plant and animal cells. This process may lead to intracellular degradation of the ligand and receptor but often involves recycling of the receptor to the cell surface (see review by Smythe and Warren, 1991). In the present study, radioac-

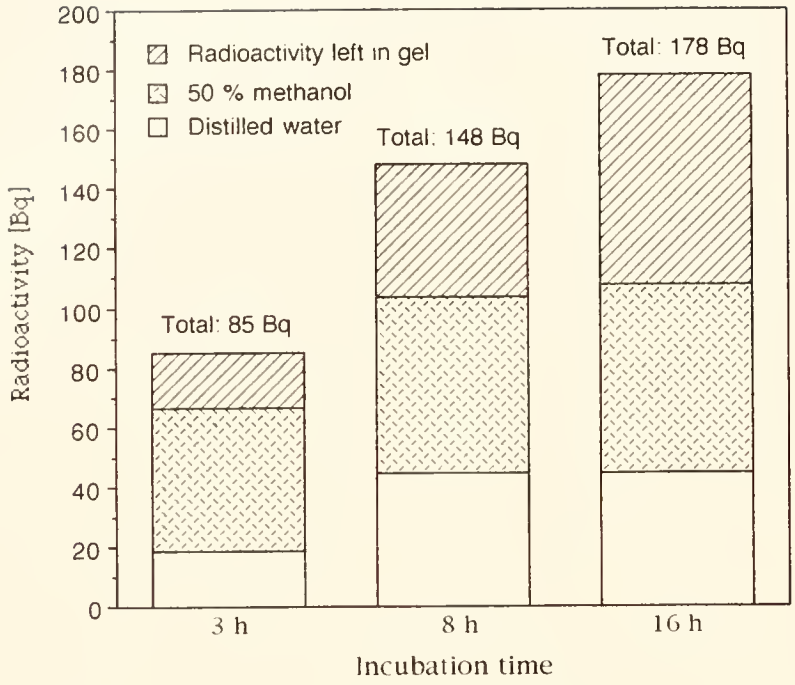

Figure 4. Radioactive fractions resulting from reversed phase chromatography of the supernatants of homogenates of buds of *Cassiopea andromeda* following 3, 8, or 16 h incubation with ^{14}C-dansyl-GPGGPA (9×10^{-6} mol/l; 17.8 kBq). Data are representative results of one out of two chromatographic separations.

tively labeled peptide was shown to be internalized rapidly by buds of *Cassiopea andromeda* when exposed to the metamorphosis-inducing oligopeptide ^{14}C-dansyl-GPGGPA. Silver grains were discovered in longitudinal sections of buds that had been incubated with the inducer for only 10 min. Counting of the labels and relating their number to the three morphological parts of the presumptive polyp (pedal disc, stalk, head) revealed that labeling was highest in the ectoderm of the pedal disc. An explanation for this degree of labeling may lie in the fact that buds and larvae swim with the aboral knob—which becomes the pedal disc upon metamorphic induction—facing forward when exploring their habitat in search of a substrate suitable for settlement. In addition, receptors for inducer peptides are also supposed to be concentrated at the aboral end of buds and larvae (Fleck and Hofmann, 1995).

Silver grains were not found to be concentrated in specific cells, which may indicate that all cell types are able to take up peptide. The uptake mechanism may be specific, nonspecific, or both.

Which chemical molecule is represented by the silver grains in the longitudinal sections? The supernatant of homogenized buds given a prior exposure to ^{14}C-dansyl-GPGGPA for 3, 8, or 16 h showed that the degradation products ^{14}C-dansyl-GP and ^{14}C-dansyl-G were present in addition to the original compound (Fig. 5). The total amount of these agents increased with the duration of the incubation. Although longitudinal sections of buds incubated with the inducer for only 10 min or 30 min were analyzed for silver grain density, cleavage products of the hexapeptide might have already occurred after these short exposures. Silver grains would then represent not only ^{14}C-dansyl-GPGGPA but also ^{14}C-dansyl-GP and ^{14}C-dansyl-G.

Two radioactive fractions isolated from bud homogenate could not be identified. The analysis of one of these fractions was impossible due to the high content of salt in the sample. The other portion of radioactivity, which increased with the duration of the incubation, could not be eluted from the gel. Compounds larger than 20 kD or very hydrophobic molecules usually cannot be eluted from the type of reversed phase gel used in this study (pers. commun., Boehringer Biochemicals, Mannheim). Therefore, the noneluable substances might reflect hexapeptide bound to large compounds such as proteins and lipids, or denatured hexapeptide. However, silver grains in the longitudinal sections may even represent products of these unidentified radioactive fractions.

It is remarkable that ^{14}C-dansyl-GP and ^{14}C-dansyl-G are not able to effect metamorphosis (Fleck, 1994). Carr *et al.* (1990) reported that degradative enzymes in chemosensory processes can change chemoactive compounds into ones that are less or more stimulatory. Signal termination can be obtained by this mechanism in organisms

Figure 5. Autoradiogram of the radioactive 50% methanol eluate obtained by reversed phase chromatography of the supernatant of homogenates of buds of *Cassiopea andromeda* exposed to ^{14}C-dansyl-GPGGPA (9×10^{-6} mol/l) for 3 h (lane B), 8 h (lane C), or 16 h (lane D). A standard of ^{14}C-dansyl-GPGGPA was applied in lane A. ◗, ^{14}C-dansyl-GPGGPA; ➤, ^{14}C-dansyl-GP; ▶, ^{14}C-dansyl-G.

including slime molds, yeast, insects, and crustaceans (Carr *et al.*, 1990). The spiny lobster *Panulirus argus* detects potential food sources by olfactory sensilla on the antennules. These sensilla contain receptors that are sensitive to exogenous nucleotides. In addition, the sensilla contain membrane-bound degradative enzymes that rapidly dephosphorylate nucleotides entering the sensillar lymph and pumps that internalize different biologically active molecules. This process results in a change of the stimulatory state of the signal (Trapido-Rosenthal *et al.*, 1987, 1989; Gleeson *et al.*, 1991, 1992).

Such degradative enzymes seem also to be present in buds of *Cassiopea andromeda*. Action of these enzymes should have degraded ^{14}C-dansyl-GPGGPA to the biologically inactive compounds ^{14}C-dansyl-GP and ^{14}C-dansyl-G. However, the experiments performed in this study did not provide any information about the chemical fate of the carboxyterminal cleavage fragments of the inducer peptide. Therefore the possibility cannot be excluded that, in addition to the products that did not evoke metamorphosis, peptidic fragments were produced (*e.g.*, GGPA) that are able to induce metamorphosis even though they are less stimulatory than ^{14}C-dansyl-GPGGPA (Hofmann *et al.*, 1996).

Degradation of the hexapeptide may take place either externally or internally of the buds, or by a combination of both processes. On the one hand, enzymes that are either membrane-bound or released into the medium may hydrolyze the inducer right after binding to receptors located in the cell membrane. Cleavage products can then be internalized by the metamorphosing buds. The presence of ^{14}C-dansyl-GP and ^{14}C-dansyl-G in the incubation

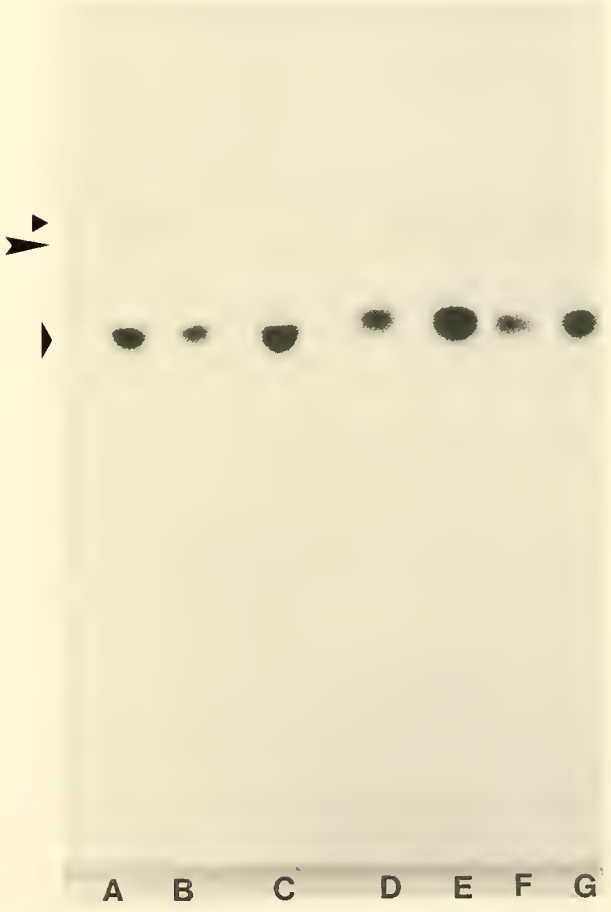

Figure 6. Autoradiogram of radioactive eluates obtained by reversed phase chromatography of the following solutions. Lane A: sample of the incubation solution of 1000 buds of *Cassiopea andromeda* exposed to ^{14}C-dansyl-GPGGPA (9×10^{-6} mol/l) for 8 h. Lanes B, C, D: ^{14}C-dansyl-GPGGPA incubated in ABS for 8 h at room temperature. Lanes E, F: ^{14}C-dansyl-GPGGPA incubated in a homogenate of 1000 buds of *Cassiopea andromeda* for 8 h at room temperature. Lane G: standard of ^{14}C-dansyl-GPGGPA. ◗, ^{14}C-dansyl-GPGGPA; ➤, ^{14}C-dansyl-GP; ▶, ^{14}C-dansyl-G.

solution after 8 h may support this hypothesis. This inactivation mechanism would reduce receptor desensitization and allow receptor activation to be renewed by subsequent pulses of the inducer peptide (Carr *et al.*, 1990). Gleeson *et al.* (1991, 1992) showed that degradative enzymatic activity in *Panulirus argus* is located in the transitional zone of the olfactory sensilla, which is the region in which the sensory neurons develop cilia and branch to form the outer dendritic segments. This demonstration might suggest that peptide-cleaving enzymes of *Cassiopea* spp. are also membrane-bound rather than released into the extracellular medium.

On the other hand, hexapeptide bound to its receptor may be taken up as a ligand-receptor complex. Degradation of the inducer and recycling of the receptor to the cell membrane as described for the epidermal growth factor (see review by Sorkin and Waters, 1993) would follow the internalization process. The presence of ^{14}C-dansyl-GP and ^{14}C-dansyl-G in the 8-h incubation solution would then indicate that buds released cleavage products of the original signal molecule. This inactivation mechanism would also allow renewal of receptor activation since a certain number of surface receptors would be re-exposed in the cell membrane after recycling. In addition, nonspecific uptake of peptide may occur during both processes described above.

Limited desensitization of receptors could be of special importance for metamorphic induction of *Cassiopea* spp. triggered by peptides. ^{14}C-dansyl-GPGGPA used in a concentration of 9×10^{-6} mol/l had to be present for 8 h to induce irreversible metamorphosis of buds in this study. Hofmann and Brand (1987) had to apply the inducer peptide Z-GPGGPA for 7 h at 1.2×10^{-5} mol/l to yield 100% metamorphosis of buds of *Cassiopea andromeda* within 24 h. However, buds treated eight times for 1 h with the same concentration of the hexapeptide also underwent metamorphosis to 100% (Hofmann and Brand, 1987). These results suggest that renewed activation of a receptor may be important for irreversible attachment and metamorphosis of buds and larvae of *Cassiopea* spp.

The radioactivity of the fraction that contained ^{14}C-dansyl-GPGGPA, ^{14}C-dansyl-GP, and ^{14}C-dansyl-G still increased after an incubation time of 8 h. Since receptor activation should no longer be required to complete metamorphosis after this time, the increase found after 16 h might have been the result of nonspecific interactions.

The findings reported here are in contrast to results published by Trapido-Rosenthal and Morse (1986) for the chemical fate of a metamorphic inducer of larvae of the mollusc *Haliotis rufescens*. These authors found that ^{3}H-baclofen, which mimics the inducing capacity of GABA as a settlement cue, was not chemically altered during interaction with the larvae.

The present paper provides data showing that a peptidic metamorphic inducer is chemically changed when exposed to vegetative buds of *Cassiopea andromeda*. The demonstration of the existence of biologically inactive fractions resulting from cleavage of ^{14}C-dansyl-GPGGPA supports the hypothesis that signal termination may be the cause of degradation of the original signal molecule.

Acknowledgments

I thank W. K. Fitt and D. K. Hofmann for critical reading of an earlier version of the manuscript. I am grateful to S. Köhler, who helped me to prepare the photographs. Thanks are also due to G. Henning and S. Höxtermann for their support with the computerized statistical analysis of the data. Contribution #008 from the Key Largo Marine Research Laboratory.

Literature Cited

Arthecker, S. 1995. Entwicklungs- und neurobiologische Untersuchungen an Entwicklungsstadien von *Cassiopea* spp. (Cnidaria, Scyphozoa). *Diplomarbeit,* Ruhr—Universität Bochum, Germany.

Bischoff, A., J. Fleck, and D. K. Hofmann. 1991. Phorbol esters induce metamorphosis in *Cassiopea andromeda* and *Cassiopea xamachana* (Cnidaria, Scyphozoa). *Verh. Dtsch. Zool. Ges.* **84:** 484.

Carr, W. E. S., H. G. Trapido-Rosenthal, and R. A. Gleeson. 1990. The role of degradative enzymes in chemosensory processes. *Chem. Senses* **15:** 181–190.

Fitt, W. K., and D. K. Hofmann. 1985. Chemical induction of settlement and metamorphosis of the reef-dwelling coelenterate *Cassiopea andromeda*. Pp. 239–244 in *Proc. 5th Int. Coral Reef Congr.* 2, Moorea.

Fitt, W. K., D. K. Hofmann, M. Wolk, and M. Rahat. 1987. Requirement of exogenous inducers for metamorphosis of axenic larvae and buds of *Cassiopea andromeda* (Cnidaria: Scyphozoa). *Mar. Biol.* **94:** 415–422.

Fleck, J. 1997. Phosphatidylinositol (PI) signaling and subsequent events in metamorphosis induction of cnidarian larvae. Pp. 1225–1229 in *Proc. 8th Int. Coral Reef Symp.* 2, Panama.

Fleck, J. 1994. Wirksamkeit modifizierter Induktorpeptide, möglicher Signaltransduktionsmechanismus und chemisches Schicksal eines biologisch aktiven Peptids bei der Auslösung der Metamorphose bei *Cassiopea* spp. (Cnidaria, Scyphozoa). *Dissertation,* Ruhr—Universität Bochum, Germany.

Fleck, J., and A. Bischoff. 1993. Protein kinase C is possibly involved in chemical induction of metamorphosis in *Cassiopea* spp. (Cnidaria: Scyphozoa). Pp. 456–462 in *Proc. 7th Int. Coral Reef Symp.* 1, Guam.

Fleck, J., and D. K. Hofmann. 1990. The efficiency of metamorphosis inducing oligopeptides in *Cassiopea* species (Cnidaria: Scyphozoa) depends on both primary structure and amino- and carboxy terminal substituents. *Verh. Dtsch. Zool. Ges.* **83:** 452–453.

Fleck, J., and D. K. Hofmann. 1995. *In vivo* binding of a biologically active oligopeptide in vegetative buds of the scyphozoan *Cassiopea andromeda:* demonstration of receptor-mediated induction of metamorphosis. *Mar. Biol.* **122:** 447–451.

Freeman, G., and E. B. Ridgway. 1990. Cellular and intracellular pathways mediating the metamorphic stimulus in hydrozoan planulae. *Roux's Arch. Dev. Biol.* **199:** 63–79.

Gleeson, R. A., L. M. McDowell, H. C. Aldrich, H. G. Trapido-Rosenthal, and W. E. S. Carr. 1991. Localization of 5′-ectonucleoti-

dase/phosphatase activity within the olfactory sensilla of the spiny lobster, *Panulirus argus*. *Cell Tissue Res.* **265:** 385–391.

Gleeson, R. A., H. G. Trapido-Rosenthal, L. M. McDowell, H. C. Aldrich, and W. E. S. Carr. 1992. Ecto-ATPase/phosphatase activity in the olfactory sensilla of the spiny lobster, *Panulirus argus:* localization and characterization. *Cell Tissue Res.* **269:** 439–445.

Hassel, M., T. Leitz, and W. A. Müller. 1996. Signals and signal-transduction systems in the control of development in *Hydra* and *Hydractinia*. *Int. J. Dev. Biol.* **40:** 323–330.

Henning, G., D. K. Hofmann, and Y. Benayahu. 1996. The phorbol ester TPA induces metamorphosis in Red Sea coral planulae (Cnidaria: Anthozoa). *Experientia* **52:** 744–749.

Hofmann, D. K., and U. Brand. 1987. Induction of metamorphosis in the symbiotic scyphozoan *Cassiopea andromeda:* role of marine bacteria and of biochemicals. *Symbiosis* **4:** 99–116.

Hofmann, D. K., and M. Hellmann. 1995. Studies in the reef-dwelling cnidarian *Cassiopea* spp.: RF-amide positive elements of the nervous system at different stages of development. *Beitr. Paläont.* **20:** 21–29.

Hofmann, D. K., and T. G. Honegger. 1990. Bud formation and metamorphosis in *Cassiopea andromeda* (Cnidaria: Scyphozoa): a developmental and ultrastructural study. *Mar. Biol.* **105:** 509–518.

Hofmann, D. K., W. K. Fitt, and J. Fleck. 1996. Checkpoints in the life-cycle of *Cassiopea andromeda:* control of metagenesis and metamorphosis in a tropical jellyfish. *Int. J. Dev. Biol.* **40:** 331–338.

Hug, H., and T. F. Sarre. 1993. Protein kinase C isoenzymes: divergence in signal transduction? *Biochem. J.* **291:** 329–343.

Pawlik, J. R. 1992. Chemical ecology of the settlement of benthic marine invertebrates. *Oceanogr. Mar. Biol. Annu. Rev.* **30:** 273–335.

Schwoerer-Böhning, B., M. Kroiher, and W. A. Müller. 1990. Signal transmission and covert prepattern in the metamorphosis of *Hydractinia echinata* (Hydrozoa). *Roux's Arch. Dev. Biol.* **198:** 245–251.

Smythe, E., and G. Warren. 1991. The mechanism of receptor-mediated endocytosis. *Eur. J. Biochem.* **202:** 689–699.

Sorkin, A., and C. M. Waters. 1993. Endocytosis of growth factor receptors. *BioEssays* **15:** 375–382.

Trapido-Rosenthal, H. G., and D. E. Morse. 1986. Availability of chemosensory receptors is down-regulated by habituation of larvae to a morphogenetic signal. *Proc. Natl. Acad. Sci. USA* **83:** 7658–7662.

Trapido-Rosenthal, H. G., W. E. S. Carr, and R. A. Gleeson. 1987. Biochemistry of an olfactory purinergic system: dephosphorylation of excitatory nucleotides and uptake of adenosine. *J. Neurochem.* **49:** 1174–1182.

Trapido-Rosenthal, H. G., W. E. S. Carr, and R. A. Gleeson. 1989. Biochemistry of purinergic olfaction: the importance of nucleotide dephosphorylation. Pp. 243–262 in *Chemical Senses Vol. 1, Receptor Events and Transduction in Taste and Olfaction*, J. G. Brand, J. H. Teeter, R. H. Cagan, and M. R. Kare, eds. Marcel Dekker, New York.

Walther, M., R. Ulrich, M. Kroiher, and S. Berking. 1996. Metamorphosis and pattern formation in *Hydractinia echinata*, a colonial hydroid. *Int. J. Dev. Biol.* **40:** 313–322.

Reference: *Biol. Bull.* **194:** 92–97. (February, 1998)

A Protein Identical to the Yolk Protein Is Stored in the Testis in Male Red Sea Urchin, *Pseudocentrotus depressus*

TATSUYA UNUMA[1,*], TOHRU SUZUKI[2], TADAHIDE KUROKAWA[2], TAKESHI YAMAMOTO[1], AND TOSHIO AKIYAMA[1]

[1] *Inland Station, National Research Institute of Aquaculture, Tamaki, Mie 519-04, Japan; and* [2] *National Research Institute of Aquaculture, Nansei, Mie 516-01, Japan*

Abstract. Female sea urchins store the major yolk protein (MYP) in ovarian nutritive phagocytes before vitellogenesis. Using immunological procedures, we detected MYP in the testicular nutritive phagocytes of *Pseudocentrotus depressus*, the red sea urchin, and then compared the distribution of MYP between sexes during gametogenesis. MYP was purified from unfertilized eggs by ion exchange chromatography (Q Sepharose) and gel filtration (Superdex 200), and an antiserum (anti-MYP) was raised against MYP. Immunoblot analysis demonstrated that immature testes, as well as ovaries, contained a large quantity of MYP. Immunohistochemistry showed that MYP was distributed in the nutritive phagocytes occupying the follicular lumen in both males and females. In both sexes, as gametogenesis proceeded, the nutritive phagocytes degenerated and the gonadal lumen filled with gametes. MYP accumulated in ripe ova as a yolk protein in the mature ovary. In contrast, MYP was not detected in mature testes, because stored spermatozoa did not react with anti-MYP. We conclude that in male *P. depressus*, MYP is stored in the testicular nutritive phagocytes and utilized as the nutrient source for spermatogenesis.

Introduction

The most abundant yolk protein found in sea urchin eggs is a glycoprotein with a molecular weight of about 180 kDa; this has been termed the major yolk protein or major yolk glycoprotein (MYP; Harrington and Easton, 1982; Kari and Rottmann, 1985; Yokota and Kato, 1988). Unlike other oviparous animals in which vitellogenin, a precursor of MYP, is female specific, sea urchins have an abundant supply of vitellogenin in the coelomic fluid of males as well as females (Harrington and Easton, 1982; Shyu *et al.*, 1986). Shyu *et al.* (1986) found that vitellogenin mRNA is expressed in the intestines and gonads of both sexes in *Strongylocentrotus purpuratus*. This suggests the possibility that in sea urchins vitellogenin performs an unidentified function required by males in addition to its role in vitellogenesis in females.

In female sea urchins, vitellogenin is reported to be incorporated into the nutritive phagocytes (accessory cells) in the previtellogenic ovary for temporary storage, and then transported to the oocytes to be accumulated as MYP (Ozaki *et al.*, 1986; Harrington and Ozaki, 1986). The gonads of male sea urchins also have nutritive phagocytes for nutrient storage (Walker, 1982). However, it is not clear whether the testicular nutritive phagocytes contain vitellogenin.

The main objective of this study is to examine whether male sea urchins store MYP-related proteins in their nutritive phagocytes. To achieve this, we purified MYP from unfertilized eggs of the red sea urchin, *Pseudocentrotus depressus*, and prepared an antiserum against MYP. We compared the distribution of MYP reactivity during gametogenesis in both sexes by immunological analysis.

Materials and Methods

Animals

Six-month-old juveniles of *P. depressus*, hatched and reared at the Fukuoka Prefectural Fish Farming Center,

Received 11 March 1997; accepted 20 October 1997.
* To whom correspondence should be addressed.
Abbreviation: MYP = major yolk protein.

were transferred to the Coastal Station of the National Research Institute of Aquaculture. They were kept in 1000-l tanks supplied with sand-filtered seawater at 30 l · min^{-1}, and reared on kelp, *Eisenia bicyclis*. The animals used for the experiment were 2 or 3 years old.

After the peristomial membrane of the animal was removed, coelomic fluid was collected with Pasteur pipettes. Coelomocytes were removed by centrifugation at 600 × *g* for 5 min. The coelomic fluid was kept at −80°C until use.

Gonads were dissected out and stored at −80°C. Small pieces were fixed in Bouin's solution for histological observations. Paraffin sections of 6-μm thickness were prepared and stained with hematoxylin and eosin. The gonadal maturity of each animal was classified according to the six stages described by Fuji (1960), with some slight modifications as described previously (Unuma *et al.*, 1996).

During the spawning season in November, eggs were obtained by coelomic injection of 20% KCl and then were stored at −80°C.

Purification of MYP

Unfertilized eggs (3 ml) were homogenized with 15 ml of 10 m*M* Tris-HCl buffer containing 10 m*M* NaCl (TBS; pH 8.0) and 0.1 m*M* phenylmethylsulfonylfluoride (PMSF) using Polytron (Kinematica, Switzerland). The homogenate was centrifuged at 25,000 × *g* for 20 min at 4°C, and the supernatant was applied to a HiLoad 16/10 Q Sepharose fast flow column (Pharmacia LKB Biotechnology, Sweden) equilibrated with TBS. After being washed with 40 ml of the same buffer, the retained proteins were eluted with a NaCl linear gradient from 10 m*M* to 1 *M* (200 ml in total) using FPLC (Pharmacia). The flow rate of the column was 2.0 ml · min^{-1}, and 4-ml aliquots of eluate were collected. Fractions rich in MYP were pooled, concentrated threefold using Molcut LGC (Millipore Corp., USA), and applied to a HiLoad 16/60 Superdex 200 column (Pharmacia) equilibrated with 10 m*M* Tris-HCl buffer containing 150 m*M* NaCl (pH 8.0). Proteins were eluted with the same buffer at a flow rate of 1 ml · min^{-1}, and fractions of 2 ml were collected. A gel filtration calibration kit (Pharmacia) was used to estimate molecular weight.

Electrophoresis

Sodium dodecylsulfate-polyacrylamide gel electrophoresis (SDS-PAGE) was performed using 5% slab gel according to Laemmli (1970). Protein bands were visualized with Coomassie brilliant blue R-250. SDS-PAGE standards (Bio-Rad Laboratories, USA) were electrophoresed for molecular weight calibration. Precast gels (NPU-5L; Atto Corp., Japan) were used for Figures 1 and 5. These gels showed double bands in the low molecular weight end, whereas the gels prepared in our laboratory showed a single band there (Fig. 4). However, Atto Corp. assures us that there is no difference between these gels in comparisons of the middle to high molecular weight ranges.

Preparation of antiserum

The peak fraction from the Superdex 200 gel filtration was electrophoresed on SDS-PAGE under nonreducing conditions. A gel slice containing the 270-kDa band was excised. The protein was eluted from the gel by an Electro Eluter (Bio-Rad), mixed with an equal volume of Freund's complete adjuvant, and then injected subcutaneously into the back of a rabbit once a week. After 4 injections, blood was collected from an ear vein. The blood was centrifuged at 1500 × *g* for 20 min, and the supernatant was collected as antiserum (anti-MYP).

Immunoblotting

Gonads were homogenized with 20-fold TBS and centrifuged at 25,000 × *g* for 20 min at 4°C. Supernatants were used as the gonadal extracts.

To detect the protein reactive with anti-MYP, coelomic fluids and the gonadal extracts were immunoblotted according to Towbin *et al.* (1979). Proteins separated by 5% SDS-PAGE were electrophoretically transferred onto a polyvinylidene difluoride (PVDF) membrane. The membrane was immunostained using anti-MYP and POD Immunostain Set (Wako Pure Chemical Industries, Ltd., Japan).

Immunohistochemistry

To visualize MYP reactivity in the gonads, immunohistochemistry was performed on paraffin-embedded gonads sectioned at 6 μm. After the paraffin was removed, sections were incubated with anti-MYP (1:2000 dilution) and then treated with Histofine SAB-PO Kit (Nichirei, Japan) as described in the manufacturer's instructions. Normal rabbit serum was substituted for anti-MYP to confirm the specificity of the immunohistochemical staining.

Results

Purification of MYP

SDS-PAGE analysis under reducing conditions showed that a 170-kDa protein occurred abundantly in *P. depressus* eggs (Fig. 1a). This protein band was reactive with periodic acid-Schiff (PAS) reagent (data not shown), similar to MYP reported for other sea urchin eggs (Harrington and Easton, 1982; Ozaki *et al.*, 1986; Yokota and Kato, 1988). We concluded that this 170-kDa protein is the MYP of *P. depressus* because of the similarity in

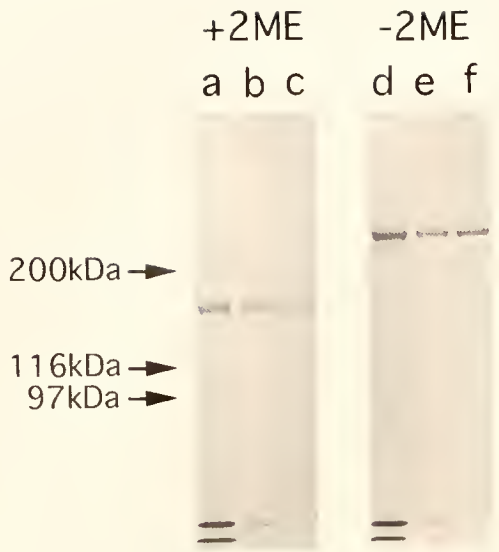

Figure 1. Five percent SDS-PAGE analysis of *Pseudocentrotus depressus* major yolk protein. Lanes a–c are under reducing conditions (+2ME), and d–f are under nonreducing conditions (−2ME). (a, d) Crude extract from unfertilized eggs; total protein = 5 μg. (b, e) Pooled fraction from Q Sepharose (Fig. 2); total protein = 1 μg. (c, f) Pooled fraction from Superdex 200 (Fig. 3); total protein = 1 μg.

molecular weight and the PAS reactivity with other MYP. Under nonreducing conditions, a large quantity of 270-kDa protein was observed instead of the 170-kDa band (Fig. 1d). This suggests that intact MYP consists of subunits.

Egg extract was applied to an ion exchange column using Q Sepharose (Fig. 2). The major protein peak eluted at 280 m*M* NaCl was revealed to be rich in MYP by SDS-PAGE (Fig. 1b, e). After concentration, the fractions were subjected to gel filtration using Superdex 200 (Fig. 3). The major peak eluted at 600 kDa gave a homogeneous 270-kDa band on SDS-PAGE under nonreducing conditions (Fig. 1f). Thus, we concluded that the MYP of *P. depressus* was isolated by a combination of ion exchange chromatography and gel filtration. Under reducing conditions, MYP gave a major 170-kDa band and four minor bands of about 100 kDa (Fig. 1c). These minor bands are probably fragments derived from the intact MYP by proteolysis.

To raise an antiserum against MYP (anti-MYP), we electronically eluted the 270-kDa band from an SDS-PAGE gel run under nonreducing conditions, then immunized a rabbit with the isolated protein (Fig. 1f).

MYP-related proteins in gonads and coelomic fluids

We used SDS-PAGE and immunoblot analyses to test the gonads and coelomic fluids of Stage 1 females and males for the presence of the protein reactive with anti-MYP. A 170-kDa protein was predominant in both female and male gonadal extracts under reducing conditions (Fig. 4b, c). These protein bands were immunoreactive with anti-MYP (Fig. 4l, m). On the basis of the molecular weight and immunoreactivity of the major protein stored in the immature ovary and testis, we concluded that it is identical to MYP. Predominant protein bands with a slightly higher molecular weight (180 kDa) than MYP were detected in the coelomic fluid of both sexes (Fig. 4d, e). In other sea urchins investigated, vitellogenin is the most abundant coelomic fluid protein; it has a molecular weight of about 200 kDa and is immunoreactive with the antiserum against MYP (Harrington and Easton, 1982; Shyu *et al.*, 1986;

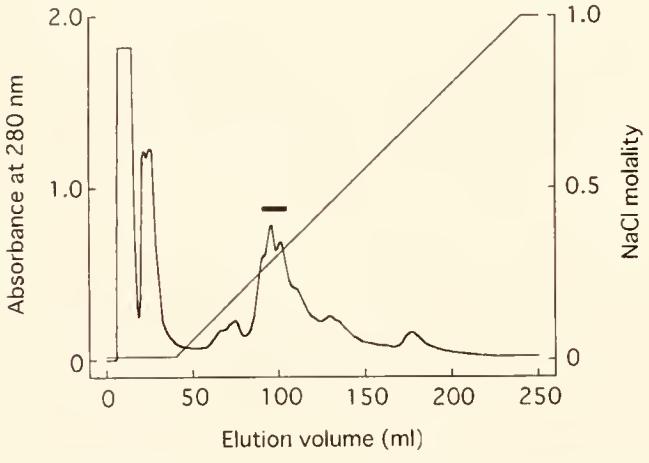

Figure 2. Q Sepharose ion exchange chromatography of extract from unfertilized eggs of *Pseudocentrotus depressus*. Fractions marked with a bar were pooled and concentrated for Superdex 200 gel filtration.

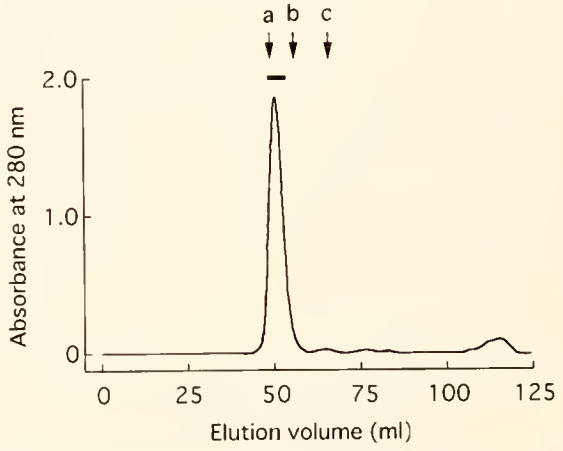

Figure 3. Gel filtration on Superdex 200 of partialy purified major yolk protein. The pooled fraction obtained by Q Sepharose (Fig. 2) was applied to Superdex 200. Fractions marked with a bar were pooled. Thyroglobulin (a; 669 kDa), ferritin (b; 440 kDa), and catalase (c; 232 kDa) were used as standards for molecular weight estimation.

Figure 4. Five percent SDS-PAGE and immunoblotting using anti-MYP of gonadal extracts and coelomic fluids of Stage 1 *Pseudocentrotus depressus*. Lanes a–e and k–o are under reducing conditions, and f–j are under nonreducing conditions. (a, f, k) Egg extract; (b, g, l) ovarian extract; (c, h, m) testicular extract; (d, i, n) female coelomic fluid; (e, j, o) male coelomic fluid. Total protein applied = 10 μg for egg extract, 2 μg for all others.

Cervello *et al.* 1994). The protein of the predominant bands of 180 kDa in the coelomic fluids was identified as vitellogenin on the basis of its reactivity with anti-MYP (Fig. 4n, o) and the similarity of its molecular weight to that of vitellogenin in other sea urchins. The protein in the gonads and coelomic fluids of both sexes appears to exist as a complex—as does MYP in unfertilized eggs—because in SDS-PAGE under nonreducing conditions bands occurred at around 270 kDa (Fig. 4f–j).

Extracts from testes at three maturational stages (Stages 1, 3, and 4) were subjected to SDS-PAGE and immunoblotting analyses (Fig. 5). As spermatogenesis progressed, the quantity of 170-kDa protein reactive with anti-MYP decreased in the testis. Mature testis (Stage 5) contained little of this protein (Fig. 5c, f).

Distribution of MYP in gonads during gametogenesis

Immunolocalization of MYP in the gonads is shown in Figure 6. The follicular lumina of immature testes and ovaries (Stage 1) were filled with nutritive phagocytes (Fig. 6A, G). The protein reactive with anti-MYP was stored in the nutritive phagocytes of both sexes (Fig. 6D, J). With the progress of gametogenesis, testes contained peripheral lines of spermatogonia and spermatocytes, and ovaries had a row of vitellogenic oocytes. The lumen of testes later filled with spermatozoa and that of ovaries with ripe ova (Fig. 6B, H). Spermatogenic cells and oocytes did not react with the anti-MYP, whereas ripe ova did (Fig. 6E, K). The nutritive phagocytes had degenerated but were still reactive with anti-MYP in Stage 3 gonads (Fig. 6E, K). In mature gonads (Stage 4), the gonadal lumina were filled with spermatozoa or ripe ova, and nutritive phagocytes were recognized only at the periphery of follicles (Fig. 6C, I). The protein disappeared

Figure 5. Five percent SDS-PAGE under reducing conditions and immunoblotting using anti-MYP of testicular extracts of *Pseudocentrotus depressus* at three maturational stages. (a, d) Stage 1; (b, e) Stage 3; (c, f) Stage 4. Amount of extract applied to each lane = 2 μl.

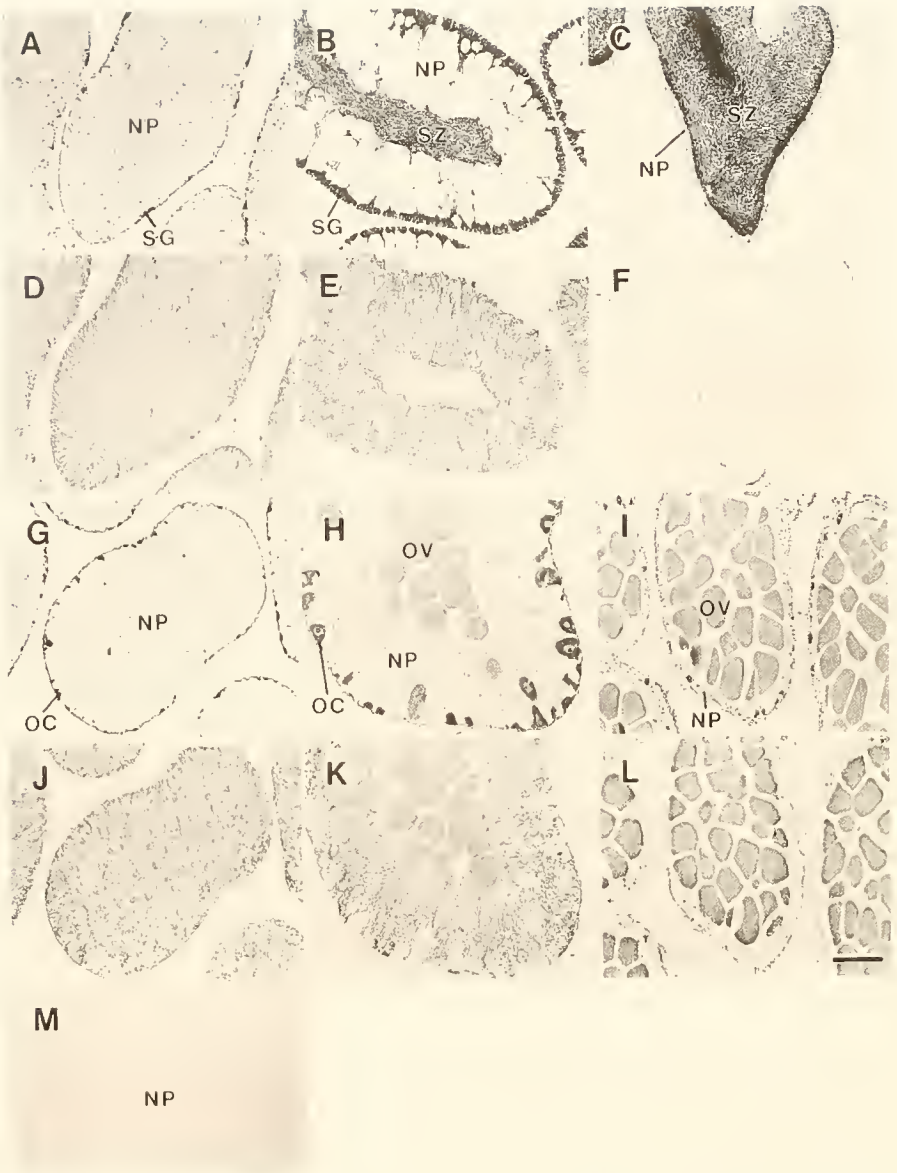

Figure 6. Immunolocalization of the protein reactive with anti-MYP in the testes (A–F and M) and ovaries (G–L) of *Pseudocentrotus depressus*. A–C and G–I were stained with hematoxylin and eosin; D–F and J–L were immunostained with anti-MYP; M was treated with normal rabbit serum instead of anti-MYP as an immunostaining control. (A, D, G, J, M) Stage 1: Nutritive phagocytes reacted with anti-MYP in both testis and ovary. (B, E, H, K) Stage 3: The spermatogenic cells and oocytes did not react with anti-MYP, but the ripe ova did react. Nutritive phagocytes were still reactive with anti-MYP. (C, F, I, L) Stage 4: The protein was not detected from the testis, but it was accumulated in the ripe ova in the ovary. NP, nutritive phagocyte; SG, spermatogonium and spermatocyte; SZ, spermatozoon; OC, oocyte; OV, ripe ovum. Scale bar = 100 μm.

from the testis (Fig. 6F), but in the ovary it accumulated in ripe ova as a yolk protein (Fig. 6L).

Discussion

This study demonstrates that prior to gametogenesis in the red sea urchin *P. depressus*, a protein identical to MYP is stored abundantly in the nutritive phagocytes of males as well as those of females. However, as gametogenesis proceeds, this protein decreases in quantity in the testis while it is accumulated in ripe ova as a yolk protein in the ovary. Histological observations have led to the suggestion that nutritive phagocytes in the testis are nutrient storage sites for spermatogenesis (Walker, 1982).

However, it is still unclear what kind of material functions as a nutrient storage in the testicular nutritive phagocytes. We propose that the MYP found in the testis functions as a nutrient for spermatogenesis in *P. depressus*. In oviparous animals, yolk protein is a nutrient source for embryogenesis and is usually found only in the female (Hara, 1987; Quinitio *et al.*, 1989, 1990; Suzuki *et al.*, 1992; Osada *et al.*, 1992). *P. depressus* is unique in apparently using a yolk protein as a nutrient for spermatogenesis.

Vitellogenin, a precursor of MYP, is abundant in the coelomic fluid of both males and females, and its role in the male sea urchin has been discussed (Harrington and Easton, 1982; Shyu *et al.*, 1986). Harrington and Easton (1982) postulated that vitellogenin performs an unknown physiological role required by both sexes, but related to the hermaphrodism observed in some echinoderms. Shyu *et al.* (1986) proposed that vitellogenin functions as an analog to the serum albumin of vertebrates, as a carrier protein, or as a store for amino acids. The possibility that male vitellogenin, like female vitellogenin, is a precursor of MYP has not been discussed because MYP storage in the testis had not been demonstrated. In female sea urchins, vitellogenin is incorporated into the nutritive phagocytes, then transported to the oocytes to be accumulated as MYP (Ozaki *et al.*, 1986; Harrington and Ozaki, 1986). We suggest that male vitellogenin is a precursor of MYP in the testis and is incorporated into the testicular nutritive phagocytes as a nutrient source for spermatogenesis. We think that the process until the incorporation into the gonad is probably the same in both sexes, although the final site for utilization is different.

MYP of *P. depressus* has a molecular weight of 170 kDa under reducing conditions, but vitellogenin has a slightly higher molecular weight (180 kDa). The same is true in *S. purpuratus:* the molecular weight of vitellogenin is 195 kDa, but that of MYP is 180 kDa (Harrington and Easton, 1982; Shyu *et al.*, 1986). Thus, a decrease in molecular weight from vitellogenins to MYPs seems to be a common phenomenon in sea urchins. It is probable that vitellogenin is slightly modified in molecular structure after its incorporation into the gonads. Shyu *et al.* (1986) presumed that this modification takes place in the oocytes, but we suggest that it occurs in the nutritive phagocytes of both sexes immediately after incorporation. We base our conclusion on the observation that the protein stored in the nutritive phagocytes is already modified to 170 kDa and little of the 180 kDa protein is detected in the gonads.

Acknowledgments

We are grateful to the Fukuoka Prefectural Fish Farming Center for providing the juvenile *P. depressus* used in this study.

Literature Cited

Cervello, M., V. Arizza, G. Lattuca, N. Parrinello, and V. Matranga. 1994. Detection of vitellogenin in a subpopulation of sea urchin coelomocytes. *Eur. J. Cell Biol.* **64:** 314–319.

Fuji, A. 1960. Studies on the biology of the sea urchin. I. Superficial and histological gonadal changes in gametogenic process of two sea urchins, *Strongylocentrotus nudus* and *S. intermedius*. *Bull. Fac. Fish. Hokkaido Univ.* **11:** 1–14.

Hara, A. 1987. Studies on female-specific serum proteins (vitellogenin) and egg yolk proteins in teleosts: immunochemical, physicochemical and structural studies. *Mem. Fac. Fish. Hokkaido Univ.* **34:** 1–59.

Harrington, F. E., and D. P. Easton. 1982. A putative precursor to the major yolk protein of the sea urchin. *Dev. Biol.* **94:** 505–508.

Harrington, F. E., and H. Ozaki. 1986. The major yolk glycoprotein precursor in echinoids is secreted by coelomocytes into the coelomic plasma. *Cell Differ.* **19:** 51–57.

Kari, B. E., and W. L. Rottmann. 1985. Analysis of changes in a yolk glycoprotein complex in the developing sea urchin embryo. *Dev. Biol.* **108:** 18–25.

Laemmli, U. K. 1970. Cleavage of structural proteins during the assembly of the head of bacteriophage T4. *Nature* **227:** 680–685.

Osada, M., T. Unuma, and K. Mori. 1992. Purification and characterization of a yolk protein from the scallop ovary. *Nippon Suisan Gakkaishi* **58:** 2283–2289.

Ozaki, H., O. Moriya, and F. E. Harrington. 1986. A glycoprotein in the accessory cell of the echinoid ovary and its role in vitellogenesis. *Roux's Arch. Dev. Biol.* **195:** 74–79.

Quinitio, E. T., A. Hara, K. Yamauchi, T. Mizushima, and A. Fuji. 1989. Identification and characterization of vitellin in a hermaphrodite shrimp, *Pandalus kessleri*. *Comp. Biochem. Physiol.* **94B:** 445–451.

Quinitio, E. T., A. Hara, K. Yamauchi, and A. Fuji. 1990. Isolation and characterization of vitellin from the ovary of *Penaeus monodon*. *Invertebr. Reprod. Dev.* **17:** 221–227.

Shyu, A.-B., R. A. Raff, and T. Blumenthal. 1986. Expression of the vitellogenin gene in female and male sea urchin. *Proc. Natl. Acad. Sci. USA* **83:** 3865–3869.

Suzuki, T., A. Hara, K. Yamaguchi, and K. Mori. 1992. Purification and immunolocalization of a vitellin-like protein from the Pacific oyster *Crassostrea gigas*. *Mar. Biol.* **113:** 239–245.

Towbin, H., T. Staehelin, and J. Gordon. 1979. Electrophoretic transfer of proteins from polyacrylamide gels to nitrocellulose sheets: procedure and some applications. *Proc. Natl. Acad. Sci. USA* **76:** 4350–4354.

Unuma, T., K. Konishi, H. Furuita, T. Yamamoto, and T. Akiyama. 1996. Seasonal changes in gonads of cultured and wild red sea urchin, *Pseudocentrotus depressus*. *Suisanzoshoku* **44**(2): 169–175.

Walker, C. W. 1982. Nutrition of gametes. Pp. 449–468 in *Echinoderm Nutrition*, M. Jangoux and J. M. Lawrence, eds. A. A. Balkema, Rotterdam.

Yokota, Y., and K. H. Kato. 1988. Degradation of yolk proteins in sea urchin eggs and embryos. *Cell Differ.* **23:** 191–200.

Ask any researcher about the Olympus line of Advanced Research Microscopes.

We did.

"The Provis Microscope simply gives me the application versatility I want," one researcher told us. "The resolution and contrast are quite spectacular. I can even see new detail when I review my older specimens. And you have all the right imaging modules and accessories I need to configure my microscope system. Your special fluorescence-excitation balancer, for instance, is a great accessory—I can now visually balance the signal between two probes!"

What about your needs? If your field is neuroscience, our BX50WI offers you the best stability and a focus mechanism that moves nothing but the nosepiece. On the other hand, your research may call for our new LSM Fluoview desktop confocal laser system. Or you may need the unparalleled light transmission of the iX70 inverted.

Whichever microscope you select, it's totally configurable to your personal specifications. So find out how our advanced microscope systems can match your requirements today and evolve for your changing needs tomorrow. Call us at 1-800-455-9236. Or fax 1-612-942-6040. We'll give you all the answers you can ask for.

OLYMPUS

RESEARCH MICROSCOPES.

The world's most custom-built microscopes.

Volume 194 Number 2

THE BIOLOGICAL BULLETIN

APRIL, 1998

Published by the Marine Biological Laboratory

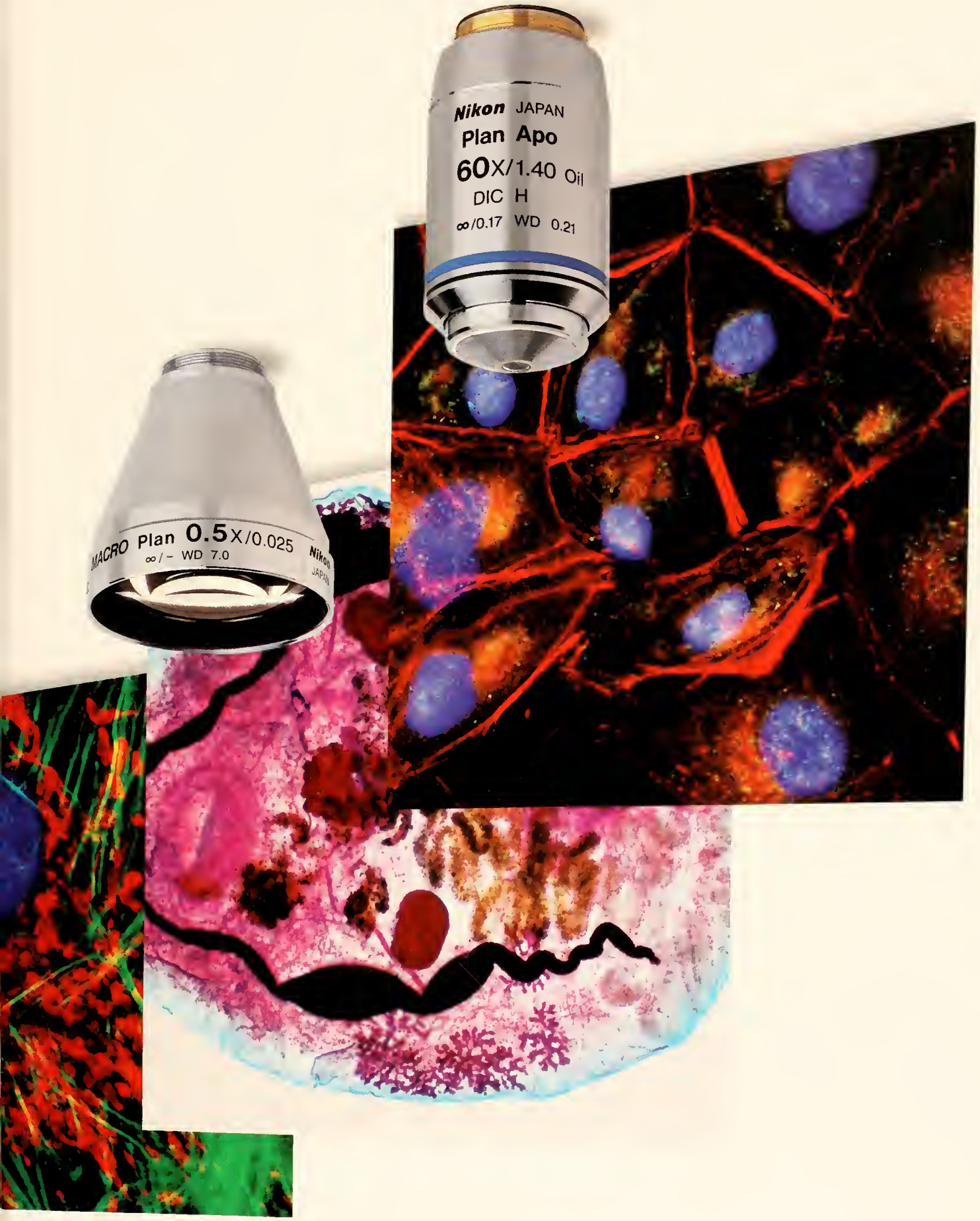
Nikon JAPAN
Plan Apo
60X/1.40 Oil
DIC H
∞/0.17 WD 0.21
MACRO Plan 0.5X/0.025
∞/- WD 7.0
Nikon
JAPAN

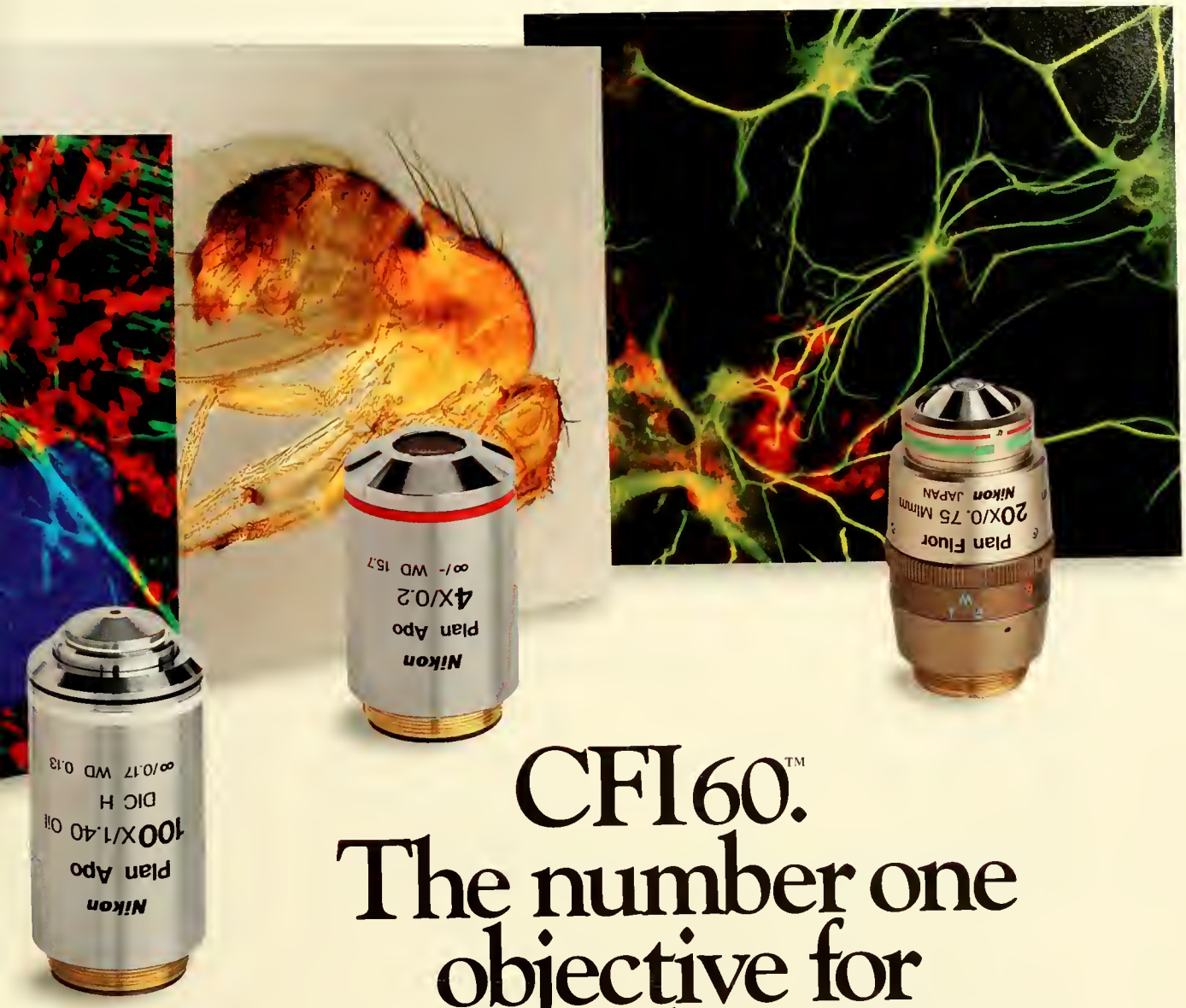

CFI60.™ The number one objective for every objective.

CFI60 ECLIPSE

The Nikon Eclipse E800™ is America's number one selling research microscope in its class.* What's the secret of our success?

Our CFI60 Technology.

The CFI60 chromatic aberration-free objectives have overcome the limitations of conventional infinity systems — with the longest working distances, highest numerical apertures, and the widest magnification range and documentation field sizes ever. Nikon's advanced technology in glass formulation, lens manufacture and coating processes have redefined infinity optics. With this technology, we have achieved higher performance levels by incorporating a 60mm objective parfocal distance, a 25mm objective thread size and a standard 25mm field of view.

Enjoy the widest range in objectives for the most diverse observation requirements.

With over 80 Nikon CFI60 objectives, including our exclusive 0.5X and the high UV transmission universal Plan Fluor series, you'll find we have the lens for you. Also available are several objectives for techniques such as confocal, microinjection and detection of GFP expression that can be utilized for phase contrast, DIC, fluorescence and brightfield. Call **1-800-52-NIKON, ext 331** today for a demonstration of our CFI60 objectives, and you'll soon find the best objective to meet your objective.

www.nikonusa.com

Nikon

Redefining Infinity

*Based on the Opto-Precision Instruments Association's (OPIA) Fourth Qtr. 1997, U.S.A. Microscope Survey

THE
BIOLOGICAL BULLETIN

PUBLISHED BY

THE MARINE BIOLOGICAL LABORATORY

APRIL, 1998

Printed and Issued by
LANCASTER PRESS, Inc.
3575 HEMPLAND ROAD
LANCASTER, PA

Cover

Time-lapse photograph showing the opisthobranch mollusc *Aplysia brasiliana* swimming. Animals in the genus *Aplysia* are normally solitary, but during the reproductive season they move into breeding aggregations where they lay eggs and mate. The eggs are a source of pheromones—both water-borne and contact—that establish and maintain the aggregation, attracting other animals to the area and facilitating reproductive activity. Egg laying can be induced by injecting atrial gland extract (a source of peptides related to egg-laying hormone) into the hemocoel. When the extract is used to induce egg laying, the investigator has control over the number of animals laying eggs, the volume of eggs laid, the timing and location of egg laying, and (to some extent) the purity of the surrounding seawater. For water-borne pheromones, this means that the investigator can regulate the amount of pheromone secreted, the timing and coordination of secretion, the number of products in the seawater that are derived from other organisms, and the amount of degradation that occurs. This approach was used by Painter *et al.* (p. 120, this issue) to isolate and characterize *attractin*, a peptide that is attractive to *Aplysia* and may induce mating behavior. Attractin is the first peptide pheromonal attractant characterized in a mollusc—or any invertebrate.

CONTENTS

THE BIOLOGICAL BULLETIN

THE BIOLOGICAL BULLETIN is published six times a year by the Marine Biological Laboratory, 7 MBL Street, Woods Hole, Massachusetts 02543.

Subscriptions and similar matter should be addressed to Subscription Manager, THE BIOLOGICAL BULLETIN, Marine Biological Laboratory, 7 MBL Street, Woods Hole, Massachusetts 02543. Subscription per year (six issues, two volumes): $195 for libraries; $95 for individuals. Subscription per volume (three issues): $97.50 for libraries; $50 for individuals. Back and single issues (subject to availability): $40 for libraries; $20 for individuals.

Communications relative to manuscripts should be sent to Michael J. Greenberg, Editor-in-Chief, or Pamela L. Clapp, Managing Editor, at the Marine Biological Laboratory, 7 MBL Street, Woods Hole, Massachusetts 02543. Telephone: (508) 289-7428. FAX: 508-457-1924. E-mail: pclapp@mbl.edu.

http://www.mbl.edu/BiologicalBulletin/

The home page for the electronic companion to THE BIOLOGICAL BULLETIN—*the Marine Models Electronic Record*—and other BIOLOGICAL BULLETIN publications is available on the World Wide Web at the address shown above.

THE BIOLOGICAL BULLETIN is indexed in bibliographic services including *Index Medicus* and MEDLINE, *Chemical Abstracts, Current Contents, CABS (Current Awareness in Biological Sciences),* and *Geo Abstracts.*

Printed on acid free paper,
effective with Volume 180, Issue 1, 1991.

POSTMASTER: Send address changes to THE BIOLOGICAL BULLETIN, Marine Biological Laboratory, 7 MBL Street, Woods Hole, MA 02543.

Periodicals postage paid at Woods Hole, MA, and additional mailing offices.
ISSN 0006-3185

INSTRUCTIONS TO AUTHORS

The Biological Bulletin accepts outstanding original research reports of general interest to biologists throughout the world. Papers are usually of intermediate length (10–40 manuscript pages). A limited number of solicited review papers may be accepted after formal review. A paper will usually appear within four months after its acceptance.

Very short, especially topical papers (less than 9 manuscript pages including tables, figures, and bibliography) will be published in a separate section entitled "Research Notes." A Research Note in *The Biological Bulletin* follows the format of similar notes in *Nature.* It should open with a summary paragraph of 150 to 200 words comprising the introduction and the conclusions. The rest of the text should continue on without subheadings, and there should be no more than 30 references. References should be referred to in the text by number, and listed in the Literature Cited section in the order that they appear in the text. Unlike references in *Nature,* references in the Research Notes section should conform in punctuation and arrangement to the style of recent issues of *The Biological Bulletin.* Materials and Methods should be incorporated into appropriate figure legends. See the article by Lohmann *et al.* (October 1990, Vol. **179:** 214–218) for sample style. A Research Note will usually appear within two months after its acceptance.

The Editorial Board requests that regular manuscripts conform to the requirements set below; those manuscripts that do not conform will be returned to authors for correction before review.

1. ***Manuscripts.*** Manuscripts, including figures, should be submitted in triplicate. (Xerox copies of photographs are not acceptable for review purposes.) The submission letter accompanying the manuscript should include a telephone number, a FAX number, and (if possible) an E-mail address for the corresponding author. The original manuscript must be typed in no smaller than 12 pitch or 10 point, using double spacing (*including* figure legends, footnotes, bibliography, etc.) on one side of 16- or 20-lb. bond paper, 8 by 11 inches. Please, no right justification. Manuscripts should be proofread carefully and errors corrected legibly in black ink. Pages should be numbered consecutively. Margins on all sides should be at least 1 inch (2.5 cm). Manuscripts should conform to the *Council of Biology Editors Style Manual,* 5th Edition (Council of Biology Editors, 1983) and to American spelling. Unusual abbreviations should be kept to a minimum and should be spelled out on first reference as well as defined in a footnote on the title page. Manuscripts should be divided into the following components: Title page, Abstract (of no more than 200 words), Introduction, Materials and Methods, Results, Discussion, Acknowledgments, Literature Cited, Tables, and Figure Legends. In addition, authors should supply a list of words and phrases under which the article should be indexed.

2. ***Title page.*** The title page consists of a condensed title or running head of no more than 35 letters and spaces, the manuscript title, authors' names and appropriate addresses, and footnotes listing present addresses, acknowledgments or contribution numbers, and explanation of unusual abbreviations.

3. ***Figures.*** The dimensions of the printed page, 7 by 9 inches, should be kept in mind in preparing figures for publication. We recommend that figures be about 1 times the linear dimensions of the final printing desired, and that the ratio of the largest to the smallest letter or number and of the thickest to the thinnest line not exceed 1:1.5. Explanatory matter generally should be included in legends, although axes should always be identified on the illustration itself. Figures should be prepared for reproduction as either line cuts or halftones. Figures to be reproduced as line cuts should be unmounted glossy photographic reproductions or drawn in black ink on white paper, good-quality tracing cloth or plastic, or blue-lined coordinate paper. Those to be reproduced as halftones should be mounted on board, with both designating numbers or letters and scale bars affixed directly to the figures. All figures should be numbered in consecutive order, with no distinction between text and plate figures and cited, in order, in the text. The author's name and an arrow indicating orientation should appear on the reverse side of all figures.

Color: The Biological Bulletin will publish color figures and plates, but must bill authors for the actual additional cost of printing in color. The process is expensive, so authors with more than one color image should—consistent with editorial concerns, especially citation of figures in order—combine them into a single plate to reduce the expense. On request, when supplied with a copy of a color illustration, the editorial staff will provide a pre-publication estimate of the printing cost.

4. ***Tables, footnotes, figure legends, etc.*** Authors should follow the style in a recent issue of *The Biological Bulletin* in preparing table headings, figure legends, and the like. Because of the high cost of setting tabular material in type, authors are asked to limit such material as much as possible. Tables, with their headings and footnotes, should be typed on separate sheets, numbered with consecutive Roman numerals, and placed after the Literature Cited. Figure legends should contain enough information to make the figure intelligible separate from the text. Legends should be typed double spaced, with consecutive Arabic numbers, on a separate sheet at the end of the paper. Footnotes should be limited to authors' current addresses, acknowledgments or contribution numbers, and explanation of unusual abbreviations. All such footnotes should appear on the title page. Footnotes are not normally permitted in the body of the text.

5. ***Literature cited.*** In the text, literature should be cited by the Harvard system, with papers by more than two authors cited as Jones *et al.*, 1980. Personal communications and material in preparation or in press should be cited in the text only, with author's initials and institutions, unless the material has been formally accepted and a volume number can be supplied. The list of references following the text should be headed Literature Cited, and must be typed double spaced on separate pages, conforming in punctuation and arrangement to the style of recent issues of *The Biological Bulletin*. Citations should include complete titles and inclusive pagination. Journal abbreviations should normally follow those of the U. S. A. Standards Institute (USASI), as adopted by BIOLOGICAL ABSTRACTS and CHEMICAL ABSTRACTS, with the minor differences set out below. The most generally useful list of biological journal titles is that published each year by BIOLOGICAL ABSTRACTS (BIOSIS List of Serials; the most recent issue). Foreign authors, and others who are accustomed to using THE WORLD LIST OF SCIENTIFIC PERIODICALS, may find a booklet published by the Biological Council of the U.K. (obtainable from the Institute of Biology, 41 Queen's Gate, London, S.W.7, England, U.K.) useful, since it sets out the WORLD LIST abbreviations for most biological journals with notes of the USASI abbreviations where these differ. CHEMICAL ABSTRACTS publishes quarterly supplements of additional abbreviations. The following points of reference style for THE BIOLOGICAL BULLETIN differ from USASI (or modified WORLD LIST) usage:

A. Journal abbreviations, and book titles, all underlined (for *italics*)

B. All components of abbreviations with initial capitals (not as European usage in WORLD LIST *e.g., J. Cell. Comp. Physiol.* NOT *J. cell. comp. Physiol.*)

C. *All* abbreviated components must be followed by a period, whole word components *must not* (*i.e., J. Cancer Res.*)

D. Space between all components (*e.g., J. Cell. Comp. Physiol.*, not *J.Cell.Comp.Physiol.*)

E. Unusual words in journal titles should be spelled out in full, rather than employing new abbreviations invented by the author. For example, use *Rit Vísindafjélags Islendinga* without abbreviation.

F. All single word journal titles in full (*e.g., Veliger, Ecology, Brain*).

G. The order of abbreviated components should be the same as the word order of the complete title (*i.e., Proc.* and *Trans.* placed where they appear, not transposed as in some BIOLOGICAL ABSTRACTS listings).

H. A few well-known international journals in their preferred forms rather than WORLD LIST or USASI usage (*e.g., Nature, Science, Evolution* NOT *Nature, Lond., Science, N.Y.; Evolution, Lancaster, Pa.*)

6. ***Reprints, page proofs, and charges.*** Authors of articles in black and white (no color figures) receive their first 50 reprints (without covers) free of charge. Color reprints and additional black-and-white reprints may be purchased; authors will receive order forms. Reprints normally will be delivered about 2 to 3 months after the issue date. Authors (or delegates for foreign authors) will receive page proofs of articles shortly before publication. They will be charged the current cost of printers' time for corrections to these (other than corrections of printers' or editors' errors). Other than these charges for authors' alterations, *The Biological Bulletin* does not have page charges.

Reference: *Biol. Bull.* **194:** 99. (April, 1998)

A New Series of Articles in a New Section of the Journal

This issue of *The Biological Bulletin* contains the first article in a series that is titled "Concepts in Imaging and Microscopy." The series was conceived of, and is supported by, the Opto-Precision Instruments Association (OPIA), an association of manufacturers and distributors of microscopes, imaging hardware and software, and related peripherals produced primarily for light microscopy.

One of the fundamental aims of the OPIA is to educate users of those instruments—scientists, students, and technical staff—about all aspects of imaging through the microscope. Moreover, because the techniques and applications of image acquisition, processing, and analysis have developed so rapidly during the past decade, and are continuing to develop, the OPIA also aims to make these advances known to a wide range of users in science and industry. The series that begins in the following pages is a means to these ends.

Optical microscopy and image analysis are featured in two courses offered at the Marine Biological Laboratory, and these methodologies are also strongly represented in the Laboratory's research programs. The editors of *The Biological Bulletin* (which is published by the MBL) are therefore pleased to join with the OPIA in disseminating this important information to the scientific community. The first article, by Dr. Kenneth R. Castleman, is about color image processing; we expect succeeding papers to be equally authoritative, interesting, and useful.

A new section of the journal—"Imaging and Microscopy"—also begins with this issue, and we are fortunate that Dr. Shinya Inoué, an MBL Distinguished Scientist, will serve as its associate editor. Of course, the OPIA series will be housed in the new section, and we hope that scientists who have developed or are using promising novel methods in imaging and microscopy will also submit papers for publication in this venue.

Abstracts of articles and papers that appear in the "Imaging and Microscopy" section will also be published electronically with the journal's home page ⟨www.mbl.edu/BiologicalBulletin/⟩.

—Michael J. Greenberg
Editor-in-Chief

Reference: *Biol. Bull.* **194:** 100–107. (April, 1998)

Concepts in Imaging and Microscopy: Color Image Processing for Microscopy

KENNETH R. CASTLEMAN

Vice-President for Research, Perceptive Scientific Instruments, Inc, 2525 South Shore Blvd., League City, Texas 77573

Abstract. Digital image analysis has long been applied to monochrome images from the light microscope. Using these techniques one can locate, measure, identify, and count the objects of interest in a microscope field of view. Since microscope images often contain color information of interest, it is now becoming more common to analyze the spectral content of images as well. Although most of the digital imaging techniques developed for monochrome microscopy work well with color images, there are a few considerations specific to the analysis of multispectral imagery. These include obtaining a properly balanced multicolor digital image, specifying the color components of the image, and compensating for imperfect separation among the color channels.

Introduction

In two-dimensional digital image processing for microscopy, images are commonly considered to have a single scalar gray level (brightness or optical density) that is a function of two spatial coordinates. With color imaging there are two or more gray levels per pixel, each corresponding to a different spectral band. When we process three spectral bands corresponding to the red, green, and blue colors to which the human visual system responds, we call it "color image processing." A tri-color image can be formed by separately sampling three spectral bands over the two spatial coordinates of an optical image. In this article we focus on tri-color image analysis, although the generalization to four or more colors is straightforward.

The legacy of human vision

The retina of the human eye is covered with photoreceptor cells that are functionally analogous to the sensor sites (picture elements, or "pixels") on the CCD chip in a television camera. These cells absorb light from the image formed on the retina by the lens and cornea, and they send nerve impulses to the brain. The photoreceptor cells are a mixture of two types, rods and cones. While the more sensitive rods provide night vision, the cones afford color vision at higher light levels.

The cones occur in three types, each having a different spectral sensitivity. They divide the visible portion of the electromagnetic spectrum into the three bands that we perceive as red, green, and blue (RGB). These, then, are the three primary colors of human vision. Figure 1 shows the sensitivity spectra of the three types of cones in the human visual system (Wald, 1964). Notice the significant degree of overlap.

Because human vision uses three color channels, the bulk of the effort in the development of electronic imaging hardware has been devoted to tri-color systems. This is particularly true for television cameras, image digitizers, display systems, and image printers. As a result, tri-color equipment is produced in high volume and is widely available at relatively low cost. Digital image analysis techniques can be applied to images having any number of primary color channels, but the tri-color model is often used, simply because of hardware availability. We focus here on tri-color imaging to illustrate the most important points. In practice, however, the nature of the problem should dictate how many color channels are used.

Color digital image analysis

A monochrome digital image can be thought of as a scalar function of two spatial dimensions (x, y). By extension, a color digital image can be viewed as a scalar function of three dimensions, two spatial and one spectral (x, y, λ). It is usually more convenient, however, to treat

Received 10 December 1997; accepted 10 February 1998.
E-mail: castleman@persci.com

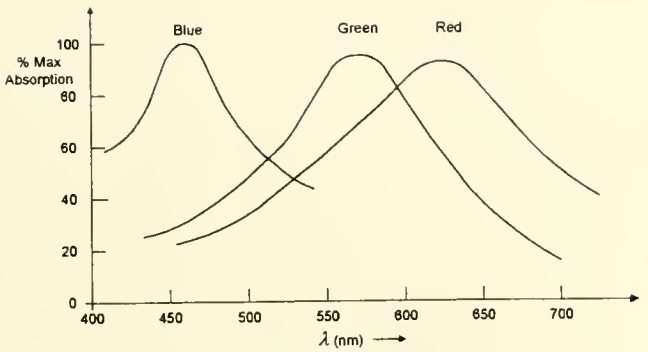

Figure 1. The spectral sensitivity of the cone photoreceptors in the human eye (after Wald, 1964).

it as a two-dimensional image having multiple gray levels (*e.g.*, red, green, and blue) at each pixel instead of only one. In other contexts it is more useful to consider it to be an overlay of monochrome digital images, each representing one of the primary colors. (We refer to these overlays as *color component images* or as the *color channels.*) The latter two viewpoints simplify the processing and analysis of color images because many of the techniques commonly applied to monochrome images can then be applied to color images with little modification.

Microscope image analysis

Three types of microscopic specimens exhibit color. Some specimens have color intrinsically. Examples are red blood cells and organic mineral samples. Other specimens take on color only as a result of staining or other chemical preparation prior to examination. A third category includes specimens given color by the optics of the microscope (polarization, birefringence, etc.).

In biomedical work, different chemical constituents of a specimen are often stained with absorbing or fluorescent dyes of different colors. In many applications the different structures are separable by color, and one wishes to visualize or measure these objects separately and in correct spatial relationship to one another.

If, for example, three chemical components of a specimen are stained, separately, with red, green, and blue fluorescent dyes, one can digitize and display a normal tri-color image of the specimen. The three color component images are registered monochrome images, each of which shows objects of a specific type. This paves the way for isolating, measuring, and classifying the objects by using standard techniques for the analysis of digital images.

Commonly, the absorption or emission spectra of the stains or fluors do not match the curves in Figure 1. Then the red, green, and blue primary colors of human vision (and of commonly available hardware) are not ideal for isolating the differently colored objects in the specimen. When it is necessary to display the specimen in its natural appearance, one must account for the spectral response of the camera and of the display unit in order to render an accurate-appearing reproduction. On the other hand, quantitative multispectral image analysis can be done using any set of (two or more) primary colors. In this case it is often advisable to abandon the RGB system and select primary colors that match the stains or fluors in use.

Color Balance

Often a digitized tri-color image will not render the various colors properly when displayed. Nonuniform illumination, combined with differing sensitivities and offsets (black levels) in the three color channels, can unbalance the three color-component images so that the objects in the field appear to be shifted in color. Most noticeably, objects that should be gray take on unwarranted color. The first test of proper color balance is that all the gray objects indeed appear gray. The second test is that the highly saturated (bright) colors must all have the proper hue (defined below).

The remedy for color imbalance is to use linear grayscale transformations (Castleman, 1996) on the individual red, green, and blue images. Normally, two of the component images are transformed to match the third, as follows. One selects two relatively uniform areas of the image, one light gray and one dark gray, and computes the mean gray level of both areas in each of the three component images. One then defines linear grayscale transformations (*i.e.*, $y = ax + b$) to make two of them (*e.g.*, red and blue) match the third (*e.g.*, green). One must solve two linear equations in two unknowns to determine a and b. This forces each of the two areas to have the same gray level in all three component images, and this will usually achieve color balance. If the camera and digitizing system are stable, the required transformations can be determined in advance by digitizing a black-and-white test target. The resulting transformations can then be used routinely throughout the digitizing session.

Color Specification

There are several ways to specify, quantitatively, the color of a pixel in a tri-color digital image. Here we discuss two of the more useful methods.

RGB format

The most common color specification simply uses the red, green, and blue brightness values scaled, for example, between zero and one. This convention is called "RGB format." The color of each pixel can be represented by the location of a point in the first quadrant of three-dimen-

sional color space (RGB-space). This is shown by the color cube in Figure 2.

The point at the origin of RGB-space represents zero brightness of all the primary colors and is thus the color black. Full brightness of all three primaries together appears as white at the corner diagonally opposite the origin of RGB-space. Three of the corners of the color cube correspond to the primary colors, red, green, and blue. The remaining three corners correspond to the secondary colors, yellow, cyan (blue-green), and magenta (purple). Equal amounts of all three color components at lesser brightness produce a shade of gray. The locus of all such points falls along the "gray line," which is the diagonal of the color cube connecting the black and white points (Fig. 2).

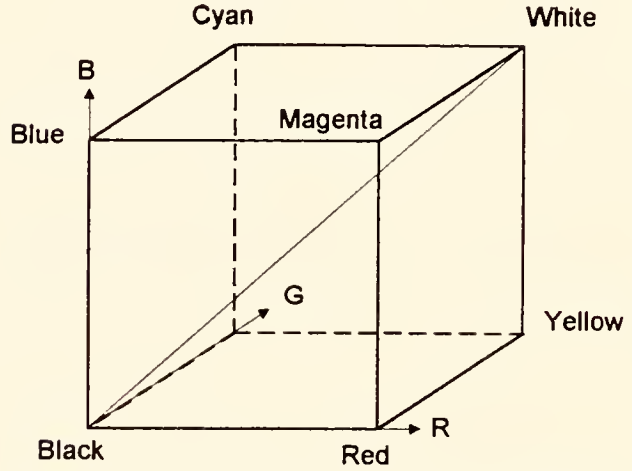

Figure 2. RGB color space. Each of the primary colors defines one axis of a three-dimensional coordinate system. Every color plots to a position in this space.

HSI format

Another useful specification scheme is called the "HSI format" (hue, saturation and intensity). It reflects the way humans perceive color, and it offers advantages for color image processing as well (Castleman, 1996; Pratt, 1991; Russ, 1995).

In HSI format the "I" stands for intensity, or brightness. It is, for our purposes, simply the sum of the R, G, and B gray level values, although different schemes with unequal weighting of the colors are also used. The intensity value specifies the overall brightness of the pixel, without regard to its color. One can convert a color image to monochrome by computing only the intensity at each point, thereby discarding the color information.

The color information is contained in two parameters that are called "hue" and "saturation," although other, equivalent terms are often used. Hue and saturation are illustrated by the color circle in Figure 3. The hue of a color refers to which spectral wavelength (color of the rainbow) it most closely matches, and is expressed as an angle. Arbitrarily, a hue of 0° is red, 120° is green, and 240° is blue. Hue traverses the colors of the visible spectrum as it goes from zero to 240 degrees. Between 240° and 360° fall the nonspectral (purple) colors that the eye perceives.

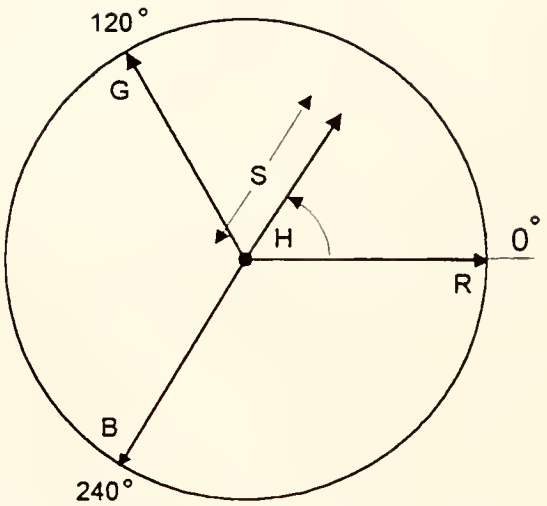

Figure 3. The color circle. Hue is an angle, and saturation is the radial variable.

The saturation parameter is the distance of the point from the origin of the color circle. The "pure" or "saturated" colors fall around the periphery of the circle, and their saturation values are unity. At the center of the color circle lie the neutral (gray) shades; that is, those with zero saturation.

The concept of saturation can be illustrated as follows. Consider a bucket of bright red paint. The color has a hue of 0° and a saturation of unity. Mixing in some white paint makes the red less intense, thereby reducing its saturation, but without making it darker (*i.e.*, reducing its intensity). Pink corresponds to a saturation of 0.5 or so. As more white is added to the mixture, the red becomes paler, and the saturation decreases, eventually approaching zero (white). If, on the other hand, black paint is mixed with the bright red paint, the intensity of the color decreases (toward black) but its hue (red) and saturation (1.0) remain constant.

The three color coordinates, taken together, define a cylindrical color space (Fig. 4). The gray shades fall along the axis from black at the bottom to white at the top. The fully bright, fully saturated colors fall on the perimeter of the top surface of the cylinder.

Many other color coordinate systems are used. Those established by the Commission Internationale de l'Eclairage (CIE), an international standards committee for light and color, are perhaps the most widely used. They are

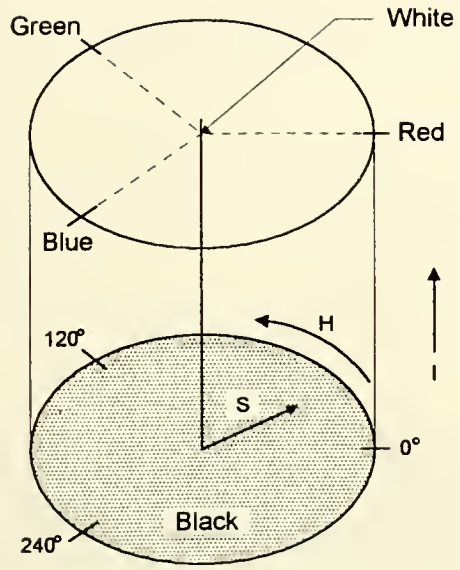

Figure 4. Cylindrical color space. Intensity is added as the axial variable. Every color plots to a position in this space.

based on experimental data from color-matching experiments conducted on human observers.

Color coordinate conversion

Some image processing techniques are intrinsically more successful when carried out in rectangular RGB-space, whereas others work best in cylindrical HSI-space. Thus it is useful to be able to convert color digital images from RGB to HSI color coordinates and back again.

RGB to HSI conversion

The conversion from RGB to HSI format can be approached as follows. Recall that the gray line is the diagonal of the color cube in RGB-space, and it is the vertical axis in cylindrical HSI-space. Thus we can begin by rotating the RGB cube in x, y, z-space so that its diagonal lies along the z-axis, and its R-axis lies in the x-z plane (Ledley *et al.*, 1990: Castleman, 1996). This is given by

$$x = \frac{1}{\sqrt{6}}[2R - G - B]$$

$$y = \frac{1}{\sqrt{2}}[G - B]$$

$$z = \frac{1}{\sqrt{3}}[R + G + B] = I \tag{1}$$

The latter of these gives the HSI intensity parameter.

We can convert to cylindrical coordinates by defining polar coordinates in the x-y plane. Then we normalize the radial variable so that the fully saturated colors (those having no more than two of the primary colors present) fall on a unit-radius circle in the x-y plane. This leads to the formula for saturation

$$S = 1 - \frac{\sqrt{3}}{I}\min(R, G, B) \tag{2}$$

We compute the angle

$$\theta = \cos^{-1}\left[\frac{\frac{1}{2}[(R - G) + (R - B)]}{\sqrt{(R - G)^2 + (R - B)(G - B)}}\right] \tag{3}$$

and the hue is

$$H = \begin{cases} \theta, & G \geq B \\ 2\pi - \theta, & G \leq B \end{cases} \tag{4}$$

Notice that black (*i.e.*, $[R, G, B] = [0, 0, 0]$) creates a problem for Eq. (3). We can assign black to $[H, S, I] = [0, 0, 0]$.

HSI to RGB conversion

The formulas for converting from HSI to RGB coordinates take on slightly different form for different sectors of the color circle (Castleman, 1996). For $0° \leq H < 120°$,

$$R = \frac{I}{\sqrt{3}}\left[1 + \frac{S\cos(H)}{\cos(60° - H)}\right]$$

$$B = \frac{I}{\sqrt{3}}(1 - S)$$

$$G = \sqrt{3}I - R - B \tag{5}$$

while for $120° \leq H < 240°$,

$$G = \frac{I}{\sqrt{3}}\left[1 + \frac{S\cos(H - 120°)}{\cos(180° - H)}\right]$$

$$R = \frac{I}{\sqrt{3}}(1 - S)$$

$$B = \sqrt{3}I - R - G \tag{6}$$

and for $240° \leq H < 360°$

$$B = \frac{I}{\sqrt{3}}\left[1 + \frac{S\cos(H - 240°)}{\cos(300° - H)}\right]$$

$$G = \frac{I}{\sqrt{3}}(1 - S)$$

$$R = \sqrt{3}I - G - B \tag{7}$$

The RGB cube (Fig. 2) does not map directly into the color cylinder of Figure 4. Instead, it defines a somewhat cone-shaped region in HSI-space, with white at the apex.

Since the entire floor of the color cylinder is the single color black, some authors prefer to consider the HSI color space to be biconic.

There are several variations of the HSI conversion formulas (Pratt, 1991), but the particular one chosen usually will not materially affect the result, as long as (1) intensity is a weighted average of R, G, and B; (2) hue is an angle; (3) hue, saturation, and intensity are independent; and (4) the transformation is accurately invertible.

Multispectral images having more than three primary colors can also be transformed into corresponding multi-dimensional color spaces. For example, one can convert from rectangular to spherical coordinates in a color space based on four or more primary colors.

Color Compensation

Available stains and fluorophores have different, often broad absorption and emission spectra, and commonly used color cameras have broad, overlapping sensitivity spectra. As a result, one seldom obtains complete isolation of three types of objects in the three component images.

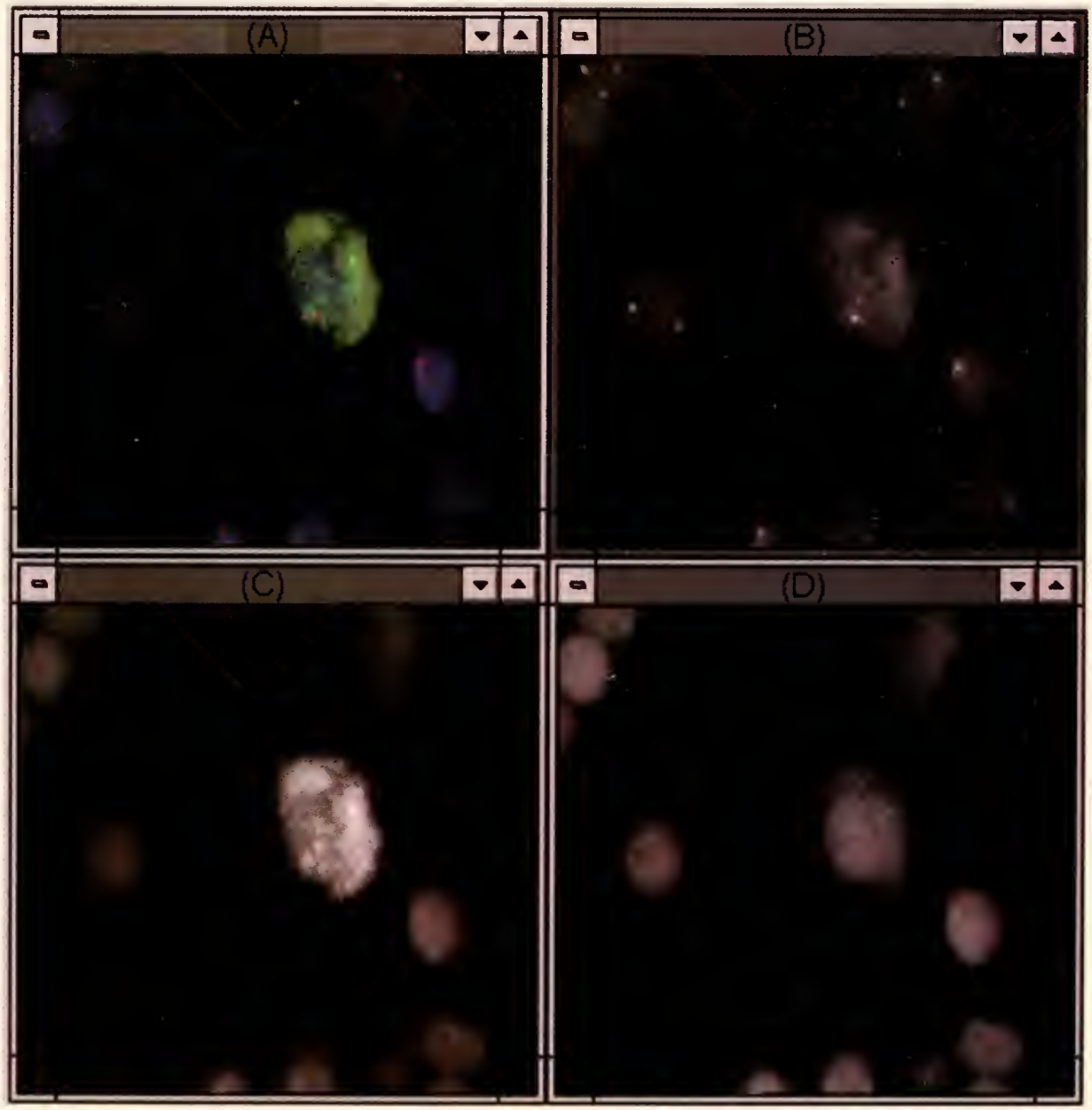

Figure 5. Three-color, fluorescently labeled bone marrow cells. (A) Color image; (B) red; (C) green; (D) blue. Notice that all structures appear in each of the R, G, and B images.

Instead, each type of object is visible in all three color-component images, although at reduced contrast in two of them (Fig. 5).

We can model the spreading of light among the color channels as a linear transformation (Castleman, 1993, 1994, 1996). Let the matrix, **C,** specify how the colors are spread among the three channels in a three-color fluorescence application (example below). Each element c_{ij} is the proportion of the brightness from fluorophore j that appears in color channel i of the digitized image. Let **x** be the 3 by 1 vector, $[R, G, B]^T$, of actual fluorophore brightness values at a particular pixel, scaled as gray levels that would be produced by an ideal color image digitizer (one with neither color spread nor black level offset). Then

$$\mathbf{y} = \mathbf{Cx} + \mathbf{b} \tag{8}$$

is the vector of RGB gray levels recorded, at that pixel, by the image digitizer. While **C** accounts for the color spread, the vector **b** accounts for the black level offset of the digitizer. That is, b_i is the gray level that corresponds to black (zero brightness) in channel i. Equation (8) is easily solved for the true brightness values by

$$\mathbf{x} = \mathbf{C}^{-1}[\mathbf{y} - \mathbf{b}] \tag{9}$$

Color spreading can thus be eliminated by first subtracting the black level from each channel, and then premultiplying the resulting RGB gray level vector for each pixel by the inverse of the color spread matrix.

Color compensation example

Figure 5 shows an RGB image of human bone marrow cells; the image was digitized with a single-chip CCD color television camera mounted on a fluorescence microscope. The camera's sensitivity spectra were similar to those in Figure 1. The cells were counterstained with DAPI (4′,6-diamidino-2-phenylindole, dihydrochloride), which fluoresces in the blue. Dividing cells also picked up the green fluorophore, FITC (fluorescein-5-isothiocyanate), which had been conjugated with BrdU (5-bromodeoxyuridine). The centromeres of the number 8 chromosomes were labeled with Texas red, a red fluorophore, attached to a DNA probe.

Ideally, the cells would appear in the blue channel, dividing cells would show up in the green channel as well, and two dots per cell (corresponding to the two number 8 chromosomes) would appear in the red channel. In Figure 5, however, all components appear in all channels because of overlap among the fluorophore emission spectra and the sensitivity spectra of the camera's three color channels.

Table I shows the color spread matrix for the system used to digitize the image in Figure 5. The values in this matrix were determined experimentally from digitized images of cells stained with single fluorophores. They represent the relative contrast of different colored objects

Table I

Color spread matrix for the image in Figure 5

	Fluorophore		
Color channel	Texas Red	FITC	DAPI
Red	0.85	0.26	0.24
Green	0.05	0.65	0.32
Blue	0.10	0.09	0.44

The columns represent the three fluorophores used, and the rows represent the three channels of the color camera. The values in the table specify the proportion of the emitted light from each fluor that appears in each color channel.

in each of the three color channels. Table I states, for example, that only 44% of a DAPI molecule's brightness is recorded in the blue channel, while 32% of it shows up in the green channel, and 24% finds its way into the red channel. The color smear in this example is relatively severe, and use of a monochrome camera with separate, optimized, color filters, for example, can produce better results. But color smear is intrinsic to the imaging process and is always present to some degree.

The inverse, $\mathbf{C}^{-1}$, of the matrix in Table I is the color compensation matrix,

$$\mathbf{C}^{-1} = \begin{bmatrix} 1.24 & -.45 & -.35 \\ 0.05 & 1.69 & -1.26 \\ -.29 & -.24 & 2.61 \end{bmatrix} \tag{10}$$

It specifies how, using Eq. (9), one can correct the color spreading. The values in the left column specify that one should, at each pixel, take 124% of the gray level in the red channel image, add 5% of the green channel value, and subtract 29% of the blue value to produce a corrected red-channel gray level. The second and third columns specify how to correct the pixels of the green and blue channels, respectively.

Figure 6 shows the result of color compensation applied to the color image in Figure 5. Here the three differently stained types of objects are effectively isolated to the images in the red, green, and blue channels. This permits more accurate segmentation and measurement of the cell and its components. Because color spread tends to "wash out" an image, color compensation tends to increase both the contrast and the saturation of the displayed color image. Since it is intended to isolate the different colored components into separate color channels, it may not produce visually realistic images upon display.

Color Image Analysis

Image segmentation

Segmentation of a tri-color image can be viewed as a process of partitioning the three-dimensional (RGB or

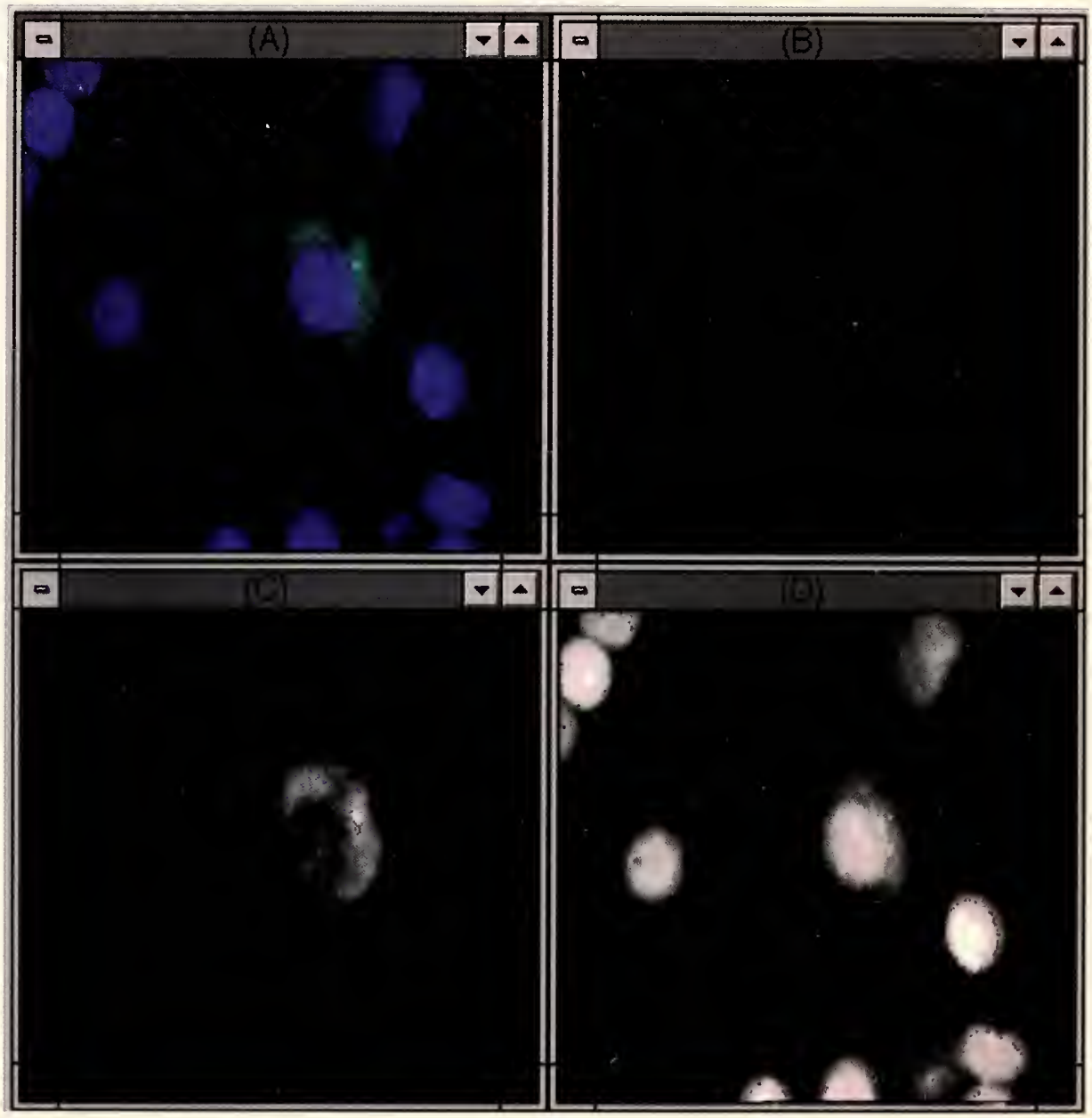

Figure 6. The effect of color compensation. This is the same image as Figure 5 after color compensation (Eq. (9)) was applied using the color smear matrix shown in Table I. (A) Color image; (B) red; (C) green; (D) blue. Notice that each of the different structures is isolated to the R, G, or B image.

HSI) color space. The different colored objects in the image correspond to separate clusters of points in color space, although the clusters corresponding to different objects may well overlap.

The hue and saturation of an object are normally dictated by the light-reactive properties of its dye or stain—how it absorbs, reflects, or emits light. The intensity, however, is seriously affected by illumination and viewing angle. Uneven illumination, for example, normally has much more effect on intensity than on the two color parameters. Thus it may be productive to segment the image in the hue-saturation plane (*i.e.*, on the color circle) rather than in three-dimensional color space, thereby ignoring intensity altogether.

Object measurement and classification

Once the objects in the image have been identified, they can usually be measured in one of the color-channel images. Sometimes two or more color-channel images can be combined to produce a monochrome image for analysis. Further, some objects may be present in different

channels and must be analyzed there. In any event, the measurement and classification of objects can usually be conducted with techniques that are commonly applied to monochrome digital images (Castleman, 1996; Pratt, 1991).

Discussion

The digital analysis of color microscopic images is becoming more important as new techniques for specimen preparation emerge. For example, each of the 24 types of human chromosomes can be painted with a distinct color by using multicolor fluorescent *in situ* hybridization (M-FISH) techniques (Speicher *et al.*, 1996, Schröck *et al.*, 1996). As the number of colors increases, and as the analytical requirements become more stringent, the demands placed on digital image analysis become more severe.

Fortunately the techniques mentioned here for tri-color images generalize readily to multispectral digital images with two, four, or more primary colors. Then the battery of techniques that have been developed for monochrome image analysis can be applied to the separate color-component images, after they have been balanced, compensated, and perhaps converted to another coordinate system.

Acknowledgments

The author thanks his colleagues Glenn Criswell, Dr. Fatima Merchant, Dr. Mark Schulze, and Dr. Qiang Wu for their contributions to this paper; Donna Call for her assistance in the preparation of the manuscript; and Dr. Jan Liang of the M. D. Anderson Cancer Center and Dr. Lisa Shaffer of the Baylor College of Medicine for providing specimens and clinical input.

This work was supported in part by Grants 1 R43 HD35411 and 2 R44 HD28849 from the National Institute of Child Health and Human Development, Grant No. 2 R44 CA58259 from the National Cancer Institute, and Contract NAS-9-19010 from the National Aeronautics and Space Administration.

Literature Cited

Castleman, K. R. 1993. Color compensation for FISH image processing. *Bioimaging* **1(3):** 159–165.

Castleman, K. R. 1994. Color compensation with unequal integration periods. *Bioimaging* **2(3):** 160–162.

Castleman, K. R. 1996. *Digital Image Processing.* Prentice-Hall, Englewood Cliffs, NJ.

Ledley, R. S., M. Buas, and T. J. Golab. 1990. Fundamentals of true-color image processing. *Proc. 10th Int. Conf. Pat. Rec.*, IEEE Comp. Soc. Press, Los Alamitos, CA (Cat. No. 90CH2898-5) **1:** 791–795.

Pratt, W. K. 1991. *Digital Image Processing.* John Wiley, New York.

Russ, J. C. 1995. *The Image Processing Handbook,* 2nd ed. CRC Press, Boca Raton, FL.

Schröck, E., S. du Manoir, T. Veldman, B. Schoell, J. Wienberg, M. A. Ferguson-Smith, Y. Ning, D. H. Ledbetter, I. Bar-Am, D. Soenksen, Y. Garini, and T. Ried. 1996. Multicolor spectral karyotyping of human chromosomes. *Science* **273:** 494–497.

Speicher, M. R., S. G. Ballard, and D. C. Ward. 1996. Karyotyping human chromosomes by combinatorial multi-fluor FISH. *Nat. Genet.* **12:** 368–375.

Wald, G. 1964. The receptors for human color vision. *Science* **145:** 1007–1017.

Reference: *Biol. Bull.* **194:** 108–115. (April, 1998)

Celestial Mechanics, Sea-Level Changes, and Intertidal Ecology

MARK W. DENNY[1,*] AND ROBERT T. PAINE[2]

[1] *Biological Sciences Department, Stanford University, Hopkins Marine Station, Pacific Grove, California, 93950; and* [2] *Department of Zoology, Box 351800, University of Washington, Seattle, Washington, 98195-1800*

Celestial mechanics has long been known to affect life on Earth, but exploration of these influences has been hampered by long temporal scales and complex biological relations. Here we report on a periodic fluctuation in tidal exposure driven by the 18.6-y oscillation of the moon's orbital inclination, which can change by almost 50% the average time that intertidal organisms are exposed to air. The temperature of nearshore water and the upper limits to mussels are shown to vary with the lunar oscillation. Such variation challenges the value of ecological and physiological generalizations based on snapshot measures, and highlights the value of long-term studies.

Mechanistic interpretations of cyclical variations in paleoclimates have been based, since the late 1800s, on celestial mechanics, especially the Earth's orbital eccentricity, orbital inclination, and axial tilt. Cycles of 41,000 and 100,000 years have characterized the periodicity of glaciation and its biological consequences for the past 2.5 million years (1, 2), and the role of such astronomical factors is a point of debate in the current concern about the reality and magnitude of anthropogenic forcing of climate, especially accelerated global warming. Although consensus has recently been reached that global warming is a reality (3), its magnitude and short-term consequences have yet to be fully determined. Warming, however, is certain to induce a rise in eustatic sea level.

Anthropologists have long recognized the importance of sea-level changes: *e.g.*, beginning in the late Pleistocene, the Bering land bridge and other human migration routes to and along coastal North America have disappeared as sea level has risen 120–150 m in the last 14,000 years (4). In contrast, ecologists studying the distribution and abundance of temperate marine organisms, and especially the dynamics underlying these patterns, have tended to ignore such shifts, either because the temporal scale is daunting, or because the complex of interactions influencing distribution patterns is too incompletely understood to be specified. In this paper we examine the interaction between a short-term (18.6 y) astronomical cycle and an ecological assemblage (the intertidal community of wave-swept rocky shores) that is capable of rapid response, and offer examples showing that the effects of celestial mechanics (beyond the obvious ties to tidal cycles and the moon's orbital period) must be identified if the magnitude of changes in community composition is to be understood.

The intertidal zone of wave-swept rocky shores has become a model system for experimentation in community ecology. Current ideas about the roles of competition, predation, succession, and disturbance are based in part on experiments on assemblages of intertidal organisms and serve as benchmarks in ecologists' understanding of how process underlies pattern (5–15).

The ecology of the intertidal zone is closely tied to its physical environment (16, 17). As the tides rise and fall, areas on the shore are alternately immersed and exposed. The concomitant change from marine to terrestrial conditions can place extreme demands on the physiology of intertidal organisms (which with few exceptions are of marine descent), and vertical zonation is often distinct (18). Any shift in the level of the tides is likely to have substantial consequences for the distribution, abundance, and interaction of intertidal plants and animals, many of

Received 3 October 1997; accepted 5 December 1997.

* To whom correspondence should be addressed. E-mail: mwdenny@leland.stanford.edu

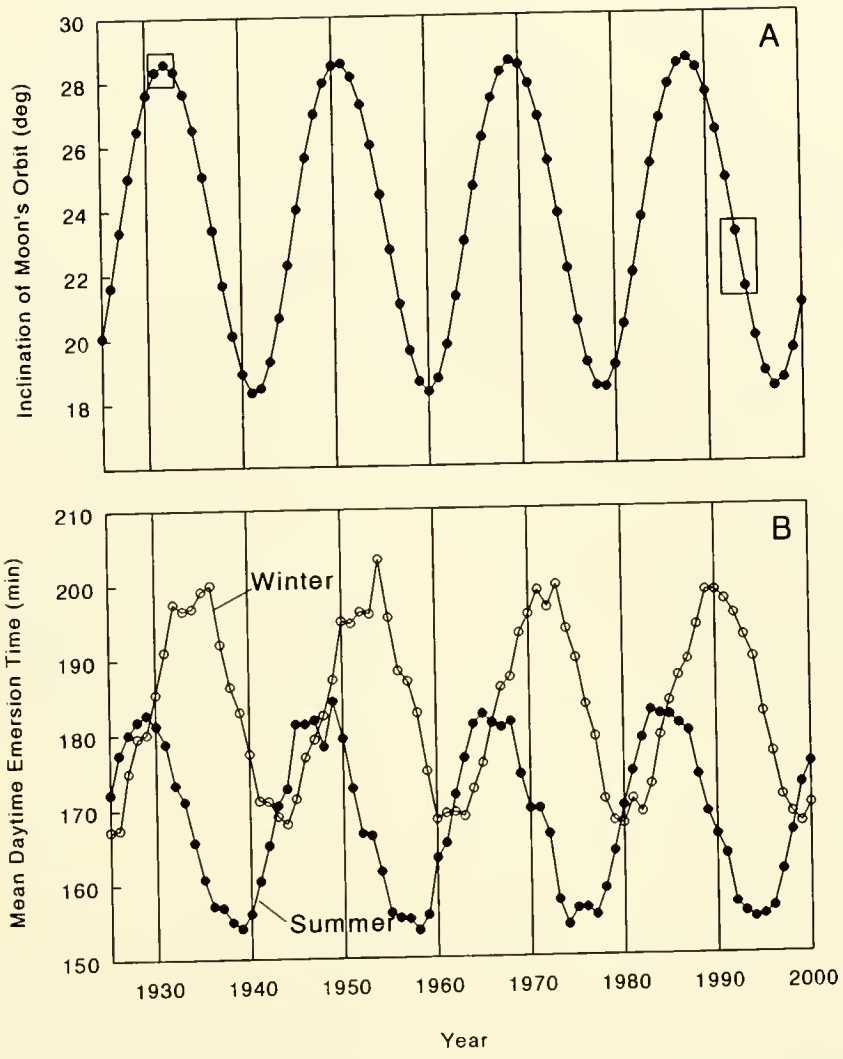

Figure 1. Variation in lunar orbital inclination (A) and seasonal variation in the average time for which intertidal organisms are exposed to air (*B*) calculated for a site 2′ above MLLW at Pacific Grove, California. The boxes in (A) enclose the data corresponding to the periods during which the transect was censused, first by Hewatt (1931–1933 [23, 24] and again by Barry *et al.* (1993–1994 [22]). We used Tides 4.01 (Walner, E. P., Nautical Shareware, 32 Barney Hill Rd., Wayland, Massachusetts 01778-3602) to calculate the tides at Pacific Grove for the period 1 Oct. 1924 through 30 Sept. 2000. From these data we measured (to the nearest minute) each period that an organism would be exposed to air during daytime hours (0600–1800 Pacific Standard Time), assuming that the organism was at a known height on the shore (−1′ to 6′ relative to MLLW). The average period of exposure was then calculated for the winter (1 Oct. to 31 Mar.) and summer months (1 Apr. to 30 Sept.) of each year. Winter of a particular year was assumed to extend from 1 Oct. of the previous year to 31 Mar. of the given year.

which are sessile as adults and thus incapable of adjusting their spatial position to counter the whims of nature. Of particular importance is the average time of emergence—the time during which intertidal organisms are exposed to a desiccating atmosphere, extremes in temperature, hypo-osmotic stress during heavy rains, or other terrestrial insults. Time of aerial exposure is controlled primarily by two factors: the vertical level of the organism on the shore (a factor under biological control) and the fluctuation of the tides (a matter of physics).

The level of the tides is governed by the action of gravitational attractions and centripetal accelerations acting on the water in the ocean, and may be modified by the topography of the local ocean basin, barometric pressure, and winds. Of particular interest here is a fluctuation in the angle between the plane of the moon's orbit and

the plane of the earth's equator (the lunar inclination), a factor that affects both the overall amplitude and the inequality of tides. The greater the inclination of the moon's orbit, the greater the difference in height between the high high and the low low tide in a given tidal cycle, and the less the difference between the low high tide and the high low tide. Variation in these tidal heights can in turn affect the period of emersion faced by an intertidal organism, the effect varying with the vertical height of the organism on the shore. The inclination of the moon's orbit varies from about 18° to 29°, with a period of 18.613 years (19, Fig. 1A). What are the effects of this fluctuation in inclination on the expected time of aerial exposure, and what are the consequences for benthic organisms?

Effects on aerial exposure

Fortunately, accurate methods for predicting the astronomical tides have been known for more than a century (20), and have recently been implemented for personal computers. We calculated the tidal height at a typical site on the west coast of North America (Pacific Grove, California, USA, 121° 53.3′ W, 36° 36.3′ N) at hourly intervals (Fig. 1B). The average duration of daytime emergence at Pacific Grove varies substantially depending on the inclination of the moon's orbit. In the example shown (shoreline height = +2′ above mean lower low water, MLLW), the average period of summertime emersion is 30 minutes longer at the maximum of an exposure cycle (184 min) than at the minimum of a cycle (154 min), a 20% increase in average emergence time relative to the minimum. A similar difference (22%) is found for wintertime exposures.

At Pacific Grove the tidal range is typically −1′ to +6′ relative to MLLW, and the periodic fluctuation in exposure time is apparent for all heights on the shore between 0 and 4 feet. Outside this range, the pattern is obscured by the large variance in exposure times. The variation in relative time of exposure is greatest at 0′ above MLLW (48.6% in summer, 31.1% in winter) and is least at 3′ (17.6% in summer, 10.5% in winter, see Table I). Note that the absolute time of exposure is low for organisms low on the shore, so that a large increase in relative exposure time does not necessarily imply a large increase in absolute exposure time (Table I).

The major period of the fluctuation in exposure time is the same as the period of oscillation in the inclination of the moon's orbit, but the fluctuation in exposure is out of phase with the moon's inclination. For example, in the period 1925–2000, predicted peaks in average summertime period of emergence at 2′ above MLLW occur 1–5 years before the peak in the inclination of the moon's orbit, and peaks in the wintertime period of emergence occur 1–4 years after the peak inclination. Fourier analysis of the time series of average periods of emergence show that exposure time is shifted on average 2.5 years ahead of the fluctuation in lunar inclination in the summer and 2.1 years back in the winter. The phase shift between the cycles of exposure and lunar inclination varies with height on the shore (Table I).

Consequences for benthic organisms

Evidence of the effects of this variation in exposure times has been found from three sources: variation in sea-surface temperatures, variation in the upper limit to mussel beds, and the coincidence of catastrophic freezes with years of maximal exposure.

Sea-surface temperature. Shoreline water temperatures at Hopkins Marine Station (Pacific Grove, CA) have been measured daily since 1919. A linear increase through time in both the minimum and maximum temperatures has

Table I

Summary data for average period of daytime emergence at Pacific Grove, California

Season	Height on shore (feet)	Period of emergence (min)					
		Mean	Maximum	Minimum	Max − Min	Max/Min	Phase (year)
Summer	0	79.80	98.38	66.20	33.18	1.486	+2.67
	1	121.65	138.72	104.13	34.59	1.332	+3.28
	2	168.75	184.32	153.61	30.71	1.200	+3.33
	3	225.62	238.00	215.43	22.57	1.105	+2.68
	4	461.67	508.76	417.25	91.51	1.219	+0.44
Winter	0	111.79	124.38	94.91	29.47	1.311	−2.43
	1	148.26	165.20	130.95	34.25	1.262	−2.47
	2	183.35	203.30	167.21	36.09	1.216	−2.05
	3	208.72	226.93	192.92	34.01	1.176	−1.85
	4	376.11	410.90	342.09	68.81	1.201	−1.75

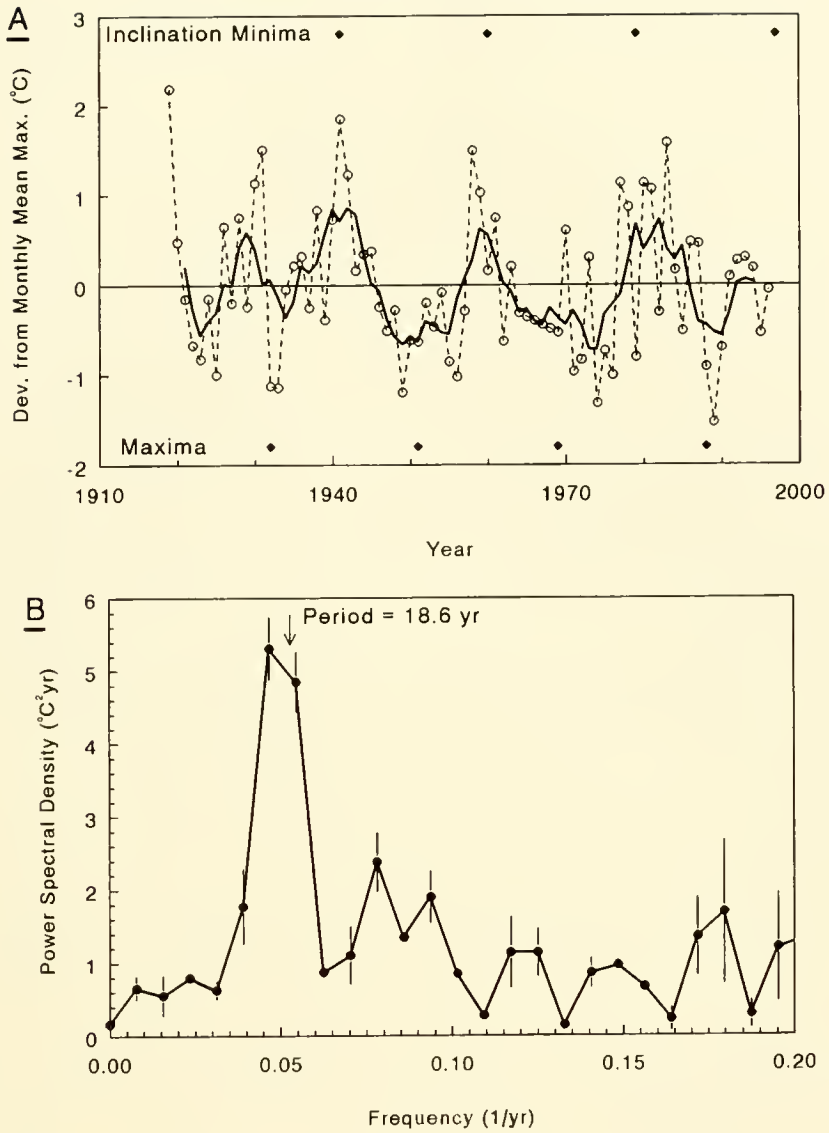

Figure 2. (*A*) Fluctuations in monthly maximum water temperature at Hopkins Marine Station (open circles). A 5-y running average of the data (solid line, not used in the calculation of periodicity) is shown to accentuate the long-term periodicity. The strong El Niño/Southern Oscillation event of 1982–1983 is evident in the unusual duration of high temperatures in the early 1980s. (*B*) Power spectrum (vertical bars = SEM) of the data shown in (A). Similar results are obtained for a time series of monthly minimum temperatures (data not shown). The power spectrum of a process that fluctuates through time apportions the variance of that fluctuation among the frequencies that contribute to the process. Thus a peak in the power spectrum at a particular frequency shows that a substantial fraction of the overall variation occurred at that frequency. See (25) for a thorough explanation of spectral analysis. Monthly maximum and minimum water temperatures were extracted from the record at Hopkins Marine Station. Two gaps in the data (1940, 1965–1968) were filled by linear interpolation, and any long-term trend in the time series for each month was removed by subtracting from the data the linear regression of temperature as a function of time. The detrended data were then tapered using a Hanning window, the time series (78 points) was padded with zeroes to a length equal to the next higher power of 2 (128, a process necessary for the application of a fast Fourier transform [FFT]), and the normalized power spectral density was calculated using the FFT procedure outlined by (28). Data shown in Figure 2A are those averaged for January and February, a time of year in which the ocean temperature at Pacific Grove is not typically influenced by oceanic upwelling. The approximately 18.6-y periodicity evident in these data is present in all months between October and March (the entire season when upwelling is absent), but is much reduced or absent during upwelling.

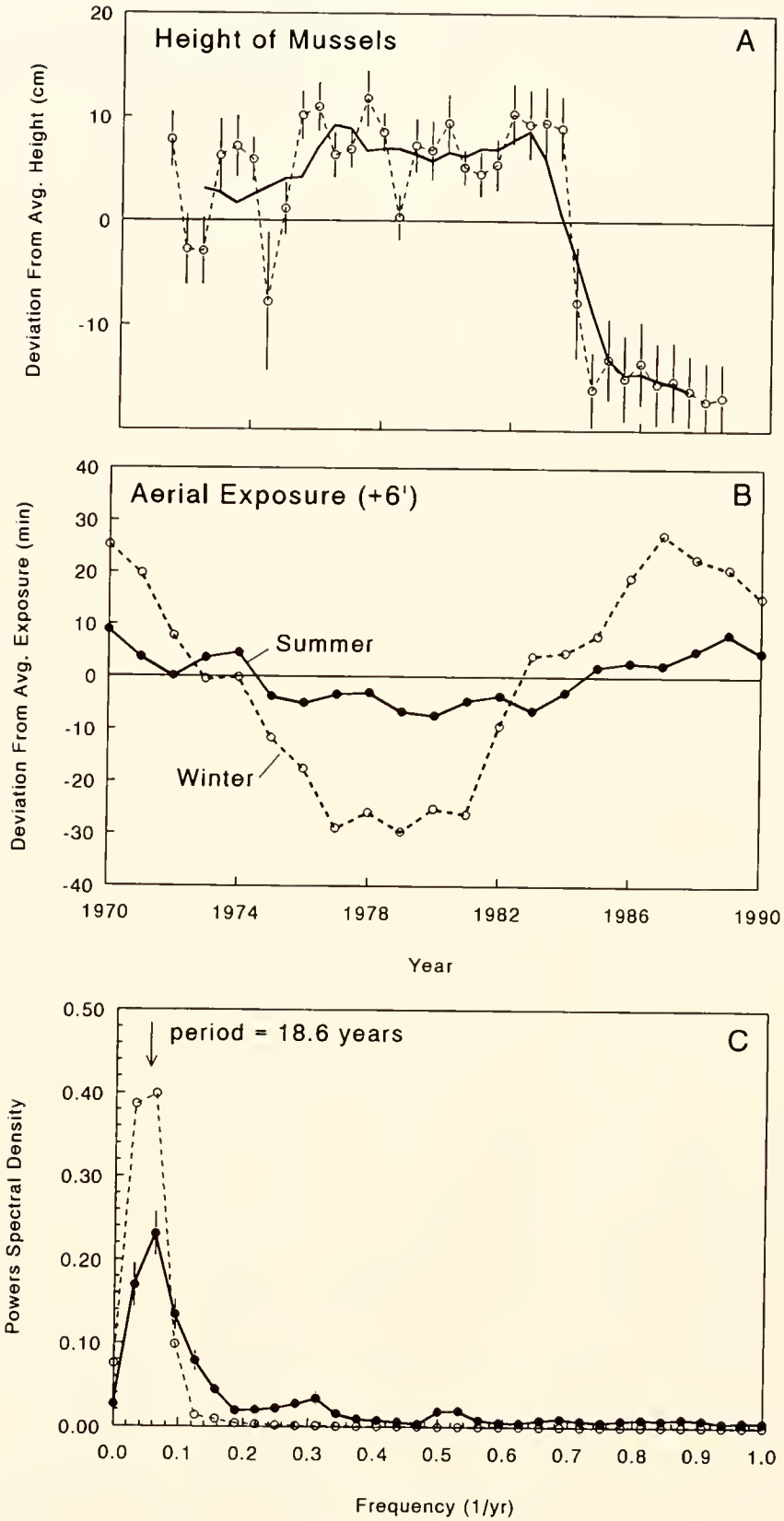
Height of Mussels
A
Deviation From Avg. Height (cm)
20
10
0
-10
Aerial Exposure (+6')
B
Deviation From Avg. Exposure (min)
40
30
20
10
0
-10
-20
-30
-40
Summer
Winter
1970
1974
1978
1982
1986
1990
Year
period = 18.6 years
C
Powers Spectral Density
0.50
0.40
0.30
0.20
0.10
0.00
0.0
0.1
0.2
0.3
0.4
0.5
0.6
0.7
0.8
0.9
1.0
Frequency (1/yr)

been noted (21, 22), but there are considerable fluctuations around this trend (Fig. 2A). These temperature anomalies have a period that is indistinguishable from 18.6 years (Fig. 2B). Temperatures are high when the lunar inclination is small (that is, when tidal fluctuations are small) and low when lunar inclination is large (see Fig. 1A). The cause of this effect is unknown, although we speculate that reduced tidal flushing (corresponding to small lunar inclinations) in the shallows surrounding the site of temperature measurement could allow resident surface water to be heated by solar radiation. Crosscorrelation analysis indicates that the maximum temperature anomaly occurs approximately 1 y after the minimum lunar inclination.

The 18.6-y cycle of lunar inclination (and the associated cycle in water temperature) may confound the interpretation of long-term trends. For example, Barry *et al.* (22) compared the species composition in 1993–1994 along an intertidal transect at Hopkins Marine Station to the composition along the same transect in 1931–1933 as recorded by Hewatt (23, 24). They noted substantial shifts in the relative frequencies of several species, in particular an increase in species commonly found to the south of Pacific Grove and a decrease in species commonly found to the north. They suggest that the long-term trend toward increasing water temperatures may have played a role in the change in species composition. Note, however, that the 1993–1994 measurements were conducted at a time of small lunar inclination (3–4 y before minimum), perhaps contributing to higher than average nearshore temperatures, whereas Hewatt's measurements were conducted in a time of high lunar inclination (bracketing the maximum, Fig. 1A) and lower than average temperatures. Therefore, what appears to be a long-term (at least 62-y) trend in species composition may be in part the result of sampling the community at different phases of the 18.6-y tidal fluctuation. This phenomenon (known as *aliasing*) is a common problem in signal analysis (25).

Upper limits To mussel beds. Beginning in September 1971, the upper limit to the mussel (*Mytilus californianus*) bed has been measured twice yearly at Tatoosh Island, Washington state (48° 24′ N, 124° 40′ W; Fig. 3A). The fluctuations in this boundary vary in synchrony with the predicted variation in aerial exposure: the bed extends higher on the shore when the predicted exposure time is less and retreats when the exposure is increased (Fig. 3B). Although the relatively short time series of boundary fluctuations does not allow for a precise measurement of the periodicity of the boundary's rise and fall, the apparent period of oscillation is consistent with that expected from the oscillation in lunar inclination (Fig. 3C).

Catastrophic freezes. The longer a sessile intertidal organism is exposed to air, the more likely it is to encounter chance extremes in terrestrial conditions. For example, intertidal organisms are more likely to freeze (a chance occurrence depending on the weather) in years of maximal exposure. In the past 47 years, four examples of catastrophic freezing have been noted in the mussel-bed community in the Pacific Northwest of the USA (1950, 1964, 1969, 1989). With the exception of the 1964 freeze, each of these events occurred near a peak of lunar inclination, and therefore near a peak of intertidal exposure. Conversely, a severe freeze in 1978 (during a minimum in lunar inclination) exterminated Winter Wrens on Tatoosh Island (26) but did not affect the upper boundary of mussels. The apparent synchronicity between catastrophic freezes and the cycle of lunar inclination may be an example of a phenomenon known as *stochastic resonance* (27). In a system exhibiting stochastic resonance, a large response is elicited whenever a periodic input signal crosses

Figure 3. (*A*) Fluctuations in the upper boundary of the mussel bed (open circles); vertical bars are the SEM among the 11 locations. The solid line is a 5-y running average, plotted to accentuate the long-term fluctuation in the boundary. (This running average is not used in calculations of periodicity.) (*B*) Predicted variation in the aerial exposure of a site 6′ above MLLW. (*C*) The power spectrum (solid line with SEM) of the boundary fluctuations shown in (A); the dashed line is the corresponding spectrum of a pure sine wave with a period of 18.6 y. The upper boundary of the mussel bed on Tatoosh Island was measured to the nearest centimeter twice yearly (Apr. and Sept.) at 11 locations at the site of previous studies on intertidal zonation (29). Data from Sept. 1971 to Sept. 1988 (17 years, 35 measurements) were averaged for each location, and the mean was subtracted from each individual value. The normalized power spectrum of each of these 11 time series was then calculated (by a method similar to that explained in the caption to Figure 2) and averaged across locations. Boundary data subsequent to Sept. 1988 were not included because a severe freeze in Feb. 1989 devastated the high intertidal mussels, lowering the upper boundary by as much as 2.6 m (8½′). Since the freeze, the bed has been steadily extending up the shore. The ability of our spectral analysis to detect an 18.6-y periodicity from 17 years of data was tested by calculating the normalized power spectral density for a pure sine wave with a period of 18.6 y (sampled twice yearly), but using only the first 17 years of the wave. Precise location of the low-frequency spectral peak would require a time series more than double the length available.

a threshold. In the absence of random noise, small input signals may never cross the threshold, and no response will result. In the presence of sufficient noise, however, the combination of a small signal and noise may cross the threshold, causing a response, and the periodicity of these responses will, on average, be the same as that of the underlying signal. It appears possible that the drastic response of mussels to low temperature (death by freezing) results in a stochastic resonance between the mussel bed community and the 18.6-y oscillation in exposure time, the coupling being enhanced by the random "noise" of the weather.

Conclusions and caveats

Our ability to detect apparent environmental and ecological signatures of the 18.6-y oscillation in lunar inclination suggests that intertidal communities may indeed be sensitive indicators of long-term environmental fluctuations. The data discussed here indicate that this lunar cycle can affect nearshore water temperature, which may, in turn, have significant implications for the growth of spores and larvae, their duration in the plankton, and possibly even post-larval performance. We have shown that the lunar cycle can influence upper distributional limits, and lower limits could be influenced as well if exposure time determined the foraging limits and effectiveness of mobile consumers. Shifts in aerial exposure due to the lunar cycle will affect how stringently the physiology of intertidal organisms (*e.g.*, their thermal and osmotic tolerance) is stressed by the environment. In these respects, the effects of the 18.6-y cycle in lunar inclination mimic the effects expected to accompany global warming and its associated change in sea level. The intertidal zone may thus serve as a convenient, fast-response system in which to test our ability to predict the ecological consequences of global change. In particular, the ability to account for the influences of predictable environmental phenomena (in this case, the tides, including the effects of the oscillation in lunar inclination) should enhance interyear comparisons within this biologically noisy system, and therefore simplify the identification of anthropogenic changes.

The tidal phenomena reported here are calculated for sites with typical, mixed semidiurnal tides. The complexity of tidal physics is such that it may be dangerous to extrapolate from these results to estimate the effects in other tidal regimes, and the time series of sea-level fluctuations should be calculated directly for each site of interest. Note too that only indirect evidence is cited here for the effect of the cycle of lunar inclination on intertidal biology. We hope, however, that this evidence will stimulate others both to search past records for direct evidence of tidal effects and to carry out long-term experiments in the future.

Acknowledgments

Support for this research was provided by the U.S. National Science Foundation (M. W. D. & R. T. P.) and the Mellon Foundation (R. T. P.). We gratefully acknowledge the Makah Tribal Council for granting access to Tatoosh Island.

Literature Cited

1. **Muller, R. A., and C. J. MacDonald. 1997.** Glacial cycles and astronomical forcing. *Science* **277:** 215–218.
2. **Muller, R. A., and C. J. MacDonald. 1997.** Spectrum of 100-kyr glacial cycle: orbital inclination not eccentricity. *Proc. Natl. Acad. Sci. U.S.A.* **94:** 8329–8334.
3. **Houghton, J. T., *et al.*, eds. 1996.** *Climate Change 1995: The Science of Climate Change.* Cambridge University Press, Cambridge, UK.
4. **Josenhans, H., D. Fedje, R. Pienitz, and J. Southon. 1997.** Early humans and rapidly changing holocene sea levels in the Queen Charlotte Islands—Hecate Strait, British Columbia, Canada. *Science* **277:** 71–74.
5. **Connell, J. H. 1961.** The influence of interspecific competition and other factors on the distribution of the barnacle *Chthamalus stellatus*. *Ecology* **42:** 710–723.
6. **Connell, J. H. 1972.** Community interactions on marine rocky intertidal shores. *Annu. Rev. Ecol. Syst.* **3:** 169–192.
7. **Connell, J. H. 1978.** Diversity in tropical rain forests and coral reefs. *Science* **199:** 1302–1310.
8. **Dayton, P. K. 1971.** Competition, disturbance, and community organization: the provision and subsequent utilization of space in a rocky intertidal community. *Ecol. Monogr.* **41:** 351–389.
9. **Paine, R. T. 1966.** Food web complexity and species diversity. *Am. Nat.* **100:** 65–75.
10. **Paine, R. T. 1974.** Intertidal community structure: experimental studies of the relationship between a dominant competitor and its principal predator. *Oecologia* **15:** 93–120.
11. **Menge, B. 1976.** Organization of the New England rocky intertidal community: role of predation, competition, and environmental heterogeneity. *Ecol. Monogr.* **46:** 355–393.
12. **Lubchenco, J. 1978.** Plant diversity in a marine intertidal community: importance of herbivore food preference and algal competitive abilities. *Am. Nat.* **112:** 23–39.
13. **Sousa, W. P. 1979.** Disturbance in marine intertidal boulder fields: the nonequilibrium maintenance of species diversity. *Ecology* **60:** 1225–1239.
14. **Paine, R. T., and R. L. Vadas. 1969.** The effects of grazing by sea urchins, *Strongylocentrotus* spp., on benthic algal populations. *Limnol. Oceanogr.* **14:** 710–719.
15. **Paine, R. T., and S. A. Levin. 1981.** Intertidal landscapes and the dynamics of pattern. *Ecol. Monogr.* **51:** 145–178.
16. **Lewis, J. R. 1964.** *The Ecology of Rocky Shores.* The English Universities Press, London.
17. **Newell, R. C. 1979.** *Biology of Intertidal Organisms.* Marine Ecological Surveys, Faversham, UK.
18. **Stephenson, T. A., and A. Stephenson. 1972.** *Life Between Tide Marks on Rocky Shores.* Freeman, San Francisco.
19. **Schureman, P. 1941.** *A Manual of the Harmonic Analysis and Prediction of Tides.* Special Publ. 98, U.S. Dept. of Commerce, Washington, DC.
20. **Darwin, G. H. 1898.** *The Tides.* Reprinted 1962. Freeman, San Francisco.

21. **Gaines, S. D., and M. W. Denny. 1993.** The largest, smallest, highest, lowest, longest, and shortest: extremes in ecology. *Ecology* **74:** 1677–1692.
22. **Barry, J. P., C. H. Baxter, R. D. Sagarin, and S. E. Gilman. 1995.** Climate-related long-term faunal changes in a California intertidal community. *Science* **267:** 672–675.
23. **Hewatt, W. G. 1934.** Ecological studies on selected marine intertidal communities of Monterey Bay. PhD thesis, Stanford University, 150 pp.
24. **Hewatt, W. G. 1937.** Ecological studies on selected marine intertidal communities of Monterey Bay. *Am. Midl. Natl.* **18:** 161–206.
25. **Bendat, J. S., and A. G. Piersol. 1986.** *Random Data: Analysis and Measurement Procedures.* 2nd ed. Wiley and Sons, New York.
26. **Paine, R. T. 1985.** Reestablishment of an insular Winter Wren population following a severe freeze. *Condor* **87:** 558–559.
27. **Wiesenfeld, K., and F. Moss. 1995.** Stochastic resonance and the benefits of noise: from ice ages to crayfish and SQUIDS. *Nature* **373:** 33–36.
28. **Press, W. H., S. A. Teukolsky, W. T. Vetterling, and B. P. Flannery. 1992.** *Numerical Recipes in FORTRAN.* 2nd ed. Cambridge University Press, Cambridge, UK.
29. **Paine, R. T. 1974.** Intertidal community structure: experimental studies of the relationship between a dominant competitor and its principal predator. *Oecologia* **15:** 93–120.

Reference: *Biol. Bull.* **194:** 116–119. (April, 1998)

Vestimentiferan on a Whale Fall

ROBERT A. FELDMAN[1,*,†], TIMOTHY M. SHANK[1], MICHAEL B. BLACK[1], AMY R. BACO[2], CRAIG R. SMITH[2], AND ROBERT C. VRIJENHOEK[1]

[1] *Center for Theoretical and Applied Genetics, Institute of Marine and Coastal Sciences, Cook College, Rutgers University, New Brunswick, New Jersey 08903-0231, and*
[2] *Biological Oceanography, Department of Oceanography, School of Ocean and Earth Science and Technology, University of Hawaii, 1000 Pope Road, Honolulu, Hawaii 96822*

Discovery of chemosynthetic communities associated with whale bones led to the hypothesis that whale falls may serve as stepping-stones for faunal dispersal between disjunct hydrothermal vents and cold seeps on the ocean floor (1). The initial observation was followed by a faunal inventory that revealed a diverse assemblage of microbes and invertebrates, supported by chemoautotrophic production, living in close proximity to whale remains (2, 3). To date, the conspicuous absence from whale falls of vestimentiferan tubeworms (a predominant constituent of eastern Pacific vent and seep habitats) has been a major objection to the stepping-stone hypothesis (4–5). We report the first evidence of a vestimentiferan tubeworm associated with a whale fall (Fig. 1). The tubeworm, Escarpia spicata, *was identified by morphological criteria and DNA sequence data from a portion of the mitochondrial cytochrome oxidase C subunit I (COI) gene. Additionally, the bacterial endosymbiont in the tubeworm possessed a 16S rRNA gene that was similar to that of endosymbionts from vestimentiferans in sedimented cold-seep environments.*

A chemosynthetic community associated with whale bones in the Santa Catalina Basin (SCB) off southern California (depth 1240 m, 33°12′N, 118°30′W) is the site of ongoing ecological studies (1, 2). We revisited the SCB site in May 1995 with the U.S. Navy's advanced tethered vehicle (ATV dive #118) and found a persistent community composed of filamentous sulfur bacteria (*Beggiatoa* sp.), vesicomyid clams (*Vesicomya*/*Calyptogena* spp.), mytilids (*Idas* sp.), limpets (*Pyropelta* spp., *Cocculina* sp.), snails (*Mitrella* sp.), and polynoid polychaetes (*Bathykurila* sp.). We also recovered a single vestimentiferan tubeworm growing near the squamosal bone of the whale skeleton (Fig. 1). The tubeworm was collected and preserved in 95% ethanol once aboard the support ship. The worm was initially identified as *Escarpia spicata* on the basis of diagnostic morphological features (6), most notably the central, slightly curved spikelike structure on the obturacular face.

DNA sequence information from a mitochondrial gene verified the identity of the SCB specimen. A 639-bp portion of the COI gene from the SCB vestimentiferan was identical to that of an *Escarpia spicata* individual sampled from cold seeps (Transform Fault) in the Gulf of California (Table I). The COI sequence of the SCB specimen differed by 0.32% from those of *Escarpia spicata* from hydrothermal vents (Guaymas Basin) in the Gulf of California (Table I). COI sequence differences less than 0.4% are consistent with intraspecific levels of divergence in vestimentiferans (7). Intergeneric COI sequence divergence in the Vestimentifera ranges from 8.5%–21.3% (7).

The bacterial endosymbiont from the SCB *E. spicata* was phylogenetically compared to other endosymbionts as part of a separate study (8). Sequence information from a 1361-bp region of the 16S rRNA gene (Genbank accession number U77842) revealed that the endosymbiont is a member of the gamma subdivision of the Proteobacteria. The SCB endosymbiont was closely related (1.45% sequence divergence) to endosymbionts found in vestimentiferans that live in sedimented seep localities; its relationship to endosymbionts from vestimentiferans found in

Received 6 January 1997; accepted 16 January 1998.

* Current address: Diversa Corporation, 10665 Sorrento Valley Road, San Diego, CA 92121.

† To whom correspondence should be addressed. E-mail: rfeldman@diversa.com

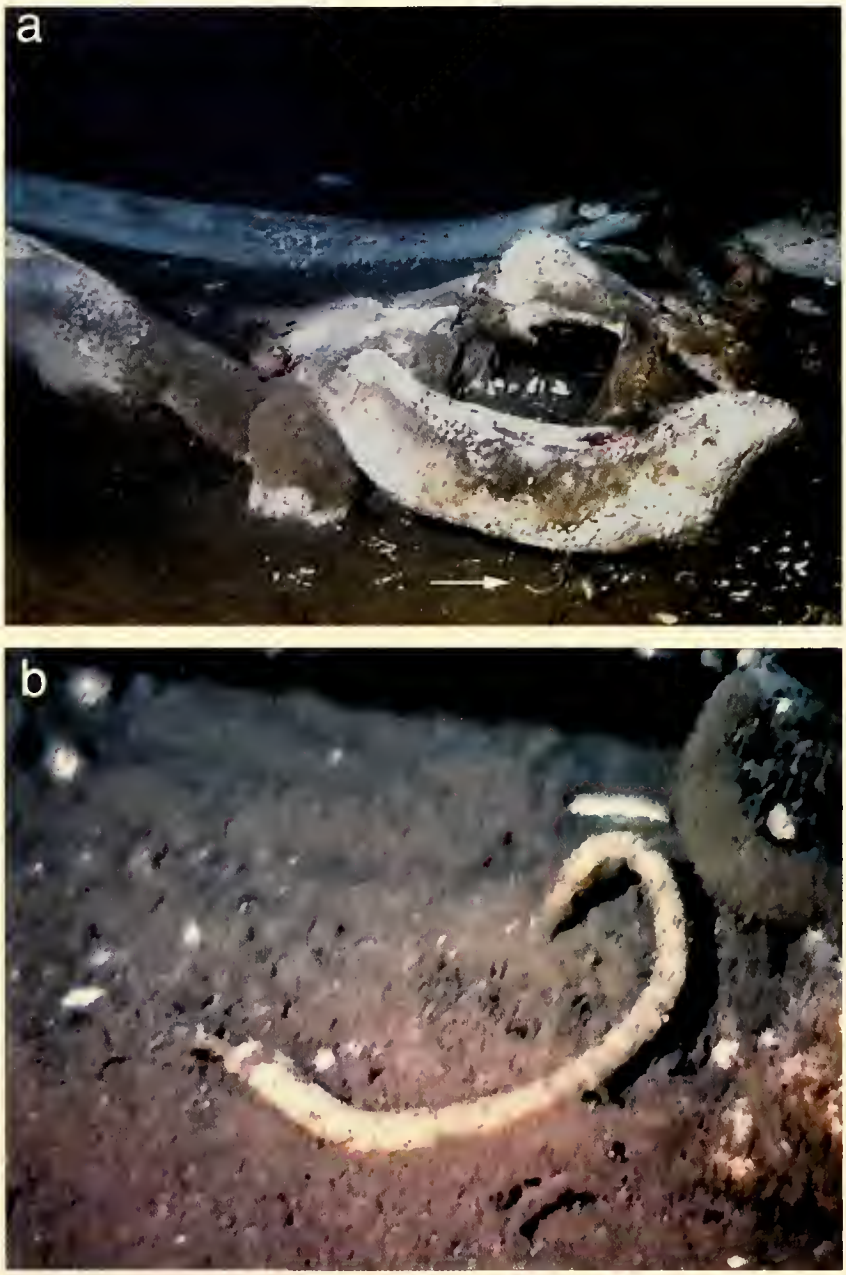

Figure 1. Skull bones of an 18-m baleanopterid skeleton, and associated chemoautotrophic community. (a) A broad view of the skull region with the first recorded adult vestimentiferan (arrow) at a whale fall (for scale, the squamosal bone in the right foreground is 80-cm long). The vestimentiferan plume (left) and posterior end of the tube (right) are visible in the magnified image (b). This individual was morphologically and genetically identified as *Escarpia spicata.* With the exception of *Lamellibrachia columna,* supplied by C. Cary (Univ. of Delaware), the specimens examined in this study were collected during oceanic cruises by one or more of the authors. DNA was extracted using the hexadecyl-trimethyl-ammonium bromide (CTAB) technique, modified from Doyle and Dickson (12). For the amplification of the mitochondrial COI gene; LCO1490: 5′-GGTCAACAAATCATAAAGATATTGG-3′ and HCO2198: 5′-ACTAAAAAACCA-GTGGGACTTCAAAT-3′ primers were used in standard conditions (13). To amplify symbiont and sequence the 16S rDNA, we used the universal bacterial primers 27F and 1492R (14); 27F: 5′-AGAGTTTGATCM-TGGCTCAG-3′, and 1492R: 5′-TACGGYTACCTTGTTACGACTT-3′ and a suite of internal primers (8). PCR products were purified and quantified on a video imaging system (Fotodyne Inc.), 100 ng of pure DNA was used as template for ABI Prism DNA sequencing reactions. The sequenced fragments were electrophoretically separated and detected using a Perkin Elmer ABI 373A DNA sequencer.

Table 1

Percent genetic distances between the Escarpia spicata *individual from the Santa Catalina Basin whale fall and related vestimentiferans for a 639-bp portion of the mitochondrial COI gene*

Species	Collection Site[1] Location	Lat Long	Substrate, Community Type	Depth (m)	Ref	Genetic Distance Matrix[2] 1	2	3	4	5
E. spicata	Guaymas Basin	27°35′N 111°28′W	sedimented, cold seep	1653	7	—				
E. spicata	Guaymas Basin	27°00′N 111°25′W	basaltic, vent	2020	7	0.32	—			
E. spicata	Santa Catalina Basin	33°12′N 118°30′W	sedimented, whale fall	1240	this study	0.00	0.32	—		
E. laminata	W. Florida Escarpment	26°02′N 84°55′W	sedimented, seep	3243	8	0.32	0.32	0.32	—	
Lamellibrachia columna	Lau Basin Hine Hina	22°32′S 176°43′W	sedimented, seep	1859	15	14.87	14.87	14.87	15.53	—

[1] Summary of collection information for all specimens analyzed.

[2] Distances are based on the Kimura 2-parameter model (16). Genbank accession numbers for these sequences are U74065, U74064, U84262, U74063, and U74061.

deep-sea hydrothermal vent habitats was more distant (4.5%).

Escarpia spicata occurs at cold-water sulfide seeps along the Louisiana Slope (9), southern California (type locality is Navy Fan, South San Clemente Basin) (6), Gulf of California (7), and in soft sediments near hydrothermal vents in the Guaymas Basin (7). Its presence in soft sediments near the Guaymas hot vents suggests that it may be an opportunistic species with a wide tolerance for habitat variation. Similarly, *Lamellibrachia barhami* is common in cold seeps in the northeastern Pacific but also occurs at new hot vents in Middle Valley (7). Vestimentiferan adults are sessile, but their larvae are free-swimming and may persist in the water column for as long as 3 weeks (10). Additionally, allozyme studies reveal that vestimentiferans have effective dispersal capabilities that maintain genetic continuity across vast distances (11). The potential for long larval life spans and the opportunistic settling habits of members of the Vestimentifera suggest that the SCB whale site is probably within the dispersal range of *E. spicata* larvae from the San Clemente Basin site.

The discovery of an adult vestimentiferan on the SCB whale fall suggests that such falls can support the recruitment and growth of at least one species of vestimentiferan. This finding, as well as the identification of seep and vent vesicomyids on whale falls, is consistent with the hypothesis that whale carcasses may serve as stepping-stones for seep and vent organisms (1). However, other models of metapopulation dynamics should also be considered, especially because we have not demonstrated the presence of a reproductive population of *E. spicata* on the SCB whale carcass. Careful analyses of the reproductive potential and persistence of whale-fall fauna are necessary to ascertain whether these animals contribute to the propagation of chemosynthetic communities in the deep sea. Alternatively, whale-fall fauna may represent sink populations that are colonized from more stable chemosynthetic source communities at nearby seeps or vents.

Acknowledgments

We gratefully acknowledge the skillful collecting efforts of the U.S. Navy advanced tethered vehicle pilots and the logistical support of the Laney Chouest crew. This is Contribution No. 98-11 of the Institute of Marine and Coastal Sciences, Rutgers University, and New Jersey Agricultural Experiment Station Publication No. 2-67175-4-98, and SOEST Publication No. 4592 supported by NOAA grant no. UAF-95-0040 to CRS, State funds and by NSF grants OCE-89-17311, OCE-92-17026, OCE-93-02205, OCE-95-29819, OCE-96-33131 and NIH Grant PHSTW00735-01 to RCV and RAL.

Literature Cited

1. **Smith, C. R., H. Kukert, R. A. Wheatcroft, P. A. Jumars, and J. W. Deming. 1989.** Vent fauna on whale remains. *Nature* **341:** 27–28.
2. **Bennett, B. A., C. R. Smith, B. Glaser, and H. L. Mayhaum. 1994.** Faunal community structure of a chemoautotrophic assemblage on whale bones in the deep northeast Pacific Ocean. *Mar. Ecol. Prog. Ser.* **108:** 205–223.
3. **Deming, J. W., A. L. Reysenbach, S. A. Macko, and C. R. Smith. 1997.** Evidence for the microbial basis of a chemoautotrophic community on a deep-sea whale skeleton: bone colonizing and animal-associated symbionts. *J. Micro. Res. Technol.* **37:** 162–170.
4. **Tunnicliffe, V., and S. K. Juniper. 1990.** Cosmopolitan underwater fauna. *Nature* **344:** 300.

5. **Jelmert, A., and O. D. Oppen-Berntsen. 1996.** Whaling and deep-sea biodiversity. *Conserv. Biol.* **10:** 653–654.
6. **Jones, M. L. 1985.** On the Vestimentifera, new phylum: Six new species, and other taxa, from hydrothermal vents and elsewhere. *Bull. Biol. Soc. Wash.* **6:** 117–158.
7. **Black, M. B., K. Halanych, P. Maas, W. R. Hoeh, J. Hashimoto, D. Desbruyères, R. A. Lutz, and R. C. Vrijenhoek. 1997.** Molecular systematics of deep-sea tube worms (Vestimentifera). *Mar. Biol.* **130:** 141–149.
8. **Feldman, R. A., M. B. Black, C. S. Cary, R. A. Lutz, and R. C. Vrijenhoek. 1997.** Molecular phylogenetics of bacterial endosymbionts and their vestimentiferan hosts. *Mol. Mar. Biol. Biotechnol.* **6**(3): 272–281.
9. **MacDonald, I. R., J. S. Boland, J. S. Baker, J. M. Brooks, M. C. Kennicutt, II, and R. R. Bidigare. 1989.** Gulf of Mexico hydrocarbon seep communities. II. Spatial distribution of seep organisms and hydrocarbons at Bush Hill. *Mar. Biol.* **101:** 235–247.
10. **Young, C. M., E. Vazquez, A. Metaxas, and P. A. Tyler. 1996.** Embryology of vestimentiferan tube worms from deep-sea methane/sulphide seeps. *Nature* **381:** 514–516.
11. **Black, M. B., R. A. Lutz, and R. C. Vrijenhoek. 1994.** Gene flow among vestimentiferan tube worm (*Riftia pachyptila*) populations from hydrothermal vents of the eastern Pacific. *Mar. Biol.* **120:** 33–39.
12. **Doyle, J. J., and E. Dickson. 1987.** Preservation of plant samples for DNA restriction endonuclease analysis. *Taxon* **36:** 715–722.
13. **Folmer, O., M. Black, W. Hoeh, R. Lutz, and R. Vrijenhoek. 1994.** DNA primers for amplification of mitochondrial cytochrome *C* oxidase subunit I from diverse metazoan invertebrates. *Mol. Mar. Biol. Biotechnol.* **3:** 294–299.
14. **Lane, D. J. 1991.** 16S/23S rRNA sequencing, Pp. 115–175 in *Nucleic Acid Techniques in Bacterial Systematics*, E. Stackebrandt and M. Goodfellow, eds. John Wiley, Chichester.
15. **Southward, E. C. 1991.** Three new species of Pogonophora, including two vestimentiferans, from hydrothermal sites in the Lau Back-arc Basin (Southwest Pacific Ocean). *J. Nat. Hist.* **25:** 859–881.
16. **Kimura, M. 1980.** A simple method for estimating evolutionary rates of base substitution through comparative studies of nucleotide sequences. *J. Mol. Evol.* **16:** 111–120.

Reference: *Biol. Bull.* **194:** 120–131. (April, 1998)

Characterization of *Aplysia* Attractin, the First Water-borne Peptide Pheromone in Invertebrates

SHERRY D. PAINTER[1,*], BRET CLOUGH[1], REBECCA W. GARDEN[2], JONATHAN V. SWEEDLER[2], AND GREGG T. NAGLE[1]

[1] *The Marine Biomedical Institute and the Department of Anatomy and Neurosciences, University of Texas Medical Branch, Galveston, Texas 77555-1043; and* [2] *School of Chemical Sciences and the Beckman Institute, University of Illinois at Urbana-Champaign, Urbana, Illinois 61801*

Abstract. Although animals in the genus *Aplysia* are solitary during most of the year, they form breeding aggregations during the reproductive season. The aggregations contain both mating and egg-laying animals and are associated with masses of egg cordons. The egg cordons are a source of pheromones that establish and maintain the aggregation, but none of the pheromonal factors have been chemically characterized. In these studies, specimens of *Aplysia* were induced to lay eggs, the egg cordons collected and eluted, and the eluates fractionated by C18 reversed-phase HPLC. Four peak fractions were bioassayed in a T-maze. All four increased the number of animals attracted to a nonlaying conspecific and were thus subjected to compositional and microsequence analysis. Each contained the same NH_2-terminal peptide sequence. The full-length peptide ("attractin") was isolated from the albumen gland, a large exocrine organ that packages the eggs into a cordon. The complete 58-residue sequence was obtained, and it matched that predicted by an albumen gland cDNA. Mass spectrometry showed that attractin is 21 wt. % carbohydrate as the result of *N*-linked glycosylation. T-maze bioassays confirmed that the full-length peptide is attractive. Attractin is the first water-borne peptide pheromone characterized in molluscs, and the first in invertebrates.

Received 13 August 1996; accepted 23 January 1998.

* To whom correspondence should be addressed. Marine Biomedical Institute, 10.104D Medical Research Building, University of Texas Medical Branch, 301 University Blvd., Galveston, Texas 77555-1043. E-mail: sdpainte@utmb.edu

Abbreviations: ASW, artificial seawater; DHB, 2,5-dihydrobenzoic acid; Endo Glu-C, endoproteinase Glu-C; HPLC, high performance liquid chromatography; MALDI-TOF MS, matrix-assisted laser desorption/ionization time-of-flight mass spectrometry; PCR, polymerase chain reaction; RP, reversed-phase.

Introduction

Pheromones play an important role in coordinating male and female reproductive behavior in many aquatic species, but relatively little is known about the identity of the water-borne factors or their specific activities. This is particularly true of water-borne peptide pheromones, which are difficult to isolate and characterize. The difficulties arise from the biological and chemical characteristics of the pheromonal system: (1) the small number of organisms that secrete the pheromone at any time; (2) the specific, but usually unknown, stimulus that induces pheromone secretion; (3) the relatively small amount of pheromone secreted; (4) the large volume of water into which secretion occurs—water that has contacted a variety of organisms and their products; and (5) the strong possibility that the pheromone may be rapidly degraded (Shimuzu, 1985).

Information generated over the last 30 years about reproductive activity in the marine opisthobranch mollusc *Aplysia* has lessened our concern about some of these problems—at least in this system. Field studies (Kupfermann and Carew, 1974; Audesirk, 1979; Susswein *et al.*, 1983, 1984) have shown that *Aplysia* is a solitary animal that moves into breeding aggregations during the summer reproductive season. The aggregations typically contain both mating and egg-laying animals and are associated with masses of recently deposited egg cordons. Most of the egg-laying animals simultaneously mate as females even though mating does not cause reflex ovulation (Blankenship *et al.*, 1983), suggesting that egg laying precedes

mating in the aggregation and that egg laying may release pheromones that establish and maintain the aggregation.

Similar observations have been made in the laboratory when animals were not individually caged (Audesirk, 1979; Blankenship *et al.*, 1983; Susswein *et al.*, 1983, 1984), and behavioral studies have shown that egg-laying animals with cordons are more attractive than sexually mature but nonlaying conspecifics (Aspey and Blankenship, 1976; Jahan-Parwar, 1976; Audesirk, 1977; Painter *et al.*, 1989). T-maze experiments demonstrate that at least some of the attractants derive from the egg cordon and are water-borne: (1) recent egg layers without egg cordons are no more attractive than nonlaying conspecifics; (2) recently deposited egg cordons are attractive, with or without the egg-laying animal, whereas sham cordons are not; and (3) both recently deposited egg cordons and their eluates increase the attractiveness of nonlaying conspecifics when placed in the adjacent seawater (Painter *et al.*, 1991; Painter, 1992). There are also contact pheromones on the egg cordon that can induce reproductive activity (Begnoche *et al.*, 1996).

Two potential tissue sources of the "cordon-derived" pheromonal attractants have been identified in T-maze experiments (Painter, 1992, 1993). The first is the albumen gland (Fig. 1), a large exocrine organ that packages the eggs into a cordon (Coggeshall, 1972); it is the first and largest exocrine organ contacted by the eggs. The second potential tissue of origin is the atrial gland (Fig. 1), a smaller exocrine organ that secretes into the oviduct (Arch *et al.*, 1980; Beard *et al.*, 1982; Painter *et al.*, 1985). The atrial gland is the last exocrine organ to contact the egg cordon, but unlike those of the albumen gland, the timing and general function of its secretion are not known.

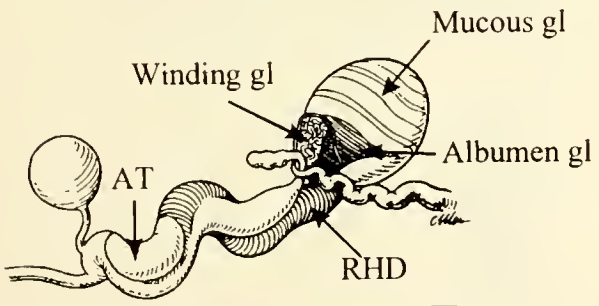

Figure 1. Schematic diagram of the reproductive tract of *Aplysia californica* rostral to the ovotestis (which would be at the far right). The labeled structures are exocrine organs that come in contact with the egg cordon during deposition. The albumen, mucous, and winding glands package the eggs into a cordon. The red hemiduct (RHD) is the functional oviduct that transports the egg cordon to the common genital aperture (which would be at the far left). The RHD secretes onto the cordon, but neither the secretory products nor their functions have been identified. The atrial gland (AT) secretes into the oviduct, but the timing of secretion is not known. T-maze experiments have identified the albumen and atrial glands as potential tissue sources of pheromonal attractants.

The current studies take advantage of two significant observations: (1) egg laying can be induced in *Aplysia* by injecting atrial gland extract into the hemocoel (Arch *et al.*, 1978); and (2) recently deposited egg cordons are a source of water-borne pheromonal attractants (Painter *et al.*, 1991). When atrial gland extract is used to induce egg laying, the number of animals laying eggs, the timing and synchronization of egg deposition, the general area where eggs are deposited, and (to some extent) the purity of the surrounding artificial seawater (ASW) can be controlled. In terms of "cordon-derived" pheromones, this means that it is possible to control the timing of pheromone secretion, the amount of pheromone secreted, and the relative amount of contaminants in the seawater.

Using this approach, we have isolated a peptide pheromonal attractant from eluates of recently deposited egg cordons, obtained a partial NH_2-terminal sequence, and used molecular techniques to identify the albumen gland as the organ of origin. The full-length peptide was isolated from the gland, and its complete 58 amino acid sequence was determined and found to match the sequence predicted from an albumen gland cDNA. *N*-linked glycosylation was demonstrated by matrix-assisted laser desorption/ionization time-of-flight mass spectrometry (MALDI-TOF MS), and attractiveness was verified in the T-maze assay.

To the best of our knowledge, this is the first water-borne peptide pheromone to be characterized in molluscs, and indeed in invertebrates. The only other water-borne peptide pheromones that have been characterized to date include a small family of structurally related mating pheromones from the ciliated protozoan *Euplotes* (*e.g.*, Raffioni *et al.*, 1988, 1992; Stewart *et al.*, 1992); several small families of mating pheromones in different genera of yeast (*e.g.*, *Saccharomyces*, Stotzler *et al.*, 1976; *Rhodospiridium*, Kamiya *et al.*, 1978); and a female attractant from the cloacal gland of male red-bellied newts (*Cynops;* Kikuyama *et al.*, 1995).

Materials, Methods, and Results

Animals

Two species of *Aplysia* were used in these studies because each has a unique characteristic that simplifies specific aspects of the experiments. This approach was feasible because the pheromonal attractants associated with the aggregation do not appear to be species-specific; breeding aggregations sometimes contain more than one species of *Aplysia* (Kupfermann and Carew, 1974; Achituv and Susswein, 1985), and the associated egg masses sometimes contain egg cordons from more than one species

(Achituv and Susswein, 1985). Only sexually mature animals, as judged by the ability to lay eggs, were used.

Aplysia brasiliana (Rang) was selected as the experimental animal for T-maze bioassays because it has lower levels of chance attraction in the maze than *A. californica* (Painter *et al.*, 1991), and it can be collected in large numbers from the south Texas coast during the reproductive season. The animals (130–390 g) were housed in individual cages in one of five large aquaria containing recirculating ASW (Instant Ocean Marine Salt, Longhorn Pet Supply, Houston, Texas). Water temperature was maintained at 20° ± 2°C; the salinity ranged from 30 to 32 ppt. A 14:10 light:dark cycle was maintained, with the light period starting at 0600 hours. Animals were fed dried laver in the late afternoon (1600–1800), after experiments had been completed. Egg-laying activity was checked twice every day (0800–0900, 1600–1800), activity recorded, and egg cordons removed.

Specimens of *Aplysia californica* (Cooper) were obtained from Alacrity Marine Biological Services (Redondo Beach, California) and maintained as described above, except that the water temperature was 14° ± 2°C. This species was used as the source of egg cordons for elutions because it lays eggs less frequently than *A. brasiliana* (Fig. 2A, B), leaving a larger proportion of animals that can be induced to lay eggs on any day, and the volume of the egg mass is larger (Fig. 2C, D; also see Dudek *et al.*, 1979; Pinsker and Parsons, 1985). *A. californica* was also used as the source of albumen glands in later experiments.

Induction of egg laying, collection of egg cordons, and elution

Procedures. Egg laying was induced by injecting 0.1 ml of atrial gland extract (made as described in Painter *et al.*, 1991) through the foot into the hemocoel. All specimens (250–500 g) of *A. californica* that had not laid eggs during the preceding 24 h were injected, the number varying in each elution, and most began laying within 30–40 min. One hour following the injection, and at 30-min intervals thereafter, egg cordons were severed a short distance from the common genital aperture and removed from the cage.

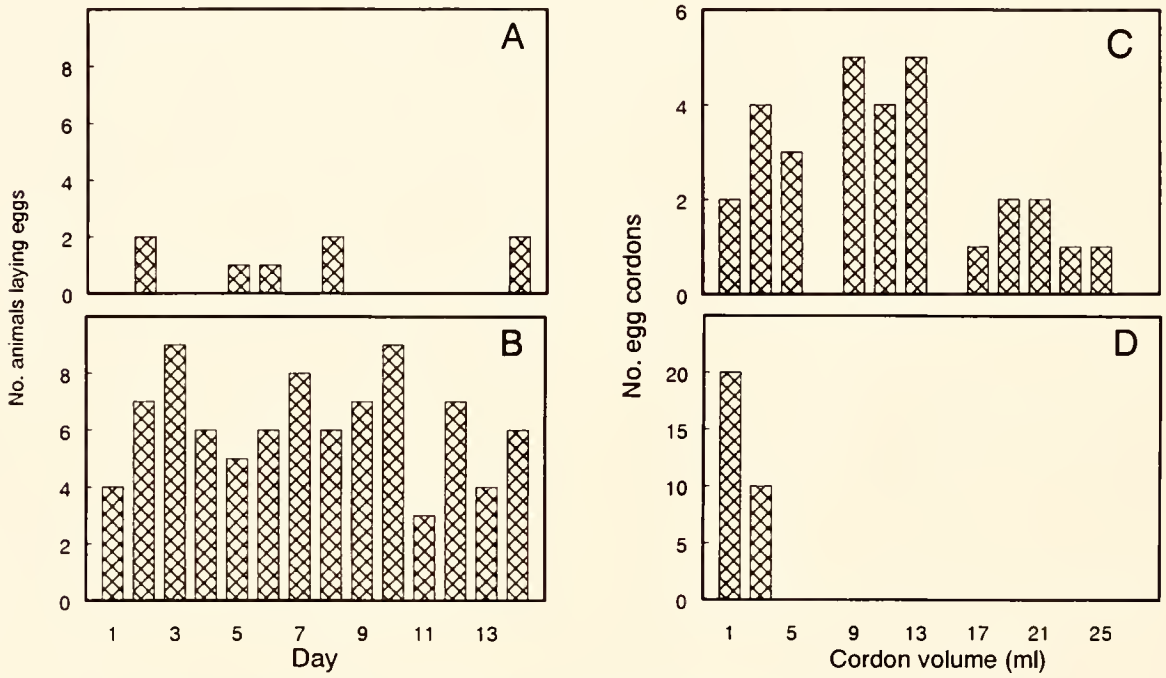

Figure 2. *Aplysia californica* lays eggs less frequently than *A. brasiliana*, and the egg cordons have a larger volume. A, B: The daily egg-laying history of *A. californica* (A) and *A. brasiliana* (B) over a 2-week period. Ten animals were present in each aquarium: all were known egg layers, and none was used in any other experiments during this time. Egg laying was checked every morning and egg cordons removed. Housing conditions differed only in water temperature. A total of 8 cordons were laid by *A. californica;* 87 cordons were laid by *A. brasiliana.* C, D: The volumes of 30 cordons laid by *A. californica* (C) and *A. brasiliana* (D); each cordon was laid by a different animal. Volume was measured by ASW displacement in a graduated cylinder. The mean volume of *A. californica* cordons was 11.1 ml, and the mean volume of *A. brasiliana* cordons was 1.5 ml.

When all of the cordons from a 30-min laying period had been collected, they were rinsed briefly in fresh ASW that had not previously contacted animals or egg cordons and then transferred to a beaker containing 200–300 ml of the fresh ASW for elution. When the volume of cordons was large (judged by eye before the rinse), two or three eluting beakers were used. Each beaker was covered and placed on a rotary shaker for 30 min. The water was at aquarium temperature when the eggs were added, and it increased by 1°–2°C during the elution period. After the elution, the cordons were carefully removed from each beaker and blotted to remove excess fluid. Cordon volume was then determined by ASW displacement in a graduated cylinder.

Several steps were taken to minimize the amount of material in the eluate that was not derived from the egg cordons. First, the ASW used for the rinses and elutions was made from isotonic salt solutions in glass-distilled water. This was necessitated by the large volumes of ASW used (small amounts of contaminants in the ASW became major components of the concentrated eluate). Second, the eluting beakers were thoroughly rinsed with this ASW and then used in two 30-min elutions comparable to those performed on the egg cordons. The first of these was discarded. The second was processed like the egg cordon eluates, and was fractionated by C18 reversed-phase (RP)-high performance liquid chromatography (HPLC). The resulting profile was used to identify water- and glassware-derived factors in the egg cordon eluates. Third, latex gloves were worn whenever egg cordons, cordon eluates, or tools that came in contact with either were handled.

Results. The number of *Aplysia* injected per elution ranged from 10 to 54, and egg deposition appeared to be normal. The injected animals continued to lay eggs for an extended period of time (4–8 h), and the mean volume of eggs laid (10.2 ml/animal; range: 9.1–15.2 ml/animal) was comparable to that of spontaneously laid egg cordons (11.1 ml/animal; Fig. 2C). The volume of cordons eluted during each period ranged from 1 to 125 ml, the variation reflecting the number of animals laying during the period and the amount of time each utilized for the activity. The volume provided a crude estimate of the amount of material and activity contained in each sample. Figure 3 shows the volume of eggs deposited during each interval of a 5-h deposition. The total volume of eggs collected for an elution ranged from 152 to 490 ml.

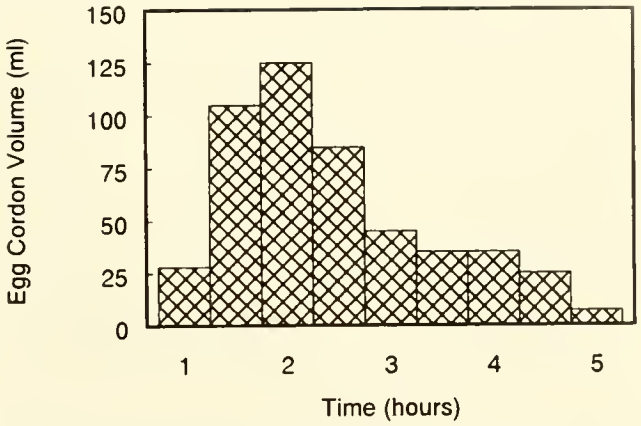

Figure 3. Time course of induced egg laying in *Aplysia californica*. In this experiment, 54 animals were injected with atrial gland extract at time zero, and most began laying eggs at about 30–40 min. Starting at 1 h post-injection, and at 30-min intervals thereafter, cordons were collected for elution. Following elution, the volume of the collected cordons was measured by ASW displacement in a graduated cylinder. The mean egg-cordon volume in this elution was 9.1 ml/animal; the mean for all elutions was 10.2 ml/animal.

Peptide purification

Procedures. After the cordons were removed, the eluates were filtered through a sterile disposable filter (0.45 μm cellulose acetate membrane; Fisher Scientific Products), acidified to 0.1% trifluoroacetic acid (TFA; VWR Scientific, reagent grade), and stored for a short time (usually less than 30 min) at 4°C in a sealed container until they could be further purified on a C18 Sep-Pak cartridge (Rainin Instrument Company). Two to three cartridges were used for each elution beaker. Each was pretreated with 3 ml of 60% acetonitrile (VWR Scientific, HPLC grade) containing 0.1% TFA, and rinsed with 5 ml of 0.1% TFA. The sample was passed through the cartridge once, and the cartridge was rinsed with 5 ml of 0.1% TFA. The peptides were then eluted with 3 ml of 60% acetonitrile containing 0.1% TFA, lyophilized, and stored at −20°C until use.

The lyophilized samples were resuspended in 1.5 ml of 0.1% heptafluorobutyric acid (HFBA; Pierce Chemical Company) and applied to a Vydac analytical C18 RP-HPLC column (0.46 × 25 cm). Both the guard and analytical columns had a 5-μm particle size. The column was eluted with a linear gradient of 0.1% HFBA and acetonitrile containing 0.1% HFBA. The column eluate was monitored at 215 nm and 1-min (1-ml) fractions collected.

Results. A representative RP-HPLC profile of an egg-cordon eluate is shown in Figure 4. Four major peaks (labeled 1–4 in the figure; referred to as C1–C4 in the text) were present in all elutions and had consistent retention times; the control RP-HPLC elution profiles showed that C1–C4 were not derived from the glassware or ASW. They were pooled based on absorbance, lyophilized, and stored at −20°C until they could be bioassayed for pheromonal attraction in the T-maze.

T-maze bioassays

Procedures. The T-maze, removable stimulus cages, and experimental protocol have been described previously

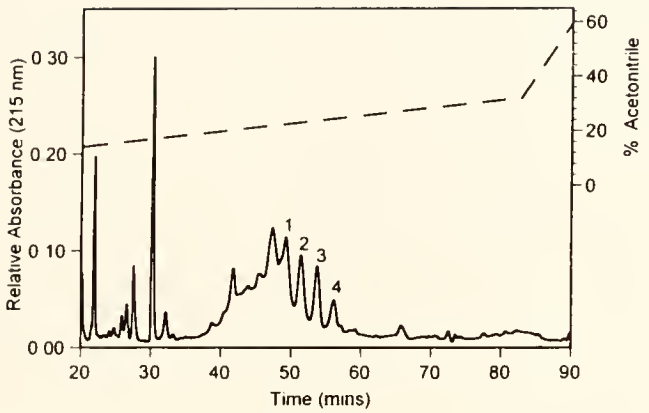

Figure 4. Representative fractionation of *Aplysia* egg-cordon eluates by C18 RP-HPLC. This eluate was from 35 ml of *A. californica* egg cordons; they were laid by 54 animals 180–210 min after injection with atrial gland extract. The fractions were eluted with a linear gradient (– – –) of 0.1% HFBA and acetonitrile containing 0.1% HFBA. Four peak fractions, C1–C4 (labeled 1–4), were pooled based on absorbance at 215 nm, and bioassayed for attraction in the T-maze.

(Painter *et al.*, 1991). Individual *A. brasiliana* for each assay were selected on the basis of four criteria: (1) the animal must be sexually mature but not have laid eggs during the preceding 24 h; (2) the animal must not have been used in a bioassay during the preceding 24 h; (3) test animals must not have been exposed previously to the fraction being tested; and (4) stimulus and test animals must be housed in the same aquarium. The potential attractants tested consisted of C1, C2, C3, or C4. The amount of material that could be recovered from 2 ml of egg cordons was tested; 2 ml is about 20% of the volume of egg cordons laid by one animal.

The test animal was placed at the base of the maze 5 min after the stimulus animal and potential attractant were placed in one of the stimulus cages. In most cases, the test animal moved directly to the top of the maze and exhibited one of two patterns of behaviors: (1) it stopped, moved its head from side to side, then either moved into one arm or returned to the base of the maze and remained there; or (2) it swam around in the maze, often visiting both cages before deciding where to stop. A response was considered to be positive if the test animal traveled to the stimulus within 20 min and maintained contact with the stimulus cage for 5 min, negative if the test animal traveled to the opposite arm and maintained contact with the cage for 5 min, and no choice if it did neither. Fifteen experiments were performed for each potential attractant, and the attractant was alternated between arms in consecutive experiments. Statistical significance was assessed by χ^2 analyses.

Results. To assess directional bias and chance levels of attraction in the maze, 15 experiments were performed in which the stimulus consisted of a nonlaying animal with nothing added to the surrounding ASW. Previous studies (Painter *et al.*, 1991) have shown that nonlaying *A. brasiliana* individuals are as attractive as empty stimulus cages. Two animals (13.3%) traveled to the right arm and remained, three (20%) traveled to the left arm and remained, and ten (66.7%) did neither. Of the five animals making a choice, only three went to the stimulus animal, one of which was in the right arm and two of which were in the left arm of the maze. These bioassays demonstrate that there was no directional bias in the maze and establish chance levels of attraction at 2–3 animals.

The positive control consisted of an extract of the atrial gland (equivalent to 0.5 gland) placed in the ASW adjacent to the stimulus animal. When the extract was present, a larger number of animals were attracted to the stimulus (11 animals; 73.3%) and fewer made negative (1 animal; 6.7%) and no-choice (3 animals; 20%) responses (Fig. 5). The change in response pattern was statistically significant [$\chi^2(2) = 7.85$; $0.01 < P < 0.025$].

A similar change in response pattern was observed when any of the fractions of egg-cordon eluate were placed in the ASW: more animals were attracted to the stimulus and fewer failed to make a choice (Fig. 5). The magnitude of the pattern changes differed among the fractions, with C1 producing the largest and most significant change: 13 of 15 animals (86.7%) were attracted to the stimulus, 1 animal (6.7%) chose the opposite arm, and 1 animal (6.7%) failed to make a choice. This change was statistically significant [$\chi^2(2) = 12.16$; $P < 0.005$]. Fewer animals were attracted by the other cordon fractions, and the resulting changes in response pattern were not statisti-

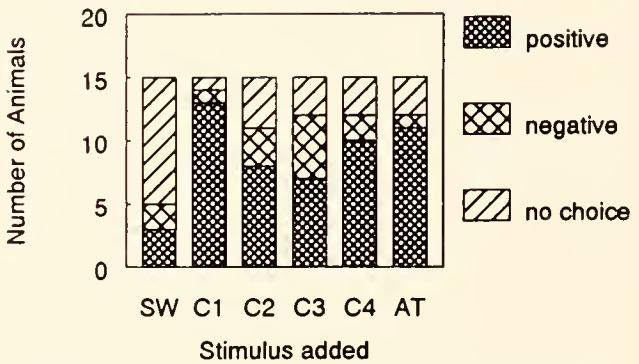

Figure 5. Fractions C1–C4 of egg-cordon eluate may contain pheromonal attractants. The number of *Aplysia brasiliana* attracted to a nonlaying conspecific (SW) was increased when any of the cordon fractions was placed in the adjacent seawater, and fewer animals failed to make a choice. The positive control (AT) is an atrial gland extract equivalent to 0.5 gland. This bar graph is based on 90 single-arm experiments, 15 per stimulus. In each experiment, animals chose between a stimulus in one arm and no stimulus in the other. The change in response pattern was statistically significant only for fraction C1 and the positive control.

cally significant [C2: $\chi^2(2) = 3.38$, $0.1 < P < 0.25$; C3: $\chi^2(2) = 4.51$, $0.1 < P < 0.25$; C4: $\chi^2(2) = 5.93$, $0.05 < P < 0.1$].

All four fractions also induced behaviors that might have resulted in male mating activity if the animals had had greater access to each other. These included eversion of the penis, attempting to enter the stimulus cage, pushing the oral veil through holes in the cage, and physically interacting with the stimulus animal. The number of times such behaviors occurred differed among the fractions, with C1 producing the largest number (Table I).

Differences in the magnitude of fraction activity could reflect differences in the amount of peptide recovered from the cordon eluate (as indicated by differences in peak area), the potency of the recovered peptides, the purity of the fractions, or some combination of the three. Because it was not easy to distinguish among these possibilities, all four fractions were subjected to biochemical analysis.

Compositional and microsequence analyses

Procedures. Reagents for these analyses were purchased from Perkin-Elmer/Applied Biosystems. Compositional analyses were performed using an Applied Biosystems 420H amino acid analyzer. For microsequence analyses, samples were applied to a Perkin Elmer/Applied Biosystems Procise 494/HT protein/peptide sequencer. The PTH derivatives of the amino acids obtained from the sequencer were identified and quantified by HPLC (Nagle *et al.*, 1986). Some samples were reduced and alkylated prior to application.

Results. The compositions of the four fractions are shown in Table II. Partial sequences, consisting of at least 24 residues for each peptide fraction, were obtained and are summarized in Table III. The sequences are identical except for length. Each has multiple cysteine residues, and one potential *N*-linked glycosylation site (Asn^8). The number of picomoles of Asn recovered at position 8 is about the same as was recovered for Gly at position 7 and for Ile at position 9, suggesting that the peptides were not glycosylated.

Table I

Potential male sexual behavior in maze assay

Stimulus	Behaviors				
	Evert penis	Enter cage	Animals interact	Stimulus animal moves to stimulus	Total animals
Non-egg-laying *Aplysia*	0	0	0	0	0
C1	3	3	1	2	9
C2	0	0	1	0	1
C3	0	0	3	2	5
C4	0	1	4	0	5
Atrial gland extract	0	1	0	0	1

Values represent number of animals exhibiting each behavior.

Table II

Amino acid composition (residues/mol peptide) of attractin-related fractions of egg-cordon eluate and of attractin from albumen gland

Amino acid	Fractions[a]				Attractin[b]
	C1	C2	C3	C4	
Cysteine	ND	ND	ND	ND	6
Aspartic acid	10.4	10.1	11.0	8.8	9
Threonine	5.3	6.0	6.2	6.3	5
Serine	2.9	2.5	1.9	1.9	4
Glutamic acid	11.4	10.0	6.8	7.4	13
Proline	1.4	1.6	1.8	2.2	1
Glycine	3.3	3.2	2.3	4.1	4
Alanine	2.8	2.7	1.9	2.5	3
Valine	1.3	1.5	1.8	2.1	1
Methionine	1.2	0.8	0.6	0.4	2
Isoleucine	4.6	4.6	4.8	4.8	4
Leucine	1.2	1.3	1.5	1.9	1
Tyrosine	0.1	0	0	0.2	0
Phenylalanine	1.0	1.0	0.8	1.0	1
Lysine	1.7	1.2	0.5	0.5	2
Arginine	0.8	0.6	0.2	0.4	1
Tryptophan	ND	ND	ND	ND	0
Histidine	0.9	0.6	0.2	0.5	1

[a] Residues determined by compositional analysis following hydrolysis. ND = not determined.

[b] Residues determined by sequence analysis following reduction and alkylation with 4-vinylpyridine.

Molecular studies to identify the organ of origin

Because of the difficulties inherent in generating egg-cordon eluates for analysis and the probability that degradation is occuring during the process, we next focused on identifying the pheromonal organ of origin; a molecular approach was used. Degenerate oligonucleotide primers corresponding to the NH_2- and COOH-terminal regions of the longest characterized peptide (C1) were used to generate an albumen-gland polymerase chain reaction (PCR) product. The PCR product was cloned and sequenced; it encoded the 46-residue peptide sequence. The corresponding cDNA was isolated from an albumen gland cDNA library and the entire 76-residue precursor sequence predicted (Fan *et al.*, 1997). The predicted sequence of the full-length 58-residue peptide ("attractin") is shown in Table IV.

The attractin cDNA was expressed in the baculovirus system, and lysates were fractionated by RP-HPLC under the same gradient conditions as the egg-cordon eluates

Table III

Sequence and quantity (in picomoles) of amino acid residues, determined by automated sequence analysis, of attractin-related fractions of egg-cordon eluate and of attractin from albumin gland

Edman cycle	C1 (U)	C2 (R/A)	C3 (U)	C3 (R/A)	C4 (U)	C4 (R/A)	Attractin 1A (R/A)	Attractin 1B (R/A)	Attractin 48–58 (D)
0*	— (1250)	— (990)	— (250)	— (205)	— (380)	— (100)	— (232)	— (320)	— (170)
1	Asp (648)	Asp (39)	Asp (20)	Asp (70)	Asp (31)	Asp (33)	Asp (71)	Asp (80)	Ser (41)
2	Gln (1028)	Gln (37)	Gln (35)	Gln (86)	Gln (34)	Gln (22)	Gln (73)	Gln (210)	Ala (119)
3	Asn (787)	Asn (38)	Asn (20)	Asn (65)	Asn (27)	Asn (23)	Asn (113)	Asn (145)	Ala (123)
4	ND —	Cys (33)	ND —	Cys (98)	ND —	Cys (15)	Cys (260)	Cys (363)	Gly (97)
5	Asp (563)	Asp (25)	Asp (15)	Asp (38)	Asp (21)	Asp (20)	Asp (82)	Asp (104)	Ser (40)
6	Ile (767)	Ile (43)	Ile (18)	Ile (88)	Ile (18)	Ile (33)	Ile (198)	Ile (280)	Thr (55)
7	Gly (592)	Gly (26)	Gly (7)	Gly (47)	Gly (15)	Gly (15)	Gly (150)	Gly (217)	Thr (57)
8	Asn (538)	Asn (36)	Asn (11)	Asn (54)	Asn (16)	Asn (20)	Asn (14)	ND —	Leu (77)
9	Ile (674)	Ile (34)	Ile (6)	Ile (71)	Ile (17)	Ile (21)	Ile (194)	Ile (274)	Gly (50)
10	Thr (460)	Thr (17)	Thr (5)	Thr (40)	Thr (9)	Thr (12)	Thr (85)	Thr (141)	Pro (37)
11	Ser (206)	Ser (9)	Ser (3)	Ser (19)	Ser (4)	Ser (10)	Ser (47)	Ser (69)	Gln (11)
12	Gln (422)	Gln (18)	Gln (7)	Gln (44)	Gln (11)	Gln (10)	Gln (95)	Gln (147)	
13	ND —	Cys (18)	ND —	Cys (42)	ND —	Cys (12)	Cys (148)	Cys (237)	
14	Gln (390)	Gln (17)	Gln (6)	Gln (32)	Gln (6)	Gln (8)	Gln (103)	Gln (146)	
15	Met (319)	Met (12)	Met (4)	Met (42)	Met (5)	Met (6)	Met (115)	Met (196)	
16	Gln (312)	Gln (15)	Gln (4)	ND —	Gln (5)	Gln (11)	Gln (83)	Gln (126)	
17	His (91	His (4)	His (1)	His (8)	His (1)	His (5)	His (35)	His (65)	
18	Lys (116)	Lys (3)	Lys (1)	Lys (6)	Lys (1)	ND —	Lys (58)	Lys (107)	
19	Asn (236)	Asn (11)	Asn (4)	Asn (27)	Asn (2)	Asn (10)	Asn (29)	Asn (58)	
20	ND —	Cys (7)	ND —	Cys (30)	ND —	Cys (8)	Cys (53)	Cys (113)	
21	Glu (124)	Glu (8)	Glu (2)	Glu (15)	Glu (2)	ND —	Glu (33)	Glu (77)	
22	Asp (95)	Asp (8)	Asp (1)	Asp (27)	Asp (2)	Asp (2)	Asp (15)	Asp (30)	
23	Ala (113)	Ala (6)	Ala (1)	Ala (16)	Ala (1)	Ala (3)	Ala (28)	Ala (54)	
24	Asn (110)	Asn (10)	Asn (1)	Asn (9)	Asn (1)	ND —	Asn (32)	Asn (31)	
25	Gly (85)	Gly (3)	Gly (2)				Gly (18)	Gly (40)	
26	ND —	Cys (2)	ND —				Cys (16)	Cys (50)	
27	Asp (36)	ND —	Asp (38)				Asp (11)	Asp (18)	
28	Thr (35)	Thr (1)	ND —				Thr (7.8)	Thr (20)	
29	Ile (42)	Ile (2)	Ile (11)				Ile (11)	Ile (33)	
30	Ile (81)	Ile (2)					Ile (29)	Ile (64)	
31	Glu (24)	Glu (3)					Glu (4.8)	Glu (20)	
32	Glu (37)						Glu (15)	Glu (35)	
33	ND —						Cys (6.8)	Cys (22)	
34	Lys (10)						Lys (5.8)	Lys (17)	
35	Thr (13)						Thr (0.4)	Thr (7.7)	
36	Ser (11)						Ser (0.9)	Ser (4.6)	
37	Met (11)						Met (3.5)	Met (14)	
38	Val (12)						Val (3.2)	Val (12)	
39	Glu (7)						Glu (0.4)	Glu (4.7)	
40	Arg (8)						Arg (3.6)	Arg (11)	
41	ND —						Cys (1.7)	Cys (10)	
42	Gln (3)						Gln (2.1)	Gln (6.4)	
43	Asn (4)						Asn (2.5)	Asn (4.6)	
44	Gln (8)						Gln (4.3)	Gln (13)	
45	Glu (1)						Glu (0.4)	Glu (5.0)	
46	Phe (4)						Phe (1.1)	Phe (6.6)	
47							ND —	Glu (4.3)	
48							Ser (0.4)	Ser (2.1)	
49							Ala (1.2)	Ala (4.4)	
50							Ala (1.2)	Ala (8.4)	
51							Gly (0.7)	Gly (1.3)	
52							ND —	Ser (0.1)	
53							ND —	Thr (1.5)	
54							ND —	Thr (1.5)	
55							Leu (1.4)	Leu (1.2)	
56								ND —	
57								Pro (2.4)	

Samples of egg-cordon eluate (C1–C4) were either untreated before sequence analysis (U) or were reduced and alkylated with 4-vinylpyridine (R/A). Samples of attractin from albumin gland were either reduced and alkylated with 4-vinylpyridine (R/A) or were digested with Endo Glu-C (D) so that the COOH-terminal fragment (residues 48–58) could be identified and sequenced. ND = not determined.

* Initial amount of peptide (picomoles) applied to sequencer.

Table IV

Amino acid sequences of Aplysia californica *peptides from attractin-related fractions of egg-cordon eluate and from attractin*

	10	20	30	40	50
Att	DQNCDIGNITSQCQMQHKNCEDANGCDTIIEECKTSMVERCQNQEFESAAGSTTLGPQ				
C1	DQN-DIGNITSQ-QMQHKN-EDANG-DTIIEE-KTSMVER-QNQEF				
C2	DQNCDIGNITSQCQMQHKNCEDANGC-TIIE				
C3	DQNCDIGNITSQCQMQHKNCEDANG-D-I				
C4	DQNCDIGNITSQCQMQHKNCEDAN				

Attractin (Att) is glycosylated at Asn^8. Fractions C2, C3, and C4 were reduced and alkylated before analysis; C1 was not.

(data not shown). The peak fraction containing full-length attractin was identified by sequence analysis, and the retention time was used in subsequent studies to identify full-length attractin in extracts of the albumen gland.

Isolation and characterization of albumen gland attractin

Procedures. Albumen glands were removed from sexually mature individuals of *A. californica*, extracted at 4°C in 0.1% HFBA using a Polytron homogenizer, and sonicated. The extract was centrifuged for 20 min at 48,000 $\times g$ (4°C) and the supernatant Sep-Pak purified. The range of acetonitrile concentrations was narrowed from 0%–60% to 10%–50% in the Sep-Pak procedure to minimize the large peaks eluting very early and very late in the RP-HPLC gradient. The purified sample was fractionated by RP-HPLC, using the same gradient conditions as the egg-cordon eluates. The peak of interest was identified from the retention time of recombinant attractin.

To verify the 46-residue NH_2-terminal sequence, aliquots of the peak fraction were reduced with 2-mercaptoethanol, alkylated with 4-vinylpyridine, and purified by RP-HPLC with TFA as counterion. The peak of interest was identified by compositional analysis and subjected to microsequence analysis. To obtain the COOH-terminal sequence, samples were digested with sequencing grade endoproteinase Glu-C (Endo Glu-C; Boehringer-Mannheim), and the resulting fragments were purified by RP-HPLC with TFA as counterion. The COOH-terminal peptide was detected by compositional analysis and subjected to microsequence analysis.

Results. A representative RP-HPLC elution profile from extracts of albumen glands from *A. californica* is shown in Figure 6A. Fraction 1 coeluted with recombinant attractin. It was reduced, alkylated, and then purified by RP-HPLC with TFA as counterion (Fig. 6B). Fractions 1A and 1B were subjected to microsequence analysis for 55 and 57 residues, respectively; the sequences were identical (Table III), but incomplete. To determine the COOH-terminal sequence, Fraction 1 (Fig. 6A) was digested with Endo Glu-C and the resulting fragments purified by RP-HPLC (Fig. 6C). The COOH-terminal fragment was identified by compositional analysis and sequenced. The sequence obtained (Table III) was identical to that predicted for residues 48–58 of attractin by nucleotide sequence analysis of the attractin cDNA (Fan *et al.*, 1997).

No major albumen gland peaks coeluted with cordon eluate fractions C1–C4, suggesting that these fractions were generated by extracellular degradation of the full-length peptide. In addition, the recovery of Asn at position 8 was reduced by several hundredfold relative to adjacent amino acids in the sequence of albumen gland attractin, but not in fractions C1–C4. This suggests that the peptide is glycosylated in the cell and that extracellular degradation removes the carbohydrate.

MALDI-TOF mass spectrometry

Procedures. *N*-linked glycosylation was investigated using MALDI-TOF MS of both the full-length native attractin and the reduced and alkylated attractin. The matrix employed (2,5-dihydroxybenzoic acid; DHB; ICN Pharmaceuticals, Costa Mesa, California) readily produces stable protonated molecular ions of glycopeptides (Harmon *et al.*, 1996). Samples were prepared by mixing a 0.5-μl aliquot of $\sim$7 μM attractin with 0.5 μl of 65 mM aqueous DHB on a metallic sample probe. The probe was dried at ambient temperature and then inserted into the mass spectrometer.

MALDI-TOF MS experiments were performed with a Voyager Elite biospectrometry research station with delayed ion extraction (PerSeptive Biosystems, Framingham, Massachusetts). A pulsed nitrogen laser (337 nm) served as the desorption/ionization source, and positively charged ions were detected in the reflectron mode using a 200-ns delay prior to acceleration at 20 kV. The laser beam was focused at the sample surface with enough energy to reach the ionization threshold. Each mass spectrum shown is the average of $\sim$100 laser pulses, with mass calibration performed externally using the known $[M + H]^+$ and $[M + 2H]^{2+}$ peaks from MALDI-TOF MS of bovine insulin (Sigma Chemical Company, St. Louis, Missouri).

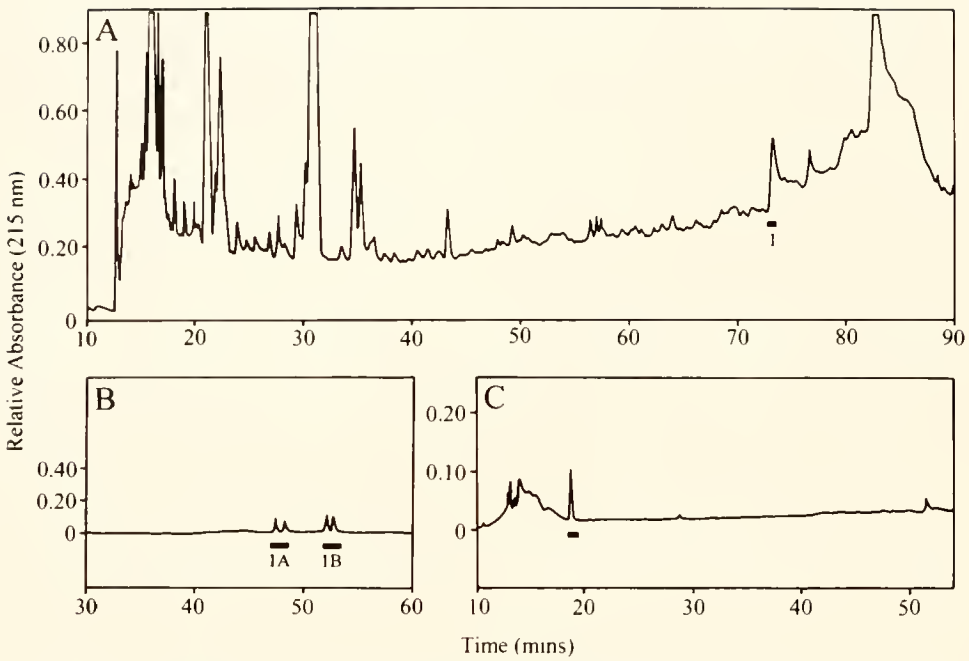

Figure 6. Representative fractionation of albumen gland extracts by RP-HPLC. (A) The extract was eluted with a linear gradient of 0.1% HFBA and acetonitrile containing 0.1% HFBA. The peak fraction 1 was pooled based on absorbance at 215 nm. (B) Fraction 1 (A) was reduced and alkylated with 4-vinylpyridine, and fractionated with a linear gradient of 0.1% TFA and acetonitrile containing 0.1% TFA. Peak fractions 1A and 1B were pooled based on absorbance and sequenced. (C) An aliquot of fraction 1 (A) was digested with Endo Glu-C and the resulting fragments fractionated with a linear gradient of 0.1% TFA and acetonitrile containing 0.1% TFA. The peak fraction indicated by the solid bar was sequenced and corresponded to attractin residues 48–58.

Results. As shown in Figure 7, MALDI-TOF MS of attractin detected singly and doubly charged components. Examining the singly charged group, inset 7A shows three major peaks at m/z 8059, 8075, and 8091. To investigate these three peaks, additional mass spectra were acquired from attractin that had been in solution at room temperature for over 3 h. This produced a similar mass spectra with differences in intensities of the three major peaks (shown in inset 7B). Several satellite peaks are observed spaced 162.1 ± 0.3 apart. Furthermore, mass spectra acquired from reduced and alkylated attractin (data not shown) contained one major peak at m/z 8696, along with two series of small peaks spaced 162.1 ± 2.3.

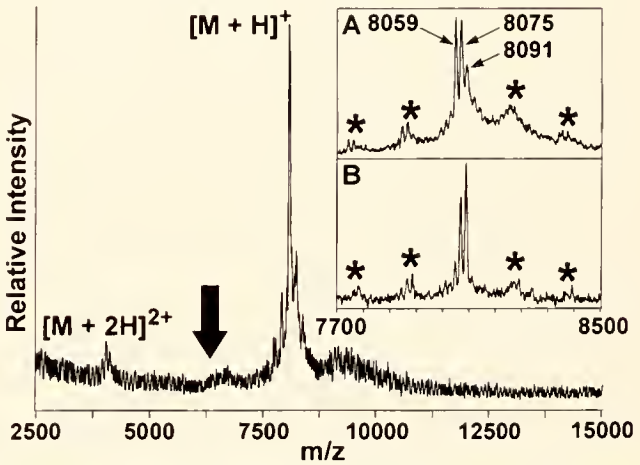

Figure 7. MALDI-TOF mass spectrometry reveals that full-length attractin is glycosylated. Mass spectra contain singly and doubly charged peaks corresponding to M_r 8059 Da for the major form. The satellite peaks (indicated by asterisks in the insets) are spaced by single hexose units. The spectrum in inset A was obtained from a freshly prepared solution, whereas the attractin in inset B had been in solution for over 3 h. Peak intensities at m/z 8075 (attractin + 16) and 8091 (attractin + 32) vary over time, confirming the presence of two readily oxidized Met residues.

T-maze bioassay

Procedures. To verify that attractin is an attractive component of fractions C1–C4 of the egg-cordon eluate, the full-length peptide was purified from the albumen gland as described above, aliquoted into 10-pmol samples, and bioassayed in the T-maze.

Results. The results are summarized in Figure 8. In the negative control (nonlaying conspecific with nothing placed in the adjacent ASW), three animals (20%) trav-

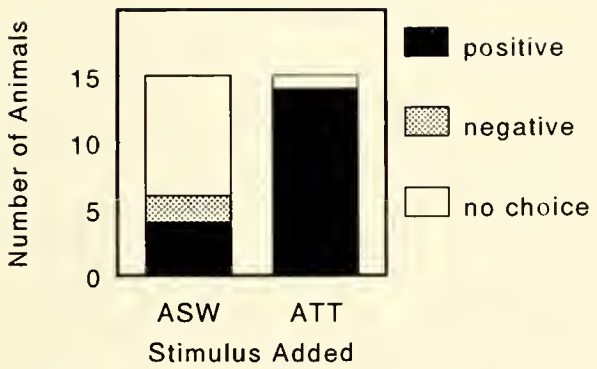

Figure 8. Attractin is a water-borne pheromonal attractant. The number of *Aplysia brasiliana* attracted to a nonlaying conspecific (ASW) was increased when full-length attractin (10 pmol) was placed in the adjacent seawater; fewer animals went to the opposite arm and fewer failed to make a choice. This bar graph is based on 30 single-arm experiments, 15 per stimulus. In each experiment, animals chose between a stimulus in one arm and no stimulus in the other. The change in response pattern is statistically significant ($\chi^2(2) = 8.04$; $0.01 < P < 0.025$).

eled to the right arm and remained, three (20%) traveled to the left arm and remained, and nine (60%) did neither. Of the six animals making a choice, only four went to the stimulus animal, two of which were in the right arm and two of which were in the left arm of the maze. These bioassays verify that there is no directional bias in the maze and establish chance levels of attraction at 4 animals.

The response pattern changed when 10 pmol of attractin was placed in the seawater adjacent to the stimulus animal (Fig. 5): 14 of 15 animals (93.3%) were attracted to the stimulus, and one (6.7%) failed to make a choice. The change was statistically significant [$\chi^2(2) = 8.04$, $0.01 < P < 0.025$]. Attractin also induced behaviors related to male approach and mating: four test animals attempted to enter the stimulus cage, one of which succeeded and mated as a male; three put their oral veil through holes in the cage; four (not including the one mating as a male) made physical contact with the stimulus animal and interacted with it. The mating animals reversed roles after about 20 min, as they normally would (Leonard and Lukowiak, 1987).

Discussion

We have isolated a water-borne pheromonal attractant for *Aplysia* from eluates of recently deposited egg cordons, and have obtained a partial 46 amino acid sequence. Degenerate oligonucleotide primers corresponding to the NH_2- and COOH-terminal regions of this peptide were used to generate an albumen gland RT-PCR product encoding the 46-residue sequence. The corresponding cDNA was isolated from an albumen gland cDNA library and the entire 76 amino acid precursor sequence predicted, including the 58-residue peptide "attractin" (Fan *et al.*, 1997).

Attractin cDNA was expressed in the baculovirus system and in lysates fractionated by C18 RP-HPLC to determine the retention time of the full-length recombinant peptide (data not shown). This information was used to identify the attractin peak in extracts of the albumen gland and to verify that the full-length peptide was not present in the egg-cordon eluates. Northern analyses showed that the albumen gland was the only source of attractin in the female reproductive tract (Fan *et al.*, 1997), suggesting that extracellular degradation occurred.

The peak that coeluted with recombinant attractin was repurified by RP-HPLC using a different counterion and bioassayed in the T-maze. Like C1, the repurified peptide attracted a larger number of animals to the nonlaying conspecific (14 rather than 4) and produced a variety of behaviors that might have resulted in male behavior if the animals had had more access to each other. The change in response pattern was statistically significant, verifying that the peptide is attractive. The amount of peptide tested (10 pmol in 6 l) is consistent with pheromonal activity and is about the same as was tested for fraction C1 (estimate based on peak area). We are currently examining the potential effect of attractin on male mating behavior.

The isolated peptide was 58 amino acids in length, and the sequence matched that predicted from the albumen gland cDNA (Fan *et al.*, 1997). It contained a potential *N*-linked glycosylation site (Asn^8) and six cysteine residues, characteristics which could contribute to the hydrophilicity and stability of the peptide. It had less than 18% sequence identity with other sequences in the Non-Redundant Genbank CDS Database, demonstrating that it is a novel peptide.

To confirm glycosylation, we characterized the peptide by MALDI-TOF MS. No ions were detected at m/z 6351 (black arrow in Fig. 7); this is the protonated M_r corresponding to the full 58-residue peptide. Instead, we observed that attractin is indeed a glycopeptide having a major form with M_r 8058 Da, an increase of 1708 Da from the predicted mass, yielding 21 wt. % carbohydrate. Mass spectra indicated the presence of not one, but a series of five peaks, separated by 162.1 Da, the M_r of a single hexose unit.

This distribution was not unexpected, as glycoforms generally exist as a set of variants exhibiting microheterogeneity with respect to the oligosaccharide composition. The branched $(mannose)_3(GlcNAc)_2$ core of *N*-linked oligosaccharides accounts for 893 Da, while the remaining 815 Da can be assigned to an additional five hexose units. Attractin with $(hexose)_5(mannose)_3(GlcNAc)_2$ attached is

within 0.06% of the observed mass, well within the mass calibration of the instrument.

The major peaks detected at m/z 8057 and 8091 are consistent with attractin containing one and two oxidized Met residues, respectively. Non-physiological oxidation of Met to Met-sulfoxide readily occurs during sample handling, and MALDI-TOF MS can be used to monitor this occurrence over time (Zhang and Capriololi, 1996). As shown in the insets of Figure 7, the intensity of the peaks corresponding to the presumed oxidized forms increases over time, consistent with oxidation. Moreover, because two oxidized forms are detected, the presence of two Met residues within attractin is confirmed.

Mass spectra were also obtained from a sample of full-length attractin that had been reduced and alkylated with 4-vinylpyridine. Again, one major component was present in addition to smaller peaks separated by ±hexose units. Because the mass change associated with the reduction and alkylation of Cys is 105 Da per residue, we confirm the presence of six Cys residues, with the calculated (8689 Da) and determined (8695 Da) M_r within 0.06%. The six Cys residues may form three intramolecular disulfide bonds, providing a compact conformation for the peptide and greater stability. Unfortunately, the mass resolution of the instrument is insufficient to confirm this structure. The question is still under investigation.

Assuming that intramolecular disulfide bonds are formed, the family of mating pheromones in the ciliate protozoan *Euplotes* may serve as a good model for *Aplysia* attractin. In the *Euplotes* family, the pheromones are slightly shorter than attractin (38–40 amino acids), but like attractin, each peptide has six cysteine residues. The cysteines form intramolecular disulfide bonds in the *Euplotes* pheromones, forming three stable loops that differ in both size and charge from one pheromone to another within the family. The differences are thought to confer mating-type specificity, whereas the conserved sequences contribute to the conserved structure and preserve function (Raffioni *et al.*, 1988, 1989, 1992).

To examine the possibility that a similar system exists within attractin, we are now isolating and characterizing attractin-related peptides from other *Aplysia* species and examining their behavioral effects. We are comparing the peptide from sets of species that have (1) overlapping ranges and are sometimes seen in (or associated with) the same aggregations; (2) overlapping ranges and are not known to associate with the same aggregations; and (3) ranges that do not overlap. We have isolated an attractin-related peptide from the *A. brasiliana* albumen gland and have obtained a partial 50-residue N-terminal sequence; it is identical to the *A. californica* sequence at 48 positions. This peptide probably serves a pheromonal function in *A. brasiliana* and accounts, at least in part, for the observed attraction in the T-maze.

Acknowledgments

We wish to thank Mr. Steve Smith for performing compositional and microsequence analyses, and Dr. Richard Fritz for conducting the BIONET searches. This work was supported by NIH grants HD28500 (S.D.P.) and NS31609 (J.V.S.), NSF Grant IBN-9511773 (G.T.N.), UTMB Small Grant 454620 (S.D.P.), and Sealy Center for Structural Biology Grant (G.T.N.). The Florence and Marie Hall Endowment for Excellence in the Biomedical Sciences provided support for the computer facilities used in these studies.

Literature Cited

Achituv, Y., and A. Susswein. 1985. Habitat selection by two Mediterranean species of *Aplysia: A. fascilata* Poiret and *A. depilans* Gmelin (Mollusca: Opisthobranchia). *J. Exp. Mar. Biol. Ecol.* **85:** 113–122.

Arch, S., T. Smock, R. Gurvis, and C. McCarthy. 1978. Atrial gland induction of the egg-laying response in *Aplysia californica. J. Comp. Physiol.* **128:** 67–70.

Arch, S., J. Lupatkin, T. Smock, and M. Beard. 1980. Evidence for an exocrine function of the *Aplysia* atrial gland. *J. Comp. Physiol.* **151:** 131–137.

Aspey, W. P., and J. E. Blankenship. 1976. *Aplysia* behavioral biology: II. Induced burrowing in swimming *A. brasiliana* by burrowed conspecifics. *Behav. Biol.* **17:** 301–312.

Audesirk, T. E. 1977. Chemoreception in *Aplysia californica.* III. Evidence for pheromones influencing reproductive behavior. *Behav. Biol.* **20:** 235–243.

Audesirk, T. E. 1979. A field study of growth and reproduction in *Aplysia californica. Biol. Bull.* **157:** 407–421.

Beard, M., L. Millechia, C. Masuoka, and S. Arch. 1982. Ultrastructure of secretion in the atrial gland of a mollusc (*Aplysia*). *Tissue Cell* **14:** 297–308.

Begnoche, V. L., S. K. Moore, N. Blum, C. vanGils, and E. Mayeri. 1996. Egg masses are a sign stimulus for release of bag cell peptides and reproductive behavior in *Aplysia. J. Neurophysiol.* **75:** 2162–2166.

Blankenship, J. E., M. K. Rock, L. C. Robbins, C. A. Livingston, and H. K. Lehman. 1983. Aspects of copulatory behavior and peptide control of egg laying in *Aplysia. Fed. Proc.* **42:** 96–100.

Coggeshall, R. E. 1972. The structure of the accessory genital mass in *Aplysia californica. Tissue Cell* **4:** 105–127.

Dudek, F. E., J. S. Cobbs, and H. M. Pinsker. 1979. Bag cell electrical activity underlying spontaneous egg laying in freely behaving *Aplysia brasiliana. J. Neurophysiol.* **42:** 804–817.

Fan, X., B. Wu, G. T. Nagle, and S. D. Painter. 1997. Molecular cloning of a cDNA encoding a potential water-borne pheromonal attractant released during *Aplysia* egg laying. *Mol. Brain Res.* **48:** 167–170.

Harmon, B. J., X. Gu, and D. I. C. Wang. 1996. Rapid monitoring of site-specific glycosylation microheterogeneity of recombinant human interferon-γ. *Anal. Biochem.* **68:** 1465–1473.

Jahan-Parwar, B. 1976. Aggregation pheromone from the egg-mass of *Aplysia. The Physiologist* **19:** 240.

Kamiya, Y., A. Sakurai, S. Tamura, N. Takahashi, K. Abe, E. Tsuchiya, S. Fukui, C. Kitada, and M. Fujino. 1978. Structure of rhodotorucine A, a novel lipopeptide, inducing mating tube formation in *Rhodosporium toruloides. Biochem. Biophys. Res. Commun.* **83:** 1077–1083.

Kikuyama, S., F. Toyoda, Y. Ohmiya, K. Matsuda, S. Tanaka, and

H. Hayashi. 1995. Sodefrin: a female-attracting peptide pheromone in newt cloacal glands. *Science* **267:** 1643–1645.

Kupfermann, I., and T. Carew. 1974. Behavior patterns of *Aplysia californica* in its natural environment. *Behav. Biol.* **12:** 317–337.

Leonard, J. L., and K. Lukowiak. 1987. The behavior of *Aplysia californica* Cooper (Gastropoda: Opisthobranchia). *Behavior* **98:** 320–360.

Nagle, G. T., S. D. Painter, J. E. Blankenship, J. D. Dixon, and A. Kurosky. 1986. Evidence for the expression of three genes encoding homologous atrial gland peptides that cause egg laying in *Aplysia*. *J. Biol. Chem.* **261:** 7853–7859.

Painter, S. D. 1992. Coordination of reproductive activity in *Aplysia:* peptide neurohormones, neurotransmitters, and pheromones encoded by the egg-laying hormone family of genes. *Biol. Bull.* **183:** 165–172.

Painter, S. D. 1993. Peptide pheromones and hormones that regulate reproductive behavior in *Aplysia.* Pp 337–349 in *Short Communications of the 1991 International Marine Biotechnology Conference, Vol. 1.*

Painter, S. D., V. K. Kalman, G. T. Nagle, R. A. Zuckerman, and J. E. Blankenship. 1985. The anatomy and functional morphology of the large hermaphroditic duct of three species of *Aplysia,* with special reference to the atrial gland. *J. Morphol.* **186:** 167–194.

Painter, S. D., A. R. Gustavson, V. K. Kalman, G. T. Nagle, and J. E. Blankenship. 1989. Induction of copulatory behavior in *Aplysia:* Atrial gland factors mimic the excitatory effects of recently deposited egg cordons. *Behav. Neural Biol.* **51:** 222–236.

Painter, S. D., M. G. Chong, M. A. Wong, A. Gray, J. Cormier, and G. T. Nagle. 1991. Relative contributions of the egg layer and egg cordon to pheromonal attraction and the induction of mating and egg-laying activity in *Aplysia*. *Biol. Bull.* **181:** 81–94.

Pinsker, H. M., and D. W. Parsons. 1985. Temperature dependence of egg laying in *Aplysia*. *J. Comp. Physiol. B* **56:** 21–27.

Raffioni, S., P. Luporini, B. T. Chait, S. S. Disper, and R. A. Bradshaw. 1988. Primary structure of the mating pheromone *Er-1* of the ciliate *Euplotes raikovi*. *J. Biol. Chem.* **263:** 18152–18159.

Raffioni, S., P. Luporini, and R. A. Bradshaw. 1989. Purification, characterization, and amino acid sequence of the mating pheromone *Er-10* of the ciliate *Euplotes raikovi*. *Biochemistry* **28:** 5250–5256.

Raffioni, S., C. Miceli, A. Vallesi, S. K. Chowdhury, B. T. Chait, P. Luporini, and R. A. Bradshaw. 1992. The primary structure of *E. raikovi* pheromones: a comparison of five sequences of pheromones of cells with variable mating interactions. *Proc. Natl. Acad. Sci. USA* **89:** 2071–2075.

Shimuzu, Y. 1985. Bioactive marine natural products, with emphasis on handling of water-soluble compounds. *J. Nat. Prod.* **42:** 223–235.

Stotzler, D., H. H. Kiltz, and W. Duntze. 1976. *Eur. J. Biochem.* **69:** 397–400.

Susswein, A. J., S. Gev, E. Feldman, and S. Markovitch. 1983. Activity patterns and time budgeting of *Aplysia fasciata* under field and laboratory conditions. *Behav. Neural Biol.* **39:** 203–220.

Susswein, A. J., S. Gev, Y. Achituv, and S. Markovitch. 1984. Behavioral patterns of *Aplysia fasciata* along the Mediterranean coast of Israel. *Behav. Neural Biol.* **41:** 7–22.

Zhang, H., and R. M. Capriololi. 1996. Oxidation of methionine-containing peptides under *in vitro* and *in vivo* conditions with analysis by MALDI MS. P. 1349 in *Proceedings of the 14th ASMS Conference on Mass Spectrometry and Allied Topics.*

Reference: *Biol. Bull.* **194:** 132–142. (April, 1998)

Role of Chemical Inducers in Larval Metamorphosis of Queen Conch, *Strombus gigas* Linnaeus: Relationship to Other Marine Invertebrate Systems

ANNE A. BOETTCHER* AND NANCY M. TARGETT

University of Delaware, Graduate College of Marine Studies, Lewes, Delaware 19958

Abstract. Chemical cues are important in the exogenous and endogenous control of metamorphosis in many marine invertebrate larvae. In the queen conch, *Strombus gigas* Linnaeus, larval metamorphosis is induced by low molecular weight compounds associated with dominant species of red algae found in conch nursery grounds; these species include the foliose rhodophyte *Laurencia poitei* (Lamouroux). The responses of conch larvae to the algal-associated cues are dependent on concentration and length of exposure, with the initial events of metamorphosis occurring within 10 min of treatment with an aqueous extract of *L. poitei*. The free amino acids valine and isoleucine mimic the effects of the natural inducer, and they may bind to and be recognized by the same sites on the larvae as the algal cues. Hydrogen peroxide, vanadate, and γ-aminobutyric acid (GABA), as well as elevated K^+ concentrations (*i.e.*, above ambient seawater levels), also induce larval metamorphosis. Acetylsalicylic acid decreases the responses of conch larvae to the algal-associated cues and to the free amino acids, but it has no effect on the induction triggered by hydrogen peroxide. The chemical induction of metamorphosis in conch larvae shares many general features with chemoreception in aquatic invertebrates. The natural inducers of metamorphosis, like the cues involved in olfactory responses in other marine organisms, are of low molecular weight and water soluble. In addition, the results of the experiments with hydrogen peroxide, vanadate, and GABA suggest that second messenger pathways are involved in conch metamorphosis.

Received 10 April 1996; accepted 23 December 1997.

* Current address: Neuroscience Research Institute, University of California, Santa Barbara, California 93106.

Introduction

Queen conch, *Strombus gigas*, are marine benthic gastropods found in seagrass beds and sand flats throughout the tropical Atlantic (Randall, 1964; Brownell and Stevely, 1981). As juveniles, conch occur primarily in seagrass beds of medium shoot density and in surrounding sandy areas where they feed on macrophytes and macrophyte epibionts (Ray and Davis, 1989; Stoner and Sandt, 1991; Stoner and Waite, 1991; Wickland *et al.*, 1991; Sandt and Stoner, 1993; Stoner and Ray, 1993; Ray and Stoner, 1994; Stoner *et al.*, 1994). The mechanisms by which conch larvae find their nursery grounds and metamorphose to juveniles are not well understood, but recent work has shown that a variety of chemical cues associated with nursery-ground substrates induce queen conch metamorphosis (Davis, 1994; Davis and Stoner, 1994; Boettcher and Targett, 1996; Stoner *et al.*, 1996). The most consistent and effective inducers are of low molecular weight (less than 1 kDa), stable, water soluble, and associated with the red algal species *Laurencia poitei* and *Fosliella* sp. (Boettcher and Targett, 1996). Crude aqueous extracts of the rhodophytes and a low molecular weight fraction (less than 1 kDa) of those extracts induce larval metamorphosis at levels comparable to those induced by the intact algae (Boettcher and Targett, 1996). These results suggest that chemical cues used by conch larvae during metamorphosis share many of the characteristics of those used by adult aquatic invertebrates. Marine invertebrates are sensitive to compounds of low molecular size, including the small peptides and amino acids that in adults serve as important cues in feeding, habitat selection, and mating, and in larvae as natural inducers of settlement and metamorphosis (Burke, 1984, 1986; Carr, 1988; Carr *et al.*, 1989; Tegtmeyer and Rittschof, 1989;

Morse, 1990; Rittschof, 1990; Morse, 1992; Leitz *et al.*, 1994; Zimmer-Faust and Tamburri, 1994).

The effects of chemical cues on metamorphosis are ideally studied with queen conch larvae. Moreover, several research facilities and one commercial facility (Caicos Conch Farm, Turks and Caicos, British West Indies) are currently involved in the culture of queen conch. By providing a better understanding of the biology of this species, detailed studies of metamorphosis in *S. gigas* could lead to improvements in the culture of this valuable mollusc (Heyman *et al.*, 1989; Boettcher *et al.*, 1997). In turn, the commercial culture of queen conch makes large numbers of larvae available for research.

In this study, the responses of *S. gigas* larvae to chemical cues were further characterized: the concentration dependency and the optimal exposure time to aqueous extracts of *L. poitei* were determined; the order of behavioral and gross morphological changes that occur in conch larvae during metamorphosis were described; and the effects of low molecular weight compounds (*e.g.*, amino acids, ions, and neuroactive compounds) on conch larvae metamorphosis were established. The results of these experiments are discussed in terms of models that have been developed to explain the transduction of cues involved in invertebrate larval metamorphosis (Burke, 1983; Baloun and Morse, 1984; Coon *et al.*, 1985; Baxter and Morse, 1987; Bonar *et al.*, 1990; Freeman and Ridgeway, 1990; Beiras and Widdows, 1995; Clare *et al.*, 1995).

Materials and Methods

Collection of algae and preparation of extracts

Specimens of *Laurencia poitei* were collected off Pine Cay, Turks and Caicos, British West Indies, and the crude aqueous extract was prepared as described in Davis (1994) and Boettcher and Targett (1996). Briefly, the alga was chopped into small pieces and ground in seawater (0.6 g alga/ml seawater) with a mortar and pestle. The sample was centrifuged at low speed in a table-top centrifuge for 10 min so that the algal pieces would pellet out of solution. The supernatant was decanted and used in all metamorphosis assays.

For amino acid analysis, the algal extract was prepared in distilled water and fractionated with a 400-ml Amicon (Amicon Division, W.R. Grace, Danvers, MA) stirred cell with 76-mm membranes. Amicon Diaflo ultrafiltration membranes (YM1) were used to separate the extract into nominal molecular sizes of less than and greater than 1 kDa (Boettcher and Targett, 1996). The fraction containing molecules smaller than 1 kDa was hydrolyzed in 6 *M* hydrochloric acid, phenol, and trifluoroacetic acid and analyzed with a single-column Beckman 6300 autoanalyzer (Tsugita *et al.*, 1987). Hereinafter, we refer to this as the < 1 kDa component of the algal extract.

Metamorphosis assay procedures

All metamorphosis assays were conducted at the Caicos Conch Farm, Providenciales, Turks and Caicos, British West Indies, according to the methods described in Boettcher and Targett (1996). Competent *Strombus gigas* larvae (19–24 days post-hatch) were provided by the Caicos Conch Farm. Techniques for their culture were as described in Davis (1994). Metamorphosis assays were run as static, no-choice experiments in 500-ml polyethylene vessels containing either 300 ml of seawater or seawater to which the appropriate treatment had been added. Seawater used in all experiments was sterilized with ultraviolet light and filtered (10 μm). Experiments were conducted at the ambient temperature (28°–29°C) and salinity (*ca.* 39 ppt), and under natural light conditions (*ca.* 12 h light: 12 h dark). The pH of the seawater was adjusted to between 8 and 8.5 with NaOH when necessary. For each assay, five replicates per treatment were used with either 15 or 25 larvae per replicate, depending on the experiment. Unless otherwise noted, the exposure time for all treatments was 5 h, after which the larvae were transferred to a fresh volume of seawater. Percent metamorphosis was determined after 24 h, and was calculated as 100 $\times$ (total number of larvae metamorphosed/total number recovered) (Pearce and Scheibling, 1990). A larva was considered to have undergone metamorphosis when it lost its velar lobes and began to use its foot to crawl (Davis, 1994). Each assay included a positive control (an aqueous extract of *L. poitei* [0.01 g wet weight/ml seawater = 20 μl extract/ml seawater]) as a measure of larval competency and a negative control (seawater only) as a test for spontaneous metamorphosis.

Mean percentages of metamorphosis among or between treatments in each experiment were compared with either a Model I ANOVA and Tukey's multiple comparison test or Student's *t* test ($\alpha = 0.05$). Plots of residuals were examined to assure that the underlying assumptions of these tests were met. Treatments in which percent metamorphosis was equal to zero for all replicates were not included in the statistical analyses.

Metamorphosis assays with algal extracts

The effects of concentration and duration of treatment on the metamorphogenic actions of crude aqueous extracts of *L. poitei* were tested according to procedures described above. In the first experiment, larvae were treated for 5 h with 11 dilutions of the *L. poitei* extract, ranging from 0.8 to 67 μl extract/ml seawater. In the second experiment, the larvae were exposed to 20 μl extract/ml seawater for 0.5, 1, 2, 3, and 5 h. As in all experiments, percentages of metamorphosis were determined after 24 h.

In an additional experiment, behavioral and morpho-

logical changes occurring in the larvae in response to the algal extract were monitored. Larvae treated with 20 μl extract/ml seawater were monitored with a compound microscope every 20 min, from time (t) = 0 to t = 3 h.

Metamorphosis assays with free amino acids

The effects of 11 free amino acids, all L-isomers (valine, leucine, isoleucine, cysteine, glycine, serine, threonine, lysine, arginine, histidine, and glutamic acid), were tested in assays of larval metamorphosis. Two criteria were used in choosing the amino acids to be tested: amino acids with basic, acidic, and neutral side chains were included, and all, except cysteine, were present in hydrolyzed samples of the less than 1 kDa component of the algal extract. Concentrations of amino acids tested ranged from 1 μ*M* to 10 m*M*. The free amino acid isoleucine (10 μ*M*) was also presented in combination with serine, histidine, and lysine (each at 10 μ*M*), and in combination with valine (each at 50 μ*M*).

Metamorphosis assays with acetylsalicylic acid

The effects of acetylsalicylic acid (aspirin, 0.1–5 m*M*), were examined alone and in combination with the algal extract (20 μl extract/ml seawater); treatments also included acetylsalicylic acid (1 m*M*) in combination with isoleucine and valine (each at 100 μ*M*). The effect of salicylic acid (1 m*M*) on the induction of metamorphosis by the algal extract was also tested. The responses of the larvae to *N*-acetyl-L-valine and to valine (both at 100 μ*M*) were compared. In an additional experiment, conch larvae were first treated with acetylsalicylic acid (1 m*M*) in combination with isoleucine (100 μ*M*), valine (100 μ*M*), or the extract, then rinsed in filtered seawater, and finally retreated for 5 h with isoleucine, valine, or extract. As a further examination of the effects of acetylsalicylic acid, the acetylsalicylic acid treatment was combined with exposure to 3-isobutyl-1-methyl xanthine (IBMX). The specific treatments in this experiment were IBMX (0.1 m*M*) or extract alone; IBMX plus acetylsalicylic acid (1 m*M*); acetylsalicylic acid plus extract; a combination of IBMX, acetylsalicylic acid, and the algal extract; and acetylsalicylic acid alone.

Metamorphosis assays with ion manipulations and neuroactive compounds

The effects on metamorphosis of elevated ion concentrations and of neuroactive compounds were examined in a series of experiments. The concentrations used were based on tests with other marine invertebrates (Baloun and Morse, 1984; Yool *et al.*, 1986; Davis *et al.*, 1990; Pires and Hadfield, 1991; Ilan *et al.*, 1993; Beiras and Widdows, 1995). Elevated concentrations of K^+, Ca^{2+}, Na^+, and Mg^{2+} (respectively 20 m*M*, 60 m*M*, 60 m*M*, and 60 m*M* above ambient seawater levels) were tested individually for their ability to induce metamorphosis. Two additional experiments focused on the concentration dependence of the response to increased K^+ concentrations (5–30 m*M*).

The responses of the larvae to the neuroactive compounds 3,4-dihydroxyphenylalanine (DOPA, 1–100 μ*M*), epinephrine (EP, 1 μ*M*), γ-aminobutyric acid (GABA, 0.1–20 m*M*), and hydrogen peroxide (50 and 100 μ*M*) were then examined. In addition, we tested the effects of compounds known to block the larval metamorphosis of other marine invertebrates (4 acetamino-4′isothiostilbene-2,2′disulfonic acid [SITS, 10 and 50 μ*M*] and tetraethylammonium chloride [TEA, 100 and 500 μ*M*]) for their effect on metamorphosis induced by algal extract (20 μl extract/ml seawater), hydrogen peroxide (50 μ*M*), and elevated K^+ concentrations (20 m*M*). SITS is an inhibitor of anion transport, and TEA is a K^+ channel blocker.

The larval responses to hydrogen peroxide (50 μ*M*) and to sodium orthovanadate (1 and 2 m*M*) were also compared. The effects of bovine catalase (5 μg/ml seawater) and acetylsalicylic acid (1 m*M*) on metamorphosis induced by hydrogen peroxide were compared with their effects on metamorphosis induced by the algal extract (20 μl extract/ml seawater).

Results

Metamorphosis assays with algal extracts

The concentration-function relationship of the response of conch larvae to the extract appeared to be hyberbolic (Fig. 1). Concentrations of algal extract lower than 5 μl/ml seawater had no significant effect on conch metamorphosis (Fig. 1). At levels greater than 13 μl/ml seawater, metamorphosis reached a plateau at about 85%. Concentrations of five μl extract/ml seawater and 6.7 μl/ml seawater induced increasing levels of conch metamorphosis (10% ± 6.0% and 37% ± 12% respectively). These two responses were significantly different from one another and from all higher ones.

The response to algal extract (20 μl/ml seawater) increased with duration of exposure (Fig. 2). The responses to the longest exposures, 3 h (76% ± 14%) and 5 h (91% ± 10%), were not significantly different. Thus, the exposure required to produce the maximal response is between 3 and 5 h.

Within 10 min of exposure to 20 μl extract/ml seawater, the velar cilia were arrested, and the conch larvae sank to the bottom of the experimental containers. Although the edges of the velar lobes started to curl, the lobes remained expanded and the cilia resumed beating

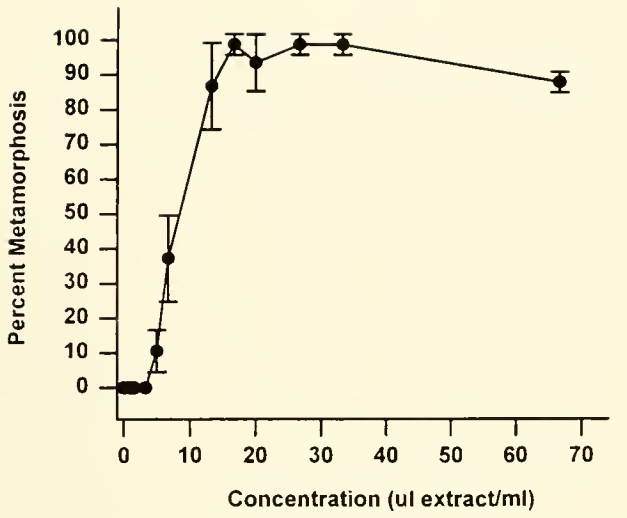

Figure 1. Percent metamorphosis of queen conch larvae in response to specific concentrations of *Laurencia poitei* extract. Points are means ± SD; $n = 5$.

after the larvae contacted the bottom. After 30 min, all larvae were on the bottom and their lobes showed increased curling; after 90 min, individual cilia and portions of the velar lobes began to drop off. Cilia on the isolated lobes continued to beat for at least 10 min. At 110 min, some of the larvae had completed metamorphosis. At this time, many still retained remnants of their velar lobes, but they had begun using the foot to crawl on the bottom of the containers. By 2 h, more than 50% of the larvae had undergone complete metamorphosis.

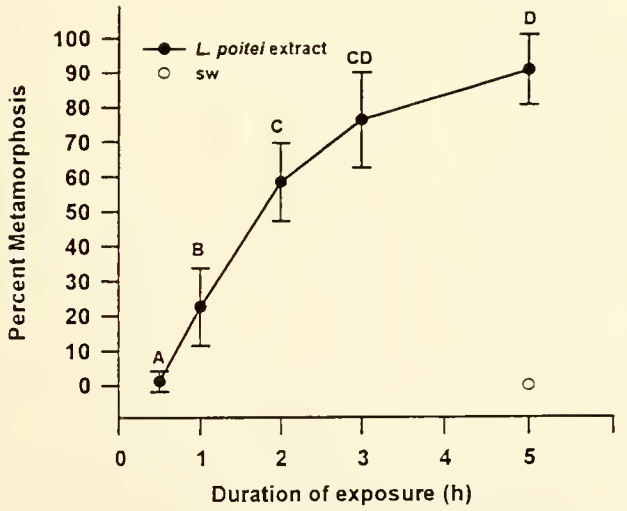

Figure 2. Percent metamorphosis of queen conch larvae in response to seawater only (sw, a negative control) for 5 h and an extract of *Laurencia poitei* (20 μl extract/ml seawater) for 0.5, 1, 2, 3, and 5 h. Points are means ± SD; $n = 5$. Data points with the same letter above the error bar are not significantly different at $P \leq 0.05$.

Amino acid composition of the algal extract

Of the 17 amino acids detected in the hydrolyzed <1 kDa component of the algal extract, the principal ones were glutamine/glutamate, glycine, alanine, and asparagine/aspartate (Table I).

Metamorphosis assays with amino acids

Of the 11 amino acids tested, only five (serine, histidine, leucine, isoleucine, and valine) induced significant levels of metamorphosis, and only two (isoleucine and valine) induced normal metamorphosis that was accompanied by normal behavior, as described above (Table II). Moreover, valine and isoleucine were present in the hydrolyzed extract at 6.6 and 4.2 μM respectively (Table I).

At 50 μM and 100 μM, the levels of metamorphosis induced by isoleucine and valine were not significantly different from those induced by the algal extract, although at the lower concentration the response to isoleucine was significantly lower than that to valine. Isoleucine at 1 mM and 10 mM, the two highest concentrations tested, was again equipotent with the extract and showed no abnormal effects. At 10 μM, isoleucine induced a high level of metamorphosis in one experiment (64% ± 18%), but a low level in a repeat of this experiment (14% ± 18%); and at the lowest concentration isoleucine had no effect (Table II), so the threshold is probably between 1 and 10 μM.

Serine, histidine, and leucine also induced significant

Table I

Concentration of amino acids detected in the hydrolyzed less than 1 kDa fraction of an aqueous Laurencia poitei *extract*

Compound	Concentration (μM)
Glutamine/Glutamate	46
Glycine	33
Alanine	19
Asparagine/Aspartate	18
Serine	14
Threonine	12
Homoserine	8.2
Valine	6.6
4-Hydroxyproline	6.2
Histidine	5.4
Leucine	4.4
Isoleucine	4.2
Hydroxylysine	3.6
Lysine	3.6
Arginine	3.0
Phenylalanine	2.8
Methionine	1.4

Only amino acids detected at concentrations greater than 1 μM are listed.

Table II

Mean percent metamorphosis of Strombus gigas *larvae treated with specific concentrations of amino acids or an aqueous* Laurencia poitei *extract (20 μl/ml seawater)*

Concentration (μM)	Serine	Histidine	Leucine	Isoleucine	Valine	Extract
10,000	85 ± 9.9A*	dead	na	93 ± 6.5A	na	87 ± 4.7A
1,000	69 ± 14A	dead	na	86 ± 9.4A	na	65 ± 25A
100	0	88 ± 9.9A*,†	na	77 ± 5.8A	na	76 ± 9.2A
100	na	na	dead	61 ± 11A	68 ± 16A	82 ± 8.0A
100	na	na	na	64 ± 8.1A	85 ± 5.9B	84 ± 14AB
100	na	na	na	73 ± 13A	73 ± 6.7A	87 ± 9.4A
50	na	na	na	23 ± 11A	53 ± 10B	33 ± 19AB
10	0	4.0 ± 6.0A	na	14 ± 18A	na	96 ± 8.9B
10	na	na	68 ± 15A*	na	na	84 ± 8.9B
10	na	na	na	64 ± 18A	na	92 ± 5.6A
1	0	0	na	0	na	96 ± 8.9

Data presented as mean ± SD, $n = 5$; na indicates that the compound was not applied. Treatment results with the same letter adjacent to the mean are not significantly different at $P \leq 0.05$; each row represents a separate experiment. Unless otherwise indicated the metamorphosis responses were normal.

* Abnormal behavior (slow moving, not using foot to crawl).

† Many dead.

levels of metamorphosis, but the behavior of the larvae in response to these amino acids did not parallel that seen in response to the natural cue (Table II). The larvae tended to be slower moving and did not attach or begin crawling on the bottom as rapidly as with the algal inducer, isoleucine, or valine, if at all. Glutamic acid, arginine, threonine, and cysteine did not induce significant levels of metamorphosis at any of the concentrations tested. At 100 μM, cysteine was toxic to the larvae. Glycine induced low levels of metamorphosis (20%–30%) at concentrations between 100 μM and 1 m*M*. Lysine also induced low levels of metamorphosis at 1 m*M* (38% ± 13%), but was toxic at concentrations greater than 1 m*M*.

The responses of the larvae to isoleucine (10 μM) in combination with serine (10 μM, 50% ± 25%) or histidine (10 μM, 58% ± 20%) were not significantly different than the response of the larvae to isoleucine alone (64% ± 18%). Isoleucine (10 μM) in combination with lysine (10 μM) was toxic; all larvae in this treatment appeared to undergo metamorphosis and then die. The response to a combination of isoleucine and valine (each at 50 μM, 27% ± 4.2%) was significantly lower than the response to valine alone (55% ± 7.3%), but not significantly different than the response to isoleucine alone (23% ± 11%).

Metamorphosis assays with acetylsalicylic acid

The response of the larvae to the algal extract was significantly decreased by 1 m*M* acetylsalicylic acid (Fig. 3). Acetylsalicylic acid concentrations of 0.1 m*M* and 0.5 m*M* had no effect either alone or in combination with the extract, and at 5 m*M* it was toxic alone or in combination with the extract. Acetylsalicylic acid at 1 m*M* also significantly decreased the responses to isoleucine and valine (Fig. 4). Salicylic acid, unlike acetylsalicylic acid, had no effect on the larval response to *L. poitei* extract (Fig. 5). As discussed above, valine induced significant levels of conch larval metamorphosis, but *N*-acetyl-L-valine had no effect on larval metamorphosis (Fig. 6). Treat-

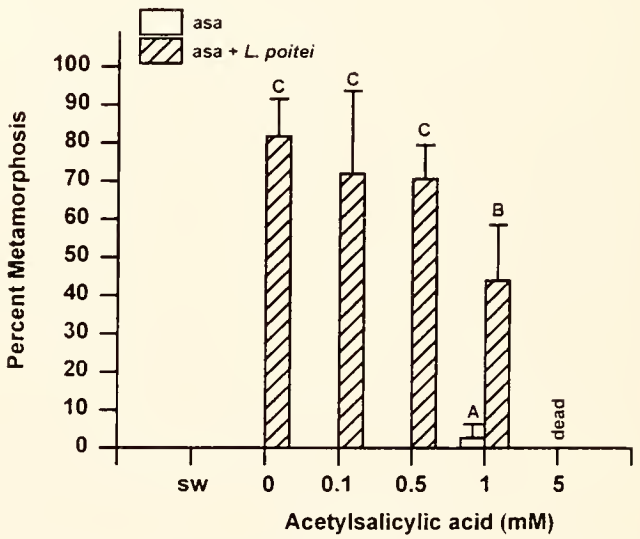

Figure 3. Percent metamorphosis of queen conch larvae in response to seawater only (sw, a negative control), acetylsalicylic acid (asa, 0–5 m*M*) alone, and to asa in combination with an extract of *Laurencia poitei* (20 μl extract/ml seawater). Points are means ± SD; $n = 5$. Data points with the same letter above the error bar are not significantly different at $P \leq 0.05$. Dead indicates all larvae in these treatments were dead at $t = 24$ h.

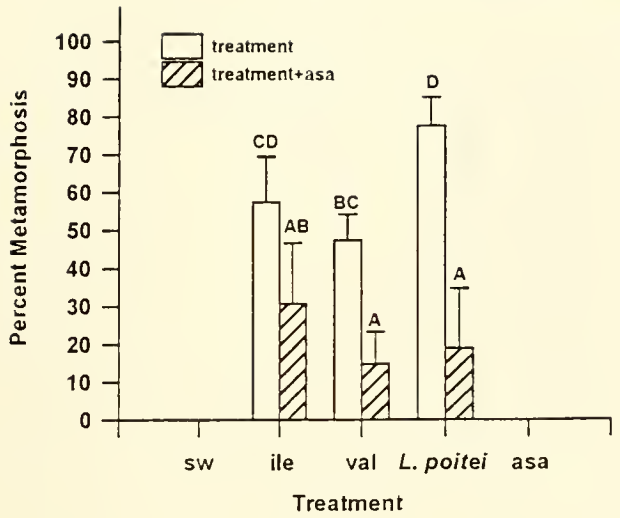

Figure 4. Percent metamorphosis of queen conch larvae in response to seawater only (sw, a negative control), isoleucine (ile, 100 μM), valine (val, 100 μM), and an extract of *Laurencia poitei* (20 μl extract/ml seawater) alone, and in combination with acetylsalicylic acid (asa, 1 mM). Asa (1 mM) alone is also shown. Points are means ± SD; n = 5. Data points with the same letter above the error bar are not significantly different at $P \leq 0.05$.

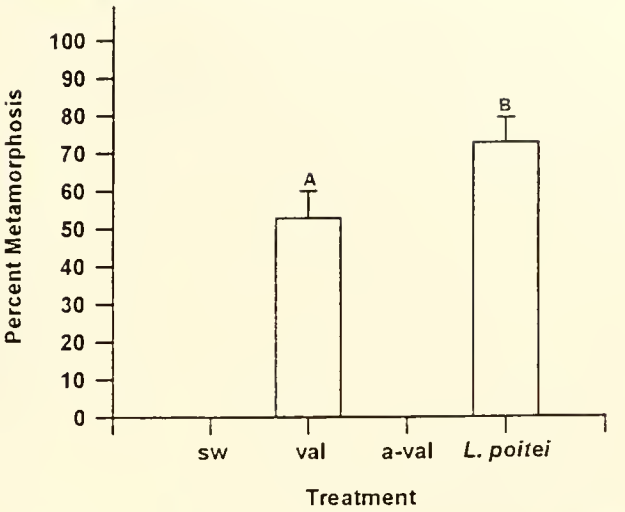

Figure 6. Percent metamorphosis of queen conch larvae in response to seawater only (sw, a negative control), valine (val, 100 μM), *N*-acetyl-L-valine (a-val, 100 μM), and an extract of *Laurencia poitei* (20 μl extract/ml seawater). Points are means ± SD; n = 5. Data points with the same letter above the error bar are not significantly different at $P \leq 0.05$.

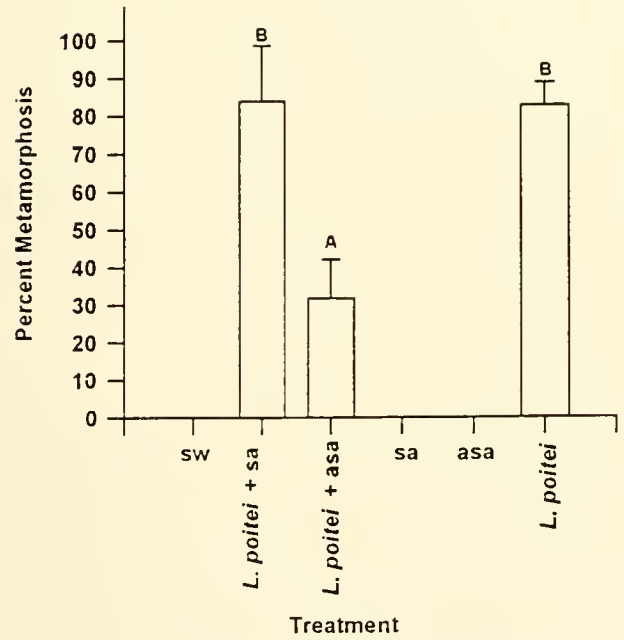

Figure 5. Percent metamorphosis of queen conch larvae in response to seawater only (sw, a negative control), an extract of *Laurencia poitei* (20 μl extract/ml seawater) in combination with salicylic acid (sa, 1 mM) or acetylsalicylic acid (asa, 1 mM). Sa, asa, and *L. poitei* extract presented alone are also shown. Points are means ± SD; n = 5. Data points with the same letter above the error bar are not significantly different at $P \leq 0.05$.

ment of larvae with isoleucine, valine, or algal extract plus acetylsalicylic acid, followed by reexposure to the appropriate cue in the absence of acetylsalicylic acid, induced levels of metamorphosis equal to or greater than those induced by treatment with the cues only. Moreover, the levels of metamorphosis induced by reexposure were significantly higher than those induced by the same cues in combination with acetylsalicylic acid and without retreatment (Fig. 7). In this experiment, the response to isoleucine alone was anomalously low.

IBMX had no effect when presented by itself or in combination with acetylsalicylic acid, but it reduced the effects of acetylsalicylic acid on the metamorphosis induced by the algal extract (Fig. 8). The response to the algal extract plus acetylsalicylic acid (26% ± 12%) was significantly lower than the response to extract alone (88% ± 9.1%). In the presence of IBMX, however, the response to extract plus acetylsalicylic acid (72% ± 7.4%) was not significantly lower than that to the extract alone. Fewer larvae were attached and crawling in the IBMX combination treatment than in the treatment with only algal extract.

Metamorphosis assays with ions and neuroactive compounds

Elevations of Ca^{2+}, Na^{+}, and Mg^{2+} concentrations (60 mM) over ambient seawater levels had no significant effect on metamorphosis. An increase in the concentration of K^{+} to 20 mM over ambient, however, induced signifi-

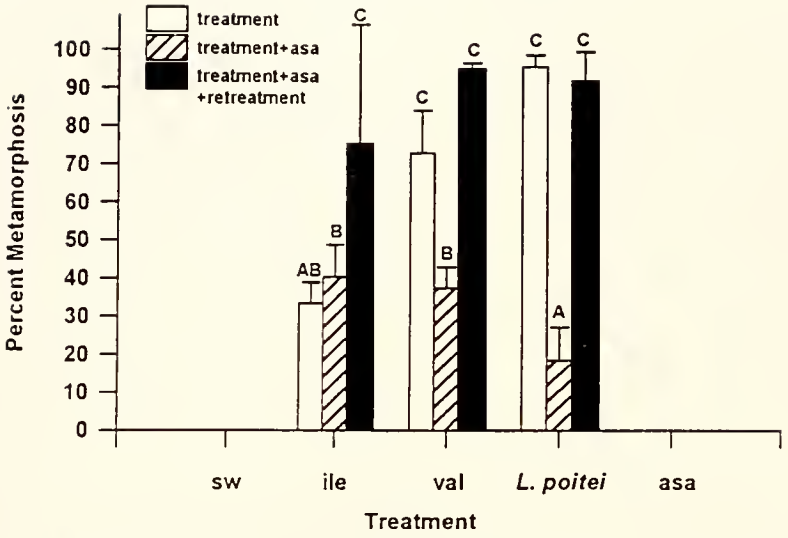

Figure 7. Mean percent metamorphosis of queen conch larvae in response to seawater only (sw, a negative control), isoleucine (ile, 100 μM), valine (val, 100 μM), and an extract of *Laurencia poitei* (20 μl extract/ml seawater) alone, and in combination with acetylsalicylic acid (asa, 1 mM) with and without reexposure to the appropriate cue. Asa (1 mM) alone is also shown. In this experiment, the response to isoleucine is anomalously low. Points are means ± SD; $n = 5$. Data points with the same letter above the error bar are not significantly different at $P \leq 0.05$.

cant levels of metamorphosis, although, as with other cues, the percentage varied among batches of larvae (Boettcher and Targett, 1996). Elevations in K^+ concentrations between 20 and 22 mM over ambient induced levels of metamorphosis equivalent to those induced by the algal extract. Concentrations ≤17 mM or ≥24 mM over ambient induced significantly lower levels of metamorphosis, and concentrations lower than 10 mM over ambient had no effect on metamorphosis.

DOPA and EP at 1 μM had no effect on metamorphosis. However, at 10 μM, DOPA induced significant levels of metamorphosis (87% ± 14%), and at 100 μM it had toxic effects. GABA induced significant levels of metamorphosis, but only at concentrations ≥ 5 mM (Fig. 9). The levels induced by GABA approached, but never were equal to, those induced by the algal extract. As reported previously, GABA at 1 and 100 μM had no significant effect on larval metamorphosis (Boettcher and Targett, 1996). Hydrogen peroxide at 50 and 100 μM induced levels of metamorphosis (54% ± 16% and 96% ± 4.0% respectively) equal to or greater than those induced by the algal extract (61% ± 5.6% and 93% ± 12%).

TEA at 100 and 500 μM had no significant effect on induction of metamorphosis caused by elevated K^+ concentrations (20 mM), hydrogen peroxide (50 μM), or the extract (20 μl extract/ml seawater), and no significant effect when presented alone (Fig. 10). SITS at 10 μM also had no effect on the above inducers; but at 50 μM, it significantly decreased the response to hydrogen peroxide and to elevated K^+ concentrations. SITS had no effect when presented alone (Fig. 10).

Vanadate (1 mM) induced levels of metamorphosis (53% ± 8.3%) equal to those induced by hydrogen peroxide (32% ± 33%) and *L. poitei* extract (56% ± 20%); but at 2 mM it was toxic to the larvae. Unlike its effects on the induction of metamorphosis by the algal extract, isoleucine, and valine, acetylsalicylic acid had no significant effect on the response of the larvae to hydrogen peroxide. Bovine catalase, however, totally blocked the larval response to hydrogen peroxide, while having no effect on the response to the extract.

Discussion

The natural inducer of larval metamorphosis in queen conch is a water-soluble cue associated with species of red algae, including *L. poitei*, commonly found in conch nursery grounds (Davis and Stoner, 1994; Boettcher and Targett, 1996). Larval responses to this cue are dependent on both concentration and exposure time, with the initiation of metamorphosis occurring within 10 min of treatment. The free amino acids isoleucine and valine, elevations in external concentrations of K^+, the neurotransmitters DOPA and GABA, as well as hydrogen peroxide and vanadate also induce larval metamorphosis.

Isoleucine and valine induce behavioral and morphogenic responses that mimic the effects of the natural inducer of conch metamorphosis. Valine and isoleucine are

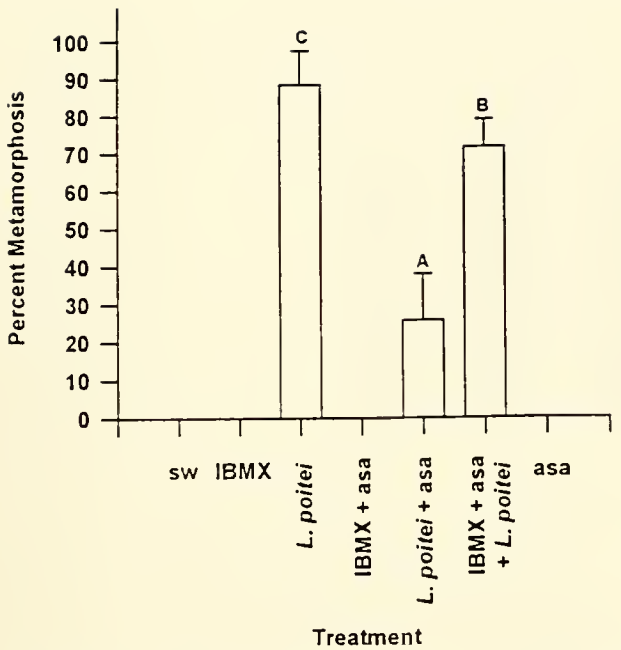

Figure 8. Percent metamorphosis of queen conch larvae in response to seawater only (sw, a negative control), isobutyl methyl xanthine (IBMX, 0.1 m*M*) and an extract of Laurencia poitei (20 μl extract/ml seawater) alone, in combination with acetylsalicylic acid (asa, 1 m*M*), and in combination with one another and asa (1 m*M*). Asa (1 m*M*) alone is also shown. Points are means ± SD; $n = 5$. Data points with the same letter above the error bar are not significantly different at $P \leq 0.05$.

similar in that they have neutral, hydrophobic, branched side chains that differ only in the length of one of the branches (Fig. 11). In leucine, the methyl group is displaced, and though this amino acid induces significant levels of metamorphosis, it does not induce normal larval behavior, and it is toxic at concentrations ≥ 100 μM. Several other amino acids also induce partial metamorphosis, but not normal larval behavior (Table II). Glutamic acid, glycine, and threonine, although found at higher concentrations than valine, isoleucine, or leucine in the <1 kDa component of hydrolyzed algal extract, induced only low levels or no metamorphosis.

The responses of conch larvae to the algal extract, valine, and isoleucine are blocked by acetylsalicylic acid (Fig. 4). In other systems (Hara, 1977), alterations of the α-amino or α-carboxyl group on amino acids through acetylation, methylation, or esterification block the activity of amino acids. Hara's results (1977) coupled with the results of our experiments on the effects of *N*-acetyl-L-valine suggest that acetylsalicylic acid may be modifying sites on either the inducer (*L. poitei* extract, valine, or isoleucine) or the larval receptors, possibly through acetylation. Acetylsalicylic acid, however, may also affect transduction of the metamorphic signal, since it indirectly affects levels of cAMP in cells (Hecker *et al.*, 1995; Payan and Katzung, 1995). Although the cAMP phosphodiesterase inhibitor IBMX does not, by itself, have an effect on conch larval metamorphosis, it does alleviate the negative effects of acetylsalicylic acid on metamorphosis (Fig. 8). Therefore, the ability of acetylsalicylic acid to modulate

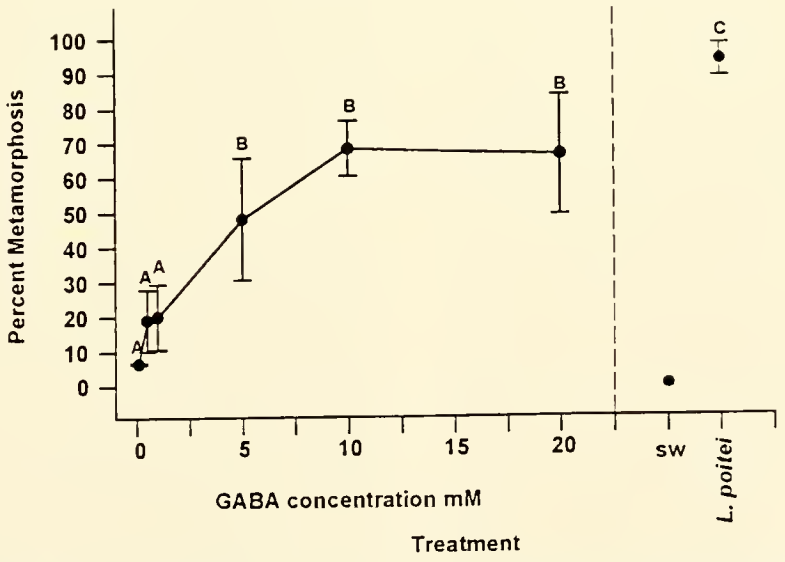

Figure 9. Percent metamorphosis of queen conch larvae in response to specific concentrations of γ-aminobutyric acid (GABA). Seawater only (sw, a negative control) and an extract of *Laurencia poitei* (20 μl extract/ml seawater) are also shown. Points are means ± SD; $n = 5$. Data points with the same letter above the error bar are not significantly different at $P \leq 0.05$.

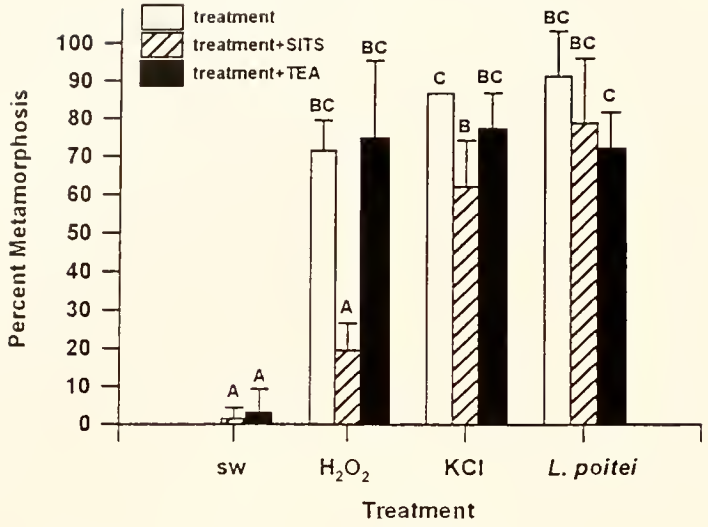

Figure 10. Percent metamorphosis of queen conch larvae in response to seawater only (sw, a negative control), hydrogen peroxide (H_2O_2, 50 μM), increased KCl (20 mM) and an extract of *Laurencia poitei* (20 μl extract/ml seawater) alone and in combination with 4-acetamino-4′isothiostilbene-2,2′disulfonic acid (50 μM, SITS) or tetraethylammonium chloride (500 μM, TEA). Points are means ± SD; $n = 5$. Data points with the same letter above the error bar are not significantly different at $P \leq 0.05$.

cAMP levels during conch metamorphosis cannot be disregarded. However, since salicylic acid (a compound that, like acetylsalicylic acid, can affect cAMP levels) has no effect on conch larval metamorphosis, and since metamorphosis induced by hydrogen peroxide is unaffected by acetylsalicylic acid, it is unlikely that the effects of acetylsalicylic acid are due to its influence on the cAMP second messenger system.

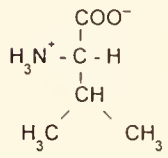

valine

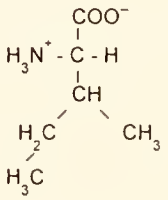

isoleucine

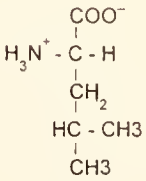

leucine

Figure 11. Structure of the amino acids valine, isoleucine, and leucine.

The responses of conch larvae to hydrogen peroxide, DOPA, vanadate, and GABA are consistent with the known roles of second messenger pathways in settlement and metamorphosis, as well as with the known activities of these compounds in other systems. Models for processes controlling the transduction of metamorphogenic signals in other marine larval systems have drawn on those developed for olfactory responses, involving primarily the adenylate cyclase (AC)/cAMP pathway, the phospholipase C (PLC)/inositol triphosphate (IP_3) pathway, or both (Leitz and Müller, 1987; Freeman and Ridgeway, 1990; Morse, 1990; Rittschof *et al.*, 1991; Anholt, 1992; Fadool and Ache, 1992; Michel and Ache, 1992; Clare *et al.*, 1995; Brunet *et al.*, 1996).

Hydrogen peroxide, vanadate, and DOPA all induce complete larval metamorphosis in the queen conch. The response of conch larvae to DOPA appears to be related to the production of hydrogen peroxide in the breakdown of this catecholamine rather than to any direct effect of DOPA itself; no response is initiated in the DOPA treatments until peroxide concentrations reach levels that alone induce metamorphosis (AAB, pers. obs.). This is similar to the response of *Phestilla sibogae* larvae to DOPA and hydrogen peroxide (Pires and Hadfield, 1991). Although hydrogen peroxide induces complete metamorphosis in the conch, only partial metamorphosis is included in *P. sibogae* (Pires and Hadfield, 1991). In other systems, hydrogen peroxide and vanadate have been shown to directly or indirectly activate Ca^{2+} release channels via oxidation of thiol groups, stimulate phospholipase C, and increase protein tyrosine phosphorylation (Paris

and Pouysségur, 1987; Ranjan and Goetz, 1990; Leitz and Wirth, 1991; Pires and Hadfield, 1991; Favero *et al.*, 1995). In addition, it has recently been hypothesized that hydrogen peroxide, like nitric oxide, may itself be an intracellular second messenger (Dong, 1995; Sundaresan *et al.*, 1995). One or several of these mechanisms may be responsible for the activities of hydrogen peroxide, DOPA, and vanadate in conch larval metamorphosis, and all suggest that these compounds influence metamorphosis by modulating second messenger pathways.

The types of chemical cues involved in conch metamorphosis and the mechanisms controlling it share general features with chemoreception in adult aquatic invertebrates (Burke, 1983; Baxter and Morse, 1987; Arkett *et al.*, 1989; Carr *et al.*, 1989; Bonar *et al.*, 1990; Freeman and Ridgway, 1990; Morse, 1990; Pawlik, 1990; Leitz, 1993; Leitz *et al.*, 1994). The red algal cues, like those that induce olfactory responses in other marine organisms, are of low molecular weight and soluble in water. It appears that the molecules of the algal cue bind to sites that also recognize and bind particular amino acids (*i.e.*, valine and isoleucine). The results of the experiments with vanadate and hydrogen peroxide suggest that metamorphosis induced by the natural cue may be triggered through a second messenger pathway. As with other marine larvae, elevated K^+ concentrations (above ambient seawater) can directly activate the metamorphosis process, presumably by depolarizing sensory cells. Studies focusing on further characterization of the natural inducer, and on the potential involvement of the PLC/DAG/IP_3 and AC/cAMP second messenger systems in conch metamorphosis, will deepen our understanding of the metamorphic process in conch and in other marine invertebrates. Electrophysiological studies directly testing the effects of morphogens on potential larval chemoreceptors would contribute further to the understanding of how metamorphosis is induced and how the signals are transduced, and would also aid in the identification of the active components of the cues.

Acknowledgments

We thank the Caicos Conch Farm for use of both larvae and laboratory space, and C. Dyer and J. Casey for laboratory assistance. K. Anderson and H. Waite are thanked for their assistance with the amino acid analyses. In addition, we thank B. Ache, T. Arnold, D. Martin, and anonymous reviewers for comments that improved the manuscript. Research was supported by grants from Lerner-Gray Fund for Marine Research and the International Women's Fishing Association to AAB. Additional support was provided by NSF Grant #OCE9314551 to NMT.

Literature Cited

Anholt, R. R. H. 1992. Molecular aspects of olfaction. Pp. 51–79 in *Science of Olfaction,* M. J. Serby and K. L. Chobor, eds. Springer-Verlag, New York.

Arkett, S. A., F-S. Chia, F. I. Goldberg, and R. Koss. 1989. Identified settlement receptor cells in a nudibranch veliger respond to specific cue. *Biol. Bull.* **176:** 155–160.

Baloun, A. J., and D. E. Morse. 1984. Ionic control of settlement and metamorphosis in larval *Haliotis rufescens* (Gastropoda). *Biol. Bull.* **167:** 124–138.

Baxter, G., and D. E. Morse. 1987. G protein and diacylglycerol regulate metamorphosis of planktonic molluscan larva. *Proc. Natl. Acad. Sci. USA* **84:** 1867–1870.

Beiras, R., and J. Widdows. 1995. Induction of metamorphosis in larvae of the oyster *Crassostrea gigas* using neuroactive compounds. *Mar. Biol.* **123:** 327–334.

Boettcher, A. A., and N. M. Targett. 1996. Induction of metamorphosis in queen conch, *Strombus gigas* Linnaeus, larvae by cues associated with red algae from their nursery grounds. *J. Exp. Mar. Biol. Ecol.* **196:** 29–52.

Boettcher, A. A., C. Dyer, J. Casey, and N. M. Targett. 1997. Hydrogen peroxide induced metamorphosis of queen conch, *Strombus gigas:* tests at the commercial scale. *Aquaculture* **148:** 247–258.

Bonar, D. B., S. L. Coon, M. Walch, R. M. Weiner, and W. Fitt. 1990. Control of oyster settlement and metamorphosis by endogenous and exogenous chemical cues. *Bull. Mar. Sci.* **46:** 484–498.

Brownell, W. N., and J. M. Stevely. 1981. The biology, fisheries, and management of the queen conch, *Strombus gigas. Mar. Fish. Rev.* **43:** 1–12.

Brunet, L. J., G. H. Gold, and J. Ngai. 1996. General anosmia caused by a targeted disruption of the mouse olfactory cyclic nucleotide-gated cation channel. *Neuron* **17:** 681–693.

Burke, R. D. 1983. The induction of metamorphosis of marine invertebrate larvae: stimulus and response. *Can. J. Zool.* **61:** 1701–1719.

Burke, R. D. 1984. Pheromonal control of metamorphosis in the Pacific sand dollar, *Dendraster excentricus. Science* **225:** 442–443.

Burke, R. D. 1986. Pheromones and the gregarious settlement of marine invertebrate larvae. *Bull. Mar. Sci.* **39:** 323–331.

Carr, W. E. S. 1988. The molecular nature of chemical stimuli in the aquatic environment. Pp. 3–27 in *Sensory Biology of Aquatic Animals,* J. Atema, R. R. Fay, A. N. Popper, and W. N. Tavolga, eds. Springer-Verlag, New York.

Carr, W. E. S., R. A. Gleeson, and H. G. Trapido-Rosenthal. 1989. Chemosensory systems in lower organisms: correlations with internal receptor systems for neurotransmitters and hormones. *Adv. Comp. Environ. Physiol.* **5:** 25–52.

Clare, A. S., R. F. Thomas, and D. Rittschof. 1995. Evidence for the involvement of cyclic AMP in the pheromonal modulation of barnacle settlement. *J. Exp. Biol.* **198:** 655–664.

Coon, S. L., D. B. Bonar, and R. M. Weiner. 1985. Induction of settlement and metamorphosis of the Pacific oyster, *Crassostrea gigas* (Thunberg), by L-DOPA and catecholamines. *J. Exp. Mar. Biol. Ecol.* **94:** 211–221.

Davis, M. 1994. Mariculture techniques for queen conch (*Strombus gigas* Linne) eggmass to juvenile stage. Pp. 231–252 in *The Biology, Fisheries, Mariculture and Management of the Queen Conch,* R. S. Appeldoorn and B. Rodriguez, eds. Fundación Científica Los Roques, Caracas.

Davis, M., and A. W. Stoner. 1994. Trophic cues induce metamorphosis of queen conch larvae (*Strombus gigas* Linnaeus). *J. Exp. Mar. Biol. Ecol.* **180:** 83–102.

Davis, M., W. D. Heyman, W. Harvey, and C. A. Withstandley. 1990. A comparison of two inducers, KCl and *Laurencia* extracts, and techniques for the commercial scale induction of metamorphosis in queen conch, *Strombus gigas* Linnaeus, 1758, larvae. *J. Shellfish Res.* **9:** 67–73.

Dong, X. 1995. Finding the missing pieces in the puzzle of plant disease resistance. *Proc. Natl. Acad. Sci. USA* **92:** 7137–7139.

Fadool, D. A., and B. W. Ache. 1992. Plasma membrane inositol 1,4,5-trisphosphate-activated channels mediate signal transduction in lobster olfactory receptor neurons. *Neuron* **9:** 907–918.

Favero, T. G., A. C. Zable, and J. J. Abramson. 1995. Hydrogen peroxide stimulates the Ca^{2+} release channel from skeletal muscle sarcoplasmic reticulum. *J. Biol. Chem.* **270:** 25557–25563.

Freeman, G., and E. B. Ridgway. 1990. Cellular and intracellular pathways mediating the metamorphic stimulus in hydrozoan planulae. *Roux's Arch. Dev. Biol.* **199:** 63–79.

Hara, T. J. 1977. Further studies on the structure-activity relationships of amino acids in fish olfaction. *Comp. Biochem. Physiol. A* **56:** 559–565.

Hecker, M., M. L. Foegh, and P. W. Ramwell. 1995. The eicosanoids: prostaglandins, thromboxanes, leukotrienes, and related compounds. Pp. 290–304 in *Basic and Clinical Pharmacology,* B. G. Katzung, ed. Appleton and Lange, Norwalk, CT.

Heyman, W. D., R. A. Dopperteen, L. A. Urray, and A. M. Heyman. 1989. Pilot hatchery for the queen conch, *Strombus gigas,* shows potential for inexpensive and appropriate technology for larval aquaculture in the Bahamas. *Aquaculture* **77:** 277–285.

Ilan, M., R. A. Jensen, and D. E. Morse. 1993. Calcium control of metamorphosis in polychaete larvae. *J. Exp. Zool.* **267:** 423–430.

Leitz, T. 1993. Biochemical and cytological bases of metamorphosis in *Hydractinia echinata. Mar. Biol.* **116:** 559–564.

Leitz, T., and W. A. Müller. 1987. Evidence for the involvement of PI-signaling and diacylglycerol second messengers in the initiation of metamorphosis in the hydroid *Hydractinia echinata* Fleming. *Dev. Biol.* **121:** 82–89.

Leitz, T., and A. Wirth. 1991. Vanadate, known to interfere with signal transduction, induces metamorphosis in *Hydractinia* (Coelenterata; Hydrozoa) and causes profound alterations of the larval and postmetamorphic body pattern. *Differentiation* **47:** 119–127.

Leitz, T., K. Morand, and M. Mann. 1994. Metamorphosin A: a novel peptide controlling development of the lower metazoan *Hydractinia echinata* (Coelenterata, Hydrozoa). *Dev. Biol.* **163:** 440–446.

Michel, W. C., and B. W. Ache. 1992. Cyclic nucleotides mediate an odor-evoked potassium conductance in lobster olfactory receptor cells. *J. Neurosci.* **12:** 3979–3984.

Morse, A. N. C. 1992. Role of algae in the recruitment of marine invertebrate larvae. Pp. 385–403 in *Plant and Animal Interoctions in the Marine Benthos,* D. M. John, S. J. Hawkins, and J. H. Price, eds. Systematics Association Special Vol. 46. Clarendon Press, Oxford.

Morse, D. E. 1990. Recent progress in larval settlement and metamorphosis: closing the gap between molecular biology and ecology. *Bull. Mar. Sci.* **46:** 465–483.

Paris, S., and J. Pouysségur. 1987. Further evidence for a phospholipase C-coupled G protein in hamster fibroblasts. *J. Biol. Chem.* **262:** 1970–1976.

Pawlik, J. R. 1990. Natural and artificial induction of metamorphosis of *Phragmatapoma lapidosa californica* (Polychaeta: Sabellariidae), with a critical look at the effects of bioactive compounds on marine invertebrate larvae. *Bull. Mar. Sci.* **46:** 512–536.

Payan, D. G., and B. G. Katzung. 1995. Nonsteroidal anti-inflammatory drugs, nonopiod analgesics; drugs used in gout. Pp. 536–559 in *Basic and Clinical Pharmacology,* B. G. Katzung, ed. Appleton and Lange, Norwalk, CT.

Pearce, C. M., and R. E. Scheibling. 1990. Induction of metamorphosis of larvae of the green sea urchin, *Strongylocentrotus droebachiensis,* by coralline red algae. *Biol. Bull.* **179:** 304–311.

Pires, A., and M. G. Hadfield. 1991. Oxidative breakdown products of catecholamines and hydrogen peroxide induce partial metamorphosis in the nudibranch *Phestilla sibogae* Bergh (Gastropoda: Opisthobranchia). *Biol. Bull.* **180:** 310–317.

Randall, J. E. 1964. Contributions to the biology of the queen conch, *Strombus gigas. Bull. Mar. Sci. Gulf Caribb.* **14:** 246–295.

Ranjan, M., and F. W. Goetz. 1990. Orthovanadate and fluorialuminate stimulate inositol phosphate production and *in vitro* ovulation in goldfish (*Carassius auratus*) follicles. *Biol. Reprod.* **43:** 323–324.

Ray, M., and M. Davis. 1989. Algae production for commercially grown queen conch (*Strombus gigas*). *Proc. Gulf Caribb. Mar. Fish. Inst.* **39:** 453–457.

Ray, M., and A. W. Stoner. 1994. Experimental analysis of growth and survivorship at a juvenile queen conch aggregation: balancing growth with safety in numbers. *Mar. Ecol. Prog. Ser.* **105:** 47–59.

Rittschof, D. 1990. Peptide-mediated behaviors in marine organisms, evidence for a common theme. *J. Chem. Ecol.* **16:** 261–272.

Rittschof, D., A. R. Schmidt, I. R. Hooper, D. J. Gerhart, D. Gunster, and J. Bonaventura. 1991. Molecular mediation of settlement of selected invertebrate larvae. Pp. 317–330 in *Bioactive Compounds from Marine Organisms with an Emphasis on the Indian Ocean,* M-F. Thompson, R. Sarojini, and R. Nagabhushanam, eds. A. A. Balkema, Rotterdam.

Sandt, V. J., and A. W. Stoner. 1993. Ontogenetic shift in habitat by early juvenile queen conch, *Strombus gigas:* patterns and potential mechanisms. *Fish. Bull. U.S.* **91:** 516–525.

Stoner, A. W., and M. Ray. 1993. Aggregation dynamics in juvenile queen conch: population structure, growth, mortality, and migration. *Mar. Biol.* **116:** 571–582.

Stoner, A. W., and V. J. Sandt. 1991. Experimental analysis of habitat quality for juvenile queen conch in seagrass meadows. *Fish. Bull. U.S.* **89:** 693–700.

Stoner, A. W., and J. M. Waite. 1991. Trophic biology of *Strombus gigas* in nursery habitats: Diets and food sources in seagrass meadows. *J. Molluscan Stud.* **57:** 451–460.

Stoner, A. W., M. D. Hanisak, N. P. Smith, and R. A. Armstrong. 1994. Large scale distribution of queen conch nursery habitats: implications for stock enhancement. Pp. 169–189 in *The Biology, Fisheries, Mariculture and Management of the Queen Conch,* R. S. Appeldoorn and B. Rodriguez, eds. Fundación Científica Los Roques, Caracas.

Stoner, A. W., M. Ray, R. A. Glazer, and K. J. McCarthy. 1996. Metamorphic responses to natural substrata in a gastropod larva: decisions related to postlarval growth and habitat preference. *J. Exp. Mar. Biol. Ecol.* **205:** 229–243.

Sundaresan, M., Z-X. Yu, V. J. Ferrans, K. Irani, and T. Finkel. 1995. Requirement for generation of H_2O_2 for platelet-derived growth factor signal transduction. *Science* **270:** 296–299.

Tegtmeyer, K., and D. Rittschof. 1989. Synthetic peptide analogs to barnacle settlement pheromone. *Peptides* **9:** 1403–1406.

Tsugita, A., T. Uchida, H. W. Mewes, and T. Akata. 1987. Rapid vapor-phase hydrolysis of peptides and proteins. *J. Biochem.* **102:** 1592–1597.

Wickland, R. I., L. J. Hepp, and G. A. Wenz. 1991. Preliminary studies on the early life history of the queen conch, *Strombus gigas,* in the Exuma Cays, Bahamas. *Proc. Gulf Caribb. Fish. Inst.* **40:** 283–298.

Yool, A. J., S. M. Grau, M. G. Hadfield, R. A. Jensen, D. A. Markell, and D. E. Morse. 1986. Excess potassium induces larval metamorphosis in four marine invertebrate species. *Biol. Bull.* **170:** 255–266.

Zimmer-Faust, R. K., and M. N. Tamburri. 1994. Chemical identity and ecological implications of a waterborne, larval settlement cue. *Limnol. Oceanogr.* **39:** 1075–1087.

Reference: *Biol. Bull.* **194:** 143–149. (April, 1998)

Zebra Mussel Spawning Is Induced in Low Concentrations of Putative Serotonin Reuptake Inhibitors

PETER P. FONG

Department of Biology, SUNY Geneseo, and Department of Biology, Gettysburg College, Gettysburg, Pennsylvania 17325

Abstract. Serotonin (5-hydroxytryptamine, 5-HT) and its receptor ligands induce both oocyte maturation and spawning in zebra mussels (*Dreissena polymorpha*). The selective serotonin reuptake inhibitors (SSRIs) fluvoxamine ("Luvox"), fluoxetine ("Prozac"), and paroxetine ("Paxil") are commonly prescribed drugs for the treatment of depression in humans. They act to increase 5-HT neurotransmission by inhibiting reuptake transport proteins at synapses. I tested the efficacy of these drugs at inducing spawning in zebra mussels. All three compounds induced spawning in both sexes at concentrations lower than that for 5-HT itself. Fluvoxamine was particularly potent, inducing spawning in 100% of both sexes at 10^{-5} and 10^{-6} *M*. The concentration that induced a significant percentage of animals to spawn was as low as 10^{-9} *M* for males and and 10^{-7} *M* for females. The lowest concentration of fluvoxamine to induce spawning was 10^{-8} *M* for females (40%) and 10^{-10} *M* for males (20%). Gametes spawned in fluvoxamine (10^{-5} *M* and lower) were viable, and swimming trochophores were formed within 20 hours. Fluoxetine was also an effective spawning inducer, causing 100% of males to spawn at 5×10^{-6} *M*. The concentration of fluoxetine required to induce a significant percentage of spawning was as low as 5×10^{-8} *M* for males and 5×10^{-6} *M* for females. In both fluvoxamine and fluoxetine, more than 60% of the males spawned within the first hour of exposure. In contrast, paroxetine was a weak spawning inducer. At concentrations of 10^{-5} and 10^{-6} *M* it induced significant, but low (50% and 40%, respectively) percentages of males to spawn. Paroxetine did not induce significant spawning in females. Thus, fluvoxamine, fluoxetine, and paroxetine can induce spawning at low concentrations, and fluvoxamine is the most powerful spawning inducer in any bivalve. These may be useful agents for stimulating invertebrate serotonergic mechanisms without applying exogenous 5-HT, and they are potentially important in bivalve aquaculture. Moreover, these results suggest, for the first time, the presence of 5-HT reuptake transporters in bivalve molluscs.

Received 7 July 1997; accepted 23 December 1997.
E-mail: pfong@gettysburg.edu

Introduction

Serotonergic mechanisms regulate a wide variety of physiological functions in molluscs. Amongst bivalve molluscs, reproductive processes including oocyte maturation (Hirai *et al.*, 1988; Krantic *et al.*, 1991; Fong *et al.*, 1994a; Gobet *et al.*, 1994), spawning (Hirai *et al.*, 1988; Ram *et al.*, 1993), and parturition (Fong and Warner, 1995; Fong *et al.*, 1996a) are regulated by serotonin (5-hydroxytryptamine, 5-HT) or a 5-HT-like compound. Exogenous application of 5-HT and 5-HT receptor ligands such as 8-OH-DPAT and alpha-methyl-5-HT induce spawning in a number of marine and freshwater bivalves (Gibbons and Castagna, 1984; Ram *et al.*, 1993; Fong *et al.*, 1993, 1996b). The serotonin pharmacology of spawning has been recently elucidated in the exotic zebra mussel, *Dreissena polymorpha* (Fong *et al.*, 1993, 1994b). Both male and female zebra mussels spawn when exposed to 10^{-4} *M* and 10^{-3} *M* 5-HT.

Fluvoxamine (5-methoxy-4′-(trifluoromethyl)valerophenone(E)-O-(2-amimoethyl)oxime maleate), fluoxetine (*N*-methyl-3[*p*-trifluoromethylphenoxy]-3-phenylpropylamine), and paroxetine {(-)-trans-4R-(4′-fluorophenyl)-3S-[93′,4′-methylenedioxyphenoxy)methyl] piperidine hydrochloride hemihydrate} are commonly prescribed antidepressants ("Luvox," "Prozac," and "Paxil," respec-

tively) in humans; they increase 5-HT neurotransmission by inhibiting 5-HT reuptake transporters (Fuller 1994; Garcia-Colunga *et al.*, 1997). Since these selective serotonin reuptake inhibitors (SSRIs) increase endogenous 5-HT neurotransmission in some species, I tested the effects of these drugs on spawning in zebra mussels. The results revealed that the three drugs, especially fluvoxamine and fluoxetine, are powerful inducers of spawning in zebra mussels, and suggest the presence of 5-HT reuptake transporters in bivalve molluscs.

Materials and Methods

Zebra mussels were collected in July 1996 and June 1997 from Conesus Lake (42° 45′ N, 78° 45′ W), Geneseo, Livingston County, New York. During the 1996 collection, the water temperature of the lake was 23°C. Mussels were transported to the laboratory and acclimated to 10°C in an incubator by reducing the temperature from 23°C at a rate of 2°C/day. Mussels were maintained without added food for 2 weeks until testing. These mussels were tested with fluoxetine only. In 1997, water temperature was 20°C during collection. Mussels were maintained without added food in a 10°C incubator and used within 3 days of collection. These animals were tested with fluvoxamine, fluoxetine, and paroxetine. Animals ranged from 13–32 mm in shell length. Fluoxetine, serotonin creatinine sulfate (both from Sigma Chemical Co., St. Louis, MO), and paroxetine (SmithKline Beecham, Philadelphia, PA) were dissolved in lake water. Fluvoxamine (Solvay-Duphar, Weesp, The Netherlands) was dissolved in 100% ETOH.

All experiments were carried out in 20-ml glass vials (1 mussel/vial) at room temperature (22°–25°C). Initially, all mussels were acclimated in either 4.5 or 9.0 ml of lake water for 20–30 min before addition of any drug. After the acclimation period, 0.5 or 1.0 ml of drug was added. Thus the final concentrations were 10-fold lower than the added concentrations. All experiments had a negative control (lake water alone or 0.1% ETOH) and a positive serotonin (10^{-3} *M*) control. Mussels were observed for evidence of spawning, and questionable spawnings were confirmed by microscopic analysis of water. In most cases, spawnings were easy to detect. Males released streams of sperm, which resulted in in cloudy water soon after. Females released oocytes in intermittent bursts; oocytes were easily seen on the bottom of vials. Experiments were run for 4 h, after which all non-spawners were dissected and their gonads examined microscopically to determine sex and reproductive maturity (Ram *et al.*, 1993). Since it is impossible to ascertain zebra mussel sex and maturity prior to experiments, the number of animals of each sex in various experimental groups varied from experiment to experiment, but each group initially consisted of at least 12 mussels. Results were analyzed statistically using Fisher's exact test (Sokal and Rohlf, 1981), and null hypotheses were rejected where $P < 0.05$.

Results

Figure 1A shows the dose-response curve for spawning in fluvoxamine. Males showed statistically significant percentages of spawning at 10^{-9} to 10^{-5} *M* (Fisher's exact test, $P < 0.0001$ for all concentrations compared with negative control). Females showed significant spawning in fluvoxamine concentrations from 10^{-7}–10^{-5} *M* (Fisher's exact test, $P < 0.003$–0.0001). As expected, 5-HT induced a high percentage of spawning compared with negative controls (Fig. 1B). At concentrations from 10^{-9} to 10^{-6} *M*, more than 60% of males spawned within the first hour, and of these, most spawned within 30 min (Fig. 2A). Females always took longer to spawn, never achieving maximum spawning in the first hour (Fig. 2B). Animals were healthy in all concentrations for the duration of the experiments. Gametes spawned in the highest concentration (10^{-5} *M*) were viable and oocytes were successfully fertilized, forming swimming trochophores within 20 h.

The spawning data for fluoxetine were pooled for 1996–1997. Fluoxetine was also an effective inducer of spawning in both sexes. A high, statistically significant percentage of males spawned from 5×10^{-7} to 5×10^{-4} *M* compared with negative controls (Fig. 3A, B). Females had a much narrower range of sensitivity, spawning at significant percentages only in 5×10^{-6} and 10^{-5} *M*. As in fluvoxamine, most males spawned within the first hour (Fig. 4A), but females lagged, achieving maximum spawning only after the second hour (Fig. 4B). Mussels exposed to high concentrations (10^{-3} *M*) of fluoxetine looked unhealthy, and sperm spawned in 10^{-3} to 5×10^{-5} *M* were not motile. But, sperm recovered motility when placed in fresh lake water. A single attempt to fertilize oocytes spawned in fluoxetine (10^{-5} *M*) was not successful.

In contrast to fluvoxamine and fluoxetine, paroxetine was only marginally effective at inducing spawning. Males spawned significantly in 10^{-6} and 10^{-5} *M*, but the highest percentage was only 50% in 10^{-6} *M* (Fig. 5A). Females did not show significant spawning at any concentration of paroxetine, although at 10^{-5} *M*, 2 of 8 females spawned. Of the 12 males that spawned in paroxetine, 6 spawned within the first hour, and 5 spawned within 2 hours. Females took at least 3 hours to spawn. Mussels exposed to high concentrations (10^{-4} *M*) of paroxetine released mucus from their siphons, and some of the sperm spawned at 10^{-5} *M* were not motile. No attempt at fertilizing paroxetine-stimulated spawned oocytes was made.

Discussion

Fluvoxamine, fluoxetine, and paroxetine increase 5-HT neurotransmission in vertebrates by inhibiting 5-HT reup-

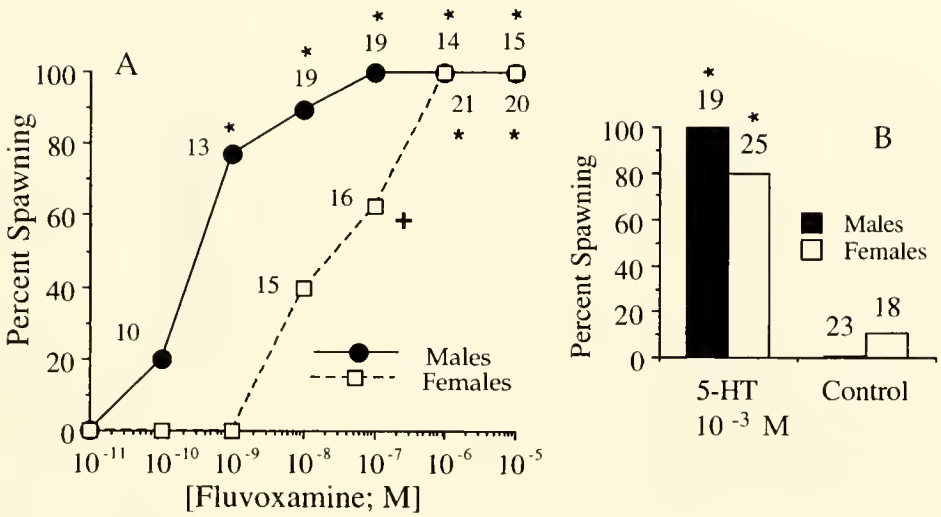

Figure 1. Dose-response experiments with fluvoxamine, June 1997. (A) Percent spawning of *Dreissena polymorpha* in different concentrations of fluvoxamine. Numbers of spawnable mussels tested are adjacent to symbols. *: $P < 0.0001$; +: $P < 0.003$ compared with negative controls. (B) Positive (5-HT) and negative (0.1% ETOH) controls for dose-response experiments. *: $P < 0.0001$. The sample sizes for females at 10^{-11}, 10^{-10}, and 10^{-9} M were 10, 10, and 7, respectively.

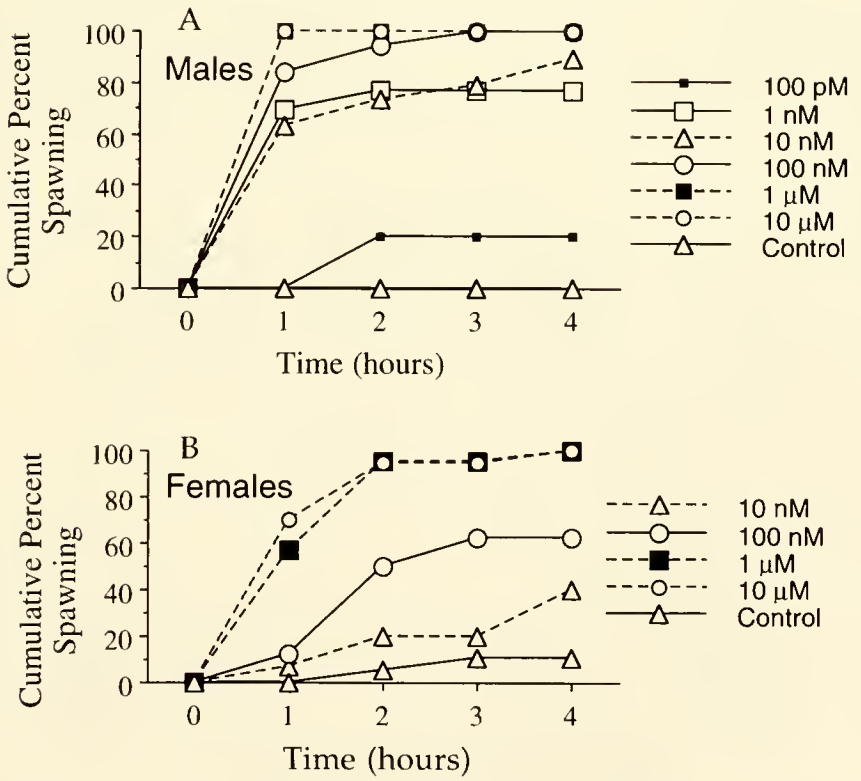

Figure 2. Cumulative percent spawning of zebra mussels over a 4-h period in different concentrations of fluvoxamine in (A) males and (B) females. Sample sizes (n) in each group range from 10 to 23 (for males) and from 15 to 21 (for females).

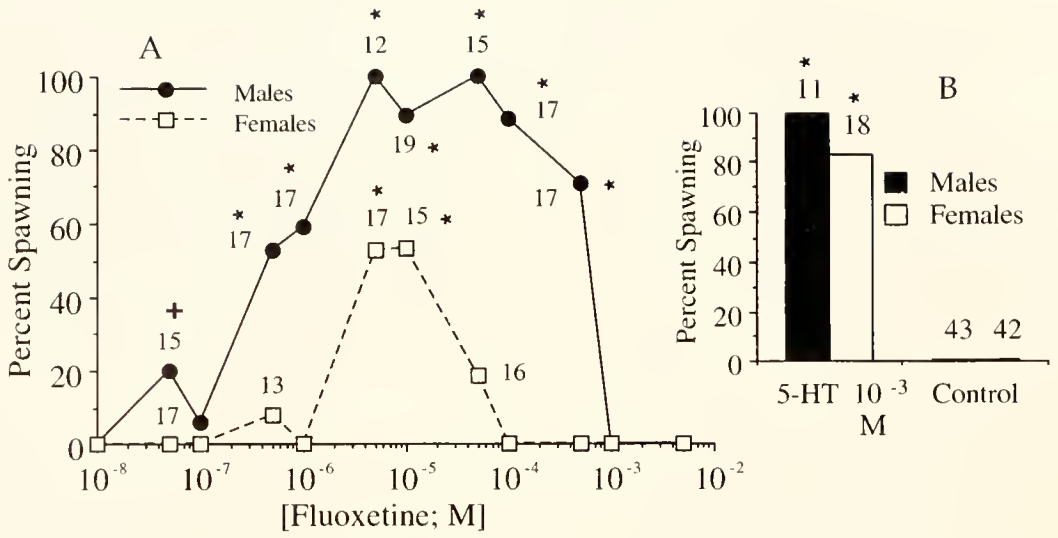

Figure 3. Dose-response experiments with fluoxetine. Data from July 1996 and June 1997 were pooled. (A) Percent spawning of *Dreissena polymorpha* in different concentrations of fluoxetine. Numbers of spawnable mussels tested are adjacent to symbols. *: $P < 0.0001$; +: $P < 0.05$ compared with negative controls. (B) Positive (5-HT) and negative (lake water) controls for dose-response experiments. *: $P < 0.0001$.

take transporters in synaptic clefts (Garcia-Colunga *et al.*, 1997). In molluscs, these compounds affect spawning (bivalves), induction and potentiation of parturition (fingernail clams; Fong *et al.*, 1998), and induction of metamorphosis (gastropod larvae; Couper and Leise, 1996). In other invertebrates such as crayfishes, ovarian growth is stimulated by both 5-HT and fluoxetine, and the latter potentiates the 5-HT effect (Kulkarni *et al.*, 1992). Similarly, fluoxetine potentiates 5-HT-stimulated testicular growth in male fiddler crabs (Sarojini *et al.*, 1993).

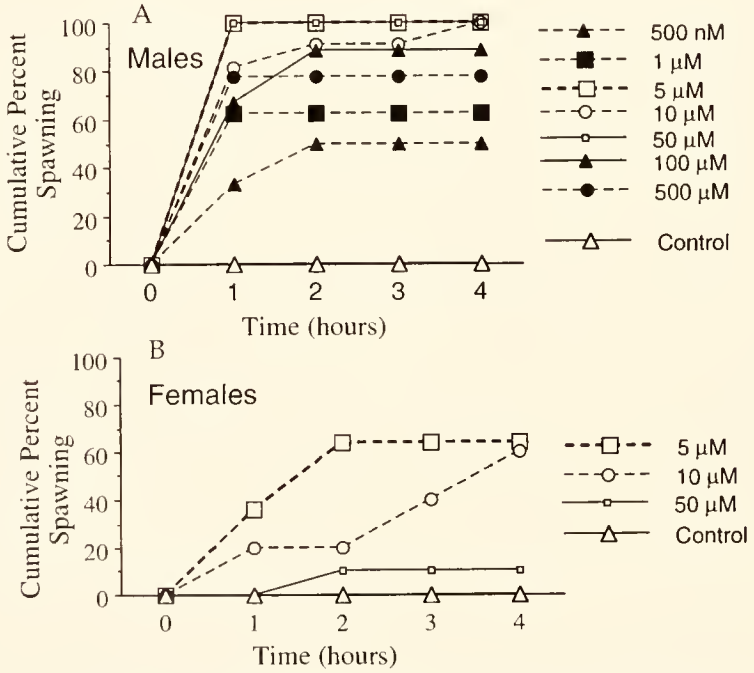

Figure 4. Cumulative percent spawning of zebra mussels over a 4-h period in different concentrations of fluoxetine in (A) males and (B) females. Sample sizes (n) in each group range from 7 to 17 (for males) and from 5 to 17 (for females). Data available for 1997 only.

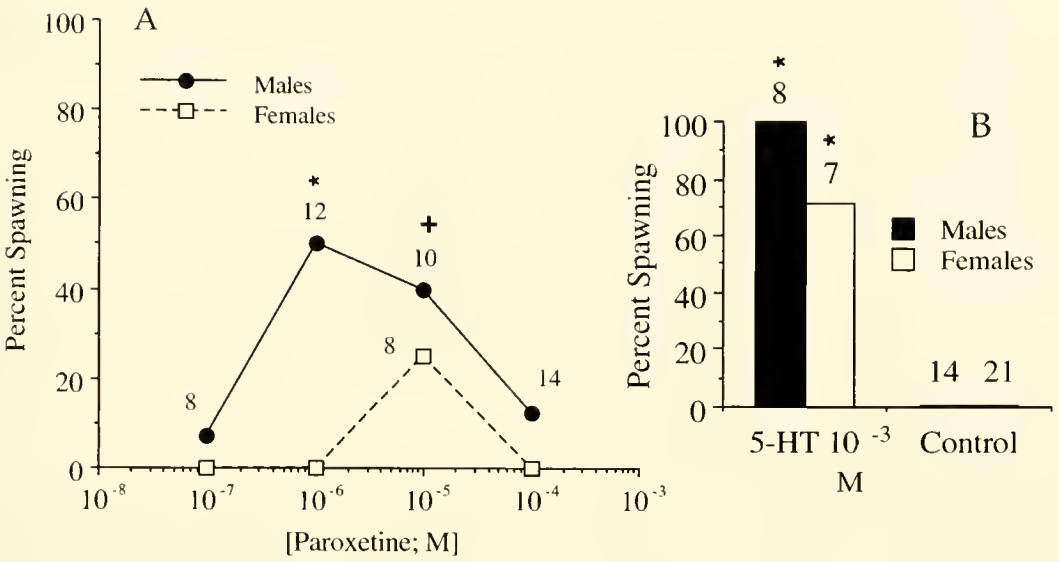

Figure 5. Dose-response experiments with paroxetine, June 1997. (A) Percent spawning of *Dreissena polymorpha* in different concentrations of paroxetine. Numbers of spawnable mussels tested are adjacent to symbols. *: $P < 0.004$; +: $P < 0.02$ compared with negative controls. (B) Positive (5-HT) and negative (lake water) controls for dose-response experiments. *: $P < 0.0002$.

As to the actual mechanism of the spawning induced in mussels by the three tested compounds in my study, two questions arise: (1) Are these compounds working as reuptake inhibitors or as ligands? and (2) How do these compounds gain entry into the animal? At this point, it is not known whether, in zebra mussels, fluoxetine, fluvoxamine, or paroxetine act as SSRIs or as ligands. Molluscan 5-HT reuptake mechanisms have been shown in snails (Osborne *et al.*, 1975) and in squids (Feldman and Dowdall, 1973). Furthermore, *Spisula* oocytes are known to have 5-HT receptors on their membranes, and 5-HT induces germinal vesicle breakdown (GVBD) (Hirai *et al.*, 1988). However, application of either fluvoxamine (10^{-5} *M*) or fluoxetine (10^{-6} and 10^{-5} *M*) to stripped *Spisula* oocytes did not induce GVBD, but 5-HT (10^{-5} *M*) did (unpubl. data). Thus there is no evidence that these compounds act as 5-HT receptor ligands in this well-known bivalve system. In lobsters, Huber *et al.* (1997a) showed reuptake of 5-HT in thoracic nerve roots and blockage of reuptake by fluoxetine. In this system, 5-HT stimulates subordinate animals to engage in fighting against dominants by reducing their willingness to retreat (Huber *et al.*, 1997b). However, injection of fluoxetine alone has no effect on fighting behavior; in fact, concommitant administration of 5-HT and fluoxetine decreased 5-HT-induced agonistic behavior (Huber *et al.*, 1997b). These authors suggested that long-term application of fluoxetine is necessary to mimic 5-HT-induced responses in their system, as is the case in the clinical treatment of depression in humans. In contrast, evidence that fluoxetine acts as a 5-HT receptor ligand has recently been reported (Ni and Miledi, 1997). In their study, fluoxetine bound to and inhibited 5-HT_{2C} receptors in *Xenopus* oocytes. There is additional evidence of fluoxetine's affinity for other neurotransmitter receptors. Garcia-Colunga *et al.* (1997) showed that fluoxetine blocks both muscle and neuronal nicotinic acetylcholine receptors in a voltage-dependent and noncompetitive fashion.

If or how the tested compounds gain entry into zebra mussels is also unknown. In fact, it is not known how externally applied 5-HT itself gains access to zebra mussels. Ram *et al.* (1993) suggested the possibilities that an external receptor is present or that 5-HT is internalized to act directly on the gonad. The concentrations of the fluvoxamine, fluoxetine, and paroxetine necessary to induce spawning in zebra mussels are many orders of magnitude lower than that of 5-HT itself (10^{-4} *M*), and are in the range of 5-HT concentrations (10^{-9} *M*) that induce inotropic (Gaddum and Paasonen, 1955) and inhibitory (Wilkens and Greenberg, 1973) effects on molluscan hearts.

To reiterate, whether fluvoxamine, fluoxetine, and paroxetine are acting as bona fide SSRIs or as 5-HT receptor ligands is unknown, as is their mode of entry. Radioligand binding studies would help elucidate if and where these drugs, when externally applied, are internalized by zebra mussels.

There is intense interest in SSRIs in mammalian vertebrates not only in the treatment of depression, but also in the treatment of conditions such as convulsive seizures (Pasini *et al.*, 1996), obsessive-compulsive behaviors associated with Tourette's syndrome (Eapen *et al.*, 1996),

and obesity in non-insulin-dependent diabetics (Daubresse *et al.*, 1996). However, the actions of putative SSRIs in invertebrates are poorly understood, even though 5-HT is a widely occurring biogenic monoamine that has been identified in a large number of invertebrates including cnidarians, platyhelminthes, nemerteans, annelids, arthropods, and especially molluscs (Welsh and Moorhead, 1960; Fujii and Takeda, 1988; Sandeman *et al.*, 1988; Linn and Roelofs, 1993).

Although some authors report enhanced fertilizability of bivalve oocytes in 5-HT (Juneja *et al.*, 1993), others report that high concentrations of 5-HT have toxic effects on zebra mussel gametes (J. Lynn, pers. comm.; pers. obs.). In the present experiments, toxic effects on mussels were noticed at high concentrations of fluoxetine and paroxetine. However, these effects were observed after most, if not all, animals in each group had already spawned. Thus the toxicity is not believed to have stimulated the spawning. The reduction in sperm motility observed in fluoxetine and paroxetine may be due to the direct action of the drugs on the sperm, since sperm transferred to fresh lake water usually recovered their motility. The mucus release seen in mussels exposed to paroxetine has also been observed in fingernail clams exposed to the same drug (pers. obs.).

Other than algal and gamete extracts (Ram *et al.*, 1996), fluvoxamine, fluoxetine, and paroxetine are the only compounds that stimulate spawning in zebra mussels which are not well-known 5-HT receptor ligands. Moreover, the lowest concentrations of any compound previously known to induce spawning in zebra mussels was 10^{-8} *M* metergoline in males (Fong *et al.*, 1994b) and 10^{-5} *M* ergotamine in females (Ram *et al.*, 1996). In the present study, fluvoxamine induced spawning in males at 10^{-10} *M* and in females at 10^{-8} *M*. Thus fluvoxamine is the most powerful spawning inducer identified not only for zebra mussels, but also for any bivalve yet tested. As powerful as fluvoxamine is, the sensitivity to this drug varies between species. The surf clam *Spisula solidissima*, one of the first bivalves to be induced to spawn with 5-HT, has a serotonin pharmacological profile similar to that of zebra mussels (Kadam *et al.*, 1991). Fluoxetine (10^{-5} and 10^{-4} *M*) induces some spawning in surf clams, but fluvoxamine (10^{-6} and 10^{-5} *M*) does not (unpubl. obs.). Although 5-HT is used to induce spawning in economically important bivalves, its high cost can prohibit its use in developing countries. Further testing of economically important bivalves with these and other putative SSRIs could uncover compounds that would induce spawning at much lower concentrations, and hence be more economically feasible, than 5-HT.

The use of fluvoxamine, fluoxetine, and paroxetine provides a possible method of stimulating serotonin-mediated responses in invertebrates without injection or external application of 5-HT or its ligands. Further experiments are needed to verify that these drugs act as SSRIs and to ascertain how widespread 5-HT reuptake transporters are in molluscs and other invertebrates.

Acknowledgments

I thank Dr. I. Bosch for use of his laboratory at SUNY Geneseo, and M. Laiosa, E. Decker, and I. Bosch for collecting and maintaining zebra mussels. I also thank three anonymous reviewers for helpful comments. Support for this work was generously provided by the Office of the Provost of Gettysburg College.

Literature Cited

Couper, J. M., and E. M. Leise. 1996. Serotonin injections induce metamorphosis in larvae of the gastropod mollusc *Ilyanassa obsoleta*. *Biol. Bull.* **191:** 178–186.

Daubresse, J. C., J. Kolanowski, G. Krzentowski, M. Kutnowski, A. Scheen, and L. Vangaal. 1996. Usefulness of fluoxetine in obese non-insulin dependent diabetics—a multicenter study. *Obesity Res.* **4:** 391–396.

Eapen, V., M. R. Trimble, and M. M. Robertson. 1996. The use of fluoxetine in Gilles-de-la-Tourette Syndrome and obsessive compulsive behaviors—preliminary clinical experience. *Prog. Neuro-psychopharmacol. Biol. Psychiatry* **20:** 737–743.

Feldman, J. L., and M. J. Dowdall. 1973. 5-Hydroxytryptamine: an uptake mechanism in synaptosomes from the optic lobe of squid (*Loligo pealeii*). *Biol. Bull.* **145:** 432–433.

Fong, P. P., and M. Warner. 1995. Serotonin-induced parturition in the fingernail clam *Sphaerium* (*Musculium*) *transversum* (Say). *J. Exp. Zool.* **272:** 163–166.

Fong, P. P., D. M. Wall, and J. L. Ram. 1993. Characterization of serotonin receptors in the regulation of spawning in the zebra mussel *Dreissena polymorpha* (Pallas). *J. Exp. Zool.* **267:** 475–482.

Fong, P. P., K. Kyozuka, H. Abdelghani, J. D. Hardege, and J. L. Ram. 1994a. *In vivo* and *in vitro* induction of germinal vesicle breakdown in a freshwater bivalve, the zebra mussel, *Dreissena polymorpha* (Pallas). *J. Exp. Zool.* **269:** 467–474.

Fong, P. P., J. Duncan, and J. L. Ram. 1994b. Inhibition and sex specific induction of spawning by serotonergic ligands in the zebra mussel *Dreissena polymorpha* (Pallas). *Experientia* **50:** 506–509.

Fong, P. P., S. Wade, and M. Rostafin. 1996a. Characterization of serotonin receptor mediating parturition in fingernail clams *Sphaerium* (*Musculium*) spp. from eastern North America. *J. Exp. Zool.* **275:** 326–330.

Fong, P. P., R. Deguchi, and K. Kyozuka. 1996b. Serotonergic ligands induce spawning but not oocyte maturation in the bivalve *Mactra chinensis* from central Japan. *Biol. Bull.* **191:** 27–32.

Fong, P. P., P. T. Huminski, and L. M. D'Urso. 1998. Induction and potentiation of parturition in fingernail clams (*Sphaerium striatinum*) by selective serotonin re-uptake inhibitors (SSRIs). *J. Exp. Zool.* (in press).

Fujii, K., and N. Takeda. 1988. Phylogenetic detection of serotonin immunoreactive cells in the central nervous system of invertebrates. *Comp. Biochem. Physiol.*, **89C (2):** 233–239.

Fuller, R. W. 1994. Uptake inhibitors increase extracellular serotonin concentration measured by brain microdialysis. *Life Sci.* **55:** 163–167.

Gaddum, J. H., and M. K. Paasonen. 1955. The use of some molluscan hearts for the estimation of 5-hydroxytryptamine. *Br. J. Pharmacol.* **10:** 474–483.

Garcia-Colunga, J., J. N. Awad, and R. Miledi. 1997. Blockage of

muscle and neuronal nicotinic acetylcholine receptors by fluoxetine (Prozac). *Proc. Natl. Acad. Sci. USA* **94:** 2041–2044.

Gibbons, M. C., and M. Castagna. 1984. Serotonin as an inducer of spawning in six bivalve species. *Aquaculture* **40:** 189–191.

Gobet, I., Y. Surocher, C. Leclerc, M. Moreau, and P. Guerrier. 1994. Reception and transduction of the serotonin signal responsible for meiosis reinitiation in oocytes of the Japanese clam *Ruditapes philippinarum*. *Dev. Biol.* **164:** 540–549.

Hirai, S., T. Kishimoto, A. L. Kadam, H. Kanatani, and S. S. Koide. 1988. Induction of spawning and oocyte maturation by 5-hydroxytryptamine in the surf clam. *J. Exp. Zool.* **245:** 318–321.

Huber, R., M. Orzeszyna, N. Pokorny, and E. A. Kravitz. 1997a. Biogenic-amines and aggression—experimental approaches in crustaceans. *Brain Behav. Evol.* **50:** 60–68.

Huber, R., K. Smith, A. Delago, K. Isaksson, and E. A. Kravitz. 1997b. Serotonin and aggressive motivation in crustaceans—altering the decision to retreat. *Proc. Natl. Acad. Sci. USA.* **94:** 5939–5942.

Juneja, R., S. J. Segal, and S. S. Koide. 1993. Promotion of fertilizability of *Spisula* oocytes with 5-hydroxytryptamine. *Invertebr. Reprod. Dev.* **24:** 103–106.

Kadam, P. A., A. L. Kadam, S. J. Segal, and S. S. Koide. 1991. Functional serotonin receptor sites on Atlantic surfclam *Spisula solidissima* (Dillwyn, 1817) oocytes and sperm. *J. Shellfish Res.* **10:** 215–219.

Krantic, S., F. Dube, R. Quiron, and P. Guerrier. 1991. Pharmacology of the serotonin-induced meiosis reinitiation in *Spisula solidissima* oocytes. *Dev. Biol.* **146:** 491–498.

Kulkarni, G. K., R. Nagabhushanam, G. Amaldoss, R. G. Jaiswal, and M. Fingerman. 1992. *In vivo* stimulation of ovarian development in the red swamp crayfish, *Procambarus clarkii* (Girard), by 5-hydroxytryptamine. *Invertebr. Reprod. Dev.* **21:** 231–240.

Linn, C. E., and W. L. Roelofs. 1993. Levels of biogenic-amines and peptides in individual corn earworm moths, *Helicoverpa zea*, using high performance liquid chromatography with electrochemical detection. *Insect Biochem. Mol. Biol.* **23:** 367–373.

Ni, Y. G., and R. Miledi. 1997. Blockage of 5-HT_{2C} receptors by fluoxetine (Prozac). *Proc. Natl. Acad. Sci. USA.* **94:** 2036–2040.

Osborne, N. N., L. Hiripi, and V. Neuhoff. 1975. The *in vitro* uptake of biogenic amines by snail (*Helix pomatia*) nervous tissue. *Biochem. Pharmacol.* **24:** 2141–2148.

Pasini, A., A. Tortorella, and K. Gale. 1996. The anticonvulsant action of fluoxetine in substantia-nigra is dependent upon endogenous serotonin. *Brain Res.* **724:** 84–88.

Ram, J. L., G. W. Crawford, J. U. Walker, J. J. Mojares, N. Patel, P. P. Fong, and K. Kyozuka. 1993. Spawning in the zebra mussel (*Dreissena polymorpha*): activation by internal or external application of serotonin. *J. Exp. Zool.* **265:** 587–598.

Ram, J. L., J. D. Hardege, M. G. Bentley, and J. Duncan. 1996. Spawning in zebra mussels: stimulation by algae- and gamete-associated factors. *Am. Zool.* **35:** 110A.

Sandeman, D. C., R. E. Sandeman, and A. R. Aitkin. 1988. Atlas of serotonin-containing neurons in the optic lobes and brain of the crayfish, *Cherax destructor*. *J. Comp. Neurol.* **269:** 465–478.

Sarojini, R., R. Nagabhushanam, and M. Fingerman. 1993. *In vivo* evaluation of 5-hydroxytryptamine stimulation of the testis in the fiddler crab, *Uca pugilator:* a presumed action on the neuroendocrine system. *Comp. Biochem. Physiol.* **106C:** 321–325.

Sokol, R. R., and F. J. Rohlf. 1981. *Biometry.* 2nd ed. W. H. Freeman, San Francisco. 859 pp.

Welsh, J. H., and M. Moorhead. 1960. The quantitative distribution of 5-hydroxytryptamine in the invertebrates, especially in their nervous systems. *J. Neurochem.* **6:** 146–169.

Wilkens, L. A., and M. J. Greenberg. 1973. Effects of acetylcholine and 5-hydroxytryptamine and their ionic mechanisms of action on the electrical and mechanical activity of molluscan heart smooth muscle. *Comp. Biochem. Physiol.* **45A:** 637–651.

Reference: *Biol. Bull.* **194:** 150–160. (April, 1998)

A Major Protein Precursor of Zebra Mussel (*Dreissena polymorpha*) Byssus: Deduced Sequence and Significance

KEVIN E. ANDERSON AND J. HERBERT WAITE*

Chemistry/Biochemistry Department and College of Marine Studies, Newark, Delaware 19716

Abstract. The zebra mussel is a nonindigenous invader of North American lakes and rivers and one of the few freshwater bivalve molluscs having a byssus—a sclerotized organ used by the mussel for opportunistic attachment to hard surfaces. We have sequenced a foot-specific cDNA whose composite protein sequence was deduced from a series of overlapping but occasionally nonidentical cDNA fragments. The overall deduced sequence matches tryptic peptides from a major byssal precursor protein—*Dreissena polymorpha* foot protein 1 (Dpfp1). The calculated mass of Dpfp1 is 49 kDa; but this is known to be extensively hydroxylated and *O*-glycosylated during maturation. Purified native Dpfp1 analyzed using matrix-assisted laser-desorption ionization mass spectrometry with time-of-flight indicates that the protein occurs as at least two size variants with masses of 48.6 and 54.5 kDa. In all probability, the sequence variants reported in this study are related to the larger mass variant. Dpfp1 has a block copolymer-like structure defined by two consensus motifs that are sharply segregated into domains. The N-terminal side of Dpfp1 has 22 tandem repeats of a heptapeptide consensus (P-[V/E]-Y-P-[T/S/δ]-[K/Q]-X); the C-terminal side has 16 repeats of a tridecapeptide motif (K-P-G-P-Y-D-Y-D-G-P-Y-D-K). Both consensus repeats are unique, with some limited homology to other proteins functioning in tension: marine mussel adhesives, plant extensins, titin, and trematode eggshell precursors.

Received 2 December 1997; accepted 10 February 1998.

* To whom correspondence should be addressed. E-mail:hwaite@udel.edu

Abbreviations: DIG, digoxigenin; Dopa, 3, 4-dihydroxyphenylalanine; Dpfp1, *Dreissena polymorpha* foot protein 1; MALDI-TOF, matrix-assisted laser desorption-ionization mass spectrometry with time-of-flight; Mefp1, *Mytilus edulis* foot protein; RACE, rapid amplification of cDNA ends; RT-PCR, reverse transcriptase-polymerase chain reaction; SDS PAGE, sodium dodecyl sulfate polyacrylamide gel electrophoresis.

Introduction

The zebra mussel, *Dreissena polymorpha* (Pallas), is a freshwater bivalve indigenous to the river basins of the Black, Baltic, and Caspian seas. Recently, it was accidentally introduced into one of the Great Lakes, and in less than 10 years, its distribution has expanded into the lakes and rivers of at least a third of the North American continent (Johnson and Padilla, 1996). The economic impact of this expansion has been profound and is due, in large part, to fouling (Roberts, 1990). Zebra mussels foul by attaching opportunistically and in large numbers to a wide variety of surfaces by means of a thread-like structure known as a byssus (Ackerman *et al.*, 1992). In this respect, they resemble marine mussels (Mytilidae), which have adopted a similar strategy.

Zebra mussel byssal threads are fibrous extracellular structures composed largely of proteins, many of which contain the post-translationally modified amino acid 3,4-dihydroxyphenylalanine (Dopa) (Rzepecki and Waite, 1993). Peptidyl Dopa is thus a convenient marker of byssal precursor proteins and is thought to play an important role in adhesion and the maturational cross-linking of byssal threads (Waite, 1990). Three polymorphic Dopa-containing protein families have previously been isolated and partially characterized from zebra mussel foot tissue, the site of byssal protein synthesis and storage. The largest of these proteins, *Dreissena polymorpha* foot protein 1 (Dpfp1), has an apparent molecular weight of 76 kDa and Dopa at levels up to 6.6 mole % (Rzepecki and Waite, 1993). Like many byssal precursors from marine mussels, Dpfp1 features Dopa residues in repeating consensus motifs. Despite this similarity, Dpfp1 is markedly different

from the marine proteins in two respects. First, members of the Dpfp1 family have acidic isoelectric points ranging from 5.3 to 6.5; marine byssal precursors, in contrast, are highly basic—many with pIs exceeding the effective resolving range of available ampholytes. Second, dreissenid byssal precursors, including Dpfp1, are glycosylated with *N*-acetylgalactosamine *O*-linked to serine and threonine residues; there is, however, no evidence for glycosylation in byssal proteins from any marine taxa. It is not known whether these differences reflect two generally valid solutions to the problem of adhesion underwater or represent genuine differences in the requirements for adhesive bond formation in freshwater and marine systems.

Our efforts to determine the complete primary sequence of Dpfp1 by traditional peptide mapping have been thwarted by the repetitive structure and protease-resistance of large regions of the protein (Rzepecki and Waite, 1993). In this study, we report on the complete primary sequence of Dpfp1 deduced using molecular techniques. cDNA sequence data reveal that Dpfp1 is a tandemly repetitive protein composed of two motifs: a novel heptapeptide sequence and a tridecapeptide consensus sequence. Unusually, these motifs are segregated to distinct regions of the protein, a fact which almost certainly has important consequences to the self-assembly of the zebra mussel byssus.

Materials and Methods

RNA extractions

All tissues used in these experiments were excised, immediately frozen in liquid nitrogen, and ground in a mortar chilled to −80°C. Tissue was homogenized in a hand-held glass homogenizer (Kontes, Vineland, NJ), and total RNA was extracted according to the methods of Chomczynski and Sacchi (1987).

Reverse transcriptase (RT)-polymerase chain reaction (PCR) and 5′ rapid amplification of cDNA ends (RACE)

mRNA was purified from total RNA using the Oligotex mRNA spin column kit (Qiagen, Chatsworth, CA). After purification, 1 μg mRNA was reverse transcribed using 20 pmoles of a primer specific to polyA tracts (polyT-LD AGAGAGATTTTTTTTTTTTTTTTVN) with 200 units of MM-LV reverse transcriptase (Superscript II, Gibco-BRL) for 2 h at 37°C in buffer supplied by the manufacturer. The reaction was quenched with 1 ml of 1 × TE, pH 7.5. One percent (v/v) of the resulting first-strand cDNA was amplified with the polymerase chain reaction (PCR) using degenerate oligonucleotide primers based on the previously determined (Rzepecki and Waite, 1993) amino acid sequence of the N-terminus of Dpfp1 (Dp1.N(+) GGIACITAYGAYTGGACNGA) and an internal peptide (Dp1.A(−) TTRTCRTAIGGICCRTCRTA). Each 50-μl reaction contained 0.25 m*M* of each dNTP, 100 pmoles of each primer, and 2.5 units of *Taq*2000 polymerase (Stratagene, La Jolla, CA), in a buffer containing 10 m*M* Tris-Cl, 1.5 m*M* $MgCl_2$, 75 m*M* KCl, and 15 m*M* $(NH_4)_2SO_4$. Samples were initially denatured at 95°C for 4 min 30 s followed by 30 cycles of amplification as follows: 95°C for 30 s, 50°C for 30 s, and 72°C for 2 min. A final extension for 5 min at 72°C was carried out to ensure addition of 3′ A overhangs. The resulting amplification product was ligated into the pCRII vector (Invitrogen, San Diego, CA) according to manufacturer's instructions. The insert from the newly constructed plasmid, pDP1.NA, was sequenced on both strands using vector-specific and degenerate oligonucleotide primers.

5′ RACE was performed to obtain cDNA sequence data upstream of the region coding for the N-terminus (Frohman *et al.*, 1988) and to independently establish the cDNA sequence of the N-terminus. All reactions were performed using reagents contained in the 5′ RACE System V2.0 (Life Technologies, Bethesda, MD) according to manufacturer's instructions. Briefly, 1 μg of *D. polymorpha* foot tissue total RNA was reverse-transcribed using a gene-specific primer (Dp1.GSP1(−) TATTTTGTAGGAGTGGG). The purified first-strand cDNA was tailed with dCTP, and PCR was performed using the supplied abridged anchor primer (GGCCACGCGTCGACTAGTACGGGIIGGGIIGGGIIG) and Dp1.GSP1(−). Each 50-μl reaction contained 0.25 m*M* of each dNTP and 20 pmoles of each primer in 1× PCR buffer (Life Technologies, Bethesda, MD) supplemented with 2 m*M* $MgCl_2$. Samples were denatured at 95°C for 4 min 30 s and equilibrated to 72°C. Two-and-one-half units of *Taq*2000 polymerase were added and amplification for 25 cycles was performed under the following conditions: 95°C for 30 s, 42°C for 30 s, and 72°C for 30 s. A final 5-min extension was performed at 72°C. A second round of PCR was performed using AAP and a nested gene-specific primer (Dp1.GSP2(−) TTGTTGTATAGTTCGGAATTTTAG). The reaction volume and component concentrations were as outlined in the previous reaction. Samples were initially denatured at 95°C for 4 min 30 s followed by 30 cycles of amplification as follows: 95°C for 30 s, 42°C for 30 s, and 72°C for 60 s. A final extension for 5 min at 72°C was carried out to ensure addition of 3′ A overhangs. The resulting amplification products were cloned into the pGEM-T vector (Promega, Madison, WI) according to manufacturer's instructions. The insert from the newly constructed plasmid, pDP1.5′UTA, was sequenced on both strands using gene-specific primers.

Probe synthesis and cDNA library screening

Two probes were created in this experiment to screen a *D. polymorpha* foot tissue cDNA library (Eddington,

1996). A digoxigenin (DIG)-labeled antisense RNA probe (probe #1) was generated from DdeI-digested pDP1.NA using T7 polymerase and the DIG-RNA labeling kit (Boehringer-Mannheim) according to manufacturer's instructions. A DIG-labeled double-stranded DNA probe (probe #2) spanning the 5′ untranslated region of Dpfp1 and the first 172 nt coding for the mature protein was generated using the PCR DIG probe synthesis kit (Boehringer-Mannheim) according to manufacturer's instructions. pDP1.5′UTA was used as a template for this reaction, and a primer specific to the 5′ untranslated region of Dpfp1 (Dp1.5′ UT(+) ATACTTCAGAGCATCAACCAA) and Dp1.GSP1(−) were used as primers. Both probes were individually incorporated at a concentration of 100 ng/ml into standard hybridization buffer + 50% formamide (5× SSC, 1% Blocking buffer (Boehringer-Mannheim), 0.1% (w/v) sarcosyl, 0.02% (w/v) SDS, 50% formamide (v/v)). Hybridizations were carried out at 60°C (probe #1) or 42°C (probe #2). Stringency washes for both probes were conducted with 0.1× SSC/0.2% (w/v) SDS at 68°C.

One million plaques generated from a λZAP-Express cDNA library (Stratagene, La Jolla, CA) were doubly screened with probes #1 and #2. No plaques positive for probe #2 were detected, suggesting that a full-length clone of Dpfp1 was not present in this library. Forty plaques positive for probe #1 were cored, eluted in SM buffer (100 m*M* NaCl, 50 m*M* Tris-Cl pH 7.5, 8 m*M* $MgSO_4$, 0.1% gelatin), and tested for insert size by PCR using vector-specific primers flanking the cDNA insert. After secondary screening, cDNA from the plaque bearing the largest insert was rescued as a phagemid using the ExAssist interference-resistant helper phage kit (Stratagene, La Jolla, CA) and sequenced using the nested deletion technique (see below).

Nested deletions

Nested deletions were performed using the double-stranded nested deletion kit (Pharmacia Biotech, Piscataway, NJ). In each case, 5 μg of template was doubly digested with EcoRI and PstI, and the restriction enzymes were heat inactivated. Digested clones were precipitated in ethanol and resuspended in a buffer containing 1.5 *M* potassium acetate, 37.5 m*M* Tris-acetate pH 7.6, 15 m*M* magnesium acetate, 750 μ*M* β-mercaptoethanol, and 15 μg/ml bovine serum albumin (BSA). A 2-μg sample of each digest was used for digestion with Exonuclease III. The reactions were carried out at 23°C and aliquots taken every 5 min. All clones yielding deletions larger than the size of the empty vector were ligated, transformed into XL1-Blue MRF′ cells (Stratagene, La Jolla, CA), purified, and sequenced using a vector-specific primer.

RNA dot blots

Ten micrograms of total RNA separately extracted from *D. polymorpha* foot, adductor mussel, mantle, and gill tissue were diluted in an equal volume of RNA dilution buffer (water: 20× SSC: formaldehyde; 5:3:2) and spotted onto a positively charged nylon membrane (MSI, Westboro, MA). The membrane was hybridized to either probe #1 as described above or to an actin-specific double-stranded DIG-labeled DNA probe (Patwary *et al.*, 1996). Hybridization with actin specific probe was performed at 37°C with a stringency wash using 0.5× SSC/0.1% (w/v) SDS at 68°C.

Northern hybridizations

Three micrograms of foot tissue mRNA were subjected to formaldehyde/agarose gel electrophoresis according to Sambrook *et al.* (1989). RNA was transferred onto a positively charged nylon membrane and hybridized overnight with probe #1.

Mass analysis of native Dpfp1

Native Dpfp1 was purified from the foot of adult zebra mussels according to Rzepecki and Waite (1993). The mass of the native protein was determined by matrix-assisted laser desorption-ionization mass spectrometry with time-of-flight (MALDI-TOF) using a PerSeptive Biosystems Voyager model in the positive ion mode and delayed extraction. A 20-μ*M* solution of Dpfp1 in 0.1% acetic acid was mixed with three volumes of a saturated sinapinic acid solution (40% acetonitrile/0.1% TFA); 2 μl of the resulting mixture (10 pmoles Dpfp1) was placed on a sample plate and allowed to air dry. The sample was inserted into a vacuum chamber (1×10^{-7} torr) and the spectra generated from 256 pulses of a 337-nm laser were averaged. The acceleration voltage was 25,000 with a 90% grid voltage and a guidewire setting of 0.1%.

Results

RNA dot blots and Northern hybridizations

The tissue specificity of Dpfp1 is demonstrated in Figure 1. RNA dot blots show that Dpfp1 mRNA transcripts were detected only in total RNA extracts from foot tissue and not in extracts from gill, adductor muscle, or mantle tissue. Identical dot blots hybridized to an actin-specific probe were positive for all tissue types although the strength of the signal varied considerably between tissue types (data not shown). These results are consistent with data obtained from other marine byssal precursor proteins (Inoue *et al.*, 1995, 1996a; Coyne *et al.*, 1997; Qin *et al.*, 1997) and support the hypothesis that Dpfp1 plays a role

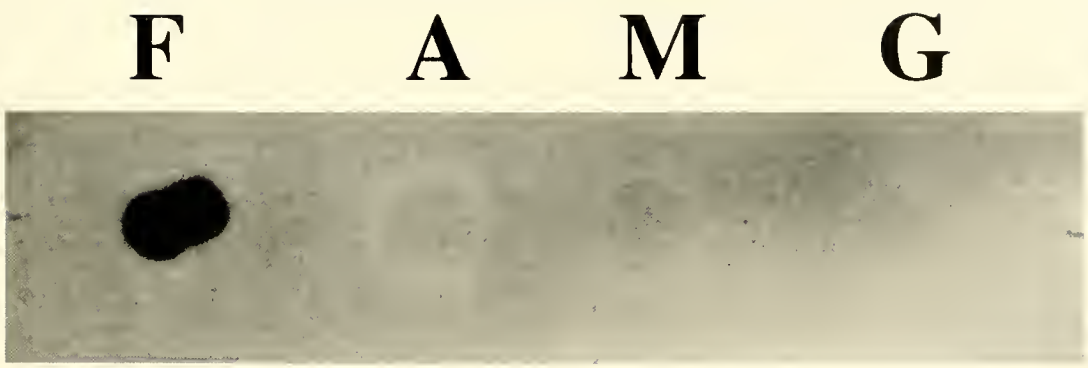

Figure 1. Total RNA dot blots of *Dreissena polymorpha* foot (F), adductor muscle (A), mantle (M), and gill (G) tissue hybridized to a digoxigenin-labeled RNA probe specific to Dpfp1. The probe was hybridized to 1 μg of total RNA from each tissue.

as a byssal structural protein. Northern blots of foot tissue mRNA indicated that Dpfp1 transcripts range in size from 1200 b to 1500 b, suggesting the presence of size variants (Fig. 2).

Dpfp1 cDNA sequence

In Figure 3 the aligned nucleotide sequence data obtained from 5′ RACE, RT-PCR with degenerate oligonucleotide primers, and from the largest cDNA clone isolated are presented. Each sequence differs slightly from the other, and therefore the consensus sequence generated from this alignment does not represent any single Dpfp1 sequence. It is likely that differences in the data sets reflect the existence of Dpfp1 variants rather than errors introduced during amplification, because each set of PCR sequence data was determined from at least two independently amplified samples. The combined transcript is 1481 bp in length and contains an open reading frame of 1332 bp coding for a protein of 443 amino acids. Included in the transcript is a start codon at nucleotide position 36 and two overlapping canonical polyadenylation signals (Kozak, 1986) at nucleotide positions 1464 and 1468. The calculated molecular weight of the deduced primary sequence is 49 kDa, with a predicted isoelectric point of 5.29.

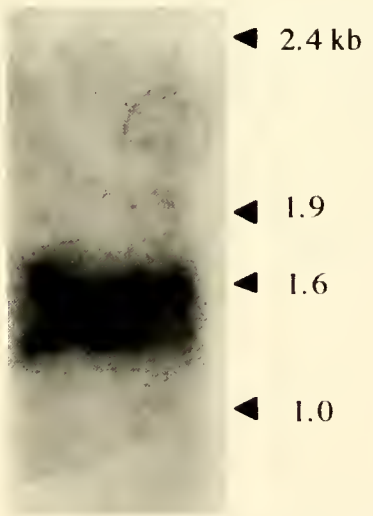

Figure 2. Northern blot of *Dreissena polymorpha* foot tissue mRNA hybridized to a digoxigenin-labeled RNA probe specific to Dpfp1; 3 μg of foot tissue mRNA was used.

The first 19 amino acids code for a putative signal peptide that conforms to the rule of von Heijne (1985). Computer-based modeling of signal peptide cleavage (Nielsen *et al.*, 1997) correctly predicts cleavage of the signal peptide preceding the previously determined N-terminal glycine residue of the mature protein (Rzepecki and Waite, 1993). The N-terminus of Dpfp1, as coded for by sequences generated using 5′ RACE, differs from the previously reported N-terminal sequence (Rzepecki and Waite, 1993) in that it substitutes serine residues for threonine at position #2, tyrosine at position #3, and aspartic acid at position #10. None of the three independently generated 5′ RACE clones exactly coded for the previously reported N-terminus of Dpfp1. N-terminal sequence data generated with degenerate oligonucleotide primers more closely resemble the previously reported N-terminal sequence but also substitute serine for aspartic acid at position #10. It is not possible to determine from these data if the N-terminal sequence deduced from cDNAs generated via degenerate oligonucleotide primers reflects a genuinely different N-terminus or is simply an artifact forced by the primers used during amplification.

The N-terminal 38 amino acids of the mature protein are relatively enriched in threonine and serine residues and quickly give way to a tandemly repeating heptapeptide. This generally basic motif (P-[V/E]-Y-P-[T/S]-[K/Q]-X) is repeated 22 times in the N-terminal half of Dpfp1

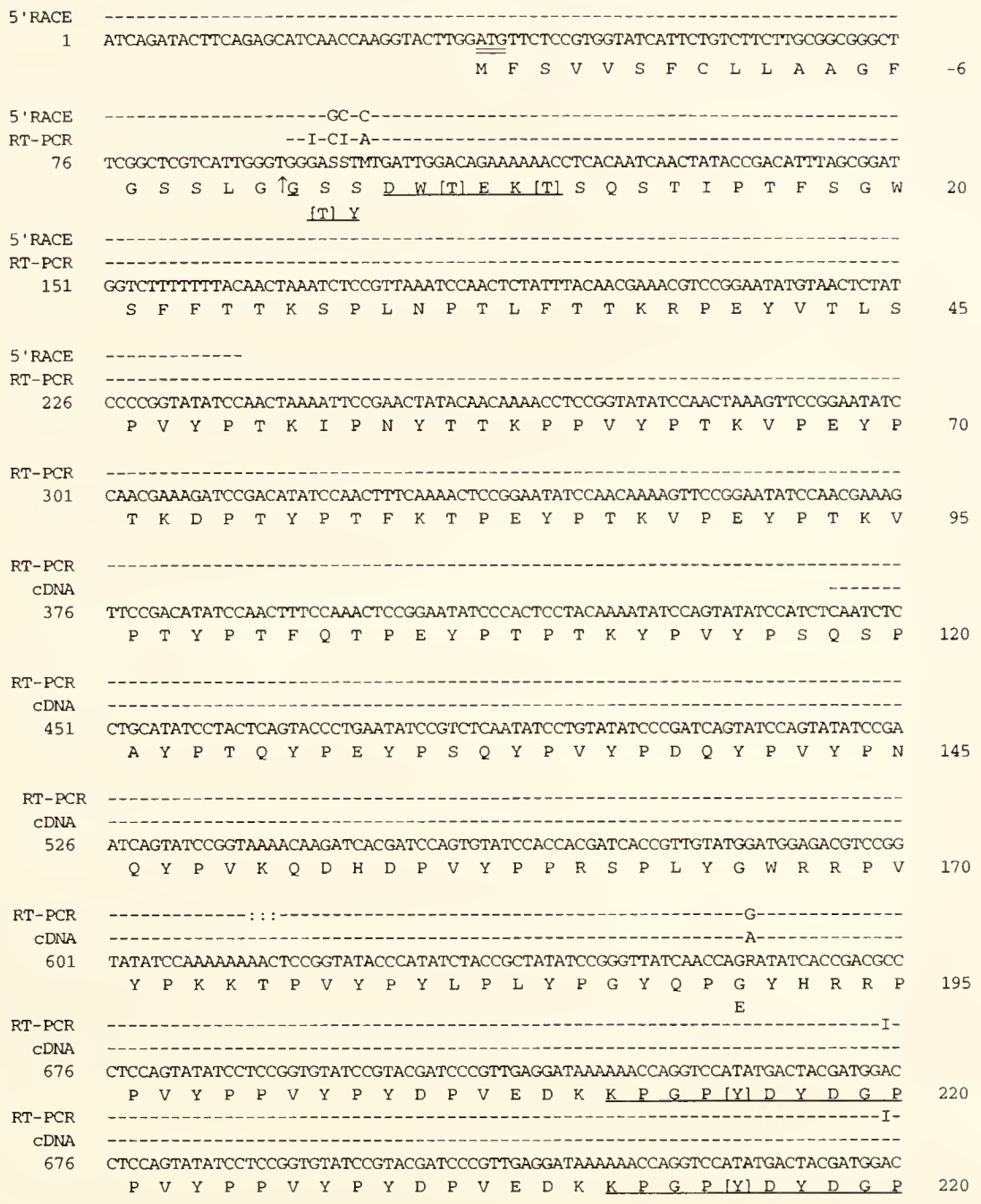
5'RACE
1 ATCAGATACTTCAGAGCATCAACCAAGGTACTTGGATGTTCTCCGTGGTATCATTCTGTCTTCTTGCGGCGGGCT
M F S V V S F C L L A A G F -6
5'RACE
RT-PCR
76 TCGGCTCGTCATTGGGTGGGASSTMTGATTGGACAGAAAAAACCTCACAATCAACTATACCGACATTTAGCGGAT
G S S L G [G] S S D W [T] E K [T] S Q S T I P T F S G W 20
[T] Y
5'RACE
RT-PCR
151 GGTCTTTTTTTACAACTAAATCTCCGTTAAATCCAACTCTATTTACAACGAAACGTCCGGAATATGTAACTCTAT
S F F T T K S P L N P T L F T T K R P E Y V T L S 45
5'RACE
RT-PCR
226 CCCCGGTATATCCAACTAAAATTCCGAACTATACAACAAAACCTCCGGTATATCCAACTAAAGTTCCGGAATATC
P V Y P T K I P N Y T T K P P V Y P T K V P E Y P 70
RT-PCR
301 CAACGAAAGATCCGACATATCCAACTTTCAAAACTCCGGAATATCCAACAAAAGTTCCGGAATATCCAACGAAAG
T K D P T Y P T F K T P E Y P T K V P E Y P T K V 95
RT-PCR
cDNA
376 TTCCGACATATCCAACTTTCCAAACTCCGGAATATCCCACTCCTACAAAATATCCAGTATATCCATCTCAATCTC
P T Y P T F Q T P E Y P T P T K Y P V Y P S Q S P 120
RT-PCR
cDNA
451 CTGCATATCCTACTCAGTACCCTGAATATCCGTCTCAATATCCTGTATATCCCGATCAGTATCCAGTATATCCGA
A Y P T Q Y P E Y P S Q Y P V Y P D Q Y P V Y P N 145
RT-PCR
cDNA
526 ATCAGTATCCGGTAAAACAAGATCACGATCCAGTGTATCCACCACGATCACCGTTGTATGGATGGAGACGTCCGG
Q Y P V K Q D H D P V Y P P R S P L Y G W R R P V 170
RT-PCR
cDNA
601 TATATCCAAAAAAAACTCCGGTATACCCATATCTACCGCTATATCCGGGTTATCAACCAGRATATCACCGACGCC
Y P K K T P V Y P Y L P L Y P G Y Q P G Y H R R P 195
E
RT-PCR
cDNA
676 CTCCAGTATATCCTCCGGTGTATCCGTACGATCCCGTTGAGGATAAAAAACCAGGTCCATATGACTACGATGGAC
P V Y P P V Y P Y D P V E D K [K P G P [Y] D Y D G P 220
RT-PCR
cDNA
676 CTCCAGTATATCCTCCGGTGTATCCGTACGATCCCGTTGAGGATAAAAAACCAGGTCCATATGACTACGATGGAC
P V Y P P V Y P Y D P V E D K [K P G P [Y] D Y D G P 220

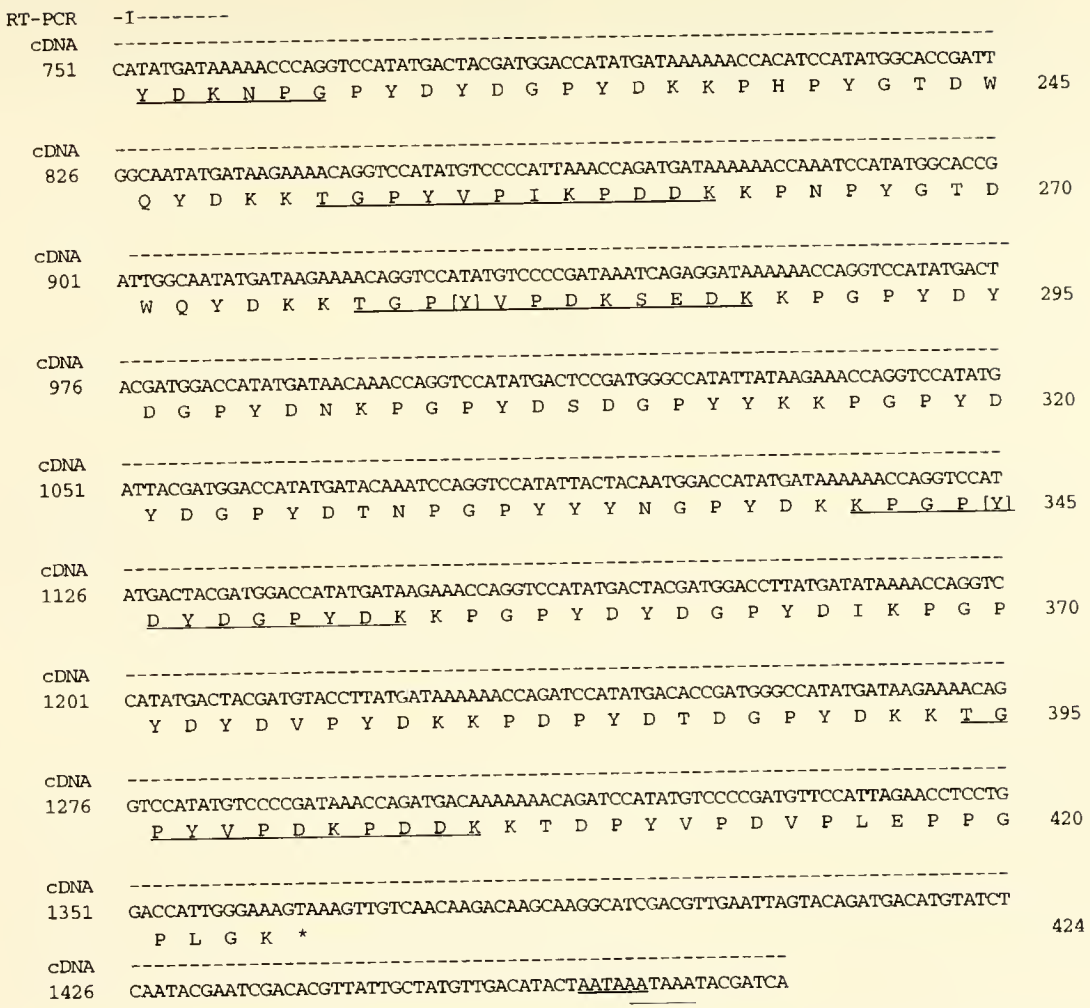

Figure 3. Composite sequence of Dpfp1 obtained by the alignment of sequences derived from 5′ RACE, RT-PCR with degenerate oligonucleotide primers, and the largest partial cDNA clone isolated. Colons (:) are gaps inserted for alignment purposes; dashes (-) indicate agreement with the consensus sequence. Positions coded for by inosine are marked as I. The consensus sequence in these regions reflects the sequence of the non-inosine-containing strand. Underlined nucleotide sequences contain the canonical polyadenylation signal (Kozak, 1986), with doubly underlined nucleotides indicating the position of the start codon. An asterisk (*) indicates a stop codon. The deduced amino acid sequence is presented with residues represented by the single letter code. ↑ indicates predicted cleavage position of signal peptide (von Heijne, 1985; Nielsen *et al.*, 1997). Underlined amino acid residues have been mapped to tryptic peptides from Rzepecki and Waite (1993). Bracketed amino acid residues represent post-translational modifications mapped from Rzepecki and Waite (1993). [T] indicates a glycosylated threonine residue; [Y] represents a Dopa residue in the mature protein.

with some variation, particularly at position #7 of the consensus sequence; however, proline residues at positions #1 and #4 and tyrosine residues at position #3 are highly conserved (Fig. 4). RT-PCR data differ from cDNA clone data in this region of the transcript by omission of threonine 175 and by a G190E substitution resulting from a transversion at nucleotide position 661.

The C-terminal half of Dpfp1 is dominated by the previously reported 13 amino acid consensus sequence: K-P-G-P-Y-D-Y-D-G-P-Y-D-K (Rzepecki and Waite, 1993). This acidic sequence is found tandemly repeated 16 times with only slight variations from the consensus (Fig. 4). The deduced amino acid composition of the composite Dpfp1 sequence, without signal peptide sequence agrees well with that of native Dpfp1 (Table I), suggesting that the composite sequence described above is representative of Dpfp1 mRNAs present in zebra mussel foot tissue. Examination of codon usage for Dpfp1 (Table II) reveals a significant degree of codon bias in amino acids that occur in conserved positions of the above-mentioned consensus sequences (*e.g.*, P, Y, D, K, T, G).

Mass analysis of native Dpfp1

MALDI-TOF analysis of native Dpfp1 indicates that the purified protein is represented by two major mass variants. The lighter of the two variants has a mass $[M + H^+]^+ = 48.6$ kDa, whereas in the heavier variant, $[M + H^+]^+ = 54.5$ kDa. No peaks were detected in the 60–80 kDa range.

Discussion

The primary structure of Dpfp1, deduced from overlapping cDNAs, represents the first complete sequence for a dreissenid byssal protein and an important advance in understanding the attachment strategy of the zebra mussel. Two observations suggest that the composite sequence generated from these data sets is likely to resemble full-length transcripts for Dpfp1. First, the size of the composite sequence (1481 bases) closely matches the size of the largest Dpfp1 transcript as determined by Northern blots of zebra mussel foot tissue mRNA hybridized to a Dpfp1-specific probe. Second, the deduced amino acid

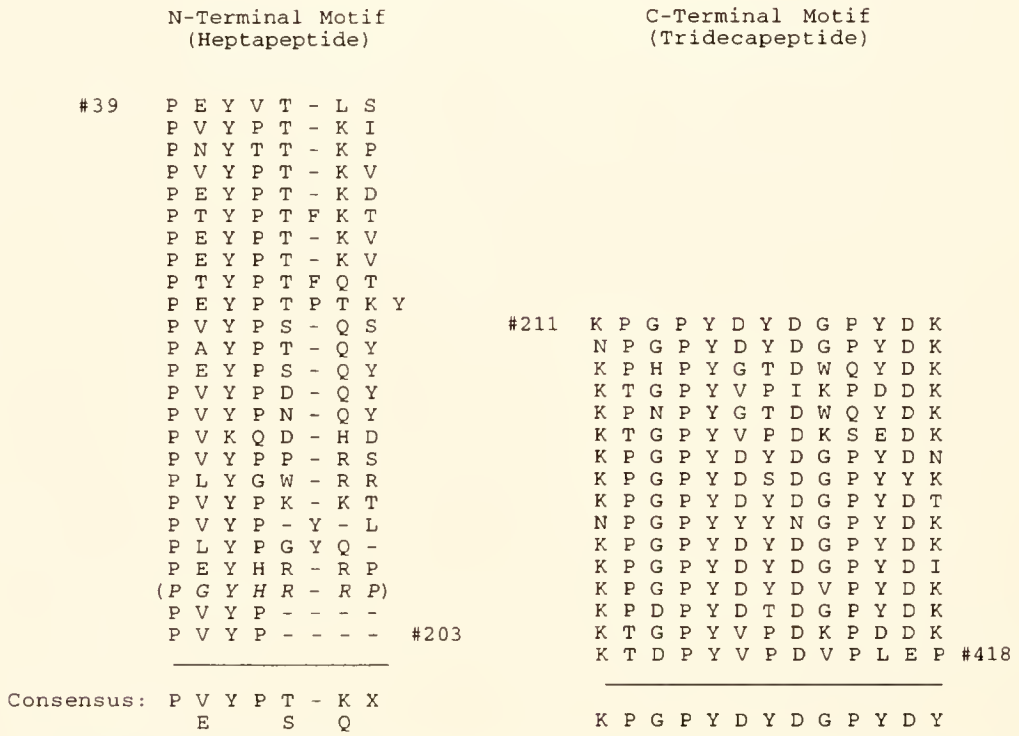

Figure 4. Aligned motifs of Dpfp1. The consensus sequences of Dpfp1 are presented as derived from the tandemly repeating motifs of the deduced primary sequence. The sequences comprising each motif are presented contiguously, and amino acids in the consensus sequence occur in the majority of aligned motifs at their respective positions. Numbers at the beginning and end of each motif represent the position of this sequence within the deduced amino acid sequence for Dpfp1 as presented in Figure 3. The motif in parentheses occurs in RT-PCR derived sequences in place of the preceding cDNA motif. Amino acids are represented by their single letter codes, and a dash (-) indicates a gap inserted for alignment purposes.

Table I

Amino acid composition of deduced and native Dpfp1

Amino acid	Native	Deduced
Asx	136.7	134.8
Thr	75.0	82.7
Ser	34.4	33.1
Glx	70.1	52.0
Pro	238.6	234.0
Gly	76.5	68.6
Ala	7.9	2.4
Val	50.4	52.0
Met	0.7	0.0
Ile	9.9	9.5
Leu	20.4	18.9
Dopa	66.6	N.D.
Tyr	84.5	165.5
Phe	9.6	14.2
His	5.1	7.1
Lys	94.8	99.3
Arg	17.0	14.2
Trp	1.8	11.8
Total:	1000.0	1000.0

The amino acid composition of deduced Dpfp1 is determined excluding signal peptide residues, and that of native Dpfp1 is from Rzepecki and Waite (1993). All values are in residues per thousand residues.

composition of the composite sequence, excluding the signal peptide, closely matches the composition of native Dpfp1 as reported in Rzepecki and Waite (1993).

Purified native Dpfp1 was subjected to MALDI-TOF analysis to resolve the conflict between the apparent and cDNA-deduced mass estimates. SDS-PAGE of native Dpfp1 established that the purified protein migrates as a doublet with apparent molecular masses of 65 and 76 kDa (Rzepecki and Waite, 1993). However, the deduced mass of Dpfp1 of 49 kDa (this work), even allowing for an additional 6.5 kDa contributed by post-translational glycosylation and hydroxylation (Rzepecki and Waite, 1993), is difficult to reconcile with the empirically determined apparent masses. According to MALDI-TOF mass spectrometric analysis, Dpfp1 exists primarily as a doublet (48.6 and 54.5 kDa) with no visible components above 60 kDa. The mass of the larger variant is in excellent agreement with the deduced mass of Dpfp1 after addition of post-translational modifications. The smaller variant may represent unmodified Dpfp1 or possibly a fully modified variant coded for by one of the smaller Dpfp1 transcripts detected during Northern blot analysis of mRNA from zebra mussel foot tissue (Fig. 2). This observation confirms that Dpfp1, like many other byssal precursor proteins (see Coyne *et al.*, 1997; Qin *et al.*, 1997; Taylor *et al.*, 1996; Papov *et al.*, 1995), migrates anomalously during SDS-PAGE.

In previous studies, isoelectric focusing of purified Dpfp1 suggested the presence of at least 10 electrophoretic variants in the polymorphic family (Rzepecki and Waite, 1993). These multiple bands may reflect differences in the primary structure of Dpfp1 variants, nonuniform post-translational modification of one or more forms of the protein, or both. At least some of the variation must arise from differences in primary structure since the N-terminus of Dpfp1 exhibited heterogeneity at two

Table II

Codon usage in Dpfp1

Amino acid	Codon	#	Amino acid	Codon	#	Amino acid	Codon	#	Amino acid	Codon	#
F	TTT	4	L	CTT	2	I	ATT	2	V	GTT	5
F	TTC	5	L	CTC	0	I	ATC	0	V	GTC	4
L	TTA	2	L	CTA	4	I	ATA	2	V	GTA	12
L	TTG	3	L	CTG	0	M	ATG	1	V	GTG	2
S	TCT	6	P	CCT	12	T	ACT	13	A	GCT	0
S	TCC	3	P	CCC	7	T	ACC	4	A	GCC	0
S	TCA	6	P	CCA	58	T	ACA	15	A	GCA	1
S	TCG	1	P	CCG	22	T	ACG	3	A	GCG	2
Y	TAT	57	H	CAT	1	N	AAT	5	D	GAT	39
Y	TAC	12	H	CAC	2	N	AAC	3	D	GAC	9
*	TAA	1	Q	CAA	8	K	AAA	39	E	GAA	9
*	TAG	0	Q	CAG	3	K	AAG	6	E	GAG	2
C	TGT	1	R	CGT	2	S	AGT	0	G	GGT	14
C	TGC	0	R	CGC	1	S	AGC	2	G	GGC	4
*	TGA	0	R	CGA	2	R	AGA	1	G	GGA	11
W	TGG	5	R	CGG	0	R	AGG	0	G	GGG	3

Amino acids are represented by their single letter codes, and an asterisk (*) indicates a stop codon. These data are compiled from the composite sequence of Dpfp1 presented in Figure 3. Where discrepancies exist in the consensus sequence, the cDNA and 5′ RACE data are used to determine codon usage at that position.

positions (#2 and #8, Fig. 3) (Rzepecki and Waite, 1993). The nucleotide sequences presented in Figure 3 suggest the existence of at least two of these variants. Differences between these variants in regions of cDNA overlap are limited to the deletion of a single codon in the RT-PCR data and a single transversion resulting in an amino acid substitution in one of the heptapeptide sequences.

An examination of the codon usage data (Table II) indicates that compositionally dominant amino acids are predominantly coded for by half of the potentially available codons for these residues. This is especially true of proline, tyrosine, aspartic acid, lysine, threonine, and glycine residues, which together account for almost 75% of the amino acid composition of Dpfp1. The pattern of codon bias in compositionally dominant residues has also been noted in other marine byssal precursor proteins—notably Mefp1 (Filpula *et al.*, 1990), Mgfp1 (Inoue and Odo, 1994), Mcfp1 (Inoue *et al.*, 1996b), and, to a lesser extent, Mgfp2 (Inoue *et al.*, 1995)—and may reflect a need to express byssal structural proteins rapidly in response to developmental cues and changing environmental conditions. It is well established that in bacterial systems, codon bias is positively correlated with the rates of gene expression (Robinson *et al.*, 1984; Varenne *et al.*, 1984; Sorensen *et al.*, 1989), presumably through selection of codons that recognize the most abundant isoaccepting tRNAs for a given amino acid. Precedence for this hypothesis can also be found among highly expressed genes in multicellular organisms such as *Drosophila melanogaster*, whose chorion genes, important eggshell components known to be highly expressed during egg development (Kafatos *et al.*, 1987), also exhibit significant codon bias (Akashi, 1994). Such a hypothesis has also been advanced to explain observed codon bias in the highly expressed silk fibroin heavy chain of the silk moth, *Bombyx mori* (Mita *et al.*, 1994).

More than 80% of the deduced primary amino acid sequence of Dpfp1 is composed of tandemly repeated and segregated motifs: one is a heptapeptide; the other, a tridecapeptide consensus motif that coincides with peptides sequenced previously (Rzepecki and Waite, 1993). The occurrence of two relatively short tandemly repeating motifs in Dpfp1 is consistent with its proposed role as a byssal structural protein. However, the absence of data on the distribution of Dpfp1 within the byssus makes it difficult to assign a specific role at this time. The repetitive nature of Dpfp1 is shared by many of the structural proteins of marine byssi. Two of three characterized Dopa-containing byssal proteins in *Mytilus* are known to be composed almost entirely of tandem repeats. Mefp1, a 110-kDa protein thought to play a role as a cuticular lacquer in the byssus of *M. edulis*, is dominated by non-segregated hexa- and decapeptide repeats (Filpula *et al.*, 1990; Waite *et al.*, 1985; Laursen, 1992). Mgfp2, a 49-kDa plaque-specific protein of *M. galloprovincialis*, is largely composed of larger, epidermal growth factor-like repeats (Inoue *et al.*, 1995).

The N-terminal half of Dpfp1 is dominated by a heptapeptide motif that is repeated 22 times with some variation, particularly at position #7 of the consensus sequence. Variability notwithstanding, the spacing of proline and tyrosine residues is well conserved, suggesting that these amino acids play an important functional role in the motif. No tryptic peptides exactly matching the deduced primary sequence could be mapped to this part of the protein; however, a fragment of one tryptic peptide (tryptic peptide #13 in fig. 6 of Rzepecki and Waite, 1993) containing the subsequence S-P-L-Y-G-W . . . is found to bridge two of the heptapeptide repeats. Although the tyrosine in this sequence is efficiently converted to Dopa, the amino acid composition of residual undigested Dpfp1 suggests that, as a whole, this region contains relatively little Dopa (Rzepecki, pers. comm.).

Given the frequency of lysine and arginine in the heptapeptide repeat region, the resistance of the repeat to cleavage by trypsin is intriguing. An examination of the deduced primary sequence indicates that K-P or R-P sequences cannot be the basis for this resistance. Interestingly, lysine and arginine residues in this domain frequently occur adjacent to threonine and serine residues. That observation, coupled with the detection of high levels of threonine and *N*-acetylgalactosamine in partially digested tryptic peptides (Rzepecki and Waite, 1993), leads to the hypothesis that Arg and Lys are protected from trypsin cleavage by adjacent glycosylated amino acids. A similar protection appears to be imparted by glycosylated residues in an extensin-like glycoprotein from *Volvox carteri* (Ertl *et al.*, 1992).

The N-terminal half of Dpfp1 differs significantly from the C-terminal domain with its repeated 13 amino acid motif (Fig. 4). Previous peptide data (Rzepecki and Waite, 1993) and the deduced sequence of Dpfp1 are consistent with the hypothesis that glycosylation is more extensive in the N-terminal region of the protein, whereas hydroxylation of tyrosine to Dopa occurs more frequently in the remaining C-terminal portion. Additionally, the average isoelectric point of Dpfp1 in the region occupied by the heptapeptide is moderately basic (pI = 8.7), whereas the C-terminal domain is quite acidic (pI = 4.7). These divergent characteristics suggest that the segregation of motifs plays a significant role in the architectural design of the zebra mussel byssus. Recently, two byssal structural proteins from *M. edulis* have also been shown to be composed of "block copolymer"-like domains. Both proteins have a central collagenous core flanked by sequences resembling either elastin (Coyne *et al.*, 1997) or silk fibroin (Qin *et al.*, 1997). The distribution of these proteins can

A. Heptapeptide comparisons

Protein	*Consensus Sequence*	*Repeats*	*Ref.*
Dpfp1	P V Y P - T - K - X	22	a
Mefp1	P S Y P P T Y K A K	75	b
Soybean PRP	P V Y - - - - K - P	43	c
Titin PEVK	P V - P - X - K	27	d

a) present data; b) Laursen (1992); c) Hong et al (1987) ; d) Labeit and Kolmerer (1995)

B. Tridecapeptide comparison

Protein	*Consensus Sequence*	*Repeats*	*Ref.*
Dpfp1	K P G P Y D Y D G P Y D K	15	a
Eggshell TRP	Y - G - Y D K Y G - Y D K	27	e

a) present data; e) Wells and Cordingly (1992)

Figure 5. Comparison of the heptapeptide (A) and tridecapeptide (B) motifs of Dpfp1 with a variety of other repetitive proteins. Shaded residues highlight identities; gaps denoted by dashes (-) are included to maximize alignment. X denotes any amino acid residue.

be used to account for the heterogeneous mechanical properties of byssus in *M. edulis* (Qin and Waite, 1995).

Although the consensus motifs of Dpfp1 do not have strong homologies with any known structural proteins, they do share some features with other proteins containing tandem repeats—*i.e.*, marine adhesives (Laursen, 1992), extensin-like proteins from plants (Kieliszewski and Lamport, 1994), and a trematode eggshell protein (Wells and Cordingley, 1992) (Fig. 5). The β-turn (Pro Val) and lysine of the heptapeptide are prominent in extension (soybean PRP) (Hong *et al.*, 1987) and adhesive protein (Waite *et al.*, 1985). In addition, although not a repeating sequence, the PEVK domain of titin, a protein of skeletal muscle, contains at least 27 occurrences of the motif $PVPX_nK$ in which X_n can be from one to three amino acids long (Labeit and Kolmerer, 1995). The tridecapeptide of Dpfp1, in contrast, shares the repeated proximity of YD with a trematode eggshell protein (Wells and Cordingley, 1992), although the latter notably lacks proline (Fig. 5). Curiously, all these proteins have one thing in common: they are significant components of structures that function in tension.

Acknowledgments

We thank Alan Jordan for year-round collections of *D. polymorpha* and the National Sea Grant Program of NOAA for support. Drs. John McDonald and Alison Hunt provided generous assistance with DNA sequencing. Dr. Lesz Rzepecki generously provided samples of native Dpfp1, and Luis Burzio provided assistance and advice regarding analysis of Dpfp1 by mass spectrometry. Research was supported by grants from the National Oceanic and Atmospheric Administration (94-3501-0115) and the Office of Naval Research (N00014-96-1-1205) to JHW. KEA was supported in part by USPHS Grant T32-GM08550. cDNA sequences have been submitted to GenBank (Accession # AF043221; AF043222; AF043223).

Literature Cited

Ackerman, J. D., C. R. Ethier, D. G. Allen, and J. K. Spelt. 1992. Investigation of zebra mussel adhesion strength using rotating disks. *J. Environ. Eng.* **118:** 708–724.

Akashi, H. 1994. Synonymous codon usage in *Drosophila melanogaster:* natural selection and translational accuracy. *Genetics* **135:** 927–935.

Chomczynski, P., and N. Sacchi. 1987. Single-step method of RNA isolation by acid guanidinium thiocyanate-phenol-chloroform extraction. *Anal. Biochem.* **162:** 156–159.

Coyne, K. J., X. X. Qin, and J. H. Waite. 1997. Extensible collagen in mussel byssus—a natural block-copolymer. *Science* **277:** 1830–1832.

Eddington, N. D. 1996. *Partial oligonucleotide sequence of a mussel byssal precursor protein,* Dreissena polymorpha *foot protein 2.* M. S. thesis, University of Delaware, Lewes.

Ertl, H., A. Hallmann, S. Wenz, and M. Sumper. 1992. A novel extensin that may organize extracellular matrix biogenesis in *Volvox carteri*. *EMBO J.* **11:** 2055–2062.

Filpula, D. R., S. M. Lee, R. P. Link, S. L. Strausberg, and R. L. Strausberg. 1990. Structural and functional repetition in a marine mussel adhesive protein. *Biotechnol. Prog.* **6:** 171–177.

Frohman, M. A., M. K. Dush, and G. R. Martin. 1988. Rapid production of full-length cDNAs from rare transcripts: amplification using a single gene-specific oligonucleotide primer. *Proc. Natl. Acad. Sci. USA* **85:** 8998–9002.

Hong, J. C., R. T. Nagao, and J. L. Key. 1987. Characterization and sequence analysis of a developmentally regulated putative cell wall protein gene isolated from soybean. *J. Biol. Chem.* **262:** 8367–8376.

Inoue, K., and S. Odo. 1994. The adhesive protein cDNA of *Mytilus galloprovincialis* encodes decapeptide repeats but no hexapeptide motif. *Biol. Bull.* **186:** 349–355.

Inoue, K., Y. Takeuchi, D. Miki, and S. Odo. 1995. Mussel adhesive plaque protein gene is a novel member of epidermal growth factor-like gene family. *J. Biol. Chem.* **270:** 6698–6701.

Inoue, K., Y. Takeuchi, D. Miki, S. Odo, S. Harayama, and J. H. Waite. 1996a. Cloning, sequencing and sites of expression of genes for the hydroxyarginine-containing adhesive-plaque protein of the mussel *Mytilus galloprovincialis*. *Eur. J. Biochem.* **239:** 172–176.

Inoue, K., Y. Takeuchi, S. Takeyama, E. Yamaha, F. Yamazaki, S. Odo, and S. Harayama. 1996b. Adhesive protein cDNA sequence of the mussel *Mytilus coruscus* and its evolutionary implications. *J. Mol. Evol.* **43:** 348–356.

Johnson, L. E., and D. K. Padilla. 1996. Geographic spread of exotic species: ecological lessons and opportunities from the invasion of the zebra mussel *Dreissena polymorpha*. *Biol. Conserv.* **78:** 23–33.

Kafatos, F. C., N. Spoerel, S. A. Mitsialis, H. T. Nguyen, C. Ramano, J. R. Lingappa, B. D. Mariani, G. C. Rodakis, R. Leganidou, and S. G. Tsitilou. 1987. Developmental control and evolution in the chorion gene families of insects. *Adv. Genet.* **24:** 223–242.

Kieliszewski, M. J., and D. T. A. Lamport. 1994. Extensin: repetitive motifs, functional sites, post-translational codes, and phylogeny. *Plant J.* **5:** 157–172.

Kozak, M. 1986. Point mutations define a sequence flanking the AUG initiator codon that modulates translation by eukaryotic ribosomes. *Cell* **44:** 283–292.

Labeit, S., and B. Kolmerer. 1995. Titins: giant proteins in charge of muscle ultrastructure and elasticity. *Science* **270:** 293–296.

Laursen, R. A. 1992. Reflections on the structure of mussel adhesive proteins. Pp. 55–74 in *Structure, Cellular Synthesis and Assembly of Biopolymers*, S. T. Case, ed. Springer Verlag, Berlin.

Mita, K., S. Ichimura, and T. C. James. 1994. Highly repetitive structure and its organization of the silk fibroin gene. *J. Mol. Evol.* **38:** 583–592.

Nielsen, H., J. Engelbrecht, S. Brunak, and G. von Heinjne. 1997. Identification of prokaryotic and eukaryotic signal peptides and prediction of their cleavage sites. *Protein Eng.* **10:** 1–6.

Papov, V. V., T. V. Diamond, K. Biemann, and J. H. Waite. 1995. Hydroxyarginine-containing polyphenolic proteins in the adhesive plaques of the marine mussel *Mytilus edulis*. *J. Biol. Chem.* **270:** 20183–20192.

Patwary, M. U., M. E. Reith, and E. L. Kenchington. 1996. Isolation and characterization of a cDNA encoding an actin gene from sea scallop (*Placopecten magellanicus*). *J. Shellfish Res.* **15:** 265–271.

Qin, X. X., and J. H. Waite. 1995. Exotic collagen gradients in the byssus of the mussel *Mytilus edulis*. *J. Exp. Biol.* **198:** 633–644.

Qin, X. X., K. J. Coyne, and J. H. Waite. 1997. Tough tendons: mussel byssus has collagen with silk-like domains. *J. Biol. Chem.* **272:** 32623–32627.

Roberts, L. 1990. Zebra mussel invasion threatens U.S. waters. *Science* **249:** 1370–1372.

Robinson, M., R. Lilley, S. Little, J. S. Emtage, G. Yamamoto, P. Stephens, A. Millican, M. Eaton, and G. Humphreys. 1984. Codon usage can affect efficiency of translation of genes in *Escherichia coli*. *Nucleic Acids Res.* **12:** 6663–6671.

Rzepecki, L. M., and J. H. Waite. 1993. The byssus of the zebra mussel, *Dreissena polymorpha*. II: structure and polymorphism of byssal polyphenolic protein families. *Mol. Mar. Biol. Biotechnol.* **2:** 267–279.

Sambrook, S., E. F. Fritsch, and T. Maniatis. 1989. *Molecular Cloning: A Laboratory Manual.* Cold Spring Harbor Laboratory Press, Cold Spring Harbor, NY.

Sorensen, M. A., C. G. Kurland, and S. Pedersen. 1989. Codon usage determines translation rate in *Escherichia coli*. *J. Mol. Biol.* **207:** 365–377.

Taylor, S. W., D. B. Chase, M. H. Emptage, M. J. Nelson, and J. H. Waite. 1996. Ferric ion complexes of DOPA-containing adhesive protein from *Mytilus edulis*. *Inorg. Chem.* **35:** 7572–7577.

Varenne, S. J., J. Buc, R. Lloubes, and C. Lazdunski. 1984. Translation is a non-uniform process. Effect of tRNA availability on the rate of elongation of nascent polypeptide chains. *J. Biol. Chem.* **180:** 549–576.

von Heijne, G. 1985. Signal sequences: the limits of variation. *J. Mol. Biol.* **184:** 99–105.

Waite, J. H. 1990. The phylogeny and chemical diversity of quinone-tanned glues and varnishes. *Comp. Biochem. Physiol.* **97B:** 19–29.

Waite, J. H., T. J. Housley, and M. L. Tanzer. 1985. Peptide repeats in a mussel glue protein: theme and variation. *Biochemistry* **24:** 5010–5014.

Wells, K. E., and J. S. Cordingley. 1992. The cell and molecular biology of eggshell formation in *Schistosoma mansoni*. Pp. 97–114 in *Structure, Cellular Synthesis and Assembly of Biopolymers*, S. T. Case, ed. Springer Verlag, Berlin.

Reference: *Biol. Bull.* **194:** 161–169. (April, 1998)

Ion Transport in the Freshwater Bivalve *Corbicula fluminea*

HUIYUAN ZHENG AND THOMAS H. DIETZ

Department of Biological Sciences, Louisiana State University, Baton Rouge, Louisiana 70803

Abstract. In freshwater bivalves such as the mussel *Corbicula fluminea,* uptake of chloride depends on the external concentration of the chloride ion. In *C. fluminea,* Cl^- uptake displayed saturation kinetics both in animals acclimated to pondwater and in those subjected to salt depletion by storage in deionized water. The transport capacity (J_{max}) was 7.00 ± 0.51 μeq g^{-1} dry tissue h^{-1} and the transport affinity (K_m) was 0.21 ± 0.08 m*M* in animals acclimated to pondwater. Animals subjected to salt depletion had a higher rate of Cl^- uptake than did animals acclimated to pondwater. After 4 weeks in deionized water, the longer the animals were salt-depleted, the higher their rate of Cl^- uptake. Na^+ and Cl^- transport were independent in pondwater-acclimated *C. fluminea.* For salt-depleted animals, Cl^- transport was Na^+-independent, but Na^+ transport depended partially on external Cl^-. Serotonin stimulated Cl^- and Na^+ transport in pondwater-acclimated animals by increasing influx while having little influence on efflux. Acetazolamide increased the Cl^- and Na^+ efflux of salt-depleted animals. Both serotonin and acetazolamide elevated the net loss of titratable base.

Introduction

Freshwater bivalves have the same osmoregulatory problems as do other freshwater animals. They must accumulate salts from the dilute environment to compensate for the loss of solutes by diffusion and excretion. *Corbicula fluminea* (Müller) belongs to the family Corbiculidae and is a relatively recent invader of fresh water (Keen and Casey, 1969). It has a different blood ionic profile than the unionid clams (Dietz, 1979; McCorkle and Dietz, 1980; Byrne *et al.,* 1989), a family that invaded fresh water millions of years earlier (Keen and Casey, 1969). Na^+ and Cl^- are the most important ions in the hemolymph of *C. fluminea,* accounting for 80%–90% of the total hemolymph solutes, compared to only about 60%–65% in unionids.

The rate of ion uptake in freshwater bivalves depends on the external ion concentration. Transport processes exhibit saturation kinetics in the freshwater bivalves that have been studied (Dietz, 1978; Dietz and Branton, 1979; McCorkle and Dietz, 1980; Dietz and Byrne, 1990; Dietz and Hagar, 1990; Wilcox and Dietz, 1995). In unionid clams, the transport capacity for Na^+, Cl^-, or K^+ is 1–2 μeq g^{-1} dry tissue h^{-1}, with a transport affinity of about 0.1 to 0.2 m*M* (Dietz, 1978; Dietz and Branton, 1979; Dietz and Byrne, 1990; Dietz and Hagar, 1990).

Blood osmolality is higher in *C. fluminea* than in the unionids (Dietz, 1979; McCorkle and Dietz, 1980; Byrne *et al.,* 1989), and the rate of ion transport is faster. Studies of Na^+ transport have shown that the transport capacity of *C. fluminea* is about 13 μeq g^{-1} dry tissue h^{-1}, or about 10 times the rate found in the unionid *Toxolasma (Carunculina) texasensis* (Dietz, 1978; McCorkle and Dietz, 1980). Potassium transport capacity in *C. fluminea* is twice that of unionids (Dietz and Byrne, 1990). The hemolymph Cl^- and Na^+ regulation of *C. fluminea* has been studied recently (Byrne and Dietz, 1997), but transport kinetics have not been reported.

The Na^+-independence of Cl^- uptake has been shown in many invertebrate and vertebrate species (Krogh, 1939; Romeu *et al.,* 1969; Stobbart, 1971; Kerstetter and Kirschner, 1972; Alvarado *et al.,* 1975; Lee and Pritchard, 1985). In the freshwater mussels that have been studied, Na^+ and Cl^- transport are independent and Cl^- uptake is thought to be *via* a Cl^-/HCO_3^- exchange pathway (Murphy and Dietz, 1976; Dietz, 1978, 1985; Dietz and Branton, 1979; Dietz and Findley, 1979; Scheide and Dietz, 1982; Henry and Saintsing, 1983).

Received 22 April 1997; accepted 22 September 1997.

In this study, we characterize the transport kinetics of Cl^- and demonstrate that Na^+ transport is partially Cl^--dependent in salt-depleted *C. fluminea*. Both salt depletion and serotonin stimulate Cl^- influx in *C. fluminea*.

Materials and Methods

Animals

Specimens of *Corbicula fluminea* were collected, under permit, from the Tangipahoa River in Mississippi. The animals were acclimated to aerated artificial pondwater (PW) containing (in m*M*) 0.5 NaCl, 0.4 $CaCl_2$, 0.2 $NaHCO_3$, and 0.05 KCl at 22°–25°C for at least 1 week before use. Salt-depleted (SD) clams were obtained by storing the animals in deionized water for at least 14 days. The deionized water was changed daily for the first 2 weeks and every other day for the rest of the salt-depletion period (McCorkle and Dietz, 1980).

Ion analysis

The animals were rinsed for about 30 min in deionized water and transferred to individual beakers with appropriate bathing medium containing either $^{36}Cl^-$ or $^{22}Na^+$. For the experiments in which the net flux of titratable base was measured, Tris (tris(hydroxymethyl)aminomethane) was added into the bathing medium at a final concentration of 0.1 m*M*, and the pH was adjusted to 7.3 with Tris-HCl for either PW or Na^+-free PW, and with Tris-H_2SO_4 for Cl^--free solutions. Choline was used to replace Na^+ in Na^+-free bathing medium, and sulfate was used to replace Cl^- in Cl^--free bathing medium. An initial (time zero) bath sample was taken after the clams began siphoning (within 10 to 15 min), with the second sample taken 2 h after time zero. Cl^- concentration in the bath samples was determined by electrometric titration, and the Na^+ concentration was assayed by flame photometry. To measure the net loss of titratable base (J_n^B), samples were sonicated to remove respiratory CO_2. The samples were titrated to pH 4.5 with standardized 5 m*M* HCl, and the difference between initial and final buffer capacity was used to calculate net base production (Dietz and Branton, 1979).

Ion transport

Unidirectional influx (J_i) was calculated from the disappearance of isotope (specific activity for $^{22}Na^+$ or $^{36}Cl^-$ was 2000 to 3000 CPM/μM) from the bathing medium, as previously described (Dietz, 1978; Graves and Dietz, 1982). Radioactivity was assayed with a liquid scintillation counter using cocktail based on Triton X-114/xylene (Wiegman *et al.*, 1975). Net flux (J_n) was estimated from the changes in bath ion concentration and normalized to g^{-1} dry weight h^{-1} (Dietz, 1978). To minimize the back flux of isotope, the bath volume was small (30 ml) to allow rapid changes in the radioactivity of the bath with limited isotope accumulating in the body fluids (Dietz, 1978).

In the study of Cl^- transport kinetics, the unidirectional Cl^- influx (J_i^{Cl}) was determined by a modification of the conventional methods described above. Because of the lack of sensitivity of the Cl^- titrator, the Cl^- net flux cannot be accurately measured if the Cl^- concentration is less than 0.2 m*M*. This problem can be overcome by using a modified procedure, in which Cl^- influx is determined from the change in $^{36}Cl^-$ in the bath divided by $^{36}Cl^-$ specific activity and normalized to grams of dry tissue. The bath Cl^- concentration was measured in the initial stock solution and dilutions were assumed to have the same specific activity. We measured Cl^- fluxes over the concentration range of 0.13 m*M* to 12.00 m*M*. To compare the two methods for determining Cl^- influx, we calculated fluxes for animals exposed to six different Cl^- concentrations and found no significant differences between these two data sets ($P > 0.25$). The agreement between these two rather independent estimates of Cl^- influx thus validates our methods.

Administration of drugs

Serotonin (5-hydroxytryptamine, 5HT) was added directly to the bathing medium at a final concentration of 0.1 m*M*. The pH of the solution was adjusted to 7.3 with NaOH after the addition of 5HT. Serotonin has been shown to stimulate Na^+ and Cl^- uptake in other freshwater bivalves (see Dietz *et al.*, 1982; Horohov *et al.*, 1992). Acetazolamide (N-(5-sulfamoyl-1,3,4-thiadiazol-2-yl)-acetamide, AZ) has been shown to alter ion fluxes in bivalves (see Henry and Saintsing, 1983). AZ was dissolved in bathing medium, and the animals were immersed in the solution at a final AZ concentration of 0.5 m*M* for 12 h before the experiments. No AZ was added to bathing medium during the flux measurement.

Statistics

Data were expressed as mean ± standard error. In the study of Cl^- transport kinetics, a rectangular hyperbolic function was chosen to fit the data (Inplot), and the Student's *t*-test was employed to examine the differences between the parameters of the function. In the studies of Cl^- and Na^+ flux relationships, we employed a two-level factorial experimental design. These data were analyzed with SAS using a general linear model or a linear regression model. Differences were considered to be significant if the corresponding *P* value was equal to or less than 0.05.

Results

Chloride transport kinetics

The rate of unidirectional Cl^- influx was dependent on the external Cl^- concentration for both pondwater-acclimated (PWA) and salt-depleted (SD) *C. fluminea* (Fig. 1). When exposed to a range of NaCl concentrations, both PWA and SD animals displayed saturation kinetics. The Cl^- uptake rate in PWA *C. fluminea* can be described by a Michaelis-Menten rectangular hyperbolic function ($R > 0.95$) with the maximum Cl^- influx being the transport capacity (J_{max}) and the Cl^- concentration at half of the J_{max} representing the transport affinity (K_m). The J_{max} for PWA animals was 7.46 ± 0.94 μeq g^{-1} dry tissue h^{-1} and the K_m was 0.22 ± 0.15 m*M*. The Cl^- influx in animals subjected to 2 weeks of salt depletion overlapped with that of PWA animals, and there was no significant difference between the two groups ($P > 0.25$). The hemolymph Cl^- and Na^+ concentrations in animals subjected to 2 weeks of salt depletion were 20.2 ± 0.20 m*M* and 26.2 ± 0.31 m*M*, respectively. There was no statistical difference in the Cl^- and Na^+ concentrations from PWA *C. fluminea* stored in the lab for the same period of time (20.9 ± 0.48 m*M* and 26.5 ± 0.31 m*M* for Cl^- and Na^+, respectively, n = 25–30, $P > 0.1$). Therefore, both data sets were combined to represent the Cl^- uptake kinetics for PWA animals. This combined transport capacity and the corresponding transport affinity were calculated to be 7.00 ± 0.51 μeq g^{-1} dry tissue h^{-1} and 0.21 ± 0.08 m*M*, respectively.

Salt depletion of 4 weeks or longer resulted in the elevation of unidirectional Cl^- uptake and a significant ($P < 0.01$) reduction in hemolymph Cl^- and Na^+ concentrations (17.1 ± 0.23 m*M* and 22.5 ± 0.19 m*M* for Cl^- and Na^+ after 4 weeks of SD, respectively, n = 25–30). The Cl^- influx of the animals subjected to salt depletion for 4 weeks or longer was consistently higher than that of the PWA animals for all Cl^- concentrations tested. Compared to PWA animals, 4-week SD animals had an estimated increase in maximal Cl^- influx (J_{max} = 10.85 ± 0.91 μeq g^{-1} dry tissue h^{-1}) of about 50%, and 8-week SD animals had about an 85% increase (J_{max} = 13.49 ± 0.16 μeq g^{-1} dry tissue h^{-1}). Animals subjected to 8 weeks of salt depletion exhibited higher net Cl^- uptake rates than those found in animals salt-depleted for 4 weeks. Although the increase of the transport capacity in SD animals was substantial, the transport affinity for Cl^- was not changed significantly.

The relationship between Cl^- and Na^+ transport and the effects of 5HT on PWA animals

Chloride transport was not affected by the absence of external Na^+ but was significantly stimulated by 5HT in PWA *C. fluminea* (Table I). With 5HT in the bath, animals displayed active siphoning, valve gaping, and extension of the foot as noted in other bivalves (Scheide and Dietz, 1984). Serotonin significantly increased influx and net flux of Cl^- with little change in efflux compared to control *Corbicula*. Cl^- net flux increased about 3.2 and 3.1 μeq g^{-1} dry tissue h^{-1} and influx about 2.0 and 2.3 μeq g^{-1} dry tissue h^{-1} in PW and Na^+-free PW bathing medium, respectively. No statistical interactions were found between external Na^+ and 5HT (Na^+/5HT), suggesting that the effect of 5HT on Cl^- transport was independent of Na^+.

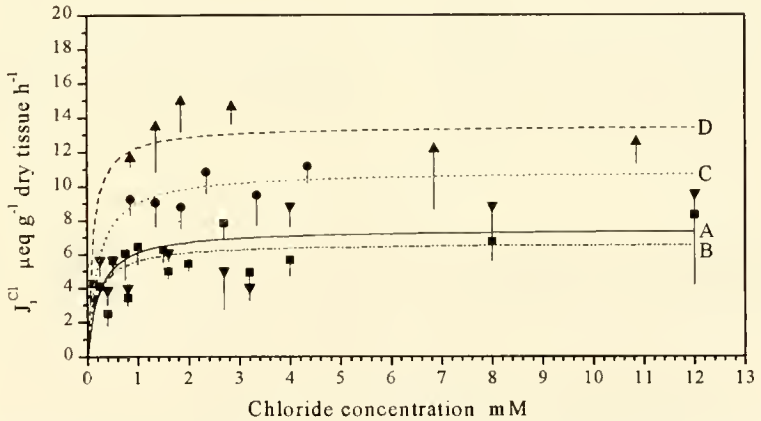

Figure 1. Effects of Cl^- concentration on the average unidirectional Cl^- influx in pondwater-acclimated (PWA) and salt-depleted (SD) *Corbicula fluminea*. Each point represents the mean and standard error of measurements for 5 animals. Down triangles (A): PWA animals, J_{max} = 7.46 ± 0.94 μeq g^{-1} dry tissue h^{-1}, K_m = 0.22 ± 0.15 m*M*; Squares (B): SD for 2 weeks, J_{max} = 6.63 ± 0.59 μeq g^{-1} dry tissue h^{-1}, K_m = 0.18 ± 0.10 m*M*; Circles (C): SD for 4 weeks, J_{max} = 10.85 ± 0.91 μeq g^{-1} dry tissue h^{-1}, K_m = 0.20 ± 0.17 m*M*; Up triangles (D): SD for 8 weeks, J_{max} = 13.49 ± 1.06 μeq g^{-1} dry tissue h^{-1}, K_m = 0.10 ± 0.12 m*M*.

Table I

The effects of serotonin (5HT) and external Na^+ on Cl^- transport and net flux of titratable base in pondwater-acclimated Corbicula fluminea; *5HT was added to the bathing solution at a final concentration of 0.1 m*M

	$+Na^+$		$-Na^+$		*F*-test		
Flux	−5HT	+5HT	−5HT	+5HT	$\pm Na^+$	±5HT	Na^+/5HT
J_n^{Cl}	−1.70 ± 0.63	1.45 ± 0.59	−2.44 ± 0.48	0.70 ± 0.93		**	
J_i^{Cl}	2.07 ± 0.30	4.07 ± 0.35	1.91 ± 0.37	4.23 ± 0.55		**	
J_o^{Cl}	3.77 ± 0.81	2.62 ± 0.82	4.35 ± 0.69	3.53 ± 0.87			
J_n^{B}	−1.78 ± 0.39	−4.19 ± 0.46	−2.51 ± 0.51	−5.73 ± 0.52	*	**	

Data are means and standard errors of measurements for 10 animals and are expressed as μeq g^{-1} dry tissue h^{-1}. J_n, net flux; J_i, influx; J_o, efflux; superscripts denote flux as either for chloride (Cl) or for titratable base (B). *: $P < 0.05$, **: $P < 0.01$. Na^+/5HT: interaction between Na^+ and 5HT.

The effect of 5HT on Na^+ transport was similar to that of Cl^- transport (Table II). Serotonin increased Na^+ net flux 2.7 and 2.4 μeq g^{-1} dry tissue h^{-1}, and influx 2.3 and 1.6 μeq g^{-1} dry tissue h^{-1} in PW and Cl^--free PW, respectively. Na^+ transport was not affected by the absence of external Cl^-. There were no statistical interactions between external Cl^- and 5HT (Cl^-/5HT), indicating that the effect of 5HT on Na^+ transport was not dependent on external Cl^-.

The loss of titratable base was significantly elevated by 5HT, but was independent of the external Na^+ or Cl^-, as indicated by the lack of effect of interactions between external Cl^- or Na^+ and 5HT (Tables II and III). Serotonin increased the net flux of base by about 1.5 μeq g^{-1} dry tissue h^{-1} and 1.6 μeq g^{-1} dry tissue h^{-1} in the presence and absence of external Cl^-, respectively. The absence of Na^+ caused a significant increase in the net loss of base. Increased loss of base was consistently observed in the absence of external Na^+ regardless of treatment with 5HT (0.73 μeq g^{-1} dry tissue h^{-1} increase in control animals and 1.54 μeq g^{-1} dry tissue h^{-1} in 5HT treated animals).

Although Cl^- and Na^+ uptakes were not directly dependent upon each other in PWA *C. fluminea*, as indicated by Tables I and II, a regression of paired Cl^- and Na^+ net fluxes revealed a significant linear relationship (Fig. 2), in which a higher Cl^- net flux correlated with a higher Na^+ net flux ($R = 0.84$; $P < 0.01$).

The relationship between Cl^- and Na^+ transport and the effects of AZ on SD animals

To study the effects of AZ on Cl^- and Na^+ transport, we used SD *C. fluminea* to increase the basal rate of Cl^- and Na^+ uptake. Studies with PWA animals were variable, and it was common to observe no effect of AZ on ion transport (data not shown). As shown in Table III, AZ was an effective inhibitor of net Cl^- transport in SD *C. fluminea*. AZ pre-treatment resulted in a significant reduction of Cl^- net flux by increasing Cl^- efflux. The increase of Cl^- efflux induced by AZ was 3.1 μeq g^{-1} dry tissue h^{-1} in the presence of Na^+ and 6.0 μeq g^{-1} dry tissue h^{-1} in the absence of Na^+. AZ exerted greater effects on Cl^- efflux when there was no Na^+ in the bathing medium, as indicated by the significant interaction effect between external Na^+ and AZ (Table III).

Table II

The effects of serotonin (5HT) and external Cl^- on Na^+ transport and net flux of titratable base in pondwater-acclimated Corbicula fluminea; *5HT was added to the bathing solution at a final concentration of 0.1 m*M

	$+Cl^-$		$-Cl^-$		*F*-test		
Flux	−5HT	+5HT	−5HT	+5HT	$\pm Cl^-$	±5HT	Cl^-/5HT
J_n^{Na}	1.31 ± 0.53	4.05 ± 0.33	1.43 ± 0.69	3.79 ± 0.51		**	
J_i^{Na}	5.88 ± 0.68	8.21 ± 0.29	5.95 ± 0.47	7.57 ± 0.86		**	
J_o^{Na}	4.57 ± 0.34	4.16 ± 0.17	4.52 ± 0.30	3.78 ± 0.44			
J_n^{B}	−2.72 ± 0.51	−4.18 ± 0.54	−2.23 ± 0.55	−3.82 ± 0.68		**	

Data are means and standard errors of measurements for 10 animals and are expressed as μeq g^{-1} dry tissue h^{-1}. J_n, net flux; J_i, influx; J_o, efflux; superscripts denote flux as either for sodium (Na) or for titratable base (B). *: $P < 0.05$, **: $P < 0.01$. Cl^-/5HT: interaction between Cl^- and 5HT.

Table III

The effects of acetazolamide (AZ) and external Na^+ on Cl^- transport and net flux of titratable base in salt-depleted Corbicula fluminea; *the animals were pre-treated for 12 h before the experiments with AZ added to the bathing solution at a final concentration of 0.5 mM (No AZ was added to the bathing solution during the experiments)*

	+Na^+		−Na^+		*F*-test		
Flux	−AZ	+AZ	−AZ	+AZ	±Na^+	±AZ	Na^+/AZ
J_n^{Cl}	3.89 ± 1.18	2.17 ± 0.88	4.46 ± 0.77	1.73 ± 0.59		*	
J_i^{Cl}	6.41 ± 1.07	7.77 ± 0.68	5.27 ± 0.57	8.55 ± 0.60		**	
J_o^{Cl}	2.52 ± 0.62	5.60 ± 0.89	0.81 ± 0.51	6.82 ± 0.73		**	*
J_n^{B}	−6.95 ± 1.37	−10.83 ± 1.08	−5.65 ± 0.69	−8.83 ± 0.48		**	

Data are means and standard errors of measurements for 10 animals and are expressed as μeq g^{-1} dry tissue h^{-1}. J_n, net flux; J_i, influx; J_o, efflux; superscripts denote flux as either for chloride (Cl) or for titratable base (B). *: $P < 0.05$, **: $P < 0.01$. Na^+/AZ: interaction between Na^+ and AZ.

Na^+ efflux was also elevated by AZ—by about 1.8 μeq g^{-1} dry tissue h^{-1} in the presence of external Cl^- and 3.6 μeq g^{-1} dry tissue h^{-1} in the absence of external Cl^- (Table IV). Net flux remained unchanged owing to the small but significant increase in Na^+ influx by AZ treatment.

Unlike PWA *C. fluminea*, in which Cl^- and Na^+ transport were independent as described above, the Cl^- and Na^+ transport in SD animals appeared to be more interrelated (Table IV). Although Cl^- uptake was Na^+-independent in SD *C. fluminea*, as indicated by the lack of alteration of Cl^- influx by the absence of external Na^+, Na^+ uptake was significantly reduced by the absence of external Cl^-. With or without exposure to AZ, there was a 3 to 4 μeq g^{-1} dry tissue h^{-1} reduction in Na^+ influx in the absence of external Cl^-, resulting in the significant decrease in the Na^+ net flux. This suggests that the component of Na^+ uptake stimulated by salt depletion is at least partially dependent on the presence of external Cl^-.

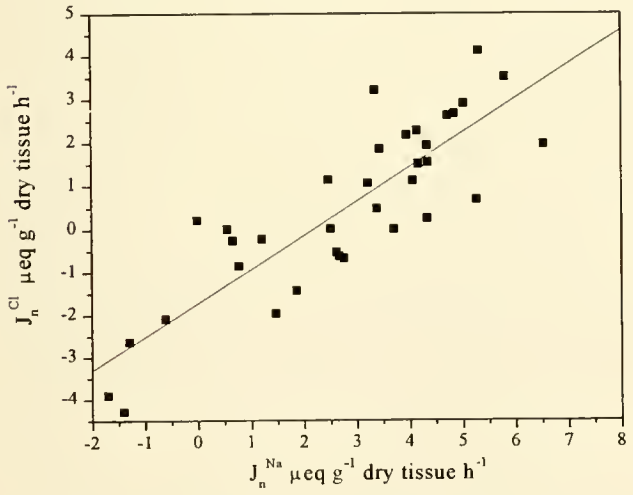

Figure 2. Relationship between net fluxes of Cl^- and Na^+ in pondwater-acclimated *Corbicula fluminea*. J_n, net flux, expressed as μeq g^{-1} dry tissue h^{-1}. $J_n^{Cl} = -1.73 + (0.79)\ J_n^{Na}$, $R = 0.85$, $n = 35$, $P < 0.01$.

As shown in Tables III and IV, the effect of AZ on base net flux was consistent in the two experiments with SD *C. fluminea*. AZ significantly increased the net loss of titratable base. The increase of net base flux was about 4 μeq g^{-1} dry tissue h^{-1} in PW medium, 3.2 μeq g^{-1} dry tissue h^{-1} in Na^+-free bathing medium, and 1.9 μeq g^{-1} dry tissue h^{-1} in Cl^--free bathing medium. No statistical interaction between external Cl^- or Na^+ and AZ was observed, indicating that the net flux of base was not affected by the absence of external Cl^- or Na^+.

In both PWA and SD *C. fluminea*, the net flux of titratable base was not affected by the absence of external Cl^-. However, a regression between Cl^- influx and net flux of base from individual animals demonstrated a significant linear relationship (Fig. 3, $R = 0.78$ and 0.82 for SD and PWA animals, respectively, $P < 0.01$). In all experiments, a greater Cl^- influx correlated with a greater base net flux. The slope of the regression for PWA animals was not statistically different from that of SD animals, suggesting that the relationship between Cl^- influx and base net flux is stoichiometrically similar in both acclimation conditions.

Discussion

The relationship between Cl^- and Na^+ transport in C. fluminea

Na^+ transport in *C. fluminea* may be Cl^--independent or Cl^--dependent, depending on the acclimation conditions. Na^+ transport and the component of Na^+ active uptake stimulated by 5HT were Cl^--independent in PWA (pondwater-acclimated) animals. However, a substantial fraction of Na^+ uptake in SD (salt-depleted) *C. fluminea* depended on the presence of external Cl^-. These data indicate that multiple pathways for Na^+ uptake may exist

Table IV

The effects of acetazolamide (AZ) and external Cl^- on Na^+ transport and net flux of titratable base in salt-depleted Corbicula fluminea; *the animals were pre-treated for 12 h before the experiments with AZ added to the bathing solution at a final concentration of 0.5 mM (no AZ was added to the bathing solution during the experiments)*

	$+Cl^-$		$-Cl^-$		*F*-test		
Flux	−AZ	+AZ	−AZ	+AZ	±Cl	±AZ	Cl/AZ
J_n^{Na}	7.75 ± 0.92	7.18 ± 0.72	5.38 ± 0.90	3.81 ± 0.83	*		
J_i^{Na}	12.33 ± 1.34	13.55 ± 1.12	8.45 ± 1.64	10.49 ± 0.87	*		
J_o^{Na}	4.58 ± 0.50	6.37 ± 0.65	3.07 ± 0.79	6.69 ± 0.82		**	
J_n^{B}	−1.47 ± 0.97	−5.74 ± 0.70	−2.46 ± 1.02	−4.33 ± 0.53		**	

Data are means and standard errors of measurements for 10 animals and are expressed as μeq g^{-1} dry tissue h^{-1}. J_n, net flux; J_i, influx; J_o, efflux; superscripts denote flux as either for sodium (Na) or for titratable base (B). *: $P < 0.05$, **: $P < 0.01$. Cl/AZ: interaction between Cl^- and AZ.

in *C. fluminea*, and that the pathway stimulated by salt depletion is different from that stimulated by 5HT. A Na^+/H^+ exchange mechanism has been considered to be a major pathway for Na^+ uptake in freshwater bivalves including *C. fluminea* (McCorkle and Dietz, 1980; Dietz, 1978, 1985; Henry and Saintsing, 1983; Byrne and Dietz, 1997). However, other Na^+ uptake pathways, such as indirect coupling to the activity of a H^+-translocating-ATPase, may also exist. Recent studies have demonstrated that Na^+ uptake in the gills of freshwater rainbow trout is energized by the electrogenic H^+-ATPase located on the apical membrane of the gill (Lin and Randall, 1995).

Serotonin stimulated the Cl^- influx by increasing the active transport component, presumably a Cl^-/HCO_3^- exchange pathway (see below). The lack of effect of external Na^+ on the stimulation of Cl^- uptake by 5HT suggests that the active uptake of Cl^- in *C. fluminea* is a Na^+-independent Cl^-/HCO_3^- exchange. Salt-depletion was reported to stimulate the activity of carbonic anhydrase (CA) in the gills of *C. fluminea* (Henry and Saintsing, 1983). The increased amount of HCO_3^- synthesized due to the CA activity may stimulate a Cl^-/HCO_3^- exchange pathway directly or indirectly by providing more HCO_3 ion. Independent transport of Cl^- and Na^+ is common in freshwater mussels (Dietz, 1978; Dietz and Branton, 1979; Dietz and Hagar, 1990). In this respect, PWA *C. fluminea* is similar to other freshwater bivalves studied.

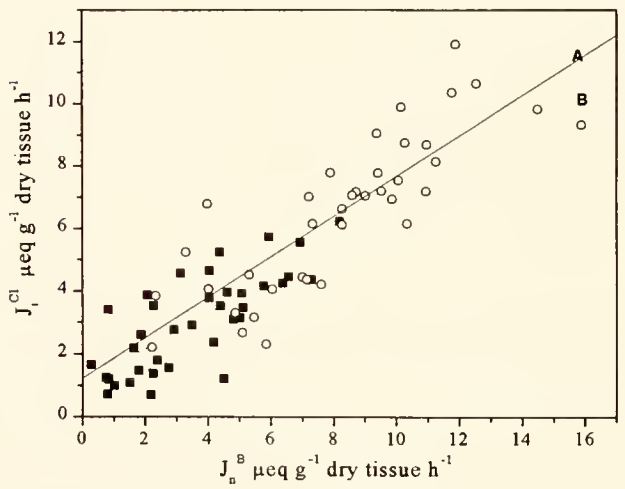

Figure 3. Relationship between Cl^- influx and net loss of titratable base in pondwater-acclimated (PWA) and salt-depleted (SD) *Corbicula fluminea*. (A) Open circle, SD animals, $J_i^{Cl} = 1.04 + (0.56)\ J_n^{B}$, $R = 0.77$, $n = 37$, $P < 0.01$. (B) Solid square, PWA animals, $J_i^{Cl} = 1.98 + (0.65)\ J_n^{B}$, $R = 0.82$, $n = 38$, $P < 0.01$. J_n, net flux, expressed as μeq g^{-1} dry tissue h^{-1}. The slopes of two lines (A = 0.65 ± 0.07; B = 0.56 ± 0.08) were not significantly different.

The effect of 5HT on ion transport in C. fluminea

The effects of 5HT on Cl^- transport in this study are similar to the results reported by Byrne and Dietz (1997). Cyclic AMP and other tested agents had no apparent effect on Cl^- net flux in *Toxolasma texasensis* and *Ligumia subrostrata* (Scheide and Dietz, 1986). Since the 5HT-stimulated Cl^- uptake was independent of external Na^+, 5HT must exert its effect directly on Cl^- uptake rather than indirectly by stimulating Na^+ uptake.

Chloride/bicarbonate exchange is an important mechanism for Cl^- uptake in the freshwater bivalves that have been studied. Stimulation of ATPase activity by chloride and HCO_3 has been demonstrated in the microsomal membranes of the gills of unionid mussel *Toxolasma texasensis* (Dietz and Findley, 1979). The highly significant correlation between Cl^- influx and the net flux of titratable base in both PWA and SD *C. fluminea* in this study also suggests the importance of this exchange mechanism in Cl^- uptake. In PWA *C. fluminea*, the active uptake component *via* Cl^-/HCO_3^- exchange and the exchange diffusion through Cl^-/Cl^- turnover both potentially contributes to total Cl^- isotope turnover. The exchange diffusion pathway was demonstrated to be important for the movement of $^{22}Na^+$ isotope in *C. fluminea* (McCorkle and

Dietz, 1980). However, exchange diffusion of Cl^- was not significant in *C. fluminea*, because 5HT significantly increased Cl^- influx and net flux with no change in Cl^- efflux. In this study we observed a stoichiometric Cl^-/HCO_3^- exchange (Fig. 3) and the small but consistent decrease of average net base flux in the absence of external Cl^- (Table II).

The stimulation of net flux of titratable base by 5HT has not been reported previously in freshwater bivalves. In this study, the net flux of titratable base was measured by determining the amount of exogenous acid required to titrate the base in the bathing solution. However, the amount of exogenous acid required can be affected by the amount of endogenous proton released from the bivalve into the bathing solution. Therefore, the net change of titratable base reflects the combined results of the activities of Cl^-/HCO_3^- exchanger, Na^+/H^+ antiporter, and H^+-ATPase in renal and extrarenal (gills) tissue. The stimulation of Na^+ uptake may extrude more protons, presumably through Na^+/H^+ antiporter or H^+-pump (or both), that would autotitrate the base in the bathing solution. The activation of Cl^- uptake would elevate the amount of base in the medium *via* Cl^-/HCO_3^- exchanger. In PWA *C. fluminea*, 5HT significantly increased the net flux of titratable base, and the increase was enhanced when Na^+ was not present in the bathing medium (Table I).

Although the increase of Na^+ and Cl^- uptake by 5HT accounts for some fraction of the alteration of net base flux, a substantial proportion of the net base flux that was stimulated by 5HT was independent of the uptake of Na^+ and Cl^-. This was indicated by the observation that in the absence of external Na^+ or Cl^- there was a persistent loss of base that was elevated by 5HT (Tables I and II). The mechanism for the elevation of base loss by 5HT is not clear. It could be an indirect result of the increased amount of HCO_3^- filtered by the renal tissue (Dietz and Byrne, 1997). 5HT appears to be a "universal" stimulator of freshwater bivalves including *C. fluminea*. Its effects on freshwater mussels include increases in gill ciliary activity, foot movement, and valve closure; gill muscle relaxation; and induction of spawning and other reproductive activities (Scheide and Dietz, 1984; Gardiner *et al.*, 1991; Fong *et al.*, 1993, 1994). The stimulation of all these activities may increase metabolic CO_2 production and result in the elevation of blood HCO_3^- due to the hydration of CO_2. Alternatively, 5HT may directly stimulate HCO_3^- excretion in the renal tissue of *C. fluminea*.

The effects of AZ on ion transport in C. fluminea

Whereas 5HT acts on the Cl^- and Na^+ uptake process in the gills of SD *C. fluminea*, AZ works predominantly on the Cl^- and Na^+ exit pathway. AZ depressed Cl^- transport of SD *C. fluminea* by exerting a greater influence on the efflux of the ion than on its influx. The significant increase in Cl^- efflux produced by AZ in this study is consistent with the results of previous studies of the freshwater mussels *Toxolasma texasensis* and *Ligumia subrostrata* (Dietz and Branton, 1979; Henry and Saintsing, 1983). An increase in Cl^- influx, on the other hand, has not been previously reported as an effect of AZ. AZ has been shown to inhibit Na^+ transport by reducing the influx in *Ligumia subrostrata* (Henry and Saintsing, 1983). In SD *C. fluminea*, however, AZ exerted its effect exclusively on the Na^+ efflux, and no evidence of a reduction in influx was observed. This disagreement may be due to the species differences in response to AZ or in the Na^+ uptake process.

The effect of AZ on the flux of titratable base has not been reported previously in freshwater bivalves. In SD *C. fluminea*, AZ significantly increased the net loss of base. Although gill epithelia are an important site for the exit of HCO_3^- and H^+ through the exchange activities, filtration and excretion by the renal tissue is also a significant process in the regulation of acid and base balance. An increase of blood HCO_3^- by AZ treatment has been demonstrated in *C. fluminea* and other freshwater mussels (Henry and Saintsing, 1983). The blockage of HCO_3^- exit pathways in the gill epithelia would result in the accumulation of HCO_3^- in the blood (Byrne and Dietz, 1997) and increase the amount of HCO_3^- being subjected to filtration and excretion by the renal tissue.

Cl^- transport kinetics

Unidirectional ion uptake depends on the corresponding external ion concentration and displays saturation kinetics in the freshwater bivalves studied (Dietz, 1978; Dietz and Branton, 1979; McCorkle and Dietz, 1980; Dietz and Byrne, 1990; Dietz and Hagar, 1990; Wilcox and Dietz, 1995). A high ion transport capacity (J_{max}) seems to be a common characteristic in *C. fluminea*. The Cl^- transport capacity is about 7 times higher in *C. fluminea* than in the unionids *Toxolasma texasensis* and *Ligumia subrostrata* (Dietz and Branton, 1979; this study).

In this study, Cl^- transport capacity was estimated to be increased 50% and 85% after salt depletion for 4 and 8 weeks, respectively. Two weeks of salt depletion is sufficient to stimulate the rate of ion uptake in most unionid clams, and even less time is required in zebra mussels (Dietz, 1985; Horohov *et al.*, 1992; Dietz *et al.*, 1994). For *C. fluminea*, however, a significant elevation of Cl^- influx requires at least 4 weeks of salt depletion. The prolonged time requirement suggests that this species has a low epithelial permeability to ions (Zheng and Dietz, 1998). The transport affinity for Cl^- that we measured in this study is about 0.2 m*M* for PWA and SD *C. fluminea*.

The elevation in ion transport capacity with little change in transport affinity suggests that more epithelial transport sites are activated during salt depletion.

Studies of transport kinetics using radioactive Rb as a substitute tracer for K in the zebra mussel, *Dreissena polymorpha,* have revealed a greater proportion of diffusive uptake at higher external Rb concentrations (Wilcox and Dietz, 1995). The ion concentrations used in transport kinetic studies in freshwater bivalves is usually under 3 m*M*. In this study, we applied Cl^- concentrations up to 12 m*M* in an attempt to identify a passive diffusion component of Cl^- uptake. Passive diffusion would appear as a linear increase in flux at higher ion concentrations (see Wilcox and Dietz, 1995). A Michaelis-Menten rectangular hyperbolic function fit the Cl^- influx data for PWA *C. fluminea* very well ($R > 0.95$), with no evidence of a diffusive component. An attempt to study fluxes at higher Cl^- concentrations (up to 20 m*M*) was unsuccessful because the animals did not open their valves.

The characteristics of Cl^- uptake in *C. fluminea* reveal differences compared with those of other freshwater bivalves such as unionids and zebra mussels (Dietz and Branton, 1979; Dietz *et al.*, 1995; Byrne and Dietz, 1997; Zheng and Dietz, 1998). The epithelium of *C. fluminea* is much "tighter" than that of unionids or zebra mussels. The tight, or low, permeability of the epithelium in this species is reflected by the longer time required for salt depletion and the lack of evidence for a passive diffusion component in Cl^- uptake. *C. fluminea* has a higher blood osmolality than do unionids and zebra mussels and has been reported to inhabit brackish water with salinities as high as 5‰ (Filice, 1958; Hayashi, 1956; Keen and Casey, 1969). In addition, this species is very tolerant of salt depletion and can be kept in deionized water for several months with little mortality (McCorkle and Dietz, 1980). Thus, *C. fluminea* can tolerate a much broader range of ambient osmolality than unionid clams and zebra mussels.

Acknowledgments

We thank Chengsung Jiang, Janice E. Horohov, Julie Cherry, Diondi Lessard, Paul Bruce, Shawn Wilcox, and Timothy Smith for technical assistance. Harold Silverman provided valuable comments. The paper was submitted to the Graduate School of Louisiana State University and A&M College in partial fulfillment of the Ph. D degree by H. Z. The research was supported in part by NSF 90-17461.

Literature Cited

Alvarado, R. H., A. M. Poole, and T. L. Mullen. 1975. Cl^- balance in *Rana pipiens*. *Am. J. Physiol.* **229:** 861–868.

Byrne, R. A., and T. H. Dietz. 1997. Ion transport and acid-base balance in freshwater bivalves. *J. Exp. Biol.* **200:** 457–465.

Byrne, R. A., R. F. McMahon, and T. H. Dietz. 1989. The effects of aerial exposure and subsequent reimmersion on hemolymph osmolarity, ion composition, and ion flux in the freshwater bivalve, *C. fluminea*. *Physiol. Zool.* **62:** 1187–1202.

Dietz, T. H. 1978. Na transport in the freshwater mussel, *Carunculina texasensis* (Lea). *Am. J. Physiol.* **235:** R35–R40.

Dietz, T. H. 1979. Uptake of Na and Cl by freshwater mussels. *Can. J. Zool.* **57:** 156–160.

Dietz, T. H. 1985. Ionic regulation in freshwater mussels: A brief review. *Am. Malacol. Bull.* **3:** 233–242.

Dietz, T. H., and W. D. Branton. 1979. Cl^- transport in freshwater mussels. *Physiol. Zool.* **52:** 520–528.

Dietz, T. H., and R. A. Byrne. 1990. K and rubidium uptake in freshwater bivalves. *J. Exp. Biol.* **150:** 395–405.

Dietz, T. H., and R. A. Byrne. 1997. Effects of salinity on solute clearance from the freshwater bivalve, *Dreissena polymorpha* Pallas. *Exp. Biol. Online* **2:** 11.

Dietz, T. H., and A. F. Hagar. 1990. Cl uptake in isolated gills of the freshwater mussel *Ligumia subrostrata*. *Can. J. Zool.* **68:** 6–9.

Dietz, T. H., and A. M. Findley. 1979. Ion-stimulated ATPase activity and NaCl uptake in the gills of freshwater mussels. *Can. J. Zool.* **58:** 917–923.

Dietz, T. H., J. I. Scheide, and D. G. Saintsing. 1982. Monoamine transmitters and cAMP stimulation of Na transport in freshwater mussels. *Can. J. Zool.* **60:** 1408–1411.

Dietz, T. H., D. Lessard, H. Silverman, and J. W. Lynn. 1994. Osmoregulation in *Dreissena polymorpha:* the importance of Na, Cl, K, and particularly Mg. *Biol. Bull.* **187:** 76–83.

Dietz, T. H., R. A. Byrne, J. W. Lynn, and H. Silverman. 1995. Paracellular solute uptake by the freshwater zebra mussel *Dreissena polymorpha*. *Am. J. Physiol.* **269:** R300–R307.

Filice, F. P. 1958. Invertebrates from the estuary portion of San Francisco Bay and some factors influencing their distribution. *Wasmann J. Biol.* **16:** 159–211.

Fong, P. P., D. M. Watt, and J. L. Ram. 1993. Characterization of 5HT in the regulation of spawning in the zebra mussel *Dreissena polymorpha*. *J. Exp. Zool.* **267:** 475–482.

Fong, P. P., J. D. Hardege, and J. L. Ram. 1994. Long-lasting, sex-specific inhibition of 5HT-induced spawning by methiothepin in the zebra mussel, *Dreissena polymorpha* (Pallas). *J. Exp. Zool.* **270:** 314–320.

Gardiner, D. B., F. S. Turner, J. M. Myers, T. H. Dietz, and H. Silverman. 1991. Long-term culture of freshwater mussel gill strips: Use of 5HT to affect aseptic conditions. *Biol. Bull.* **181:** 175–180.

Graves, S. Y., and T. H. Dietz. 1982. Cyclic AMP stimulation and prostaglandin inhibition of Na transport in freshwater mussels. *Comp. Biochem. Physiol.* **71A:** 65–70.

Hayashi, Y. 1956. On the variation of *Corbicula* due to environmental factors. *Venus* **19:** 54–60.

Henry, R. P., and D. G. Saintsing. 1983. Carbonic anhydrase activity and ion regulation in three species of osmoregulating bivalve molluscs. *Physiol. Zool.* **56:** 274–280.

Horohov, J., H. Silverman, J. W. Lynn, and T. H. Dietz. 1992. Ion transport in the freshwater zebra mussel, *Dreissena polymorpha*. *Biol. Bull.* **183:** 297–303.

Keen, M., and R. Casey. 1969. Family Corbiculidae. Pp. 665–669 in *Treatise on Invertebrate Paleontology,* Pt. N, R. C. Moore, ed. Geological Society of America, Boulder, Colorado.

Kerstetter, T. H., and L. B. Kirschner. 1972. Active chloride transport by the gills of rainbow trout (*Salmo gairdneri*). *J. Exp. Biol.* **56:** 263–272.

Krogh, A. 1939. *Osmotic Regulation in Aquatic Animals.* Cambridge University Press, London. 242 pp.

Lee, S. H., and J. B. Pritchard. 1985. Bicarbonate-Cl exchange in gill plasma membrane of blue crab. *Am. J. Physiol.* **249:** R544–R550.

Lin, H., and D. Randall. 1995. Proton pumps in fish gills. Pp. 229–255 In *Cellular and Molecular Approaches to Fish Ionic Regulation.* C. M. Wood and T. J. Shuttleworth, eds. Academic Press, Santiago.

McCorkle, S., and T. H. Dietz. 1980. Na transport in the freshwater Asiatic clam *Corbicula fluminea. Biol. Bull.* **159:** 325–336.

Murphy, W. A., and T. H. Dietz. 1976. The effects of salt depletion on blood and tissue ion concentration in the freshwater mussel, *Ligumia subrostrata* (Say). *J. Comp. Physiol.* **108:** 233–242.

Romeu, F. G., A. Salibian, and S. Pezzani-Hernandez. 1969. The nature of the *in vivo* Na and Cl uptake mechanisms through the epithelium of the Chilean frog *Calyptocephalella gayi* (Dum. et. Bibr., 1841). *J. Gen. Physiol.* **53:** 816–835.

Scheide, J. I., and T. H. Dietz. 1982. The effects of independent sodium and chloride depletion on ion balance in freshwater mussels. *Can. J. Zool.* **60:** 1676–1682.

Scheide, J. I., and T. H. Dietz. 1984. The effects of calcium on serotonin-stimulated adenylate cyclase in freshwater mussels. *Biol. Bull.* **166:** 594–607.

Scheide, J. I., and T. H. Dietz. 1986. 5HT regulation of gill cAMP production, Na, and water uptake in freshwater mussels. *J. Exp. Zool.* **240:** 309–314.

Stobbart, R. H. 1971. Evidence for Na^+/H^+ and Cl^-/HCO_3^- exchange during independent Na and Cl uptake by the larva of the mosquito *Aedes aegypti* (L.). *J. Exp. Biol.* **54:** 19–27.

Wiegman, T., M. G. Woldring, and J. J. Pratt. 1975. A new cocktail for liquid scintillation counting of aqueous radioimmunoassay samples. *Clin. Chim. Acta.* **59:** 347–356.

Wilcox, S. J., and T. H. Dietz. 1995. K transport in the freshwater bivalve *Dreissena polymorpha. J. Exp. Biol.* **198:** 861–868.

Zheng, H., and T. H. Dietz. 1998. Paracellular solute uptake in the freshwater bivalves *Corbicula fluminea* and *Toxolasma texasensis. Biol. Bull.* **194:** 170–177.

Reference: *Biol. Bull.* **194:** 170–177. (April, 1998)

Paracellular Solute Uptake in the Freshwater Bivalves *Corbicula fluminea* and *Toxolasma texasensis*

HUIYUAN ZHENG AND THOMAS H. DIETZ

Department of Biological Sciences, Louisiana State University, Baton Rouge, Louisiana 70803

Abstract. Two species of freshwater bivalve were exposed to hyperosmotic solutions of various nonelectrolytes to compare the paracellular permeability of their gill epithelia. In *Corbicula fluminea*, exposure resulted in an elevation of blood solutes that was primarily due to dehydration. After 36 h of exposure, the concentration of Na in the blood decreased precipitously, and the nonelectrolyte accumulated. When lanthanum was added to the solution as a diffusion tracer, its electron-dense precipitate was rarely observed to penetrate the paracellular spaces of the gill epithelial cells in the absence of hyperosmotic stress. In contrast, precipitated lanthanum was commonly observed in the paracellular junctional complexes of the gill in animals that were subjected to hyperosmotic conditions.

When the second species, *Toxolasma texasensis*, was exposed to hyperosmotic solutions of nonelectrolyte, dehydration appeared to be minimal and a seemingly normal concentration of ions was maintained in the blood. This, however, was because of the simultaneous loss of ions and water and a small gain in nonelectrolytes. Longer exposure (12 h or more) produced a precipitous decrease in most blood solutes and an extensive accumulation of nonelectrolyte. More lanthanum precipitate was seen in the paracellular spaces of both control and hyperosmotically stressed *T. texasensis* than in identically treated *C. fluminea*. We conclude that the epithelial junctions found in *C. fluminea* are relatively tight, which probably contributes to the ability of this species to maintain the solute in its body fluid at concentrations higher than are possible in *T. texasensis*.

Introduction

The paracellular pathway is the site of the high electrical conductance of "leaky" epithelia in vertebrates (Frömter and Diamond, 1972). This particular pathway is usually limited by tight junctions, and can operate as a simple "gate" in several epithelia (Diamond, 1977). Paracellular movement of solute has been demonstrated in the epithelia of vertebrate gallbladder, small intestine, and proximal renal tubules (Boulpaep, 1971; Barry *et al.*, 1971; Frömter and Diamond 1972). In molluscs and some other invertebrates, the septate junction performs a function similar to that of the vertebrate tight junction (Lord and DiBona, 1976). When dehydrated, the terrestrial slug *Lehmannia valentiana* displays rapid water uptake and accumulates nonelectrolytes (mannitol and inulin) through paracellular pathways in the foot epithelium (Uglem *et al.*, 1985). In the intestine of the sea slug *Aplysia juliana*, the paracellular pathway constitutes the major conductive route for both Na and Cl (Gerencser, 1982).

In recent studies, the gill epithelia of *Dreissena polymorpha* (zebra mussel) have demonstrated unusually "leaky" characteristics (Dietz *et al.*, 1995; Dietz *et al.*, 1997). When exposed to solutions that were hyperosmotic to their blood, individuals of this freshwater species experienced substantial solute movement through paracellular pathways. Following exposure to hyperosmotic but low ionic strength solutions (100 m*M*) of mannitol, glucose, or sucrose, *D. polymorpha* specimens lost 80%–85% of their blood Na and Cl within 12 h, with concomitant accumulation of the nonelectrolytes from the bathing medium through the paracellular pathway (Dietz *et al.*, 1995; Dietz *et al.*, 1997). Finally, *D. polymorpha* also has a substantial diffusive uptake of Rb from hyposmotic solutions (Wilcox and Dietz, 1995). Paracellular solute movement has not been assessed in any other species of freshwater bivalve.

Corbicula fluminea (Müller) belongs to the family Corbiculidae and entered fresh water during the Pleistocene (Keen and Casey, 1969). *C. fluminea* has been reported to inhabit brackish water up to 5‰ salinity although it is

Received 11 September 1997; accepted 16 January 1998.

considered to be a freshwater species (Filice, 1958; Hayashi, 1956). *C. fluminea* has a higher blood osmolality, a higher rate of ion transport, and a different blood ionic composition than unionid mussels (McCorkle and Dietz, 1980; Dietz 1985; Dietz *et al.*, 1996; Zheng and Dietz, 1998). In contrast to the corbiculids, the unionid bivalves invaded fresh water in the Triassic (Keen and Casey, 1969). The unionid *Toxolasma texasensis* (Lea) and the corbiculid *C. fluminea* may have evolved different epithelial characteristics and, thus, were chosen as bivalve models for a comparative study of paracellular permeability.

In this study, we demonstrate that *C. fluminea* epithelia were relatively non-leaky during a 36-h exposure to a hyperosmotic nonelectrolyte challenge. After the 36-h hyperosmotic challenge the epithelia became selectively leaky, allowing the mussel to gain nonelectrolytes and lose ions, primarily Na. In contrast, *T. texasensis* specimens subjected to similar hyperosmotic conditions had relatively leaky epithelia; they gained nonelectrolytes within 4 h and lost most of the ions from their blood within 12 h.

Materials and Methods

Animals

Corbicula fluminea was collected, under permit, from the Tangipahoa river in Mississippi. Most *Toxolasma* (*Carunculina*) *texasensis* and some *C. fluminea* were obtained under permit from ponds in Louisiana. The animals were acclimated to an aerated artificial pondwater (PW) containing (in m*M*) 0.5 NaCl, 0.4 $CaCl_2$, 0.2 $NaHCO_3$, and 0.05 KCl at 22°–25°C for at least 1 week before use.

Blood analyses

Blood was collected anaerobically by cardiac puncture (Fyhn and Costlow, 1975) and centrifuged 1 min at 8000 × *g*. The supernatant was used for solute determinations. Total solute was measured by freezing point depression on undiluted samples. Concentrations of K and Na were measured by flame photometry, Cl by electrometric titration, and Ca and Mg by atomic absorption spectrophotometry on samples diluted with LaO_3/HCl. The nonspecific phenol/sulfuric acid method was used for rapidly measuring total sugar concentration in large numbers of samples (Montgomery, 1957), and glucose was measured, using a specific glucose kinase procedure (Sigma Chemical), for some samples. Mannitol concentration was determined by HPLC separation using a normal phase APS-hypersil column and a refractive index detector (Gäde, 1991; Dietz *et al.*, 1995). A 5-μl sample of blood in 45 μl of acetonitrile was injected onto the column. Mannitol concentrations calculated from the HPLC chromatography peak area had less than 5% error.

Ion transport

Net ion flux (J_n) was calculated from the change in ion concentration of the bath (Dietz, 1978). The animals were rinsed with deionized water for about 30 min, then each specimen was transferred to a separate 50-ml beaker with appropriate bathing medium. Bath samples were collected at 6-h intervals, and J_n was calculated and expressed as μeq g^{-1} dry tissue h^{-1}.

Hyperosmotic conditions and paracellular permeability

Artificial pondwater containing 100 m*M* mannitol or glucose was used to establish an osmotic gradient without the confounding effect of an elevation of ion concentration in the bath. Each specimen was placed in a separate 50-ml beaker with the indicated bathing medium during an experiment. All animals opened their valves, siphoned the medium, and survived the treatment in hyperosmotic nonelectrolyte solutions. In some experiments, sucrose was used as an osmotic stressor and lanthanum was added to the PW as an electron-dense diffusion tracer to stain the paracellular spaces for electron microscopy (Dietz *et al.*, 1995; 1997). Animals were exposed to CO_2-free PW containing 0.1 m*M* $LaCl_3$ and 100 m*M* sucrose for 2 h or 12 h. Lanthanum carbonate forms an insoluble precipitate at the site of La contact with endogenous HCO_3. The total solute was measured on blood samples collected from the sucrose-treated animals and from controls exposed to the same solution without sucrose. Gills were excised and fixed for 2 h in 2% glutaraldehyde prepared with a phosphate buffer that was isosmotic with the blood of each specimen, and adjusted to pH 7.3 (Gardiner *et al.*, 1991). Tissues were rinsed with a buffer, exposed to 1% osmium tetroxide for 1 h, and dehydrated in an ethanol series. The tissues were infiltrated with 50% LR White resin in ethanol overnight, transferred to 100% LR White resin (2–3 changes), and polymerized at 59°C overnight. Tissues were thin sectioned with an ultramicrotome (50–70 nm), and examined with a JEOL CX-100 transmission electron microscope operating at 40 or 80 keV without further contrasting with heavy metals.

Statistical analyses

Data were expressed as the mean ± the standard error of the mean, with the number of animals in parentheses. Statistical significance was determined by one-way ANOVA or Student's *t* test. For some data sets in which larger variances were unequal, the data were transformed by the natural log (Ln) for the statistical analysis.

Results

The responses of C. fluminea *to hyperosmotic stress*

Mannitol. Analysis of the blood from animals exposed to 100 m*M* mannitol in pondwater demonstrated that hy-

perosmotic stress induced an elevation in the ion concentrations, increasing the total solute concentration (Table I). After 12 h exposure to 100 m*M* mannitol in PW, osmolality and all ion concentrations in the blood of the animals were significantly elevated, with the exception of K. The average net flux of Na and Cl was unchanged during the initial 12 h of the experiment [control: $J_n^{Na} = 0.30 \pm 0.20$, $J_n^{Cl} = 0.78 \pm 0.16$ ($n = 6$); treated: $J_n^{Na} = 0.13 \pm 0.12$, $J_n^{Cl} = 0.63 \pm 0.09$ ($n = 6$) μeq g^{-1} dry tissue h^{-1}], indicating that the rise in body-fluid solute concentrations was primarily due to dehydration.

A small amount of mannitol was detected in the blood after 12 h of exposure to 100 m*M* mannitol, but after 24 h of exposure the mannitol concentration increased significantly (Table I). These data suggest that the permeability of the epithelium changed after prolonged exposure to the hyperosmotic 100 m*M* mannitol solution. Although the Na concentration in the blood rose further during the 12- to 24-h exposure to hyperosmotic mannitol, there was no difference between the 12-h and 24-h treatment groups for the other ions. These data are consistent with a prolonged osmotic loss of water and a dehydration-induced elevation of ion concentrations in the blood. The penetration of mannitol into the body fluids was likely *via* paracellular routes (see below).

Glucose. Glucose was selected as an alternate nonelectrolyte to induce a hyperosmotic challenge as it allowed more rapid chemical analysis. In most cases the changes of ion concentration in the blood that were induced within 24 h of exposure to hyperosmotic glucose solutions were similar to those produced by mannitol (Table II). At 12 h of exposure to 100 m*M* glucose, the osmolality and the concentrations of all ions except K were significantly elevated in the blood. With the exception of calcium, which continued to rise during the 24 h of exposure, the other ions in the blood showed no further concentration changes until 48 h, at which time a critical alteration in epithelial permeability apparently occurred. Small amounts of glucose entered the blood during 12–36 h of exposure to hyperosmotic glucose media. These data are consistent with a dehydration-induced elevation of blood ion concentration over the 36-h treatment.

Although all of the animals lived and appeared to be in normal condition after prolonged hyperosmotic stress, the major ions showed acute concentration decreases concomitant with a rapid rise in blood glucose during 36 to 48 h of exposure (Table II). During this period, 70% of blood Na and 18% to 26% of Cl, Ca, and Mg were lost. Concurrently, the amount of glucose in the blood increased about 8-fold. The concentration of K in the blood was so low that it was below the detection limit (0.05 m*M*) after 48 h of exposure. These data suggest an acute change in permeability of the epithelial tissue following prolonged exposure to hyperosmotic stress.

The blood became isosmotic within a 24-h exposure to the hyperosmotic glucose solution—primarily because of the dehydration-induced elevation of ion concentrations and a rather small amount of glucose entering the blood (Table II). Although most of the ion concentrations in the blood decreased during 36 to 48 h of exposure, the osmolality remained isosmotic to the bathing solution because of the simultaneous accumulation of glucose.

In PW-acclimated animals, the osmolality of *C. fluminea* (about 60–70 mOsm) is higher than that of *T. texasensis* (about 40–50 mOsm). A glucose concentration of 100 m*M* in the bathing medium is more than double the osmolality of the blood of *T. texasensis* (see below). To compare the responses of these two species to an equivalent level of hyperosmotic stress, 140 m*M* glucose was added to PW to challenge *C. fluminea* with an osmolality more than twice the normal level of its blood. After 12 h exposure to glucose in PW, animals in both the 100 m*M* and 140 m*M* glucose treatments had significantly higher blood osmolality [91 ± 1 ($n = 5$); 96 ± 3 ($n = 5$) mOsm, respectively] than the PW controls [68 ± 2 ($n = 5$) mOsm]. However, neither the osmolality nor the major blood ions (with the exception of Ca and Mg; data not shown) in animals from the 100 m*M* treatment group (Na, 47.3 ± 0.4 m*M;* Cl, 34.9 ± 0.5 m*M*) differed significantly ($P > 0.05$) from these in animals exposed to 140 m*M* glucose (Na, 48.4 ± 1.5 m*M;* Cl, 35.7 ± 1.9 m*M*). Likewise, the higher glucose gradient did not significantly change the amount of glucose that entered the blood after 12 h of treatment (3.6 ± 1.8 m*M;* 3.9 ± 0.5 m*M*, respectively).

Table I

Comparisons of ion concentrations, total solute, and the accumulation of mannitol in the blood of C. fluminea *over different periods of exposure to 100 m*M *mannitol in pondwater*

Solute	Control ($n = 24$)*	100 m*M* mannitol	
		12 h ($n = 18$)	24 h ($n = 15$)
Na	28.1 ± 0.2[a]	38.0 ± 0.7[b]	43.2 ± 1.0[c]
Cl	23.3 ± 0.5[a]	30.7 ± 0.6[b]	31.1 ± 1.2[b]
Ca	9.0 ± 0.5[a]	14.6 ± 1.5[b]	16.9 ± 1.4[b]
K	0.8 ± 0.0[a]	0.9 ± 0.0[a]	0.8 ± 0.0[a]
Mannitol		1.6 ± 1.1[a]	13.9 ± 3.3[b]
Total	61.5 ± 0.6[a]	85.8 ± 2.2[b]	97.1 ± 2.0[c]

Concentrations are the means ± the standard error, expressed as m*M* or mOsm. In each row, values that are significantly different ($P < 0.05$) are indicated by superscript letters.

* For Na, $n = 23$.

The responses of T. texasensis *to hyperosmotic stress*

Mannitol. After 24 h exposure to 100 m*M* mannitol in PW, *T. texasensis* experienced a significant decrease in the concentration of all ions in its blood (Table III). Dur-

Table II

Comparisons of ion concentrations, total solute, and the accumulation of glucose in the blood of C. fluminea *over different exposure times to 100 m*M *glucose in pondwater*

		100 m*M* glucose			
Solute	Control	12 h	24 h	36 h	48 h
Na	29.7 ± 0.5[b]	44.2 ± 0.9[c]	45.4 ± 1.0[c]	43.5 ± 0.8[c]	13.2 ± 1.5[a]
Cl	27.6 ± 0.4[a]	35.1 ± 0.5[b]	32.5 ± 1.0[b]	32.1 ± 1.3[b]	26.3 ± 3.0[a]
Ca	8.9 ± 0.7[a]	13.6 ± 1.0[b]	19.8 ± 1.8[c]	14.6 ± 1.0[b]	12.0 ± 1.3[b]
Mg	2.8 ± 0.3[a]	5.2 ± 0.4[b]	5.0 ± 0.4[b]	4.5 ± 0.3[b]	3.3 ± 0.4[a]
K	0.6 ± 0.0[b]	0.6 ± 0.0[b]	0.1 ± 0.0[a]	0.1 ± 0.0[a]	0.0 ± 0.0[a]
Glucose	0.7 ± 0.1[a]	4.4 ± 0.8[b]	10.1 ± 2.3[b]	5.5 ± 0.5[b]	44.0 ± 8.0[c]
Total	64.7 ± 1.0[a]	86.6 ± 0.9[b]	96.6 ± 0.9[c]	94.7 ± 1.4[c]	95.0 ± 5.1[c]

Concentrations are the mean plus or minus the standard error of the mean, expressed as m*M* or mOsm. In each row, values that are significantly different ($P < 0.05$) are indicated by superscript letters; $n = 10$.

ing the hyperosmotic challenge, mannitol accumulated in the blood and accounted for about 71% of the osmolality. In a separate study we monitored the net flux of Na and Cl in *T. texasensis* during a 12-h exposure to 100 m*M* mannitol in PW. The treated mussels displayed a significant ($P < 0.01$) loss of ions during the study [control: $J_n^{Na} = 0.52 \pm 0.22$, $J_n^{Cl} = 0.04 \pm 0.14$ ($n = 6$); treated: $J_n^{Na} = -2.29 \pm 0.34$, $J_n^{Cl} = -1.82 \pm 0.23$ ($n = 6$) μeq g^{-1} dry tissue h^{-1}].

Glucose. For *T. texasensis* exposed to 100 m*M* glucose in PW for 24 h, Table IV shows the time course of change in blood solute concentration and the accumulation of glucose. During the 4- to 8-h exposure, animals were able to maintain the concentrations of ions in their blood within the normal range. During this period, there was a small but significant amount of glucose entering the blood. Total solute in the blood was significantly increased due to the slight elevation of the individual ions and the accumulation of glucose from the bathing medium. After exposure of 12 h or longer, there was a precipitous decrease in ion concentrations with concomitant accumulation of glucose in the blood. At the end of a 12-h exposure to 100 m*M* glucose, the concentration of glucose in the blood was about 70 m*M*, accounting for 80% to 90% of blood osmolality.

Table III

Comparisons of ion concentrations, total solute, and the accumulation of mannitol in the blood of T. texasensis *before and after 24 h exposure to 100 m*M *mannitol in pondwater*

Solute	Control ($n = 9$)	Treated ($n = 6$)
Na	16.9 ± 1.0[b]	2.4 ± 1.2[a]
Cl	9.9 ± 0.8[b]	2.0 ± 0.6[a]
Ca	3.1 ± 0.3[b]	1.8 ± 0.5[a]
K	0.6 ± 0.0[b]	0.2 ± 0.0[a]
Mannitol		61.5 ± 11.0
Total	40.3 ± 2.6[a]	86.8 ± 10.1[b]

Concentrations are the means ± the standard error, expressed as m*M* or mOsm. In each row, values that are significantly different ($P < 0.05$) are indicated by superscript letters.

Localization of electron-dense lanthanum carbonate

To exclude the possible, but unlikely, existence of an epithelial glucose-transport system in the gills of these animals, we used sucrose instead of glucose as the hyperosmotic osmolyte in lanthanum studies (Dietz *et al.*, 1997). Preliminary studies had demonstrated that both *C. fluminea* and *T. texasensis* behaved the same in sucrose-induced hyperosmotic stress as in glucose treatment (data not shown).

C. fluminea *exposed to lanthanum.* Exposure of *C. fluminea* to 0.1 m*M* lanthanum in HCO_3-free PW (control animals) for 2 h (not shown) or 12 h resulted either in no deposits of electron-dense lanthanum carbonate, or in only trace amounts in a few locations in the junctional complexes of the gill epithelial cells (Fig. 1A). Only one out of eight control animals was found to contain lanthanum precipitate after either 2 or 12 h of exposure. In contrast, addition of 100 m*M* sucrose to the bathing medium—all other conditions remaining the same as in the controls—and exposure of four *C. fluminea* resulted in the appearance of lanthanum precipitate in the intercellular spaces between many epithelial cells in all the gill sections examined (Fig. 1B, C). More interestingly, some lanthanum deposits were found to be inside the vesicles or "blister-like" structures inside the epithelial cells of the gill filaments and in the intercellular spaces between the cells (Fig. 1D). The lanthanum-containing blisters were more prominent in the 12-h hyperosmotic treatment than in the 2-h treatment. These blisters were probably formed by the deformation of the lateral membranes of the epithelial cells due to the hyperosmotic-induced dehy-

Table IV

Comparisons of blood ion concentrations, total solute, and the accumulation of glucose in T. texasensis *over different exposure times to 100 m*M *glucose in pondwater*

Solute	Control	100 m*M* glucose			
		4 h	8 h	12 h	24 h
Na	17.2 ± 0.8^{b}	19.0 ± 2.2^{b}	20.1 ± 1.0^{b}	1.6 ± 0.8^{a}	0.0 ± 0.0^{a}
Cl	10.4 ± 0.5^{c}	11.3 ± 1.4^{c}	11.5 ± 0.5^{c}	2.4 ± 0.4^{b}	0.8 ± 0.2^{a}
Ca	3.6 ± 0.5^{b}	5.6 ± 0.9^{b}	3.9 ± 0.3^{b}	1.1 ± 0.1^{a}	1.4 ± 0.1^{a}
Mg	0.3 ± 0.1^{b}	0.4 ± 0.0^{b}	0.2 ± 0.0^{b}	0.0 ± 0.0^{a}	0.2 ± 0.0^{b}
K	0.5 ± 0.0^{b}	0.6 ± 0.0^{b}	0.5 ± 0.1^{b}	0.0 ± 0.0^{a}	0.0 ± 0.0^{a}
Glucose	3.5 ± 0.4^{a}	10.4 ± 5.5^{b}	10.5 ± 3.2^{b}	73.2 ± 7.6^{c}	66.6 ± 8.8^{c}
Total	40.6 ± 1.8^{a}	53.0 ± 4.9^{b}	64.0 ± 3.4^{b}	80.3 ± 6.0^{c}	83.4 ± 9.4^{c}

Concentrations are the mean plus or minus the standard error of the mean, expressed as m*M* or mOsm. In each row, values that are significantly different ($P < 0.05$) are indicated by superscript letters; $n = 5–10$.

dration. This inference was supported by evidence of tissue condensation in the gill filament (Fig. 1D), and by the dehydration-induced elevation of blood solute concentrations observed under hyperosmotic glucose or mannitol challenge (Tables I and II). Deposition of lanthanum in the paracellular spaces of gill epithelial cells was more extensive after 12 h of hyperosmotic stress than after 2 h, indicating a time dependence of the hyperosmotic induction of paracellular leakage.

T. texasensis *exposed to lanthanum.* Animals exposed to HCO_3-free PW containing 0.1 m*M* lanthanum for 2 h (not shown) or 12 h showed only a few locations, in one of the six controls, containing a limited amount of lanthanum deposit in the junctional complexes of the gill epithelial cells (Fig. 1E). When animals were exposed to 0.1 m*M* lanthanum in HCO_3-free PW containing 100 m*M* sucrose for 2 or 12 h, lanthanum was found to penetrate intercellular spaces between many epithelial cells in all the gill sections examined (Fig. 1F, G). Longer exposure to hyperosmotic conditions always resulted in a larger quantity of lanthanum precipitate. In some sections from the animals treated for 12 h, lanthanum precipitate was found within blisters, as observed in *C. fluminea.*

Both the quantity of lanthanum and the number of locations of lanthanum precipitate in the intercellular spaces of *T. texasensis* were greater than in *C. fluminea* after the same treatment time. These data suggest that the paracellular pathways between epithelial cells were more sensitive to hyperosmotic stress in *T. texasensis* than in *C. fluminea.*

Discussion

Under short-term hyperosmotic challenge, the epithelia of *C. fluminea* were relatively "tight" and resistant to the penetration of nonelectrolytes compared to those of another freshwater bivalve, *D. polymorpha* (Dietz *et al.*, 1995, 1997). The initial response of *C. fluminea* to 100 m*M* hyperosmotic stress was an increase, due to dehydration, in the concentration of ions in the blood. During the initial period, *C. fluminea* tolerated a 20% to 50% increase in osmolality and in concentration of the major ions without a significant change in the permeability of its gill epithelia to the nonelectrolytes. The increase in total solute concentration was primarily due to dehydration, as indicated by the lack of any change in the net flux of Na or Cl. However, small but significant amounts of nonelectrolytes were able to diffuse into the blood. That diffusion was probably a result of paracellular leakiness in gill epithelia, which was demonstrated by the presence of lanthanum carbonate precipitates between the cells of the gill filaments after 12 h of exposure to hyperosmotic stress.

Prolonged exposure to hyperosmotic conditions apparently induced a distinct change in epithelial permeability. This is suggested by the acute decrease of ion concentrations and the concomitant rise in glucose observed in the blood of *C. fluminea* after 36 h of exposure to hyperosmotic glucose. The observed changes in solute composition in the blood were most likely due to the increase of paracellular permeability through which glucose or mannitol diffused into the body fluids. It is interesting that the decrease in blood concentration of ions was more pronounced for Na than for any other ion. As much as 70% of the Na, but only 18% to 26% of other ions (Cl, Ca, or Mg), was lost from the blood during 36 to 48 h of exposure to hyperosmotic conditions. The reason for this selectivity was not clear. Perhaps the paracellular pathway is more permeable to monovalent cations and constitutes some proportion of diffusive loss of Na in *C. fluminea,* even under normal conditions. Nevertheless, even after the significant increase of paracellular leakage, the animals were still able to stabilize their blood ion concentrations, except for Na and K, at about control levels. All of the animals survived the treatment regimen, so the

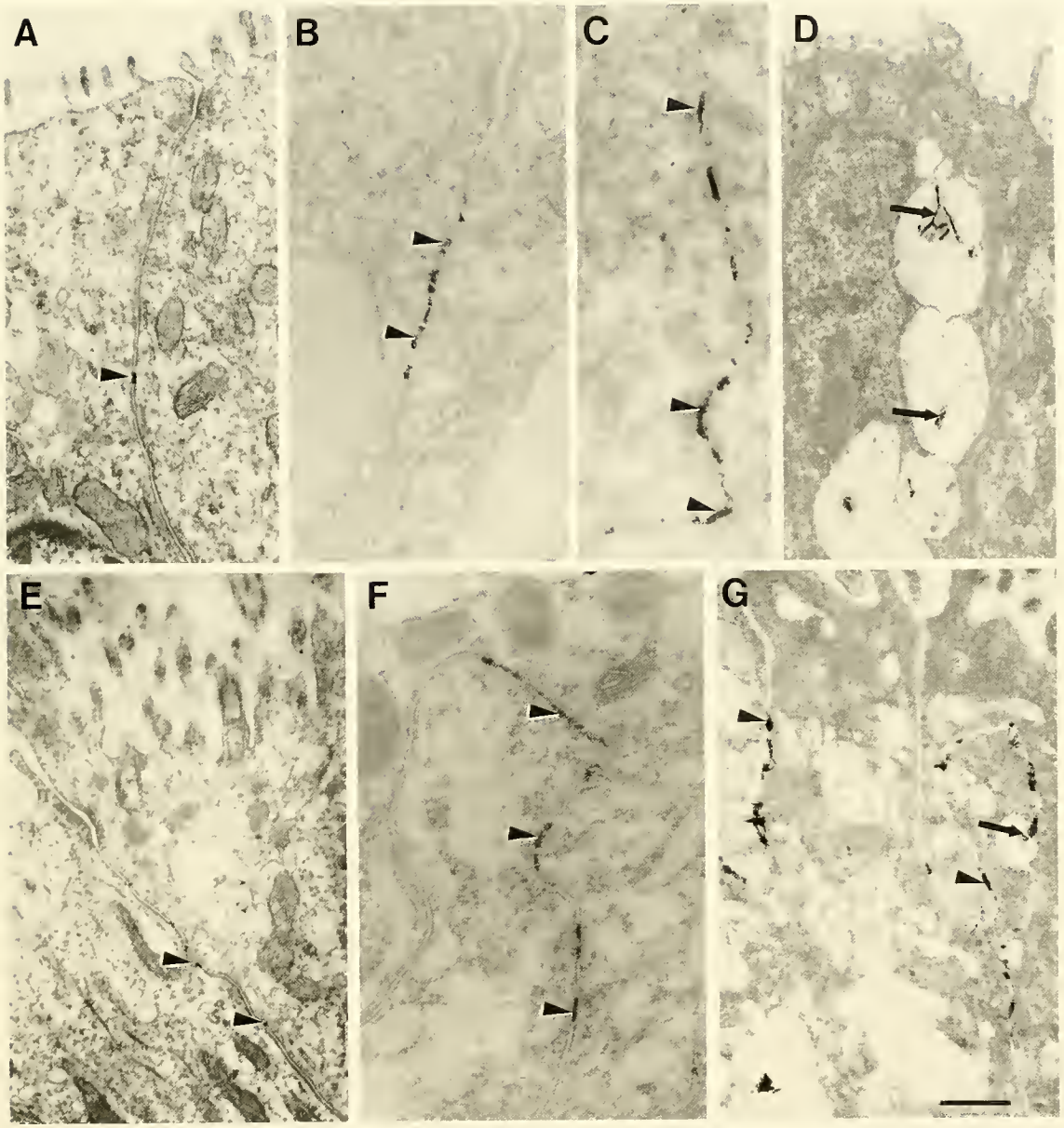

Figure 1. Transmission electron micrographs of gills from *Corbicula fluminea* (A–D) and *Toxolasma texasensis* (E–G) exposed to solutions containing 0.1 m*M* lanthanum. All sections are unstained, and the apical surface is at the top of each micrograph. The calibration bar for all micrographs is at the bottom right corner. (A) Gill epithelium from a *C. fluminea* specimen that was exposed to lanthanum in pondwater for 12 h (control). A small deposit of electron-dense lanthanum precipitate is in the lateral (paracellular) space between cells in the center of the micrograph (arrowhead); bar = 0.46 μm. (B) Gill epithelium from an animal that was exposed to 100 m*M* sucrose in pondwater for 2 h. Small amounts of lanthanum deposits are noticeable in the space between cells (arrowheads); bar = 0.23 μm. (C) Gill epithelium from an animal that was exposed to 100 m*M* sucrose in pondwater for 12 h. Extensive electron-dense lanthanum deposits are present in the space between cells (arrowheads); bar = 0.24 μm. (D) A different region of the same tissue appears more condensed, and a series of lanthanum-containing "blisters" are seen in the lateral membrane region between the epithelial cells (arrows). These blisters may appear as vesicles that are incorporating portions of lateral membranes; bar = 0.89 μm. (E) Gill epithelium from a *T. texasensis* specimen that was exposed to lanthanum in pondwater for 12 h (control). Close to the bottom of the micrograph are lanthanum deposits in the lateral space between cells (arrowheads); bar = 0.49 μm. (F) Gill epithelium from an animal that was exposed to 100 m*M* sucrose in pondwater for 2 h. Electron-dense lanthanum deposits are present in the paracellular space between cells (arrowheads); bar = 0.31 μm. (G) Gill epithelium from an animal that was exposed to 100 m*M* sucrose in pondwater for 12 h. Extensive electron-dense precipitates of lanthanum are found in the paracellular spaces (arrowheads). Lanthanum-containing blisters are present on the right side of the micrograph (arrow); bar = 0.31 μm.

changes were not due to deterioration of the cells or tissues. We have observed that although *Dreissena polymorpha* has the highest paracellular permeability to nonelectrolytes among the bivalves that have been studied, it will survive for more than 2 weeks in 100 m*M* mannitol with little mortality (unpubl. obs.).

The most notable difference between *T. texasensis* and *C. fluminea* is that the former has a lower resistance to long-term hyperosmotic challenge; the difference is probably due to the relative leakiness of the epithelia in the two species. The major change in epithelial permeability occurred after only 8 h of exposure of *T. texasensis* to hyperosmotic glucose, at which time an acute decrease of solutes occurred concomitant with the rapid rise of glucose concentration in the blood. The leakiness was confirmed by the high net loss of Na and Cl from the mussels. As in *C. fluminea*, the increased epithelial permeability was mostly paracellular, as suggested by the increase in lanthanum precipitates between the intercellular spaces after hyperosmotic treatments. Unlike *C. fluminea*, *T. texasensis* was not able to retain its blood ions after the abrupt change of epithelial permeability. After 12 h of exposure to the hyperosmotic glucose, more than 75% of the ionic solutes were lost from the blood. Furthermore, the loss of the solutes from the blood was relatively nonselective.

Another significant difference is that instead of experiencing an elevation in concentration of the ions in the blood due to dehydration, *T. texasensis* maintained a nearly normal ion concentration for a short exposure (up to 8 h) to a hyperosmotic challenge of glucose. The apparent maintenance of the ion concentration in the blood was coupled with a comparatively low accumulation of glucose in the blood, suggesting that the paracellular permeability was initially relatively low. The slightly increased osmolality was attributed to the small amount of glucose that accumulated in the blood. Despite the dehydrating hyperosmotic conditions, there was no evidence of an elevation in the concentration of ions in the blood of *T. texasensis*. These results suggest that the mussels were losing body fluids so that there was a concomitant loss of solutes and water, as was observed previously in *D. polymorpha* (Dietz *et al.*, 1995). This hypothesis is consistent with the net loss of Na and Cl observed during the hyperosmotic challenge.

The physiological responses of *T. texasensis* to hyperosmotic stress are intermediate, but more similar to those of *D. polymorpha* (Dietz *et al.*, 1995) than of *C. fluminea*. In *D. polymorpha*, approximately 80% to 85% of the Na and Cl in the blood was lost after 12 h of exposure to 100 m*M* mannitol or glucose in pondwater. Within 4 h of exposure to hyperosmotic conditions, total solute was elevated due to the gain of glucose or mannitol in the blood and not to a dehydration-induced elevation of ion concentration. The responses of *T. texasensis* to hyperosmotic challenge are similar to those of *D. polymorpha* in at least two respects. For short-term hyperosmotic exposure, in neither species was there a significant elevation in the concentration of ions in the blood by dehydration. In addition, during 12 h of hyperosmotic challenge both species displayed a substantial increase in the paracellular permeability of the epithelium, allowing the outward loss of electrolytes and the simultaneous inward diffusion of nonelectrolytes from the bathing medium.

In both species, the concentration of potassium in the blood either remained constant as the concentration of other ions increased, or it decreased. These results are consistent with a redistribution of K to the intracellular compartment to provide solute for regulating cellular volume. Similar results were observed in *D. polymorpha* subjected to hyperosmotic challenge (Dietz *et al.*, 1997, 1998). The elevated Ca concentration in the blood of *C. fluminea* likely represents a mobilization of Ca from the shell (Byrne *et al.*, 1989).

The tolerance of freshwater bivalves to an osmotic challenge might reflect their habitats and possibly their origin. *C. fluminea* has been reported to inhabit brackish water up to 5‰ salinity, although it is a freshwater species (Filice, 1958; Hayashi, 1956). Compared to unionid clams, corbiculids are able to maintain a higher osmolality (Dietz, 1979; McCorkle and Dietz, 1980; Zheng and Dietz, 1998). The characteristics of relatively lower paracellular permeability of the epithelia and higher ion transport rates allow *C. fluminea* to maintain the solutes in its blood at a higher concentration than that found in the unionid clam *T. texasensis*. Thus, *C. fluminea* is less sensitive than *T. texasensis* to osmotic stress and more resistant to environmental osmotic challenges.

Acknowledgments

We thank Chengsung Jiang, Janice E. Horohov, Julie Cherry, Diondi Lessard, Paul Bruce, Shawn Wilcox, and Timothy Smith for technical assistance. Harold Silverman provided valuable comments. We thank Ron Bouchard from the M. D. Socolofsky Microscopy Center for his able assistance. This paper was submitted to the Graduate School of Louisiana State University and A&M College in partial fulfillment of the Ph. D. degree by H. Z. The research was supported, in part, by NSF 90-17461, and by Louisiana Sea Grant NOAA 46RG00960 Project R/ZMM-1.

Literature Cited

Barry, P. H., J. M. Diamond, and E. M. Wright. 1971. The mechanism of cation permeation in rabbit gallbladder: dilution potentials and bi-ionic potentials. *J. Membr. Biol.* **4:** 358–394.

Boulpaep, E. 1971. Electrophysiological properties of the proximal tubule: importance of cellular and intercellular transport pathways. Pp. 91–112 in *Electrophysiology of Epithelial Cells*, G. Giebisch and F. K. Schattauer, eds. Springer-Verlag, Stuttgart.

Byrne, R. A., R. F. McMahon, and T. H. Dietz. 1989. The effects of aerial exposure and subsequent reimmersion on hemolymph osmolality, ion composition and ion flux in the freshwater bivalve, *Corbicula fluminea*. *Physiol. Zool.* **62:** 1187–1202.

Diamond, J. M. 1977. The epithelial junction: bridge, gate, and fence. *Physiologist* **20:** 10–18.

Dietz, T. H. 1978. Sodium transport in the freshwater mussel, *Carunculina texasensis* (Lea). *Am. J. Physiol.* **235:** R35–R40.

Dietz, T. H. 1979. Uptake of sodium and chloride by freshwater mussels. *Can. J. Zool.* **57:** 156–160.

Dietz, T. H. 1985. Ionic regulation in freshwater mussels: a brief review. *Am. Malacol. Bull.* **3:** 233–242.

Dietz, T. H., R. A. Byrne, J. W. Lynn, and H. Silverman. 1995. Paracellular solute uptake by the freshwater zebra mussel *Dreissena polymorpha*. *Am. J. Physiol.* **269:** R300–R307.

Dietz, T. H., S. J. Wilcox, R. A. Byrne, J. W. Lynn, and H. Silverman. 1996. Osmotic and ionic regulation of North American zebra mussels (*Dreissena polymorpha*). *Am. Zool.* **36:** 364–372.

Dietz, T. H., S. J. Wilcox, R. A. Byrne, and H. Silverman. 1997. Effects of hyperosmotic challenge on the freshwater bivalve, *Dreissena polymorpha:* Importance of K^+. *Can. J. Zool.* **75:** 697–705.

Dietz, T. H., D. S. Neufeld, H. Silverman, and S. H. Wright. 1998. Cellular volume regulation in freshwater bivalves. *J. Comp. Physiol.* **168:** 87–95.

Filice, F. P. 1958. Invertebrates from the estuarine portion of San Francisco Bay and some factors influencing their distribution. *Wasmann. J. Biol.* **16:** 159–211.

Frömter, E., and J. Diamond. 1972. Route of passive ion permeation in epithelia. *Nat. New Biol.* **235:** 9–13.

Fyhn, H. J., and J. D. Costlow. 1975. Anaerobic sampling of body fluids in bivalve molluscs. *Comp. Biochem. Physiol.* **52A:** 266–268.

Gäde, G. 1991. Hyperglycaemia or hypertrehalosaemia? The effect of insect neuropeptides on haemolymph sugars. *J. Insect Physiol.* **37:** 483–487.

Gardiner, D. B., H. Silverman, and T. H. Dietz. 1991. Musculature associated with the water canals in freshwater mussels and response to monoamines *in vitro*. *Biol. Bull.* **180:** 453–465.

Gerencser, G. A. 1982. Paracellular transport characteristics of *Aplysia juliana* intestine. *Comp. Biochem. Physiol.* **72A:** 721–725.

Hayashi, Y. 1956. On the variation of *Corbicula* due to environmental factors. *Venus* **19:** 54–60.

Keen, A. M., and R. Casey. 1969. Family Corbiculidae, Gray 1847. Pp. 665–669 in *Treatise on Invertebrate Paleontology,* Pt. N, N. R. C. Moore, ed. Geological Society of America, Boulder, Colorado.

Lord, B. A. P., and D. R. DiBona. 1976. Role of the septate junction in the regulation of paracellular transepithelial flow. *J. Cell. Biol.* **71:** 967–972.

McCorkle, S., and T. H. Dietz. 1980. Sodium transport in the freshwater Asiatic clam *Corbicula fluminea*. *Biol. Bull.* **159:** 325–336.

Montgomery, R. 1957. Determination of glycogen. *Arch. Biochem. Biophys.* **67:** 378–386.

Uglem, G. L., D. J. Prior, and S. D. Hess. 1985. Paracellular water uptake and molecular sieving by the foot epithelium of terrestrial slugs. *J. Comp. Physiol. B.* **156:** 285–289.

Wilcox, S. J., and T. H. Dietz. 1995. Potassium transport in the freshwater bivalve *Dreissena polymorpha*. *J. Exp. Biol.* **198:** 861–868.

Zheng, H., and T. H. Dietz. 1998. Ion transport in the freshwater bivalve *Corbicula fluminea*. *Biol. Bull.* **194:** 161–169.

Reference: *Biol. Bull.* **194:** 178–186. (April, 1998)

Gastrovascular Circulation in an Octocoral: Evidence of Significant Transport of Coral and Symbiont Cells

DANIEL GATEÑO,* ALVARO ISRAEL, YAEL BARKI, AND BARUCH RINKEVICH

National Institute of Oceanography, Israel Oceanographic and Limnological Research, P.O. Box 8030, Haifa 31080, Israel

Abstract. The gastrovascular system in the Red Sea soft coral *Parerythropodium fulvum fulvum* comprises two interconnected networks of canals filled with fluid and circulating cells. The first network is composed of narrow canals (50–80 μm in width) located below the upper ectodermal layer; the second network includes larger canals (300–500 μm in width) that are located deeper in the coral tissue. Particle movement in the second network is faster than in the superficial network, but in both, coral cells with and without healthy zooxanthellae circulate freely. To investigate the movement of metabolites and cellular components within the colony, coral fragments were exposed to ^{14}C-labeled seawater for 24 h in the laboratory and *in situ* under saturating photosynthetic photon flux and then grafted back to their original colonies. Grafts fused after 24 h. In the laboratory experiment, up to 45% of the fixed ^{14}C was translocated to the unlabeled colony within 48 h after fusion. In the *in situ* experiment, significant translocation of labeled materials occurred at the furthest parts of the colonies, 390 mm away from the fusion line, in 24 h. Even though the amount of labeling varied between colonies, labeled material spread throughout all the unlabeled parts. It thus appears that the gastrovascular system in *Parerythropodium fulvum fulvum* functions as an effective circulatory apparatus for fast translocation of organic compounds and cellular components within the colony.

Introduction

Corals are mostly colonial cnidarians composed of modular units (polyps) that, in a single colony, are physically connected and generally share similar physiological and biochemical environments. Translocation of organic compounds between polyps could result from diffusion down a concentration gradient (Pratt, 1905; Murdoch, 1978a; Fang *et al.*, 1989) or from active transport in the fluid of the gastrovascular system (Gladfelter, 1983; Schlichter, 1991, 1992).

Gastrovascular systems have been studied in several cnidarian groups including hydromedusae (Roosen-Runge, 1967), hydroids (Rees *et al.*, 1970; Blackstone, 1996), gorgonians (Murdoch, 1978a, b), pennatulids (Musgrave, 1909; Parker, 1920; Brafield, 1969), hexacorallians (Gladfelter, 1983; Schlichter, 1991, 1992), and soft corals (Pratt, 1905). These systems have been suggested to function as (1) a hydrostatic skeleton allowing the colony to expand or retract (Chapman, 1974; Fautin and Mariscal, 1991), (2) a transport system for the distribution of substances between polyps in which extracellular digestion of organic material also takes place (Gladfelter, 1983; Schlichter, 1991, 1992), (3) a transport system for exchange of gases such as oxygen and carbon dioxide (Brafield and Chapman, 1967; Chapman, 1972), (4) an excretion system for waste metabolites (Schlichter, 1991), and (5) a system that controls the morphological development of colonies (Dudgeon and Buss, 1996). Gastrovascular systems have been described as ramified canal networks with blind ends and with back-and-forth movement of the internal fluid (Blackstone, 1996) propelled by either flagella (Gladfelter, 1983) or other mechanisms (Schierwater *et al.*, 1992). In some corals, the gastrovascular cavity is a flow-through system with many pores that are located near the crests of the sclerosepta of the external body wall and allow uni-directional movement of fluids (Schlichter, 1991, 1992). Anthozoan and hydrozoan gastrovascular systems are distinguished one from the other

Received 17 March 1997; accepted 9 December 1997.

* To whom correspondence should be addressed. E-mail: dani@ocean.org.il

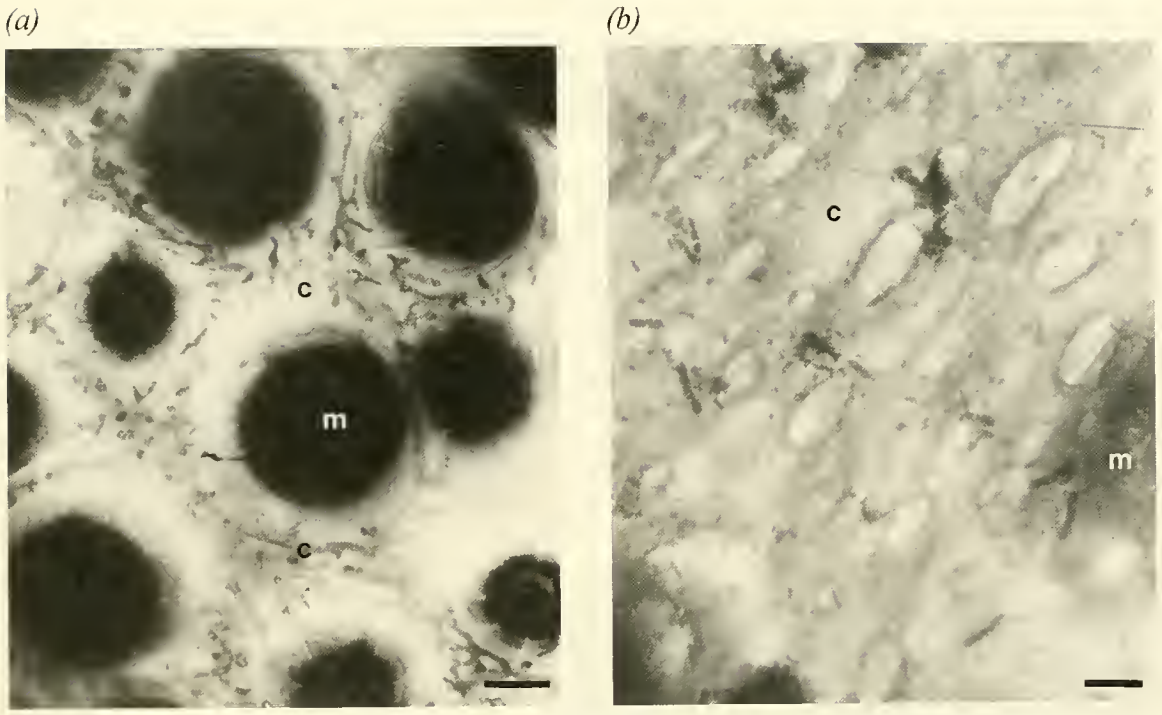

Figure 1. General morphology of the gastrovascular system of *Parerythropodium fulvum fulvum*. Superficial (a) and deep (b) network of canals in live specimens growing on glass slides. In photograph (b) the coral was positioned upside down with a strong back light to make the canals visible. m = mouth of a polyp, c = canal. Scale bars = 500 μm.

primarily by the presence of flagellated endodermal cells lining the entire internal gastrovascular epithelium of the anthozoans. This study refers mainly to the anthozoans.

Parerythropodium fulvum fulvum (Forskål, 1775), a symbiotic alcyonarian soft coral characterized by an encrusting growth form, a thin coenenchyme, and short polyp cavities, is common in shallow waters of the Israeli Red Sea coast (Benayahu and Loya, 1983). To further reveal the role of the gastrovascular system in this species, we investigated the structure and some physiological functions of this system. Here we document the free circulation of living animal cells and zooxanthellae within the gastrovascular system and the rapid transport of organic substances between different parts of the colony. These results suggest that the gastrovascular system in *P. f. fulvum* is a functional circulatory apparatus.

Materials and Methods

Collection and maintenance of corals

Colonies of *Parerythropodium fulvum fulvum* were collected at depths between 3 and 12 m in the Red Sea, next to the H. Steinitz Marine Biology Laboratory, Eilat, Israel. This encrusting coral is about 6-mm thick when growing on a straight surface; polyps emerge 3 to 10 mm from the base when expanded and have an average density of 22.6 polyps cm^{-2} (SD = 6.2; n = 8 different colonies). Colonies were carefully peeled off the substrate, reattached to glass slides by cotton threads, and transported to the National Institute of Oceanography at Haifa, Israel.

The corals were grown in the laboratory in 17-l aerated aquaria filled with running, 20-μm-filtered seawater at 24° ± 1°C. Photosynthetic photon flux (PPF) was provided by 500 W halogen lamps on a 12:12 h (light:dark) regime. On the surface of the aquaria the PPF, measured with a quantum meter (LI-COR, North Carolina), averaged 150 μmol photon m^{-2} s^{-1}, which is approximately the irradiance at a depth of 10 m in the Red Sea. Corals were fed twice a day with either 50-μm microcapsules of artificial plankton (Argent, Redmond, Washington), *Artemia nauplii* (Neptune Industries, Salt Lake City, Utah), or lyophilized rotifers.

Morphology

Specimens growing on the glass slides were observed with a binocular dissecting microscope at magnifications from 10× to 63×. For light microscopy, samples were fixed in 2.5% glutaraldehyde for 24 h, decalcified with formic acid and sodium citrate for 30 min (Rinkevich and Loya, 1979), dehydrated with ethanol, and embedded in glycol methacrylate plastic. Histological sections (width 2–3 μm) were stained with hematoxylin and eosin (Ban-

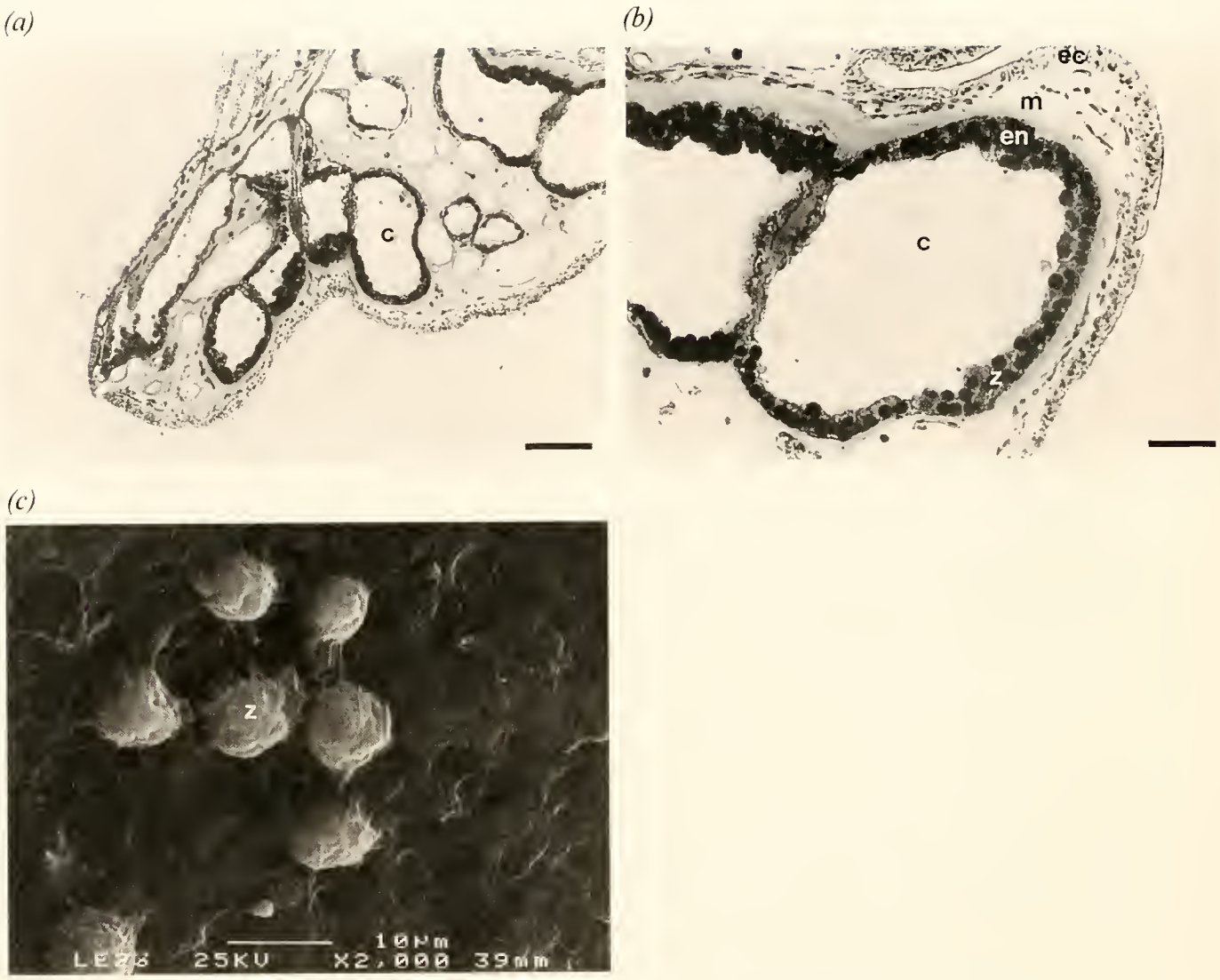

Figure 2. Detailed morphology of the gastrovascular system of *Parerythropodium fulvum fulvum.* (a, b) Cross-sections of the deeper canals inside the coral tissue. (c) Scanning electron micrograph showing algal cells embedded in endoderm within the inner wall of the canals. c = canal, ec = ectoderm, en = endoderm, m = mesoglea, z = zooxanthellae. Scale bars: a = 500 μm; b = 30 μm; c = 10 μm.

croft and Stevens, 1990). For scanning electron microscopy, specimens were fixed in 2.5% glutaraldehyde (electron microscopy grade) in filtered seawater, and sections were prepared following Bancroft and Stevens (1990).

Circulation of free cells

The presence of free circulating cells in the gastrovascular system was determined in three ways: (1) by collecting gastrovascular fluid from the mouth of the polyps and from inside the canals (fluid was obtained using a micromanipulator [Narishige, Japan], a microinjector [Narishige, IM 300, Japan] and a micropipette with a tip diameter of 30 μm) and viewing it with a light microscope (100×–1000×); (2) by analyzing histological cross-sections of the gastrovascular canals; and (3) by using a sharp razor blade to injure live corals in the periphery of the colony and observing the outcoming fluid under the light microscope.

To measure the movement of free cells in the canals, corals growing on glass slides were observed under the binocular dissecting microscope with strong background light. The movement rate of particles inside the gastrovascular system was timed by using a built-in grid located in the ocular of the dissecting microscope.

^{14}C labeling

Coral fragments from six colonies growing in the laboratory and six large colonies growing in the field were

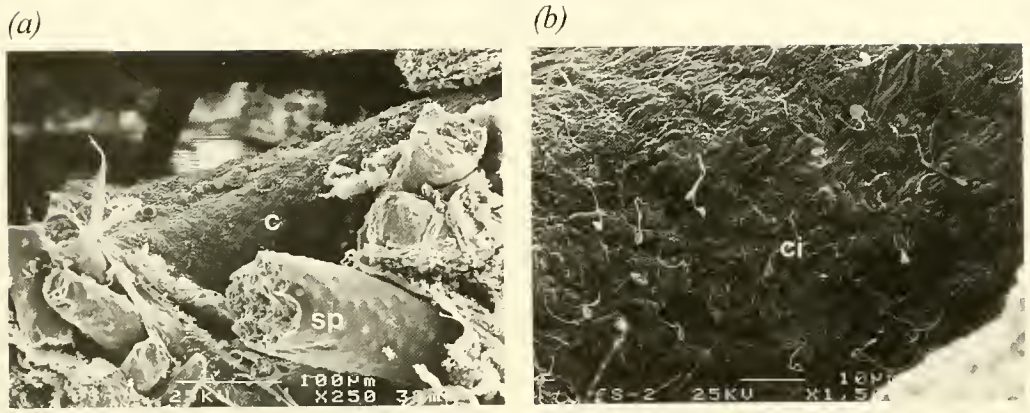

Figure 3. Scanning electron micrograph of the inner walls of a canal from the gastrovascular system of *Parerythropodium fulvum fulvum*. (a) This sample was frozen and then fractured to show the inner part of a canal. (b) Closer view of the inner wall covered with cilia. c = canal, ci = cilia, sp = spicula. Scale bars: a = 100 μm; b = 10 μm.

cut 24 to 48 h before starting the experiments. The fragments were incubated for 24 h in closed, transparent 1-l plastic chambers filled with filtered (2 μm) seawater containing $NaH^{14}CO_3$ (Amersham, Netherlands; 0.01 μCi ml^{-1}) at 25°C under continuous illumination (300 μmol photon m^{-2} s^{-1}) and gentle stirring. Incubation was followed by two to three rinses with ^{14}C-free seawater and placement in the dark to eliminate unfixed ^{14}C. The seawater was changed daily until no traces of radioactivity were found in the medium, usually 2 days, and then the labeled fragments were grafted in the laboratory or *in situ* to their original colonies.

Within the next 24 h, the fragments usually reattached to the substrate and fused, which included the connection of the canals, with tissue of the original colonies (see Frank *et al.*, 1996). Tissue from the labeled fragments and the unlabeled colonies was sampled with a 5-mm-diameter metal cork-borer (0.196 cm^2) 12, 24, and 48 h after fusion for the laboratory experiments and 24 h after fusion for the field experiments. The distance of each sample from the fusion line was recorded. The samples were solubilized in 1 ml Soluene-350 (Packard, England) at 37°C for 24 h. To eliminate any remaining unfixed ^{14}C, 0.5 ml of a 1 *N* solution of HCl was added, followed by gentle aeration for 4 h. Radioactivity was measured with a liquid scintillation spectrophotometer (Kontron) using 4 ml of scintillation fluid (Optifluor, Packard, England). To evaluate possible passage of ^{14}C to the unlabeled fragment through the water, similar control colonies were placed close (2–3 mm) to but not in contact with the labeled grafts and later sampled as above.

Results

Morphology of the canal system

Observations of live colonies on glass slides revealed that the gastrovascular system in *Parerythropodium fulvum fulvum* comprises two distinctive, interconnected types of canals (Fig. 1) filled with moving fluid. The first type is superficial, lying just below the outer ectoderm layer and surrounding the polyps (Fig. 1a). The canals in this area were 50–80 μm in width, with abundant dead ends; the average speed of the particles in the fluid was 1.2 cm h^{-1} (n = 8; SD = 0.9) to either direction. The second type is deeper in the coenosarc and close to the base of the colony (Fig. 1b). These canals were 300–500 μm in width and the speed of their particles was much faster, averaging 3.4 cm min^{-1} (n = 10; SD = 1.1). In the superficial canals, zooxanthellae and coral cells were seen forming patches, but in deeper canals they moved freely with no apparent directionality.

Measurements on histological cross-sections (Fig. 2a, b), indicated that the gastrovascular cavity accounts for an average of 45% (n = 5; SD = 12.2) of the animal's volume. The inner wall of the canals is lined with endodermal cells possessing abundant zooxanthellae (Fig. 2b, c), with cilia covering most of the canal inner surface (Fig. 3a, b).

Circulation of free cells

Histological cross-sections from the gastrovascular cavity confirmed the presence of large quantities of free cells (Fig. 4a) inside the canals (Fig. 4b, c). Two types of cells circulated freely in the gastrovascular fluid collected from either polyp mouths or canals. Most (81.6%; SD = 5.4, n = 20 different coral colonies; 50 to 100 cells counted in each sample) were coral cells containing zooxanthellae, and the rest were coral cells without zooxanthellae. In addition, amorphous particles that may correspond to partly digested food were commonly seen in the gastrovascular fluid. When corals were slightly injured at the edge of the colony, large amounts of zooxanthellae

(a)

(b)

(c)

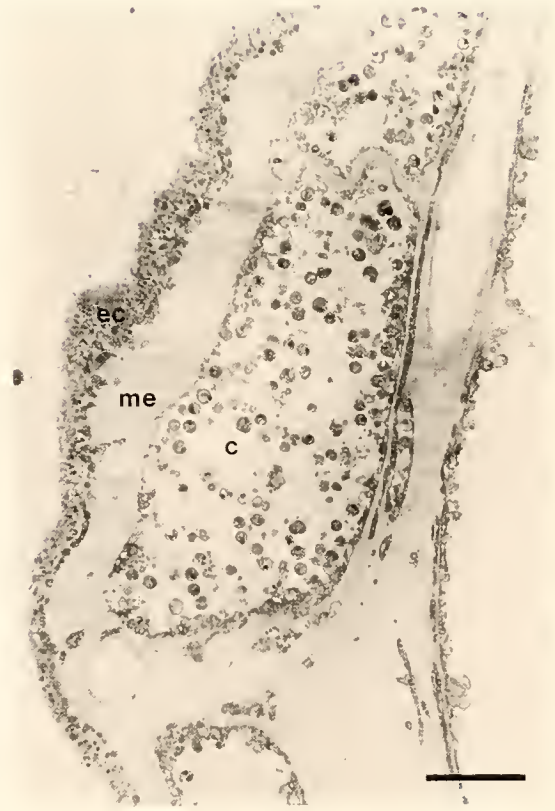

(d)

Table I

Translocation of ^{14}C over time in the laboratory experiment following fusions between the labeled fragments and their respective unlabeled coral colonies; (n) is the number of corer samples analyzed

Colony no.	Fragment size (cm^2)		Total ^{14}C (DPM)*		Time (h)	^{14}C transported (%)
	Labeled (n)	Unlabeled (n)	Labeled	Unlabeled		
1	3.28 (4)	18.28 (26)	157,442	2,756	12	1.7
2	4.97 (7)	52.56 (63)	288,025	12,092	12	4.0
3	0.79 (2)	1.52 (3)	341,095	24,194	24	6.6
4	5.28 (5)	17.81 (7)	329,453	72,842	24	18.1
5	3.12 (3)	19.57 (6)	1,346,105	312,022	24	18.8
6	1.01 (2)	2.32 (4)	360,677	299,836	48	45.4

* DPM = disintegrations per minute.

and coral cells were continuously expelled outwards for several minutes (Fig. 4d).

^{14}C-labeling

In the laboratory experiment, translocation of ^{14}C from the labeled to the unlabeled fragment occurred shortly (12–24 h) after fusion (Table I). The percentage of translocated ^{14}C from the total fixed carbon was calculated using the formula: $100 \times U/(L + U)$, where U and L are the total disintegrations per minute (DPM) for the unlabeled and labeled fragments, respectively. The transport of ^{14}C from the labeled to the unlabeled fragment of the colony averaged 2.8% (SD = 1.6; n = 2) to 14.5% (SD = 6.9; n = 3), 12 to 24 h after fusion, respectively, and increased to 45.4% (n = 1) 48 h after fusion (Table I). The coefficient of variability (CV) was high for both the 12-h (CV = 57%) and the 24-h colonies (CV = 47%). The detailed results for tissue samples taken from the unlabeled parts of colonies 5 and 6 (Table I) are provided in Figure 5. ^{14}C-labeled materials extended virtually throughout the unlabeled colonies within 24 to 48 h of fusion, but two neighboring samples differed by 2- to 3-fold, indicating uneven distribution of the ^{14}C-labeled compounds (Fig. 5a, b).

Colonies used in field experiments were much larger than those used in laboratory experiments. Because of the extremely irregular morphology of colonies in nature their actual size could not be estimated; therefore, these colonies were used only in evaluating the translocation distances 24 h after fusion. We recorded ^{14}C in the most distant part of the unlabeled colony, 390 mm away from the fusion line (Fig. 6). However, the amounts of ^{14}C that were recovered within the range of 1–150 mm from the fusion line were significantly higher than the amounts recorded farther away (ANOVA; df = 227; F = 16.68; $P < 0.01$). No traces of radioactivity were found in the control colonies for laboratory or field experiments, thus indicating that ^{14}C was not being passed from labeled fragments to the unlabeled parts of the colony through the water.

Discussion

The results presented here show that the gastrovascular system in the soft coral *Parerythropodium fulvum fulvum* is a complex, interconnected network of canals that facilitates the rapid transport of fluid, organic particles, and cells between distant parts of the colony. The movement of the fluid in gastrovascular systems of cnidarians could be driven by contractions of the epitheliomuscular cells (Van Winkle and Blackstone, 1997) or contractile vacuoles (Schierwater *et al.*, 1992), or by the activity of cilia. Since we never observed signs of canal contractions in *P. f. fulvum*, we may conclude that the third possibility, ciliar action, is probably the main mechanism of fluid propulsion in this species, as it is in other anthozoans (Gladfelter, 1983). Furthermore, the gastrovascular system of *P. f. fulvum* may function not only as an internal water system, as previously suggested for other cnidarians

Figure 4. Freely circulating cells in the gastrovascular system of *Parerythropodium fulvum fulvum*. (a) Photomicrograph of the coral cells and zooxanthellae collected from inside the canals of the gastrovascular system. (b) Histological section through the gastrovascular system just below the mouth of a polyp, showing the presence of large numbers of free cells (arrows) inside the gastrovascular system. (c) Closer view of a cross-section of one superficial canal showing the free cells. (d) "Bleeding" of zooxanthellae and coral cells 2 min after injury to the edge of the colony. a = animal cell, b = bleeding, c = canal, ec = ectoderm, en = endoderm, gv = gastrovascular cavity, m = mouth of the polyp, me = mesoglea, z = zooxanthellae. Scale bars: a = 4 μm; b = 200 μm; c = 100 μm; d = 1000 μm.

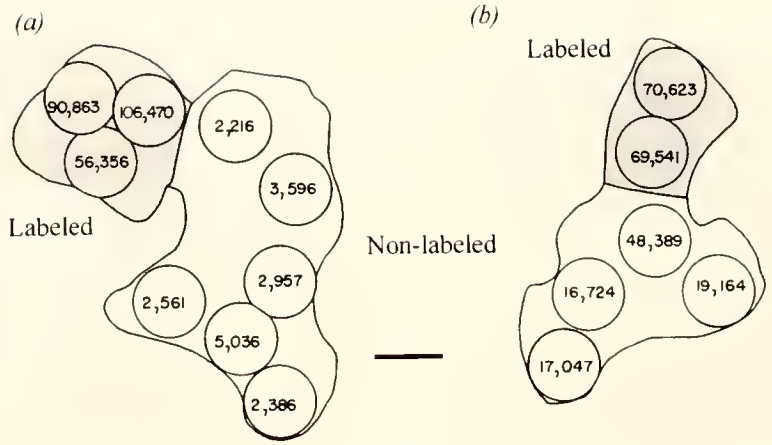

Figure 5. ^{14}C distribution within fused labeled and unlabeled fragments on two laboratory colonies of *Parerythropodium fulvum fulvum:* (a) Colony 5 (Table 1) 24 h after fusion. (b) Colony 6 (Table 1) 48 h after fusion. Circles represent cork-bored samples (0.196 cm^2). Numbers are the disintegrations per minute per sample. Scale bar = 5 mm.

(Chapman, 1974; Fautin and Mariscal, 1991), but also as an effective circulatory apparatus, analogous to a primitive vascular system. The transport of metabolites within *P. f. fulvum* colonies to several tens of centimeters in 24 h is faster than recorded for other corals (Pearse and Muscatine, 1971; Taylor, 1977; Gladfelter, 1983; Rinkevich and Loya, 1983a, b; Rinkevich, 1991) in which transport has been attributed to simple diffusion (Pratt, 1905; Murdoch, 1978a; Fang *et al.*, 1989). This rules out the possibility that the recorded translocation is the result of a process other than gastrovascular transport, as it is in the marine bryozoan *Membranipora membranacea* (Miles *et al.*, 1995).

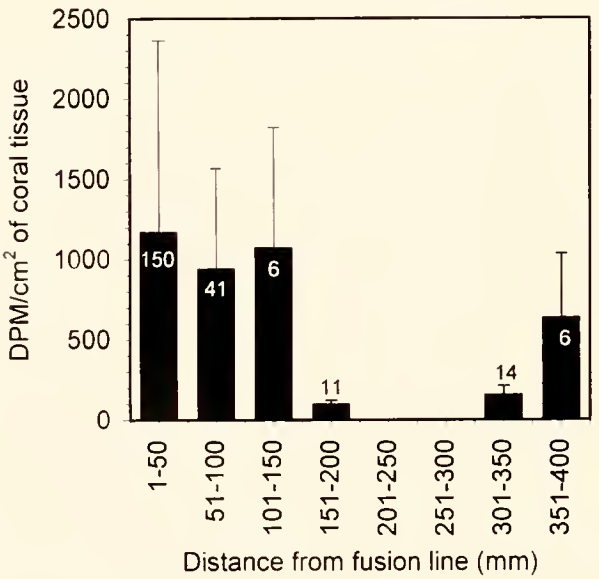

Figure 6. Distribution of ^{14}C within the unlabeled colony of *Parerythropodium fulvum fulvum* in the field experiments (n = 6) 24 h after fusion. Bars indicate the mean number of disintegrations per minute (DPM) per square centimeter of coral tissue (± 1 SD) for the distance range from the fusion line. Numbers at the top of each bar are the sample sizes for each range of distances. No samples were taken between 201 and 300 mm from the fusion line.

The presence of the two distinct networks of canals indicates that they may have different functions. We propose that an important function of the superficial network, which is located just under the upper ectodermal layer and is characterized by narrow canals, slow particle movement, and many dead ends, is to increase the exposure of the algal symbionts to light. The inner network, with larger canals and faster particle movement, is the part of the gastrovascular system responsible for the rapid transport of cells, particles, and substances throughout the colony.

The high variability seen within the 12-h and 24-h measurements of the amounts of ^{14}C translocated from labeled to unlabeled fragments could be due to differences between colonies in the number of functional canal interconnections or the rates of transport. Nevertheless, samples taken from the same colony 24 and 48 h after fusion showed similar levels of fixed ^{14}C, indicating that most of the translocated labeled materials were distributed throughout the unlabeled colony within short periods after fusion. Moreover, the percentage of the total fixed ^{14}C that is translocated is greater if the zooxanthellae that are embedded in the endodermal layer of the labeled fragment, and therefore do not move, are considered. Photosynthates are therefore being transported either inside the circulating algae or as dissolved materials in the gastrovascular fluid.

It is commonly accepted that zooxanthellae are located only in the endodermal layer (Glider *et al.*, 1980; Rinkevich and Loya, 1983a, b; Muscatine, 1990; Gates *et al.*, 1992), whereas free algal cells circulating in the gastro-

vascular system are assumed to be partly digested senescent zooxanthellae or algae in the process of being expelled outside the colony (Trench, 1987; Titlyanov *et al.*, 1996). Our observations suggest that large populations of apparently healthy zooxanthellae within coral cells and animal cells move freely in the gastrovascular system of *P. f. fulvum;* a similar phenomenon is occasionally seen in the hermatypic coral *Acropora cervicornis* (Gladfelter, 1983). Many questions regarding the floating cells remain to be investigated—for example, the digestive behavior of the *P. f. fulvum* gastrovascular system, how healthy living cells are kept from being digested, how long a specific animal cell (with or without symbiontic algae) continues to circulate, and what is the origin of these cells.

Algal circulation probably facilitates metabolite exchange between symbionts and enhances light capture since it acts as a regulatory mechanism for algae. Active intracolonial transport is an important feature of colonial organisms: it allows the reallocation of resources such as oxygen (unpubl. data) and photosynthates, helping to maintain the health of the colony in case of injury or when not all polyps succeed in capturing food or light (Taylor, 1977; Hughes, 1989).

We also have evidence to support the idea (*e.g.*, Buss and Vaisnys, 1993) that the gastrovascular system plays an important role in the bleaching of coral. Previous studies have shown that bleaching may be controlled by extremes of temperature, salinity, and light intensity (Buddemeier and Fautin, 1993). We found that after 1 h of exposure to high temperature (30°C), polyps of *P. f. fulvum* expelled large quantities of zooxanthellae through the mouth (unpubl. data). The mechanisms involved in the regulation of the free-circulating zooxanthellae and animal cells through the mouth of the polyp are not yet understood.

The gastrovascular system in the alcyonarian coral *Parerythropodium fulvum fulvum,* and probably in other cnidarians, plays an important role in the physiology and the development of the colonies, and it may still have other unknown functions, such as that of freely circulating cells.

Acknowledgments

We thank the staff and the personnel of the Steinitz Interuniversity Marine Biology Institute in Eilat for the use of their facilities. This study is part of the research done in the Minerva Center for Marine Invertebrate Immunology and Developmental Biology, and was also supported by EC Grant (INCO) ERB3514 PL950184.

Literature Cited

Bancroft, J. D., and A. Stevens. 1990. *Theory and Practice of Histological Techniques.* 3rd ed. Churchill Livingstone, Edinburgh.

Benayahu, Y., and Y. Loya. 1983. Surface brooding in the Red Sea soft coral *Parerythropodium fulvum fulvum* (Forskål, 1775). *Biol. Bull.* **165:** 353–369.

Blackstone, N. W. 1996. Gastrovascular flow and colony development in two colonial hydroids. *Biol. Bull.* **190:** 56–68.

Brafield, A. E. 1969. Water movements in the pennatulid coelenterate *Pteroides griseum. J. Zool. (Lond.)* **158:** 317–325.

Brafield, A. E., and G. Chapman. 1967. The respiration of *Pteroides griseum* (Bohadsch), a pennatulid coelenterate. *J. Exp. Biol.* **46:** 97–104.

Buddemeier, R. W., and D. G. Fautin. 1993. Coral bleaching as an adaptive mechanism. A testable hypothesis. *Bioscience* **43:** 320–326.

Buss, L. W., and J. R. Vaisnys. 1993. Temperature stress induces dynamical chaos in a cnidarian gastrovascular system. *Proc. R. Soc. Lond. B* **252:** 39–41.

Chapman, D. M. 1974. Cnidarian histology. Pp. 1–92 in *Coelenterate Biology. Reviews and New Perspectives,* L. Muscatine and H. M. Lenhoff, eds. Academic Press, New York.

Chapman, G. 1972. A note on the oxygen consumption of *Renilla kollikeri,* Pfeffer. *Comp. Biochem. Physiol. A.* **42:** 863–866.

Dudgeon, S. R., and L. W. Buss. 1996. Growing with the flow: on the maintenance and malleability of colony form in the hydroid *Hydractinia. Am. Nat.* **147:** 667–691.

Fang, L.-s., Y.-w. J. Chen, and C.-s. Chen. 1989. Why does the white tip of stony coral grow so fast without zooxanthellae? *Mar. Biol.* **103:** 359–363.

Fautin, D. G., and R. N. Mariscal. 1991. Cnidaria: Anthozoa. Pp. 267–358 in *Microscopic Anatomy of Invertebrates, Volume 2: Placozoa, Porifera, Cnidaria, and Ctenophora,* F. W. Harrison and J. A. Westfall, eds. Wiley-Liss, New York.

Frank, U., R. P. M. Bak, and B. Rinkevich. 1996. Allorecognition responses in the soft coral *Parerythropodium fulvum fulvum* from the Red Sea. *J. Exp. Mar. Biol. Ecol.* **197:** 191–201.

Gates, R. D., G. Baghdasarian, and L. Muscatine. 1992. Temperature stress causes host cell detachment in symbiotic cnidarians: implications for coral bleaching. *Biol. Bull.* **182:** 324–332.

Gladfelter, E. H. 1983. Circulation of fluids in the gastrovascular system of the reef coral *Acropora cervicornis. Biol. Bull.* **165:** 619–636.

Glider, W. V., D. Phipps, and R. L. Pardy. 1980. Localization of symbiontic dinoflagellate cells within tentacle tissue of *Aiptasia pallida* (Coelenterata, Anthozoa). *Trans. Am. Microsc. Soc.* **99:** 426–438.

Hughes, R. N. 1989. *A Functional Biology of Clonal Animals.* Chapman and Hall, New York. 331 pp.

Miles, J. S., C. D. Harvell, C. M. Griggs, and S. Eisner. 1995. Resource translocation in a marine bryozoan: quantification and visualization of ^{14}C and ^{35}S. *Mar. Biol.* **122:** 439–445.

Murdoch, G. R. 1978a. Digestion, assimilation, and transport of food in the gastrovascular cavity of a gorgonian octocoral (Cnidaria: Anthozoa). *Bull. Mar. Sci.* **28:** 354–362.

Murdoch, G. R. 1978b. Circulation and digestion of food in the gastrovascular system of gorgonian octocorals (Cnidaria: Anthozoa). *Bull. Mar. Sci.* **28:** 363–370.

Muscatine, L. 1990. The role of symbiotic algae in carbon and energy flux in reef corals. Pp. 75–87 in *Coral Reefs,* Z. Dubinsky, ed. Elsevier, Amsterdam.

Musgrave, E. M. 1909. Experimental observations on the organs of circulation and powers of locomotion in pennatulids. *Q. J. Microsc. Sci.* **54:** 443–482.

Parker, G. H. 1920. Activities of colonial animals. 1. Circulation of water in *Renilla. J. Exp. Zool.* **31:** 342–367.

Pearse, V. P., and L. Muscatine. 1971. Role of symbiotic algae (zooxanthellae) in coral calcification. *Biol. Bull.* **141:** 350–363.

Pratt, E. M. 1905. The digestive organs of the Alcyonaria and their

relation to the mesogleal cell plexus. *Q. J. Microsc. Sci.* **49:** 327–362.

Rees, J., L. Y. Davis, and H. M. Lenhoff. 1970. Paths and rates of food distribution in the colonial hydroid *Pennaria. Comp. Biochem. Physiol.* **34:** 309–316.

Rinkevich, B. 1991. A long-term compartmental partitioning of photosynthetically fixed carbon in a symbiotic reef coral. *Symbiosis* **10:** 175–194.

Rinkevich, B., and Y. Loya. 1979. The reproduction of the Red Sea coral *Stylophora pistillata.* I. Gonads and planulae. *Mar. Ecol. Prog. Ser.* **1:** 133–144.

Rinkevich, B., and Y. Loya. 1983a. Oriented translocation of energy in grafted reef corals. *Coral Reefs* **1:** 243–247.

Rinkevich, B., and Y. Loya. 1983b. Short-term fate of photosynthetic products in a hermatypic coral. *J. Exp. Mar. Biol. Ecol.* **73:** 175–184.

Roosen-Runge, E. C. 1967. Gastrovascular system of small hydromedusae: Mechanisms of circulation. *Science* **156:** 74–76.

Schierwater, B., B. Piekos, and L. W. Buss. 1992. Hydroid stolonal contractions mediated by contractile vacuoles. *J. Exp. Biol.* **162:** 1–21.

Schlichter, D. 1991. A perforated gastrovascular cavity in *Leptoseris fragilis.* A new strategy to improve heterotrophic nutrition in corals. *Naturwissenschaften* **78:** 467–469.

Schlichter, D. 1992. A perforated gastrovascular cavity in the symbiontic deep-water coral *Leptoseris fragilis:* a new strategy to optimize heterotrophic nutrition. *Helgol. Meeresunters.* **45:** 423–443.

Taylor, D. L. 1977. Intra-colonial transport of organic compounds and calcium in some Atlantic reef corals. *Proc. 3rd Int. Coral. Reef Symp.* **1:** 431–436.

Titlyanov, E. A., T. V. Titlyanova, V. A. Leletkin, J. Tsukahara, R. van Woesik, and K. Yamazato. 1996. Degradation of zooxanthellae and regulation of their density in hermatypic corals. *Mar. Ecol. Prog. Ser.* **139:** 167–178.

Trench, R. K. 1987. Dinoflagellates in non-parasitic symbiosis. Pp. 531–570 in *The Biology of Dinoflagellates,* F. J. R. Taylor, ed. Blackwell Scientific, Oxford.

Van Winkle, D. H., and N. W. Blackstone. 1997. Video microscopical measures of gastrovascular flow in colonial hydroids. *Invertebr. Biol.* **116:** 6–16.

Reference: *Biol. Bull.* **194:** 187–193. (April, 1998)

Cloning by Ophiuroid Echinoderm Larvae

ELIZABETH J. BALSER

Illinois Wesleyan University, Department of Biology, Bloomington, Illinois 61702-2900

Abstract. Larvae of the brittle star *Ophiopholis aculeata*, common to the North Pacific coast of the United States, and an unidentified species of ophiuroid, collected from waters off the eastern coast of Florida, undergo asexual reproduction of the primary larva to produce a secondary larval clone. Generation of a secondary larva begins with the release of the larval posterolateral arms, which are initially retained by the settled juvenile. In *O. aculeata*, the released arms regenerate all the structures typical of the primary ophiopluteus. Tissue and energy reserves required for formation of the secondary feeding larva appear to be supplied by the absorption and reorganization of part of the posterolateral arms. Various developmental stages of the unidentified ophiopluteus were collected from plankton samples taken off the coast of Florida. These included just-released posterolateral arms, plutei, and metamorphosed juveniles with the posterolateral arms still attached. The identification of regenerating arms from the plankton demonstrates that asexual reproduction by ophiuroid larvae is not restricted to a single, laboratory-cultured species. In both *O. aculeata* and the unidentified Atlantic ophiopluteus, cloning involves the dedifferentiation of primary larval tissue and a developmental progression similar to that followed by the zygote, although it is not known whether the formation of the secondary larva follows the same pathway utilized by the primary larva or a novel developmental program. Asexually produced secondary larvae of *O. aculeata* undergo metamorphosis, settle to the benthos, and initiate a tertiary larval generation, indicating that cloned larvae could be added to the population as long as environmental conditions could support a planktonic existence. This phenomenon represents an unusual potential to increase the geographic range and the number of juveniles of a given parentage in future generations without additional reproductive input from the adult.

Received 15 August 1997; accepted 22 December 1997.
E-mail: sbalser@titan.iwu.edu

Introduction

In 1921, Mortensen reported the appearance of unusual brittle star larvae in plankton tows taken from the waters surrounding the islands of the West Indies. He speculated that these larvae were asexual clones originating from the released posterolateral arms of settled juveniles. MacBride (1921), renowned for his contributions to echinoderm embryology, strongly rejected this interpretation, and Mortensen's observation remained unconfirmed for the next 75 years (Mladenov and Burke, 1994).

Larval cloning is a rare event in the life history of nonparasitic planktonic invertebrate larvae, but is reported for a number of species of asteroid echinoderms (Bosch *et al.*, 1989; Rao *et al.*, 1993; Jaeckle, 1994). In asteroid larvae, the formation of the asexually produced secondary propagule results from the differentiation and release of some part of the primary larval body. The propagule develops into a secondary larva that is morphologically identical to the primary larva. It is not known if the secondary larvae of asteroids are capable of settlement and metamorphosis or if continued cycles of asexual reproduction are possible.

The work presented here confirms Mortensen's (1921) earlier observations that ophiuroid larvae undergo asexual reproduction to produce secondary clones. Like asteroids, secondary larvae of *Ophiopholis aculeata* and of an unidentified ophiopluteus collected from the Western Atlantic Ocean off the coast of Florida originate from the release and development of primary larval structures, specifically, the posterolateral arms. The released arms undergo gastrulation and development similar to that of the primary embryo, but development of secondary larvae follows from the reorganization of larval tissues instead of from embryonic cells. This raises significant questions

concerning the flexibility of developmental pathways and the initiation and control of morphogenesis.

In *O. aculeata*, asexually produced secondary larvae undergo metamorphosis, settle to the benthos, and initiate a tertiary larval generation. Asexual reproduction of larval propagules has potential evolutionary and ecological ramifications. For each juvenile that survives to settlement, an additional larva is produced that not only increases the number of individuals of a given genetic lineage, but also enhances the dispersal potential of the species.

Methods and Materials

Adult specimens of *Ophiopholis aculeata* were collected during the summer of 1996 from the intertidal and subtidal zones of various sites along the shores of San Juan Island, Washington. The animals were transported to the Friday Harbor Laboratories, Friday Harbor, Washington, where spawning was induced by alternating light and dark exposure. Fertilization and culturing of the embryos and larvae followed methods outlined by Strathmann (1987). Feeding ophioplutei were kept in 2 l of 5-μm-filtered seawater in glass jars at 10C°, stirred gently by paddles, and fed cultured cells of the alga *Rhodomonas* sp. Juveniles suspended between the posterolateral arms and free-swimming released arms were removed from the jars and maintained in culture dishes. Clean filtered seawater and algae were provided every other day, and the cultures were stirred gently with a pipette several times a day to suspend food and larvae in the water column. A Wild M-5 dissecting scope and a Nikon Optiphot-2 compound microscope were used to take photographs on T-Max 100 (Kodak) film.

During May and June of 1997, plankton was collected approximately 1 mile off the coast of Ft. Pierce, Florida, by towing a 202-μm-mesh plankton net at a depth of less than 10 m. The samples were transported to the Smithsonian Marine Station in Ft. Pierce and examined for ophioplutei. In some samples, an unidentified ophiopluteus was the most abundant organism present. Plutei, juveniles with attached posterolateral arms, and free-swimming posterolateral arms in various stages of development were collected and maintained in culture dishes in filtered seawater. Larvae were fed cells of *Rhodomonas* sp. Larvae and regenerating arms were photographed with a Zeiss Photomicroscope II and T-Max 100 film.

Results

Larvae of Ophiopholis aculeata

The development of primary larvae of *O. aculeata* follows that described for other planktotrophic ophioplutei (Hendler, 1991). The onset of metamorphosis is indicated by the appearance of the five hydrocoelic lobes of the presumptive primary podia. Metamorphosis continues while the larva remains in the water column, eventually resulting in a juvenile suspended between the two outer posterolateral arms (Fig. 1A). The juvenile retains the posterolateral arms for some undetermined period after settlement. During this time the transverse rods appear to shorten and contact is made between the proximal tip of each posterolateral arm. The posterolateral arms are released from the settled juvenile (Fig. 1B) and, with

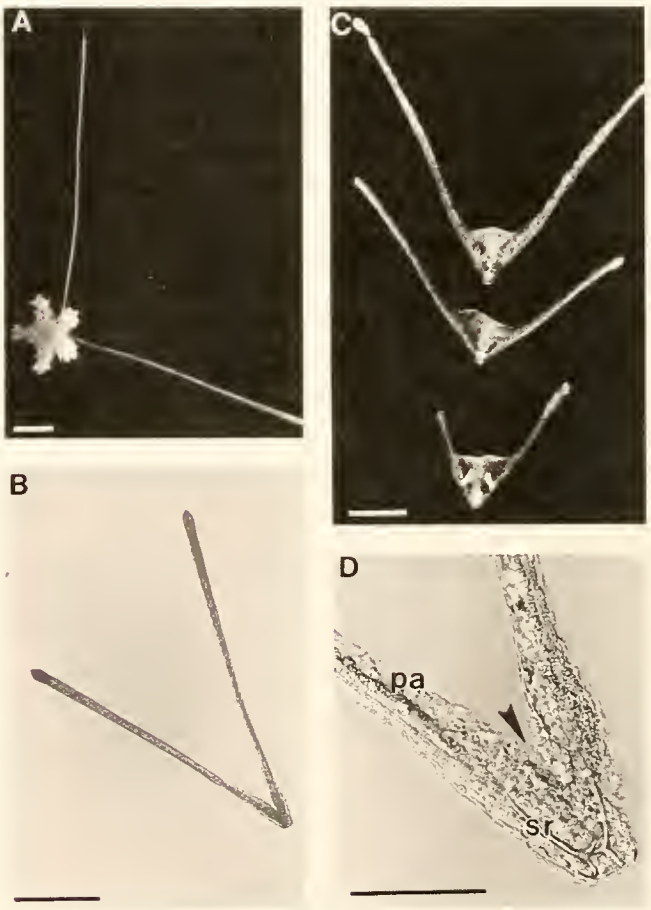

Figure 1. (A) Light photomicrograph of a juvenile *Ophiopholis aculeata* suspended between the outer posterolateral arms. (B) Recently released posterolateral arms from a settled juvenile. (C) A developmental series of three different asexually produced secondary larvae arranged chronologically from top to bottom. (D) Gastrulation of released posterolateral arms. After settlement, the juvenile releases the posterolateral arms (B) which swim using the ciliated epidermis covering the arms (originally part of the primary larval ciliated band). The posterolateral arms (pa) are supported internally by skeletal rods (sr), seen in D. An event similar to gastrulation begins with the invagination of the epidermis (arrowhead) in the vee of the arms. Formation of the secondary pluteus (shown in series in C), is characterized by a shortening of the outer arms and a concentration of tissue between the arms. Scale bars = 0.1 mm.

ciliary band intact, swim off the bottom of the culture dish and into the water column.

The free arms consist of the skeletal rods, mesenchymal cells, a ciliated epidermis, and the blastocoel of the primary larva's posterolateral arms. Within 24 h of release, the tissue forming the inner vee of the arms undergoes a process similar to gastrulation. This results in the production of an archenteron that continues to develop, forming a new larval gut (Figs. 1C, D and 2A). As in development of the primary larva, the archenteron gives rise to an anterior coelom that divides and grows to produce the right and left axohydrocoels (Fig. 2B). The formation of the somatocoels in both primary and secondary larvae is, at present, unclear. Over the course of 3 to 4 days, the posterolateral arms regenerate the structures typical of an ophiopluteus, including the gut, the coeloms, and additional feeding arms (Figs. 1C, 2C).

Prior to feeding in the secondary larva, tissue and energy resources appear to be supplied by the posterolateral arms, as indicated by a decrease in the length of the arms

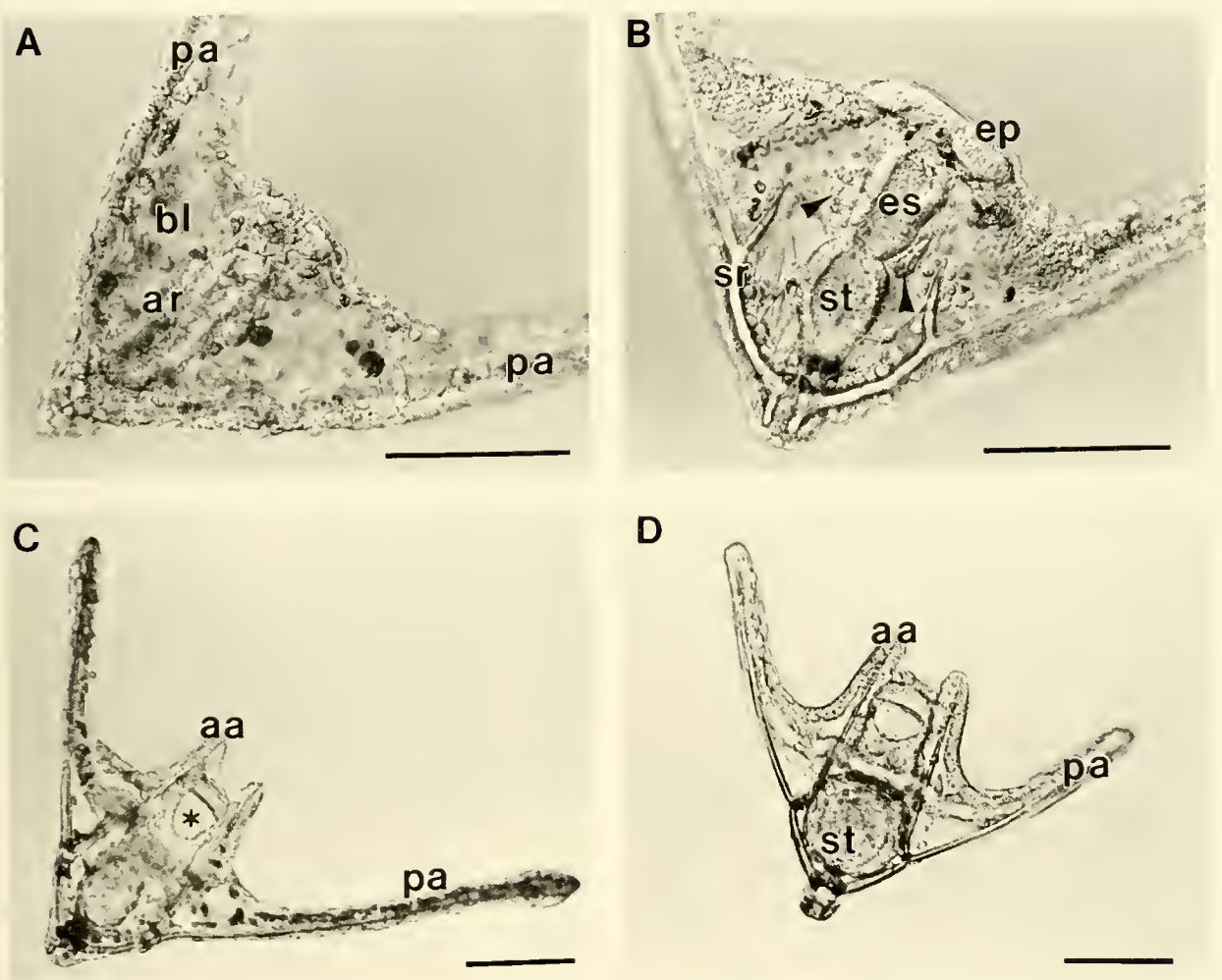

Figure 2. (A, B) Light photomicrographs of the formation of the larval gut in 2-arm clones of *Ophiopholis aculeata*. (C) Photomicrograph of a 4-arm pluteus produced from released posterolateral arms of primary juvenile. (D) Photomicrograph of a primary pluteus resulting from fertilization of an ovum and development of the zygote. In cloned larvae, the archenteron (ar) gives rise to the esophagus (es), stomach (st), and intestine (not shown). The mouth (asterisk) opens from the exterior into the esophagus, but it is not known if it forms at the opening of the archenteron (blastopore analog) or elsewhere. As in primary larvae, the anterior coelom arises from the tip of the archenteron and later divides to form the right and left axohydrocoels (arrowheads). The 4-arm asexually produced pluteus (C) is morphologically similar to a primary pluteus (D) except for increased pigment in the epidermis (seen as dark spots in this micrograph) and disproportionately longer posterolateral arms (pa). aa, anterolateral arm; bl, blastocoel; ep, epidermis; sr, skeletal rod. Scale bars = 0.1 mm.

(Fig. 1C). The average total length (sum of left and right arm lengths) for arms just released from the juvenile was 620 ± 71 μm (mean ± 1 SD, $n = 6$); in contrast, the mean total arm length of 2-arm prefeeding secondary larvae was 374 ± 82 μm ($n = 6$). This 40% difference represents a significant decrease ($t = 5.53$, $P < 0.001$) in the average total arm length. During reformation of the secondary pluteus, the epidermis covering the arms appears to be pulled towards the inner vee of the arms, presumably providing the cells for invagination and formation of the archenteron. The epidermis appears buckled along the length of the arms and is pulled away from the ends of the skeletal rods. In some larvae, the reduction in arm length was not symmetrical, with one arm being shorter than the other (Fig. 1C). The reason for this asymmetry is not known, but it apparently has no adverse effect on development. These larvae formed normal plutei and the asymmetry disappeared as development progressed.

Within 5 days, a feeding 4-arm pluteus is formed (Fig. 2C). This larval clone is morphologically indistinct from a primary larva except for having more of a characteristic orange pigment in its epidermis (seen in fully developed primary larvae) and disproportionately long posterolateral arms (compare Fig. 2C with 2D). Continued growth and morphogenesis results in an 8-arm pluteus that is indistinguishable from the primary larva at the same developmental stage. Metamorphosis of the secondary larva begins with the formation of the hydrocoelic lobes and follows a morphogenic pattern similar to that of the primary larva. At the time of settlement, the secondary juvenile retains the posterolateral arms but, as in the primary larva, eventually releases them. The free arms return to the water column and begin a tertiary cycle of development that results in another planktonic ophiopluteus.

Ophioplutei collected from plankton tows

Plankton tows taken off the coast of Ft. Pierce, Florida, contained a series of developmental stages of an unknown ophiuroid larva. These stages included 8-arm plutei (Fig. 3A), metamorphosed juveniles suspended between the posterolateral arms, free-swimming posterolateral arms (Fig. 3B), and various stages of regenerating posterolateral arms (Fig. 3C, D). Juveniles maintained in culture dishes eventually settled and released the posterolateral arms which, as in *O. aculeata*, began morphogenetic changes consistent with regeneration of the larva.

Stages collected from the plankton showed a progressive series from recently released arms (Fig. 3B) to an early 4-arm pluteus (Fig. 3D). In some, but not all, of the recently released stages the two arms were of different lengths (Fig. 3B). This asymmetry had no noticeable adverse effect on swimming or development and disappeared by the 4-arm stage. In plankton-collected clones, no asymmetry in arm length was observed in 4-arm secondary larvae.

Gastrulation by posterolateral arms of this east coast species may not occur as it does in *O. aculeata*. At the junction of the two posterolateral arms, the transverse rods form a spherical cage (Fig. 3C). Although not clearly seen in Figure 3C, the lumen of this cage is filled with cells. It is not known from where these cells originate or if they reform the larval gut, and subsequently the larval coeloms. Asexually produced 4-arm plutei appeared to have disproportionately longer posterolateral arms than those expected for primary plutei at a similar developmental stage, but without direct comparison, this remains a subjective observation. Beyond the 4-arm stage, secondary plutei were indistinguishable from primary larvae.

Discussion

In *O. aculeata*, tissues in the asexually produced larvae appear to originate from dedifferentiation and redifferentiation of the epidermis covering the posterolateral arms. Mesenchymal cells are present in the blastocoel (of the arms), but are associated with the skeletal rods and do not seem to contribute to the formation of the archenteron or the axohydrocoels. This developmental sequence is similar to that seen in the blastula of *O. aculeata* and raises questions concerning the ontogeny of larval morphogenesis. Principally, do the clones follow the same genetic and morphogenetic pathways as the primary larva or do they use a novel developmental pattern?

Specific questions about the development of asexually produced larvae are how the larval body axes are established in the clone and what mechanisms are involved in differentiation of endoderm and subsequently mesoderm from the ectodermal epithelium covering the free-swimming arms. In both primary and secondary larvae, the archenteron forms along the long axis of the larval skeleton (anterior-posterior axis), but it is not yet known if the mouth in the secondary larva forms at the site of invagination or at a point 90 degrees from the advancing tip of the archenteron, as in the primary larva. If, after invagination of the arm epithelium, the cells forming the archenteron in the cloned pluteus are embryologically equivalent to those of the primary gastrula, formation of endodermal and mesodermal structures could simply repeat the developmental program of the primary embryo.

O. aculeata and the ophiuroid species collected from the plankton may not follow the same developmental sequence in forming a secondary larva—specifically with respect to gastrulation. Although multiple modes of asexual reproduction are reported for asteroid larvae (Jaeckle, 1994), gastrulation appears to proceed from an invagi-

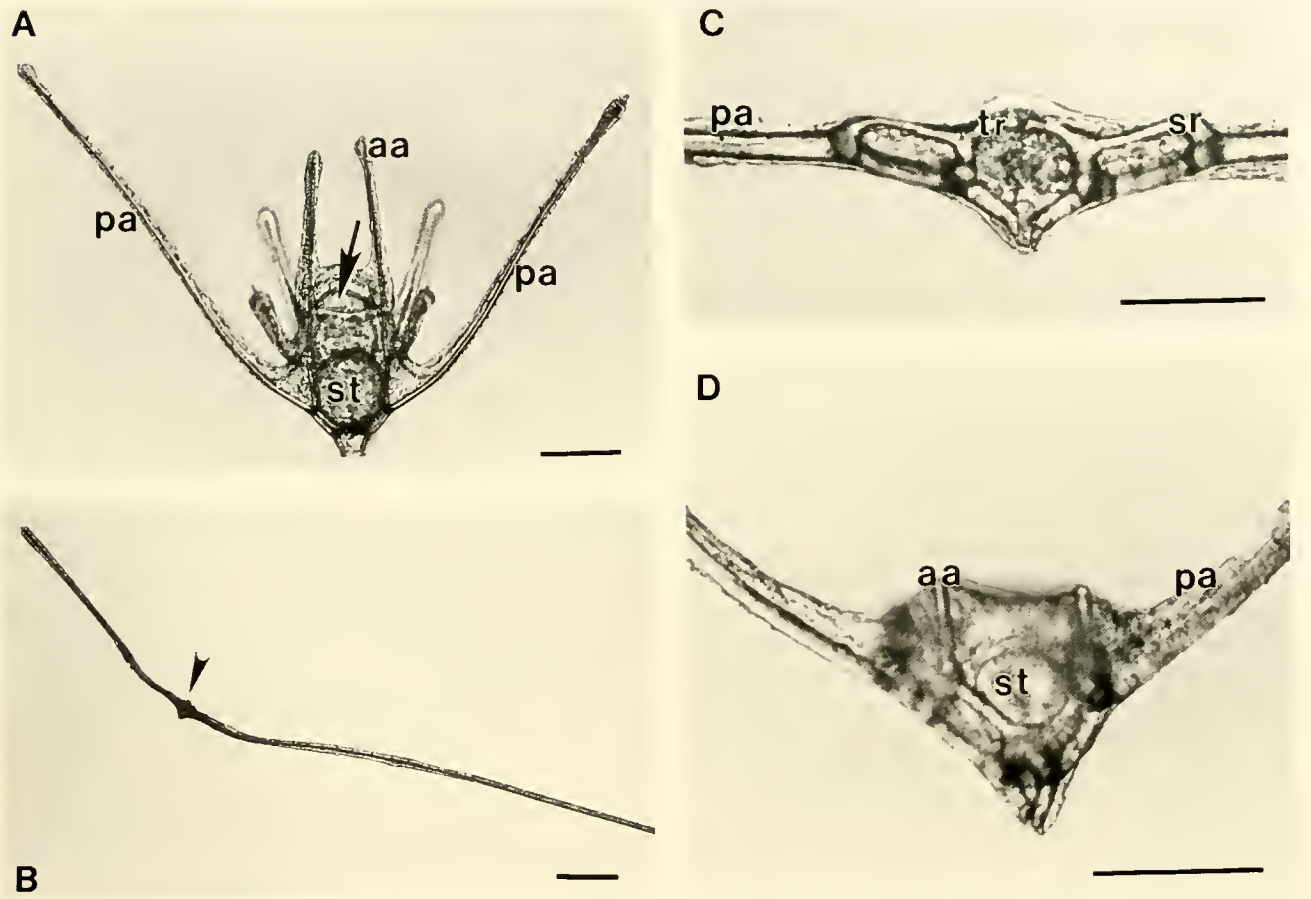

Figure 3. Light micrographs of an ophiopluteus (A), released posterolateral arms (B), and apparently regenerating larvae (C, D) collected from plankton samples taken off the east coast of Florida. Similarities in the larval skeleton and in pigmentation suggest that these specimens represent one species. aa, anterolateral arm; pa, posterolateral arm; st, stomach; sr, skeletal rod; tr, transverse rod; arrowhead, concentration of tissue at the point of contact of the two posterolateral arms. Scale bars = 0.1 mm.

nation of the outer (epidermal) epithelium of the propagule (Bosch *et al.*, 1989; Jaeckle, 1994). The origin of the cells in the vee of the released arms of this unidentified secondary ophiopluteus is at present unknown. They may have originated from invagination of the epidermis of the arms or, alternatively, from mesenchymal cells of the primary larva. If the latter hypothesis is true, the development of the secondary larva deviates from that described for asteroids and for *O. aculeata.*

In ophiuroids, asexually produced larvae can complete metamorphosis and initiate another generation of planktonic larvae. The formation of tertiary larvae suggests that the production of asexual larval clones could continue indefinitely as long as environmental conditions could support a planktonic existence. Development of secondary larvae is known for *Ophiopluteus opulentus* (Mortensen, 1921) and *Ophiopholis aculeata* (this manuscript). Mladenov (1979) reported the release of the posterolateral arms by the settled juveniles of *Ophiothrix oerstedi.* In this species, however, the arms did not develop and eventually died. The unidentified pluteus collected off the coast of Florida may be the same larva described by Mortensen (1921) from the West Indies and designated as *O. opulentus* species c. Similarities in the larval skeleton of both larvae and the confluence between the West Indies and the Florida coastline provided by the flow of the Florida Current of the Gulf Stream system raise the possibility that the unidentified larva is *O. opulentus.* Nevertheless, the potential for larval cloning is evident in possibly three species of planktotrophic ophioplutei (although *O. opulentus* is known only from larval stages), and may represent an important life history strategy for planktonic ophiuroid larvae.

The impact of asexual reproduction by larvae on the life history of a species is dependent on the cloned individuals' ability to produce viable gametes, which, in turn,

requires the formation of germ cells. The origin of the primary germ cells in ophiuroids, and in general in echinoderms, is equivocal. Germ cells in echinoderms are thought to arise either from secondary mesenchymal cells or from a proliferation or outgrowth of cells from the epithelial lining of the somatocoel (Gemmill, 1914; Nieuwkoop and Sutasurya, 1981; Delavault, 1966; Houk and Hinegardner, 1980, 1981; Hendler, 1991; Holland, 1991). In ophiuroids, as in other echinoderms, the primary germ cells are not evident in the larval body until late in development, usually just prior to or after metamorphosis (Gemmill, 1914; Houk and Hinegardner, 1980, 1981; Smiley, 1986; Hendler, 1991; Holland, 1991). The "absence" of germ cells in earlier developmental stages suggests, concurrently or alternatively, a delay in the induction of the expression of germ cell characteristics and an origin of the primary germ cells from structures not formed until later in development.

The formation of primary germ cells in asexually reproduced larvae has not been demonstrated, but the following three hypotheses are possible. The cloned larvae lack the ability to produce germ cells and, therefore, form sterile adults. Primary germ cells are sequestered from a population of stem cells in the primary larva and are transferred to the secondary (or subsequent) propagule prior to its release from the primary larva. Finally, the primary germ cells could arise *de novo* from the somatocoelic epithelium, which apparently arises anew in the cloned larva. The latter two hypotheses are consistent with the formation of the germ cells in primary larvae either from mesenchyme or from the epithelium of the somatocoel.

Provided that the juveniles resulting from cloned larvae can produce viable gametes, asexual reproduction of larval propagules increases the effective population size without additional reproductive cost to the primary adult. Further, asexual reproduction by larvae may produce a larger increase in the number of juveniles than could be realized from an equivalent increase in the number of eggs released by the female. The loss of individuals during larval development (mortality rate > 0) requires that the number of eggs released by the female exceed the number of juveniles produced.

Cloned larvae, which enter the water column at a size equivalent to the arm-span of an 8-arm pluteus, may experience a decrease in predation (Rumrill *et al.*, 1985; Pennington *et al.*, 1986; Rumrill, 1987), and thus a lower mortality rate, compared to less developed stages. The reduction may, however, depend on the type of predator encountered. In the presence of arthropod and chaetognath predators, blastulae and prism stages of *O. aculeata* were more susceptible than 4-arm plutei, which were more susceptible than 8-arm plutei (Rumrill, 1987). In contrast, when larvae were presented to a copepod or hydromedusa predator, a greater percentage of later larval stages was lost to predation (Rumrill, 1987). Nevertheless, decreased predation resulting from morphological or behavioral characteristics of more advanced larval stages (Pennington *et al.*, 1986) may in some cases improve the survivorship of asexually produced plutei.

For each juvenile that survives to settlement, an additional larva is produced; this not only increases the number of individuals of a given genetic lineage, but also enhances the dispersal potential of the species. Subsequent generations of asexually produced larvae have the potential to increase the distance of dispersal by at least as much as the primary larva. Dispersal promotes genetic connectivity between populations geographically isolated by distance and allows recruitment to new habitats (Chia, 1974; Crisp, 1974; Strathmann, 1974; Scheltema, 1986). Asexual reproduction by planktonic larvae increases the life span of a genetically identical cohort and distributes the timing of the attainment of competence to settle. If appropriate settlement sites are randomly distributed along a dispersal axis, then asexual propagation—by producing more larvae that can spread over a wider area—increases the likelihood that a competent larva will locate a suitable settlement site.

Acknowledgments

I thank Bruno Pernet, Chris Lowe, and Dr. William Jaeckle for their assistance in collecting adults and culturing primary larvae of *O. aculeata*. My appreciation is also extended to Dr. Dennis Willows and Friday Harbor Laboratories, Friday Harbor, Washington, for laboratory space and technical support. I am grateful to Dr. Mary Rice and the Smithsonian Marine Station, Ft. Pierce, Florida, for use of the Marine Station facilities. I offer a special thanks to Sherry Reed for her assistance in collecting plankton. This work was supported, in part, by an Artistic and Scholarly Development Grant provided to the author by Illinois Wesleyan University. Smithsonian Contribution Number 437.

Literature Cited

Bosch, I., R. B. Rivkin, and S. P. Alexander. 1989. Asexual reproduction by oceanic planktotrophic echinoderm larvae. *Nature* **337:** 169–170.

Chia, F. S. 1974. Classification and adaptive significance of developmental patterns of marine invertebrates. *Thalassia Jugosl.* **10:** 121–130.

Crisp, D. J. 1974. The role of pelagic larvae. Pp. 145–155 in *Perspectives on Experimental Biology*, Vol. 1, P. Spencer-Davies, ed. Pergamon Press, Oxford.

Delavault, R. 1966. Determinism of sex. Pp. 615–638 in *Physiology of Echinodermata*, R. A. Boolootian, ed. Wiley-Interscience, New York.

Gemmill, J. F. 1914. The development and certain points in the adult

structure of *Asterias rubens*. *Philos. Trans. Zool. Soc. London* **20:** 1–17.

Hendler, G. 1991. Echinodermata: Ophiuroidea. Pp. 355–511 in *Reproduction of Marine Invertebrates*, Vol. 6, A. C. Giese, J. S. Pearse, and V. B. Pearse, eds. The Boxwood Press, Pacific Grove, California.

Holland, N. D. 1991. Echinodermata: Crinoidea. Pp. 247–299 in *Reproduction of Marine Invertebrates*, Vol. 6, A. C. Giese, J. S. Pearse, and V. B. Pearse, eds. The Boxwood Press, Pacific Grove, California.

Houk, M. S., and R. T. Hinegardner. 1980. The formation and early differentiation of sea urchin gonads. *Biol. Bull.* **159:** 220–294.

Houk, M. S., and R. T. Hinegardner. 1981. Cytoplasmic inclusions specific to the sea urchin germ line. *Dev. Biol.* **86:** 94–99.

Jaeckle, W. B. 1994. Multiple modes of asexual reproduction by tropical and subtropical sea star larvae: an unusual adaptation for genet dispersal and survival. *Biol. Bull.* **186:** 62–71.

MacBride, E. W. 1921. Echinoderm larvae and their bearing on classification. *Nature* **108:** 529–530.

Mladenov, P. V. 1979. Unusual lecithotrophic development of the Caribbean brittle star *Ophiothrix oerstedi*. *Mar. Biol.* **55:** 55–62.

Mladenov, P. V., and R. D. Burke. 1994. Echinodermata: asexual propagation. Pp. 339–383 in *Reproductive Biology of Invertebrates*, K. G. and R. G. Adiyodi, eds., Oxford and IBH Publishing, New Delhi.

Mortensen, T. 1921. Studies of the development and larval forms of echinoderms. *G.E.C. Gad., Copenhagen.* 1–261 pp.

Nieuwkoop, P. D., and L. A. Sutasurya. 1981. *Primordial Germ Cells in the Invertebrates: From Epigenesis to Preformation.* Cambridge University Press, Cambridge. 258 pp.

Pennington, J. T., S. S. Rumrill, and F. S. Chia. 1986. Stage-specific predation upon embryos and larvae of the Pacific sand dollar, *Dendraster excentricus*, by 11 species of common zooplankton predators. *Bull. Mar. Sci.* **39:** 234–240.

Rao, P. S., K. H. Rao, and K. Shyamasundari. 1993. A rare condition of budding in bipinnaria larvae (Asteroidea). *Curr. Sci.* **65:** 792–793.

Rumrill, S. S. 1987. Differential predation upon embryos and larvae of temperate Pacific echinoderms. Ph.D. Dissertation, University of Alberta. 432 pp.

Rumrill, S. S., J. T. Pennington, and F. S. Chia. 1985. Differential susceptibility of marine invertebrate larvae: Laboratory predation of sand dollar, *Dendraster excentricus*, embryos by zoeae of the red crab, *Cancer productus*. *J. Exp. Mar. Biol. Ecol.* **90:** 193–208.

Scheltema, R. S. 1986. On dispersal and planktonic larvae of benthic invertebrates: an eclectic overview and summary of problems. *Bull. Mar. Sci.* **39:** 290–322.

Smiley, S. 1986. Metamorphosis of *Stichopus californicus* (Echinodermata: Holothuroidea) and its phylogenetic implications. *Biol. Bull.* **171:** 611–631.

Strathmann, M. F. 1987. *Reproduction and Development of Marine Invertebrates of the Northern Pacific Coast.* University of Washington Press, Seattle. 670 pp.

Strathmann, R. R. 1974. The spread of sibling larvae of sedentary marine invertebrates. *Am. Nat.* **108:** 29–44.

Reference: *Biol. Bull.* **194:** 194–223. (April, 1998)

Evaluation of the Effects of Extremely Low Frequency Electromagnetic Fields on Movement in the Marine Diatom *Amphora coffeaeformis*

MARK S. DAVIES[1,2,3,*], RICHARD DIXEY[1], AND J. C. GREEN[2]

[1] *Department of Medical Electronics, St. Bartholomew's Hospital, West Smithfield, London, EC1A 7BE, UK;* [2] *Plymouth Marine Laboratory, Citadel Hill, Plymouth, PL1 2PB, UK; and* [3] *Ecology Centre, University of Sunderland, Sunderland, SR1 3SD, UK*

Abstract. Published work has shown that population motility in the marine diatom *Amphora coffeaeformis* can be influenced by externally applied electromagnetic fields (EMFs). Here we report attempts to repeat these experiments, which have been proposed as a model for assessing the effects of EMFs on biological systems. Susceptibility to EMFs was tested using five strains of diatoms on agar plates at a very broad range of field conditions, but no effect on population motility was demonstrated. Exposure period to the EMFs, cell density, and position in the cell cycle had no effect on EMF susceptibility, and the direction and distance moved by the diatoms were not affected by EMFs. When tested after at least a month of pre-incubation at 20 μT, diatoms of strains #2038, III_B, and III_F did show an EMF-induced increase in population motility over control cells (up to ~20%) at conditions predicted by the "ion cyclotron resonance" model, but this effect was ephemeral. Later, III_B showed a similar increase that was abolished when (1) non-pre-incubated cells were used, (2) the EMF-producing coils were not energized, and (3) even harmonics were used. On observing the response of diatoms to EMFs in real time, a significant increase (~2-fold) in diatom speed over control cells was evident at "ion cyclotron resonance" conditions, using strain #2038 (pre-incubated at 20 μT). The effect was abolished at an even harmonic. We conclude that EMFs can modulate diatom motility, but that the system is, as yet, not consistently reproducible.

Introduction

Despite a vast literature describing the effects of externally applied, non-ionizing, extremely low frequency (< 100 kHz) electromagnetic fields (ELF EMFs) on biological systems, this branch of science is neither well known nor understood. The reasons for this are probably threefold. Firstly, there is no well-accepted mechanism, based on empirical studies, by which EMFs can influence and modify a biological or biochemical process. Any interaction mechanism must describe how fields with energy levels less than that of thermal noise (k_T) can exert an effect (Male, 1992). Secondly, experimentation paying proper attention to both biological *and* physical variables is necessary, but is not common. Thirdly, there is no "tried-and-tested" model system that can be used to test new developments in bioelectromagnetic science. The acceptance of empirical evidence is usually determined by the ability of others to replicate research findings, and investigation to this end has yet to produce a robust system, independently replicable in different laboratories. Here we report attempts to replicate the findings of experiments describing EMF-induced increased motility in populations of the marine diatom *Amphora coffeaeformis* Agardh (McLeod *et al.*, 1987a; Smith *et al.*, 1987a, b).

Amphora coffeaeformis is a common benthic marine pennate diatom (Round *et al.*, 1990) whose motility is well documented (Cooksey and Cooksey, 1980; Round *et al.*, 1990). Motility can be observed by light microscopy in real time and is easily measured on agar plates because the diatoms leave visible trails of mucus. The mucus is produced via a channel, or raphe, running along the long axis of the diatom (Edgar, 1980). In *A. coffeaeformis* the raphe is restricted to one side of the diatom only. Diatoms have many advantages as biological models: they are easy to maintain in culture; have a short generation time (<1 day, Round *et al.*, 1990); are single-celled and eukaryotic; and commonly reproduce asexually, giving a large population of cloned individuals. Motility in *A. coffeaeformis* depends on external [Ca] (Cook-

Received 24 June 1997; accepted 5 December 1997.

* To whom correspondence should be directed. E-mail: mark.davies@sunderland.ac.uk

sey and Cooksey, 1980), and this property was exploited by McLeod *et al.* (1987a) and Smith *et al.* (1987a, b) who demonstrated that populations of *A. coffeaeformis* on agar containing a [Ca] that normally checked motility could be induced to move when exposed to specific ELF EMFs. Amongst the many studies of bioelectromagnetic effects, these were important because they used a biological system that was potentially easy to re-create in other laboratories, thus allowing replication studies, and they demonstrated that, in common with most bioelectromagnetic effects, a dose-dependent response was not apparent; rather the effect was maximal around specific field amplitudes and frequencies, the latter as predicted by a theoretical model ("ion cyclotron resonance"; Liboff, 1985). In effect, McLeod *et al.* (1987a) and Smith *et al.* (1987a, b) putatively 'tuned' the applied fields to stimulate Ca^{2+} ion activity. Thus the studies provided a clue to the interaction mechanism between living systems and EMFs.

"Ion cyclotron resonance" theory can be used to predict the frequency of EMF that will stimulate any ion, dependent on its charge-to-mass ratio, according to the formula

$$f = \frac{1}{2\pi} \frac{q}{m} B,$$

where f is the stimulation frequency, q/m the charge-to-mass ratio and B the static magnetic field (Liboff, 1985). Extrapolating from the model, stimulation at even harmonics should abolish the effect, and in terms of diatom motility, this was what was found (McLeod *et al.*, 1987b). In addition, McLeod *et al.* (1987b) found that stimulating at "ion cyclotron resonance" conditions for the K^+ ion reduced diatom motility, which again centered on predicted field amplitudes and frequencies.

Clearly the "diatom system" presented a testable model and suggested an interaction mechanism. Not surprisingly, several groups then attempted to replicate the original findings (Reese *et al.*, 1991; Parkinson and Sulik, 1992; Saalman *et al.*, 1992; Prasad *et al.*, 1994; Florig, pers. comm.) and, with one exception, all failed. Reese *et al.* (1991) reported a partial replication in that diatom population motility was increased on EMF stimulation in some, but not all, experiments (15/19 at 0.25 m*M* Ca). Here we report the most thorough attempt at repeating the original findings of the diatom system to date, testing a wide range of both biological and EMF conditions. Our aim is to assess the repeatability of the original experiments, implicating a potential interaction mechanism, and to examine the usefulness of the diatom system as a model for bioelectromagnetic phenomena in general.

Materials and Methods

Because our primary aim was to investigate the repeatability of the results of McLeod *et al.* (1987a) and Smith *et al.* (1987a, b) our methods follow theirs as closely as possible.

Diatoms

Five strains of *Amphora coffeaeformis* were used. Mixed cell-size cultures of strains #2036, #2038, and #2039 were obtained from the Culture Collection of Algae at the University of Texas (Starr and Zeikus, 1987). A mixed cell-size culture of strain III_B (referred to here as III_F) was obtained from the University of Southern California. A narrow size-range (21–23 μm along the long axis) culture of strain III_B was obtained from B. Cooksey at Montana State University. These latter two strains are claimed to be descendants of the strain referred to in the original publications (McLeod *et al.*, 1987a; Smith *et al.*, 1987a, b) on diatom/EMF interaction (B. Cooksey, pers. comm.).

Although these strains are conspecific, there is considerable variation in their gross morphology (Fig. 1); they show differences in upper lethal temperature (Davies, unpubl. data), and they produce differently shaped growth mats in liquid culture (Davies, unpubl. data). Gallagher (1986 and pers. comm.) advocates a reexamination of the taxon *Amphora coffeaeformis* with a view to splitting it into numerous species. Thus, it is important that strain types and their origin be specified in studies such as this (see Wood and Leatham, 1992).

Diatoms were grown in the ASP2 medium of Provasoli *et al.* (1957), modified to contain 0.25 m*M* Ca (Smith *et al.*, 1987a). Reserve stocks of diatoms were kept on 2% w/v Sigma 'A' agar in modified ASP2 slants in polystyrene tubes at 15°C. Diatoms for experimental use were grown either (a) in an incubator at 20°C at 3000 lux (~58.8 μE s^{-1} m^{-2}) illumination from fluorescent lights on a 12-h light-dark cycle where the horizontal component of the magnetic field, B_H = 4.7 μT; the vertical component, B_V = 14 μT; and the oscillating fields were negligible; or (b) in a water bath at 25°C at 3000 lux continuous fluorescent illumination (B_H = 23 μT, B_V = 20 μT; when a thermostatically controlled heater was operating, B_{Hac} = 13 μT peak-peak at 50 Hz, B_{Vac} = 3 μT peak-peak at 50 Hz). Cultures were periodically (about every 4 months) treated with an antibiotic solution (see Stein, 1973) to maintain axenicity.

A second water bath constructed of acrylic plastic with polystyrene insulation was used for EMF pre-incubation experiments and was enclosed by near-Helmholtz coils (see *Exposure apparatus*). Water was pumped to this bath by, and recirculated to, a Lauda-thermostat recirculating water bath sited 1.5 m from the acrylic bath. Diatoms were grown here at 25°C at 1000 lux (~19.6 μE s^{-1} m^{-2}) illumination from DC lamps for at least 1 month prior to experimentation.

Aseptic techniques were practiced throughout.

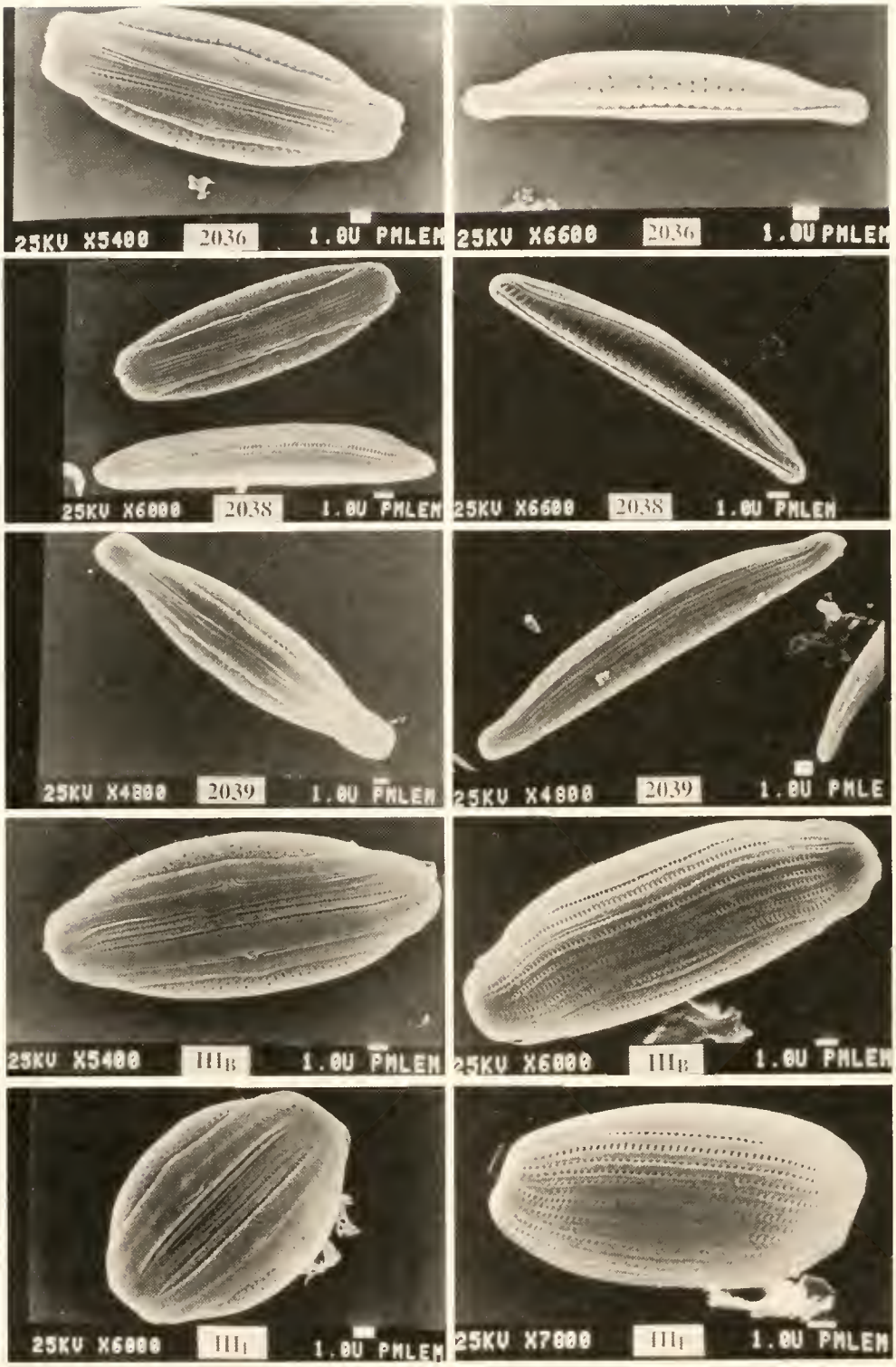

Figure 1. Strains #2036, #2038, #2039, III_B and III_F of *Amphora coffeaeformis*. Left, views of the raphed surface; right, lateral views. Scale bar is 1 μm in each case.

Exposure apparatus

Two pairs of coils (each 295-mm internal diameter) were mounted in a PVC frame at 90° to each other in a near-Helmholtz configuration. One of the pairs (260-mm separation) had its magnetic axis along the z-axis and controlled the vertical (static) component (B_V) of the EMF within the coils. This pair was supplied with current

from a Kingshill 50V2C constant-voltage supply. The second pair (135-mm separation) had its magnetic axis along the *x*-axis (north-south) and controlled the horizontal (both static, B_H, and alternating, B_{Hac}) components of the EMF within the coils. This pair was driven by a Farnell stabilized power supply E30/2 coupled to a Farnell synthesized digital signal generator DSG2 whose outputs were fed through a Hewlett-Packard 6826A bipolar power supply/amplifier acting as a variable gain amplifier. The output of this latter device was used to energize the coil pair. The EMF in the *y*-axis (east-west) was brought to zero by aligning the *x*-axis along the earth's north-south magnetic maximum. Thus we could control the magnitude of the vertical (static) component (B_V), the magnitude of the horizontal static component (B_H), and the magnitude and frequency of the sinusoidally oscillating component (B_{Hac}) of the EMF within the coils.

The EMFs generated were measured at the center of the coils using a Domain SAM3 single-axis fluxgate magnetometer, whose analog display was used to record the static field components. This magnetometer was coupled to an Iso-tech ISR420 oscilloscope that was used to check the magnitude and frequency of the oscillating field components.

Experimental samples were placed at the center of the coils on a platform that could be raised or lowered, depending on the number of samples introduced. The coils were placed on a table at least 1 m away from any metal object. The geomagnetic field components within the coils were identical to those at the site chosen for the control (sham) exposure 2 m away ($B_H = 16.5\ \mu T$, $B_V = 44\ \mu T$). Lighting over both coil and sham sites was provided by DC lamps producing a flux density of 500 lux ($\sim 9.8\ \mu E\ s^{-1}\ m^{-2}$) at sample level. Experimental (room) temperature was 23 ± 1°C. The laboratory chosen for experimental work (at the Plymouth Marine Laboratory, Citadel Hill, Plymouth) was electromagnetically quiet: no EMF interference could be detected at nT levels.

A second set of two coil pairs (each 300-mm internal diameter) was employed in EMF pre-incubation of cells and enclosed a water bath. The coils were mounted in a wooden frame at 90° to each other in a near-Helmholtz configuration. The coils controlling the horizontal field were separated by 150 mm; those controlling the vertical field by 210 mm. The EMF in the *y*-axis was again brought to zero utilizing the geomagnetic maximum. Both coil pairs were driven by a Farnell E30-1BT dual power supply such that the EMF in the center of the coils was set to $B_H = 20\ \mu T$, $B_V = 0\ \mu T$, negligible oscillating components.

Agar plate experiments

There is some confusion over the type of agar used by McLeod *et al.* (1987a) and Smith *et al.* (1987a, b). Although McLeod, Smith, and K. Cooksey (pers. comms.) maintain that Difco Noble agar was used, our experiments with this agar demonstrated that its Ca content was too high to produce the prerequisite Ca-limiting effect on motility (Fig. 2). Figure 2 also shows a Ca-curve prepared using Difco Noble agar from the same container as was claimed to be used in the original experiments (McLeod, Smith, and K. Cooksey, pers. comms.). This latter curve was produced by one of us (MD) on a study visit to Montana State University. Subsequent spectrophotometric analysis showed Difco Noble agar (UK batch) to contain ~62 m*M* Ca. For routine work we have therefore used Sigma 'A' agar (~6 m*M* Ca) which gives Ca-curves consistent with those of McLeod *et al.* (1987a) and Smith *et al.* (1987a, b).

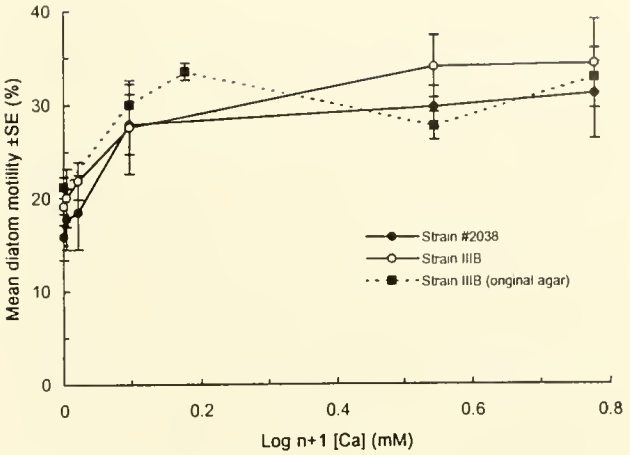

Figure 2. Diatom motility response to external [Ca] on Difco Noble agar. In each case $n = 3$ agar plates with 100 diatoms counted per plate.

Agar (Sigma 'A') was introduced at 2% (w/v) to various maintenance media (the minimal medium [M-M] of Smith *et al.* [1987a]) each containing 308 m*M* NaCl, 8.1 m*M* KCl, 20.2 m*M* $MgSO_4$, 8.3 m*M* Tris-HCl and adjusted to pH 7.6–7.7, but varying in their Ca (as $CaCl_2$) content (0–10 m*M*). After each mixture was autoclaved for 5 min at 121°C, agar plates were made by pipetting 2 ml of the molten agar into each 50-mm-diameter polystyrene petri dish required. Thus a series of plates could be prepared containing 0–10 m*M* added Ca. Plates were wrapped in aluminum foil, stored at 4°C, and used 3–21 days after pouring. Plates used less than 3 days after pouring gave poor diatom tracks.

Diatoms were harvested by centrifugation (1000 × *g*) for 5 min at incubation temperature before being both washed and recentrifuged twice in Ca-free maintenance medium to ensure a Ca-free pellet of diatoms. The cells were then adjusted, using a hemacytometer, to a density of $1.5 \times 10^5\ ml^{-1}$. In later experiments, in accordance with a revised protocol supplied from Montana State University (McLeod, pers comm.), cells were then returned

to the incubator for 30 min prior to plating. This step was introduced to the revised protocol putatively to allow diatom membranes ruptured during centrifugation to heal (Smith, pers. comm.).

McLeod *et al.* (1987a) and Smith *et al.* (1987a, b) used a paintbrush to introduce diatoms to the agar. The volume of suspension applied in this way was not constant, and it was difficult not to disturb the agar surface. We substituted a technique in which a 5-μl drop of density-adjusted cell suspension was introduced to the agar on each plate at one end of a 30-mm line marked on the underside of the plate. The drop was then drawn along the length of the line with an inoculation loop whose tip had been squared to present a 3-mm bar to the agar surface. Care was taken not to touch the loop to the agar.

After experimental exposure, diatoms on the plates were killed by introducing a few drops of 2% (w/v) OsO_4 to the inside of the lid of each plate. This procedure ensured that there was no additional time after the termination of plate exposure during which the diatoms could move.

Diatom movement on each plate was scored by counting 100 diatoms in random fields viewed with a phase-contrast microscope. Diatoms were scored as motile or nonmotile depending on the presence or absence of a track visible at either pole of the frustule. Only spatially individual diatoms were counted: diatoms that appeared in clumps or whose track originated in a clump were not scored. If these latter diatoms had been scored as motile, then all clumped diatoms would need to be scored as nonmotile. Diatoms were also not scored if they could be clearly seen to be lying with a lateral surface touching the agar. These diatoms are incapable of movement (pers. obs.) because the raphe system is not in contact with the substratum.

(i) Growth curves. Growth curves were produced for each strain of *A. coffeaeformis* by introducing a 1.5×10^5-cell inoculum in modified ASP2 into a polystyrene tube and making the total volume up to 5 ml with modified ASP2. Growth, measured daily by hemacytometer (two chambers counted) was monitored for 8 days in three tubes for each diatom strain. Diatoms were incubated at either 20°C in the incubator or 25°C in the water bath.

(ii) Age-dependent motility. To investigate the relationship between age of culture and diatom motility, cells of each strain were harvested (see above) at 1–8 days after inoculation (1.5×10^5 cells in 5 ml) and streaked onto three agar plates each containing 5 m*M* added Ca. Motility on the plates was scored after 1 h in the incubator at 20°C. Again diatoms were used from both incubator (20°C) and water bath (25°C).

(iii) Ca curves. The relationship between extracellular [Ca] and motility was investigated for all five strains of diatom by preparing a series of agar plates containing a range of [Ca] from 0–5 m*M*. Diatoms of each strain were harvested when in their most motile phase of growth as determined from the results of the age-dependent motility tests (3 days for #2036, #2038, and #2039, and 2 days for III_F and III_B) and introduced to three plates at each [Ca]. Motility was scored after 1 h in the incubator at 20°C. Diatom cultures were grown in the water bath (25°C).

(iv) Effect of light intensity. McLeod (pers. comm.) and Parkinson and Sulik (1992) found that light intensity during diatom exposure influenced the proportion of diatoms showing motility. To test this we harvested a 6-day-old incubator-grown #2038 culture and seeded its diatoms onto 15 agar plates containing 5 m*M* added Ca. Plates, in triplicate, were placed in illumination at <0.625 (inside a drawer), 21.4, 500, 1190, and 2740 lux (<0.01, 0.4, 9.8, 23.3, and 53.7 $\mu E\ s^{-1}\ m^{-2}$, respectively). After 1 h of exposure, the diatoms were killed and scored for motility.

(v) EMF experiments. In all cases we searched for EMF-induced motility using plates with 0.25 m*M* or 0.5 m*M* added Ca. Diatoms in logarithmic growth were seeded onto six replicate plates for each experiment. Three plates served as treatment (EMF-exposed) plates and three as control (sham-exposed) plates. Control and treatment plates for each experiment were always run simultaneously and were seeded from the same diatom culture at its most motile phase of growth (Parkinson and Sulik, 1992). Using diatoms from more than one culture would have introduced confounding factors. A positive control in the form of a plate with 5 m*M* added Ca was always placed with the sham-exposed plates to check that the diatoms were motile at high [Ca]. Each exposure lasted 1 h. To allow for geomagnetic disturbance, experiments conducted on days when large fluctuations in the earth's magnetic field occurred (data from Hartland Monthly Bulletin, British Geological Survey) were repeated at a later date. "Large fluctuations" was arbitrarily defined as a variation greater than 30 nT in either horizontal or vertical intensity during any experimental period.

All strains were exposed to calcium "ion cyclotron resonance" conditions, which produced the greatest field effect for McLeod *et al.* (1987a) and Smith *et al.* (1987a, b). These were: $B_V = 0\ \mu T$, $B_H = 20.9\ \mu T$, $B_{Hac} = 41.8\ \mu T$ peak-peak at 16 Hz.

Subsequently a set of permutations of field conditions was developed that covered all possible avenues of approach in attempting to reproduce the results of Smith *et al.* (1987a, b) and was designed to allow the detection of any ELF-EMF effect on diatom motility. These conditions were tested both with strain III_F, which was claimed to be the same strain as used by Smith *et al.* (1987a), and strain #2038, with which a partial replication of the original results has been achieved (Reese *et al.*, 1991). Each permutation was tested twice. In all experiments, except

those in (7) below, the vertical component of the earth's field was nulled ($B_V = 0$).

The following permutations were used (the amplitude of B_{Hac} is expressed as peak-peak).

(1) Frequency response. $B_H = 20.9\ \mu T$; $B_{Hac} = 41.8\ \mu T$ at frequencies from 1 to 24 Hz in 1-Hz steps. This was an attempt to demonstrate the frequency window for cell motility shown by Smith *et al.* (1987a).

(2) Amplitude response. $B_H = 20.9\ \mu T$; B_{Hac} varied from 5 to 140 μT (in 5-μT steps to 30 μT, 10-μT steps to 80 μT, and 20-μT steps to 140 μT) at 16 Hz. This was an attempt to demonstrate the amplitude window for cell motility shown by Smith *et al.* (1987a).

(3) Amplitude response. $B_H = (B_{Hac})/2$; B_{Hac} varied from 5 to 140 μT (in 5-μT steps to 30 μT, 10-μT steps to 80 μT, and 20-μT steps to 140 μT) at 16 Hz.

(4) Amplitude response. B_H = ambient; B_{Hac} varied from 5 to 140 μT (in 5-μT steps to 30 μT, 10-μT steps to 80 μT, and 20-μT steps to 140 μT) at 16 Hz.

(5) Amplitude response. $B_H = 0\ \mu T$; B_{Hac} varied from 5 to 140 μT (in 5-μT steps to 30 μT, 10-μT steps to 80 μT, and 20-μT steps to 140 μT) at 16 Hz.

In (2), (3), (4), and (5), plates with 5 m*M* added Ca were also used as treatment and control plates (again in triplicate) in an attempt to reproduce the reduction in motility reported by Smith *et al.* (1987a) at high EMF amplitudes.

(6) $B_H = (B_{Hac})/2$ = ambient at 16, 12.5, and 6.25 Hz. These latter frequencies are the predicted cyclotron resonance frequency and an even harmonic, respectively, of the unhydrated calcium ion in the ambient horizontal field in our laboratory. This follows from Blackman *et al.* (1985) and Leal *et al.* (1986), whose work suggested that the ambient field is important in inducing an EMF effect.

(7) Switched field axes at ion cyclotron resonance conditions. $B_H = 0\ \mu T$; $B_V = 20.9\ \mu T$; $B_{Vac} = 41.8\ \mu T$ at 16 Hz. Switching field axes altered field quantities within the plates (see McLeod *et al.*, 1983).

(vi) Effect of exposure period. McLeod *et al.* (1987a) and Smith *et al.* (1987a, b) used an exposure period of 1 h. In our search for an EMF effect we tried extending this period. We harvested a 6-day-old #2038 culture and a 4-day-old III_F culture (both grown in the incubator) and seeded their diatoms onto six replicate plates with 0.25 m*M* added Ca and one plate with 5 m*M* added Ca. Three of the plates with 0.25 m*M* added Ca plus the plate with 5 m*M* added Ca were placed at the sham-exposure site; the remainder were placed at the EMF-exposure site and subjected to Ca ion cyclotron resonance EMF conditions. At 1, 2, 4, 6, 8, 12, 16, 24, 34, and 58 h after the exposure commenced, each plate was removed from exposure or sham-exposure, its diatoms were scored for motility as above, and the plate was returned to the exposure or sham-exposure site.

(vii) Effect of cell density. To test whether the density of the diatom cells on the agar plates had an effect on motility or susceptibility to EMFs (see Aarholt *et al.*, 1981; Carson *et al.*, 1990), a 6-day-old incubator-grown #2038 culture was harvested and its cells were seeded onto 5 plates with m*M* added Ca. Quadruplicate plates were prepared at each cell density used (5×10^4, 1×10^5, 1.5×10^5, 1×10^6, 2×10^6 cells ml^{-1}). Two of each four were placed in Ca ion cyclotron resonance EMF conditions and two were sham-exposed. After 1 h of exposure, the diatoms were killed and scored for motility.

(viii) Effect of position in cell cycle. To test for EMF susceptibility of diatoms at different stages of their cell cycle, cells (III_F) were acclimatized (2 weeks) to a regime of 12 h light/dark at 20°C in the incubator. Following this, on one day cells were inoculated in the usual manner into polystyrene tubes at intervals of 2 h for a total of 16 h. Each culture was then simultaneously harvested 4 days later when in logarithmic growth and seeded on to triplicate sham-exposed and triplicate Ca ion cyclotron resonance-exposed plates with 0.5 m*M* added Ca plus a plate with 5 m*M* added Ca as a positive control. After 1 h of exposure, the cells were scored in the usual way.

(ix) Effect of EMF on distances moved. During the frequency-response test above, the distances moved by III_F cells during the 1-h exposure period were recorded using a calibrated eyepiece graticule attached to the microscope. The distances moved by 10 motile diatoms were recorded on each triplicate sham-exposed and each triplicate EMF-exposed plate (each 0.5 m*M* added Ca) in each experiment. The frequency of B_{Hac} was varied from 1 to 24 Hz in 1-Hz steps, $B_{Hac} = 41.8\ \mu T$, $B_H = 20.9\ \mu T$, $B_V = 0$.

(x) Effect of EMF on direction of movement. The direction of cell movement was also recorded during the frequency-response test using strain III_F. An eyepiece graticule was divided into twelve 30° sectors. Each motile diatom scored was assigned to a sector depending on its initial direction of movement (0° = north). In this way, 100 diatoms per triplicate plate with 0.5 m*M* added Ca were scored in EMF-exposure and sham-exposure conditions at each frequency tested. Direction of movement was tested for nonrandomness using χ^2 tests.

(xi) Effect of EMF pre-incubation. After at least a month of pre-incubation (subculturing every 4–5 days) in a water bath at $B_H = 20\ \mu T$ (see *Exposure apparatus*), 1-, 2-, 3-, 4- and 5-day-old cells of each strain of *A. coffeaeformis* were exposed at Ca ion cyclotron resonance EMF conditions. Exposures lasted for 1 h on triplicate agar plates for each treatment. Treatment plates ranged from 0 to 5 m*M* in added Ca. Those experiments that indicated a positive response to the EMFs in terms of motility were repeated. Five replicate experiments were

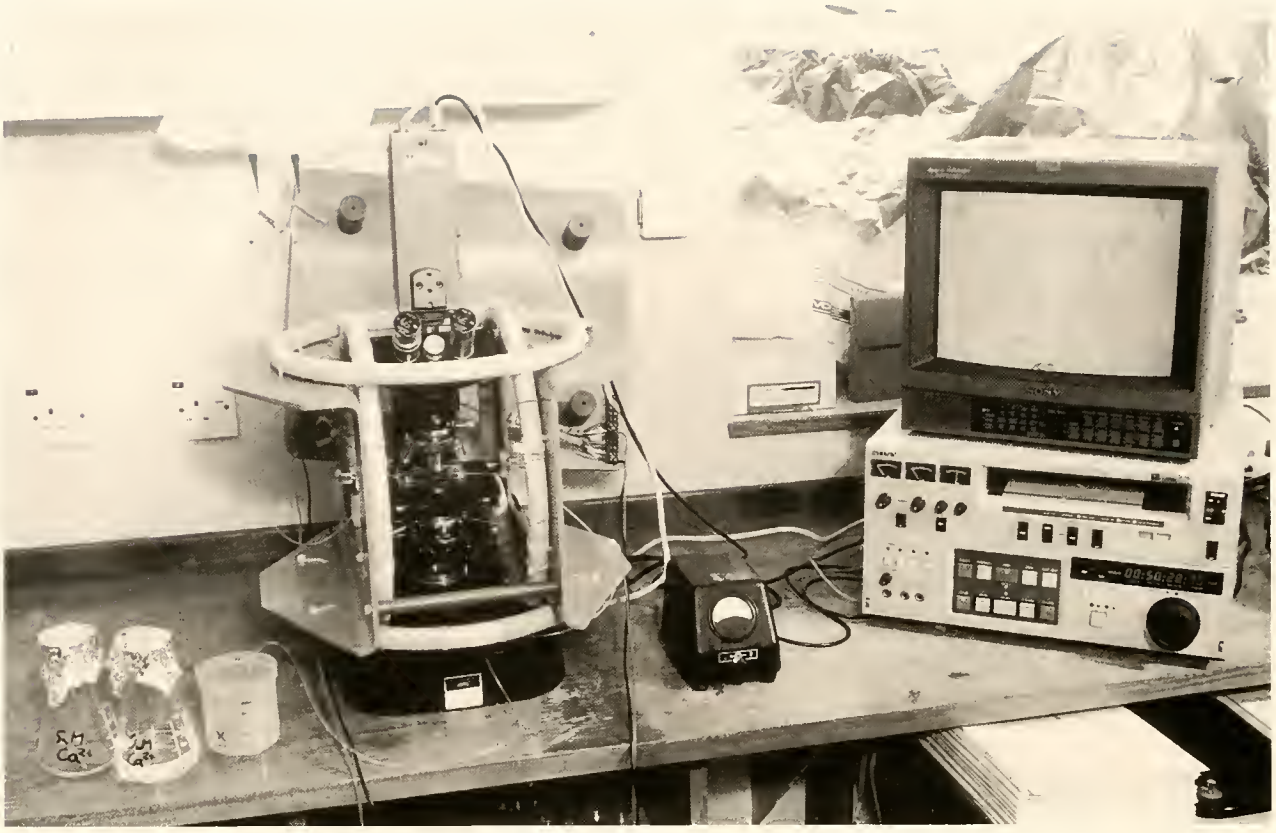

Figure 3. Equipment used in perfusion experiments. Near-Helmholtz coils arranged around microscope stage. Video display of diatoms in perfusion chamber.

also conducted with 3-day-old diatoms (in logarithmic growth) of strain III_B under three conditions: (1) using cells that were not pre-incubated (grown at ambient: B_H = 16.5 μT, B_V = 44 μT); (2) where the near-Helmholtz coils were disconnected from their supply (which remained switched on); and (3) at the even harmonics of 8 and 32 Hz (other field conditions remained the same). According to Smith *et al.* (1987a), shifting to even harmonics should abolish any EMF effect. The experiments were conducted not in the order listed but in a random order, determined using random number tables.

Perfusion experiments

All perfusion experiments were performed on cultures of strain #2038 that had been incubated at B_H = 20 μT for at least one month (see above). Perfusion media were at room temperature (23 ± 1°C).

(i) Equipment. The near-Helmholtz coils used for experimental EMF exposure were placed around a Reichert Zetopan microscope so that the microscope stage was at the center of the coils. The microscope was set for phase contrast and was linked to a U-matic video recorder and monitor *via* a Panasonic CL700 CCD video camera (Fig. 3). The coils were again aligned along the geomagnetic maximum (see above) and, when energized, the field at stage level was at Ca ion cyclotron resonance conditions. The sensing head of the fluxgate magnetometer (56 × 48 × 22 mm) was too large to fit on the stage with the objective lens cluster in place, so the latter was removed during EMF measurement. However, the introduction of the objective lens cluster next to the sensing head within energized coils caused no more than 1 μT deviation in magnetic flux density. During perfusion, diatoms were viewed through a long-working-distance 20× phase-contrast objective lens and displayed on the video monitor.

A perfusion chamber was created from two small glass plates separated by a 30-mm diameter O-ring and clamped together with bulldog clips. Two hollow (hypodermic) needles (0.55-mm diameter) were inserted through the O-ring at points 180° to each other to act as fluid entry and exit ports. Polyethylene tubing was connected to these ports. Two 60-ml syringes acted as reservoirs from which perfusion fluid flowed under gravity through silicone rubber tubing and then polyethylene tubing to the perfusion chamber on the microscope stage. Flow from each reservoir was controlled using a clip on the silicone rubber tubing. An acrylic plastic junction unit allowed flow into the chamber from one reservoir only. In a chamber flooded with water, the time taken from switching to a

flow of food coloring until the central area of the chamber was flooded with color was 50 s.

(ii) Effects of Ca levels on motility. Since the examination of diatom motility in a perfusion chamber was a novel technique, we initially assessed the effects of [Ca] in the perfusion medium. Three-day-old cells were harvested by a single centrifugation (5 min at 1000 × *g*) at 25°C and resuspended in 5 m*M* added Ca minimal medium (M-M). A drop of this cell suspension was introduced into the center of the perfusion chamber. Following a 5-min period allowing for diatoms to adhere to the glass substratum, the chamber was perfused for 10 min with 5 m*M* added Ca M-M. Perfusion was then switched to 0 m*M* added Ca M-M for 5 min; switched back to 5 m*M* added Ca M-M for 5 min; to 0 m*M* added Ca M-M for 5 min; and finally to 5 m*M* added Ca M-M for 5 min. Video recordings of one field of view were made during the whole of this procedure. Diatom speed was estimated by measuring, on screen, the distance moved by each motile diatom in the 10-s period prior to each switching of perfusion medium and in each 10-s period following 1 min of perfusion (except the initial perfusion with 5 m*M* added Ca M-M).

(iii) EMF experiments. The procedure for EMF experiments closely followed the Ca-response experiments above. Cells (3 days old) were again pelleted by a single centrifugation and resuspended in 5 m*M* added Ca M-M. A drop of diatom suspension was introduced into the perfusion chamber. Perfusion with 5 m*M* added Ca M-M commenced after 10 min. Diatoms that showed motility were then observed during the remainder of the procedure. After 10 min, perfusion was switched to 1 m*M* added Ca M-M (a Ca level suboptimal for diatom motility). Motility was measured as before, after 2 min. The EMFs were applied and motility was remeasured after a further 3 min. EMFs were then discontinued and motility was remeasured after a further 3 min.

The above procedure was repeated until a total of 30 diatoms had been recorded during each treatment, with 3–10 diatoms (depending on the number visible on the monitor screen) recorded during each procedure. Control experiments were performed by following the procedure but not applying any EMF. Each treatment and its control were performed during one 3-h period on diatoms from the same culture. Two treatments were used. One employed EMFs at Ca ion cyclotron resonance conditions. The second (conducted 2 days later) involved a manipulation of frequency to an even harmonic which should, according to ion cyclotron resonance theory, abolish any EMF effect. We used $B_V = 0\ \mu T$, $B_H = 20.9\ \mu T$, $B_{Hac} = 41.8\ \mu T$ peak-peak at 32 Hz—*i.e.*, the same conditions for ion cyclotron resonance but at double the frequency.

Paramagnetic investigations

To assess whether the response of diatoms to EMFs was owing to paramagnetism, each strain of *A. coffeaeformis* was grown in polystyrene tubes or glass flasks from 30 000 cells ml^{-1} until stationary phase was attained. Diatoms were harvested by centrifugation (1000 × *g* for 5 min) a minimum of 2 weeks after inoculation and were then washed and recentrifuged four times in deionized (17.4 $M\Omega\ cm^{-1}$) water. Diatom pellets were then lyophilized for 2 days. At no time did the diatoms come into contact with any metal object. To minimize contamination from ferrous particles, both the modified ASP2 and the deionized water used were kept in glass flasks atop a large strong permanent magnet for at least 1 month prior to use (a technique employed by J. Kirschvink, pers. comm.). These liquids were carefully pipetted from the flasks for use.

Samples of freeze-dried diatoms of all strains were sent for analysis to the laboratory of Dr J. Kirschvink (University of California Institute of Technology, USA) where a superconducting quantum interference device (SQUID) was used to detect the presence of biogenic magnetite or ferrous material in the diatoms. For further information on this method, see Kirschvink *et al.* (1992). We had hoped to obtain a sample of diatoms from the group (Reese *et al.*, 1991) that achieved a partial replication of the results of McLeod *et al.* (1987a) and Smith *et al.* (1987a, b), but none were available.

Results

Agar plate experiments

(i) Growth and motility. During growth in culture, each strain of diatom exhibited maximal motility on agar during the logarithmic phase of its growth. This was true whether cultures were grown at 20°C (Fig. 4) or 25°C (Fig. 5), although the time taken to reach logarithmic growth, and hence maximal motility, was shorter at 25°C than at 20°C. These data were used to determine when to harvest cells for maximal motility in the rest of the experiments.

The maximum motilities of #2036, #2038, and #2039 seem independent of growth temperature, whereas those of III_B and III_F increase with increased temperature (maximum mean motilities: III_B at 20°C = 51% ± 7 SE, 25°C = 78% ± 9 SE; III_F at 20°C = 42% ± 4 SE, 25°C = 72% ± 6 SE). The maximum motility recorded on any agar plate during the experiments was for III_B (98%). The higher growth temperature also apparently allows a greater carrying capacity for each strain in culture. Within each temperature treatment the growth curves can be split into two groups: III_B and III_F showed a short logarithmic phase and a small carrying capacity; #2036, #2038, and #2039 showed a longer logarithmic phase and a higher carrying capacity (Figs. 4 and 5).

(ii) Ca curves. In Figure 6, the motility response of our diatoms to external [Ca] is compared with the results obtained by Smith *et al.* (1987a). Our results show that

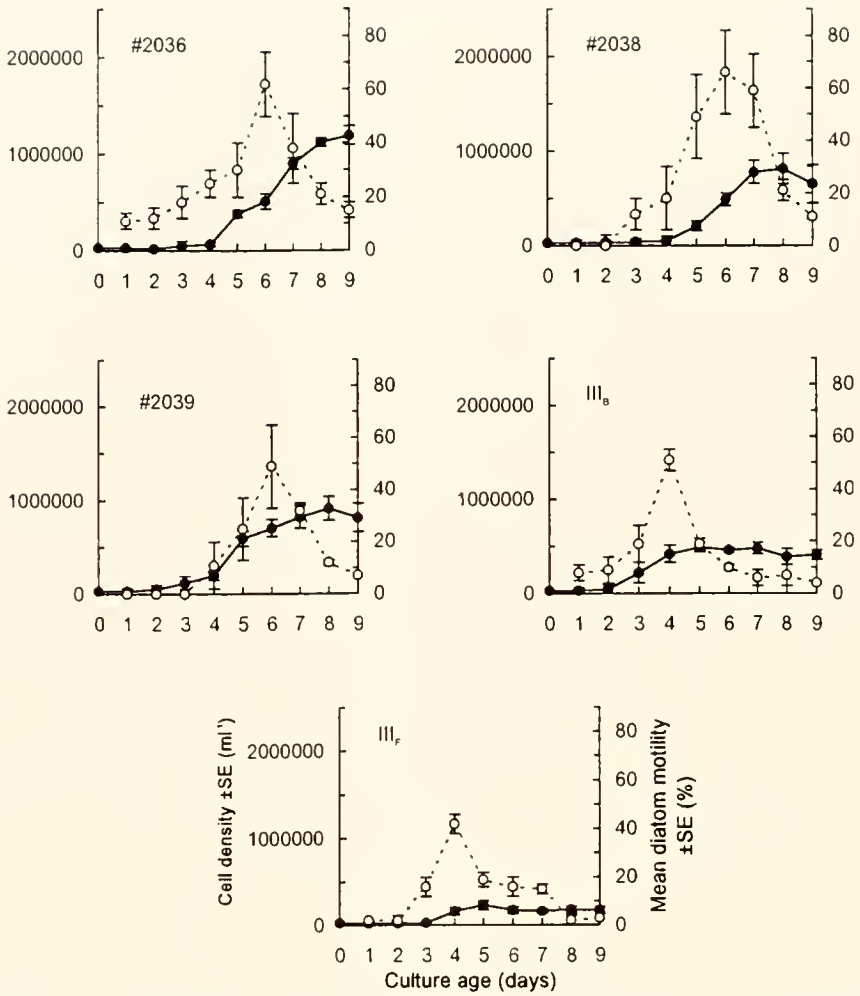

Figure 4. Growth (unfilled circles) and motility (filled circles) of five strains of *Amphora coffeaeformis* at 20°C. In each case $n = 3$.

A. coffeaeformis is incapable of movement in a medium without calcium and that motility increases sharply between 0.25 and 2.5 m*M* external [Ca]. The motility curves for strains III_B and III_F were very similar and showed saturation (of ~70% motility) at about 5 m*M* external [Ca]. The other strains did not show saturation. Strains #2036 and #2038 showed a similar motility response, rising to ~60% at 5 m*M* external [Ca], and #2039 gave a relatively poor response to millimolar Ca levels (40.1% at 5 m*M* external [Ca]). In each case the motility on plates with 0.25 m*M* added Ca was of the order of a few percentage points. This is a prerequisite for the detection of an EMF effect with this system.

(iii) Effect of light intensity. Varying the photon flux density from <0.01 to 53.7 $\mu E\ s^{-1}\ m^{-2}$ had no effect on the motility of #2038 diatoms (Table I).

(iv) EMF experiments. The results of EMF experiments are presented in Tables II–XII. Most data were analyzed by *t*-tests as pairs of control and EMF-exposed groups. Most data were not suitable for multivariate or factorial analyses as cell motility in each experiment was largely determined by the position of the diatoms in their growth curve. Although a very broad range of EMF conditions were employed—including those purported to produce ion cyclotron resonance—and in most cases each was tested twice, a significant difference in diatom motility between exposed and control plates was not demonstrated in any case. No amplitude or frequency window was found. There was no reduction in motility at high EMF amplitudes (Tables IV–VII).

For diatoms of strains #2038 and III_F, extending the exposure period up to 58 h did not produce an EMF effect at ion cyclotron resonance conditions (Fig. 7). Diatom motility reached a maximum within 12 h of exposure.

Varying the cell density of #2038 from 5×10^4 to $2 \times 10^6\ ml^{-1}$ prior to plating had no effect on the motility of either control diatoms or those exposed to ion cyclotron resonance EMFs (Table IX). Similarly, the position of

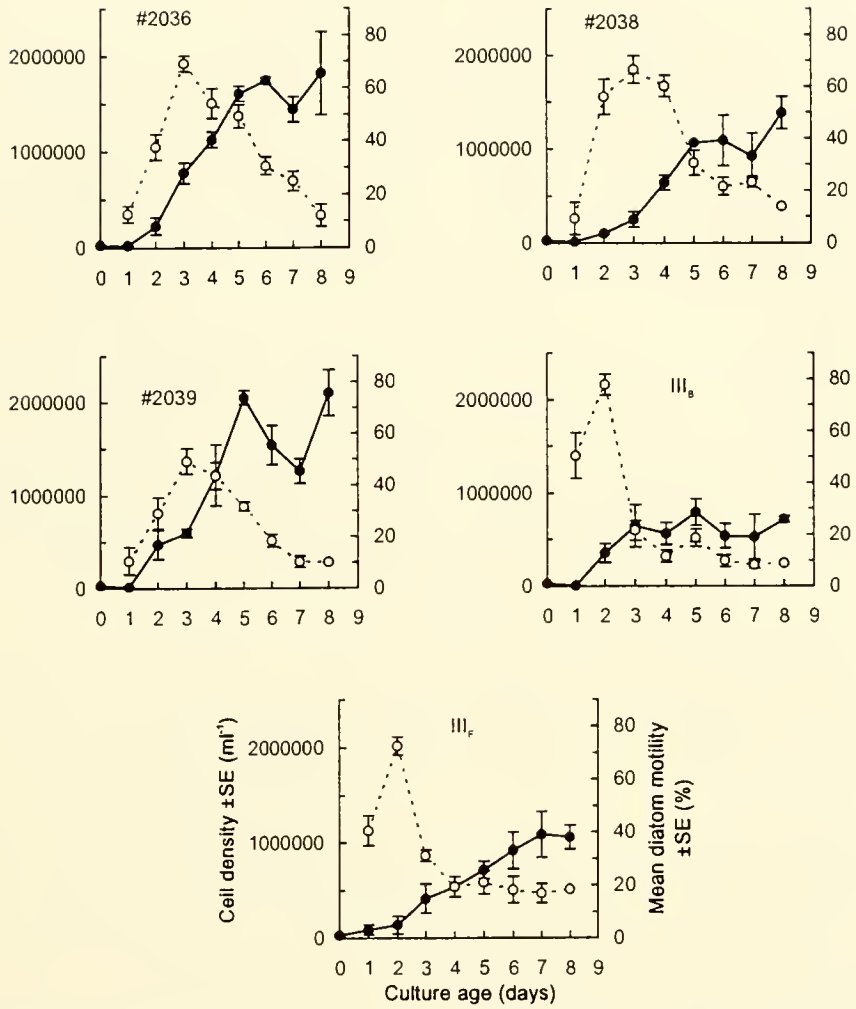

Figure 5. Growth (unfilled circles) and motility (filled circles) of five strains of *Amphora coffeaeformis* at 25°C. In each case $n = 3$.

III_F diatoms in their cell cycle had no effect on population motility at ion cyclotron resonance EMFs (Table X).

The overall mean distance moved by motile III_F diatoms in 1 h was 36.1 μm $\pm$ 0.8 SE, $n = 1440$. Neither the presence of an EMF nor its frequency had an effect on distance moved (Table XI). Table XII shows that EMFs at frequencies from 1 to 24 Hz could not elicit directionality in the movement of III_F diatoms. In each case, the initial direction of diatom movement was randomly distributed about the compass.

(v) Effect of EMF pre-incubation. When diatoms (all strains) were tested under Ca ion cyclotron resonance conditions, the initial experiments showed a poor motility response to Ca; this proved to be a result of technical difficulties with cell culture. However, if the EMF had no effect, we would expect that the number of EMF-exposed/control pairs of cell counts showing an increase in cell motility would, on average, equal the number showing a decrease. A significant proportion (71%) of count pairs showed an increase in cell motility on EMF-exposure ($\chi^2 = 57.4$, $P < 0.001$, $n = 322$), although this increase was usually <10% in population motility.

When a good motility response had been established, three strains aged 2 days or older (cultures tested at ages of 2–5 days) showed a positive response to the Ca ion cyclotron resonance EMFs when Ca-dependent motility curves were constructed (Fig. 8). The most marked responses (~20% increase in cell motility) were shown by 2- and 3-day-old cultures of strain #2038 on agar with 2.5 m*M* added Ca. Smaller increases were also shown by older #2038 cultures and by strains III_B and III_F. Strains #2036 and #2039 did not show a positive EMF-response. Our culture of #2038 then went into decline, and fresh material from a reserve stock was pre-incubated at $B_H = 20$ μT, $B_V = 0$ μT for 1 month. In a further three sets of experiments, this fresh #2038 responded positively to EMF (Fig. 9); however, subsequent attempts, including experiments with the other strains, showed no effect. The greatest positive effect

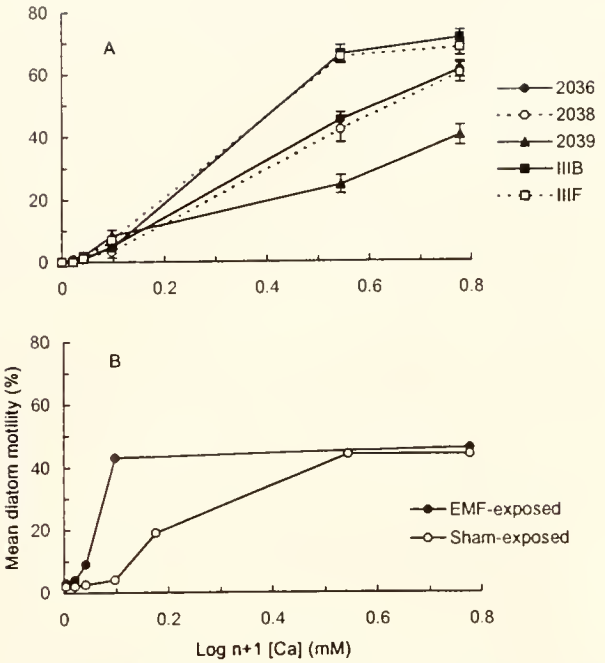

Figure 6. Motility response of *Amphora coffeaeformis* in logarithmic growth to external [Ca]. (A) Present results using five strains of *A. coffeaeformis* (bars are SE, $n = 3$). (B) Results of Smith *et al.* (1987), including an EMF-induced effect for comparison.

(~30% increase in motility) was shown by a 1-day-old culture on plates with 2.5 m*M* added Ca (Fig. 9).

Material from reserve stocks was again pre-incubated at $B_H = 20\ \mu T$, $B_V = 0\ \mu T$, this time for at least 3 months. Strain #2038 again declined, but III_B grew as expected and was used in the following experiments (each repeated five times). Under ion cyclotron resonance conditions, each experiment showed an EMF effect (Fig. 10), the maximum difference in motility between exposed and sham-exposed cells occurring at 2.5 m*M* added Ca (mean increase = +22.1% ± 1.8 SE, $n = 15$). No experiment at Ca ion cyclotron resonance conditions failed to show an EMF effect (Fig. 10), although the percentage shift in motility was smaller, and the [Ca] at which an effect occurred was higher, than in the other experiments using pre-incubation reported above. The EMF effect was abolished when diatoms were grown in the earth's field prior to experimentation (Fig. 11: mean increase in motility at 2.5 m*M* added Ca = −1.8% ± 1.8 SE, $n = 15$) and when the coils were not energized during experimentation (Fig. 12; mean increase = −3.4% ± 0.9 SE, $n = 15$). The effect was also abolished when even harmonics at 8 Hz (mean increase = +1.4% ± 1.1 SE, $n = 15$) and 32 Hz (mean increase = −0.8% ± 1.5 SE, $n = 15$) were used (Figs. 13 and 14). Experimentation was recommenced after a break of 1 month and subsequent experiments, under conditions above that produced an effect, indicated no EMF effect.

Perfusion experiments

(i) Effects of Ca levels on motility. In conditions of 5 m*M* added Ca M-M, all observed diatoms were motile. When the perfusion medium was switched to 0 m*M* added Ca M-M, all diatoms either stopped moving or greatly slowed their movement. When switched back to 5 m*M* added Ca M-M, the diatoms resumed motility. A further switching to 0 m*M* added Ca M-M abolished or reduced motility in all diatoms. Example observations are shown in Figure 15. All diatoms observed regained motility in 5 m*M* added Ca M-M at the end of the procedure.

(ii) EMF experiments. At ion cyclotron resonance conditions (at 16 Hz), a significant increase (approximately 2-fold, over the control) in diatom speed was ob-

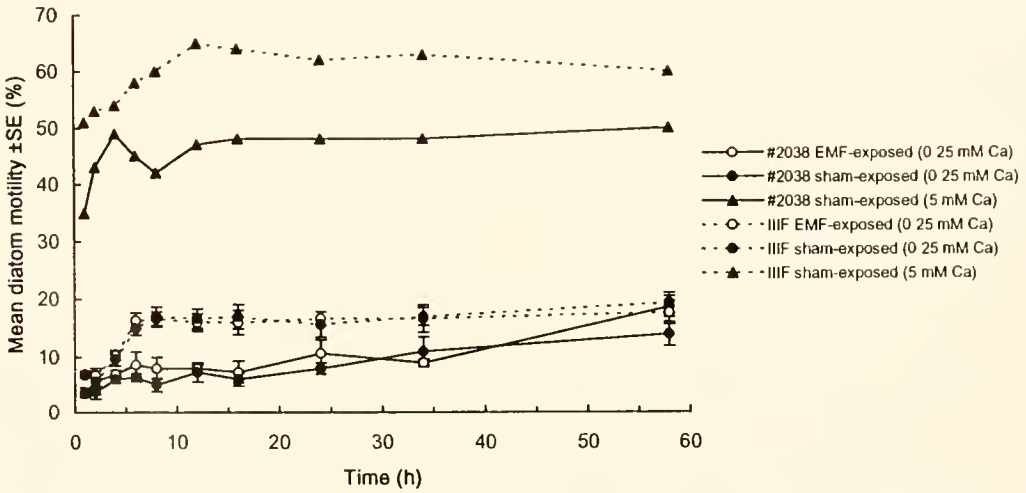

Figure 7. Effect of exposure period on susceptibility of *Amphora coffeaeformis* strains #2038 and III_F to EMFs at ion cyclotron resonance conditions on agar plates. [Ca] refer to levels of added Ca in agar; $n = 3$, except for 5 m*M* Ca plates where $n = 1$.

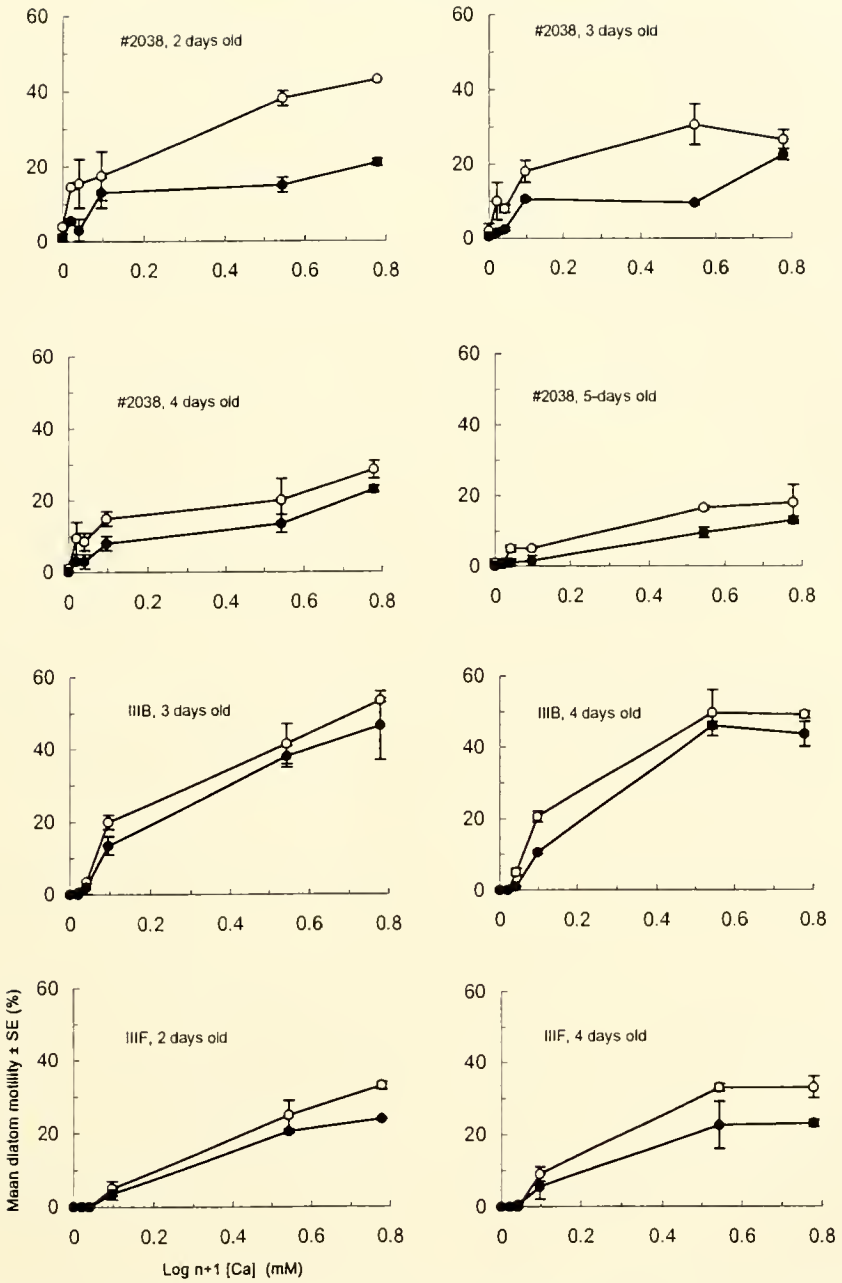

Figure 8. Motility response of strains #2038, III_B, and III_F (pre-incubated at $B_V = 0$, $B_H = 20$ μT for at least 1 month) to external [Ca] in EMF experiments at ion cyclotron resonance conditions ($B_V = 0$, $B_H = 20.9$ μT, $B_{Hac} = 41.8$ μT peak-peak at 16 Hz). Unfilled circles = EMF-exposed; filled circles = sham-exposed; $n = 3$ in each case. Time indicated is culture age. Results shown only where an EMF-induced effect is apparent. Strains #2036, #2039, III_B at 2 and 5 days old, and III_F at 3 and 5 days old showed no effect.

served on application of the EMFs (Mann-Whitney test, $U = 286$, $P = 0.012$; Fig. 16). Such an increase was not apparent either before or after application of EMFs in comparison with the controls (Mann-Whitney tests: $U = 416$, $P = 0.548$; $U = 358$, $P = 0.153$, respectively, Fig. 16); and the pre-exposure, during-exposure, and post-exposure speeds of the control diatoms were not significantly different from each other (Kruskall-Wallis test, $H = 1.44$, $P = 0.486$). A shift to an even harmonic (32 Hz) abolished the EMF effect (Fig. 16): there was no significant difference in speed between diatoms exposed to the EMF and control diatoms either before ($U = 411$, $P = 0.513$), during ($U = 432$, $P = 0.758$), or after ($U = 424$, $P = 0.664$) EMF application. Again the control diatoms showed no significant variation in speed during the experiment ($H = 1.5$, $P = 0.472$).

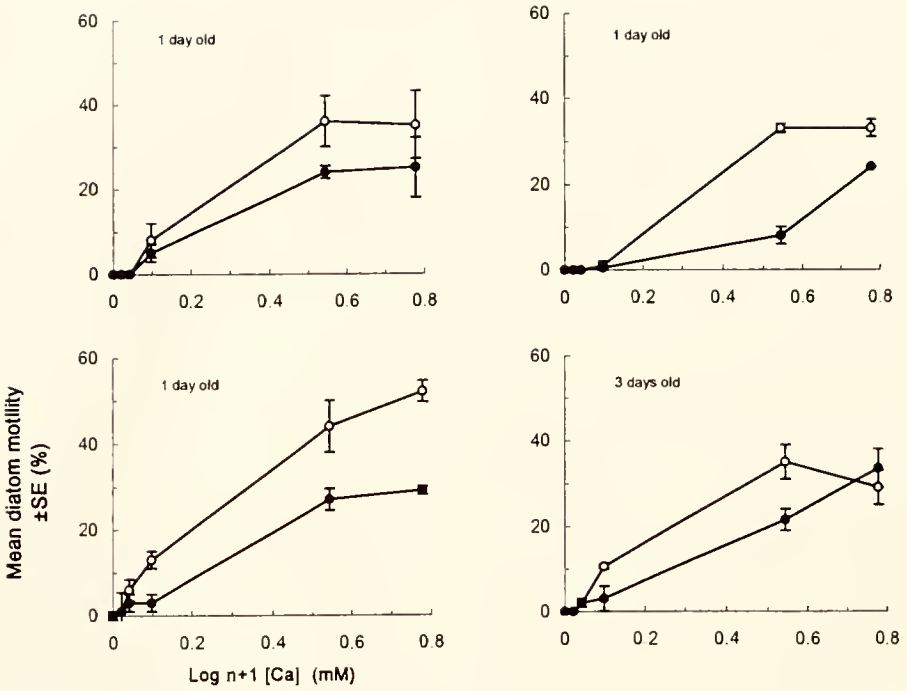

Figure 9. Motility response of strain #2038 (pre-incubated at $B_V = 0$, $B_H = 20\ \mu T$ for at least 3 months) to external [Ca] in EMF experiments at ion cyclotron resonance conditions ($B_V = 0$, $B_H = 20.9\ \mu T$, $B_{Hac} = 41.8\ \mu T$ peak-peak at 16 Hz). Unfilled circles = EMF-exposed; filled circles = sham-exposed; $n = 3$ in each case.

Paramagnetic investigations

The diatoms exhibited no detectable ferromagnetic properties.

Discussion

In the exploration of the interaction between biological systems and EMFs, the use of diatoms and the 'diatom system' was originally seen as potentially reproducible in different laboratories. The system was heralded as one that could effectively and easily demonstrate an EMF effect (McLeod *et al.*, 1987a, Smith *et al.*, 1987a, b). In addition, by indicating effects only at specific frequency-windows and amplitude-windows, the results of McLeod *et al.* (1987a) and Smith *et al.* (1987a, b) pointed to an interaction mechanism (originally ascribed to ion cyclotron resonance), and this is probably the reason that so many (Reese *et al.*, 1991; Parkinson and Sulik, 1992; Saalman *et al.*, 1992; Prasad *et al.*, 1994; Florig, pers. comm.) have attempted to repeat the original work. However, as we and many of those who have attempted replication have found, the system is more complex than originally thought.

It is apparent from Figures 1, 4, and 5 that the different strains of *A. coffeaeformis* vary considerably in morphology and physiology (see also Parkinson and Sulik, 1992). There are also variations in upper lethal temperature and in the shape of the growth mat in liquid culture (Davies, unpubl. data). Clearly the classification of the diatoms we used as strains or variants of *A. coffeaeformis* is in doubt and there is a need to reexamine the taxon *Amphora coffeaeformis* (Gallagher, 1986, 1987). The variations may in part be owing to the culturing of diatoms over many years in laboratories where selection pressures may differ, and to the process of subculturing in which a small number of cells (often only one) is used to start a new population, producing genetic bottlenecks. In only one (Saalman *et al.*, 1992) of the other attempts to reproduce the findings of McLeod *et al.* (1987a) and Smith *et al.* (1987a, b) were the diatoms of the same strain as used in the original experiments, and this may contribute to a lack of repeatability. If the diatom system is indeed dependent on the use of a single strain of one species, or possibly, the presence of a single gene (which might be lost during subculturing), then its value as a reproducible system is in doubt. Large genetic variation in intraspecific variants of photosynthetic microbes is an acknowledged problem for experimentalists (see, for example, Gallagher, 1980; Medlin *et al.*, 1996; Paasche *et al.*, 1996).

Diatom motility shows a sharp peak during exponential growth (Figs. 4 and 5), and although the physiological explanation for this remains unknown, diatoms clearly must be in exponential growth (show motility) before they can display sensitivity to EMFs. Whether this was the case in the other attempts at replication is not apparent (Reese *et al.*, 1991; Parkinson and Sulik, 1992; Saalman *et al.*, 1992; Prasad *et al.*, 1994). McLeod *et al.* (1987a)

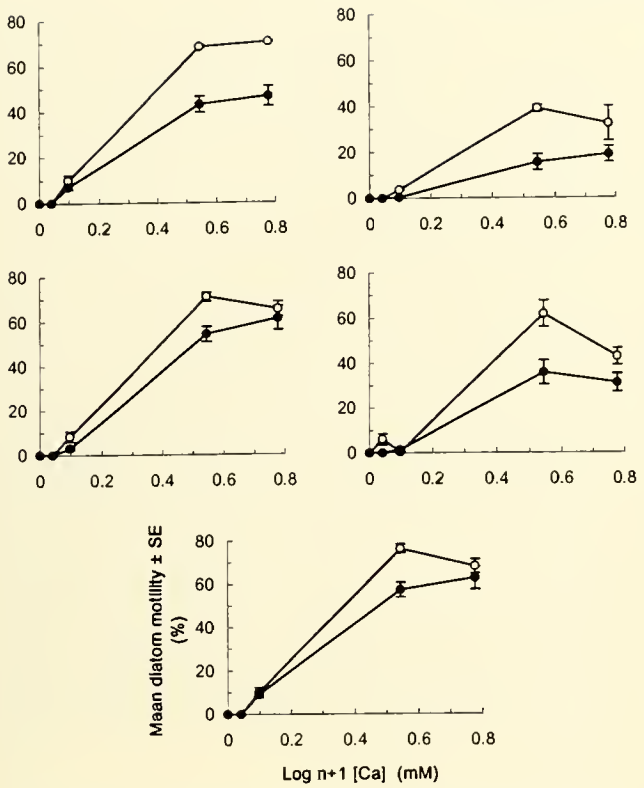

Figure 10. Motility response of strain III_B (pre-incubated at B_V = 0, B_H = 20 μT for at least 3 months) to external [Ca] in EMF experiments at ion cyclotron resonance conditions (B_V = 0, B_H = 20.9 μT, B_{Hac} = 41.8 μT peak-peak at 16 Hz). Unfilled circles = EMF-exposed; filled circles = sham-exposed; n = 3 in each case.

and Smith *et al.* (1987a) observed a maximum motility of ~45% within any diatom population, ascribing this to the presence of the raphe system on one diatom valve only. We (and Reese *et al.*, 1991, and Saalman *et al.*, 1992) noted that population motility can exceed 50%, perhaps as a result of our plating technique, which allows time for the diatoms to orient themselves in liquid culture before they contact the surface of the agar. In our motility assays, in common with Parkinson and Sulik (1992) and Saalman *et al.* (1992), we counted only diatoms that were not in contact with any others. This condition was set because motility in one diatom may trigger motility in an adjoining diatom, thus producing non-independence of measurements (Saalman *et al.*, 1992). McLeod *et al.* (1987a) and Smith *et al.* (1987a, b) counted some diatoms that were in clumps and some counts may have included (immotile) diatoms whose lateral surfaces were in contact with the agar (Smith, pers. comm.). Thus, it is not surprising that our Ca curves (Fig. 6) do not agree with those of McLeod *et al.* (1987a) and Smith *et al.* (1987a, b). Nevertheless, although diatoms of strains III_B and III_F showed greater motility than those in the original experiments, the shape of the Ca response curves is similar, supporting the contention that these strains are descendants of diatoms used in the original experiments. Cooksey and Cooksey (1980), Parkinson and Sulik (1992), and McLeod (pers. comm.) observed a reduction or abolition of diatom population motility in the dark. We (Table I), on the other hand, in common with Saalman *et al.* (1992), observed motility in the dark, suggesting the existence of a store of energy in diatoms (probably as a pool of ATP). Again our results may be different because we may have used a different strain of *A. coffeaeformis* (#2038) from those of Cooksey and Cooksey (1980) (presumably III_B) and Parkinson and Sulik (1992) (strain not indicated).

Experiments using externally applied EMFs (Tables II–X) showed wide variability in the proportion of diatoms exhibiting motility under putatively the same control conditions. This we can only ascribe to slight variations in population age and culture conditions, of diatoms, which could produce diatoms at slightly different stages of the growth-cycle at the start of the experiments. Clearly control experiments must be concurrent with exposure experiments in this system. Our initial inability to demonstrate an EMF effect using a wider range of field conditions than any previously published, extending the period of exposure, varying the

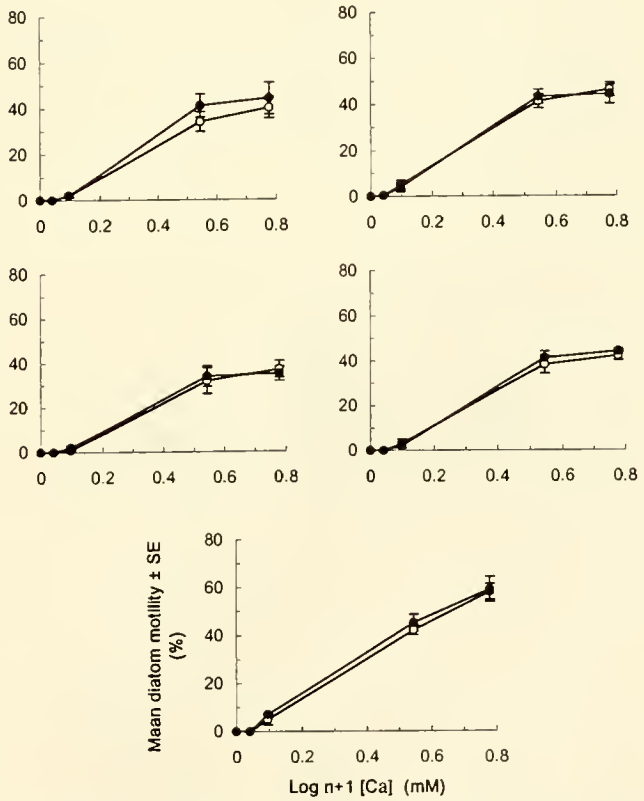

Figure 11. Motility response of strain III_B to external [Ca] in EMF experiments at ion cyclotron resonance conditions (B_V = 0, B_H = 20.9 μT, B_{Hac} = 41.8 μT peak-peak at 16 Hz). Unfilled circles = EMF-exposed; filled circles = sham-exposed; n = 3 in each case. Diatoms were not pre-incubated before use, but were grown in ambient EMF.

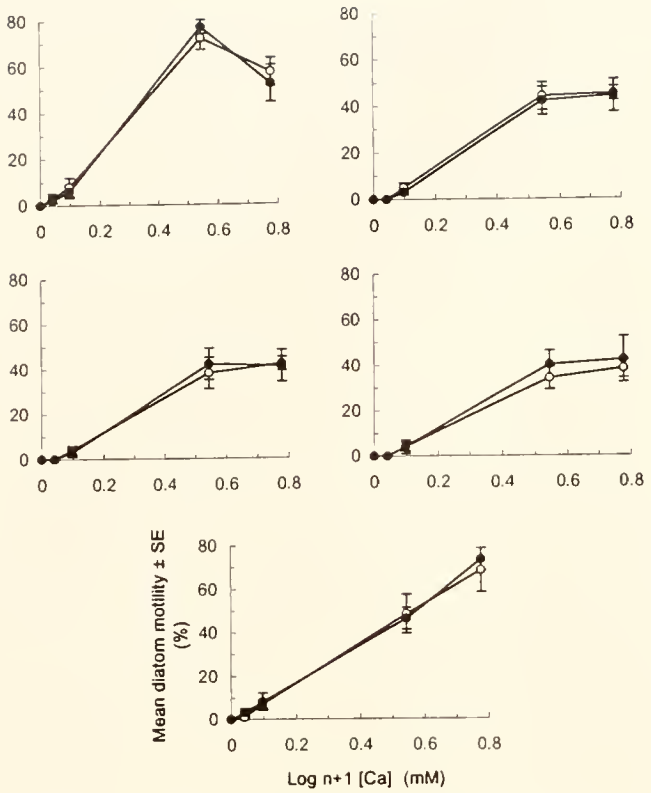

Figure 12. Motility response of strain III_B (pre-incubated at B_V = 0, B_H = 20 μT for at least 3 months) to external [Ca] in EMF experiments in which electrical equipment was set to give ion cyclotron resonance conditions (B_V = 0, B_H = 20.9 μT, B_{Hac} = 41.8 μT peak-peak at 16 Hz), but the coils were not energized. Unfilled circles = EMF-exposed; filled circles = sham-exposed; n = 3 in each case.

cell density and position in the cell-cycle, and assessing the distance and direction moved by diatoms militates against the potential of diatoms as a useful model for EMF effects. However, the increase (compared to paired controls) in population motility exhibited by a significant proportion of EMF-exposed diatoms (all strains) on agar at ion cyclotron resonance conditions indicates that diatoms are susceptible to the effects of EMFs, but only when they have experienced a defined EMF environment prior to experimentation. Significant increases in motility of EMF-exposed over sham-exposed diatoms were observed in single experiments (Figs. 8–10), although again only where diatoms had been "pre-incubated" in specific EMFs. The abolition of the effect when the EMF-producing coils were disconnected (Fig. 12) gives clear evidence for the role of extraneous fields in producing the effect, and the abolition at even harmonics (Figs. 13 and 14) does not rule out the presence of a frequency window. Blackman *et al.* (1985, 1990) and Leal *et al.* (1986) reported EMF effects that were modulated by the intensity of the geomagnetic field. In our experiments we effectively modified the Earth's field to create defined conditions ($B_H \cong B_H$ used in the experiments at ion cyclotron resonance conditions) during diatom growth, as originally suggested by Smith *et al.* (1987b). Neither we nor Smith *et al.* (1987b) offer an explanation for this phenomenon, but it is unlikely to be owing to any paramagnetism within the diatoms because none was detected. Clearly our initial failure (and that of others) to replicate the original findings may be owing to a lack of appreciation of the effect of the Earth's field. Before using the pre-exposure system, we grew diatoms in conventional incubators with complex spatiotemporal EMF conditions, and a lack of reproducibility of EMF effects in general may be caused by the complex EMFs to which cells and organisms are exposed *prior* to experimentation. Our results support those of Blackman *et al.* (1988) in suggesting that prior treatment of experimental organisms is an important variable in bioelectromagnetic science. Even our experiments involving ambient fields (Table VIII) used diatoms grown in a conventional incubator. The ability of McLeod *et al.* (1987a), Smith *et al.* (1987a, b), and many other workers to observe a response to EMFs without pre-incubation of the test organism may be owing to the continued culture, over many generations, of the test organism in the environment in which experiments are subsequently performed; again, however, the rationale for this effect is not apparent.

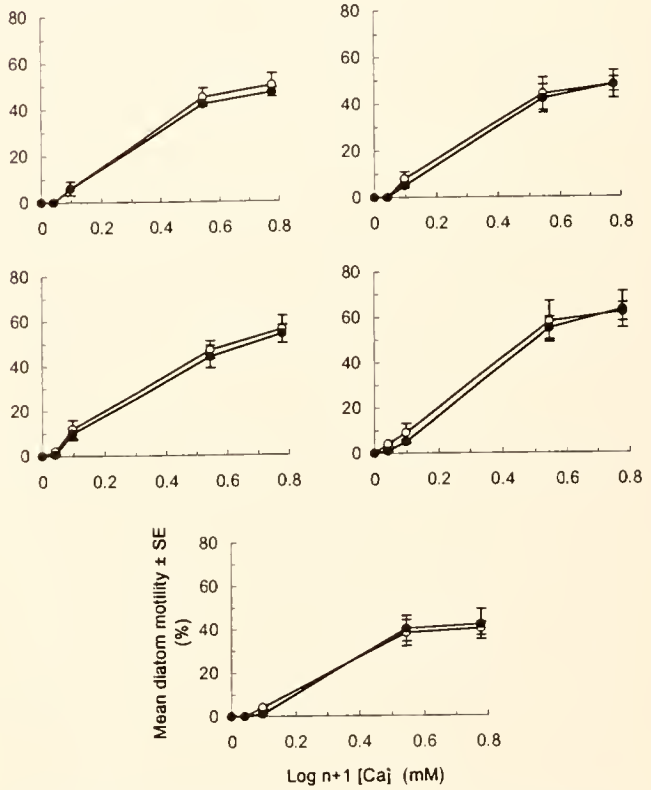

Figure 13. Motility response of strain III_B (pre-incubated at B_V = 0, B_H = 20 μT for at least 3 months) to external [Ca] in EMF experiments at an even harmonic of ion cyclotron resonance conditions (B_V = 0, B_H = 20.9 μT, B_{Hac} = 41.8 μT peak-peak at 8 Hz). Unfilled circles = EMF-exposed; filled circles = sham-exposed; n = 3 in each case.

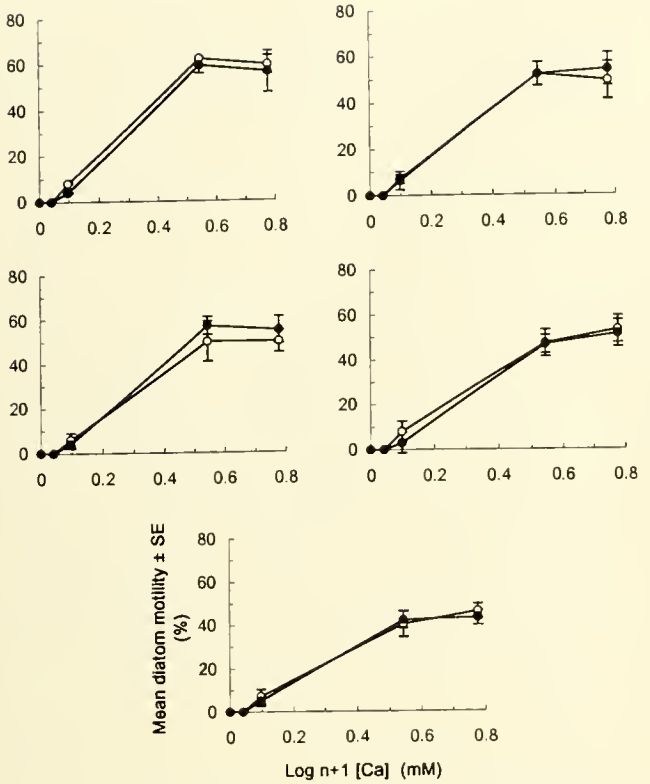

Figure 14. Motility response of strain III_B (pre-incubated at B_V = 0, B_H = 20 μT for at least 3 months) to external [Ca] in EMF experiments at an even harmonic of ion cyclotron resonance conditions (B_V = 0, B_H = 20.9 μT, B_{Hac} = 41.8 μT peak-peak at 32 Hz). Unfilled circles = EMF-exposed; filled circles = sham-exposed; n = 3 in each case.

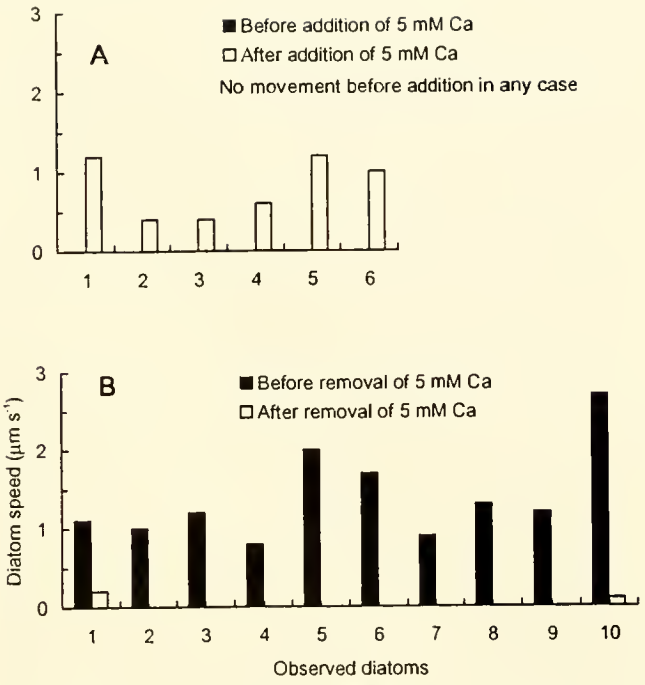

Figure 15. Mean (±SE) diatom speed recorded in real time on addition (A) and removal (B) of 5 mM Ca to the perfusion chamber. Measurements made in 10-s period prior to addition or removal and in 10-s period 1 min after addition or removal (see text).

When the pre-incubation step was used, three strains of *A. coffeaeformis* (#2038, III_B, and III_F) showed a population motility response to EMFs. Strains III_B and III_F might be expected to respond since they are putative descendants of the strain used in the original experiments. That #2038 showed a response and #2036 and #2039 did not may indicate intraspecific genetic variation in susceptibility to EMFs—variation that presumably involves the metabolism of Ca. Any susceptibility may already be lost, however, because of the influence of selection and genetic bottleneck effects on genetic drift (see above). Indeed, with the exception of the experiments on strain III_B (Figs. 10–14), EMF effects were generally ephemeral and the controlling factor (be it genetic or environmental) is, as yet, unknown. Reese *et al.* (1991) also reported an ephemeral response with strain #2038. All these observations further emphasize the importance of using a responsive strain of *A. coffeaeformis* for these experiments, but they also highlight the limitations of *A. coffeaeformis* as a model for assessing EMF interactions with living systems.

We developed the system involving perfusion of media over diatoms as a method for quantitatively monitoring the movements of diatoms exposed to EMFs. The system has

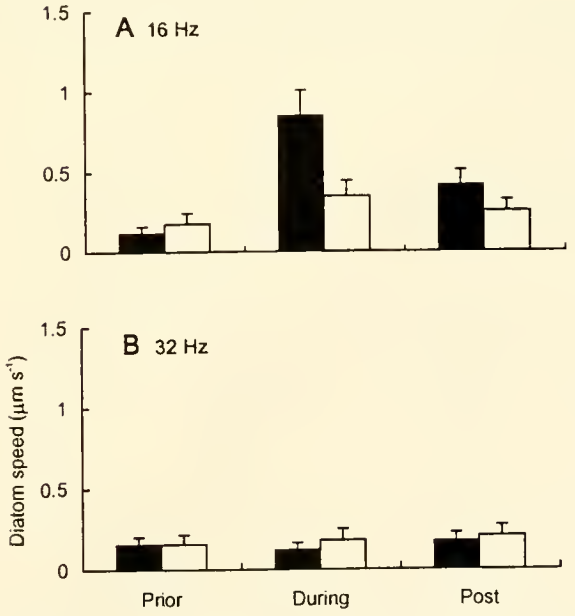

Figure 16. Mean (±SE) speed of 2-day-old #2038 cells in perfusion experiments prior to, during, and after EMF exposure (see text). Filled bars = EMF-exposure; open bars = sham-exposure. EMF before objective lens in place: B_H = 20.9 μT, B_{Hac} = 41.8 μT peak-peak at (A) 16 Hz and (B) 32 Hz, B_V = 0.

several advantages over the agar plate method: it allows real-time *in vivo* recordings to be made of diatom speed and direction while EMF stimulation takes place; diatoms remain alive at the end of the procedure and can be tested again, if necessary; the activities of numerous diatoms can be followed on repeated EMF exposure; positive control tests (motility at high [Ca]; no motility at low [Ca]) can be performed on diatoms at the start and end of each procedure; and the time required for both experimentation and analysis is reduced. Results using this system demonstrated that external [Ca] can be manipulated to limit diatom motility (Fig. 15) and that EMFs at ion cyclotron resonance conditions, but not at an even harmonic (using pre-incubated #2038 cells), increase the speed of motile diatoms (Fig. 16). EMFs therefore act both to increase the proportion of motile diatoms within a population and to increase the speed of those diatoms that show motility.

The positive results reported are consistent with ion cyclotron resonance as the mode of interaction, although tests designed to assess the validity of this mode of interaction were not performed. However, there are theoretical reasons why ion cyclotron resonance is unlikely to be a plausible mechanism (Halle, 1988; Male, 1992). The present results are also consistent with later theories of "ion precession" (Lednev, 1991; Edmonds, 1993), although our experiments give no indication of mechanism, but merely report a possible frequency window. That the Ca^{2+} ion is involved in the process of susceptibility of diatoms to EMFs is not in doubt, and this ion has been implicated in many other studies involving EMF interactions (*e.g.*, Fitzsimmons *et al.*, 1994; Stefano *et al.*, 1994; Gamaley *et al.*, 1995; see Goldberg and Creasey, 1991, and Michaelson, 1985, for reviews). McLeod *et al.* (1992) suggest that biological systems in transition, or those that are working suboptimally, may be most susceptible to EMFs; clearly the diatom system—motility limited by Ca—fits this hypothesis. Nevertheless, the attention paid by workers to the importance of Ca (see Michaelson, 1985) may be unfounded because Ca is a common second messenger in cellular systems (Alberts *et al.*, 1994) and is likely to be involved in the regulation of many cellular processes. Thus the Ca^{2+} ion may not be the link in the biochemical chain that is directly influenced by EMFs, but merely the ion used in destabilizing a system to look for EMF effects and the ion deliberately made rate-limiting. Evidence supporting Ca as the natural rate-limiter in biological processes that can be modulated by EMFs is weak.

In conclusion, we have found the mediation of diatom motility by EMFs to be at best ephemeral and reliant upon the pre-incubation of cells in a specific electromagnetic environment. (Nevertheless, independent replication of bioelectromagnetic phenomena is rare and any such replicability can only help establish bioelectromagnetic science.) In addition, sensitivity to EMFs was demonstrated in only three of five strains of *A. coffeaeformis* tested. It is our opinion that although the "diatom system" may still constitute a useful cellular model for demonstrating bioelectromagnetic effects, further development to identify and control subtle etiological factors is required before the system can be regarded as readily reproducible.

Acknowledgments

This work was generously supported by The National Grid Company, UK. S. D. Smith, K. and B. Cooksey, and especially B. R. McLeod gave advice and assistance. Thanks to Caroline Palmer and Mariata Jutson for technical assistance.

Table I

Effect of light intensity on the motility of diatom strain #2038 exposed for 1 h on 5 mM added Ca plates (n = 3 *in each case*)

Flux density ($\mu E\ s^{-1}\ m^{-2}$)	Diatom motility (%)	
	mean	SE
<0.01	32.33	1.45
0.40	37.00	1.53
9.80	31.33	4.41
23.30	32.00	4.16
53.70	33.00	2.52

Analysis of variance table (performed on arcsine-square root transformed data)

Source of variation	d.f.	SS	MS	*F*	*P*
Light intensity	4	0.00704	0.00176	0.52	0.723
Error	10	0.03377	0.00338		
Total	14	0.04081			

Table II

EMF test results (mean % motilities ± SE on agar plates, n = 3*) at ion cyclotron resonance conditions (B_V = 0 μT, B_H = 20.9 μT, B_{Hac} = 41.8 μT peak-peak at 16 Hz).* t = t-*value of arcsine square-root transformed motility data from exposed and sham-exposed 0.25 mM added Ca plates*

Diatom strain	Exposed 0.25 m*M* Ca	Control 0.25 m*M* Ca	*t*	*P*	Control 5 m*M* Ca
#2036	1.33 ± 0.88	1.33 ± 0.88	0.00	1.00	46
	3.33 ± 0.88	1.33 ± 0.67	1.61	0.25	40
#2038	3.00 ± 1.53	3.67 ± 1.45	0.32	0.77	42
	4.00 ± 1.15	4.67 ± 0.88	0.50	0.65	44
#2039	3.00 ± 1.53	3.00 ± 1.15	0.30	0.79	41
	3.33 ± 0.33	2.33 ± 0.33	2.17	0.12	34
III_B	6.00 ± 1.15	6.00 ± 1.73	0.07	0.95	61
	7.67 ± 0.88	7.33 ± 1.76	0.24	0.83	52
III_F	4.67 ± 1.33	6.33 ± 0.88	1.04	0.41	60
	3.00 ± 1.00	1.33 ± 0.33	1.79	0.22	66

Table III

EMF test results (mean % motilities ± SE on agar plates, n = 3): frequency response. t = t-*value of arcsine square-root transformed motility data from exposed and sham-exposed 0.25 m*M *added Ca plates*

Diatom strain	Exposed 0.25 m*M* Ca	Control 0.25 m*M* Ca	*t*	*P*	Control 5 m*M* Ca
B_V = 0 μT, B_H = 20.9 μT, B_{Hac} = 41.8 μT peak-peak at 1 Hz					
#2038	7.67 ± 0.88	6.67 ± 0.88	0.79	0.49	46
	4.33 ± 0.88	4.67 ± 1.45	0.10	0.93	42
III_F	6.67 ± 0.33	6.00 ± 1.53	0.51	0.66	56
	3.67 ± 1.20	3.33 ± 0.33	0.14	0.90	52
B_V = 0 μT, B_H = 20.9 μT, B_{Hac} = 41.8 μT peak-peak at 2 Hz					
#2038	7.67 ± 0.88	7.00 ± 1.00	0.50	0.65	49
	8.33 ± 0.33	7.00 ± 0.58	1.98	0.14	51
III_F	2.00 ± 0.58	3.00 ± 1.00	0.72	0.52	58
	1.00 ± 1.00	2.33 ± 0.88	1.38	0.30	54
B_V = 0 μT, B_H = 20.9 μT, B_{Hac} = 41.8 μT peak-peak at 3 Hz					
#2038	2.67 ± 0.88	1.33 ± 0.88	1.14	0.34	44
	2.33 ± 1.20	2.00 ± 1.15	0.12	0.91	49
III_F	5.33 ± 1.33	5.00 ± 0.58	0.16	0.89	56
	4.33 ± 0.33	6.00 ± 0.58	2.57	0.08	50
B_V = 0 μT, B_H = 20.9 μT, B_{Hac} = 41.8 μT peak-peak at 4 Hz					
#2038	4.67 ± 1.33	5.00 ± 1.00	0.25	0.82	46
	1.33 ± 0.88	1.67 ± 0.88	0.19	0.86	48
III_F	4.67 ± 1.76	7.33 ± 0.67	1.45	0.29	50
	10.00 ± 0.58	8.00 ± 1.53	1.27	0.33	52
B_V = 0 μT, B_H = 20.9 μT, B_{Hac} = 41.8 μT peak-peak at 5 Hz					
#2038	1.33 ± 0.33	2.00 ± 0.58	0.97	0.41	46
	0.67 ± 0.33	0.67 ± 0.33	0.00	1.00	47
III_F	2.67 ± 0.67	3.00 ± 1.00	0.24	0.83	50
	4.67 ± 2.19	5.33 ± 1.76	0.28	0.80	51
B_V = 0 μT, B_H = 20.9 μT, B_{Hac} = 41.8 μT peak-peak at 6 Hz					
#2038	4.33 ± 0.88	4.67 ± 1.20	0.19	0.86	39
	2.67 ± 0.33	2.00 ± 0.58	1.03	0.41	46
III_F	7.00 ± 1.00	6.33 ± 0.33	0.61	0.60	56
	4.67 ± 0.33	6.33 ± 0.88	1.82	0.21	58
B_V = 0 μT, B_H = 20.9 μT, B_{Hac} = 41.8 μT peak-peak at 7 Hz					
#2038	3.33 ± 0.88	4.67 ± 1.86	0.42	0.71	47
	5.67 ± 1.20	5.33 ± 0.33	0.19	0.87	42
III_F	7.00 ± 3.06	6.67 ± 2.73	0.04	0.97	56
	5.00 ± 1.53	6.33 ± 1.76	0.54	0.63	48
B_V = 0 μT, B_H = 20.9 μT, B_{Hac} = 41.8 μT peak-peak at 8 Hz					
#2038	1.67 ± 0.88	1.00 ± 1.00	0.60	0.59	36
	6.33 ± 0.33	6.33 ± 0.33	0.00	1.00	38
III_F	1.00 ± 0.58	2.00 ± 1.15	0.46	0.68	49
	4.67 ± 1.86	5.00 ± 1.53	0.21	0.85	50
B_V = 0 μT, B_H = 20.9 μT, B_{Hac} = 41.8 μT peak-peak at 9 Hz					
#2038	5.00 ± 1.00	4.00 ± 1.53	0.63	0.57	46
	0.67 ± 0.67	1.67 ± 1.20	0.71	0.53	49
III_F	5.00 ± 1.53	4.00 ± 1.53	0.45	0.68	59
	1.33 ± 0.88	1.00 ± 1.00	0.43	0.69	43
B_V = 0 μT, B_H = 20.9 μT, B_{Hac} = 41.8 μT peak-peak at 10 Hz					
#2038	5.00 ± 2.08	3.33 ± 2.03	0.75	0.51	47
	0.33 ± 0.33	0.67 ± 0.67	0.24	0.83	41
III_F	2.00 ± 1.53	1.67 ± 0.67	0.23	0.84	51
	2.00 ± 0.58	0.33 ± 0.33	2.66	0.08	49
B_V = 0 μT, B_H = 20.9 μT, B_{Hac} = 41.8 μT peak-peak at 11 Hz					
#2038	1.33 ± 0.33	0.33 ± 0.33	2.23	0.16	42
	0.67 ± 0.67	1.33 ± 0.33	1.35	0.31	36
III_F	7.67 ± 0.88	7.67 ± 1.33	0.04	0.97	43
	6.33 ± 1.76	5.00 ± 1.53	0.54	0.63	39
B_V = 0 μT, B_H = 20.9 μT, B_{Hac} = 41.8 μT peak-peak at 12 Hz					
#2038	7.33 ± 0.88	6.33 ± 1.76	0.58	0.62	42
	2.67 ± 0.33	3.00 ± 0.58	0.45	0.68	38
III_F	8.00 ± 1.15	8.33 ± 2.33	0.03	0.98	51
	7.33 ± 1.76	7.33 ± 0.67	0.10	0.93	56
B_V = 0 μT, B_H = 20.9 μT, B_{Hac} = 41.8 μT peak-peak at 13 Hz					
#2038	0.33 ± 0.33	1.00 ± 0.58	0.88	0.44	44
	1.67 ± 0.88	1.00 ± 1.00	0.60	0.59	44
III_F	8.00 ± 1.00	6.00 ± 1.15	0.06	0.14	56
	6.67 ± 1.45	5.33 ± 1.86	0.63	0.58	60
B_V = 0 μT, B_H = 20.9 μT, B_{Hac} = 41.8 μT peak-peak at 14 Hz					
#2038	3.00 ± 1.53	5.67 ± 1.45	1.33	0.28	49
	6.33 ± 0.33	4.00 ± 2.00	1.08	0.39	53
III_F	6.33 ± 1.45	6.33 ± 1.45	0.00	1.00	48
	0.67 ± 0.67	1.67 ± 1.20	0.71	0.53	51
B_V = 0 μT, B_H = 20.9 μT, B_{Hac} = 41.8 μT peak-peak at 15 Hz					
#2038	1.00 ± 0.58	2.67 ± 1.76	0.59	0.60	48
	0.67 ± 0.67	0.67 ± 0.33	0.34	0.76	57
III_F	3.67 ± 1.20	2.67 ± 0.67	0.71	0.53	39
	4.33 ± 1.20	5.33 ± 2.03	0.33	0.76	46
B_V = 0 μT, B_H = 20.9 μT, B_{Hac} = 41.8 μT peak-peak at 17 Hz					
#2038	11.33 ± 0.88	10.00 ± 0.58	1.27	0.29	61
	4.67 ± 1.33	5.00 ± 2.08	0.19	0.19	53
III_F	5.67 ± 0.33	4.67 ± 1.20	0.90	0.47	51
	8.67 ± 0.67	8.33 ± 0.33	0.43	0.71	60

Table III (*Continued*)

Diatom strain	Exposed 0.25 m*M* Ca	Control 0.25 m*M* Ca	*t*	*P*	Control 5 m*M* Ca
$B_V = 0\ \mu T$, $B_H = 20.9\ \mu T$, $B_{Hac} = 41.8\ \mu T$ peak-peak at 18 Hz					
#2038	5.00 ± 1.15	4.67 ± 1.20	0.21	0.85	38
	0.67 ± 0.67	1.00 ± 0.58	0.53	0.63	37
III_F	3.67 ± 0.88	3.33 ± 1.76	0.50	0.67	71
	7.33 ± 0.88	5.33 ± 2.03	0.99	0.43	64
$B_V = 0\ \mu T$, $B_H = 20.9\ \mu T$, $B_{Hac} = 41.8\ \mu T$ peak-peak at 19 Hz					
#2038	0.67 ± 0.67	1.33 ± 0.88	0.64	0.57	41
	1.67 ± 0.82	2.00 ± 2.00	0.23	0.83	43
III_F	9.00 ± 1.73	9.00 ± 2.00	0.01	0.99	42
	5.33 ± 1.20	3.67 ± 2.19	0.85	0.49	40
$B_V = 0\ \mu T$, $B_H = 20.9\ \mu T$, $B_{Hac} = 41.8\ \mu T$ peak-peak at 20 Hz					
#2038	4.00 ± 2.65	6.33 ± 0.88	1.04	0.41	46
	0.67 ± 0.67	1.00 ± 0.58	0.53	0.63	36
III_F	1.67 ± 1.67	2.33 ± 1.86	0.39	0.72	50
	1.00 ± 0.58	1.33 ± 0.88	0.16	0.88	42
$B_V = 0\ \mu T$, $B_H = 20.9\ \mu T$, $B_{Hac} = 41.8\ \mu T$ peak-peak at 21 Hz					
#2038	1.00 ± 0.58	1.67 ± 0.88	0.36	0.74	40
	2.67 ± 2.67	4.00 ± 2.00	0.55	0.62	36
III_F	10.67 ± 0.88	8.33 ± 1.20	1.53	0.22	61
	6.00 ± 0.58	6.00 ± 0.58	0.00	1.00	54
$B_V = 0\ \mu T$, $B_H = 20.9\ \mu T$, $B_{Hac} = 41.8\ \mu T$ peak-peak at 22 Hz					
#2038	2.00 ± 0.58	2.33 ± 1.20	0.20	0.86	34
	1.67 ± 1.67	2.00 ± 1.15	0.41	0.71	41
III_F	5.00 ± 2.08	6.00 ± 1.73	0.45	0.68	56
	8.67 ± 0.33	9.67 ± 1.20	0.78	0.52	59
$B_V = 0\ \mu T$, $B_H = 20.9\ \mu T$, $B_{Hac} = 41.8\ \mu T$ peak-peak at 23 Hz					
#2038	3.00 ± 1.53	5.00 ± 1.00	1.19	0.32	46
	5.33 ± 0.33	4.33 ± 1.20	0.85	0.49	40
III_F	3.67 ± 1.67	5.00 ± 1.15	0.77	0.50	72
	8.33 ± 1.20	7.67 ± 0.67	0.44	0.69	59
$B_V = 0\ \mu T$, $B_H = 20.9\ \mu T$, $B_{Hac} = 41.8\ \mu T$ peak-peak at 24 Hz					
#2038	0.67 ± 0.33	0.67 ± 0.67	0.34	0.76	48
	3.00 ± 0.58	2.67 ± 1.20	0.41	0.72	34
III_F	8.00 ± 2.00	7.33 ± 0.67	0.24	0.83	60
	8.33 ± 2.33	6.33 ± 1.20	0.67	0.55	71

Table IV

EMF test results (mean % motilities ± SE on agar plates, n = 3): amplitude response 1. t = t-value of arcsine square-root transformed motility data from exposed and sham-exposed 0.25 mM added Ca plates and exposed and sham-exposed 5 mM added Ca plates

Diatom strain	Exposed 0.25 m*M* Ca	Control 0.25 m*M* Ca	*t*	*P*	Exposed 5 m*M* Ca	Control 5 m*M* Ca	*t*	*P*
		B_V = 0 μT, B_H = 20.9 μT, B_{Hac} = 5 μT peak-peak at 16 Hz						
#2038	3.67 ± 1.20	3.00 ± 0.58	0.43	0.70	38.00 ± 2.31	43.00 ± 2.08	1.61	0.21
	3.67 ± 2.19	3.67 ± 1.45	0.09	0.93	47.00 ± 1.00	48.00 ± 2.08	0.43	0.71
III_F	10.00 ± 0.58	9.67 ± 1.76	0.25	0.83	67.00 ± 1.00	69.67 ± 1.86	1.27	0.29
	8.33 ± 0.33	8.33 ± 0.88	0.04	0.97	53.00 ± 3.51	57.30 ± 1.86	1.09	0.36
		B_V = 0 μT, B_H = 20.9 μT, B_{Hac} = 10 μT peak-peak at 16 Hz						
#2038	1.00 ± 0.58	1.00 ± 1.00	0.32	0.77	49.33 ± 0.88	47.67 ± 1.20	1.12	0.34
	1.67 ± 1.20	0.67 ± 0.67	0.71	0.53	50.33 ± 0.88	48.33 ± 2.30	0.80	0.51
III_F	3.33 ± 1.45	4.33 ± 20.3	0.32	0.77	61.00 ± 0.58	56.33 ± 1.86	2.41	0.14
	8.67 ± 1.76	9.67 ± 0.88	0.57	0.63	52.67 ± 1.76	51.67 ± 2.19	0.36	0.75
		B_V = 0 μT, B_H = 20.9 μT, B_{Hac} = 15 μT peak-peak at 16 Hz						
#2038	3.33 ± 1.45	3.33 ± 1.45	0.00	1.00	41.00 ± 1.53	46.00 ± 1.15	2.61	0.08
	5.33 ± 0.33	6.33 ± 1.45	0.60	0.61	45.67 ± 2.73	48.00 ± 3.00	0.57	0.61
III_F	7.00 ± 0.58	7.67 ± 0.67	0.76	0.50	61.33 ± 0.88	62.33 ± 1.20	0.67	0.55
	11.30 ± 1.76	10.30 ± 1.33	0.43	0.70	49.67 ± 2.73	56.33 ± 3.18	1.59	0.21
		B_V = 0 μT, B_H = 20.9 μT, B_{Hac} = 20 μT peak-peak at 16 Hz						
#2038	6.33 ± 0.33	6.00 ± 1.73	0.32	0.78	43.00 ± 3.51	47.33 ± 4.10	0.81	0.48
	8.67 ± 0.67	9.67 ± 1.20	0.72	0.52	44.33 ± 2.85	44.00 ± 2.00	0.09	0.93
III_F	6.33 ± 0.33	7.00 ± 0.58	0.99	0.39	55.33 ± 2.60	53.33 ± 3.38	0.47	0.67
	7.67 ± 0.67	7.33 ± 0.33	0.43	0.71	43.67 ± 0.88	42.67 ± 1.76	0.51	0.66
		B_V = 0 μT, B_H = 20.9 μT, B_{Hac} = 25 μT peak-peak at 16 Hz						
#2038	3.33 ± 1.76	4.33 ± 0.33	0.78	0.52	48.33 ± 0.88	43.33 ± 2.40	1.95	0.19
	6.00 ± 0.58	7.67 ± 0.88	1.57	0.21	42.00 ± 1.15	44.00 ± 2.52	0.72	0.55
III_F	2.33 ± 0.88	5.67 ± 1.45	2.00	0.14	62.67 ± 1.76	54.33 ± 3.84	1.97	0.19
	8.00 ± 0.58	8.00 ± 0.58	0.00	1.00	57.67 ± 2.03	54.67 ± 3.18	0.79	0.49
		B_V = 0 μT, B_H = 20.9 μT, B_{Hac} = 30 μT peak-peak at 16 Hz						
#2038	0.33 ± 0.33	1.00 ± 0.58	0.88	0.44	36.33 ± 2.19	38.67 ± 1.45	0.89	0.44
	1.00 ± 1.00	1.00 ± 1.00	0.00	1.00	46.00 ± 2.31	44.33 ± 3.18	0.43	0.70
III_F	9.00 ± 2.52	8.33 ± 0.88	0.17	0.88	53.67 ± 2.33	51.67 ± 0.33	0.85	0.48
	8.67 ± 1.76	9.33 ± 0.67	0.43	0.71	59.67 ± 0.88	57.67 ± 0.88	1.60	0.21
		B_V = 0 μT, B_H = 20.9 μT, B_{Hac} = 40 μT peak-peak at 16 Hz						
#2038	3.33 ± 1.76	2.00 ± 2.00	0.60	0.59	39.00 ± 2.89	44.67 ± 2.40	1.51	0.23
	1.00 ± 0.58	1.67 ± 1.20	0.28	0.80	48.00 ± 2.08	49.00 ± 1.53	0.39	0.72
III_F	7.33 ± 0.88	6.33 ± 2.67	0.52	0.65	51.33 ± 1.86	51.67 ± 2.03	0.12	0.91
	3.33 ± 1.76	1.00 ± 0.58	0.79	0.49	47.33 ± 1.76	49.00 ± 1.73	0.67	0.55
		B_V = 0 μT, B_H = 20.9 μT, B_{Hac} = 50 μT peak-peak at 16 Hz						
#2038	4.33 ± 1.67	3.00 ± 0.58	0.50	0.67	44.67 ± 1.76	46.33 ± 1.86	0.65	0.56
	6.67 ± 1.86	4.33 ± 0.33	1.10	0.39	52.33 ± 2.03	52.33 ± 1.86	0.00	1.00
III_F	6.33 ± 0.33	7.33 ± 0.88	1.06	0.40	50.00 ± 3.46	50.33 ± 3.48	0.07	0.95
	2.67 ± 1.76	3.33 ± 0.33	0.74	0.54	49.67 ± 0.67	51.33 ± 2.40	0.67	0.57

Table IV (*Continued*)

Diatom strain	Exposed 0.25 m*M* Ca	Control 0.25 m*M* Ca	*t*	*P*	Exposed 5 m*M* Ca	Control 5 m*M* Ca	*t*	*P*
		$B_V = 0\ \mu T$, $B_H = 20.9\ \mu T$, $B_{Hac} = 60\ \mu T$ peak-peak at 16 Hz						
#2038	5.67 ± 0.33	7.33 ± 0.88	1.81	0.21	40.00 ± 0.58	42.00 ± 0.58	2.45	0.09
	2.00 ± 0.58	3.00 ± 0.88	1.23	0.31	46.00 ± 1.73	46.33 ± 1.86	0.13	0.91
III_F	5.67 ± 0.33	7.00 ± 1.53	0.74	0.54	57.00 ± 2.00	56.67 ± 1.76	0.13	0.91
	7.33 ± 1.67	5.00 ± 1.53	1.02	0.38	48.67 ± 1.45	51.00 ± 0.58	1.49	0.27
		$B_V = 0\ \mu T$, $B_H = 20.9\ \mu T$, $B_{Hac} = 70\ \mu T$ peak-peak at 16 Hz						
#2038	1.00 ± 1.00	0.33 ± 0.33	0.37	0.74	41.67 ± 1.45	46.00 ± 1.53	2.06	0.13
	1.67 ± 0.88	2.00 ± 1.15	0.11	0.92	47.33 ± 1.33	43.67 ± 1.20	2.04	0.13
III_F	6.33 ± 0.33	6.67 ± 0.33	0.71	0.52	61.33 ± 0.88	66.00 ± 2.52	1.75	0.22
	2.00 ± 1.15	3.00 ± 0.58	0.93	0.45	80.33 ± 3.18	83.33 ± 1.76	0.80	0.48
		$B_V = 0\ \mu T$, $B_H = 20.9\ \mu T$, $B_{Hac} = 80\ \mu T$ peak-peak at 16 Hz						
#2038	4.00 ± 1.15	3.00 ± 0.58	0.70	0.54	43.00 ± 1.53	45.67 ± 1.67	1.60	0.25
	7.00 ± 1.00	5.00 ± 0.58	1.80	0.17	40.00 ± 0.58	42.67 ± 1.76	1.44	0.29
III_F	0.67 ± 0.67	1.67 ± 1.23	0.71	0.53	57.33 ± 0.88	60.33 ± 0.88	2.40	0.10
	6.00 ± 0.58	7.00 ± 1.00	0.87	0.45	58.33 ± 1.33	61.67 ± 1.20	0.85	0.16
		$B_V = 0\ \mu T$, $B_H = 20.9\ \mu T$, $B_{Hac} = 100\ \mu T$ peak-peak at 16 Hz						
#2038	2.00 ± 0.58	4.67 ± 0.88	2.52	0.09	43.00 ± 1.53	43.33 ± 1.33	0.17	0.88
	6.33 ± 1.45	8.33 ± 0.67	1.27	0.33	42.67 ± 2.73	43.00 ± 2.85	0.17	0.88
III_F	2.67 ± 1.20	5.67 ± 1.45	1.62	0.20	72.33 ± 1.76	75.33 ± 2.73	0.94	0.41
	8.67 ± 0.88	6.33 ± 0.33	2.53	0.13	70.00 ± 3.46	75.33 ± 3.18	1.14	0.34
		$B_V = 0\ \mu T$, $B_H = 20.9\ \mu T$, $B_{Hac} = 120\ \mu T$ peak-peak at 16 Hz						
#2038	6.33 ± 0.67	4.67 ± 1.20	1.26	0.33	42.33 ± 0.88	44.33 ± 0.33	2.12	0.17
	5.33 ± 1.76	3.67 ± 0.88	0.72	0.52	47.33 ± 0.67	46.33 ± 0.88	0.90	0.43
III_F	8.33 ± 1.20	7.67 ± 0.88	0.41	0.71	73.33 ± 0.88	74.67 ± 2.60	0.51	0.66
	8.67 ± 0.33	8.67 ± 0.33	0.00	1.00	54.00 ± 2.31	51.33 ± 0.88	1.08	0.39
		$B_V = 0\ \mu T$, $B_H = 20.9\ \mu T$, $B_{Hac} = 140\ \mu T$ peak-peak at 16 Hz						
#2038	0.33 ± 0.33	0.67 ± 0.67	0.24	0.83	46.67 ± 1.20	45.00 ± 1.53	0.86	0.45
	3.33 ± 1.30	3.00 ± 1.73	0.45	0.70	49.33 ± 0.67	50.33 ± 1.20	0.73	0.52
III_F	9.67 ± 0.33	10.67 ± 1.20	0.78	0.51	55.67 ± 2.91	54.67 ± 2.03	0.29	0.79
	7.00 ± 1.15	6.67 ± 1.33	0.21	0.85	48.00 ± 1.53	49.00 ± 0.58	0.61	0.60

Table V

EMF test results (mean % motilities ± SE on agar plates, n = 3): amplitude response 2. t = t-value of arcsine square-root transformed motility data from exposed and sham-exposed 0.25 mM added Ca plates and exposed and sham-exposed 5 mM added Ca plates

Diatom strain	Exposed 0.25 m*M* Ca	Control 0.25 m*M* Ca	*t*	*P*	Exposed 5 m*M* Ca	Control 5 m*M* Ca	*t*	*P*
			B_V = 0 μT, B_H = 2.5 μT, B_{Hac} = 5 μT peak-peak at 16 Hz					
#2038	0.67 ± 0.67	1.67 ± 0.20	0.71	0.53	46.67 ± 0.33	44.67 ± 1.33	1.45	0.28
	3.67 ± 0.67	4.67 ± 0.88	0.88	0.44	46.67 ± 0.67	45.00 ± 1.00	1.39	0.26
III_F	10.67 ± 0.88	10.00 ± 1.53	0.42	0.70	60.00 ± 0.58	60.33 ± 0.88	0.32	0.77
	7.33 ± 0.33	6.67 ± 0.67	0.93	0.45	59.00 ± 0.58	61.33 ± 1.33	1.60	0.25
			B_V = 0 μT, B_H = 5 μT, B_{Hac} = 10 μT peak-peak at 16 Hz					
#2038	2.33 ± 0.33	3.00 ± 0.58	0.98	0.40	47.67 ± 1.45	47.67 ± 1.20	0.00	1.00
	6.33 ± 0.33	6.67 ± 1.20	0.20	0.86	42.33 ± 1.45	41.33 ± 1.20	0.53	0.63
III_F	2.33 ± 0.88	4.00 ± 1.15	1.16	0.33	52.00 ± 1.15	54.67 ± 0.88	1.84	0.16
	8.67 ± 1.20	7.00 ± 0.88	0.47	0.69	54.67 ± 2.40	53.67 ± 2.91	0.26	0.81
			B_V = 0 μT, B_H = 7.5 μT, B_{Hac} = 15 μT peak-peak at 16 Hz					
#2038	0.67 ± 0.67	2.67 ± 0.88	1.98	0.14	38.00 ± 1.15	39.67 ± 1.45	0.90	0.44
	7.67 ± 0.88	6.33 ± 0.33	1.40	0.30	45.33 ± 1.33	45.00 ± 0.58	0.23	0.84
III_F	11.00 ± 1.00	10.67 ± 1.20	0.22	0.84	59.67 ± 0.88	57.00 ± 1.15	1.84	0.16
	7.33 ± 0.33	7.33 ± 0.33	0.00	1.00	48.33 ± 1.20	49.00 ± 0.58	0.50	0.67
			B_V = 0 μT, B_H = 10 μT, B_{Hac} = 20 μT peak-peak at 16 Hz					
#2038	4.00 ± 1.15	4.00 ± 1.00	0.04	0.97	44.67 ± 1.33	46.33 ± 1.76	0.75	0.51
	6.67 ± 1.20	6.00 ± 1.15	0.41	0.71	43.00 ± 1.00	44.33 ± 1.86	0.63	0.57
III_F	2.33 ± 0.88	2.67 ± 0.88	0.25	0.82	45.00 ± 0.00	45.00 ± 0.00	0.00	1.00
	6.00 ± 0.58	8.00 ± 1.00	1.71	0.19	62.33 ± 0.67	62.67 ± 1.76	0.18	0.87
			B_V = 0 μT, B_H = 12.5 μT, B_{Hac} = 25 μT peak-peak at 16 Hz					
#2038	7.33 ± 0.33	7.67 ± 0.67	0.43	0.71	46.00 ± 0.58	46.00 ± 1.00	0.00	1.00
	4.00 ± 1.15	3.33 ± 1.20	0.43	0.69	50.33 ± 1.45	50.33 ± 0.88	0.00	1.00
III_F	10.00 ± 2.00	9.33 ± 1.33	0.22	0.84	49.33 ± 0.88	50.67 ± 2.40	0.52	0.65
	6.33 ± 1.33	7.67 ± 0.88	0.88	0.44	58.67 ± 1.33	57.00 ± 1.73	0.76	0.50
			B_V = 0 μT, B_H = 15 μT, B_{Hac} = 30 μT peak-peak at 16 Hz					
#2038	8.33 ± 0.88	9.33 ± 0.67	0.92	0.43	50.33 ± 1.45	51.00 ± 1.00	0.38	0.73
	4.00 ± 1.00	4.00 ± 1.15	0.04	0.97	43.67 ± 1.86	47.33 ± 1.33	1.60	0.21
III_F	6.00 ± 1.15	6.33 ± 1.33	0.19	0.86	55.33 ± 1.30	56.00 ± 1.53	0.33	0.76
	7.00 ± 0.58	3.33 ± 2.40	1.49	0.27	55.67 ± 0.67	54.33 ± 2.03	0.62	0.60
			B_V = 0 μT, B_H = 20 μT, B_{Hac} = 40 μT peak-peak at 16 Hz					
#2038	7.67 ± 0.67	7.67 ± 0.88	0.02	0.98	51.33 ± 0.67	48.00 ± 1.15	2.50	0.09
	6.33 ± 0.67	4.00 ± 1.53	1.30	0.32	43.00 ± 2.89	43.33 ± 2.96	0.08	0.94
III_F	10.00 ± 1.15	9.33 ± 0.33	0.51	0.66	56.33 ± 0.33	58.00 ± 0.58	2.50	0.09
	11.67 ± 1.20	12.33 ± 1.45	0.35	0.75	52.67 ± 1.86	54.33 ± 1.86	0.64	0.57
			B_V = 0 μT, B_H = 25 μT, B_{Hac} = 50 μT peak-peak at 16 Hz					
#2038	4.67 ± 1.45	5.00 ± 1.73	0.11	0.92	41.00 ± 1.53	40.67 ± 0.67	0.20	0.86
	5.67 ± 0.88	4.33 ± 2.40	0.73	0.54	40.67 ± 0.67	40.67 ± 0.33	0.00	1.00
III_F	7.67 ± 0.88	8.33 ± 0.67	0.61	0.69	53.67 ± 0.88	56.33 ± 1.33	1.67	0.19
	6.00 ± 0.58	7.33 ± 0.33	1.98	0.14	54.67 ± 3.48	57.67 ± 4.10	0.56	0.61

Table V (*Continued*)

Diatom strain	Exposed 0.25 m*M* Ca	Control 0.25 m*M* Ca	*t*	*P*	Exposed 5 m*M* Ca	Control 5 m*M* Ca	*t*	*P*
		$B_V = 0\ \mu T$, $B_H = 30\ \mu T$, $B_{Hac} = 60\ \mu T$ peak-peak at 16 Hz						
#2038	3.00 ± 0.58	3.00 ± 0.58	0.00	1.00	44.67 ± 2.19	44.33 ± 1.76	0.12	0.91
	2.33 ± 0.67	1.67 ± 0.67	0.71	0.52	46.67 ± 0.33	44.00 ± 1.53	1.71	0.23
III_F	3.33 ± 0.67	3.33 ± 0.33	0.08	0.95	56.33 ± 1.45	52.00 ± 1.15	2.33	0.10
	10.00 ± 0.57	8.00 ± 1.15	1.54	0.26	61.00 ± 0.58	63.33 ± 1.76	1.26	0.33
		$B_V = 0\ \mu T$, $B_H = 35\ \mu T$, $B_{Hac} = 70\ \mu T$ peak-peak at 16 Hz						
#2038	2.00 ± 1.15	3.00 ± 0.58	0.93	0.45	46.67 ± 1.20	45.33 ± 1.76	0.63	0.58
	5.33 ± 0.33	5.00 ± 2.00	0.34	0.76	50.00 ± 1.00	50.00 ± 0.58	0.00	1.00
III_F	8.33 ± 0.33	10.00 ± 0.58	2.54	0.09	57.33 ± 1.67	59.00 ± 0.58	0.94	0.44
	10.30 ± 1.20	10.30 ± 0.33	0.05	0.97	52.33 ± 0.67	52.67 ± 0.67	0.35	0.74
		$B_V = 0\ \mu T$, $B_H = 40\ \mu T$, $B_{Hac} = 80\ \mu T$ peak-peak at 16 Hz						
#2038	6.33 ± 0.33	7.33 ± 0.88	1.06	0.40	41.00 ± 1.53	43.67 ± 1.20	1.37	0.26
	4.33 ± 0.67	4.67 ± 2.19	0.03	0.98	41.67 ± 1.86	40.00 ± 1.00	0.79	0.49
III_F	7.67 ± 0.67	7.67 ± 0.67	0.00	1.00	59.33 ± 0.67	60.67 ± 0.88	1.21	0.31
	10.00 ± 0.58	8.67 ± 0.67	1.53	0.22	59.00 ± 0.58	60.67 ± 0.67	1.89	0.16
		$B_V = 0\ \mu T$, $B_H = 50\ \mu T$, $B_{Hac} = 100\ \mu T$ peak-peak at 16 Hz						
#2038	5.67 ± 0.33	6.33 ± 0.33	1.41	0.25	57.00 ± 0.58	54.33 ± 0.88	2.53	0.90
	1.33 ± 0.88	1.00 ± 0.58	0.16	0.88	49.67 ± 1.86	49.33 ± 0.33	0.16	0.89
III_F	10.33 ± 0.88	10.67 ± 1.33	0.18	0.87	59.67 ± 0.33	57.33 ± 2.33	0.99	0.43
	10.00 ± 0.58	9.33 ± 0.88	0.65	0.56	66.33 ± 2.60	67.00 ± 1.53	0.21	0.85
		$B_V = 0\ \mu T$, $B_H = 60\ \mu T$, $B_{Hac} = 120\ \mu T$ peak-peak at 16 Hz						
#2038	1.00 ± 1.00	1.67 ± 1.20	0.52	0.64	39.67 ± 1.20	44.00 ± 1.15	2.60	0.08
	0.67 ± 0.67	1.00 ± 1.00	0.14	0.90	45.33 ± 0.88	51.33 ± 3.38	1.72	0.23
III_F	8.00 ± 1.00	8.33 ± 0.33	0.36	0.76	54.33 ± 0.67	52.67 ± 1.67	0.93	0.45
	11.33 ± 0.67	8.67 ± 1.76	1.44	0.29	49.00 ± 1.00	52.00 ± 2.00	1.34	0.31
		$B_V = 0\ \mu T$, $B_H = 70\ \mu T$, $B_{Hac} = 140\ \mu T$ peak-peak at 16 Hz						
#2038	2.33 ± 0.88	2.67 ± 0.88	0.25	0.82	41.67 ± 3.48	43.67 ± 0.88	0.57	0.63
	0.67 ± 0.33	1.67 ± 0.88	0.61	0.58	42.67 ± 0.67	42.33 ± 1.86	0.17	0.88
III_F	7.33 ± 0.88	7.33 ± 1.67	0.08	0.94	53.33 ± 1.45	55.00 ± 0.58	1.06	0.40
	5.33 ± 0.33	4.00 ± 1.15	1.14	0.37	60.33 ± 0.33	59.00 ± 0.58	2.00	0.14

Table VI

EMF test results (mean % motilities ± SE on agar plates, n = 3): amplitude response 3, t = t-value of arcsine square-root transformed motility data from exposed and sham-exposed 0.25 mM added Ca plates and exposed and sham-exposed 5 mM added Ca plates

Diatom strain	Exposed 0.25 m*M* Ca	Control 0.25 m*M* Ca	*t*	*P*	Exposed 5 m*M* Ca	Control 5 m*M* Ca	*t*	*P*
		B_V = 0 μT, B_H = ambient (~16.5 μT), B_{Hac} = 5 μT peak-peak at 16 Hz						
#2038	1.33 ± 1.33	1.33 ± 0.88	0.29	0.79	37.67 ± 0.88	37.33 ± 1.67	0.18	0.87
	0.67 ± 0.67	0.33 ± 0.33	0.24	0.83	41.00 ± 0.58	43.00 ± 1.15	1.55	0.26
III_F	9.00 ± 0.58	8.67 ± 0.33	0.48	0.66	53.67 ± 2.19	58.33 ± 1.20	1.87	0.16
	6.33 ± 1.45	6.33 ± 0.33	0.10	0.93	61.00 ± 0.58	60.67 ± 0.33	0.50	0.65
		B_V = 0 μT, B_H = ambient (~ 16.5 μT), B_{Hac} = 10 μT peak-peak at 16 Hz						
#2038	3.33 ± 1.76	3.67 ± 1.45	0.38	0.73	38.00 ± 0.58	37.67 ± 0.67	0.38	0.73
	0.33 ± 0.33	0.33 ± 0.33	0.00	1.00	35.33 ± 1.45	33.67 ± 2.19	0.64	0.57
III_F	3.67 ± 0.67	4.33 ± 0.88	0.60	0.59	61.67 ± 0.67	59.33 ± 0.88	2.11	0.13
	3.00 ± 1.15	2.67 ± 0.33	0.09	0.94	54.33 ± 0.67	55.00 ± 0.58	0.76	0.50
		B_V = 0 μT, B_H = ambient (~ 16.5 μT), B_{Hac} = 15 μT peak-peak at 16 Hz						
#2038	1.33 ± 0.33	2.00 ± 1.00	0.54	0.64	39.33 ± 0.88	40.67 ± 1.45	0.78	0.49
	7.00 ± 0.58	7.00 ± 1.00	0.04	0.97	42.33 ± 1.67	42.00 ± 1.00	0.17	0.88
III_F	4.67 ± 0.67	2.33 ± 0.86	2.08	0.13	57.33 ± 0.88	58.67 ± 0.88	1.07	0.36
	4.33 ± 0.88	2.67 ± 0.88	1.33	0.28	58.00 ± 0.58	58.33 ± 0.33	0.50	0.65
		B_V = 0 μT, B_H = ambient (~ 16.5 μT), B_{Hac} = 20 μT peak-peak at 16 Hz						
#2038	2.33 ± 0.88	5.00 ± 0.58	2.39	0.14	45.67 ± 2.03	40.67 ± 2.73	1.47	0.24
	3.67 ± 1.45	3.00 ± 1.53	0.32	0.77	50.33 ± 1.33	49.33 ± 0.67	0.67	0.57
III_F	9.33 ± 0.67	8.33 ± 0.88	0.92	0.43	56.00 ± 0.58	55.67 ± 0.33	0.50	0.65
	7.00 ± 1.00	6.00 ± 0.58	0.82	0.47	52.67 ± 0.88	53.33 ± 1.20	0.45	0.68
		B_V = 0 μT, B_H = ambient (~ 16.5 μT), B_{Hac} = 25 μT peak-peak at 16 Hz						
#2038	4.33 ± 2.03	4.67 ± 2.33	0.07	0.95	42.67 ± 1.45	37.00 ± 2.65	1.87	0.16
	4.67 ± 0.33	4.67 ± 0.33	0.00	1.00	47.00 ± 1.15	46.33 ± 1.33	0.38	0.73
III_F	8.33 ± 1.20	6.33 ± 1.33	1.14	0.34	49.33 ± 0.33	49.67 ± 0.88	0.35	0.76
	11.33 ± 0.67	12.00 ± 1.15	0.48	0.67	53.67 ± 0.88	53.67 ± 0.33	0.00	1.00
		B_V = 0 μT, B_H = ambient (~ 16.5 μT), B_{Hac} = 30 μT peak-peak at 16 Hz						
#2038	4.33 ± 0.33	4.67 ± 0.33	0.71	0.52	45.00 ± 2.00	44.67 ± 1.86	0.12	0.91
	1.00 ± 0.58	1.33 ± 0.88	0.16	0.88	42.00 ± 2.52	42.33 ± 1.20	0.12	0.91
III_F	10.67 ± 1.20	11.33 ± 1.20	0.39	0.72	52.33 ± 0.88	52.00 ± 1.53	0.19	0.86
	9.00 ± 0.58	10.33 ± 1.67	0.68	0.57	59.33 ± 0.67	60.33 ± 0.88	0.91	0.43
		B_V = 0 μT, B_H = ambient (~ 16.5 μT), B_{Hac} = 40 μT peak-peak at 16 Hz						
#2038	0.67 ± 0.67	1.33 ± 1.33	0.24	0.82	40.00 ± 0.58	44.33 ± 2.73	1.55	0.26
	4.00 ± 1.00	5.00 ± 1.00	0.71	0.52	47.33 ± 0.88	47.33 ± 0.33	0.00	1.00
III_F	3.00 ± 1.15	4.00 ± 1.00	0.73	0.52	52.33 ± 0.88	54.00 ± 1.53	0.95	0.41
	9.00 ± 0.58	9.33 ± 0.67	0.37	0.74	57.00 ± 1.00	56.67 ± 0.67	0.28	0.80
		B_V = 0 μT, B_H = ambient (~ 16.5 μT), B_{Hac} = 50 μT peak-peak at 16 Hz						
#2038	3.00 ± 1.15	2.67 ± 0.88	0.17	0.88	39.67 ± 0.67	40.67 ± 0.88	0.90	0.43
	2.33 ± 0.88	2.00 ± 1.15	0.50	0.67	44.67 ± 1.20	45.33 ± 0.88	0.45	0.68
III_F	10.67 ± 0.67	10.00 ± 1.15	0.53	0.67	51.33 ± 1.45	52.67 ± 1.33	0.68	0.55
	7.00 ± 1.15	7.33 ± 0.33	0.34	0.77	47.33 ± 0.88	47.00 ± 1.00	0.25	0.82

Table VI *(Continued)*

Diatom strain	Exposed 0.25 m*M* Ca	Control 0.25 m*M* Ca	*t*	*P*	Exposed 5 m*M* Ca	Control 5 m*M* Ca	*t*	*P*
		B_V = 0 μT, B_H = ambient (~ 16.5 μT), B_{Hac} = 60 μT peak-peak at 16 Hz						
#2038	2.00 ± 0.58	3.33 ± 1.45	0.74	0.54	44.00 ± 1.15	44.33 ± 0.88	0.23	0.83
	4.67 ± 1.86	3.67 ± 1.20	0.28	0.80	48.00 ± 1.00	48.00 ± 0.58	0.00	1.00
III_F	5.67 ± 0.67	5.33 ± 1.20	0.31	0.79	57.67 ± 1.33	57.00 ± 0.58	0.46	0.69
	7.67 ± 0.67	6.67 ± 0.33	1.36	0.27	51.00 ± 0.57	53.00 ± 1.53	1.23	0.35
		B_V = 0 μT, B_H = ambient (~ 16.5 μT), B_{Hac} = 70 μT peak-peak at 16 Hz						
#2038	2.00 ± 2.00	1.67 ± 1.20	0.18	0.87	42.67 ± 0.67	43.00 ± 0.58	0.38	0.73
	3.00 ± 1.15	2.00 ± 1.53	0.78	0.49	50.33 ± 0.88	49.67 ± 0.88	0.53	0.62
III_F	9.00 ± 0.58	8.67 ± 0.33	0.48	0.66	58.33 ± 1.20	57.00 ± 0.58	1.00	0.42
	9.67 ± 0.33	8.00 ± 0.58	2.45	0.09	52.67 ± 0.88	53.67 ± 0.88	0.80	0.47
		B_V = 0 μT, B_H = ambient (~ 16.5 μT), B_{Hac} = 80 μT peak-peak at 16 Hz						
#2038	0.33 ± 0.33	0.33 ± 0.33	0.00	1.00	41.67 ± 1.20	39.00 ± 0.58	2.01	0.18
	1.67 ± 1.20	0.67 ± 0.67	0.71	0.53	41.00 ± 0.58	40.67 ± 0.67	0.38	0.73
III_F	8.00 ± 0.58	7.33 ± 0.33	0.99	0.39	56.00 ± 1.00	56.00 ± 1.15	0.00	1.00
	10.00 ± 0.58	8.33 ± 0.33	2.54	0.09	56.67 ± 0.33	58.00 ± 0.58	2.00	0.14
		B_V = 0 μT, B_H = ambient (~ 16.5 μT), B_{Hac} = 100 μT peak-peak at 16 Hz						
#2038	2.67 ± 0.88	2.33 ± 1.20	0.48	0.68	37.67 ± 0.88	38.67 ± 0.88	0.80	0.48
	4.33 ± 2.19	0.67 ± 0.67	1.27	0.29	42.67 ± 0.33	41.33 ± 0.88	1.42	0.29
III_F	12.67 ± 0.33	11.00 ± 0.58	2.47	0.09	60.67 ± 0.67	60.00 ± 0.58	0.76	0.50
	12.00 ± 1.15	11.00 ± 1.53	0.55	0.62	48.67 ± 0.88	48.00 ± 0.58	0.63	0.57
		B_V = 0 μT, B_H = ambient (~ 16.5 μT), B_{Hac} = 120 μT peak-peak at 16 Hz						
#2038	1.67 ± 0.67	2.00 ± 0.58	0.43	0.70	33.67 ± 0.88	38.00 ± 1.15	0.46	0.68
	4.67 ± 0.88	3.00 ± 0.58	1.56	0.22	42.33 ± 1.20	42.33 ± 0.88	0.00	1.00
III_F	8.00 ± 1.53	6.33 ± 0.88	0.89	0.44	46.67 ± 0.33	46.67 ± 0.33	0.00	1.00
	7.33 ± 0.67	9.00 ± 0.58	1.86	0.16	59.00 ± 0.58	60.33 ± 0.33	2.00	0.14
		B_V = 0 μT, B_H = ambient (~ 16.5 μT), B_{Hac} = 140 μT peak-peak at 16 Hz						
#2038	1.33 ± 0.88	1.00 ± 1.00	0.43	0.69	39.00 ± 1.15	39.67 ± 1.20	0.40	0.72
	4.67 ± 1.33	3.67 ± 1.45	0.52	0.64	43.33 ± 0.67	42.00 ± 0.58	1.51	0.23
III_F	7.67 ± 0.67	6.67 ± 1.76	0.62	0.60	55.00 ± 1.53	56.00 ± 0.58	0.61	0.60
	8.67 ± 0.33	8.67 ± 0.33	0.00	1.00	57.67 ± 0.67	57.00 ± 0.58	0.76	0.50

Table VII

EMF test results (mean % motilities ± SE on agar plates, n = 3); amplitude response 4, t = t-value of arcsine square-root transformed motility data from exposed and sham-exposed 0.25 mM added Ca plates and exposed and sham-exposed 5 mM added Ca plates

Diatom strain	Exposed 0.25 m*M* Ca	Control 0.25 m*M* Ca	*t*	*P*	Exposed 5 m*M* Ca	Control 5 m*M* Ca	*t*	*P*
			$B_V = 0\ \mu T$, $B_H = 0\ \mu T$, $B_{Hac} = 5\ \mu T$ peak-peak at 16 Hz					
#2038	1.00 ± 1.00	1.67 ± 1.20	0.52	0.64	35.33 ± 1.76	38.33 ± 0.88	1.52	0.27
	1.67 ± 0.88	2.00 ± 0.58	0.58	0.62	46.00 ± 1.00	43.67 ± 2.73	0.81	0.50
III_F	5.33 ± 0.88	6.33 ± 0.67	0.92	0.42	59.67 ± 0.88	60.33 ± 0.33	0.71	0.55
	7.00 ± 1.00	6.67 ± 1.20	0.24	0.82	54.67 ± 2.03	57.33 ± 0.88	1.21	0.35
			$B_V = 0\ \mu T$, $B_H = 0\ \mu T$, $B_{Hac} = 10\ \mu T$ peak-peak at 16 Hz					
#2038	2.00 ± 0.58	2.00 ± 0.58	0.00	1.00	41.33 ± 0.88	42.33 ± 1.20	0.67	0.55
	3.67 ± 0.33	3.00 ± 0.58	1.02	0.38	47.67 ± 0.88	47.67 ± 0.67	0.00	1.00
III_F	6.33 ± 0.88	8.00 ± 0.58	1.59	0.21	53.33 ± 0.88	52.67 ± 0.67	0.60	0.59
	6.67 ± 0.33	6.67 ± 0.33	0.00	1.00	52.67 ± 1.45	54.67 ± 1.86	0.85	0.46
			$B_V = 0\ \mu T$, $B_H = 0\ \mu T$, $B_{Hac} = 15\ \mu T$ peak-peak at 16 Hz					
#2038	3.00 ± 0.58	3.33 ± 0.88	0.27	0.80	47.33 ± 0.88	47.00 ± 2.00	0.15	0.89
	4.00 ± 0.58	5.66 ± 0.67	1.92	0.15	48.67 ± 0.88	47.33 ± 0.33	1.41	0.29
III_F	2.33 ± 0.88	3.67 ± 0.33	1.45	0.28	52.33 ± 2.03	54.00 ± 0.58	0.79	0.51
	7.33 ± 0.33	6.00 ± 0.58	1.98	0.14	63.33 ± 1.45	63.33 ± 0.67	0.01	1.00
			$B_V = 0\ \mu T$, $B_H = 0\ \mu T$, $B_{Hac} = 20\ \mu T$ peak-peak at 16 Hz					
#2038	2.67 ± 0.33	1.00 ± 1.00	1.78	0.22	48.33 ± 1.20	48.00 ± 1.00	0.21	0.85
	1.00 ± 0.58	0.67 ± 0.67	0.53	0.63	42.67 ± 0.88	41.00 ± 1.15	1.15	0.33
III_F	9.67 ± 0.33	10.33 ± 0.88	0.69	0.56	62.67 ± 1.76	62.67 ± 1.76	0.00	1.00
	8.33 ± 0.33	8.67 ± 0.67	0.43	0.71	58.33 ± 0.88	57.00 ± 0.58	1.26	0.30
			$B_V = 0\ \mu T$, $B_H = 0\ \mu T$, $B_{Hac} = 25\ \mu T$ peak-peak at 16 Hz					
#2038	2.33 ± 0.88	2.67 ± 0.67	0.39	0.72	47.33 ± 0.33	46.00 ± 0.58	2.00	0.14
	4.33 ± 0.88	4.67 ± 1.33	0.11	0.92	46.67 ± 0.67	43.67 ± 1.20	2.18	0.12
III_F	7.33 ± 0.33	7.33 ± 0.88	0.04	0.97	51.33 ± 0.88	53.33 ± 0.33	2.12	0.17
	8.00 ± 0.58	8.33 ± 0.67	0.37	0.74	61.33 ± 0.88	60.67 ± 0.67	0.60	0.59
			$B_V = 0\ \mu T$, $B_H = 0\ \mu T$, $B_{Hac} = 30\ \mu T$ peak-peak at 16 Hz					
#2038	4.33 ± 1.33	4.00 ± 0.58	0.14	0.90	46.67 ± 0.33	45.00 ± 0.58	2.50	0.09
	3.67 ± 0.33	4.33 ± 0.88	0.66	0.58	42.33 ± 0.67	41.67 ± 0.33	0.89	0.47
III_F	10.33 ± 0.33	12.00 ± 0.58	2.53	0.09	59.33 ± 0.67	58.33 ± 0.88	0.90	0.43
	10.00 ± 1.53	11.00 ± 1.00	0.58	0.60	50.00 ± 0.58	53.00 ± 1.15	2.32	0.15
			$B_V = 0\ \mu T$, $B_H = 0\ \mu T$, $B_{Hac} = 40\ \mu T$ peak-peak at 16 Hz					
#2038	3.00 ± 1.53	5.00 ± 1.00	1.19	0.32	46.33 ± 0.33	44.67 ± 1.20	1.34	0.31
	4.00 ± 1.15	3.33 ± 0.67	0.42	0.70	45.67 ± 2.03	47.00 ± 1.00	0.59	0.61
III_F	8.67 ± 0.33	8.33 ± 0.67	0.46	0.69	51.33 ± 0.67	54.00 ± 1.15	2.00	0.14
	6.00 ± 0.58	6.00 ± 0.58	0.00	1.00	52.00 ± 1.00	51.33 ± 1.33	0.40	0.72
			$B_V = 0\ \mu T$, $B_H = 0\ \mu T$, $B_{Hac} = 50\ \mu T$ peak-peak at 16 Hz					
#2038	5.33 ± 1.20	3.67 ± 0.67	1.16	0.33	49.67 ± 0.88	48.00 ± 0.58	1.58	0.21
	4.33 ± 0.33	4.00 ± 0.58	0.54	0.63	40.67 ± 0.88	42.67 ± 0.33	2.12	0.17
III_F	5.33 ± 1.33	5.67 ± 1.20	0.21	0.85	56.00 ± 2.52	56.33 ± 0.88	0.12	0.91
	5.00 ± 1.00	5.67 ± 0.33	0.67	0.57	50.00 ± 1.00	49.33 ± 0.67	0.55	0.62

Table VII *(Continued)*

Diatom strain	Exposed 0.25 m*M* Ca	Control 0.25 m*M* Ca	*t*	*P*	Exposed 5 m*M* Ca	Control 5 m*M* Ca	*t*	*P*
			$B_V = 0\ \mu T$, $B_H = 0\ \mu T$, $B_{Hac} = 60\ \mu T$ peak-peak at 16 Hz					
#2038	5.67 ± 0.37	6.33 ± 0.33	0.94	0.45	47.33 ± 0.88	48.00 ± 1.00	0.50	0.65
	6.33 ± 0.33	6.00 ± 0.58	0.52	0.64	43.33 ± 0.88	45.67 ± 1.20	1.57	0.22
III_F	7.67 ± 0.67	8.00 ± 0.58	0.39	0.72	51.33 ± 0.67	53.00 ± 1.15	1.25	0.30
	10.00 ± 0.58	9.33 ± 0.67	0.75	0.51	58.00 ± 0.58	56.33 ± 0.88	1.58	0.21
			$B_V = 0\ \mu T$, $B_H = 0\ \mu T$, $B_{Hac} = 70\ \mu T$ peak-peak at 16 Hz					
#2038	2.67 ± 0.67	3.67 ± 0.33	1.40	0.30	49.00 ± 1.15	50.33 ± 2.40	0.50	0.67
	3.00 ± 0.58	2.67 ± 0.88	0.40	0.72	47.00 ± 1.15	49.00 ± 1.15	1.22	0.31
III_F	7.00 ± 0.58	7.67 ± 0.67	0.76	0.50	61.00 ± 0.58	58.33 ± 1.76	1.44	0.29
	9.67 ± 0.88	9.33 ± 0.67	0.28	0.79	62.33 ± 1.86	60.00 ± 1.15	1.07	0.36
			$B_V = 0\ \mu T$, $B_H = 0\ \mu T$, $B_{Hac} = 80\ \mu T$ peak-peak at 16 Hz					
#2038	1.00 ± 0.58	0.67 ± 0.67	0.53	0.63	43.33 ± 1.45	41.67 ± 0.88	0.98	0.40
	3.00 ± 1.73	5.00 ± 0.58	1.13	0.38	45.67 ± 1.67	49.00 ± 1.73	1.39	0.26
III_F	10.33 ± 0.88	10.67 ± 0.67	0.32	0.77	58.00 ± 0.58	58.67 ± 0.88	0.63	0.57
	8.67 ± 0.33	9.67 ± 1.20	0.78	0.52	53.67 ± 1.76	57.00 ± 1.15	1.68	0.21
			$B_V = 0\ \mu T$, $B_H = 0\ \mu T$, $B_{Hac} = 100\ \mu T$ peak-peak at 16 Hz					
#2038	1.67 ± 0.33	1.33 ± 0.33	0.71	0.52	45.67 ± 2.03	45.33 ± 1.86	0.12	0.91
	2.33 ± 0.88	2.00 ± 0.58	0.25	0.82	41.00 ± 1.15	41.33 ± 1.76	0.15	0.89
III_F	9.33 ± 0.33	10.33 ± 0.33	2.14	0.12	54.33 ± 1.20	53.00 ± 0.58	1.00	0.42
	11.67 ± 0.88	13.00 ± 0.58	1.26	0.30	54.67 ± 1.76	51.00 ± 1.53	1.57	0.21
			$B_V = 0\ \mu T$, $B_H = 0\ \mu T$, $B_{Hac} = 120\ \mu T$ peak-peak at 16 Hz					
#2038	3.33 ± 0.67	2.67 ± 0.33	0.81	0.48	46.33 ± 1.76	46.33 ± 0.67	0.00	1.00
	3.00 ± 0.58	3.33 ± 0.33	0.55	0.62	47.33 ± 1.76	46.67 ± 1.20	0.31	0.78
III_F	7.33 ± 0.33	7.33 ± 0.88	0.04	0.97	57.67 ± 1.33	57.67 ± 1.20	0.00	1.00
	9.33 ± 0.88	9.33 ± 0.33	0.03	0.98	52.00 ± 0.58	50.67 ± 1.20	1.00	0.42
			$B_V = 0\ \mu T$, $B_H = 0\ \mu T$, $B_{Hac} = 140\ \mu T$ peak-peak at 16 Hz					
#2038	2.67 ± 0.33	3.00 ± 0.58	0.45	0.68	47.33 ± 0.88	45.00 ± 1.00	1.75	0.18
	5.67 ± 0.33	4.33 ± 0.88	1.44	0.29	44.00 ± 1.15	45.67 ± 1.20	1.00	0.39
III_F	7.67 ± 0.88	9.00 ± 0.58	1.26	0.30	49.67 ± 1.45	49.33 ± 0.88	0.20	0.86
	7.33 ± 0.88	8.33 ± 0.67	0.92	0.43	51.00 ± 1.00	53.33 ± 1.20	1.49	0.23

Table VIII

EMF test results (mean % motilities ± SE on agar plates, n = 3) at (a) ion cyclotron resonance conditions for the ambient horizontal field at Plymouth, an even harmonic and at 16 Hz; and (b) at switched field axes at ion cyclotron resonance conditions. t = t-*value of arcsine square-root transformed motility data from exposed and sham-exposed 0.25 mM added Ca plates*

Diatom strain	Exposed 0.25 m*M* Ca	Control 0.25 m*M* Ca	*t*	*P*	Control 5 m*M* Ca
(a)					
$B_V = 0\ \mu T$, $B_H = (B_{Hac})/2$ = ambient (16.5 μT) at 16 Hz					
#2038	1.00 ± 0.58	1.67 ± 0.88	0.36	0.74	47
	0.67 ± 0.67	2.00 ± 0.15	0.88	0.44	42
III_F	6.00 ± 0.58	7.00 ± 0.58	1.23	0.31	56
	9.00 ± 1.53	8.33 ± 0.67	0.36	0.75	59
$B_V = 0\ \mu T$, $B_H = (B_{Hac})/2$ = ambient (16.5 μT) at 12.5 Hz					
#2038	1.67 ± 0.67	2.33 ± 0.88	0.60	0.59	46
	1.67 ± 0.33	1.67 ± 1.20	0.46	0.69	49
III_F	8.33 ± 0.33	7.00 ± 0.58	1.98	0.14	59
	6.00 ± 0.58	7.67 ± 0.67	1.91	0.15	61
$B_V = 0\ \mu T$, $B_H = (B_{Hac})/2$ = ambient (16.5 μT) at 6.25 Hz					
#2038	4.67 ± 0.33	5.00 ± 0.58	0.47	0.67	51
	4.00 ± 0.58	3.00 ± 0.58	1.23	0.31	43
III_F	7.00 ± 1.00	6.33 ± 0.33	0.56	0.63	55
	5.33 ± 0.33	5.67 ± 1.33	0.12	0.92	60
(b)					
$B_V = 0\ \mu T$, $B_V = 20.9\ \mu T$; $B_{Vac} = 41.8\ \mu T$ at 16 Hz					
#2038	1.33 ± 0.88	1.00 ± 1.00	0.43	0.69	49
	1.67 ± 1.20	1.67 ± 0.88	0.06	0.96	49
III_F	5.67 ± 0.33	6.67 ± 0.33	2.09	0.13	56
	6.00 ± 0.58	7.00 ± 0.58	1.23	0.31	58

Table IX

Effect of cell density on the motility of diatom strain #2038 exposed at ion cyclotron resonance EMFs for 1 h on 5 mM added Ca plates (n = 2 in each case)

Cell density (cells ml^{-1})	Diatom motility (mean % ± SE)	
	Exposed	Control
5×10^4	40.5 ± 1.5	41.5 ± 1.5
1×10^5	41.5 ± 1.5	43.5 ± 0.5
1.5×10^5	43.0 ± 2.0	40.5 ± 1.5
1×10^6	41.0 ± 3.0	42.5 ± 0.5
2×10^6	45.0 ± 1.0	41.5 ± 0.5

Two-factor analysis of variance table (performed on arcsine-square root transformed data)

Source of variation	d.f.	SS	MS	*F*	*P*
EMF on/off	1	0.000044	0.000044	0.090	>0.25
Cell density	4	0.001202	0.000300	0.612	>0.25
Interaction	4	0.002596	0.000649	1.325	>0.25
Error	10	0.004896	0.000490		
Total	19	0.008738			

Table X

Effect of position in cell cycle on the motility of diatom strain III_F exposed at ion cyclotron resonance for 1 h (mean % motilities ± SE on agar plates. n = 3). t = t-*value of arcsine square-root transformed motility data from exposed and sham-exposed 0.25 mM added Ca plates*

Time of inoculation (h after light commenced at 0700)	Culture age (h)	Exposed 0.25 m*M* Ca	Control 0.25 m*M* Ca	*t*	*P*	Control 5 m*M* Ca
0	101	7.00 ± 0.58	8.00 ± 1.00	0.82	0.47	56
2	99	8.33 ± 0.88	9.00 ± 0.58	0.66	0.56	59
4	97	6.67 ± 0.67	6.33 ± 0.88	0.33	0.76	51
6	95	7.00 ± 1.15	5.67 ± 0.67	0.98	0.40	56
8	93	9.33 ± 0.67	7.67 ± 0.88	1.48	0.23	54
10	91	6.67 ± 0.88	7.67 ± 1.33	0.57	0.61	59
12	89	6.67 ± 1.20	9.33 ± 1.20	1.57	0.21	60
14	87	8.33 ± 1.33	8.33 ± 0.88	0.03	0.98	53
16	85	9.00 ± 0.58	7.67 ± 1.33	0.92	0.45	58

Table XI

Effect of EMFs at frequencies from 1 to 24 Hz (B_V = 0 μT, B_H = 20.9 μT, B_{Hac} = 41.8 μT) on the distance moved by diatoms of strain III_F exposed for 1 h on 0.5 mM added Ca plates (distance data pooled from triplicate plates; n = 30 in each case)

EMF frequency (Hz)	Mean distance moved by diatoms ± SE (μm)	
	Exposed	Control
1	46.9 ± 9.3	46.4 ± 10.1
2	28.7 ± 4.3	26.7 ± 4.3
3	33.5 ± 4.6	34.9 ± 5.4
4	25.0 ± 3.2	35.0 ± 5.9
5	35.6 ± 4.4	33.7 ± 4.8
6	38.2 ± 6.9	27.6 ± 3.8
7	34.0 ± 5.4	37.0 ± 7.1
8	37.5 ± 5.6	36.8 ± 7.3
9	35.3 ± 5.7	33.9 ± 5.8
10	37.8 ± 4.8	38.7 ± 6.6
11	46.2 ± 7.8	36.8 ± 6.1
12	35.0 ± 7.8	34.3 ± 6.7
13	38.2 ± 8.4	33.8 ± 5.1
14	35.3 ± 5.3	30.3 ± 4.9
15	35.1 ± 4.7	35.4 ± 6.9
16	36.2 ± 5.5	39.1 ± 6.5
17	37.9 ± 5.1	36.9 ± 6.3
18	35.2 ± 4.1	36.0 ± 6.2
19	41.4 ± 6.3	38.9 ± 6.1
20	32.9 ± 4.3	40.7 ± 5.8
21	33.4 ± 4.5	39.3 ± 5.9
22	39.4 ± 6.8	36.2 ± 5.3
23	37.4 ± 5.1	36.6 ± 5.2
24	38.5 ± 5.0	32.3 ± 4.3

Two-factor analysis of variance table

Source of variation	d.f.	SS	MS	*F*	*P*
EMF on/off	1	424	424	0.40	>0.5
Frequency	23	17930	780	0.74	>0.5
Interaction	23	7490	326	0.31	>0.5
Error	1392	1458958	1048		
Total	1439	1484801			

Table XII

χ^2 values of effect of EMFs at frequencies from 1 to 24 Hz (B_V = 0 μT, B_H = 20.9 μT, B_{Hac} = 41.8 μT) on the initial direction of movement (into one of twelve 30° sectors) of diatoms of strain III_F exposed for 1 h on 0.5 mM added Ca plates (direction data pooled from triplicate plates; n = 300 in each case)

EMF frequency (Hz)	Exposed χ^2 value	*P*	Control χ^2 value	*P*
1	17.83	>0.05	9.43	>0.5
2	10.39	>0.5	15.68	>0.5
3	4.64	>0.9	17.36	>0.05
4	7.28	>0.5	15.92	>0.1
5	6.80	>0.5	12.56	>0.1
6	2.24	>0.99	9.92	>0.5
7	14.96	>0.1	11.84	>0.1
8	2.24	>0.99	5.84	>0.5
9	8.00	>0.5	3.68	>0.9
10	5.12	>0.9	12.32	>0.1
11	14.96	>0.1	3.20	>0.9
12	4.64	>0.9	8.96	>0.5
13	0.80	>0.99	2.00	>0.99
14	0.80	>0.99	9.92	>0.5
15	0.80	>0.99	4.88	>0.9
16	7.52	>0.5	7.76	>0.5
17	8.00	>0.5	5.36	>0.9
18	7.76	>0.5	5.36	>0.9
19	4.16	>0.9	5.84	>0.5
20	3.20	>0.9	1.52	>0.99
21	6.80	>0.5	2.24	>0.99
22	8.48	>0.5	9.20	>0.5
23	4.16	>0.9	7.04	>0.5
24	5.36	>0.9	11.36	>0.1

Literature Cited

Aarholt, E., E. A. Flinn, and C. W. Smith. 1981. Magnetic fields affect the lac operon system. *Phys. Med. Bull.* **21:** 606–610.

Alberts, B., D. Bray, and J. Lewis. 1994. *Molecular Biology of the Cell.* Garland Publishing, New York.

Blackman, C. F., S. G. Benane, J. R. Rabinowitz, D. E. House, and W. T. Joines. 1985. A role for the magnetic field in the radiation-induced efflux of calcium ions from brain tissue in vitro. *Bioelectromagnetics* **6:** 327–337.

Blackman, C. F., D. E. House, S. G. Benane, W. T. Joines, and R. J. Spiegel. 1988. Effect of ambient levels of power-line-frequency electric fields on a developing vertebrate. *Bioelectromagnetics* **9:** 129–140.

Blackman, C. F., S. G. Benane, D. E. House, and D. J. Elliott. 1990. Importance of alignment between local DC magnetic field and an oscillating magnetic field in responses of brain tissue in vitro and in vivo. *Bioelectromagnetics* **11:** 159–167.

Carson, J. J. L., F. S. Prato, D. J. Drost, L. D. Diesbourg, and S. J. Dixon. 1990. Time-varying magnetic fields increase cytosolic free Ca^{2+} in HL-60 cells. *Am. J. Physiol.* **28:** C687–C692.

Cooksey, B., and K. E. Cooksey. 1980. Calcium is necessary for motility in the diatom *Amphora coffeaeformis. Plant Physiol.* **65:** 129–131.

Edgar, L. A. 1980. Mucilage secretions of moving diatoms. *Protoplasma* **118:** 44–48.

Edmonds, D. T. 1993. Larmor precession as a mechanism for the detection of static and alternating magnetic fields. *Bioelectrochem. Bioenerg.* **30:** 3–12.

Fitzsimmons, R. J., J. T. Ryaby, F. P. Magee, and D. J. Baylink. 1994. Combined magnetic fields increased net calcium flux in bone cells. *Calcif. Tissue Int.* **55:** 376–380.

Gallagher, J. C. 1980. Population genetics of *Skeletonema costatum* (Bacillariophyceae) in Narragansett bay. *J. Phycol.* **16:** 464–474.

Gallagher, J. C. 1986. Population genetics of microalgae. *Nova Hedwigia* **83:** 6–14.

Gallagher, J. C. 1987. Genetic variation in oil-producing microalgae. Pp. 321–337 in *Proceedings of the Aquatic Species Program Annual Review Meeting 1986.* Solar Energy Research Institute, Golden, Colorado.

Gamaley, I., K. Augsten, and H. Berg. 1995. Electrostimulation of macrophage NADPH oxidase by modulated high-frequency electromagnetic fields. *Bioelectrochem. Bioenerg.* **38:** 415–418.

Goldberg, R. B., and W. A. Creasey. 1991. A review of cancer in-

duction by extremely low frequency electromagnetic fields. Is there a plausible mechanism? *Med. Hypotheses* **35:** 265–274.

Halle, B. 1988. On the cyclotron resonance mechanism for magnetic field effects on transmembrane ion conductivity. *Bioelectromagnetics* **9:** 381–385.

Kirschvink, J. L., A. Kobayashi-Kirschvink, and B. J. Woodford. 1992. Magnetite biomineralization in the human brain. *Proc. Natl. Acad. Sci. USA* **89:** 7683–7687.

Leal, J., M. A. Trillo, A. Ubeda, V. Abraira, K. Shamsaifar, and L. Chacon. 1986. Magnetic environment and embryonic development: a role for the earth's field. *IRCS Med. Sci.* **14:** 1145–1146.

Lednev, V. V. 1991. Possible mechanism for the influence of weak electromagnetic fields on biological systems. *Bioelectromagnetics* **12:** 71–75.

Liboff, A. R. 1985. Cyclotron resonance in membrane transport. Pp. 281–296 in *Interactions Between Electromagnetic Fields and Cells*, A. Chiabrera, C. Nicolini, and H. P. Schwan, eds. Plenum Press, New York.

Male, J. 1992. Biological effects of magnetic fields: a possible mechanism? *Biologist* **39:** 87–89.

McLeod, B. R., A. A. Pilla, and M. W. Sampsel. 1983. Electromagnetic fields induced by helmholtz aiding coils inside saline-filled boundaries. *Bioelectromagnetics* **4:** 357–370.

McLeod, B. R., S. D. Smith, K. E. Cooksey, and A. R. Liboff. 1987a. Ion cyclotron resonance frequencies enhance Ca^{++}-dependent motility in diatoms. *J. Bioelectr.* **6:** 1–12.

McLeod, B. R., S. D. Smith, and A. R. Liboff. 1987b. Calcium and potassium cyclotron resonance curves and harmonics in diatoms (*A. coffeaeformis*). *J. Bioelectr.* **6:** 153–168.

McLeod, B. R., A. R. Liboff, and S. D. Smith. 1992. Biological systems in transition: sensitivity to extremely low-frequency fields. *Electro-Magnetobiol.* **11:** 29–42.

Medlin, L. K., G. L. A. Barker, L. Campbell, J. C. Green, P. K. Hayes, D. Marie, S. Wrieden, and D. Vaulot. 1996. Genetic characterisation of *Emiliania huxleyi* (Haptophyta). *J. Mar. Sys.* **9:** 13–31.

Michaelson, S. M. 1985. Perspective on windows and calcium efflux studies. Pp. 499–519 in *Interactions Between Electromagnetic Fields and Cells*, A. Chiabrera, C. Nicolini, and H. P. Schwan, eds. Plenum Press, New York.

Paasche, E., S. Brubak, S. Skattebøl, J. R. Young, and J. C. Green. 1996. Growth and calcification in the coccolithophorid *Emiliania huxleyi* (Haptophyceae) at low salinities. *Phycologia* **35:** 394–403.

Parkinson, W. C., and G. L. Sulik. 1992. Diatom response to extremely low-frequency magnetic fields. *Radiat. Res.* **130:** 319–330.

Prasad, A. V., M. W. Miller, C. Cox, E. L. Carstensen, H. Hoops, and A. A. Brayman. 1994. A test of the influence of cyclotron resonance exposures on diatom motility. *Health Phys.* **66:** 305–312.

Provasoli, L., J. J. A. McLaughlin, and M. R. Droop. 1957. The development of artificial media for marine algae. *Arch. Mikrobiol.* **25:** 392–428.

Reese, J. A., M. E. Frazier, J. E. Morris, R. L. Buschhorn, and D. L. Miller. 1991. Evaluation of changes in diatom mobility after exposure to 16-Hz electromagnetic fields. *Bioelectromagnetics* **12:** 21–25.

Round, F. E., R. M. Crawford, and D. G. Mann. 1990. *The Diatoms.* Cambridge University Press, Cambridge.

Saalman, E., S. Galt., Y. Hamnerius, and B. Norden. 1992. Diatom motility: replication study in search of cyclotron resonance effects. Pp. 280–292 in *Interaction Mechanisms of Low-level Electromagnetic Fields in Living Systems*, B. Norden and C. Ramel, eds. Oxford University Press, Oxford.

Smith, S. D., B. R. McLeod, A. R. Liboff, and K. E. Cooksey. 1987a. Calcium cyclotron resonance and diatom mobility. *Bioelectromagnetics* **8:** 215–227.

Smith, S. D., B. R. McLeod, A. R. Liboff, and K. E. Cooksey. 1987b. Calcium cyclotron resonance and diatom motility. *Stud. Biophys.* **119:** 131–136.

Starr, R. C., and J. A. Zeikus. 1987. UTEX—the culture collection of algae at the University of Texas at Austin. *J. Phycol.* **23**(suppl.): 1–42.

Stefano, G. B., M. B. Teoh, A. Grant, C. Reid, H. Teoh, and T. K. Hughes. 1994. Electric field exposure activates immunocytes: evidence for calcium dependency. *Electro-Magnetobiol.* **13:** 123–136.

Stein, J. R. 1973. *Handbook of Phycological Methods.* Cambridge University Press, Cambridge.

Wood, A. M., and T. Leatham. 1992. The species concept in phytoplankton ecology. *J. Phycol.* **28:** 723–729.

Reference: *Biol. Bull.* **194:** 224–230. (April, 1998)

Minerals of the Radular Apparatus of *Falcidens* sp. (Caudofoveata) and the Evolutionary Implications for the Phylum Mollusca

RENATO CRUZ[1,*], ULYSSES LINS[2], AND MARCOS FARINA[3,†]

[1] *Instituto de Biofísica Carlos Chagas Filho, Universidade Federal do Rio de Janeiro, Cidade Universitária, 21949-900, Rio de Janeiro, RJ, Brasil;* [2] *Instituto de Microbiologia Professor Paulo de Góes, Setor de Microscopia Eletrônica e Departamento de Microbiologia Geral, Universidade Federal do Rio de Janeiro, Cidade Universitária, 21941-590, Rio de Janeiro, RJ, Brasil; and* [3] *Departamento de Anatomia, Centro de Ciências da Saúde, Universidade Federal do Rio de Janeiro, 21941-590, Rio de Janeiro, RJ, Brasil*

Abstract. Minerals have been found in the radular teeth of molluscs from the classes Caudofoveata, Polyplacophora, Monoplacophora, and Gastropoda (Patellogastropoda: Acmaeidae, Patellidae). Here we report the discovery of amorphous iron oxide and hydroxyapatite in the highly modified radular apparatus of *Falcidens* sp. (Caudofoveata). The mineralization process in *Falcidens* sp. is unique: the components of the radular apparatus, unlike those of other molluscs, are not renewed during the animal's lifetime. We propose that the presence of mineralized teeth among the molluscs is not necessarily connected to their manner of obtaining food and suggest that the molluscan common ancestor had mineralized teeth.

Introduction

The radula is one of the most characteristic organs of the phylum Mollusca, lacking only in the class Bivalvia. The function of the radula is to obtain food. The basic pattern of most radulae consists of several to numerous transverse rows of radular teeth with bilateral symmetry relative to the main axis, supported by a thin radular membrane. The radula lies within the radular sac, an invagination of the buccal cavity, where it is continuously produced at the proximal end (Brusca and Brusca, 1990). In some molluscan groups, mineralized compounds are associated with the organic matrix of the teeth. Best known among the groups that have mineralized teeth are the limpets (Gastropoda: Acmaeidae, Patellidae) and chitons (Polyplacophora). In chitons, the second lateral tooth is mineralized primarily by magnetite (Fe_3O_4) (Lowenstam, 1962a). However, ferrihydrite ($5\ Fe_2O_3.9\ H_2O$), lepidocrocite (γ-FeOOH), maghemite (γ-Fe_2O_3), goethite (α-FeOOH), and apatite (crystalline calcium phosphate) also occur (Lowenstam, 1967; Towe and Lowenstam, 1967; Kim *et al.*, 1989; St. Pierre *et al.*, 1992). In limpets, the radular teeth are impregnated only with goethite and opal ($SiO_2.nH_2O$) (Lowenstam, 1962b, 1971).

The Caudofoveata (=Aplacophora; Chaetodermomorpha) is a class of marine worm-like molluscs. Until recently the class had received little attention (Scheltema *et al.*, 1994; Ivanov, 1996) and the only known mineralized structures were the spicules that cover the body. These spicules present different morphologies in different regions of the body surface and are composed of the crystalline calcium carbonate polimorph aragonite ($CaCO_3$). On the other hand, precipitates rich in aluminum, calcium, phosphorus, and iron have been reported in the teeth of *Chevroderma turnerae* (Prochaetodermatidae) (Tillier and Cuif, 1986). In its jaws, sodium, magnesium, aluminum, phosphorus, calcium, and small quantities of iron have been detected (Tillier and Cuif, 1986). Another class

Received 5 March 1997; accepted 22 December 1997.

* Present address: Universidade Santa Úrsula, Rua Jornalista Orlando Dantas 59, 22231-010, Rio de Janeiro, RJ, Brasil.

† To whom correspondence should be addressed. E-mail: mfarina@ibccf.biof.ufrj.br

only recently studied which has mineralized compounds in its teeth is the Monoplacophora (= Tryblidiida) (iron oxide, Lindberg, 1986; Haszprunar, 1988; McLean, 1990). These results suggest that the more primitive molluscan classes (*e.g.*, Caudofoveata and Monoplacophora) should be investigated as potential models for the study of biomineralization. In the present study, we report the discovery, through analytical electron microscopy, of mineralized compounds in the radular apparatus of *Falcidens* sp. (Caudofoveata:Chaetodermatidae), and we propose some interpretations of these results from an evolutionary perspective.

Materials and Methods

The specimens of *Falcidens* sp. (Rios, 1994) were collected in 1986 on the continental slope (22° 55′ S, 42° 00′ W and 23° 05′ S, 42° 20′ W) off Rio de Janeiro State, Brazil, at depths between 25 and 97 m. They were immediately fixed in buffered formaldehyde at 4% for 24 h and stored in 70% ethanol.

Scanning electron microscopy (SEM)

Radular apparatuses were placed under a light microscope and dissected. They were then cleaned in 1 N NaOH for 2 h at 70°C, rinsed in distilled water, dehydrated in an ethanol series, critical-point dried, and gold sputtered. Finally, they were examined with a Zeiss DSM 940.

Transmission electron microscopy (TEM)

Radular apparatuses were viewed under a light microscope and extracted, then embedded in Spurr resin. Ultrathin (≈ 90–100 nm) sections were mounted on copper grids and examined without any stain. Transmission electron micrographs and electron spectroscopic diffraction (ESD) patterns (Reimer *et al.*, 1990; Barckhauss *et al.*, 1991) were obtained with an energy filtering electron microscope (Zeiss CEM 902) operating at 80 kV.

Energy dispersive X-ray analysis (EDXA)

Unstained, ultrathin sections were examined in the TEM mode of a Zeiss EM 912 analytical electron microscope, operating at 100 kV and equipped with a silicon/lithium detector (Oxford). Selected areas down to 0.1 μm were analyzed for 100 s.

Electron spectroscopic images (ESI)

Unstained, ultrathin (≈ 40–60 nm) sections were mounted on copper grids. To determine the net element composition of a specific area, electron spectroscopic images (Bauer, 1988) were recorded using the Zeiss CEM 902 operating at 80 kV (energy-selecting slit: 20 eV) and a digital analyzer (Kontron-Zeiss).

Results

The radular apparatus of the family Chaetodermatidae is highly modified when compared to the basic pattern found in most molluscs (Scheltema, 1972, 1976, 1981; Salvini-Plawen, 1988). The first complete light microscopy description of the *Falcidens* radula was made by Scheltema (1972). In *Falcidens* sp. (Fig. 1, A, B, C) the radular apparatus is constituted by one pair of teeth accompanied by a second denticle-like pair. These teeth are attached to the end of a cone-shaped piece (radular cone). Two lateral membranes extend almost one-third the length of the radular cone. In the main region of the radular apparatus are a circular structure known as the axial plate and one pair of bar-shaped apophyses. Transmission electron micrographs of transverse sections of the unstained radular apparatus of *Falcidens* sp. (Fig. 1D) reveal that the axial plate in fact is composed of two parallel, electron-dense plates. These plates are connected to the radular lateral membrane near the radular cone (Fig. 1E).

EDXA analysis of sections containing the axial plate shows deposits rich in iron, silicon, oxygen, sulfur, phosphorus, and calcium (Fig. 2A). The denticles (Fig. 2B) and the second denticle-like pair also contain these elements. The radular cone, the periphery of the axial plate, and the periphery of the denticles and denticle-like pair do not exhibit mineralized compounds. Frontal sections of a denticle (Fig. 3A) show that the entire tooth is electron dense, except at the periphery, and in some internal regions dark precipitates are observed. When viewed at higher magnification, the dark precipitates are seen as several needlelike crystals (Fig. 3B) oriented parallel to the organic fibers. ESI of iron in sections from the sample in Figure 3A show that this element occurs mainly in the core of the denticle (Fig. 3C). Oxygen was found to be distributed in the whole section of the denticle (Fig. 3D). By the same technique, phosphorus (Fig. 3E) and calcium (Fig. 3F) were shown to be restricted to the periphery, where the precipitates are more electron dense. The association of iron with oxygen is interpreted as iron oxide in an amorphous state, since no diffraction spots were detected by ESD. Diffraction patterns of the regions rich in calcium, phosphorus, and also oxygen are compatible with hydroxyapatite, $Ca_5(PO_4)_3(OH)$ (Fig. 4).

Discussion

The morphology and the mineralization process in the radular apparatus of *Falcidens* sp. are markedly different from those of chitons and limpets. The radulae of those two groups have several rows of teeth in different stages

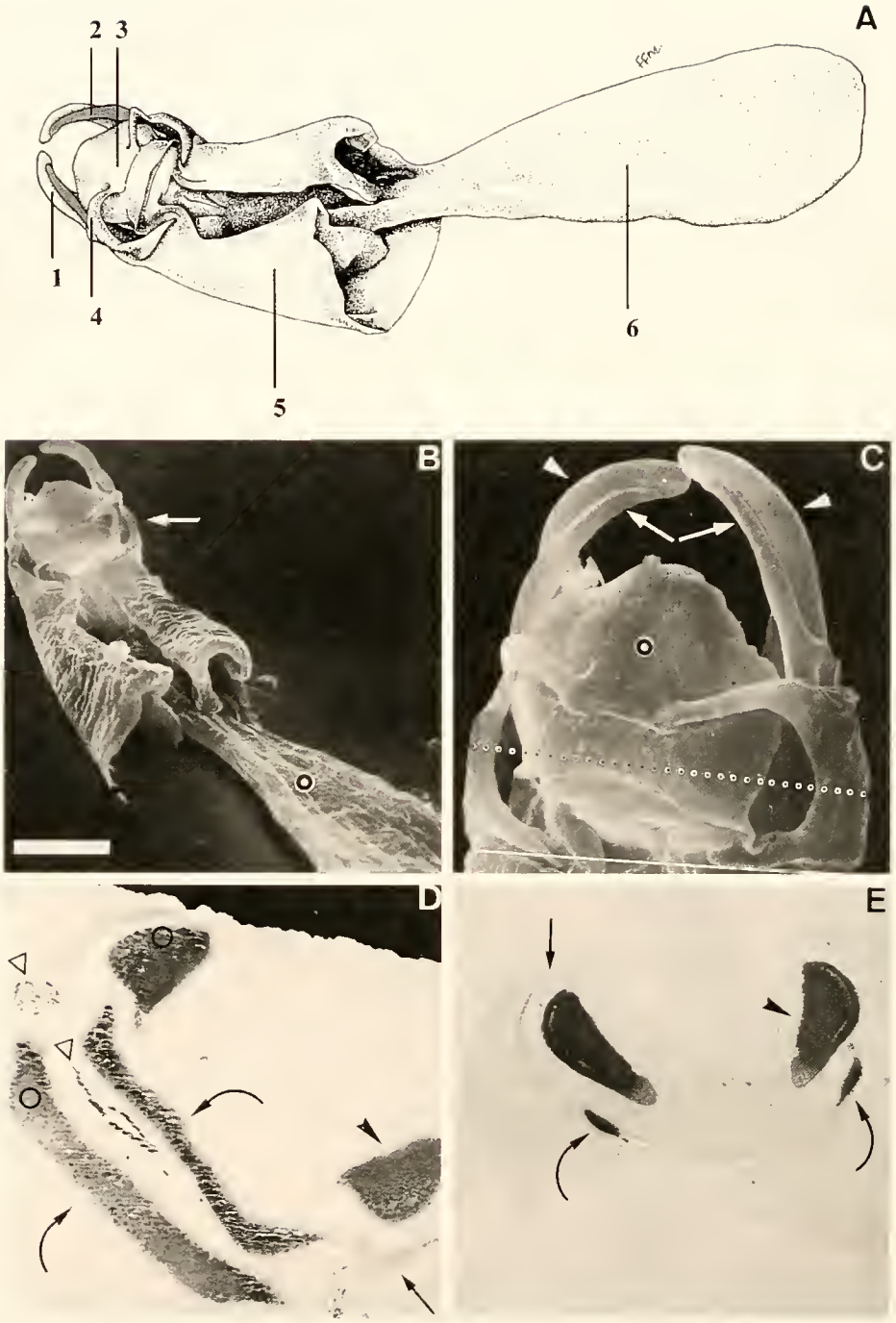

Figure 1. The radular apparatus of *Falcidens* sp. (A) Representative drawing of the apparatus showing denticles (1), second denticle-like pair (2), axial plate (3), bar-shaped apophyses (4), lateral membrane (5), and radular cone (6). (B) Scanning electron micrograph showing the radular cone (open circle) and lateral membrane (arrow). Scale bar in (B), 20 μm. (C) Anterior view of radular apparatus showing a denticle pair (arrowheads), second denticle-like pair (arrows), and axial plate (open circle). The scale bar in (B) represents 4.5 μm in (C). (D) Transmission electron micrograph (TEM) of a transverse section through a region indicated in (C) by the dotted line. Curved arrows show the components of the axial plate; also shown are denticles (arrowhead), second denticle-like pair (arrow), and particles of marine sediments (open arrowheads) that have been retained in the radular apparatus. The open circles indicate the regions selected for energy dispersive X-ray analysis. (E) TEM of a transverse section through the region indicated in (C) by the continuous line. Denticle (arrowhead), second denticle-like pair (arrow), and axial plate (curved arrows) are seen. The scale bar in (B) represents 4.9 μm in (D) and (E).

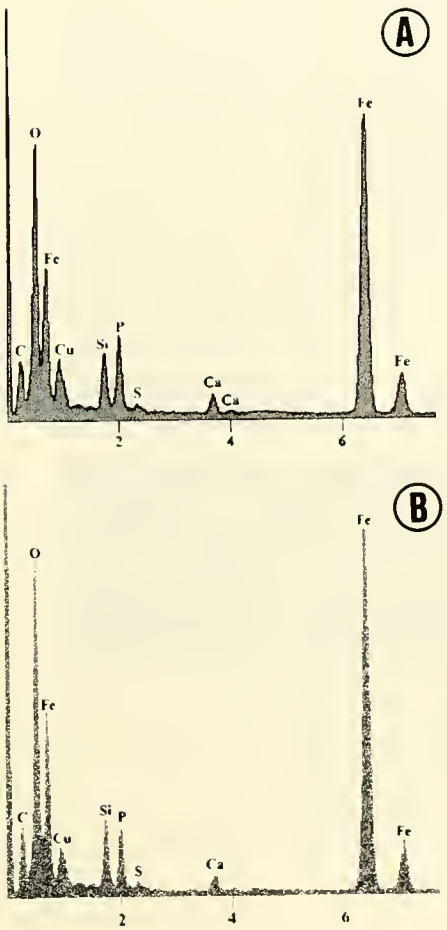

Figure 2. Energy dispersive X-ray analysis spectrum representing the elemental composition of the axial plate (A) and denticle (B) of *Falcidens* sp. The same elements are present in both structures. The *x* axis represents X-ray energies in kiloelectron volts. The *y* axis represents counts per second (arbitrary scale for qualitative comparison). The copper peak comes from the grid bar.

of mineralization, ranging from immature teeth (containing only soft organic structures) to fully mineralized mature teeth (Kirschvink and Lowenstam, 1979; Lowenstam and Weiner, 1985; Mann *et al.*, 1986). Most of these animals are herbivorous scrapers (Steneck and Watling, 1982) whose teeth are abraded and broken during feeding (Webb *et al.*, 1989) and are continuously replaced (Webb *et al.*, 1990). The Chaetodermatidae, however, are selective carnivores (Scheltema, 1981), and their denticles, axial plate, and lateral membrane persist throughout their life span (Luitfried von Salvini-Plawen, pers. comm.). Since these structures are not renewed, it seems that a continuous process of mineralization does not occur, in contrast to chitons (Kirschvink and Lowenstam, 1979) and limpets (Mann *et al.*, 1986).

Impregnation of the denticles of *Falcidens* sp. with a crystalline phosphorous mineral, hydroxyapatite, constitutes an unusual example of mineralization in invertebrates. The great majority of invertebrates exhibit calcium phosphates only in the amorphous state (Taylor and Simkiss, 1994). Among the invertebrate structures reported to have crystalline phosphorous minerals (apatite) are the radular teeth of the Polyplacophora (Lowenstam, 1967), the shells of inarticulate brachiopods (LeGeros *et al.*, 1985), and the shell plates of certain barnacles (Lowenstam *et al.*, 1992). The presence of amorphous iron oxide as a final product of mineralization in the denticles and axial plate of *Falcidens* sp. is also unusual and does not occur among chitons and limpets. In those two groups, the final form of the iron biomineral is invariably crystalline, although the presence of soluble silicon in limpets can dramatically retard the process of iron oxide crystallization in some areas of the tooth (Mann *et al.*, 1986). The presence of silicon associated with iron may account for the amorphous state of the iron in the denticles and axial plate of *Falcidens* sp.

Unlike most chitons (Lowenstam, 1962a; Steneck and Watling, 1982) and limpets (Steneck and Watling, 1982; Van der Wal, 1989), which graze on hard rocks in the intertidal and near-tidal regions, *Falcidens* sp. does not show a clear association between the presence of minerals in its teeth and its manner of obtaining food. In *Falcidens* sp., the denticles are thought to act as a pincers, grasping the food (*e.g.*, foraminifers) with precision (Scheltema, 1981). In fact, the great majority of Caudofoveata (including the genus *Falcidens*) obtain food without performing or enduring any kind of abrasive action in their radular teeth (Scheltema, 1981, 1988). The presence of mineralized compounds in the teeth of nongrazing species also occurs among the Polyplacophora: some carnivorous species in that class have teeth mineralized by magnetite even though they are not used to scrape the substrate (Lowenstam and Weiner, 1989). The deep-sea chitons (deposit feeders) that consume marine sediments to extract the nutritional contents also have mineralized teeth, although they do not graze (Lowenstam and Weiner, 1989). However, the buccal musculature in these species is greatly reduced in comparison with that of grazing species from shallow water (Menzies *et al.*, 1973). These observations suggest that the presence of mineralized teeth among the molluscs is not necessarily related solely to grazing. The hypothesis that the mineralization could increase the stiffness of the denticles and thus be an advantage also for nongrazing individuals such as *Falcidens* sp. cannot be rejected.

In a recent phylogenetic study of the extant Mollusca (Scheltema, 1993), the existence of two separate evolutionary molluscan lineages was proposed. The Solenogastres (=Neomeniomorpha), Caudofoveata (=Chaetoder-

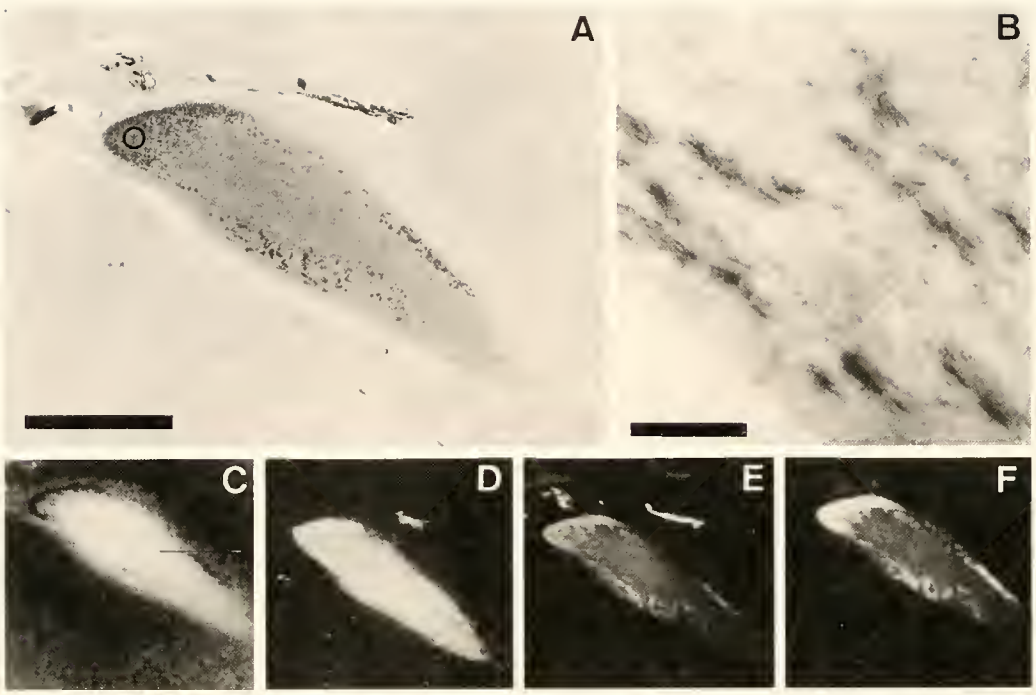

Figure 3. Frontal sections of the denticle of *Falcidens* sp. (A) Transmission electron micrograph of a frontal section showing regions with highly electron-dense precipitates peripheral to less electron-dense region in the core. (B) High magnification of a denticle section showing the presence of several needlelike crystals aligned with the organic fibers. (C–F) Electron spectroscopic images from the section in (A), showing the presence of iron (C), oxygen (D), phosphorus (E), and calcium (F). A comparison of (E) and (F) suggests that the phosphorus is associated with the calcium. Scale bar in (A), 1.25 μm. Scale bar in (B), 90 nm.

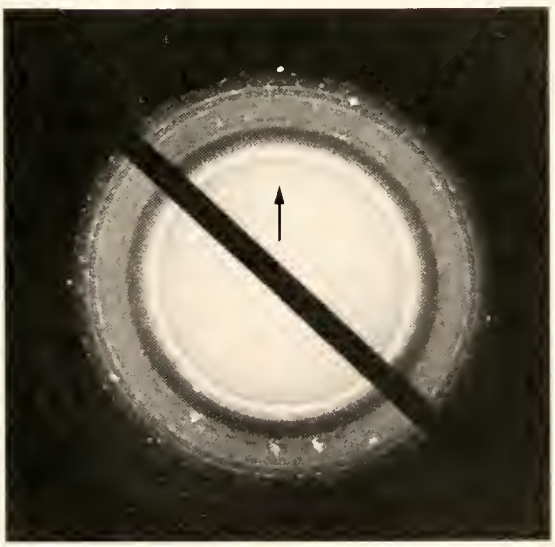

Figure 4. Electron spectroscopic diffraction pattern of the dark region (open circle) in Figure 3 A, showing Debye-Scherrer rings of hydroxyapatite. Black arrow indicates hydroxyapatite {002} lattice planes.

momorpha), and Polyplacophora were grouped in the subphylum Aculifera, and the Monoplacophora, Bivalvia, Gastropoda, Scaphopoda, and Cephalopoda were placed in the subphylum Conchifera. The Solenogastres, Caudofoveata, Polyplacophora, and Monoplacophora are considered "primitive" groups (Salvini-Plawen, 1980; Haszprunar, 1988; Scheltema, 1993). Based on the retention of ancestral characters in its radular apparatus (docoglossate radula), the order Patellogastropoda (=Docoglossa)—including the Acmaeidae and Patellidae—is considered to be the earliest offshoot of Gastropoda (Haszprunar, 1988; McLean, 1990). The ancestral characters mentioned above are a stereoglossate radula apparatus with a weakly developed rhachis tooth and mineralized lateral teeth (Haszprunar, 1988). These characters are also present in the Polyplacophora and Monoplacophora (Wingsrand, 1985; Haszprunar, 1988; McLean, 1990). Apart from monoplacophorans and limpets, the Conchifera show no evidence of mineralized compounds in the radulae (Jones *et al.*, 1935; Lowenstam, 1962a; Haszprunar, 1988). We suggest that the presence of mineralized compounds in the radula may be a plesiomorphic character in the phylum Mollusca. The existence of a common molluscan ancestor

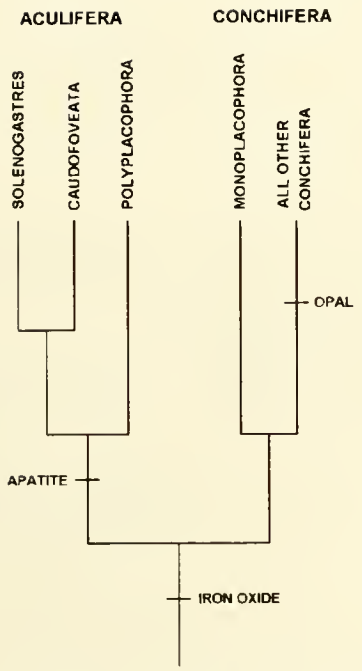

Figure 5. Phylogeny of the extant Mollusca (adapted from Scheltema, 1993). Biogenic minerals in the radular teeth of Mollusca: common molluscan ancestor with mineralized teeth (probably iron oxide); Solenogastres, should be investigated; Caudofoveata, presence of iron oxide and apatite (this work); Polyplacophora, presence of iron oxide and apatite (Lowenstam, 1962a; Lowenstam, 1967); Monoplacophora, presence of iron oxide (Lindberg, 1986); the presence of iron oxide and opal (Lowenstam, 1962b, 1971) was reported only in the families Acmaeidae and Patellidae (Patellogastropoda:Gastropoda). All Other Conchifera refers to the classes Bivalvia, Gastropoda, Scaphopoda, and Cephalopoda. Iron oxide is present in all of the groups that have mineralized teeth.

with mineralized teeth would satisfactorily explain the presence of mineralized compounds in the radulae of different extant molluscan classes (Fig. 5). This hypothesis would be reinforced if mineralized compounds could be found in the teeth of the Solenogastres.

The presence of apatite, a rare mineral among invertebrates, in the same structure (radular teeth) of two distinct groups (Caudofoveata and Polyplacophora) reinforces the evidence that the mineralization of molluscan teeth did not appear independently in these groups, and suggests that this is a heritable character from a common molluscan ancestor.

Acknowledgments

R. C. thanks L. v. Salvini-Plawen for comments and B.Sc. Flávia Moreira Leite for drawing. We thank Laboratório de Biologia Celular e Tecidual (UENF) for EDXA facilities and M. Sorenson for contributions to the final version of the manuscript. This work was supported by the Brazilian agencies CAPES, FINEP, and CNPq (PRONEX).

Literature Cited

Barckhauss, R. H., H. J. Höling, I. Fromm, P. Hirsch, and L. Reimer. 1991. Electron spectroscopic diffraction and imaging of the early and mature stages of calcium phosphate formation in the epiphyseal growth plate. *J. Microsc.* **162:** 155–169.

Bauer, R. 1988. Electron spectroscopic imaging: an advanced technique for imaging and analysis in transmission electron microscopy. *Methods Microbiol.* **20:** 113–146.

Brusca, R. C., and G. J. Brusca. 1990. *Invertebrates.* Sinauer, Sunderland, MA. 992 pp.

Haszprunar, G. 1988. On the origin and evolution of major gastropod groups, with special reference to the Streptoneura. *J. Molluscan Stud.* **54:** 367–441.

Ivanov, D. L. 1996. Origin of Aculifera and problems of monophyly of higher taxa in molluscs. Pp. 59–65 in *Origin and Evolutionary Radiation of the Mollusca,* J. Taylor, ed. London Press, Oxford.

Jones, E. I., R. A. McCance, and I. R. B. Shacketon. 1935. The role of iron and silica in the structure of the radular teeth of certain marine molluscs. *J. Exp. Biol.* **12:** 59–65.

Kim, K.-S., D. J. Macey, J. Webb, and S. Mann. 1989. Iron biomineralization in the radula teeth of the chiton *Acanthopleura hirtosa. Proc. R. Soc. Lond. Ser. B* **237:** 335–346.

Kirschvink, J. L., and H. A. Lowenstam. 1979. Mineralization and magnetization of chiton teeth: paleomagnetic, sedimentologic, and biological implications of organic magnetite. *Earth Planet. Sci. Lett.* **44:** 193–204.

LeGeros, R. Z., C.-M. Pan, S. Suga, and N. Watabe. 1985. Crystallo-chemical properties of apatite in atremate shell. *Calcif. Tissue Int.* **37:** 98–100.

Lindberg, D. R. 1986. Radula evolution in the Patellogastropoda [Abstract]. *Am. Malacol. Bull.* **4:** 115.

Lowenstam, H. A. 1962a. Magnetite in denticle capping in recent chitons (Polyplacophora). *Geol. Soc. Am. Bull.* **73:** 435–438.

Lowenstam, H. A. 1962b. Goethite in radular teeth of recent marine gastropods. *Science* **137:** 279–280.

Lowenstam, H. A. 1967. Lepidocrocite, an apatite mineral, and magnetite in teeth of chitons (Polyplacophora). *Science* **156:** 1373–1375.

Lowenstam, H. A. 1971. Opal precipitation by marine gastropods (Mollusca). *Science* **171:** 487–490.

Lowenstam, H. A., and S. Weiner. 1985. Transformation of amorphous calcium phosphate to crystalline dahlite in the radula teeth of chitons. *Science* **227:** 51–53.

Lowenstam, H. A., and S. Weiner. 1989. *On Biomineralization.* Oxford University Press, New York. 324 pp.

Lowenstam, H. A., S. Weiner, and W. A. Newman. 1992. Carbonate apatite-containing shell plates of a barnacle (Cirripedia). Pp. 73–83 in *Chemistry and Biology of Mineralized Tissues,* H. Slavkin and P. Price, eds. Elsevier, Amsterdam.

Mann, S., C. C. Perry, J. Webb, B. Luke, and R. J. P. Williams. 1986. Structure, morphology, composition and organization of biogenic minerals in limpet teeth. *Proc. R. Soc. Lond. Ser. B* **227:** 179–190.

McLean, J. H. 1990. Neolepetopsidae, a new docoglossate limpet family from hydrothermal vents and its relevance to patellogastropod evolution. *J. Zool. (Lond.)* **222:** 485–528.

Menzies, R. J., R. Y. George, and G. T. Rowe. 1973. *Abyssal Environment and Ecology of the World's Oceans.* Wiley-Interscience, New York.

Reimer, L., I. Fromm, and I. Naundorf. 1990. Electron spectroscopic diffraction. *Ultramicroscopy* **32:** 80–91.

Rios, E. C. 1994. *Seashells of Brazil.* FURG, Rio Grande do Sul. 368 pp.

Salvini-Plawen, L. v. 1980. A reconsideration of systematics in the Mollusca (phylogeny and higher classification). *Malacologia* **19:** 249–278.

Salvini-Plawen, L. v. 1988. The structure and function of molluscan digestive systems. In *The Mollusca,* vol. 11, E. R. Trueman and M. R. Clarke, eds. Academic Press. London.

Scheltema, A. H. 1972. The radula of the Chaetodermatidae (Mollusca, Aplacophora). *Z. Morphol. Tiere* **72:** 361–370.

Scheltema, A. H. 1976. Two new species of *Chaetoderma* from off West Africa (Aplacophora, Chaetodermatidae). *J. Molluscan Stud.* **42:** 223–234.

Scheltema, A. H. 1981. Comparative morphology of the radulae and alimentary tracts in the Aplacophora. *Malacologia* **20:** 361–383.

Scheltema, A. H. 1988. Ancestors and descendents: relationships of the Aplacophora and Polyplacophora. *Am. Malacol. Bull.* **6:** 57–68.

Scheltema, A. H. 1993. Aplacophora as progenetic aculiferans and the coelomate origin of mollusks as the sister taxon of Sipunculida. *Biol. Bull.* **184:** 57–78.

Scheltema, A. H., M. Tscherkassky, and M. Kuzirian. 1994. Aplacophora. In *Microscopic Anatomy of Invertebrates, 5: Mollusca,* F. W. Harrison and A. J. Kohn, eds. John Wiley, New York.

St. Pierre, T. G., L. A. Evans, and J. Webb. 1992. Non stoichiometric magnetite and maghemite in the mature teeth of the chiton *Acanthopleura hirtosa. Hyperfine Interaction* **71:** 1275–1278.

Steneck, R. S., and L. Watling. 1982. Feeding capabilities and limitations of herbivorous molluscs: a functional group approach. *Mar. Biol.* **68:** 299–319.

Taylor, M. G., and K. Simkiss. 1994. Cation substitutions in phosphate biominerals. *Bull. Inst. oceanogr. (Monaco)* **no spécial 14:** 75–79.

Tillier, S., and J. P. Cuif. 1986. L'animal-conodonte est-il un mollusque aplacophore? *C. R. Acad. Sci. Paris* **303:** 627–632.

Towe, K. M., and H. A. Lowenstam. 1967. Ultrastructure and development of iron mineralization in the radula teeth of *Cryptochiton steleri* (Mollusca). *J. Ultrastruct. Res.* **17:** 1–13.

Van der Wal, P. 1989. Structural and material design of mature mineralized radula teeth of *Patella vulgata* (Gastropoda). *J. Ultrastruct. Mol. Struct. Res.* **102:** 147–161.

Webb, J., D. J. Macey, and S. Mann. 1989. Biomineralization of iron in molluscan teeth. Pp. 345–387 in *Biomineralization,* S. Mann, J. Webb, and R. J. P. Williams eds. VCH Verlagsgesellschaft, Weinheim.

Webb, J., T. G. St. Pierre, and D. J. Macey. 1990. Iron biomineralization in invertebrates. Pp. 193–220 in *Iron Biominerals,* R. B. Frankel and R. P. Blakemore eds. Plenum Press, New York.

Wingstrand, K. G. 1985. On the anatomy and relationships of recent Monoplacophora. *Galathea Rep.* **16:** 1–94.

Reference: *Biol. Bull.* **194:** 231–240. (April, 1998)

Carbohydrates of the Organic Shell Matrix and the Shell-Forming Tissue of the Snail *Biomphalaria glabrata* (Say)

JULIA C. MARXEN*, MAREN HAMMER, TILMAN GEHRKE, AND WILHELM BECKER

University of Hamburg, Department of Zoology, Martin-Luther-King-Platz 3, D-20146 Hamburg, Germany

Abstract. Sulfated carbohydrates may play a role in the biomineralization of the molluscan shell. The carbohydrates of the extracted water-insoluble organic shell matrix (IM) of the freshwater snail *Biomphalaria glabrata* were identified as glucose, mannose, galactose, and *N*-acetyl-glucosamine, whereas the water-soluble organic matrix (SM) additionally contained *N*-acetyl-galactosamine. A specific lectin binding pattern of the matrix was obtained. One prominent protein of the SM, with a size of 19.6 kDa and a pI of 7.4, was shown to be a glycoprotein with terminal glucosyl or mannosyl moieties. The acidic constitutents of the matrix showed a variety of possible terminal sugars, indicating a heterogenous mixture of proteoglycans or glycosaminoglycans (GAGs) and glycoproteins.

At the shell-forming mantle edge, an alcian-blue-positive material was observed in the periostracum groove (PG), the belt, and apically in the cells of the outer mantle epithelium (OME). With the help of lectins, all sugars in question were detected in the PG and the belt, whereas the OME was bound by glucose/mannose- and GlcNac-specific lectins only. Although the complete set of GAGs will be produced in the PG and the belt, a very acidic fraction of GAGs and the 19.6-kDa protein can also be delivered by the OME.

Introduction

The biomineralization of the molluscan shell is controlled to a high degree by the organic shell matrix. The processes that have to be controlled are the crystal nucleation and then the modification, morphology, and size of the growing crystals. Macromolecules from the molluscan water-soluble organic matrix (SM) can modify calcium carbonate crystals *in vitro* (Belcher *et al.*, 1996; Falini *et al.*, 1996). Furthermore, acidic macromolecules from the SM can influence the crystal morphology by stereoselective binding (Addadi and Weiner, 1985).

The shell-building tissue of molluscs, the mantle, secretes all shell material into the extrapallial space below the periostracum. Here, the shell is formed in a way that is still scarcely understood. The mantle edge of pulmonates can be morphologically and physiologically divided into five zones (Timmermanns, 1969; Bielefeld *et al.*, 1993a), which should reflect functional units. If the exact function of each unit could be defined successfully, the sequence of the functional units would allow us to draw conclusions about the chronology of the mineralization process. Therefore, it is of special interest to localize the production site of specific matrix components at the mantle edge.

In the past, analysis of molluscan shell matrices concentrated mainly on the proteins, and minor attention was paid to its carbohydrates. The interest focused primarily on chitin, which is found in the water-insoluble organic matrix (IM) of many molluscs (*e.g.*, Poulicek *et al.*, 1991) and could play a special role in the structural framework of the shell (Weiner and Traub, 1984; Falini *et al.*, 1996). But other carbohydrates, especially in the SM, should be investigated because they might provide sulfate groups, which possibly concentrate calcium in the shell (Addadi *et al.*, 1987).

In the SM of several oysters, hexosamines or hexoses and uronic acids are found in combination with sulfate (Crenshaw, 1972; Samata and Krampitz, 1982). Similarly,

Received 28 April 1997; accepted 1 December 1997.

* To whom correspondence should be addressed. E-mail: fb4a010@rrz-cip-1.rrz.uni-hamburg.de

Abbreviations: GAG, glycosaminoglycan; IM, water-insoluble organic matrix; IME, inner mantle epithelium; OME, outer mantle epithelium; PG, periostracum groove; SM, water-soluble organic matrix.

in the SM of the aragonitic cross-lamellar structured shell of the freshwater gastropod *Biomphalaria glabrata,* the amounts of hexosamines, hexoses, uronic acids, and sulfate were 8.8%, 12.7%, 2.1%, and 14% (w/w), respectively (Marxen and Becker, 1997). After SDS-electrophoresis, the SM showed considerable material stained positively with Stains-all and alcian blue. These stained areas probably represent glycosaminoglycans (GAGs) bound to proteins. Prominent among the matrix proteins of *B. glabrata* was one that, with a size of 19.6 kDa, an isoelectrical point of 7.4, and a hydrophobic *N*-terminus (Marxen and Becker, 1997), might be a glycoprotein.

Our approach in this study was the biochemical identification of the carbohydrates in the organic shell matrix of *B. glabrata,* and the detection of glycoproteins. We expected that the histochemical localization of carbohydrates at the shell-building mantle edge would reveal where the glycosylated components of the organic shell matrix are secreted.

Materials and Methods

Animals

Between 200 and 300 snails of the species *Biomphalaria glabrata* (Say, 1818) (Basommatophora, Planorbidae) were kept in 80-l aquaria with a water exchange of about 200 l of dechlorinated tap water per day. The water was preheated to 28 ± 1°C, and the illumination cycle was 12 h light to 12 h dark. The animals were fed *ad libidum* with a food prepared according to Standen (1951).

Extraction of the shell matrix

The organic matrix of the shell was extracted as described elsewhere (Marxen and Becker, 1997). Briefly: 100 g of powdered shell, including the periostracum, was suspended in 50 ml 10^{-5} *M* HCl. The shell powder was decalcified with HCl under continuous stirring at +4°C, the pH never dropping below 5.0. Each time the volume reached 250 ml, the pH was adjusted to 7.4 and the preparation was allowed to rest for 30 min., then centrifuged for 20 min. at 16,000 × *g*. The supernatants were stored, and the preservatives NaN_3 and AEBSF (4-(2-aminoethyl) benzenesulfonyl fluoride) added. The pellet remaining after decalcification was washed, lyophilized, and termed insoluble matrix (IM). All supernatants from the decalcification were combined and dialyzed with 20 changes of the sixfold volume against bidistilled water. Material that precipitated during dialysis was removed by centrifugation at $10^5 \times g$ for 30 min. This pellet had an intermediate degree of solubility in water and was not further investigated. The volume of the supernatant of the 10^5-*g* centrifugation was reduced by lyophilization to 20 ml and further desalted on a P-2 column (Bio-Rad). The void volume was lyophilized and termed the soluble matrix (SM).

Determination of alkali-resistant hexosamines

Protein was removed by boiling the matrix samples for 6 h in 0.5 *M* NaOH and then washing with 1 *M* HCl, 95% (v/v) ethanol, acetone, and 100% ethanol (Jeuniaux, 1963). In the alkali-resistant residue, hexosamines were quantified using Ehrlich's reagent as described by Elson and Morgan (1933) and modified by Kabat and Meyer (1961).

Infrared spectrometry

A KBr pill of the soluble or insoluble organic matrix of *B. glabrata* was prepared according to the method of Günzler and Böck (1983), using 1% of dried organic shell matrix, and analyzed on a Perkin Elmer 841 infrared spectrometer. For a better detection of chitin, protein was removed from some samples of the IM, as described above.

Gas chromatography

Sugars were identified with gas chromatography (Hewlett Packard, Model 437A) using a 10 m × $^1/_8$ inch column packed with 3% silicone OV 225 on Chromosorb W HP 80–100 mesh. Samples were prepared according to Chaplin (1982). An optimal methanolysis was achieved with 2 *M* HCl for 16 h at 85°C. The dry, methanolyzed samples were dissolved in 500 μl waterfree methanol and mixed with 10 μl pyridine and 50 μl acetic anhydride. After 15 min of incubation at room temperature, the samples were dried overnight (Kozulic *et al.,* 1979). The reacetylated samples were mixed with 100 μl silylation reagent (trimethylsilyl imidazole : *N,O*-bis-(trimethylsilyl)-acetamide : trimethylchlorosilane = 3:3:2) (Sweeley *et al.,* 1963), and incubated for 15 min at 70°C and for 45 min at room temperature. Inositol was used as an internal standard. Injector and detector temperatures were 250°C, and the elution program was 2 min at 120°C, rising by 6°C/min. to 220°C.

Lectin binding to the soluble matrix

For the visualization of the lectin binding to the SM, an assay analogous to an ELISA was used. Between all subsequent steps the microtiter plate was washed three times with wash solution (150 m*M* NaCl + 0.1% (v/v) Tween 20), 200 μl/well. A 96-well microtiter plate was coated with SM, each well with 10 μg protein/50 μl 0.2 *M* sodium carbonate buffer, pH 9.5. Unspecific binding was blocked with 200 μl/well blocking buffer: 1% (w/v) carbohydrate-free BSA in 50 m*M* Tris/HCl + 150 m*M* NaCl, pH 7.5. Stock solutions of the biotinylated lectins (Vector, Burlingame, CA) were prepared in a concentration of 1 mg/ml in 10 m*M* PBS + 150 m*M* NaCl, pH 7.4 + 0.25% (w/v) BSA + 0.1% (w/v) NaN_3. The lectins of the stock solutions were diluted 1:100 with dilution buffer:

50 m*M* Tris/HCl + 150 m*M* NaCl, pH 7.5 + 0.5% (w/v) BSA + 0.05% (v/v) Tween 20. This lectin test solution (50 μl/well) was incubated with the SM for 30 min at 37°C. Thirty minutes prior to use, the complex of avidin and biotinylated peroxidase (ABC) (Vector) was prepared; each component was diluted 1:200 in the dilution buffer. The ABC was incubated 50 μl/well for 30 min at 37°C. As a final step, 50 μl/well of the substrate solution were incubated for 30 min at 37°C in the dark. ABTS (2,2′-azinobis(3-ethylbenzthiazoline-6-sulfonic acid) in a concentration of 95.3 mg/100 ml substrate buffer was used as a chromogene. The substrate buffer was 50 mg sodium perborate trihydrate + 836 mg citric acid monohydrate + 1068 mg disodium hydrogen phosphate dihydrate filled up to 100 ml with bidistilled water, pH 4.5. The optical densities at 405 nm were measured with a microplate reader. The quality of all lectins was tested with appropriate neoglycoproteins, which replaced the SM in these controls. The unspecific binding of the lectins to the microtiter plate was tested, leaving some wells uncoated. The specificity of the lectin binding to the SM was tested by preincubating the lectins with suitable carbohydrates for 30 min. The binding was considered specific only when an inhibiting effect was observed.

Lectin binding to the insoluble matrix

The investigation of the lectin binding to the IM was carried out in small plastic centrifuge vials. All buffers and reagents were as described for the lectin binding to the soluble matrix, except that the lectin stock solutions were diluted 1:200, and the ABC-complex 1:400, with dilution buffer. The sample solution was 1 mg/ml dilution buffer. The vials were filled completely with blocking buffer, kept overnight at 4°C, and then emptied. Next, 25 μl of the constantly stirred sample solution plus 100 μl of diluted lectin was placed in the emptied vials and incubated for 30 min at 37°C. The vials were washed three times with 300 μl wash solution and centrifuged at 8000 $\times$ *g* for 3 min in between. A 100-μl sample of the ABC was incubated and washed in the same way. After incubation with 100 μl of substrate solution for 15 min, 50 μl was pipetted into a microplate for measuring the optical densities at 405 nm.

Isoelectrical focusing

The isoelectrical focusing (IEF) was performed according to the recommendations of Serva (Heidelberg, FRG). Servalyt precotes (125 $\times$ 125 mm) with a polyacrylamide layer of 150 μm and a pH gradient from pH 3.0 to 10.0 were used. After 30 min of prefocusing, the samples were loaded and separated for 1.5 h with a maximum of 2000 V, 6 mA, and 4 W at 4°C.

Lectin binding to the isoelectric focusing gel

When the IEF run was finished, biotinylated lectins were applied directly to the gel according to a procedure modified from Allen *et al.* (1976). The gel was fixed with 12.5% (v/v) TCA for 15 min and washed three times with wash solution (see *Lectin binding to the soluble matrix*). The gel was incubated under constant shaking for 1.5 h at room temperature with lectins from the stock solutions, diluted 1:100 with 50 m*M* Tris/HCl + 150 m*M* NaCl, pH 7.5, + 0.1% (v/v) Tween 20, and washed three times. ABC, diluted 1:50 in the same solution 30 min prior to use, was incubated for 1 h. AEC (3-amino-9-ethylcarbazole), dissolved in DMF (dimethylformamide) 4 mg/ml, was used as a chromogene. The freshly prepared substrate solution contained 76 ml of 0.05 *M* acetate buffer, pH 5.0, 4 ml of AEC in DMF, and 400 μl 3% (v/v) H_2O_2. The gel was incubated in the dark with the substrate solution until intense red bands appeared.

Histological detection of mucus

Pieces of the mantle edge were fixed by three methods. Method 1: Fixation for 28 h at room temperature in 2% (v/v) glutardialdehyde in 0.05 *M* cacodylate buffer, pH 7.4. Method 2: Fixation for 24 h at room temperature in 4% (v/v) formaldehyde in 0.067 *M* phosphate buffer, pH 7.4, with 0.5% (w/v) cetylpyridinium chloride added. Method 3: Fixation for 18 h at 4°C in 4% (v/v) formaldehyde in picric-acid-saturated ethanol with 5% (v/v) acetic acid. After embedding in paraplast, sections of 5-μm thickness were cut, and the Paraplast was removed. Mucus and mucus cells were stained with 1% (w/v) alcian blue 8GX in 3% (v/v) acetic acid at pH 2.5 and counterstained with either Kernechtrot or PAS. For the differentiation between carboxylic and sulfate groups, the alcian blue staining at pH 1.0 (Lev and Spicer, 1964) and the critical electrolyte concentration (Scott and Dorling, 1965) were carried out.

Lectin histochemistry

Pieces of the mantle edge were fixed for 26 h at room temperature in 2% (v/v) formaldehyde in a solution of 25% (v/v) ethanol, 25% (v/v) ethyl acetate, 5% (v/v) acetic acid, and 0.5% (w/v) picric acid. From sections of 7-μm thickness, embedded in Paraplast, the Paraplast was removed, and the endogenous peroxidase was blocked with 1% (v/v) H_2O_2 in 100% methanol. Unspecific binding was blocked with 2% (w/v) BSA in PBS (150 m*M* NaCl, buffered with 10 m*M* phosphate, pH 7.4). The sections were incubated with biotinylated lectins (Vector Laboratories, Burlingame, CA), in dilutions from 1:50 to 1:1600 in PBS, pH 7.4, containing 0.25% (w/v) BSA and 0.1% (w/v) NaN_3 for 18 h at 4°C in a moistened chamber. After careful rinsing with PBS, the avidin-biotin-peroxi-

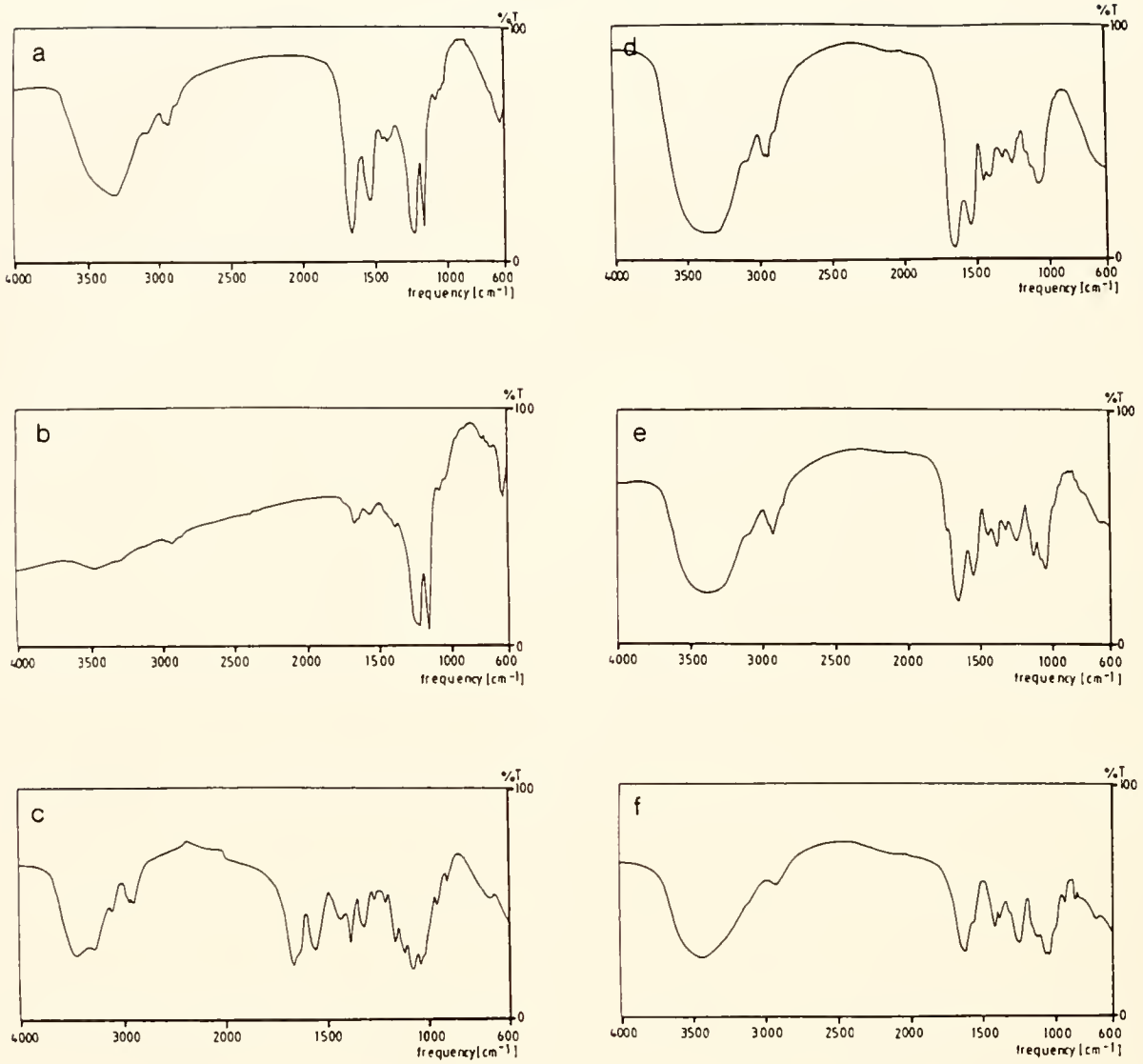

Figure 1. The infrared absorption spectra from (a) the extracted water-insoluble organic matrix fraction of the *Biomphalaria glabrata* shell; (b) the alkali-treated, protein-free water-insoluble organic matrix; (c) chitin from crabshell; (d) the extracted water-soluble organic matrix fraction of the *B. glabrata* shell; (e) mucin from bovine submaxillary glands; (f) chondroitin sulfate A from bovine trachea.

dase complex (Vector) was incubated for 30 min at room temperature. After rinsing with PBS, the staining was carried out with 0.08% (w/v) DAB, 0.075% (w/v) $NiCl_2$, and 0.01% (v/v) H_2O_2 in Tris-buffered solution, pH 7.4, for 20 min at room temperature. Controls: (1) without lectin, (2) without ABC, (3) without DAB, (4) lectins preincubated with their specific sugar.

Results

Hexosamine quantification and infrared spectrometry

In this preparation, the IM of *B. glabrata* included the periostracum. Of the hydrolyzable part of the IM (63.5% [w/w]), 3.4% (w/w) was composed of hexosamines. After a previous alkaline treatment, alkali-resistant hexosamines represented 2.9% (w/w) of the IM—that is, 85% (w/w) of the total hexosamines. The hexosamines of the SM were not alkali-resistant.

The finding of alkali-resistant hexosamines in the IM hinted at the occurrence of chitin. The infrared absorption spectra of the IM and SM of the *Biomphalaria glabrata* shell (Fig. 1) were examined to see whether chitin was visible in the IM and whether the occurrence of GAGs in the SM could be confirmed. The main absorption bands are listed in Table I.

The pattern of the IM (Fig. 1a) differed from that of

Table I

Positions of the main infrared absorption bands of the extracted water-soluble organic matrix fraction of the Biomphalaria glabrata *shell (SM), mucin from bovine submaxillary glands, chondroitin sulfate A from bovine trachea, the water-insoluble matrix fraction (IM), the alkali-treated protein-free IM, and chitin from crabshell; appropriate functional groups are suggested in the left column*

Functional group	SM	Mucin	Chondroitin sulfate	IM	Protein-free IM	Chitin
-OH/H_2O	3336	3395	3436	3309	(3463)	3451
-COOH	2933	2927	2927	2930	—	2884
Amide I	1657	1655	1616*	1656	1659	1656
Amide II	1534	1546	—	1528	1553	1562
$-COO^-$ symm.	1448	1441	—	—	—	—
	1404	—	1412	1410	—	—
C-H bending	—	1377	1376	—	—	1376
Amide III	1311	1316	—	—	—	1307
Sulfate	1241	1238	1241	1228	—	—
-C-O single bonding	—	—	—	—	1214	(1201)
	—	—	—	1153	1152	1158
-OH sugar	—	1124	—	—	—	1113
	1066	—	1065	1073	—	1067
	—	1042	—	—	—	1030
Sulfate	—	—	926	—	—	—
	—	—	855	—	—	—
Amide IV	—	—	—	622	623	—

( ) = weak band.
* Probably due to *N*-acetyl group.

the soluble matrix (Fig. 1d). The IM showed a strong protein peak (amide I) at 1656 cm^{-1} and a medium band (amide II) at 1528 cm^{-1}. Although no amide III band and just one symmetric COO^- vibration appeared, a band indicating a -C-O bonding came out at 1153 cm^{-1}. The band at 1228 cm^{-1} may point to sulfate, and the absorption at 1073 cm^{-1} to carbohydrates. Any chitin present should have become apparent in the IM samples from which protein had been removed (Fig. 1b), but this was not the case. A comparison with chitin from crabshell (Fig. 1c) showed a strikingly different pattern. The alkaline treatment removed the carboxylic, hydroxylic, and sulfate bands preferentially, so that the "unmasked" residue of the insoluble matrix probably consisted of sclerotized proteins only.

Table II

The gas-chromatographically identified sugars in the extracted water-soluble (SM) and insoluble (IM) organic matrix fractions of the Biomphalaria glabrata *shell*

	SM	IM
Glucose	+	+
Galactose	+	+
Mannose	+	+
N-Acetyl-Glucosamine	+	+
N-Acetyl-Galactosamine	+	−
Small unidentified peaks	2 plus 1	2

The SM (Fig. 1d) showed a strong protein peak (amide I) at 1657 cm^{-1}, a medium band (amide II) at 1534 cm^{-1}, and a weak band (amide III) at 1311 cm^{-1}. The absorption bands at 1448 and 1404 cm^{-1} were probably due to carboxylic groups, while carbohydrates were responsible for the band at 1066 cm^{-1}. Since sulfate is indicated by bands between 1250 and 1230 as well as 925 and 850 cm^{-1}, the band at 1241 cm^{-1} can be interpreted as a sulfate band. In contrast, the pure GAG chondroitin sulfate A (Fig. 1f) contained no amide bands—the band at 1616 cm^{-1} was probably due to *N*-acetyl groups located on the galactosamine—but all sulfate bands. Mucin from bovine submaxillary glands (Fig. 1e), which consists of protein-bound GAGs, showed amide bands very similar to those of the soluble shell matrix: just one sulfate band at 1238 cm^{-1}, one symmetric carboxylic band, but two different carbohydrate bands. The infrared spectra from bovine mucin and the extracted shell matrix were almost identical, indicating the occurrence of protein-bound GAGs in the shell.

Carbohydrates of the organic matrix

The sugars of the soluble and the insoluble shell matrix of *B. glabrata* were identified gas-chromatographically as listed in Table II. In the SM and IM, two identical plus one additional peak in the SM remained unidentified. These unidentified peaks were not *N*-acetyl-mannosamine, arabinose, fucose, fructose, galactosamine, galacturonic acid,

Table III

The binding pattern of lectins to the extracted water-soluble (SM) and insoluble (IM) organic matrix fractions of the Biomphalaria glabrata *shell*

Lectin	Specificity*	Inhibitor	SM	IM
UEA-I	L-Fuc $\alpha 1 \rightarrow 2$ Gal	—	−	n.t.
LTA	L-Fuc $\alpha 1 \rightarrow 2$ Gal	—	−	n.t.
DBA	GalNac $\alpha 1 \rightarrow 3$ GalNac	—	−	−
SBA	GalNac α or $\beta 1 \rightarrow 3$ Gal	1.0 *M* GalNac	(+)	−
MPA	Gal $\beta 1 \rightarrow 3$ GalNac > GalNac $\alpha 1 \rightarrow 6$ Gal	0.5 *M* Gal or 0.5 *M* GalNac	+++	+++
PNA	Gal $\rightarrow \beta 1 \rightarrow 3$ GalNac	0.025 *M* Gal	(+)	−
RCA1	Gal $\beta 1 \rightarrow 4$ GlcNac	0.050 *M* Gal	+	(+)
ConA	Man $\alpha 1 \rightarrow$ > Glc $\alpha 1 \rightarrow$	0.100 *M* Man	++	+++
WGA	$(GlcNac\ \beta 1 \rightarrow 4)_n$ ($n = 5 > 4 > 3 > 2$)	0.005 *M* Chitotriose	++	+++

Lectins: UEA-I = *Ulex europaeus* agglutinin; LTA = *Lotus tetragonolobus* agglutinin; DBA = *Dolichus biflorus* agglutinin; SBA = *Glycine max* agglutinin; MPA = *Maclura pomifera* agglutinin; PNA = *Arachis hypogaea* agglutinin; RCA1 = *Ricinus communis* agglutinin; ConA = *Concanavalia ensiformis* agglutinin; WGA = *Triticum vulgaris* agglutinin.

* Preferred specificity according to Wu *et al.* (1988).

n.t. = not tested.

(+) = weak bond.

glucosamine, glucuronic acid, mannosamine, mannuronic acid, rhamnose, or xylose. The recovery of uronic acids was generally poor.

Terminal sugar moieties were identified with the help of lectins, binding to the water-soluble and water-insoluble matrix (Table III). No terminal fucose was observed. The GalNac-specific lectins DBA and SBA were negative or just weakly positive. The high amount of sugar, which was necessary to inhibit the binding of SBA, indicated an unspecific binding. Since MPA with a lower preference also binds to GalNac, the occurrence of this sugar in a terminal position cannot be absolutely excluded for the SM. The strong binding of MPA, in combination with the weakly positive reactions of PNA and RCA1, indicated that both the SM and the IM contained terminal galactosyl moieties. The binding of ConA can be due to glucose or mannose, which were both found to be constituents of the matrix (Table II). Also, terminal GlcNac was identified in both matrix fractions by the binding of WGA.

The binding of lectins to glycoproteins and proteoglycans of the organic matrix after isoelectrical focusing is demonstrated in Figure 2. The matrix protein of *B. glabrata* with a size of 19.6 kDa and a pI of 7.4 was bound by ConA only, referring to terminal glucosyl or mannosyl moieties. ConA with a lower preference also binds to GlcNac, but the occurrence of this sugar in terminal position at the 19.6 kDa protein is excluded because of the negative reaction with WGA. Furthermore, the 19.6 kDa protein was not bound by PNA and RCA1 (Table IV)—results that were obtained after SDS electrophoresis and blot transfer (not shown).

In the acidic range between pI 5.4 and 3.3, where the alcian-blue-positive material was found, ConA, bound to two bands at pI 5.0 and 4.5, indicated terminal glucosyl or mannosyl moieties. WGA, bound to a band with a pI of 3.5, indicated terminal GlcNac; MPA, bound to 10 bands in the range between pI 4.5 and 3.3, indicated terminal galactosyl or GalNac moieties.

Carbohydrates at the mantle edge

The appearance of mucus at the shell-forming mantle edge was detected by alcian blue staining. All three fixations gave satisfactory results, but the use of CPC (method 2) resulted in the best preservation of lighter stained minor amounts of mucus, especially in the belt and the outer mantle epithelium (OME). The results are combined in a schematic drawing (Fig. 3). Staining at pH 2.5, which indicates carboxylic groups, gave a strong reaction with mucus cells at the base of the PG, a weaker reaction in the middle of the belt, and was seen as a thin apical layer at the cells of the OME. Furthermore, mucus cells, which secrete their contents towards the inner mantle epithelium (IME), gave strong positive reactions with alcian blue at pH 2.5 and 1.0, indicating carboxylated as well as sulfated mucus.

The results of all lectins applied to the shell-forming mantle edge and the shell matrix of *B. glabrata* are summarized in Table IV. The lectins UEA-I, SBA, RCA1, PNA, ConA, and WGA bound specifically to the periostracum groove (PG) (Zone 1). All lectins reacted, with different strengths, with the distal belt (Zones 2 and 3). The binding of SBA (Fig. 4), WGA (Fig. 5), and ConA (Fig. 6) is shown. At the proximal belt (Zone 4) and at the OME (Zone 5), a thin layer of material that reacted with WGA (Fig. 5) and ConA (Fig. 6) was seen, but only apically. The mucus cells of the IME reacted almost like

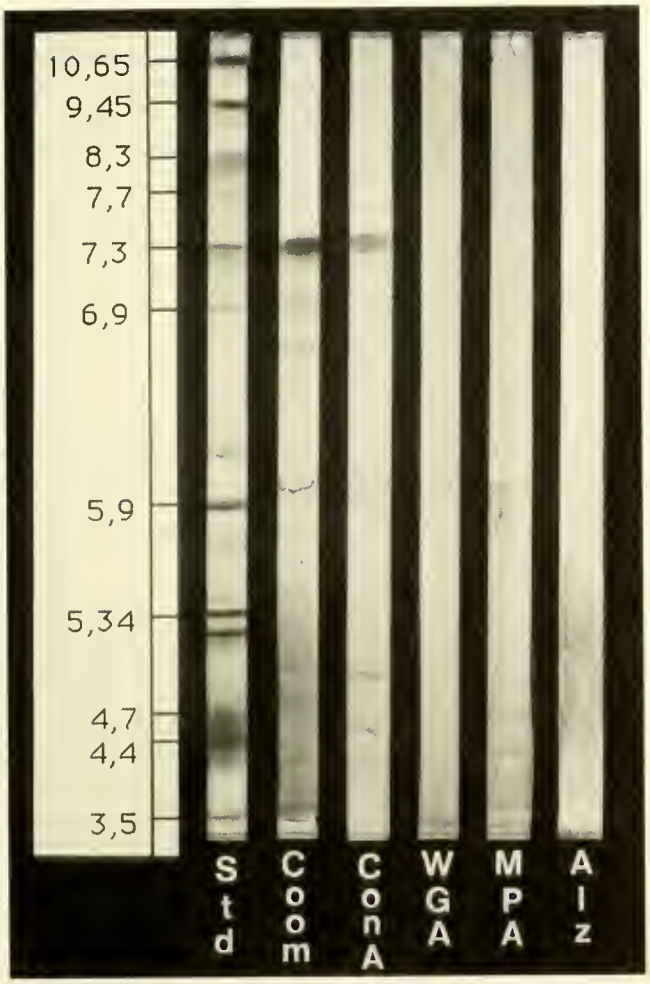

Figure 2. Isoelectrical focusing of the extracted water-soluble organic matrix fraction of the *Biomphalaria glabrata* shell and application of lectins. Std = standard proteins; Coom = matrix, stained with Coomassie brilliant blue; ConA, WGA, and MPA = lectins; Alz = matrix, stained with alcian blue.

the belt. The calcium cells in the interstitium bound almost all lectins, but no inhibition by the specific sugars occurred, indicating merely an unspecific reaction.

Discussion

Chitin

The hexosamines of the IM were mainly alkali-resistant, so the matrix could contain chitin. The infrared spectrometry could not, however, confirm this assumption (Fig. 1b). Bielefeld *et al.* (1993a), using electron microscopy, found WGA binding sites in the periostracum of *B. glabrata.* After a chitinase digestion, the reactivity of these sites was reduced, but not negative. The cells at the PG and the belt, however, were not affected by chitinase. The results indicate that chitin is one of the GlcNac-positive components of the periostracum of *B. glabrata,* but the amount may be considered rather low.

Glycoproteins and proteoglycans

Prominent among the proteins of the SM of *B. glabrata* is one that has a size of 19.6 kDa and an isoelectrical point of 7.4. *N*-terminal microsequencing revealed that 15 or 16 of the 24 amino acids identified in the 19.6-kDa protein were hydrophobic (Marxen and Becker, 1997). Because of its high pI, this protein cannot be directly involved in the binding of calcium. As demonstrated by the binding of lectins to the IEF gel (Fig. 2, Table IV), this protein is glycosylated with glucosyl and mannosyl moieties, singly or in combination. Thus, this glycoprotein contains hydrophobic as well as hydrophilic domains and may have evolved from a membrane protein. In the SM of *Mytilus edulis,* Keith *et al.* (1993) found a protein with a size of 21 kDa and a highly hydrophobic *N*-terminus with a sequence that was identical in the positions 7, 8, and 9 to that of the 19.6-kDa protein of *B. glabrata.* It is not known, however, whether the 21-kDa protein from *M. edulis* is glycosylated. Mann *et al.* (1988) observed a change in the modification of calcium carbonate crystals under a stearic acid monolayer. The hydrophobic and hydrophilic parts of the 19.6-kDa protein (and perhaps also the 21-kDa protein from *M. edulis*) could give molecules of this kind a detergent-like quality, by which they might—among other possible functions—play a role in the determination of the crystal modification.

The acidic material of the SM of *B. glabrata* shows a variety of possible terminal sugar moieties at various isoelectrical points (Fig. 2, Table IV). Although the main part with a broad range of isoelectrical points is bound by the Gal- or GalNac-specific MPA, only a very acidic component is detected by the GlcNac-specific WGA. A lower acidic part is detected by ConA, pointing to Man or Glc, which are not common sugars in GAGs. The results indicate the occurrence of several different GAGs and glycoproteins. Mixtures of GAGs are common in vertebrates (Volpi, 1996) as well as in molluscan tissues (Dietrich *et al.,* 1983). Cottrell *et al.* (1994) detected a large number of hexoses and hexosamines in the body mucus of the slug (*Arion ater*) and showed that—in addition to the main fraction, which probably is heparan sulfate—other, unidentified GAGs unknown in vertebrates must also be present. Moreover, in invertebrates the variable glycosylation of one core protein is possible (Har-El and Tanzer, 1993).

Mucopolysaccharides have been found in other molluscan shells as well (Simkiss, 1965; Worms and Weiner, 1986), but their function in the shell remains questionable. Sulfated polysaccharides have been discussed as possible calcium-binding sites (Wilbur, 1976) and, because of their appearance in the center of nacreous tablets, could play a role in the nucleation and the growth inhibition of the mineral (Crenshaw and Ristedt, 1976).

Table IV

The binding pattern of lectins to the periostracum groove (PG), the belt, and the outer mantle epithelium (OME) of Biomphalaria glabrata, *the extracted water-soluble organic matrix fraction (SM), the 19.6-kDa protein, and the acid IEF bands of the* B. glabrata *shell*

Lectin	Specificity	PG	Belt	OME	Whole SM	19.6 kDa protein	Acidic IEF bands
UEA-I	Fuc	(+)	(+)	−	−	n.t.	n.t.
DBA	GalNac	−	(+)	−	−	n.t.	n.t.
SBA	GalNac	++	+++	−	(+)	n.t.	−
MPA	Gal, GalNac	−	++	−	+++	−	+++
PNA	Gal	+	+	−	(+)	−	n.t.
RCA1	Gal	(+)	++	−	+	−	n.t.
ConA	Man, Glc	++	+++	$+_a$	++	++	+
WGA	GlcNac	+++	++	$+_a$	++	−	++

Lectins = UEA-I: *Ulex europaeus* agglutinin; DBA = *Dolichus biflorus* agglutinin; SBA = *Glycine max* agglutinin; MPA = *Maclura pomifera* agglutinin; PNA = *Arachis hypogaea* agglutinin; RCA1 = *Ricinus communis* agglutinin; ConA = *Concanavalia ensiformis* agglutinin; WGA = *Triticum vulgaris* agglutinin.

n.t. = not tested.

a = positive reaction apically.

(+) = weak bond.

Histological observations

In the shell-forming tissue, alcian-blue-positive material was found in cells of the PG, the belt and, as a thin apical border, the OME (Fig. 3). Surprisingly, no sulfated mucopolysaccharides were detected here, although a considerable amount of sulfate is found in the shell matrix (Crenshaw, 1972; Marxen and Becker, 1997). Also, in the freshwater mussel *Anodonta californiensis*, sulfate was observed in those parts of the mantle edge that correspond to the IME of *B. glabrata*, but not in the outer fold, which corresponds to the belt and OME (Hovingh and Linker, 1993). Thus, the origin of the sulfate in the organic shell matrix remains questionable.

Eight lectins reacted positively—most strongly so—with the belt (Zones 2 and 3), although their reactions with the PG were generally weaker or partly negative, indicating that the sugar concentrations were higher in the belt. The question remains, why GalNac-specific lectins, especially SBA, bound to the shell-forming tissue but not to the organic matrix of the shell.

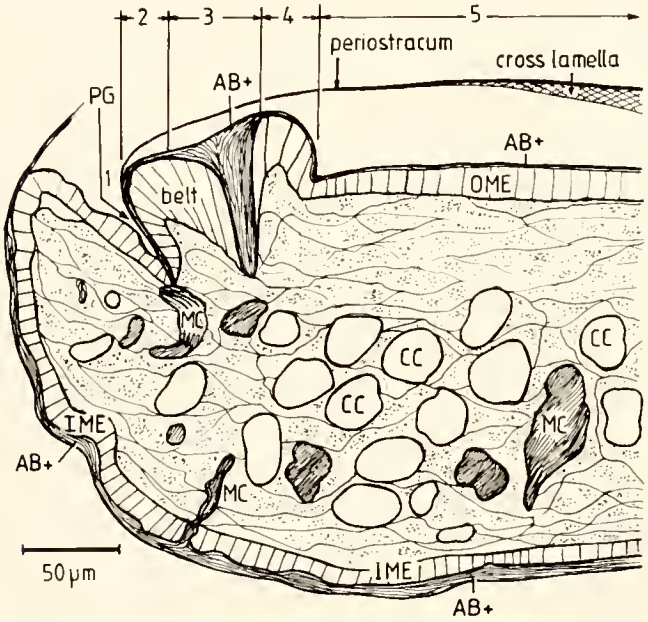

Figure 3. Drawing of the shell-forming mantle edge of *Biomphalaria glabrata*, showing the combined results after fixing the tissue with three different methods and staining with alcian blue. Zones 1–5 are facing the shell. A strongly positive reaction product appears in the mucus cells (MC) and the periostracum groove (PG) after staining with alcian blue at pH 2.5 (AB+, hatched areas). A more lightly stained reaction product descends to the basis of the high prismatic cells of the belt and is detected apically in the cells of the outer mantle epithelium (OME). A thick layer of mucus secreted from the mucus cells can be seen on the cells of the inner mantle epithelium (IME). The tissue is filled with calcium cells (CC).

Figure 4. Binding of the lectin SBA (1:200) to the mantle edge of *Biomphalaria glabrata*. A positive reaction product is visible in the cells of the periostracum groove (PG), Zones 2 and 3 of the belt, mucus cells (MC) near the inner mantle epithelium (IME), and at a mucous border on the IME. No reaction product is found in the outer mantle epithelium (OME).

All the glycosylated components of the matrix can be produced in cells of the PG (Zone 1) and the distal belt (Zones 2 and 3). In contrast to Zones 1 to 3, the proximal belt (Zone 4) and the OME (Zone 5) exhibited only terminal GlcNac and Man/Glc, respectively pointing to the production of a GAG with a pI of 3.5 and to the less acidic glycosylated material, the 19.6-kDa glycoprotein, or both. The lectin binding pattern of the mantle edge indicates a functional differentiation among the various kinds of GAGs, but the same GAG has different functions depending on the location of its production.

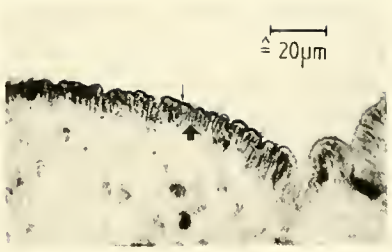

Figure 6. Binding of the lectin ConA (1:200) to the outer mantle epithelium of *Biomphalaria glabrata.* The positive reaction product can be seen apically (small arrow); the gray appearance of the cell bodies is caused by their natural orange color (large arrow).

Conclusions

The striking difference in the lectin binding pattern between the distal part (Zones 1 to 3) and the proximal part (Zones 4 and 5) of the shell-forming tissue gives new emphasis to a strict functional separation between these parts.

In Zones 1, 2, and 3 of the mantle edge of freshwater snails, a phenol oxidase activity has been observed (Timmermanns, 1969; Bielefeld *et al.,* 1993a). This enzyme may be responsible for the sclerotization and tanning of the periostracum (Waite, 1984) and the matrix (Gordon and Carriker, 1980), which thus become water-insoluble. The sugar patterns in the SM and IM of *B. glabrata* are very similar, indicating that GAGs are trapped in the network of sclerotized proteins.

In Zones 4 and 5, a strong alkaline phosphatase activity (Timmermanns, 1969; Bielefeld *et al.,* 1993b) and a carbonic anhydrase activity were detected (Timmermanns, 1969; Boer and Witteveen, 1980); both enzymes are thought to be closely related to the mineralization process (Wilbur, 1964; Watabe, 1984). Because calcium has also been localized at these proximal zones in *B. glabrata* (Bielefeld *et al.,* 1992), this site can be considered to be the region where the calcification of the organic matrix of the shell takes place.

The periostracum is produced by the groove and the distal belt (Bielefeld *et al.,* 1993a). Furthermore, the belt seems to be the production site for those GAGs and proteins that form the structural framework of the organic matrix. Here, the proteins will be partly linked by the phenol oxidase, trapping acidic polysaccharides. Matrix constituents that may be directly involved in the calcification process of the shell seem to be produced, in addition, by the mineralizing region of the mantle. In *B. glabrata,* these constituents presumably include the very acidic WGA-positive part of the GAGs, the less acidic ConA-positive material, and the 19.6-kDa protein. Because components of the SM are known to enhance crystal nucleation when immobilized but inhibit crystal growth when free in solution (*e.g.,* Wheeler and Sikes, 1989), the function of the acidic polysaccharides may vary depending on their place of origin. Distally produced, immobilized GAGs may provide nucleation sites, while the proximally produced ones could instead be involved in regulating crystal growth.

Figure 5. Binding of the lectin WGA (1:200) to the mantle edge of *Biomphalaria glabrata.* A positive reaction product shows in the cells of the periostracum groove (PG), Zones 2 and 3 of the belt, apically in the cells of the transitional Zone 4 and the outer mantle epithelium (OME). The mucus cells near the inner mantle epithelium (IME) are slightly stained, and the calcium cells (CC) of the interstitium give an unspecific reaction.

Acknowledgments

We thank Mrs. V. Wagschal for her excellent technical assistance. This project was financially supported by the German Ministry for Research and Technology (BMFT) (50 WB 9112).

Literature Cited

Addadi, L., and S. Weiner. 1985. Interactions between acidic proteins and crystals: Stereochemical requirements in biomineralization. *Proc. Natl. Acad. Sci. USA* **82:** 4110–4114.

Addadi, L., J. Moradian, E. Shay, N. G. Maroudas, and S. Weiner. 1987. A chemical model for the cooperation of sulfates and carboxylates in calcite crystal nucleation: Relevance to biomineralization. *Proc. Natl. Acad. Sci. USA* **84:** 2732–2736.

Allen, R. C., S. S. Spicer, and D. Zehr. 1976. Concanavalin-A-horse-

radish peroxidase bridge staining of α-1-glycoproteins separated by isoelectric focusing on polyacrylamide gel. *J. Histochem. Cytochem.* **24:** 908–914.

Belcher, A. M., X. H. Wu, R. J. Christensen, P. K. Hansma, G. D. Stucky, and D. E. Morse. 1996. Control of crystal phase switching and orientation by soluble mollusc-shell proteins. *Nature* **381:** 56–58.

Bielefeld, U., K. Zierold, K. H. Körtje, and W. Becker. 1992. Calcium localization in the shell-forming tissue of the freshwater snail, *Biomphalaria glabrata:* a comparative study of various methods for localizing calcium. *Histochem. J.* **24:** 927–938.

Bielefeld, U., W. Peters, and W. Becker. 1993a. Ultrastructure and cytochemistry of periostracum and mantle edge of *Biomphalaria glabrata* (Gastropoda, Basommatophora). *Acta Zool.* **74(3):** 181–193.

Bielefeld, U., K. H. Körtje, H. Rahmann, and W. Becker. 1993b. The shell-forming mantle epithelium of *Biomphalaria glabrata* (Pulmonata): ultrastructure, permeability and cytochemistry. *J. Molluscan Stud.* **59:** 323–338.

Boer, H. H., and J. Witteveen. 1980. Ultrastructural localization of carbonic anhydrase in tissues involved in shell formation and ionic regulation in the pond snail *Lymnaea stagnalis. Cell Tissue Res.* **209:** 383–390.

Chaplin, M. F. 1982. A rapid and sensitive method for the analysis of carbohydrate components in glycoproteins using gas-liquid chromatography. *Anal. Biochem.* **123:** 336–341.

Cottrell, J. M., I. F. Henderson, and D. J. Wright. 1994. Studies on the glycosaminoglycan component of trail mucus from the terrestrial slug, *Arion ater* L. *Comp. Biochem. Physiol.* **107B:** 285–296.

Crenshaw, M. A. 1972. The soluble matrix from *Mercenaria mercenaria* shell. *Biomineralization* **6:** 6–11.

Crenshaw, M. A., and H. Ristedt. 1976. Histochemical localization of reactive groups in septal nacre from *Nautilus pompilius.* Pp. 355–367 in *The Mechanisms of Mineralization in the Invertebrates and Plants,* N. Watabe and K. M. Wilbur, eds. The University of South Carolina Press, Columbia.

Dietrich, C. P., V. M. P. Paiva, S. M. B. Jerònimo, T. M. O. C. Ferreira, M. G. L. Medeiros, J. F. Paiva, and H. B. Nader. 1983. Characteristic distribution of heparan sulfates and chondroitin sulfates in tissues and organs of the ampularidae *Pomacea* sp.*. *Comp. Biochem. Physiol.* **76B:** 695–698.

Elson, L. A., and W. T. J. Morgan. 1933. A colorimetric method for the determination of glucosamine and chondrosamine. *Biochem. J.* **27:** 1824–1828.

Falini, G., S. Albeck, S. Weiner, and L. Addadi. 1996. Control of aragonite or calcite polymorphism by mollusk shell macromolecules. *Science* **271:** 67–69.

Gordon, J., and M. R. Carriker. 1980. Sclerotized protein in the shell matrix of a bivalve mollusc. *Mar. Biol.* **57:** 251–260.

Günzler, H., and H. Böck. 1983. *IR-Spektroskopie.* Verlag Chemie, Weinheim.

Har-El, R., and M. L. Tanzer. 1993. Extracellular matrix 3: Evolution of the extracellular matrix in invertebrates. *FASEB J.* **7:** 1115–1123.

Hovingh, P., and A. Linker. 1993. Glycosaminoglycans in *Anodonta californiensis,* a freshwater mussel. *Biol. Bull.* **185:** 263–276.

Jeuniaux, C. 1963. *Chitine et Chitinolyse. Un chapitre de la Biologie Moléculaire.* Masson, Paris.

Kabat, E. A., and O. M. Mayer. 1961. *Kabat and Mayer's Experimental Immunochemistry.* Thomas, Springfield, IL.

Keith, J., S. Stockwell, D. Ball, K. Remillard, D. Kaplan, T. Thannhauser, and R. Sherwood. 1993. Comparative analysis of macromolecules in mollusc shells. *Comp. Biochem. Physiol.* **105B:** 487–496.

Kozulic, B., B. Ries, and P. Mildner. 1979. N-Acetylation of amino sugar methyl glycosides for gas-liquid chromatographic analysis. *Anal. Biochem.* **94:** 36–39.

Lev, R., and S. S. Spicer. 1964. Specific staining of sulfate groups with alcian blue at low pH. *Histochem. Cytochem.* **12:** 309.

Mann, S., B. R. Heywood, S. Rajam, and J. D. Birchall. 1988. Controlled crystallization of $CaCO_3$ under stearic acid monolayers. *Nature* **334:** 692–695.

Marxen, J., and W. Becker. 1997. The organic shell matrix of the freshwater snail *Biomphalaria glabrata. Comp. Biochem. Physiol.* **118B:** 23–33.

Poulicek, M., M. F. Voss-Foucart, and C. Jeuniaux. 1991. Regressive shell evolution among opisthobranch gastropods. *Malacologia* **32:** 223–232.

Samata, T., and G. Krampitz. 1982. Ca^{2+}-binding polypeptides in oyster shells. *Malacologia* **22:** 225–233.

Scott, J. E., and J. Dorling. 1965. Differential staining of acid glycosaminoglycans (mucopolysaccharides) by alcian blue in salt solution. *Histochemistry* **5:** 221–233.

Simkiss, K. 1965. The organic matrix of the oyster shell. *Comp. Biochem. Physiol.* **16:** 427–435.

Standen, O. D. 1951. Some observations upon the maintenance of *Australorbis glabratus* in the laboratory. *Ann. Trop. Med. Parasitol.* **45:** 80–83.

Sweeley, C. C., R. Bentley, M. Makita, and W. W. Wells. 1963. Gas-liquid chromatography of trimethylsilyl derivatives of sugars and related substances. *J. Am. Chem. Soc.* **85:** 2497–2507.

Timmermanns, L. P. M. 1969. Studies on shell formation in molluscs. *Neth. J. Zool.* **19:** 417–523.

Volpi, N. 1996. Electrophoresis separation of glycosaminoglycans on nitrocellulose membranes. *Anal. Biochem.* **240:** 114–118.

Waite, J. H. 1984. Quinone-tanned scleroproteins. Pp. 467–504 in *The Mollusca, Vol 1: Metabolic Biochemistry and Molecular Biomechanics,* P. W. Hochachka, ed. Academic Press, San Diego, CA.

Watabe, N. 1984. Shell. Pp. 448–485 in *Biology of the Integument, Vol. 1: Invertebrates,* J. Bereiter-Hahn, A. G. Matoltsy, and K. S. Richards, eds. Springer-Verlag, Berlin.

Weiner, S., and W. Traub. 1984. Macromolecules in mollusc shells and their functions in biomineralization. *Philos. Trans. R. Soc. Lond. B* **304:** 425–434.

Wheeler, A. P., and C. S. Sikes. 1989. Matrix-crystal interactions in $CaCO_3$ biomineralization. Pp. 95–131 in *Biomineralization—Chemical and Biochemical Perspectives,* S. Mann, J. Webb, and R. J. P. Williams, eds. VCH, New York.

Wilbur, K. M. 1964. Shell formation and regeneration. Pp. 243–282 in *Physiology of the Mollusca,* Vol. 1, K. M. Wilbur and C. M. Yonge, eds. Academic Press, New York.

Wilbur, K. M. 1976. Recent studies of invertebrate mineralization. Pp. 79–108 in *The Mechanisms of Mineralization in the Invertebrates and Plants,* N. Watabe and K. M. Wilbur, eds. The University of South Carolina Press, Columbia.

Worms, D., and S. Weiner. 1986. Mollusc shell organic matrix: Fourier transform infrared study of the acidic macromolecules. *J. Exp. Zool.* **237:** 11–20.

Wu, A. M., S. Sugii, and A. Herp. 1988. A table of lectin carbohydrate specificities. Pp. 723–740 in *Lectins—Biology, Biochemistry, Clinical Biochemistry,* Vol 6, T. C. Bög-Hansen and D. L. J. Freed, eds. Sigma Chem. Comp., St. Louis, Missouri.

Optical Microscopy and Imaging in the Biomedical Sciences

October 7 – October 15, 1998

Application Deadline:
August 4, 1998

Admission to MBL courses is competitive; student selection is determined by review committees appointed for each individual course.

Course Fee:
1998 course fee to be determined. 1997 course fee was $1,950 with room & board provided at no additional charge.

For application forms and information, contact:
Carol Hamel
Admissions Coordinator
Marine Biological Laboratory
7 MBL Street
Woods Hole, MA 02543-1015
(508) 289-7401
<admissions@mbl.edu>
WWW: http://www.mbl.edu

This course is designed primarily for research scientists, physicians, postdoctoral trainees, and advanced graduate students in animal, plant, medical, and material sciences. Non-biologists seeking a comprehensive introduction to microscopy and video imaging will benefit greatly from the course. There are no specific prerequisites, but an understanding of the basic principles of optics is desirable. Limited to 24 students.

Topics to be covered include:

- principles of microscope design and image formation
- bright and dark-field, phase contrast, polarized light, differential interference contrast, interference reflection, and fluorescence microscopy
- confocal scanning microscopy, multiphoton excitation fluorescence microscopy, digital image restoration, and 3-D reconstruction
- video imaging, recording, enhancement, and intensification
- analog and digital image processing and analysis
- fluorescent probes and ratiometric-imaging
- use of laser tweezers and scissors

Application of the optical methods to live cells will be emphasized. Other specimens will also be covered.

Director: Colin S. Izzard, State University of New York, Albany.

Faculty: Robert Hard, SUNY, Buffalo; Brian Herman, University of North Carolina; Frederick R. Maxfield, Cornell University; John M. Murray, University of Pennsylvania; John W. Sedat, University of California, San Francisco; Kenneth R. Spring, NIH; and others to be named.

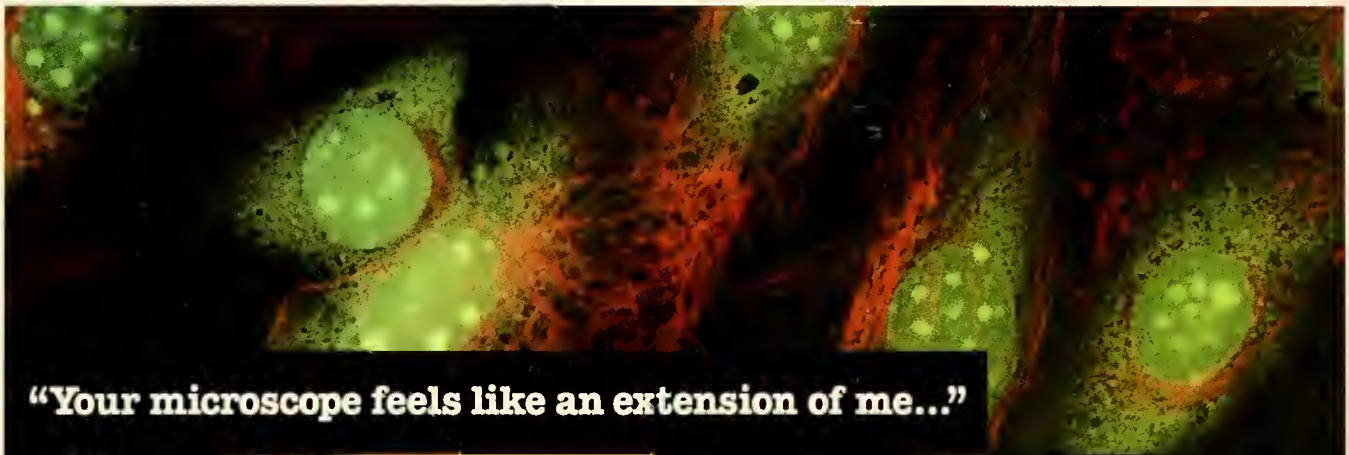

"Your microscope feels like an extension of me..."

Ask any researcher about the Olympus line of Advanced Research Microscopes.

We did.

"The Provis Microscope simply gives me the application versatility I want," one researcher told us. "The resolution and contrast are quite spectacular. I can even see new detail when I review my older specimens. And you have all the right imaging modules and accessories I need to configure my microscope system. Your special fluorescence-excitation balancer, for instance, is a great accessory—I can now visually balance the signal between two probes!"

What about your needs? If your field is neuroscience, our BX50WI offers you the best stability and a focus mechanism that moves nothing but the nosepiece. On the other hand, your research may call for our new LSM Fluoview desktop confocal laser system. Or you may need the unparalleled light transmission of the iX70 inverted.

Whichever microscope you select, it's totally configurable to your personal specifications. So find out how our advanced microscope systems can match your requirements today and evolve for your changing needs tomorrow. Call us at 1-800-455-3236. Or fax 1-612-942-6340. We'll give you all the answers you can ask for.

OLYMPUS

RESEARCH MICROSCOPES.

The world's most custom-built microscopes.

Volume 194 Number 3

THE BIOLOGICAL BULLETIN

JUNE, 1998

Published by the Marine Biological Laboratory

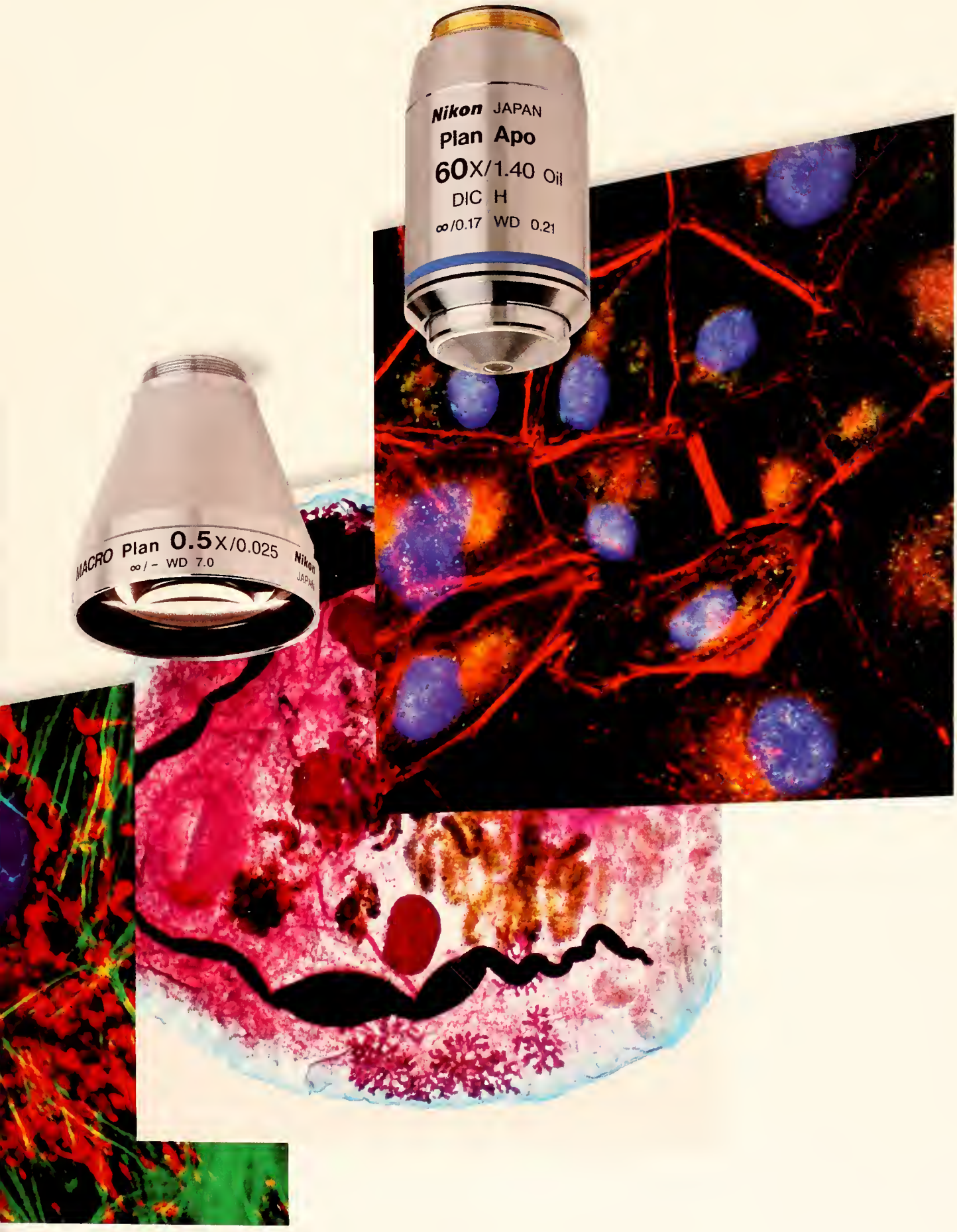
Nikon JAPAN
Plan Apo
60X/1.40 Oil
DIC H
∞/0.17 WD 0.21
MACRO Plan 0.5X/0.025
∞/- WD 7.0
Nikon
JAPAN

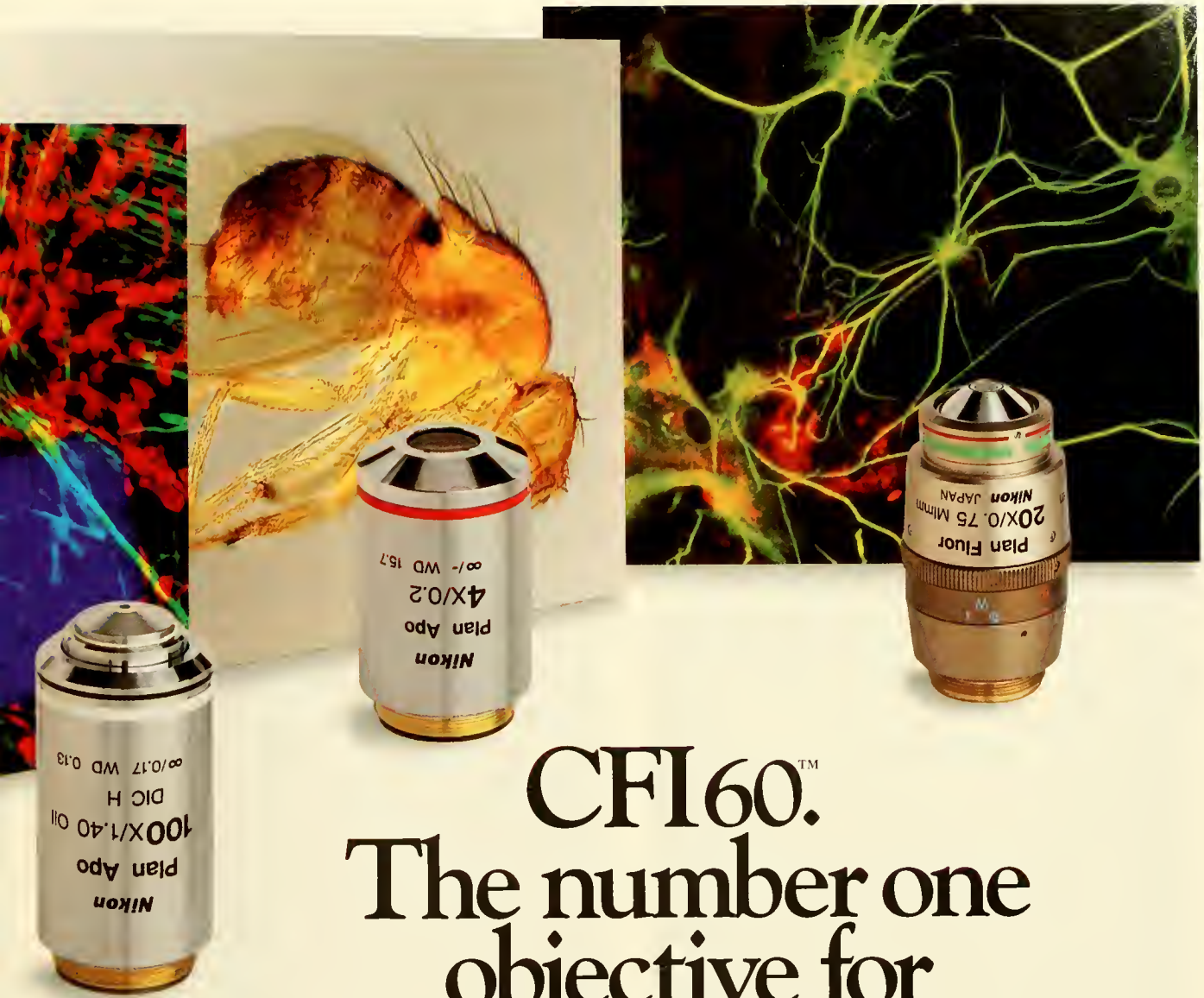

CFI60.™ The number one objective for every objective.

CFI60 ECLIPSE

The Nikon Eclipse E800™ is America's number one selling research microscope in its class.* What's the secret of our success?

Our CFI60 Technology.

The CFI60 chromatic aberration-free objectives have overcome the limitations of conventional infinity systems — with the longest working distances, highest numerical apertures, and the widest magnification range and documentation field sizes ever. Nikon's advanced technology in glass formulation, lens manufacture and coating processes have redefined infinity optics. With this technology, we have achieved higher performance levels by incorporating a 60mm objective parfocal distance, a 25mm objective thread size and a standard 25mm field of view.

Enjoy the widest range in objectives for the most diverse observation requirements.

With over 80 Nikon CFI60 objectives, including our exclusive 0.5X and the high UV transmission universal Plan Fluor series, you'll find we have the lens for you. Also available are several objectives for techniques such as confocal, microinjection and detection of GFP expression that can be utilized for phase contrast, DIC, fluorescence and brightfield. Call **1-800-52-NIKON, ext 331** today for a demonstration of our CFI60 objectives, and you'll soon find the best objective to meet your objective.

www.nikonusa.com

Nikon

Redefining Infinity

*Based on the Opto-Precision Instruments Association's (OPIA) Fourth Qtr. 1997, U.S.A. Microscope Survey

THE
BIOLOGICAL BULLETIN

PUBLISHED BY

THE MARINE BIOLOGICAL LABORATORY

JUNE, 1998

Printed and Issued by
LANCASTER PRESS, Inc.
3575 HEMPLAND ROAD
LANCASTER, PA

Cover

Top: A specimen of a sea cucumber, *Stichopus japonicus*. The animal's body wall comprises a thin epidermis covering a thick, collagenous, connective tissue dermis. The mechanical properties of the dermis—reflecting the viscosity of its extracellular materials—are variable and under neural control. Neuropeptides play an important role in this regulation, and now peptides that change the stiffness of the dermis have been isolated from *S. japonicus* and chemically characterized (see Birenheide *et al.*, this issue).

Bottom: The spectacular changes in mechanical properties characteristic of the holothurian dermis are illustrated in two photographs, taken at an interval of one minute. At left is the sea cucumber *Stichopus chloronotus* in its stiff state; mechanical stimulation is being applied by rubbing between the hands. At right, the same animal is seen a minute later in its relaxed state; with continued rubbing, the dermis has softened so much that the sea cucumber appears to have "melted." The hands applying the stimulation are those of Professor Tatsuo Motokawa, who has been studying the variable connective tissue of echinoderms for nearly 20 years.

CONTENTS

Intermediate Filaments, Hemidesmosomes, and Desmosomes

Biological Interactions of the Cytoskeleton

Biochemical Properties of the Cytoskeleton

* * *

THE BIOLOGICAL BULLETIN

THE BIOLOGICAL BULLETIN is published six times a year by the Marine Biological Laboratory, 7 MBL Street, Woods Hole, Massachusetts 02543.

Subscriptions and similar matter should be addressed to Subscription Manager, THE BIOLOGICAL BULLETIN, Marine Biological Laboratory, 7 MBL Street, Woods Hole, Massachusetts 02543. Subscription per year (six issues, two volumes): $195 for libraries; $95 for individuals. Subscription per volume (three issues): $97.50 for libraries; $50 for individuals. Back and single issues (subject to availability): $40 for libraries; $20 for individuals.

Communications relative to manuscripts should be sent to Michael J. Greenberg, Editor-in-Chief, or Pamela L. Clapp, Managing Editor, at the Marine Biological Laboratory, 7 MBL Street, Woods Hole, Massachusetts 02543. Telephone: (508) 289-7428. FAX: 508-457-1924. E-mail: pclapp@mbl.edu.

http://www.mbl.edu/BiologicalBulletin/

The home page for the electronic companion to THE BIOLOGICAL BULLETIN—*the Marine Models Electronic Record*—and other BIOLOGICAL BULLETIN publications is available on the World Wide Web at the address shown above.

THE BIOLOGICAL BULLETIN is indexed in bibliographic services including *Index Medicus* and MEDLINE, *Chemical Abstracts, Current Contents, CABS (Current Awareness in Biological Sciences),* and *Geo Abstracts.*

Printed on acid free paper,
effective with Volume 180, Issue 1, 1991.

POSTMASTER: Send address changes to THE BIOLOGICAL BULLETIN, Marine Biological Laboratory, 7 MBL Street, Woods Hole, MA 02543.

Periodicals postage paid at Woods Hole, MA, and additional mailing offices.
ISSN 0006-3185

INSTRUCTIONS TO AUTHORS

The Biological Bulletin accepts outstanding original research reports of general interest to biologists throughout the world. Papers are usually of intermediate length (10–40 manuscript pages). A limited number of solicited review papers may be accepted after formal review. A paper will usually appear within four months after its acceptance.

Very short, especially topical papers (less than 9 manuscript pages including tables, figures, and bibliography) will be published in a separate section entitled "Research Notes." A Research Note in *The Biological Bulletin* follows the format of similar notes in *Nature.* It should open with a summary paragraph of 150 to 200 words comprising the introduction and the conclusions. The rest of the text should continue on without subheadings, and there should be no more than 30 references. References should be referred to in the text by number, and listed in the Literature Cited section in the order that they appear in the text. Unlike references in *Nature,* references in the Research Notes section should conform in punctuation and arrangement to the style of recent issues of *The Biological Bulletin.* Materials and Methods should be incorporated into appropriate figure legends. See the article by Lohmann *et al.* (October 1990, Vol. **179:** 214–218) for sample style. A Research Note will usually appear within two months after its acceptance.

The Editorial Board requests that regular manuscripts conform to the requirements set below; those manuscripts that do not conform will be returned to authors for correction before review.

1. ***Manuscripts.*** Manuscripts, including figures, should be submitted in triplicate. (Xerox copies of photographs are not acceptable for review purposes.) The submission letter accompanying the manuscript should include a telephone number, a FAX number, and (if possible) an E-mail address for the corresponding author. The original manuscript must be typed in no smaller than 12 pitch or 10 point, using double spacing (*including* figure legends, footnotes, bibliography, etc.) on one side of 16- or 20-lb. bond paper, 8 by 11 inches. Please, no right justification. Manuscripts should be proofread carefully and errors corrected legibly in black ink. Pages should be numbered consecutively. Margins on all sides should be at least 1 inch (2.5 cm). Manuscripts should conform to the *Council of Biology Editors Style Manual,* 5th Edition (Council of Biology Editors, 1983) and to American spelling. Unusual abbreviations should be kept to a minimum and should be spelled out on first reference as well as defined in a footnote on the title page. Manuscripts should be divided into the following components: Title page, Abstract (of no more than 200 words), Introduction, Materials and Methods, Results, Discussion, Acknowledgments, Literature Cited, Tables, and Figure Legends. In addition, authors should supply a list of words and phrases under which the article should be indexed.

2. ***Title page.*** The title page consists of a condensed title or running head of no more than 35 letters and spaces, the manuscript title, authors' names and appropriate addresses, and footnotes listing present addresses, acknowledgments or contribution numbers, and explanation of unusual abbreviations.

3. ***Figures.*** The dimensions of the printed page, 7 by 9 inches, should be kept in mind in preparing figures for publication. We recommend that figures be about 1 times the linear dimensions of the final printing desired, and that the ratio of the largest to the smallest letter or number and of the thickest to the thinnest line not exceed I:1.5. Explanatory matter generally should be included in legends, although axes should always be identified on the illustration itself. Figures should be prepared for reproduction as either line cuts or halftones. Figures to be reproduced as line cuts should be unmounted glossy photographic reproductions or drawn in black ink on white paper, good-quality tracing cloth or plastic, or blue-lined coordinate paper. Those to be reproduced as halftones should be mounted on board, with both designating numbers or letters and scale bars affixed directly to the figures. All figures should be numbered in consecutive order, with no distinction between text and plate figures and cited, in order, in the text. The author's name and an arrow indicating orientation should appear on the reverse side of all figures.

Color: The Biological Bulletin will publish color figures and plates, but must bill authors for the actual additional cost of printing in color. The process is expensive, so authors with more than one color image should—consistent with editorial concerns, especially citation of figures in order—combine them into a single plate to reduce the expense. On request, when supplied with a copy of a color illustration, the editorial staff will provide a pre-publication estimate of the printing cost.

4. ***Tables, footnotes, figure legends, etc.*** Authors should follow the style in a recent issue of *The Biological Bulletin* in preparing table headings, figure legends, and the like. Because of the high cost of setting tabular material in type, authors are asked to limit such material as much as possible. Tables, with their headings and footnotes, should be typed on separate sheets, numbered with consecutive Roman numerals, and placed after the Literature Cited. Figure legends should contain enough information to make the figure intelligible separate from the text. Legends should be typed double spaced, with consecutive Arabic numbers, on a separate sheet at the end of the paper. Footnotes should be limited to authors' current addresses, acknowledgments or contribution numbers, and explanation of unusual abbreviations. All such footnotes should appear on the title page. Footnotes are not normally permitted in the body of the text.

5. ***Literature cited.*** In the text, literature should be cited by the Harvard system, with papers by more than two authors cited as Jones *et al.*, 1980. Personal communications and material in preparation or in press should be cited in the text only, with author's initials and institutions, unless the material has been formally accepted and a volume number can be supplied. The list of references following the text should be headed Literature Cited, and must be typed double spaced on separate pages, conforming in punctuation and arrangement to the style of recent issues of *The Biological Bulletin*. Citations should include complete titles and inclusive pagination. Journal abbreviations should normally follow those of the U. S. A. Standards Institute (USASI), as adopted by BIOLOGICAL ABSTRACTS and CHEMICAL ABSTRACTS, with the minor differences set out below. The most generally useful list of biological journal titles is that published each year by BIOLOGICAL ABSTRACTS (BIOSIS List of Serials; the most recent issue). Foreign authors, and others who are accustomed to using THE WORLD LIST OF SCIENTIFIC PERIODICALS, may find a booklet published by the Biological Council of the U.K. (obtainable from the Institute of Biology, 41 Queen's Gate, London, S.W.7, England, U.K.) useful, since it sets out the WORLD LIST abbreviations for most biological journals with notes of the USASI abbreviations where these differ. CHEMICAL ABSTRACTS publishes quarterly supplements of additional abbreviations. The following points of reference style for THE BIOLOGICAL BULLETIN differ from USASI (or modified WORLD LIST) usage:

A. Journal abbreviations, and book titles, all underlined (for *italics*)

B. All components of abbreviations with initial capitals (not as European usage in WORLD LIST *e.g., J. Cell. Comp. Physiol.* NOT *J. cell. comp. Physiol.*)

C. *All* abbreviated components must be followed by a period, whole word components *must not* (*i.e., J. Cancer Res.*)

D. Space between all components (*e.g., J. Cell. Comp. Physiol.*, not *J.Cell.Comp.Physiol.*)

E. Unusual words in journal titles should be spelled out in full, rather than employing new abbreviations invented by the author. For example, use *Rit Vísindafjélags Islendinga* without abbreviation.

F. All single word journal titles in full (*e.g., Veliger, Ecology, Brain*).

G. The order of abbreviated components should be the same as the word order of the complete title (*i.e., Proc.* and *Trans.* placed where they appear, not transposed as in some BIOLOGICAL ABSTRACTS listings).

H. A few well-known international journals in their preferred forms rather than WORLD LIST or USASI usage (*e.g., Nature, Science, Evolution* NOT *Nature, Lond., Science, N.Y.; Evolution, Lancaster, Pa.*)

6. ***Reprints, page proofs, and charges.*** Authors of articles in black and white (no color figures) receive their first 50 reprints (without covers) free of charge. Color reprints and additional black-and-white reprints may be purchased; authors will receive order forms. Reprints normally will be delivered about 2 to 3 months after the issue date. Authors (or delegates for foreign authors) will receive page proofs of articles shortly before publication. They will be charged the current cost of printers' time for corrections to these (other than corrections of printers' or editors' errors). Other than these charges for authors' alterations, *The Biological Bulletin* does not have page charges.

VOLUME CONTENTS

No. 1, February 1998

No. 2, April 1998

No. 3, June 1998

Physical Properties of the Cytoskeleton

Structural, Mechanical, and Biological Properties of the Cytoskeleton

Microtubules and Viscoelasticity of Actin

Intermediate Filaments, Hemidesmosomes, and Desmosomes

Biological Interactions of the Cytoskeleton

Biochemical Properties of the Cytoskeleton

* * *

Reference: *Biol. Bull.* **194:** 241–243. (June, 1998)

Evolutionary Implications of FGF and Distal-Less Expressions During Proximal-Distal Axis Formation in the Ampulla of a Direct-Developing Ascidian, *Molgula pacifica*

WILLIAM R. BATES

Bamfield Marine Station, Bamfield, British Columbia, Canada VOR 1BO, and the Department of Biology, University of Victoria, Victoria, British Columbia, Canada V8W 2Y2

The present results provide the first evidence of a fibroblast growth factor (FGF) family protein in a urochordate. Anti-FGF2 immunoreactive hemoblast cells were detected at day 3 of juvenile development in a direct-developing urochordate ascidian, Molgula pacifica. *The detection of FGF in hemoblast cells coincided with the appearance of distal-less protein along the proximal-distal axis of growing ampullae. Ampullae are limb-like, fluid-filled ectodermal appendages that contain hemoblast cells and have holdfast, respiratory, and immunological functions (1). Given the evolutionary conservation of the genes encoding FGF (2), their receptors (2), and distal-less (3), the present results suggest that the formation of non-homologous ascidian appendages shares genetic elements in common with proximal-distal axis formation in arthropod limbs and vertebrate limbs (4,5). The possible evolutionary implications of these findings are discussed.*

Members of the fibroblast growth factor (FGF) family of proteins have multiple functions in organizing the patterns of diverse kinds of tissues.[2] One member of this family, FGF2, has been implicated in mesoderm induction in amphibians (6) and in the initiation of limb development in chick embryos (7) and in mouse embryos (8,9). FGF2 does not function alone, but acts with other regulatory molecules including Wg/Wnt (7). In *Drosphilia,* it was recently reported that Wg can induce distal-less, a highly conserved homeoprotein, during the proximal-distal outgrowth of a fly's leg (4). Distal-less is a highly conserved gene that functions in the development of diverse kinds of appendages from onychophoran lobopods to mammalian limbs, and this gene is thought to have evolved in the pre-Cambrian ancestor of protostomes and deuterostomes (3).

In the present study, juveniles of the invertebrate ascidian chordate *Molgula pacifica* (belonging to the subphylum Urochordata), in which five ectodermal ampullar appendages grow out from the body wall of an early juvenile, were examined for two proteins that are known to be involved in the outgrowth of arthropod and vertebrate limbs. Histological sections of *M. pacifica* juveniles were stained with FGF2 antibody at days 2, 3, 4, and 5 of development. Anti-FGF2 staining was first observed at day 3 of development, exclusively in newly formed hemoblast cells, and the detection of these cells coincided with the appearance of distal-less proteins expressed along the proximal-distal axis of growing ampullae (Fig. 1A, B; Table I).

Prior to hemoblast cell formation, anti-FGF2 stained cells were not detected (50 serially sectioned juveniles were examined), and anti-EGF immunoreactive cells were not observed at day 2 or day 5 of development (30 serially sectioned juveniles were examined). Anti-FGF2 staining intensified in a subpopulation of hemoblast cells at days 4 and 5 of development (Fig. 1C). At day 5, the average number of hemoblast cells stained with FGF2 antibody was three to four cells per juvenile (a total of 132 juveniles were serially sectioned and stained with FGF2 antibody).

This is the first report in which an endogenous growth factor belonging to the FGF superfamily has been detected in a urochordate. Furthermore, the present results demonstrate that anti-FGF2 staining is restricted to hemoblast cells. In an indirect-developing ascidian, hemoblast

Received 1 October 1997; accepted 2 March 1998.
E-mail: bbates@bms.bc.ca

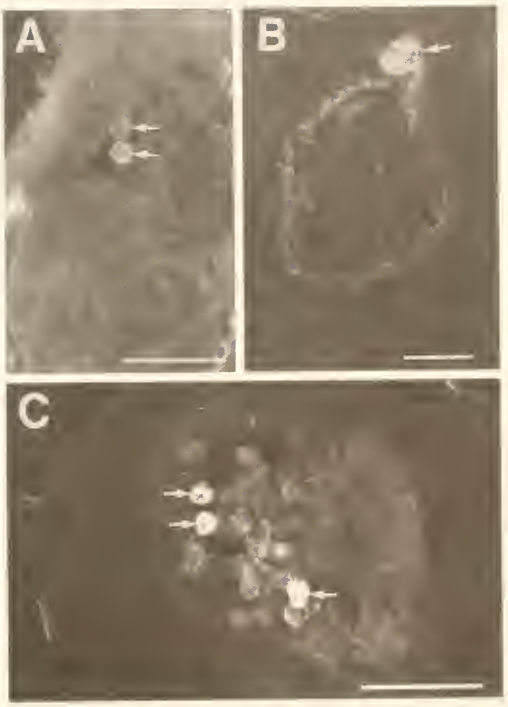

Figure 1. Immunocytochemical detection of FGF and distal-less proteins during the proximal-distal outgrowth of *Molgula pacifica* ampullae. *M. pacifica* adults were collected by scuba in the Barkley Sound region located along the west coast of Vancouver Island, British Columbia, Canada, near Bamfield Marine Station, Bamfield, British Columbia. Sperm and oocytes were obtained by the dissection of gonads. Oocytes were washed with large volumes of seawater and allowed to undergo germinal vesicle breakdown in seawater prior to their insemination with non-self sperm. Fertilized eggs were washed with large volumes of seawater and cultured at 11°C in glass Syracuse dishes on sea tables containing fresh, flowing seawater. *M. pacifica* juveniles at days 2, 3, 4, and 5 of development were fixed for 20 minutes in absolute methanol at −20°C followed by a 20-minute immersion in absolute ethanol at −20°C and then embedded in polyester wax for sectioning. Embedded specimens were cut into 8-μm-thick sections and floated on distilled water droplets placed on gelatin-coated shards of glass. After the sections dried overnight at room temperature, they were de-waxed and equilibrated with phosphate buffered saline (PSB) by immersing the shards with adhered sections through a graded series of ethanol followed by three washes with PBS. Prior to immersion into antibody solutions, sections were immersed in a blocking solution (1% BSA (Sigma Chemical Company) in PBS) for 30 min at room temperature. Shards with adhered sections were transferred to a moist chamber for antibody incubations. Anti-bovine FGF2 antibody was purchased from Sigma Chemical Company and diluted 1:60 with PBS containing 0.5% BSA. Sections stained with primary antibody for 1 h at room temperature in a moist chamber were immersed in FITC-labeled anti-rabbit secondary antibody diluted 1:60 with PBS. Bovine FGF2 was purchased from Sigma Chemical Company to preabsorb anti-FGF2 prior to immunochemistry for a control experiment. Sections probed with anti-FGF2 that was preabsorbed with FGF2 showed no fluorescence. Epidermal growth factor antibody was purchased from Sigma Chemical Company and diluted 1:60 with PBS containing 0.5% BSA. EGF incubation times and detection methods were the same as those used for the detection of FGF2. The distal-less antibody, kindly provided by Dr. Grace Panganiban, was used as previously described by Panganiban *et al.* (3), except that the specimens were fixed in methanol and ethanol, sectioned, and the primary antibody was detected using FITC-secondary antibody. Fluorescence was not detected when sections were incubated in secondary antibody without prior treatment with the primary antibody.

(A) Sections through a day 3 juvenile showing anti-FGF2 immunoreactive hemoblast cells (see arrows) situated within the hemocoel and (B) a day 3 ampulla (see arrow) stained with distal-less antibody. (C) Section through a day 5 juvenile showing intense anti-FGF2 stained hemoblast cells (see arrows). Scale bars in each frame equal 50 μm.

Table I

Hemoblast cell-specific immunoreactivity using anti-FGF2 in Molgula pacifica *juveniles*

Antibody	Stage (Day)	Cell type* and staining†				
		me	tu	ae	hb	ccm
FGF2	2	−	−	−	−	−
	3	−	−	−	+	−
	4	−	−	−	++	−
	5	−	−	−	+++	−
EGF	2	−	−	−	−	−
	5	−	−	−	−	−

* Me, mantle epidermis; tu, tunic; ae, ampullar epidermis; hb, hemoblast cells; ccm, central cell mass.

† −, unstained; +, weak staining; ++, intermediate staining; +++, intense staining.

cells were shown to be derived from larval trunk lateral cells (TLCs), decendents of the A7.6 lineage of a 110-celled embryo (10). Cell lineage studies, now in progress, will examine whether the anti-FGF2 immunoreactive hemoblast cells are derived from the A7.6 lineage or from another cell lineage of *M. pacifica* embryos.

The results of a previous experiment suggest that FGF may play a role earlier in ascidian development (11). When notochord progenitor cells were isolated from embryos and then immersed in FGF2, some of the descendants of these cells expressed a notochord-specific protein, termed "Not-1." Although these results suggest that FGF2 receptors may be present in notochord cells of indirect-developing embryos, it was not reported whether endogenous FGF2 actually exists in the embryo at the time of notochord induction. In *M. pacifica*, detailed light and electron microscopy studies failed to detect the presence of a notochord placode (12,13). The absence of this structure suggests that notochord cell fates were eliminated in this species, an event that may have been caused by a modification of an FGF-mediated inductive interaction, if it is assumed that the ancestor of *M. pacifica* was an indirect-developer.

Several intriguing evolutionary questions are raised by the present results. What are these conserved regulatory proteins for limb development doing in presumably non-homologous, limb-like ampullae? One possibility is that urochordate FGF and distal-less proteins, along with other limb-patterning regulatory proteins, repre-

sent some of the ancestral vertebrate genetic elements that are utilized in a modified manner during the development of a complex vertebrate limb. As previously described in detail (1), hemoblast cells are pumped into the lumen of growing ampullae by rhythmic contraction waves generated by the ampullar walls, and hemoblast cells are often observed in the tip region of ampullae. These contractions may bring FGF into close proximity with target FGF receptors that may be present on ampulla ectoderm cells. FGF may function as a mitogen along with distal-less and other regulatory proteins to promote ampullar outgrowth and patterning. A direct comparison can be made with limb development in salamanders. Mullen *et al.* (14) showed that the apical ectodermal cap cells of a salamander limb transcribe large amounts of Dlx3, a homolog of distal-less, and that Dlx3 expression is regulated by FGF2.

A second possibility is that evolutionary co-option for ampulla expression may have occurred in that FGF and distal-less proteins were appropriated for functions other than limb formation during their evolution. The resolution of these questions may be possible when urochordate FGF and distal-less genes are characterized and their signaling pathways, which likely involve other limb-patterning genes, are better understood. In conclusion, the expression of two conserved limb-patterning proteins, FGF and distal-less, during the outgrowth of ascidian ampullae represents an exciting experimental system for investigating the evolutionary development of animal appendages.

Acknowledgments

The author wishes to thank Dr. Grace Panganiban for providing him with the distal-less antibody. This project was supported by an operating grant awarded to the author by the Natural Sciences and Engineering Research Council of Canada.

Literature Cited

1. **Bates, W. R. 1991.** Ampulla morphogenesis in anural and urodele molgulid ascidians. *Dev. Growth Differ.* **33:** 401–411.
2. **Mason, I. J. 1994.** Meeting Review: the ins and outs of fibroblast growth factors. *Cell* **78:** 547–552.
3. **Panganiban, G., S. M. Irvine, C. Lowe, H. Roehl, L. S. Corley, B. Sherbon, J. K. Grenier, J. F. Fallon, J. Kimble, M. Walker, G. A. Wray, B. J. Swalla, M. Q. Martindale, and S. B. Carroll. 1997.** The origin and evolution of animal appendages. *Proc. Natl. Acad. Sci. USA* **94:** 5162–5166.
4. **Lecuit, T., and S. M. Cohen. 1997.** Proximal-distal axis formation in the *Drosophila* leg. *Nature* **388:** 139–145.
5. **Shubin, N., C. Tabin, and S. Carroll. 1997.** Fossils, genes and the evolution of animal limbs. *Nature* **388:** 639–648.
6. **Slack, J. M. W., B. G. Darlington, J. K. Heath, and S. F. Godsave. 1987.** Mesoderm induction in early *Xenopus* embryos by heparin-binding growth factors. *Nature* **326:** 197–200.
7. **Cohn, M. J., J. C. Izpisua-Belmonte, H. Abud, J. K. Heath, and C. Tickle. 1995.** Fibroblast growth factors induce additional limb development from the flank of chick embryos. *Cell* **80:** 739–746.
8. **Peters, K. G., S. Werner, G. Chen, and L. T. Williams. 1992.** Two FGF receptor genes are differentially expressed in epithelial and mesenchymal tissues during limb formation and and organogenesis in the mouse. *Development* **114:** 233–243.
9. **Yamaguchi, T. P., and J. Rossant. 1995.** Fibroblast growth factors in mammalian development. *Curr. Opin. Genet. Dev.* **5:** 485–491.
10. **Nishide, K., T. Nishikata, and N. Satoh. 1989.** A monoclonal antibody specific to embryonic trunk-lateral cells of the ascidian *Halocynthia roretzi* stains coelomic cells of juvenile and adult basophilic blood cells. *Dev. Growth Differ.* **31:** 595–600.
11. **Nakatani, Y., H. Yasuo, N. Satoh, and H. Nishida. 1996.** Basic fibroblast growth factor induces notochord formation and the expression of As-T, a Brachyury homolog, during ascidian embryogenesis. *Development* **122:** 2023–2031.
12. **Bates, W. R., and J. E. Mallett. 1991.** Anural development in the ascidian *Molgula pacifica*. *Can. J. Zool.* **69:** 618–627.
13. **Bates, W. R., and J. E. Mallett. 1991.** Ultrastructural and histochemical study of anural development in the ascidian *Molgula pacifica*. *Roux's Arch. Dev Biol.* **200:** 193–201.
14. **Mullen, L. M., S. V. Bryant, M. A. Torok, B. Blumberg, and D. M. Gardiner. 1996.** Nerve dependency of regeneration: the role of Distal-less and FGF signaling in amphibian limb regeneration. *Development* **122:** 3487–3497.

Reference: *Biol. Bull.* **194:** 244–252. (June, 1998)

Luciferase of the Scyphozoan Medusa *Periphylla periphylla*

OSAMU SHIMOMURA[1,*] AND PER R. FLOOD[2]

[1] *Marine Biological Laboratory, Woods Hole, Massachusetts 02543; Department of Physiology, Boston University School of Medicine, Boston, Massachusetts 02118; and* [2] *Bathybiologica A.S., N-5030 Landås, Bergen, Norway*

Abstract. Two types of luciferase that catalyze the luminescent oxidation of coelenterazine were isolated from the marginal exumbrella epithelium (lappet) and the ovary of *Periphylla periphylla;* they were designated luciferase-L and luciferase-O, respectively. Luciferase-L (M_r 32,000), probably derived from highly specialized photocytes, was very resistant to heat, and its activity was little affected by boiling; but it was unstable in solutions of low ionic strength if bovine serum albumin was not included in the solvent. Luciferase-O (M_r 75,000) occurred in the eggs in association with particulate matter, and was solubilized and extracted with a buffer containing 2 *M* guanidine hydrochloride; the enzyme was highly stable in this strongly denaturing solvent. The intensities of the coelenterazine luminescence catalyzed by both luciferases were maximal at pH 7.8 and in the presence of about 1 *M* NaCl. The quantum yield of coelenterazine was estimated to be 0.14 with luciferase-L (emission max. at 465 nm) and 0.12 with luciferase-O (emission max. at 470 nm). The luminescence caused by both luciferases was strongly inhibited by Cu^{2+} and thiol compounds.

Introduction

All three classes of the phylum Cnidaria contain bioluminescent species. In the class Hydrozoa, all reported cases of luminescence are caused by Ca^{2+}-sensitive photoproteins such as aequorin, found in the jellyfish *Aequorea aequorea* (Shimomura *et al.,* 1962), and obelin, obtained from the hydroid *Obelia* sp. (Morin and Hastings, 1971a, b; Campbell, 1974; Visotskii *et al.,* 1989). In the class Anthozoa, light emission is produced by luciferin-luciferase type reactions, such as those of the sea pansy *Renilla* sp. (Cormier, 1978), the sea cactus *Cavernularia obesa,* and the sea pen *Ptilosarcus gruneyi* (Shimomura and Johnson, 1979). The bioluminescence of the class Scyphozoa has never been biochemically studied. In the phylum Ctenophora, many species are bioluminescent, and two of them—*Mnemiopsis* sp. and *Beroë ovata*—contain Ca^{2+}-sensitive photoproteins, mnemiopsin and berovin, respectively (Ward and Seliger, 1974a, b). These proteins are photosensitive and inactivated by exposure to visible light; thus they are distinctly different from the hydrozoan photoproteins.

The luminophore of the photoprotein-based bioluminescence systems of hydrozoans and ctenophores is coelenterazine (Anctil and Shimomura, 1984; Shimomura, 1985). Moreover, this same compound serves as the luciferin (substrate) in the coelenterazine-luciferase system of the luminescent anthozoans (Shimomura and Johnson, 1975; Cormier, 1978). Although the coelenterazine-luciferase system also occurs in many kinds of luminous organisms, including fishes, shrimps, copepods, squids, and coelenterates (Shimomura *et al.,* 1980; McCapra and Hart, 1980; Campbell and Herring, 1990), coelenterazine luciferase has been isolated and investigated in detail from only two of them: *i.e.,* the sea pansy *Renilla* (Matthews *et al.,* 1977) and the decapod shrimp *Oplophorus* (Shimomura *et al.,* 1978).

In a recent study, the luminescence of the scyphozoan jellyfish *Periphylla periphylla* was found to be associated with two distinct sources: one represented by minute, irregularly shaped cytoplasmic granules in the cortical layer of maturing ovarian eggs; the other represented by clusters of even smaller, mostly spherical grains within the cytoplasm of highly specialized photocytes that are

Received 19 September 1997; accepted 17 March 1998.

* To whom correspondence should be addressed. E-mail: shimomura@mbl.edu

less than 1 mm apart and distributed throughout the exumbrellar epithelium of the medusae (Herring, 1990; Flood *et al.*, 1996). These photocytes are most concentrated along the margin of the umbrella, which is divided into 16 even-sized lappets by deep groves that lead to the bases of 12 tentacles and 4 sensory organs (Russell, 1970).

We have isolated two luciferases that catalyze the luminescent oxidation of coelenterazine. In correspondence with the findings discussed above, one is from the ovary (luciferase-O) and the other from the lappet (luciferase-L). Although these luciferases are not yet completely pure, they have some extraordinary properties. In the present paper, we report the purification method and some of the properties of these unusual luciferases.

Materials and Methods

Specimens of *Periphylla periphylla* were collected individually, at night, from surface waters of the Lurefjorden north of Bergen, Norway, and placed into 10-liter buckets. The collections were made during December 1995 and March 1996 on board the research vessel *Håkon Mosby* (see Fosså, 1992; Flood *et al.*, 1996; Herring *et al.*, 1996). Lappets and ovarian tissue were cut from the medusae with minimal mechanical disturbance and rapidly frozen at −20°C. After the cruise, the tissues were transferred to a −70°C freezer and were stored at that temperature until used. All experiments were performed at room temperature, except as noted. Bovine serum albumin (BSA) was purchased from Calbiochem (La Jolla, CA); KCl and NaCl were from Fisher Scientific (Pittsburgh, PA); guanidine hydrochloride, Tris, and the protein standards for molecular weight determination were from Sigma (St. Louis, MO).

Measurement of luminescence and luciferase activity

Luminescence intensity and total light were measured with a modified MacNichol-type integrating photometer Model 8020 (Pelagic Electronics, Falmouth, MA) calibrated with the *Cypridina* bioluminescence reaction (Shimomura and Johnson, 1970). The determination of luciferase activity was based on the rate of the light emission caused by the addition to a sample of luciferase (2–50 μl) of 3 ml of 20 m*M* Tris-HCl buffer, pH 7.8, containing 1 *M* NaCl, 0.05% BSA, and 5 μl of 0.2 m*M* methanolic coelenterazine ($A_{430\,nm,\,1\,cm}$ 1.8); exceptions are noted. A full-scale deflection of the meter at the highest sensitivity was defined as one light unit (L.U.) and corresponded to 6×10^8 quanta, except as noted.

Purification of Periphylla *luciferase from lappets*

Lappets (100 g) were thawed and homogenized with a Bamix mixer M 122 (Clark National Products, San Dimas, CA) in 130 ml of 0.05% BSA in water. After its pH was adjusted to 7.2, the homogenate was centrifuged, all at 0°C. Most of the luciferase activity was found in the supernatant, and this activity was purified by four steps of chromatography, as follows. Acetate buffer (10 m*M*, pH 4.8) was used as the basic buffer throughout the purification.

First step. The supernatant (220 ml), having a luminescence activity of 100,000 L.U. (light units), was diluted with 3 volumes of the acetate buffer containing 0.05% BSA, then filtered through a column of Toyopearl SP-650M cation exchanger (Supelco, Bellefonte, PA; 2.5 cm × 7 cm). The luciferase, adsorbed at the top part of the column, was eluted by a stepwise increase (0.1 *M* increments) of KCl concentration, from 0.1 *M* to 0.5 *M* in a pH 4.8 acetate buffer containing 0.05% BSA. The effluent was fractionated.

Second step. The fractions containing luciferase activity (30 ml; 75,000 L.U.) were combined, diluted with 200 ml of the acetate buffer containing 0.05% BSA, and filtered through a column of Toyopearl SP-650M (1.5 cm × 5 cm). The luciferase adsorbed was then eluted by an increasing concentration gradient of KCl, from 0.1 *M* to 0.5 *M*, in an acetate buffer lacking BSA. The luciferase fractions were combined, saturated with ammonium sulfate, and centrifuged.

Third step. The precipitate containing luciferase (55,000 L.U.) was dissolved in 1 ml of the acetate buffer and divided into two parts. Each part was chromatographed by gel filtration on a column of Superdex 200 prep (1 cm × 28 cm; Pharmacia); an acetate buffer containing 1 *M* KCl was used as the solvent.

Fourth step. The combined luciferase fraction (35,000 L.U.) was saturated with ammonium sulfate, then centrifuged. The precipitated luciferase was re-chromatographed on the same column and with the same solvent as used in the third step; the elution curve is shown in Figure 1.

Extraction and purification of Periphylla *luciferase from ovary*

The frozen ovaries (10 g) were thawed and homogenized with about 10 volumes of phosphate buffer (pH 7.0), and centrifuged at 5,000 × *g* for 10 min. The precipitate and floating material were discarded; the cloudy supernatant was saved. The supernatant contained luciferase (500,000 L.U.) in two forms: about 20%–25% was in a dissolved form, and the rest was in an insoluble form that was associated with particulate matter. The supernatant was frozen at −70°C, then thawed and centrifuged at 20,000 × *g* for 20 min. The precipitate that contained the insoluble luciferase was suspended in 5 ml of 10 m*M* Tris-HCl buffer, pH 7.5, containing 0.5 *M* NaCl, and then

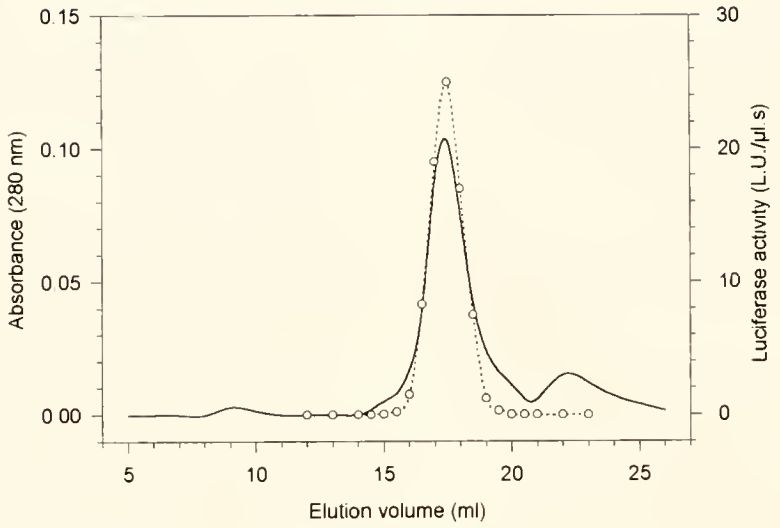

Figure 1. The last step in purification of *Periphylla* luciferase-L on a column of Superdex 200 Prep (1 cm × 28 cm) with 10 m*M* acetate buffer, pH 4.8, containing 1 *M* KCl. Eluent fractions between 16.5 ml and 18 ml were pooled and used as the purified luciferase. Solid line: absorbance measured with a 1-cm light-path cuvette; dotted line: luminescence activity measured at a photometer sensitivity of 3 × 10^9 quanta/L.U.

centrifuged at 20,000 × *g* for 20 min. The supernatant was discarded. The precipitate was mixed with 5 ml of 10 m*M* Tris-HCl buffer, pH 7.7, containing 2 *M* guanidine hydrochloride, 1 *M* KCl and 1% glucose, then sonicated briefly. The mixture, containing a total activity of 350,000 L.U., was centrifuged at 20,000 × *g* for 20 min. The supernatant contained solubilized luciferase (70,000 L.U.), and the precipitate contained the luciferase that remained insoluble (about 200,000 L.U.; not used in the present study). Thus, we estimated that the activity of the insoluble form of luciferase had decreased to about 50% by solubilization. One-fifth of the supernatant (1 ml; 14,000 L.U.) was purified by gel filtration on a column of Superose 6 prep grade (Pharmacia; 1 cm × 19 cm) in 10 m*M* Tris buffer, pH 7.7, containing 2 *M* guanidine hydrochloride, 1 *M* KCl and 0.5% glucose. The elution curve is shown in Figure 2. The gel filtration was repeated four more times to purify the rest of the supernatant.

Results and Discussion

Purification of Periphylla *luciferases*

The luciferase of the lappets (luciferase-L) could easily be extracted with neutral saline solutions. The luciferase activity was sufficiently stable during purification in neutral and acidic media (even at pH 3.0 and below) at 0°C, but was drastically reduced by dilution with water—*i.e.*, by a decrease in the ionic strength. The activity loss was, however, completely prevented, sometimes even reversed, by the addition of 0.05% BSA to the media. The activity of luciferase-L was unstable at a pH higher than 9.0. Thus, the whole process of purification was carried out in a pH 4.8 buffer containing (when appropriate) 1 *M* KCl. In addition, 0.05% BSA was added to the buffer during the cation exchange chromatography as a precaution against inactivation.

The luciferase extracted from the ovary consisted of two types: one was extractable with saline solution and was probably luciferase-L; the other was insoluble in most buffer solutions, even in the presence of 1 *M* KCl, and its activity was associated with tiny particles that were completely retainable on a 0.2-μm filter, but not on a 2-μm filter. The activity of the insoluble enzyme was not easily destroyed by the acidity of pH 1.0, or by a temperature of 90°C. The activity could be extracted from the particles only under very drastic conditions, such as 40% acetonitrile containing 0.2% trifluoroacetic acid; 2% Triton X-100 in 10 m*M* Tris-HCl containing 1 *M* KCl; and 2 *M* guanidine hydrochloride in Tris-HCl buffer containing 1 *M* KCl; but the extraction was partial in all three methods. The last cited solvent was found to be most efficient, solubilizing about 50% of the luciferase activity in one step of extraction; thus, it was used in the present study in the extraction and chromatography of ovarian luciferase (luciferase-O). The relationship between the amount of activity extracted and that retained in the particulate matter indicated that the solubilization causes a decrease of luciferase activity to about half.

The luciferase-L obtained appears to be highly pure on the basis of the chromatogram shown in Figure 1, al-

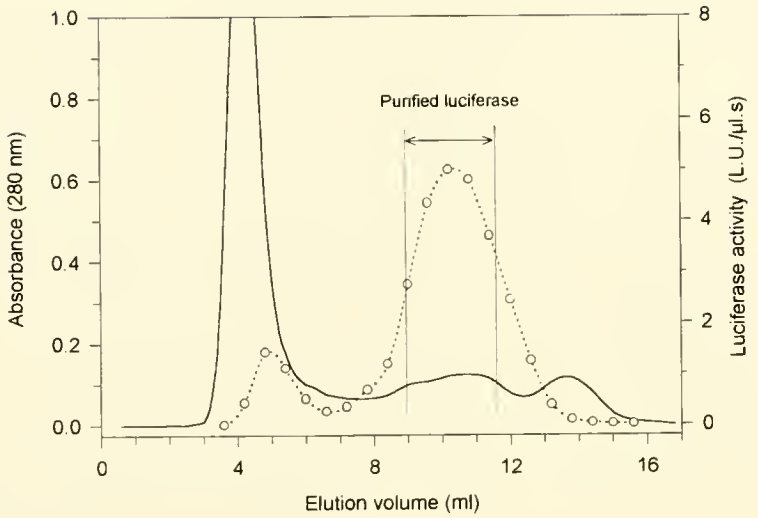

Figure 2. Purification of *Periphylla* luciferase-O by gel filtration on a column of Superose 6 Prep grade (1 cm × 19 cm) using 10 m*M* Tris-HCl buffer, pH 7.7, containing 1 *M* KCl, 2 *M* guanidine hydrochloride, and 0.5% glucose. Solid line: absorbance measured with a 0.5-cm light-path cuvette; dotted line: luminescence activity measured at a photometer sensitivity of 1.1×10^9 quanta/L.U.

though it possibly contained some inactivated luciferase (also see the discussion below in connection with the measurement of quantum yield). The purity of the luciferase-O obtained must be lower than that of the luciferase-L, because the purification method involved only one step of chromatography. The molecular weights of luciferase-L and luciferase-O, as estimated by gel filtration, were about 32,000 and 75,000, respectively (Fig. 3).

Enzymatic properties of the luciferase

The relationship between the intensity of emitted light and the pH of the buffer used (Fig. 4) indicates that

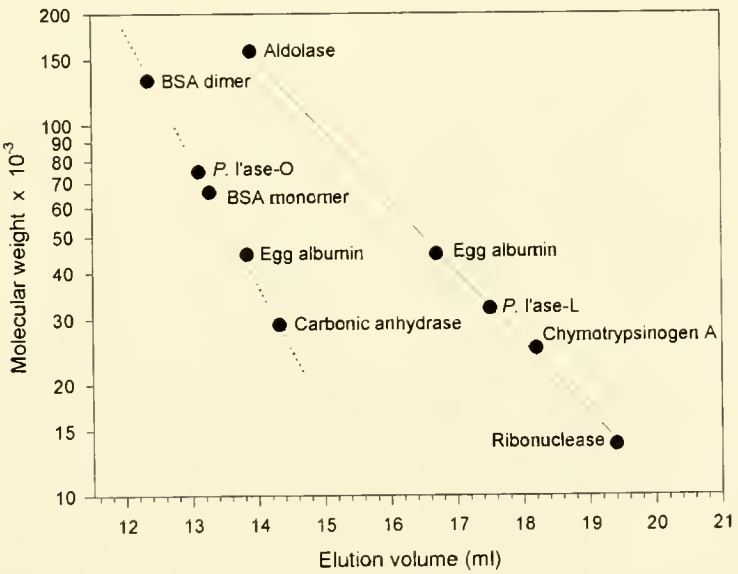

Figure 3. Determination of the molecular weights of luciferase-L (*P.* l'ase-L; solid line) and luciferase-O (*P.* l'ase-O; dotted line) by gel filtration. Luciferase-L was measured on a Superdex 200 Prep column (1 cm × 28 cm) in 10 m*M* acetate buffer, pH 4.8, containing 1 *M* KCl, and luciferase-O on a Superose 6 Prep grade column (1 cm × 21 cm) in 10 m*M* Tris-HCl buffer, pH 7.7, containing 2 *M* guanidine hydrochloride, 1 *M* KCl, and 0.5% glucose. Protein standards used are indicated at appropriate points on the solid and dotted lines.

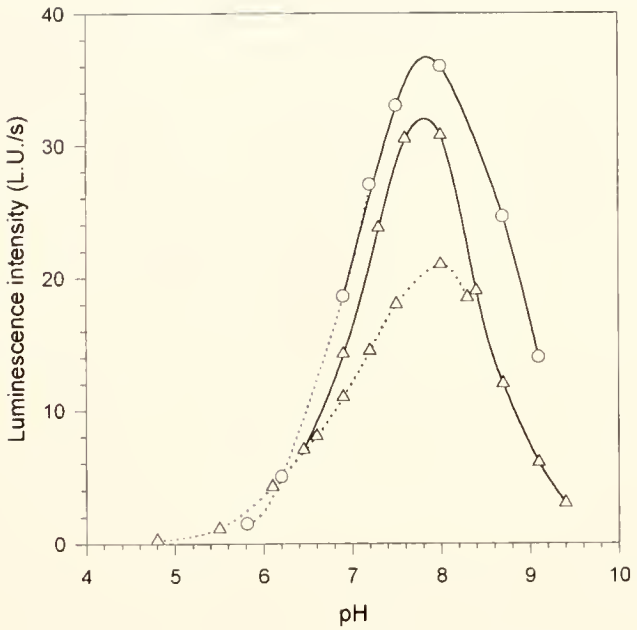

Figure 4. Influence of pH on the intensity of coelenterazine luminescence catalyzed by luciferase-L (○) and luciferase-O (△), in 20 m*M* Tris-HCl buffer containing 1 *M* NaCl (solid lines) and 20 m*M* phosphate buffer containing 1 *M* NaCl (dotted lines); in addition, all solutions used for luciferase-L contained 0.05% BSA.

luminescence intensity is maximal at pH 7.8 for both luciferase-L and luciferase-O. With regard to the effect of salt concentration, the experimental results (Fig. 5) show that luciferase-L has an optimum at about 1 *M* NaCl, whereas the activity of luciferase-O reaches a plateau at about 1 *M* NaCl and stays constant at least up to 3 *M* NaCl. The effect of KCl was essentially the same as that of NaCl. The effect of guanidine hydrochloride was similar when luciferase-O was tested; the optimum concentration was at about 0.6 *M*, indicating that luciferase-O is resistant to this denaturant. In contrast, an increase of guanidine hydrochloride simply decreased the luminescence intensity of luciferase-L, showing no optimum concentration.

The effect of temperature on luciferase-L is highly unusual and intriguing (Fig. 6). The activity of luciferases in catalyzing light emission, *i.e.* luminescence intensity, progressively decreased when the temperature was raised beyond the optimum (about 0°C for luciferase-L; 20°C for luciferase-O), which would be quite normal. In the case of luciferase-L, subsequent cooling of the sample to room temperature (about 25°C) caused an increase of luminescence intensity to the level seen before the temperature was raised. Thus, the inactivation was rapidly reversed upon cooling, so the activity of the luciferase-L was not lost or affected by exposure to the elevated temperature. When a sample was heated at 100°C for 1 min under the conditions described in Figure 6, followed by cooling to room temperature, no loss in the luciferase activity was detected as judged by the intensity of luminescence caused by the addition of coelenterazine; when heated for 15 min at 100°C, the activity decreased by about 20%. Thus, luciferase-L must be a highly thermostable enzyme. The solubilized form of luciferase-O did not have this property, but the insoluble form associated with the particulate matter in the eggs was, like luciferase-L, highly thermostable.

Properties of the luminescence reaction of coelenterazine catalyzed by Periphylla *luciferase*

The spectrum of coelenterazine luminescence catalyzed by luciferase-L (maximum at 465 nm) and that catalyzed by luciferase-O (maximum at 470 nm) are closely similar (Fig. 7). The slight difference found in the emission maxima might indicate that the environment of the coelenterazine binding site is more hydrophobic in luciferase-L molecules than in luciferase-O molecules; this conclusion is based on various data on the emission maximum of aequorin luminescence (Shimomura, 1995a). The slight shoulders seen in the luminescence spectrum measured with purified luciferase-O (550 nm and 620 nm) became much higher and turned into peaks when a less purified preparation was examined (Fig. 7). Probably the peaks were caused by the presence in the sample of unidentified

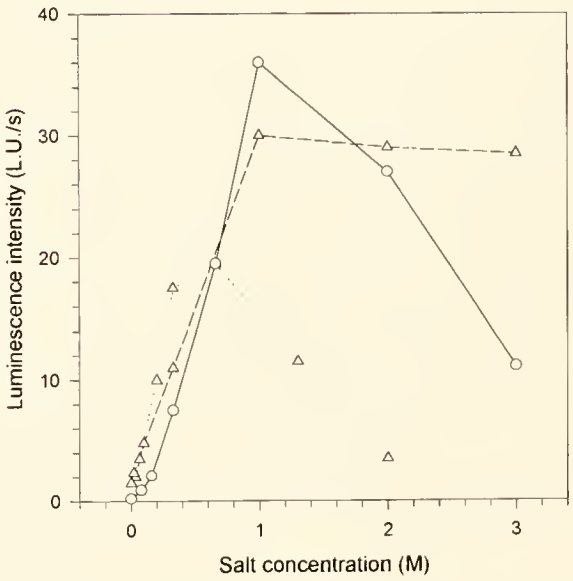

Figure 5. Effect of salt concentration on the intensity of luminescence catalyzed by luciferase-L (○) and luciferase-O (△). Salts used: NaCl, in 20 m*M* Tris-HCl containing 0.05% BSA, pH 7.8 (solid line); NaCl, in 50 m*M* Tris-HCl, pH 7.8 (broken line); guanidine hydrochloride, in 50 m*M* Tris-HCl, pH 7.8 (dotted line).

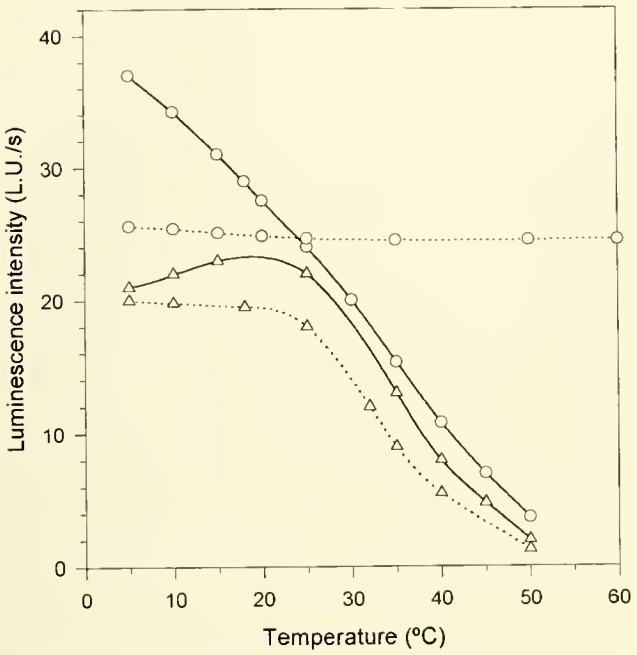

Figure 6. Effect of temperature on the luminescence intensity (solid lines) and the stability of luciferases at various temperatures (dotted lines) in the luminescence of coelenterazine catalyzed by luciferase-L (○) and luciferase-O (△). The luminescence with luciferase-L was measured in 20 m*M* phosphate buffer, pH 7.8, containing 1 *M* NaCl and 0.05% BSA, and the luminescence with luciferase-O was in 10 m*M* phosphate buffer, pH 7.8, containing 1 *M* NaCl. In the measurement of the stability data, the luciferase in the buffer in a test tube was exposed to the indicated temperature for 1 min, then the test tube was equilibrated in a water bath at room temperature for 2–5 min before luminescence was initiated by the addition of coelenterazine.

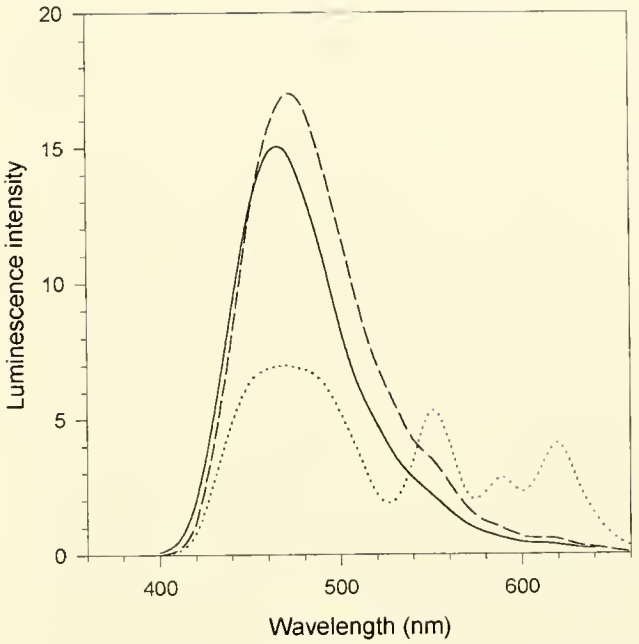

Figure 7. Luminescence spectra of coelenterazine catalyzed by purified *Periphylla* luciferase-L (solid line), purified luciferase-O (broken line), and a crude preparation of luciferase-O (dotted line) in 20 m*M* Tris-HCl buffer, pH 7.8, containing 1 *M* NaCl and 0.05% BSA.

fluorescent substances with corresponding emission maxima. A previously reported observation that the clusters of the grains in the exumbrellar photocytes, but not the grains in the cortex layer of eggs, show a pinkish fluorescence that rapidly fades under UV light (Flood *et al.*, 1996) is apparently not in accord with the present results. One explanation for the discrepancy is that a pink fluorescent substance is more abundant in the lappet photocytes than in the ovarian photocytes, but that the fluorescent substance in lappets easily dissociates from luciferase-L molecules during the extraction process, whereas that in eggs does not dissociate from luciferase-O. In our actual experimental procedure, the lappet fluorescent substance might have dissociated from luciferase-L, even when the frozen lappets were thawed and the cells were broken. In any event, the bioluminescence spectrum of *Periphylla* is probably not affected significantly by these fluorescent substances, because the bioluminescence spectrum of live *Periphylla* was previously reported to be a single peak with a maximum at 470–475 nm (Herring, 1983; Widder *et al.*, 1983).

The luminescence intensity of coelenterazine catalyzed by luciferase was affected by the concentration of coelenterazine up to 3 μM, as shown in Figure 8. From the data in the figure, the Michaelis constant of this enzyme is

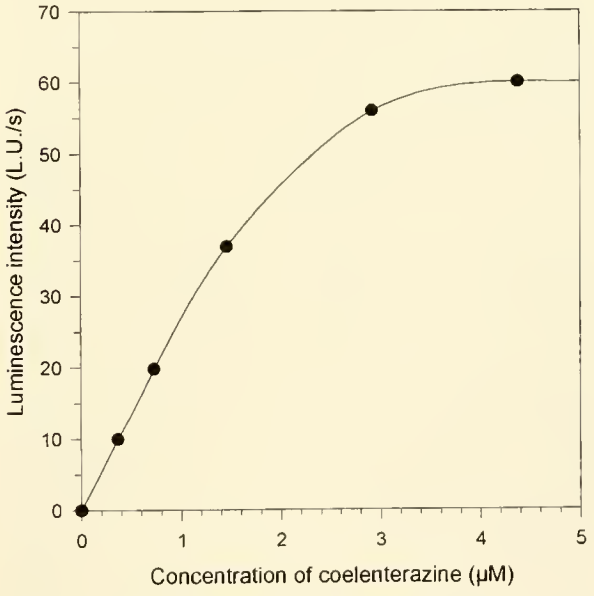

Figure 8. Effect of coelenterazine concentration on the intensity of luminescence when the reaction was catalyzed by *Periphylla* luciferase-L. The concentration of coelenterazine represents the final concentration.

estimated to be about 1.1 μM. The maximum specific activity (the specific activity measured in the presence of a saturating concentration, about 5 μM, of coelenterazine) of the purest luciferase-L preparation was 8.0×10^{13} quanta/mg · s, assuming an $A_{280\,nm,\,1\,cm}$ value of 1.0 for 1 mg/ml solution of this enzyme. For luciferase-O, the Michaelis constant and the maximum specific activity of luciferase-O were estimated to be 0.2 μM and 5.5×10^{12} quanta/mg · s, respectively (data not shown). The activity of luciferase-O is highly variable, dependent on the environment and the composition of buffer solution; the activity is almost certainly much greater in the insoluble form that originally existed in association with particulate matter. In any case, the values given above for specific activity must be considered as minimal values, because the luciferase preparations used were not completely pure. For comparison, the specific activities of *Renilla* luciferase (M_r 35,000; Matthews *et al.*, 1977) and *Oplophorus* luciferase (M_r 130,000; Shimomura *et al.*, 1978) under comparable conditions were 1.9×10^{13} quanta/mg · s and 1.34×10^{14} quanta/mg · s, respectively (Inouye and Shimomura, 1997).

A problem arose in the determination of the quantum yield of coelenterazine in the presence of luciferase-L. The purified luciferase-L apparently contained a trace impurity that inactivated coelenterazine by binding it tightly or by oxidizing it without light emission. This impurity eluted from the Superdex 200 column in the final step of purification (Fig. 1) immediately after the peak of luciferase; thus it could not be completely eliminated from the purified luciferase. The effect of this coelenterazine-inactivating impurity was reduced greatly, but not completely, by heating luciferase-L in the assay buffer at 100°C for 10 min. The complete elimination of the effect of this impurity was achieved only by pretreating the luciferase-L with coelenterazine. Thus, the quantum yield of coelenterazine was measured by repeated additions of a small amount of coelenterazine (5 μl of 0.2 mM methanolic solution) to a solution of luciferase-L; each new addition of coelenterazine was made only after the light emission from the previous addition had been completed. In this way, the total light emitted in each addition of coelenterazine successively increased, reaching a constant, maximum value after five or six additions. The quantum yield of coelenterazine calculated for the last addition was 0.14; this value was taken as the quantum yield of coelenterazine catalyzed by luciferase-L. Luciferase-O contained no significant inhibitor, and the quantum yield of coelenterazine catalyzed by luciferase-O was 0.12. For reference, the quantum yield of coelenterazine in the presence of *Renilla* luciferase was 0.069 (Hart *et al.*, 1979) and 0.11 (Inouye and Shimomura, 1997); the quantum yield in the presence of *Oplophorus* luciferase was 0.34 at 22°C (Shimomura *et al.*, 1978).

Inhibitors of the luminescence reaction

Periphylla luciferase was strongly inhibited in different fashions by two types of compounds, cupric salts and thiol compounds. The inhibition of coelenterazine luminescence by Cu^{2+} was instantaneous and very strong. The luminescence catalyzed by luciferase-L was inhibited by 25% with 10 μM Cu^{2+} and 85% with 30 μM Cu^{2+}; when catalyzed by luciferase-O, the inhibition was 70% with 1 μM Cu^{2+} and 97% with 10 μM Cu^{2+}. Various enzymes are inhibited by heavy metals, but *Periphylla* luciferase was inhibited by Cu^{2+} almost specifically; *i.e.*, much more strongly than by other metals (such as Ba^{2+}, Cd^{2+}, Zn^{2+}, and Pb^{2+}). The significance of this finding is unknown.

The inhibition by thiols is not instantaneous. The loss in the activity of luciferase-L in the presence of 0.3 mM 2-mercaptoethanol was 60% after incubation for 20 h at 0°C; in the presence of 1 mM, the loss was 95%. With luciferase-O, under the same conditions (after 20 h at 0°C), the activity loss was 27% in the presence of 1 mM 2-mercaptoethanol and 92% in the presence of 10 mM. The inhibition was probably caused by the reduction of a functional S-S bond to thiol groups in the luciferase molecules. *Cypridina* luciferase is similarly inhibited by 2-mercaptoethanol (unpubl. data).

Significance of the existence of two different luciferases

To find two or more isoenzymes in a single species of organisms is not unusual. In the case of the hydrozoan jellyfish *Aequorea aequorea*, eight slightly different forms of the photoprotein aequorin have been isolated (Shimomura, 1986), although a photoprotein is not an enzyme in a strict sense. In the case of *Periphylla* luciferase, however, the designation of isoenzymes does not fit well for luciferase-L (M_r 32,000) and luciferase-O (M_r 75,000), because of the large difference in their molecular sizes. Based on their molecular weights, it is possible that luciferase-O is a derivative of luciferase-L; luciferase-O might be a dimer of luciferase-L or a conjugate of luciferase-L and an unrelated protein molecule.

As judged by their light emission, luciferase-L in live specimens of *P. periphylla* exists in photocytes scattered in the exumbrellar epithelium of the dome and lappet, whereas luciferase-O occurs in the cortical layer of eggs (Flood *et al.*, 1996). The bioluminescence response of the exumbrellar photocytes may have some practical functions—serving as a physiologically controlled defense mechanism, for example (Herring *et al.*, 1996); but the possible light emission from the eggs inside the ovaries of the adult medusae is difficult to rationalize. Although these ovaries and eggs are easily visible from below the medusa, light emission has never been observed in response to mechanical and electrical stimuli that readily elicit bioluminescence from the exumbrellar epithelium.

Only strong mechanical stimuli (rough rubbing) or strong osmotic shock (immersion in tap water), which is likely to disrupt the cell membrane, have proven effective in causing the eggs to luminesce (Flood, unpubl. data). The bioluminescence of eggs of certain hydromedusae, such as *Phialidium gregarium* and *Mitrocoma cellularia,* has been reported to rely on photoprotein systems (Freeman and Ridgway, 1987).

In the ovary of *Periphylla,* luciferase-O exists in an insoluble form bound to particulate matter; the enzyme is unusually stable and highly resistant to inactivation under various conditions. Indeed it is far more stable than luciferase-L, luciferase-O (soluble), *Oplophorus* luciferase, or *Renilla* luciferase, under all the conditions tested: heating at 90°C; adding guanidine hydrochloride, detergents, or organic solvents (methanol, ethanol, acetonitrile, etc); and leaving at room temperature for more than 2 weeks. The high stability of the insoluble form of luciferase-O, as well as its insolubility, might have evolved through an adaptation to the fat-rich ovarian environment, for the purpose of preserving the luciferase until oocytes begin to develop and stimulable bioluminescence becomes functional in early embryos.

Conclusions

The bioluminescence system of the scyphozoan jellyfish *Periphylla periphylla* was shown to be a coelenterazine-luciferase system; it is the first fully confirmed example in luminous jellyfishes. The *Periphylla* bioluminescence system is remarkable in two ways: First, the system involves two apparently different luciferases, luciferase-L and luciferase-O, that occur separately in two different types of cells in a single animal. Second, these luciferases are highly resistant to certain drastic processes of inactivation: luciferase-L withstands boiling at 100°C, and luciferase-O functions normally in denaturing environments containing 2 *M* guanidine hydrochloride. This high resistance to inactivation, however, is not indicative of a high stability at normal experimental conditions; the stabilities of luciferase solutions at neutral pH are similar to those of *Oplophorus* luciferase and *Renilla* luciferase when left for an extended period at room temperature (Shimomura, unpubl. data).

The heat resistance of luciferase-L is far greater than that of any luciferase previously known. Most other luciferases, including those of the luminous bacteria, the ostracod *Cypridina,* the limpet *Latia,* and the krill *Euphausia,* are inactivated rapidly and irreversibly between 30°C and 50°C; the most heat-resistant examples known previously are the partially purified preparations of *Oplophorus* luciferase, which withstand temperatures up to about 70°C (Shimomura *et al.,* 1978; Shimomura, 1995b). A structural study of *Periphylla* luciferase molecules, to clarify the cause of their unusual stabilities, together with studies of other luminous scyphozoans such as *Atolla* and *Pelagia,* would be important and interesting next problems.

Acknowledgments

The *Periphylla* material for this work was collected aboard the R/V *Håkon Mosby,* when PRF served as a professor of zoology at the University of Bergen. Financial support was received from the U.S. National Science Foundation (MCB-9303842 and MCB-9403183) and the Norwegian Research Council.

Literature Cited

Anctil, M., and O. Shimomura. 1984. Mechanism of photoinactivation and re-activation in the bioluminescence system of the ctenophore *Mnemiopsis. Biochem. J.* **221:** 269–272.

Campbell, A. K. 1974. Extraction, partial purification and properties of obelin, the calcium-activated luminescent protein from the hydroid *Obelia geniculata. Biochem. J.* **143:** 411–418.

Campbell, A. K., and P. J. Herring. 1990. Imidazopyrazine bioluminescence in copepods and other marine organisms. *Mar. Biol.* **104:** 219–225.

Cormier, M. J. 1978. Comparative biochemistry of animal systems. Pp. 75–108 in *Bioluminescence in Action,* P. J. Herring, ed. Academic Press, London.

Flood, P. R., J.-M. Bassot, and P. J. Herring. 1996. The microscopical structure of the bioluminescence system in the medusa *Periphylla periphylla.* Pp. 149–153 in *Bioluminescence and Chemiluminescence; molecular reporting with photons,* J. W. Hastings, L. J. Kricka, and P. E. Stanley, eds. John Wiley, Chichester.

Fosså, J. H. 1992. Mass occurrence of *Periphylla periphylla* (Scyphozoa, Coronatae) in a Norwegian fjord. *Sarsia* **77:** 237–251.

Freeman, G., and E. B. Ridgway. 1987. Endogenous photoproteins, calcium channels and calcium transients during metamorphosis in hydrozoans. *Roux's Arch. Dev. Biol.* **196:** 30–50.

Hart, R. C., J. C. Matthews, K. Hori, and M. J. Cormier. 1979. *Renilla reniformis* bioluminescence: luciferase-catalyzed production of nonradiating excited states from luciferin analogues and elucidation of the excited state species involved in energy transfer to *Renilla* green fluorescent protein. *Biochemistry* **18:** 2204–2210.

Herring, P. J. 1983. The spectral characteristics of luminous marine organisms. *Proc. R. Soc. Lond B.* **220:** 183–217.

Herring, P. J. 1990. Bioluminescence responses of the deep-sea scyphozoan *Atolla wyvillei. Mar. Biol.* **196:** 413–417.

Herring, P. J., J.-M. Bassot, and P. R. Flood. 1996. Bioluminescence responses of the scyphozoan *Periphylla periphylla* from a Norwegian fjord. Pp. 154–157 in *Bioluminescence and Chemiluminescence; molecular reporting with photons,* J. W. Hastings, L. J. Kricka, and P. E. Stanley, eds. John Wiley, Chichester.

Inouye, S., and O. Shimomura. 1997. The use of *Renilla* luciferase, *Oplophorus* luciferase, and apoaequorin as bioluminescent reporter protein in the presence of coelenterazine analogues as substrate. *Biochem. Biophys. Res. Commun.* **233:** 349–353.

Matthews, J. C., K. Hori, and M. C. Cormier. 1977. Purification and properties of *Renilla reniformis* luciferase. *Biochemistry* **16:** 85–90.

McCapra, F., and R. Hart. 1980. The origins of marine bioluminescence. *Nature* **286:** 660–661.

Morin, J. G., and J. W. Hastings. 1971a. Biochemistry of the bioluminescence of colonial hydroids and other coelenterates. *J. Cell. Physiol.* **77:** 305–312.

Morin, J. G., and J. W. Hastings. 1971b. Energy transfer in a bioluminescent system. *J. Cell. Physiol.* **77:** 313–318.

Russell, F. S. 1970. *The Medusae of British Isles. Vol. II: Pelagic Scyphozoa with a Supplement to the First Volume on Hydromedusae.* Cambridge University Press, London, 284 pp.

Shimomura, O. 1985. Bioluminescence in the sea: photoprotein systems. *Symp. Soc. Exp. Biol.* **39:** 351–372.

Shimomura, O. 1986. Isolation and properties of various molecular forms of aequorin. *Biochem. J.* **234:** 271–277.

Shimomura, O. 1995a. Cause of spectral variation in the luminescence of semisynthetic aequorins. *Biochem. J.* **306:** 537–543.

Shimomura, O. 1995b. The roles of the two highly unstable components F and P involved in the bioluminescence of euphausiid shrimps. *J. Biolumin. Chemilumin.* **10:** 91–101.

Shimomura, O., and F. H. Johnson. 1970. Mechanisms in the quantum yield of *Cypridina* bioluminescence. *Photochem. Photobiol.* **12:** 291–295.

Shimomura, O., and F. H. Johnson. 1975. Chemical nature of bioluminescence systems in coelenterates. *Proc. Natl. Acad. Sci. USA* **72:** 1546–1549.

Shimomura, O., and F. H. Johnson. 1979. Comparison of the amounts of key components in the bioluminescence systems of various coelenterates. *Comp. Biochem. Physiol.* **64B:** 105–107.

Shimomura, O., F. H. Johnson, and Y. Saiga. 1962. Extraction, purification and properties of aequorin, a bioluminescent protein from the luminous hydromedusan, *Aequorea*. *J. Cell. Comp. Physiol.* **59:** 223–240.

Shimomura, O., T. Masugi, F. H. Johnson, and Y. Haneda. 1978. Properties and reaction mechanism of the bioluminescence system of the deep-sea shrimp *Oplophorus gracilorostris*. *Biochemistry* **17:** 994–998.

Shimomura, O., S. Inoue, F. H. Johnson, and Y. Haneda. 1980. Widespread occurrence of coelenterazine in marine bioluminescence. *Comp. Biochem. Physiol.* **65B:** 435–437.

Vysotskii, E. S., V. S. Bondes, and V. N. Letunov. 1989. Extraction and purification of obelin, a calcium-activated photoprotein from the hydroid polyp *Obelia longissima*. *Biokhimiya* **54:** 965–973.

Ward, W. W., and H. H. Seliger. 1974a. Extraction and purification of calcium-activated photoproteins from the ctenophores *Mnemiopsis* sp. and *Beroë ovata*. *Biochemistry* **13:** 1491–1499.

Ward, W. W., and H. H. Seliger. 1974b. Properties of mnemiopsin and berovin, calcium-activated photoproteins from the ctenophore *Mnemiopsis* sp. and *Beroë ovata*. *Biochemistry* **13:** 1500–1510.

Widder, E. A., M. I. Latz, and J. F. Case. 1983. Marine bioluminescence spectra measured with an optical multichannel detection system. *Biol. Bull.* **165:** 791–810.

Reference: *Biol. Bull.* **194:** 253–259. (June, 1998)

Peptides Controlling Stiffness of Connective Tissue in Sea Cucumbers

R. BIRENHEIDE[1,*], M. TAMORI[1], T. MOTOKAWA[1], M. OHTANI[2], E. IWAKOSHI[2], Y. MUNEOKA[2], T. FUJITA[3], H. MINAKATA[3], AND K. NOMOTO[3]

[1] *Basic Biology, Faculty of Bioscience and Biotechnology, Tokyo Institute of Technology, Ookayama 2-12-1, Meguro, Tokyo 152, Japan;* [2] *Faculty of Integr. Arts and Sciences, Hiroshima University, Higashi-Hiroshima 739, Japan; and* [3] *Suntory Institute for Bioorganic Research, Osaka 618, Japan*

Abstract. We present the first evidence of a system of four bioactive peptides that affect the stiffness of sea cucumber dermis. The body wall dermis of sea cucumbers consists of catch connective tissue that is characterized by quick and drastic stiffness changes under nervous control. The peptides were isolated from the body wall, their amino acid sequences determined, and identical peptides synthesized. Two peptides, which we named holokinins, are homologous with bradykinin. We tested the effect of the peptides on the mechanical properties of sea cucumber dermis. Both of the holokinins softened the dermis, and a pentapeptide that we designated as NGIWYamide stiffened it. Both effects were reversibly suppressed by anesthesia with menthol. We called the fourth peptide stichopin; it had no direct effect on the stiffness of the dermis but suppressed action of the neurotransmitter acetylcholine reversibly. The results suggest that the peptides are neuropeptides and are part of a sophisticated system of neurotransmitters and neuromodulators that controls the connective tissue stiffness of sea cucumber dermis.

Introduction

One key character of echinoderms is their unique catch connective tissue (CCT, Motokawa, 1984a; mutable connective tissue, Wilkie, 1984). This connective tissue can change its mechanical properties dramatically in response to various stimuli. The response, which can be stiffening or softening, is under nervous control.

The body wall of sea cucumbers consists of a thin epidermis, an extensive dermis, and inner muscles composed of a sheet of ring muscles and five bands of longitudinal muscles. In most species the dermis makes up by far the biggest part of the body wall. The dermis consists of pure CCT and can change its properties to the extent that the animal can be very stiff to the touch at one moment and practically melt a few seconds later (Motokawa, 1988); in extreme cases, drastic softening leads to autotomy. A number of studies reported different stimuli that lead to stiffness changes (Motokawa, 1981, 1982c, 1984b, 1984c, 1987; Hayashi and Motokawa, 1986). Among them are acetylcholine (ACh) and cholinergic agonists/antagonists. Other common vertebrate neurotransmitters did not have any effect. The holothurian nervous system is very poorly known, and—like all echinoderm nervous systems—it seems to lack synapses. The site of action of ACh is unknown, as is the mechanism of neural transmission in echinoderms.

Many studies of vertebrates have shown the importance of neuropeptides in neural transmission. In echinoderms, only a few peptides have been isolated and classified as neuropeptides. The sea star *Asterias rubens* has two peptides: S1 (Gly-Phe-Asn-Ser-Ala-Leu-Met-Phe-NH_2) and S2 (Ser-Gly-Pro-Tyr-Ser-Phe-Asn-Ser-Gly-Leu-Thr-Phe-NH_2) (Elphick *et al.*, 1991). The second of these (S2) has a relaxing effect on the cardiac stomach of *A. rubens* (Elphick *et al.*, 1995). The sea cucumber *Holothuria glaberrima* has two peptides: SGYSVLYamide and GFSKLYFamide (Diaz-Miranda *et al.*, 1992). The latter induces relaxation of the intestinal muscles and the longitudinal body wall muscles of *H. glaberrima.* No other bioactive peptides are known at present, and no study has investigated the effects of peptides on connective tissue stiffness. However, there are pioneering studies that sug-

Received 19 November 1997; accepted 27 March 1998.

*To whom correspondence should be addressed. E-mail: rbirenhe@bio.titech.ac.jp

gest the presence of low molecular weight factors controlling the stiffness of echinoderm connective tissues (Smith and Greenberg, 1973; Motokawa, 1981, 1982a, 1982c, 1984b). These studies reported a stiffening factor and a softening factor in coelomic fluids and body wall of echinoderms but did not analyze its chemical structure.

On the other hand, Iwakoshi *et al.* (1995) isolated a number of peptidic bioactive substances from the body wall of the sea cucumber *Stichopus japonicus* and determined the structures of four peptides. They did not, however, test the influence of those peptides on the connective tissue of sea cucumber. We recently made further attempts to isolate bioactive peptides from the body wall of sea cucumber and found 14 peptides, including the four obtained in the previous study. A preliminary account of the identification process is given in Ohtani *et al.* (1998). These peptides have been tested on the connective tissue of the sea cucumber. To date, we have found that four of them (termed holokinin 1 and 2, NGIWYamide, and stichopin) have considerable effects on the stiffness of the body wall connective tissue; these effects are reported here.

Materials and Methods

Specimens of the sea cucumber *Stichopus japonicus* were collected in the Seto Inland Sea near Hiroshima and in the Japan Sea near the Noto peninsula. Specimens of *Holothuria leucospilota* were collected in Okinawa. The animals were kept in aquaria with circulating seawater at 18°C and 25°C, respectively.

Isolation and structure determination of peptides

Body walls, including longitudinal muscles, from a 5-kg sample of *S. japonicus* were cut into small pieces, frozen in liquid nitrogen, and pulverized. The pulverized material was boiled for 10 min in 10 volumes of water, then homogenized with a Waring blender and a Polytron. The homogenate was centrifuged (13,000 × *g*, 40 min, 4°C). The supernatant was concentrated to 200 ml with an evaporator. To the concentrated supernatant, 20 ml of 1 *N* HCl was added and the precipitate was centrifuged off. Next, the supernatant was forced through a series of five C18 cartridges (Varian Mega Bond-Elut). The retained material was eluted with 10% and then with 60% methanol. The 60% methanol eluate was subjected to HPLC purification. The four peptides used in the present experiments were purified through five or six HPLC steps with two kinds of C18 reversed-phase columns (Asahikasei ODP-50 and Tosoh ODS-80TM) and a cation-exchange column (Tosoh SP-5PW). After each purification step, the bioactivity of the obtained fractions was assayed on longitudinal muscle and intestine of *S. japonicus*. Details concerning the purification of the four active peptides found in this study are given in the Results.

Bioassay

A longitudinal muscle (10-mm length) was dissected out, tied with cotton thread at each end, and mounted in a chamber (2.5 ml) filled with artificial seawater (ASW). The ASW used in the bioassay was of the following composition: 445 m*M* NaCl, 10 m*M* KCl, 10 m*M* $CaCl_2$, 55 m*M* $NaCl_2$, and 10 m*M* Tris-HCl (pH 7.6). Twitch contraction of the muscle was elicited by stimulating it with an electrical pulse (20 V, 3 ms) at 10-min intervals. The stimulation was delivered in air after removing the ASW in the chamber. After each recording of twitch contraction, the chamber was again filled with ASW. Peptide samples were dissolved in ASW and applied to the muscle 8 min before stimulation. The intestine (75-mm length) was mounted in another chamber. Peptide samples were dissolved in 0.1 ml ASW and applied to the intestine by injection into the aerated ASW.

Mechanical tests

For oscillatory strain tests, tissue samples (1 mm × 1 mm × 5 mm) were cut from the interambulacral white dermis with a razor blade. The long axis of the sample corresponded to the long axis of the animal. The samples were glued to a holder in a trough filled with ASW or experimental solutions. The samples were connected to a force gauge (LVS-20GA, Kyowa), whose position oscillated between 0 and 800 μm at a rate of 0.3 Hz. The samples were thus periodically stretched and relaxed along their long axis. The oscillator was adjusted so that the sample was totally relaxed in one half cycle but was never compressed. The samples developed a counterforce that oscillated with the same period as the strain. The counterforce was recorded with a microcomputer at a rate of 7 or 10 Hz. Chemicals were diluted in ASW and added to the trough.

For creep tests, samples similar to those used for oscillatory strain tests were glued to a holder in a trough. Loads between 0.09 g and 5 g were applied *via* a lever system to ensure constant elongation of the sample. The elongation of the sample was measured with a laser displacement sensor (3Z4M-S01, Omron) and recorded with a microcomputer. Chemicals were diluted in ASW to a concentration of 10^{-6} *M* (for most experiments) or 10^{-5} *M* (in a few cases) and added to the trough. Relative viscosity was calculated as the reciprocal value of strain rate normalized by the same value at application of test solutions.

The samples of body wall tissue used in the mechanical tests were taken from at least 5 animals for each neuropeptide. We could not find statistically significant differences in responses between animals or between samples from the same animal.

Results

Purification and bioassay of peptides

At the first step of HPLC purification, the column (reversed-phase, ODP-50) was eluted with a 120-min linear gradient of 0%–60% acetonitrile (ACN) in 0.1% trifluoroacetic acid (TFA) at pH 2.2. The results of bioassay experiments showed that most fractions obtained between 10% and 34% ACN had effects on the contractility of both the longitudinal muscle and the intestine. Therefore, we divided the active fractions into six groups. Two of the four peptides used in the present study were purified from group 1, which was obtained between 10% and 14% ACN. The other two were purified from group 2, which was obtained between 14% and 18% ACN.

Group 1 was applied to a cation-exchange column, and the column was eluted with a 70-min linear gradient of 0–0.7 *M* NaCl in 10 m*M* phosphate buffer at pH 7.1. An active peak (P1), which was found to have an inhibitory effect on the twitch contraction of the radial muscle but no effect on spontaneous contractions of the intestine, eluted at about 0.15 *M* NaCl. Another active peak (P2), which was found to have a contractile effect on both muscle tissues, eluted at about 0.25 *M* NaCl. P1 was applied to another kind of reversed-phase column (ODS-80TM), and an active peak eluted at about 18% ACN. The peak was applied to the same column, and the column was eluted isocratically with 16% ACN. To purify the active substance of the peak, isocratic elution was repeated under the same conditions. P2 was also applied to the ODS-80TM column. The active peak eluted at about 20% ACN. Next, the peak was again applied to the cation-exchange column. Although the conditions of elution were the same as in the second step, the active peak eluted at about 0.1 *M* NaCl. To purify the active substance of P2, isocratic elution was performed twice with the ODS-80TM column at 19% ACN.

Group 2 was also applied to the cation-exchange column, and the column was eluted under the same conditions as for group 1. An active peak, which was found to have an inhibitory effect on twitch contraction of the radial muscle and a contractile effect on the intestine, eluted at about 0.3 *M* NaCl. The peak was then applied onto an ODS-80TN column. Two overlapping active peaks (P3 and P4) eluted at about 22% ACN. Both peaks showed similar activities. Next, P3 was applied to the same column, and the column was eluted isocratically with 21% ACN. The isocratic elution was again performed and the P3 substance was purified. To purify the P4 substance, similar isocratic elution with 21.5% ACN was performed twice.

The purified peptidic substances were subjected to amino acid sequence analysis and fast atom bombardment mass spectrometry (FAB-MS). The results of the analyses of the substances and their structures predicted from the results are shown in Figure 1. P1 was suggested to be a heptadecapeptide having a disulfide bond. The peptide was named stichopin. P2 was suggested to be a pentapeptide with an amidated C-terminus. The peptide was named NGIWYamide according to its structure. P4 was suggested to be a bradykinin-related heptapeptide. Its predicted structure is the same as holokinin 1 found in a previous study (Iwakoshi *et al.*, 1995). P3 was suggested to be Met(O)^5-holokinin 1; that is, the peptide has an oxidized methionine at the fifth position of holokinin 1. This peptide has also been found in the previous study and was termed holokinin 2. It cannot be ruled out that

Holokinin 1

Sequence Pro-Leu-Gly-Tyr-Met-Phe-Arg

FAB-MS 883.5 $(M + H)^+$

Structure Pro-Leu-Gly-Tyr-Met-Phe-Arg

Holokinin 2

Sequence Pro-Leu-Gly-Tyr-Met-Phe-Arg

FAB-MS 899.4 $(M + H)^+$

Structure Asn-Gly-Ile-Trp-Tyr-NH_2

NGIWYamide

Sequence Asn-Gly-Ile-Trp-Tyr

FAB-MS 651.2 $(M + H)^+$

Structure Asn-Gly-Ile-Trp-Tyr-NH_2

Stichopin

Sequence Asp-Arg-Gln-Gly-Trp-Pro-Ala-Xaa-Tyr-Asp-Ser-Lys-Gly-Asn-Tyr-Lys

FAB-MS 1989.7 $(M + H)^+$

Structure

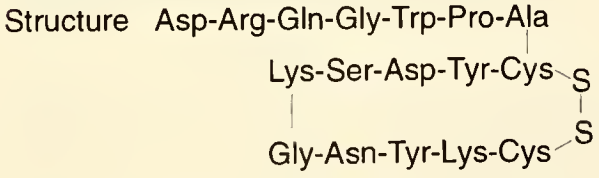

Figure 1. Results of amino acid sequence analysis and fast atom bombardment mass spectrometry (FAB-MS) of the purified peptides, and the structures predicted from the results.

the oxidization occurred during the purification of holokinin 1, though holokinin 2 (oxidized holokinin 1) had an almost identical effect on the muscle tissues and connective tissue.

Peptides with the predicted structures were synthesized. The behavior of each synthetic peptide on reversed-phase and cation-exchange HPLC was confirmed to be identical with that of the corresponding native peptide. Further, the effects of each synthetic peptide on the radial muscle and the intestine were also confirmed to be identical with those of the corresponding native peptides.

Figure 1 shows the results of amino acid sequence and FAB-MS analysis as well as the predicted structure of the four peptides isolated from the body wall of *Stichopus japonicus*. We used synthetic peptides to test whether they have an influence on the stiffness of sea cucumber connective tissue either by themselves, or by influencing the effect of ACh. Dermis samples of *S. japonicus* were in general softer than those of *H. leucospilota*. However, this did not influence the reactivity of the samples, and we did not observe any significant differences among the species.

Mechanical tests

The holokinins had a softening effect, whereby the effect of a concentration of $10^{-5}M$ did not differ significantly from that of $10^{-6}M$. The effect could be observed within 30 s after application of holokinins in both kinds of test. In oscillating tests (Figs. 2, 4) the samples developed a maximal counterforce that was more or less constant without stimulation. When holokinins were applied the counterforce dropped sharply, indicating that the tissue softened. In creep tests (Figs. 3, 5), creep velocity increased after application of holokinins, shown in our graphs as a decrease of relative viscosity compared to viscosity at time of application.

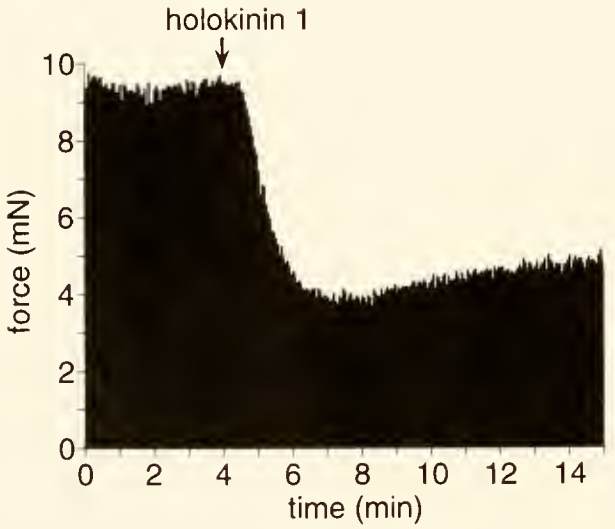

Figure 2. Effect of holokinin 1 ($10^{-6}M$) on stiffness of the dermis of *Holothuria leucospilota* in the oscillatory strain test. The maximal counterforce decreased rapidly after the holokinin 1 was applied. In this graph and in Figures 4 and 6, the time axis is compressed so that it does not resolve each oscillating cycle of the counterforce. Therefore the space between no force and maximal force is blackened entirely in the graphs.

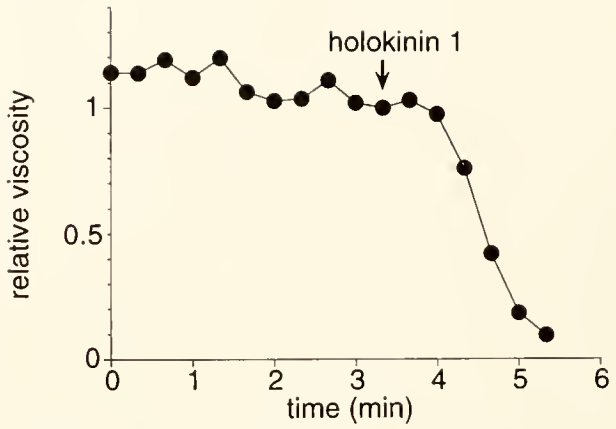

Figure 3. Effect of holokinin 1 ($10^{-6}M$) on the relative viscosity of a dermis sample of *Stichopus japonicus* in the creep test. Relative viscosity was calculated as the reciprocal value of strain rate normalized by the same value at the time when holokinin 1 was applied.

Holokinin 1 at concentrations of $10^{-6}M$ and $10^{-5}M$ softened 19 out of 41 samples. The effect was seen with dermis strips of *H. leucospilota* (Fig. 2) and *S. japonicus* (Fig. 3). Relative viscosity dropped to maximally about 10% in creep tests. Most of the samples stayed soft after holokinin 1 was washed out with ASW. In some cases a slight stiffening (recovery) was observed, but never to the level before application of holokinin 1. In oscillation tests, maximal counterforce dropped maximally to 40% with the application of holokinin 1, and no recovery was observed after washing out with ASW.

Holokinin 2 was slightly less effective, softening 7 out of 24 samples of *H. leucospilota* (Fig. 4) and *S. japonicus* (Fig. 5). In creep tests, relative viscosity dropped to maximally 10% without recovery, and in oscillation tests, maximal counterforce was reduced to 23% after application of holokinin 2.

When we treated samples for 10 min in ASW saturated with menthol, the softening reaction of both holokinins was suppressed, but recovered at least partly after extensive washing in ASW.

The neuropeptide bradykinin, common in vertebrates and wasps (Elliott *et al.*, 1960; Nakajima, 1988) was also tested, because it is partly homologous in sequence to the holokinins. However, it had no effect on the stiffness of holothurian dermis, nor did it suppress or enhance the effect of ACh.

NGIWYamide had the opposite effect from that of the

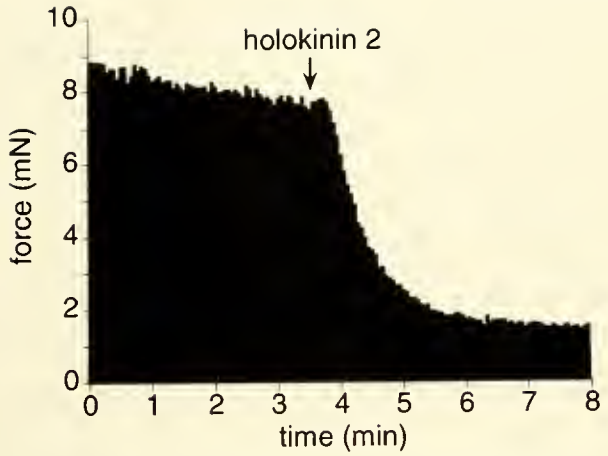

Figure 4. Effect of holokinin 2 (10^{-6} *M*) on the stiffness of the dermis of *Holothuria leucospilota* in the oscillatory strain test.

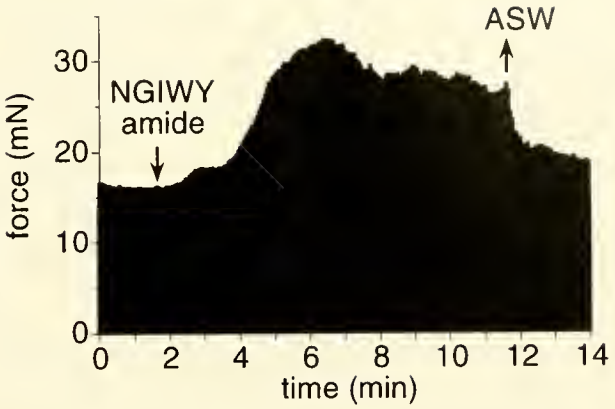

Figure 6. NGtWYamide (10^{-6} *M*) stiffened the dermis of *Holothuria leucospilota* as seen here by an increase in counterforce in the oscillatory strain test. Washing with artificial seawater (ASW) lowered the counterforce to nearly the initial value.

holokinins: it stiffened the dermis in 52 out of 120 samples of both sea cucumber species. Compared to the holokinins, NGIWYamide had a longer reaction time (the reaction occurring within 100 s of application), the reaction was often slower, and the extent of stiffening was very variable. In oscillation tests the maximal counterforce increased, showing a stiffening of the sample (Fig. 6) to maximal 194%. Recovery (*i.e.*, softening of the sample) occurred frequently after washing with ASW. In creep tests (Fig. 7) relative viscosity increased to maximal 220% of the initial value, without recovery after washing with ASW.

As in holokinins, anesthesia for 10 min in ASW saturated with menthol blocked the effect of NGtWYamide reversibly.

Stichopin by itself had no effect on dermal stiffness during our tests. However, when samples were treated with stichopin at 10^{-5} or 10^{-6} *M* for 30 min, the effect of ACh was blocked in creep tests and in forced vibration tests of both sea cucumber species (Fig. 8). In controls, ACh had a stiffening effect or a biphasic effect—first stiffening, then softening. Altogether, stichopin completely blocked the effect of ACh in 27 out of 36 cases, and reduced the effect in the remaining 9 cases. When samples were washed with ASW for at least 1 h, the reactivity of ACh recovered to some extent but never regained the levels seen before treatment with stichopin.

Discussion

The amino acid sequences of holokinins are homologous with those of bradykinins in vertebrates and wasps (Elliott *et al.*, 1960; Nakajima, 1988). Vertebrate bradykinins have a wide range of effects, mainly on the central nervous system and on smooth muscles. Bradykinins from

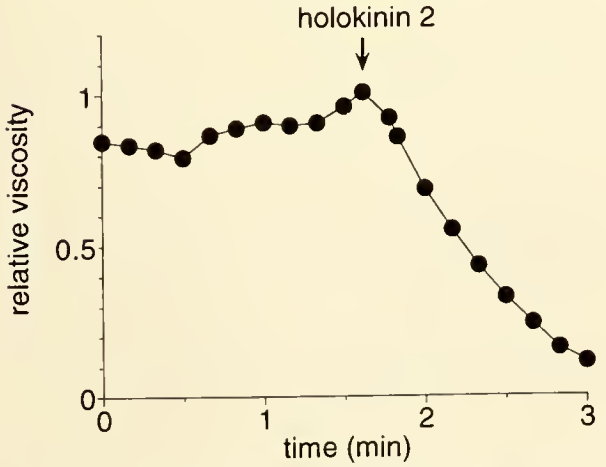

Figure 5. Creep test showing the softening effect of holokinin 2 (10^{-6} *M*) on the stiffness of the dermis of *Stichopus japonicus*.

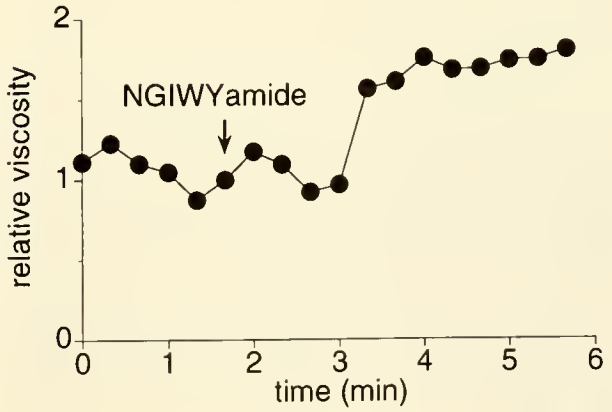

Figure 7. Creep test showing the stiffening effect of NGtWYamide (10^{-5} *M*) on the dermis of *Stichopus japonicus*. Relative viscosity increased *ca.* 1.5-fold.

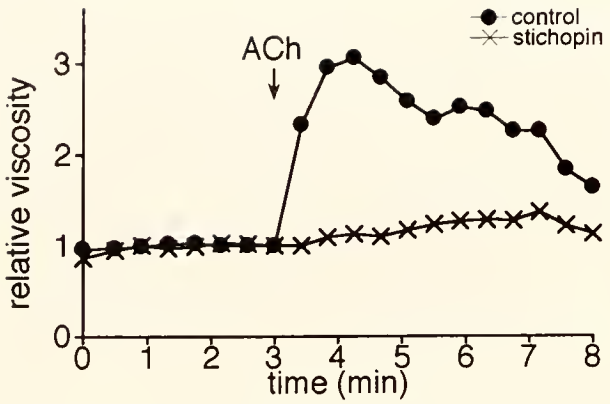

Figure 8. Influence of stichopin on the effect of acetylcholine (ACh) on relative viscosity in the creep test with a sample of *Holothuria leucospilota*. Stichopin was applied at the start of the experiment. At 3 min, 10^{-5} *M* ACh was applied but had no effect (crosses). After washing the sample for 1 h in artificial seawater (ASW), it was tested again as control (circles). Now ACh had a clear stiffening effect, indicating that the suppressive influence of stichopin had disappeared.

wasp venoms show some variation, but the basic bradykinin sequence is well preserved (Nakajima, 1988).

The sequence homology between the holokinins and bradykinin points to the possibility of a common ancestral molecule, although the softening reaction of the sea cucumber connective tissue is unique. Moreover, bradykinin itself did not affect the stiffness of holothurian dermis, so functionally the two peptides are different. The nervous system of sea cucumbers is almost unknown, and speculations about its evolution must wait until more details are available.

Effects

The effect of the peptides was not constant throughout our tests. Dermis samples were previously reported to have different initial physiological states that result in variable responses to the same stimuli (Motokawa, 1984b). These initial states most likely cause variability of responses to peptides.

To test the responses of the dermis, we used two methods that differed in the way the force was applied and in the speed at which the samples elongated. The oscillation test employed repeated stretch-relax cycles and the elongation speed was typically about 500 μm/s. The creep test applied a constant load and the speeds ranged between 0.1 and 3 μm/s. This difference of two orders of magnitude makes it likely that the two tests measure stresses of different parts of the complex molecular network of the connective tissue. The effect of the agents tested did not differ between the test methods, indicating that the peptides affect basic properties of the material that influence tissue mechanics.

Holokinins had the most prominent effect among the peptides tested here and are the first fully characterized softening agent for sea cucumber dermis. Until now, ACh was the only neurotransmitter known to affect dermal stiffness, and its effect is biphasic: that is, it first stiffens and then softens the dermis. As the only identified softening agents, the holokinins are unique. Their effect was easily suppressed by menthol, indicating that they can be classified as neuropeptides.

NGIWYamide is a short peptide and worked antagonistically to the holokinins—it stiffened the dermis. Anesthesia suppressed the effect of NGIWYamide, classifying it as a neuropeptide.

Stichopin lacked an effect when used alone, but suppressed the reaction of sea cucumber dermis to ACh. This suggests that NGIWYamide is also a neuropeptide, modulating the action of ACh.

Studies on factors controlling the stiffness of sea cucumber dermis were pioneered by Smith and Greenberg (1973), who found an evisceration factor with a molecular weight between 131 and 181 in the sea cucumber *Thyone briareus*. Among its other effects, this factor softened the connective tissue of the introvert during evisceration. Later, Motokawa published a series of papers about a softening and a stiffening factor in the coelomic fluid of the sea cucumber *Stichopus chloronotus* (Motokawa, 1981, 1982a, 1982c) and a stiffening factor in the sea cucumber *S. japonicus* (Motokawa, 1984b). The softening factor is heat stable, of low molecular size, and methanol insoluble. The stiffening factor is also heat stable and of low molecular size, but it is methanol soluble. We cannot decide whether the factors found in those studies are identical with the neuropeptides described here, but heat stability and low molecular weight (Iwakoshi *et al.*, 1995) are common characteristics of our neuropeptides. Therefore it seems possible that the two groups are similar or even identical.

Catch connective tissue is unique to echinoderms and characterized by its ability to change stiffness quickly under nervous control without the involvement of muscle cells. The connective tissue of sea cucumber dermis lacks muscle cells entirely, so the observed effects can be attributed to changes of the connective tissue alone. Our data show that four peptides (holokinins, NGIWYamide, and stichopin) compose a system of neuropeptides that can soften and stiffen the dermis and modulate the action of the neurotransmitter ACh. Such a system has not been reported in echinoderms.

It would be interesting to know which cells synthesize and secrete the neuropeptides. Localization of the peptides would probably require specifically tailored antibodies and was far beyond the scope of the present study. Our samples consisted of the white connective tissue of the dermis. Former studies (Motokawa, 1982b; Matsuno and Motokawa, 1992) have shown that this tissue consists of extracellular matrix interspersed with minute processes

of granule-containing cells of various types that resemble vertebrate neurosecretory cells. The peptides in our experiments most likely affected these cells. In a similar fashion, cholinergic drugs evoke stiffness changes in samples of connective tissue (Motokawa, 1987), probably by acting on the same cells. The effect of anesthetics on the action of both peptides and cholinergic drugs (Motokawa, 1987) supports the idea that the granule-containing cells are functionally linked to neural elements. It seems likely that the neuropeptides are synthesized and secreted by these cells in order to closely control the stiffness of sea cucumber dermis.

Other echinoderms

Control of connective tissue stiffness by a peptide or peptide-containing factor has been reported only for the starfish *Pycnopodia helianthoides* (Mladenov *et al.*, 1989). The body fluids of this species contain an autotomy-promoting factor that is most likely a peptide or has a peptide component with a molecular weight of about 1200 daltons. Because of its ability to evoke softening of connective tissue during autotomy, this factor might be similar to the peptides described in our study, although its amino acid composition is unknown.

The other neuropeptides found in echinoderms evoke stomach eversion in starfish (Elphick *et al.*, 1995) or muscle relaxation in sea cucumbers (Diaz-Miranda and Garcia-Arraras, 1995). The latter authors proposed that both the neuropeptides of starfish and the neuropeptide they found in sea cucumbers belong to a family of neuropeptides with a common periodic sequence that includes serine, leucine, and phenylalanine (Diaz-Miranda *et al.*, 1992). The peptides of our study do not fit this amino acid pattern, and we thus conclude that ours are novel neuropeptides different from any known in echinoderms.

Acknowledgments

We thank the staff of Noto Marine Biological Station, University of Kanazawa, and the staff of Sesoko Marine Science Center, University of the Ryukyus, for providing specimens.

Literature Cited

Diaz-Miranda, L., and J. Garcia-Arraras. 1995. Pharmacological action of the heptapeptide GFSKLYFamide in the muscle of the sea cucumber *Holothuria glaberrima* (Echinodermata). *Comp. Biochem. Physiol. C* **110:** 171–176.

Diaz-Miranda, L., D. A. Price, M. J. Greenberg, T. D. Lee, K. E. Doble, and J. E. Garcia-Arraras, 1992. Characterization of two novel neuropeptides from the sea cucumber *Holothuria glaberrima*. *Biol. Bull.* **182:** 241–247.

Elliott, D., G. Lewis, and E. Horton. 1960. The structure of bradykinin—a plasma kinin from ox blood. *Biochem. Biophys. Res. Commun.* **3:** 87–91.

Elphick, M. R., D. A. Price, T. D. Lee, and M. C. Thorndyke. 1991. The SALMFamides: a new family of neuropeptides isolated from an echinoderm. *Proc. R. Soc. Lond. B* **243:** 121–127.

Elphick, M., S. Newman, and M. Thorndyke. 1995. Distribution and action of SALMFamide neuropeptides in the starfish *Asterias rubens*. *J. Exp. Biol.* **198:** 2519–2525.

Hayashi, Y., and T. Motokawa. 1986. Effects of ionic environment on viscosity of catch connective tissue in holothurian body wall. *J. Exp. Biol.* **125:** 71–84.

Iwakoshi, E., M. Ohtani, T. Takahashi, Y. Muneoka, T. Ikeda, T. Fujita, H. Minakata, and K. Nomoto. 1995. Comparative aspects of structure and action of bioactive peptides isolated from the sea cucumber *Stichopus japonicus*. Pp. 261–264 in *Peptide Chemistry 1994*, M. Ohno, ed. Protein Research Foundation, Osaka.

Maisuno, A., and T. Motokawa. 1992. Evidence for calcium translocation in catch connective tissue of the sea cucumber *Stichopus chloronotus*. *Cell Tissue Res.* **267:** 307–312.

Mladenov, P. V., S. Igsoura, S. Asotra, and R. D. Burke. 1989. Purification and partial characterization of an autotomy-promoting factor from the seastar *Pycnopodia helianthoides*. *Biol. Bull.* **176:** 169–175.

Motokawa, T. 1981. The stiffness change of the holothurian dermis caused by chemical and electrical stimulation. *Comp. Biochem. Physiol.* **70:** 41–48.

Motokawa, T. 1982a. Factors regulating the mechanical properties of holothurian dermis. *J. Exp. Biol.* **99:** 29–41.

Motokawa, T. 1982b. Fine structure of the dermis of the body wall of the sea cucumber, *Stichopus chloronotus*, a connective tissue which changes its mechanical properties. *Galaxea* **1:** 55–64.

Motokawa, T. 1982c. Rapid change in mechanical properties of echinoderm connective tissues caused by coelomic fluid. *Comp. Biochem. Physiol. C* **73:** 223–229.

Motokawa, T. 1984a. Connective tissue catch in echinoderms. *Biol. Rev. Camb. Philos. Soc.* **59:** 255–270.

Motokawa, T. 1984b. The viscosity change of the body-wall dermis of the sea cucumber *Stichopus japonicus* caused by mechanical and chemical stimulation. *Comp. Biochem. Physiol. A* **77:** 419–423.

Motokawa, T. 1984c. Viscosity increase of holothurian body wall in response to photic stimulation. *Comp. Biochem. Physiol. A* **79:** 501–503.

Motokawa, T. 1987. Cholinergic control of the mechanical properties of the catch connective tissue in the holothurian body wall. *Comp. Biochem. Physiol. C* **86:** 333–337.

Motokawa, T. 1988. Catch connective tissue: a key character for echinoderms' success. Pp. 39–54 in *Echinoderm Biology*. R. D. Burke, P. V. Mladenov, P. Lambert, and R. L. Parsley, eds. A. A. Balkema, Rotterdam.

Nakajima, T. 1988. Active peptides of nonmammalian origin. Pp. 1–26 in *Physiologically Active Peptides*, T. Nakajima, N. Yanaihara, and T. Miyazawa, eds. Kodansha Ltd., Tokyo.

Ohtani, M., E. Iwakoshi, Y. Muneoka, H. Minakata, and K. Nomoto. 1998. Isolation and characterization of bioactive peptides from the sea cucumber, *Stichopus japonicus*. In *Proceedings of the 1st International Peptide Symposium*, Y. Shimonishi, ed. Kluwer Academic Publishers B. V., The Netherlands. In press.

Smith, G., and M. Greenberg. 1973. Chemical control of the evisceration process in *Thyone briareus*. *Biol. Bull.* **144:** 421–436.

Wilkie, I. C. 1984. Variable tensility in echinoderm collagenous tissues: a review. *Mar. Behav. Physiol.* **11:** 1–34.

Reference: *Biol. Bull.* **194:** 260–266. (June, 1998)

Nitric Oxide Function in an Echinoderm

MAURICE R. ELPHICK* AND RICHARD MELARANGE

School of Biological Sciences, Queen Mary and Westfield College, University of London, Mile End Road, London E1 4NS, UK

Abstract. In vertebrates, nitric oxide (NO) is synthesized from L-arginine by NO synthase (NOS) and regulates relaxation of smooth muscle by activating the cyclic-GMP (cGMP) generating enzyme soluble guanylyl cyclase (SGC). Here we show that the NO-cGMP pathway mediates relaxation of the cardiac stomach in the starfish *Asterias rubens*. The NO-donors hydroxylamine, *S*-nitrosoglutathione (SNOG) and *S*-nitroso-*N*-acetylpenicillamine (SNAP) and the NOS substrate L-arginine cause relaxation of the cardiac stomach. The relaxing effect of SNAP is blocked by the SGC inhibitor 1H-[1,2,4]-oxadiazolo[4,3-a]quinoxalin-1-one (ODQ), and the relaxing effect of L-arginine is inhibited by ODQ and the NOS inhibitor N^{ω}-monomethyl-L-arginine (L-NMMA). ODQ and methylene blue also cause contraction, which may be due to inhibition of the relaxing action of NO produced by cells in the cardiac stomach. These results suggest that NO is synthesized in the cardiac stomach and regulates relaxation by activating SGC. NO-cGMP-mediated relaxation of the cardiac stomach may be important during feeding in starfish where the relaxed stomach is everted through an oral opening and over the digestible parts of prey. The discovery of NO-cGMP-mediated relaxation in an echinoderm demonstrates that regulation of smooth muscle tone by this signaling pathway also occurs in animals other than vertebrates.

Introduction

Nitric oxide (NO) is one of a class of gaseous chemicals that have been identified as signaling molecules in the nervous system (Dawson and Snyder, 1994). NO is synthesized in neurons by a Ca^{2+}/calmodulin-activated, NADPH-dependent enzyme known as nitric oxide synthase (NOS). NO diffuses from sites of synthesis into adjacent cells and exerts effects by activating the enzyme soluble guanylyl cyclase (SGC) to generate the second messenger cGMP (Garthwaite, 1991). This NO-cGMP signaling pathway appears to be evolutionarily ancient because it is present in a wide range of animal groups including cnidarians (Colasanti *et al.*, 1995; Salleo *et al.*, 1996), nematodes (Bascal *et al.*, 1995), annelids (Leake and Moroz, 1996), molluscs (Jacklet and Gruhn, 1994), arthropods (Müller, 1997), and vertebrates (Nilsson and Söderström, 1997). Moreover, diverse functions for the NO-cGMP pathway have been identified, including roles in learning and memory (Schuman and Madison, 1994; Robertson *et al.*, 1996), feeding (Colasanti *et al.*, 1995; Elphick *et al.*, 1995b; Salleo *et al.*, 1996), olfaction (Gelperin, 1994; Müller and Hildebrandt, 1995), and regulation of mammalian smooth muscle tone (Palmer *et al.*, 1987; Bult *et al.*, 1990).

One major invertebrate phylum in which the NO-cGMP signaling system has remained largely unexamined is the echinoderms. In fact, the only evidence of the existence of the NO-cGMP pathway in this phylum is an immunocytochemical study using an antiserum to rat brain NOS in which NOS-like immunoreactive neurons were detected in the cardiac stomach of the starfish *Marthasterias glacialis* (Martinez *et al.*, 1994). Interestingly, one of the functions of NO in vertebrates is to cause relaxation of smooth muscle in the gut (Olsson and Holmgren, 1997). The detection of NOS-like immunoreactivity in neurons of the starfish cardiac stomach suggests that NO may regulate muscle tone in this organ. The relaxing effect of NO on smooth muscle has been observed in a variety of vertebrate preparations, but it is not known whether NO has a similar role in invertebrates. Echinoderms occupy

Received 15 January 1998; accepted 20 March 1998.

* To whom correspondence should be addressed. E-mail: M.R.Elphick@qmw.ac.uk

Abbreviations: NOS, nitric oxide synthase; SGC, soluble guanylyl cyclase; SNOG, *S*-nitrosoglutathione; SNAP, *S*-nitroso-*N*-acetylpenicillamine; ODQ, 1H-[1,2,4]oxadiazolo[4,3-a]quinoxalin-1-one; L-NMMA, N^{ω}-monomethyl-L-arginine.

an interesting position in animal evolution. Although they are invertebrates, echinoderms have a deuterostomian mode of development like the vertebrates. For this reason the echinoderms and a few other invertebrate deuterostomian phyla are recognized as being more closely related to vertebrates than the protostomian invertebrate phyla such as arthropods, molluscs, and annelids. Therefore, comparative analysis of NO function in echinoderms is of particular interest.

In the present study we have investigated the role of the NO-cGMP pathway in the cardiac stomach of the starfish *Asterias rubens*. To do this a variety of drugs that interact with components of the NO-cGMP signaling system were tested for their effects on the contractility of an *in vitro* preparation of the cardiac stomach. The results indicate that NO is involved in regulating the starfish cardiac stomach by causing relaxation of muscle tone. This effect of NO may be important during feeding in starfish where the relaxed cardiac stomach is everted through an oral opening and over the digestible parts of prey animals such as mussels and oysters.

Materials and Methods

Specimens of *Asterias rubens* were purchased from the University Marine Biological Station at Millport, Scotland, and kept in a seawater aquarium at Queen Mary and Westfield College. Cardiac stomach preparations were dissected and linked to a transducer as described by Elphick *et al.* (1995a). The preparation was suspended in a 20-ml organ bath containing aerated seawater maintained at 11°C and was then left to equilibrate for about 15 min. To investigate the effects of drugs that interact with the NO-cGMP pathway, the seawater (which contains about 10 m*M* K^+) was replaced with seawater containing 30 m*M* added KCl. These depolarizing conditions induce sustained but sub-maximal contracture of the cardiac stomach, making it possible to observe the effects of drugs that cause relaxation.

Cardiac stomach movement was recorded using a Harvard isotonic transducer (0.5 g load) linked to a Harvard twin-channel Universal oscillograph. A range of gain settings on the oscillograph were used depending on the responsiveness of the preparation. Each of the recordings illustrated in the figures are accompanied in the figure legend with the gain setting to enable comparison of responses.

Drugs tested included the NO-donors hydroxylamine, *S*-nitrosoglutathione (SNOG) and *S*-nitroso-*N*-acetylpenicillamine (SNAP). *N*-acetylpenicillamine (NAP) was used as a negative control for SNAP to establish whether effects observed could be attributed to SNAP's ability to release NO. The substrate for NOS, L-arginine, was tested using D-arginine as a negative control. Test compounds that inhibit NO-cGMP signaling included methylene blue, an inhibitor of both NOS and SGC (Miki *et al.*, 1987; Mayer *et al.*, 1993); the NOS inhibitor N^{ω}-monomethyl-L-arginine (L-NMMA) (Moncada *et al.*, 1991); and 1H-[1,2,4]oxadiazolo[4,3-a]quinoxalin-1-one (ODQ), a compound recently identified as a selective inhibitor of SGC (Garthwaite *et al.*, 1995).

All of the drugs were tested on at least three different preparations and representative responses are illustrated in the figures. Where enzyme inhibitors were used, the percent inhibition was calculated from three or more experiments as the mean ± standard error of the mean.

Drugs were obtained from Sigma (Poole, Dorset, UK) except SNAP, SNOG, and L-NMMA, which were gifts from the Wellcome Research Laboratories, and ODQ, which was purchased from Tocris Cookson (Bristol, UK). Drugs were prepared as aqueous solutions except ODQ, which was dissolved in DMSO and diluted in water with the final concentration of DMSO in the organ bath not exceeding 0.12%. Drugs were added to the organ bath in volumes of 10–100 μl to achieve the bath concentrations shown in the figures.

Results

The NO-donors hydroxylamine, SNOG, and SNAP caused relaxation of the cardiac stomach (Fig. 1). The relaxing effect of SNOG (10 μM) was rapidly reversed on washing (Fig. 1b), whereas hydroxylamine (1 m*M*) and SNAP (10 μM) had longer lasting effects as several washes were required before basal tone was restored (Fig. 1a, c). Differences in the reversibility of the relaxing effects of the NO donors may reflect their relative permeability in cardiac stomach tissue. The magnitude of the relaxing effect of the NO-donors was dose-dependent as illustrated for SNAP in Figure 1c. If three chemically unrelated NO-donors cause relaxation of the cardiac stomach, then it is likely that their effects are attributable to their ability to release NO rather than to some other chemical property of these compounds. Nevertheless, we addressed this question by testing NAP which, except for the absence of an NO moiety, is otherwise chemically identical to SNAP. NAP did not cause relaxation of the cardiac stomach when tested at a concentration (10 μM) at which SNAP causes marked relaxation (Fig. 1d).

Methylene blue caused dose-dependent contraction of the cardiac stomach (Fig. 2a). However, this compound inhibits both NOS and SGC, which makes interpretation of results difficult. ODQ, a selective inhibitor of SGC, has low solubility in water, and DMSO was used as a solvent to prepare stock solutions. In some preparations, however, the DMSO-containing vehicle had a contracting effect on the cardiac stomach. Therefore, we have illustrated here experiments in which the DMSO-containing

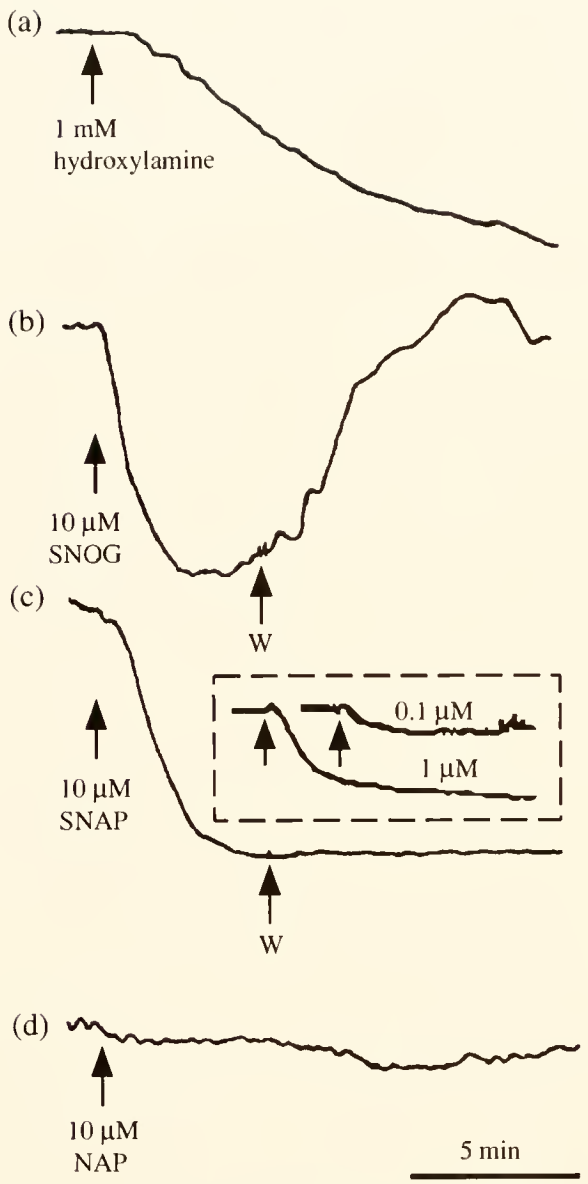

Figure 1. NO-donors cause relaxation of the cardiac stomach. (a) Hydroxylamine; gain 1. (b) SNOG; gain 5. (c) SNAP; gain 7. (d) NAP, which is chemically identical to SNAP apart from the absence of a NO moiety, does not cause relaxation; gain 5. [W = wash] In (c) and (d) there is a slight decrease in baseline tension during the course of the experiments, but the responses to SNAP and NAP, respectively, are clearly very different.

vehicle had no effect on muscle tone. Doses of 1 μM and 3 μM ODQ had no effect on cardiac stomach tone, but 10 μM ODQ consistently caused contraction (Fig. 2b). However, the delay in the onset of contraction and the rate of contraction with 10 μM ODQ were quite variable in different preparations.

The contractions caused by ODQ on the cardiac stomach suggest that ODQ is exerting this effect through inhibition of SGC activation by endogenous NO. To investigate the mode of action of ODQ on the cardiac stomach, we tested ODQ in combination with exogenous NO released by the NO-donor SNAP. First SNAP was tested alone at a concentration (10 μM) at which it consistently causes relaxation of the cardiac stomach (Fig. 3a). Then, after washing, the cardiac stomach was incubated with 10 μM ODQ for 15 min before applying a second dose of 10 μM SNAP (Fig. 3b). ODQ caused almost complete inhibition (94.8% in Fig. 3b) of the relaxing effect of SNAP. After washing out of the ODQ, SNAP was tested a third time and in the absence of ODQ the normal relaxing effect of 10 μM SNAP was restored (Fig. 3c). The mean percentage inhibition by 10 μM ODQ on the relaxing effect of 10 μM SNAP in five experiments on different preparations was 88.7 ± 2.3% (Fig. 3d). A mean inhibition of 56.6% was observed in two other experiments using 3 μM ODQ (data not shown).

The experiments described so far indicate that NO causes relaxation of the cardiac stomach by activating SGC. In the presence of the SGC inhibitor ODQ, the relaxing effect of endogenous NO is blocked, leading to contraction. However, this provides only indirect evi-

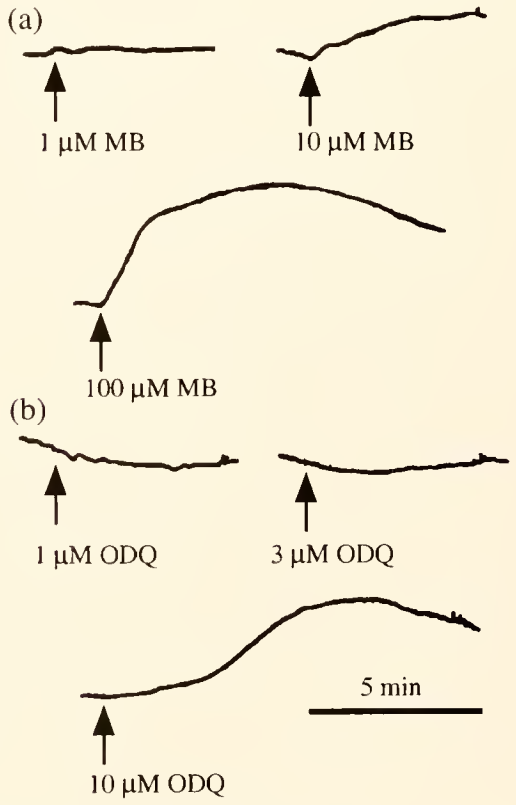

Figure 2. The NO-cGMP pathway inhibitors methylene blue and ODQ cause contraction of the cardiac stomach. (a) Methylene blue (MB); gain 5. (b) ODQ; gain 4.

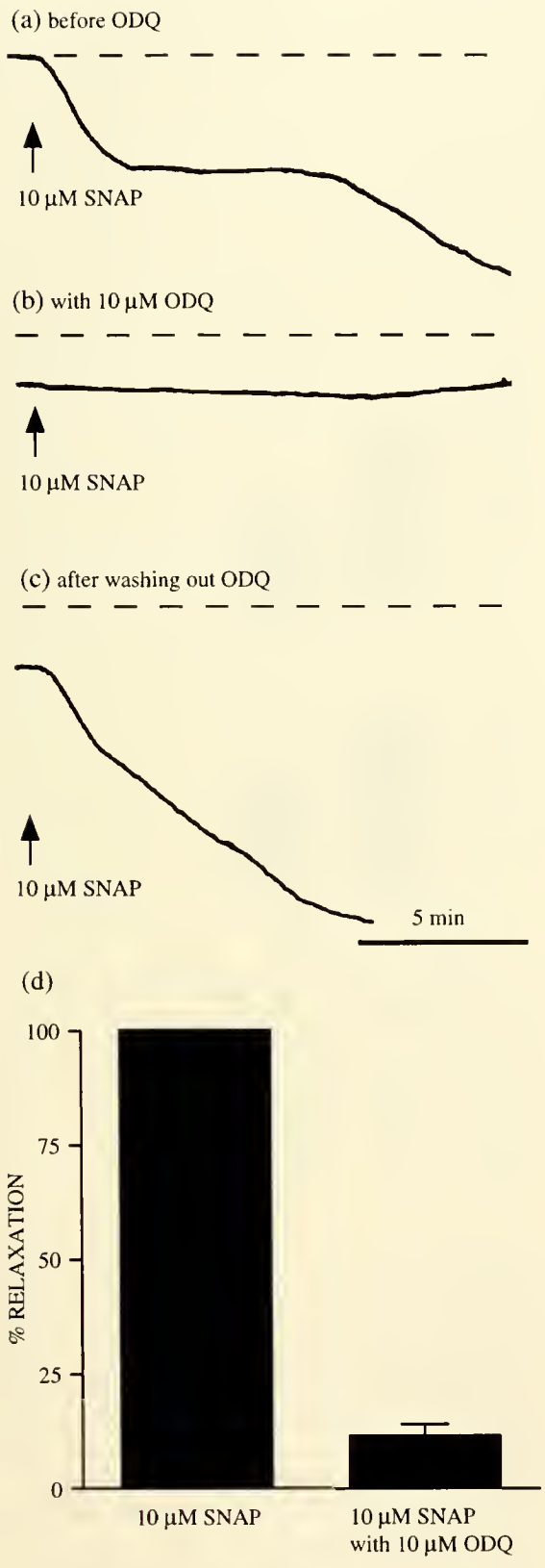

dence that NO is synthesized and released by cells in the cardiac stomach. We tested for NO production by NOS in the cardiac stomach by examining the effects of its substrate L-arginine. We also tested the NOS inhibitor L-NMMA.

L-arginine caused relaxation of the cardiac stomach when tested at 0.1 m*M* and 1 m*M*. In the experiments illustrated in Figure 4a and b, first the D-isomer of arginine was tested at 0.1 m*M*; this had no effect on muscle tone (Fig. 4a), whereas the L-isomer tested at the same concentration caused a marked relaxation of the cardiac stomach (Fig. 4b). At 1 m*M*, however, D-arginine sometimes caused slight relaxation of the cardiac stomach. This may be due to the presence of small amounts of L-arginine in our D-arginine stock. Alternatively, D-arginine may produce effects at 1 m*M* due to the action of an isomerase that converts D-arginine to L-arginine.

In each preparation, consistent dose-dependent relaxation was observed with L-arginine. However, preparations varied in the shape and magnitude of their responses to L-arginine. For example, some preparations relaxed rapidly and then partially restored basal tone prior to washing (Fig. 4b) and others responded with a slow but sustained relaxation that was only reversed on washing (Fig. 4c). Differences in responses among preparations probably reflect natural variability in the motility and metabolic state of the cardiac stomach in starfish.

L-NMMA did not have a consistent effect on cardiac stomach tone when tested alone, although we observed a gradual and slight increase in tone in some preparations. However, in preparations pre-incubated with L-NMMA for 30 min, the relaxing effect of L-arginine (Fig. 4c) was partially inhibited (56%; Fig. 4d). The mean percentage inhibition of 1 m*M* L-arginine-induced relaxation by 0.1 m*M* L-NMMA from three experiments performed on different preparations was 60.0 ± 9.9% (Fig. 4e).

We further investigated the mode of action of L-arginine on the cardiac stomach by testing the effect of ODQ on L-arginine responses. Ten μM ODQ caused partial inhibition (41.4%) of the relaxing effect of L-arginine (Fig. 4f) as illustrated in Figure 4g. In three experiments

Figure 3. ODQ inhibits SNAP-induced relaxation of the cardiac stomach. (a) SNAP-induced relaxation before application of ODQ. (b) Incubation in 10 μM ODQ for 15 min prior to application of SNAP inhibits (94.8%) the relaxing effect of SNAP. (c) After washing (60 min), the relaxing effect of SNAP is restored. The dashed line in each section of the figure indicates basal tone in the preparation prior to application of the first sample of SNAP in (a). The biphasic nature of the response to SNAP in (a) but not in (c) was not seen in all preparations tested, but we have shown it here because it reflects natural variability that is typical for this preparation. The gain is 2 in (a), (b), and (c). (d) Graph showing the mean and standard error of the inhibitory effect of ODQ on SNAP-induced relaxation from five experiments on different preparations.

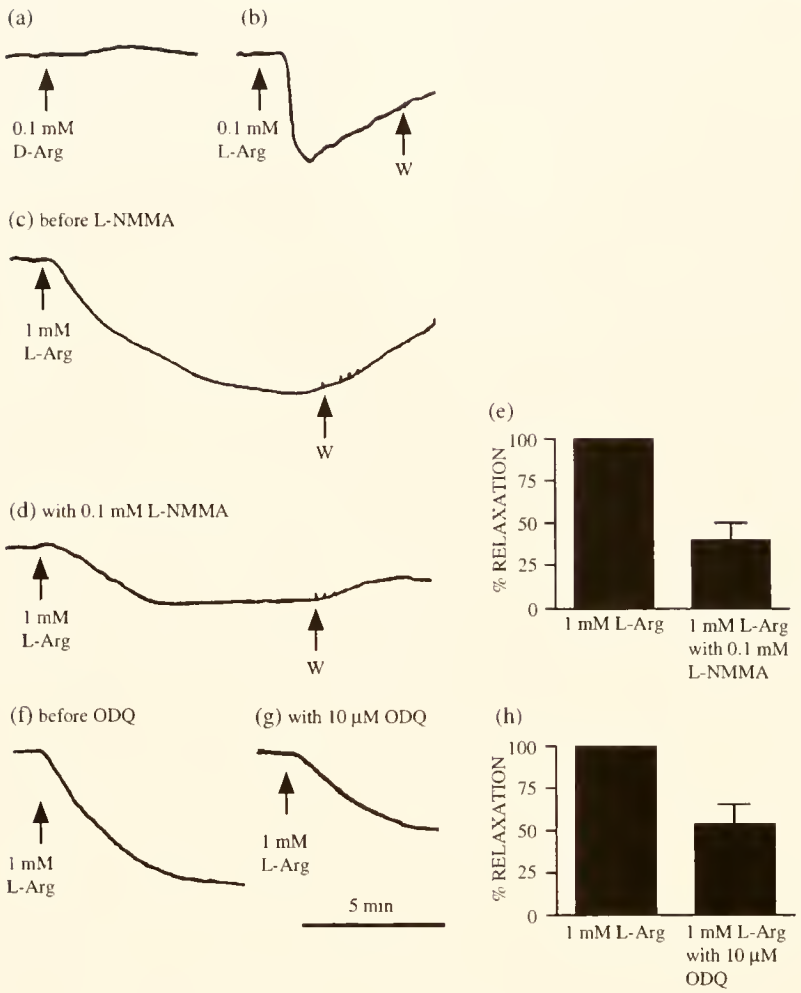

Figure 4. L-NMMA and ODQ inhibit L-arginine-induced relaxation of the cardiac stomach. (a) D-arginine has no effect on a cardiac stomach preparation in which (b) L-arginine causes relaxation; gain 5. (c) L-arginine-induced relaxation is (d) inhibited (56%) when the preparation is pre-incubated with 0.1 m*M* L-NMMA for 30 min; gain 3. (e) Graph showing the mean and standard error of the inhibitory effect of 0.1 m*M* L-NMMA on 1 m*M* L-arginine-induced relaxation from three experiments on different preparations. (f) L-arginine-induced relaxation is (g) inhibited (41.4%) when the preparation is pre-incubated with 10 μM ODQ for 15 min; gain 3. (h) Graph showing the mean and standard error of the inhibitory effect of 10 μM ODQ on 1 m*M* L-arginine-induced relaxation from three experiments on different preparations.

performed on different preparations, the mean percentage inhibition of 1 m*M* L-arginine-induced relaxation by 10 μM ODQ was 46.5 ± 11.6% (Fig. 4h).

Discussion

The results of the experiments described here demonstrate that NO causes relaxation of the starfish cardiac stomach and indicate the presence of a NO-cGMP signaling pathway in the cardiac stomach. Three chemically distinct NO-donors, hydroxylamine, SNOG, and SNAP, caused relaxation of the cardiac stomach while NAP, which is chemically identical to SNAP apart from the absence of a NO moiety, had no effect on the cardiac stomach. This provides clear evidence that NO causes relaxation of the starfish stomach. However, it is more difficult to demonstrate that NO is naturally released by cells in the cardiac stomach to regulate muscle tone. Nevertheless, by testing a range of NO-cGMP pathway inhibitors and the substrate for NOS, L-arginine, we have obtained a series of consistent responses, all of which support the notion that NO is a natural regulator of muscle contractility in the starfish cardiac stomach.

Methylene blue causes contraction of the cardiac stomach in a dose-dependent manner, but we cannot be certain of the mode of action of this compound because it inhibits

both of the key enzymic components of the NO-cGMP pathway, NOS and SGC (Miki *et al.*, 1987; Mayer *et al.*, 1993). Therefore, inhibition of basal NO production by NOS or inhibition of the activation of SGC by endogenous NO could account for the contracting effect of methylene blue on the cardiac stomach. The effects of ODQ on the cardiac stomach, however, can be attributed to its property as a selective inhibitor of SGC (Garthwaite *et al.*, 1995). ODQ causes contraction of the cardiac stomach, suggesting that it is blocking activation of SGC by endogenous NO. Evidence that ODQ exerts its effects by inhibiting activation of SGC by endogenous NO is provided by experiments in which ODQ blocked the relaxing effect of exogenous NO in the form of the NO-donor SNAP. ODQ also partially inhibits the relaxing effect of the NOS substrate L-arginine, indicating that endogenous production of NO regulates cardiac stomach tone by activating SGC. Likewise, the NOS inhibitor L-NMMA partially inhibits the relaxing effect of L-arginine, indicating the presence of NOS in the cardiac stomach.

Therefore, collectively the experiments described here indicate that NO is synthesized by NOS in the cardiac stomach and regulates this organ by activating SGC to generate cGMP, which leads to relaxation. The cellular location of the enzymic components of this NO-cGMP pathway in the cardiac stomach is not known. However, the presence of NOS-like immunoreactivity in basiepithelial neurons of cardiac stomach (Martinez *et al.*, 1994) suggests that NO is released by neurons. It seems most likely that NO is released in the basiepithelial nerve plexus, which is separated in the cardiac stomach from a smooth muscle layer by a thin layer of connective tissue (see Moore and Thorndyke, 1993, for diagrams). The most likely location for SGC is in the smooth muscle cells of the cardiac stomach, as in the mammalian gut (Boeckxstaens and Pelckmans, 1997). Here activation of SGC by NO would cause increased cGMP levels, which in turn could act as an intracellular signal mediating relaxation.

The proposed anatomy of NO-cGMP signaling in the cardiac stomach may explain some of the results obtained with NO-cGMP pathway inhibitors. The SGC inhibitor ODQ caused contraction of the cardiac stomach. We attribute this to inhibition of SGC activation by endogenously released NO. If this is correct, then one could predict that the NOS inhibitor L-NMMA would also cause contraction by inhibiting endogenous NO production. However, with L-NMMA we did not observe contractions like those seen with ODQ, although in some preparations a gradual increase in tone was observed. How can this be explained? It may simply reflect the relative permeability of the two drugs in cardiac stomach tissue and the depth of tissue they must penetrate to reach their molecular targets. The molecular target of ODQ (SGC) is likely to be located in the superficial muscle layer, whereas the molecular target of L-NMMA (NOS) is apparently located in neurons (Martinez *et al.*, 1994) that are separated from the bathing medium by several layers of cells and connective tissue.

It should be recognized, however, that although the function of the NO-cGMP pathway in the starfish cardiac stomach may be similar to its role in the mammalian gut, the anatomy of the innervation is quite different. In mammals, NO is released by inhibitory non-adrenergic non-cholinergic (NANC) nerves of the peripheral autonomic nervous system (Boeckxstaens and Pelckmans, 1997). Homologs of NANC nerves are not present in echinoderms, and innervation of the starfish cardiac stomach consists solely of an intrinsic basiepithelial nerve plexus. Moreover, NO is only one of a number of molecules that are considered to function as inhibitory NANC neurotransmitters in mammals. Other substances that may act in series or in parallel with NO include the neuropeptide vasoactive intestinal peptide and ATP (Boeckxstaens and Pelckmans, 1997).

The discovery of a NO-cGMP signaling system in the starfish cardiac stomach is interesting for a number of reasons. This is the first study, to the best of our knowledge, that has investigated NO function in an echinoderm. Moreover, NO-cGMP-mediated relaxation of smooth muscle has thus far been described only in vertebrates. The presence of this pathway in a stomach preparation from an echinoderm indicates that NO-cGMP-mediated smooth muscle relaxation may be widespread in the animal kingdom.

The presence of the NO-cGMP pathway in the starfish cardiac stomach is of particular interest because of the role this organ plays in the unusual feeding behavior of these animals. Starfish like *Asterias rubens* feed by everting their cardiac stomach through an oral opening and over digestible parts of prey such as mussels and oysters. Very little is known about how eversion of the cardiac stomach is controlled, but it is clear that the stomach must be relaxed for eversion to be accomplished (Anderson, 1954). Recently, a neuropeptide (S2) belonging to a family of echinoderm peptides known as SALMFamides was identified as a potent relaxant of the starfish cardiac stomach (Elphick *et al.*, 1991, 1995a). In the present study we show that the NO-cGMP pathway also mediates relaxation of the cardiac stomach. This indicates that cardiac stomach relaxation and eversion is controlled by several neuronal signaling systems that may act in parallel or in series. The complexity of the pharmacology of the cardiac stomach is therefore comparable with the aforementioned NANC innervation of the mammalian gut. In the future we plan to investigate possible interactions between the SALMFamide neuropeptide system and the

NO-cGMP pathway in regulating relaxation of the starfish cardiac stomach.

Acknowledgments

This work was supported by a research grant (17912) awarded to M.R.E. by the Royal Society (UK). We are grateful to Helen Dawson, who did some preliminary experiments in our laboratory that showed that hydroxylamine and SNAP cause relaxation of strips of the starfish cardiac stomach.

Literature Cited

Anderson, J. M. 1954. Studies on the cardiac stomach of the starfish *Asterias forbesi*. *Biol. Bull.* **107:** 157–173.

Bascal, Z. A., A. Montgomery, L. Holden-Dye, R. G. Williams, and R. J. Walker. 1995. Histochemical mapping of NADPH diaphorase in the nervous system of the parasitic nematode *Ascaris suum*. *Parasitology* **110:** 625–637.

Boeckxstaens, G. E., and P. A. Pelckmans. 1997. Nitric oxide and the non-adrenergic non-cholinergic neurotransmission. *Comp. Biochem. Physiol.* **118A:** 925–937.

Bult, H., G. E. Boeckxstaens, P. A. Pelckmans, F. H. Jordaens, Y. M. Van Maercke, and A. G. Herman. 1990. Nitric oxide as an inhibitory non-adrenergic non-cholinergic neurotransmitter. *Nature* **345:** 346–347.

Colasanti, M., G. M. Lauro, and G. Venturini. 1995. NO in hydra feeding response. *Nature* **374:** 505.

Dawson, T. M., and S. H. Snyder. 1994. Gases as biological messengers: nitric oxide and carbon monoxide in the brain. *J. Neurosci.* **14:** 5147–5159.

Elphick, M. R., D. A. Price, T. D. Lee, and M. C. Thorndyke. 1991. The SALMFamides: a new family of neuropeptides isolated from an echinoderm. *Proc. Roy. Soc. Lond. B* **243:** 121–127.

Elphick, M. R., S. J. Newman, and M. C. Thorndyke. 1995a. Distribution and action of SALMFamide neuropeptides in the starfish *Asterias rubens*. *J. Exp. Biol.* **198:** 2519–2525.

Elphick M. R., G. Kemenes, K. Staras, and M. O'Shea. 1995b. Behavioral role for nitric oxide in chemosensory activation of feeding in a mollusc. *J. Neurosci.* **15:** 7653–7664.

Garthwaite, J. 1991. Glutamate, nitric oxide and cell-cell signalling in the nervous system. *Trends Neurosci.* **14:** 60–67.

Garthwaite, J., E. Southam, C. L. Boulton, E. B. Nielsen, K. Schmidt, and B. Mayer. 1995. Potent and selective inhibition of nitric oxide-sensitive guanylyl cyclase by 1H-[1,2,4]oxadiazolo[4,3-a]quinoxalin-1-one. *Mol. Pharmacol.* **48:** 184–188.

Gelperin, A. 1994. Nitric oxide mediates network oscillations of olfactory interneurons in a terrestrial mollusc. *Nature* **369:** 61–63.

Jacklet, J. W., and M. Gruhn. 1994. Nitric oxide as a putative transmitter in *Aplysia* neural circuits and membrane effects. *Neth. J. Zool.* **44:** 524–534.

Leake, L. D., and L. L. Moroz. 1996. Putative nitric-oxide synthase (NOS)-containing cells in the central-nervous-system of the leech, *Hirudo medicinalis*—NADPH-diaphorase histochemistry. *Brain Res.* **723:** 115–124.

Martinez, A., V. Riveros-Moreno, J. M. Polak, S. Moncada, and P. Seesma. 1994. Nitric oxide (NO) synthase immunoreactivity in the starfish *Marthasterias glacialis*. *Cell Tissue Res.* **275:** 599–603.

Mayer, B., F. Brunner, and K. Schmidt. 1993. Inhibition of nitric oxide synthase by methylene blue. *Biochem. Pharmacol.* **45:** 367–374.

Miki, N., Y. Kawabe, and K. Kuriyama. 1987. Activation of cerebral guanylate cyclase by nitric oxide. *Biochem. Biophys. Res. Commun.* **75:** 851–856.

Moncada, S., R. M. J. Palmer, and E. A. Higgs. 1991. Nitric oxide—physiology, pathophysiology and pharmacology. *Pharmacol. Rev.* **43:** 109–142.

Moore, S. J., and M. C. Thorndyke. 1993. Immunocytochemical mapping of the novel echinoderm neuropeptide SALMFamide 1 (S1) in the starfish *Asterias rubens*. *Cell Tissue Res.* **274:** 605–618.

Müller, U. 1997. The nitric oxide system in insects. *Prog. Neurobiol.* **51:** 368–381.

Müller, U., and H. Hildebrandt. 1995. The nitric oxide/cGMP system in the antennal lobe of *Apis melifera* is implicated in integrative processing of chemosensory stimuli. *Eur. J. Neurosci.* **7:** 2240–2248.

Nilsson, G. E., and V. Söderström. 1997. Comparative aspects on nitric oxide in brain and its role as a cerebral vasodilator. *Comp. Biochem. Physiol.* **118A:** 949–958.

Olsson, C., and S. Holmgren. 1997. Nitric oxide in fish gut. *Comp. Biochem. Physiol.* **118A:** 959–964.

Palmer, R. M. J., A. G. Ferrige, and S. Moncada. 1987. Nitric oxide release accounts for the biological activity of endothelium-derived relaxing factor. *Nature* **327:** 524–526.

Robertson, J. D., J. Bonaventura, A. Kohm, and M. Hiscat. 1996. Nitric oxide is necessary for visual learning in *Octopus vulgaris*. *Proc. Roy. Soc. Lond. B* **263:** 1739–1743.

Salleo, A., G. Musci, P. F. A. Barra, and L. Calabrese. 1996. The discharge mechanism of acontial nematocytes involves the release of nitric oxide. *J. Exp. Biol.* **199:** 1261–1267.

Schuman, E. M., and D. V. Madison. 1994. Nitric oxide and synaptic function. *Ann. Rev. Neurosci.* **18:** 283–317.

Reference: *Biol. Bull.* **194:** 267–280. (June, 1998)

Comparative Morphology of the Eyes of Postlarval Bresiliid Shrimps From the Region of Hydrothermal Vents

E. GATEN[1,*], P. J. HERRING[2], P. M. J. SHELTON[1], AND M. L. JOHNSON[1]

[1]*Department of Biology, University of Leicester, University Road, Leicester LE1 7RH, UK; and* [2]*Southampton Oceanography Centre, Empress Dock, Southampton, SO14 3ZH, UK*

Abstract. The structure and ultrastructure of the eyes of postlarval vent shrimps provisionally designated '*Alvinocaris*' and '*Chorocaris*' are described. The eyes of the postlarval '*Alvinocaris*' are cylindrical, borne on short stalks, and contain closely packed rhabdoms. The ommatidia lack dioptric apparatus and have rhabdoms extending almost to the cornea. The rhabdoms consist of orthogonal layers of microvilli typical of crustacean rhabdoms. The eyes of the '*Chorocaris*' are similar, but the rhabdom layer extends back through the reduced eyestalks and covers some of the dorsal surface of the cephalothorax. The rhabdoms from both the anterior and the thoracic regions consist of layered microvilli. The eyes of a slightly smaller postlarval vent shrimp, termed 'Type A', differ. Although clearly related to the other vent shrimps, Type A has stalked eyes held at an angle to the head. The eye displays a gradient of ommatidial development, with the older ommatidia closely resembling those seen in the other postlarval types. Between the cornea and the rhabdom layer, the youngest ommatidia possess quadripartite crystalline cones similar to those seen in related families of caridean shrimps; these are absent in the more mature ommatidia. The external structure of the anterior and thoracic eyes of juvenile *Rimicaris exoculata* (after settlement at the vent site) is also described. Juveniles up to 9 mm in carapace length have anterior corneas similar to those seen in postlarvae, whereas in larger specimens the corneas are progressively replaced by an ocular plate.

Received 16 September 1997; accepted 19 March 1998.

* To whom correspondence should be addressed. E-mail: gat@leicester.ac.uk

Introduction

Hydrothermal vents are generally found in the region of tectonic plate boundaries such as the mid-Atlantic ridge and the Galapagos rift. The emission of super-heated water (350°C) rich in minerals has led to the establishment of communities of animals that live around these vents and feed primarily on chemoautotrophic bacteria (Segonzac *et al.*, 1994). Such communities are dominated on the mid-Atlantic ridge by caridean shrimps of the family Bresiliidae (Williams and Rona, 1986). In the present study, the structure and ultrastructure of the eyes of postlarval shrimps obtained in the dark by trawling above a vent field in the mid-Atlantic ridge are described. In addition, the progressive reduction in size and disappearance of the anterior eyes during development is described in juvenile specimens of *Rimicaris exoculata* obtained from two vent sites sampled using a submersible vehicle.

The commonest vent shrimps recorded from the mid-Atlantic ridge are *Rimicaris exoculata, Chorocaris chacei,* and *Alvinocaris markensis* (Segonzac *et al.*, 1994), although there may be other species present. Although lacking conventional compound eyes, adult specimens of *R. exoculata* possess a large white photosensitive organ (thoracic eye) beneath the dorsal surface of the carapace (Van Dover *et al.*, 1989). It has been suggested that this thoracic eye is used for detecting light emitted from the vents (Pelli and Chamberlain, 1989; Van Dover *et al.*, 1994). In the present study we found that, in their early stages, postlarval *R. exoculata* possess eyes of a conventional appearance, but that these gradually disappear during development. Because the eyes do not contain any dioptric apparatus during the later stages of development,

they are referred to below as anterior eyes (if located in the position normally occupied by the eyestalks) and dorsal or thoracic eyes (if located on the dorsal surface of the cephalothorax). The structure of the thoracic eye has been described for *R. exoculata* (O'Neill *et al.*, 1995) and for a new unidentified species of *Rimicaris* (Nuckley *et al.*, 1996). The evolutionary origins of the thoracic eye are not immediately obvious, although possible clues to its provenance may come from studies of vent shrimps possessing eyes of a more conventional appearance. *Alvinocaris markensis* has no thoracic eye but does possess small anterior eyes, although it has been reported that the latter contain no photoreceptors (Wharton *et al.*, 1997). *Chorocaris chacei* and *Chorocaris fortunata* not only have reduced anterior eyes but also have thoracic eyes that may be contiguous with them (Lakin *et al.*, 1997; Kuenzler *et al.*, 1997). Hypotheses about the relationship of the thoracic organ to the usual decapod compound eye have been put forward (O'Neill *et al.*, 1995; Nuckley *et al.*, 1996; Lakin *et al.*, 1997; Kuenzler *et al.*, 1997), but the development of vent shrimp eyes has not been investigated. In the current study, the structure of both anterior and thoracic eyes is described in various postlarval and juvenile stages of vent shrimps. The term *postlarvae* is used here to designate post-zoeal stages bearing the full complement of abdominal appendages (Herring and Dixon, 1998).

Because the eyes of deep-sea decapod crustaceans are adapted to maximize sensitivity, they are susceptible to light-induced damage when they are exposed to light levels significantly higher than ambient (Loew, 1976; Shelton *et al.*, 1985). The damage manifests itself as irreversible rhabdom breakdown and changes to other structures in the eye (Gaten *et al.*, 1990). The thoracic eyes of adult vent shrimps described at the ultrastructural level in previous studies were obtained from animals that had been illuminated by the floodlights of a submersible vehicle during capture and sometimes by other light sources afterwards (O'Neill *et al.*, 1995; Nuckley *et al.*, 1996; Lakin *et al.*, 1997; Kuenzler *et al.*, 1997). This is likely to lead to light-induced structural damage, making it difficult to be certain that the appearance of the rhabdoms in such material is normal. Thoracic eye rhabdoms are described as lacking the orthogonally orientated layers of microvilli typical of rhabdoms in other Crustacea, and they often contain irregular arrays of microvilli—some of which may be expanded to form vesicles within the rhabdom (Van Dover *et al.*, 1989; O'Neill *et al.*, 1995; Nuckley *et al.*, 1996; Kuenzler *et al.*, 1997). To confirm that this appearance is not artifactual, it is necessary to examine material that has not been exposed to visible light. The postlarval shrimps used for ultrastructural analysis in the present study were obtained by trawling. Consequently they had not encountered lights from a submersible vehicle, and they were not exposed to white light at any stage during capture. This has enabled us to investigate rhabdom structure in specimens that have definitely not been damaged by light. The results show that in the postlarval stages at least, the rhabdom structures in both anterior and thoracic eyes have the banded appearance typical of other crustaceans.

The shrimps we examined were taken from a collection made during a mid-Atlantic survey carried out during Charles Darwin cruise 95 (Herring, 1996). Although no classification of postlarval bresiliid shrimps is currently available, the collection was found to contain three morphologically distinct types: postlarvae of the genus *Alvinocaris*, a group classified as '*Chorocaris*' type, and a group of morphologically indistinguishable younger postlarvae that were arbitrarily designated 'Type A' (Herring, 1996). A DNA analysis of selected specimens from the collection concluded that the *Alvinocaris* postlarvae were probably *A. markensis*, while those identified as '*Chorocaris*' type postlarvae were indeed mainly *Chorocaris* sp. but included occasional specimens of *Rimicaris* (Dixon and Dixon, 1996). The same study found that the Type A specimens included individuals from three genera: *Alvinocaris*, *Chorocaris*, and *Rimicaris*. Whatever the final assignation of the specimens, the present paper represents the first description of developing stages of anterior and thoracic eyes in vent shrimps. It also shows that the thoracic eyes are anatomically continuous with the anterior eyes in postlarval stages and are almost certainly derived from them.

Materials and Methods

Most of the postlarval shrimps described were obtained by trawling above a known hydrothermal vent site (Broken Spur—29°10′N) in the mid-Atlantic ridge (segment 17) during cruise 95 of the RRS *Charles Darwin*. The maximum depth in the region of the vent field is 3200 m. A multiple rectangular midwater trawl (Roe and Shale, 1979) was used to fish the nets above the vent region at depths ranging from 2000 to 3050 m. A total of 232 postlarval vent shrimps, all between 13 mm and 23 mm total length, were taken, mostly within 1000 m of the vent. Although abundances decreased both vertically and horizontally away from the vents, some shrimps were taken at more than 100 km from known vents (Herring, 1996). The nets were hauled after dark, the opaque codends were protected from light, and the shrimps were sorted under dim red light to avoid light-induced damage.

Whole shrimps, heads, or eyes were fixed in the dark in 3% glutaraldehyde in 0.1 *M* phosphate buffer, pH 7.2. Some specimens were embedded on board ship (through

a graded ethanol series and into Taab E-Mix resin *via* propylene oxide), whilst others were stored in fixative and embedded ashore up to 3 months later (dehydrated in acetone and embedded in Spurr's resin). Semithin (1 μm) sections were taken for light microscopy and pale gold sections for electron microscopy. Semithin sections were stained in 1% toluidine blue in 4% borax and mounted in resin under a thin coverslip. Ultrathin sections were mounted on grids, stained by standard techniques in uranyl acetate and lead citrate, and observed on a JEOL CX100 transmission electron microscope. Other specimens were dehydrated, critical point dried in carbon dioxide, and coated with gold/palladium for observation using a Cambridge S100 scanning electron microscope.

Quantitative measurements were made from both electron micrographs (diameters of microvilli) and light micrographs (rhabdom volume density and microvillar surface area). To determine the rhabdom volume density, rhabdom areas were measured on micrographs of transverse and longitudinal sections of the retinular cell layer and recorded as a proportion of the total area. The surface area of microvillar membrane was calculated assuming that the microvilli are cylindrical and hexagonally packed; the values are recorded as square micrometers of membrane per cubic micrometer of rhabdom.

A limited number of large juvenile shrimps were obtained by net from a submersible at the Broken Spur (29°10′N) and TAG (26°8.25′N) sites during the Russian/British BRAVEX/94 program. They were fixed in buffered formalin solution, without having been protected from light during capture.

Results

External appearance

The '*Chorocaris*' type postlarvae (Fig. 1A) and the *Alvinocaris markensis* postlarvae (Fig. 1C) are similar in general appearance, differing primarily in the lengths of the rostra and in the presence of a thoracic eye in the former. '*Chorocaris*' has anterior eyes that are almost cuboid, largely because the anterior medial surfaces of the two eyes are flattened where they abut each other and the ventral surfaces of the eyes are flattened where they abut the underlying carapace. The lateral and anterior surfaces of the eye are also relatively flat. Both anterior eyes are almost hidden beneath the short, blunt rostrum; they are sessile and, although separate at anterior levels, they are fused in the midline more posteriorly. A small papilla is present on the medio-dorsal region of the cornea. The anterior eyes do not show regular external facetting, but roughly square arrays of ommatidial units are visible in fresh specimens. This pattern extends seamlessly behind the eye and into the thorax, where the retina extends to form thoracic eye lobes on either side of the midline beneath the dorsal carapace. The thoracic eyes are white in freshly caught animals, but turn dark following extended fixation. The *Alvinocaris markensis* postlarvae have a long, pointed rostrum with anterior eyes that are rounded and sessile. They also possess a corneal papilla. There is no sign of any external facetting on the cornea (Fig. 1B) and no extension of the retina into the thoracic region to form thoracic eyes.

Type A postlarvae differ from the preceding types principally in the structure of the eyes. These are borne on eyestalks projecting forward at an angle of about 45° to the antero-posterior axis and are located on either side of the long, pointed rostrum (Fig. 1D). In this orientation the functional parts of the eye face laterally and anteriorly. The carapace covers most of the medial face of the eyestalk. As in the other two taxa, a papilla is present on each eyestalk. Scanning electron micrographs revealed traces of external facetting on the cornea even though the soft cornea in most of the specimens had been damaged during capture or subsequent processing. The facets are hexagonal over most of the eye (Fig. 1E), although some postero-ventral facets are square (Fig. 1F). There is no sign of a thoracic eye. The anterior eyes of the juvenile shrimps obtained from Broken Spur and TAG varied in the extent to which they were developed, with the smaller individuals possessing the most pronounced anterior eyes. In the largest specimens, anterior eyes were replaced by a fused ocular plate as in adult *R. exoculata* (Segonzac *et al.*, 1994). In addition to the variability in eye appearance, these specimens revealed differences in the degree of reduction of the rostra and the inflation and forward expansion at the rounded anterolateral margins of the carapace. They all possessed a thoracic eye, and the first cheliped had the slender shape and chela structure typical of *R. exoculata* (Williams and Rona, 1986). Although in certain respects they resembled juvenile *Chorocaris chacei*, the antennal scale completely lacked the external tooth characteristic of that species. In addition, they possessed rounded eyes rather than the cuboidal ones seen in juvenile *Chorocaris*. On the basis of the antennal scale characteristics and the structure of the first cheliped, we are confident that these juvenile vent shrimps obtained from the Broken Spur and TAG sites are *R. exoculata*. Because of their variable appearance, the anterior eye, carapace, and rostrum are not reliable characteristics for the separation of juvenile *Rimicaris* and *Chorocaris*. At the earlier postlarval stage, *R. exoculata* and *C. chacei* are morphologically inseparable but genetically distinct (Dixon and Dixon, 1996). As they mature, juveniles of *R. exoculata* apparently undergo a progressive reduction in the anterior eyes and rostra.

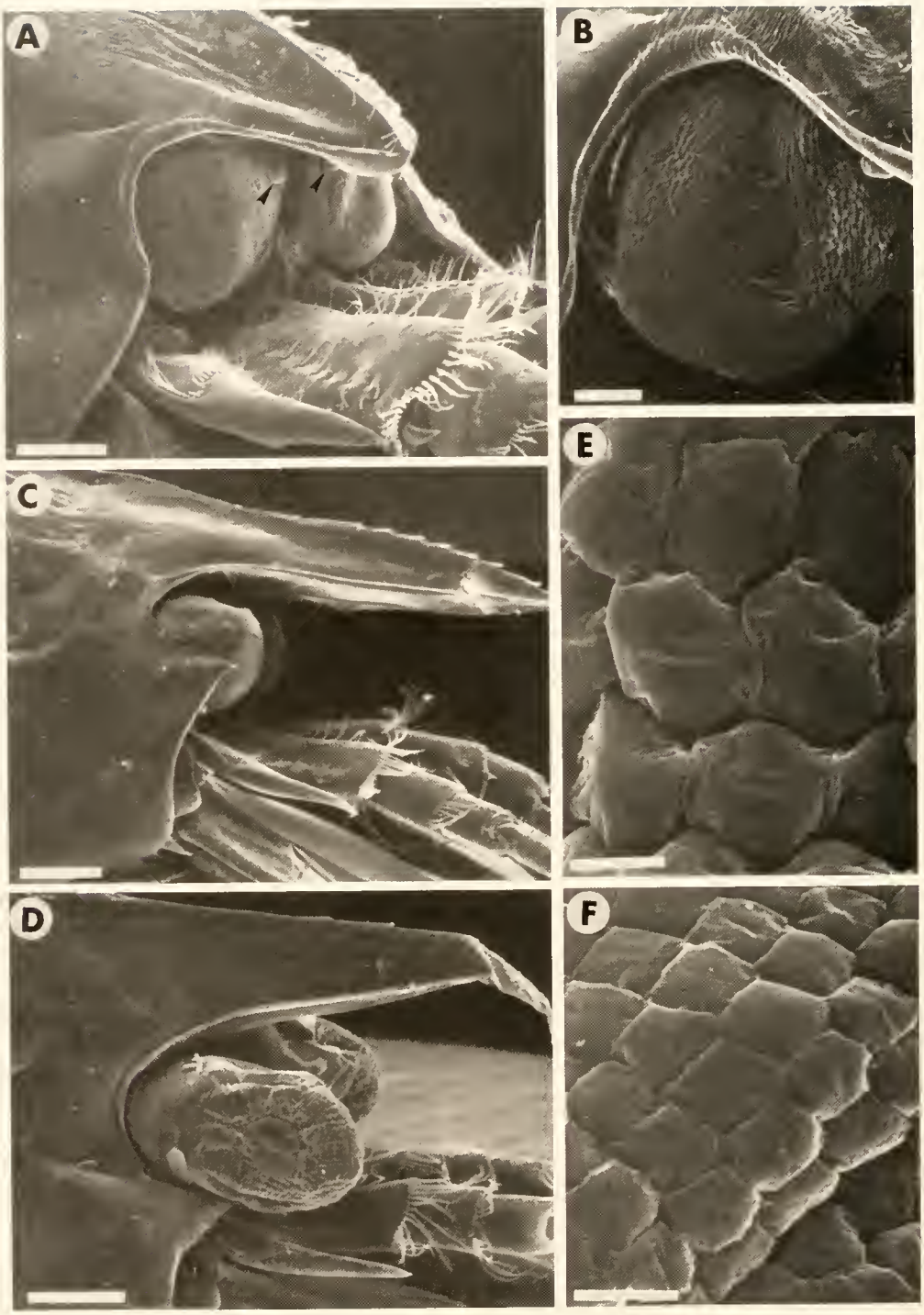

Figure 1. Scanning electron micrographs of postlarval vent shrimps. (A) Antero-lateral view of '*Chorocaris*' showing the eyes almost hidden beneath the short blunt rostrum. Papillae (arrowed) are present on each eyestalk. (B) Anterior view of the right eye of the same species. Although the surface of the cornea is sculptured, there is no visible facetting. (C) Lateral view of *Alvinocaris* showing the much longer rostrum. (D) In this lateral view of Type A it can be seen that the eyestalks protrude either side of the long rostrum. External facetting is seen in this species, usually arranged hexagonally (E) but including areas of square facets ventrally (F). Scale bars: A = 250 μm, B = 100 μm, C = 500 μm, D = 500 μm, E = 25 μm, F = 50 μm.

Specimens up to 9 mm in carapace length retain distinct anterior corneas with the rostrum extending forward to their anterior limit (Fig. 2A). In larger specimens (carapace length 9.5 mm and above) the corneas are replaced by an ocular plate, and the rostrum is reduced and rounded (Fig. 2B). This reduction continues as the animals mature (Fig. 2C; carapace length 18 mm). Although adults of this species lack the cylindrical eyestalk seen in most caridean shrimp, it has been suggested that the ocular plate (Fig. 2C) is a reduced, flattened modification of the fused eyestalks of related vent shrimps (Martin and Hessler, 1990).

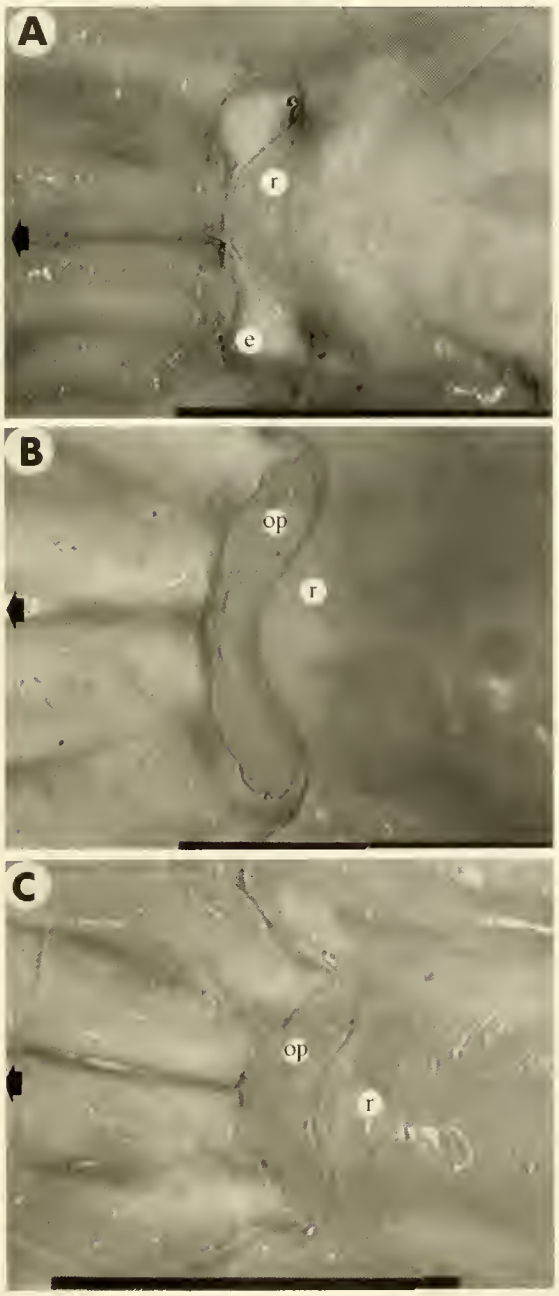

Figure 2. Light micrographs showing the dorsal view of the cephalothorax of *Rimicaris* sp. at various stages of development (arrow points to anterior). (A) Juvenile (9-mm carapace length) with separate eyes (e) and protruding rostrum (r). (B) Juvenile (9.5-mm c.l.) with fused ocular plate (op) and a reduced rostrum. (C) The reduction of the ocular plate and rostrum continues in the adult (18-mm c.l.). Scale bar: A = 2 mm, B = 2 mm, C = 5 mm.

Internal structure

'Chorocaris' *type.* In sagittal sections, the anterior rostrum can be seen to extend forward over the anterior eye (Fig. 3A). The latter is bounded externally by a thin, unfacetted cornea anteriorly and laterally. However, where the cornea is opposed by carapace it is covered by extensive plumose cuticular protrusions. A thin layer of cells (presumed to be corneagenous cells) is present below the cornea (Fig. 3C). There are no crystalline cones. The rest of the eye is dominated by hypertrophied rhabdoms that fill most of the space between the cornea and the basement membrane (Fig. 3A, C). The rhabdom layer extends backward beneath the dorsal carapace of the cephalothorax without interruption to form the thoracic eye (Fig. 3A). The rhabdoms in all parts of the system are lobed, usually x-shaped in cross-section, and not arranged consistently in either a square or hexagonal array (Fig. 3B). Many of the rhabdoms within the anterior eye point in an anterior direction, with the result that vertical sections show rhabdoms with the same shape in cross-section (Fig. 3B). The rhabdoms in the thoracic eye are more variable in their arrangement but are usually at right angles to the carapace (Fig. 3C). Within the photoreceptor layer, the rhabdoms occupy about 75% of the available volume. The rhabdoms consist of microvilli that have a mean diameter of 0.079 μm (SD = 0.006; n = 20) and are arranged in alternating layers, both in the anterior eye (Fig. 3D) and in the thoracic eye (Fig. 3E). The microvilli are generally at right angles to the rhabdom surface, so each layer is not necessarily arranged orthogonal to the adjacent layer, especially in the dorsal eye. The average density of microvillar membrane was 50.8 $\mu m^2/\mu m^3$ of rhabdom.

A tapetum formed of reflecting pigment cells (creamy white in life) lies beneath the rhabdom layer, and the tapetal cells surround the bases of the rhabdoms (Fig. 4A, B). The retinular cells contain shielding pigment granules. Although a few of these granules may be found in the retinular cell cytoplasm adjacent to the rhabdoms, most of them are proximal to the photoreceptor nucleus and the tapetum (Fig. 4A). Lipid droplets are also abundant in the cells in this region. All of these cellular inclusions are found in both the anterior and thoracic parts of the visual system.

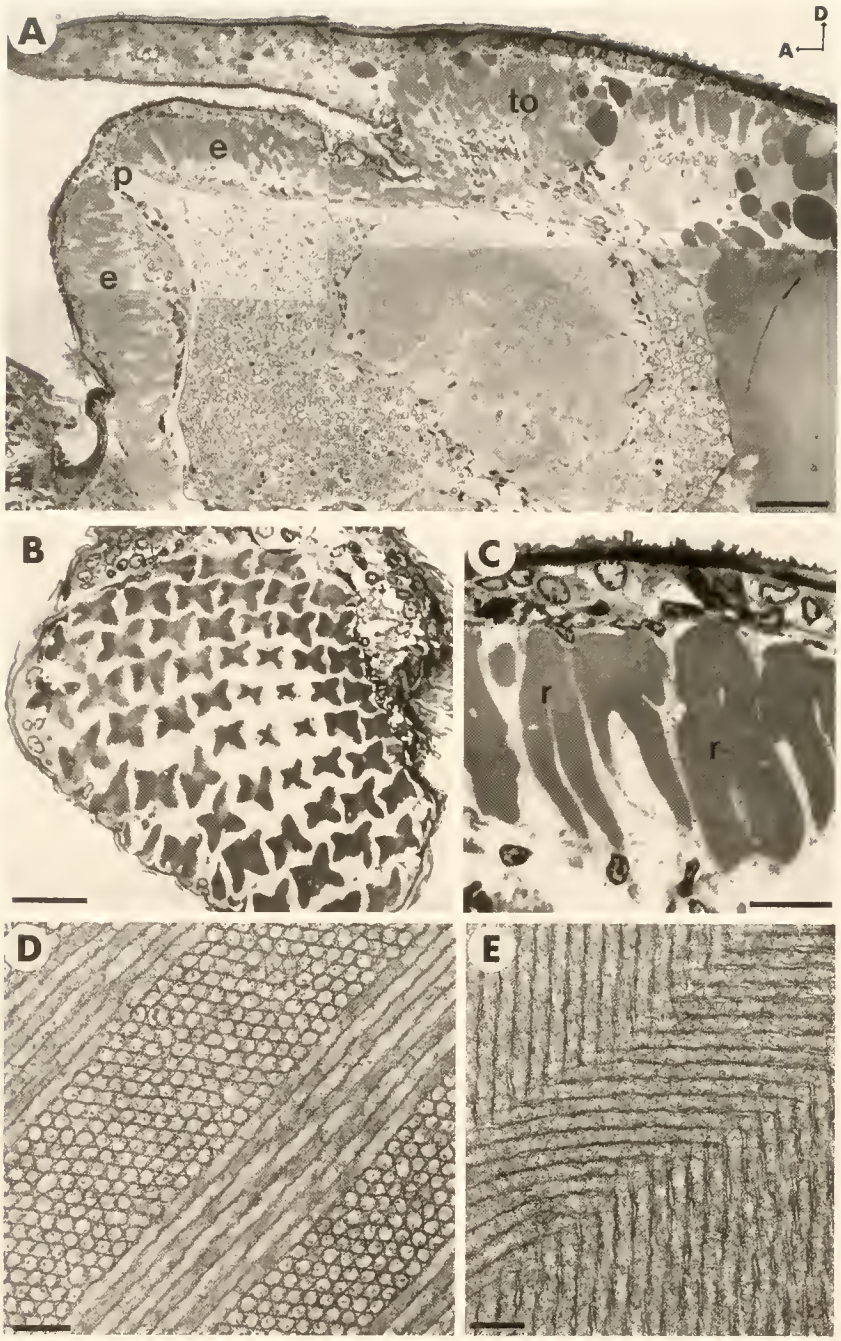

Figure 3. '*Chorocaris*' postlarvae (arrows point to Dorsal and Anterior). (A) Sagittal section showing rhabdoms extending in an almost uninterrupted row around the eye (e) and posteriorly beneath the dorsal carapace to form the thoracic organ (to). The only area in which rhabdoms are missing is where the connection from the sensory papilla (p) to the brain passes through the rhabdom layer. (B) Vertical section through the anterior region of an eye showing the x-shaped cross-sections of anteriorly directed rhabdoms. (C) Rhabdoms (r) in the thoracic organ (seen in longitudinal section) are irregular in shape and extend almost to the cornea. Electron micrographs of rhabdoms show the typical decapod layered arrangement of microvilli, both in the anterior eye (D) and in the thoracic organ (E). Scale bars: A = 100 μm, B = 100 μm, C = 25 μm, D = 0.2 μm, E = 0.2 μm.

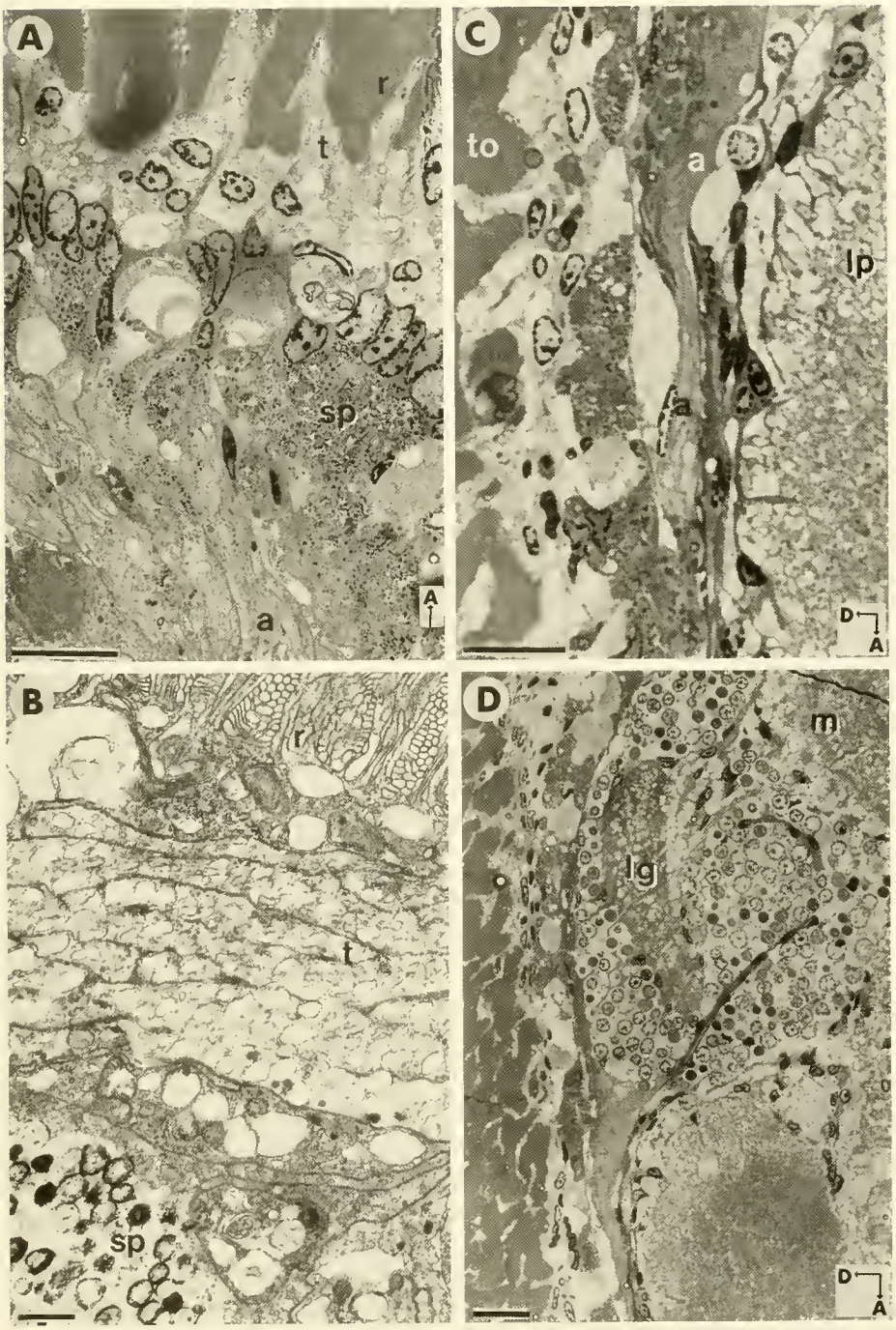

Figure 4. '*Chorocaris*' postlarvae (arrows point to Dorsal and Anterior). (A) Light micrograph showing the proximal rhabdom region (r), tapetum (t), proximal shielding pigment (sp), and the retinular cell axons (a). (B) Electron micrograph of a rhabdom (r), tapetal cell (t) and proximal shielding pigment (sp). (C) Posterior to the anterior eye, retinular cell axons (a) pass between the thoracic organ (to) and the lateral protocerebrum (lp). (D) The retinular axons eventually project onto the lamina ganglion (lg) and the medulla externa (m). Scale bars: A = 25 μm, B = 0.5 μm, C = 25 μm, D = 25 μm.

The retinular cell projection is modified in '*Chorocaris*' by its distinctive brain morphology. In most decapods with stalked eyes, the optic neuropiles are located within the eyestalks in optic lobes that form the most anterior parts of the brain. They form outgrowths of the protocerebrum and lie immediately behind the eye, where they are innervated by retinular cell axons that pass directly through the basement membrane to project to the underlying lamina ganglion. In '*Chorocaris*' postlarvae the eyestalks are greatly reduced and the optic neuropiles are within the main body of the protocerebrum. In addition, the optic lobes do not form the most anterior structure but are displaced posteriorly by the hypertrophied lateral protocerebral neuropile region with its associated cell bodies. It is this protocerebral region that lies immediately behind the basement membrane of the eyes. Because the optic neuropiles are displaced, the retinular cell axons have to travel a considerable distance posteriorly before reaching the lamina ganglion. Together the axons form a distinct optic nerve surrounded by neurilemma that is intimately associated with the basement membrane (Fig. 4C). On entering the protocerebrum, the optic nerve terminates in the lamina ganglion (Fig. 4D).

'Alvinocaris' *type.* The anterior eye is similar in general organization to that of '*Chorocaris*'; the rhabdoms occupy much of the eye, and the crystalline cones are absent. However, in *A. markensis* the rhabdom layer does not extend into the cephalothorax to form a thoracic eye. The rhabdoms are more regular in outline than in '*Chorocaris*' and are often square in cross-section (Fig. 5A). The rhabdoms occupy about 62% of the volume of the retinula cell layer. They point anteriorly over much of the eye with an interommatidial angle of around 3° (Fig. 5B) and taper posteriorly, where they are surrounded by seven retinular cells (Fig. 5C). The rhabdoms show the alternating, orthogonally orientated rows of microvilli characteristic of decapod crustacean eyes (Fig. 5E). The microvilli have a mean diameter of 0.062 μm (SD = 0.002, n = 20), giving a surface area of 66.7 $\mu m^2/\mu m^3$ of rhabdom. Occasional rhabdoms show some evidence of rhabdom breakdown or turnover (Hafner *et al.*, 1980) in the form of multivesicular bodies and lamellar bodies (Fig. 5F). Tapetal reflecting pigment, retinular cell shielding pigment, and lipid are present behind the rhabdom layer in a pattern similar to that seen in '*Chorocaris*'. At the back of the eye, the retinular cell axons combine to form an optic nerve similar in all respects to that in '*Chorocaris*' (Fig. 5D). Once again, the optic nerve travels posteriorly alongside the lateral protocerebrum before joining the brain laterally and terminating in the lamina ganglion.

Type A. Examination of sections of the eye confirms the external observations that the photoreceptor cells are localized in the anterior and lateral regions of the eyestalk (Fig. 6A) and that there is no thoracic eye. In Type A, in contrast to the other two types of postlarvae, the eyestalk contains the neuropile layers of the optic lobes and other anterior protocerebral regions (Fig. 6B). Once again, the retinular cell axons are grouped together to form a distinctive optic nerve. This travels over the surface of the optic lobes to innervate the lamina ganglion (Fig. 6B). Large accumulations of lipid droplets are also found within the eyestalk (Fig. 6A). Unlike the other two species, Type A has crystalline cone cells in some ommatidia, particularly towards the posterior end of the eye (Fig. 6A). In this region the crystalline cones have a fine-grained appearance typical of crustacean eyes, and they abut the layered rhabdom (Fig. 6C). In anterior ommatidia, the rhabdoms extend virtually to the cornea, although the remnants of some indeterminate cells are found distal to the rhabdoms. The rhabdoms are generally square in cross-section (Fig. 6D) and consist of orthogonally orientated layers of microvilli (Fig. 6E). The latter have an average diameter of 0.066 μm (SD = 0.003, n = 20). The volume density of rhabdoms within the photoreceptor layer is about 68%, with a microvillar membrane area of 61.3 $\mu m^2/\mu m^3$ of rhabdom.

Discussion

Structure of the eye

In comparison with other caridean shrimps, the bresiliids described in this paper exhibit a considerable reduction in most of the structures normally found in the decapod eye (summarized in Fig. 7). The ommatidia of most decapod eyes each consist of a corneal facet secreted by two corneagenous cells, a single crystalline cone formed by four cone cells, eight retinular cells forming a single rhabdom, and a number of tapetal cells. In the larval vent shrimps, most of the eye between the cornea and basement membrane is filled with hypertrophied rhabdoms. As in other decapods, the bulk of the rhabdom appears to be formed by seven retinular cells. Although we were not able to identify an eighth retinular cell in the postlarval specimens, a distinct R8 cell has been observed in prezoea larvae of *Chorocaris fortunata* (Gaten, unpubl. data). Most of the cornea is thin, apparently contains no internal lens, and displays an external facet pattern only in Type A. The mixture of hexagonal and square facets is similar to that seen in postlarval oplophorid shrimps during the transformation from apposition to superposition optics (Gaten and Herring, 1995). Apparently, the zoeal eyes of all decapods have hexagonal facets (Nilsson, 1983). If reflecting superposition eyes, with their characteristic square array of facets, represent the primitive condition in adult decapods (Gaten, 1998), then remnants of the square facets might be expected even though these optics

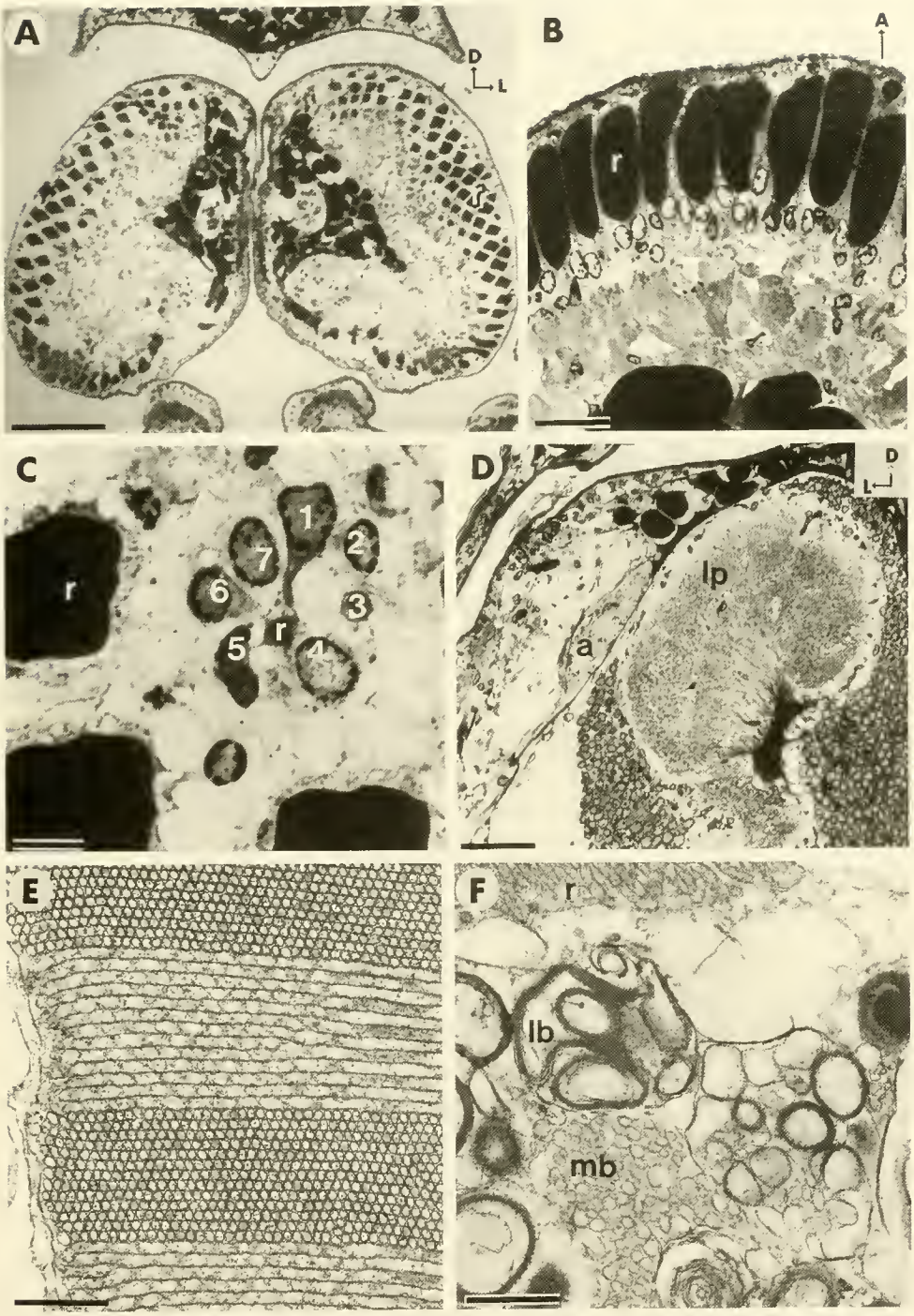

Figure 5. *Alvinocaris* postlarvae (arrows point to Dorsal, Lateral, and Anterior). Light micrographs show the anteriorly directed rhabdoms (r) in vertical transverse sections (A) and in sagittal sections (B) of the eye. (C) The rhabdoms are generally square in cross-section and are surrounded at their base by seven retinular cell nuclei (1–7). (D) Posterior to the eye, the axons (a) remain distal to the basement membrane, still separate from the lateral protocerebrum (lp). Electron micrographs show the layered appearance typical of decapod rhabdoms (E), although there is some evidence of rhabdom turnover (F) in the form of multivesicular bodies (mb) and lamellar bodies (lb). Scale bars: A = 250 μm, B = 50 μm, C = 10 μm, D = 100 μm, E = 0.5 μm, F = 0.5 μm.

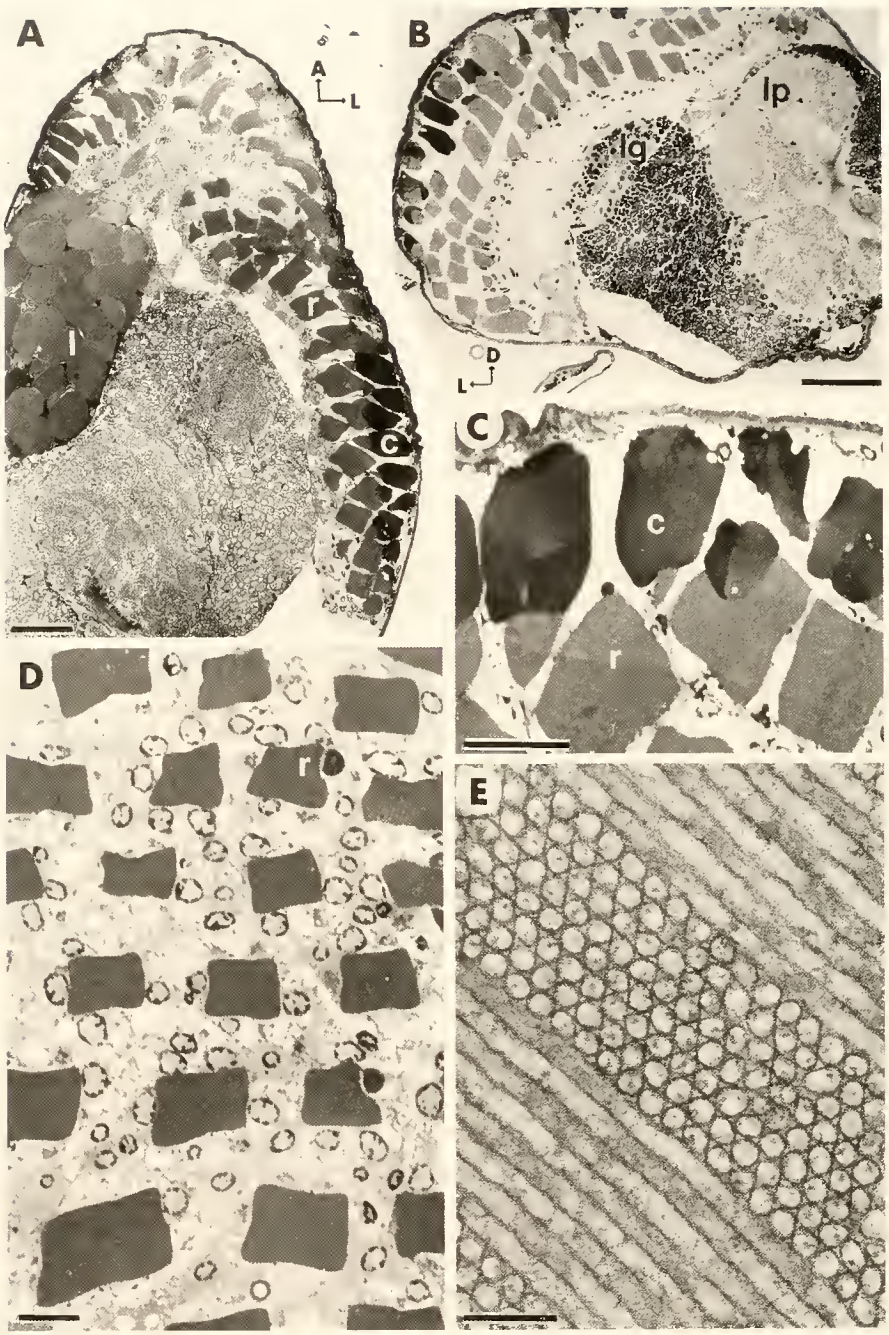

Figure 6. Type A postlarvae (arrows point to Dorsal, Lateral, and Anterior). (A) In horizontal sections, the eyestalks show a region of rhabdoms extending over the anterior and lateral regions. Crystalline cones (c) are present in lateral ommatidia. Lipid (l) fills much of the eyestalk. (B) This cross-section of the eyestalk shows the presence of lateral protocerebral neuropile (lp) and lamina ganglion (lg) below the basement membrane. (C) Crystalline cones (c) are present in lateral regions of the eye between the rhabdoms and the cornea. (D) The rhabdoms (r) are generally square in cross-section. (E) An electron micrograph showing the orthogonal layers of microvilli in the rhabdom. Scale bars: A = 100 μm, B = 100 μm, C = 50 μm, D = 25 μm, E = 0.2 μm.

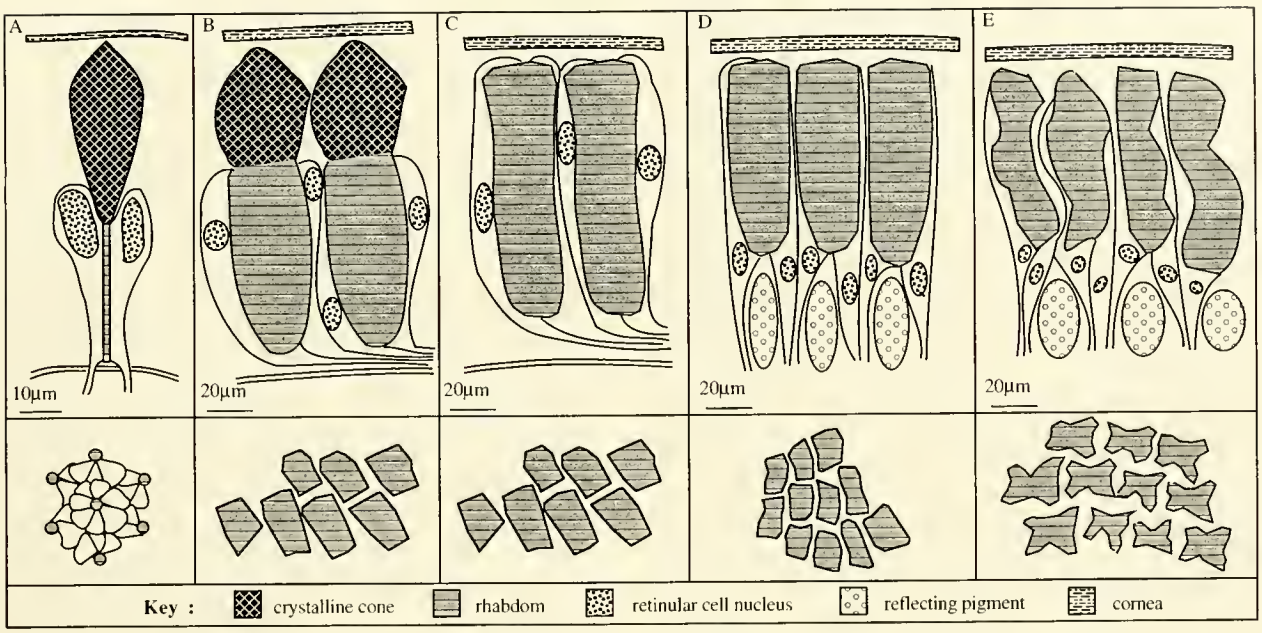

Figure 7. Semi-schematic diagram summarizing the ommatidial structure of the postlarval shrimps described. (A) Prezoea of *Chorocaris fortunata.* (B) Type A lateral ommatidia. (C) Type A anterior ommatidia. (D) *Alvinocaris* type. (E) '*Chorocaris*' type. The distribution of the rhabdoms in transverse section is also shown for each type.

are not used in vent shrimps. In some areas of the eyes of more mature postlarvae, the surface of the cornea bears plumose protrusions that are presumably related to the specialized feeding habits of vent shrimps (Segonzac *et al.,* 1994). Identifiable crystalline cone cells are absent except in the posterior regions of the eye of Type A. Retinular cell shielding pigment is absent from the distal regions of all the eyes examined but is present proximally in reduced amounts. A proximal reflecting layer is prominent, consisting of an extensive array of tapetal cells. An abundance of lipid around the basement membrane probably contributes to the reflecting layer.

The reduction seen in parts of the ommatidia is mirrored to some extent within the Oplophoridae, which are considered to be closely related to the Bresiliidae (Christoffersen, 1990). In the Oplophoridae, eye structure changes with depth. The ommatidia of species from the upper mesopelagic zone, such as *Oplophorus spinosus* (Land, 1976), contain the full range of cells. Species from deeper water, such as *Acanthephyra purpurea,* have very little retinular cell screening pigment, and the rhabdoms interdigitate to form a continuous layer with no optical isolation of rhabdoms (Gaten *et al.,* 1992). In *Hymenodora glacialis,* a species found below the photic zone, the hypertrophied rhabdoms fill the space between the basement membrane and the cornea (Welsh and Chace, 1937).

However, a major departure from the usual decapod pattern is apparent in the position of the optic neuropiles in '*Chorocaris*' and *A. markensis* postlarvae. The optic neuropiles are normally located within the eyestalks, between the eye and the brain. Only in the Type A postlarvae were the optic ganglia found within the eyestalk, although the ganglia were displaced ventrally by the presence of lateral protocerebral neuropile. Compared to the prominent eyestalks of Type A, the eyestalks in the other taxa are greatly reduced. In the latter cases, the region behind the eye is occupied by the prominent lobes of the lateral protocerebrum, and the optic lobes are displaced posteriorly. This is similar to the arrangement in *Birgus latro,* a species in which the optic lobes are located within the body of the protocerebrum (Sandeman *et al.,* 1993). The function of the protocerebral neuropiles within the anterior lobes of the brain is unknown (Sandeman *et al.,* 1993); in '*Chorocaris*' and *A. markensis* these neuropiles extend forward into the bases of the sensory papillae located on the cornea. The optic neuropiles are often relocated from the eyestalks to the head capsule in the Anomura, Brachyura, and Caridea (Sandeman *et al.,* 1993), but the ommatidia remain at the extremity of the eyestalks. It is the reduction of the eyestalk, bringing the marginal ommatidia close to the dorsal carapace of the cephalothorax, that allows the ommatidia to extend backwards to form the thoracic organ.

The main difference between the postlarval eyes de-

scribed here and the thoracic eyes described in published accounts of the genera *Rimicaris* and *Chorocaris* concerns the appearance of the rhabdoms. The eyes of postlarval Type A and *A. markensis* have the orthogonal layers of microvilli typical of most decapod rhabdoms, with all of the microvilli closely packed and of similar diameter (ranging from 0.062 to 0.067 μm). In '*Chorocaris*' postlarvae, the microvilli are larger (about 0.079 μm in diameter) and, although the rhabdoms lack the regular orthogonal arrangement of the layers, the individual microvilli are neatly packed. In contrast, the rhabdoms of the adult eyes described so far (O'Neill *et al.*, 1995; Nuckley *et al.*, 1996; Lakin *et al.*, 1997; Kuenzler *et al.*, 1997) contain larger microvilli (0.09 to 0.12 μm in diameter) that generally lack the orthogonal layering and often show vesiculation towards the edge of the rhabdoms. This unusual appearance of the rhabdoms could reflect some degenerative process occurring in the adults or it could indicate light-induced damage. In deep-sea species, short exposures (as little as 10 s) to daylight can initiate irreversible damage. Although the full morphological impact is not seen for 24 h or more, changes in rhabdom structure are detectable within minutes of exposure (Shelton *et al.*, 1985). If the searchlights employed by the submersible had initiated such damage, the rhabdoms of animals fixed at the surface might show some structural changes. To resolve this question, it is clearly necessary to obtain adult shrimp that have not been exposed to excess light to compare directly with the postlarval rhabdoms described here.

The volume density of rhabdoms within the retinular cell layer varies from 62% in *Alvinocaris markersis* to 75% in '*Chorocaris*'. Similar values—ranging from 60% in *Chorocaris chacei* (Lakin *et al.*, 1997) to 85% in *Rimicaris* sp. (Nuckley *et al.*, 1996)—were recorded for adult vent shrimps. The smaller microvillar diameters and tight packing seen in the postlarval shrimps produce a larger surface area of photosensitive membrane (per unit volume of rhabdom) than has been recorded in the adult shrimps. The values for '*Chorocaris*' (50.76 $\mu m^2/\mu m^3$), *Alvinocaris markensis* (66.66 $\mu m^2/\mu m^3$), and Type A (61.34 $\mu m^2/\mu m^3$) are all higher than the values of 30.7 $\mu m^2/\mu m^3$ for adult *Chorocaris chacei* (Lakin *et al.*, 1997) and 40.3 $\mu m^2/\mu m^3$ for adult *Rimicaris* sp (Nuckley *et al.*, 1996). Nevertheless, the total volume of the rhabdoms is much smaller in the postlarval shrimps than in the adults, making it unlikely that the sensitivity of the eye is any greater in the postlarval shrimps than in adult *Rimicaris exoculata* (Pelli and Chamberlain, 1989).

Optics

The image in decapod eyes is normally focused by the cornea with its internal lens and by the crystalline cone (*e.g.*, Gaten, 1994). In the eyes of vent shrimps, the crystalline cone is absent in all but the smaller postlarval stages, and the cornea is thin and appears to lack an internal lens. Although there is no mechanism for forming a focused image, there may be some directional sensitivity due to the optical isolation of individual rhabdoms. In deep-sea oplophorids such as *Acanthephyra purpurea*, the rhabdoms interdigitate and are contiguous (Gaten *et al.*, 1992), so there can be no optical isolation of the ommatidia. In the eyes of *Alvinocaris markensis* postlarvae, the anteriorly pointing rhabdoms in the anterior eye have an inter-ommatidial angle of about 3° and are separated from one another by a layer of cytoplasm. As a result, any incident rays at angles up to 12.5° from the ommatidial axis will be retained within the rhabdom, assuming that the refractive indices of the rhabdoms and the surrounding retinular cells are similar to those of other decapods (*e.g.*, Gaten, 1994). The presence of reflecting and shielding pigments behind the rhabdoms may contribute to optical isolation of the rhabdoms. Although most deep-sea crustaceans retain the capacity for all-round vision, the orientation of the rhabdoms in a single direction (anteriorly in *Alvinocaris markensis* and dorsally in *Rimicaris exoculata*) is not unique. Most common, however, when crustacean eyes are highly directional (Land *et al.*, 1979; Land, 1989) is that the visual systems are specialized for upward vision in specimens found at the limit of the downwelling irradiance. Similarly, the presence of highly directional eyes in *A. markensis* and *R. exoculata* suggests that they are specialized for detecting dim light sources from anterior or dorsal directions respectively.

Although the lack of sophisticated optics suggests that image formation is not particularly important in vent shrimps, any directional sensitivity is likely to be relevant to their behavior. The hydrothermal vents are located well below the depths to which light penetrates, but it has been suggested that vent shrimps may be able to see the blackbody radiation associated with the heated plumes (Van Dover *et al.*, 1989, 1994; Pelli and Chamberlain, 1989). The relative development of the anterior and thoracic eyes suggests that the vent shrimps may rely on visual cues to maintain their orientation with respect to the vent. Postlarval specimens seeking a vent site may be aided by the possession of anteriorly directed rhabdoms. After settlement, the developing stages of *Rimicaris exoculata* lose the separate corneas of the anterior eyes, whilst the thoracic eye becomes more prominent in the adult. The adults of this species swarm around the base of the vent chimneys, and the presence of only thoracic eyes suggests that these organs are used solely to view the light emitted from the vent (Van Dover *et al.*, 1989, 1994). In contrast, the other genera are less dependent on the vents (Segonzac *et al.*, 1994) and so do not rely solely on the thoracic

organ for location of, and orientation toward, the vent. An alternative explanation may be that the species with more prominent anterior eyes are those that do not form dense swarms, whereas species such as *R. exoculata,* whose anterior ends are buried under swarms, rely on dorsal eyes (S. Chamberlain, pers. comm.).

The presence of orthogonal layers of microvilli in decapod rhabdoms is generally associated with the analysis of polarized light. Such an arrangement was found in the Type A and *Alvinocaris markensis* postlarvae, although in the '*Chorocaris*' postlarvae the arrangement of layers was less regular. Such differences may be depth-related, or they may be associated with the development of the shrimps. In oplophorid shrimps, sensitivity to polarized light may be present in animals from the upper mesopelagic zone, but absent in those active under aphotic conditions (Gaten *et al.,* 1992). This would imply that the early postlarvae were living at shallow depths where the analysis of polarized light would be advantageous. Unfortunately we have no information about the depths at which the early developmental stages are found, although all of the postlarvae in this study were caught in the same depth range (2000 m to 3050 m). Alternatively, it may be that all larval and postlarval decapods have orthogonal layering of the rhabdoms, but that it is lost in the later stages of species for which the analysis of polarized light confers no advantage.

Life history

One of the most intriguing questions concerning vent shrimps is how they maintain a viable population at an existing vent while employing a dispersal strategy that enables them to locate and colonize new vent sites. The eggs are microlecithal, and they hatch at the zoeal stage with apposition eyes (P. J. Herring, unpubl. obs.). In contrast, the zoeal stages of shrimps with macrolecithal eggs are completed within the egg, and the eye of the newly hatched postlarva is capable of using superposition optics (Gaten and Herring, 1995). Through the generosity of Dr. M. Segonzac (IFREMER), we obtained prezoeas of the related *Chorocaris fortunata* from eggs about to hatch. The eyes of these very late embryos have crystalline cones (Fig. 7) and appear to be capable of using apposition optics (supported by recent observations on laboratory-hatched first zoeas: P. J. Herring, unpubl. data). This finding suggests that these shrimp could have passed through their early developmental stages in a photic environment; furthermore, there is some evidence that the lipid distributed throughout the bodies of the shrimps is of planktonic origin (Dixon and Dixon, 1996). The fact that the eyes of the Type A postlarvae described here have crystalline cones suggests that they, too, may have spent their early life history in the photic zone. Although we have no definitive evidence, we postulate that the postlarval shrimps were returning to vent sites following a planktotrophic zoeal phase.

In view of the large distances involved and the difficulties inherent in locating a vent site, it seems likely that the sense organs of postlarval vent shrimps are adapted for the detection of vent sites, whether by sensing light, temperature, or sulfide concentration. It has been suggested that the eyes of postlarval shrimps are primarily concerned with assembling the large array of photoreceptors found in the eyes of the adult (S. Chamberlain, pers. comm.). However, the optically isolated and anteriorly pointing rhabdoms in the anterior eye imply that it is adapted to enhance directional sensitivity, whilst the reduced optics are typical of the eyes of animals that need to maximize sensitivity at the expense of resolution. We suggest that the eye of the postlarval vent shrimp functions as an extremely sensitive and highly directional photoreceptor, adapted to detect quanta emitted from a hydrothermal vent.

Acknowledgments

We thank Mrs. E. M. Roberts, Leicester University Electron Microscope Unit, for her valuable assistance. The study was supported by NERC grant GST/02/1125 to PJH under the NERC BRIDGE initiative and by NERC grant GR9/0119A to PMJS.

Literature Cited

Christoffersen, M. L. 1990. A new superfamily classification of the Caridea (Crustacea: Pleocyemata) based on phylogenetic pattern. *Z. Zool. Syst. Evolutionforsch.* **28:** 94–106.

Dixon, D. R., and L. R. J. Dixon. 1996. Results of DNA analyses conducted on vent-shrimp postlarvae collected above the Broken Spur vent field during the CD95 cruise, August 1995. *BRIDGE Newsletter* (British Mid-Ocean Ridge Initiative, Univ. of Leeds) **11:** 9–15.

Gaten, E. 1994. Geometrical optics of a galatheid compound eye. *J. Comp. Physiol. A* **175:** 749–759.

Gaten, E. 1998. Optics and phylogeny: Is there an insight? *Contrib. Zool.* **67** (in press).

Gaten, E., and P. J. Herring. 1995. The morphology of the reflecting superposition eyes of larval oplophorid shrimps. *J. Morphol.* **225:** 19–29.

Gaten, E., P. M. J. Shelton, C. J. Chapman, and A. M. Shanks. 1990. Depth-related variation in structure and functioning of the compound eyes of the Norway lobster *Nephrops norvegicus. J. Mar. Biol. Assoc. U.K.* **70:** 343–355.

Gaten, E., P. M. J. Shelton, and P. J. Herring. 1992. Regional morphological variations in the compound eyes of mesopelagic decapods in relation to their habitat. *J. Mar. Biol. Assoc. U.K.* **72:** 61–75.

Hafner, G. S., G. Hammond-Soltis, and T. Tokarski. 1980. Diurnal changes of lysosome-related bodies in the crayfish photoreceptor cells. *Cell Tissue Res.* **206:** 319–332.

Herring, P. J. 1996. Travelling shrimp. *BRIDGE Newsletter* (British Mid-Ocean Ridge Initiative, Univ. of Leeds) **11:** 6–8.

Herring, P. J., and D. R. Dixon. 1998. Extensive distribution of postlarval shrimp from a hydrothermal vent. *Deep-Sea Res.* (in press).

Kuenzler, R. O., J. T. Kwasniewski, R. N. Jinks, R. C. Lakin, B.-A. Battelle, E. D. Herzog, L. Kass, G. H. Renninger, and S. C. Chamberlain. 1997. Retinal anatomy of new bresiliid shrimp from the Lucky Strike and Broken Spur hydrothermal vent fields on the mid-Atlantic ridge. *J. Mar. Biol. Assoc. U.K.* **77:** 707–725.

Lakin, R. C., R. N. Jinks, B.-A. Battelle, E. D. Herzog, L. Kass, G. H. Renninger, and S. C. Chamberlain. 1997. Retinal anatomy of *Chorocaris chacei,* a deep-sea hydrothermal vent shrimp from the Mid-Atlantic ridge. *J. Comp. Neurol.* **384:** 1–12.

Land, M. F. 1976. Superposition images are formed by reflection in the eyes of some oceanic decapod Crustacea. *Nature* **263:** 764–765.

Land, M. F. 1989. The eyes of hyperiid amphipods: relations of optical structure to depth. *J. Comp. Physiol. A* **164:** 751–762.

Land, M. F., F. A. Burton, and V. B. Meyer-Rochow. 1979. The optical geometry of euphausiid eyes. *J. Comp. Physiol. A* **130:** 49–62.

Loew, E. R. 1976. Light, and photoreceptor degeneration in the Norway lobster, *Nephrops norvegicus* (L.). *Proc. R. Soc. Lond. B* **193:** 31–44.

Martin, J. W., and R. R. Hessler. 1990. *Chorocaris vandoverae,* a new genus and species of hydrothermal vent shrimp (Crustacea, Decapoda, Bresiliidae) from the western Pacific. *Contrib. Sci. (Los Angel.)* **417:** 1–11.

Nilsson, D.-E. 1983. Evolutionary links between apposition and superposition optics in crustacean eyes. *Nature* **302:** 818–821.

Nuckley, D. J., R. N. Jinks, B.-A. Battelle, E. D. Herzog, L. Kass, G. H. Renninger, and S. C. Chamberlain. 1996. Retinal anatomy of a new species of bresiliid shrimp from a hydrothermal vent field on the Mid-Atlantic Ridge. *Biol. Bull.* **190:** 98–110.

O'Neill, P. J., R. N. Jinks, E. D. Herzog, B.-A. Battelle, L. Kass, G. H. Renninger, and S. C. Chamberlain. 1995. The morphology of the dorsal eye of the hydrothermal vent shrimp, *Rimicaris exoculata. Visual Neurosci.* **12:** 861–875.

Pelli, D. G., and S. C. Chamberlain. 1989. The visibility of 350°C blackbody radiation by the shrimp *Rimicaris exoculata* and man. *Nature* **337:** 460–461.

Roe, H. S. J., and D. M. Shale. 1979. A new multiple rectangular midwater trawl (RMT 1 + 8M) and some modifications to the Institute of Oceanographic Sciences' RMT 1 + 8. *Mar. Biol.* **50:** 283–288.

Sandeman, D. C., G. Scholtz, and R. E. Sandeman. 1993. Brain evolution in decapod Crustacea. *J. Exp. Zool.* **265:** 112–133.

Segonzac, M., M. de Saint Laurent, and B. Casanova. 1994. L'énigme du comportement trophique des crevettes Alvinocarididae des sites hydrothermaux de la dorsale médio-atlantique. *Cah. Biol. Mar.* **34:** 535–571.

Shelton, P. M. J., E. Gaten, and C. J. Chapman. 1985. Light and retinal damage in *Nephrops norvegicus* (L.). *Proc. R. Soc. Lond. B* **211:** 217–236.

Van Dover, C. L., E. Z. Szuts, S. C. Chamberlain, and J. R. Cann. 1989. A novel eye in 'eyeless' shrimp from hydrothermal vents of the mid-Atlantic ridge. *Nature* **337:** 458–460.

Van Dover, C. L., J. R. Cann, C. Cavanaugh, S. Chamberlain, J. R. Delaney, D. Janecky, J. Imhoff, and J. A. Tyson. 1994. Light at deep sea hydrothermal vents. *Eos, Trans. Am. Geophys. Union* **75:** 44–45.

Welsh, J. H., and F. A. Chace. 1937. Eyes of deep-sea crustaceans. I Acanthephyridae. *Biol. Bull.* **72:** 57–74.

Wharton, D. N., R. N. Jinks, E. D. Herzog, B.-A. Battelle, L. Kass, G. H. Renninger, and S. C. Chamberlain. 1997. Morphology of the eye of the hydrothermal vent shrimp, *Alvinocaris markensis. J. Mar. Biol. Assoc. U. K.* **77:** 1097–1108.

Williams, A. B., and P. A. Rona. 1986. Two new caridean shrimps (Bresiliidae) from a hydrothermal field on the Mid-Atlantic Ridge. *J. Crustac. Biol.* **6:** 446–462.

Reference: *Biol. Bull.* **194:** 281–296. (June, 1998)

Exogenous Retinoic Acid During Gastrulation Induces Cartilaginous and Other Craniofacial Defects in *Fundulus heteroclitus*

MARK W. VANDERSEA[1], ROBERT A. McCARTHY[1,2], PAUL FLEMING[1,2], AND DENICE SMITH[1,*]

[1] *Grice Marine Biological Laboratory, University of Charleston, 205 Fort Johnson, Charleston, South Carolina 29412; and* [2] *Department of Cell Biology and Anatomy, Medical University of South Carolina, Charleston, South Carolina 29401*

Abstract. Embryonic levels of retinoic acid (RA) and the response of cells to RA are critical to the normal development of vertebrates. To understand the effects of RA signaling in *Fundulus heteroclitus*, we exposed embryos to a range of RA concentrations for 2 h during gastrulation. Embryos exposed to low concentrations of RA (10^{-10}–10^{-7} *M*) develop normally, whereas those exposed to higher concentrations (5×10^{-7}–10^{-4} *M*) develop characteristic dose-dependent defects. We describe, in detail, four stages of development that represent morphological effects of RA on (1) cell death and defects in the brain, heart, and eye, (2) relative size and differentiation, (3) duplications of pectoral fins, and (4) deletions in craniofacial cartilage elements. Analysis of cartilaginous skeletal elements demonstrates distinct patterns of deletions in the neurocranium and pharyngeal skeleton in response to increasing concentrations of RA. In *F. heteroclitus*, RA treatment during gastrulation results in five highly consistent phenotypes, which we have incorporated into an index of embryonic RA defects. This index should be valuable in the genetic analysis of RA pathways and in evaluating chemicals that interfere with embryonic RA signaling.

Introduction

Retinoic acid (RA), a derivative of vitamin A, is reported to be an important signaling molecule that plays a crucial role in establishing anterior-posterior patterning in vertebrate embryos (for review see Means and Gudas, 1995). Endogenous RA has been detected in many vertebrate organisms (Durston *et al.*, 1989; Chen *et al.*, 1992; Hogan *et al.*, 1992) including *Xenopus laevis*, in which developing embryos exhibit a gradient of RA (Chen *et al.*, 1994). RA binds to receptors that are members of a large superfamily of steroid and thyroid hormone binding receptors (Lohnes *et al.*, 1995). RA and the receptors then recognize DNA response elements that influence gene expression by promoting or inhibiting transcription (Marshall *et al.*, 1994; Zilliacus *et al.*, 1995). Developmental target genes include Hox genes (Langston and Gudas, 1992; Studer *et al.*, 1994; Lohnes *et al.*, 1995), which impart important anterior-posterior positional information along the axis of the developing embryo (Kessel and Gruss, 1991; Kessel, 1992; and Krumlauf, 1994).

The distribution of RA in the embryo is heterogeneous and the concentration is both limiting and critical because patterning defects can be induced by both RA excess (Holder and Hill, 1991) and RA deficiency (Schuh *et al.*, 1993). Embryos respond to RA in a dose-dependent and stage-specific manner (Durston *et al.*, 1989; Sive *et al.*, 1990; Holder and Hill, 1991; Wood *et al.*, 1994). The sensitivity of vertebrate embryos to RA is well documented in mouse (Wood *et al.*, 1994; Leonard *et al.*, 1995), *Xenopus* (Durston *et al.*, 1989; Minucci *et al.*, 1996; Sive *et al.*, 1990), chicken (Gale *et al.*, 1996), and zebrafish (Holder and Hill, 1991; Stainier and Fishman, 1992; Hill *et al.*, 1995). Exposure of zebrafish embryos to RA during gastrulation results in deletions of the midbrain-hindbrain border regions; defects in the eye, retina,

Received 18 September 1997; accepted 13 February 1998.

* Author to whom correspondence should be addressed. E-mail: smithde@ashley.cofc.edu

and heart; deformities of the tail; and abnormalities in the cartilaginous skeletal elements of the head (Holder and Hill, 1991; Stainier and Fishman, 1992; Alexandre *et al.*, 1996). Administered later in development, exogenous RA can disrupt the patterning of the fin (Akimenko and Ekker, 1995). In chicken and quail embryos, application of RA to the anterior of a limb bud often results in a mirror-image duplication of digits (Tickle, 1995; Tabin, 1995). This suggests that a delicate balance of RA is critical to the proper patterning of embryonic structures and that disruption of this signaling pathway results in a variety of skeletal and anatomical malformations.

In vertebrates, much of the head skeleton is derived from neural crest precursors that migrate into the pharyngeal arches from the midbrain and specific rhombomeres of the hindbrain (Langille and Hall, 1988, 1993). Specific populations of neural crest cells that contribute to the skeletal elements in the head have been identified in mapping studies (Couly *et al.*, 1993; Schilling and Kimmel, 1994). Among different vertebrates, the similarities of neural crest contributions to skeletal elements suggests that the patterning mechanisms that direct these cells are also well conserved (Koentges and Lumsden, 1996; Schilling and Kimmel, 1994; Noden, 1975). The molecular mechanism by which the craniofacial skeleton is patterned is not fully understood. However, interactions between rhombomeric segments of the hindbrain, neural crest cells, and branchial arches are thought to be influenced by overlapping expression domains of Hox genes; moreover, the anterior-posterior patterning of the head is regulated by a Hox code in the branchial region (Hunt *et al.*, 1991) that may be influenced by endogenous RA.

In this study we exposed *F. heteroclitus* embryos to a range of RA concentrations during gastrulation, and we describe defects in the treated embryos as they appear at four distinct developmental stages. In other species, a large variation of phenotypes is produced in response to a single RA concentration (Holder and Hill, 1991; Marshall *et al.*, 1992), but the protracted development of *F. heteroclitus* has allowed for the selection of highly synchronous embryos that respond more uniformly. We show that disruption of endogenous levels of RA during gastrulation results in deletions of the midbrain-hindbrain border region and, at higher concentrations, to deletion of the eyes, shortening of the trunk, and duplications of the pectoral fins. Analysis of cartilage in these embryos suggests that RA differentially affects the patterning of subpopulations of neural crest cells and the formation of specific cartilage elements, resulting in very different patterns of deletions in the neurocranium and the pharyngeal skeleton.

Bent body axes, fin defects, heart defects, eye malformations, and craniofacial defects are common in fish embryos that have been exposed to heavy metals and other xenobiotics during gastrulation (Weis and Weis, 1977; Sharp and Neff, 1980, 1985; Weis and Weis, 1989). These defects are similar to those induced by RA excess or deficiency, suggesting that xenobiotics may interfere with embryonic RA signaling pathways. Therefore, one objective of this study was to utilize *F. heteroclitus*—an estuarine species widely used in toxicity studies—as a model with which to establish an index of defects that occur in response to disruption of RA signaling. The index we describe should therefore help identify and evaluate the sensitivity of embryos to the effects of xenobiotics on RA-regulated pathways.

Materials and Methods

In vitro fertilization of F. heteroclitus

Adult fish were captured from a *Spartina* marsh adjacent to the Grice Marine Biological Laboratory, Charleston, South Carolina. Fish were anesthetized with 1.5×10^{-4} *M* 3-aminobenzoic acid ethyl ester (MS-222) in filtered seawater. Eggs were collected from gravid females, in a dry dish, and then fertilized with 15 μl of sperm activated in 20 ml of filtered seawater. Eggs were then rinsed (15 min post-fertilization) and incubated in a moist chamber at 25°C. Only embryos that showed normal cell cleavage were used experimentally. At 10 days post-fertilization, the eggs were immersed in filtered seawater, which initiated hatching.

Staging series of F. heteroclitus

Embryos from *in vitro* fertilizations (about 100–300 eggs/fertilization) were raised at 25°C, a temperature relevant to the warm coastal waters of South Carolina. Their development was recorded and characterized from before fertilization until 2 days after hatching (12 days post-fertilization). Observations of anatomical features at different stages were compared with descriptions produced by Armstrong and Child (1965), Oppenheimer (1937), and Solberg (1938), and a staging series at 25°C was constructed.

Retinoic acid treatment

Stock solutions of 2×10^{-2} *M* were made in dimethyl sulfoxide (DMSO) from all-*trans*-retinoic acid (Sigma Chemical Co.) and stored at −20°C. Experimental concentrations were prepared by serial dilution with filtered seawater (FSW). Embryos at 50% epiboly (from *in vitro* fertilizations; stage 17, 21.5 h post-fertilization (hpf) at 25°C) were exposed to concentrations of RA ranging from 10^{-10} *M* to 10^{-4} *M* for 2 h in the dark. DMSO control embryos were exposed to 0.1% DMSO in FSW, and untreated control embryos were incubated in FSW. All embryos were then rinsed for 10 min several times with large

Table I

Comparison of embryonic development at 20°C[1] and 25°C

	Time (h:min)			Time (h:min)	
Stage	20°C	25°C	Stage	20°C	25°C
1	0	0	21	52:00	32:00
2	1:75	1:00	22	56:00	34:30
3	2:50	2:00	23	66:00	40:00
4	3:25	2:45	24	74:00	45:00
5	4:25	3:10	→25	84:00	51:00
6	5:00	3:40	26	92:00	63:00
7	6:00	4:30	27	112	73:00
8	7:50	6:00	28	128	82:30
9	9:00	7:00	→29	144	90:00
10	10:00	8:45	30	156	99:00
11	11:00	9:45	31	168	120
12	15:00	11:15	32	192	142
13	20:00	12:00	33	216	166
14	24:00	14:00	34	228	188
15	27:00	16:00	35	252	205
16	30:00	19:00	36	288	220
→17	33:00	21:30	→37	336	245
18	37:00	24:30	38	360	270
19	40:00	27:30	→39	384	296
20	46:00	30:00			

[1] Data from Armstrong and Child, 1965.
Arrows indicate stages and times relevant to this study.

volumes of FSW and allowed to develop at 25°C in a moist chamber.

Skeletal preparations of embryos, and photography

Skeletal preparations of stage 39 larvae were prepared by the method of Dingerkus and Uhler (1977), except that a 0.05% solution of trypsin in saturated sodium borate was used to digest the embryonic tissues. Camera lucida drawings of whole-mounted larvae stained with alcian blue were prepared with the aid of a drawing tube attached to a Nikon Optiphot 2 microscope. Drawings of live larvae were used to depict differences in size, overall morphology, and extent of development, and to serve as illustrations for the different levels of the RA index. Other images were obtained photographically with a Nikon SMZ-U dissecting microscope and Kodak film, digitized, and compiled with Adobe Photoshop software.

Results

During early development the embryo changes rapidly; thus, comparisons of the effects of RA on development demand precise staging and rearing of embryos. The developmental stages of *F. heteroclitus* raised at 20°C have been previously described by Armstrong and Child (1965). In our study, embryos were staged and raised at 25°C, reducing the time to hatching by about 4 days. Table I compares the development at 20°C to development at 25°C, based on the staging descriptions of Armstrong and Child. To determine the effects of exogenous RA on *F. heteroclitus* at 50% epiboly (stage 17, Table I), embryos were exposed for 2 h to concentrations of RA ranging from 10^{-10} *M* to 10^{-4} *M* and then allowed to develop at 25°C. Such embryos undergo gastrulation in the same manner as control embryos, and there are no immediate signs of cell death or toxic response. The overall axial dimensions of treated and control embryos are similar until stage 25, some 27 h after RA exposure, when embryos show normal trunk muscle development and slow muscle contractions.

We compared the development of RA-treated embryos and untreated embryos at four embryonic stages. At stage 25 (about 50 hpf; Table I), when an embryonic axis is completed, circulation begins, and head structures including the eyes and optic tecta are well formed. The overall dimensions of treated and untreated embryos are similar, but there are discernible differences in axial patterning. By stage 29 (about 90 hpf; Table I), dose-dependent effects of RA exposure are more pronounced, both in the relative size of the embryo and in organ differentiation. At stage 37 (about 245 hpf), untreated embryos and those exposed to 10^{-10}–10^{-7} *M* RA hatch, allowing observation of swimming movements and fin structure and comparisons of external morphology. Finally, at stage 39 (296 hpf), the cranial cartilage is well established and can be stained with alcian blue.

Stage 25: Early effects on eye, heart, and the midbrain-hindbrain region

1×10^{-6} M RA. At stage 25 (Fig. 1A) control embryos possess several anatomical landmarks useful for assessing the effects of RA. A small telencephalic ventricle (tv) is present in the forebrain. Embryos have well-defined eyes (arrows), optic tecta (ot), and a hindbrain (hb). Blood cells circulate in vessels on the yolk sac, and the heart is a broad tube with no defined chambers (not shown). Embryos exposed to low concentrations of RA (10^{-10} to 10^{-7} *M*) appear normal (compare Fig. 1A–E). In embryos treated with 10^{-6} *M* RA (Fig. 1F), the telencephalon (t) is present, although the telencephalic ventricle has not expanded (compare Fig. 1E and F), and the embryos display a slight anterior and ventral rotation of the eyes with the lenses incompletely filling the optic cups (arrows, Fig. 1F). Embryos exposed to this concentration lack well-defined optic tecta (asterisk, Fig. 1F). Moreover, most of the midbrain region appears deleted, and the hindbrain (hb) appears to have shifted slightly anteriorly (compare Fig. 1A and F). Using darkfield microscopy, cell death is apparent as white-opaque cells (Grunwald *et al.*, 1988; Stainier and Fishman, 1992) in the midbrain-hindbrain border region and along the trunk and tail (black arrow-

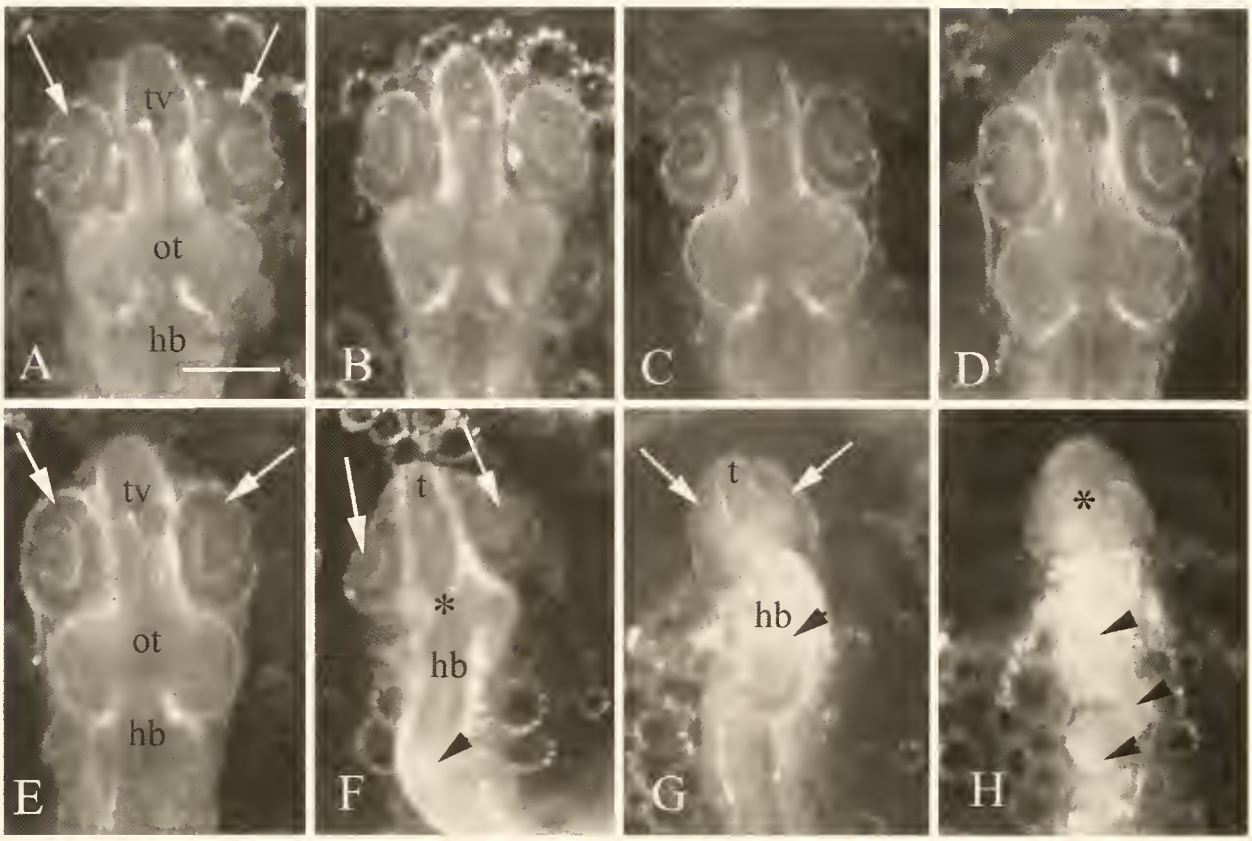

Figure 1. At stage 25, embryos exposed to retinoic acid (RA) during gastrulation show defects in the development of head structures. Control embryos (A) and embryos treated with low concentrations of RA—10^{-10} *M* (B), 10^{-9} *M* (C), 10^{-8} *M* (D), and 10^{-7} *M* (E)—form an expanded telencephalic ventricle (tv, A and E) in the forebrain, optic tecta (ot) in the midbrain, and a well-developed hindbrain (hb). Embryos treated at gastrulation with 10^{-6} *M* RA (F) show defects in the eyes (arrows), telencephalon (t), and midbrain (asterisk). At 10^{-5} *M* (G), the telencephalon (t) and the eyes (arrows) are obscure. Note that the position of the hindbrain (hb, E, F, and G) assumes a progressively more anterior position. Cell death is indicated by black arrowheads (F, G, and H). Anterior is to the top. Scale bar = 200 μm.

head, Fig. 1F). Although not shown in Figure 1F, heart defects range from complete deletion of the heart to the development of a small, thin, tube heart. In those treated embryos that have a heart, circulation is not observed, even though cardiac contractions occur. Pericardial edema extends anteriorly over a large portion of the yolk, and blood cells pool in islands at the tip of the tail. The overall embryonic axis is slightly truncated, but muscular movements occur, and tails are often curled at the tips and are partially detached from the yolk.

1 × 10^{-5} M *RA*. Embryos exposed to 10^{-5} *M* RA show additional anterior head defects (Fig. 1G). Portions of the forebrain region and telencephalon (t) are present, but no telencephalic ventricle forms. The optic cups are ambiguous (arrows), and the midbrain-hindbrain border region is absent. The hindbrain (hb) lies immediately posterior to the forebrain region, and cell death is evident in the hindbrain region and along a posterior region of the trunk (black arrowhead). Large pericardial edemas occur; the heart is deleted; and blood cells pool at the tip of the tail, which is still attached to the yolk (not shown). Although the embryo is truncated, muscular contractions occur.

1 × 10^{-4} M *RA*. Embryos exposed to 10^{-4} *M* RA show few forebrain and eye structures (asterisk, Fig. 1H). The embryonic axis is twisted and exhibits extensive degenerating white-opaque cells (black arrowheads). Muscular contractions of the trunk do not occur in the embryos at this stage. The heart is absent, but there is a large pericardial cavity, and blood cells are pooled posteriorly at the base of the tail.

Stage 29: Effects on relative size and differentiation

1 × 10^{-6} M *RA*. At stage 29 (Fig. 2) the embryonic head in control embryos has grown considerably; measurements of the area of the head indicate an enlargement

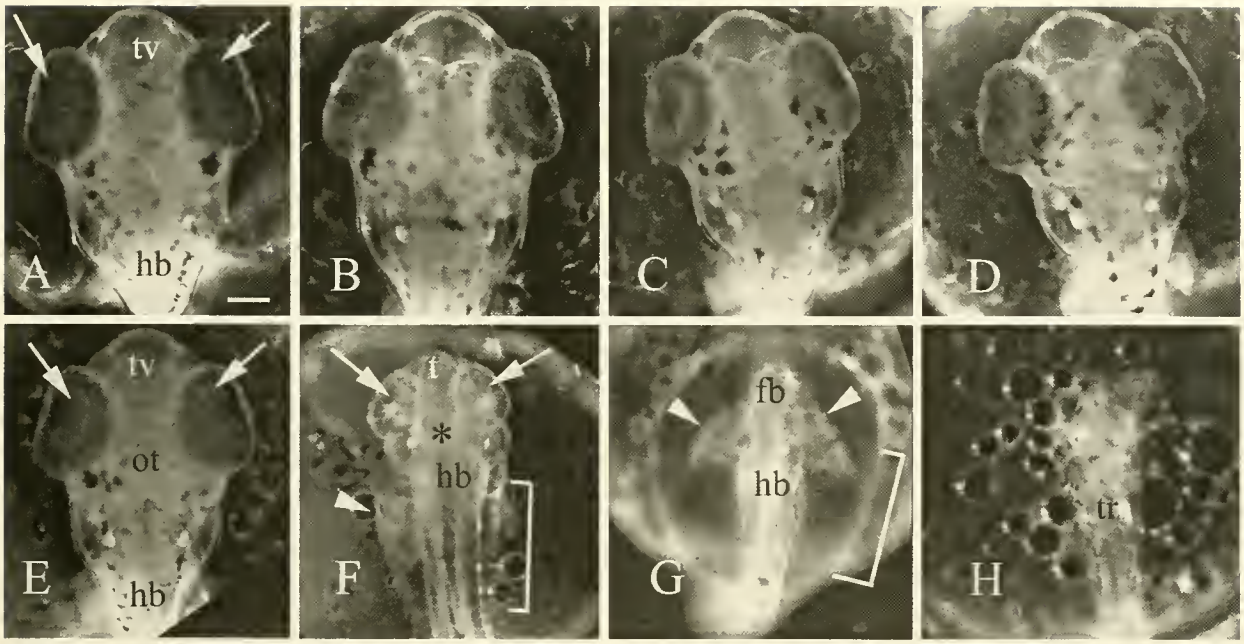

Figure 2. Dorsal views of stage 29 embryos show the effects of retinoic acid (RA) on relative size and head development. In control embryos (A) and embryos exposed to low concentrations of RA—10^{-10} *M* (B), 10^{-9} *M* (C), 10^{-8} *M* (D), and 10^{-7} *M* (E), the eyes are lightly pigmented (arrows, A and E) and the telencephalic ventricle (tv, A and E) and optic tecta (ot, E) anterior to the hindbrain (hb, A and E) has expanded. Embryos exposed to 10^{-6} *M* RA lack retinal pigment in the eyes (arrows, F), show abnormalities of the brain (asterisk, F) anterior to the hindbrain (hb, F), pectoral fin development (arrowhead, F), and an expansion of the visceral cavity (bracket, F). At 10^{-5} *M* RA embryos show abnormal pectoral fin development (arrows, G), and have severe malformations in the forebrain (fb, G), and an expanded visceral cavity (bracket, G). At 10^{-4} *M* RA exposure, embryos consist only of a thin trunk (tr, H). Anterior is to the top. Scale bar = 200 μm.

greater than 3.5-fold between stages 25 and 29. The telencephalic ventricle (Fig. 2A, tv) of the forebrain has widened, the eyes are pigmented (arrows), and the optic tecta (ot) have enlarged posterior to the eyes. Embryos exposed to low concentrations (10^{-7}–10^{-10} *M*) of RA (Fig. 2B–E) are morphologically normal. In contrast, embryos treated with 10^{-6} *M* RA have optic cups that are malformed and rotated anteriorly (arrows, Fig. 2F). The head has enlarged only 2.5-fold over stage 25 embryos. The optic tecta are greatly reduced (asterisk), and the hindbrain (hb) region is shifted anteriorly. The visceral cavity is expanding and appears to be proportionately larger than in control embryos (bracket, Fig. 2F). Other defects also occur in embryos (not shown). The otocysts contain smaller otoliths, and they are irregular in shape; the heart tube is attached by a thin strand of cells to the pericardial wall; and blood cells pool on the ventral side of the embryo at the level of the hindbrain and along the length of the tail. The pectoral fins of control embryos develop just posterior to the vitelline veins, whereas the pectoral fins in RA-treated embryos are posterior and lateral to the otocysts and are slightly smaller (arrowhead, Fig. 2F). In all embryos, frequent muscle movements occur, and the small, bilobed urinary bladder is developing at the base of the trunk where it is attached to the yolk sac.

1×10^{-5} M *RA.* Embryos exposed to 10^{-5} *M* RA (Fig. 2G) lack well-defined eyes and are missing large portions of the midbrain. From stage 25 to stage 29, the area of the head increases only 1.3-fold, remaining similar to that of a stage 25 embryo (compare Figs. 2G and 1G). The visceral cavity is abnormally large relative to the size of the head and trunk, and it covers much of the yolk (bracket). The gut, however, appears normal. A small portion of the forebrain may be present (fb), and some embryos may develop lenses and retinal pigment (not shown). Lenses, in some cases, lie freely exposed on the anterior of the head (not shown). The hindbrain (hb) develops just posterior to any retinal tissue, but the otocysts have been deleted. The pectoral fins develop in an extreme anterior position, such that they are almost lateral to any retinal tissue. Furthermore, the fin structure is abnormal, appearing as thin columns of tissue that extend laterally from the trunk (arrowheads, Fig. 2G). The length of the embryonic axis has increased and, in some embryos, the tip of the tail has detached from the yolk where the small, bilobed urinary bladder is developing (not shown). Blood

Figure 3. At stage 37, dorsal views of control larvae (A) and larvae exposed at gastrulation to low concentrations of retinoic acid (RA)—10^{-10} *M* (B), 10^{-9} *M* (C), 10^{-8} *M* (D), and 10^{-7} *M* (E)—show well-developed eyes (arrows, A and E) and pectoral fins (arrowheads, A and E). Larvae exposed at gastrulation to 10^{-6} *M* RA (F) show anterior and ventral rotation of the eyes (arrows), normal fin development (arrowheads), pericardial edema (pe), and shortened trunks and curled tails (asterisk, F). At 10^{-5} *M* RA, larvae display multiple pectoral fins (arrowheads, G), a heavily pigmented trunk (tr), and curled tail (asterisk, G). A lateral view of a larva treated at 10^{-4} *M* RA (H) shows a shortened trunk (tr) atop the yolk. Anterior is to the top (A–G) and to the left (H). Scale bar = 200 μm.

cells are pooled around the urinary bladder, and muscular contractions occur in the trunk, but not as frequently as in the control embryos.

1 × 10^{-4} M *RA.* Embryos exposed to 10^{-4} *M* RA (Fig. 2H) lack obvious head structures and appear only as a thin trunk (tr) set on an expanded visceral cavity and gut. Pectoral fins are absent. The urinary bladder is surrounded by blood cells at the base of the trunk where the bladder meets the yolk sac (not shown). Muscular movements occur in some embryos, and a small, stubby tail projects from the trunk (not shown).

Stage 37: Multiple fin phenotypes

1 × 10^{-6} M *RA.* At stage 37, controls and larvae that have been exposed as gastrulae to 10^{-10} to 10^{-7} *M* RA are normal in appearance (Fig. 3A–E) and can be induced to hatch at 10 days post-fertilization. Embryos exposed to greater concentrations of RA do not hatch but survive for an extended period. These larvae are smaller and retain a large volume of yolk (compare Fig. 3A–E with 3F–H). Embryos exposed to 10^{-6} *M* RA develop into larvae with smaller than normal eyes that display more ventral and anterior rotation than the controls (arrows, Fig. 3F). The pectoral fins, however, approximate normal size (arrowheads, compare Fig. 3A and F) and exhibit a high rate of motor activity. Control larvae and larvae of embryos treated with low concentrations of RA (10^{-10}–10^{-7} *M*) possess a functional mouth (m, Fig. 3A and E) and jaw, and exhibit rapid opercular movements. The mouths of larvae treated with 10^{-6} *M* RA as embryos are small and are tucked underneath the forebrain and against the yolk or a large pericardial edema; it is unclear whether

the mouths are functional. The tails are short and curled, and do not exhibit fin development (asterisk, Fig. 3F). Not shown in Figure 3F, the otocysts are irregular in size and shape and are just posterior to the eyes. This is probably due to the midbrain-hindbrain deletion, which causes an anterior shift of the otocysts. The visceral cavity has expanded laterally, and internal organs have developed. The heart, usually located ventrally at the level of the operculum, is contractile but smaller and lies anterior to the gut in a large, balloon-like pericardial edema (pe, Fig. 3F).

1 × 10^{-5} M. Exposure to 10^{-5} *M* RA at gastrulation results in larvae that lack most of the forebrain, midbrain, and hindbrain (Fig. 3G). The most prominent feature of these larvae is the development of multiple pectoral fins (arrowheads, Fig. 3G). The supernumerary fins often show a variation in phenotype. Some larvae have two to three pairs of well-developed fins that are often overlapping and move independently of one another (arrowheads, Fig. 3G). Other larvae have more extreme fin phenotypes: *i.e.,* small stubby fins that are fused by soft tissue at the base of the pectoral girdle. Detailed analysis of the multiple-fin phenotype has been described elsewhere (Vandersea *et al.,* in press). The body axis is shortened and the trunk is wide (tr, Fig. 3G); some larvae possess a small, curled tail (asterisk, Fig. 3G) but no ventral, dorsal, or caudal fins. Lenses often lie freely exposed in the anterior head region of the larvae (not shown). The visceral cavities and gut are greatly expanded over the yolk sac. These larvae live for as long as 22 days postfertilization.

1 × 10^{-4} M *RA.* Larvae exposed to 10^{-4} *M* RA (Fig. 3H) are very susceptible to bacterial or fungal infections, and about 50% die between stages 29 and 37; but others live for as long as 15 days. In these larvae the tail, pectoral fins, and all of the anterior head structures are absent. A larva viewed laterally (Fig. 3H), rather than dorsally, shows that the trunk (tr) is largely intact. The gut and other internal organs have formed in the visceral cavity, and some larvae possess the remains of a tail, which protrudes as a small stump from the trunk (not shown). The trunk exhibits muscular movements.

Stage 39: Craniofacial and pectoral fin cartilage defects

To determine the effects, at gastrulation, of increasing concentrations of RA on cartilage patterning in the head and fins, larvae were stained with alcian blue at stage 39 (Fig. 4). Camera lucida drawings of the stained larvae were used to aid in the analysis of cranial cartilage and pectoral girdles. For clarity of presentation, we have depicted the elements that make up the braincase as the neurocranial cartilage (Fig. 4E–H), whereas those elements derived from the seven pharyngeal arches (the mandibular, hyoid, and five branchial arches) and from the pectoral girdle are presented as the pharyngeal-pectoral cartilage (Fig. 4I–L). The identification of cartilage elements was based on comparative descriptions of skull development (de Beer, 1937) and on skull development in medaka (Langille and Hall, 1987) and zebrafish (Cubbage and Mabee, 1996; Schilling and Kimmel, 1997). Abbreviations used in labeling the cartilaginous elements in Figure 4 are listed in Table II (abv). Alcian blue staining of larvae treated during gastrulation with increasing concentrations of RA reveals an overall reduction in the development of cartilage in the head (compare Fig. 4A–D) consistent with the descriptions of the anatomical effects of RA at the earlier stages described above.

At stage 39 in the normal neurocranium (Fig. 4E), the ethmoid plate (ep) joins the lamina orbitonasalis (lo) and trabeculae (t). The epiphyseal bar (eb) joins both the anterior and posterior orbital cartilage (ao, po). Posteriorly, the parachordals (pc) form the base of the neurocranium and fuse with the hypophyseal plate (hp) joining the polar cartilage (pl) with the auditory capsules (ac). Embryos exposed to 5×10^{-7} *M* RA develop (as larvae) a neurocranium that contains all the normal cartilage elements, but is reduced in size (compare Fig. 4E and F). In some cases, the hypophyseal and polar cartilage are slightly malformed (hp and pl, Fig. 4F). Embryos exposed to 10^{-6} *M* RA develop a neurocranium that lacks an epiphyseal bar, as well as anterior and posterior orbital cartilage (Fig. 4G). Notice that the lamina orbitonasalis and trabeculae are only slightly smaller than normal, and the ethmoid plate is present. Furthermore, these elements develop in a more ventral position, close to the level of the pharyngeal skeleton. The posterior neurocranium develops similarly in size and organization in embryos exposed to either 5×10^{-7} *M* RA or 10^{-6} *M* RA (compare Fig. 4F and G). Embryos treated with 10^{-5} *M* RA develop only one neurocranial element—the parachordals (pc, Fig. 4H), which form the posterior base of the neurocranium at the anterior end of the notochord (nc, Fig. 4D).

The pharyngeal-pectoral cartilage at stage 39 (Fig. 4I) consists anteriorly of Meckel's cartilage (mc) which articulates with the pterygoid (p), the quadrate (q), and the hyosymplectic (hs) to form the jaw. In the gill region, the basihyal (bh) and ceratohyals (ch) lie anterior to the centrally located basibranchials (bb) and the three pairs of hypobranchials (hb). Within the branchial arches, five pairs of ceratobranchials (cb) lie ventrally to four paired epibranchials and the pharyngobranchials (not shown). The coracoscapulae (cs) and the proximal radials (pr) compose the pectoral girdle.

Larvae of embryos treated with 5×10^{-7} *M* (Fig. 4J) and 10^{-6} *M* RA (Fig. 4K) do not develop the major cartilage components of the jaw. Although small cartilaginous

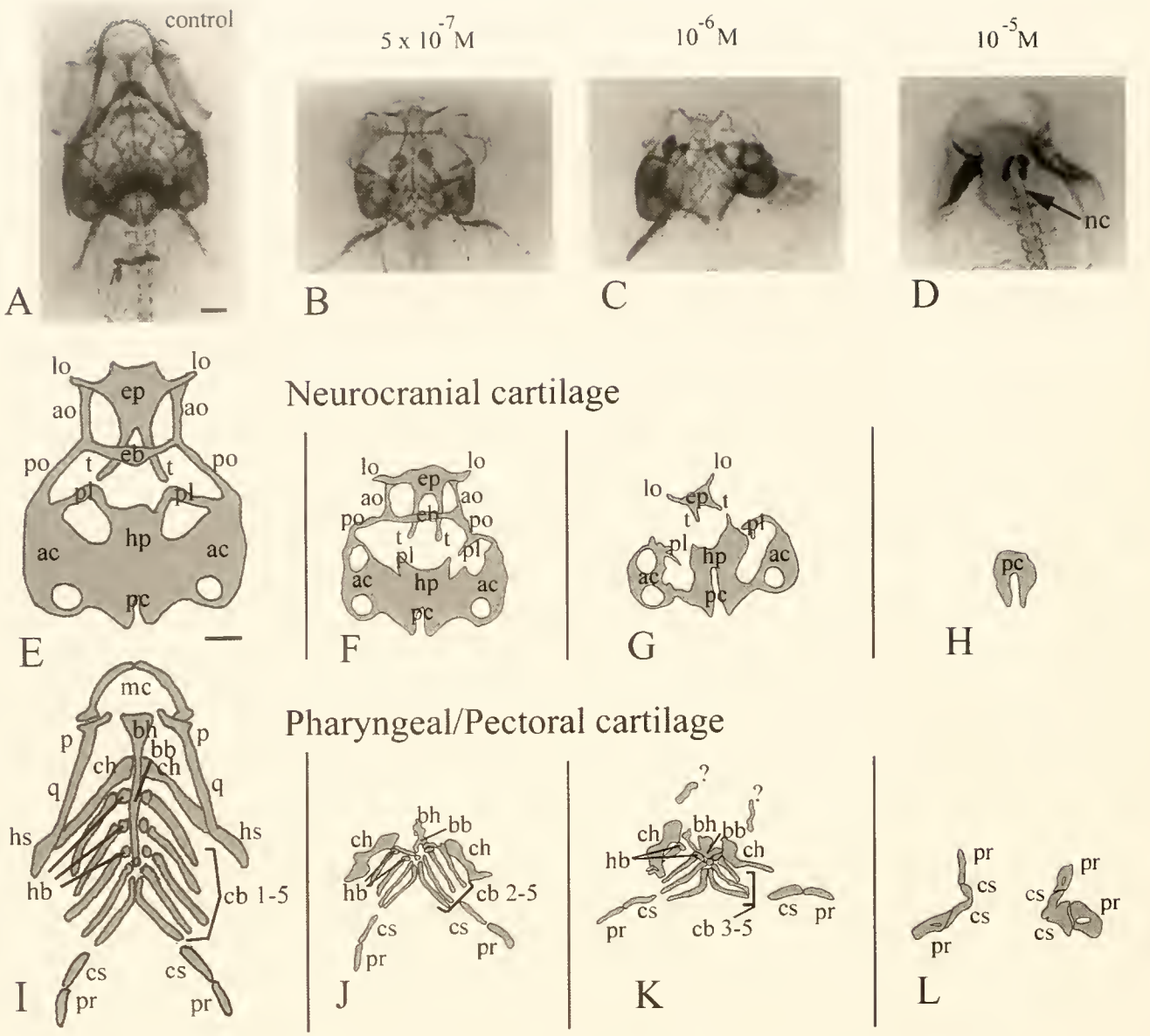

Figure 4. Light micrographs of alcian blue staining (A–D) and camera lucida drawings (E–L) of cartilage elements at stage 39. The figure shows the cartilage elements of control larvae (A, E, and I) and larvae of embryos exposed to retinoic acid (RA) at 5×10^{-7} *M* (B, F, and J), 10^{-6} *M* (C, G, and K), and 10^{-5} *M* (D, H, and L). Camera lucida drawings, which depict a dorsal view of the neurocranial cartilage (E–H) and a ventral view of pharyngeal/pectoral cartilage (I–L), show a progressive loss and malformation of cartilage to increasing concentrations of RA. Abbreviations for cartilage elements are listed in Table II, nc = notochord. Anterior is to the top. Scale bar (A) = 200 μm (A–D) and (E) = 200 μm (E–L).

elements that could represent Meckel's cartilage (question marks, Fig. 4K) are often present, the morphological characteristics of these elements are incomplete, so positive identification is difficult. The basihyal, ceratohyals, and basibranchials are present but shorter and thicker (Fig. 4J and K); moreover, the number of ceratobranchials and hypobranchials that develop may vary. In less extreme cases anterior ceratobranchials are deleted (Fig. 4J and K), but the posterior elements develop. In the most extreme phenotypes, the ceratobranchials and hypobranchials do not form. The order of the ceratobranchials is distinguished by their associations with the hypobranchials, their position relative to the pectoral girdle cartilage (which develops normally), and the presence of pharyngeal teeth on the fifth ceratobranchial. At both concentrations of RA the epibranchials and pharyngobranchials are

Table II

Analysis of retinoic acid effects on cartilage formation in the head and pectoral girdle

Origin		Skeletal element	Abv[1]	Concentration of retinoic acid			
				5×10^{-7} *M*	10^{-6} *M*	10^{-5} *M*	10^{-4} *M*
Neural[2] Crest	Mandibular Arch	Quadrate	(q)	A	A	A	A
		Pterygoid	(p)	A	A	A	A
		Meckel's	(mc)	M/A	M/A	(?)	A
	Hyoid Arch	Hyosymplectic	(hs)	A	A	A	A
		Basihyal	(bh)	M	M	A	A
		Ceratohyals	(ch)	M	M	(?)	A
	Branchial Arches	Epibranchials	—	A	A	A	A
		Pharyngobranchials	—	A	A	A	A
		Basibranchials	(bb)	RN	RN	A	A
		Hypobranchials	(hb)	RN	RN	A	A
		Ceratobranchials	(cb)	RN	RN	A	A
	Neurocranium	Ethmoid plate	(ep)	P	P	(?)	A
		Lamina orbitonasalis	(lo)	P	P	A	A
		Trabeculae	(t)	P	M	(?)	A
		Epiphyseal bar	(eb)	P	A	A	A
		Anterior orbital	(ao)	P	A	A	A
		Posterior orbital	(po)	P	A	A	A
Non-Neural[2] Crest		Polar cartilage	(pl)	P	P	A	A
		Hypophyseal plate	(hp)	P	P	A	A
		Auditory capsule	(ac)	P	M	A	A
		Parachordals	(pc)	P	P	P	A
	Pectoral Girdle	Coracoscapulae	(cs)	P	P	D	A
		Proximal radials	(pr)	P	P	D	A

[1] Abbreviations used in Figure 4.
[2] Based on Langille and Hall, 1988; Schilling and Kimmel, 1997.
Key: P = Present and normal; M = Malformed; RN = Reduced in number; A = Absent; D = Duplicated; ? = Unidentified cartilage.

absent (not shown). Most larvae of embryos exposed to 10^{-5} *M* RA lack pharyngeal cartilage, but 94% of these larvae possess multiple fins with two or more pairs of coracoscapulae and proximal radials (Fig. 4L, and Vandersea *et al.*, in press).

Table II lists the cartilaginous skeletal elements that are present in control larvae and in larvae that were exposed, as gastrulating embryos, to increasing concentrations of RA. To aid in the analysis of RA-induced defects, skeletal elements have been grouped according to their embryological origin and their position within the neurocranium or the pharyngeal skeleton. The presence (P) or absence (A) of individual elements is noted, as well as whether the cartilages are malformed (M) or reduced in number (RN). Duplications (D) and unidentified cartilage (?) are also indicated. Elements of the neurocranium are listed in order of their position along the axis, with the anteriormost element, the ethmoid plate, listed first and the posterior elements, the parachordals, listed last. RA causes concentration-dependent deletions of central neurocranial elements at the lowest concentrations of RA and the deletion of more anterior and posterior elements at higher concentrations of RA.

Table II also shows a distinct pattern of deletions in the pharyngeal skeleton which appears to comprise an iterated, segmental set of homologous arches (Romer and Parsons, 1977; Schilling and Kimmel, 1997). In the branchial or gill arches, the epibranchials and pharyngobranchials are the dorsal elements, and the ceratobranchials are the ventral elements. In the mandibular arch the quadrate and pterygoid are considered to be the dorsal homologs, while Meckel's cartilage is believed to correspond to the ventral homolog. The hyosymplectic and ceratohyal cartilages are believed to correspond to the dorsal and ventral homologs, respectively, in the hyoid arch. Notice that dorsal elements in all pharyngeal arches are deleted at lower concentrations of RA than more ventral elements.

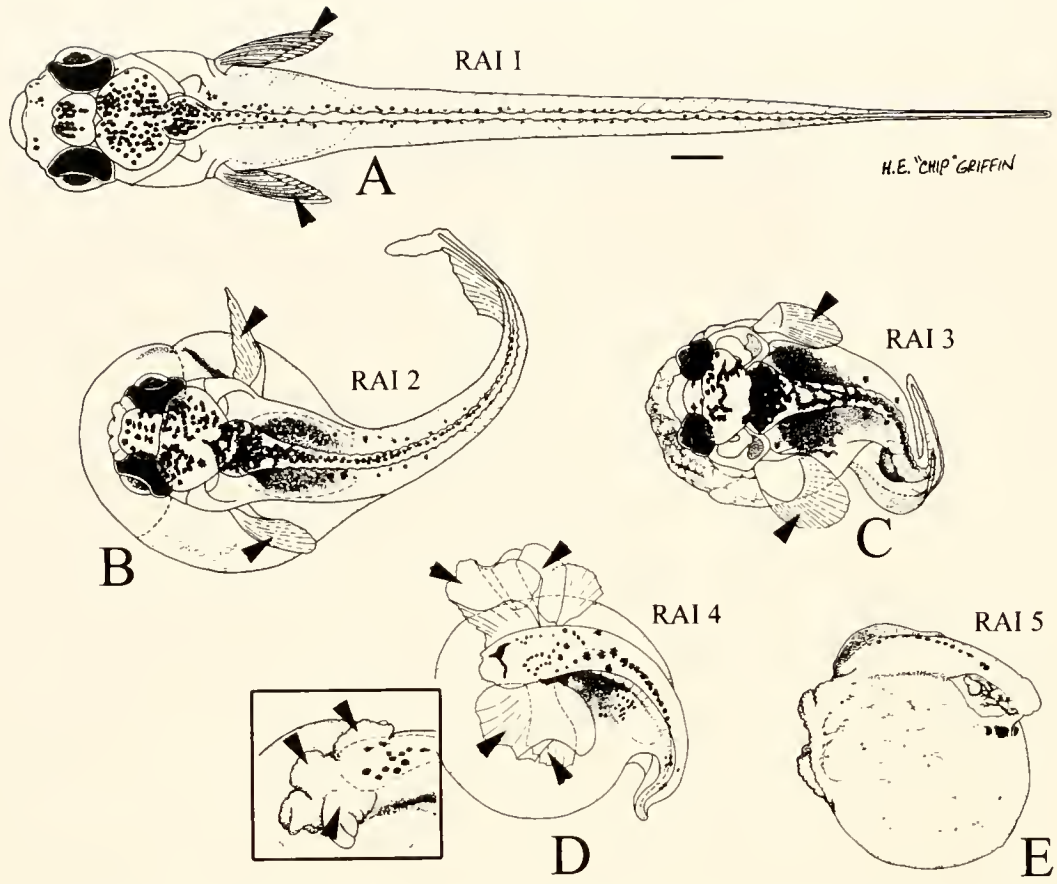

Figure 5. Illustrations of live larvae corresponding to the five retinoic acid (RA) index levels (RAI 1–5). Stage 37 larvae are representative of RAI 1 (A), and larvae with increasing severity of defects due to RA exposure at gastrulation are shown for RAI 2 (B), RAI 3 (C), RAI 4 (D), and RAI 5 (E). Inset (D) shows the variation of duplicated pectoral fins of RAI 4. Arrowheads denote pectoral fins. Dorsal views are shown in A–D and a lateral view in E. Anterior is to the left. Scale bar (A) = 400 μm.

An index of retinoic acid defects

Larvae of *F. heteroclitus* that were exposed at gastrulation to a range of RA concentrations exhibit five distinct phenotypes. We have incorporated these phenotypes into an index of RA defects (RAI). Larvae representative of each level of the index are illustrated in Figure 5 and described (on the basis of morphological observations and alcian blue staining of cartilage) in Table III.

Briefly, RAI 1 represents larvae that are morphologically normal and contain all head and pectoral fin cartilage (Fig. 5A and Table III). RAI 2 larvae show partial deletions of the midbrain-hindbrain border region, with slightly curved tails, normal pectoral fins, and deletions of the cartilage that form in the jaw and anterior gill arches (Fig. 5B and Table III). RAI 3 larvae show additional deletions of structures in the forebrain and midbrain-hindbrain border region, severe truncation of the axis, expansion of the visceral cavity, a thin tubular heart, and malformations of the cartilages of the neurocranium and anterior gill arches (Fig. 5C and Table III). The most obvious characteristic of RAI 4 larvae is the development of multiple fins, which can range from fully independent pairs of pectoral fins (arrowheads, Fig. 5D) to stubby, malformed pairs of fins (arrowheads, Fig. 5D, inset). RAI 4 larvae also lack forebrain and midbrain-hindbrain border structures and most of the craniofacial cartilage. RAI 5 larvae consist of a muscular trunk with a well-formed gut, but no cartilaginous elements (Fig. 5E and Table III).

To determine whether the phenotypes reflected in the RAI are dependent on the concentration of RA to which the embryos are exposed, we scored 1452 embryos from seven RA experiments and compared the RAI with the level of RA exposure (Fig. 6). Between 97% and 98% of control embryos, DMSO-treated embryos, and embryos exposed to 10^{-7} *M* RA have an RAI of 1 (Fig. 6, RAI 1). Figure 6 also shows that each exposure concentration between 5×10^{-7} and 10^{-4} *M* RA exhibits a dominant

Table III

Retinoic acid index

Index level	Description[1]
RAI 1	Larvae appear normal; craniofacial cartilage identical to untreated control embryos.
RAI 2	Partial deletions and distortions of midbrain/hindbrain border region (MB/HB); eyes slightly closer together; axis slightly truncated; heart smaller with pericardial edema, otocysts slightly closer to MB/HB; tail slightly curled; deletions of the quadrate, pterygoid, and hyosymplectic cartilage; malformations of Meckel's cartilage, ceratohyals and the basihyal.
RAI 3	Partial deletion of forebrain (FB); broad deletion of MB/HB border region; eyes smaller, closer together, and ventrally and anteriorly rotated; otocysts shifted anterior; axis severely truncated; curled tail; visceral cavity expanded; thin tube heart with contractions but no circulation; blood cells pooled posteriorly; deletions of the quadrate, pterygoid, hyosymplectic, orbital, epiphyseal, and basibranchial cartilage; malformations or deletion of Meckel's cartilage; malformation of the ethmoid, ceratohyals, basihyal, auditory capsule, basibranchials, hypobranchials, and ceratobranchials.
RAI 4	Broad deletion of FB, MB/HB; otocysts absent; most retinal pigment deleted; heavy pigment on expanded visceral cavity wall; multiple pectoral fins; axis severely truncated and tail curled; urinary bladder and gut present; heart absent; deletions of most craniofacial cartilage; remnants of Meckel's or the ceratohyals may be present; parachordals present; multiple coracoscapulae and proximal radials present.
RAI 5	Major deletions of head and tail with only trunk remaining; urinary bladder and gut present; blood cells pooled posteriorly; muscular movements of trunk present; no cartilaginous staining present.

[1] Descriptions are summaries of the larval anatomy at stage 37 and cartilage staining at stage 39.

index level that includes most of the embryos exposed to that concentration at gastrulation: 5×10^{-7} *M* RA, 90% of embryos fall into RAI 2; 10^{-6} *M* RA, 88% in RAI 3; 10^{-5} *M* RA, 91% in RAI 4; 10^{-4} *M* RA, 93% in RAI 5. The ability of RA to induce reproducible phenotypes in a large number of embryos makes *F. heteroclitus* an important embryonic model for the understanding of molecular and genetic interactions of the RA signaling pathways.

Discussion

We have described brain, craniofacial, and pectoral fin defects arising from the exposure of *F. heteroclitus* embryos to increasing concentrations of exogenous retinoic acid during gastrulation. RA-treated embryos, like control embryos, gastrulate and form an axis, but by stage 25, they demonstrate dose-dependent differences in axial patterning. Moderate RA exposure during gastrulation leads to axial patterning defects in the tail, heart, midbrain-hindbrain, and the craniofacial cartilage. High concentrations of RA further disrupt the pectoral fins, otocysts, forebrain, and posterior hindbrain structures (including cartilage). However, patterning of the gut and trunk appear normal, even at high RA exposures. We have used RA phenotypes to establish an RA index that shows low inter-experimental variability. The index should be useful in understanding RA signaling pathways.

Cellular events that may contribute to RA-induced phenotypes

Gastrulation and neural induction. Embryos exposed to exogenous RA at 50% epiboly continue to gastrulate and show no immediate signs of cell death or toxic response. The overall patterns of development of treated and control embryos at 25°C are similar prior to stage 25, some 27 hours after RA exposure. Other responses to RA argue against an immediate toxic response: *i.e.*, embryos exposed to the highest RA concentrations live for more than 2 weeks, show normal gut and somatic trunk muscle development, and exhibit frequent muscle contractions.

Although we have not examined in detail the effects of RA on gastrulation, it is possible that the patterning defects we observe stem, in part, from subtle changes in cellular migration patterns during gastrulation. Gastrulation in *F. heteroclitus* occurs by the ingression of superficial deep cells at the margin of the blastoderm during early epiboly (stage $13–13^{1/2}$, 12 hpf at 25°C; Trinkaus, 1996). The detailed studies of Trinkaus and colleagues provide background information on development in this species, and the large size and transparency of the embryo contribute to ease of observation. Together, these factors make *F. heteroclitus* embryos excellent candidates for lineage studies to determine whether RA leads to altered migration patterns of cells during gastrulation.

Exposure to RA may disrupt the interactions that occur between mesoderm and ectoderm during gastrulation—interactions shown by classical embryological and recent molecular studies to be critical for normal neural induction of the brain and spinal cord (Spemann and Mangold, 1924; Tanabe and Jessell, 1996; Elinson and Kao, 1993). It has been shown in *X. laevis*, that treatment with RA during gastrulation affects both mesoderm (Cho and De Robertis, 1990; Sive *et al.*, 1990; Sive and Cheng, 1991;

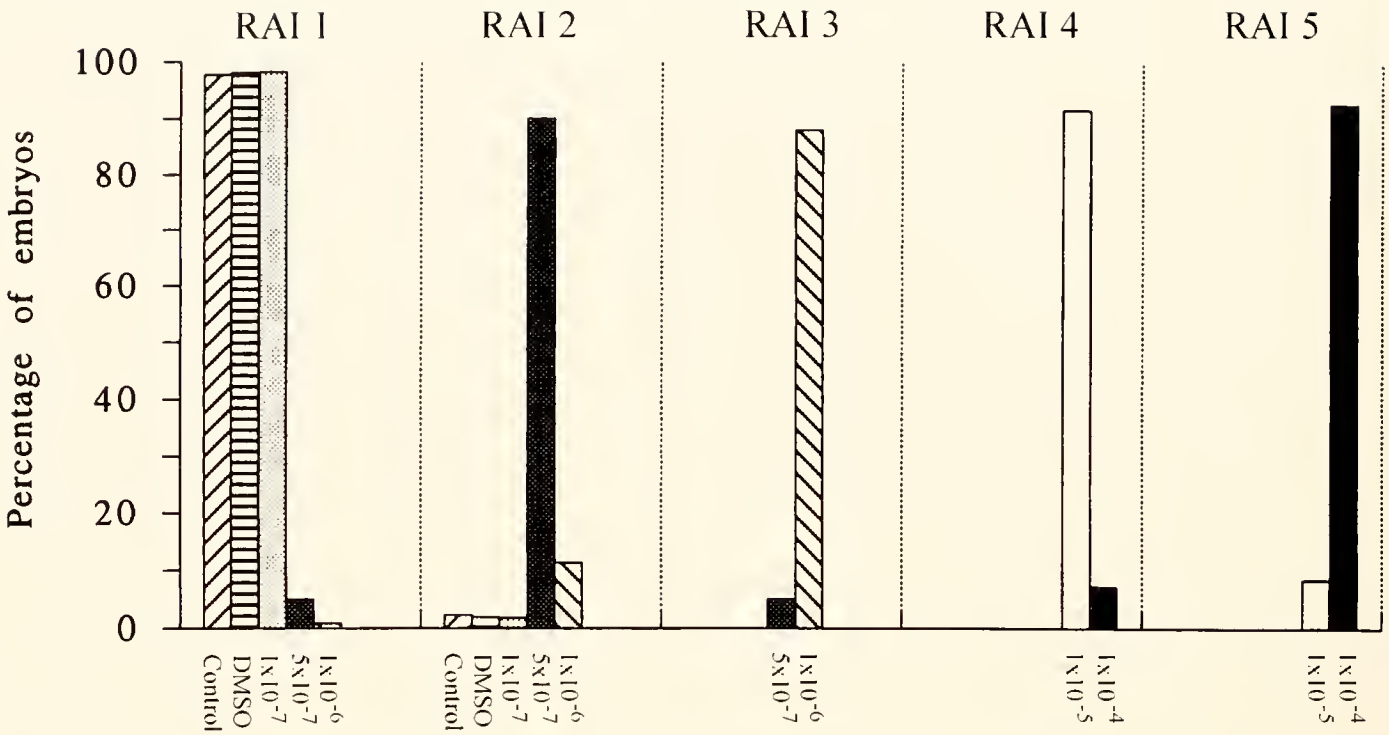

Figure 6. Distributions of embryos categorized by retinoic acid (RA) index level. The graph shows the percentage of control larvae (n = 205) and larvae treated at gastrulation with DMSO (n = 192) or RA at 10^{-7} M (n = 214), 5×10^{-7} M (n = 100), 10^{-6} M (n = 231), 10^{-5} M (n = 280), 10^{-4} M (n = 230) that fall within each RAI level.

Ruiz i Altaba and Jessell, 1991a) and ectoderm (Ruiz i Altaba and Jessell, 1991b). Transplantation experiments, as pioneered in *F. heteroclitus* by Oppenheimer (1936), between RA-treated and control ectoderm and mesoderm may resolve which of these effects on ectoderm or mesoderm is the more relevant to the midbrain-hindbrain deletions and craniofacial defects we observe.

Cell death and cell proliferation. Proper patterning of early development depends on both embryonic growth and programmed cell death. Studies carried out in zebrafish have shown that RA exposure leads to midbrain-hindbrain deletions, demonstrated by the absence of cells expressing the marker protein, engrailed, which is diagnostic for this region (Holder and Hill, 1991). Stainier and Fishman (1992) have suggested, from separate observations of RA-treated zebrafish, that opaque cells found in the affected midbrain-hindbrain region correspond to cells undergoing cell death. We find that *F. heteroclitus* embryos exposed to concentrations of RA greater than 10^{-7} M gastrulate and form an axis similar to that of control embryos. However, at stage 25, RA-treated embryos show localized opaque zones in the brain and tail, similar to those described in zebrafish. In subsequent stages, the opaque regions are cleared from the embryo, and structures are deleted within these regions. Cell death in opaque zones may partially account for the severe truncation of the axis that is evident in older embryos.

A comparison of normal and RA-exposed embryos shows differences that may not be fully explained by localized cell death. At stage 25, control and RA-treated embryos display only slight overall differences in size; by stage 29, however, considerable size differences are obvious. For example, head structures in control embryos have enlarged relative to stage 25 embryos, whereas similar structures in RA-treated embryos have not. Therefore, increased levels of RA may also disrupt signaling events necessary for cellular proliferation in the embryo. Thus, our observations point to two developmental periods at which effects produced by RA exposure during gastrulation lead to changes in embryonic size: (1) between stage 21 and stage 25, cell death may be increased in RA-treated embryos; (2) between stages 25 and 29, cell proliferation may be decreased in RA-exposed embryos. Further investigations in *F. heteroclitus* by TUNEL assays for cell death and BrdU assays for cell proliferation should clarify the effects of RA exposure at gastrulation on later development.

Effects of RA on axial specification and cartilage patterning

RA-treated embryos survive for up to 22 days and show extensive development of cartilaginous skeletal elements. This has permitted a more detailed analysis of RA-induced craniofacial and pectoral fin skeletal defects than has been undertaken for other species. Our results show that the development of many craniofacial and pectoral fin cartilage elements is altered in response to RA exposure during gastrulation. Dose-dependent deletions occur in both neurocranial and pharyngeal skeletal elements, while duplications and deletions are observed for pectoral girdle and fin elements.

In the neurocranium, the orbitals and epiphyseal bar, which are cartilage elements centrally located along the anterior-posterior (A/P) axis, are deleted at lower concentrations of RA than are the ethmoid plate and the parachordals, which are elements at the anterior and posterior extremes. These results suggest that RA has a concentration-dependent effect, either on the developmental regulation of specific neural cranial elements, or on the specification of their ultimate position along the A/P axis. Although patterning of the craniofacial region is generally believed to be conserved in evolution, the origin of the neurocranium—whether from mesoderm or neural crest—is a matter of contention. Extirpation of neural crest cells in medaka embryos results in defects of the craniofacial cartilage (Langille and Hall, 1988), demonstrating the importance of neural crest for normal head development. These studies suggest that the anteriormost elements of the neurocranium, the ethmoid plate and trabeculae, are derived from neural crest cells that migrate from the mesencephalon, whereas the more centrally located elements, orbitals and epiphyseal bar, receive neural crest contributions from both the mesencephalon and the preotic rhombencephalon (Langille and Hall, 1988). Posterior elements of the neurocranium are believed to be derived from mesoderm (Langille and Hall, 1988). However, recent quail-chick transplantation studies suggest that most of the neurocranium is mesoderm-derived (Couly *et al.*, 1993), except for specific neural-crest-derived regions corresponding to sites at which craniofacial muscles attach (Koentges and Lumsden, 1996). The patterns of deletions of cartilaginous elements we observe at moderate RA concentrations seem to be unrelated to their embryological origin—whether that is neural crest or mesoderm. Thus, RA is more likely to be affecting positional information given to cells along the A/P axis.

The pharyngeal skeleton consists of a set of seven segmented arch homologs, each consisting of dorsal and ventral elements that give rise to specific cartilage elements (Romer and Parsons, 1977; Schilling and Kimmel, 1997). We observe two patterns of cartilage deletions in response to increasing concentrations of RA. First, the dorsal cartilage elements in each of the arches are deleted at a lower concentration of RA than the more ventral cartilage elements. For example, in the neurocranial cartilage of larvae exposed to 5×10^{-7} *M* RA as gastrulae, the ventral elements of all seven arches can be found (Meckel's cartilage in the mandibular arch, the ceratohyal in the hyoid arch, and the ceratobranchials in the branchial arches). The more dorsal elements (quadrate and pterygoid in the mandibular arch, hyosymplectic in the hyoid arch, and epibranchials or pharyngobranchials in the branchial arches) are all absent.

The second pattern involves the deletion of ventral elements of each arch and occurs in a noncontiguous fashion with respect to the A/P axis. Larvae treated as gastrulae with 5×10^{-7} *M* RA show deletions of one pair of ceratobrachials, whereas the ceratohyals in the hyoid arch and, in many cases, Meckel's cartilage in the mandibular arch remain. All of these cartilages are ventral elements, with the ceratohyals more centrally located along the A/P axis of the head. Although the order of the deleted ceratobranchials cannot be established definitively, they are not the tooth-bearing fifth pair of ceratobranchials, which are still present. The discontinuity of deleted ventral cartilages, relative to their position along the A/P axis, is seen at higher concentrations of RA where Meckel's cartilage and one or more additional pair of ceratobranchials are eliminated before the ceratohyals. To emphasize this important point, the cartilage derived from the ventral element of the second arch is formed; but the ventral elements of first and third or fourth arches are deleted.

The effects of exogenous RA on embryos have been explained by disruption of endogenous gradients of RA on the early patterning of embryonic tissues (Durston *et al.*, 1989). In vertebrates, RA has been shown to be important in patterning the embryonic axis (Sive *et al.*, 1990; Kessel, 1992; Conlon, 1995). All of the cartilage elements of the pharyngeal skeleton are believed to be derived from neural crest cells that migrate from midbrain and from specific rhombomeres of the hindbrain (Langille and Hall, 1988, 1993; Lumsden *et al.*, 1991; Couly *et al.*, 1993). However, different skeletal elements in the same arch, and even a single cartilage element within an arch, may receive contributions of neural crest cells from more than one specific axial level (Koentges and Lumsden, 1996). Recent studies in zebrafish suggest that dorsal and ventral elements in a given arch originate from separate sites of chondrification within the same condensation of precartilage cells (Schilling and Kimmel, 1997). In the mandibular arch, for example, the quadrate and Meckel's cartilage both arise from a single precartilage condensation, with the quadrate forming before Meckel's cartilage (Schilling and Kimmel, 1997). Our results suggest that the dorsal and ventral cartilage elements of the pharyngeal arches

are differentially sensitive to early exposure to RA and may originate from different populations of neural crest cells along the embryonic axis. Furthermore, the noncontiguous pattern of deletions of ventral elements indicates a more complex regulation or axial organization than previously recognized.

Although most of the RA-induced patterning defects we describe in this study represent deletions of specific structures, exposure of *F. heteroclitus* embryos to 1×10^{-5} *M* RA during gastrulation causes duplications of pectoral fins (described in further detail in Vandersea *et al.*, in press). Parallel studies in zebrafish also show duplicated pectoral fins at defined RA concentrations (Vandersea *et al.*, in press). Lower body and limb duplications have been shown to be induced by RA when administered during pregastrulation stages to mouse embryos (Rutledge *et al.*, 1994). Our results demonstrate that the phenotypic response to RA at gastrulation may be evolutionarily conserved and suggest that RA may be an early signaling molecule for axial specification of vertebrate limbs. The induction of duplications of specific structures is consistent with current ideas that the mechanism by which exogenous RA disrupts developmental patterning is mis-expression of patterning genes, such as Hox and Otx2 genes (Conlon, 1995).

Molecular aspects of RA action—Hox gene involvement

RA is an endogenous regulator of patterning in vertebrate embryos; at the molecular level, RA is believed to exert its patterning influences by the temporal and spatial regulation of Hox and other homeobox-containing genes (Simeone *et al.*, 1990; Papalopulu *et al.*, 1991; Langston and Gudas, 1992; and Studer *et al.*, 1994). In this paper we have shown that brain and skeletal elements of the *F. heteroclitus* head exhibit dose-dependent deletions in response to RA exposure during gastrulation. By supplying excess RA, we are disrupting the natural levels of RA in the embryos; this in turn may alter homeobox and Hox gene expression, resulting in developmental defects (Taira *et al.*, 1994; Conlon, 1995; Hill *et al.*, 1995; Alexandre *et al.*, 1996). Our work provides a model species that permits large numbers of synchronous embryos to be treated with RA at gastrulation. RA-treated *F. heteroclitus* embryos develop with distinct, reproducible phenotypes that may be useful in resolving the molecular details of RA-signaling pathways and the role of Hox gene expression.

RA signaling pathways may be sensitive to disruption by xenobiotics

The craniofacial defects we have characterized in this study of *F. heteroclitus* are similar to defects that have been described in fish and other vertebrates exposed to various xenobiotics (Weis and Weis, 1989). RA is critical for normal patterning of the craniofacial region and the heart (Means and Gudas, 1995; Conlon, 1995), and defects induced in these regions by various xenobiotics suggest that they may act by disrupting RA signaling pathways. RA acts by binding to receptors that are members of a large superfamily of steroid and thyroid hormone receptors (Leid *et al.*, 1993). Certain xenobiotics may mimic RA or disrupt the RA signaling pathway by binding or interfering with this class of receptors. For example, the insect growth regulator methoprene is teratogenic in mice (Unsworth *et al.*, 1974) and can activate one class of retinoid receptors in expression assays (Harmon *et al.*, 1995).

In this paper we have established a dose-response index describing the phenotypes resulting from increasing doses of RA. Similar index phenotypes are also identifiable in RA-exposed zebrafish embryos (Vandersea *et al.*, in press; and unpubl. data), suggesting that the mechanism by which RA induces defects is evolutionarily conserved. *F. heteroclitus* and zebrafish are, respectively, estuarine and freshwater fish species that are widely used in toxicology studies. The index we describe should be useful in embryo-based assays for toxicological and environmental monitoring studies by permitting xenobiotic effects to be ranked and quantified in exposed embryos whose defects resemble those resulting from RA exposure. This index should also aid in defining the mechanisms by which xenobiotics act and the concentrations that can be tolerated in the environment.

Acknowledgments

We thank J. Spruill for assistance with digital imaging, M. Tomblin for careful reading of the manuscript, and Chip Griffin for drawings of embryos. This is contribution #142 from Grice Marine Biological Laboratory. The study was supported by College of Charleston grants to D. S., by NIH Project Program Grant NIHLB P01 HL52813 to R.M., and by South Carolina Sea Grant NA46R-G0454AM.6 to R.M. and D.S. This paper is dedicated to investigators who pioneered the use of *Fundulus heteroclitus* and other fish for embryological studies, including William Ballard, J. P. Trinkaus, and the late Jane Oppenheimer.

Literature Cited

Akimenko, M. A., and M. Ekker. 1995. Anterior duplication of the sonic hedgehog expression pattern in the pectoral fin buds of zebrafish treated with retinoic acid. *Dev. Biol.* **170:** 243–247.

Alexandre, D., J. D. W. Clarke, E. Oxtoby, Y-L. Yan, T. Jowett, and N. Holder. 1996. Ectopic expression of *Hoxa-1* in the zebrafish alters the fate of the mandibular arch neural crest and phenocopies a retinoic acid-induced phenotype. *Development* **122:** 735–746.

Armstrong, P. B., and J. S. Child. 1965. Stages in the normal development of *Fundulus heteroclitus*. *Biol. Bull.* **123:** 143–168.

Chen, Y., L. Huang, A. F. Russo, and M. Solursh. 1992. Retinoic acid is enriched in Hensen's node and is developmentally regulated in the early chick embryo. *Proc. Natl. Acad. Sci. USA* **89:** 10056–10059.

Chen, Y., L. Huang, and M. Solursh. 1994. A concentration of retinoids in the early *Xenopus laevis* embryo. *Dev. Biol.* **161:** 70–76.

Cho, K. W. Y., and E. M. De Robertis. 1990. Differential activation of *Xenopus* homeobox genes by mesoderm-inducing growth factors and retinoic acid. *Genes Dev.* **4:** 1910–1916.

Conlon, R. A. 1995. Retinoic acid and pattern formation in vertebrates. *Trends Genet.* **11:** 314–319.

Couly, G. F., P. M. Coltey, and N. M. Le Douarin. 1993. The triple origin of skull in higher vertebrates: a study in quail-chick chimeras. *Development* **117:** 409–429.

Cubbage, C. C., and P. M. Mabee. 1996. Development of the cranium and paired fins in the zebrafish *Danio rerio* (Ostariophysi, Cyprinidae). *J. Morphol.* **229:** 1–40.

de Beer, G. R. 1937. *The Development of the Vertebrate Skull.* Oxford University Press, Oxford, UK. Reprinted 1985. Chicago University Press, Chicago, IL.

Dingerkus, G., and D. L. Uhler. 1977. Enzyme clearing of Alcian Blue stained whole small vertebrates for demonstration of cartilage. *Stain Technol.* **52:** 229–231.

Durston, A. J., J. P. M. Timmermans, W. J. Hage, H. F. J. Hendriks, N. J. de Vries, M. Heideveld, and P. D. Nieuwkoop. 1989. Retinoic acid causes an anteroposterior transformation in the developing central nervous system. *Nature* **340:** 140–144.

Elinson, R. P., and K. R. Kao. 1993. Axis specification and head induction in vertebrate embryos. Pp. 1–41 in *The Skull,* J. Hanken and B. K. Hall, eds. University of Chicago Press, Chicago, IL.

Gale, E., V. Prince, A. Lumsden, J. Clarke, N. Holder, and M. Maden. 1996. Late effects of retinoic acid on neural crest and aspects of rhombomere identity. *Development* **122:** 783–793.

Grunwald, D. J., C. B. Kimmel, M. Westerfield, C. Walker, and G. Streisinger. 1988. A neural degeneration mutation that spares primary neurons in the zebrafish. *Dev. Biol.* **126:** 115–125.

Harmon, M. A., M. F. Boehm, R. A. Heyman, and D. J. Mangelsdorf. 1995. Activation of mammalian retinoid X receptors by the insect growth regulator methoprene. *Proc. Natl. Acad. Sci. USA* **92:** 6157–6160.

Hill, J., J. D. W. Clarke, N. Vargesson, T. Jowett, and N. Holder. 1995. Exogenous retinoic acid causes alterations in the development of the hindbrain and midbrain of the zebrafish embryo including positional respecification of the Mauthner neuron. *Mech. Dev.* **50:** 3–16.

Hogan, B., C. Thaller, and G. Eichele. 1992. Evidence that Hensen's node is a site of retinoic acid synthesis. *Nature* **359:** 237–241.

Holder, N., and J. Hill. 1991. Retinoic acid modifies development of the midbrain-hindbrain border and affects cranial ganglion formation in zebrafish embryos. *Development* **113:** 1159–1170.

Hunt, P., M. Gulisano, M. Cook, M. Sham, A. Faiella, D. Wilkinson, E. Boncinelli, and R. Krumlauf. 1991. A distinct Hox code for the branchial region of the head. *Nature* **353:** 861–864.

Kessel, M. 1992. Respecification of vertebral identities by retinoic acid. *Development* **115:** 487–501.

Kessel, M., and P. Gruss. 1991. Homeotic transformations of murine vertebrae and concomitant alteration of Hox codes induced by retinoic acid. *Cell* **67:** 89–104.

Koentges, G., and A. Lumsden. 1996. Rhombencephalic neural crest segmentation is preserved throughout craniofacial ontogeny. *Development* **122:** 3229–3242.

Krumlauf, R. 1994. Hox genes in vertebrate development. *Cell* **78:** 191–201.

Langille, R. M., and B. K. Hall. 1987. Development of the head skeleton of the Japanese medaka, *Oryzias latipes* Teleostei. *J. Morphol.* **193:** 135–158.

Langille, R. M., and B. K. Hall. 1988. Role of the neural crest in development of the cartilaginous cranial and visceral skeleton of the medaka, *Oryzias latipes* Teleostei. *Anat. Embryol.* **177:** 297–305.

Langille, R. M., and B. K. Hall. 1993. Pattern formation and the neural crest. Pp. 77–111 in *The Skull,* J. Hanken and B. K. Hall, eds. University of Chicago Press, Chicago, IL.

Langston, A. W., and L. J. Gudas. 1992. Identification of a retinoic acid responsive enhancer 3′ of the murine homeobox gene *Hox 1.6*. *Mech. Dev.* **38:** 217–228.

Leid, M., P. Kastner, B. Durand, A. Krust, P. Leroy, R. Lyons, C. Mendelsohn, S. Nagpal, H. Nakshatri, C. Reibel, M. Saunders, and P. Chambon. 1993. Retinoic acid signal transduction pathways. *Annals N.Y. Acad. Sci.* **684:** 19–34.

Leonard, L., C. Horton, M. Maden, and J. A. Pizzey. 1995. Anteriorization of CRABP-I expression by retinoic acid in the developing mouse central nervous system in its relationship to teratogenesis. *Dev. Biol.* **168:** 514–528.

Lohnes, D., M. Mark, C. Mendelsohn, P. Dolle, D. Decimo, M. LeMeur, A. Dierich, P. Gorry, and P. Chambon. 1995. Developmental roles of the retinoic acid receptors. *J. Steroid Biochem. Mol. Biol.* **53:** 475–486.

Lumsden, A., N. Spawson, and A. Graham. 1991. Segmental origin and migration of neural crest cells in the hindbrain region of the chick embryo. *Development* **8:** 329–335.

Marshall, H., S. Nonchev, M. H. Sham, I. Muchamore, A. Lumsden, and R. Krumlauf. 1992. Retinoic acid alters hindbrain Hox code and induces transformation of rhombomeres 2/3 into a 4/5 identity. *Nature* **360:** 737–741.

Marshall, H., M. Studer, H. Popperl, S. Aparicio, A. Kuroiwa, S. Brenner, and R. Krumlauf. 1994. A conserved retinoic acid response element required for early expression of the homeobox gene *Hox b-1*. *Nature* **370:** 567–571.

Means, A. L., and L. J. Gudas. 1995. The roles of retinoids in vertebrate development. *Annu. Rev. Biochem.* **64:** 201–233.

Minucci, S., J. P. Saint-Jeannet, R. Toyama, G. Scita, L. M. DeLuca, M. Tiara, A. A. Levin, K. Ozato, and I. B. Dawid. 1996. Retinoid X receptor-selective ligands produce malformations in *Xenopus* embryos. *Proc. Natl. Acad. Sci. USA* **93:** 1803–1807.

Noden, D. M. 1975. An analysis of the migratory behavior of avian cephalic neural crest cells. *Dev. Biol.* **42:** 106–130.

Oppenheimer, J. 1936. Transplantation experiments on developing teleosts (*Fundulus* and *Perca*). *J. Exp. Zool.* **72:** 409–437.

Oppenheimer, J. 1937. The normal stages of *Fundulus heteroclitus*. *Anat. Rec.* **68:** 1–15.

Papalopulu, N., R. Lovell-Badge, and R. Krumlauf. 1991. The expression of murine *Hox-2* genes is dependent on the differentiation pathway and displays a collinear sensitivity to retinoic acid in F9 cells and *Xenopus* embryos. *Nucleic Acids Res.* **19:** 5497–5506.

Romer, A. S., and T. S. Parsons. 1977. *The Vertebrate Body.* Saunders College Publishing, Philadelphia.

Ruiz i Altaba, A., and T. M. Jessell. 1991a. Retinoic acid modifies mesodermal patterning in early *Xenopus* embryos. *Genes Dev.* **5:** 175–187.

Ruiz i Altaba, A., and T. M. Jessell. 1991b. Retinoic acid modifies the pattern of cell differentiation in the central nervous system of neurula stage *Xenopus* embryos. *Development* **112:** 945–958.

Rutledge, J. C., A. G. Shourbaji, L. A. Hughes, J. E. Polifka, Y. P. Cruz, J. B. Bishop, and W. M. Generoso. 1994. Limb and lower-

body duplications induced by retinoic acid in mice. *Proc. Natl. Acad. Sci. USA* **91:** 5436–5440.

Schilling, T. F., and C. B. Kimmel. 1994. Segment and cell type lineage restrictions during pharyngeal arch development in the zebrafish embryo. *Development* **120:** 483–494.

Schilling, T. F., and C. B. Kimmel. 1997. Musculoskeletal patterning in the pharyngeal segments of the zebrafish embryo. *Development* **124:** 2945–2960.

Schuh, T. J., B. L. Hall, J. C. Kraft, M. L. Privalsky, and D. Kimelman. 1993. v-erb A and citral reduce the teratogenic effects of all-trans retinoic acid and retinol, respectively, in *Xenopus* embryos. *Development* **119:** 785–795.

Sharp, J. R., and J. M. Neff. 1980. Effects of the duration of exposure to mercuric chloride on the embryogenesis of the estuarine teleost, *Fundulus heteroclitus*. *Mar. Environ. Res.* **3:** 195–203.

Sharp, J. R., and J. M. Neff. 1985. Age-dependent response differences of *Fundulus heteroclitus* embryos following chronic exposure to mercury. P. 281 in *Marine Pollution and Physiology: Recent Advances*, P. J. Vernberg, F. P. Thurberg, A. Calabrese, and W. B. Vernberg, eds. University of South Carolina Press, Columbia, SC.

Simeone, A., D. Acampora, L. Arcioni, P. W. Andrews, E. Boncinelli, and F. Mavilio. 1990. Sequential activation of HOX2 homeobox genes by retinoic acid in human embryonal carcinoma cells. *Nature* **346:** 763–766.

Sive, H. L., and P. F. Cheng. 1991. Retinoic acid perturbs the expression of *Xhox.lab* genes and alters mesodermal determination in *Xenopus laevis*. *Genes Dev.* **5:** 1321–1332.

Sive, H. L., B. W. Draper, R. M. Harland, and H. Weintraub. 1990. Identification of a retinoic acid-sensitive period during primary axis formation in *Xenopus laevis*. *Genes Dev.* **4:** 932–942.

Solberg, A. N. 1938. The development of a bony fish. Pp. 378–379 in *Experimental Embryology Techniques and Procedures*, R. Rugh, ed. Burgess Publishing Co. Minneapolis, MN.

Spemann, H., and H. Mangold. 1924. Induction of embryonic primordia by implantation of organizers from a different species. Pp. 144–184 in *Foundations of Experimental Embryology*, B. H. Willier and J. M. Oppenheimer, eds. Hafner, New York.

Stainier, D. Y. R., and M. C. Fishman. 1992. Patterning the zebrafish heart tube: acquisition of anteroposterior polarity. *Dev. Biol.* **153:** 91–101.

Studer, M., H. Popperl, H. Marshall, A. Kuroiwa, and R. Krumlauf. 1994. Role of a conserved retinoic acid response element in rhombomere restriction of *Hox b-1*. *Science* **265:** 1729–1732.

Tabin, C. 1995. The initiation of the limb bud: growth factors, Hox genes and retinoids. *Cell* **80:** 671–674.

Taira, M., M. Jamrich, P. J. Good, and I. B. Dawid. 1994. The LIM domain-containing homeobox gene XLIM-1 is expressed specifically in the organizer region of *Xenopus* gastrula embryos. *Genes Dev.* **6:** 356–366.

Tanabe, Y., and T. M. Jessell. 1996. Diversity and pattern in the developing spinal cord. *Science* **274:** 1115–1122.

Tickle, C. 1995. Vertebrate limb development. *Curr. Opin. Genet. Dev.* **5:** 478–484.

Trinkaus, J. P. 1996. Ingression during early gastrulation of *Fundulus*. *Dev. Biol.* **177:** 356–370.

Unsworth, B., S. Hennen, and A. Krishnakumaran. 1974. Teratogenic evaluation of terpenoid derivatives. *Life Sci.* **15:** 1649–1655.

Vandersea, M. W., P. Fleming, R. A. McCarthy, and D. Smith. 1998. Fin duplications and deletions induced by disruption of retinoic acid signaling. *Dev. Genes Evol.* (in press).

Weis, P., and J. S. Weis. 1977. Methylmercury teratogenesis in the killifish, *Fundulus heteroclitus*. *Teratology* **16:** 317–326.

Weis, J. S., and P. Weis. 1989. Effects of environmental pollutants on early fish development. *Rev. Aquat. Sci.* **1:** 45–73.

Wood, H., G. Pall, and G. Morriss-Kay. 1994. Exposure to retinoic acid before or after the onset of somitogenesis reveals separate effects on rhombomeric segmentation and 3′ *HoxB* gene expression domains. *Development* **120:** 2279–2285.

Zilliacus, J., A. P. H. Wright, J. Carlstedt-Duke, and J. Gustafsson. 1995. Structural determinants of DNA-binding specificity by steroid receptors. *Mol. Endocrinol.* **9:** 389–399.

Reference: *Biol. Bull.* **194:** 297–303. (June, 1998)

Predation on Bivalve Veligers by Polychaete Larvae

KEVIN B. JOHNSON[1,*] AND LAURA A. BRINK[2]

[1] *Oregon Institute of Marine Biology, P.O. Box 5389, Charleston, Oregon 97420; and* [2] *Horn Point Laboratory, Cambridge, Maryland 21613*

Abstract. Polychaete larvae from several families are thought to be natural predators upon planktonic bivalve larvae. However, little direct evidence of interactions between these predators and prey is available. We conducted predator-prey experiments on laboratory roller tables for five putative predatory polychaete larvae, representing four families (metatroch-less larvae of the Polynoidae and metatrochophore larvae of the Spionidae, the Magelonidae, and the Phyllodocidae). D-hinge veliger larvae of the oyster *Crassostrea gigas* were offered as prey. Predation was monitored over a range of prey densities and in the presence and absence of background plankton. "Background plankton" are any naturally occurring plankton assemblages found in whole, unfiltered seawater at ambient concentrations. For all polychaete larvae examined, when natural *C. gigas* densities *and* background plankton were used, no predation was observed. Magelonids and phyllodocids did not consume any *C. gigas* larvae, regardless of conditions. Polynoid and spionid trochophores consumed *C. gigas* veligers at both the "natural" and unnaturally high prey densities in filtered seawater. The addition of background plankton eliminated the predation at all natural prey densities and significantly reduced the predation observed at high prey densities.

Introduction

Predation in the plankton is a source of mortality that may control the presence and abundance of the planktonic larvae of benthic marine invertebrates (Thorson, 1950). Observations of predation upon meroplanktonic invertebrate larvae are recorded from as far back as the 1920s. For example, Lebour (1922) noted bivalve veliger larvae in the guts of the larval polychaete *Magelona papillicornis* (Magelonidae). Other biologists have also observed bivalve veligers within the guts of field-caught *Magelona* sp. larvae (Thorson, 1946; Smidt, 1951; Kühl, 1974; Wilson, 1982). Lebour (1922), Smidt (1951), and Kühl (1974) recorded only bivalve larvae as prey for magelonids, but Thorson (1946) and Wilson (1982) observed that *M. papillicornis* also consumed other planktonic organisms. In spite of these many observations and the general impression that larval polychaetes of the genus *Magelona* are specialist predators of bivalve veligers (*e.g.*, Todd *et al.*, 1996), a natural predator-prey relationship between larval polychaetes and bivalve larvae has yet to be definitively shown. There are problems also with the anecdotal nature of some past observations on wild-caught plankton: when planktonic predators and prey are concentrated in the cod-end of a plankton net for several minutes or more, as is usually the case when plankton samples are being collected, it is not possible to differentiate natural predation from that occurring in the cod-end under very abnormal conditions, which we refer to as "artifactual predation."

Predation upon bivalve veligers by polychaete trochophores (metatroch-less trochophores and metatrochophores) has also been observed for representatives of other polychaete families, including the Polynoidae (Yokouchi, 1991), the Nephtyidae (Mileikovski, 1959; Yokouchi, 1991), the Phyllodocidae (Yokouchi, 1991), and the Spionidae (Daro and Polk, 1973; K. B. Johnson, unpubl. data). These observations of predation are remarkable in two ways. First, it is very seldom that a larva has been observed to be the primary food consumed by a planktonic suspension-feeding predator that consumes its prey one individual at a time. Unlike cases in which predators (*e.g.*, some scyphozoans and clupeid fish) indiscriminately feed on many planktonic prey, consistent observations of a given prey item in the gut of such a "single-

Received 29 July 1997; accepted 12 March 1998.

* To whom correspondence should be addressed. E-mail: kjohnson@oimb.uoregon.edu

particle predator" may indicate a strongly specific predator-prey relationship and provide insight into predator behavior. Second, bivalve veligers consumed by polychaete larvae are often surprisingly large relative to the predator's body diameter and apparent mouth size (see Fig. 1).

Examining the mechanism underlying particle ingestion by polychaete larvae, Phillips and Pernet (1996) fed larvae of the polychaetes *Serpula vermicularis* (Serpulidae) and *Arctonöe vittata* (Polynoidae) polystyrene beads and plankton at a range of sizes. *S. vermicularis* larvae were apparently not equipped to handle food particles greater than 12 μm in diameter (Phillips and Pernet, 1996). *A. vittata* larvae less than 100 μm in diameter were observed to ingest large particles (polystyrene beads and phytoplankton) up to 60 μm in diameter, a common size for small bivalve larvae. The larvae of *A. vittata*, a scaleworm, likely include relatively large particles in their natural diet. Does this diet include larval bivalves? Bivalve veligers have been observed in the guts of field-caught polynoid larvae (Yokouchi, 1991). Like the larvae of *Magelona* sp., the larvae of polynoids and several other polychaete families may be natural predators upon bivalve veligers.

We examined the potential predator-prey relationship between several larval polychaetes and bivalve veliger larvae. The relationship was examined using a combination of field observations (plankton samples) and laboratory experiments. In plankton samples, trochophores representing several families were observed with bivalve veligers in their guts. More important for this study, however, field samples helped determine densities used in laboratory experiments. Densities of predators and prey reflected field densities from samples in which predation was observed. Laboratory experiments used five types of larval polychaetes as predators: *A. vittata* (metatroch-less trochophore, Polynoidae), *Magelona* sp. (metatrochophore, Magelonidae), and unidentified species from the families Polynoidae (metatroch-less trochophore), Spionidae (metatrochophore), and Phyllodocidae (metatrochophore). D-hinge veliger larvae of the oyster *Crassostrea gigas* were offered as prey. Experiments were conducted at two prey densities and in the presence or absence of background plankton. The presence of background plankton (by which we mean naturally occurring phyto- and zooplankton ever-present in the field but often excluded in laboratory experiments) is potentially important because it may act as a substitute food for predators or obscure prey from detection (Johnson and Shanks, 1997).

Materials and Methods

Field observations

During August 1994, plankton samples were collected from within 10 km of the shore of Duck, North Carolina. Using a 100-μm-mesh plankton net and an on-board electric centrifugal pump, samples were collected for 3 min at 227.1 l min^{-1}, for a final sample volume of approximately 680 liters. Between 3 and 5 sampling depths were chosen at each station, depending upon the station depth. After pumping was complete, samples were rinsed from the cod-ends and preserved with 10% $CaCO_3$-buffered formalin for later sorting. Plankton samples were sorted under a dissection microscope with polarized light to aid in locating bivalves. For a more detailed description of collection and sorting methods, see Brink (1997).

Bivalve veligers were tallied when observed in the guts of predatory polychaete larvae. The total density of bivalve larvae and polychaete larvae was determined for each sample in which bivalve predation was observed. These densities were considered when deciding upon predator and prey densities to be used in the laboratory experiments described below.

Culture of predators and prey

Adult specimens of the scaleworm *Arctonöe vittata*, commensal with the keyhole limpet *Diodora aspera*, were collected with their host from the west shore rocky intertidal of San Juan Island, Washington. Individuals of *A. vittata* were spawned and larvae were cultured using the methods described by Phillips and Pernet (1996) with the addition of *Coscinodiscus radiatus* (CCMP 310) as a food source. Fertilized eggs were cultured in 600-ml beakers at densities of ~500 l^{-1}. Larvae approximately 21 days old were used as predators in experiments.

All other larval polychaetes used as predators were collected at high tide near the mouth of Coos Bay, Oregon, by slowly towing a 150-μm-mesh plankton net equipped with a large, blind cod-end (Reeve, 1981). Pipettes (3-mm-bore) were used to immediately remove predators from the plankton sample and isolate them in 250 ml of filtered seawater. Experiments began within 6 hours of predator collection.

D-hinge veligers of the oyster *Crassostrea gigas*, 5 to 10 days old (greatest linear dimension 70–90 μm), were used as prey in all laboratory experiments. The oyster larvae were obtained from Whiskey Creek Oyster Farms, Tillamook, Oregon, and maintained in 1-gallon jars on a diet of *Isochrysis galbana* and *Rhodomonas* sp.

Roller table experiments

One laboratory experiment, with four treatments, was conducted for each of the five species of larval polychaete (Table I). Two densities of prey were used. The first prey density (Treatments A and B) was designed to approximate natural field concentrations and was set at 33 bivalve larvae l^{-1} on the basis of the highest value we found in the literature (Carriker, 1951). The second prey density

Table I

Mean number of Crassostrea gigas *veliger larvae in individual guts of predatory larval polychaetes according to treatment (prey density and the presence or absence of background plankton) ± the 95% confidence interval*

	Treatment			
	Near-natural prey density (33 prey l^{-1})		High prey density (1000 prey l^{-1})	
Larval polychaete (body length in parentheses)	Filtered seawater A	Background plankton **B**	Filtered seawater C	Background plankton D
Magelona sp. (2–3 mm)	0	**0**	0	0
Phyllodocid A (300–360 μm)	0	**0**	0	0
A. vittata (260–290 μm)	1.05 ± 0.37	**0**	4.17 ± 0.64	0.72 ± 0.38
Polynoid A (280–310 μm)	0.83 ± 0.41	**0**	6.17 ± 0.79	1.33 ± 0.44
Spionid A (400–500 μm)	0.08 ± 0.16	**0**	1.33 ± 0.37	0.50 ± 0.38

Results of Treatment B, the most natural treatment in regard to prey density and the presence of background plankton, are in bold.

(Treatments C and D) was chosen to represent an unnaturally high concentration (1000 l^{-1}) and thus increase the likelihood that the prey would be encountered and ingested by predators. Each prey density was presented to predators in either filtered seawater (Treatments A and C) or with background plankton (Treatments B and D). Background plankton was collected by filling buckets with whole, unfiltered seawater at the high tide immediately preceding the start of an experiment. To fill background treatment tanks, the seawater in buckets was stirred gently, suspending settled plankton, and then poured into tanks.

For each experiment, all treatments and replicates were conducted simultaneously. Cylindrical 3-l tanks (19 cm dia. × 10.5 cm ht.) were placed on a roller table (Omori and Ikeda, 1984; Larson and Shanks, 1996) maintained at 12°C in a constant temperature room with a 14:10 light:dark cycle. The slow (1 rpm) rotation of the tanks kept the plankton from settling, and the experiments were of short duration (24 h) to prevent oxygen depletion (Larson and Shanks, 1996). At the close of the experiments, the water in the roller table tanks was filtered through a partially submerged 20-μm-mesh Nitex filter, and each tank was rinsed twice to ensure that all polychaete larvae were retrieved. Within 2.5 min of filtration, polychaetes were located and isolated in filtered seawater. Consumed bivalve larvae, visible through the polychaete larva's transparent body, were then counted.

The experiment using *Arctonöe vittata* larvae as predators was conducted at Friday Harbor Laboratories (Friday Harbor, Washington). A predator density of 2 l^{-1} (6 predators per tank) was chosen based upon the upper range of polychaete trochophore densities from our field samples in which predation upon bivalve larvae had been observed. Each tank was replicated three times. Thus, a total of 18 polychaete larvae were used as predators for each treatment.

All other experiments were conducted at the Oregon Institute of Marine Biology (Coos Bay, Oregon). The four species of larval polychaetes used as predators were *Magelona* sp. (metatrochophores) and three unidentified species representing the families Polynoidae (metatroch-less trochophores), Spionidae (metatrochophores), and Phyllodocidae (metatrochophores). The unidentified genera will be referred to as polynoid A, spionid A, and phyllodocid A, respectively. All predator densities in Coos Bay experiments were 1 l^{-1} (3 predators per tank) and, for each treatment, tanks were replicated four times.

Results

Field observations

Of 150 samples, 18 had at least one polychaete larva that had preyed upon a bivalve veliger. A total of 30 bivalves were observed in the guts of 25 polychaete larvae (20 trochophores and 5 metatrochophores). The number of bivalves consumed by each of the 20 metatroch-less trochophores was variable: 1 trochophore larva had 3 bivalves, 2 trochophore larvae had 2 bivalves each, and 17 trochophore larvae had 1 bivalve each. Trochophores were typically large (mean body length = 237 μm, SD = 35 μm) and robust in form (for examples of body shape, see illustrations of polynoids, phyllodocids, or nephtyids in Bhaud and Cazaux, 1987). Detailed identification of

these metatroch-less trochophores was often not possible, but the following families may have been represented: Phyllodocidae, Hesionidae, early Nephtyidae, Polynoidae, and Chrysopetalidae. Of those metatrochophores that had bivalves, 3 were *Magelona* sp. with 1 bivalve each. The last 2 metatrochophores were likely either phyllodocids or hesionids; one (380 μm in length) had 2 bivalves in its gut, while the other (368 μm in length) had 1 bivalve. In addition, a single metatroch-less polychaete larva was observed with a gastropod veliger in its gut.

For the 18 samples in which bivalves were observed in polychaete larva guts, densities ranged from 42 to 1193 polychaete larvae sample^{-1} ($\bar{x}$ = 277.2, SD = 324.3). The range of larval bivalve densities in these same samples was from 419 to 1949 larvae sample^{-1} ($\bar{x}$ = 1217.6, SD = 494.2). Therefore, at least 42 trochophores and 419 bivalve larvae were concentrated together in the cod-end bucket (about 200 ml of seawater) when a sample was complete.

Roller table experiments

Table I summarizes the results of the roller table experiments. For the larvae of *Magelona* sp. and phyllodocid A, predation on bivalve veligers was not observed in the laboratory under any conditions. The larvae of *Arctonöe vittata*, polynoid A, and spionid A, however, did consume *Crassostrea gigas* veligers (Fig. 1). These three polychaetes exhibited low levels of predation when veliger larvae were presented at near-natural densities and in filtered seawater (Table I, Treatment A). When background plankton was used with this same near-natural prey density, predation was always absent (Table I, Treatment B). Predation was most frequent when densities of *C. gigas* were high in filtered seawater (Table I, Treatment C). Notably, the polynoid larvae, *A. vittata* and polynoid A, consumed the greatest numbers of veligers in Treatment C. The most extreme was polynoid A, averaging 6.17 bivalve veligers gut^{-1} with two of the individuals consuming 8 veligers each. Presenting prey at high densities in the presence of background plankton (Table I, Treatment D) reduced, but did not eliminate, the predation observed at the same densities in Treatment C.

Polynoid trochophores, which consumed numerous veligers in Treatment C, voided their gut contents through a large posterior rupture. This rupture quickly heals and the unburdened trochophore suffers no obvious permanent damage. Veliger valves sometimes remain attached at the hinge after passage through the gut. Intact veligers that passed through the guts of larval polychaetes were isolated in filtered seawater, but no consumed veligers revived. Thus, although digestion by trochophores can be incomplete, predation does appear to result in mortality for bivalve larvae.

Discussion

None of the larval polychaete species we tested consumed any bivalve larvae when laboratory conditions were the closest to natural (*i.e.*, near-natural prey density with background plankton present; Table I, Treatment B). We did observe predation in the treatments that used unnatural prey density or filtered seawater. One explanation for the lack of predation in Treatment B could be that larval polychaetes are not natural predators of bivalve veliger larvae. In that case, previously published observations of bivalve veligers in the guts of larval polychaetes might be an artifact of the concentration of predators and prey in cod-end buckets during plankton tows. Such artificial conditions can alter the behavior of predators and prey and increase the probability of encounters between them, resulting in unnatural ingestion. Cod-end predation is well documented for other planktonic predators, such as chaetognaths (Feigenbaum and Maris, 1984), and may mislead observers about predator-prey relationships.

Low encounter rates might also explain the absence of predation under the most natural laboratory conditions used in this study. Predators and prey may simply not encounter one another during the experiment. Natural prey densities, which tend to be relatively low, and the presence of background plankton can both decrease the number of encounters between predators and prey (Johnson and Shanks, 1997). For example, lack of encounters may explain the low predation by *Arctonöe vittata* on *Crassostrea gigas* under the most natural conditions (Table I, Treatment B). This explanation is supported by comparisons between observed predation by *A. vittata* and encounter model estimates (K. B. Johnson, unpubl. data): the estimates produced by two models (Gerritsen and Strickler, 1977, and a simple clearance rate model) were statistically indistinguishable from the minimum known encounters of *A. vittata* with *C. gigas* (*i.e.*, observed predation events). This bolsters the argument that larval polychaetes naturally prey upon bivalve veligers during relatively infrequent encounters. Indeed, the many published observations of predation (*e.g.*, Thorson, 1946; Smidt, 1951; Kühl, 1974; Wilson, 1982) may reflect relatively rare field encounters rather than artifactual cod-end predation. Predator-prey encounters in these previously published studies can, however, be difficult to estimate. Field densities, swimming speeds, and encounter radiuses, essential components of encounter rate models, are often unknown. Finally, the hypothesis that these polychaetes may, upon infrequent encounters, be natural predators of bivalve larvae is also supported by an observation of a spionid larva with one *C. gigas* veliger in its gut (K. B. Johnson, unpubl. data). This metatrochophore larva was fixed only seconds after being collected in a 120-l sample

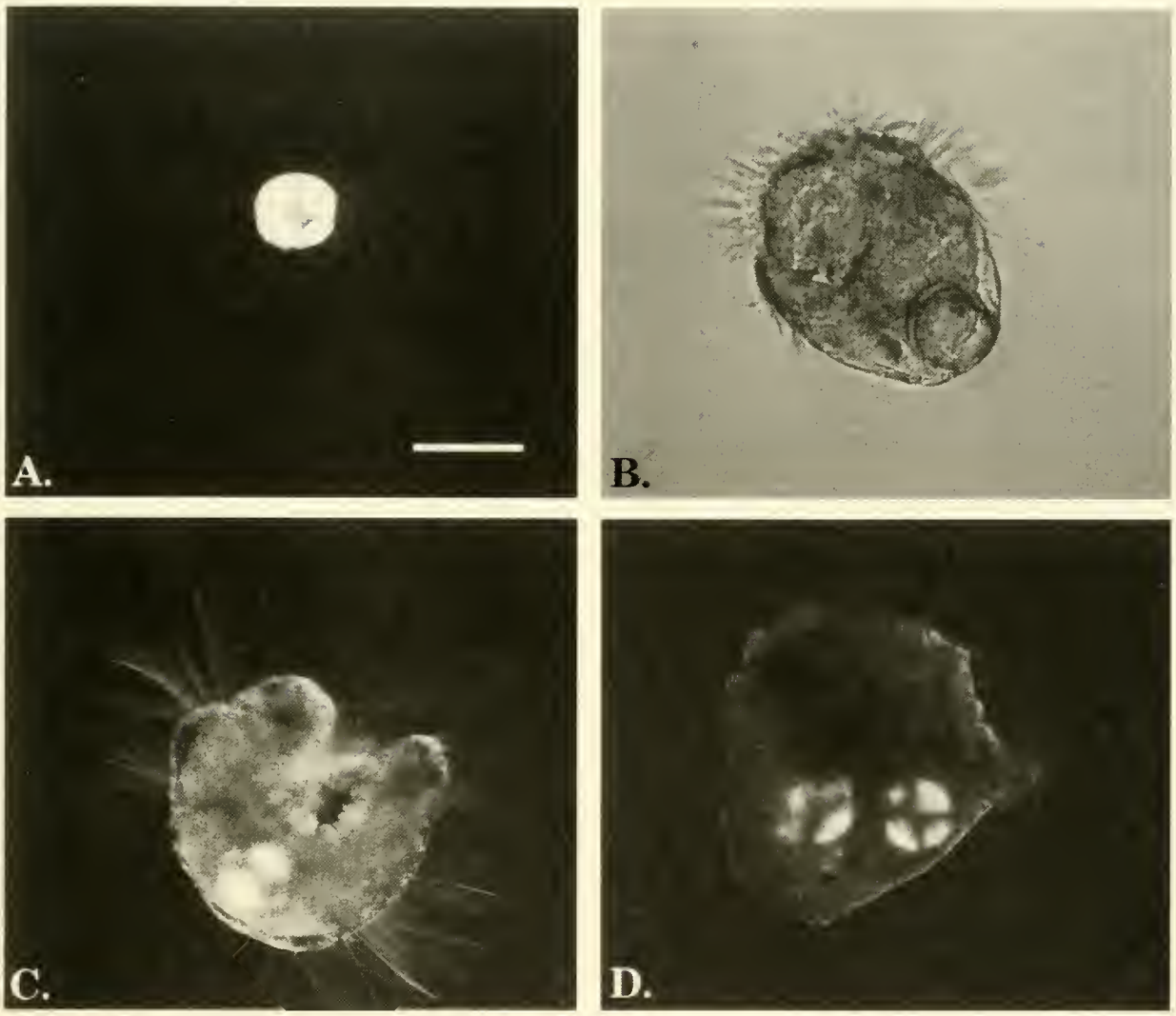

Figure 1. (A) D-hinge veliger of the oyster *Crassostrea gigas*. (B) Trochophore larva of the polynoid *Arctonöe vittata* with a veliger of the oyster *C. gigas* in its gut. (C) Metatrochophore larva of spionid A with a *C. gigas* veliger in its gut. (D) Trochophore larva of polynoid A with two *C. gigas* veligers in its gut. A, C, and D are viewed with cross-polarized light. Scale bar = 100 μm.

of seawater. No plankton net was towed; the water was collected in a plastic bag, then immediately concentrated and fixed. This method allowed little time for artifactual predation.

The true frequency of encounters between predators and prey in the field may, however, be far greater than estimated by models or from laboratory experiments if natural densities are greater than those recorded by investigators. The effect of plankton patchiness on sampling accuracy has received some attention (Hamner and Carleton, 1979; Omori and Hamner, 1982) and could cause underestimation of field densities. Plankton can be highly concentrated in a localized area—for example, through behavior-related aggregation (*e.g.*, Alldredge and Hamner, 1980; Ueda *et al.*, 1983) or the accumulation of plankton in a front (Stommel, 1949; Bray, 1953; George and Edwards, 1973). A net towed through such a patch and then through a sparsely populated region would collect a sample with an apparent density lower than the actual density within the front or aggregation. Furthermore, bivalve veligers are known to associate with marine snow (Green and Dagg, 1997; Shanks and Walters, 1997), creating localized high larval densities. Larval polychaetes can also be strongly associated with marine snow (Shanks and del Carmen, 1997) and, as a result, may encounter potential prey items such as bivalve veligers more frequently. Published observations of predation upon bivalve veligers by larval polychaetes may thus re-

flect natural predation in concentrated patches of predators and prey.

In spite of the fact that we never observed predation on bivalve veligers by *Magelona* larvae in laboratory experiments, published observations of this predator-prey relationship are numerous and should not be summarily dismissed. Wilson (1982) mentions that three species of *Magelona* are known to be carnivorous in later stages and includes descriptions of late-stage metatrochophore larvae > 4 mm in length. The *Magelona* metatrochophore larvae used in our experiments were 2—3 mm long. At a later stage, with larger palps and mouths, these larvae may be more effective at capturing bivalve larvae. It should be noted, however, that a larva of *Magelona papillicornis*, lacking long palps and only 1 mm in length, is depicted by Todd *et al.* (1996) with a bivalve veliger in its gut. Experiments analogous to ours should be conducted with later stage *Magelona* larvae to clarify the relationship of this predator with potential bivalve prey.

Summary

Certain larval polychaetes may be significant natural predators upon bivalve veligers. This investigation, however, provides laboratory evidence that natural predation on bivalve larvae by polychaete larvae is absent or uncommon, possibly because the predators and prey have few encounters in the field (assuming that published larval bivalve densities accurately reflect natural densities).

Published reports of bivalve veligers in the guts of larval polychaetes suggest a natural predator-prey relationship and are seemingly incongruous with our results. One possible explanation is that polychaete larvae consumed the veligers while in the cod-end of a plankton net, making the predation an artifact of the collection method.

When polychaete larvae consumed bivalve veligers in our laboratory experiments, the use of near-natural prey densities with natural background plankton completely eliminated predation. This lack of predation may be due to a reduction in the number of encounters with prey (published data indicates that natural densities of bivalve larvae are relatively low) or to the role of background plankton as a substitute food for predators or a screen to obscure prey from detection. In short, our results suggest that a natural predator-prey relationship between polychaete larvae and bivalve veligers may not exist. If a relationship does exist, then the frequency of interaction and its ecological importance may be less than expected on the basis of published observations.

Acknowledgments

We thank Bruno Pernet for valuable culture assistance, Friday Harbor Laboratories for providing cold room space, and Whiskey Creek Oyster Farms (Tillamook, Oregon) for supplying oyster larvae. The manuscript benefited from the input of B. Pernet, S. S. Rumrill, A. L. Shanks, and two anonymous reviewers. Field work was supported by NSF grant #OCE-9123514 to A. L. Shanks, Oregon Institute of Marine Biology. Laboratory work was funded by NSF grant #OCE-9521093 to ALS and by an award from the Lerner-Gray Fund for Marine Research to KBJ.

Literature Cited

Alldredge, A. L., and W. M. Hamner. 1980. Recurring aggregation of zooplankton by a tidal current. *Estuarine Coastal Mar. Sci.* **10:** 31–37.

Bhaud, M., and C. Cazaux. 1987. Description and identification of polychaete larvae; their implications in current biological problems. *Oceanis* **13:** 596–753.

Bray, B. M. 1953. Sea-water discoloration by living organisms. *N. Z. J. Sci. Technol. B* **34:** 393–407.

Brink, L. A. 1997. *Cross-shelf transport of planktonic larvae of inner shelf benthic invertebrates.* M. S. Thesis, University of Oregon, Eugene.

Carriker, M. R. 1951. Ecological observations on the distribution of oyster larvae in New Jersey estuaries. *Ecol. Monogr.* **21:** 19–38.

Daro, M. H., and P. Polk. 1973. The autecology of *Polydora ciliata* along the Belgian coast. *Neth. J. Sea Res.* **6:** 130–140.

Feigenbaum, D. L., and R. C. Maris. 1984. Feeding in the Chaetognatha. *Oceanogr. Mar. Biol. Annu. Rev.* **22:** 343–392.

George, D. G., and R. W. Edwards. 1973. *Daphnia* distribution within langmuir circulations. *Limnol. Oceanogr.* **18:** 798–800.

Gerritsen, J., and J. R. Strickler. 1977. Encounter probabilities and community structure in zooplankton: a mathematical model. *J. Fish. Res. Board Can.* **34:** 73–82.

Green, E. P., and M. J. Dagg. 1997. Mesozooplankton associations with medium to large marine snow aggregates in the northern Gulf of Mexico. *J. Plankton. Res.* **19:** 435–447.

Hamner, W. H., and J. H. Carleton. 1979. Copepod swarms: attributes and role in coral reef ecosystems. *Limnol. Oceanogr.* **24:** 1–14.

Johnson, K. B., and A. L. Shanks. 1997. The importance of prey densities and background plankton in studies of predation on invertebrate larvae. *Mar. Ecol. Prog. Ser.* **158:** 293–296.

Kühl, H. 1974. Über vorkemmen und nahrung der larven von *Magelona papillicornis* O. F. Müller (Polychaeta Sedentaria) im Mündungsgebiet von Elbe, Weser und Ems. *Ber. Dtsch. Wiss. Komm. Meeresforsch.* **23:** 296–301.

Larson, E. T., and A. L. Shanks. 1996. Consumption of marine snow by two species of juvenile mullet and its contribution to their growth. *Mar. Ecol. Prog. Ser.* **130:** 19–28.

Lebour, M. V. 1922. The food of planktonic organisms. *J. Mar. Biol. Assoc. U.K.* **12:** 644–677.

Mileikovski, S. A. 1959. Interrelations between the pelagic larvae of *Nephtys ciliata* (O. F. Müller), *Macoma baltica* and *Mya arenaria* of the White Sea. *Zool. Zh.* **38:** 1889–1891.

Omori, M., and W. M. Hamner. 1982. Patchy distribution of zooplankton: Behavior, population assessment and sampling problems. *Mar. Biol.* **72:** 193–200.

Omori, M., and T. Ikeda. 1984. *Methods in Marine Zooplankton Ecology,* John Wiley, New York, 332 pp.

Phillips, N. E., and B. Pernet. 1996. Capture of large particles by suspension-feeding scaleworm larvae (Polychaeta: Polynoidae). *Biol. Bull.* **191:** 199–208.

Reeve, M. R. 1981. Large cod-end reservoirs as an aid to the live collection of delicate zooplankton. *Limnol. Oceanogr.* **26:** 577–580.

Shanks, A. L., and K. A. del Carmen. 1997. Larval polychaetes are strongly associated with marine snow. *Mar. Ecol. Prog. Ser.* **154:** 211–221.

Shanks, A. L., and K. Walters. 1997. Holoplankton, meroplankton, and meiofauna associated with marine snow. *Mar. Ecol. Prog. Ser.* **156:** 75–86.

Smidt, E. L. B. 1951. Animal production in the Danish Waddensea. *Medd. Dan. Fisk.-Havunders.* **11(6):** 151 pp.

Stommel, H. 1949. Trajectories of small bodies sinking slowly through convection cells. *J. Mar. Res.* **8:** 24–29.

Thorson, G. 1946. Reproduction and larval development of Danish marine bottom invertebrates, with special reference to the planktonic larvae in the sound (Øresund). *Medd. Dan. Fisk.-Havunders. Serie: Plankton* **4:** 7–523.

Thorson, G. 1950. Reproductive and larval ecology of marine bottom invertebrates. *Biol. Rev. Camb; Philos. Soc.* **25:** 1–45.

Todd, C. D., M. S. Laverack, and G. A. Boxshall. 1996. *Coastal Marine Zooplankton,* 2nd ed. Cambridge University Press, New York.

Ueda, H., A. Kuwahara, M. Tanaka, and M. Azeta. 1983. Underwater observations on copepod swarms in temperate and subtropical waters. *Mar. Ecol. Prog. Ser.* **11:** 165–171.

Wilson, D. P. 1982. The larval development of three species of *Magelona* (Polychaeta) from the localities near Plymouth. *J. Mar. Biol. Assoc. U.K.* **62:** 385–401.

Yokouchi, K. 1991. Seasonal distribution and food habits of planktonic larvae of benthic polychaetes in Volcano Bay, Southern Hokkaido, Japan. *Ophelia* **5:** 401–410.

Reference: *Biol. Bull.* **194:** 304–316. (June, 1998)

Oyster Shell Protein and Atomic Force Microscopy of Oyster Shell Folia

C. S. SIKES[1,*], A. P. WHEELER[2], A. WIERZBICKI[3], R. M. DILLAMAN[4], AND L. DE LUCA[2]

[1] *The Mineralization Center, Department of Biological Sciences, and* [3] *Department of Chemistry, University of South Alabama, Mobile, Alabama 36688;* [2] *Department of Biological Sciences, Clemson University, Clemson, South Carolina 29634-1903; and* [4] *Department of Biological Sciences, University of North Carolina at Wilmington, Wilmington, North Carolina 28403-3297*

Abstract. The organic layers within biominerals often are viewed as sheets that may function in part to limit and define the underlying crystal structure, as well as to promote formation of the next mineral layer. Some insights into the nature of the sheets were revealed by atomic force microscopy (AFM) of surfaces of freshly cleaved fragments of oyster shell folia. Visible in the micrographs were arrays of globular structures that resembled the globules seen in isolated oyster shell protein bound to calcite, mica, and glass. The results of chemical treatment showed that the foliar globules slowly dissolved in 5.25% NaOCl or 1 *N* NaOH, reacted with an antibody prepared against an isolated oyster shell protein, and were hydrolyzed by several proteolytic enzymes. These morphological and chemical observations suggested that protein was a significant component of the foliar globules. Although they might also have a significant mineral content, the foliar globules were not effective as nucleators of $CaCO_3$ crystal formation at low levels of supersaturation in artificial seawater. Overall, the results suggested that molecules of oyster shell protein may agglomerate and combine with mineral to form a surface of complex topography that coats the calcite laths but exhibits no obvious correspondence to any specific crystallographic plane.

Introduction

Information about the organization of shell and regulation of its growth is not only central to biomineralogy but also has increasingly attracted the attention of materials scientists (Wheeler and Koskan, 1993; Mann, 1996; Stupp and Braun, 1997; Weiner and Addadi, 1997). For example, there is interest in nanoscale approaches to making composite materials that have increased durability, elevated resistance to fracture, and other desirable properties. In shell, such properties are thought to be derived from the interplay of the mineral phases with the organic layers; the latter are viewed mainly as sheets that may nucleate the original crystal phase, then regulate and limit its growth so that a specific morphology results.

The organic and inorganic phases of the carbonate biominerals that occur in shells are well suited to atomic-level imaging by atomic force microscopy (AFM), as shown by a number of studies that probed the hard, flat mineral surfaces (Friedbacher *et al.*, 1991; Hilner *et al.*, 1992; Drake *et al.*, 1992; Donachy *et al.*, 1992; Sikes *et al.*, 1993). There also have been AFM observations of protein molecules isolated from calcite oyster shell, as well as of peptide analogs of the protein, bound to specific surfaces of calcite (Wierzbicki *et al.*, 1994; Sikes and Wierzbicki, 1995a, b). The isolated oyster shell protein had an ellipsoid, globular appearance when attached to calcite grown *in vitro* and viewed by AFM.

The polygonal crystalline arrays of aragonite from molluscan nacre also have been studied by AFM (Giles *et al.*, 1994, 1995; Manne *et al.*, 1994). The emphasis in these studies was on bleached biominerals, which thus were presumably free of the associated proteins. Although logically interpreted as composed of mineral only, many globules were observed that at least resembled the globules of isolated matrix proteins that we had reported, as

Received 30 April 1997; accepted 6 March 1998.

* To whom correspondence should be addressed. E-mail: ssikes@usamail.usouthal.edu

mentioned above. Along these lines, Gutmannsbauer and Hanni (1994) viewed nacreous tablets by a variety of techniques and interpreted both the X-ray reflections and the AFM images as showing an ordered layer of organic globules that coats each tablet. Shell organic layers have also been described in detail in many electron microscopy studies over the years.

For example, Watabe and coworkers studied transmission electron micrographs of Formvar replicas taken from the whole, inner surface of oyster shell (1958), Formvar replicas of fracture surfaces of oyster shell (1961), and diamond-knife sections of pieces of foliar layers of oyster shell with and without a decalcification treatment (1965), usually with silicon monoxide or carbon coatings. The images revealed distinct relationships between the organic and inorganic layers, in some cases including the presence of organic layers at the fracture surfaces. Although the spatial resolution of the surface topography was necessarily affected by the limitations of electron microscopy, especially when replicated and coated specimens were examined, the clarity of the images was nonetheless excellent, making possible the detection of globular and "reticular" structures on the foliar surfaces. Assignments of spatial dimensions of organic layers were made only of cross-sections and not of surface views; the assignments were based on the relative electron density of the layers. By this approach, the width of the proteinaceous layer between adjacent folia was estimated to be 12 to 20 nm.

Similarly, Taylor *et al.* (1969) and Carriker and coworkers (1979, 1980) used transmission and scanning electron microscopy (SEM) of coated replicas, diamond-wheel sections, and fracture surfaces in monographic studies of oyster shell ultrastructure. Many high-resolution images of all layers of the shell were produced. The large inner layer of calcite sheets, or folia, was one area of emphasis. Spatial relationships again were evident between the organic and inorganic constituents, with the observations and interpretations consistent with earlier studies. In a number of the images, globules are apparent on the surfaces of the folia, but no particular attention was drawn to them.

Previously, we reported AFM images of folia from the inner layer of oyster shell. Foliar chips, which are produced in abundance when a shell is cracked open, evidently cleave mainly along the interfaces where the proteins occur rather than through the mineral itself, and therefore might be coated with protein (Watabe, 1965; Taylor *et al.*, 1969; Carriker and Palmer, 1979; Carriker *et al.*, 1980; Kuhn-Spearing *et al.*, 1996). We had observed that the foliar surface contained globular ellipsoids resembling the globules of isolated oyster shell protein imaged both in fluids and dry on calcite, glass, and mica (Sikes and Wierzbicki, 1995a, b; 1996). Moreover, the foliar globules were susceptible to enzymatic hydrolysis (Sikes *et al.*, 1997).

The purpose of the present investigation was to establish the identity of the foliar globules more clearly as proteinaceous, mineral, or perhaps a combination of both. Approaches included chemical, enzymatic, and immunologic treatments together with AFM and SEM observations. In addition, the possible function of the foliar globules and their relationship to the adjacent mineral phases was investigated by AFM and SEM studies of nucleation of calcite on foliar chips. The results suggested that the proteinaceous layer of oyster shell folia is itself a composite of undefined mineral and agglomerations of individual protein molecules, which together form a layer of complex topography, rather than a linearized sheet, that overlies the calcite laths. As nucleators of crystal growth, the foliar globules were less effective than the areas of exposed calcite that may occur on the foliar surfaces. No obvious relationship of the foliar globules to specific crystallographic planes was found, although several possibilities were considered.

Materials and Methods

Oyster shell folia

The outer surface of freshly shucked shells of the American oyster, *Crassostrea virginica*, was ground using a hand-held Dremel to remove residual periostracum and outer prismatica. The shell was then fractured with a hammer. White, pearlescent foliated chips were separated from pigmented and chalky chips and stored dry in a vial. The chips were several millimeters in linear dimensions; they typically weighed between 20 and 30 mg, and did not exceed 100 mg.

Chemical treatments

Foliar chips were incubated in 10 ml of 1 *N* NaOH or 5.25% NaOCl (Clorox) in a glass vial for 3 weeks. The solution was changed daily. At intervals, a chip was removed with forceps, placed on a glass-fiber filter, and washed under gentle vacuum with 10 ml of 0.1 m*M* NaOH. Next, the chip was soaked for 10 min, 3 times, in 10 ml of an aqueous solution saturated with respect to calcite. This solution was the supernatant of a slurry of reagent-grade calcite crystal, 25 g/liter of water, stirred for 3 weeks. The chip then was placed on a piece of absorbent paper, air-dried for 1 h, and glued to a 12-mm glass disc by gently placing it on 10 μl of 3:1 dichloromethane and commercial polyurethane (Minwax), just after the dichloromethane had mostly evaporated, leaving a flat, nonwicking adhesive surface. This produced a firm,

insoluble attachment to the glass disc, which had been previously attached with superglue (cyanoacrylate) to an electron-microscopy stub. Epoxy was also acceptable for adhering the chips to glass, but superglue was not because it dissolved during aqueous imaging.

Control chips were incubated in calcite-saturated water and washed as above prior to viewing. They also were imaged directly, with no treatment, to ensure that the soaking and washing did not affect the control morphology. Some chips and control crystals of calcite also were rinsed in distilled water rather than calcite-saturated water. This had no effect on the overall appearance of the folia, but did etch the surface of the control crystals. Therefore, for AFM imaging at the atomic level, the calcite-saturated solution was preferable for rinsing. However, if the saturated solution was not quickly absorbed into the paper, the samples would occasionally exhibit ectopic crystals that formed from drying droplets.

Enzymatic treatments

Foliar chips were incubated for 48 h in 0.5 ml of phosphate buffer (0.05 *M*, pH 7.5) that contained 1.95 units of carboxypeptidase B (Sigma), 2 units of endoproteinase glu-C (Boehringer-Mannheim), or 1.5 units of subtilisin (Boehringer-Mannheim). Carboxypeptidase is a general protease of peptide bonds at the C-terminus. Endoproteinase glu-C and subtilisin both cleave internal peptide bonds, particularly of acidic residues, which are common in the oyster shell protein.

The chips were rinsed with distilled water and air dried prior to gluing onto the glass disc and AFM stub. Control chips were incubated in buffer alone.

Immunohistochemical treatments

An ELISA assay was performed directly on foliar chips, using an antibody prepared against a 48-kD protein band obtained by SDS-PAGE of whole, soluble protein extracts of folia (Myers *et al.*, 1996). The electroeluted protein was mixed 1:2 with Freunds incomplete adjuvant and injected intramuscularly (three injections) into single-comb white leghorn hens to stimulate antibody production. Approximately 2 weeks after the final injection, IgG was chloroform-extracted from egg yolks and purified by ethanol precipitation (after Mohammed *et al.*, 1986). Standard ELISA confirmed the reactivity of the extracted antibody with the 48-kD antigen and demonstrated cross-reactivity of the antibody with other isolated oyster shell matrix proteins (Johnstone and Wheeler, unpubl. data). The antibody did not react with β-lactoglobulin or BSA, which served as negative controls.

Foliar chips were incubated for 1 h in 1% BSA to block nonspecific binding, washed in two changes of TBS (Tris-buffered saline, pH 7.4), and then transferred to a 1:200 solution of the soluble matrix primary antibody. After 1 h, the chips were washed twice with TBS and transferred for 1 h to a 1:1200 solution of horseradish-peroxidase-conjugated goat anti-chicken secondary antibody (Sigma). After a final TBS wash, the DAB system (Sigma) was used to detect antibody binding to the foliar chips. Additional blocked (BSA-incubated) and unblocked (no BSA incubation) chips, incubated with secondary antibody only and developed using the DAB system, confirmed that there was very little nonspecific binding of the secondary antibody to the foliar shell.

Matched foliar chips were pretreated for 24 h with 1 ml of 0.1 *M* NaOH or 0.08 *M* EDTA solution (pH about 9.0) and then assayed as above. The EDTA solution was prepared so as to dissolve no more than 10% of the 80 mg of foliar shell. These treatments yielded ELISA results that were nearly as dark as those for untreated chips, indicating that most sites for primary antibody binding were still available. The slightly diminished reactivity of the treated chips suggested that some binding sites had been altered or removed via dissolution of protein or shell.

Foliar chips to be imaged by AFM were incubated in primary antibody only.

Atomic force microscopy

Constant-force, contact-mode AFM (Nanoscope III, Digital Instruments) was used to image foliar chips, both dry and in calcite-saturated artificial seawater (ASW: again, the supernatant of a slurry of calcite crystals as above, but prepared in 0.5 *M* NaCl, 0.011 *M* KCl, pH 8.3). Tapping-mode AFM was not needed for foliar images because the imaged surfaces and adsorbates were firm and stationary to contact-mode AFM. However, tapping-mode images were obtained for the various treatments and, in all cases, revealed morphologies similar to those obtained by contact mode. The images reported herein were all obtained by contact-mode AFM. Standard tips of Si_3N_4 were used for contact mode and tips of etched silica for tapping mode (both from Digital Instruments). The tip forces in contact mode were minimized at $\sim 10^{-9}$ N; however, the samples were stable under higher forces as well. The AFM scanner was adapted for use of SEM stubs.

Procedures to guard against artifacts included variation of the scan angle to make sure that the image rotated accordingly. In addition, for contact-mode imaging, tips were first used to obtain an atomic image of mica to be sure that the tip was performing optimally before imaging a sample. This procedure was repeated after an imaging session, as well as during a session if questionable features began to appear, to confirm that the tip was still

capable of producing images at the angstrom level. Tips that would not generate an atomic pattern of mica were discarded.

Morphology at the micrometer level as seen by AFM was corroborated by direct comparison of AFM and SEM images of similar surfaces. This was more satisfactory than use of several commercial and shareware deconvolution programs to remove any tip-related features from AFM images. These programs often yielded images of oyster shell folia or fields of randomly oriented crystals of calcite that conflicted with images of the same materials viewed by SEM.

AFM crystal growth assay

Metastable and spontaneously nucleating solutions of calcite-supersaturated ASW were gently pumped through a fluid cell (Digital Instruments, volume ~150 μl) by use of a peristaltic pump (Cole-Parmer) at a flow rate of ~150 μl/min. The calcium concentration was 10 m*M*, with total dissolved inorganic carbon (DIC) varied from 2 to 10 m*M*. The solutions were first prepared in a three-necked, 50-ml round-bottom flask by addition of 30 ml of ASW, with smooth magnetic stirring. To this was added 0.3 ml of 1.0 *M* $CaCl_2 \cdot 2H_2O$, followed by appropriate volumes of 0.5 *M* $NaHCO_3$. The pH was adjusted to 8.30 with microliter amounts of 1 *N* NaOH and monitored by pH electrode and meter (Fisher 911) equipped with a strip chart (Cole-Parmer). The apparatus was not thermostated, but room temperature was recorded at 23° ± 2°C. At the initiation of the experiment, the fluid from the flask was pumped through the flow-cell of the AFM. The foliar chip was already in place and being imaged in calcite-saturated ASW.

In separate experiments, the metastability of the fluids was demonstrated by growth of 15 mg of $CaCO_3$ seeds, added to the flask as 1.5 ml of a 10 mg/ml seed suspension in saturated ASW. The primary stock of calcite seeds was prepared by stirring 100 g of reagent-grade calcite (Baker) in 1 l of ASW for at least 3 weeks (Wheeler *et al.*, 1991). In the absence of seed crystals, at 2 to 5 m*M* DIC, the solutions exhibited no spontaneous crystal formation over periods of at least 2 h of most imaging sessions. However, these solutions were shown to be supersaturated and were defined as metastable because crystal growth did occur in the presence of seed crystals. The growth was observed as a downward drift in pH resulting from incorporation of CO_3^{2-} ions into the seed-crystal lattice.

At a concentration of 7 m*M* DIC at pH 8.3, the calcite crystals did spontaneously nucleate after an induction period of 15 to 20 min. At concentrations of DIC higher than 7 m*M*, the induction of crystal growth, again monitored by downward pH drift, became increasingly more rapid, making real-time monitoring by AFM more difficult. In addition to rapid crystal formation over large regions of the foliar chip, the turbid suspension of calcite crystals at these concentrations of DIC interfered with the laser signal of the AFM.

Scanning electron microscopy

Foliar chips were dehydrated by vacuum at 1 mTorr for 15 min, then coated with a layer of approximately 20 nm of gold palladium in a Polaron sputter coater. Specimens were viewed with an ISI SX40 scanning electron microscope operated at 30 kV.

Results

Atomic force micrographs of dry, control, untreated foliar chips of oyster shell are shown in Figures 1, 3, 5, and 6. The folia are composed of individual crystalline laths lying side-by-side to form a sheet. Laths are typically about 2 μm in width, with lath heights in the imaged areas varying from 150 to 350 nm. Figures 1 and 3 are comparable in magnification to Figures 2 and 4, which are scanning electron micrographs of control, untreated foliar chips. Both Figures 1 and 2 are low magnifications that show the arrays of folia revealed by the fracturing process. Figures 3 and 4 show individual folia and reveal randomly broken ends, straight foliar margins, and a granular surface texture. Figures 5 and 6 are higher magnification AFM images that resolve the surface texture, identified in the lower magnification images from both SEM and AFM, into a continuous layer of discrete globules. These foliar globules typically were about 10 to 15 nm in height, but ranged up to about 40 nm.

The susceptibility of the foliar globules to dissolution in 1 *N* NaOH is shown in Figure 7. The foliar globules were seen to be relatively resistant to the NaOH treatment at 5 days. However, by 10 days (not shown), the globules were reduced to remnants with indistinct edges and heights of 1 to 3 nm instead of the typical globular height of about 10 to 15 nm on control foliar surfaces.

The effect of NaOCl treatment on the foliar globules as viewed by AFM is shown in Figures 8 and 9. After 1 day, the globules remained relatively intact. By 5 days, the globules were blurred and reduced in height to a range of 3 to 8 nm. In both the NaOH and NaOCl treatments, the surfaces became smoother and relatively featureless with time.

Treatment of foliar chips for 48 h with the proteolytic enzymes (carboxypeptidase B, endoproteinase glu-C, and subtilisin) also led to the partial removal of the foliar globules. In each case, as illustrated for carboxypeptidase B (Figs. 10 and 11), the globules became indistinct and reduced in height relative to control globules.

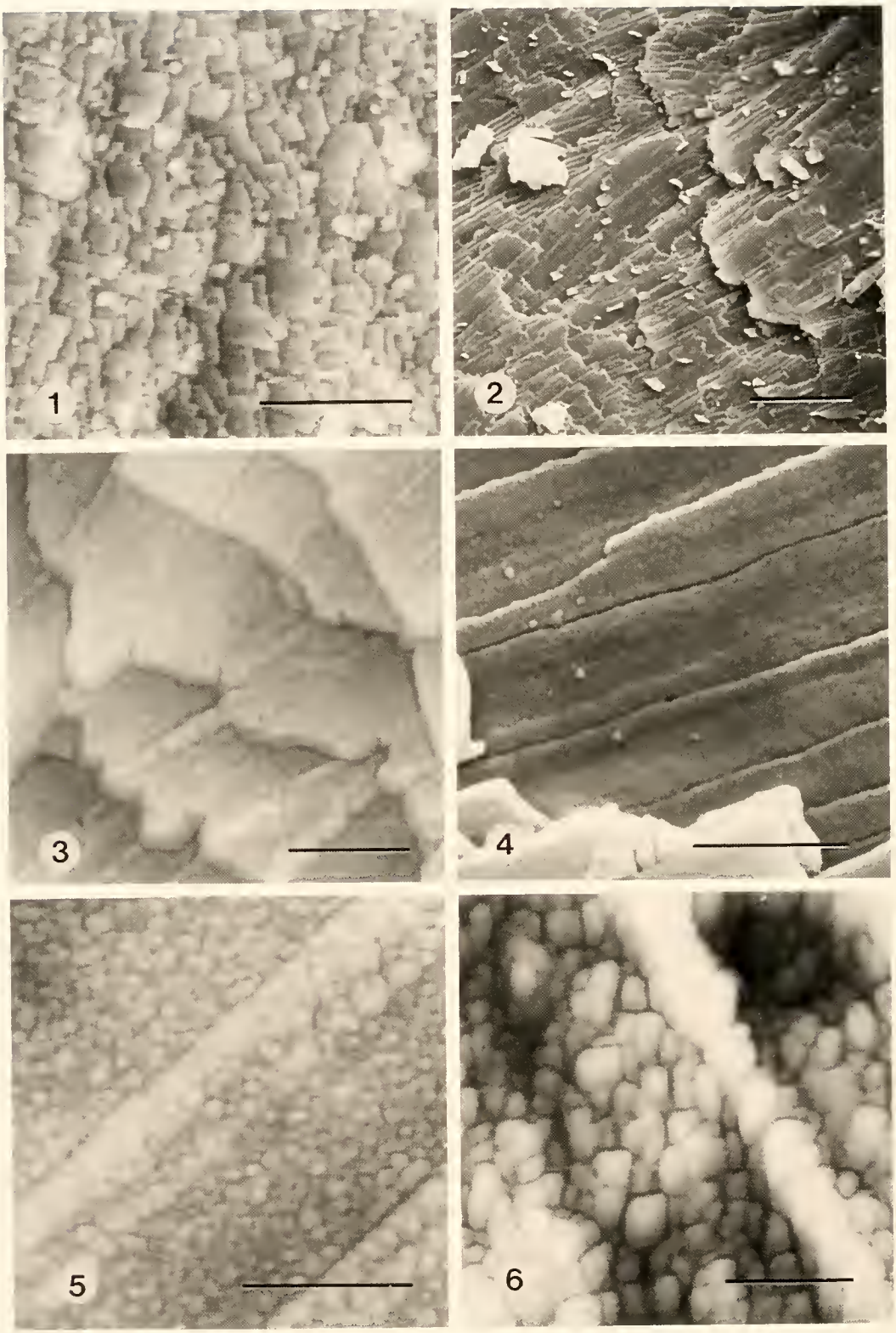

Figures 1–6. Micrographs of untreated (control) chips of oyster shell folia.

The surfaces of foliar chips that had been treated with the antibody to the oyster shell protein were coated with globular material as seen by AFM (Figs. 12 and 13). These globules of immunoglobulins were 4 to 5 times as large as the untreated foliar globules (compare Figs. 6 and 13).

AFM and SEM images of a foliar chip on which calcite crystals were grown can be compared (Figs. 14–16). In both types of micrographs, the newly formed crystals appeared to be very smooth and to emerge from the foliar surface at an oblique angle. Because these ectopic crystals were not coated with protein, the atomic pattern of the lattice surface could be resolved by AFM (Fig. 17).

The spacings and angles between the positions of hundreds of atoms of the surface of crystal growth were measured directly on several images by manual placement of the cursor onscreen and use of the measurement tools of the software. In addition, Fourier analysis was applied to the average periodicities of the entire images. The AFM software readily supplies measurements by both of these approaches.

The measured atomic spatial relationships were then compared to the theoretical spatial relationships generated by computer models of various possible surfaces of calcite (Cerius^2, molecular modeling software, Molecular Simulations, Inc.). A similar approach has been helpful in identifying other calcite surfaces such as the (104) cleavage surface of control calcite rhombohedrons and the (001) basal plane of calcite nucleated on glass (Sikes *et al.*, 1994), as well as the (1 −1 0) surface of calcite crystals that were stabilized by the presence of polyaspartate (Sikes and Wierzbicki, 1996).

The first identifiable surface of the ectopic foliar crystals appeared to be the (1 −1 0) plane of calcite. The AFM atomic image (Fig. 17) was compared to a computer model of the (1 −1 0) surface (Fig. 18). The measured spacings and angles between the various atomic positions matched within 5% of the theoretical values in all cases, as explained in the legend of Figure 18.

Discussion

The results supported the identity of the foliar globules, at least in part, as molecules of oyster shell protein, rather than only mineral material. That is, the globules exhibited (1) slow dissolution in NaOH and NaOCl, (2) reactivity to an antibody specific to oyster shell protein, (3) partial hydrolysis by proteolytic enzymes, and (4) morphological similarity to ellipsoids and globules of isolated protein from oyster shell as observed in prior studies.

The correspondence in size and appearance between the foliar globules and the isolated molecules of the protein was evident in AFM images that were prepared in a variety of ways. For example, the isolated protein was bound to calcite and viewed by AFM both in fluids and on rinsed, then dried crystals. The protein exhibited ellipsoid and globular morphologies with lengths and widths in the range of 50 to 100 nm, similar to those of the foliar globules (Donachy *et al.*, 1992; Wierzbicki *et al.*, 1994; Sikes *et al.*, 1994). The isolated protein also exhibited comparable morphologies when viewed either bound on glass and mica in fluids or when dried onto these substrates (Sikes and Wierzbicki, 1995a, b; 1996; Sikes *et al.*, 1997).

The protein used in the prior studies was obtained as a distinct, reversed-phase peak from the EDTA-soluble, proteinaceous matrix of the shells (Wheeler *et al.*, 1988; Wheeler and Sikes, 1989; Rusenko *et al.*, 1991). The peak is polydisperse, with an estimated gel-permeation molecular mass of approximately 50 kD. The protein is anionic with about 30% of the residues being aspartate and nearly 30% being serine, much of which is phosphorylated.

If the foliar globules are proteinaceous in part, they would of necessity seem to be agglomerations. That is, the AFM volume ($4/3\ \pi\ abc$) of the foliar globular ellipsoids of about 100 nm length (a = 50 nm), 50 nm width (b = 25 nm), and 10 nm height (c = 5 nm) is 2.62×10^{-17} cm^3. The theoretical molecular volume ($4/3\ \pi\ r^3$) of a globular protein of the size of a typical soluble oyster shell protein (M_w 50 kD, diameter ~5.4 nm; Cantor and Schimmel, 1980) is about 8.24×10^{-20} cm^3. Comparison of these values, assuming for the moment that the globules are entirely protein, yields an estimate of about 318 molecules of oyster shell protein per globule. Lower estimates would result if larger proteins of the shell matrix were

Figure 1. Atomic force micrograph of a dry, untreated chip. Range of lath heights: 150–350 nm. Scale bar = 15 μm.

Figure 2. Scanning electron micrograph of an untreated chip. Scale bar = 25 μm.

Figure 3. Atomic force micrograph of a dry, untreated chip. Range of lath heights: 150–250 nm. Scale bar = 2 μm.

Figure 4. Scanning electron micrograph of an untreated chip. Scale bar = 2 μm.

Figure 5. Atomic force micrograph of a dry, untreated chip. Total range of elevation within the imaged area = 70 nm. Scale bar = 1 μm.

Figure 6. Atomic force micrograph of a dry, untreated chip. Typical globular height = 10 to 15 nm; maximum globular height in the imaged area = 40 nm. Scale bar = 250 nm.

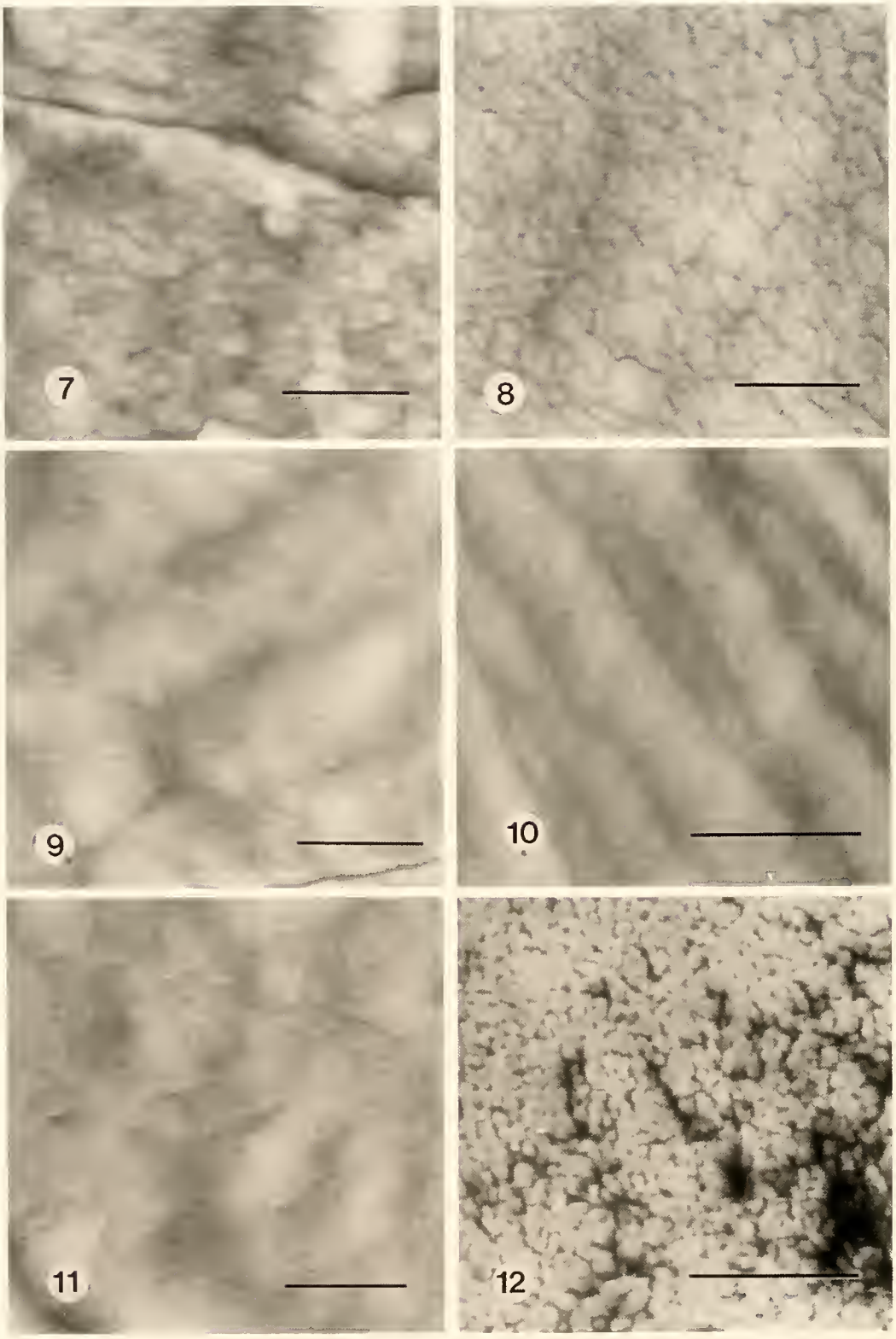

Figures 7–12. Atomic force micrographs of dry chips of oyster shell folia treated with various substances.

considered. For example, the proteins from oyster shell exhibit a continuum of molecular weights that ranges into the millions for soluble fractions. Also present are insoluble fractions with an amino acid composition similar to that of the soluble proteins (Wheeler *et al.*, 1988).

Phosphoproteins similar to the oyster shell protein are known to form micellar agglomerations in solution. For example, Marsh (1989a, b) reviewed the associative behavior of casein and other phosphoproteins and demonstrated that the phosphophoryn from tooth dentin forms agglomerations that are held together *via* ionic interactions with cations such as calcium and magnesium. Phosphophoryn, which—like the oyster shell protein—is highly enriched in phosphoserine and aspartic acid, formed particles of about 25 nm in diameter that contained perhaps 75 monomers per particle.

AFM and TEM observations by Fincham *et al.* (1994, 1995) of 15–20 nm "nanospheres" on the calcium phosphate surfaces of developing enamel have also been interpreted as proteinaceous, composed of amelogenin proteins. The amelogenins are smaller (~20 kD) and more hydrophobic than the typical oyster shell protein. The amelogenic nanospheres are thought to be agglomerations of greater than 100 monomers.

Globular ellipsoids in the range of 100 nm have also been observed on the surfaces of $CaCO_3$ otoconia from the inner ear of a newt (Hallworth *et al.*, 1995). The otoconia were isolated intact and are known to have associated proteins. Observed with AMF, the otoconial surface globules were quite like the foliar globules in appearance and were attributed to crystal formation as mediated by the otoconial proteins.

Our results indicate that the foliar globules are probably not composed solely of protein. The comparative images revealed that the foliar globules were generally taller at 10 to 40 nm than the ellipsoids and globules of isolated protein on calcite, mica, and glass, which had heights generally in the range of a few nanometers. Furthermore, the foliar globules resisted dissolution in NaOCl and NaOH. Mutvei (1977, 1978) also reported the presence of hypochlorite-resistant, "calcified" organic matrices associated with the surfaces of nacreous tablets of molluscan shell, and Towe (1990) commented on the resistance to household bleach of some matrix-like organic molecules, particularly if they were intimately associated with the mineral. Thus it seems that, in addition to protein, the foliar globules may contain a phase of mineral salts and perhaps water, as discussed below.

One assignment of the relative amounts of the mineral and organic phases of shell can be made by quantifying the weight of each component. Another assignment can be made by comparing the volumes of each layer, taken from the linear dimensions of each phase as seen in both SEM and AFM images, correcting for density differences of the mineral and the proteinaceous material. The observed linear dimensions as determined by SEM and AFM, although subject to different kinds of artifacts, were in agreement, lending credence to the estimates.

The protein content of oyster shell has been variously measured as ranging from perhaps a few tenths of 1% to no more than 3% by weight in whole shells (Korringa, 1951; Weiner and Hood, 1975; Price *et al.*, 1976; Rusenko, 1988; Rusenko *et al.*, 1991), with the protein content of the foliar layers alone placed at <1%. A lower protein content for foliar layers is consistent with the electron microscopic observations, all of which revealed that the foliar layer lacks the thicker, "interlamellar" organic layer of the prismatic regions of shell.

Given this range of values reported for protein content, an analysis of the apparent, relative volumes of "nonmineral" and mineral layers in a foliar lath as seen in both electron micrographs and atomic force micrographs yields an estimate of nonmineral content that is too high to be attributable only to organic matter. For example, Watabe and Wilbur (1961) and Watabe (1965) in electron microscopic studies observed the laths to be composed of crystal blocks that were surrounded by "intercrystalline" organic material. The dimensions of each block ranged from 10 to 40 nm in width, 15 to 200 nm in height, and ~4 μm in length. The dimensions of the organic matrix ranged

Figure 7. Treatment: 1 *N* NaOH for 5 days. Total range of elevation within the imaged area = 80 nm; range of globular heights = 4 to 30 nm. Scale bar = 500 nm.

Figure 8. Treatment: 5.25% NaOCl for 24 hours. Total range of elevation within the imaged area = 18 nm; heights of globular remnants = 3 to 6 nm. Scale bar = 250 nm.

Figure 9. Treatment: 5.25% NaOCl for 5 days. Total range of elevation within the imaged area = 16 nm; heights of globular remnants = 2 to 4 nm. Scale bar = 250 nm.

Figure 10. Treatment: Carboxypeptidase B for 48 hours. Total range of elevation within the imaged area = 30 nm, heights of globular remnants = 3 to 5 nm. Scale bar = 1 μm.

Figure 11. Treatment: Carboxypeptidase B for 48 hours. Total range of elevation within the imaged area = 15 nm. Scale bar = 250 nm.

Figure 12. Treatment: An antibody to the isolated oyster shell protein. Foliar laths are obscured by copiously bound antibody molecules. Scale bar = 5 μm.

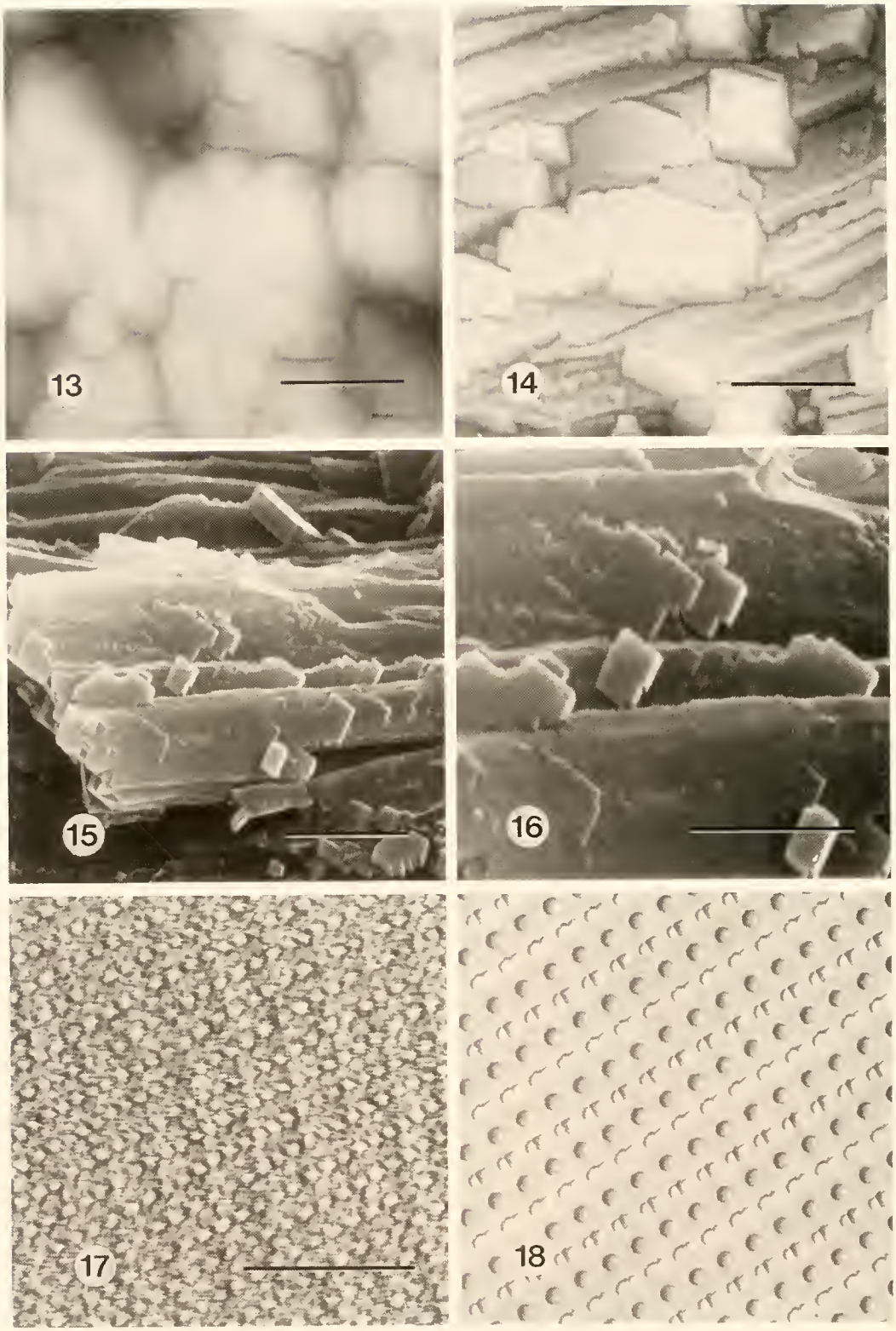

Figures 13–18

from 12 nm to 20 nm, as also later recorded by Taylor *et al.* (1969). These values for the dimensions both of the crystal blocks and of the organic layers are similar to the dimensions of the crystal laths and the foliar globules observed by AFM and recorded herein.

Based on average values of these dimensions and a simple calculation of the volume of the crystal block and the volume of the encapsulating proteinaceous layer, corrected for the density of calcite (2.71; Weast *et al.*, 1988) and typical proteins (~1.35; White *et al.*, 1973), the protein content would be about 17% by weight, which of course is too high. A plausible explanation for the high estimate is that the foliar globules seen with AFM and the organic layer seen in electron micrographs might consist of both protein and mineral, with the latter filling in spaces around and between the molecules of protein.

Another possible complication is that actual volumes of the foliar globules and the AFM volumes might be different, as sometimes occurs in AFM studies. The discrepancy is most likely to reflect an overestimate of the length and width of molecules. This kind of tip artifact results when the inverted pyramidal AFM tip slides up and down the sides of objects that are actually sharp, giving a smoothed and widened appearance (Hansma *et al.*, 1995; Giles *et al.*, 1994, 1995) and perhaps exaggerating the length or width by about 20%.

This convolution phenomenon is not a simple function and does not always occur: as demonstrated by the comparison of the micrographs produced by SEM and AFM, AFM showed true foliar morphology. Similarly, AFM micrographs of peptides bound to calcite (Wierzbicki *et al.*, 1994; Sikes *et al.*, 1993, 1994, 1997) and of various other molecules bound to flat substrates—for example, DNA to mica (Hansma and Hoh, 1994; Hansma *et al.*, 1995)—revealed molecular morphologies that were consistent with theory.

The height measurements at the top of an elevation, particularly of firm surfaces such as the foliar globules, are considered to be generally reliable, depending on the method of standardization. We calibrate our scanners at the micrometer level by use of commercial standards (Digital Instruments) and at the angstrom level by use of well-characterized crystals such as mica for the x and y axes, and calcite [the step height of the cleavage surface (104)] for the z axis.

Overall, the results and analysis suggest that the foliar globules are composed in significant part of protein. An undefined mineral phase that fills in the spaces around and within the foliar globules also may be a significant component, along with water, gases, and other mineral salts as minor components. In fact, Galtsoff (1964) viewed initiation of oyster shell growth as crystallization

---

Figure 13. Atomic force micrograph of a dry chip of oyster shell folia that was treated with an antibody to the isolated oyster shell protein. Total range of elevation within the imaged area = 150 nm (compare to Fig. 6, a control chip at the same magnification). Scale bar = 250 nm.

Figure 14. Atomic force micrograph of calcite crystals that were nucleated on an untreated chip of oyster shell folia at 10 m*M* Ca^{2+}, 7 m*M* inorganic carbon, initial pH 8.3, in artificial seawater (imaged in this fluid). Height of the central ectopic crystal = 340 nm, with a plane angle $<10°$ between the crystal surface and the underlying foliar surfaces. Scale bar = 2.5 μm.

Figure 15. Scanning electron micrograph of calcite crystals that were nucleated on the oyster shell foliar surface of Figure 14. Scale bar = 3 μm.

Figure 16. Scanning electron micrograph of calcite crystals that were nucleated on the oyster shell foliar surface of Figure 14. Scale bar = 2 μm.

Figure 17. Atomic force micrograph of the lattice atoms of the surface of the central crystal of Figure 14, imaged in fluid as above. Total range of elevation within the imaged area = 3 Å. Scale bar = 5 nm.

Figure 18. Computer diagram of the (1 −1 0) surface of calcite showing calcium atoms (grey) and carbonate groups (with white oxygens) in alternating rows. The spacing between lattice positions in the rows (diagonal upward, left to right) of both calcium atoms and carbonate groups is 4.99 Å. The spacing between lattice positions perpendicular to the rows (that is, between a calcium atom and the nearest oxygen of an adjacent carbonate group) is 4.265 Å. Both of these distances matched the spacings observed in the AFM of Figure 17. The computer model showed that an oxygen of each carbonate group is elevated ~1 Å relative to the plane of calcium atoms, and therefore the most distinct and separate atoms of Figure 17 are thought to be oxygen atoms. The specific carbonate oxygens that are most protuberant in each row differ in alternating rows, creating a slight zig-zag pattern (the oxygens of alternating rows do not line up exactly along the diagonal from upper left to lower right). This is visible in both the image of Figure 17 and the model. Similarly, the lower atoms were measured in Figure 17 to be in agreement with theory at ~1 Å below the plane of the higher atoms, and thus are thought to be calcium atoms that blended together somewhat in the image, probably owing to the interaction between the AFM tip and the lattice during imaging in the troughs. The agreement between these and other features of the experimental image (Fig. 17) and the theoretical model (Fig. 18) lead to the assignment of the surface of the crystal as most likely the (1 −1 0) surface of calcite.

within a gelatinous organic secretion of the mantle, with the mineral imbedded within the matrix of organic matter (see also Carriker *et al.,* 1980; Crenshaw, 1990).

Certainly, an important function of the oyster shell protein might be to nucleate calcite from the extrapallial fluid, which would be supersaturated during shell formation. However, the foliar globules were not particularly effective as crystal nucleators. That is, under metastable conditions in the AFM assay at 2 to 5 m*M* DIC, which readily supported growth of calcite seeds, there was no crystal growth associated with the globules. Furthermore, under the metastable conditions, exposed regions of mineral on fracture surfaces at the sides or ends of laths did exhibit crystal growth when the organic-coated foliar surfaces did not. Even after 2 h at 5 m*M* DIC when crystals had spontaneously nucleated and could be seen flowing past the probe during scanning, (via the top-view videomicroscopy capability of the AFM system) crystal growth was not observed in association with the foliar globules.

It seems clear that a preexisting mineral phase would be the best nucleator for further lattice formation of that phase. In an AFM study of bivalve shell, Giles *et al.* (1995) noted that aragonite growth of the molluscan nacreous layer could have been nucleated by small regions of uncoated mineral on nacreous tablets. Watabe (1981) and later Manne *et al.* (1994) had previously offered this as a mechanism for continued nucleation during growth of nacre. In summary, it may be that the issue is not so much the nucleation of calcite on the foliar surface, but rather exactly how the foliar morphology is continually sustained layer-upon-layer during growth of the shell.

If the nucleation of a new layer of calcite occurs on exposed regions of calcite, the lack of ready nucleation on the foliar surfaces suggests either that the putative mineral phase of the foliar globules was not exposed to the metastable fluid or that, if exposed, the mineral phase is not crystalline calcite. An analogous arrangement of phosphoproteins and a mineral phase has been observed in some molluscs. For example, agglomerations of phosphoproteins and mineral salts (sometimes an amorphous calcium phosphate phase) of about 40-nm diameter have been reported as part of a nonmineralizing, organic lamella that contacts the shells of some molluscs (Marsh and Sass, 1983, 1984). These particles also occur in the fluids that bathe the shell in some molluscs, but they were not observed in the American oyster (Marsh and Sass, 1985). Again, neither these globules nor the aforementioned agglomerations of dentin phosphophoryn, which also are thought to contain an amorphous mineral phase, seemed to act as nucleators of the crystalline mineral phase of shell or teeth (Marsh, 1986, 1989a, b, 1994).

The crystallographic identity of the foliar surface of oyster shell has been studied by several authors with different results. For example, on the basis of X-ray data, Wada (1963, 1968) and Watabe (1965, 1981) assigned the foliar surfaces as the basal plane (001), with the sides probably hexagonal planes, essentially similar to the crystallographic arrangement of molluscan prismatic nacre. In this case, the *c*-axis would be perpendicular to the foliar surface, with the hexagonal planes parallel to the *c*-axis. The oyster shell protein is thought to have high affinity for each of these surfaces (Sikes *et al.*, 1993, 1994; Sikes and Wierzbicki, 1995a, b, 1996; Wierzbicki *et al.*, 1994, including references to other workers).

In contrast, Taylor *et al.* (1969) used optical measurements and X-ray patterns to suggest that the plane of foliation was not (001) and that the *c*-axis was inclined to the foliar plane at a shallow angle (26° in *Placuna placenta*). These authors also theorized that there may, in fact, be no definable crystallographic plane of initial foliation of each layer in that the foliar crystals are not planar on top when viewed in both surface and cross-sectional electron micrographs. Giles *et al.* (1995) further considered the rounded globules of hypochlorite-treated nacre as inorganic, aragonite surfaces that possibly consisted of many steps at the nanoscale, thus suggesting a complex mechanism of crystal growth.

Runnegar (1984) also made extensive X-ray and optical assessments of the crystallography of foliar layers from various bivalves, including *C. virginica.* From these studies, he noted an inclination of the *c*-axis relative to the foliar plane. Using scanning electron micrographs and aluminum models of calcite rhombohedrons ectopically grown from hypochlorite-treated foliar chips, he further demonstrated this inclination by the tilted appearance of the crystals and models relative to the foliar surface. The oyster shells of his study exhibited folia with more than one type of inclination of the *c*-axis, even within a single shell. Runnegar acknowledged that the reports of (001) foliar surfaces in some specimens by other workers also seemed to be correct, although he did not observe this arrangement.

Our observations of calcite crystals grown on untreated chips of oyster shell folia at 7 m*M* DIC in the AFM assay support the findings of both Taylor *et al.* (1969) and Runnegar (1984). Even the early stages of crystal formation often exhibited an inclination of the ectopic crystals relative to the foliar surface. The (1 −1 0) plane of calcite appeared as a principal surface identifiable by AFM during the early growth of the crystals. This plane is parallel to the *c*-axis, and therefore its angle of inclination is the same as that of the *c*-axis. By use of the plane-angle function of the AFM imaging software, which is designed for first designating planes of interest and then calculating the angles between them, angles between the foliar plane and the ectopic crystal surfaces were measured. In a few

cases, angles close to 64° (Runnegar's type 3 arrangement) were observed. However, much shallower angles were frequently seen as well.

The (1 −1 0) surface of calcite is one of several surfaces that are likely to be expressed during ectopic crystal growth, particularly at the higher of the supersaturations used herein, which actually were significantly lower than those of Runnegar (1984). Although crystals did not appear to nucleate on the foliar globules at our lower supersaturations (≤5 m*M* DIC), the higher supersaturations (≥7 m*M* DIC) did result in rapid and widespread crystal growth on the foliar surfaces. Even so, the precise site of nucleation was not easily discernible because the ectopic crystals usually spanned more than one lath, as well as the sides of laths. The exact spatial and crystallographic relationships, if any, between the foliar globules and calcite nucleation will require further study under controlled conditions of metastable supersaturation that reflect conditions *in vivo*.

Acknowledgments

This work was supported by grants EHR-9108761 from the National Science Foundation, C-3662 from the Research Corporation, and R/MX-6 from the South Carolina Sea Grant Consortium.

Literature Cited

Cantor, C. R., and P. R. Schimmel. 1980. *Biophysical Biochemistry. Part I. The Conformation of Biological Molecules.* W. H. Freeman, San Francisco.

Carriker, M. R., and R. E. Palmer. 1979. Ultrastructural morphogenesis of prodissoconch and early dissoconch valves of the oyster *Crassostrea virginica*. *Proc. Natl. Shellfish. Assoc.* **69:** 103–128.

Carriker, M. R., R. E. Palmer, and R. S. Prezant. 1980. Functional ultramorphology of the dissoconch valves of the oyster *Crassostrea virginica*. *Proc. Natl. Shellfish. Assoc.* **70:** 139–183.

Crenshaw, M. A. 1990. Biomineralization mechanisms. Pp. 1–9 in *Skeletal Biomineralization: Patterns, Processes, and Evolutionary Trends. Volume I.* J. G. Carter, ed. Van Nostrand Reinhold, New York.

Donachy, J. E., B. Drake, and C. S. Sikes. 1992. Sequence analysis and atomic force microscopy of a matrix protein from the shell of the oyster *Crassostrea virginica*. *Mar. Biol.* **114:** 423–428.

Drake, B., R. Hellmann, C. S. Sikes, and M. L. Ocelli. 1992. Atomic scale imaging of albite feldspar, calcium carbonate, rectorite, and bentonite using atomic force microscopy. *SPIE Proc.* **1639:** 151–159.

Fincham, A. G., J. Moradian-Oldak, J. P. Simmer, P. Sarte, E. C. Lau, T. Diekwisch, and H. C. Slavkin. 1994. Self-assembly of a recombinant amelogenin protein generates supramolecular structures. *J. Struct. Biol.* **112:** 103–109.

Fincham, A. G., J. Moradian-Oldak, and H. C. Slavkin. 1995. Evidence for amelogenin "nanospheres" as functional components of secretory-stage enamel matrix. *J. Struct. Biol.* **115:** 50–59.

Friedbacher, G., P. K. Hansma, E. Ramli, and G. D. Stucky. 1991. Imaging powders with the atomic force microscope: from biominerals to commercial materials. *Science* **253:** 1261–1263.

Galtsoff, P. S. 1964. The American oyster *Crassostrea virginica* Gmelin. *Fish. Bull.* **64:** 1–480.

Giles, R., S. Manne, C. M. Zaremba, A. Belcher, S. Mann, D. E. Morse, G. D. Stucky, and P. K. Hansma. 1994. Imaging single nacreous tablets with the atomic force microscope. *Mater. Res. Soc. Symp. Proc.* **332:** 413–422.

Giles, R., S. Manne, S. Mann, D. E. Morse, G. D. Stucky, and P. K. Hansma. 1995. Inorganic overgrowth of aragonite on molluscan nacre examined by atomic force microscopy. *Biol. Bull.* **188:** 8–15.

Gutmannshauer, W., and H. A. Hänni. 1994. Structural and chemical investigations on shells and pearls of nacre forming salt- and fresh-water bivalve molluscs. *J. Gemmology* **24:** 241–252.

Hallworth, R., M. L. Wiederhold, J. B. Camphell, and P. S. Steyger. 1995. Atomic force microscope observations of otoconia in the newt. *Hear. Res.* **85:** 115–121.

Hansma, H. G., and J. H. Hoh. 1994. Biomolecular imaging with the atomic force microscope. *Annu. Rev. Biophys. Biomol. Struct.* **23:** 115–139.

Hansma, H. G., D. E. Laney, M. Bezanilla, R. L. Sinsheimer, and P. K. Hansma. 1995. Applications for atomic force microscopy of DNA. *Biophys. J.* **68:** 1672–1677.

Hilner, P. E., A. J. Gratz, S. Manne, and P. K. Hansma. 1992. Atomic scale imaging of calcite growth and dissolution in real time. *Geology* **20:** 359–362.

Korringa, P. 1951. On the nature and function of "chalky" deposits in the shell of *Ostrea edulis* Linnaeus. *Proc. Calif. Acad. Sci.* **27:** 133–158.

Kuhn-Spearing, L. T., H. Kessler, and S. M. Spearing. 1996. Fracture mechanisms of the *Strombus gigas* conch shell: implications for design of brittle laminates. *J. Mater. Sci.* **31:** 6583.

Mann, S. (ed.). 1996. *Biomimetic Approaches in Materials Science,* VCH Publishers, New York.

Manne, S., C. M. Zaremba, R. Giles, L. Huggins, D. A. Walters, A. Belcher, D. E. Morse, G. D. Stucky, J. M. Didymus, S. Mann, and P. K. Hansma. 1994. Atomic force microscopy of the nacreous layer in mollusc shells. *Proc. R. Soc. Lond. B Biol. Sci.* **256:** 17–23.

Marsh, M. E. 1986. Biomineralization in the presence of calcium-binding phosphoprotein particles. *J. Exp. Zool.* **239:** 207–220.

Marsh, M. E. 1989a. Self-association of calcium and magnesium complexes of dentin phosphophoryn. *Biochemistry* **28:** 339–345.

Marsh, M. E. 1989b. Binding of calcium and phosphate ions to dentin phosphophoryn. *Biochemistry* **28:** 346–352.

Marsh, M. E. 1994. Polyanions and biomineralization. *Bull. Inst. Oceanogr. (Monaco)* **14(1):** 121–128.

Marsh, M. E., and R. L. Sass. 1983. Calcium-binding phosphoprotein particles in the extrapallial fluid and innermost shell lamella of clams. *J. Exp. Zool.* **226:** 193–203.

Marsh, M. E., and R. L. Sass. 1984. Phosphoprotein particles: calcium and inorganic phosphate binding structures. *Biochemistry* **23:** 1448–1456.

Marsh, M. E., and R. L. Sass. 1985. Distribution and characterization of mineral-binding phosphoprotein particles in bivalvia. *J. Exp. Zool.* **234:** 237–242.

Mohammed, H. D., R. Yamamoto, T. E. Carpenter, and H. B. Ortmayer. 1986. A statistical model to optimize enzyme-linked immunosorbent assay parameters for detection of *M. gallisepticum* and *M. synoviae* antibodies in egg yolk. *Avian Dis.* **30:** 389–397.

Mutvei, H. 1977. The nacreous layer in *Mytilus, Nucula,* and *Unio* (Bivalvia). *Calcif. Tissue Res.* **24:** 11–18.

Mutvei, H. 1978. Ultrastructural characteristics of the nacre in some gastropods. *Zool. Scr.* **7:** 287–296.

Myers, J. M., A. Veis, B. Sahsay, and A. P. Wheeler. 1996. A

method for enhancing the sensitivity and stability of stains-all for phosphoproteins separated in sodium dodecyl sulfate-polyacrylamide gels. *Anal. Biochem.* **240:** 300–302.

Price, T. J., G. W. Thayer, M. W. LaCroix, and G. P. Montgomery. 1976. The organic content of shells and soft tissues of selected estuarine gastropods and pelecypods. *Proc. Natl. Shellfish. Assoc.* **65:** 26–31.

Runnegar, B. 1984. Crystallography of the foliated calcite shell layers of bivalve molluscs. *Alcheringa* **8:** 273–290.

Rusenko, K. W. 1988. Studies on the structure and function of shell matrix proteins from the American oyster, *Crassostrea virginica*. Ph.D. Dissertation, Clemson University, Clemson, SC. 287 pp.

Rusenko, K. W., J. E. Donachy, and A. P. Wheeler. 1991. Purification and characterization of a shell matrix phosphoprotein from the American oyster. Pp. 107–124 in *Surface Reactive Peptides and Polymers: Discovery and Commercialization,* C. S. Sikes and A. P. Wheeler, eds. ACS Symposium Series 444. ACS Books, Washington, DC.

Sikes, C. S., and A. Wierzbicki. 1995a. Mechanisms of regulation of crystal growth in selected biological systems. Pp. 183–206 in *Mineral Scale Formation and Inhibition,* Z. Amjad, ed. Plenum Press, New York.

Sikes, C. S., and A. Wierzbicki. 1995b. Atomic force microscopy and molecular modeling of protein bound to calcite. *SPIE Proc.* **2547:** 164–174.

Sikes, C. S., and A. Wierzbicki. 1996. Polyamino acids as antiscalants, dispersants, antifreezes, and absorbent gelling materials. Pp. 249–278 in *Biomimetic Approaches in Materials Science,* S. Mann, ed. VCH Publishers, New York.

Sikes, C. S., E. Mueller, J. D. Madura, B. Drake, and B. J. Little. 1993. Polyamino acids as antiscalants, corrosion inhibitors, and dispersants: atomic force microscopy and mechanisms of action. *Corrosion 93,* paper **465:** 1–21.

Sikes, C. S., A. Wierzbicki, and V. Fabry. 1994. From atomic to global scales in biomineralization. *Bull. Inst. Oceanogr. (Monaco)* **14(1):** 1–49.

Sikes, C. S., F. Martin, A. Wierzbicki, and A. P. Wheeler. 1997. Atomic force microscopy and enzymatic degradation of oyster shell protein and polyaspartate. *Macromol. Symp.* **123:** 85–92.

Stupp, S. I., and P. V. Braun. 1997. Molecular manipulation of microstructures: biomaterials, ceramics, and semiconductors. *Science* **277:** 1242–1248.

Taylor, J. D., W. J. Kennedy, and A. Hall. 1969. The shell structure and mineralogy of the bivalvia. Introduction. Nuculacea-Trigonacea. *Bull. Br. Mus. (Nat. Hist.) Zool., Supplement* **3:** 1–125, plates 1–29.

Towe, K. M. 1990. Overviews of biomineralization. *Paleobiology* **16:** 521–526.

Wada, K. 1963. Studies on the mineralization of the calcified tissue in molluscs. VI. Crystal structure of the calcite grown on the inner surface of calcitostracum. *J. Electron Microsc.* **12:** 224–227.

Wada, K. 1968. Spiral growth of calcitostracum. *Nature* **219:** 62.

Watabe, N. 1965. Studies on shell formation. XI. Crystal-matrix relationships in the inner layers of mollusk shells. *J. Ultrastruct. Res.* **12:** 351–370.

Watabe, N. 1981. Crystal growth of calcium carbonate in the invertebrates. *Prog. Crystal Growth Charact.* **4:** 99–147.

Watabe, N., and K. M. Wilbur. 1961. Studies on shell formation. IX. An electron microscope study of crystal layer formation in the oyster. *J. Biophys. Biochem. Cytol.* **9:** 761–771.

Watabe, N., D. G. Sharp, and K. M. Wilbur. 1958. Studies on shell formation. VIII. Electron microscopy of crystal growth of the nacreous layer of the oyster *Crassostrea virginica*. *J. Biophys. Biochem. Cytol.* **4:** 281–284, plates 152–156.

Weast, R. C., M. J. Astle, and W. H. Beyer (eds.). 1988. *CRC Handbook of Chemistry and Physics,* CRC Press, Boca Raton, FL.

Weiner, S., and L. Addadi. 1997. Design strategies in mineralized biological materials. *J. Mater. Chem.* **7:** 689–702.

Weiner, S., and L. Hood. 1975. Soluble protein of the organic matrix of mollusk shells: a potential template for shell formation. *Science* **190:** 987–989.

Wheeler, A. P., and L. P. Koskan. 1993. Large scale thermally synthesized polyaspartate as a biodegradable substitute in polymer applications. *Mater. Res. Soc. Symp. Proc.* **292:** 277–283.

Wheeler, A. P., and C. S. Sikes. 1989. Matrix-crystal interactions in $CaCO_3$ biomineralization. Pp. 95–133 in *Biomineralization: Chemical and Biochemical Perspectives,* S. Mann, J. Webb, and R. J. P. Williams, eds. VCH Publishers: Weinheim, FRG.

Wheeler, A. P., K. W. Rusenko, D. M. Swift, and C. S. Sikes. 1988. Regulation of $CaCO_3$ formation by fractions of oyster shell matrix. *Mar. Biol.* **98:** 71–80.

Wheeler, A. P., K. C. Low, and C. S. Sikes. 1991. $CaCO_3$ crystal-binding properties of peptides and their influence on crystal growth. Pp. 72–84 in *Surface Reactive Peptides and Polymers: Discovery and Commercialization,* C. S. Sikes and A. P. Wheeler, eds. ACS Symposium Series 444. ACS Books, Washington, DC.

White, A., P. Handler, and E. L. Smith. 1973. *Principles of Biochemistry,* McGraw Hill, New York.

Wierzbicki, A., C. S. Sikes, B. Drake, and J. Madura. 1994. Atomic force microscopy and molecular modeling of protein and peptide binding to calcite. *Calcif. Tissue Int.* **54:** 133–141.

The Cytoskeleton: Mechanical, Physical, and Biological Interactions

Proceedings
of a workshop
sponsored by
the Center for Advanced Studies
in the Space Life Sciences
at the MBL

15–17 November 1996

Marine Biological Laboratory,
Woods Hole, Massachusetts

Funded by
the National Aeronautics
and Space Administration
under Cooperative Agreement
NCC 2-896

CONTENTS

The Cytoskeleton:
Mechanical, Physical, and Biological Interactions

Reference: *Biol. Bull.* **194:** 321–322. (June, 1998)

Introduction

This workshop, entitled "The Cytoskeleton: Mechanical, Physical, and Biological Interactions," was sponsored by the Center for Advanced Studies in the Space Life Sciences at the Marine Biological Laboratory. This Center was established through a cooperative agreement between the MBL and the Life Sciences Division of the National Aeronautics and Space Administration. The Center is charged to act as an interface between NASA and the basic science community, promoting interactions and discussions in areas of basic biology that are of mutual interest. To achieve these goals, the Center sponsors a series of workshops on various topics in the life sciences, including cell biology, developmental biology, evolutionary biology, molecular biology, neurobiology, plant biology, and systems biology.

Elements of the cytoskeleton have been implicated in the effects of gravity on the growth of plants and fungi. An intriguing finding in this regard is the report by Wayne *et al.* (1992) indicating that an integrin-like protein may be the gravireceptor in the internodal cells of *Chara.* Involvement of the cytoskeleton in cellular graviperception of the basidiomycete *Flammulina velutipes* has also been reported (Monzer, 1995). Although the responses of mammalian cells to gravity are not well documented, Ingber (1991) has proposed that integrins—which are involved in both transmembrane signaling and the formation of structural connections between the extracellular matrix and the cytoskeleton (Sastry and Horwitz, 1993)—can act as mechanochemical transducers in mammalian cells. Ever increasing evidence supports this notion (Shyy and Chien, 1997).

At a previous workshop at the MBL, on the "Future of Aquatic Research in Space," Baxter attempted to reconcile the differences between theoretical predictions and empirical findings about gravity-dependent changes in cellular activities (Baxter and Byrne, 1997). A potential similarity between the effects of microgravity and shear stress on mammalian cells (Schmitt *et al.*, 1996; Hu and Chien, 1997) may provide the clues we require to resolve this apparent dichotomy. Thus, whereas Schmitt *et al.* (1996) have shown that the distribution of protein kinase C in human leukocytes is altered in microgravity, Hu and Chien (1997) have shown that shear stress affects the distribution of protein kinase C in endothelial cells.

Mechanical stress induced by shear force produces a rapid reorganization of the cytoskeleton, including rearrangement of actin and vimentin filaments in endothelial cells (Davies *et al.*, 1997; Goldman, discussion at this workshop). This cellular response to mechanical stress is reminiscent of alterations in the cytoskeleton detected in response to heat shock (Morimoto, at this workshop [See list, "Published by Title Only"]; Welch *et al.*, 1985; Walter *et al.*, 1990) and related stress (Haskin *et al.*, 1993). In his introductory remarks at this workshop on the cytoskeleton, Bob Goldman pointed out that understanding the molecular bases of the cellular responses to mechanical stress in ground-based studies is currently the best available approach to delineating the potential role of microgravity at the cellular level. Goldman further indicated that since little is known about the integrated mechanical and physical properties of cytoplasm, this workshop would be the best place to begin developing interdisciplinary approaches to the effects of mechanical stresses on cells and on their most likely responsive cytoplasmic elements—the fibrous proteins comprising the cytoskeleton.

The program for this meeting, arranged by Bob Goldman and Paul Janmey, brought many of the world's leading authorities to Woods Hole in an attempt to establish communication links amongst physicists, biochemists, and cell biologists, all approaching this problem from different perspectives.

This paper was originally presented at a workshop titled *The Cytoskeleton: Mechanical, Physical, and Biological Interactions.* The workshop, which was held at the Marine Biological Laboratory, Woods Hole, Massachusetts, from 15–17 November 1996, was sponsored by the Center for Advanced Studies in the Space Life Sciences at MBL and funded by the National Aeronautics and Space Administration under Cooperative Agreement NCC 2-896.

Bob Goldman concluded his introduction to the meeting with the following statement:

> It is especially appropriate that this meeting is being held here at the Marine Biological Laboratory—and in this particular Lillie Auditorium, since this is the place in which Jacques Loeb, Frank Lillie, Charles Whitman and others first attempted to integrate chemistry and physics into studies of cellular structure.

E.A. Dawidowicz
Center for Advanced Studies in the Space Life Sciences at the MBL
Woods Hole, Massachusetts

Literature Cited

Baxter, D. A., and J. H. Byrne. 1997. Complex oscillations in simple neural systems. *Biol. Bull.* **192:** 167–169.

Davies, P. F., K. A. Barbee, M. V. Volin, A. Robotewsky, J. Chen, L. Joseph, M. L. Griem, M. N. Wernick, E. Jacobs, D. C. Polacek, N. DePaola, and A. I. Barakat. 1997. Spatial relationships in early signaling events of flow-mediated endothelial mechanotransduction. *Annu. Rev. Physiol.* **59:** 527–549.

Haskin, C. L., K. A. Athanasiou, R. Klehe, and I. L. Cameron. 1993. A heat-shock-like response with cytoskeletal disruption occurs following hydrostatic pressure in MG-63 osteosarcoma cells. *Biochem. Cell. Biol.* **71:** 361–371.

Hu, Y-L., and S. Chien. 1997. Effects of shear stress on protein kinase C distribution in endothelial cells. *J. Histochem. Cytochem.* **45:** 237–249.

Ingber, D. 1991. Integrins as mechanochemical transducers. *Curr. Opin. Cell Biol.* **3:** 841–848.

Monzer, J. 1995. Actin filaments are involved in cellular graviperception of the basidiomycete *Flammulina velutipes*. *Eur. J. Cell Biol.* **66:** 151–156.

Sastry, S. K., and A. F. Horwitz. 1993. Integrin cytoplasmic domains: mediators of cytoskeletal linkages and extra- and intra-cellular initiated transmembrane signaling. *Curr. Opin. Cell Biol.* **5:** 819–831.

Schmitt, D. A., J. Hatton, C. Emond, D. Chaput, H. Paris, T. Levade, J-P. Cazenave, and L. Schafar. 1996. The distribution of protein kinase C in human leukocytes is altered in microgravity. *FASEB J.* **10:** 1627–1634.

Shyy, J. Y-J., and S. Chien. 1997. Role of integrins in cellular responses to mechanical stress and adhesion. *Curr. Opin. Cell Biol.* **9:** 707–713.

van Bergen en Henegouwen, P. M., and A. M. Linnemans. 1987. Heat shock gene expression and cytoskeletal alterations in mouse neuroblastoma cells. *Exp. Cell Res.* **171:** 367–375.

Walter, M. F., N. S. Petersen, and H. Biessmann. 1990. Heat shock causes the collapse of the intermediate filament cytoskeleton in *Drosophila* embryos. *Dev. Gen.* **11:** 270–279.

Wayne, R., M. P. Staves, and A. C. Leopold. 1992. The contribution of the extracellular matrix to gravisensing in characean cells. *J. Cell Sci.* **101:** 611–623.

Welch, W. J., J. R. Feramisco, and S. H. Blose. 1985. The mammalian stress response and the cytoskeleton: alterations in intermediate filaments. *Ann. N. Y. Acad. Sci.* **455:** 57–67.

Reference: *Biol. Bull.* **194:** 323–327. (June, 1998)

Cellular Basis of Mechanotransduction

DONALD E. INGBER

Departments of Pathology and Surgery, Children's Hospital and Harvard Medical School, Boston, Massachusetts 02115

Physical forces, such as those due to gravity, are fundamental regulators of tissue development. To influence morphogenesis, mechanical forces must alter growth and function. Yet little is known about how cells convert mechanical signals into a chemical response. This presentation attempts to place the potential molecular mediators of mechanotransduction within the context of the structural complexity of living cells.

Our experimental approach is based on the hypothesis that cells use tensegrity architecture to structure themselves (Ingber, 1993, 1998; Ingber and Jamieson, 1985). Most man-made structures gain their stability through continuous compression; one element weighs down on the element below due to the force of gravity. In contrast, tensegrity structures stabilize themselves through continuous tension that is distributed across all of the structural elements and balanced by a subset of these elements that resist compression locally. These internal struts generate an internal tension or "prestress" that mechanically stabilizes the entire structure. Tensegrity cell models composed of sticks and elastic string (Fig. 1) predict many complex cell behaviors, including how cells change shape when they adhere to rigid or flexible extracellular matrices (Ingber, 1993, 1998; Ingber and Jamieson, 1985). Tensegrity models also predict that cells and nuclei are hard-wired to respond immediately to mechanical stresses transmitted over cell surface receptors that physically couple the cytoskeleton to the extracellular matrix and to other cells.

We recently developed a technique to apply controlled mechanical forces (rotational shear stresses) to cell surface receptors in living cells. In brief, magnetic microspheres are coated with specific receptor ligands and are thus bound to the cell surface. The microspheres are magnetically twisted, and their rotation (angular strain) is simultaneously quantified. Using this method, magnetic twisting cytometry (Wang *et al.*, 1993; Wang and Ingber, 1995), we have been able to confirm that extracellular matrix receptors, such as integrins, and cell-cell adhesion receptors (*e.g.*, E-selectin) provide preferred paths for mechanical signal transfer across the cell surface and to the internal cytoskeleton (Wang *et al.*, 1993; Wang and Ingber, 1995; Yoshida *et al.*, 1996). We also were able to show directly that living cells behave mechanically as if they were tensegrity structures. Our evidence includes a demonstration of linear stiffening behavior; results indicating that cell stiffness depends on internal prestress in the cytoskeleton; and data showing that microtubules resist lateral compression in the cytoplasm (Wang *et al.*, 1993; Wang and Ingber, 1994, 1995; Stamenovic *et al.*, 1996; Maniotis *et al.*, 1997; Tagawa *et al.*, 1997; Lee *et al.*, 1998). In addition, we have been able to demonstrate that pulling on cell surface integrins with matrix-coated micropipettes in living cells results in immediate realignment of cytoskeletal filaments, as well as tension-dependent changes in structure inside the nucleus (Maniotis *et al.*, 1997). This latter finding directly confirms the existence of hard-wiring (mediated by intermediate filaments and actin microfilaments) in cells and emphasizes that conventional biomechanical models of the cell based on a viscous cytosol surrounded by an elastic membrane are not accurate or useful when considering the molecular basis of cell mechanics.

The finding that integrins mediate the transfer of mechanical signals across cellular membranes is important for tissue physiology because integrins also coordinate other forms of signal transduction in the cell. Many sig-

This paper was originally presented at a workshop titled *The Cytoskeleton: Mechanical, Physical, and Biological Interactions.* The workshop, which was held at the Marine Biological Laboratory, Woods Hole, Massachusetts, from 15–17 November 1996, was sponsored by the Center for Advanced Studies in the Space Life Sciences at MBL and funded by the National Aeronautics and Space Administration under Cooperative Agreement NCC 2-896.

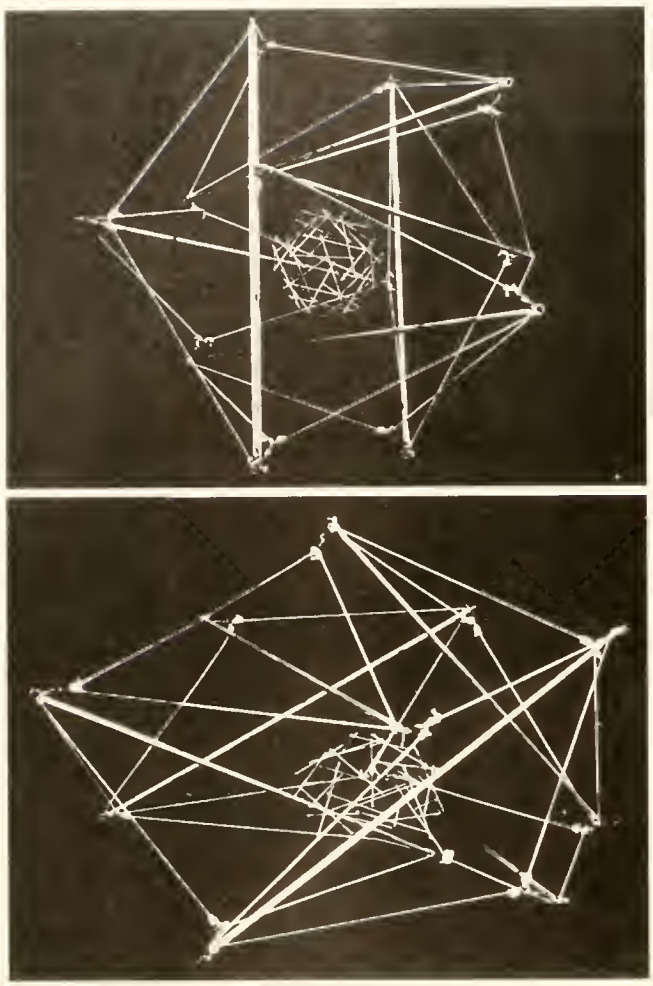

Figure 1. A tensegrity model composed of sticks and elastic strings. This model rounds up on a flexible substrate (upper panel), but it spreads when attached to a rigid foundation (lower panel), much like a living cell (Ingber, 1993, 1998; Ingber and Jamieson, 1985).

nal-transducing molecules associate with cytoskeletal scaffolds within the focal adhesion complex and appear to concentrate at the site of integrin binding (Plopper *et al.*, 1995). Importantly, these same signaling components mediate the cellular effects of soluble growth factors and insoluble extracellular matrix, as well as mechanical forces. Thus, integrins are perfectly poised to mediate mechanochemical transduction. We have found, in fact, that cells can be switched between programs of growth, differentiation, and apoptosis by changing the balance of forces across cell surface integrins and thus altering cell shape (Ingber and Folkman, 1989; Ingber, 1990; Singhvi *et al.*, 1994; Chen *et al.*, 1997). These results demonstrate that while extracellular matrix, growth factors, and mechanical forces all contribute to cellular regulation, mechanical signals are the dominant regulators.

Mechanical stresses may be integrated with other environmental signals and transduced into a biochemical response through force-dependent changes in cytoskeletal scaffold geometry or through local changes in molecular shape that alter chemical potential and thereby influence thermodynamic parameters (Ingber, 1997; Chicurel *et al.*, 1998a). For example, we have recently found that increasing tension across integrins results in cytoskeletal restructuring events that lead to the creation of a cellular microcompartment specialized for local protein synthesis at the site of integrin binding (Chicurel *et al.*, 1998b). Taken together, our results suggest that tensegrity provides a mechanism to focus mechanical energy on critical molecular transducers and to both orchestrate and tune the cellular response to mechanical stress (Ingber, 1993, 1997, 1998; Chicurel *et al.*, 1998a). Tensegrity also may explain how stresses are transmitted through tissues, and how cellular responses are integrated within the hierarchical complexity of living tissues and organs (Ingber and Jamieson, 1985; Ingber, 1993, 1998; Chen and Ingber, 1998).

Acknowledgments

This work was supported by grants from NASA and NIH.

Literature Cited

Chen, C. S., and D. E. Ingber. 1998. Tensegrity and mechanoregulation: from skeleton to cytoskeleton. *Osteoarthritis Articular Cartilage* (in press).

Chen, C. S., M. Mrksich, S. Huang, G. Whitesides, and D. E. Ingber. 1997. Geometric control of cell life and death. *Science* **276:** 1425–1428.

Chicurel, M., C. S. Chen, and D. E. Ingber. 1998a. Cellular control lies in the balance of forces. *Curr. Opin. Cell Biol.* **10:** 232–239.

Chicurel, M. E., R. H. Singer, C. J. Meyer, and D. E. Ingber. 1998b. Integrin binding and mechanical tension induce movement of mRNA and ribosomes to focal adhesions. *Nature* **392:** 730–733.

Ingber, D. E. 1990. Fibronectin controls capillary endothelial cell growth by modulating cell shape. *Proc. Natl. Acad. Sci. USA* **87:** 3579–3583.

Ingber, D. E. 1993. Cellular tensegrity: defining new rules of biological design that govern the cytoskeleton. *J. Cell Sci.* **104:** 613–627.

Ingber, D. E. 1997. Tensegrity: The architectural basis of cellular mechanotransduction. *Annu. Rev. Physiol.* **59:** 575–599.

Ingber, D. E. 1998. The architecture of life. *Sci. Am.* **278:** 48–57.

Ingber, D. E., and J. Folkman. 1989. Mechanochemical switching between growth and differentiation during fibroblast growth factor-stimulated angiogenesis in vitro: role of extracellular matrix. *J. Cell Biol.* **109:** 317–330.

Ingber, D. E., and J. D. Jamieson. 1985. Cells as tensegrity structures: architectural regulation of histodifferentiation by physical forces transduced over basement membrane. Pp. 13–32 in *Gene Expression During Normal and Malignant Differentiation*, L. C. Andersson, C. G. Gahmberg, and P. Ekblom, eds. Academic Press, Orlando, FL.

Lee, K.-M., K. Tsai, N. Wang, and D. E. Ingber. 1998. Extracellular matrix and pulmonary hypertension: control of vascular smooth muscle cell contractility. *Am. J. Physiol.* **274:** H76–H82.

Maniotis, A., C. Chen, and D. E. Ingber. 1997. Demonstration of mechanical connections between integrins, cytoskeletal filaments and nucleoplasm that stabilize nuclear structure. *Proc. Natl. Acad. Sci. USA* **94:** 849–854.

Plopper, G., H. McNamee, L. Dike, K. Bojanowski, and D. E. Ingber. 1995. Convergence of integrin and growth factor receptor signaling pathways within the focal adhesion complex. *Mol. Biol. Cell* **6:** 1349–1365.

Singhvi, R., A. Kumar, G. Lopez, G. N. Stephanopoulos, D. I. C. Wang, G. M. Whitesides, and D. E. Ingber. 1994. Engineering cell shape and function. *Science* **264:** 696–698.

Stamenovic, D., J. Fredberg, N. Wang, J. Butler, and D. Ingber. 1996. A microstructural approach to cytoskeletal mechanics based on tensegrity. *J. Theor. Biol.* **181:** 125–136.

Tagawa, H., N. Wang, T. Narishige, D. E. Ingber, M. R. Zile, and G. Cooper IV. 1997. Cytoskeletal mechanics in pressure overload cardiac hypertrophy. *Circ Res.* **80:** 281–289.

Wang, N., and D. E. Ingber. 1994. Control of cytoskeletal mechanics by extracellular matrix, cell shape, and mechanical tension. *Biophys. J.* **66:** 2181–2189.

Wang, N., and D. E. Ingber. 1995. Probing transmembrane mechanical coupling and cytomechanics using magnetic twisting cytometry. *Biochem. Cell Biol.* **73:** 1–9.

Wang, N., J. P. Butler, and D. E. Ingber. 1993. Mechanotransduction across the cell surface and through the cytoskeleton. *Science* **260:** 1124–1127.

Yoshida, M., W. F. Westlin, N. Wang, D. E. Ingber, A. Rosenweig, N. Resnick, and M. Gimbrone. 1996. Leukocyte adhesion to vascular endothelium induces e-selectin association with the actin cytoskeleton. *J. Cell Biol.* **133:** 445–455.

Discussion

BORISY: How do you imagine that the nucleus is receiving and transmitting the mechanical signal into a chemical signal, especially since there are no intermediate filaments, microtubules, or actin filaments within the nucleus?

INGBER: We believe that mechanical connections to the nucleus effect changes in chemical signals at the plasma membrane. There are also data suggesting that nuclear pore size and nuclear transport rates are being affected at the nucleus. Some studies suggest that the nuclear pores are distorted when nuclei spread, affecting the efficiency of nuclear transport. This is of interest to us because we find that cells need to spread late in G1 to get into S phase, and nuclear transport of large enzyme complexes is a requirement for S phase entry late in G1. We can harpoon the nucleus, pull out all of the nucleoplasm on a string in interphase or pull out all the chromosomes on a string in metaphase, then add a small amount of magnesium, and all these structures unwind. After dilution of the magnesium, they all rewind to reconstruct their original form and position (Maniotis *et al.*, 1997. *J. Cellul. Biochem.* **65:** 114–130). This effect is not nonspecific; rather it is DNA-based. The structure of DNA and its nuclear matrix scaffoldings are being affected. The literature tells how DNA is wound on the nuclear matrix, which dictates its regulation. I think that there are things in the nucleus that are load-bearing and by pulling on them we may change their kinetics and thermodynamics. This also may increase the efficiency, possibly allowing specific transcription factors to enter certain sites on parts of transcriptionally active DNA near the nuclear matrix. But it is not going to be a simple on–off process. We need to continue developing the techniques to study these effects.

MACINTOSH: Are there any other ways to look for the development of nonrandom networks of this kind? Obviously one could look for order of some kind. My second question relates to prestressed fibers. How do you visualize prestressed fibers in a network where many of the crosslinks are highly dynamic and transient?

INGBER: Our view of the cytoskeleton is almost exclusively based on the use of immunofluorescence microscopy, which presents a problem of limited resolution. We think that actin stress fibers are "floating" in a black sea of cytoplasm. That sea is filled with a continuous network of actin filaments in loose polygonal arrangements, perhaps more actin than in stress fibers. Dynamic polymerization on a stress fiber can be described in terms of a molecular rope made up of many smaller ropes, with the group in the middle maintaining mechanical connectedness as the outer rope components "polymerize" on and off. In terms of cross-links and dynamics, I believe that the actin cytoskeleton is a tensegrity structure which immediately responds to a quick pull on its attachments to the cell surface by slightly realigning all its elements; through tensegrity you get flexibility out of a structure, even when it contains nonextensible or rigid elements. There also may be some regions that exhibit relatively increased distortion which may change molecular shape and thus alter local thermodynamic parameters and, hence, influence molecular biochemistry (Ingber, 1997. *Annu. Rev. Physiol.* **59:** 575–599). For example, this could influence rates of cross-link breakage and reformation or alter cytoskeletal filament polymerization as has been observed for microtubules. If the mechanical stress is sustained, as might be expected for an adhesive interaction with a substrate, then this process would proceed in an iterative manner and result in progressively greater levels of cytoskeletal restructuring as is observed in spreading cells.

In response to your first question about patterns: there is a lot of order in the cytoskeleton. Mathematical descriptions of our tensegrity model predict the linear stiffening behavior we observe in living cells whether the models incorporate elastic elements and rigid struts or nonextensible tensile elements and buckleable struts. I believe this latter configuration is really how

it works with microtubules or cross-linked bundles of actin filaments acting as the buckleable struts. This is now clear from the work of Andrew Matus (Kaech *et al.*, 1996. *Neuron* **17:** 1189–1199). Intermediate filaments are also coils that are basically extensible structures that can change in length and that mechanically couple the nucleus to cell surface receptors (Maniotis *et al.*, 1997. *Proc. Natl. Acad. Sci. USA* **94:** 849–854). Many cells also contain titin, which is a highly elastic molecule. I think the cell builds hierarchically; it's not just six struts in a cell. That's why after a cell is cut with a microneedle, each piece has the properties of the whole system, such as the ability to move, as shown many years ago by Gunter Albrecht-Buehler.

STEWART: It seems to me that there are two elements in this about the idea of mechanical transduction in the nucleus. What concerns me is that the elements in the nucleus that are involved in gene expression are not likely to be bearing the loads that are going to come down through the nucleus.

INGBER: We have data to show that we reorient the mitotic spindle by pulling on integrins in a mitotic cell. So we are getting force to every chromosome.

STEWART: Yes, but the mitotic spindle is not involved in transcription.

INGBER: I showed pictures where we have analyzed SC35 splicing sites. Don Coffey and co-workers have shown (Pienta *et al.*, 1991. *Crit. Rev. Eukaryot. Gene Expr.* **1:** 355–385) that the parts of the genome actively involved in transcription are on the nuclear matrix. He has mapped the genes on a prostate cell that is sensitive to androgen and finds that they are all at the base of DNA loops on the nuclear matrix, which is probably part of a load-bearing scaffolding. After castration the animal loses androgen sensitivity, becoming estrogen sensitive within hours. Within a matter of hours, those same genes are at the tip of the loop. These genes that have been turned on were at the bottom, in physical interconnection with the load-bearing system. You may have your conception, but I believe that we have actual data to show that it is not correct.

STEWART: How can this happen by just applying a mechanical stress? It seems to me that there are well-documented pathways involving chemical messages that could easily come from the cytoskeleton. One of the principal regulatory roles in terms of communication between the nucleus and the cytoplasm is that elements are immobilized on the cytoskeleton—NFkappaB, for example. You could easily imagine that being released and transported.

INGBER: I completely agree with that. That is why the first thing I said in answer to your question was that the initial effect of mechanical force is to change chemicals in the cytoplasm. It is not one or the other, it is both. I think most cells have specialized structures, like mechanoreceptor cells, to take the load. A pressure-sensitive cell in your skin has lots of matrix so when you press once it feels it, then the stress dissipates. Different cells are structured so that stress may never get to the nucleus, in terms of causing a change. I'm not saying that when you stretch the nucleus you make it grow. In G2 phase the nucleus spreads all the time, you don't get S phase. My point is that if you have all the chemicals coming from the cytoplasm, you don't get the same result; it will depend on the structure of the nucleus. All of these factors are necessary, but not sufficient; and they are all interdependent. This is just another potential way to feed in information. Half of my lab work is based on what you are talking about (that is, chemical signaling) because we think it is equally important.

STEWART: To make it plausible you need to first show that the forces are being distributed to the elements that are working, as opposed to the nucleus itself. You have to provide some sort of mechanism whereby those forces can produce realistic effects. You need to think of the magnitude of the forces compared to the elements that are involved in actually changing the structure of the chromatin. I am concerned that the forces that are involved and are going to produce the regulatory changes of the nucleus are rather large compared to the mechanical forces that you are likely to be able to concentrate.

INGBER: We don't necessarily have to distort anything to affect function. If you have a spring that vibrates and you change the center of gravity of that spring, you change its vibration; you change kinetics. If you slightly distort the spring you can change kinetics without having to distort the whole thing. But I agree with you. It has taken a number of years for me to reach this point. We have had to combat the arguments that you can't get force to the nucleus, by testing it. Right now, I don't know how this works at the level of transcription. However, my only point is that forces applied to the cell surface can get to the nucleus. Just because we can't envision a mechanism doesn't mean that it doesn't happen.

FORGACS: I wish to propose an alternative idea which is based on percolative networks. This is more random than tensegrity. Tensegrity structures appear more ordered than percolative structures. I would like to point out that the linear stress-strain relationship is a generic feature of connective networks. Percolative structures possess exactly the same behavior.

INGBER: Only if they are prestressed, and we are talking about linear stress-stiffness curves here, not linear stress-strain.

FORGACS: Percolative structure can basically produce the same thing once you fix the network somehow, which you may refer to as prestressed. My question concerns how mechanical forces can induce relevant changes. We had the model calculation which shows that mechanical forces of the magnitude that can be produced in percolative networks can really kick molecules bound to the cytoskeleton and bring them from one molecular or quantum energy level to another. I interpret this as going from one conformation to another. It would be nice if someone would design an experiment to test this theoretical possibility.

INGBER: Percolation presents a complementary view to understand the connectivity of these networks: how you go from losing connections to having connections, and how signals transmit over this. However, I don't think that percolation can predict the patterning and mechanical response of these structures in living cells (Ingber, 1998. *Proceedings of the Les Houches Meeting on Dynamical Networks in Physics and Biology*. France, Springer-Verlag. In press).

GUNDERSEN: As a biochemist, I believe there are mechanical effects on cells and that this is an important component of how cells respond to their environment. Your tensegrity models seem to predict fairly well some of the basic properties of cells. However, you never labeled your models. What are the struts and what are the elements tying them? I am interested in whether there is a 1:1 correspondence between your rods and the tie elements to some cytoskeletal structure? Is this a good representation of the behavior of those elements in the cell? Is it possible that there may be other things in the cell, for example, the dynamics of the filaments, that contribute to the behavior of your tensegrity models?

INGBER: In the video I showed, our modeled networks of actomyosin and those individual struts are 3.6 μm in length. The geodesic nets and linear stress fibers created by those models exhibit structural features that are exactly those predicted from analysis of the actomyosin network in living cells based on thin section transmission electron microscopy (Lazarides, 1976. *J. Cell Biol.* **68:** 202–219; Osborn *et al.*, 1978. *Cell* **14:** 477–488). Our model is exactly precise, strut for strut, vertex for vertex, at least in this context. In terms of the compression elements, Steve Heidemann and co-workers (Joshi *et al.*, 1985, *J. Cell Biol.* **101:** 697–705) have shown that bundles of microtubules in the neurite act like compression struts. Andrew Matus has recently shown this directly in cells containing microtubules labeled with green fluorescent protein. They are being pulled by actin and balanced by matrix tethers, just as we are saying here. The matrix itself consists of local compression struts, due to the distribution of forces between focal adhesion at either end of the same stress fiber, resulting in the stability of the whole cell, which is globally tensile. Thus the cell is a tensegrity structure, based on definition at the whole cell level. I have shown you that connecting single microtubules with many actomyosin filament nets with dimensions of 3.6 μm creates hierarchical structures, again with tensegrity-based mechanical stability. We are just beginning to develop testable hypotheses. If that is true, we should be able to determine curvature of a microtubule on a specific size scale and ranges of amplitude, and how changing contractility affects that. That is where we are heading.

GUNDERSEN: Do you think you could isolate, in a biochemical sense, something that would behave like your stick and strut models? What I am asking is, can you do the biochemistry behind the tensegrity models? Do you think that is possible?

INGBER: Steve Heidemann has used tensegrity to define a thermodynamic model that explains how microtubule polymerization is regulated. This also explains microtubule polymerization in hepatocytes, as we have published. I must emphasize that as cells stick and spread they go from round to a pancake. We have measured this and find no correlation between the total amount of actin, microtubule or intermediate filaments, and spreading.

GUNDERSEN: Maybe it is in their dynamics. The dynamics of all these filaments is very sensitive to all kinds of different changes.

INGBER: What I am saying is that actin polymerization goes up 20-fold when an isolated hepatocyte attaches to a matrix-coated dish, with no change in shape. It then goes down 20-fold, with no change in shape. When the cell goes from round to a pancake, microtubules are constant; intermediate filaments are constant. You could argue that it is changing in a local domain. This may be so, but it is not a global, viscous polymerization. It does change when the cell is moving and forming ruffling edges; I totally agree with that. However, I don't believe that it is possible to explain mechanotransduction and higher order integration on the basis of a single molecule. If you are asking whether we can identify an assemblage of these elements that have certain mechanical properties, my answer is "I hope so." One possible approach would be to look at self-assembly reactions in whole cell extracts. This has been done with the mitotic spindle, which we believe behaves in similar ways; that is, it is a unit that stiffens by global transmission of tensile forces that are resisted internally by multiple microtubule struts.

BARAKAT: There is evidence that small forces, such as shear stresses over endothelial cells of a magnitude less than 1, and even as low as 0.1 dyne per square centimeter, can elicit biochemical responses. These forces are thought to be significantly smaller than what is required to induce mechanical deformation in certain cytoskeletal elements. Do you think that the fact that these small forces elicit biochemical responses is consistent with the notion of tensegrity?

INGBER: Is there any knowledge about the frequency of those stimulations? One can change the harmonics without changing the deformation and get some of the same things. These structures are coupled harmonic oscillators; by banging the whole cell the nucleus starts moving with the same frequency.

Reference: *Biol. Bull.* **194:** 328–330. (June, 1998)

Surface Tension and Viscoelastic Properties of Embryonic Tissues Depend on the Cytoskeleton

GABOR FORGACS

Departments of Physics and Biology, Clarkson University, Potsdam, New York 13676

A number of morphogenetic phenomena in early development, as well as *in vitro* experiments, suggest that embryonic tissues in many respect behave as liquids. A small chunk of such tissue, originally of arbitrary shape, will eventually assume an almost perfectly spherical shape when left alone in the medium. When two such tissues are placed contiguously, a state reminiscent of that of immiscible fluids of different surface tensions (in the absence of gravity) is reached: one tissue spreads, engulfs, and eventually surrounds the other. The same final configuration can be attained in a sorting out assay, when the cells of the two tissues are initially intermixed. The properties leading to the final states in the engulfment and sorting out experiments are transitive: if tissue A is spread upon by tissue B, and B spread upon by C, then A will be spread upon by C if the two tissues are mutually adhesive. The prediction of transitivity in the mutual spreading preferences of embryonic tissues was the basis of a test of the "differential adhesion hypothesis (DAH) (Steinberg, 1970); *i.e.,* the liquid-like behavior of cell populations is attributed to the surface tensions of the tissues, which is postulated to arise from adhesive and cohesive interactions of their component cells. Surface and interfacial tensions are equilibrium properties governing the final configurations assumed by the tissues. If embryonic tissues indeed possess liquid properties, it is their viscoelastic characteristics that determine how equilibrium is reached.

Here I describe a method for defining and simultaneously measuring the surface tensions and viscoelastic properties of tissues. Spherical cell aggregates are placed between the plates of a specifically designed parallel plate apparatus (Fig. 1), compressed with a known force, and allowed to equilibrate (Fig. 2). The surface tension is determined from the equilibrium force and the change in shape of the aggregate using Laplace's equation (Foty *et al.,* 1994). Measurements of the surface tension of several embryonic tissues are presented and correlated with the mutual spreading behavior of these tissues (Foty *et al.,* 1996). It is demonstrated that tissue surface tension is indeed a well-defined intensive physical parameter: it does not depend on sample variability or the specific conditions under which it is measured. In particular, it is independent of the size of the aggregate and the magnitude of the compressive force.

Viscoelastic properties are modeled by a generalized Kelvin body, extensively used to interpret viscoelasticity in biological materials (Fung, 1993). The Kelvin body is an appropriately constructed circuit of springs (to model elasticity) and dashpots (to model viscosity). The prediction of the model is compared with the force relaxation curve obtained after compression. The analysis shows that embryonic tissues are very well characterized in terms of two relaxation times: a shorter one defined by the early elastic response, and a longer one defined by the later viscous response.

As postulated in the differential adhesion hypothesis, the surface tension is correlated with the number of cell adhesion molecules, most of which are transmembrane proteins attached to the cytoskeleton. Recent experimental results suggest that the measured values of the tensions may strongly depend on the state of the cytoskeleton, the interconnected, intracellular, filamentous structure of macromolecules. The measured physical parameters (surface tension, viscosity, elastic constants, and relaxation times) can be related to biologically relevant quantities

This paper was originally presented at a workshop titled *The Cytoskeleton: Mechanical, Physical, and Biological Interactions.* The workshop, which was held at the Marine Biological Laboratory, Woods Hole, Massachusetts, from 15–17 November 1996, was sponsored by the Center for Advanced Studies in the Space Life Sciences at MBL and funded by the National Aeronautics and Space Administration under Cooperative Agreement NCC 2-896.

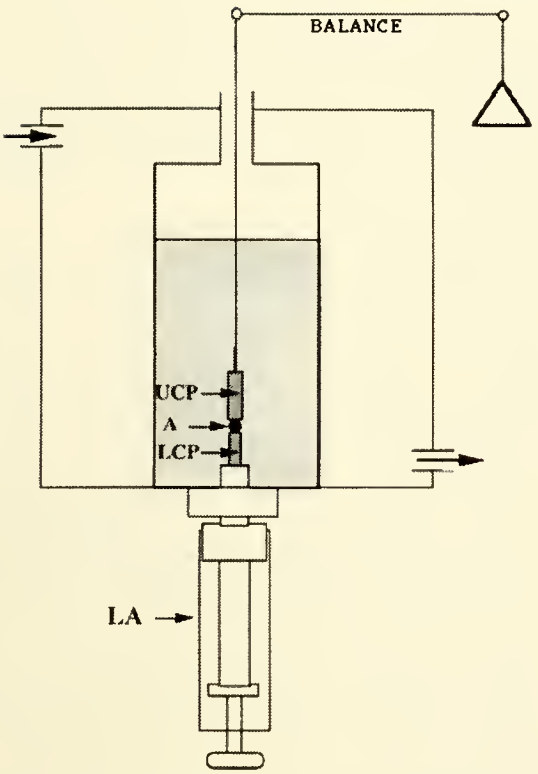

Figure 1. Schematic representation of the compression plate apparatus. Spherical cell aggregates (A) are positioned between the upper and lower compression plates (UCP and LCP, respectively). The UCP is suspended from the arm of an electrobalance, which records the compressive force that is exerted on the aggregate when the lower assembly (LA) is turned. The evolution of the compressive force with time is continuously recorded by a computer.

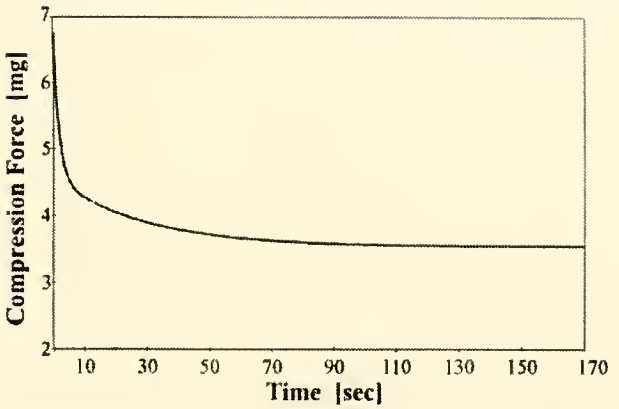

Figure 2. A characteristic compressive relaxation curve as recorded by the computer. The one shown comes from a chick embryonic heart aggregate. This curve is matched with the one predicted by the Kelvin body in terms of the physical parameters mentioned in the text.

like the strength of binding between cell adhesion molecules and their characteristic lifetimes.

Literature Cited

Foty, R., G. Forgacs, C. M. Pleger, and M. Steinberg. 1994. Liquid properties of embryonic tissues: measurement of interfacial tensions. *Phys. Rev. Lett.* **72:** 2298–2301.

Foty, R., C. M. Pleger, G. Forgacs, and M. Steinberg. 1996. Surface tension of embryonic tissues predict their mutual envelopment behavior. *Development* **122:** 1611–1620.

Fung, Y. C. 1993. *Biomechanics.* Springer–Verlag, New York.

Steinberg, M. S. 1970. Does differential adhesion govern self-assembly processes in histogenesis? Equilibrium configurations and the emergence of a hierarchy among populations of embryonic cells. *J. Exp. Zool.* **173:** 395–434.

Discussion

SCHWARTZ: How do you know whether cytochalasin lowers surface tension by reducing tension inside the cell or by affecting cadherins and cell-cell adhesion?

FORGACS: Since cadherins are known to be coupled to the actin cytoskeleton, I believe cytochalasin affects them both.

COULOMBE: How much time is required for these cells to sort out? Does this require *de novo* gene expression, or *de novo* protein synthesis? Does it occur in the presence of cyclohexamide?

FORGACS: I can tell you that it takes about 20 h for these cells to divide under the conditions of the experiment, and it takes anywhere from 2 to 15 h for the compression force to fully relax, depending on the tissue type; neural retina, for example, relaxes in about 2 h. We have not performed experiments in the presence of cyclohexamide.

BRUINSMA: Your finding that the effect of surface tension for all these cells is proportional to the number of cadherins would naively suggest that cadherins are not cooperative but work independently of one another. (Forgacs: Not necessarily.) It has been shown that cadherins have a strong tendency to aggregate in strings. In general, with focal adhesion you wouldn't expect the effect of tension to be proportional to the number of adhesion molecules.

FORGACS: Those experiments show that this tension, which we call effective surface tension, is linearly proportional to the number of cadherins. You are correct in saying that there is

strong evidence that cadherins bundle up. When we use fluorescence microscopy to look at the cell surface to see what happens to the cadherins during relaxation, we detect fluorescent patches over the whole surface. This could reflect how the aggregates are prepared, which may not be the same as in the body. I expect that the connections are stronger when there are more cadherins in a focal contact. Even when cadherins are bundled, the overall cohesiveness of the tissue manifested in the value of the measured surface tension may still be proportional to the number of cadherins. Attachment of cadherins to the cytoskeleton is also a factor.

JANMEY: In your model, it looks as though recovery of shape soon after deformation is the result of passive mechanical or elastic recovery. In that case, you might be able to separate the cytochalasin effect from its effect on selectin efficiency or function by determining whether cytochalasin alters the first elastic recovery. If this sits for a long time, recovery to the spherical state requires cell migration and reformation of cell-cell contacts that are not necessary after the quick recovery. If you look at those two kinds of relaxations, do you see systematic differences?

FORGACS: These findings are recent. We have not checked the effect of cytochalasin on viscosity. We do see the early response in terms of the short relaxation time, which I interpret as an elastic response. We also see much longer relaxation times, which I interpret in terms of viscous relaxation. Our ability to fit these experimental results with two relaxation times, two exponentials, fits nicely with local changes at the level of a single cell followed by cooperative phenomena as the cells line up with each other.

BORISY: I would like you to go into the formalism of surface tension and viscosity. I am worried that unless we penetrate the formalism and try to explain it in molecular terms, the formalism may be misleading. Could you comment on what you think is responsible for the behavior that gives rise to this formalism? Surface tension could be a counter for some minimization or maximization principle. With an oil droplet in water, for example, we can talk about maximization of hydrogen bonds of water molecules as driving the spherical shape. There may be a similar principle that can account for the behavior of cells in these aggregates which could also be described in terms of surface tension. What we would like to understand is what are these minimization principles? What is operating? What do you think is responsible for this formalism?

FORGACS: You are asking a difficult question. The ultimate goal, of course, is to relate measurable physical properties such as surface tension to molecular mechanisms. At this point we take the physicists' attitude, namely we use the simplest possible formalism to explain our experimental results, and that is surface tension. What about the molecular details? Recent experimental results suggest that the number of cadherins and the resultant strength of cohesion are important contributions to what we call surface tension, but this is not the full story. Although we have some idea of the forces involved, we are unable, at this point, to interpret surface tension in terms of these forces alone. This does not mean that our formalism is wrong; it means that there are certain factors that we don't understand. We do not know, for example, how to quantify the effect of cytoskeletal attachments.

CHEN: I am trying to extend your analysis to understand what is going on. By analogy with properties of liquids, I think that your measurements of surface tension reflect attractive forces between cells, and that your determinations of viscosity are a measure of how easily the cells can move past one another. It seems that the sorting process you describe may be considered a diffusion-limited process of sorting in a highly viscous fluid. Have you looked at the rate of sorting as some measure of diffusion?

FORGACS: This is precisely what we are now doing. We have learned from following the sorting process as a function of time that the process is basically nucleation, which is diffusion limited. I don't want to present our final results, but it is interesting that standard theories of nucleation hold true. I believe that we can learn a great deal from these studies.

Reference: *Biol. Bull.* **194:** 331–333. (June, 1998)

Two-Dimensional Cytoskeletons Under Stress

DAVID H. BOAL

Department of Physics, Simon Fraser University, Burnaby, British Columbia, V5A 1S6, Canada

Planar triangular networks under stress are predicted to have several interesting properties: a first-order transition to a collapsed state for a range of compressive stresses, and a negative Poisson ratio for a range of tensions (*i.e.*, they expand transversely when stretched longitudinally). When these two-dimensional nets are allowed to fluctuate in three dimensions, they are predicted to be asymptotically rigid at long length scales and to have a universally negative Poisson ratio, even at zero stress (reviewed in Boal, 1996). There are many examples of two-dimensional networks in nature: auditory outer hair cells (Tolomeo *et al.*, 1996) and bacterial cell walls (Ghuysen, 1968) contain few or many layers of networks with square or honeycomb symmetry. Further, not all networks are isotropic: the peptidoglycan network of the bacterial cell wall is anisotropic in the network plane, being stiff in one direction but soft in the other.

One well-studied network is the membrane-associated cytoskeleton of the human red blood cell—a two-dimensional network whose elements are tetramers of the protein spectrin. Although the contour length of a spectrin tetramer is approximately 200 nm, the average separation between the sixfold junctions linking the tetramers is closer to 70 nm (Steck, 1989). Thus, one picture of the erythrocyte cytoskeleton is that of a triangular network of convoluted chains, as shown by the simulation in Figure 1. By mechanically manipulating the erythrocyte, measurements can be made of the shear modulus μ and compression modulus K_a of its cytoskeleton in the lipid bilayer plane to which the network is attached (Discher *et al.*, 1994).

This paper was originally presented at a workshop titled *The Cytoskeleton: Mechanical, Physical, and Biological Interactions.* The workshop, which was held at the Marine Biological Laboratory, Woods Hole, Massachusetts, from 15–17 November 1996, was sponsored by the Center for Advanced Studies in the Space Life Sciences at MBL and funded by the National Aeronautics and Space Administration under Cooperative Agreement NCC 2-896.

Although the cytoskeleton chains appear convoluted in the simulation, the chain junctions (the white disks in Fig. 1) fluctuate only slightly around their mean positions. Indeed, the junctions in the simulation behave like those of a spring network with a reduced temperature of $k_BT/K_{sp}S_o^2 = 1/30$, where k_B is Boltzmann's constant, K_{sp} is the network spring constant, and S_o is the equilibrium spring length. At low temperature, the elastic moduli of such a network are $\mu/K_{sp} = \sqrt{3}\,(1 - \sqrt{3}\cdot P/K_{sp})/4$, and $K_a/K_{sp} = \sqrt{3}\,(1 + P/[\sqrt{3}K_{sp}])/2$, where P is the in-plane pressure, defined to be negative for networks under tension. These expressions are in rough agreement with experiment if K_{sp} is estimated from the properties of polymer chains. When stretched, the erythrocyte cytoskeleton is predicted to lie close to the bilayer plane and to restrict

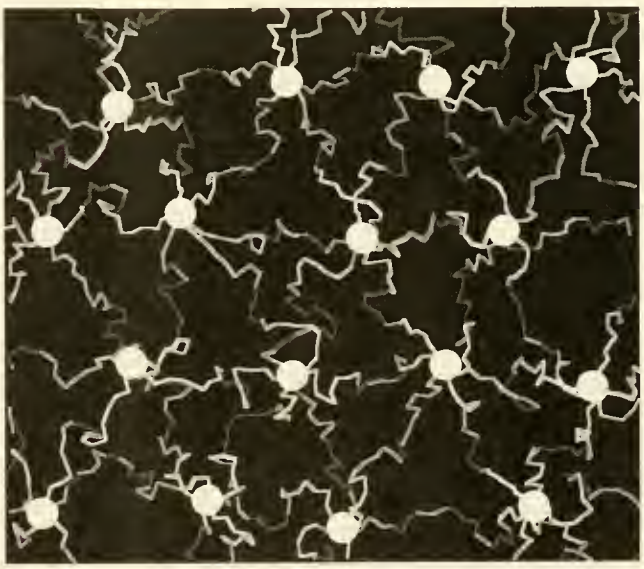

Figure 1. Polymer chain model of the erythrocyte cytoskeleton. The large white disks indicate the locations of the sixfold junction vertices of the chains.

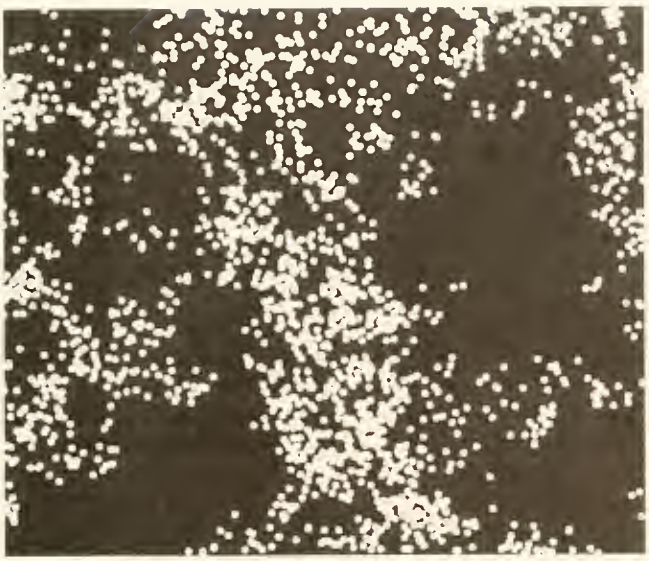

Figure 2. Simulation of randomly diffusing proteins in the bilayer plane, showing locations of the proteins separated by constant time intervals. The proteins are segregated into corrals by their interaction with the cytoskeleton.

the motion of membrane proteins that extend significantly into the cytoplasm. As shown in Figure 2, membrane proteins that are otherwise freely diffusing may become restricted to localized "corrals" because of their repulsive interactions with the cytoskeleton.

Biological networks contain defects that may alter the mechanical properties from those of networks with perfect triangular, square, or honeycomb symmetry. For example, while a network whose connectivity is sixfold on average may have near-ideal properties, bond-depleted networks may be weak to the point of failure (Mohandas and Evans, 1994). Percolation theory has provided a qualitative description of how the elastic moduli decrease as the average connectivity of the network decreases (reviewed in Saxton, 1990).

Literature Cited

Boal, D. H. 1996. Statistical physics of membranes and lamellar systems. Pp. 541–562 in *Encyclopedia of Applied Physics*, Vol. 19, G. Trigg, ed. VCH Publishers and American Institute of Physics, New York.

Discher, D. E., N. Mohandas, and E. A. Evans. 1994. Molecular maps of red cell deformations: hidden elasticity and *in situ* connectivity. *Science* **266:** 1032–1035.

Ghuysen, J.-M. 1968. Use of bacteriolytic enzymes in determination of wall structure and their role in cell metabolism. *Bacteriol. Rev.* **32:** 425–464.

Mohandas, N., and E. A. Evans. 1994. Mechanical properties of the red cell membrane in relation to molecular structure and genetic defects. *Annu. Rev. Biophys. Biomol. Struct.* **23:** 787–818.

Saxton, M. 1990. The membrane skeleton of erythrocytes: a percolation model. *Biophys. J.* **57:** 1167–1177.

Steck, T. L. 1989. Red cell shape. Pp. 205–246 in *Cell Shape: Determinants, Regulation and Regulatory Role*, W. Stein and F. Bronner, eds. Academic Press, New York.

Tolomeo, J. A., C. R. Steele, and M. C. Holley. 1996. Mechanical properties of the lateral cortex of mammalian auditory outer hair cells. *Biophys. J.* **71:** 421–429.

Discussion

TAYLOR: Could you clarify what you mean by low temperature in relationship to spectrin?

BOAL: If you look at the motion of the nodes rather than the floppy chains and follow the movement of those nodes, the rms (root mean square) dispersion in the position of these nodes resembles motions at low temperature. The energy scale in this system is provided by $K_{sp}S_o^2$, where K_{sp} is the effective spring constant of the network and S_o is the equilibrium spring length. In these units, the temperature kT is equal to 1/30, which is very low.

SCHWARTZ: I want to see if I understand the implication of your model. When the cytoskeletal network is under stress, and the density of sites restricting diffusion increases, you would predict that molecular diffusion would slow. On the other hand, if molecules were confined in a restricted area, would reaction rates increase by stretching the network?

BOAL: Yes, there is an increase in the local density of proteins, and hence there would be an increase in the reaction rates.

SCHWARTZ: In principle, you could effect signaling by molecules that are not actually attached to the cytoskeletal network?

BOAL: Yes. Let me comment on diffusion. There are two effects in Figure 2: the network is stretched out compared to the equilibrium configuration, so the overall protein density is lower; however, the proteins are concentrated in corrals, so their local density may be higher. One can expect that some effect would arise from the stretching of the network alone. The corralling phenomenon is real.

SCHWARTZ: For those of us who think of signaling molecules as being attached to those networks, that is an interesting implication.

BOAL: If these molecules are attached to the net, they are

going to spread out more. On the other hand, if they are corralled, they will bump into each other frequently.

STEWART: I want to follow up on Ed Taylor's question. In your equation $\beta K_{sp} S_o^2 \sim 30$, what are the units you used? Is the spring constant (K_{sp}) in that expression on the order of kT? Or, depending upon the units, is it much less than kT, perhaps two or more orders of magnitude less?

BOAL: K_{sp} and kT have different units. K_{sp} is in joules/square meter, so one must use an appropriate length scale to make K_{sp} and kT comparable. The product $K_{sp}S_o^2$, which is an energy, is 30 times kT. The compression modulus K_a, and the shear modulus μ, are both within a factor of two of K_{sp}.

STEWART: If we applied the sort of energy involved in kT to the system, would this produce a large or small change in terms of the difference between nodes?

BOAL: A small change. Basically, the nodes are vibrating around slowly, although the chains themselves are oscillating wildly.

GUNDERSEN: I am very interested in the effect of stretching on the potential corralling of molecules. When vesicles pinch off from membranes—for example, in the flow of proteins from endoplasmic to Golgi reticulum—such a corralling of molecules may occur. I'm wondering if you have any comments on this?

BOAL: I cannot comment on that in my own research, but I am familiar with experiments on normal rat kidney cells. These cells show a strong tendency to form corals or domains. The domains are typically 500–700 nm, reflecting the fact that the cytoskeletons in these kidney cells are presumably much looser, or of a much larger scale system, than in the erythrocyte. However, similar measurements of domain size in erythrocytes are not possible because the size of the beads used in these experiments is comparable to the domain size in the erythrocyte.

GUNDERSEN: With respect to the pinching off of vesicles, proteins on the vesicles may actually be affecting the clustering phenomenon.

MACKINTOSH: Although your talk focused primarily on spectrin networks, you also mentioned anisotropic stresses. Can you look at anisotropic stresses in the lamellopodium?

BOAL: Not yet. We have done some general work on anisotropic stresses. The statistical mechanics have not been sufficiently investigated and, before studying biological systems, that is where my laboratory has been focusing. In principle, there is no reason why we cannot study these stiffer, longer systems, such as the lamellopodium.

MACKINTOSH: Several people have suggested that you can create defects in polymer networks, removing cross-links and enhancing the modulus, without weakening the material. These are rather special cases, yet they are supported by simulations. This is a fundamental property of entropic elasticity.

BOAL: There has been a lot of work on generic changes to the triangulation of triangulated nets; for example, having fivefold and sevenfold coordinated sites. This produces modest changes in the moduli, but not the huge differences seen when the nets are depleted.

MACKINTOSH: The examples that I'm thinking of are networks that have zero shear modulus at zero temperature, like a square lattice.

INGBER: Studies on lipid domains and stretch-activated ion channels are looking for the type of information that you have. It might be interesting to see how your kinetic phenomena match up with some of those channel systems. In the type of experiments you have described, it seems that most investigators pull on the outer curvature of the red blood cell. Does the dimple in the middle of the cell have the same mechanical properties as the outer rim?

BOAL: I do not think they differ at all. Even in our studies, there is a slightly different average connectivity at the edges compared to the center. But when you inflate the cell first and then pull, there are no differences. A question would be, has the cytoskeleton relaxed during the inflation process such that an initially inhomogeneous connectivity has relaxed away?

INGBER: There must be some prestress or internal stress, to maintain that kind of curvature.

BOAL: If we compare our stretched cytoskeletons with aspiration experiments (involving huge deformations), we have to add some prestress to the stretched cytoskeletons, in order to get better agreement.

SHAFRIR: You cited discrete percolation theory, but from what I saw in your picture of this network (Fig. 1), it does not appear to be discrete. Did you try to simulate that (Boal: That is not my work.) with a continuous percolation model?

BOAL: Mike Saxton, at University of California—Davis, has looked at a variety of percolation models. As I recall, in no cases did the predicted value of the shear modulus agree with the experimentally observed value for spectrin-depleted erythrocytes. This may just mean that percolation theory can't be applied to this system because of the structure of the spectrin network. For example, connectivity in spectrin-depleted red blood cells may be different from that in the normal blood cell. However, there may be some experimental bias in these measurements. When researchers collect the samples on which to conduct the aspiration, they select blood cells where they can attach the micropipette onto the surface. Even though the sample has a global average spectrin content, the specific cells chosen for investigation may not have the same spectrin content as the global average.

Reference: *Biol. Bull.* **194:** 334–336. (June, 1998)

Cytoskeletal Networks and Filament Bundles: Regulation by Proteins and Polycations

PAUL A. JANMEY, JOSEF KÄS, JAGESH V. SHAH, PHILIP G. ALLEN, AND JAY X. TANG

Experimental Medicine Division, Brigham and Women's Hospital, Harvard Medical School, 221 Longwood Avenue, Boston, Massachusetts 02115

The three-dimensional polymer network formed by the cytoskeleton is the main determinant of cellular mechanics (Elson, 1988; Maniotis *et al.*, 1997) and is required for the cell to resist external forces as well as to generate and transmit the forces used during cell motility (Stossel, 1994). Three types of protein filaments—microtubules, F-actin, and intermediate filaments—form the basis of the cytoskeleton. Certain types of polymers tend to concentrate in separate regions of the cell; typically actin is concentrated at the cell cortex, whereas the microtubules and intermediate filaments are more centrally localized. However, the three types of cytoskeletal filaments can also interpenetrate and form contacts with each other and with specialized structures in cell membranes to provide mechanical continuity throughout the cell. The architecture of these networks depends on local activation of specific regulatory elements, and the variety of structures they form have distinct mechanical characteristics (Satcher and Dewey, 1996). Two distinct types of cytoskeletal assembly are open meshworks of single filaments, and asymmetric assemblies of filament bundles.

The viscoelastic properties of networks formed by F-actin, microtubules, and various intermediate filament types (*e.g.*, vimentin and neurofilaments) differ strongly from each other, as shown in Figure 1. At biologically relevant stresses (*e.g.*, from the 10 dyne/cm^2 of fluid shear stress at the artery wall, to the greater stresses needed for phagocytosis and locomotion) the different types of purified cytoskeletal polymer networks exhibit very different mechanical responses. At a constant weight concentration (2 mg/ml), microtubule networks deform to the largest extent, presumably because there are no bonds to keep the rigid polymers from sliding past each other. In contrast, networks of long actin filaments or of short actin filaments linked to each other by the divalent ABP280 crosslinker initially exhibit very little deformation, but at larger stresses these networks appear to rupture. Vimentin intermediate filaments are more deformable at smaller stresses than F-actin but resist much larger stresses without rupture. This ability to deform without damage, and the downward curvature of the strain/stress plot indicative of strain hardening is also observed in the extracellular fibrin network. The mechanical differences suggest some aspects of the possible biological function of these cytoskeletal elements; they also suggest the molecular basis of the elasticity of such networks, which differs radically from the viscoelastic properties of rubber-like materials (MacKintosh *et al.*, 1995; Kroy and Frey, 1996; Maggs, 1997).

Bundles of filamentous polymers are also a common feature of biological tissues, ranging from partly ordered structures (such as stress fibers), to well-ordered structures (such as sarcomeres and the paracrystalline arrays of actin filaments in microvilli and microtubules in flagella). The formation of such structures *in vivo* is generally thought to be orchestrated by the activity of specific binding proteins (Otto, 1994); but the thermodynamic driving force for the formation of bundles is largely unknown (Grazi, 1994; Tang *et al.*, 1997). Like DNA, all of the cytoskeletal filaments are anionic, with linear charge densities sufficiently high to stabilize electrostatic interactions with polyanions even at physiological ionic strength

This paper was originally presented at a workshop titled *The Cytoskeleton: Mechanical, Physical, and Biological Interactions.* The workshop, which was held at the Marine Biological Laboratory, Woods Hole, Massachusetts, from 15–17 November 1996, was sponsored by the Center for Advanced Studies in the Space Life Sciences at MBL and funded by the National Aeronautics and Space Administration under Cooperative Agreement NCC 2-896.

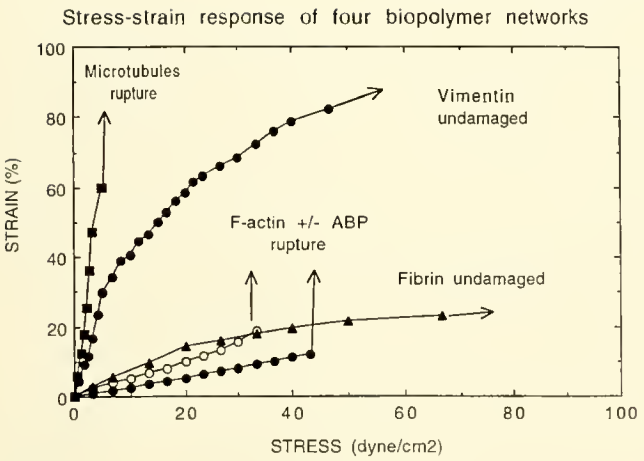

Figure 1. Shear strain of 2 mg/ml samples of polymerized biopolymer networks. The measurements were made 10 s after a range of shear stresses were imposed with a torsion pendulum, as previously described (Janmey, 1991).

(Tang *et al.*, 1996). Theories of polyelectrolytes developed to account for cation-induced condensation of DNA (1) apply equally well to F-actin, microtubules, intermediate filaments, and some filamentous viruses; and these theories provide an explanation for the ability of specific polycationic proteins to be efficient bundling factors for all of these diverse filament types. The effects of metal ions and polyvalent protein ligands on the structure and rheology of cytoskeletal networks likewise provide data relevant to both the biological function of the networks and the molecular structures underlying their mechanical properties.

Literature Cited

Anderson, C. F., and M. J. Record. 1990. Ion distributions around DNA and other cylindrical polyions: theoretical descriptions and physical implications. *Annu. Rev. Biophys. Biophys. Chem.* **19:** 423–465.

Elson, E. L. 1988. Cellular mechanics as an indicator of cytoskeletal structure and function. *Annu. Rev. Biophys. Biophys. Chem.* **17:** 397–430.

Grazi, E. 1994. Cytoskeleton, motile structures and macromolecular crowding. *Adv. Exp. Med. Biol.* **358:** 123–30.

Janmey, P. A. 1991. A torsion pendulum for measurement of the viscoelasticity of biopolymers and its application to actin networks. *J. Biochem. Biophys. Methods* **22:** 41–53.

Kroy, K., and E. Frey. 1996. Force-extension relation and plateau modulus for wormlike chains. *Phys. Rev. Lett.* **77:** 306–309.

MacKintosh, F., J. Käs, and P. Janmey. 1995. Elasticity of semiflexible biopolymer networks. *Phys. Rev. Lett.* **75:** 4425–4428.

Maggs, A. 1997. Two plateau moduli for actin gels. *Phys. Rev. A.* **55:** 7396–7400.

Maniotis, A. J., C. S. Chen, and D. E. Ingber. 1997. Demonstration of mechanical connections between integrins, cytoskeletal filaments, and nucleoplasm that stabilize nuclear structure. *Proc. Natl. Acad. Sci. USA* **94:** 849–854.

Otto, J. J. 1994. Actin-bundling proteins. *Curr. Opin. Cell Biol.* **6:** 105–109.

Satcher, R., and C. Dewey. 1996. Theoretical estimates of mechanical properties of the endothelial cell cytoskeleton. *Biophys. J.* **71:** 109–118.

Stossel, T. P. 1994. The machinery of cell crawling. *Sci. Am.* **271:** 54–55, 58–63.

Tang, J., S. Wong, P. Tran, and P. Janmey. 1996. Counterion induced bundle formation of rodlike polyelectrolytes. *Ber. Bunsenges. Phys. Chem.* **100:** 796–806.

Tang, J. X., T. Ito, T. Tao, P. Traub, and P. A. Janmey. 1997. Opposite effects of electrostatics and steric exclusion on bundle formation by f-actin and other filamentous polyelectrolytes. *Biochemistry* **36:** 12600–12607.

Discussion

COULOMBE: I have a question about the behavior of individual filaments in a network of similar filaments. If the filament surface is charged, how do you explain node formation at discrete points along the length of the network?

JANMEY: If the filaments are all anionically charged, you might expect them to be so electrostatically repulsive that they would never come near enough to one another to make nodes. There are two possibilities. One is that some of those nodes are simply kinks in which two filaments, that may be repulsive to each other, are caught in something like a local knot. What we are then looking at is the time it takes for that kind of knot to unravel. A second possibility is that, although the filaments repel each other in a vacuum, when they are in a medium full of counter ions attractive interactions can be created between polymers with like charges. The attraction could be based on the sharing of counterion clouds, or on fluctuations in that cloud. In this way, dipole-dipole interactions may in some cases overcome electrostatic repulsion between the polymers. This is an experimental surprise to us, but it holds up consistently.

FORGACS: If you shear or deform a microfilament network, is it possible to change some rate of polymerization?

JANMEY: I'm not sure that is known for actin. In the case of microtubules, there is evidence that assembly and disassembly rates of tubulin dimers on the microtubule end can be affected by something that looks like a force-generating mechanism. In an actin system it is more likely that you would generate breakage of actin filaments, and accelerate either polymerization or

depolymerization. The short answer to your question is that we do not really know.

FORGACS: You mentioned that microtubule and actin networks do not interact in your assays, whereas intermediate filaments and actin do. Do we know anything about these interactions in the cell?

JANMEY: The filament systems are intimately related to one another—it is very difficult to manipulate one without manipulating the others. The question is whether that kind of connectivity is directly mediated by polymer-polymer contact, or whether it works through specific regulatory proteins that mediate this "talking" of one filament system to another. That is the kind of question we would like to address. In the case of microtubules and actin, it looks as though the interaction must be mediated by some third protein.

FORGACS: If those filaments are all negatively charged, is it possible that some signaling molecules, which are positively charged, can slide or diffuse within those filaments, thereby contributing to their stability?

JANMEY: That is an appealing concept, but I do not know if it has been experimentally tested and verified. There is an interesting split in thinking of the cytoskeleton from a purely mechanical view, which is our lab's prejudice, dissociating it from the connectivity made by a percolated network. That is why the split between making a connective network or a structure rigid enough to resist or support a mechanical stress presented in David Boal's talk is so interesting. We do not know how to separate those two features.

CHEN: Does tagging the actin with a fluorescent group change its stiffness or affect surface interactions with other actin polymers?

JANMEY: That is a really good question. We cannot detect differences in flexibility between a fluorescently tagged actin filament and a non-tagged filament by using techniques such as dynamic light scattering or electron microscopy. Some fluorophores carry their own electrostatic charge. Therefore, we should be able to assemble populations of filaments consisting of the same protein, yet differing by 10%–20% in electrostatic surface charge, due to the fluorophore that we couple to them. If the hypothesis regarding surface charges is correct, then the fluorescently tagged filament types should behave differently. We have yet to test this. In answer to your question, there is no obvious alarm that fluorescent tagging of actin filaments is a problem.

GOLDMAN: Did you mix microtubules and intermediate filaments, especially neurofilaments?

JANMEY: Yes, we have mixed them. One of our problems with intermediate filaments and other filament types is how to take polymerized systems and instill another polymer into them. We start by placing preformed neurofilaments and preformed microtubules next to each other and gently trying to get them to interpenetrate. One of the really interesting findings, which Shah will present, concerns vimentin. We have tried to polymerize vimentin around very low concentrations of labeled actin filaments. The polymerization process breaks the filaments into small pieces. This surprising result might be an interesting mechanical problem. We know it is not simply due to a chemical poison effect, because before the vimentin subunits form a network they don't do anything to destabilize the actin. Only after vimentin begins to polymerize and form a visco-elastic network does it break up the actin filaments. We can polymerize tubulin around actin, but we cannot polymerize vimentin around actin without breaking up the actin. Therefore, it is possible that some of the work of polymerization has the consequence of breaking actin filaments.

TAYLOR: Actin and myosin subfragments have a net negative charge, yet they still interact because of local charge distributions on a protein surface.

Reference: *Biol. Bull.* **194:** 337–341. (June, 1998)

Actin: Dissecting the Structural Basis of Its Oligomerization, Polymerization, and Polymorphism

MICHEL O. STEINMETZ, DANIEL STOFFLER, AND UELI AEBI

M.E. Müller Institute, Biozentrum, Basel University, CH-4056, Basel, Switzerland

At first glance, the "actin polymerization" problem may appear to have been solved: that is, it involves a simple nucleation-condensation mechanism following pseudo-first-order assembly kinetics leading to a steady state (Oosawa *et al.*, 1975; Carlier, 1991). Although there is general agreement that one of the first steps in the polymerization reaction of G-actin into F-actin filaments involves dimerization of a significant fraction of the monomer pool, evidence has been presented that this dimer—called the "lower dimer" (LD)—is in a G-like conformation and is, by itself, unable to polymerize into F-actin filaments (Millonig *et al.*, 1988). Hence LD formation may represent an unproductive side reaction similar to the "ring" formation occurring during the oscillating cycle of assembly and disassembly seen in microtubules (Mandelkow *et al.*, 1991).

We have now demonstrated that LD, while being unproductive by itself, can add to growing F-actin filaments *via* one of its subunits (Steinmetz *et al.*, 1997a). Slowly but definitely, the surplus monomers dissociate from these partially "LD-decorated" filaments to yield, eventually, *bona fide* F-actin filaments at steady state. Taken together, these findings strongly suggest that F-actin polymerization may involve multiple pathways rather than a simple nucleation-condensation mechanism. The role of the LD should therefore be seriously considered in any future model or mechanism that attempts to describe the polymerization of G-actin into F-actin filaments. The functional significance of the LD is also supported by the occurrence of actin-binding proteins and molecules that bind to an LD-type dimer with high affinity (Hesterkamp *et al.*, 1993; Bubb *et al.*, 1994, 1995).

The Gd^{3+}-induced polymorphic crystalline actin sheets (Aebi *et al.*, 1981; Smith *et al.*, 1983) are made from actin dimers thought to be in an LD-like conformation (Millonig *et al.*, 1988); we have therefore computed 3-D reconstructions from tilt series of negatively stained crystalline actin tubes. We are now in the process of building an atomic model of the actin sheet dimer by fitting the atomic structure of the actin molecule (Kabsch *et al.*, 1990) into its EM-based 3-D mass density map (Bremer *et al.*, 1994).

When phalloidin (a bicyclic heptapeptide toxin of the toadstool *Amanita phalloides*) was present in a 2:1 molar excess over actin, we observed a drastic enhancement of the nucleation rate, with a more minor effect on the elongation rate. Moreover, this effect occurred regardless of the divalent cation (*i.e.*, Mg^{2+}, Ca^{2+}, or none) bound to the high-affinity binding site (HAS) of the G-actin monomer. We also found that slow polymerization of Mg-G-actin into filaments could also be achieved with stoichiometric amounts of phalloidin, even without K^+. These data indicate that the mechanisms of action of K^+ and phalloidin on the polymerization reaction of G-actin into F-actin filaments are very different. As phalloidin does not bind to monomeric actin, it appears not to activate G-actin significantly under low-salt conditions. However, halloidin tightly binds to, and thereby strongly stabilizes, nuclei and growing filaments (*i.e.*, by a "locking-in" mechanism), so that slowly but definitely the net equilibrium is shifted toward F-actin filament formation.

Moreover, we have systematically investigated the effect of the divalent cation (*i.e.*, Mg^{2+}, Ca^{2+}, or none) bound to the HAS of the G-actin molecule in terms of

This paper was originally presented at a workshop titled *The Cytoskeleton: Mechanical, Physical, and Biological Interactions.* The workshop, which was held at the Marine Biological Laboratory, Woods Hole, Massachusetts, from 15–17 November 1996, was sponsored by the Center for Advanced Studies in the Space Life Sciences at MBL and funded by the National Aeronautics and Space Administration under Cooperative Agreement NCC 2-896.

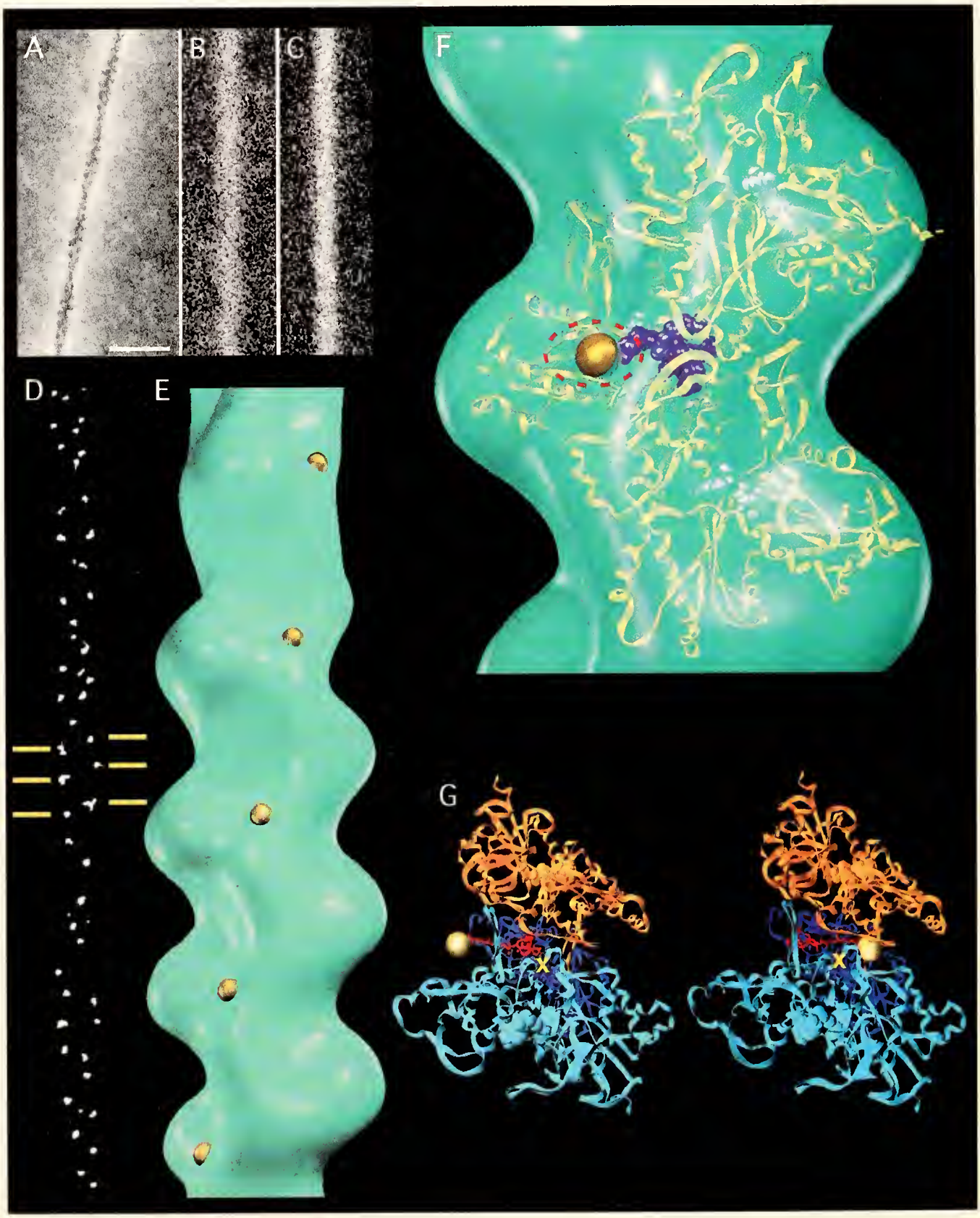
A
B
C
D
E
F
G

the mechanical properties and 3-D structure of the resulting F-actin filaments (*i.e.*, polymerized in the presence of 100 m*M* KCl). Judged from 3-D helical reconstructions, the overall filament conformation appears rather robust to this variation at the 25 Å resolution level. In accord with a recent report (Isambert *et al.*, 1995), but at variance with earlier results (Orlova and Egelman, 1993), we were unable to depict any significant dependence of the apparent persistence length of the resulting F-actin filaments on the divalent cation present in the HAS. But compared with native filaments, phalloidin-stabilized F-actin filaments appeared stiffer, as judged by a typically 2-fold increase of their apparent persistence length. As suggested first by EM data (Bremer *et al.*, 1991) and proposed later by an atomic model (Lorenz *et al.* 1993), 3-D helical reconstructions of negatively stained phalloidin-stabilized F-actin filaments yielded subtle but significant and reproducible changes in their intersubunit contact pattern both along and between the two long-pitch helical strands (Steinmetz *et al.*, 1997a).

To determine the exact location and orientation of the stoichiometrically bound phalloidin molecule within the F-actin filament, we collaborated with Dr. Faulstich (Max-Planck Institute for Medical Research, Heidelberg, Germany) in chemically engineering an undeca-gold (Au_{11})-tagged phalloidin derivative (Au_{11}-phalloidin). F-actin filaments—unstained freeze-dried native (Fig. 1B), and Au_{11}-phalloidin-stabilized (Fig. 1C)—were then imaged in a scanning transmission electron microscope (STEM) by the annular dark-field (ADF) detector at high magnification. To our surprise, the 11-gold-atom cluster was directly visible at distinct sites every 5.5 nm along the two long-pitch helical strands of derivatized F-actin filaments (Fig. 1D; see also Steinmetz *et al.*, 1997b). Moreover, 3-D reconstructions (Fig. 1E) of negatively stained Au_{11}-phalloidin-stabilized filament stretches (Fig. 1A), compared to un-tagged phalloidin-stabilized filaments, revealed a highly significant increase in mass density at distinct sites located near the interface between the two long-pitch helical strands (Steinmetz *et al.*, 1998). The phalloidin-binding site within F-actin, as thus identified, agrees well with the site proposed by the atomic model of Lorenz *et al.* (1993). However, atomic modeling of the Au_{11}-phalloidin derivative within the refined and averaged filament reconstruction (Fig. 1F) yields an orientation of the toxin within its binding site that is distinct from that obtained by Lorenz *et al.* (1993). As demonstrated in Figure 1G, if the Au_{11}-cluster, which is linked to the phalloidin moiety by a spacer of about 17 Å, is not to collide with an adjacent intersubunit contact, the phalloidin molecule must be rotated by roughly 180° around an axis parallel to the filament axis compared to the orientation proposed by Lorenz *et al.* (1993).

Literature Cited

Aebi, U., W. E. Fowler, G. Isenberg, T. D. Pollard, and P. R. Smith. 1981. Crystalline actin sheets: their structure and polymorphism. *J. Cell Biol.* **91:** 340–351.

Bremer, A., R. C. Millonig, R. Sütterlin, A. Engel, T. D. Pollard, and U. Aebi. 1991. The structural basis for the intrinsic disorder of the F-actin filament: the lateral slipping model. *J. Cell Biol.* **115:** 689–703.

Bremer, A., C. Henn, K. N. Goldie, A. Engel, P. R. Smith, and U. Aebi. 1994. Towards atomic interpretation of 3-D reconstructions of F-actin filaments. *J. Mol. Biol.* **242:** 683–700.

Figure 1. Locating the phalloidin-binding site within F-actin filaments by stoichiometric binding of an undeca-gold (Au_{11})-tagged phalloidin derivative (Au_{11}-PHD) to the filaments (A–E), and orientation of the PHD moiety within its F-actin-binding site (F, G). STEM (scanning transmission electron microscope) annular dark-field (ADF) micrographs of (A) a negatively stained (*i.e.*, with 0.75% uranyl formate, pH 4.25) Au_{11}-PHD stabilized F-actin filament stretch; (B) a freeze-dried and unstained PHD stabilized F-actin filament stretch; and (C) a freeze-dried and unstained Au_{11}-PHD stabilized F-actin filament stretch. (D) Same data as in (C) but contrast adjusted (*i.e.*, by top/bottom slicing) to display the highest intensities only, which correspond to single undeca-gold clusters (diameter ~1 nm). The image reveals single gold clusters about every 5.5 nm along the two long-pitch helical strands which are staggered by 2.75 nm (see yellow bars). (E) An averaged and refined 3-D helical reconstruction computed from negatively stained Au_{11}-PHD stabilized F-actin filament stretches (see A) has been surface-rendered to include 100% of its nominal molecular mass. The location of the undeca-gold clusters has been determined from a difference map (*i.e.*, Au_{11}-PHD stabilized F-actin filament reconstruction minus PHD stabilized F-actin filament reconstruction) and visualized by 1-nm-diameter gold spheres. (F) Alignment and overlay of an atomic PHD:F-actin trimer (yellow ribbon; data from Lorenz *et al.*, 1993) on the Au_{11}-PHD:F-actin 3-D reconstruction displayed in (E). Compared to the orientation proposed by Lorenz *et al.* (1993), the PHD molecule was rotated by ~180° about an axis roughly parallel to the filament axis and then replaced by our Au_{11}-PHD derivative (violet CPK with a golden sphere). The experimentally determined Au_{11} density peak is marked by the red dashed contour. (G) On the left, a top view of the atomic Au_{11}-PHD:F-actin trimer as displayed in (F) is shown; on the right, the same F-actin trimer is displayed, but this time with the PHD moiety oriented as proposed by Lorenz *et al.* (1993). In this latter orientation, the Au_{11} cluster collides with an actin monomer near the filament axis (yellow cross). Scale bar, 20 nm (A–C).

Bubb, M. R., J. R. Knutson, D. K. Porter, and E. D. Korn. 1994. Actobindin induces the accumulation of actin dimers that neither nucleate polymerization nor self-associate. *J. Biol. Chem.* **269:** 25592–25597.

Bubb, M. R., I. Spector, A. D. Bershadsk, and E. D. Korn. 1995. Swinholide A is a microfilament disrupting marine toxin that stabilizes actin dimers and severs actin filaments. *J. Biol. Chem.* **270:** 3463–3466.

Carlier, M.-F. 1991. Actin: protein structure and filament dynamics. *J. Biol. Chem.* **266:** 1–4.

Hesterkamp, T., A. G. Weeds, and H. G. Mannherz. 1993. The actin monomers in the ternary gelsolin: 2 actin complex are in an antiparallel orientation. *Eur. J. Biochem.* **218:** 507–513.

Isambert, H., P. Venier, A. Maggs, A. Fattoum, R. Kassab, D. Pantaloni, and M.-F. Carlier. 1995. Flexibility of actin filaments derived from thermal fluctuations. *J. Biol. Chem.* **270:** 11437–11444.

Kabsch, W., H. G. Mannherz, D. Suck, E. Pai, and K. C. Holmes. 1990. Atomic structure of the actin: DNase I complex. *Nature* **347:** 37–44.

Lorenz, M., D. Popp, and K. C. Holmes. 1993. Refinement of the F-actin model against X-ray fiber diffraction data by the use of a directed mutation algorithm. *J. Mol. Biol.* **234:** 826–836.

Mandelkow, E.-M., E. Mandelkow, and R. A. Milligan. 1991. Microtubule dynamics and microtubule caps: a time resolved cryo-electron microscopy study. *J. Cell Biol.* **114:** 977–991.

Millonig, R. C., H. Salvo, and U. Aebi. 1988. Probing actin polymerization by intermolecular crosslinking. *J. Cell Biol.* **106:** 785–796.

Oosawa, F., and S. Askura. 1975. *Thermodynamics of the Polymerization of Proteins.* Academic Press, New York.

Orlova, A., and E. H. Egelman. 1993. A conformational change in the actin subunit can change the flexibility of the actin filament. *J. Mol. Biol.* **232:** 334–341.

Smith, P. R., W. E. Fowler, T. D. Pollard, and U. Aebi. 1983. Structure of the actin molecule determined from electron micrographs of crystalline actin sheets with a tentative alignment of the molecule in the actin filament. *J. Mol. Biol.* **167:** 641–660.

Steinmetz, M., K. N. Goldie, and U. Aebi. 1997a. A correlative analysis of actin filament assembly, structure and dynamics. *J. Cell Biol.* **138:** 559–574.

Steinmetz, M., D. Stoffler, A. Hoenger, A. Bremer, and U. Aebi. 1997b. Actin filaments: From cell biology to atomic detail. *J. Struct. Biol.* **119:** 295–320.

Steinmetz, M. O., D. Stoffler, S. A. Müller, W. Jahn, B. Wolpensinger, K. N. Goldie, A. Engel, H. Faulstich, and U. Aebi. 1998. Evaluating atomic models of F-actin with an undecagold-tagged phalloidin derivative. *J. Mol. Biol.* **276:** 1–6.

Discussion

GUNDERSEN: Have you looked to see if any actin-binding proteins affect the distribution of lower or upper dimers?

AEBI: No, we have not done this yet. Using the cross-linking assay, we are currently looking for this type of protein in extracts from various cells. Although it is present, I cannot provide quantitative data at this stage. As I indicated, other researchers have shown that the gelsolin segment 2 acts *in vitro* to stabilize the lower dimer rather than an F-actin oligomer (Hesterkamp *et al.,* 1993. *Eur J. Biochem.* 218: 507–513).

CHISHOLM: There is at least one proposal for an alternative structure of actin filaments. Could the lower dimers that you see relate to that alternative structure?

AEBI: We were very interested in this structure proposed by Schutt and co-workers (1995. *Biophys. J.* **69:** 12S–18S) where actin in a 1:1 complex with profilin forms a "ribbon." Schutt *et al.* believe that this ribbon is structurally related to the helical actin filament and may undergo a transition into the helical actin filament. In fact, Schutt *et al.* think that such ribbon-to-helix transitions may have a more specific application in a new theory of force generation (see also Schutt *et al.,* 1997. *Nat. Struct. Biol.* **4:** 169–172). We have looked very carefully and find that these ribbons cannot be made out of lower dimers. However, we can assemble actin into a type of folded ribbons which are built of this dimer (Millonig *et al.,* 1988. *J. Cell Biol.* **106:** 785–796; see also Steinmetz *et al.,* 1997. *J. Struct. Biol* 119:295–320). In fact, by solving the 3-D structure of our Gd^{3+}-induced crystalline actin sheets by electron crystallography we have built an atomic model of the lower dimer that I did not present here (Steinmetz *et al.,* 1998. *J. Mol. Biol.* **278:** 703–711).

ALLEN: The reduced fluorescence at steady state for calcium and/or EGTA compared to magnesium that you described for polymerization—was that due to a reduced critical concentration?

AEBI: There is a very small, reproducible attenuation of the fluorescence at steady state for Ca^{2+}- and EGTA-actin compared to Mg^{2+}-actin, but I don't know what this means. It could be a quenching effect.

ALLEN: Does that imply differences in structure that are smaller than your resolution?

AEBI: There are probably significant structural differences between Mg-G-actin and Ca-G-actin. However, once actin has switched from its G- to its F-conformation, the structural differences between Mg-F-actin and Ca-F-actin appear to be rather small so that we cannot depict them at 25 Å resolution.

ALLEN: Is there any evidence that the divalent cations influence the generation of the lower dimer?

AEBI: Yes, as we have previously shown (Millonig *et al.,* 1988. *J. Cell Biol.* **106:** 785–796), cations do influence generation of the lower dimer. For example, when actin is polymerized

with 2 m*M* $CaCl_2$, the yield of lower dimer is significantly larger than when the same polymerization is conducted in the presence of 2 m*M* $MgCl_2$. Also, when Mg-G-actin is polymerized with phalloidin alone (*i.e.*, without addition of any salt), we cannot detect any significant amounts of lower dimer during the course of polymerization (Steinmetz *et al.*, 1997. *J. Cell Biol.* 138: 559–574). The lower dimer, which is not a filament dimer, has been observed by many techniques. There are conditions (*e.g.*, polymerization with 50 m*M* $CaCl_2$) where more than 95% of the actin forms lower dimer during the first few seconds. In fact, under sheet- or ribbon-forming conditions, 100% of the actin forms lower dimer.

ALLEN: Is there any possibility that the gold-labeled phalloidin has a different structure from native phalloidin?

AEBI: According to all our criteria, coupling of undeca-gold (Au_{11}) to phalloidin *via* a 17-Å-long spacer has no significant effect on its structure or conformation. The spacer is long enough so that the binding affinity of phalloidin to actin is only an order of magnitude lower than that of native phalloidin but short enough that you do not get significant delocalization of the undeca-gold cluster. I would guess from the strength of its binding that it is in the right position. However, as I showed during my talk, for the undeca-gold cluster to be in the right position (*i.e.*, as revealed by 3-D reconstruction of Au_{11}-phalloidin labeled F-actin filaments), we had to rotate the phalloidin moiety by roughly 180° about an axis parallel to the filament axis compared to the orientation proposed by Lorenz *et al.* (1993. *J. Mol. Biol.* **234:** 826–836).

BORISY: In your introduction you describe actin as a passive molecule. The researchers in this area who study actin dynamics, as opposed to structure, might disagree. They might point out that actin polymerization is the driving force for cell protrusion, listerial locomotion, and other viral and bacterial particles, and for acrosome extension.

AEBI: I agree with you. It is just a matter of the right semantics. I use "passive" to refer to the actin-myosin type of force generation. You can generate a lot of force through polymerization in non-muscle cells. Murray Stewart will show in his talk that motility can be generated without motors.

Reference: *Biol. Bull.* **194:** 342–344. (June, 1998)

Amoeboid Motility Without Actin: Insights into the Molecular Mechanism of Locomotion Using the Major Sperm Protein (MSP) of Nematodes

MURRAY STEWART*, THOMAS M. ROBERTS†, JOSEPH E. ITALIANO, JR.†, KAREN L. KING†, ROBIN HAMMEL†, G. PARATHASATHY†, TIMOTHY L. BULLOCK*, AIRLEE J. MCCOY*, HELEN KENT*, ANDREAS HAAF*, AND DAVID NEUHAUS*

** Medical Research Council Laboratory of Molecular Biology, Hills Road, Cambridge, CB2 2QH, England; and †Department of Biological Science, Florida State University, Tallahassee, Florida, 32306*

Because of their simplicity and specialization, nematode sperm are a powerful system with which to investigate the molecular principles underlying amoeboid cell motility (reviewed by Theriot, 1996; Roberts and Stewart, 1995, 1997). These sperm crawl at up to 50 μm/min by extending a pseudopod packed with bundles of cytoskeletal filaments that can be observed *in vivo* by light microscopy (Roberts and Stewart, 1995, 1997).

The cytoskeleton in nematode sperm is based on the 14-kD major sperm protein (MSP) rather than on actin. Locomotion in this system is generated by the vectorial assembly of MSP filaments and their bundling into macrofibers, and motor proteins do not appear to play a major role (Roberts and Stewart, 1997). MSP filaments are formed *in vivo* and *in vitro* from two helical subfilaments that wrap around one another. Because of their unique structure, MSP filaments have an inherent capacity to form bundles (King *et al.*, 1994; Stewart *et al.*, 1994), and this is crucial to their function. In solution, MSP forms stable dimers (Haaf *et al.*, 1996), and X-ray crystallography shows that the MSP polypeptide chain fold is based on a seven-stranded beta sandwich that closely resembles the fold of immunoglobulins, and especially that of the bacterial chaperonin PapD (Bullock *et al.*, 1996a, b). X-ray crystallography has also been used to determine the structure of the helices of the MSP dimers; these dimers are indistinguishable from the subfilaments from which filaments are constructed (Bullock *et al.*, 1998). Because these filaments have no overall polarity, pseudopod extension is not likely to be generated by motor proteins acting on MSP filaments (Bullock *et al.*, 1998). To investigate the polymerization and bundling of MSP in greater detail, we constructed an *in vitro* motility system in which MSP filament assembly and bundling is able to move membrane vesicles (Italiano *et al.*, 1996). With this system we have shown that locomotion requires a soluble factor in addition to MSP, membrane vesicles derived from the sperm plasma membrane, and ATP. Hydrostatic pressure reduces the rate of polymerization *in vitro* and inhibits whole sperm locomotion. When the pressure is increased, fewer MSP filaments are produced more slowly (Roberts *et al.*, 1998). Moreover, these pressure studies show that MSP polymerization is restricted to the immediate vicinity of the membrane vesicle and appears to require the generation of an activated species, MSP*, through the interaction of a soluble factor with a protein associated with the vesicle surface (Roberts *et al.*, 1998).

The way in which nematode sperm crawl is closely analogous to the way in which actin-based amoeboid cells move over substrates. Moreover, the *in vitro* MSP-based motility system closely resembles the "comet tails" by which *Listeria* generates motility (see Theriot, 1996). Therefore, both actin-based and MSP-based systems probably generate protrusive force by similar mecha-

This paper was originally presented at a workshop titled *The Cytoskeleton: Mechanical, Physical, and Biological Interactions.* The workshop, which was held at the Marine Biological Laboratory, Woods Hole, Massachusetts, from 15–17 November 1996, was sponsored by the Center for Advanced Studies in the Space Life Sciences at MBL and funded by the National Aeronautics and Space Administration under Cooperative Agreement NCC 2-896.

nisms. Our studies on the molecular mechanism of nematode sperm amoeboid motility have emphasized the contributions made by vectorial assembly and filament bundling, and it is likely that these features also make a major contribution to motility in actin-based systems (Roberts and Stewart, 1995, 1997).

Acknowledgments

Supported in part by NIH GM 29994.

Literature Cited

Bullock, T. L., S. Parthasarathy, H. M. Kent, T. M. Roberts, and M. Stewart. 1996a. New crystal forms of the motile major sperm protein (MSP) of *Ascaris suum*. *J. Struct. Biol.* **116:** 432–437.

Bullock, T. L., T. M. Roberts, and M. Stewart. 1996b. 2.5 Å resolution crystal structure of the motile major sperm protein (MSP) of *Ascaris suum*. *J. Mol. Biol.* **263:** 284–296.

Bullock, T. L., A. J. McCoy, H. M. Kent, T. M. Roberts, and M. Stewart. 1998. Structural basis for amoeboid motility in nematode sperm. *Nature Struct. Biol.* **5:** 184–189.

Haaf, A., P. J. G. Butler, T. M. Roberts, D. Neuhaus, and M. Stewart. 1996. The motile major sperm protein (MSP) from *Ascaris suum* is a symmetric dimer in solution. *J. Mol. Biol.* **260:** 251–260.

Italiano, J. E., T. M. Roberts, M. Stewart, and C. A. Fontana. 1996. Reconstitution *in vitro* of the motile apparatus from the amoeboid sperm of *Ascaris*: direct evidence that filament assembly and bundling move membranes. *Cell.* **84:** 105–114.

King, K. L., M. Stewart, and T. M. Roberts. 1994. Supramolecular assemblies of the *Ascaris suum* major sperm protein associated with amoeboid cell motility. *J. Cell Sci.* **107:** 631–638.

Roberts, T. M., and M. Stewart. 1995. Nematode sperm locomotion. *Curr. Opin. Cell Biol.* **7:** 13–17.

Roberts, T. M., and M. Stewart. 1997. Nematode sperm: amoeboid movement without actin. *Trends Cell Biol.* **7:** 368–373.

Roberts, T. M., E. D. Salmon, and M. Stewart. 1998. Hydrostatic pressure shows that lamellipodial motility in *Ascaris* sperm requires membrane-associated major sperm protein filament nucleation and elongation. *J. Cell Biol.* **140:** 367–375.

Stewart, M., K. L. King, and T. M. Roberts. 1994. The motile major sperm protein of *Ascaris suum* forms filaments constructed from two helical subfilaments. *J. Mol. Biol.* **243:** 60–71.

Theriot, J. 1996. Worm sperm and advances in cell locomotion. *Cell* **84:** 1–4.

Discussion

CHISHOLM: If there is filament assembly at the front end of the cell, and disassembly at the rear end, how do the monomers get back to the front end?

STEWART: I think part of it can get back by diffusion. In addition, the amount of the MSP (major sperm protein) that is assembled at any one time will be as great as it seems when observed by light microscopy—probably about 10%–20% of the total MSP. We think that enough diffusion can occur by recycling alone, because the cells themselves are moderately small. At the moment, we haven't been forced to postulate something more involved than that.

CHISHOLM: Even when the sperm move at the rate that you stated—35 μm/min?

STEWART: They move at 35 μm/min, but this means that a small amount of protein is just being added at the front each time and taken off at the back. I think this can probably be done without having to transport the protein.

WADE: Is there a relationship between the membrane and the fiber in terms of phosphorylation?

STEWART: The generation of fibers in our *in vitro* system is very intimately associated with that membrane vesicle. When we use pH jump experiments *in vivo*, we can see that growth of new material is very intimately associated with the leading edge of the pseudopod. I am somewhat skeptical of a mechanism that invokes a molecule on the membrane taking in individual monomers and polymerizing them. I think that the process is mediated by a molecule present on that vesicle, possibly transmembrane integrin-like molecules or receptor-like molecules. We do not have smoking-gun evidence for that. We do have a 70-Kd protein on a gel, but no sequence. A protein like that could interact through GTP-binding proteins to stimulate polymerization in the immediate vicinity. At the moment we can't distinguish between these two possible models.

SCHWARTZ: Does this 70-Kd protein bind GTP?

STEWART: We are currently trying to test that by isolating large quantities of protein to determine the direct binding of GTP.

JANMEY: Could you comment on the hydrostatic pressure experiments? Are you suggesting that the effect of the hydrostatic pressure might be the release of water associated with the polymerization process? Do you think there is something involved in the protrusion of the vesicle at the edge of the bundle?

STEWART: Most proteins have a large shell of water that is bound moderately strongly around the surface. Some people refer to this as crystallizing around the surface. The volume of these bound water molecules is significantly lower than that of free water in solution. When two molecules come together and form a polymer, they usually do so by combining hydrophobic

faces with the exclusion of water. A large amount of water is released in the process, resulting in a transient volume change. That would be a way of rectifying a thermal-action-type mechanism. There are a whole series of variations on these mechanisms that George Oster has proposed. Another aspect may be important: if a transient volume change occurs in this immediate vicinity—particularly since the rest of the cytoplasm is a gel—then this volume change might be used to move the membrane more readily, making it easier to put in another molecule. I do not want to give you the impression that we have definitive data to support this suggestion. But the idea would be consistent with the pressure effect; increasing pressure would tend to decrease effects that rely on positive volume changes, according to Le Chatelier's Principle. We can actually stop the cells moving with about 70 atm pressure. This pressure is rather low compared to an actin-based system.

TAYLOR: I am still confused about the energy source. Actin treadmilling is possible because that is coupled to ATP hydrolysis.

STEWART: You are correct. We can't say how ATP is being used by MSP.

TAYLOR: The subunits have to diffuse to the front of the cell, which would result in a higher concentration at the back of the cell. This suggests a linkage. What is the G-protein doing? Is it in the GTP-bound state and released later?

STEWART: Even though this is cell biology, it is unwise to violate the first and second laws of thermodynamics. It is reassuring that energy must be added to make this system work. What puzzles me is how the energy is actually being utilized. We have not been able to show that it is directly utilized by the MSP. There is no evidence of any nucleotide binding to MSP. We suspect that the energy is being used in the form of ATP, but it could also be used in the form of GTP with an exchange system in the cell. Recent evidence indicates that GTP, not ATP, is used in nuclear cytoplasmic transport. The energy could be used by the G-protein cycling between two states. A large number of G-proteins and motor proteins switch between two states. It is not clear whether these proteins produce motion via such a process. It could be that the G-protein is switching and activating some other protein that could be breaking the MSP dimer into monomers. We do not know whether the filaments are made up from MSP monomers or dimers. Although our prejudice is dimers, the energy could be used to form monomers. The energy could be used to phosphorylate MSP, which would result in a small cap of phosphorylated MSP. We have been trying to demonstrate phosphorylation of MSP but without success, although this may be due to technical difficulties. Less than 0.1% of the MSP is actually in the fibers, even though these are seen everywhere in our *in vitro* assay. The bottom line is, we don't know exactly where the energy is being used, but at least it is being used, which is better than violating the laws of thermodynamics.

GUNDERSEN: A treadmilling model suggests a polar filament. Are these filaments polar?

STEWART: We don't know. We know that the MSP exists as a dimer in solution, with a twofold rotation axis. Based on symmetry, the filament will lack polarity if that twofold rotation axis is perpendicular to the axis of the filament. In the models that we have generated from our C2 crystals, this twofold axis is close to being perpendicular to the axis of the filament. Therefore, it may well be that the filaments have no net polarity. If that was the case it would be very difficult to imagine how motor proteins might function, because they wouldn't know which way to go. We still have to establish that fact. It looks as if there is not much polarity here; however, there may be polarity, but it's just below the level of detection.

GUNDERSEN: How does the cell determine to start the filament at its front end? Do you know of any treatments that disorganize this?

STEWART: Acids disorganize this. There is a chemotactic response. These cells know where the eggs are and crawl after them, but this has not been characterized in molecular terms. When sperm are removed from the vas deferens, they begin to crawl after treatment with a PBS extract of the vas deferens. The mechanism of activation is not understood, although it is probably chemotactic. Once cell movement is established, it appears that there are molecules present in the leading edge that maintain the movement.

Reference: *Biol. Bull.* **194:** 345–347. (June, 1998)

Role of Ponticulin in Pseudopod Dynamics, Cell-Cell Adhesion, and Mechanical Stability of an Amoeboid Membrane Skeleton

ELIZABETH J. LUNA[1], ANNE L. HITT[1], DAMON SHUTT[2], DEBORAH WESSELS[2], DAVID SOLL[2], PAT JAY[3], CHRIS HUG[3], ELLIOT L. ELSON[3], ALEX VESLEY[4], GREGORY P. DOWNEY[4], MICHAEL WANG[5], STEVEN M. BLOCK[5], WADE SIGURDSON[6], AND FREDERICK SACHS[6]

[1] University of Massachusetts Medical Center, Worcester Foundation Campus, 222 Maple Ave, Shrewsbury, Massachusetts 01545; [2] Department of Biological Sciences, University of Iowa, Iowa City, Iowa 52242; [3] Department of Biological Chemistry, Washington University School of Medicine, St. Louis, Missouri 63110; [4] Department of Medicine, University of Toronto, Ontario, ON M5S 1A8, Canada; [5] Department of Molecular Biology, Princeton University, Princeton, New Jersey 08544; and [6] Department of Biophysics, SUNY at Buffalo, Buffalo, New York 14214

Ponticulin is a transmembrane protein that constitutes the major high-affinity link between the actin cytoskeleton and the plasma membrane of the soil amoeba *Dictyostelium discoideum*. As one of the few membrane proteins known to contain both a cytoplasmic domain and a glycosyl anchor, ponticulin accounts for about 90% of the actin-binding and actin-nucleating activities of isolated plasma membranes.

The function of ponticulin *in vivo* is being deduced by analyzing mutant amoebae in which the single-copy ponticulin gene has been disrupted by homologous recombination. These cells are deficient in high-affinity actin-membrane binding, as determined by co-sedimentation of actin and membrane vesicles from freshly broken cells, electron microscopic analysis, and *in vitro* assays of actin-membrane binding and membrane-mediated actin nucleation. Thus ponticulin's role as a major link between the actin cytoskeleton and the plasma membrane has been confirmed both *in vivo* and *in vitro*. Because ponticulin is an integral membrane protein, its absence is expected to affect only the integrity of the membrane attachment to the underlying cortex, and not the extent of cross-linking between cortical actin filaments. This property distinguishes ponticulin from other well-known proteins of the membrane skeleton, such as spectrin, dystrophin, and filamin, all of which are structural elements of both the membrane skeleton and the subjacent cortical cytoskeleton.

The role of ponticulin, and thus of the membrane skeleton, in cell behaviors is being explored in a number of functional and mechanical assays. Cells lacking ponticulin are less efficient in migrating up chemotactic gradients, apparently due to a loss of positional control of both anterior and lateral pseudopods. The pseudopods in ponticulin-minus cells appear to form normally; but during cell movement they undergo dramatic shifts in position relative to the substratum, a behavior never seen in cells containing ponticulin.

Despite their reduced chemotactic ability, ponticulin-minus cells can aggregate sooner than the parental strain during starvation-induced multicellular development. Solution changes that enhance cell adhesiveness cause all cells, mutant and wild type, to aggregate with the faster, mutant time course. These observations suggest that one role of the ponticulin-based membrane skeleton is to modulate or to negatively regulate cell-cell adhesion.

This paper was originally presented at a workshop titled *The Cytoskeleton: Mechanical, Physical, and Biological Interactions*. The workshop, which was held at the Marine Biological Laboratory, Woods Hole, Massachusetts, from 15–17 November 1996, was sponsored by the Center for Advanced Studies in the Space Life Sciences at MBL and funded by the National Aeronautics and Space Administration under Cooperative Agreement NCC 2-896.

In other experiments, we have been analyzing the role of the membrane skeleton during cellular resistance to various types of mechanical stress. Parental cells and mutants lacking ponticulin have been prodded with glass rods and forced through Nucleopore filters, techniques that apply forces downward into the cell and parallel to the membrane-cortex boundary, respectively. Outward forces have been applied by using optical trapping of membrane-attached silica beads and suction pipetting. To date, no significant difference between parental and mutant cells has been observed. Given the large differences in membrane-actin attachment observed in cells lacking ponticulin, these results suggest that all of the mechanical techniques employed measure structural properties of the cell cortex, rather than of the membrane skeleton. Ongoing research is focused on understanding the function and regulation of ponticulin during cell movement and adhesion and on the identification of structural and functional analogs of ponticulin in higher organisms.

Bibliography

Chia, C. P., A. L. Hitt, and E. J. Luna. 1991. Direct binding of F-actin to ponticulin, an integral membrane glycoprotein. *Cell Motil. Cytoskel.* **18:** 164–179.

Chia, C. P., A. Shariff., S. A. Savage, and E. J. Luna. 1993. The integral membrane protein, ponticulin, acts as a monomer in nucleating actin assembly. *J. Cell Biol.* **120:** 909–922.

Hitt, A. L., J. H. Hartwig, and E. J. Luna. 1994. Ponticulin is the major high-affinity link between the plasma membrane and the cortical actin network in *Dictyostelium. J. Cell Biol.* **126:** 1433–1444.

Hitt, A. L., T. H. Lu, and E. J. Luna. 1994. Ponticulin is an atypical membrane protein. *J. Cell Biol.* **126:** 1421–1431.

Shariff, A., and E. J. Luna. 1990. *Dictyostelium discoideum* plasma membranes contain an actin-nucleating activity that requires ponticulin, an integral membrane glycoprotein. *J. Cell Biol.* **110:** 681–692.

Shutt, D. C., D. Wessels, K. Wagenknecht, A. Chandrasekhar, A. Hitt, E. J. Luna, and D. R. Soll. 1995. Ponticulin plays a role in the positional stabilization of pseudopods. *J. Cell Biol.* **131:** 1495–1506.

Wuestehube, L. J., and E. J. Luna. 1987. F-actin binds to the cytoplasmic surface of ponticulin, a 17kD glycoprotein from *Dictyostelium discoideum* plasma membranes. *J. Cell Biol.* **105:** 1741–1751.

Discussion

CHISHOLM: You suggested that your assay measures cortical rather than membrane effects.

LUNA: That is one possibility; there may be others.

CHISHOLM: In that case, the idea would be that ponticulin anchors the cortex to the membrane. Do you think that the cortex and membrane are floating completely independently of each other?

LUNA: We are trying to figure out what is slipping. It appears that the whole pseudopod is moving when we look at the images of the flying pseudopods with DIC (differential interference contrast). It does not appear that the membrane is moving over the pseudopod. Our studies have been hampered because we do not have an extracellular epitope unique to ponticulin. Antibodies to the outside of the protein react with carbohydrates that are present on most glycosylated membrane proteins. Dr. Anne Hitt has generated transfected cells that we hope will express Myc-tagged ponticulin, with Myc on the outside surface. We plan to follow what is moving by using fluorescence quenching or activation of fluorescence using antibodies directed against that epitope. Poking the cell would not give us an effect, because this measures cortical stiffness. I would have thought that pushing the cells through filters might have made a difference. I'm really perplexed by the action of the suction pipette. If anything would pull a membrane away from an underlying cortex, I would have thought that it would be the suction pipette, although the high forces generated by this technique may well be acting on deeper cortical structures.

CHISHOLM: Is there really 10%–20% of the nucleation activity remaining or is that just the limit of the assay?

LUNA: This is hard to measure reproducibly. Maybe another way of looking at it is to say that what we have left might be the *Dictyostelium* equivalent of the big sticks in Don Ingber's model for tensegrity. Perhaps what we have done is remove some of the small elastic moduli that are right at the membrane. Maybe the big sticks are what matter when pulling vectorially and for a relatively long time frame, relative to the cell's ability to remodel its cortex. However, this is obviously all speculation.

INGBER: You are basically correct. The magnetic twisting technique used by our group produces results that are different from those produced by techniques that non-specifically poke or pull on the surface membrane, such as those that you tried. In the same cells, we have used our method, and then Eliot Elson's group used their poking technique, which only measures cortical stiffness. Since we can obtain different measurements with different receptors in the same cell, we know that we are measuring membrane stiffness with metabolic receptor ligands and internal cytoskeletal stiffness with integrin ligands. You presented human analogies of how cells move with "elbows," and perhaps that is what is going on. There may be different structurally stabilized microdomains that are coordinated by some orienting scaffolding provided by the membrane. An analogy would be if my arm system was working but wasn't coordinated with my nervous system. You need a way to measure the mechanics of the microdomains of the cortex rather than the

whole cell, to determine whether each has its own frequencies of movement, which act as one integrated system after insertion of your protein.

LUNA: If we can use the anti-Myc antibody as a probe of the external domain of ponticulin, and also perform comparative confocal microscopy with this antibody and with our existing antibody against the cytoplasmic domain, we can find out by difference where ponticulin is bound to the actin cytoskeleton. This is what we really want to know—where it is functional, not just where it is.

JANMEY: By analogy with the membrane of the red blood cell, you may expect that if you detach the lipid bilayer from any kind of protein meshwork you will either increase the flickering motion of the lipid bilayer or you will increase the amount of surface area in contact with a smooth substrate. In the *Dictyostelium* mutants, have you ever looked at the number of cells that are in close contact with a glass surface?

LUNA: There is a lot of wobble in the front end of these cells: they look really sloppy when they move, compared to the normal cells. I do not know if that is because the front end of the cell has a series of pseudopods and extensions that are just not well organized. However, we never see extensive smooth areas with rounded contours that I would call "blebs." Looking at the percentage of surface area in close contact with a glass surface is a really good idea, but we haven't tried it yet.

Reference: *Biol. Bull.* **194:** 348–350. (June, 1998)

Cell Locomotion and Focal Adhesions Are Regulated by the Mechanical Properties of the Substrate

ROBERT J. PELHAM JR. AND YU-LI WANG

Department of Physiology, University of Massachusetts Medical School, Worcester Foundation Campus, 222 Maple Ave, Shrewsbury, Massachusetts 01545

Cell-cell adhesion and cell-substrate adhesion are important interactions that modulate intracellular signaling pathways, as well as various cellular events from gene expression to cell locomotion (Juliano and Haskill, 1993). The full response to adhesion seems to involve not only the cross-linking of integrins but also mechanical input through these receptors (Craig and Johnson, 1996; Wang *et al.*, 1993; Ingber, 1993; Chrzanowska-Wodnika and Burridge, 1996; Choquet *et al.*, 1997). To explore this possibility, we have examined the motility and cytoskeletal organization of NRK epithelial cells and 3T3 fibroblasts cultured on substrates having varying mechanical properties (Pelham and Wang, 1997).

Flexible, optically clear substrates were prepared by covalently linking type I collagen to polyacrylamide sheets. The flexibility of the substrate was manipulated by maintaining the acrylamide concentration at 10% while varying the bis-acrylamide contents between 0.03% and 0.26%. In this manner, we were able to maintain a constant chemical environment regardless of substrate flexibility. The Young's Modulus of the substrate, determined by measuring the extent of stretching in response to known applied forces, showed a 13-fold difference between sheets of 0.26% and 0.03% bis-acrylamide. When probed microscopically with a calibrated microneedle, the substrates showed 16-fold difference in compliance ($\sim 7.3 \times 10^{-7}$ newtons/μm *versus* $\sim 4.6 \times 10^{-8}$ newtons/μm).

On more rigid substrates, both NRK epithelial cells and 3T3 fibroblasts were well spread and appeared indistinguishable from those cultured on glass or plastic surfaces. However, when cells were cultured on increasingly flexible substrates, there was a corresponding change in morphology: NRK cells became less well spread and irregularly shaped. Highly active, phase-dense ruffles appeared, not only along the periphery, but on the ventral surface of the cell. 3T3 cells lost most of their stress fibers and became increasingly spindle-shaped, with a concomitant increase in the rate of locomotion.

These observations suggest that cellular motility is regulated according to the mechanical properties of the surrounding environment. The initial response likely originates at cell-substrate adhesion sites, where mechanical input can be translated into intracellular signals. Indeed, microinjection of fluorescent vinculin showed that focal adhesions in cells cultured on highly flexible substrates become irregular in morphology and much less stable than those in cells on rigid substrates. Similar differences were found when cells were immunostained for phosphotyrosine. In addition, immunoblots with anti-phosphotyrosine Py20 antibody indicated that the overall extent of phosphorylation on flexible substrates was greatly reduced in comparison with that of cells plated on plastic or rigid surfaces.

Treatment of cells on flexible substrates with phenylarsine oxide, a tyrosine phosphatase inhibitor, resulted in the formation of normal focal adhesions. Conversely, treatment of cells on firm substrates with myosin II/myosin light chain kinase inhibitors 2,3-butanedione monoxime or KT5926 caused large focal adhesions to disappear, as on flexible substrates. These results are consistent with the idea that cells use an actin-myosin-based push-pull mechanism at their integrin receptors to probe their mechanical environment. The responses then affect the level of tyrosine phosphorylation on the cytoplasmic side, which in turn regulates the formation and stability of focal adhesions and possibly motile activities (Fig. 1).

The present results, together with a growing list of observations suggesting that cells can respond to both the

This paper was originally presented at a workshop titled *The Cytoskeleton: Mechanical, Physical, and Biological Interactions.* The workshop, which was held at the Marine Biological Laboratory, Woods Hole, Massachusetts, from 15–17 November 1996, was sponsored by the Center for Advanced Studies in the Space Life Sciences at MBL and funded by the National Aeronautics and Space Administration under Cooperative Agreement NCC 2-896.

magnitude and distribution of adhesion forces, strongly indicate that communication through physical signals is as important as communication mediated by chemical messengers. Physiologically, the mechanical properties of a cell's surrounding environment could be modulated by the synthesis or degradation of ECM proteins, by the movement of surrounding cells, or by the pressure or fluid shear of blood flow. Such events are likely to occur frequently during embryonic development and wound healing, and may play an important role in guiding cell movement and regulating cell functions.

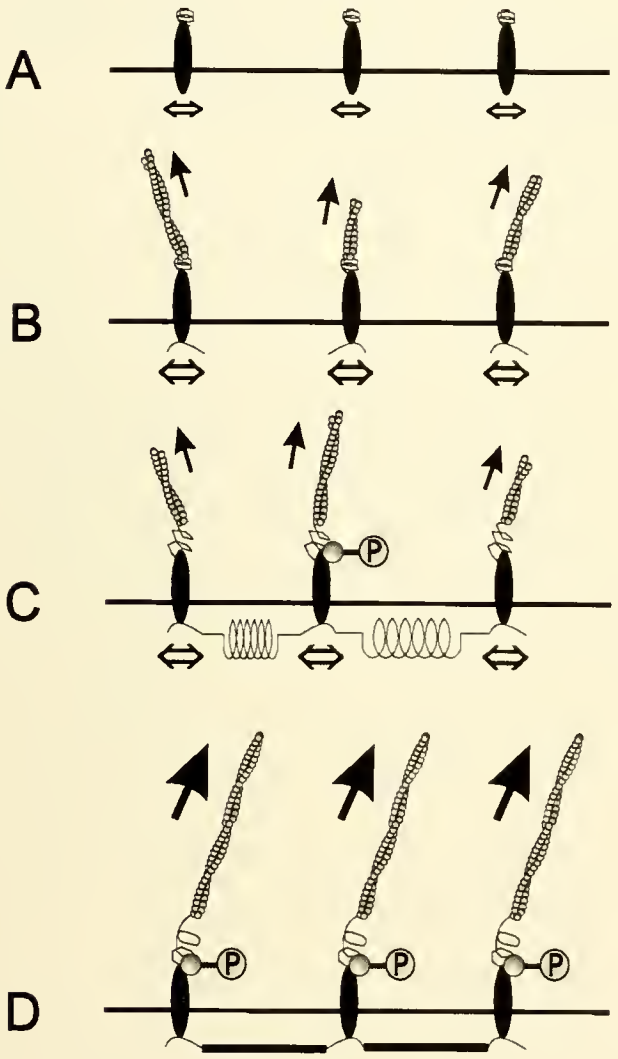

Figure 1. Model of anchorage-tension mediated signal transduction. We propose that integrins diffuse along the plasma membrane (A) and, on their cytoplasmic phase, are associated with a tension-sensitive signal transduction complex. The occupancy of extracellular matrix binding sites causes the actin-myosin cytoskeleton to associate with integrins and start to exert motile or tensile forces (B and C, small solid arrows). However, with soluble extracellular matrix components, (B, represented by thin line), or on highly flexible substrates (C, represented by spring), the association with the cytoskeleton is unstable, and the force on the tension-sensitive complex is weak. Thus, the tension-sensitive complex remains in a largely unphosphorylated state. When integrins become anchored to rigid substrates (D, represented by thick rod), the tension on the cytoplasmic phase increases (D, large solid arrows), causing activation of an associated tyrosine kinase. Tyrosine phosphorylation of proteins, in turn, leads to the amplification and stabilization of cytoskeletal association and multiple downstream responses. The mobility of integrins is indicated with hollow arrows.

Literature Cited

Choquet, D., D. P. Felsenfeld, and M. P. Sheetz. 1997. Extracellular matrix rigidity causes strengthening of integrin-cytoskeletal linkages. *Cell* **88:** 39–48.

Chrzanowska-Wodnika, M., and K. Burridge. 1996. Rho-stimulated contractility drives the formation of stress fibers and focal adhesions. *J. Cell Biol.* **133:** 1403–1415.

Craig, S. W., and R. P. Johnson. 1996. Assembly of focal adhesions: progress, paradigms, and portents. *Curr. Opin. Cell Biol.* **8:** 74–85.

Ingber, D. E. 1993. Cellular tensegrity: defining new rules of biological design that govern the cytoskeleton. *J. Cell Sci.* **104:** 613–627.

Juliano, R. L., and S. Haskill. 1993. Signal transduction from the extracellular matrix. *J. Cell Biol.* **120:** 577–585.

Pelham, R. J. Jr., and Y-l. Wang. 1997. Cell locomotion and focal adhesions are regulated by substrate flexibility. *Proc. Natl. Acad. Sci. USA* **94:** 13661–13665.

Wang, N., J. P. Butler, and D. E. Ingber. 1993. Mechanotransduction across the cell surface and through the cytoskeleton. *Science* **260:** 1124–1127.

Discussion

SCHWARTZ: Does phenyl arsine oxide inhibit ruffling and motility?

WANG: Yes.

SCHWARTZ: If cells are on a matrix that has a gradient of rigidity, can you predict which end the cells should move towards?

WANG: That is a good question. If a cell is on the rigid side of the matrix, I can argue that when the pseudopod stretches into the softer side of the matrix it will become more active, whereas the pseudopod in the rigid side will become less active. This predicted increase in activity should direct or stabilize the pseudopod, driving the cell to the soft flexible end of the substrate. Conversely, I can turn the argument around. The cell could use a temporal sensing mechanism similar to bacterial

chemotaxis. When motile cells that are on the flexible side of the matrix enter the rigid side, they could become immobilized. This would lead to accumulation of cells on the rigid side of the matrix. The answer to your question must come from the experiments.

BRUINSMA: You said that the cell is sensing the shear modulus of the polyacrylamide gel. (Wang: That is correct). If you destroy the cross linking in the polyacrylamide gel to form a very viscous polymer melt, what would happen? Do the cells only sense the shear modulus, or do they perhaps also sense regions of different viscosity?

WANG: Based on our current observations, where we have been looking at a rigid surface, I cannot predict what will happen with changes in viscosity. We haven't looked at cells plated on a viscous fluid, which is what it would take to answer your question. The experiment that you suggest is a good one. This will require a substrate where we can modulate flexibility to follow cell behavior from the entirely cross linked to the fluid state.

Reference: *Biol. Bull.* **194:** 351–353. (June, 1998)

Theoretical Models of Viscoelasticity of Actin Solutions and the Actin Cortex

F. C. MACKINTOSH

Department of Physics and Biophysics Research Division, University of Michigan, Ann Arbor, Michigan 48109-1120

The elastic response of plant and animal cells depends on a network of protein filaments that form the cytoskeleton. This is a complex and highly dynamic composite of filamentous proteins, together with a range of accessory proteins for initiating and terminating polymerization, introducing cross-links, and forming lateral arrays or bundles of filaments (Alberts, 1994). A principal component of this is the actin cortex, which is itself an entangled and cross-linked network of F-actin. This cortex appears to be responsible for the mechanical stability and resistance of eukaryotic cells to external stresses. Coordinated assembly and disassembly of this network in response to cellular signals also appears to play a crucial role in cell locomotion (Stossel, 1994).

The actin cortex, consisting of entangled or cross-linked actin filaments (F-actin), resembles solutions and gels of common synthetic polymers. However, the actin cortex *in vivo*—as well as *in vitro* models of the actin cortex, consisting of solutions of reconstituted F-actin—exhibit unique properties that cannot be accounted for by the well-established models of synthetic polymer gels and solutions (DeGennes, 1979; Doi, 1988). For instance, the elastic moduli (specifically, the shear modulus) of actin networks can be several orders of magnitude larger than for comparable synthetic polymer systems (*e.g.*, at the same concentration). This is a key property of actin networks, as many types of cells must withstand shear stresses as large as 1000 Pa, or even more. Furthermore, the results of several experiments in which different elements of the cytoskeleton were disrupted suggest that the mechanical stability of cells and their elastic resistance to such applied stresses is primarily due to the actin cortex. Thus, the origin of high-shear moduli of the actin cortex poses an important problem for cell biology.

Progress has been made, recently, in defining the unusual rheology (including the elastic shear modulus) of solutions containing actin filaments purified from muscle; and theoretical models have been devised to explain the viscoelastic properties of these systems (MacKintosh, 1995; Isambert, 1996; Krov, 1996; Satcher, 1996). All of these models are based, in part, on the known rigidity of actin filaments, as compared with conventional polymer systems. This rigidity (or semi-flexibility) is characterized by a *persistence length*—the typical length at which thermal fluctuations begin to bend the polymer in different directions. For actin, this length is several micrometers (Gittes, 1993; Ott, 1993). However, rigid constituent filaments do not necessarily produce entangled solutions or gels with increased rigidity. Indeed, increased polymer stiffness can actually *reduce* dramatically the shear modulus of a solution (Isambert, 1996), and this is due to reduced entanglement (Semenov, 1986).

Here, we describe a model that can account for the large shear moduli observed for actin networks. Specifically, we predict a shear modulus

$$G \propto \frac{\kappa^2}{kT}\,\xi^{-5} \propto \frac{\kappa^2}{kT}(ac_A)^{5/2}$$

for densely crosslinked gels, where κ is the filament stiffness, k is Boltzmann's constant, T is the temperature, ξ is the so-called mesh size (or typical spacing between polymers), c_A is the concentration of actin monomers of size a comprising the filaments. For entangled (un-

This paper was originally presented at a workshop titled *The Cytoskeleton: Mechanical, Physical, and Biological Interactions.* The workshop, which was held at the Marine Biological Laboratory, Woods Hole, Massachusetts, from 15–17 November 1996, was sponsored by the Center for Advanced Studies in the Space Life Sciences at MBL and funded by the National Aeronautics and Space Administration under Cooperative Agreement NCC 2-896.

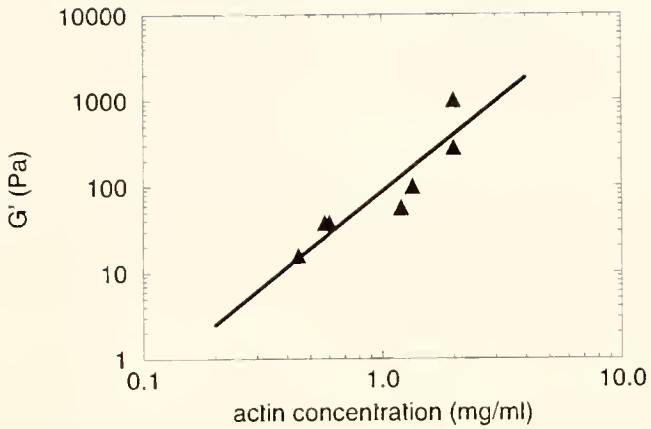

Figure 1. The measured shear elastic modulus G of actin networks as a function of concentration in mg/ml (Janmey, 1991). The predicted scaling of modulus with concentration c_A is shown as the solid line (MacKintosh, 1995). Here, $G \propto c_A^{11/5}$.

crosslinked) filaments, somewhat weaker concentration and filament stiffness dependencies are predicted:

$$G \propto \kappa \left(\frac{\kappa}{kT}\right)^{2/5} (ac_A)^{11/5}.$$

The latter concentration dependence of the shear modulus is in accord with recent experiments on *in vitro* solutions of F-actin (Janmey, 1991); see Figure 1.

We also report on ongoing experimental and theoretical characterizations of local viscoelasticity of actin solutions, as observed with embedded micrometer-size particles. These methods can be used to measure the shear and compression moduli, as well as the dynamics of solutions and gels at the micrometer scale. Small, inert, spherical beads of 0.5 to 5.0 μm diameter are placed in actin and polyacrylamide (used as control) gels. Through sensitive detection (resolution about 1 nm) of the thermal motion of individual beads, over frequencies ranging from 0.1 Hz to 10 kHz, both storage and loss shear moduli can be determined as functions of frequency (Gittes, 1997: Schnurr, 1997).

Literature Cited

Alberts, B., D. Bray, J. Lewis, M. Raff, K. Roberts, and J. D. Watson. 1994. *Molecular Biology of the Cell.* Garland, New York.

DeGennes, P.-G. 1979. *Scaling Concepts in Polymer Physics.* Cornell Univ. Press, Ithaca, NY.

Doi, M., and S. F. Edwards. 1988. *The Theory of Polymer Dynamics.* Clarendon, Oxford.

Gittes, F., B. Mickey, J. Nettleton, and J. Howard. 1993. Flexural rigidity of microtubules and actin filaments measured from thermal fluctuations in shape. *J. Cell Biol.* **120:** 923–934.

Gittes, F., B. Schnurr, P. D. Olmsted, F. C. MacKintosh, and C. F. Schmidt. 1997. Microscopic viscoelasticity: shear moduli of soft materials determined from thermal fluctuations. *Phys. Rev. Lett.* **79:** 3286–3289.

Isambert, H., and A. C. Maggs. 1996. Dynamics and rheology of actin solutions. *Macromolecules* **29:** 1036–1040.

Janmey, P. A., U. Euteneuer, P. Traub, and M. Schliwa. 1991. Viscoelastic properties of vimentin compared with other filamentous biopolymer networks. *J. Cell Biol.* **113:** 155–160.

Kroy, K., and E. Frey. 1996. Force-extension relation and plateau modulus for wormlike chains. *Phys. Rev. Lett.* **77:** 306–309.

MacKintosh, F. C., J. Kas, and P. A. Janmey. 1995. Elasticity of semiflexible biopolymer networks. *Phys. Rev. Lett.* **75:** 4425–8.

Ott, A., M. Magnasco, A. Simon, and A. Libchaber. 1993. Measurement of the persistence length of polymerized actin using fluorescence microscopy. *Phys. Rev. E (Statistical Physics, Plasmas, Fluids, and Related Interdisciplinary Topics)* **48:** R1642–R1645.

Satcher, R. L., and C. F. Dewey. 1996. Theoretical estimates of mechanical properties of the endothelial cell cytoskeleton. *Biophys. J.* **71:** 109–118.

Schnurr, B., F. Gittes, P. D. Olmsted, C. F. Schmidt, and F. C. MacKintosh. 1997. Determining microscopic viscoelasticity in flexible and semiflexible polymer networks from thermal fluctuations. *Macromolecules* **30:** 7781–7792.

Semenov, A. N. 1986. Dynamics of concentrated solutions of rigid-chain polymers, part 1: Brownian motion of persistent macromolecules in isotropic solution. *J. Chem. Soc. Faraday Soc. Trans. 2.* **82:** 317–329.

Stossel, T. P. 1994. The machinery of cell crawling. *Sci. Am.* **271:** 54–63.

Discussion

BOAL: A similar ideal expression for the shear modulus is applied in studies of two-dimensional polymeric nets. The shear is proportional to the density of nodes. But when steric interactions and the self-avoidance of polymers are accounted for, then the proportionality changes from density to the power one to density to the power 1.2 or 1.25. You showed a plot of the shear modulus as a function of density. You did not comment on what the exponent was, or what the scaling factor is. Is it very much different from one?

MACKINTOSH: The change that you mentioned is not quite as dramatic in three dimensions. The scaling of the modulus with concentration for polymer chains in a good solvent in three dimensions, as predicted by established models of flexible polymers, is with a power of about 2.2. Specifically, the shear modulus G should be proportional to $c^{2.2}$. The model I presented predicts an exponent of 2.5 for densely crosslinked networks of filaments such as actin. I mentioned an interesting subtlety about going from cross-linked networks to entangled networks. For conventional (flexible) polymer systems, there is no difference between the two in the scaling exponent with concentration. For systems such as actin, I get an exponent of about $^{11}/_{5}$

= 2.2 if there are no cross-links—*i.e.*, a different exponent from that predicted for cross-linked actin networks. In this case, the power law, not just the amplitude, changes. The figure I showed was for an exponent of $^{11}/_{5}$, the exponent predicted for entangled semiflexible chains such as actin. This apparent qualitative distinction between entangled and crosslinked semiflexible polymers is a subtle point that is not yet well understood. But, I think it is a subtle problem to pursue.

CHIEN: You measure the microviscosity in a dynamic way, but the macro-rheology is done in a static way. Did you also do the dynamic measurement to see how phase angle and viscoelasticity compare with the micro measurements?

MACKINTOSH: Measurements for solutions of this kind by conventional macroscopic rheology techniques, as carried out, for example, by Paul Janmey's group, can be done only for frequencies less than 100 Hz at most. To my knowledge no measurements of any kind have been made for actin above this range, although in principle it can be done with more specialized instruments. The frequency dependence of the shear moduli was studied by the Munich group in the range below 100 Hz. The data were quite limited, but a small increase with frequency was reported. The reported frequency dependence is not inconsistent with the behavior expected for conventional polymer networks (*e.g.*, a power law dependence on frequency with exponent of about 0.5), even though the magnitude of the shear modulus is way off relative to conventional polymers. This is one of the interesting puzzles, for which no one yet seems to have a very good microscopic understanding. Although the origin of elasticity is quite different, the dynamics turn out to be very similar at high frequency. A value for the exponent of 0.7 is distinguishable from conventional systems. Generalization of the model that predicts an increase of the shear modulus with the power 0.5 frequency to semi-flexible systems would predict a power of 0.25. That is still surprising to me.

CHIEN: It is known that with shear the endothelial cell will reorganize its cytoskeletal fibers. In your model, how does the organization affect the shear modulus—for example, alignment of the fibers with flow?

MACKINTOSH: What I have been talking about is the linear response of the network to small strains. The effect you mentioned is one of two things. It is either a nonlinear response (as evidenced by the alignment that results from shearing the network beyond a certain amount), or low-frequency behavior in which the network responds and flows. I did not try to address either of those limits. I only discussed the linear response of the network to small strains and at moderately high frequencies, relative to the effects you mentioned.

STEWART: What you have described seems to be a wonderful explanation in accounting for actin at 1 mg/ml. I was wondering how easily this can be extrapolated to the actin concentrations that might be found in a cell where the free water concentration will be down to 5–10 *M*. Can this be extrapolated to 10–20 mg/ml F-actin?

MACKINTOSH: As you probably know, if you take these networks and concentrate them they form an equilibrium nematic phase of aligned filaments. The reason for this is that the molecular weight in these *in vitro* models is much higher than in the cell. If you break the filaments down to smaller molecular weight, formation of the nematic phase doesn't become a problem, even at elevated concentrations. That is one way of extrapolating our model to higher concentrations while maintaining isotropic networks. The network is also highly dynamic, but that is beyond the scope of our current work where we are simply interested in understanding the basic polymeric-like responses of the networks.

BRIUNSMA: What would happen if you had stiff impurities in your actin system, such as randomly dispersed microtubules? How would the elastic properties of such an inhomogeneous system differ from the homogeneous structure? Could the stiffness that results from the presence of stiff rods of microtubules be magnified elsewhere in the system?

MACKINTOSH: You might imagine that a shear response would result from bending the microtubule filaments. However, if you apply a uniform macroscopic strain to the sample, you get no bending of such inclusions. It may seem counterintuitive, but filaments do not bend when subject to uniform strain. If the strain is not uniform, the response may be nonlinear, since the degree of nonuniformity would itself be an increasing function of strain. Therefore, I would expect a change in the nonlinearities of the response, but not necessarily in the linear response.

Reference: *Biol. Bull.* **194:** 354–357. (June, 1998)

Stabilization and Functional Modulation of Microtubules by Microtubule-Associated Protein 4

H. L. NGUYEN, D. GRUBER, T. MCGRAW, M. P. SHEETZ, AND J. C. BULINSKI

Departments of Anatomy and Cell Biology and Pathology, Columbia University, College of Physicians and Surgeons, New York, New York 10032

Microtubules (MTs) are hollow cytoplasmic fibers that are composed of a dimeric protein called tubulin, as well as several MT-associated proteins (MAPs) bound along their surface. MTs are believed to play important roles in a variety of cellular processes, including mitosis, cell motility, and intracellular vesicle transport. Both *in vitro* and *in vivo*, individual MTs are dynamic; that is, they undergo alternating periods of polymerization and depolymerization from their ends, a process known as dynamic instability. The dynamic behavior of MTs is thought to play an important role both in cell cycle events and in cell differentiation.

MAPs have been postulated to function as *in vivo* regulators of the dynamics and functions of MTs. Based on *in vitro* studies, several MAPs have been classified as assembly-promoting MAPs, because they stimulate MT polymerization. Tau and MAP2 are assembly-promoting MAPs expressed almost exclusively in nervous tissue; MAP4, the subject of our research, is another assembly-promoting MAP of ~210 kDa, which is expressed throughout all tissues of all vertebrate organisms that have been examined. MAP4 is the most abundant non-tubulin component of MTs in proliferating cells and non-neuronal tissues, but it is down-regulated in its expression during neuronal differentiation. Because MAP4 is present along the length of MTs that are performing functions as diverse as organizing and transporting organelles and vesicles in interphase cells, rearranging the MT array and altering MT dynamics for mitosis, changing cell shape, and specifying directional motility, we and others have hypothesized that MAP4 plays roles in the regulation of MT dynamics, MT organization, and MT-based transport processes *in vivo*. In turn MAP4, itself, is subject to regulation as the MT system adapts to changes in the cell cycle or the cell's environment.

To investigate the *in vivo* functions of MAP4, we prepared stably transfected clonal mouse L^{tk-} cell lines expressing either full-length MAP4 (L-MAP4 cells) or its MT-binding domain (L-MTB cells); see Figure 1. Although transfectants showed no dramatic defect in morphology or level of MT polymer, as compared with naïve L^{tk-} cells or L-MOCK cells (transfected with vector alone), MTs in L-MAP4 and L-MTB cells showed greater stability than those in control cells. Stability was monitored by the level of post-translationally detyrosinated α-tubulin and by a quantitative nocodazole-resistance assay. *In vivo*, the MT-binding domain of MAP4 stabilized MTs less potently than full-length MAP4, in contrast to the equivalent efficacy demonstrated previously in studies of *in vitro* MT polymerization. L-MAP4 and L-MTB cells grew significantly more slowly than control cells; this growth inhibition was not due to mitotic arrest or cell death. L-MAP4 and L-MTB cells also exhibited greater tolerance to the MT-depolymerizing agent nocodazole, but not to the MT-polymerizing agent taxol. Results with these transfected cell lines demonstrated that MAP4 and its MT-binding domain are capable of MT stabilization *in vivo*, and that increasing the intracellular level of MAP4 affects cell growth parameters.

The L^{tk-} cell lines we have generated, which inducibly overexpress different levels and domains of MAP4, have allowed us to address further questions about the

This paper was originally presented at a workshop titled *The Cytoskeleton: Mechanical, Physical, and Biological Interactions*. The workshop, which was held at the Marine Biological Laboratory, Woods Hole, Massachusetts, from 15–17 November 1996, was sponsored by the Center for Advanced Studies in the Space Life Sciences at MBL and funded by the National Aeronautics and Space Administration under Cooperative Agreement NCC 2-896.

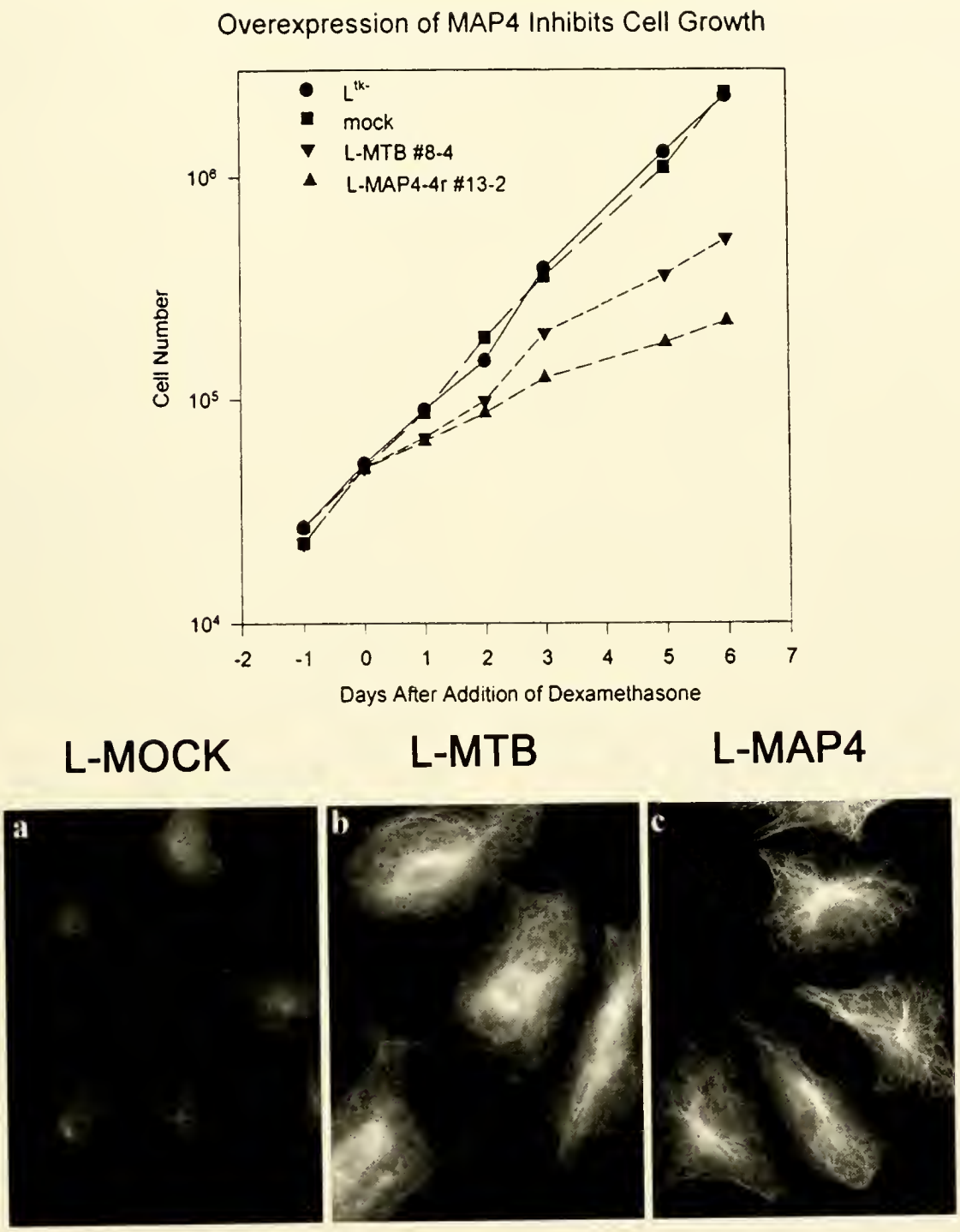

Figure 1. The top portion of the figure shows a growth curve of naiive L^{tk-} cells and those expressing empty plasmid, MAP4-MTB, and full-length MAP4 (called L-MOCK or MOCK, L-MTB #8-4, and L-MAP4-4r #13-2, respectively). The cells expressing MAP4 constructs are clearly inhibited in their growth. Expression of MAP4 in the transfectants can be visualized in the immunofluorescence micrographs shown at the bottom of the figure. Cells were stained with a primate-specific antibody to MAP4; the MAP4-MTB and full-length MAP4 present in L-MTB and L-MAP4 cells respectively display bright microtubule staining, while those cells expressing only plasmid (L-MOCK cells) exhibit only dimmer, diffuse staining with the MAP4 antibody.

functional interactions of MAP4 *in vivo*. For example, we examined the distribution of various organelles in L-MAP4 and L-MTB cells, hoping that any alterations in cytoplasmic organization would suggest binding interactions of MAP4, which we could then test. In these studies, we noted no change in organelle position, cytoplasmic organization, or cell morphology when we labeled L-MAP4 or L-MTB cells with anti-mannose-6-P, wheat germ agglutinin, anti-cytochrome *c*, anti-actin, or anti-vimentin antibodies to localize various organelles.

Previous *in vitro* work had demonstrated that assembly-promoting MAPs can inhibit organellar trafficking along MTs, by sterically hindering kinesin or dynein motility (Lopes and Sheetz, 1993; and unpubl. data, same authors). Thus, we reasoned that, although the steady-state distribution of cellular organelles might appear to be normal, there might nonetheless be defects in *in vivo* organellar trafficking. Such a defect might affect cell growth, perhaps partially explaining the cell growth defects we had measured. Yet, since the deficit in organellar trafficking predicted from *in vitro* work would be a kinetic decrease rather than a permanent blockage, no obvious defect in morphology or organellar distribution would be expected.

We tested this hypothesis by examining *in vivo* organelle motility in L-MAP4 and L-MTB cells under high resolution DIC. In both high- and low-expressing L-MAP4 and L-MTB cells, movements of organelles were severely decreased, as compared with L-MOCK or L^{tk-} cells, and the inhibition was greater in the lines that expressed higher levels of MAP4 or MTB. MTB was almost as effective at inhibiting *in vivo* motility as L-MAP4, but was not as potent as the full-length molecule. We next asked whether *in vivo* vesicle motility was inhibited by the presence of MTB or MAP4, *per se*, or whether the inhibition could be ascribed to MT stabilization alone. To answer this question, we treated cells with several concentrations of the MT stabilizing drug taxol. Our results showed that MT stabilization alone was not nearly as effective as MAP4 or MTB at inhibiting movement.

To elucidate the types of transport events altered by overexpression of MAP4 or MTB, we used fluorescent markers to perform several assays of cell-sorting functions. We noted defects or retardation in endocytosis (monitoring recycling of Cy3-transferrin), LDL uptake and processing (using di-I LDL), and sorting to lysosomes (observing movement and intensity of FITC-dextran). These data suggested that either MAP4 or MTB, coated onto cellular MTs, was capable of inhibiting normal MT-based transport events *in vivo*.

As before, we asked whether the inhibition of cellular activities dependent on organellar motility was attributable to the presence of extra MAP4 or MTB, or whether it was due to the MAP-induced alteration in MT stability. Again, we found that the former possibility was the correct one, because concentrations of taxol that produced equivalent MT stability had virtually no effect on trafficking events. This was particularly exciting to us, for two reasons: First, our results suggested that cells could regulate transport along individual MTs in a single cell by producing high or low local concentrations of MAP4 along different fibers. Moreover, at least one kinase capable of releasing MAP4 from MTs, called MARK (MT-affinity regulating kinase; Drewes *et al.*, 1997), has been described. Alternatively, however, extensive end dynamics, in which MTs depolymerize near their ends and MAP4 rebinds at higher concentration to the shortened MT, could provide a stochastic heterogeneity in MAP4 composition that would be capable of altering transport efficiency on individual MTs. Indeed, heterogeneity in MAP4 level along MTs has been observed previously (Chapin and Bulinski, 1994). The second exciting aspect of these results is that the observed inhibition of transport properties does not appear in the absence of MTs or at the expense of MT dynamics. In most previous studies, by contrast, inhibition of vesicle transport or trafficking events has been measured in the presence of concentrations of nocodazole or taxol that, respectively, completely depolymerize or stabilize MTs. Our data suggest that the control of MAP4 content along an MT is a potential regulator of transport events along that fiber; this is an area of current study in our laboratory.

In summary, we have used a system in which human MAP4 or its MT-binding domain is inducibly overexpressed in a cultured line of rodent cells to investigate the *in vivo* functions of MAP4. We have found that overexpressed MAP4 can contribute to MT stabilization, can affect cell growth parameters, and can inhibit vesicle motility *in vivo*. Our results suggest that alterations in MAP4 expression, or MT stabilization itself, may be physiologically significant mechanisms for altering cell growth and intracellular transport *in vivo*; these MAP4 alterations may occur during the cell growth or development, or during experimental manipulations or pathologies.

Acknowledgments

Portions of this work have been published in Bulinski *et al.* (1997) and Nguyen *et al.* (1997).

Literature Cited

Bulinski, J. C., T. McGraw, D. Gruber, H. L. Nguyen, and M. P. Sheetz. 1997. Overexpression of MAP4 inhibits organelle motility *in vivo*. *J. Cell. Sci.* **110:** 3055–3064.

Chapin, S., and J. C. Bulinski. 1994. Cellular microtubules heterogeneous in their content of MAP4 (210d MAP). *Cell Motil. Cytoskel.* **27:** 133–149.

Drewes, G., A. Ebneth, U. Preuss, E.-M. Mandelkow, and E. Mandelkow. 1997. MARK, a novel family of protein kinases that phos-

phorylate microtubule-associated proteins and trigger microtubule disruption. *Cell* **89:** 297–308.

Lupez, L., and M. P. Sheetz. 1993. Steric inhibition of cytoplasmic-dynein and kinesin motility by MAP2. *Cell Motil. Cytoskel.* **24:** 1–16.

Nguyen, H.-L., S. Chari, D. Gruber, C.-M. Lue, S. J. Chapin, and J. C. Bulinski. 1997. Overexpression of full- or partial-length MA4 stabilizes microtubules and alters cell growth. *J. Cell Sci.* **110:** 281–294.

Discussion

GOLDMAN: Have you looked at the rate of individual organelle translocations, or did you say fewer particles move in cells that overexpress MAP4? A second question is, do any of the motor molecules compete with MAP4 for binding sites on microtubules?

BULINSKI: We don't have the resolution to look at rate of organelle translocations. In answer to your second question, we have not yet done the work to see whether motor molecules compete with MAP4 for those binding sites. Since the microtubule-binding domain of MAP4 is homologous to those of MAP2 and Tau, we can extrapolate from studies done on those MAPs. However, there is a conflict in the literature about this. In the original research, Lopez and Sheetz compared three molecules: full-length MAP2, microtubule-binding domain of MAP2 created by protease digestion, and Tau, which has the same microtubule-binding domain but only a small projection domain. They found virtually no inhibition by Tau or the MAP2 microtubule-binding domain, and concluded that inhibition was due to steric factors. However, these studies were conducted at a very low ratio of MAP to tubulin. There is contradictory evidence in another paper from a different group. However, there are other experiments that show fairly good competition data. In our cells we have a high ratio of MAP to tubulin. We've calculated that if the vesicle is 0.1 μm in diameter and there are 50 MAP4 molecules along a microtubule, the vesicle will run into a number of the MAP4 molecules as it transits along the microtubule. In the cells where we have increased MAP content sevenfold, this movement will be inhibited.

GOLDMAN: Could that account for saltatory movement?

BULINSKI: We cannot see the individual tracks the vesicle moves on *in vivo*. This can be seen in the *in vitro* system where one can measure run time, the time that the vesicle stays on a microtubule before it falls off. The presence of MAP molecules decreases this run time.

LIAO: Are these microtubule-dependent transport events?

BULINSKI: Yes, they are similar to transferrin receptor movements, which have been studied with microtubule active drugs. There was no vesicle movement for the *in vivo* motility when the cells were treated with nocadazole. There was decreased movement when they were treated with vanadate, an inhibitor of dynein. These events are microtubule-based movement.

LUNA: Are there lower levels of MAP4 or other MAPs in the melanocytes? Could this represent an instance of microtubule motors run amok? Controlling access to the number of binding sites through steric hindrance would slightly reduce motility of a vesicle along a microtubule; consequently, you would expect it to cause greater reduction in the ability of the vesicles to serve as multivalent crosslinkers.

BULINSKI: We don't know anything about the level of non-motor MAPs, also called assembly-promoting MAPs or structural MAPs (such as MAP4) in melanocytes. I have discussed MAP4 in my presentation. However, there are other MAPs in these cells that may have the same or similar properties. When we increase the level of one MAP, this doesn't tell us about the other MAPs that are present and may function in the same way. There are also kinases, such as MARK (microtubule-affinity regulating) kinase, that can phosphorylate a single site on MAP4 and remove it from the microtubule. If that is a regulated event, it could help pigment transport or process formation.

ALBRECHT-BUEHLER: Is it cause or effect that is observed, and could it be that you found the handle on the cellular clock?

BULINSKI: The cyclin people think that they have the corner on the market of the cell cycle. I don't think it is likely that cells would normally regulate their growth this way. But it is a possibility, I suppose, that regulation of MAPs on MTs could have an effect on cell growth. I was hoping that significant effects on transport would be produced by stabilizing the microtubules. That would have had implications for how some of these chemotherapeutic drugs work, at concentrations lower than those required to alter mitosis, by altering growth-related transport phenomena. So in some ways I was disappointed that microtubule stability had so little effect.

CHEN: You had no trouble loading LDL or transferrin, which implies that the kinesin pathway works fine, but the dynein does not.

BULINSKI: When we've used iodinated transferrin or iodinated LDL, they both seem to load up fairly rapidly. That suggests that it's not microtubule-based transport, or that it would not be very inhibitory to the dynein motor. But it's still not clear that an hour would be a limiting time frame for a kinetic limitation of transport by MAPs.

Reference: *Biol. Bull.* **194:** 358–360. (June, 1998)

Microtubules as Determinants of Cellular Polarity

GREGG G. GUNDERSEN, GERI KREITZER, TIFFANI COOK, AND GUOJUAN LIAO

Departments of Cell Biology & Anatomy and Pathology, Columbia University, New York, New York 10032

Most eukaryotic cells respond to developmental or environmental stimuli with a change in their polarity. Inherent in this behavior is the ability of the cell to detect the extracellular cue, to transmit a signal across a plasma membrane, and to translate the signal into molecules that can produce the requisite architecture of change. The overall response could be modulated by the expression of new genes, but since many such responses can be generated without new genetic input, this is not an essential feature of the response. We and others have been asking, in particular, how elements of the cytoskeleton, especially microtubules (MTs), contribute to the generation of cellular polarity by responding to environmental cues and transmitting the information to other cellular constituents. Unlike other signal transduction systems (*e.g.*, growth factor activation of gene expression), the one involving MTs mediates a cellular response that reflects the spatial information provided by the original extracellular cue. Individual elements of this MT system will be described, and the possible mechanisms by which cells achieve functional polarity will be discussed.

The biological system that we use in most of our studies is an *in vitro* wound-healing model. Fibroblasts are grown in culture until confluent, and narrow strips of cells are then scraped off the substratum. The cells at the wound edge are initially unpolarized, but in response to wounding, they become polarized with their long axis perpendicular to the wound and with an active leading edge at the portion of the cell facing the cell-free area. As a result of this polarization, the cells are able to move directionally into the wound. This model system has a number of advantages for the study of cell polarization: the cellular response is rapid (on the order of minutes); the cells respond synchronously; and polarization can be measured both structurally (cell shape parameters) and functionally (cell migration parameters).

The state of the MTs in cultured fibroblasts before wounding is typical of the MTs in many nonpolarized cells grown in culture. The MTs radiate from a central focus near the nucleus and fill the cytoplasm without any particular bias to one portion of the cell. By directly imaging MTs in cells that have been microinjected with a fluorescent rhodamine-derivative of tubulin (the subunit protein of MTs), we observed that MTs in cells exhibit dynamic instability (periods of growth and shrinkage, with infrequent and rapid transitions between the two phases), a condition similar to that exhibited by MTs in many nonpolarized cells. The dynamic instability of MTs in nonpolarized cells is thought to contribute to the short half-life of these MTs, which has been reported to be 5–10 min (Saxton *et al.*, 1984; Schulze and Kirschner, 1986).

One of the first responses to wounding is the stabilization of a subset of dynamic MTs. In particular, MTs that are oriented toward the wound become stabilized (Gundersen and Bulinski, 1988; Nagasaki *et al.*, 1992; Gundersen *et al.*, 1994). With a rapid assay to detect MT stabilization, we have observed the formation of stable MTs in as little as 5 min after the addition of growth factors to wounded monolayers of serum-starved cells. This suggests that MTs are poised to respond rapidly to extracellular cues and can function on a time scale that is consistent with many cell behaviors. We are currently trying to identify the factors that are involved in stabilizing the MTs in a localized area and have found that activated rho (a ras-related, small

This paper was originally presented at a workshop titled *The Cytoskeleton: Mechanical, Physical, and Biological Interactions*. The workshop, which was held at the Marine Biological Laboratory, Woods Hole, Massachusetts, from 15–17 November 1996, was sponsored by the Center for Advanced Studies in the Space Life Sciences at MBL and funded by the National Aeronautics and Space Administration under Cooperative Agreement NCC 2-896.

GTPase) is both necessary and sufficient to mediate the selective stabilization of MTs at the wound edge (Cook *et al.*, 1998). We propose that rho is part of a signaling cascade that locally activates or recruits MT stabilizing factors in the leading edge of the cell. We are attempting to identify other factors in this signaling pathway, as well as the factors mediating the MT stabilization.

Shortly after the MTs become stabilized, they accumulate a post-translationally modified form of tubulin known as detyrosinated tubulin. This modification involves the removal of a tyrosine residue from the C-terminus of α-tubulin by a specific tubulin carboxypeptidase, and this occurs predominantly on polymeric tubulin (Hallak *et al.*, 1977). Detyrosination is reversible, and tyrosine is re-added by a second enzyme, tubulin tyrosine ligase (Raybin and Flavin, 1977). This enzyme is active only on soluble tubulin and is responsible for keeping the monomer pool of tubulin completely tyrosinated *in vivo* (Gundersen *et al.*, 1987). In cells, therefore, newly polymerized MTs are composed of tyrosinated tubulin. If these MTs turn over rapidly, they are not significantly detyrosinated by the carboxypeptidase, but if they are stabilized, the carboxypeptidase can generate MTs with high levels of detyrosinated tubulin. A subset of MTs with elevated levels of detyrosinated tubulin (termed Glu MTs after the C-terminal *Glu*tamate residue of detyrosinated tubulin) has been demonstrated; and these MTs are also stable (reviewed in Bulinski and Gundersen, 1991). In the wound-edge cells, the Glu MTs are oriented toward the wound. Thus, the stabilization of MTs at the leading edge of wounded cells generates a polarized array of MTs that are biochemically distinct from the randomly distributed dynamic MTs.

What is the consequence of detyrosinating the tubulin that constitutes stable MTs? Recently, we have found that intermediate filaments, another type of cytoskeletal filament, are preferentially aligned with the Glu MTs in wound-edge cells (Gurland and Gundersen, 1995). This preferential coalignment was disrupted by microinjecting cells with antibodies to detyrosinated tubulin, but not with antibodies to tyrosinated tubulin. More recently, we have found that a nonpolymerizable form of detyrosinated tubulin acts as a dominant negative inhibitor of the intermediate filament-MT interaction when microinjected into cells (Kreitzer and Gundersen, pers. comm). Nonpolymerizable tyrosinated tubulin had no effect when microinjected. Since the nonpolymerizable detyrosinated tubulin remained in the monomer pool and did not affect the endogenous, stable Glu MTs, these results show directly that detyrosination is involved in signaling or in recruiting intermediate filaments onto stable Glu MTs. The functional consequence of the association of intermediate filaments with Glu MT is unknown, but it may rigidify the leading lamella of the cell so that it is able to resist fluid flow or other mechanical stresses. In any case, the paradigm we have established for intermediate filaments may be applicable to other organelles that are known to depend on MTs for their location in cells.

To identify the molecules that specifically recognize detyrosinated tubulin and mediate the interaction between MTs and intermediate filaments, we attempted to block the binding of proteins to MTs with antibodies to detyrosinated or tyrosinated tubulin. We added crude preparations of brain MT-associated proteins (MAPs) or MT motor proteins to MTs composed of a mixture of detyrosinated and tyrosinated tubulin, together with saturating levels of antibody to either detyrosinated or tyrosinated tubulin. Neither antibody significantly affected the binding of brain MAPs. But antibody to detyrosinated tubulin did block the MT-binding of a protein of ~120 kD from the brain MT motor preparations (Liao and Gunderson, 1998). We identified this protein as a kinesin based on its apparent molecular weight, its reactivity with several kinesin antibodies, and its ATP-dependent binding to MTs. To test directly whether kinesin would bind preferentially to detyrosinated tubulin, we examined the binding of a recombinant kinesin head fragment to detyrosinated and tyrosinated tubulin from cultured HeLa cells. We found that there is a 2- to 3-fold tighter binding of kinesin to detyrosinated tubulin (Liao and Gunderson, 1998). These data suggest that detyrosination of tubulin may regulate the interaction of kinesin with MTs, and they support the idea that kinesin may mediate the interaction between MTs and intermediate filaments. We are currently determining whether kinesin moves differently on detyrosinated and tyrosinated tubulin, and whether kinesin can move intermediate filaments along MTs.

In summary, our data support a model in which MTs play a central role in generating cellular polarity. The rapid dynamics of MTs allows MTs to act as a sensor for changes in the extracellular milieu. In a process that we still do not understand completely, dynamic MTs are converted to stabilized MTs in portions of the cell adjacent to the extracellular stimulus. After stabilization, the MTs are modified by post-transitional modification. This step does not alter the three-dimensional information resident in the array of stabilized MTs. Rather, it translates the change in MT dynamics into a biochemical signal that can be interpreted by other cellular constituents. It also ensures that the other cellular constituents are not able to interfere with the process of MT dynamics; *i.e.*, the other cellular constituents are incapable of interacting with tyrosinated tubulin monomer or with newly polymerized MTs. There are at last six other tubulin post-translational modifications, and we suggest that these may also be involved in regulating MT interactions.

Literature Cited

Bulinski, J. C., and G. G. Gundersen. 1991. Stabilization of post-translational modification of microtubules during cellular morphogenesis. *Bioessays* **13:** 285–293.

Cook, T. A., T. Nagasaki, and G. G. Gunderson. 1998. Rho guanosine triphosphatase mediates the selective stabilization of microtubules induced by lysophosphatidic acid. *J. Cell Biol.* **141:** 175–185.

Gundersen, G. G., and J. C. Bulinski. 1988. Selective stabilization of microtubules oriented toward the direction of cell migration. *Proc. Natl. Acad. Sci. USA* **85:** 5946–5950.

Gundersen, G. G., S. Khawaja, and J. C. Bulinski. 1987. Postpolymerization detyrosination of α-tubulin: a mechanism for the subcellular differentiation of microtubules. *J. Cell Biol.* **105:** 251–264.

Gundersen, G. G., I. Kim, and C. J. Chapin. 1994. Induction of stable microtubules in 3T3 fibroblasts by TGF-β and serum. *J. Cell Sci.* **107:** 645–659.

Gurland, G., and G. G. Gundersen. 1995. Stable, detyrosinated microtubules function to localize vimentin intermediate filaments in fibroblasts. *J. Cell Biol.* **131:** 1275–1290.

Hallak, M. E., J. A. Rodriguez, H. S. Barra, and R. Caputto. 1977. Release of tyrosine from tyrosinated tubulin. Some common factors that affect this process and the assembly of tubulin. *FEBS Lett.* **73:** 147–150.

Liao, G., and G. G. Gunderson. 1998. Kinesin is a candidate for crossbridging microtubules and intermediate filaments: selective binding of kinesin to detyrosinated tubulin and vimentin. *J. Biol. Chem.* **273:** 9797–9803.

Nagasaki, T., C. J. Chapin, and G. G. Gundersen. 1992. Distribution of detyrosinated microtubules in motile NRK fibroblasts is rapidly altered upon cell-cell contact: implications for contact inhibition of cell locomotion. *Cell Motil. Cytoskel.* **23:** 45–60.

Raybin, D., and M. Flavin. 1977. Enzyme which specifically adds tyrosine to the alpha chain of tubulin. *Biochemistry* **16:** 2189–2194.

Saxton, W. M., D. L. Stemple, R. J. Leslie, E. D. Salmon, M. Zavortink, and J. R. McIntosh. 1984. Tubulin dynamics in cultured mammalian cells. *J. Cell Biol.* **99:** 2175–2186.

Schulze, E., and M. Kirschner. 1986. Microtubule dynamics in interphase cells. *J. Cell Biol.* **102:** 1020–1031.

Discussion

GOLDMAN: Is there evidence that vimentin binds kinesin?

GUNDERSEN: We have done the experiment and can detect kinesin sedimenting with the intermediate filaments. We haven't done experiments to test whether this reflects a specific interaction, but kinesin doesn't sediment by itself.

GREEN: Several laboratories have published data that the tumor-suppressor gene-product APC binds to microtubules. Recent research has produced some evidence that this association occurs at the leading edge of cells, and it may have something to do with motility. Have you looked at where APC is located with respect to stable microtubules?

GUNDERSEN: Yes, we have, and we are very interested in the mechanism by which the microtubules are selectively stabilized. We have indirect evidence for a specific capping phenomenon: during time-lapse recordings of microtubules in cells, we have observed microtubules to contact something and then stop their dynamics. This may be why stable microtubules behave as they do when diluted. Their ends are no longer active, so they don't lose subunits. We don't know yet what is capping the microtubules. It does not seem to be APC. James Nelson has provided us with an antibody to APC, and we have colocalized APC with Glu microtubules in a number of different cell types. We have not seen a correspondence between APC staining and the ends of Glu microtubules.

TAYLOR: How big is the kinesin that you were using to show binding to the intermediate filament?

GUNDERSEN: I believe it was 110 kDa. It is the major kinesin in our crude motor preparations.

TAYLOR: But that's the whole molecule.

GUNDERSEN: Yes. It appears that the kinesin heavy chain is behaving this way.

TAYLOR: With something else attached to the bottom of that heavy chain?

GUNDERSEN: I don't know. The recombinant head alone binds differentially to Glu and Tyr tubulin. Thus, I don't think we need to invoke a light chain or some other associated molecule to account for the difference in binding to Glu and Tyr tubulin. We do not know, at this point, whether kinesin heavy chain interacts with intermediate filaments or whether it's a light chain or some other associated subunit that is responsible. We are looking into this question.

Reference: *Biol. Bull.* **194:** 361–363. (June, 1998)

Intermediate Filament Cytoskeletal System: Dynamic and Mechanical Properties

R. D. GOLDMAN, S. CLEMENT, S. KHUON, R. MOIR, A. TREJO-SKALLI, T. SPANN, AND M. YOON

Department of Cell and Molecular Biology, Northwestern University Medical School, 303 E. Chicago Avenue, Chicago, Illinois 60611

Intermediate filaments (IF) are major cytoskeletal constituents of animal cells. For many years they were thought to be the most stable of all of the different cytoskeletal systems. Recently, however, IF have been shown to be in a state of dynamic equilibrium in growing cells. In fibroblasts and epithelial cells, this has been demonstrated *in vivo* by the finding that microinjected, soluble vimentin and keratin subunits are incorporated into endogenous IF (Vikstrom *et al.*, 1989; Miller *et al.*, 1991). Other experiments involving fluorescence recovery after photobleaching (FRAP) have demonstrated the existence of a steady-state equilibrium between polymerized IF and their subunits *in vivo* (Vikstrom *et al.*, 1992). Furthermore, the exchange between IF subunits and their polymers appears to be regulated by phosphorylation catalyzed by different kinases and dephosphorylation catalyzed by phosphatases (Eriksson *et al.*, 1992). Recently, we have exploited this equilibrium state *in vivo* through the use of mimetic peptides that are known to both drive vimentin IF disassembly and to inhibit subunit polymerization into IF at 1:1 molar ratios *in vitro*. The sequence of these peptides is derived from the helix 1A initiation domain of the central rod region of either keratin or vimentin. The same 1A peptide carrying a single point mutation has no obvious effect on vimentin IF assembly *in vitro* up to a 10-fold molar excess. We have also shown that there are no detectable effects of the wild-type peptide on either the stability or polymerization of microtubules and actin at 3–5 molar excesses *in vitro*. When these peptides are injected into live cells containing vimentin IF, they rapidly induce the disassembly of IF networks. This disassembly of IF *in vivo* is accompanied by dramatic changes in cell shape and mechanical properties. More specifically, cells lose their asymmetric shapes within 15–45 min as they are transformed into a round shape. Under these conditions, cell-substrate adhesions are lost and there is an induction of microtubule and microfilament disassembly. The rounded cells exhibit active blebbing for short time intervals, but within 4–5 h they have respread into their normal shapes and have reestablished their cell-substrate contacts. These latter changes are coincident with the reassembly of IF, microtubule, and microfilament networks. An important control for these experiments has involved the microinjection of the mutant peptide at the same concentrations. The results demonstrate no significant changes in IF assembly, cell shape, or microtubules and microfilaments (Goldman *et al.*, 1996).

We have also carried out numerous additional controls to make certain that the peptides are primarily targeting IF. One of these controls has involved treatment of 3T3 cells with colchicine to depolymerize microtubules. Thirty minutes after the addition of colchicine, microtubules are not detected, and many IF remain extended from the nuclear region to the cell surface. If the 1A peptide is injected into these cells, the effect on cell shape and on actin-microfilaments appears to be the same as in untreated cells. Therefore, the effects on cell shape do not depend on polymerized microtubules. The 1A peptide has also been injected into fibroblasts derived from vimentin knockout mice. These cells contain no detectable IF, but they do contain extensive arrays of microtubules and mi-

This paper was originally presented at a workshop titled *The Cytoskeleton: Mechanical, Physical, and Biological Interactions.* The workshop, which was held at the Marine Biological Laboratory, Woods Hole, Massachusetts, from 15–17 November 1996, was sponsored by the Center for Advanced Studies in the Space Life Sciences at MBL and funded by the National Aeronautics and Space Administration under Cooperative Agreement NCC 2-896.

crofilaments. When the peptide is injected, no changes in cell morphology are detected, and the microtubule and microfilament systems remained unperturbed. All of these experimental observations indicate that the peptide-induced disruption is specific for IF and has no obvious effects on microtubules and microfilaments. Therefore, in growing cells containing IF, the induction of their disassembly leads to alterations in the stability of the other major cytoskeletal components and a dramatic loss of cellular mechanical properties and shape. These observations could be in part due to IF associated proteins (IFAPs) that form bridges between IF and other cytoskeletal components. For example, BPAG1n/dystonin and plectin both have actin binding domains as well as IF binding domains (for review see Chou *et al.*, 1997).

It has been suggested that the injection of these 1A peptides *in vivo* might lead to toxic side effects due to the sudden release of large amounts of small oligomers and monomers of vimentin. This does not appear to be the case. For example, in 3T3 cells we have calculated that molar ratios of 1:20 (peptide:vimentin) *in vivo* are very effective in disassembling the IF network, altering cell shape and microtubule/microfilament assembly (Goldman *et al.*, 1996). At this concentration, we are quite certain that the IF network disassembles into large oligomeric complexes that should not have a significant deleterious effect on overall cell physiology. This is also indicated by the fact that cells treated with the peptide fully recover within a few hours. In contrast, it has also been demonstrated that the perturbation of the normal organization of IF networks by a variety of different agents does not have similar effects on cell shape and cytoskeletal integrity. These include the reorganization of IF following the disassembly of microtubules with inhibitors such as colchicine, the microinjection of IF antibodies and protein kinase A, and following heat shock (for discussion see Goldman *et al.*, 1997). However, these treatments do not specifically disassemble IF networks; rather they appear to induce the relocation of existing polymerized IF. The latter changes do not mimic the profound changes in IF assembly states that occur following peptide injection. Based on these considerations, we feel that the 1A peptide is a reliable probe for studying the functions of IF *in vivo*.

Acknowledgments

This work is supported by the NIGMS.

Literature Cited

Chou, Y. -H., O. Skalli, and R. D. Goldman. 1997. Intermediate filaments and cytoplasmic networking: new connections and more functions. *Curr. Opin. Cell Biol.* **9:** 49–53.

Eriksson, J. E., D. L. Brautigan, R. Vallee, J. Olmsted, H. Fujiki, and R. D. Goldman. 1992. Cytoskeletal integrity in interphase cells requires protein phosphatase activity. *Proc. Nat. Acad. Sci. USA* **89:** 11093–11097.

Goldman, R. D., S. Khuon, Y.-H. Chou, P. Opal, and P. M. Steinert. 1996. The function of intermediate filaments in cell shape and cytoskeletal integrity. *J. Cell Biol.* **134:** 971–983.

Miller, R. K., K. Vikstrom, and R. D. Goldman. 1991. Keratin incorporation into intermediate filament networks is a rapid process. *J. Cell Biol.* **113:** 843–855.

Vikstrom, K. L., G. G. Borisy, and R. D. Goldman. 1989. Dynamic aspects of intermediate filament networks in BHK-21 cells. *Proc. Nat. Acad. Sci. USA* **86:** 549–553.

Vikstrom, K. L., S. S. Lim, R. D. Goldman, and G. G. Borisy. 1992. Steady state dynamics of intermediate filament networks. *J. Cell Biol.* **118:** 121–129.

Discussion

GREEN: What are the differences in mechanical properties between keratin filaments and type III filaments? Can we distinguish differences in mechanical properties in the bundles *versus* individual keratin filaments?

GOLDMAN: Paul Janmey is just beginning those experiments. I can tell you one interesting preliminary finding. When we inject the 1A peptide into an epithelial cell, like a PTK cell which normally does not move, the cells round up. All focal adhesions disappear and the cells migrate numerous cell diameters to another part of the cover slip. It looks as though the motor systems can turn on when we disassemble keratin, and the cells become actively migratory. As the keratin network reassembles, because it is quite reversible, we get a static cell again. These epithelial cells usually grow in little islands and are very stable; consequently, they don't move very much. So it's possible that keratin could be acting as a brake on motility. That's an important function because most tissue cells don't move. In fact, they are terminally differentiated. My guess is that a lot of the dynamic activities that we see, including those of all cytoskeletal systems, are more related to actively growing cells in culture.

FORGACS: At this meeting good evidence has been presented to show that the microtubule and the intermediate filament network interconnect directly. You have shown us that actin and intermediate filaments colocalize. Do you have any evidence that this is more than just colocalization? If they do interact, what would be the culprit for that?

GOLDMAN: One interesting candidate, recently discovered by Brown *et al.* (1995. *Nat. Genetics*, **10:** 301–306) is dystonin.

Mutation in this gene is responsible for *Dystonia musculorum*, a mutation in mice, which is a severe nervous disorder. In a recent paper from Elaine Fuchs' lab (Yang *et al.* 1996. *Cell* **86:** 655–65), BPAG1, a neuronal variant of bullous pemphigoid antigen, is described as the same gene. The gene product has never been isolated, but it has an actin-binding domain and an intermediate filament-binding domain. So there is at least one possible cross-bridging element in addition to plectin. Research presented by Gerhard Wiche and Gary Borisy and others at this meeting show that it is very important to begin looking for interactions among the different cytoskeletal systems.

CHEN: When you inject the peptide, the intermediate filaments disassemble, all the other polymers disassemble, and the cells round up. In contrast, the vimentin-free cells show the opposite reaction. Can you interpret these results?

GOLDMAN: The vimentin-free cells don't have any intermediate filaments, so there's nothing to disassemble. This serves as a control for our peptide experiment. It looks to us as if the cells have a compensatory system which allows them to overexpress other cytoskeletal proteins.

CHEN: Why is that not happening when you depolymerize the intermediate filaments in the normal cells?

GOLDMAN: Because these reactions occur in 30 minutes, and the recovery takes place in a few hours. Everything is already there, and the cell just goes through a rapid reversal.

GUNDERSEN: In previous studies of intermediate filament function, antibodies to intermediate filaments were injected into cells, causing the collapse of the intermediate filaments back toward the nucleus. In these experiments, cell motility was not affected, and the microtubules were fine. In your experiments, when you injected a peptide it disrupted the intermediate filaments, producing all these effects. Why do you think these two experiments give such really disparate results?

GOLDMAN: In our hands antibody injections do not retract all of the intermediate filaments towards the nucleus (unpubl. obs). Approximately 20% to 30% of the intermediate filament population is resistant, even when treated with colchicine or other antimitotic drugs. Perhaps you don't need many filaments to provide appropriate mechanical properties at the periphery of the cell. Furthermore, the IF polymer doesn't appear to change when you inject antibodies; only its organization changes. It is still present in cells. This is very different from the disassembly effects of the peptides.

STEWART: When you disassemble intermediate filaments *in vitro* with your peptide, have you observed them with electron microscopy to see what it looks like?

GOLDMAN: I'll let Peter (Steinert) answer that.

STEINERT: Yes, we have. The filaments basically unravel and fall apart into subfilamentous units.

Reference: *Biol. Bull.* **194:** 364–366. (June, 1998)

Type I Keratin 16 Forms Relatively Unstable Tetrameric Assembly Subunits With Various Type II Keratin Partners: Biochemical Basis and Functional Implications

PIERRE A. COULOMBE, MATTHEW WAWERSIK, RUDOLPH D. PALADINI, AND ERICK NOENSIE

Departments of Biological Chemistry and Dermatology, The Johns Hopkins University School of Medicine, Baltimore, Maryland 21205

Type II keratin 6 (K6) and type I keratins 16 and 17 (K16 and K17) are intermediate-filament (IF) proteins that are induced in wound-edge keratinocytes as early as 4–6 h after injury to skin, either human or mouse. This induction occurs at the expense of the keratin proteins that are normally expressed in differentiating epidermal keratinocytes. Correlated with these changes in protein expression, keratinocytes—for 24 h following injury—undergo major cytoarchitectural alterations that affect their shape, intracellular organization, surface morphology, and adhesion properties. We recently proposed that the intrinsic properties of K16 are compatible with a direct role in "keratinocyte activation" at the wound edge (Paladini *et al.*, 1996). Unlike K14, a related type I keratin that is constitutively expressed in epidermis, we found that K16 forms *unstable* heterotetramer subunits that polymerize into shorter filaments when paired with a variety of type II keratin partners (*e.g.*, K5, K6b, K8). Such properties are of particular interest because it has been shown in a number of studies that the tetramer subunit predominates in the soluble pool of IF subunits in epithelial and nonepithelial cell lines in culture. The tetramer-forming properties of K16 may thus influence its dynamic partitioning between the polymer and soluble pools and, as such, play a key role in determining the overall impact of its presence on the cytoarchitecture of epidermal keratinocytes.

The main objective of this study was to determine the biochemical basis of the unique tetramer-forming properties of K16 as a first step toward a full understanding of its significance in the regulation and function of this keratin. We showed that K16-containing tetramers are not only less stable than K14-containing ones, but also less stable than K17- and K19-containing ones, irrespective of the type II keratin partner used. We exploited the remarkable degree of primary sequence identity between K14 and K16 to construct a series of chimeric K14–K16 cDNAs, obtaining the corresponding proteins in a purified recombinant form and testing them for tetramer formation using anion-exchange chromatography and chemical cross-linking under denaturing buffer conditions. These studies allowed us to define a segment, of about 200 amino acid residues, within the central α-helical rod domain (310 amino acid residues) that is responsible for the difference in stability. Such a finding was expected, as the rod domain has been identified as the main determinant in the assembly of coiled-coil parallel dimer and anti-parallel tetramer subunits. Alignment of the sequences for human K14, K16, K17, and K19 over this 200-residue segment led to the identification of a candidate residue, ^{188}Pro, which is unique to K16 and has properties that are consistent with a local disruption of the α-helical secondary structure. Consistent with this prediction, site-directed

This paper was originally presented at a workshop titled *The Cytoskeleton: Mechanical, Physical, and Biological Interactions.* The workshop, which was held at the Marine Biological Laboratory, Woods Hole, Massachusetts, from 15–17 November 1996, was sponsored by the Center for Advanced Studies in the Space Life Sciences at MBL and funded by the National Aeronautics and Space Administration under Cooperative Agreement NCC 2-896.

mutagenesis revealed that ^{188}Pro accounts quantitatively for the instability of K16-containing heterotetramers under denaturing conditions. Of note, introduction of a proline residue at corresponding positions in K14 (^{186}Val→Pro) and K17 (^{155}Ile→Pro) rendered these keratins K16-like in their tetramer-forming properties. We believe that ^{188}Pro contributes to the properties and functions of K16, either by influencing its partitioning between the soluble and polymer pools in the cytoplasm, or by causing it to enter the assembly pathway as a heterodimer instead of a heterotetramer. In addition, these data provide insights into the assembly-productive conformation of the keratin tetramer, a matter of contention in the literature, as well as into the unique interdependency of type I and type II keratin sequences for their assembly into 10-nm filaments.

Acknowledgments

These studies were supported by grants from the NIH and NSF.

Bibliography

Coulombe, P. A. 1997. Towards a molecular definition of keratinocyte activation after acute injury to stratified epithelia. *Biochem. Biophys. Res. Comm.* **236:** 231–238.

Fuchs, E., and K. Weber. 1994. Intermediate filaments: structure, dynamics, function, and disease. *Ann. Rev. Biochem.* **63:** 345–382.

Heins, S., and U. Aebi. 1994. Making heads and tail of intermediate filament assembly, dynamics, and networks. *Curr. Opin. Cell Biol.* **6:** 25–33.

Paladini, R. D., K. Takahashi, N. S. Bravo, and P. A. Coulombe. 1996. Onset of re-epithelialization after skin injury correlates with a reorganization of keratin filaments in wound edge keratinocytes: defining a potential role for keratin 16. *J. Cell. Biol.* **132:** 381–398.

Discussion

GREEN: In tissues where keratin K16 is expressed at a low level, how much of that is in an insoluble pool in the filament system, and how much is in another type of pool that it is not capable of being incorporated into?

COULOMBE: This is something we really have to look into. From our findings one could predict that the partitioning of K16-containing subunits between the polymer pool and the soluble pool should be different from other epidermal keratins. This issue needs to be formally examined in an appropriate set of experiments.

AEBI: The destabilization of your tetramers by proline 188 in keratin 16 suggests that these tetramers are really N,N-type half-stacked tetramers.

COULOMBE: Yes, I would agree with that. This particular proline mutation could tell us that the type of tetramer conformation you are referring to is dominant. Conversely, this substitution may favor the formation of other tetramer conformations that would have different assembly properties. This may explain why K16 forms relatively short filaments. These issues need to be examined.

AEBI: When you get this overexpression of keratin K16, either in your transfected cells or after wounding, what happens to K1 and K6, which form the heterodimers? Does this also increase?

COULOMBE: Yes, they do go up. It's K16, K17 as type I keratins, as well as K6, a type II keratin. Now we know that if you make K5, K6, K14, K16, and K17 compete for one another under conditions such that the type II are limiting, the one that is left out as type I is 16. The monomer fractions in a wounded keratin site must be looked at to see which keratin is going to be predominant in the soluble pool. That's another issue we need to examine.

GOLDMAN: Can you speculate about what this might mean in terms of cell physiology? What you are proposing is that K16 is almost a keratin poison. It makes shorter, poorly structured filaments, which might increase motility during wound healing. Why go to all this trouble when there are other ways to do this?

COULOMBE: Your work has shown that phosphorylation could produce comparable changes in filament structure. Gregg Gundersen showed data at this meeting that suggest that one might promote such reorganization of keratin filaments in a fashion completely independent of keratin *de novo* synthesis, simply by disrupting the interaction with microtubules. I think that the polymer pool and the unpolymerized pool might have separate functions. If one were to look at the *in vivo* peptide disruption experiment that was performed in your laboratory, I think that a possible mechanism for reorganization of the entire cytoskeleton is that a soluble pool of tremendous size is suddenly created which the cell normally never sees. This causes the other polymer systems to eventually come apart. In my opinion, the application of molecular genetic approaches will reveal that tetramers are binding to all kinds of cellular components.

LUNA: If keratins, or possibly all intermediate filaments, are inherently apolar, how do you get motility? How do you get the kinds of movements that Bob Goldman saw? Are there motors, interactions with microtubules, or is this the kind of collapse of biopolymers that we heard about earlier?

COULOMBE: It's clear that intermediate filaments in general

lack polarity, which likely makes them unsuitable for use as tracks for motor-based translocation. Moreover, they are very convoluted, so it would be very inefficient for the cell to use them as a track for specific transport events.

GREEN: Do we really know that for all of the intermediate filaments?

COULOMBE: Yes, I think so. The only possible polymeric exceptions are neurofilaments, since it features those side arms sticking out. What that means in terms of polarity might depend on the way the subunits are integrated along the filament wall. In terms of the basic character of the intermediate filament fiber, it is an apolar structure because the two dimers come together in antiparallel fashion to form a tetramer.

GOLDMAN: I think the use of the term "collapse" is incorrect. Firstly, it requires energy to move the filaments back, and this takes a long time. They don't collapse; it's not like a rubber band. Secondly, keratin does not respond to colchicine or any other antimitotic drug the way other intermediate filaments do.

STEWART: The fact that you have the two chains antiparallel means that it is possible that the filaments lack polarity. It does not mean that they lack polarity—they can still be quite polar with the chains antiparallel. It is very important to realize that.

ALBRECHT-BUEHLER: A quick comment. I want to remind you that many epithelial cells migrate as groups of 8–10 cells tied together, not as single cells. I showed this in tissue culture years ago. My point is that if you look for migration, you may not find it in the single cells; you may find it in a whole group of cells. Any changes in the keratin and intermediate filaments may be expressed in the group and not in a single cell in the usual way.

COULOMBE: Although I did not talk about migration of PTK_2 cells, your point is well taken. As I mentioned in my presentation, epidermal keratinocytes do migrate into a wound site as a stratified epithelial sheet.

Reference: *Biol. Bull.* **194:** 367–370. (June, 1998)

Structural-Mechanical Integration of Keratin Intermediate Filaments With Cell Peripheral Structures in the Cornified Epidermal Keratinocyte

PETER M. STEINERT

Laboratory of Skin Biology, National Institute of Arthritis and Musculoskeletal and Skin Diseases, NIH, Bethesda, Maryland 20892-2752

The outermost visible layer of the skin consists of terminally differentiated, flattened, dead, cornified cells (squames). These squames consist predominantly of keratin intermediate filaments (KIF) embedded in a matrix of filaggrin, and these are contained within a specialized thickened insoluble cell peripheral structure termed the cornified cell envelope (CE). The primary function of these cells is to provide a barrier against the environment. We are interested in how these components are assembled and integrated, since it now seems that any defect in either component will cause a serious epidermal disorder, generally an ichthyosiform disease.

One approach has been to study the structure of the CE. The CE is a 15–20 nm-thick layer of insoluble protein formed on the inside of the plasma membrane during terminal differentiation in the epidermis (as well as in other stratified squamous epithelia). It constitutes about 10% of the mass of the cornified cell. Its insolubility is largely attributable to cross-linking of certain structural proteins by a series of transglutaminase (TGase) enzymes which form an $N^{\epsilon}(\gamma$-glutamyl)lysine isopeptide bond between the γ-amide sidechain of a donor glutamine residue and the ϵ-NH_2 sidechain group of an acceptor lysine residue. Since this bond cannot be cleaved in nature, the result is an insoluble macromolecular complex. In addition, a series of ω-hydroxy ceramides become attached by ester linkages to the cross-linked proteins on the extracellular surface of the cornified cells. This composite protein-lipid CE structure replaces the plasma membrane, and its integrity is vital for barrier function.

Using limited proteolysis procedures, we have isolated and sequenced large numbers of peptides that contain cross-links, and have addressed such questions as which proteins are involved; which glutamine and lysine residues are used on what parts of the proteins; what is the temporal order of protein deposition; and what is the mechanism of assembly of the CE. Quantitatively, most cross-links are intra- and inter-chain links between loricrin, which is the most abundant CE protein (70%–80%). This protein is unusual in that its content of glycine residues is the highest of any known protein in biology. The glycine sequences are clustered into domains that are thought to be configured as highly flexible loops, interspersed by glutamine and lysine rich domains that are the sites of cross-linking. In addition, some cross-links are between loricrin and representatives of the small proline-rich protein (SPR) class (about 5% of total). Most of these linkages suggest that the SPRs serve as cross-bridging proteins. The SPRs contain more proline than any proteins known in biology, and include least 10 different proteins that are differentially expressed in the epidermis of different body sites. The prolines are distributed among peptide repeats of 8 or 9 residues; the repeats are located in a central domain, and each domain comprises from about 3 (smallest SPR protein) to 23 (largest SPR protein) repeats. These peptide repeats are thought to form a relatively stiff structure. The glutamines and lysines used for cross-linking are located on the head (amino-terminal) and tail

This paper was originally presented at a workshop titled *The Cytoskeleton: Mechanical, Physical, and Biological Interactions.* The workshop, which was held at the Marine Biological Laboratory, Woods Hole, Massachusetts, from 15–17 November 1996, was sponsored by the Center for Advanced Studies in the Space Life Sciences at MBL and funded by the National Aeronautics and Space Administration under Cooperative Agreement NCC 2-896.

(carboxy-terminal) domains of the SPRs. Together, loricrin and the SPRs constitute 85% of the protein mass of the CE of the epidermis. Protein expression data show that loricrin and the SPR proteins are located on the intracellular side of the CE; thus these proteins must have been accumulated onto the CE structure during the last stages of its assembly. Thus the bulk of the CE consists of a "solution" of SPRs in loricrin. Although the total amount of loricrin + SPRs remains constant in the epidermis of different body sites, we find the content of SPRs is highest in the epidermis of the palms and soles, with decreasing amounts in elbows, lips, foreskin, and trunk. This series is correlated with decreasing epidermal thickness and with the relative amount of mechanical stress or trauma that these epidermal sites undergo during their normal function.

This variability in composition is familiar to materials science, wherein variations in the amounts of a minor cross-bridging component can greatly change the mechanical properties of a composite material. We therefore speculate that the differential expression of the SPRs reflects the required biomechanical properties of the epidermis of different body sites.

When the ceramide lipids were removed by mild alkaline hydrolysis, we found that a number of other CE proteins were exposed for immunogold electron microscopy. These proteins presumably represent the innermost components of the CE, corresponding to its initial stages of assembly. By additional proteolysis and sequencing, we have found many cross-links within involucrin and between such proteins as involucrin and desmoplakin, or cystatin α, or envoplakin, or loricrin and SPRs.

Some cross-linking also involved the type II keratins K1, K2e, K5, and K6. Only one lysine residue in these keratin chains was used for cross-linking: it is located in a conserved stretch of sequences in the V1 head domain. This residue is important in two ways. First, in *in vitro* crosslinking reactions, TGase enzymes specifically utilize this lysine residue to cross-link synthetic peptides. Second, we have discovered a family with autosomal dominant non-epidermolytic palmar plantar keratoderma whose affected members have a single point mutation that results in the loss of this residue. The patients have a severe scaling disorder of their palms and soles and of other thickened epidermal sites. When viewed by electron microscopy, the affected cornified cells are highly irregular in shape, and there is an abnormal accumulation and distribution of the lamellar granules that export the lipids. The failed distribution of the lipids is presumably the cause of the hyperkeratosis and scaling phenotype.

Together, these data suggest that CE assembly is initiated at, or near, the site where KIF meet desmosomes. In addition, they suggest that certain proteins can mediate an indirect association between KIF and desmoplakin. Moreover, these studies offer a mechanism by which the KIF cytoskeleton of the cornified cell is mechanically integrated with the CE. We conclude that the terminal differentiation program exploits the existing KIF cytoskeleton-desmosome machinery to build the novel and vital CE barrier structure. Failure to implement proper attachment by cross-linking has resulted in severe mechanical and biological consequences.

Bibliography

Candi, E., E. Tarcsa, J. J. DiGiovanna, J. G. Compton, P. M. Elias, L. N. Marekov, and P. M. Steinert. 1998. Identification of a highly conserved lysine residue on type II keratins which is essential for the structural coordination of keratin intermediate filaments and the cornified cell envelope through isopeptide crosslinking by transglutaminases. *Proc. Natl. Acad. Sci. USA* **95:** 2067–2072.

Hohl, D., U. Lichti, M. L. Turner, D. R. Roop, and P. M. Steinert. 1991. Characterization of human loricrin: structure and function of a new class of epidermal cell envelope proteins. *J. Biol. Chem.* **266:** 6626–6636.

Jarnik, M., T. Kartasova, P. M. Steinert, U. Lichti, and A. C. Steven. 1996. Differential expression and cell envelope incorporation of small proline rich protein 1 in different cornified epithelia. *J. Cell Sci.* **109:** 1381–1391.

Kartasova, T., Y. Kohno, H. Koizumi, S. Osada, N. Huh, U. Lichti, P. M. Steinert, and T. Kuroki. 1996. Sequence and expression patterns of mouse SPR1: correlation of expression with epithelial function. *J. Invest. Dermatol.* **106:** 294–304.

Kimonis, V., J. J. DiGiovanna, J.-M. Yang, S. Z. Doyle, S. J. Bale, and J. G. Compton. 1994. A mutation in the V1 end domain of keratin 1 causing non-epidermolytic palmar-plantar keratoderma. *J. Invest. Dermatol.* **103:** 764–769.

Steinert, P. M., and L. N. Marekov. 1995. The proteins elafin, filaggrin, keratin intermediate filaments, loricrin and SPRs are isodipeptide crosslinked components of the human epidermal cornified cell envelope. *J. Biol. Chem.* **270:** 17702–17711.

Steinert, P. M., and L. N. Marekov. 1997. Involucrin is an important early component in the assembly of the epidermal cornified cell envelope. *J. Biol. Chem.* **272:** 2021–2030.

Steinert, P. M., E. Candi, T. Kartasova, and L. N. Marekov. 1998. Small Proline Rich Proteins are cross-bridging proteins in the cornified cell envelopes of stratified squamous epithelia. *J. Struct. Biol.* (in press).

Steinert, P. M., T. Kartasova, and L. N. Marekov. 1998. Biochemical evidence that the small proline rich proteins and trichohyalin function in epithelia by modulation of the biochemical properties of their cornified cell envelopes. *J. Biol. Chem.* **273:** 11758–11769.

Discussion

COULOMBE: Am I correct that non-epidermal PPK features hyper-proliferation in the basal compartment?

STEINERT: Yes.

COULOMBE: Since the structural defect involved in this disease is a late event, in terms of the differentiation pathways, there must be some means of signaling between suprabasal cells and basal cells in the absence of lysis. Would you care to speculate on this?

STEINERT: I can only speculate. Dr. Peter Elias, a skin biologist and lipid expert, believes that there is a complex interplay between lipid synthesis in these lamellar granules and cell proliferation. He is particularly interested in ceramides, a major lipid component of the lipid envelope, which are known to be second messengers.

GOLDMAN: This is remarkable remodeling of already existing cellular components. The speed at which a cell becomes enucleated, presumably by going through some part of apoptosis, and then reutilizes all of these proteins by cross-linking to become a part of that fortified envelope structure is quite remarkable. Desmosomal components, and keratin, and other normal components are being reorganized into a highly cross-linked structure that bears very little resemblance to desmosomes and other structures in the super basal cells. Can you speculate on how long it takes to go through the process?

STEINERT: On the basis of our studies of cross-linking and immunogold electron microscopy, I believe that we can make intelligent guesses as to how assembly of this complex structure is initiated. We think that this occurs at the site of the desmosome. What probably happens first is association of things like envoplakin and involucrin to the site of the desmosome by cross-linking—more specifically, to the tail of desmoplakin, which extends 100 nm from the main plaque of the desmosome into the cytoplasm. Proteins such as involucrin and envoplakin then form interdesmosomal sheets at the focal points of envelope assembly. This produces a layer of protein in the granular layer of the epidermis. At about this time mayhem breaks loose and everything within the cell is dissolved. This includes all of the cytoplasmic constituents and the plasma membrane. These events are finalized by the addition of loricrin to the existing involucrin-envoplakin scaffold. We do not yet understand when and how the lipid granules, which are of critical importance to both extra- and intracellular lipids, can escape before the whole structure closes down.

GREEN: You mentioned a compromised keratin attachment, but you place more emphasis on the role of the lipid organization problem. Am I correct in presuming that these are two separate functions? If so, what are their related roles for the amino terminus?

STEINERT: I assume you are referring to the amino terminus of desmoplakin? We have no information about its cross-linking to the cell envelope. Perhaps this is buried and may be lost before the envelope is assembled. We have seen only certain desmoplakin sequences near its carboxy terminus, which you have predicted project far into the cytoplasm. However, I want to answer a slightly different question that is important because it bears on what you ask. The amount of keratin cross-linked to the cell envelope represents only about 0.1% of the envelope protein mass. We have calculated what this means in terms of the extent of cross-linking of keratin filaments. Assuming that keratin filaments are 15 nm wide, and assuming a model in which the filaments completely line the intracellular surface of the cell envelope, we calculate about one crosslink per 100 nm of filament length. This is actually a high level, and it suggests that the keratin filament cytoskeleton really gets glued tightly and permanently onto the cell periphery. We have also seen that the amount of keratin cross-linked to the cell envelope of mouse forestomach tissue is about 10 times higher, which is really an incredible amount. This must reflect the biomechanical requirements of a tissue that is subjected to extraordinarily rigorous stresses and trauma. Also, the disease we talk about is autosomal dominant, so we don't know what would happen if both alleles were knocked out—perhaps not a viable fetus. To check this experimentally is of course difficult because, in cell culture, you get upregulation of K5 and K6. A mouse with this lysine residue knocked out in both alleles could be made. We believe that to make only 50% of the cross-links seriously compromises the structural interface between the cytoplasmic keratin filament network and the cell periphery, or the growing cell envelope. It is highly convoluted, which increases the surface area of the cellular connections. Peter Elias hypothesizes that this greater surface area prevents lipids from distributing properly, resulting in decreased barrier function and thus a hyperkeratotic response.

JANMEY: Is the transglutaminase, which crosslinks the proteins together, constitutively active?

STEINERT: Yes the transglutaminase enzymes are very active during the stages when the cell envelope barrier is assembled. The transglutaminase story is complicated. There are a number of different enzymes functioning simultaneously. Some of these enzymes exist in multiple different post-translationally modified forms, each possibly with a different function. What we are trying to unravel now is which enzyme does what. Preliminary data suggest that transglutaminase 3 strongly favors cross-linking of loricrin and SPRs. Apparently one or two forms of trans-

glutaminase 1 are involved in the earlier stages of cross-linking of involucrin and envoplakin to the tails of desmoplakin. We also have data that transglutaminase 1 works synergistically with transglutaminase 3 to cross-link loricrin and SPRs. The studies needed here involve systematic *in vitro* analyses of the preferences of the enzymes for the numerous substrate proteins, and comparisons with the *in vivo* data. If the transglutaminase 1 enzyme is knocked out you get the naturally occurring, autosomal recessive human disease called lamellar ichthyosis. This is a life-threatening disease because it produces a serious loss of skin barrier function. The mouse knockout model results in death of the newborn within 6 hours of birth because of dehydration; that is, there has been complete breakdown of skin barrier function.

BORISY: We are cheered by this presentation. If intermediate filaments have no purpose in life, they now have a purpose after death.

Reference: *Biol. Bull.* **194:** 371–373. (June, 1998)

What Links Laminin-5 to the Keratin Cytoskeleton in Epithelial Cells?

JONATHAN C. R. JONES, OMAR SKALLI, ROBERT D. GOLDMAN, AND SCOTT E. BAKER

Cell and Molecular Biology, Northwestern University Medical School, 303 E. Chicago Avenue, Chicago, Illinois 60611

The extracellular matrix plays an important role in tissue morphogenesis. It does so, in part, by interacting with a family of heterodimeric cell surface receptors called integrins. Indeed, the integrins are considered to play an important role, not only in adhesion of cells to matrix, but also in signal transduction between the matrix and the cells (Hynes, 1992). Signal transduction *via* integrins involves the cytoskeleton and cytoskeleton-associated proteins which bind to the cytoplasmic domain of the integrin subunits.

Our particular interest is in the $\alpha 6\beta 4$ integrin heterodimer. This integrin is unusual because it is involved in keratin intermediate filament (IF)/cell surface anchorage at the site of hemidesmosomes—structures that play an important role in epithelial cell-matrix linkage (Quaranta and Jones, 1991; Jones *et al.*, 1994). Since the major matrix element of the hemidesmosome is the laminin isoform called laminin-5, we have been investigating the molecular links between the keratin cytoskeleton, integrins, and laminin-5 matrix. In the current analyses, we have used FG epithelial cells, derived from a pancreatic tumor.

FG cells characteristically grow in mounds and fail to flatten efficiently onto their substrate. In such cells, keratin intermediate filaments (IFs) are concentrated in the perinuclear region. Furthermore, the IF-associated protein IFAP300 (a relative of plectin and possibly identical to a protein termed HD1) primarily localizes along these keratin bundles. Additionally, $\alpha 6\beta 4$ integrin heterodimers localize in streaks or spots towards the free edges of cells, whereas $\alpha 3\beta 1$ integrin is predominant at the opposed surfaces of adjacent cells; neither integrin shows any obvious interaction with IF. Note that these FG cells express very little, if any, laminin-5, the matrix ligand for both the $\alpha 6\beta 4$ and $\alpha 3\beta 1$ integrin receptors.

We have discovered that we can induce a reorganization of the cytoskeleton of FG cells, as well as an association of IF with integrins, by simply adding rat laminin-5 to the medium in which we grow the FG cells (Baker *et al.*, 1997). When FG cells are plated into this medium, they no longer form mounds, but rapidly adhere and spread onto the substrate. They do so, apparently by "capturing" rat laminin-5 and placing it basally in circles or arcs at areas of cell-substrate interaction. Double-label immunofluorescence microscopy reveals that IFAP300, $\alpha 6\beta 4$ integrin, and $\alpha 3\beta 1$ integrin are all colocalized with the polarized laminin-5, indicating that the FG cells are using these receptors to interact with the exogenously added laminin-5 protein. Concomitantly, $\alpha 6$ integrin undergoes dephosphorylation on serine residue 1041; we are intrigued by the possibility that this event plays a crucial role in mediating subsequent cytoskeleton rearrangement.

Rapid adhesion, induced by laminin-5, can be blocked by antibodies against the $\alpha 3$ integrin subunit. In contrast, although antibodies raised to $\alpha 6$ integrin do not block laminin-5-induced rapid adhesion, they do prevent FG cells from assuming an epithelial-like morphology. This suggests that $\alpha 3\beta 1$ and $\alpha 6\beta 4$ integrins have distinct functions: $\alpha 3\beta 1$ integrin appears to mediate rapid adhesion

This paper was originally presented at a workshop titled *The Cytoskeleton: Mechanical, Physical, and Biological Interactions.* The workshop, which was held at the Marine Biological Laboratory, Woods Hole, Massachusetts, from 15–17 November 1996, was sponsored by the Center for Advanced Studies in the Space Life Sciences at MBL and funded by the National Aeronautics and Space Administration under Cooperative Agreement NCC 2-896.

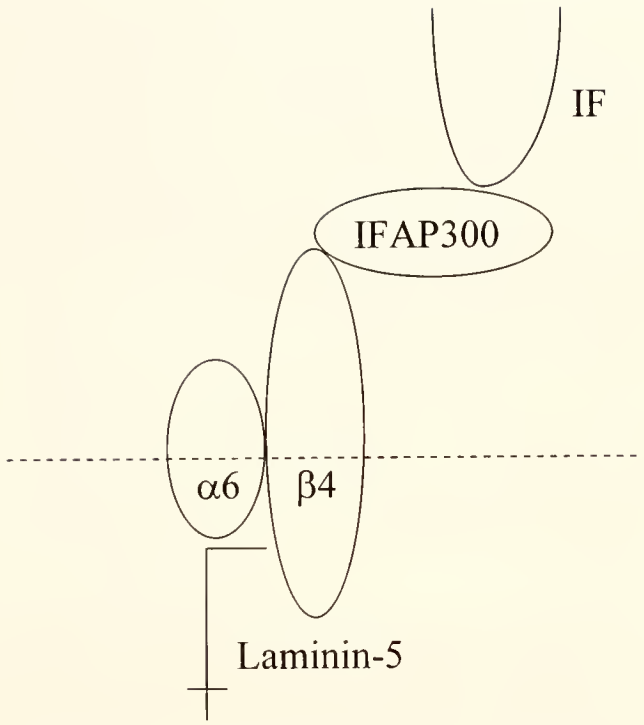

Figure 1. FG cells maintained in a laminin-5-rich medium "capture" the laminin-5 and incorporate it into their extracellular matrix. The molecular interactions of the captured laminin-5 are indicated here. Laminin-5 (represented as an inverted t) binds the extracellular domain of the $\alpha 6\beta 4$ integrin. The cell membrane is represented by a dashed line. In this scheme, IFAP300 interacts with the cytoplasmic domain of the $\beta 4$ integrin subunit and mediates the interaction of the IF cytoskeleton with the cell surface.

of FG cells to laminin-5, whereas $\alpha 6\beta 4$ integrin appears to mediate cell-spreading on the laminin-5 matrix.

In FG cells maintained in laminin-5-containing medium, keratin IF bundles "move" from their perinuclear location and are induced to associate with IFAP300-$\alpha 6\beta 4$/$\alpha 3\beta 1$ integrin complexes along the surface of the cell that is attached to the substratum. Furthermore, the results of coprecipitation experiments suggest that, within IFAP300-integrin complexes, IFAP300 is associated with the $\beta 4$ integrin subunit. Based on our results and on evidence that IFAP300 binds keratin *in vitro* (Skalli *et al.*, 1994), we propose that, when $\alpha 6\beta 4$ integrin binds to its matrix ligand laminin-5, IFs indirectly interact with the cytoplasmic domain of $\alpha 6\beta 4$ integrin at the cell surface. The latter interaction is mediated by IFAP300. In other words, we have identified one potential series of molecules that link laminin-5 indirectly to the IF cytoskeleton. We show this putative interaction diagrammatically in Figure 1.

Acknowledgments

Supported by the NIH.

Literature Cited

Baker, S. E., O. Skalli, R. D. Goldman, and J. C. R. Jones. 1997. Laminin-5 and modulation of keratin cytoskeleton arrangement in FG pancreatic carcinoma cells: involvement of IFAP300 and evidence that laminin-5/cell interactions correlate with a dephosphorylation of α6A integrin. *Cell Motil. Cyto.* **37:** 271–286.

Hynes, R. O. 1992. Integrins: versatility, modulation, and signaling in cell adhesion. *Cell* **69:** 11–25.

Jones, J. C. R., J. Asmuth, S. E. Baker, M. Langhofer, S. I. Roth, and S. B. Hopkinson. 1994. Hemidesmosomes: extracellular matrix/intermediate filament connectors. *Exp. Cell Res.* **213:** 1–11.

Quaranta, V., and J. C. R. Jones. 1991. The internal affairs of an integrin. *Trends Cell Biol.* **1:** 2–4.

Skalli, O., J. C. Jones, R. Gagescu, and R. D. Goldman. 1994. IFAP300 is common to desmosomes and hemidesmosomes and is a possible linker of intermediate filaments to the junctions. *J. Cell Biol.* **125:** 159–170.

Discussion

COULOMBE: Would you agree that the recent work of Elaine Fuchs' lab shows that BAG1 or BP230, the bullous pemphigoid antigen, is involved in anchoring keratin filaments at the cell surface with sites of hemidesmosomes?

JONES: Yes, I think that is true. If you knock out BP230, her pictures would imply that there is a reduction in intermediate filaments at that site in transgenic mouse skin. However, we have used FG cells since they don't possess any of their own BP230. Thus the filament associations that we have described were in the absence of BP230. We speculate that there could be cooperation between IFAP300 and BP230, in that there may be multiple proteins linking intermediate filaments at the cell surface in intact, complete hemidesmosomes.

WICHE: Do you have evidence for direct interaction of $\beta 4$ with IFAP300?

JONES: No.

KOWALCZYK: You showed that when the cells adhere to laminin-5, there was dephosphorylation of $\alpha 6$. Can you get that to

happen in suspension, or do the cells have to adhere to the immobilized substrate?

JONES: We haven't done it in suspension, so I don't know.

BORISY: Could you expand a little bit on the functional significance of that peripheral association of the IFAP300 in the cells grown on laminin-5? What is its function for the cell?

JONES: At the cell periphery, laminin-5 binds to $\alpha 6\beta 4$ integrin, which itself binds to IFAP300, which then is bound to the filament cytoskeleton. Presumably a firmer attachment to substrates is established when this molecular interaction occurs.

BORISY: Is laminin-5 captured from solution?

JONES: We don't think that the laminin-5 has been captured from solution. We think, in fact, that laminin-5 possibly rapidly coats the surface upon which the cell sits. The cell then reorganizes the laminin-5, and pulls it in. What we observe is the initial aspects of pulling in this laminin-5, which is why this protein is located more toward the cell periphery at that time.

Reference: *Biol. Bull.* **194:** 374–377. (June, 1998)

Desmosomes: Integrators of Mechanical Integrity in Tissues

KATHLEEN J. GREEN, ANDREW P. KOWALCZYK, ELAYNE A. BORNSLAEGER, HELENA L. PALKA, AND SUZANNE M. NORVELL

Department of Pathology, Northwestern University Medical School, Chicago, Illinois 60611

The most prominent cell surface attachment site for intermediate filaments (IF) at epithelial cell-cell interfaces is the desmosome (reviewed in Collins and Garrod, 1994; Schmidt *et al.*, 1994; Garrod *et al.*, 1996; Green and Jones, 1996); see Figure 1. By anchoring IF at sites of strong intercellular adhesion, desmosomes create a transcellular network throughout the tissue, and this network is thought to resist forces of mechanical stress. The importance of the IF-cell surface complex has been highlighted by the discovery of mutations in genes encoding IF structural proteins, as well as cell junction proteins that result in blistering diseases of the skin (Steinert and Bale, 1993; Fuchs, 1994; McLean and Lane, 1995). Furthermore, autoimmune antibodies that specifically attack the desmosomal cadherin component of desmosomes result in a family of blistering diseases of the skin and oral cavity known as pemphigus (Stanley, 1995). Thus, these cell-cell adhesive structures and their underlying cytoskeletal attachments are clearly important for the integrity of tissues.

Desmosomes are related to another class of adhesive junctions called adherens junctions, which mediate attachment of the microfilament cytoskeleton to the cell surface (Kowalczyk and Green, 1996). In adherens junctions, classic calcium-dependent cell-cell adhesion molecules (*e.g.*, E-cadherin) are anchored to the actin cytoskeleton through a complex that includes the armadillo protein family member β-catenin. β-catenin binds directly to both E-cadherin and to the actin-associated protein α-catenin. In desmosomes, two classes of desmosomal cadherins, the desmogleins and desmocollins, bind to the β-catenin-related protein called plakoglobin. Unlike classic cadherins, desmogleins and desmocollins have not yet been experimentally demonstrated to be adhesion molecules. To examine the adhesive potential of desmosomal cadherins, we expressed desmogleins and desmocollins along with their associated protein plakoglobin, individually and together, in normally nonadherent L cell fibroblasts. Unlike E-cadherin, desmoglein and desmocollin were unable to confer adhesive properties on these cells in several adhesion assays, including formation of cell-cell aggregates in suspension (Kowalczyk *et al.*, 1996). This may be due to the complexity of cadherin forms, both within a single desmosome and within tissues; it could also reflect the requirement for additional noncadherin molecules in the adhesive complex.

Co-immunoprecipitation of myc-tagged proteins from L cell lines revealed that plakoglobin binds with an unusual 6:1 stoichiometry to desmoglein, whereas it binds with a 1:1 stoichiometry to desmocollin (Kowalczyk *et al.*, 1996). The functional significance of this dramatic difference in stoichiometry is currently unknown; but cells expressing dominant negative mutants of plakoglobin that affect the ratio of binding to desmoglein also exhibit alterations in desmosome structure, consistent with a role in desmosome assembly. Plakoglobin can also bind directly to α-catenin and E-cadherin, which leads us to ask how specificity of filament attachment is achieved during junction assembly. We have demonstrated that α-catenin is not associated with plakoglobin bound to either desmoglein or desmocollin. Along with observations from other labs demonstrating that the α-catenin binding site on plakoglobin overlaps with that for desmosomal cadherins, these data suggest a possible means of achieving cytoskeletal specificity.

Although the mechanism by which the desmosomal cadherin-plakoglobin complex is coupled specifically to

This paper was originally presented at a workshop titled *The Cytoskeleton: Mechanical, Physical, and Biological Interactions.* The workshop, which was held at the Marine Biological Laboratory, Woods Hole, Massachusetts, from 15–17 November 1996, was sponsored by the Center for Advanced Studies in the Space Life Sciences at MBL and funded by the National Aeronautics and Space Administration under Cooperative Agreement NCC 2-896.

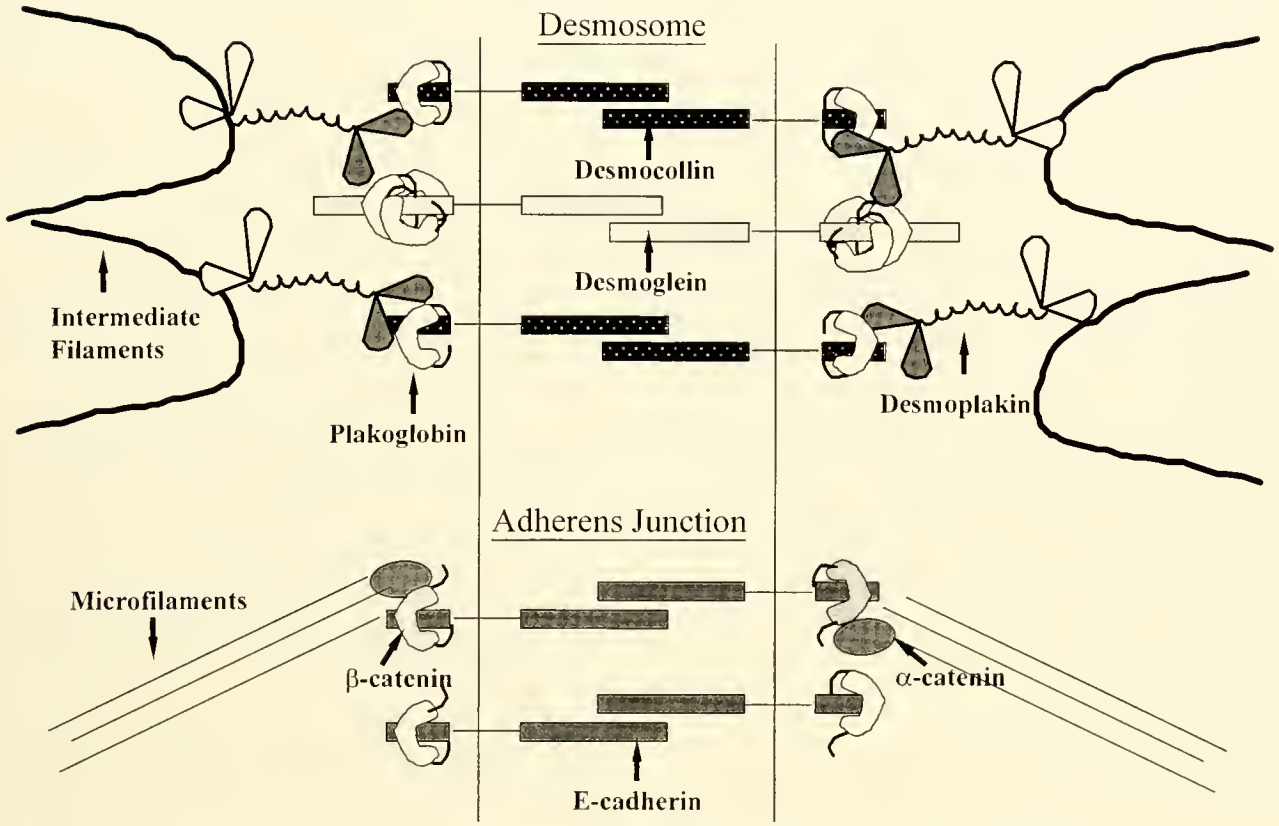

Figure 1. Diagram comparing the major molecular constituents of the two intercellular adhesive junctions found in epithelial tissues. The adhesion molecules in both junctions are members of the larger cadherin family of calcium-dependent cell adhesion molecules. These are desmogleins and desmocollins in the desmosome (top), and classic cadherins, such as E-cadherin, in the adherens junction (bottom). Members of the armadillo gene family, plakoglobin and β-catenin, associate with the cytoplasmic tails of the cadherins and link the membrane molecules to the cytoskeleton through adapter proteins. In the desmosome, desmoplakin is an adapter protein that anchors the cadherin complex specifically to the intermediate filament cytoskeleton, and in the adherens junction α-catenin anchors the cadherin complex specifically to the microfilament cytoskeleton.

the IF cytoskeleton is unknown, desmoplakin (DP) is a putative link. Our previous work demonstrated that the DP C-terminus associates with IF networks, whereas the DP N-terminus is required for incorporation into desmosomes. To directly test whether DP is required to link IF to the desmosome, a dominant negative mutant comprising 70 kDa of the DP N-terminus (DP-NTP) was stably expressed in A-431 epithelial cells (Bohnslaeger *et al.*, 1996). DP-NTP dramatically perturbed endogenous DP, likely by competing for interaction with transmembrane adhesive complexes. Ultrastructural analysis revealed junctional structures that were largely lacking associated IF bundles. Adherens junction components, such as α-catenin and E-cadherin, coassembled into these structures, along with desmosomal components and DP-NTP. This observation suggests that sequences in full length DP, not present in DP-NTP, and perhaps anchorage to the IF cytoskeleton, are required for the normal segregation of desmosomal and classic cadherins during junction assembly.

To begin examining whether DP-NTP could associate directly with the desmosomal cadherin-plakoglobin complex, junction proteins were coexpressed in L cell fibroblasts lacking desmosomal components. In cell lines without DP-NTP, plakoglobin codistributed diffusely along the membrane with desmosomal cadherins. But in cells coexpressing DP-NTP, desmosomal cadherins and plakoglobin were redistributed into punctate structures containing DP-NTP. The similarity of these clusters to nascent junctional plaques was more easily assessed by employing a chimeric molecule containing both the E-cadherin extracellular domain and a desmosomal cadherin cytoplasmic domain. When we expressed an E-cadherin/Dsg1 chimera along with plakoglobin and DP-NTP, plaque-like structures reminiscent of epithelial cell desmosomes were observed at some cell-cell interfaces. Fur-

thermore, an antibody directed against the DP N-terminus co-immunoprecipitated plakoglobin in a complex with DP-NTP, suggesting that plakoglobin provides a link to the cadherin-based desmosomal core. Plakoglobin deletions in which the N- or C-terminus was removed also associated with DP, indicating that the central armadillo repeats of plakoglobin contain sequences that mediate complex formation. Together, these results suggest, not only that desmosomal cadherins and plakoglobin form a complex with DP-NTP, but that DP-NTP is also capable of clustering these transmembrane desmosomal cadherin complexes.

The results summarized here provide insights into the protein-protein interactions required for the assembly of a normal desmosome and for anchoring IF to the desmosomal plaque. Further experiments, currently underway, are targeting dominant negative mutations of desmosomal molecules to the epidermis of transgenic mice. This work is helping define the importance of IF-cell surface attachment for the integrity of complex epithelia, and will provide a framework for understanding the underlying basis of certain inherited skin diseases.

Literature Cited

Bornslaeger, E. B., C. M. Corcoran, T. S. Stappenbeck, and K. J. Green. 1996. Breaking the connection: Displacement of the desmosomal plaque protein desmoplakin from cell-cell interfaces disrupts anchorage of intermediate filament bundles and alters intercellular junction assembly. *J. Cell Biol.* **134:** 985–1002.

Collins, J. E., and D. R. Garrod. 1994. *Molecular Biology of Desmosomes and Hemidesmosomes.* Pp. 1–131. R. G. Landes, Austin, TX.

Fuchs, E. 1994. Intermediate filaments and disease: mutations that cripple cell strength. *J. Cell Biol.* **125:** 511–516.

Garrod, D., M. Chidgey, and A. North. 1996. Desmosomes: differentiation, development, dynamics and disease. *Curr. Opin. Cell Biol.* **8:** 670–678.

Green, K. J., and J. C. R. Jones. 1996. Desmosomes and hemidesmosomes: structure and function of molecular components. *FASEB J.* **10:** 871–881.

Kowalczyk, A. P., and K. J. Green. 1996. The desmosome: a component system for adhesion and intermediate filament attachment. *Curr. Top. Membr.* **43:** 187–209.

Kowalczyk, A. P., J. E. Borgwardt, and K. J. Green. 1996. Analysis of desmosomal cadherin-adhesive function and stoichiometry of desmosomal cadherin-plakoglobin complexes. *J. Invest. Dermatol.* **107:** 293–300.

McLean, W. H. I., and E. B. Lane. 1995. Intermediate filaments in disease. *Curr. Opin. Cell Biol.* **7:** 118–125.

Schmidt, A., H. W. Heid, S. Schafer, U. A. Nuber, R. Zimbelmann, and W. W. Franke. 1994. Desmosomes and cytoskeletal architecture in epithelial differentiation: cell type-specific plaque components and intermediate filament anchorage. *Eur. J. Cell Biol.* **65:** 229–245.

Stanley, J. R. 1995. Autoantibodies against adhesion molecules and structures in blistering skin diseases. *J. Exp. Med.* **181:** 1–4.

Steinert, P. M., and S. J. Bale. 1993. Genetic skin diseases caused by mutations in keratin intermediate filaments. *Trends Genet.* **9:** 280–284.

Discussion

BORISY: Could you explain the terms "armadillo" and "armadillo repeat" for the benefit of our physics colleagues?

GREEN: Armadillo is the name of a gene product involved in the "wingless" signaling pathway that governs the establishment of segment polarity in *Drosophila.* It is now known that the vertebrate proteins β-catenin and plakoglobin are both very similar to armadillo. This growing protein family functions both in cell-cell junctions as well as in signaling during development and likely in the adult as well. These proteins consist of a central domain made up of multiple copies of a repeating motif, the "arm" repeat, named after the armadillo gene product. The arm repeats contain binding sites for a number of structural and signaling proteins, and it is thought that the identity of binding partners regulates their function in the junction or in signaling.

BAKER: Do L cells express the catenins? If so, are they catenins found in those junctions, or where you see the cell-cell staining?

GREEN: L cells can express α- and β-catenin if you transfect a classic cadherin into them. Normally L cells don't exhibit cadherin-mediated function or adhesion. However, if E-cadherin is expressed in L cells, α- and β-catenin are stabilized, and the adhesive complex is reconstituted. Presumably the mRNA is being made, but the protein breaks down unless you transfect in E-cadherin.

BAKER: What about desmosomal cadherins?

GREEN: There is a very minute amount of plakoglobin in L cells. Transfection of desmosomal cadherins leads to stabilization of this endogenous plakoglobin. But to detect some of the things that we see, we must increase the level of plakoglobin by transfection because there's just vanishingly small amounts of this protein in these cells. Desmosomal cadherins do not stabilize α- or β-catenin at all.

GUNDERSEN: Am I correct that, in your desmoplakin dominant negative cell line, the intermediate filaments do not extend out to the cell periphery?

GREEN: Yes.

GUNDERSEN: We know that keratin intermediate filaments do not redistribute to a perinuclear area—that is, collapse—when you break down microtubules. One possible reason for that

might be that they're connected to junctional proteins. If you break down microtubules in your cell lines, do the intermediate filaments redistribute to a perinuclear area?

GREEN: We haven't done that. We have looked at microtubules just to make sure that we weren't also affecting other filament systems, but we have not treated these cells with colchicine or nocodazole.

ALBRECHT-BUEHLER: When you speak of the clustering of these components, it sounds as though you envision a model where the components are free to float laterally in the membrane, meet by accident, then cluster and interact. Is that what you have in mind?

GREEN: That could be one way of interpreting it. We do know that, in epithelial cells maintained in low calcium, for instance, cadherins are constantly being synthesized, are translocated to the cell surface where they are present in a diffuse distribution, and are then rapidly turned over. This could be due to the fact that clustering and metabolic stabilization do not occur under these conditions.

ALBRECHT-BUEHLER: In the pictures that I have seen, the clusters seem to appear only on the edges of cells. Have you ever seen them floating around on the dorsal or ventral side?

GREEN: Yes, in the L cell system clusters do appear on all surfaces. Although in normal epithelial cells the protein is usually seen at lateral margins, half desmosomes have been observed to recycle in and out of epithelial cells under certain conditions, and these can be seen on the dorsal surface. So, to answer the question: yes, you can see them.

IP: Is anything known about how plakoglobin binds to two classes of cadherins in terms of their sequence and domains?

GREEN: Yes. Several laboratories have mapped plakoglobin binding sites for classic and desmosomal cadherins.

IP: Are they very different?

GREEN: Yes. The plakoglobin binding site for desmosomal cadherins appears to be at the ends of the plakoglobin armadillo repeats, whereas classic cadherins bind to the more central armadillo repeats.

QUESTION: Is the actin-mediated adherens junction disrupted by the presence of desmosomal cadherins that shouldn't be able to link up? I picture these two islands of cadherins, which are normally separate, coming together. Do they come together as islands, or do they interpenetrate?

GREEN: Based on immunogold EM observations, we think that they coassemble into the same type of junction. We're trying to look at the actual assembly properties during that process, and think that desmosome and adherens junction components are intimately intermingled. We think that they form a new, mixed type of junction. Along these lines it is interesting to note that in knockout mice lacking plakoglobin, "mixed junctions" containing both desmosomal and adherens junction components were also observed. This is somewhat different from our system, where plakoglobin is still present but the IF cytoskeleton is detached.

LIAO: Do cells with intermediate filaments detach from the junction? Did you check the organization of microtubules? Is it disrupted?

GREEN: We have looked at microtubules, and although there may be subtle changes that we did not detect with fluorescence, they don't appear to be significantly altered. We have yet to treat them with colchicine or nocodazole.

Reference: *Biol. Bull.* **194:** 378–380. (June, 1998)

Protein-Protein Interactions in Intermediate Filament Structure and Anchorage to the Cell Surface

JIN-JUN MENG*, ELAYNE BORNSLAEGER†, KATHLEEN J. GREEN†, AND WALLACE IP*

** Department of Cell Biology, Neurobiology and Anatomy, University of Cincinnati College of Medicine; and † Department of Pathology, Northwestern University Medical School*

Many biological processes involve dramatic changes in cellular morphology. These changes are attributable, in large measure, to dynamic remodeling that occurs as a result of interactions between the plasma membrane and the underpinning filamentous cytoskeleton. How the plasma membrane interacts with actin-containing microfilaments has been studied extensively, but considerably less is known about how it interacts with the other two classes of cytoskeletal elements—microtubules and intermediate filaments (IFs). Understanding how IFs are built and how they interact with the cell surface has been a focus of our laboratories for the past several years.

IFs are widely believed to perform structural functions, such as maintaining cell and tissue integrity. The evidence for this is twofold. First, mutations in keratin genes that abolish the ability of the proteins to assemble into IFs are the genetic basis for many hereditary skin blistering diseases. The second kind of evidence comes from studies of the physical characteristics of gels made *in vitro* from actin, tubulin, and vimentin. Of these three classes of cytoskeletal elements, the rheologic properties of IF networks are the most compatible with a role in structural support; moreover, mixed IF and actin networks produce a degree of resiliency and strength unattainable by either of the two alone.

This paper was originally presented at a workshop titled *The Cytoskeleton: Mechanical, Physical, and Biological Interactions.* The workshop, which was held at the Marine Biological Laboratory, Woods Hole, Massachusetts, from 15–17 November 1996, was sponsored by the Center for Advanced Studies in the Space Life Sciences at MBL and funded by the National Aeronautics and Space Administration under Cooperative Agreement NCC 2-896.

The family of proteins that make up IFs share a common structural motif that features a central α-helical rod domain and globular head and tail domains. The assembly of these highly asymmetrical molecules into 10-nm-wide filaments takes place in several experimentally identifiable steps; these include the formation of dimers, tetramers, and higher order oligomers, although a continuum of oligomers is more likely to exist beyond the dimer stage. Many kinds of interactions among the three domains of the IF polypeptide occur during IF assembly. The most well known of these is the lateral association of the α-helical rod domains through hydrophobic interactions to form dimeric coiled-coils. Equally significant are electrostatic interactions among charged zones on the surface of dimeric coiled-coils; these drive the formation of tetramers and higher order structures. Using a two-hybrid cloning approach, we recently attempted to identify regions along the IF protein molecule that undergo true protein-protein interactions leading to filament formation. These studies showed that the rod domain—especially helices 1B and 2B—had the highest propensity to form homotypic dimers and tetramers, whereas interactions involving the head and tail domains were considerably weaker. These results suggest that growth in filament length and girth are largely a function of the overlap of the rod domain alone. The end domains may play a role in other aspects of filament assembly, but their contribution to filament growth is likely to be minimal.

In many tissues, IFs associate with the cell surface at desmosomes. This association between the IF cytoskeleton and these adhesive cell surface specializations is the structural basis for a transcellular cytoskeleton-plasma

membrane superstructure that stabilizes the entire tissue. Yet, although the IF-desmosome association provides mechanical integrity in every tissue, the interactions between desmosomes and IF proteins from particular tissues appear to have different structural requirements. The interaction between the C-terminus of desmoplakin—the major protein in the cytoplasmic portion of the desmosomes (DP.CT)—and various IF family members has been accessed by yeast two-hybrid analyses. These studies have revealed the most robust interaction to be that between DP.CT and an epidermal keratin. In agreement with previous reports, this interaction requires participation of the head domain of the keratin polypeptide. Interaction between DP.CT and epithelial keratins is weaker and requires that both a Type I and Type II keratin be present, suggesting that dimerization is a prerequisite. In contrast to the case of the epidermal keratin, this interaction does not appear to be mediated by the head domains of either the Type I or Type II keratin. DP.CT also interacts with the Type III IF proteins vimentin and desmin, but these interactions are also weaker than that involving an epidermal keratin. Whether dimerization of the Type III IF protein is required for this interaction is not known.

These observations have begun to reveal interesting information as to how IFs are constructed, and how they interact with other cytoplasmic components to bring about mechanical stabilization of cells and tissues. They also raise the possibility that, although IFs are believed to serve primarily a structural function in all tissues in which they are found, the underlying molecular basis for each case may be different. Identifying such differences should bring new insights to the larger problem of tissues formation and maintenance.

Bibliography

Fuchs, E., and K. Weber. 1994. Intermediate filaments: structure, dynamics, function and disease. *Annu. Rev. Biochem.* **63:** 345–382.

Meng, J.-J., S. A. Khan, and W. Ip. 1996. Intermediate filament domain interaction during assembly as revealed by two-hybrid cloning. *J. Biol. Chem.* **271:** 1599–1604.

Meng, J.-J., E. B. Bornslaeger, K. J. Green, P. M. Steinert, and W. Ip. 1997. Two hybrid analysis reveals fundamental differences in direct interactions between desmoplakin and cell type specific intermediate filaments. *J. Biol. Chem.* **272:** 21495–21503.

Discussion

CHEN: In your two-hybrid system you only use the C-terminus of desmoplakin. Do you think your results would change if you put the C-terminus in the context of the whole molecule? Do you think that you would have more or less interaction with vimentin or the keratins?

IP: This presents a technical problem. We are already pushing the limits of the size of the cDNA construct in these yeast two-hybrid vectors, by inserting the largest construct reported in the literature. Since dimerization of desmoplakin is mediated by dimerization of its rod domain, we had hoped that expression of the entire rod domain plus the C-terminus would enhance the activity somewhat. However, that's a total of over 1800 amino acids. Although we have cloned it into the vectors, the constructs have not worked.

LIAO: Based on measurements of fluorescence intensity, you deduced which of these interactions is weaker than the other. It is difficult to conclude that certain interactions are stronger than the others without normalizing the expression level, because the level of proteins that you have in the cells are probably very different.

IP: I agree that this is a complex issue. The data are not meant to provide absolute measures of the strength of individual interactions, but to compare the relative strengths of a series of related interactions. As demonstrated nicely by Estojak *et al.* (1995. *Mol. Cell. Biol.* 15:5820–5829), there is not a reporter in two hybrid assays for which the amount of gene expression linearly reflects affinity measured *in vitro*, but the level of gene expression does provide an indication of the strength of the interaction. Thus, reporter gene expression levels of, say, 300, 200, and 100 cannot be taken to mean interaction strengths of 3×, 2× and 1×, but it does mean that the first interaction is the strongest, the third one is the weakest, and the second is in between. This is particularly useful for comparing a series of interactions of the type $(X + Y)$, $(X + Y')$, $(X + Y'')$, and $(X + Y''')$, where Y', Y'', and Y''' are derivatives of Y. That is what we have tried to do.

It is important to bear in mind that GAL4 is a transcription factor. For this reason, the amount of GAL4 reconstituted by interaction of TA and DB fusion proteins is not as important as the length of time that the reconstituted GAL4 stays reconstituted, provided that enough of it is expressed to activate transcription. The stronger the protein-protein interaction, the more robust is the reconstituted GAL4 and the longer (statistically) it will reside on the DNA to activate transcription, which in turn leads to higher levels of reporter gene expression.

COULOMBE: How can you draw conclusions about tetramer structure based on the two-hybrid system? I can see the direct relevance to dimer formation, but I would like you to explain

that for tetramers. Secondly, do you know for a fact that the so-called serine 23 is phosphorylated in yeast?

IP: In our 1996 paper (Meng *et al.* 1996. *J. Biol. Chem.* 271: 1599–1604) we showed that both dimers and tetramers are formed in transformed yeast cells. This was shown by expanding a positive colony, making a cytosolic extract of the yeast cells, chemically cross-linking it with glutaraldehyde, and then identifying the oligomeric species by western blotting. We found species with molecular sizes consistent with vimentin dimers as well as tetramers.

Regarding phosphorylation of ser-23, the serine at position -23 from the C-terminus: we do not have direct evidence that it is phosphorylated in yeast cells. However, Stappenbeck *et al.* (1994. *J. Biol. Chem.* 269: 29351) showed that this residue is phosphorylated in mammalian cells. Ser-23 is situated within an A kinase consensus sequence, and forskolin stimulates its phosphorylation; these observations suggest that the kinase responsible is A kinase. While we cannot say whether ser-23 is phosphorylated in yeast, A kinase certainly is found in yeast cells.

COULOMBE: What about dimers *versus* tetramers?

IP: We did try that. We picked a positive colony, made a yeast extract followed by cross-linking, and tried to identify the species present using a western blot analysis. From that analysis we know that both the tetramer and dimer exist.

CHISHOLM: When you add the Type I and Type II keratin together with the desmoplakin tail, is the idea that you are actually forming a dimer between those two, and that somehow that dimer is now providing the DNA-binding domain together with the desmoplakin tail and the activating domain?

IP: This study is described in detail in our 1997 paper (Meng *et al.* 1997. *J. Biol. Chem.* 272: 21495–21503). Briefly, the Type I and Type II keratins (K18 and K8 in this case) were expressed as separate fusion proteins with the trans-activating domain (TA), and the desmoplakin tail was expressed as a fusion with the DNA-binding domain (DB). We know from previous studies that the two keratins interact, but in this experiment the keratin interaction would not activate reporter gene transcription because they were both fused with the activating domain only. We also know from previous studies that neither K8 nor K18 alone would interact with the DP tail. Therefore, if β-galactosidase activity is elevated in the three-hybrid transformation, it must result from interaction among all three fusion proteins, the K8-TA, K18-TA, and DP,CT-DB.

CHISHOLM: But they're expressed as separate polypeptides. You're forming a dimer; therefore the argument would be that you require that dimer in order to get enough of the activating domain together with the binding domain.

IP: That is correct.

CHISHOLM: A second question concerns your interpretation of the negative result—when you don't see fluorescence. This has to do with the geometry of association of the DNA-binding domain with the activating domain. If the two proteins were to associate, let's say, in one direction—parallel—I can imagine that you would have the activating domain and the DNA-binding domain in one relationship to each other. If the proteins were to bind anti-parallel, I would imagine that those two activities would be in another physical disposition to each other. Is there any reason to think that they could lead to a negative result in the case of a direct protein-protein interaction?

IP: The scenario you describe could conceivably occur if the molecules involved are highly extended (*e.g.*, very long) rods. In the case of IF proteins and the DP tail, it is unlikely for two reasons. First, IF proteins dimerize in parallel and in axial register. Since, in our constructs, the IF protein/domain is always fused to the N-terminus of either the GAL4 TA or DB domain, dimerization of an IF protein always puts the GAL4 domains in close proximity to one another regardless of how large the IF protein is. Second, DP.CT is not highly extended.

AEBI: As you certainly know, you can often get false positives with the two-hybrid system. It is therefore important when working at this level to evaluate a positive interaction by *in vitro* binding assays with the expressed proteins. Have you expressed your positive constructs in *E. coli,* for example, and then performed *in vitro* binding experiments?

IP: We have done the filament assembly experiment. We haven't done this with desmoplakins.

Reference: *Biol. Bull.* **194:** 381–383. (June, 1998)

Domain Structure and Transcript Diversity of Plectin

GERHARD WICHE

Institute of Biochemistry and Molecular Cell Biology, University of Vienna, Dr. Bohrgasse 9, A-1030 Vienna, Austria

Plectin, a cytoskeleton-associated protein of exceptionally large size, is abundantly expressed in a wide variety of mammalian tissues and cell types. It is codistributed with different types of intermediate filaments (IFs) and is prominently located at the plasma membrane attachment sites of IFs and of microfilaments, such as hemidesmosomes (Wiche *et al.*, 1984), Z-line structures and dense plaques of striated and smooth muscle (Wiche *et al.*, 1983), intercalated discs of cardiac muscle (Zernig and Wiche, 1985), and focal contacts (Seifert *et al.*, 1992). Furthermore, in several tissues, including brain (Errante *et al.*, 1994) and kidney (Yaoita *et al.*, 1996), plectin expression is prominent in cells forming tissue layers at the interface of tissue and fluid-filled cavities. These observations are consistent with a model in which the role of plectin is to strengthen cells against mechanical stress both along their surfaces and at their internal anchorage sites for cytoskeletal filaments. This concept is supported by recent reports demonstrating defective expression of plectin in epidermolysis bullosa simplex (EBS)-Ogna, an autosomal dominant disease that produces severe skin blistering (Koss-Harnes *et al.*, 1997), and EBS-MD, an autosomal recessive disease, characterized by skin blistering combined with muscular dystrophy (Gache *et al.*, 1996; MacLean *et al.*, 1996; Smith *et al.*, 1996).

We have cloned and sequenced plectin from rat (Wiche *et al.*, 1991) and man (Liu *et al.*, 1996). Secondary structure predictions based on the deduced amino acid sequences of cDNAs and genomic clones, as well as on electron microscopy of the protein (Foisner and Wiche, 1987), revealed a multi-domain structure composed of a central ~200 nm long, α-helical coiled-coil structure flanked by large globular domains. The structure of the carboxy-terminal domain is dominated by six highly homologous repeats that also occur in lesser number in desmoplakin (3 repeats; Green *et al.*, 1990), bullous pemphigoid antigen (BPAG) 1 (2 repeats; Sawamura *et al.*, 1991), and the recently identified envoplakin (1 repeat; Ruhrberg *et al.*, 1996). Analysis of the human gene locus revealed a complex organization of 32 exons spanning 31 kb of DNA located in the telomeric region (q24) of chromosome 8 (Liu *et al.*, 1996).

On the molecular level, plectin binds to a variety of cytoskeletal proteins, including cytoplasmic and nuclear IF subunit proteins (vimentin, GFAP, cytokeratins, neurofilament proteins, lamin B), subplasma membrane proteins (fodrin and α-spectrin), and high molecular weight microtubule-associated proteins MAP1 and MAP2 (Herrmann and Wiche, 1987; Foisner *et al.*, 1988; Wiche *et al.*, 1993). The expression of mutant forms of plectin in cell lines transiently transfected with cDNA constructs led to the conclusion that the C-terminal globular domain of plectin is involved in the binding to IFs (Foisner *et al.*, 1991). Recently, we mapped the binding site of plectin to vimentin, and to keratinocyte cytokeratins, to a stretch of ~50 amino acid residues within plectin's terminal repeat 5-domain; and a basic amino acid residue cluster within a functional nuclear targeting sequence motif was identified as an essential element of this site (Nikolic *et al.*, 1996). Moreover, we found that a dystrophin/β-spectrin-like, actin-binding domain of plectin—located in its aminoterminal region (encoded by exons 2–8)—is functional.

Plectin is characterized by versatile binding activities,

This paper was originally presented at a workshop titled *The Cytoskeleton: Mechanical, Physical, and Biological Interactions.* The workshop, which was held at the Marine Biological Laboratory, Woods Hole, Massachusetts, from 15–17 November 1996, was sponsored by the Center for Advanced Studies in the Space Life Sciences at MBL and funded by the National Aeronautics and Space Administration under Cooperative Agreement NCC 2-896.

prominence at distinct strategically important locations within the cytoarchitecture (such as cytoskeleton anchorage junctions), complex exon-intron organization, and differential staining of tissues and cells as revealed by a battery of monoclonal antibodies raised to the protein. These features suggest that different plectin isoforms exist, that they perform different cellular tasks and, thus, have different subcellular localizations. Recently, we have found several such variant transcripts in rat and man. Of particular interest was the identification of four distinct first coding exons, all of which splice into a common successive exon 2. RNase protection mapping of transcripts containing three of the four identified alternative first exons revealed their coexpression in rat glioma C6 cells, and in a series of different rat tissues. However, significant variations in the expression levels of first exons indicated tissue-specific promoters for at least some of them. Multiple transcriptional start sites and a preceding, nontranscribed GC-rich sequence lacking any TATA element suggested that expression of exon 1 transcripts involves a promoter characteristic of housekeeping genes. In addition, plectin splice variants lacking exon 31 (>3 kb), which encodes the entire rod domain of the molecule, were identified by RT-PCR in a variety of cells and tissues. These findings lend further support to the hypothesis that plectin is a versatile organizing element of the cytoskeleton, and they provide first insights into a complex gene regulatory machinery.

Literature Cited

Errante, L. D., G. Wiche, and G. Shaw. 1994. Distribution of plectin, an intermediate filament-associated protein, in the adult rat central nervous system. *J. Neurosci. Res.* **37:** 515–528.

Foisner, R., and G. Wiche. 1987. Structure and hydrodynamic properties of plectin molecules. *J. Mol. Biol.* **198:** 515–531.

Foisner, R., F. E. Leichtfried, H. Herrmann, J. V. Small, D. Lawson, and G. Wiche. 1988. Cytoskeleton-associated plectin: *in situ* localization, *in vitro* reconstitution, and binding to immobilized intermediate filament proteins. *J. Cell Biol.* **106:** 723–733.

Foisner, R., P. Traub, and G. Wiche. 1991. Protein kinase A- and protein kinase C-regulated interaction of plectin with lamin B and vimentin. *Proc. Natl. Acad. Sci. USA* **88:** 3812–3816.

Gache, Y., S. Chavanas, J. P. Lacour, G. Wiche, K. Owaribe, G. Meneguzzi, and J. P. Ortonne. 1996. Defective expression of plectin/HD1 in epidermolysis bullosa simplex with muscular dystrophy. *J. Clin. Invest.* **97:** 2289–2298.

Green, K. J., D. A. D. Parry, P. M. Steinert, M. L. A. Virata, R. M. Wagner, B. D. Angst, and L. A. Nilles. 1990. Structure of the human desmoplakins. Implications for function in the desmosomal plaque. *J. Biol. Chem.* **265:** 2603–2612.

Herrmann, H., and G. Wiche. 1987. Plectin and IFAP-300K are homologous proteins binding to microtubule-associated proteins 1 and 2 and to the 240-kilodalton subunit of spectrin. *J. Biol. Chem.* **262:** 1320–1325.

Koss-Harnes, D., F. L. Jahnsen, G. Wiche, E. Soyland, P. Brandtzaeg, and T. Gedde-Dahl, Jr. 1997. Plectin abnormality in epidermolysis bullosa simplex Ogna: non-responsiveness of basal keratinocytes to some anti-rat plectin antibodies. *Exp. Dermatol.* **6:** 41–48.

Liu, C.-g., C. Maercker, M. J. Castañón, R. Hauptmann, and G. Wiche. 1996. Human plectin: organization of the gene, sequence analysis, and chromosome localization (8q24). *Proc. Natl. Acad. Sci. USA* **93:** 4278–4283.

MacLean, W. H. I., L. Pulkkinen, F. D. J. Smith, E. L. Rugg, E. B. Lane, F. Bullrich, R. E. Burgeson, S. Amano, D. L. Hudson, K. Owaribe, J. A. McGrath, J. R. McMillan, R. A. J. Eady, I. M. Leigh, A. M. Christiano, and J. Uitto. 1996. Loss of plectin causes epidermolysis bullosa with muscular dystrophy: cDNA cloning and genomic organization. *Genes Dev.* **10:** 1724–1735.

Nikolic, B., E. MacNulty, B. Mir, and G. Wiche. 1996. Basic amino acid residue cluster within nuclear targeting sequence motif is essential for cytoplasmic plectin-vimentin network junctions. *J. Cell Biol.* **134:** 1455–1467.

Ruhrberg, C., M. A. Nasser Hajibagheri, M. Simon, T. P. Dooley, and F. M. Watt. 1996. Envoplakin, a novel precursor of the cornified envelope that has homology to desmoplakin. *J. Cell Biol.* **134:** 715–729.

Sawamura, D., K. Li, M.-L. Chou, and J. Uitto. 1991. Human bullous pemphigoid antigen (BPAG1). Amino acid sequences deduced from cloned cDNA's predict biologically important peptide segments and protein domains. *J. Biol. Chem.* **266:** 17784–17790.

Seifert, G. J., D. Lawson, and G. Wiche. 1992. Immunolocalization of the intermediate filament-associated protein plectin at focal contacts and actin stress fibers. *Eur. J. Cell Biol.* **59:** 138–147.

Smith, F. J. D., R. A. J. Eady, I. M. Leigh, J. R. McMillan, E. L. Rugg, D. P. Kelsell, S. P. Bryant, N. K. Spurr, J. F. Geddes, G. Kirtschig, G. Milana, A. G. de Bono, K. Owaribe, G. Wiche, L. Pulkkinen, J. Uitto, W. H. I. McLean, and E. B. Lane. 1996. Plectin deficiency results in muscular dystrophy with epidermolysis bullosa. *Nat. Genet.* **13:** 450–457.

Wiche, G., R. Krepler, U. Artlieb, R. Pytela, and H. Denk. 1983. Occurrence and immunolocalization of plectin in tissues. *J. Cell Biol.* **97:** 887–901.

Wiche, G., R. Krepler, U. Artlieb, R. Pytela, and W. Aberer. 1984. Identification of plectin in different human cell types and immunolocalization at epithelial basal cell surface membranes. *Exp. Cell Res.* **155:** 43–49.

Wiche, G., B. Becker, K. Luher, G. Weitzer, M. J. Castañón, R. Hauptmann, C. Stratowa, and M. Stewart. 1991. Cloning and sequencing of rat plectin indicates a 466-kD polypeptide chain with a three-domain structure based on a central alpha-helical coiled coil. *J. Cell Biol.* **114:** 83–99.

Wiche, G., D. Gromov, A. Donovan, M. J. Castañón, and E. Fuchs. 1993. Expression of plectin mutant cDNA in cultured cells indicates a role of COOH-terminal domain in intermediate filament association. *J. Cell Biol.* **121:** 607–619.

Yaoita, E., G. Wiche, T. Yamamoto, K. Kawasaki, and I. Kihara. 1996. Perinuclear distribution of plectin characterizes visceral epithelial cells of rat glomeruli. *Am. J. Pathol.* **149:** 319–327.

Zernig, G., and G. Wiche. 1985. Morphological integrity of single adult cardiac myocytes isolated by collagenase treatment: immunolocalization of tubulin, microtubule-associated proteins 1 and 2, plectin, vimentin, and vinculin. *Eur. J. Cell Biol.* **38:** 113–122.

Discussion

LUNA: You said your plectin knockout mice had a severe phenotype; would you elaborate on that?

WICHE: They have a severe phenotype, with skin blistering from which they die within two days after birth. We are looking to see if they show additional phenotypes.

ALBRECHT-BUEHLER: Plectin seems to be a dangerous molecule for a cell to have. As you described it, it acts basically like a fixative, so a cell must control this molecule if it wants to live. The isoforms you describe are one of the possible ways for taking advantage of the multivalency of such a fixative. I would expect that there is much more to it. Is there any evidence for some kind of chaperone, some kind of sequestering proteins, that deliver plectin to places rather than letting it freely fix any protein that it meets? Have you ever looked for something like this?

WICHE: No we haven't.

BORISY: You talked about all of the different molecules that plectin interacts with, and then you told us about the possibility of many plectin isoforms. Do you think that individual plectin molecules can bind to all of the different targets, or do you think that the spectrum of binding of a particular isoform is more limited, with some of the multiplicity of binding being due to different isoforms?

WICHE: Yes, I would predict that the spectrum of binding of the molecule is limited. Different molecules have different tasks; one molecule cannot do everything. By forming complexes, even by dimerization of different isoforms, different functional properties of the formed molecule may be obtained.

BORISY: A second question is, if intermediate filament proteins are the major binding partner for plectins, how do you explain the phenotype of the vimentin knockout mouse reported in the literature?

WICHE: I wouldn't say that intermediate filaments are necessarily the major interaction partner. That was the conclusion based on early experiments, where we found and isolated isoforms of plectin due to their binding to intermediate filaments. When we characterize more of these forms, this picture will probably change. Regarding the vimentin knockout mouse, perhaps plectin is more important than the vimentin in this. We have studied plectin expression and organization in the cytoplasm of vimentin-negative cells. Plectin is there as a network, even without vimentin.

Reference: *Biol. Bull.* **194:** 384–386. (June, 1998)

Response of Vascular Endothelial Cells to Fluid Flow

KEIGI FUJIWARA, MICHITAKA MASUDA, MASAKI OSAWA, KAZUO KATOH, YUMIKO KANO, NOBORU HARADA, AND ROSANGELA B. LOPES

Department of Structural Analysis, National Cardiovascular Center Research Institute, Suita, Osaka, 565-8565 Japan

Fluid flow triggers a variety of responses in vascular endothelial cells (ECs), such as initiation of signal transduction, modulation of gene expression, and remodeling of cytoskeletal and related structures. However, the primary steps of mechanosensing are not known. Because fluid flow is a mechanical (thus vectorial) stimulus, we decided to study how ECs respond in a vectorial manner. Among the various types of responses (for review, see Davies, 1995), those involving the cytoskeleton are clearly vectorial.

Using a parallel plate flow chamber mounted on a light microscope, we first analyzed morphological responses of ECs to laminar flow (Masuda and Fujiwara, 1993a, b). We found that, in addition to the already known morphological responses of ECs to flow (*i.e.*, the elongation and alignment of ECs parallel to the direction of flow and alignment of stress fibers in the flow direction), flow induced preferential development of lamellipodia in the direction of flow. This latter response caused ECs to migrate preferentially in the flow direction. Although it takes many hours for both the cell shape change and the alignment responses to become recognizable, the motility pattern change was detectable in 5–10 min. This is the fastest morphology-related response of ECs exposed to flow.

ECs exhibit little morphologically detectable responses when exposed to fluid shear stress of less than 0.4 Pa (4 dyn/cm^2), although it is known that many signal-transducing events and gene expressions are activated by much smaller levels of flow. To consistently cause the reorganization of stress fibers, the cell elongation-alignment, and the preferential migration in the flow direction, ECs have to be exposed to a fluid shear stress of over 0.6 Pa. To identify biochemical events occurring during these morphological responses, we have investigated changes in the phosphorylation level of some membrane proteins.

We have found that a 128-kDa glycoprotein is tyrosine-phosphorylated within minutes when cultured bovine ECs are exposed to the levels of fluid flow (*i.e.*, >0.5 Pa) that elicit morphological responses (Harada *et al.*, 1995). This protein is now purified and partially sequenced, and using RT-PCR, we have cloned a 3.4-kb cDNA encoding the protein (Osawa *et al.*, 1997). The amino acid and cDNA sequence data show that it is a bovine homolog of platelet endothelial cell adhesion molecule-1 (PECAM-1), consisting of 738 amino acids and showing 71% and 63% identity with human and mouse PECAM-1, respectively. Because it has been shown that fluid flow deforms the cell surface (Liu *et al.*, 1994), we used osmotic changes to deform the cell surface. Although there are various ways to cause deformation of cells, this is the easiest way. We found that PECAM-1 was also tyrosine-phosphorylated in ECs that were placed in a hyper- or hypo-osmotic medium. However, PECAM-1 is not phosphorylated when ECs are treated with chemical reagents such as thrombin, acetylcholine, ATP, IL-1, TNF-alpha, Ca-ionophores, PMA and various growth factors, suggesting that this phosphorylation occurs specifically when ECs are mechanically stimulated.

An autophosphorylatable band comigrating with c-Src is present in the anti-PECAM-1 immunoprecipitate, and c-Src phosphorylates and binds to a GST fusion protein containing the PECAM-1 cytoplasmic domain. A spliced

This paper was originally presented at a workshop titled *The Cytoskeleton: Mechanical, Physical, and Biological Interactions.* The workshop, which was held at the Marine Biological Laboratory, Woods Hole, Massachusetts, from 15–17 November 1996, was sponsored by the Center for Advanced Studies in the Space Life Sciences at MBL and funded by the National Aeronautics and Space Administration under Cooperative Agreement NCC 2-896.

mRNA form lacking the amino acid residues 703–721 in the cytoplasmic domain is also expressed in bovine ECs. Present within this missing domain is one of the six tyrosine residues, and c-Src fails to phosphorylate and bind to a GST fusion protein containing the cytoplasmic region of the spliced form. Because a GST fusion protein containing an SH2 domain of Fyn can bind to PECAM-1 but an SH3 domain of Fyn cannot, the SH2 domain of c-Src appears to be involved in c-Src binding to tyrosine-phosphorylated PECAM-1. These results suggest that the YSEI motif in the PECAM-1 sequence, which includes Tyr 713, is the site of tyrosine phosphorylation by the Src family kinase as well as the site of SH2 binding. They also suggest that both PECAM-1 and the Src family kinases are involved in signal transduction of mechanical stimuli in ECs.

The simplest mechanism for transmitting information from the cell surface to the interior of the cell about the direction of flow would enlist a structure that runs between the apical cell surface and other parts of the cell such as the basal surface. We have shown that although the majority of stress fibers are associated with focal adhesions located in the basal portion of cells (the basal stress fiber), some terminate at the apical surfaces (the apical stress fiber). Apical stress fibers are anchored to the apical plasma membrane at a structure similar to the focal adhesion, and we have proposed to call this apical stress fiber attachment site the apical plaque. The molecular composition of the apical plaque is surprisingly similar to that of the focal adhesion, but some differences are apparent, such as the absence of FAK and vitronectin receptors in the apical plaque (Katoh *et al.*, 1995). Our immunofluorescence and electron microscope studies show that both apical stress fibers and apical plaques are present in ECs *in situ* (Kano *et al.*, 1996). At present, we are investigating the precise location of the other end of the apical stress fiber. Locations we are particularly interested in are the adhesion plaque where ECs attach firmly to the substrate and the cell-cell adhesion site where PECAM-1 is localized.

The PECAM-1 tyrosine phosphorylation does not occur when ECs are treated with cytochalasin D. ECs treated with an actin filament stabilizing agent phalloidin and then stimulated by mechanical means showed a greatly increased level of PECAM-1 tyrosine phosphorylation. Cholchicine did not change the PECAM-1 phosphorylation level. These results suggest that the actin cytoskeleton is involved in the PECAM-1 tyrosine phosphorylation induced by mechanical stimuli. We are now analyzing what role the actin cytoskeletal system plays in the PECAM-1 tyrosine phosphorylation.

Literature Cited

Davies, P. F. 1995. Flow-mediated endothelial mechanotransduction. *Physiol. Rev.* **75:** 519–560.

Harada, N., M. Masuda, and K. Fujiwara. 1995. Fluid flow and osmotic stress induce tyrosine phosphorylation of an endothelial cell 128 kDa surface glycoprotein. *Biochem. Biophys. Res. Commun.* **214:** 69–74.

Kano, Y., K. Katoh, M. Masuda, and K. Fujiwara. 1996. Macromolecular composition of stress fiber plasma membrane attachment sites in endothelial cells *in situ*. *Circulation Res.* **79:** 1000–1006.

Katoh, K., M. Masuda, and K. Fujiwara. 1995. Focal adhesion proteins associated with apical stress fibers of human fibroblasts. *Cell Motil. Cytoskel.* **31:** 177–195.

Liu, S. Q., M. Yen, and Y. G. Fung. 1994. On measuring the third dimension of cultured endothelial cells in shear flow. *Proc. Nat. Acad. Sci. USA* **91:** 8782–8786.

Masuda, M., and K. Fujiwara. 1993a. The biased lamellipodium development and microtubule organizing center position in vascular endothelial cells migrating under the influence of fluid flow. *Biol. Cell.* **77:** 237–245.

Masuda, M., and K. Fujiwara. 1993b. Morphological responses of single endothelial cells exposed to physiological levels of fluid shear stress. *Front. Med. Biol. Eng.* **5:** 79–87.

Osawa, M., M. Masuda, N. Harada, R. B. Lopes, and K. Fujiwara. 1997. Tyrosine phosphorylation of platelet endothelial cell adhesion molecule-1 (PECAM-1, CD31) in mechanically stimulated vascular endothelial cells. *Eur. J. Cell Biol.* **72:** 229–237.

Discussion

BRUINSMA: I was somewhat surprised by the high variation in surface stresses you showed in your talk. Did you determine those stresses from a theoretical estimate?

FUJIWARA: It's an estimate generated by computer; we made the contour map of a cell and then applied known flow over it.

BRUINSMA: How is the stress sensing taking place? Is it because PECAM is an adhesion molecule, and the shear stress, or osmotic stress, puts tension on the cell-cell contact, and the PECAM senses stress between the cells? Or, can the PECAM independently sense stress by shear flow applied to a free PECAM on the surface?

FUJIWARA: We don't know the answer to any of those questions. Our thinking is that there are several places where the force from fluid shear stress could be concentrated, like the site of cell-cell or cell-substrate adhesion. Mechanical sensors may be present at these sites. We are also thinking about stress fibers

that are attached to the luminal surface. These stress fibers are contractile structures that are always under tension. If they can be moved, the bottom and the rest of the cell can directly sense which way the thing is moving. We envision a very simple mechanical thing, but have no idea how PECAM-1 phosphorylation fits in.

SHYY: This is a wonderful model. You show that alignment of the extracellular matrix can be regulated by flow, both *in vivo* and *in vitro*. What mechanism for shear stress regulates the alignment of extracellular matrix molecules that are located underneath the endothelial cells?

FUJIWARA: Dick Hynes showed, a long time ago, that stress fibers and fibronectin fibers are nicely aligned in tissue culture cells under certain circumstances. Therefore, I would think that stress fiber organization is related to fibronectin organization underneath the cell.

LUNA: When I see the staining, and knowing that PECAM is also isolated on microvilli, I think of stereocilia, which are long projections involved in how we perceive sound. I wonder if this is related to stereocilia, and could it be the microvilli and the motion of these small projections that is the real sensing element?

FUJIWARA: It is possible. We tried to locate those microvilli, but they are very few. However, we haven't ruled out the possibility that they may be involved.

ALBRECHT-BUEHLER: You have ignored intermediate filaments. Research on the guinea pig aorta and in other vascular endothelia revealed a prominent ring of intermediate filaments surrounding the nucleus parallel to the surface of the epithelium. This is very enigmatic because it is not found anywhere else except in these high flow situations. Is it possible that these rings, or intermediate filaments in particular, play a role?

FUJIWARA: We have not studied intermediate filaments. There are some studies on microtubules which suggest that centriole positions are interesting—their position in the blood vessel. As far as our motility assays are concerned, we can treat the cells with colchicine, and they respond in a normal way. They can sense the flow. Microtubules are not that important, in terms of sensing this flow stimulus. I don't know about intermediate filaments.

CHISHOLM: Which comes first, reorganization of fibronectin or reorganization of actin?

FUJIWARA: We have followed developing vessels: organization of actin stress fibers comes first, followed by organization of fibronectin.

BARAKAT: Do you see evidence of an adaptive mechanism in the phosphorylation? Does it ever go back down to baseline with sustained flow?

FUJIWARA: We have not done long-term studies. It does appear to come down a bit in a span of about 20 to 30 minutes.

BARAKAT: The comment has been raised regarding possible deformation of the sensors by flow. If you do a Stokes flow-calculation around a sphere that is a typical distance away from the cell surface, you find that the extent of mechanical deformation is smaller than thermal fluctuations. I don't think that will be a major player in the sensing of the initial signal.

BRUINSMA: I think your molecule is smarter than you think it is. You suggest that it is just measuring the surface stress. However, this molecule moves left or right depending on the flow. Surface stress is identical if you reverse the flow from left to right. Your molecule must be doing more than measuring surface stress—it measures a direction as well, and it must do this by measuring a tension gradient on the surface created by viscous stress along the cell. It even has to measure the difference in tension between the front and back part of the cell in order to move.

FUJIWARA: We are thinking about two things. The level of fluid shear stress may be monitored by this molecule by phosphorylation. The direction may be sensed mechanically by using these stress fibers that run from the top to the bottom.

TAYLOR: You said that stress fibers seem to exert a force. Do you have any information that supports this?

FUJIWARA: We have isolated stress fibers. We can just take them out from the cell, add ATP, and they contract at the rate of about 10 μm/min.

TAYLOR: When you remove the force by stopping the flow, do your cells start to contract?

FUJIWARA: Dr. Chien has information on that. You can see the movement on the surface of the cell. Whether there is this change, I do not know.

WANG: Do endothelial cells normally move inside the blood vessel *in vivo*?

FUJIWARA: That is an interesting question. We have labeled a section of blood vessels. When we opened them after a few months we saw that the labeled area does not disperse. They did not go toward the upstream. If they do move, they move very little in the direction of flow.

GOLDMAN: I would like to make a comment. We have done some of these shear experiments with Peter Davies at the University of Chicago. In collaboration with a colleague of mine, Eric Flitney from Scotland, we find that the intermediate filaments of the vimentin system are exquisitely sensitive to shear. In fact, you can see changes in the IF earlier than you see changes in actin. It looks like the first reaction is disassembly and then reorganization or reassembly. This seems to be coincident and prerequisite to shape changes.

Reference: *Biol. Bull.* **194:** 387–389. (June, 1998)

A Role for pp125^{FAK} in Suppression of Apoptosis in Fibroblasts

CAROL A. OTEY

Department of Cell Biology, University of Virginia, Charlottesville, Virginia 22908

Integrins are the transmembrane receptors that serve to anchor the cell to the extracellular matrix. Integrins are found clustered in specialized membrane domains called focal adhesions. In addition to cell-to-matrix adhesion, a number of functions have been attributed to focal adhesions, including anchorage of the actin cytoskeleton to the membrane and bi-directional signal transduction across the membrane. The integrins are thought to participate in all of these functions; but integrins do not possess any endogenous catalytic activity. Therefore, the signal transduction function of integrins must involve binding partners that can serve to generate second messengers within the cytoplasm. pp125^{FAK} is a tyrosine kinase that may be involved in such a secondary messenger cascade. FAK colocalizes with integrins in the focal adhesions, and FAK's kinase activity is up-regulated when integrins bind to the extracellular matrix as cells are spreading. The precise downstream functions of FAK are not known, but they could include the initiation of focal adhesion assembly or the regulation of actin attachment to integrins (for review, see Otey, 1996).

Because the FAK-binding site on the cytoplasmic tail of the integrin β_1 subunit was recently mapped (Schaller *et al.,* 1995), we reasoned that such a peptide would be able to bind to FAK but would not contain sufficient conformation to activate FAK. Thus, the peptide might function as a "dominant negative" form of integrin. The synthetic integrin peptide was coupled to carrier protein and injected into freshly plated fibroblasts while the cells were still rounded. Two hours after injection, the cells were fixed and stained with rhodamine phalloidin to determine whether peptide-injected cells could assemble actin stress fibers and focal adhesions. It was observed that cells injected with the integrin peptide failed to spread and failed to assemble stress fibers and focal adhesions, whereas cells injected with a scrambled control peptide had spread normally in the same period. We also observed that the nuclei of cells injected with the integrin peptide appeared to be condensed and lobular, an indication that these cells might be in an early stage of apoptosis. Since cleavage of DNA is a defining characteristic of apoptotic cells, peptide-injected cells were stained with a reagent (Apoptag) that detects free DNA ends and thus stains apoptotic nuclei with great specificity. This staining protocol revealed that 95% of cells injected with the integrin peptide were apoptotic. None of the control-injected cells were found to be apoptotic. These results suggest that FAK plays a role in cell spreading and in the assembly of focal adhesions and stress fibers; in addition, FAK activation may be required to suppress apoptotic death in anchorage-depended cells.

To confirm these conclusions, cells were injected with a monoclonal antibody specific for the C-terminus of FAK (antibody 2A7, a gift from Dr. J. Thomas Parsons). The epitope for this antibody is proximal to the FAK localization sequence, a region in the FAK C-terminal domain that is required for efficient recruitment of FAK to the focal adhesions. When rounded cells were injected with the 2A7 antibody, they spread partially, but then began to apoptose. An unrelated control antibody had no effect on cell spreading or cell survival. This result supports the interpretation that one of the most important roles for FAK may be to convey signals from the focal adhesions to the nucleus; these signals inform the nucleus that the

This paper was originally presented at a workshop titled *The Cytoskeleton: Mechanical, Physical, and Biological Interactions.* The workshop, which was held at the Marine Biological Laboratory, Woods Hole, Massachusetts, from 15–17 November 1996, was sponsored by the Center for Advanced Studies in the Space Life Sciences at MBL and funded by the National Aeronautics and Space Administration under Cooperative Agreement NCC 2-896.

cell is attached to the extracellular matrix. In the absence of the FAK signal, anchorage-dependent cells are programmed to undergo apoptosis as a default pathway.

If this interpretation is correct, then one would predict that constituitive activation of FAK would release cells from anchorage dependency. In other words, if the FAK signal to the nucleus is always on, regardless of integrin occupancy, then cells would be able to survive in suspension. This prediction was tested by Stephen Frisch and co-workers (Frisch *et al.*, 1996), who transfected cultured epithelial cells with a constituitively active form of FAK and found that the cells could then survive in suspension and were also tumorigenic in nude mice. These results are in good agreement with those of the Cance lab (Xu *et al.*, 1996), who found higher levels of FAK expression in many types of human tumors. Collectively, these data support the following model: normal cells bind to the extracellular matrix through integrins, which results in the activation of FAK, which then signals the nucleus to suppress apoptosis. The latter signal is perhaps conveyed by the assembled actin cytoskeleton. Tumorigenic cancer cells possess higher levels of active FAK, which suppresses apoptosis regardless of cell attachment, and permits the cells to survive and grow in suspension.

Bibliography

Frisch, S. M., K. Vuori, E. Ruoslahti, and P. Y. Chan-Hui. 1996. Control of adhesion-dependent cell survival by focal adhesion kinase. *J. Cell Biol.* **134:** 793–799.

Hungerford, J. E., M. T. Compton, M. L. Matter, B. G. Hoffstrom, and C. A. Otey. 1996. Inhibition of pp125^{FAK} in cultured fibroblasts results in apoptosis. *J. Cell Biol.* **135:** 1383–1390.

Otey, Carol A. 1996. pp125^{FAK} in the focal adhesion. *Inter. Rev. Cytol.* **167:** 161–183.

Schaller, M. D., C. A. Otey, J. Hildebrand, and J. T. Parsons. 1995. Focal adhesion kinase and paxillin bind to peptides mimicking β integrin cytoplasmic domains. *J. Cell Biol.* **130:** 1181–1188.

Xu, L.-H., L. V. Owens, G. C. Sturge, X. Y. Yang, E. T. Liu, R. J. Craven, and W. G. Cance. 1996. Attenuation of the expression of the focal adhesion kinase induces apoptosis in tumor cells. *Cell Growth Differ.* **7:** 413–418.

Discussion

JANMEY: It seems that the kinase activity of FAK is important, either for sending the signal to the nucleus or for sequestering some factor and preventing it from going into the nucleus and turning some process on. Can you distinguish between those two?

OTEY: In our experiments we can't distinguish between them. We don't know what pathways are being affected downstream from FAK activation. At this meeting, Martin Schwartz showed that Abl seems to have a similar property in regulating anchorage dependency (see list, "Published by Title Only"). His slides showed that Abl is being translocated to the nucleus. An appealing model is that FAK activation is perhaps the proximal event at the membrane, and Abl activation then occurs downstream from FAK and transmits the information to the nucleus. We don't know that to be the case; it is simply wild conjecture.

WADE: In the cells that overexpress the FAK, is actin playing any role in signal transduction?

OTEY: Actin seems to play a role in FAK activation. This has been studied using mainly growth factors in the absence of serum, because different factors present in serum may activate FAK. We don't know if this happens through the integrins or is independent of integrins, but we know that these growth factor effects only occur when the actin cytoskeleton is intact.

WADE: What about the signal going to the nucleus?

OTEY: We don't know whether those serum factors are activating these exact same FAK-mediated pathways that the integrins are activating. I think it would be interesting to ask Don Ingber if he thinks that actin can be playing a role in activating FAK and transmitting a signal to the nucleus.

ALLEN: In the expression of the constitutively active FAK, cells in suspension did not apoptose. Were they able to grow in suspension, or is that a separate pathway?

OTEY: That is the work of Steven Frisch (Frisch *et al.* 1996 *J. Cell Biol.* **134:** 793–799), who found that these cells were not only able to grow in suspension in soft agar, but were also able to generate tumors in nude mice. So, it seems they have almost generated a metastatic phenotype by constitutively activating FAK.

ALLEN: You have done all of your microinjections in cells that are round or spreading and are obviously low in focal adhesions. Do you get the same results if the cells have already established many focal adhesions?

OTEY: When cells are fully spread before we inject and they already have focal adhesions and stress fibers, there is no apparent effect of either the peptide or the antibody.

ALLEN: Does FAK leave the focal adhesion under those conditions?

OTEY: No, FAK is still there. Possibly, when a cell is fully

spread, the focal adhesions are crowded with the protein. Perhaps once the focal adhesions are made, the focal adhesion kinase is no longer accessible to binding by the antibody.

ALBRECHT-BUEHLER: I hope I did not misunderstand you. You are not saying that any cell in soft agar will automatically die? (OTEY: No, I am not saying that.). The cells didn't proliferate in any of these assays, but they didn't die. If you change the adhesiveness of substrates and do the same thing, will you get the same result? You can have cells that spread to different extents depending on how you coat substrates. Do you get the whole effect or half effects? Is it an all-or-none situation?

OTEY: I don't know the answer to your question. We've only done injection experiments on rigid planar substrates coated with fibronectin. Most of what is known about FAK, including FAK activation when cells are spreading, has been studied in cells that were plated onto rigid planar substrates coated with fibronectin. I don't know whether FAK would even be activated if cells were spreading on a more flexible substrate.

ALBRECHT-BUEHLER: It's not the flexibility that I'm after. If you use bacterial plates, for example, where the cells would adhere very poorly, you will get one result. If you use metalized plates or sulfonated plates, you obtain very different results even though you have the same inhibitor concentration.

OTEY: I don't know the answer to your question.

WANG: You mentioned that Keith Burridge's group have microinjected pre-spread cells and yet they can see the FAK.

OTEY: Andy Gilmore (who is present at this meeting) did those injection experiments, so maybe he would like to comment on this question. [Addressing Andrew Gilmore] Andy, he's asking about your experimental design. You injected cells that were spread and then you rounded them up, and plated them down again, correct? That was a little different from the way that we did it.

GILMORE: Yes; however, we have also injected cells that were rounded and in the process of spreading.

WANG: You rounded the cells artificially and then let them spread out?

GILMORE: Yes. If we inject as the cells spread, leave them spread and don't round them up, we still see a reduction in tyrosine phosphorylation and focal adhesions (Gilmore and Romer. 1996. *Mol. Biol. Cell* **7:** 1209–1224). It doesn't seem to have any effect whether or not the cells are forming new focal adhesions or whether they are just left as they are.

WANG: My second question concerns a publication on FAK knockout.

OTEY: Yes, a FAK knockout mouse has been made. That experiment shows us that FAK is important because it was an embryonic lethal; the FAK knockout mouse died at about day 8. From that knockout we know that FAK is important. Results obtained using cells grown out from those embryos were confusing. Cells grown from early embryos had more than the normal number of focal adhesions. This is somewhat confusing because these cells, which lacked focal adhesion kinase, had a tremendous number of focal adhesions. I think it's hard to draw any conclusions; we don't know what is going on.

GILMORE: I would like to comment on FAK knockout cells. To get cells to grow out of the FAK knockout mice they had to mutate and knock out P53.

OTEY: Basically, they have to immortalize the cells.

GILMORE: Yes, which could have profound implications for the ability of the cell to proliferate and resist apoptosis, so I don't think we can really make comparisons.

OTEY: There's no question that FAK knockout cells are certainly able to make focal adhesions.

Reference: *Biol. Bull.* **194:** 390–393. (June, 1998)

Effects of Hemodynamic Forces on Gene Expression and Signal Transduction in Endothelial Cells

SHU CHIEN AND JOHN Y. J. SHYY

Department of Bioengineering and Institute for Biomedical Engineering, University of California, San Diego, La Jolla, California

Vascular endothelial cells respond to mechanical forces, such as shear stress, by expressing a number of immediate early genes. One of these genes encodes monocyte chemotactic protein-1 (MCP-1, Shyy *et al.*, 1994), which plays a significant role in atherogenesis. This presentation summarizes the work done in our laboratory on the effects of shear stress on signal transduction and on the expression of the MCP-1 gene. Human umbilical vein endothelial cells and many other cell types respond to arterial level of shear stress (10–30 dynes/cm^2) with a transient increase of MCP-1 gene expression that peaks at 1.5 h (Shyy *et al.*, 1994). Sequential deletion of the 5′ promoter region of the MCP-1 gene and site-specific mutation of the *cis*-elements show that one of the two copies of the putative TPA-responsive elements (TRE), with the sequence TGACTCC, is critical for shear-stress induction of the MCP-1 gene (Shyy *et al.*, 1994). Transactivation assays indicate that activating protein-1 (AP-1, composed of Jun-Fos heterodimer or Jun-Jun homodimer) is the nuclear binding protein responsible for shear activation of MCP-1.

The signal transduction pathways leading to the activation of AP-1/TRE by shear stress have been investigated with protein kinase assays and dominant negative mutants of signaling molecules in the pathways of the c-jun NH_2 terminal kinases (JNK) and the extracellular signal-regulated kinases (ERK). JNK(K-R) and MEKK(K-M), the catalytically inactive mutants of, respectively, JNK1 and MEKK in the JNK pathway, attenuate the shear-induced TRE responses. The dominant negative mutant of Ha-Ras blocks the shear-activation of JNK and the downstream TRE. These results indicate that shear stress activates primarily the Ras-MEKK-JNK pathway in inducing MCP-1 gene expression (Li *et al.*, 1996, 1997).

Shear stress rapidly and transiently increases the association between growth factor receptor-2 (Grb2) and Son of sevenless (Sos) in bovine aortic endothelial cells. Shear stress also augments the tyrosine phosphorylation of FAK and its association with Grb2. FAK(F397Y) and FAK(F925Y), the negative mutants of FAK, attenuate the shear-stress induction of the kinase activity of HA-JNK (Li *et al.*, 1997). Similarly, the shear-stress-induced activities of luciferase (Luc) reporter gene linked to MCP-1 or 4×TRE promoters are decreased by these FAK mutants. Thus, the Tyr-397 (autophosphorylation site) and the Tyr-925 (binding site for Grb2 src homology domain 2 [SH2]) of FAK are critical for its activation in response to shear stress. pGrb2-SH2, which encodes the SH2 domain of Grb2, and pΔmSos1, in which the guanine nucleotide exchange domain has been deleted, also attenuate induction of HA-JNK, MCP1-Luc, and 4×TRE-Luc by shear stress. These results indicate that the FAK-Grb2-Sos-Ras-MEKK-JNK system is a major signaling pathway mediating the shear-induced gene expression (Fig. 1). Other signaling mechanisms may also be involved; *e.g.*, we have found that shear stress causes an increase of protein kinase C, especially in the cortical region, in the endothelial cell (Hu and Chien, 1997).

This paper was originally presented at a workshop titled *The Cytoskeleton: Mechanical, Physical, and Biological Interactions.* The workshop, which was held at the Marine Biological Laboratory, Woods Hole, Massachusetts, from 15–17 November 1996, was sponsored by the Center for Advanced Studies in the Space Life Sciences at MBL and funded by the National Aeronautics and Space Administration under Cooperative Agreement NCC 2-896.

List of abbreviations: AP, activating protein; EC, endothelial cell; ECM, extracellular matrix; ERK, extracellular signal regulated kinase; FAK, focal adhesion kinase; JNK, Jun amino-terminal kinase; MAPK, mitrogen-activated protein kinase; MCP, monocyte chemotactic protein; MEKK, MAPK/ERK kinase-kinase; PDGF, platelet-derived growth factor; TRE, TPA-responsive elements; VSMC, vascular smooth muscle cell.

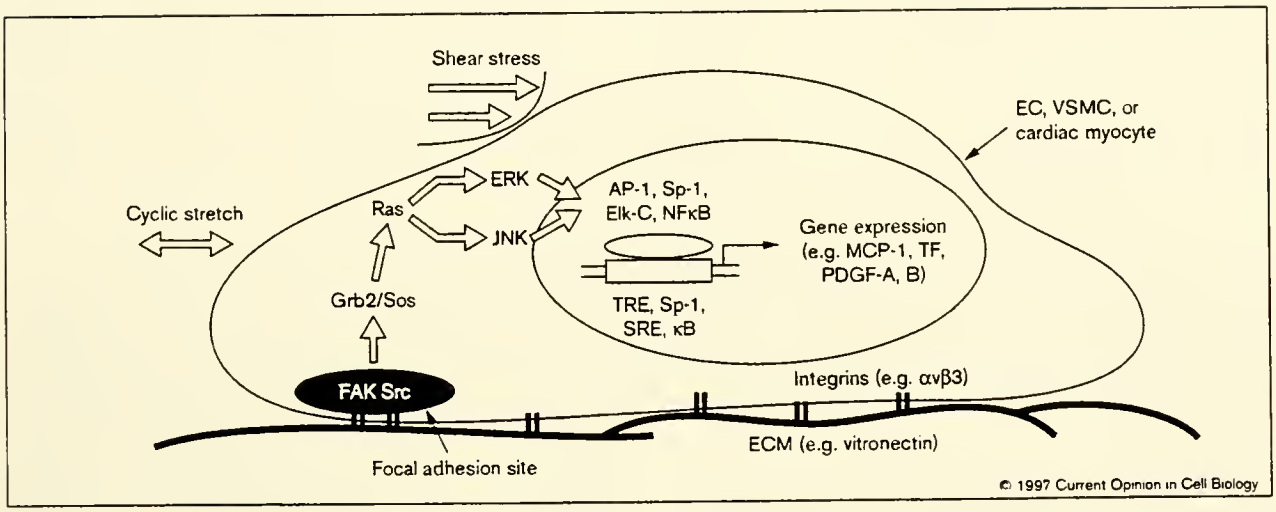

Figure 1. Proposed mechanotransduction pathways in cells such as ECs, VSMCs and cardiac myocytes in response to mechanical stresses such as shear stress and cyclic stress. This diagram shows only the proposed involvement of the molecules in focal adhesion sites, including integrins, ECM proteins, FAK, Src, *et cetera*, in mechanotransduction. The activated chemical signals can be transduced from these molecules through SH2-containing docking proteins such as Grb2 to activate the small GTPase Ras. Downstream to Ras, cytoplasmic MAPKs such as JNK and ERK are activated and they, in turn, cause the activation of nuclear transcription factors such as AP-1, Sp-1, Elk-C, and NFκB. Interactions of these transcription factors with their corresponding *cis* elements (*i.e.*, TRE [12-*O*-tetradecanoylphorbol 13-acetate-responsive element], Sp-1, SRE [serum-response element] and κB, respectively) lead to the activation of appropriate genes, for example, those encoding monocyte chemotactic protein-1 (MCP-1), tissue factor (TF) and PDGF-A and B. Not shown in this diagram is the involvement of other molecules such as the G proteins, receptor tyrosine kinases, and possibly ion channels and cytoskeletal proteins in mechanotransduction. [Figure and legend reprinted, with permission, from John Y.-J. Shyy and Shu Chien. 1997. *Current Opinion in Cell Biology* **9:** 707–713.]

Studies on the tissue factor gene show that the shear-stress-responsive element is Sp1 in the GC rich region of its promoter and that the two copies of TREs there are not critical (Lin *et al.*, 1997). Coupled with the finding by Resnick *et al.* (1993) that the nucleotide sequence GAGACC is the shear-stress-responsive element for the platelet-derived growth factor B chain, our results indicate that shear stress activates different *cis*-elements in different genes (Shyy *et al.*, 1995). The orchestration of various *cis*-elements and signaling pathways may play an important role in determining the complex gene regulation in response to mechanical forces in health and disease, including those induced by microgravity.

Acknowledgments

Supported by NIH Research Grant HL-44147.

Bibliography

Hu, Y. L., and S. Chien. 1997. Effects of shear stress on protein kinase C distribution in endothelial cells. *J. Histochem. Cytochem.* **45:** 237–249.

Li, Y. S., J. Y. J. Shyy, S. Li, J. D. Lee, B. Su, M. Karin, and S. Chien. 1996. The Ras/JNK pathway is involved in shear-induced gene expression. *Mol. Cell. Biol.* **16:** 5947–5954.

Li, S., M. Kim, D. D. Schlaepfer, T. Hunder, J. Y. J. Shyy, and S. Chien. 1997. The fluid shear stress induction of JNK pathway is mediated through FAK-Grb2-sos. *J. Biol. Chem.* **272:** 30455–30462.

Lin, M. C., F. Almus-Jacobs, H.-H. Chen, G. C. N. Parry, N. Mackman, J. Y. J. Shyy, and S. Chien. 1997. Shear stress induction of tissue factor gene expression and phosphorylation of SP1. *J. Clin. Invest.* **99:** 737–744.

Resnick, N., T. Collins, W. Atkinson, D. J. Bonthron, F. Dewey, Jr., and M. A. Gimbrone, Jr. 1993. Platelet-derived growth factor B chain promoter contains a cis-acting fluid shear-stress-responsive element. *Proc. Natl. Acad. Sci. USA.* **90:** 4591–4595.

Shyy, Y.-J., and S. Chien. 1997. Role of integrins in cellular response to mechanical stress and adhesion. *Curr. Opin. Cell Biol.* **9:** 707–713.

Shyy, Y.-J., H.-J. Hsieh, S. Usami, and S. Chien. 1994. Fluid shear stress induces a biphasic response of human monocyte chemotactic protein-1 gene expression in vascular endothelium. *Proc. Nat. Acad. Sci. USA* **91:** 4678–4682.

Shyy, Y. J., Y. S. Li, M. C. Lin, H. Gregersen, W. Chen, S. Yuan, F. Almus, S. Usami, and S. Chien. 1995. The shear stress-mediated gene expression and the *cis*-elements involved. *J. Biomechanics* **28:** 1451–1457.

Shyy, Y.-J., M. C. Lin, J. Han, Y. Lu, M. Petrime, and S. Chien. 1995. TPA responsive element as a common cis-acting element for mechanical and chemical stimuli. *Proc. Nat. Acad. Sci. USA.* **92:** 8069–8073.

Discussion

KOWALCZYK: Are the cells exposed to fresh medium or serum at the beginning of the experiment? Do you rinse them before flow is initiated? A lot of the changes you describe resemble transient effects associated with growth factor addition. Perhaps the initiation of flow over the cells is changing local concentrations of growth factors or metabolites near the cell surface.

CHIEN: Cells were washed with serum-free culture medium before initiation of flow. The responses I have described are not serum-dependent. Chemical stimuli such as TPA and mechanical stimulation can mutually affect each other. If you pretreat the cell with TPA to down-regulate the pathway to JNK, and then stimulate with mechanical shear, you get much less response, suggesting that both effects share the same pathway.

COULOMBE: Would you repeat the changes that are taking place in the three filament systems of the cells, and also speculate on the kinetics as these relate to the signaling events that you described?

CHIEN: The mRNA response starts within an hour or so, but cytoskeletal reorganization takes a long time. Thus, the shear-induced gene expression occurs much earlier than detectable reorganization of the cytoskeletal fibers. All the responses in the pathway occur in the correct sequence. Ras is activated upstream in less than 1 min. Activation of JNK occurs within a few minutes, and the MCP-1 gene is activated later. Thus, there is a sequential activation. The morphological changes of cytoskeletal reorganization are the long-term change; they do not precede the changes in signal transduction and gene expression. Now there may be some subtle changes in the cytoskeletal proteins that are responsible for the signaling and gene expression, but these cannot be seen morphologically at an early stage. Actin seems to be playing a role here. The actin filaments, which were present as peripheral bands in the static condition, gradually disappear after shear and reorganize themselves into long stress fibers. These fibers tend to move from the basal side toward the top of the cell. Using confocal microscopy we observed that the microtubules and the intermediate filaments, which were originally around the nuclei, began to move toward the base after shearing. The nature of the association of these cytoskeletal elements with each other has been mentioned several times during this workshop.

BAKER: You showed a peak of activity for many factors right after you start your shear stress. Is there a physiological static state, and does this apply to starting exercise, where the body sees a sudden, greater stress?

CHIEN: What we have shown here is not a physiological response, because we start from a static situation. This only applies to a pathological state, like re-perfusion after stoppage of flow. In the physiological state, long-term shear occurs in the straight part of the vasculature. As shown in my first slide, the vasculature in the straight part of the thoracic aorta is sheared all the time, and the MCP-1 gene is therefore down-regulated, and monocytes tend not to be attracted there. At branch points, the flow is unsteady and there are flow reattachment areas near the bifurcation. These reattachment areas don't stay at the same spot; they move back and forth. The spatial effects were discussed by Dr. Fujiwara. It is my belief that the spatial and temporal variations are very important. At one moment there is no shear; then there is shear in one direction; then there is shear in another direction. The endothelial cells in these areas can sense what is going on. Our preliminary results, using an *in vitro* analog of those branch points, do confirm the hypothesis that the reattachment areas in the branch regions are vulnerable. Concerning your question on exercise, I think during exercise shear increases, not only in the straight part of the aorta, but this increase also invades the bifurcation. The exposure of these regions to fairly steady high shear may down-regulate the genes. This may be why physicians always tell us to exercise three times a day, at least 30 min each time. I think that's what it takes for the down-regulation to occur.

CHEN: I'm wondering why the experiments do not start with a constant shear flow which is then changed. Do you use turbulent flows? I would imagine there is recirculation at those bifurcation points.

CHIEN: We are doing these experiments with recirculation and reattachment.

CHEN: Is there anything known about that?

CHIEN: Yes. The reattachment area seems to be very important. In the vicinity there are eddies, secondary flows, and stagnation. These are the sites of action. You ask why we don't start with a baseline flow. We are doing these experiments, and other groups are also doing them. Those studies have more physiological relevance, but it is much easier to see the effect if you start from zero. If you want to work out the pathway from the point of view of molecular biology, again it is simpler to start from zero. You can then go to a more physiologically relevant system.

BRUINSMA: You showed a physical stimulus that produces a gene response; then you show two parallel pathways, each containing eight steps. Why is this so complex? I can imagine that a number of amplification steps cross-link to other stimuli. Can you comment on this?

CHIEN: They are cross-linked to other pathways. I have presented a simplification which you say is complex. In fact, it is like a neural network, where there are layers and layers of interactions. The cells in our body have complex interacting pathways, and we are not dealing with simple situations. To deal with our daily environment and to adjust to microgravity, we must have a very finely tuned system, with redundancy and delicacy of controls.

BRUINSMA: Is there intertalk between the pathways? Do you see saturation?

CHIEN: If you vary the shear stress, you do see a saturation effect. We don't see any differences beyond about 10 dynes/cm^2. We are very interested in the kinetics of this process. We are interested in modeling all of this, but it's too complex, and we don't have sufficient data to do the modeling. There is crosstalk among the pathways. Although we have some kinetic data describing how quickly each step happens in one pathway, we have no good means of manipulating every step so as to examine how the next step behaves. We need to establish the transfer function for each station. We're not getting that yet. With data from experiments being done in a number of labs, we hope that we can start to look into that.

STEWART: Continuing on with the complexity of the signaling pathways, one of the difficulties, always, is knowing which part is being stimulated, because quite often one pathway will stimulate an adjacent pathway. I was wondering whether two classes of experiment that you have done might help to distinguish where the signal is actually coming from. The first one would be to introduce the constitutively active Ras mutants. Strictly, putting in the N17 is wiping out the GEF, rather than actually showing the positive involvement of Ras. Then, wondering backwards, is the signal actually deriving from a surface receptor, or not? I know you mentioned, for example, that the EGF receptor was phosphorylated. That would make me wonder whether, if you treated these sort of cells with EGF, you would actually get the induction of the MCP-1 protein that you are measuring. Or is it that there is some other part of the cell that is sensing the pressure and that there might be a difference, then, in the response in stimulating a surface receptor to say, FAK?

CHIEN: These are excellent questions. To answer the question about whether the protein is induced, it is indeed. Not only is the protein induced, it is also functional. We get enhancement of monocyte adhesion after applications of shear stress. We are doing experiments with over-expression of the wild type, and the results do fit in.

GOLDMAN: I just want to make one comment. We have done experiments with Peter Davies in which we shear cells and then detect very significant changes in the cytoskeleton within 60 min. There are profound changes in the organization. It does not take 12 to 24 hours for us to see this effect.

CHIEN: What I meant was that you need that long to see the kind of morphological changes I showed.

GOLDMAN: The shape changes take a long time, but the cytoskeletal changes begin very quickly.

CHIEN: That's right. Actually they do not go to this final state; they go through a whole series of contortions. They may first align perpendicular to flow or swirling patterns, as mentioned by Dr. Fujiwara. That's what I meant. I agree with you completely, but to get to the picture I showed, it did take 12–24 hours of shearing. In fact, I said that the actin plays a role, and there may be changes occurring in less than 60 min that we cannot even see morphologically.

GOLDMAN: I would say within minutes.

CHIEN: I agree with you completely. One other thing I wanted to mention is that the mechanical force probably activates many types of molecules, including receptors and channels. These effects must be summed to give the final response. That's why, whenever we try to block these responses, we can never block them completely. It is a summation effect of many responses. Each may be nonspecific and weak, but the sum total gives us a significant response. This is one of the differences from chemical stimulation, where the ligand-receptor interaction is specific.

Reference: *Biol. Bull.* **194:** 394–399. (June, 1998)

Effect of Flow on Gene Regulation in Smooth Muscle Cells and Macromolecular Transport Across Endothelial Cell Monolayers

LARRY V. MCINTIRE[1], JOHN E. WAGNER[1], MARIA PAPADAKI[1], PEGGY A. WHITSON[2], AND SUZANNE G. ESKIN[3]

[1] *Institute of Biosciences & Bioengineering, Rice University, Houston, Texas 77251;* [2] *Medical Sciences Division, NASA/Johnson Space Center, Houston, Texas 77058; and* [3] *Cell Biology Department, Texas Biotechnology Corporation, Houston, Texas 77030*

Introduction

Endothelial cells line all of the vessels of the circulatory system, providing a non-thrombogenic conduit for blood flow; they regulate many complex functions in the vasculature, such as coagulation, fibrinolysis, platelet aggregation, vessel tone and growth, and leukocyte traffic; and they form the principal barrier to transport of substances between the blood and the surrounding tissue space. The permeability of endothelial cells changes with environmental stimuli; shear stress, in particular, applied either *in vivo* or *in vitro*, induces changes in protein expression and secretion of vasoactive factors by endothelial cells (Nollert *et al.*, 1991; McIntire, 1994; Papadaki and Eskin, 1997). The ability to study the effects of shear on the macromolecular permeability of the cerebral vasculature is particularly important, since in no other place is the barrier function of the endothelium more important than in the brain. The endothelial cells of this organ have developed special barrier properties that keep the cerebral system from experiencing any drastic change in composition; together with glial cells, they form the blood brain barrier (BBB). We have studied the effect of flow on bovine BBB using flow chambers and tissue culture systems.

This paper was originally presented at a workshop titled *The Cytoskeleton: Mechanical, Physical, and Biological Interactions.* The workshop, which was held at the Marine Biological Laboratory, Woods Hole, Massachusetts, from 15–17 November 1996, was sponsored by the Center for Advanced Studies in the Space Life Sciences at MBL and funded by the National Aeronautics and Space Administration under Cooperative Agreement NCC 2-896.

Recent modeling studies indicate that, not only the endothelium, but also the underlying smooth muscle cells (SMC) in the vasculature are exposed to significant shear stresses that arise from interstitial flow driven by transmural pressure gradients (Wang and Tarbell, 1995). In response to vascular injury, the medial SMCs of arteries proliferate and migrate to the intima (Schwartz, 1993). Moreover, it has been hypothesized that the SMC are directly exposed to blood flow when the integrity of the endothelial monolayer is disrupted, and that their healing behavior is then modulated by the local hemodynamic environment (Kohler *et al.*, 1991; Kohler and Jawien, 1992). Presumably, however, the effects of this environment on the SMC are not only mediated by flow, but also by small messenger molecules whose rate of production may be modulated by flow.

Nitric oxide (NO) is such a molecule; among its diverse biological functions are vasorelaxation, reduction of platelet aggregability, inhibition of adhesion of inflammatory molecules in the vascular wall, and cytostatic or cytotoxic actions in various cell types (Sessa, 1994; Koprowski and Maeda, 1995). To date, three major subtypes of nitric oxide synthase (NOS) have been identified. One subtype is the inducible NOS (NOS II), which is regulated at the transcriptional level and produces high levels of NO for extended periods. NO II is present in macrophages, SMC, and endothelial cells upon stimulation with cytokines. The other two isoforms are constitutively expressed and normally produce low levels of NO; they are termed NOS I (in neuronal, epithelial cells) and NOS III (in endothelial cells, cardiac myocytes, and skeletal muscle) (Koprowski and Maeda, 1995). Recent findings

indicate that mechanical deformation of the endothelium by shear stress or by cyclic stretching increases NOS III mRNA, protein and enzymatic activity (Sessa, 1994). We have investigated the effects of fluid shear stress on the growth kinetics of cultured human aortic SMC (hASMC) and on NO released by these cells.

Materials and Methods

Cell culture

Brain microvessel endothelial cells (BMECs) were isolated by a two-step enzymatic process. Briefly, a fresh bovine brain was obtained from a local slaughterhouse, and the isolation was begun within 18 h post-mortem. The gray matter was separated from the white matter, collected, blended (Tekmar Instrument Co. stomacher), and digested with 0.5% dispase (Boehringer-Mannheim) for 3 h at 37°C. The solution was then centrifuged on a dextran (Sigma) gradient, washed, and redigested with 1 mg/ml collagenase/dispase (Boehringer-Mannheim) for 5 h at 37°C. The microvascular endothelial cells were separated from the other cells by centrifugation (1000 × *g*) on a preformed 50% Percoll (Sigma) gradient. The second layer (containing the cells) was removed, washed, and frozen in liquid nitrogen for later use. After thawing, the isolated BMECs were grown on surfaces that were treated with both type I rat tail collagen and human fibronectin. The culture media contained MEM/F-12 (Sigma) supplemented with 10% plasma derived horse serum (Hyclone), 0.1 mg/ml penicillin G/streptomycin (Gibco), 2.5 mg/ml fungizone (Gibco), and 0.1 mg/ml heparin (Sigma).

A hASMC line initiated with cells from the abdominal aorta of a 9-year-old kidney transplant donor was used in all the experiments performed in this study (Papadaki *et al.*, 1996); the culture medium was Dulbecco's modified Eagle's medium (DMEM) supplemented with 20% fetal bovine serum (FBS), 2 mmol L-glutamine, 200 U/ml penicillin, and 100 μg/ml streptomycin. Phenol-red-free DMEM was used in the nitrite experiments to prevent color interference with the fluorometric assay. hASMC (P2-P10) were plated at a subconfluent density of 2.5 × 10^4 cells/cm^2, on fibronectin-coated glass slides (75 × 38 mm). Twenty-four hours after seeding, hASMC were exposed to physiological levels of venous and arterial laminar stress (5 to 25 dyn/cm^2) in parallel plate flow chambers connected to recirculating flow loops (Papadaki *et al.*, 1996). The experiments were run in a humidified room at 37°C and the system was gassed with 5% CO_2. For the growth studies, the flow experiments were carried out for 24 h. At the end of each experiment, the cells were removed from the slide with the 0.05% typsin-EDTA, and the number of cells was determined with a Coulter Counter.

Permeability

The marker molecules for the permeability experiments were fluoroisothiocynate (FITC) dextran (Pharmacia for all molecular weights except 2 million). The 70 and 2000 kD probes were dialyzed extensively before use. The dextrans were also tested for purity on thin-layer chromatography (70% chloroform; 25% methanol and 5% acetic acid, on silica gel plates, as recommended by Molecular Probes). Permeability was measured in a modified parallel plate flow chamber according to methodology described earlier (Nollert *et al.*, 1991; McIntire, 1994; Casnocha *et al.*, 1989; Wagner *et al.*, 1997).

Nitrate assay

Samples of the conditioned media samples were collected at different times, and nitrite, as an index of nitric oxide production, was measured with a quantitative fluorometric assay (Misko *et al.*, 1993, Papadaki *et al.*, 1998). This assay is based on the reaction of nitrite with an acid form of 2,3-diaminonaphthalene to form the highly fluorescent product 1-(H)-naphthotriazole. The intensity of the fluorescent product was maximized by the addition of 2.8 N NaOH, and the signal was measured with a fluorescent 96-well plate reader, with excitation of 365 nm and emission read at 460 nm.

Western blotting

NOS protein was detected in total cell lysates. Cells were harvested from both the control and flow cultures in 150 μl of lysis buffer (0.5% SDS, 50 m*M* Tris/Cl, pH 7.4, leupeptin 1 mg/ml, pepstatin 1 mg/ml, 0.1 *M* phenylmethylsufonyl fluoride). Cell homogenates were centrifuged for 20 min at 14,000 × *g* at 4°C to remove insoluble material, and the viscosity of the supernatant was then reduced by several passages through a 26-gauge needle. Protein concentration was measured in a small aliquot of sample with the micro BCA method. The samples were further diluted, at a ratio of 3:1 in a 4× sample buffer (0.2 m*M* TrisCl, pH 6.8, 4% SDS, 40% glycerol, 0.4% bromophenol blue, 10% β-mercaptoethanol) and boiled for 5 min. Equal amounts of protein were loaded in a 7.5% SDS-polyacrylamide minigel and electrophoresed at a constant current of 15 mA for 2 hours. The separated proteins were transferred to nitrocellulose membranes, and the blots were incubated for 1 h with 5% nonfat dry milk in Dulbecco's phosphate buffered saline (PBS) and 0.05% Tween-20, (PBS-T) to block nonspecific binding of the antibody. The membranes were incubated overnight with primary monoclonal and polyclonal antibodies against all isoforms of NOS protein (Transduction Laboratories); the antibodies were diluted 1:500 in PBS-T. Blots were washed (PBS-T × 5) and then incu-

Table I

Increase in permeability over baseline[a]

	1 dyne/cm^2		10 dyne/cm^2	
MW KDa	18 h	30 h[b]	18 h	30 h[b]
2000	76	4	34	2.3
70	20	0.8	11	−0.4
4	2	1.2	3.4	1.4*

[a] Increases shown are multiples of baseline values.
[b] Not significantly larger than baseline values, except (*).

bated for 1 h with a donkey anti-rabbit secondary antibody conjugated to horseradish peroxidase and used at a dilution 1:1000 in PBS-T. Nitric oxide synthase immunoreactivity was detected by the enhanced chemiluminescence (ECL) method, followed by autoradiography.

Results

Permeability

The permeability of BMECs under shear stresses of 1 dyne/cm^2 or 10 dyne/cm^2 rose rapidly at first, became maximal between 10 and 18 h, and had largely recovered by 30 h (Table I).

Smooth muscle cell metabolism

Our results demonstrated that fluid shear stress decreased the proliferation rate of hASMC (Fig. 1). The cell number at high shear-stress levels (> 17.5 dyn^a/cm^2) was significantly lower than at low levels of shear stress (> 15 dyn^a/cm^2). Furthermore, at all shear-stress levels tested, the growth rate was reduced relative to stationary control cultures (Papadaki *et al.*, 1996). The flow-related reduction in the cell number was not due to cell injury, as demonstrated by the equality of lactate dehydrogenase (LDH) activity in the conditioned media of control and sheared cultures (results not shown). The LDH concentration in the medium of the stationary cell (3.5 ± 0.8 U/L) was not different from those in the media containing cells at all different shear stress levels used (2.4 ± 1.5 U/L) (Papadaki *et al.*, 1996). In addition, indirect immunofluorescence for the proliferating cell nuclear antigen (PCNA) provided further evidence that, in the range of shear stresses used and for the time course of these experiments, the growth of the cell population was not arrested. Control cultures had more PCNA-positive nuclei ($37\% \pm 6\%$) than cultures exposed to flow, and this difference was essentially the same as that seen for cell density ($35\% \pm 6\%$). This comparison suggests that the reduction in the cell number observed with shear stress is due to slower movement of cells through the cell cycle (Papadaki *et al.*, 1996).

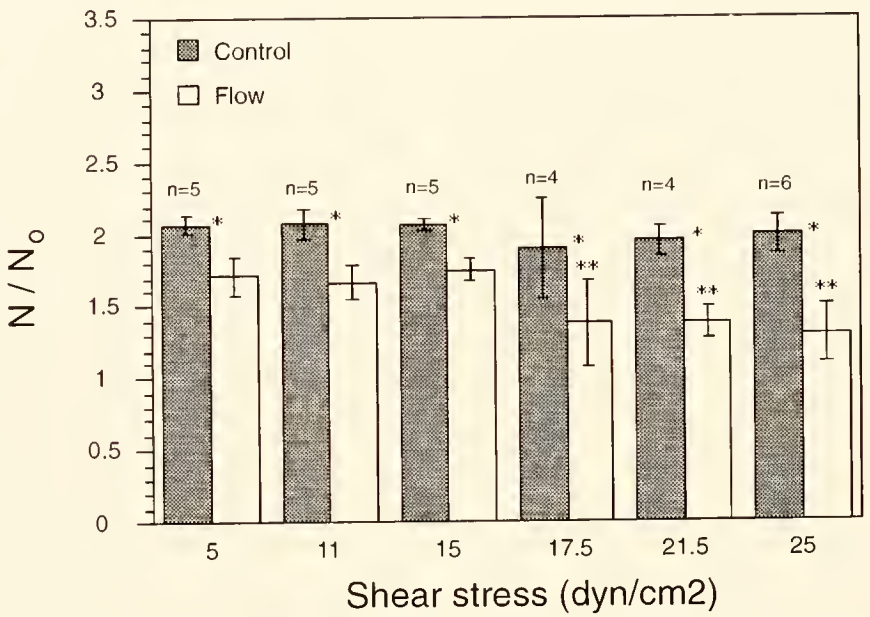

Figure 1. Effect of shear stress on the growth rate of human aortic smooth muscle cells (hASMC). Results are expressed as the mean ± SD. Multiple comparisons were made by one-way ANOVA followed by Fisher's least-squares difference ($P < 0.05$). N/N_0 is the ratio of cells per square centimeter at the end of an experiment to that 24 h after seeding (at the initiation of flow). *, significantly different from the control; **, significantly different from 5, 11, 15 dyne/cm^2.

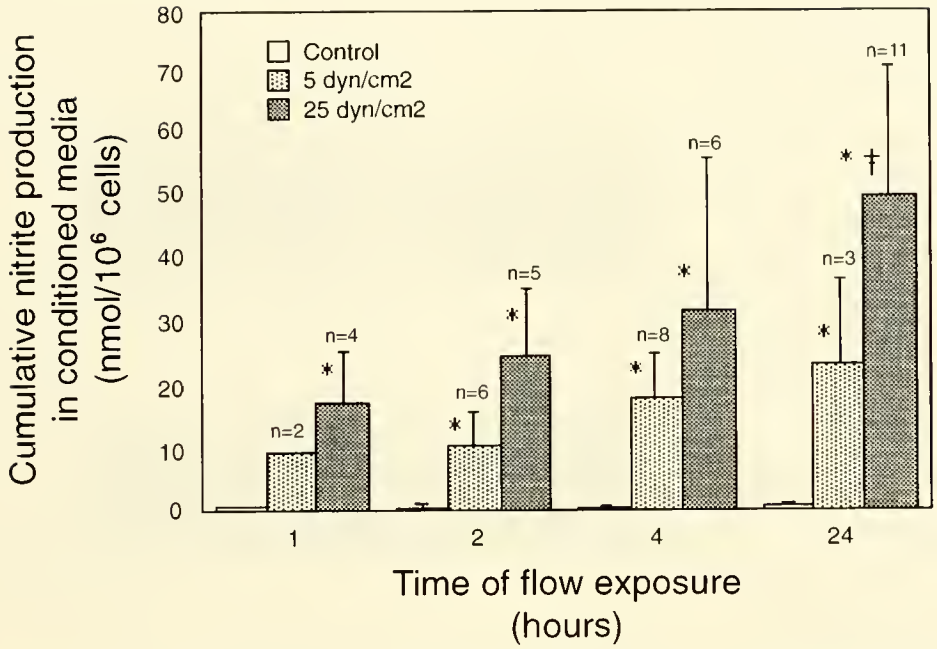

Figure 2. Nitrite production in human aortic smooth muscle cells in the presence of shear stress. Results are expressed as mean ± SEM. Multiple comparisons were made by one-way ANOVA followed by Fisher's least-squares difference ($P < 0.05$); (n = 7–9 for control cultures). *, significantly different from the control; †, significantly different from 5 dyn/cm^2.

The effects of flow on nitrite production by hASMC are shown on Figure 2. Shear stress significantly increased nitrite levels in the conditioned media, whereas the levels present in the stationary control cells were almost undetectable (Papadaki *et al.*, 1998). Cumulative nitrite production in conditioned media increased with the duration of flow exposure and with shear. However, nitrite production rates were inversely correlated with time. An initial burst in nitrite production rate, detected as early as 1 h after flow exposure, was followed by a gradual decrease with time. Similar experiments with endothelial cells have shown similar trends in nitrite production rates (Kuchan and Frangos, 1994). This result was the first indication that the NOS isoform responsible for shear-induced NO production is not NOS II; *i.e.*, activation of NOS II results in sustained nitrite production rates for extended periods (up to 72 h after addition of stimulant). Treatment with 100 μM N^G-amino-L-arginine (L-NAA) for 30 min before and during exposure to shear stress (25 dynes/cm^2) completely abolished the flow-induced release of nitrite without affecting release from stationary cultures. L-NAA is a potent amino-substituted NOS inhibitor (Kuchan and Frangos, 1994). The complete inhibition of the nitrite signal in the presence of inhibitor provided evidence that the NO production in response to shear stress comes from the enzymatic reaction of L-arginine to L-citrulline, and is not a result of cell debris.

To identify the NOS isoform involved, cultures were incubated with 1 μM dexamethasone (DM) 24 h before and during exposure to shear stress (Papadaki *et al.*, 1998). DM is a steroid that blocks transcription of NOS II by interfering with the binding of transcription factors to the promoter region of the gene (Rees *et al.*, 1990). Dexamethasone had no effect on the nitrite levels in either the controls or the flow cultures. This result provided further evidence that NOS II plays no role in flow-induced nitrite production by hASMC. Monoclonal or polyclonal antibodies against NOS II showed no immunoreactivity with Western blot analysis (Fig. 3), which verified that the inducible isoform was not present, either in control or sheared hASMC cultures. On the other hand, polyclonal antibodies against the constitutively expressed isoform of neuronal NOS (NOS I) gave specific products in all stationary control and flow samples (Fig. 3). The intensities of the control and shear NOS I bands are identical at 6 h, indicating that cultured hASMC express a constitutive NOS I protein whose enzymatic activity, rather than the amount of protein, is modulated by shear stress. Endothelial NOS (NOS III) was found in neither control nor sheared hASMC (Fig. 3).

Summary and Conclusions

BMECs in static culture have a swirling spindoidal morphology. After exposure to flow for 10–18 h, BMECs

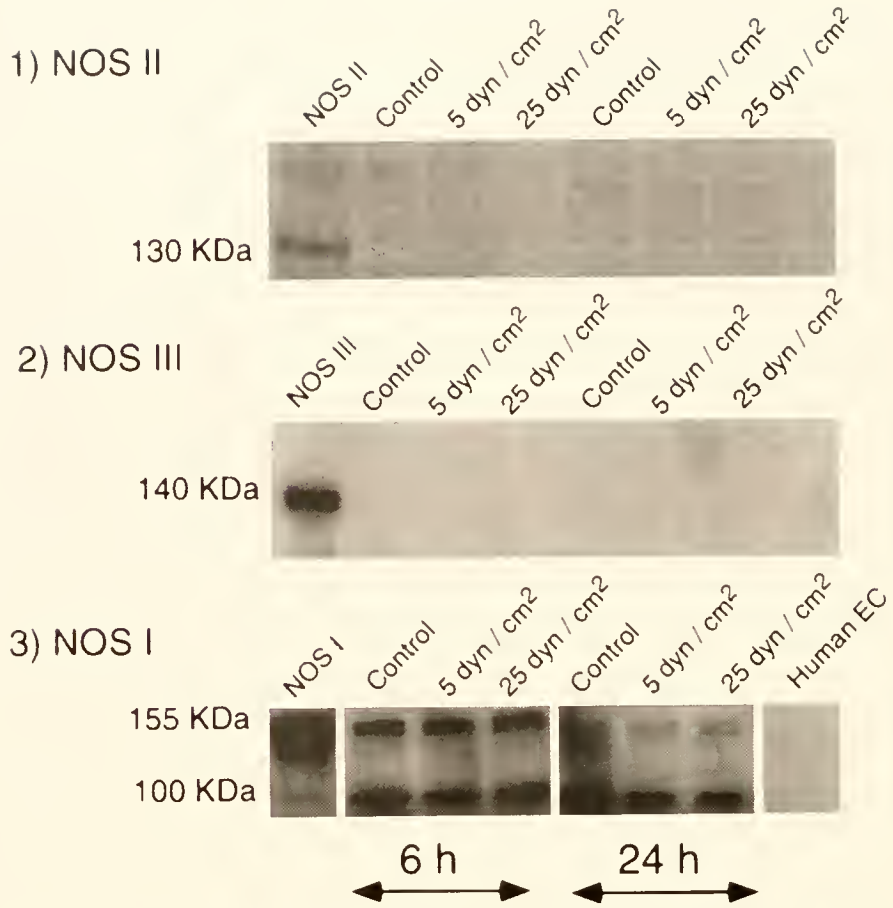

Figure 3. Western blot of nitric oxide synthase (NOS) protein in total cell lysates of hASMC. (1) Blot was incubated with a monoclonal NOS II antibody. *Lane 1*, positive control for NOS II (human glioblastoma cell line, incubated with cytokines); *lanes 2–4*, representative samples of a 6-h experiment; *lanes 5–7*, representative samples of a 24-h experiment. (2) Blot was incubated with a monoclonal NOS III antibody. *Lane 1*, positive control for NOS III (human endothelial cells); *lanes 2–4*, representative samples of a 6-h experiment; *lanes 5–7*, representative samples of a 24-h experiment. (3) Blot was immunoblotted with a monoclonal NOS I antibody. *Lane 1*, positive control for NOS I (rat pituitary tumor cell line); *lanes 2–4*, representative samples of a 6-h experiment; *lanes 5–7*, representative samples of a 24-h experiment; *lane 8*, human endothelial cell (EC) lysate used as a negative control.

appeared rounded with no preferred orientation. Further application of 10 dynes/cm^2, but not 1 dyne/cm^2, induced the cells to elongate in the direction of flow (data not shown). We demonstrated that BMECs initially respond to either of 1 dyne/cm^2 or 10 dynes/cm^2 shear stress with a dramatically increased macromolecular permeability. Maximum permeabilities were obtained between 10 and 18 h in the shear field for both shear rates, and these timepoints corresponded to the most rounded morphology. Continued application of the shear field led to a partial recovery in the permeability of the cerebral endothelial cells to macromolecules. The initial increase in permeability and the recovery was most dramatic for the higher molecular weight dextran markers.

We have also shown that the flow-induced shear stress stimulates NO production in hASMC due to activation of a constitutively expressed NOS I enzyme. The constitutive expression of NOS I in SMC, and its concomitant activation by flow-induced shear stress, may play a regulatory role in the blood vessel wall in the absence of endothelium due to vascular injury. Shear-induced NO production from vascular SMC may inhibit excessive adhesion of platelets and other inflammatory molecules at the injury site, and may regulate the release of mitogenic factors by activated blood cells. In vascular wall homeostasis, constitutive NO production by underlying SMC, modulated due to transmural flow, may act in concert with endothelial-cell-derived NO to regulate vascular tone and maintain a non-proliferative phenotype for SMC.

Literature Cited

Casnocha, S. A., S. G. Eskin, E. R. Hall, and L. V. McIntire. 1989. Permeability of human endothelial cell monolayers: effect of vasoactive agonists and cAMP. *J. Appl. Physiol.* **87:** 1997–2005.

Kohler, T. R., and A. Jawien. 1992. Flow affects development of intimal hyperplasia after arterial injury in rats. *Arterioscler. Thromb.* **12:** 963–971.

Kohler, T. R., T. R. Kirkman, L. W. Krais, B. K. Ziegler, and A. W. Clowes. 1991. Increased blood flow inhibits neointimal hyperplasia in endothelialized vascular grafts. *Circ. Res.* **69:** 1557–156.

Koprowski, H., and H. Maeda. 1995. *The Role of Nitric Oxide in Physiology and Pathophysiology.* Springer-Verlag, New York.

Kuchan, M. J., and J. A. Frangos. 1994. Role of calcium and calmodulin in flow-induced nitric oxide production in endothelial cells. *Am. J. Physiol.* **35:** C628–C636.

McIntire, L. V. 1994. Bioengineering and vascular biology. *Ann. Biomed. Eng.* **22:** 2–13.

Misko, T. P., R. J. Schilling, D. Salvemini, W. M. Moore, and M. G. Currie. 1993. A fluorometric assay for the measurement of nitrite in biological samples. *Anal. Biochem.* **214:** 1–6.

Nollert, M. U., S. L. Diamond, and L. V. McIntire. 1991. Hydrodynamic shear stress and mass transport modulation of endothelial cell metabolism. *Biotechnol. Bioeng.* **38:** 588–602.

Papadaki, M., and S. G. Eskin. 1997. Effects of fluid shear stress on gene replication in vascular cells. *Biotechnol. Prog.* **13:** 209–221.

Papadaki, M., L. V. McIntire, and S. G. Eskin. 1996. Effects of shear stress on the growth kinetics of human aortic smooth muscle cells *in vitro*. *Biotechnol. Bioeng.* **50:** 555–561.

Papadaki, M., R. G. Tilton, S. G. Eskin, and L. V. McIntire. 1998. Effects of shear stress on nitric oxide production by human aortic smooth muscle cells. *Am. J. Phys.* **274:** H616–H626.

Rees, D. D., R. M. J. Palmer, and S. Moncada. 1990. Dexamethasone prevents the induction by endotoxin of a nitric oxide synthase and the associated effects on vascular tone, an insight into endotoxin shock. *Biochem. Biophys. Res. Com.* **173:** 541–547.

Schwartz, R. S. 1993. *Coronary Restenosis.* Blackwell Scientific, Cambridge, MA.

Sessa, W. C. 1994. The nitric oxide synthase family of proteins. *J. Vas. Res.* **31:** 131–143.

Wagner, J. E., L. V. McIntire, and P. A. Whitson. 1997. Macromolecular permeability of bovine brain endothelial cells monolayers subjected to shear stress *in vitro*. *Am. J. Physiol.* (in press).

Wang, D. M., and J. M. Tarbell. 1995. Modeling interstitial flow in an artery wall allows estimation of wall shear stress on smooth muscle cells. *J. Biomech. Eng.* **117:** 358–363.

Discussion

LUNA: Did you say that there is a 36-fold increase for high molecular weight species and only a 2-fold increase for the low molecular weights?

MCINTIRE: Yes, 36- to 70-fold for high molecular weight species and 2- to 4-fold for low molecular weight species.

LUNA: Can you speculate on what kind of hole would be opening up that would allow the bigger molecules through, or is it some kind of transcytosis through the cell?

MCINTIRE: We think that there is a cytoskeletal rearrangement that leads to a change in the junction integrity. This would allow larger molecular weight species through, whereas the lower molecular weight species are going through relatively fast anyway.

FUJIWARA: Do you have any explanation for the fact that the mololayer with the round cell shape has increased permeability?

MCINTIRE: Those time points happen to coincide with the high flow. At the lower shear stress we see even bigger changes in permeability; but we don't see changes in gross cell shape because we don't see any realignment at very low stress. I assume this to mean there are various cytoskeletal rearrangements occurring even at the low stresses, but they don't lead to alignment in the direction of the flow, because the flow forces aren't forcing the cells to do that. I don't know why the maximum permeability occurs for that rounded shape at that particular time.

FUJIWARA: We are looking at the motility of cells in the monolayer, and when cells are round they move at lot more. Perhaps movement breaks the cell-cell adhesion more frequently than in the aligned area, contributing to the increased permeability.

MCINTIRE: Yes, that's possible.

Reference: *Biol. Bull.* **194:** 400–401. (June, 1998)

Identification of a Functional Domain in Laminin-5

SCOTT E. BAKER* AND JONATHAN C. R. JONES†

Department of Cell and Molecular Biology, Northwestern University Medical School, 303 E. Chicago, Chicago, Illinois 60611

Laminin-5, a trimer composed of $\alpha 3$, $\beta 3$, and $\gamma 2$ subunits, is an important component of epithelial basement membranes and is spatially associated with cell-substrate adhesion structures called hemidesmosomes (Rouselle *et al.*, 1991; Jones *et al.*, 1994). Hemidesmosomes are associated with keratin filaments and are therefore considered linkers of the extracellular matrix and the intermediate filament cytoskeleton (Jones *et al.*, 1994).

A laminin-5-rich matrix is capable of inducing rapid cell adhesion as well as hemidesmosome assembly in a squamous cell carcinoma line (SCC12) (Langhofer *et al.*, 1993; Baker *et al.*, 1996). Two members of the integrin family of cell matrix receptors, $\alpha 3\beta 1$ and $\alpha 6\beta 4$, bind laminin-5 and are involved in these processes (Carter *et al.*, 1991; Langhofer *et al.*, 1993). $\alpha 3\beta 1$ integrin is involved in rapid cell adhesion to laminin-5, whereas $\alpha 6\beta 4$ is involved in hemidesmosome formation and cell spreading on laminin-5-rich substrates (Jones *et al.*, 1991; Langhofer *et al.*, 1993; Baker *et al.*, 1997). We have taken an immunological approach to defining the domains of laminin-5 involved in epithelial cell-substrate interactions.

A panel of monoclonal antibodies to the $\alpha 3$, $\beta 3$, and $\gamma 2$ subunit chains of the laminin-5 heterotrimer was generated (Langhofer *et al.*, 1993; Plopper *et al.*, 1996). Two of these antibodies, 5C5 and CM6, recognized the $\alpha 3$ laminin-5 subunit (Langhofer *et al.*, 1993; Plopper *et al.*, 1996; Baker *et al.*, 1996). We assessed, by electron microscopy, the ability of these antibodies to block laminin-5-induced hemidesmosome assembly in SCC12 cells. When the laminin-5 matrix was treated with CM6 antibody, SCC12 cells plated on this substrate lacked hemidesmosomes (Baker *et al.*, 1996). This indicated that CM6 antibodies block the ability of laminin-5 to nucleate hemidesmosome formation in SCC12 cells. In contrast, when SCC12 cells were plated onto 5C5 antibody-treated matrix, there were many hemidesmosomes at the basal aspect of these cells (Baker *et al.*, 1996). These results indicate that the epitope recognized by the CM6 antibodies plays an important role in hemidesmosome formation.

To characterize the epitopes of the CM6 and 5C5 antibodies, laminin-5 was purified from conditioned medium of epithelial cells, incubated with each antibody, and analyzed by rotary shadowing. Purified non-antibody-treated laminin-5 is a Y-shaped molecule with a long (about 110 nm) arm (Baker *et al.*, 1996). Rotary shadowed images of laminin-5 incubated with the 5C5 antibody showed that this antibody bound to the long rod domain of laminin-5. Interestingly, the function-blocking antibody, CM6, localized to the globular or G domain of the laminin-5 heterotrimer (Baker *et al.*, 1996).

Our results indicate that the G domain of laminin-5 appears to be essential for both epithelial cell interaction and nucleation of hemidesmosome assembly. This conclusion is consistent with studies of laminin-1, whose G domain has also been shown to mediate a number of important processes (Skubitz *et al.*, 1991; Yurchenco *et al.*, 1993; Matter and Laurie, 1994). Our study provides the first direct evidence that the G domain of laminin-5 is not only a structural component of the extracellular matrix-cytoskeleton link, but also a crucial player in its formation.

* Present address: Dept. Molecular and Cellular Biology, Life Sciences South Bldg, University of Arizona, Tucson AZ 85721.

† Author for correspondence.

This paper was originally presented at a workshop titled *The Cytoskeleton: Mechanical, Physical, and Biological Interactions.* The workshop, which was held at the Marine Biological Laboratory, Woods Hole, Massachusetts, from 15–17 November 1996, was sponsored by the Center for Advanced Studies in the Space Life Sciences at MBL and funded by the National Aeronautics and Space Administration under Cooperative Agreement NCC 2-896.

Acknowledgments

This work was supported by NIH and ACS.

Literature Cited

Baker, S. E., S. B. Hopkinson, M. Fitchmun, G. L. Andreason, F. Grasier, G. Plopper, V. Quaranta, and J. C. R. Jones. 1996. Laminin-5 and hemidesmosomes: role of the $\alpha 3$ subunit in hemidesmosome stability and assembly. *J. Cell Sci.* **109:** 2509–2520.

Baker, S. E., O. Skalli, R. D. Goldman, and J. C. R. Jones. 1997. Laminin-5 and modulation of keratin cytoskeleton arrangement in FG pancreatic carcinoma cells: involvement of IFAP300 and evidence that laminin-5/cell interactions correlate with a dephosphorylation of $\alpha 6$A integrin. *Cell Motil. Cytoskel.* **37:** 271–286.

Carter, W. G., M. C. Ryan, and P. J. Gahr. 1991. Epiligrin, a new cell adhesion ligand for integrin $\alpha 3\beta 1$ in epithelial basement membranes. *Cell* **65:** 599–610.

Jones, J. C. R., J. Asmuth, S. E. Baker, M. Langhofer, S. I. Roth, and S. B. Hopkinson. 1994. Hemidesmosomes: extracellular matrix/intermediate filament connectors. *Exp. Cell Res.* **213:** 1–11.

Jones, J. C. R., M. A. Kurpakus, H. M. Cooper, and V. Quaranta. 1991. A function for the integrin alpha 6 beta 4 in the hemidesmosome. *Cell Reg.* **2:** 427–438.

Langhofer, M., S. B. Hopkinson, and J. C. R. Jones. 1993. The matrix secreted by 804G cells contains laminin-related components that participate in hemidesmosome assembly *in vitro*. *J. Cell Sci.* **105:** 753–764.

Matter, M. L., and G. W. Larurie. 1994. A novel laminin E8 cell adhesion site required for lung alveolar formation *in vitro*. *J. Cell Biol.* **124:** 1083–1090.

Plopper, G., J. Falk-Marzillier, S. Glaser, M. Fitchmun, G. Giannelli, T. Romario, J. C. R. Jones, and V. Quaranta. 1996. Changes in expression of monoclonal antibody epitopes on laminin-5r induced by cell contact. *J. Cell Sci.* **109:** 1965–1973.

Rousselle, P., G. P. Lunstrum, D. R. Keene, and R. E. Burgeson. 1991. Kalinin: an epithelium-specific basement membrane adhesion molecule that is a component of anchoring filaments. *J. Cell Biol.* **12:** 205–214.

Skubitz, A. P., P. C. Letourneau, E. Wayner, and L. T. Furcht. 1991. Synthetic peptides from the carboxy-terminal domain of the A chain of laminin: their ability to promote cell adhesion and neurite outgrowth, and interact with heparin and the beta 1 integrin subunit. *J. Cell Biol.* **115:** 1137–1148.

Yurchenco, P. D., U. Sung, M. D. Ward, Y. Yamada, and J. J. O'Rear. 1993. Recombinant laminin G domain mediates myoblast adhesion and heparin binding. *J. Biol. Chem.* **268:** 8356–8365.

Reference: *Biol. Bull.* **194:** 402–405. (June, 1998)

Interaction of Vimentin With Actin and Phospholipids

JAGESH V. SHAH*†, LOUISE Z. WANG†, PETER TRAUB‡, AND PAUL A. JANMEY†

**Harvard-MIT Division of Health Sciences and Technology,† Division of Experimental Medicine, Brigham and Women's Hospital, Harvard Medical School, Boston, Massachusetts; and ‡Max-Planck Institute for Cell Biology, Heidelberg, Germany*

Vimentin intermediate filaments are a major cytoskeletal constituent of cells of mesenchymal origin. They have been colocalized with a variety of intracellular structures such as actin filaments and the plasma membrane. Labeled actin filaments, observed *in vitro* by fluorescence microscopy, break in the presence of polymerizing vimentin; the time course is consistent with stopped-flow measurements of vimentin polymerization. This breakage phenomenon appears to be specific for vimentin. Inhibition of vimentin network formation was observed with phosphatidyl inositol phosphate (PI(4)P) and phosphatidyl inositol bisphosphate (PI(4,5)P_2), but not phosphatidyl choline (PC), phosphatidyl serine (PS), or phosphatidyl inositol (PI). Taken together, these results indicate a specific interaction of vimentin with F-actin and polyphosphoinositide lipids.

Introduction

Vimentin-type intermediate filaments are a major cytoskeletal constituent of cells of mesenchymal origin. Theories as to their function vary from maintenance of cellular integrity (Lazarides, 1980) to gene regulation (Traub and Shoeman, 1994). There is *in vivo* evidence for vimentin colocalization with other cytoskeletal elements, such as actin (Brown and Binder, 1992; Cary *et al.*, 1994; and Tint *et al.*, 1991) and microtubules (Gurland and Gunderson, 1995; Gyoeva and Gelfand, 1991), as well as with cellular organelles, such as the plasma membrane and the nucleus. Here we present *in vitro* studies indicating that vimentin interacts directly with both F-actin and polyphosphoinositide lipids.

This paper was originally presented at a workshop titled *The Cytoskeleton: Mechanical, Physical, and Biological Interactions.* The workshop, which was held at the Marine Biological Laboratory, Woods Hole, Massachusetts, from 15–17 November 1996, was sponsored by the Center for Advanced Studies in the Space Life Sciences at MBL and funded by the National Aeronautics and Space Administration under Cooperative Agreement NCC 2-896.

Materials and Methods

Purification of actin and vimentin

Actin was purified by the method of Spudich and Watt (1971) with slight modifications. Actin was stored in G-buffer (2 m*M* Tris, 0.2 m*M* $CaCl_2$, 0.5 m*M* ATP, 0.5 m*M* DTT, pH 8.0) at −80°C; it was polymerized at a concentration of 5 μM by the addition of a ten-times concentrated solution of F-buffer (1×:20 m*M* Tris, 150 m*M* KCl, 2 m*M* $MgCl_2$, 0.2 m*M* $CaCl_2$, 0.5 m*M* ATP, 0.5 m*M* DTT, pH 7.4) and was stabilized by the addition of equimolar TRITC-phalloidin (Sigma Chemicals, St. Louis, MO). Vimentin was purified from Ehrlich ascites tumor cells by the method of Nelson *et al* (1982). Vimentin was extensively dialyzed against non-polymerizing buffer (10 m*M* Tris, 6 m*M* DTT, pH 7.6) to remove residual urea and was polymerized by the addition of KCl to 150 m*M*. All reagents were purchased from Sigma Chemicals (St. Louis, MO).

F-actin-vimentin interactions

F-actin, under either polymerizing or non-polymerizing conditions, and stabilized by TRITC-phalloidin (10 n*M*), was visualized by fluorescence microscopy in the presence of 20 μM unpolymerized vimentin. A large number of fields were recorded to videotape over time, and the average length of F-actin—based on at least 200 filament traces—was calculated.

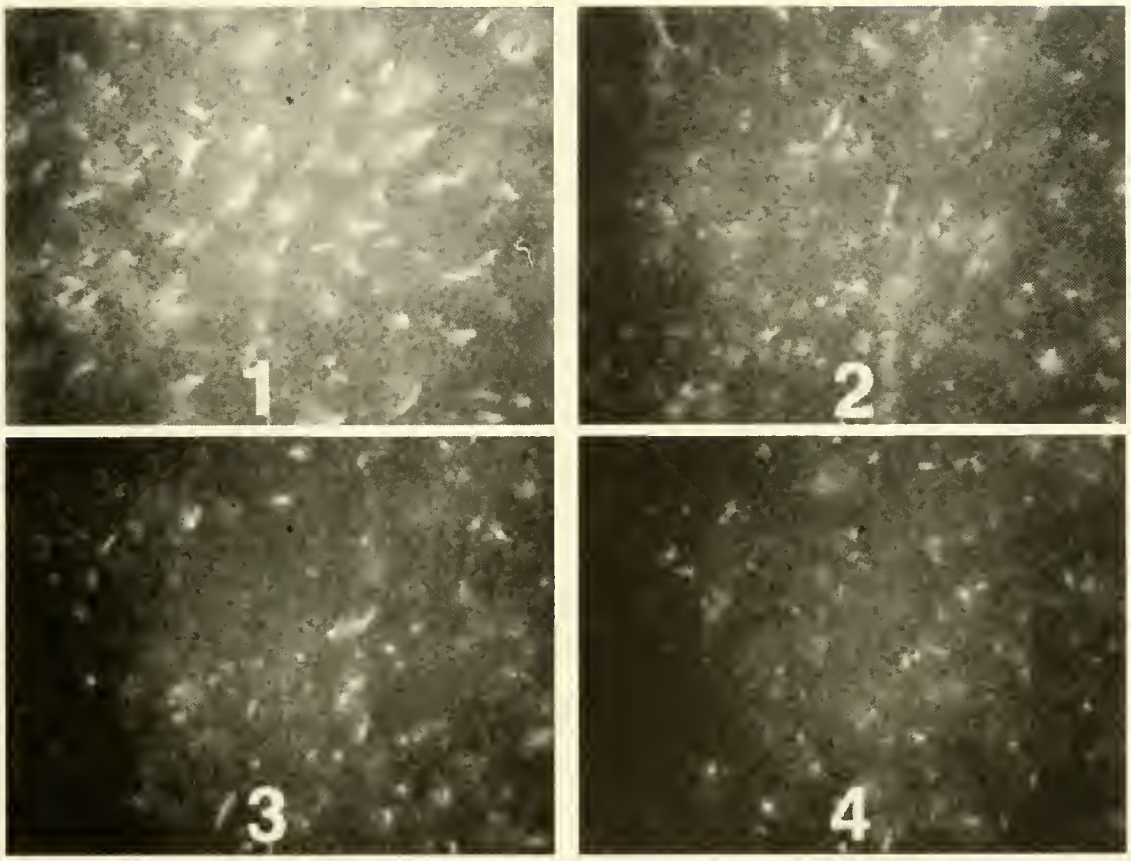

Figure 1. With increasing time, the average length of F-actin decreases in the presence of polymerizing vimentin. Labeled, phalloidin-stabilized actin filaments (10 n*M*) are visible by fluorescence microscopy in a sample containing 18 μM (1 mg/ml) unlabeled vimentin before and after addition of KCl to initiate vimentin polymerization. The dimension of each image is 50 μm in width, and the image in panel 4 was taken 25 min after polymerization.

Rheology of vimentin networks

Rheology of vimentin networks was carried out as described previously (Janmey *et al.*, 1991). Oscillatory measurements of elastic modulus were made with a Rheometrics RFS II fluids spectrometer (Rheometrics, Piscataway, NJ) at a frequency of 1 rad/s and a strain amplitude of 1%.

Results

F-actin-vimentin interactions

Labelled actin filaments were examined *in vitro* by fluorescence microscopy and were seen to break in the presence of polymerizing vimentin. Figure 1 shows a panel of four video frames; the fluorescent filaments are F-actin in a matrix of polymerizing unlabeled vimentin filaments. Such breakage was not seen under non-polymerizing conditions, indicating that polymerization is required. The decrease in average F-actin length is shown

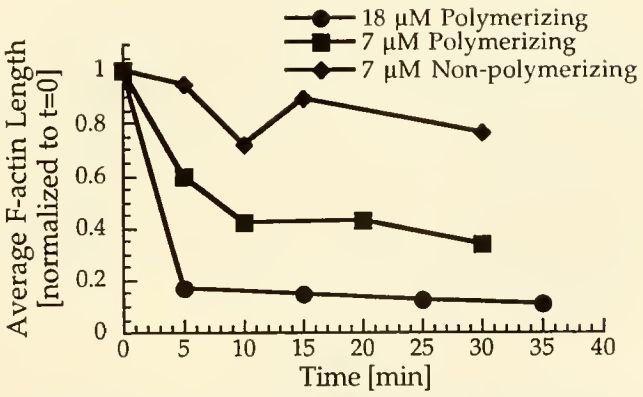

Figure 2. Average length of F-actin decreases in the presence of polymerizing vimentin filaments. Higher concentrations of vimentin result in faster rate of length decrease. Unpolymerized vimentin does not cause a decrease in F-actin length.

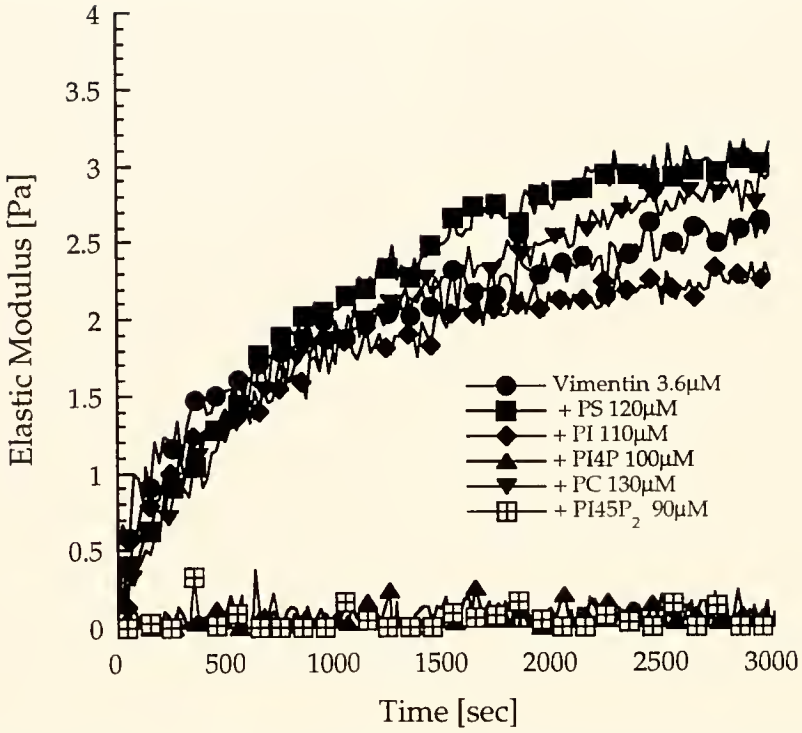

Figure 3. Rheology of vimentin networks disrupted by polyphosphoinositide lipids. Other phospholipids, such as phosphatidyl serine, phosphatidyl choline, and phosphatidyl inositol, had no significant effect on vimentin polymerization.

in Figure 2 as a function of vimentin polymerization and concentration. The time course is consistent with stopped flow measurements of vimentin polymerization (data not shown). This breakage phenomenon appears to be specific for vimentin, since no breakage is seen with microtubules in actin, or with actin in microtubules or fibrin (data not shown).

Vimentin-phospholipid interactions

The interaction of vimentin and phospholipids was measured by rheological methods and showed that polyphosphoinositide lipids inhibit the formation of an elastic network. Inhibition was observed with PI(4)P and PI(4,5)P_2, and to a lesser extent with PI (Fig. 3). Inhibition was not observed with PC or PS. These results are consistent with early studies by Perides *et al.* (1986) showing that phospholipid vesicles, especially those containing PIP and PIP_2, inhibit vimentin polymerization and depolymerize preformed vimentin filaments.

Conclusions

Fluorescent actin filaments decrease in length in the presence of polymerizing vimentin. Filament breakage was not observed in other biopolymer systems, indicating that the interaction is specific.

PIP and PIP_2 inhibit the polymerization of vimentin as measured by rheological methods. This evidence points to a specific interaction between vimentin and polyphosphoinositide lipids.

Acknowledgments

The authors thank Jay Tang, Zeno Guttenburg, and Wolfgang Goldman for performing the kinetic stopped-flow measurements. This work was sponsored by the NIH grant AR38910 (P.A.J.) and the National Science and Engineering Research Council of Canada (J.V.S.).

Literature Cited

Brown, K. D., and L. I. Binder. 1992. Identification of the intermediate filament-associated protein gyronemin as filamin. Implications for a novel mechanism of cytoskeletal interaction. *J. Cell Sci.* **102:**19–30.

Cary, R. B., M. W. Klymkowsky, R. M. Evans, A. Domingo, J. A. Dent, and L. E. Backhus. 1994. Vimentin's tail interacts with actin-containing structures in vivo. *J. Cell Sci.* **107:**1609–1622.

Gurland, G., and G. G. Gundersen. 1995. Stable, detyrosinated microtubules function to localize vimentin intermediate filaments in fibroblasts. *J. Cell Biol.* **131:** 1275–1290.

Gyoeva, F. K., and V. I. Gelfand. 1991. Coalignment of vimentin intermediate filaments with microtubules depends on kinesin. *Nature* **353:** 445–448.

Janmey, P. A., U. Euteneuer, P. Traub, and M. Schliwa. 1991. Visco-

elastic properties of vimentin compared with other filamentous biopolymer networks. *J. Cell Biol.* **113:** 155–160.

Lazarides, E. 1980. Intermediate filaments as mechanical integrators of cellular space. *Nature* **283:** 249–256.

Nelson, W. J., C. E. Vorgias, and P. Traub. 1982. A rapid method for the large scale purification of the intermediate filament protein vimentin by single-stranded DNA-cellulose affinity chromatography. *Biochem. Biophys. Res. Commun.* **106:** 1141–1147.

Perides, G., A. Scherbarth, and P. Traub. 1986. Influence of phospholipids on the formation and stability of vimentin-type intermediate filaments. *Eur. J. Cell Biol.* **42:** 268–280.

Spudich, J., and S. Watt. 1971. The regulation of rabbit skeletal muscle contraction. I. Biochemical studies of the interaction of the tropomyosin-troponin complex with actin and the proteolytic fragments of myosin. *J. Biol. Chem.* **246:** 4866–4871.

Tint, I. S., P. J. Hollenbeck, A. B. Verkhovsky, I. G. Surguchcva, and A. D. Bershadsky. 1991. Evidence that intermediate filament reorganization is induced by ATP-dependent contraction of the actomyosin cortex in permeabilized fibroblasts. *J. Cell Sci.* **98:**375–384.

Traub, P., and R. L. Shoeman. 1994. Intermediate filament and related proteins: potential activators of nucleosomes during transcription initiation and elongation? *Bioessays* **16:** 349–355.

Reference: *Biol. Bull.* **194:** 406–408. (June, 1998)

Two Distinct Mechanisms of Actin Bundle Formation

JAY X. TANG AND PAUL A. JANMEY

Brigham and Women's Hospital, Harvard Medical School, 221 Longwood Ave., LMRC 301, Boston, Massachusetts 02115

Actin filaments (F-actin)—one of the major types of cytoskeletal filament—can be induced to form bundles by the addition of any of a number of polycations, including divalent metal ions, trivalent hexaminecobalt, or basic polypeptides. The general features of bundle formation, as detected by light scattering, centrifugation, optical and electron microscopy, are largely independent of the specific structure of the bundling agent used. The formation of lateral aggregates of actin filaments in response to polycations begins at a threshold concentration that varies strongly with the valence of the cation and increases with the ionic strength of the solution. Polyanions, such as nucleoside phosphates and acidic polypeptides, disperse actin bundles into single filaments. These features are similar to those associated with DNA condensation and can be explained analogously by polyelectrolyte theory (Tang and Janmey, 1996; Tang *et al.*, 1996). The general behavior is dictated by the polyelectrolyte nature of F-actin, which causes a class of nonspecific binding by ligands that carry several net, opposite charges. Such a bundling mechanism can be applied to a class of cationic actin-bundling proteins, including smooth muscle calponin and the microtubule-associated proteins tau and Map2c.

One direct consequence of this model of bundling is that neither dual binding sites nor dimerization of a protein with a single binding site is required to bundle F-actin (Tang *et al.*, 1997b). This alternative and somewhat counterintuitive concept may help explain why some actin-bundling and cross-linking proteins have only a single identifiable actin-binding site, and the purified proteins exist in solution as monomers. Smooth muscle calponin and a 25-amino-acid actin-binding peptide (aa 151–175) derived from the myristoylated, alanine-rich, C kinase substrate (MARCKS) are two examples among polycations that appear to induce actin-bundle formation mainly by an electrostatic mechanism (Tang and Janmey, 1996; Tang *et al.*, 1997b).

A different type of actin bundle is formed by solution crowdedness, the thermodynamic basis of which is to maximize the entropy of the solution, including all solute and solvent molecules. Two equivalent terms—the excluded volume effect (Onsager, 1949) and steric exclusion (Arakawa and Timasheff, 1985)—have been used in the literature to describe the restriction that two macromolecules cannot overlap their positions in solution. At high concentrations, such a constraint may lead to various forms of self-assembly or other aggregation phenomena (Herzfeld, 1996). For the case of an F-actin solution, high concentrations of noninteracting proteins like ovalbumin, and inert polymers like polyethylene glycol, facilitate lateral aggregation of F-actin (Suzuki *et al.*, 1989). This type of actin-bundle formation has different features than that induced by polycations, including an opposite dependence on the ionic strength of the solution (Tang *et al.*, 1997a) and an opposite dependence on the concentration of actin (Suzuki *et al.*, 1989; Tang *et al.*, 1997a; Tang and Janmey, 1996), which by itself contributes to the solution crowdedness.

The optical images in Figure 1 show examples of actin bundles formed by the two different mechanisms. Panel A shows bundling induced by 50 m*M* $MgCl_2$, representative of excess polycation concentration. Panel B shows bundles induced by 8% polyethylene glycol [molecular

This paper was originally presented at a workshop titled *The Cytoskeleton: Mechanical, Physical, and Biological Interactions.* The workshop, which was held at the Marine Biological Laboratory, Woods Hole, Massachusetts, from 15–17 November 1996, was sponsored by the Center for Advanced Studies in the Space Life Sciences at MBL and funded by the National Aeronautics and Space Administration under Cooperative Agreement NCC 2-896.

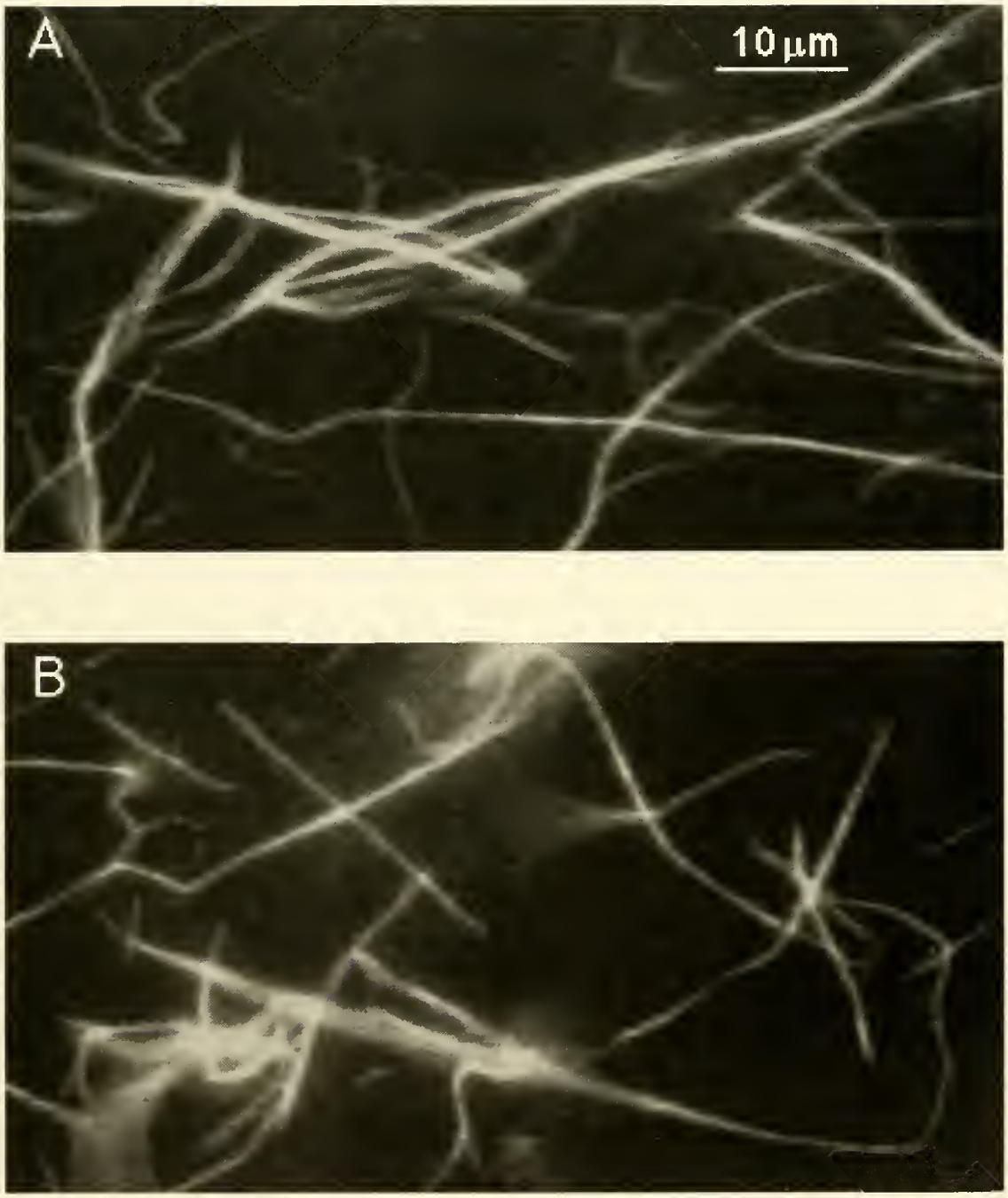

Figure 1. Comparison of actin bundles formed by excess polycations (A) and by solution crowdedness (B). Panel A: large bundles of F-actin induced by 50 m*M* $MgCl_2$. Panel B: actin bundles formed by 8% (wt) polyethylene glycol of average molecular weight 8000 dalton (PEG-8000).

weight approximately 8000 (PEG-8000)], illustrating the effect of solution crowding. Bundles of both types were visualized by the fluorescent labeling of F-actin with rhodamine phalloidin. The pair of images illustrates the general observation that the two types of bundles are virtually identical in appearance at this level of resolution. The only subtle difference is that the Mg-actin bundles tend to reach a larger size than PEG-actin bundles, and the difference is more apparent by phase-contrast microscopy (data not shown). Both types of actin bundles have also been examined by electron microscopy, and the general morphology is indistinguishable. In cells, various poly-

cations and cationic proteins are abundant, and the cytoplasm is also crowded with other macromolecules that may or may not directly interact with F-actin. Therefore, the two distinct mechanisms may jointly play pivotal roles in forming the functional arrays of bundled actin filaments found in many cell types.

Literature Cited

Arakawa, T., and S. N. Timasheff. 1985. Mechanism of poly(ethylene glycol) interaction with proteins. *Biochemistry* **24:** 6756–6762.

Herzfeld, J. 1996. Entropically driven order in crowded solutions: from liquid crystals to cell biology. *Accounts Chem. Res.* **29:** 31–37.

Onsager, L. 1949. The effects of shape on the interaction of colloidal particles. *Ann. NY Acad. Sci.* **51:** 627–659.

Suzuki, A., M. Yamazaki, and T. Ito. 1989. Osmoelastic coupling in biological structures: formation of parallel bundles of actin filaments in a crystalline-like structure caused by osmotic stress. *Biochemistry* **28:** 6513–6518.

Tang, J. X., and P. A. Janmey. 1996. Polyelectrolyte nature of F-actin and mechanism of actin bundle formation. *J. Biol. Chem.* **271:** 8556–8563.

Tang, J. X., S. Wong, P. T. Tran, and P. A. Janmey. 1996. Counter-ion induced bundle formation of rodlike polyelectrolytes. *Ber. Bunsenges. Phys. Chem.* **100:** 796–806.

Tang, J. X., T. Ito, T. Tao, P. Traub, and P. A. Janmey. 1997a. Opposite effects of electrostatics and steric exclusion on bundle formation by F-actin and other filamentous polyelectrolytes. *Biochemistry* **36:** 12600–12607.

Tang, J. X., P. Szymanski, P. A. Janmey, and T. Tao. 1997b. Electrostatic effects of smooth muscle calponin on actin assembly. *Eur. J. Biochem.* **247:** 432–440.

Reference: *Biol. Bull.* **194:** 409–410. (June, 1998)

Plectin Sidearms Mediate Interactions of Intermediate Filaments With Microtubules and Other Components of the Cytoskeleton

TATYANA M. SVITKINA, ALEXANDER B. VERKHOVSKY, AND GARY B. BORISY

Laboratory of Molecular Biology, University of Wisconsin, Madison, Wisconsin 53706

The IF-associated protein plectin has been proposed to be a cytoplasmic cross-linker (Foisner and Wiche, 1991). We recently reported unique "millipede-like" structures in mammalian cell cytoskeletons revealed after removal of actin by treatment with gelsolin (Svitkina *et al.*, 1995, 1996). Here we demonstrate, by immunogold labeling, that the millipede structures are composed of cores of vimentin IFs with sidearms containing plectin. The dimensions of the sidearms (up to 200 nm long and 2–3 nm wide) match the size of plectin molecules (Foisner and Wiche, 1987), suggesting that sidearms are made of individual plectin molecules, or a few of them in register. These plectin sidearms connect IFs to microtubules, the actin-based cytoskeleton, and possibly to membrane components. Plectin binding to microtubules is significantly increased in cells from transgenic mice lacking IFs (MFT-16 cell line, courtesy of Dr. R. Evans). Numerous sidearms are associated with microtubules in these cells, giving them an unusual "hairy" appearance. After microinjection of exogenous vimentin in MFT-16 cells, IFs of variable length are formed within 3 h; the IFs have a very high density of associated plectin, whereas microtubules lose most of their plectin sidearms. These results suggest the existence of a pool of plectin that preferentially associates with IFs, but that may also be competed for by microtubules. The association of IFs with microtubules shows no preference for Glu-tubulin. Nor does it depend upon the presence of MAP4; indeed plectin links were retained after specific immunodepletion of MAP4.

The IF-plectin complexes also displayed extensive association with stress-fibers. The actin-binding domain identified in the plectin sequence (McLean *et al.*, 1996) may play a role in this interaction. However, plectin binding to stress-fibers survives actin depletion by gelsolin, revealing structural association with myosin II minifilaments, the major non-actin component of stress-fibers. These results suggest that myosin II minifilaments, or components closely associated with them, may play a role as plectin targets. An additional association partner of plectin seen in our cytoskeleton preparations consists of material with irregular granular and fibrillar substructure. This material, as yet unidentified, may represent protein remnants of membrane structures, such as plasma membrane or membrane organelles.

In conclusion, our results provide direct structural evidence for the hypothesis that IF-plectin complexes comprise an extensive cross-linking of cellular components (Fig. 1) and provide a structural framework for the integration of cytoplasm. In this model, IFs provide the core while plectin forms peripheral linkers that connect to MTs, the actin-based cytoskeleton, and membrane structures. However, IFs and plectin do not seem to be equal partners in performing their functions. The absence of obvious phenotype in vimentin-null mice (Colucci-Guyon *et al.*, 1994) suggests that vimentin's role in cytoplasmic organization is not essential. In contrast, plectin seems to play a key role in maintaining tissue integrity, as has been demonstrated by analysis of a human hereditary disorder (epidermolysis bullosa with muscular dystrophy) showing plectin deficiency (McLean *et al.*, 1996; Smith *et al.*,

This paper was originally presented at a workshop titled *The Cytoskeleton: Mechanical, Physical, and Biological Interactions*. The workshop, which was held at the Marine Biological Laboratory, Woods Hole, Massachusetts, from 15–17 November 1996, was sponsored by the Center for Advanced Studies in the Space Life Sciences at MBL and funded by the National Aeronautics and Space Administration under Cooperative Agreement NCC 2-896.

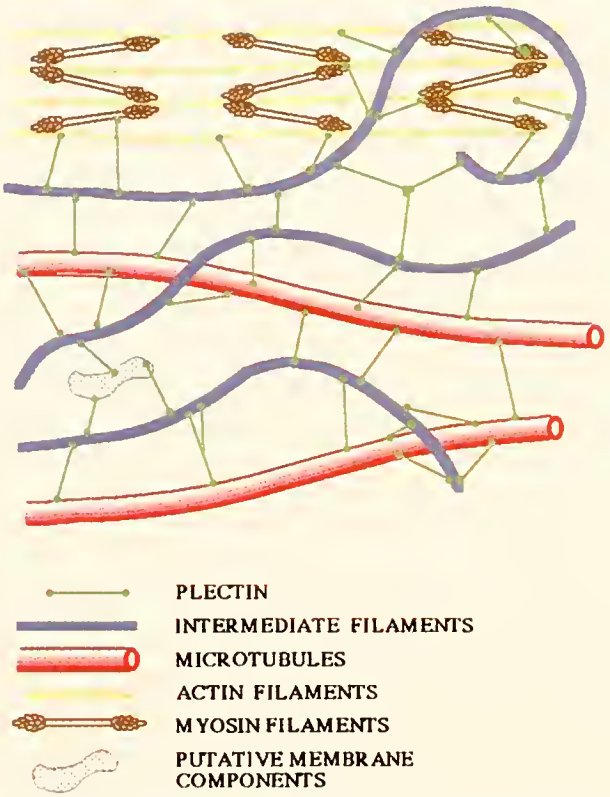

Figure 1. Diagram illustrating integration of the cytoskeleton. Plectin sidearms on IFs link them to microtubules, myosin II minifilaments, actin filaments, and putative membrane components, thus mechanically connecting various cellular structures.

1996). Though plectin prefers to associate with IFs, it can cross-link cytoskeletal structures in the absence of vimentin. Consequently, plectin may be able to maintain cytoplasmic integrity independently of IFs.

Literature Cited

Colucci-Guyon, E., M.-M. Porteir, I. Dunia, D. Paulin, S. Pourin, and C. Babinet. 1994. Mice lacking vimentin develop and reproduce without an obvious phenotype. *Cell* **79:** 679–694.

Foisner, R., and G. Wiche. 1987. Structure and hydrodynamic properties of plectin molecules. *J. Mol. Biol.* **198:** 515–531.

Foisner, R., and G. Wiche. 1991. Intermediate filament-associated proteins. *Curr. Opin. Cell Biol.* **3:** 75–81.

McLean, W. H. I., L. Pulkkinen, F. J. D. Smith, E. L. Rugg, E. B. Lane, F. Bullrich, R. E. Burgeson, S. Amano, D. Hudson, K. Owaribe, J. A. McGrath, J. R. McMillan, R. A. J. Eady, I. M. Leigh, A. M. Christiano, and J. Uitto. 1996. Loss of plectin causes epidermolysis bullosa with muscular dystrophy: cDNA cloning and genomic organization. *Genes Devel.* **10:** 1724–1735.

Smith, F. J. D., R. A. J. Eady, I. M. Leigh, J. R. McMillan, E. L. Rugg, D. P. Kelsell, S. P. Bryant, N. K. Spurr, J. F. Geddes, G. Kirtschig, G. Milana, A. G. de Bono, K. Owaribe, G. Wiche, L. Pulkkinen, J. Uitto, W. H. I. McLean, and E. B. Lane. 1996. Plectin deficiency results in muscular dystrophy with epidermolysis bullosa. *Nature Genet.* **13:** 450–457.

Svitkina, T. M., A. B. Verkhovsky, and G. G. Borisy. 1995. Improved procedures for electron microscopic visualization of the cytoskeleton of cultured cells. *J. Struct. Biol.* **115:** 290–303.

Svitkina, T. M., A. B. Verkovsky, and G. G. Borisy. 1996. Plectin sidearms mediate interaction of intermediate filaments with microtubules and other components of the cytoskeleton. *J. Cell Biol.* **135:** 991–1007.

Reference: *Biol. Bull.* **194:** 411. (June, 1998)

Concluding Remarks

This has been an interesting few days for many of us who have not had the opportunity to meet each other in this kind of context before. It has forced us to think of other areas that we normally don't study and the complexity of those different systems. With respect to complexity, some of the terms that have been used in this meeting demonstrate that communication is one of the major problems we face. However, the important prospect for this meeting is that it is the beginning of a series of multidisciplinary communications that we hope NASA will perpetuate, because they have an interesting niche to fill in the life sciences. I would therefore like to thank NASA for supporting this workshop.

In concluding, I would like to present a typical molecular biologist's view of signalling in the cell. A signal is depicted by a lightning bolt which interacts with a receptor and is followed by a response within the nucleus. A cell biologist who works on microtubules depicts the cell as consisting primarily of microtubules; we have seen this many times at this meeting. Then there is the way I look at the cell—as containing intermediate filaments. Someone working with actin portrays a cell with only actin. We all use different antibodies and different probes, which suggests to our audience that there is only one major component inside the cell, because each of our images is filled with our own protein. In turn, each of us tries to explain signal transduction in light of our own interests.

We know, however, that there is a lot of cross-talk amongst these different elements. One of the most intriguing things that has come up several times at this meeting is that a cell can be stimulated in various ways if it is stressed. Some refer to this stimulation simply as stress, while others call it signaling. There are also many ways to describe the response. Whether stimulated by heat shock, mechanical stress, or some toxic compound, cells behave in interesting ways, from the moment that some signal impinges on the cell surface. I will just remind you of what Rick Morimoto told us very briefly at this meeting. That is, if you stress a cell by using heat shock or some poisonous divalent cation, or any of a whole spectrum of different agents, they all produce this kind of response in which cytoskeletal systems such as intermediate filaments collapse back to the nucleus, or actin paracrystals form inside the nucleus. These responses happen in minutes, and it takes time for the cell to recover. At the same time, heat-shock transcription factors, which are normal constituents of the cytoplasm, enter the nucleus to form structures inside it which alter gene expression in some way. At this meeting we heard about the effect of shear stress on endothelial cells. Peter Davies has shown, and Keigi Fujiwara described to us this morning, that an endothelial cell exposed to shear elongates, and stress fibers proliferate—or at least they get longer, more abundant, and thicker.

Any drug that reacts with one of the cytoskeletal elements will change the others. However, if experiments are narrowly focused on one cytoskeletal element, the action of the drug appears to be very specific. I think we are learning that there is a lot of cross-talk amongst the cytoskeletal systems which form extremely complex interacting networks. Nevertheless, although a very close look at just actin in solution, or even solubilized actin containing interdigitated intermediate filaments, may seem simplistic, in fact, this is probably the only way to begin learning how these systems interact.

I think that cell biologists must begin to communicate with physicists if we are to get a handle on the exquisite sensitivity of these systems to external perturbations. Perhaps everything starts as a mechanical stimulus at the cell surface and is then transmitted through these elements to the nucleus and back again to the surface of the cell. I hope that this meeting will be only the first exchange in a dialog addressing these issues. I thank NASA again for giving us the opportunity to get together.

Robert D. Goldman
Woods Hole, Massachusetts
November 1996

This paper was originally presented at a workshop titled *The Cytoskeleton: Mechanical, Physical, and Biological Interactions.* The workshop, which was held at the Marine Biological Laboratory, Woods Hole, Massachusetts, from 15–17 November 1996, was sponsored by the Center for Advanced Studies in the Space Life Sciences at MBL and funded by the National Aeronautics and Space Administration under Cooperative Agreement NCC 2-896.

Reference: *Biol. Bull.* **194:** 412. (June, 1998)

Published by Title Only

Albrecht-Buehler, Guenter
The conceptual challenge of cellular gravi-sensing.

Borisy, Gary G., and Vladimir I. Rodionov
Self organization of cytoplasm.

Jansen, N., J. Mashl, W. Gelbart, and R. Bruinsma
Electrostatic interactions and collapse of biopolymers.

Kowalczyk, A. P., J. E. Borgwardt, E. A. Bornslaeger, H. L. Palka, A. S. Dhaliwal, and K. J. Green
The amino-terminal domain of desmoplakin clusters desmosomal cadherin-plakoglobin complexes: implications for desmosome assembly and intermediate filament attachment.

Morimoto, Richard I.
Effects of stress and protein damage on the mammalian cell shape and function.

Oschman, James L.
The nuclear, cytoskeletal, and extracellular matrices: a continuous communication network.

Palacek, Sean P., Joseph C. Loftus, Mark H. Ginsberg, Alan F. Horwitz, and Douglas A. Lauffenburger
Changes in cell-substratum adhesiveness regulate cell migration rate.

Schwartz, Martin A.
Tho and C-Abl as mediators of integrin signaling.

Reference: *Biol. Bull.* **194:** 413–415. (June, 1998)

Chairs and Speakers

Workshop Chair
Robert D. Goldman
Department of Cell, Molecular and Structural Biology
Northwestern University Medical School
303 E. Chicago Avenue
Chicago, IL 60611

Ueli Aebi
Am Biozentrum der Universität Basel
Klingelbergstr 70
Basel, CH-4056
Switzerland
E-mail: aebi@ubaclu.unibas.ch

Guenter Albrecht-Buehler
Department of Cell, Molecular and Structural Biology
Northwestern University Medical School
303 E. Chicago Avenue
Chicago, IL 60611
E-mail: g-buehler@nwu.edu

David Boal
Department of Physics
Simon Fraser University
Burnaby, British Columbia
Canada V5A 1S6
E-mail: David__Boal@sfu.ca

Gary G. Borisy
Department of Molecular Biology and Zoology
University of Wisconsin
1525 Linden Drive
Madison, WI 53706-1514
E-mail: ggborisy@facstaff.wisc.edu

Robijn Bruinsma
Department of Physics
University of California
Los Angeles, CA 90024
E-mail: bruinsma@physics.ucla.edu

J. Chloe Bulinski
Department of Anatomy and Cell Biology
Columbia University College of Physicians and Surgeons
630 W. 168th Street
New York, NY 10032-3702
E-mail: jcb4@columbia.edu

Shu Chien
Department of Bioengineering
University of California
9500 Gilman Drive
La Jolla, CA 92093-0412
E-mail: schien@bioeng.ucsd.edu

Pierre A. Coulombe
Department of Biological Chemistry
The Johns Hopkins University
School of Medicine
725 N. Wolfe Street
Baltimore, MD 21205
E-mail: pacoulom@welchlink.welch.jhu.edu

Gabor Forgacs
Department of Physics
Clarkson University
Potsdam, NY 13676
E-mail: forgacs@polaris.clarkson.edu

Keigi Fujiwara
Department of Structural Analysis
National Cardiovascular Center Research Inst.
Fujishiro-dai, Suita
Osaka 565
Japan
E-mail: keigi@jsc.ri.ncvc.go.jp

Kathleen J. Green
Department of Pathology
Northwestern University Medical School
303 E. Chicago Avenue
Chicago, IL 60611
E-mail: kgreen@nwu.edu

Gregg G. Gundersen
Department of Anatomy and Cell Biology
Columbia University College of Physicians and Surgeons
630 W. 168th Street
New York, NY 10032-3702
E-mail: ggg1@columbia.edu

Donald Ingber
Department of Surgical Research
Enders 1007
Children's Hospital
300 Longwood Avenue
Boston, MA 02116-5737
E-mail: ingber@a1.tch.harvard.edu

Wallace Ip
Department of Cell Biology, Neurobiology, and Anatomy
University of Cincinnati College of Medicine
231 Bethesda Avenue
P.O. Box 670521
Cincinnati, OH 45267-0521
E-mail: wallace.ip@uc.edu

Paul Janmey
Experimental Medicine Division
Brigham and Women's Hospital
LMRC #302
221 Longwood Avenue
Boston, MA 02115
E-mail: janmey@calvin.bwh.harvard.edu

Jonathan C. R. Jones
Department of Cell and Molecular Biology
Northwestern University Medical School
303 E. Chicago Avenue, Ward Building
Chicago, IL 60611
E-mail: jjones@worms.cmb.nwu.edu

Elizabeth Luna
University of Massachusetts Medical Center
Worcester Foundation Campus
222 Maple Avenue
Shrewsbury, MA 01545-2795
E-mail: luna@sci.wfbr.edu

Frederick C. MacKintosh
Department of Physics
2071 Randall Lab
University of Michigan
Ann Arbor, MI 48109-1120
E-mail: fcm@umich.edu

Larry V. McIntire
Institute of Biosciences and Bioengineering
Rice University
Houston, TX 77251-1892
E-mail: mcintir@rice.edu

Richard I. Morimoto
Department of Biochemistry, Molecular, and Cell Biology
Northwestern University
2159 N. Campus Drive
Evanston, IL 60208-3500
E-mail: morimoto@casbah.acns.nwu.edu

Carol A. Otey
Department of Anatomy and Cell Biology
University of Virginia School of Medicine
Box 439
Charlottesville, VA 22908-0439
E-mail: cao2a@uva.pcmail.virginia.edu

Martin A. Schwartz
Department of Vascular Biology VB-4
Scripps Research Institute
10666 N. Torrey Pines Road
La Jolla, CA 92037
E-mail: schwartz@scripps.edu

Peter M. Steinert
Laboratory of Skin Biology
NIAMS/NIH
Building 6, Room 425
Bethesda, MD 20892-2755
E-mail: pemast@helix.nih.gov

Murray Stewart
Medical Research Council
Laboratory of Molecular Biology
MRC Centre
Hills Road
Cambridge
United Kingdom CB2 2QH
E-mail: ms@mrc-lmb.cam.ac.uk

Edwin Taylor
Dept. of Molec. Genetics and Cell Bio.
University of Chicago
920 E 58th Street
Chicago, IL 60637
E-mail: ewt1@midway.uchicago.edu

GERHARD WICHE
Institute of Biochemistry and Molecular Cell Biology
University of Vienna
Dr. Bohrgasse 9
A-1030 Wien
Austria
E-mail: Wiche@abc.univie.ac.at

YU-LI WANG
University of Massachusetts Medical School
Worcester Foundation Campus
222 Maple Avenue
Shrewsbury, MA 01545-2795
E-mail: wang@sci.wfeb.edu

Reference: *Biol. Bull.* **194:** 416–418. (June, 1998)

Participants

Philip Allen
Experimental Medicine Division
Brigham and Women's Hospital
LMRC #302
Boston, MA 02115

Scott Baker
Dept. of Cell and Molecular Biology
Northwestern University Medical School
303 E. Chicago Avenue
Ward Building
Chicago, IL 60611

Abdul Barakat
Dept. of Mechanical and Aeronautical Eng.
University of California
Davis, CA 95616

Joseph D. Cassidy
The Priory of St. Thomas Aquinas
Providence College
Providence, RI 02918-0001

Winston Chang
Dept. of Anatomy and Cell Biology
Columbia University College of Physicians and Surgeons
630 W. 168th Street
New York, NY 10032-3702

Chris Chen
Enders 1007—Surgical Research
Children's Hospital
300 Longwood Avenue
Boston, MA 02115

Rex Chisholm
Dept. of Cell and Molecular Biology
Northwestern University
303 E. Chicago Avenue
Chicago, IL 60611

Magnus Edlund
Dept. of Anatomy and Cell Biology
University of Virginia School of Medicine
Box 439
Charlottesville, VA 22908-0439

Suzanne Eskin
Cell Biology Department
Texas Biotechnology Corporation
Houston, TX 77030

Andrew Gilmore
Dept. of Cell Biology and Anatomy
University of North Carolina
Chapel Hill, NC 27599

Diane Heck
Dept. of Pharmacology and Toxicol.
Rutgers University
Piscataway, NJ 08855

Anne Hitt
University of Massachusetts Medical Center
Worcester Foundation Campus
222 Maple Ave
Shrewsbury, MA 01545-2795

Francis Hoskin
Marine Biological Laboratory
Home address:
8 Meyer Terrace
Canton, MA 02021

Andrew Kowalczyk
Dept. of Dermatology
Northwestern University Medical School
303 E. Chicago Avenue
Chicago, IL 60611

Leonard Laster
University of Massachusetts Medical Ctr.
120 Front St., Suite 800
Worcester, MA 01608

Paul Letourneau
Dept. of Cell Biol. and Neuroanatomy
4-135 Jackson Hall
University of Minnesota Medical School
Minneapolis, MN 55455

Guojuan Liao
Dept. of Anatomy and Cell Biology
Columbia University College of Physicians and Surgeons
630 W. 168th St.
New York, NY 10032

Eduardo Macagno
Dept. of Biological Sciences
1003B Fairchild, MC 2442
Columbia University
New York, NY 10027

Robert D. MacElroy
NASA
Ames Research Center
239-23
Moffett Field, CA 94035

Anthony Mahowald
Dept. Mol. Genetics and Cell Biology
University of Chicago
920 E. 58th Street
Chicago, IL 60637

Andrew Maniotis
Enders 1007—Surgical Research
Children's Hospital
300 Longwood Avenue
Boston, MA 02115

Alexande Mogilner
Department of Mathematics
University of California
Davis, CA 95616

Paul O'Lague
Department of Biology
UCLA
Los Angeles, CA 90024

James Oschman
Nature's Own Research Assoc.
P.O. Box 5101
Dover, NH 03821-5101

Sean Palacek
Dept. of Chem. Engineering and Center for Biomed. Engineering
MIT
Cambridge, MA 02139

Wayne Patton
Department of Biology
Boston University
5 Cummington St.
Boston, MA 02215-2406

Robert Pelham
University of Massachusetts Medical Center
Worcester Foundation Campus
222 Maple Ave
Shrewsbury, MA 01545-2795

Nancy Rafferty
Marine Biological Laboratory
7 MBL St.
Woods Hole, MA 02543

Robert Rice
Box 219
Woods Hole, MA 02543

Birgit Rose
Lab. of Cell Communication
Marine Biological Laboratory
7 MBL St.
Woods Hole, MA 02543

Tom Scott
Life and Biomed. Sci and Applications Div.
NASA Headquarters
Washington, DC 20546

Nancy Searby
NASA
Ames Research Center
MS 236-5
Moffett Field, CA 94035

Yinon Shafrir
Department of Physics
Clarkson University
Potsdam, NY 13699

Jagesh Shah
Experimental Medicine Division
Brigham and Women's Hospital
221 Longwood Ave. LMRC #301
Boston, MA 02115

David Shepro
Microvascular Research Lab
Boston University Medical School
Boston, MA 02215

John Shyy
Department of Bioengineering
University of California at San Diego
La Jolla, CA 92093-0412

Marvin Solit
212 Concord Ave
Cambridge, MA 02138

Timothy Spann
Dept. of Cell and Mol. Biol.
Northwestern University Medical School
303 Chicago Ave
Chicago, IL 60611

Alfred Stracher
Dept. of Biochemistry
SUNY Health Sci. Ctr at Brooklyn
450 Clarkson Ave
Brooklyn, NY 11203

Tatyana Svitkina
Lab. of Molecular Biology
University of Wisconsin
1525 Linden Drive
Madison, WI 53706–1514

Sidney Tamm
Department of Biology
Boston University
5 Cummington St.
Boston, MA 02215

Jay Tang
Div. of Experimental Medicine
Brigham and Women's Hospital
221 Longwood Ave. LMRC #301
Boston, MA 02115

Charles Wade
NASA
Ames Research Center
Life Sciences MS-239-11
Moffett Field, CA 94965

Julia Wulfkuhle
University of Massachusetts Medical Center
Worcester Foundation Campus
222 Maple Ave.
Worcester, MA 01545-2795

INDEX

D

E

F

G

H

I

J

K

L

M

N

O

P

Q

R

S

T

U

V

W

Y

Z

Ask any researcher about the Olympus line of Advanced Research Microscopes.

We did.

"The Provis Microscope simply gives me the application versatility I want," one researcher told us. "The resolution and contrast are quite spectacular. I can even see new detail when I review my older specimens. And you have all the right imaging modules and accessories I need to configure my microscope system. Your special fluorescence-excitation balancer, for instance, is a great accessory—I can now visually balance the signal between two probes!"

What about your needs? If your field is neuroscience, our BX50WI offers you the best stability and a focus mechanism that moves nothing but the nosepiece. On the other hand, your research may call for our new LSM Fluoview desktop confocal laser system. Or you may need the unparalleled light transmission of the iX70 inverted.

Whichever microscope you select, it's totally configurable to your personal specifications. So find out how our advanced microscope systems can match your requirements today and evolve for your changing needs tomorrow. Call us at 1-800-455-8236. Or fax 1-612-942-6940. We'll give you all the answers you can ask for.

OLYMPUS

RESEARCH MICROSCOPES.

The world's most custom-built microscopes.